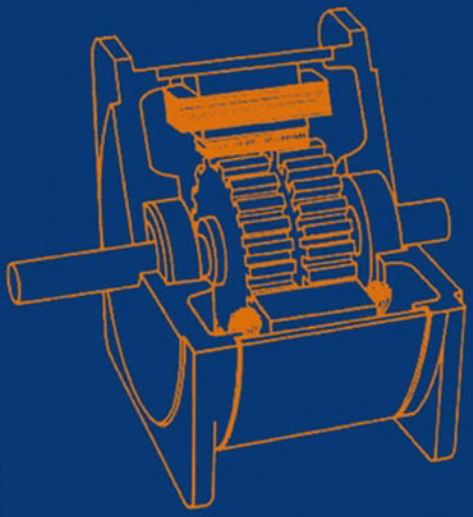
IEEE Series on Power Engineering M. E. El-Hawary, Series Editor

Modeling and High-Performance Control of Electric Machines



ftp://
SITE AVAILABLE

JOHN CHIASSON

www.EngineeringEBooksPdf.com

MODELING AND HIGH-PERFORMANCE CONTROL OF ELECTRIC MACHINES

www.EngineeringEBooksPdf.com

This Page Intentionally Left Blank

www.EngineeringEBooksPdf.com

MODELING AND HIGH-PERFORMANCE CONTROL OF ELECTRIC MACHINES

www.EngineeringEBooksPdf.com

Books in the IEEE Press Series on Power Engineering

Rating of Electric Power Cables in Unfavorable Thermal Environments
George J. Anders

Power System Protection
P. M. Anderson

Understanding Power Quality Problems: Voltage Sags and Interruptions
Math H. J. Bollen

Modeling and High-Performance Control of Electric Machines
John Chiasson

Electric Power Applications of Fuzzy Systems
Edited by M. E. El-Hawary

Principles of Electric Machines with Power Electronic Applications,
Second Edition
M. E. El-Hawary

Pulse Width Modulation for Power Converters: Principles and Practice
D. Grahame Holmes and Thomas Lipo

Analysis of Electric Machinery and Drive Systems, Second Edition
Paul C. Krause, Oleg Wasynczuk, and Scott D. Sudhoff

Risk Assessment for Power Systems: Models, Methods, and Applications
Wenyan Li

Optimization Principles: Practical Applications to the Operations and Markets of the Electric Power Industry
Narayan S. Rau

Electric Economics: Regulation and Deregulation
Geoffrey Rothwell and Tomas Gomez

Electric Power Systems: Analysis and Control
Fabio Saccomanno

Electrical Insulation for Rotating Machines: Design, Evaluation, Aging, Testing, and Repair
Greg Stone, Edward A. Boulter, Ian Culbert, and Hussein Dhirani

www.EngineeringEBooksPdf.com

MODELING AND HIGH-PERFORMANCE CONTROL OF ELECTRIC MACHINES

JOHN CHIASSON



IEEE Press Series on Power Engineering
Mohamed E. El-Hawary, *Series Editor*

IEEE

The Institute of Electrical and Electronics Engineers, Inc., New York

WILEY-INTERSCIENCE

A JOHN WILEY & SONS, INC., PUBLICATION

www.EngineeringEBooksPdf.com

Copyright © 2005 by John Wiley & Sons, Inc. All rights reserved.

Published by John Wiley & Sons, Inc., Hoboken, New Jersey.
Published simultaneously in Canada.

No part of this publication may be reproduced, stored in a retrieval system or transmitted in any form or by any means, electronic, mechanical, photocopying, recording, scanning or otherwise, except as permitted under Section 107 or 108 of the 1976 United States Copyright Act, without either the prior written permission of the Publisher, or authorization through payment of the appropriate per-copy fee to the Copyright Clearance Center, Inc., 222 Rosewood Drive, Danvers, MA 01923, (978) 750-8400, fax (978) 646-8600, or on the web at www.copyright.com. Requests to the Publisher for permission should be addressed to the Permissions Department, John Wiley & Sons, Inc., 111 River Street, Hoboken, NJ 07030, (201) 748-6011, fax (201) 748-6008.

Limit of Liability/Disclaimer of Warranty: While the publisher and author have used their best efforts in preparing this book, they make no representation or warranties with respect to the accuracy or completeness of the contents of this book and specifically disclaim any implied warranties of merchantability or fitness for a particular purpose. No warranty may be created or extended by sales representatives or written sales materials. The advice and strategies contained herein may not be suitable for your situation. You should consult with a professional where appropriate. Neither the publisher nor author shall be liable for any loss of profit or any other commercial damages, including but not limited to special, incidental, consequential, or other damages.

For general information on our other products and services please contact our Customer Care Department within the U.S. at 877-762-2974, outside the U.S. at 317-572-3993 or fax 317-572-4002.

Wiley also publishes its books in a variety of electronic formats. Some content that appears in print, however, may not be available in electronic format.

Library of Congress Cataloging-in-Publication Data:

Chiasson, John Nelson.
Modeling and high performance control of electric machines / John Chiasson.
p. cm. — (IEEE Press series on power engineering)
Includes bibliographical references and index.
ISBN 0-471-68449-X (cloth)
1. Electric machinery—Automatic control—Mathematical models. I. Title. II. Series.
TK2181.C43 2005
621.31'042—dc22 2004021739

Printed in the United States of America.

10 9 8 7 6 5 4 3 2 1

www.EngineeringEBooksPdf.com

To My Parents

and to

Marc Bodson

Pour son soutien et son aide jour après jour durant une période très difficile de ma carrière

Amro El-Jaroudi
Mahmoud El Nokali

إِلَى اصدقَائِي الذينَ وَقَفُوا بِجَانِبِي في تِلكَ الأَوقَاتِ العَصيبَةِ مِن حَيَاتِي

James B. Lieber

על שתמיד האמנת בי ועל עזרתך הרבה בשעתי הקשה בקריירה האקדמית שלי

www.EngineeringEBooksPdf.com

This Page Intentionally Left Blank

www.EngineeringEBooksPdf.com

Contents

I DC Machines, Controls, and Magnetics **1**

1 The Physics of the DC Motor **3**
1.1 Magnetic Force . . . 3
1.2 Single-Loop Motor . . . 5
1.2.1 Torque Production . . . 6
1.2.2 Commutation of the Single-Loop Motor . . . 9
1.3 Faraday's Law . . . 11
1.3.1 The Surface Element Vector $d\vec{\mathbf{S}}$ . . . 12
1.3.2 Interpreting the Sign of ξ . . . 13
1.3.3 Back Emf in a Linear DC Machine . . . 14
1.3.4 Back Emf in the Single-Loop Motor . . . 15
1.3.5 Self-Induced Emf in the Single-Loop Motor . . . 18
1.4 Dynamic Equations of the DC Motor . . . 20
1.5 Microscopic Viewpoint . . . 23
1.5.1 Microscopic Viewpoint of the Single-Loop DC Motor 26
1.5.2 Drift Speed . . . 28
1.6 Tachometer for a DC Machine*[1] . . . 29
1.6.1 Tachometer for the Linear DC Machine . . . 29
1.6.2 Tachometer for the Single-Loop DC Motor . . . 30
1.7 The Multiloop DC Motor* . . . 31
1.7.1 Increased Torque Production . . . 32
1.7.2 Commutation of the Armature Current . . . 32
1.7.3 Armature Reaction . . . 38
1.7.4 Field Flux Linkage and the Air Gap Magnetic Field 40
1.7.5 Armature Flux Due to the External Magnetic Field 41
1.7.6 Equations of the PM DC Motor . . . 43
1.7.7 Equations of the Separately Excited DC Motor . . . 44
Appendices . . . 47
Rotational Dynamics . . . 47
Gears . . . 52
Problems . . . 57

2 Feedback Control **71**
2.1 Model of a DC Motor Servo System . . . 71

[1] Sections marked with an asterisk (*) may be skipped without loss of continuity.

www.EngineeringEBooksPdf.com

2.2 Speed Estimation 77
2.2.1 Backward Difference Estimation of Speed 77
2.2.2 Estimation of Speed Using an Observer 79
2.3 Trajectory Generation 82
2.4 Design of a State Feedback Tracking Controller 86
2.5 Nested Loop Control Structure* 90
2.6 Identification of the DC Motor Parameters* 96
2.6.1 Least-Squares Approximation 99
2.6.2 Error Index 103
2.6.3 Parametric Error Indices 103
2.7 Filtering of Noisy Signals* 108
2.7.1 Filter Representations 111
2.7.2 Causality 112
2.7.3 Frequency Response 112
2.7.4 Low-Pass Filters with Linear Phase 113
2.7.5 Distortion 114
2.7.6 Low-Pass Filtering of High-Frequency Noise 114
2.7.7 Butterworth Filters 116
2.7.8 Implementation of the Filter 118
2.7.9 Discretization of Differential Equations 120
2.7.10 Digital Filtering 122
2.7.11 State-Space Representation 124
2.7.12 Noncausal Filtering 126
Appendix - Classical Feedback Control 129
Tracking and Disturbance Rejection 129
General Theory of Tracking and Disturbance Rejection . . . 144
Internal Model Principle 149
Problems 151

3 Magnetic Fields and Materials **177**
3.1 Introduction 177
3.2 The Magnetic Field $\vec{\mathbf{B}}$ and Gauss's Law 183
3.2.1 Conservation of Flux 186
3.3 Modeling Magnetic Materials 190
3.3.1 Magnetic Dipole Moments 192
3.3.2 The Magnetization $\vec{\mathbf{M}}$ and Ampère's Law 194
3.3.3 Relating $\vec{\mathbf{B}}$ to $\vec{\mathbf{M}}$ 201
3.4 The Magnetic Intensity Field Vector $\vec{\mathbf{H}}$ 205
3.4.1 The $B-H$ Curve 207
3.4.2 Computing $\vec{\mathbf{B}}$ and $\vec{\mathbf{H}}$ in Magnetic Circuits 211
3.4.3 $\vec{\mathbf{B}}$ is Normal to the Surface of Soft Magnetic Material 217
3.5 Permanent Magnets* 219
3.5.1 Hysteresis Loss 223
3.5.2 Common Magnetic Materials 225
Problems 226

www.EngineeringEBooksPdf.com

II AC Machine Theory **235**

4 Rotating Magnetic Fields **245**
4.1 Distributed Windings 245
4.2 Approximate Sinusoidally Distributed $\vec{\mathbf{B}}$ Field 249
4.2.1 Conservation of Flux and $1/r$ Dependence 254
4.2.2 Magnetic Field Distribution Due to the Stator Currents 256
4.3 Sinusoidally Wound Phases 257
4.3.1 Sinusoidally Wound Rotor Phase 257
4.3.2 Sinusoidally Wound Stator Phases 258
4.4 Sinusoidally Distributed Magnetic Fields 259
4.4.1 Sinusoidally Distributed Rotating Magnetic Field . 262
4.5 Magnetomotive Force (mmf) 264
4.6 Flux Linkage 266
4.7 Azimuthal Magnetic Field in the Air Gap* 269
4.7.1 Electric Field $\vec{\mathbf{E}}_{Sa}$ 275
4.7.2 The Magnetic and Electric Fields $\vec{\mathbf{B}}_{Sa}, \vec{\mathbf{E}}_{Sa}, \vec{\mathbf{B}}_{Sb}, \vec{\mathbf{E}}_{Sb}$ 276
Problems 277

5 The Physics of AC Machines **293**
5.1 Rotating Magnetic Field 293
5.2 The Physics of the Induction Machine 296
5.2.1 Induced Emfs in the Rotor Loops 297
5.2.2 Magnetic Forces and Torques on the Rotor 299
5.2.3 Slip Speed 302
5.3 The Physics of the Synchronous Machine 302
5.3.1 Two-Phase Synchronous Motor with a Sinusoidally Wound Rotor 303
5.3.2 Emfs and Energy Conversion 309
5.3.3 Synchronous Motor with a Salient Rotor 313
5.3.4 Armature and Field Windings 315
5.4 Microscopic Viewpoint of AC Machines* 315
5.4.1 Rotating Axial Electric Field Due to the Stator Currents 316
5.4.2 Induction Machine in the Stationary Coordinate System 317
5.4.3 Faraday's Law and the Integral of the Force per Unit Charge 323
5.4.4 Induction Machine in the Synchronous Coordinate System 326
5.4.5 Synchronous Machine 334
5.5 Steady-State Analysis of a Squirrel Cage Induction Motor* 334
5.5.1 Rotor Fluxes, Emfs, and Currents 336
5.5.2 Rotor Torque 337
5.5.3 Rotor Magnetic Field 342

www.EngineeringEBooksPdf.com

5.5.4 Comparison with a Sinusoidally Wound Rotor . . . 344
Problems . . . 346

6 Mathematical Models of AC Machines 363
6.1 The Magnetic Field $\vec{\mathbf{B}}_R(i_{Ra}, i_{Rb}, r, \theta - \theta_R)$ . . . 364
6.2 Leakage . . . 366
6.3 Flux Linkages in AC Machines . . . 370
6.3.1 Flux Linkages in the Stator Phases . . . 370
6.3.2 Flux Linkages in the Rotor Phases . . . 375
6.4 Torque Production in AC Machines . . . 380
6.5 Mathematical Model of a Sinusoidally Wound Induction Machine . . . 383
6.6 Total Leakage Factor . . . 385
6.7 The Squirrel Cage Rotor . . . 386
6.8 Induction Machine With Multiple Pole Pairs . . . 387
6.9 Mathematical Model of a Wound Rotor Synchronous Machine . . . 388
6.10 Mathematical Model of a PM Synchronous Machine . . . 390
6.11 The Stator and Rotor Magnetic Fields of an Induction Machine Rotate Synchronously* . . . 391
6.12 Torque, Energy, and Co-energy* . . . 393
6.12.1 Magnetic Field Energy . . . 393
6.12.2 Computing Torque From the Field Energy . . . 396
6.12.3 Computing Torque From the Co-energy . . . 397
Problems . . . 401

7 Symmetric Balanced Three-Phase AC Machines 413
7.1 Mathematical Model of a Three-Phase Induction Motor . . . 413
7.2 Steady-State Analysis of the Induction Motor . . . 434
7.2.1 Steady-State Currents and Voltages . . . 434
7.2.2 Steady-State Equivalent Circuit Model . . . 436
7.2.3 Rated Conditions . . . 440
7.2.4 Steady-State Torque . . . 441
7.2.5 Steady-State Power Transfer in the Induction Motor 444
7.3 Mathematical Model of a Three-Phase PM Synchronous Motor . . . 449
7.4 Three-Phase, Sinusoidal, 60-Hz Voltages* . . . 458
7.4.1 Why Three-Phase? . . . 458
7.4.2 Why AC? . . . 471
7.4.3 Why Sinusoidal Voltages? . . . 472
7.4.4 Why 60 Hz? . . . 474
Problems . . . 475

8 Induction Motor Control 493
8.1 Dynamic Equations of the Induction Motor . . . 493

www.EngineeringEBooksPdf.com

8.1.1 The Control Problem 494
8.2 Field-Oriented and Input-Output Linearization Control of an Induction Motor 497
8.2.1 Current-Command Field-Oriented Control 501
8.2.2 Experimental Results Using a Field-Oriented Controller 506
8.2.3 Field Weakening 509
8.2.4 Input-Output Linearization 511
8.2.5 Experimental Results Using an Input-Output Controller 514
8.3 Observers 519
8.3.1 Flux Observer 519
8.3.2 Speed Observer 521
8.3.3 Verghese–Sanders Flux Observer* 524
8.4 Optimal Field Weakening* 528
8.4.1 Torque Optimization Under Current Constraints . . 529
8.4.2 Torque Optimization Under Voltage Constraints . . 530
8.4.3 Torque Optimization Under Voltage and Current Constraints 537
8.5 Identification of the Induction Motor Parameters* 548
8.5.1 Linear Overparameterized Model 549
8.5.2 Nonlinear Least-Squares Identification 552
8.5.3 Calculating the Parametric Error Indices 556
8.5.4 Mechanical Parameters 557
8.5.5 Simulation Results 558
8.5.6 Experimental Results 560
Appendix 565
Elimination Theory and Resultants 565
Problems 568

9 PM Synchronous Motor Control **591**
9.1 Field-Oriented Control 591
9.1.1 Design of the Reference Trajectory and Inputs . . . 592
9.1.2 State Feedback Controller 595
9.1.3 Speed Observer 597
9.1.4 Experimental Results 598
9.1.5 Current Command Control 606
9.2 Optimal Field Weakening* 608
9.2.1 Formulation of the Torque Maximization Problem . 608
9.2.2 Speed Ranges and Transition Speeds 609
9.2.3 Two Examples 615
9.3 Identification of the PM Synchronous Motor Parameters* . 624
9.3.1 Experimental Results 627
9.4 PM Stepper Motors* 632
9.4.1 Open-Loop Operation of the Stepper Motor 635

www.EngineeringEBooksPdf.com

9.4.2 Mathematical Model of a PM Stepper Motor 639
9.4.3 High-Performance Control of a PM Stepper Motor . 641
Appendices 641
Two-Phase Equivalent Parameters 641
Current Plots 643
Problems 645

10 Trapezoidal Back-Emf PM Synchronous Motors (BLDC) 651
10.1 Construction 651
10.2 Stator Magnetic Field $\vec{\mathbf{B}}_S$ 654
10.3 Stator Flux Linkage Produced by $\vec{\mathbf{B}}_S$ 657
10.4 Stator Flux Linkage Produced by $\vec{\mathbf{B}}_R$ 661
10.5 Emf in the Stator Windings Produced by $\vec{\mathbf{B}}_R$ 666
10.6 Torque 668
10.7 Mathematical Model 671
10.8 Operation and Control 673
10.8.1 The Terminology "Brushless DC Motor" 677
10.9 Microscopic Viewpoint of BLDC Machines* 679
10.9.1 Axial Electric Field $\vec{\mathbf{E}}_R$ 679
10.9.2 Emf Induced in the Stator Phases 681
Problems 684

Trigonometric Table and Identities 687
Trigonometric Table 687
Trigonometric Identities 688

References 691

Index 701

www.EngineeringEBooksPdf.com

Preface

This book is intended to be an exposition of the modeling and control of electric machines, specifically, the direct current (DC) machine and the alternating current (AC) machines consisting of the induction motor, the permanent magnet (PM) synchronous motor, and the brushless DC motor. The particular emphasis here is on techniques used for high-performance applications, that is, applications that require both rapid and precise control of position, speed, and/or torque. Traditionally, DC motors were reserved for high-performance applications (positioning systems, rolling mills, traction drives, etc.) because of their relative ease of control compared to AC machines. However, with the advances in control methods, computing capability, and power electronics, AC motors continue to replace DC motors in high-performance applications. The intent here is to carefully derive the mathematical models of the AC machines and show how these mathematical models are used to design control algorithms that achieve high performance.

Electric machines are a particularly fascinating application of basic electricity and magnetism. The presentation here relies heavily on these basic concepts from Physics to develop the models of the motors. Specifically, Faraday's law ($\xi = -d\phi/dt$, where $\phi = \int_S \vec{\mathbf{B}} \cdot d\vec{\mathbf{S}}$), the magnetic force law ($\vec{\mathbf{F}} = i\vec{\boldsymbol{\ell}} \times \vec{\mathbf{B}}$ or, $\vec{\mathbf{F}} = q\vec{\mathbf{v}} \times \vec{\mathbf{B}}$), Gauss's law ($\oint \vec{\mathbf{B}} \cdot d\vec{\mathbf{S}} = 0$), Ampère's law ($\oint \vec{\mathbf{H}} \cdot d\vec{\boldsymbol{\ell}} = i_{\text{free}}$), the relationship between $\vec{\mathbf{B}}$ and $\vec{\mathbf{H}}$, properties of magnetic materials, and so on are reviewed in detail and used extensively to derive the currently accepted nonlinear differential equation models of the various AC motors. The author made his best attempt to make the modeling assumptions as clear as possible and to consistently show that the magnetic and electric fields satisfy Maxwell's equations (as, of course, they must). The classical approach to teaching electric machinery is to present their equivalent circuit models and to analyze these circuit models ad nauseam. Further, the use of the basic Physics of electricity and magnetism to explain their operation is minimized if not omitted. However, the equivalent circuit is a result of assuming constant-speed operation of the machine and computing the sinusoidal steady-state solution of the nonlinear differential equation model of the machine. Here, the emphasis is on explaining how the machines work using fundamental concepts from electricity and magnetism, and on the derivation of their nonlinear differential equation models. The derivation of the corresponding equivalent circuit assuming steady-state conditions is then straightforward.

Electric machines also provide fascinating examples to illustrate con-

www.EngineeringEBooksPdf.com

cepts from electromagnetic field theory (in contrast to electricity and magnetism). In particular, the way the electric and magnetic fields change as one goes between reference frames that are in relative motion are vividly illustrated using AC machines. For this reason, optional sections are included to show how the electric and magnetic fields change as one goes between a coordinate system attached to the stator to a coordinate system that rotates with the rotating magnetic field produced by the stator currents or a frame attached to the rotor. Also given in an optional section is the derivation of the axial electric and azimuthal magnetic fields in the air gap.

This is also a book on the control of electric machines based on their differential equation models. With the notable exception of the sinusoidal steady-state analysis of the induction motor in Chapter 7, very little attention is given to the classical equivalent circuits as these models are valid only in steady state. Rather, the differential equation models are used as the basis to develop the notions of field-oriented control, input-output linearization, flux observers, least-squares identification methods, state feedback trajectory tracking, and so on. This is a natural result of the emphasis here on high-performance control methods (e.g., field-oriented control) as opposed to classical methods (e.g., V/f, slip control, etc.).

There are of course many good books in the area of electric machines and their control. The author owes a debt of gratitude to Professor W. Leonhard for his book [1] (see the most recent edition [2]), from which he was educated in the modeling and control of electric drives. The present book is narrower in focus with an emphasis on the modeling and operation of electric machines based on elementary classical physics and an emphasis on high-performance control methods using a state-space formulation. The books by P. C. Krause [3] and P. C. Krause et al. [4] are complete in their derivation of the mathematical models of electric machines while C. B. Gray [5] presents electromagnetic theory in the context of electric machines. A comprehensive treatment using SIMULINK to simulate electric machinery is given in C-M. Ong's book [6]. The graduate level books by D. W. Novotny and T. A. Lipo [7], P. Vas [8], J. M. D. Murphy and F. G. Turnbull [9], I. Boldea and S. A. Nasar [10], B. Adkins and R. G. Harley [11], A. M. Trzynadlowski [12], M. P. Kazmierkowski and H. Tunia [13], B. K. Bose [14], and R. Krishnan [15] all cover the modeling and control of electric machines while the books by R. Ortega et al. [16], D. M. Dawson et al. [17], and F. Khorrami et al. [18] emphasize advanced control methods.

The introductory-level books by S. J. Chapman [19], H. Woodson and J. Melcher [20], L. W. Matsch and J. D. Morgan [21], G. McPherson and R. D. Laramore [22], D. V. Richardson [23], P. C. Krause and O. Wasynczuk [24], N. Mohan [25], G. R. Slemon and A. Straughn [26], J. Sokira and W. Jaffe [27], G. J. Thaler and M. L. Wilcox [28], V. Deltoro [29], M. El-Hawary [30], P. C. Sen [31], and G. R. Slemon [32] are among the many books on electric machines from which this author has benefited.

www.EngineeringEBooksPdf.com

The beautifully written textbooks *PSSC Physics* by the Physical Science Curriculum Study [33], *Physics* by D. Halliday and R. Resnick [34], *Principles of Electrodynamics* by M. Schwartz [35], and *Electromagnetic Fields* by R. K. Wangness [36] are used as references for the theory of electricity and magnetism.

This book borrows from these above works and hopefully makes its own contribution to the literature on electric machines.

Part I of the book consists of the first three chapters. Chapters 1 and 2 present a detailed review of the basic concepts of electricity and magnetism in the context of DC machines and an introduction to control methods, respectively, which will be used extensively in the remaining chapters. The third chapter on magnetic fields and magnetic materials is intended to be a detailed introduction to the subject. For example, most textbooks assume that the reader understands Ampère's law in the form $\oint \vec{\mathbf{H}} \cdot d\vec{\boldsymbol{\ell}} = i_{\text{free}}$ and that $\vec{\mathbf{B}} = \mu \vec{\mathbf{H}}$ in (soft) magnetic materials, yet it is the experience of the author that students do not have a fundamental understanding of these concepts.

These first three chapters are elementary in nature and were written to be accessible to undergraduates. The reason for this is that often control engineers do not have any background in electric machinery while power/electric-machine engineers often do not have any background in basic state-space concepts of control theory. Consequently, it is hoped that these chapters can bring the reader "up to speed" in these areas.

Chapter 1 reviews the basic ideas of electricity and magnetism that are needed to model electric machines. In particular, the notions of magnetic fields, magnetic force and Faraday's law are reviewed by using them to derive the standard model of a DC motor.

Chapter 2 provides an elementary introduction to the control techniques required for the high-performance control of electric machines. This includes an elementary presentation of state feedback control, observers, and identification theory as applied to DC machines to prepare the reader for the subsequent chapters.

Chapter 3 goes into the modeling of magnetic materials in terms of their use in electric machines. The fundamental result of this chapter is the modification of Ampère's law $\oint_C \vec{\mathbf{B}} \cdot d\vec{\boldsymbol{\ell}} = \mu_0 i$ so that it is valid in the presence of magnetic material. This introduces the magnetic intensity field $\vec{\mathbf{H}}$ and its relationship to magnetic induction field $\vec{\mathbf{B}}$ via the magnetization vector $\vec{\mathbf{M}}$ to obtain the more general version of Ampère's law $\oint \vec{\mathbf{H}} \cdot d\vec{\boldsymbol{\ell}} = i_{\text{free}}$. All of this requires a significant discussion of the modeling of magnetic materials. The approximation $\vec{\mathbf{H}} = 0$ in magnetic materials is discussed, and then it is shown how this approximation along with Ampère's law can be used to find the radial component of $\vec{\mathbf{B}}$ in the air gap of electric machines. Also presented is Gauss's law for $\vec{\mathbf{B}}$; this leads to the notion of conservation of flux, as well as the fact that $\vec{\mathbf{B}}$ is normal to the surface of

www.EngineeringEBooksPdf.com

soft magnetic materials. This chapter should be read, but the reader should not get "bogged down" in the chapter. Rather, the main results should be remembered.

Part II consists of Chapters 4 through 10 and presents the modeling and control of AC machines.

Chapter 4 uses the results of Chapters 1 and 3 to explain how a radially directed rotating magnetic field can be established in the air gap of AC machines. In particular, the notions of distributed windings and of sinusoidally wound turns (phase windings) are explained. Ampère's law is then used to show that a sinusoidal (spatially) distributed radial magnetic field is established in the air gap by the currents in the phase windings. The concept of flux linkage in distributed windings is explained, and the chapter ends with an optional section on the azimuthal magnetic field in the air gap.

Chapter 5 explains the fundamental Physics behind the working of induction and synchronous machines. Specifically, this chapter uses a simplified model of the induction motor and shows how voltages and currents are induced in the rotor loops by the rotating magnetic field established by the stator currents. Then it is shown how torque is produced on these induced currents by the same stator rotating magnetic field that induced them introducing the idea of slip. Similarly, the synchronous machine is analyzed to show how the rotating radial magnetic field established by the stator currents produces torque on a rotor carrying constant current.

An optional section on the microscopic point of view of the Physics of the induction motor is also presented. This includes a discussion of how the electric and magnetic fields change as one goes between coordinate systems that are rotating with respect to each other and how one reinterprets the Physics of the machine's operation. The chapter ends with another optional section of the steady-state behavior of an induction machine with a squirrel cage rotor.

Chapter 6 derives the systems of differential equations that mathematically model the two-phase induction and synchronous machines. The concept of leakage is presented and accounted for in the derived models. These models are the accepted models used throughout the literature and form the basis for high-performance control of these machines. In an optional section it is shown that the stator and rotor *magnetic fields* of an induction motor rotate synchronously together as they do in a synchronous machine. The chapter ends with another optional section on the concepts of field energy and co-energy, and how the expression for the torque of an electric machine can be derived using these notions.

Chapter 7 presents the derivation of the models of three-phase AC machines and their two-phase equivalent models. These derivations readily follow from the results of Chapter 6. The classical steady-state analysis of the induction motor is also presented including its equivalent circuit. The chapter ends with a discussion of why the standard power system is an AC

www.EngineeringEBooksPdf.com

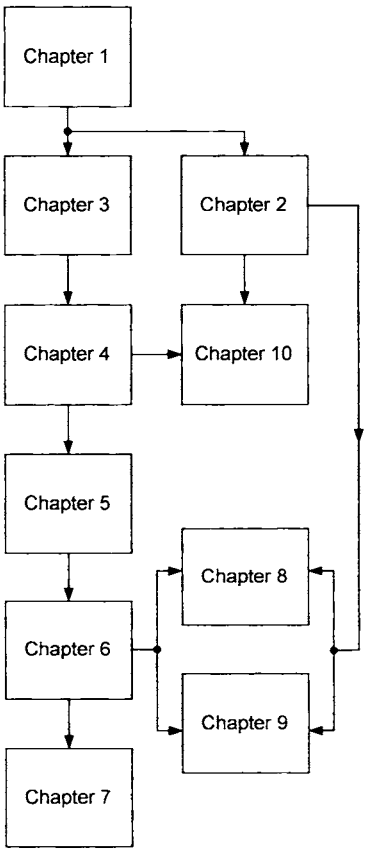
sinusoidal three-phase 60-Hz (or 50-Hz) system.

Chapter 8 covers the control of induction motors presenting both field-oriented control and input-output linearization control. Flux observers, field weakening, and speed observers are also presented along with experimental results. The chapter ends with an optional section on how to identify the induction motor parameters using a nonlinear least-squares technique.

Chapter 9 covers the control of synchronous motors describing field-oriented control, field weakening, speed observers and identification methods. The operation and modeling of permanent magnet stepping motors is also covered.

Chapter 10 covers the modeling and control of PM synchronous motors with trapezoidal back emf, which are also known as brushless DC (BLDC) motors.

The logical dependence of the chapters is shown in the block diagram below assuming that the optional sections are *not* covered.



Logical dependence of the chapters.

www.EngineeringEBooksPdf.com

Finally, the author's intent for this book was for the reader to understand how electric machines are modeled and to understand the basic techniques in their control. The references at the end of the book are only those directly referenced in the book and are *not* representative of (nor give proper recognition to) the many important contributions made by researchers throughout the world. The reader is referred to Professor Leonhard's book [2] for a much more extensive reference list.

Comments on the Use of the Book

In using this book in a one-semester graduate-level course, the following material was usually covered:

Chapter 1, Sections 1.1–1.7
Chapter 2, Sections 2.1–2.4
Chapter 3, Sections 3.1–3.4
Chapter 4, Sections 4.1–4.5
Chapter 5, Sections 5.1–5.3
Chapter 6, Sections 6.1–6.10
Chapter 7, Sections 7.1–7.3
Chapter 8, Sections 8.1–8.3
Chapter 9, Section 9.1

Sections marked with an asterisk (*) may be omitted without loss of continuity. Some of these optional sections assume familiarity with Maxwell's equations in *differential* form.

Acknowledgments

There are many people that I would to acknowledge for their help in my work in the control of electric machines.

I did my Ph.D. thesis in Algebraic Systems Theory which is quite far from the area of Electric Machines. Nevertheless, I am most grateful to my advisor, Professor E. Bruce Lee, who has always shown me his kindness over the years.

Professor Edward W. Kamen (formerly at the University of Pittsburgh) along with Mr. Stephen Botos (President of Aerotech, Inc.) were instrumental through their enthusiasm and financial support at the University of Pittsburgh, through which many of the results presented here were funded. I am very grateful to Mike Aiello (chief design engineer at Aerotech) for both designing and building our hardware platform, resulting in a successful set of experiments.

I would like to thank The Oak Ridge National Laboratory in particular, Don Adams and Laura Marlino, for funding the recent results on the identification of the induction motor parameters presented in Chapter 8.

www.EngineeringEBooksPdf.com

Shortly after I arrived at the University of Pittsburgh, I started to work with Marc Bodson (formerly at Carnegie Mellon University) and I want to express my deep gratitude to him for this collaboration, which led to many of the new theoretical and experimental results presented in Chapters 8 and 9.

Also, shortly after I arrived at the University of Tennessee, I began to work with Leon M. Tolbert, and I am very grateful for this collaboration as well.

Mohamed Zribi was the first student I worked with in this area, leading to a paper on feedback linearization control of stepper motors. Ron Rekowski suffered through our first attempts to do some experiments for which I am grateful. My Ph.D. student Bob Novotnak continued this work and did the experiments on the control of the stepper and induction motors presented in Chapters 8 and 9 of this book. Through his skill we were able to obtain experimental results demonstrating very high performance. Jennifer Stephans (Marc Bodson's student) did the early work on identification for the induction motor while my student Kaiyu Wang did the identification experiments for the induction motor given in Chapter 8. Andy Blauch (Marc Bodson's student) did the identification experiments for the PM stepper motor presented in Chapter 9.

I first taught (and learned!) induction motor control using the book by Professor Werner Leonhard, and I am very grateful for his writing that book. I later had the opportunity to visit his institute in Braunschweig Germany from which I left with even more enthusiasm for the field.

I would like to thank the many students who suffered under the early versions of this book, or suffered with me as their advisor, or both. These include Mohamed Zribi, Bob Novotnak, Eric Shook, Ron Rekowski, Walt Barie, Joe Matesa, Chellury Sastry, Gary Campbell, David Schuerer, Atul Chaudhari, Jason Mueller, Samir Mehta, Pete Hammond, Dick Osman, Jim Short, Vincent Allarouse, Marc Aiello, Sean West, Baskar Vairamohan, Yinghui Lu, Zhong Tang, Mengwei Li, Kaiyu Wang, Yan Xu, Madhu Chinthavali, Jianqing Chen, Nivedita Alluri, Zhong Du, Faisal Khan, Pankaj Pandit, Hui Zhang, Wenjuan Zhang, Ben Sooter, Keith McKenzie, Rebin Zhou, Ann Chee Tan, Jesse Richmond, SeongTaek Lee, and all my other students.

I am very grateful to Thomas Keller for teaching me about real time simulators.

I would like to thank my colleagues Leon Tolbert, Saul Gelfand, Joachim Böcker, Miguel Vélez-Reyes, Michel Fliess, Thomas Keller, George Verghese, Jeff Lang, David Taylor, Ray DeCarlo, Mark Spong, Steve Yurkovich, Jessy Grizzle, Henk Nijmeijer, Chaouki Abdallah, Doug Birdwell, Gerardo Espinosa-Pérez, Romeo Ortega, Yih-Choung Yu, Gerardo Escobar-Valderrama, Daniel Campos-Delgado, Ricardo Fermat-Flores, Jesús Alvarez, Jesús Leyva-Ramos, Jeffrey Mayer, Kai Mueller, Henrik Mosskull, Stanislaw Żak, Samer Saab, Burak Özpineci, and Alex Stanković for their

www.EngineeringEBooksPdf.com

words of encouragement.

This book was written in LaTeX using SCIENTIFIC WORD from Mackichan Software (see *http://www.mackichan.com*). I would especially like to thank John McKendrick and Alan Green of Mackichan Software for their help with my many questions.

I would like thank my editor Valerie Moliere as well as my production editor Lisa Vanhorn of John Wiley & Sons for stepping me through the process of getting this book published. Bob Golden, who copy edited the manuscript of this book, is gratefully acknowledged for fixing many errors and inconsistencies.

I am very grateful to Sharon Katz for her drawings of Figures 1.8(a)−(d), 1.25, 1.41−1.47, 9.31, 9.34, 9.35(a)−(e) and for her help, suggestions and encouragement of the artwork in this book and for actually setting me on the path to getting the figures drawn. I would also like to thank Bret Wilfong, who drew Figures 4.1, 5.4(b), 5.7(b), and 5.8(b).

John Wiley & Sons maintains an ftp site at

ftp://ftp.wiley.com/public/sci_tech_med/high_performance_control

for downloading an errata sheet for the book. Instructors, upon obtaining password privileges, will also be able to download the simulation files that go with this textbook. A solutions manual is available to instructors by contacting their local Wiley representative.

Any comments, criticisms, and corrections are most welcome and may be sent to the author at *chiasson@ieee.org*.

John Chiasson

www.EngineeringEBooksPdf.com

MODELING AND HIGH-PERFORMANCE CONTROL OF ELECTRIC MACHINES

www.EngineeringEBooksPdf.com

This Page Intentionally Left Blank

www.EngineeringEBooksPdf.com

Part I

DC Machines, Controls, and Magnetics

www.EngineeringEBooksPdf.com

This Page Intentionally Left Blank

www.EngineeringEBooksPdf.com

1

The Physics of the DC Motor

The principles of operation of a direct current (DC) motor are presented based on fundamental concepts from electricity and magnetism contained in any basic physics course. The DC motor is used as a concrete example for reviewing the concepts of magnetic fields, magnetic force, Faraday's law, and induced electromotive forces (emf) that will be used throughout the remainder of the book for the modeling of electric machines. All of the Physics concepts referred to in this chapter are contained in the book *Physics* by Halliday and Resnick [34].

1.1 Magnetic Force

Motors work on the basic principle that magnetic fields produce forces on wires carrying a current. In fact, this experimental phenomenon is what is used to define the magnetic field. If one places a current carrying wire between the poles of a magnet as in Figure 1.1, a force is exerted on the wire. Experimentally, the magnitude of this force is found to be proportional to both the amount of current in the wire and to the length of the wire that is between the poles of the magnet. That is, F_{magnetic} is proportional to ℓi. The direction of the magnetic field $\vec{\mathbf{B}}$ at any point is defined to be the direction that a small compass needle would point at that location. This direction is indicated by arrows in between the north and south poles in Figure 1.1.

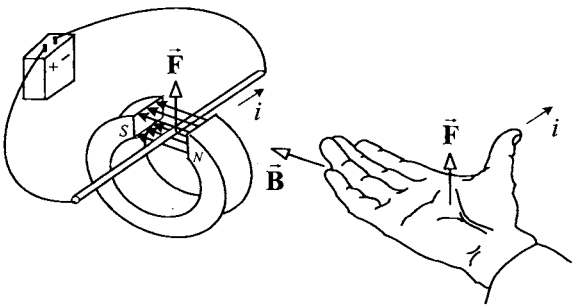


FIGURE 1.1. Magnetic force law. From *PSSC Physics*, 7th edition, by Haber-Schaim, Dodge, Gardner, and Shore, published by Kendall/Hunt, 1991.

www.EngineeringEBooksPdf.com

With the direction of $\vec{\mathbf{B}}$ perpendicular to the wire, the strength (magnitude) of the *magnetic induction field* $\vec{\mathbf{B}}$ is defined to be

$$B = \ |\vec{\mathbf{B}}| \ \triangleq \frac{F_{\text{magnetic}}}{\ell i}$$

where F_{magnetic} is the magnetic force, i is the current, and ℓ is the length of wire perpendicular to the magnetic field carrying the current. That is, B is the proportionality constant so that $F_{\text{magnetic}} = i\ell B$. As illustrated in Figure 1.1, the direction of the force can be determined using the right-hand rule. Specifically, using your right hand, point your fingers in the direction of the magnetic field and point your thumb in the direction of the current. Then the direction of the force is out of your palm.

Further experiments show that if the wire is parallel to the $\vec{\mathbf{B}}$ field rather than perpendicular as in Figure 1.1, then no force is exerted on the wire. If the wire is at some angle θ with respect to $\vec{\mathbf{B}}$ as in Figure 1.2, then the force is proportional to the *component* of $\vec{\mathbf{B}}$ perpendicular to the wire; that is, it is proportional to $B_\perp = B\sin(\theta)$. This is summarized in the *magnetic force law*: Let $\vec{\ell}$ denote a vector whose magnitude is the length ℓ of the wire in the magnetic field and whose direction is defined as the positive direction of current in the bar; then the magnetic force on the bar of length ℓ carrying the current i is given by

$$\vec{\mathbf{F}}_{\text{magnetic}} = i\vec{\ell} \times \vec{\mathbf{B}}$$

or, in scalar terms, $F_{\text{magnetic}} = i\ell B\sin(\theta) = i\ell B_\perp$. Again, $B_\perp \triangleq B\sin(\theta)$ is the component of $\vec{\mathbf{B}}$ perpendicular to the wire.[1]

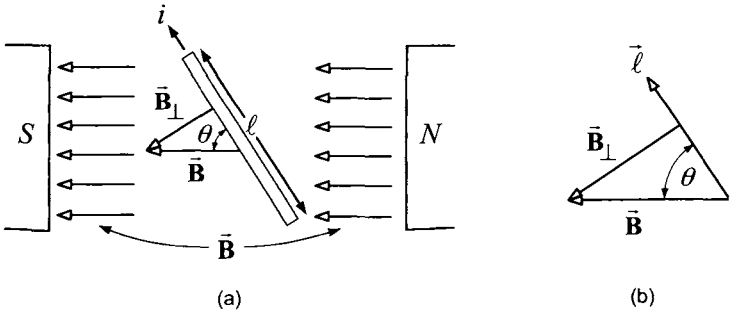


FIGURE 1.2. Only the component $B_\perp$ of the magnetic field which is perpendicular to the wire produces a force on the current.

[1] Motors are designed so that the conductors are perpendicular to the external magnetic field.

www.EngineeringEBooksPdf.com

Example *A Linear DC Machine* [19]

Consider the simple linear DC machine in Figure 1.3 where a sliding bar rests on a simple circuit consisting of two rails. An external magnetic field is going through the loop of the circuit up out of the page indicated by the $\otimes$ in the plane of the loop. Closing the switch results in a current flowing around the circuit and the external magnetic field produces a force on the bar which is free to move. The force on the bar is now computed.

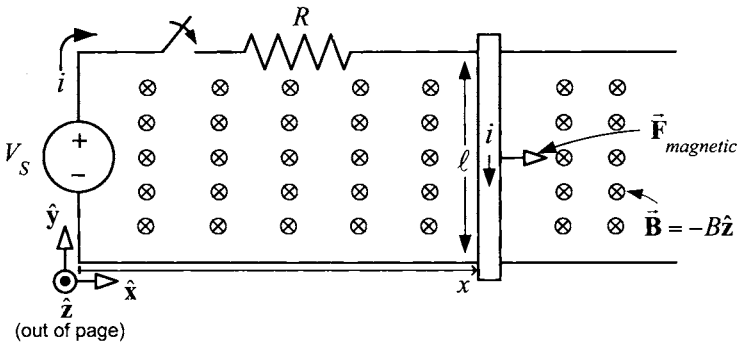


FIGURE 1.3. A linear DC motor.

The magnetic field is constant and points into the page (indicated by $\otimes$) so that written in vector notation, $\vec{\mathbf{B}} = -B\hat{\mathbf{z}}$ with $B > 0$. By the right hand rule, the magnetic force on the sliding bar points to the right. Explicitly, with $\vec{\boldsymbol{\ell}} = -\ell\hat{\mathbf{y}}$, the force is given by

$$\begin{aligned} \vec{\mathbf{F}}_{\text{magnetic}} &= i\vec{\boldsymbol{\ell}} \times \vec{\mathbf{B}} = i(-\ell\hat{\mathbf{y}}) \times (-B\hat{\mathbf{z}}) \\ &= i\ell B\hat{\mathbf{x}}. \end{aligned}$$

To find the equations of motion for the bar, let f be the coefficient of viscous (sliding) friction of the bar so that the friction force is given by $F_f = -f dx/dt$. Then, with m_ℓ denoting the mass of the bar, Newton's law gives

$$i\ell B - f dx/dt = m_\ell d^2x/dt^2.$$

Just after closing the switch at $t = 0$, but before the bar starts to move, the current is $i(0^+) = V_S(0^+)/R$. However, it turns out that as the bar moves the current does *not* stay at this value, but instead decreases due to electromagnetic induction. This will be explained later.

1.2 Single-Loop Motor

As a first step to modeling a DC motor, a simplistic single-loop motor is considered. It is first shown how torque is produced and then how the

www.EngineeringEBooksPdf.com

current in the single loop can be reversed (commutated) every half turn to keep the torque constant.

1.2.1 *Torque Production*

Consider the magnetic system in Figure 1.4, where a cylindrical core is cut out of a block of a permanent magnet and replaced with a soft iron core. The term "soft" iron refers to the fact that material is easily magnetized (a permanent magnet is referred to as "hard" iron).

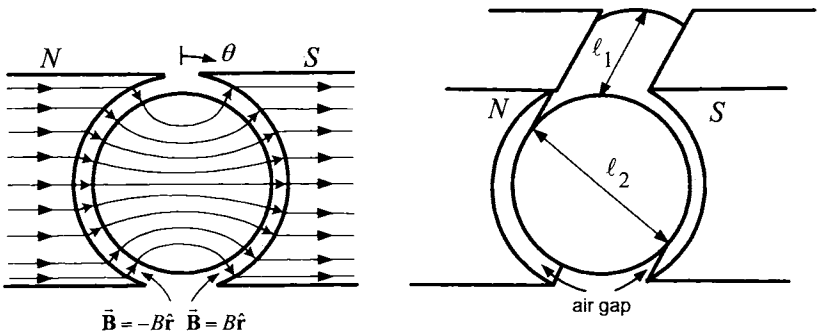


FIGURE 1.4. Soft iron cylindrical core placed inside a hollowed out permanent magnet to produce a radial magnetic field in the air gap.

An important property of soft magnetic materials is that the magnetic field at the surface of such materials tends to be normal (perpendicular) to the surface. Consequently, the cylindrical shape of the surfaces of the soft iron core and the stator permanent magnet has the effect of making the field in the air gap *radially* directed; furthermore, it is reasonably constant (uniform) in magnitude. A mathematical description of the magnetic field in the air gap due to the permanent magnet is simply

$$\vec{\mathbf{B}} = \begin{cases} +B\hat{\mathbf{r}} & \text{for } 0 < \theta < \pi \\ -B\hat{\mathbf{r}} & \text{for } \pi < \theta < 2\pi \end{cases}$$

where $B > 0$ is the magnitude or strength of the magnetic field and θ is an arbitrary location in the air gap.[2]

Figure 1.5 shows a rotor loop wound around the iron core of Figure 1.4. The length of the rotor is ℓ_1 and its diameter is ℓ_2. The torque on this rotor loop is now calculated by considering the magnetic forces on sides a and a' of the loop. On the other two sides of the loop, that is, the front and

[2] Actually it will be shown in a later chapter that the magnetic field must be of the form $\vec{\mathbf{B}} = \pm B(r_0/r)\hat{\mathbf{r}}$ in the air gap, that is, it varies as $1/r$ in the air gap. However, as the air gap is small, the $\vec{\mathbf{B}}$ field is essentially constant across the air gap.

www.EngineeringEBooksPdf.com

back sides, the magnetic field has negligible strength so that no significant force is produced on these sides. As illustrated in Figure 1.5(b), the rotor angular position is taken to be the angle θ_R from the vertical to side a of the rotor loop.

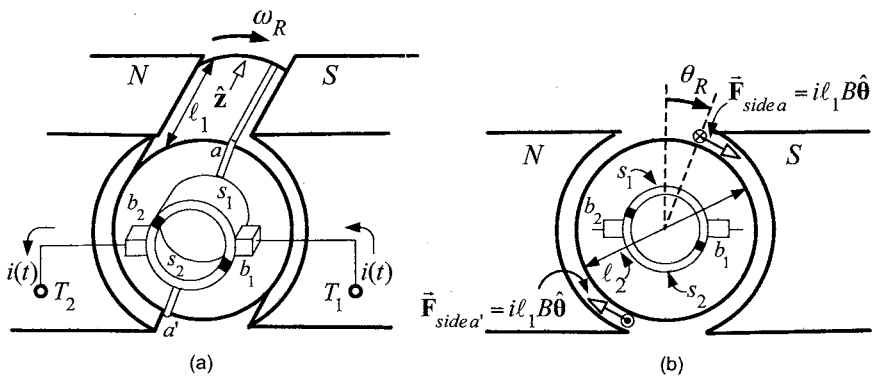


FIGURE 1.5. A single-loop motor. From *Electromagnetic and Electromechanical Machines*, 3rd edition, L. W. Matsch and J. Derald Morgan, 1986. Reprinted by permisson of John Wiley & Sons.

Figure 1.6 shows the cylindrical coordinate system used in Figure 1.5. Here $\hat{\mathbf{r}}, \hat{\boldsymbol{\theta}}, \hat{\mathbf{z}}$ denote unit cylindrical coordinate vectors. The unit vector $\hat{\mathbf{z}}$ points along the rotor axis into the paper in Figure 1.5(b), $\hat{\boldsymbol{\theta}}$ is in the direction of increasing θ, and $\hat{\mathbf{r}}$ is in the direction of increasing r.

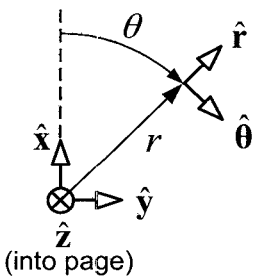


FIGURE 1.6. Cylindrical coordinate system used in Figure 1.5.

Referring back to Figure 1.5, for $i > 0$, the current in side a of the loop is going into the page (denoted by $\otimes$) and then comes out of the page (denoted by $\odot$) on side a'. Thus, on side a, $\vec{\boldsymbol{\ell}} = \ell_1 \hat{\mathbf{z}}$ (as $\vec{\boldsymbol{\ell}}$ points in the direction of positive current flow) and the magnetic force $\vec{\mathbf{F}}_{\text{side } a}$ on side a

www.EngineeringEBooksPdf.com

is then

$$\begin{aligned}\vec{\mathbf{F}}_{\text{side } a} &= i\vec{\boldsymbol{\ell}} \times \vec{\mathbf{B}} \\ &= i(\ell_1 \hat{\mathbf{z}}) \times (B\hat{\mathbf{r}}) \\ &= i\ell_1 B\hat{\boldsymbol{\theta}}\end{aligned}$$

which is tangential to the motion as shown in Figure 1.5(b). The resulting torque is

$$\begin{aligned}\vec{\boldsymbol{\tau}}_{\text{side } a} &= (\ell_2/2)\hat{\mathbf{r}} \times \vec{\mathbf{F}}_{\text{side } a} \\ &= (\ell_2/2)i\ell_1 B\hat{\mathbf{r}} \times \hat{\boldsymbol{\theta}} \\ &= (\ell_2/2)i\ell_1 B\hat{\mathbf{z}}.\end{aligned}$$

Similarly, the magnetic force on side a' of the rotor loop is

$$\begin{aligned}\vec{\mathbf{F}}_{\text{side } a'} &= i\vec{\boldsymbol{\ell}} \times \vec{\mathbf{B}} \\ &= i(-\ell_1 \hat{\mathbf{z}}) \times (-B\hat{\mathbf{r}}) \\ &= i\ell_1 B\hat{\boldsymbol{\theta}}\end{aligned}$$

so that the corresponding torque is then

$$\begin{aligned}\vec{\boldsymbol{\tau}}_{\text{side } a'} &= (\ell_2/2)\hat{\mathbf{r}} \times \vec{\mathbf{F}}_{\text{side } a'} \\ &= (\ell_2/2)i\ell_1 B\hat{\mathbf{r}} \times \hat{\boldsymbol{\theta}} \\ &= (\ell_2/2)i\ell_1 B\hat{\mathbf{z}}.\end{aligned}$$

The total torque on the rotor loop is then

$$\begin{aligned}\vec{\boldsymbol{\tau}}_m &= \vec{\boldsymbol{\tau}}_{\text{side } a} + \vec{\boldsymbol{\tau}}_{\text{side } a'} \\ &= 2(\ell_2/2)i\ell_1 B\hat{\mathbf{z}} \\ &= \ell_1\ell_2 B i\hat{\mathbf{z}}.\end{aligned}$$

The torque points along the z axis, which is the axis of rotation. In scalar form,

$$\tau_m = K_T i$$

where $K_T \triangleq \ell_1\ell_2 B$. The force is proportional to the strength B of magnetic field $\vec{\mathbf{B}}$ in the air gap due to the permanent magnet.

In order to increase the strength of the magnetic field in the air gap, the permanent magnet can be replaced with a soft iron material with wire wound around the periphery of the magnetic material as shown in Figure 1.7(a). This winding is referred to as the *field winding*, and the current it carries is called the *field current*. In normal operation, the field current is held constant. The strength of the magnetic field in the air gap is then proportional to the field current i_f at lower current levels (i.e., $B = K_f i_f$) and then saturates as the current increases. This may be written as $B =$

www.EngineeringEBooksPdf.com

$f(i_f)$ where $f(\cdot)$ is a saturation curve satisfying $f(0) = 0, f'(0) = K_f$ as shown in Figure 1.7(b).

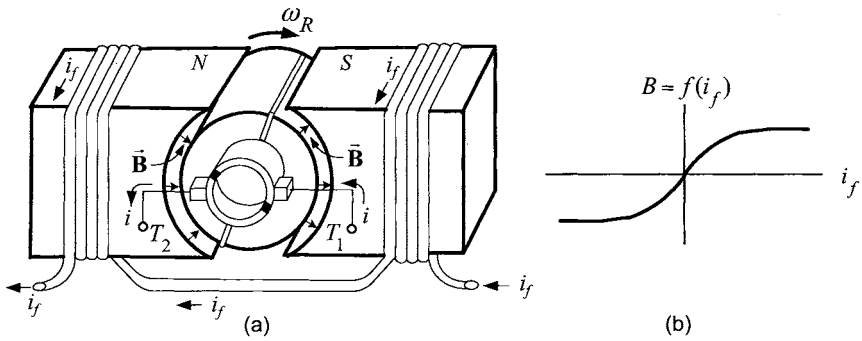


FIGURE 1.7. (a) DC motor with a field winding. (b) Radial magnetic field strength in the air gap produced by the field current.

1.2.2 *Commutation of the Single-Loop Motor*

The above derivation for the torque $\tau_m = K_T i$ assumes that the current in the side of the rotor loop[3] under the south pole face is into the page and the current in the side of the loop under the north pole face is out of the page as in Figure 1.8(a). In order to make this assumption valid, the direction of the current in the loop must be changed each time the rotor loop passes through the vertical.

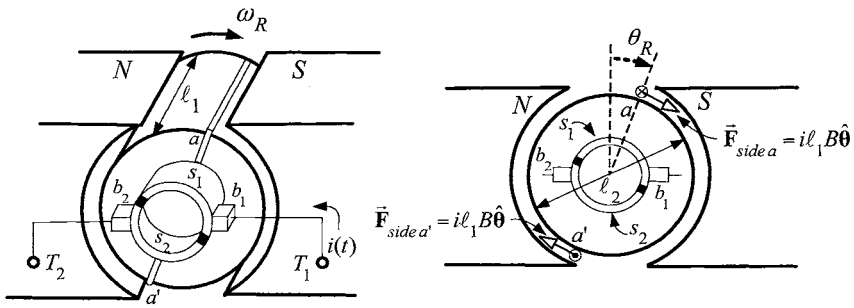


FIGURE 1.8. (a) $0 < \theta_R < \pi$. From *Electromagnetic and Electromechanical Machines,* 3rd edition, L. W. Matsch and J. Derald Morgan, 1986. Reprinted by permisson of John Wiley & Sons.

[3]The rotor loop is also referred to as the *armature* winding and the current in it as the *armature* current.

www.EngineeringEBooksPdf.com

The process of changing the direction of the current is referred to as *commutation* and is done at $\theta_R = 0$ and $\theta_R = \pi$ through the use of the slip rings s_1, s_2 and brushes b_1, b_2 drawn in Figure 1.8. The slip rings are rigidly attached to the loop and thus rotate with it. The brushes are fixed in space with the slip rings making a sliding electrical contact with the brushes as the loop rotates.

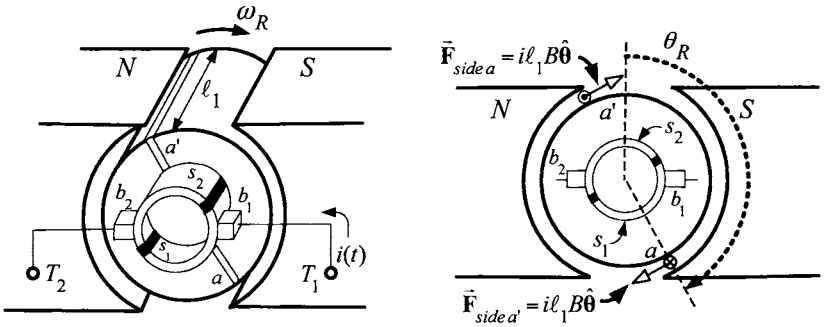


Figure 1.8(b) Rotor loop just prior to commutation where $0 < \theta_R < \pi$.

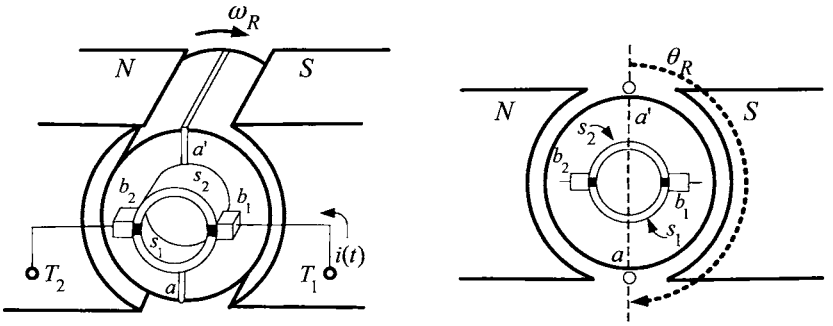


Figure 1.8(c) The ends of the rotor loop are shorted when $\theta_R = \pi$.

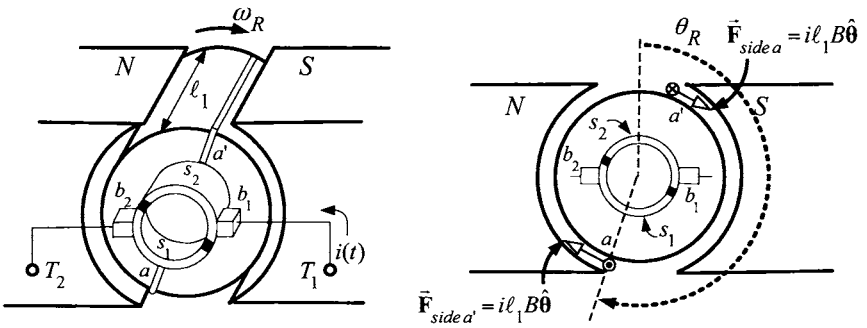


Figure 1.8(d) Rotor loop just after commutation where $\pi < \theta_R < 2\pi$.

www.EngineeringEBooksPdf.com

To see how the commutation of the current is accomplished using the brushes and slip rings, consider the sequence of Figures 1.8(a)–(d). As shown in Figure 1.8(a), the current goes through brush b_1 into the slip ring s_1. From there, it travels down (into the page $\otimes$) side a of the loop, comes back up side a' (out of the page $\odot$) into the slip ring s_2, and, finally, comes out the brush b_2. Note that side a of the loop is under the south pole face while side a' is under the north pole face. Figure 1.8(b) shows the rotor loop just before commutation where the same comments as in Figure 1.8(a) apply.

Figure 1.8(c) shows that when $\theta_R = \pi$, the slip rings at the ends of the loop are shorted together by the brushes forcing the current in the loop to drop to zero. Subsequently, as shown in Figure 1.8(d), with $\pi < \theta_R < 2\pi$, the current is now going through brush b_1 into slip ring s_2. From there, the current travels down (into the page $\otimes$) side a' of the loop and comes back up (out of the page $\odot$) side a. In other words, the current has *reversed* its direction in the loop from that in Figures 1.8(a) and 1.8(b). This is precisely what is desired, as side a is now under the north pole face and side a' is under the south pole face. As a result of the brushes and slip rings, the current direction in the loop is reversed every half-turn.

1.3 Faraday's Law

Figure 1.9 shows a magnet moving upwards into a wire loop producing a changing magnetic flux in the loop.

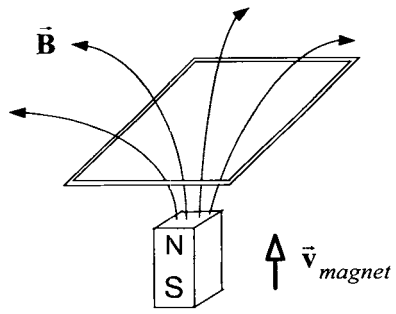


FIGURE 1.9. A magnet moving upwards produces a changing flux in the loop which in turn results in an induced emf and current in the loop.

Recall that a changing flux within a loop produces an induced *electro-*

www.EngineeringEBooksPdf.com

motive force (emf) ξ in the loop according to Faraday's law.[4] That is,

$$\xi = -d\phi/dt$$

where

$$\phi = \int_S \vec{\mathbf{B}} \cdot d\vec{\mathbf{S}}$$

is the flux in the loop and S is any surface with the loop as its boundary. Faraday's law is now reviewed in some detail.

1.3.1 *The Surface Element Vector* $d\vec{\mathbf{S}}$

The surface element $d\vec{\mathbf{S}}$ is a vector whose magnitude is a differential (small) element of area dS and whose direction is normal (perpendicular) to the surface element. As there are two possibilities for the normal to the surface, one must choose the normal in a consistent manner. In particular, depending on the particular normal chosen, a convention is used to characterize the positive and negative directions of travel around the surface boundary. To describe this, consider Figure 1.10(a) which shows a small surface element with the normal direction taken to be up in the positive z direction. In this case, with $\hat{\mathbf{n}} = \hat{\mathbf{z}}$, $dS = dxdy$, the surface element vector is defined by

$$d\vec{\mathbf{S}} \triangleq dxdy\hat{\mathbf{z}}.$$

The corresponding direction of travel around the surface boundary is indicated by the curved arrow in the figure.

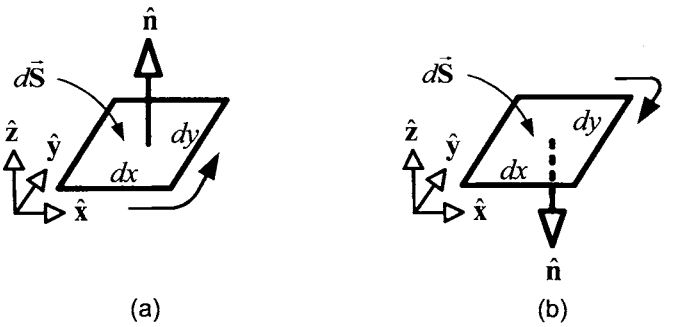


FIGURE 1.10. (a) Positive direction of travel around a surface element with the normal up. (b) Positive direction of travel around a surface element with the normal down.

[4] ξ is the Greek letter "xi" and is pronounced "ksi".

www.EngineeringEBooksPdf.com

In Figure 1.10(b) a surface element with the normal direction taken to be down in the negative z direction is shown. In this case $\hat{\mathbf{n}} = -\hat{\mathbf{z}}, dS = dxdy$ so that the surface element vector is defined as

$$d\vec{\mathbf{S}} = -dxdy\hat{\mathbf{z}}.$$

The direction of positive travel around the surface element is indicated by the curved arrow in Figure 1.10(b) and is opposite to that of Figure 1.10(a).

As illustrated in Figure 1.10, the vector differential surface element $d\vec{\mathbf{S}}$ is defined to be a vector whose magnitude is the area of the differential surface element and whose direction is normal to the surface. One may choose either normal, and the corresponding direction of positive travel around the surface is then determined.

Two surface elements may be connected together as in Figure 1.11 and travel around the total surface is defined as shown. Note that along the common boundary of the two joined surface elements, the directions of travel "cancel" out each other, resulting in a net travel path around both surface elements. The normals for the surface elements must both be up or both be down; that is, the normal must be continuous as one goes from one surface element to the next.

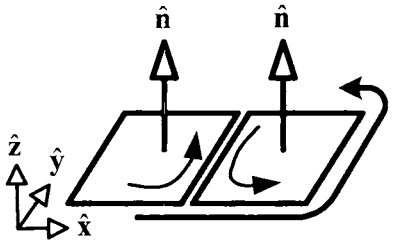


FIGURE 1.11. Positive direction of travel around two joined surface elements.

1.3.2 Interpreting the Sign of ξ

The interpretation of positive and negative values of the induced electromotive force ξ is now explained. Faraday's law says that the induced emf (voltage) in a loop is given by

$$\xi = -d\phi/dt$$

where

$$\phi = \int_S \vec{\mathbf{B}} \cdot d\vec{\mathbf{S}}.$$

If $\xi > 0$, the induced emf will force current in the positive direction of travel around the surface while if $\xi < 0$, the induced emf will force current in the

www.EngineeringEBooksPdf.com

opposite direction. As illustrated in problems 1 and 2, this sign convention for Faraday's law is just a precise mathematical way of describing Lenz's law: *"In all cases of electromagnetic induction, an induced voltage will cause a current to flow in a closed circuit in such a direction that the magnetic field which is caused by that current will oppose the change that produced the current"* (pages 873–877 of Ref. [34]).

Faraday's law is now illustrated by some examples. Specifically, it is used to compute the induced emf in the linear DC machine, the induced emf in the single-loop machine and the self-induced voltage in the single-loop machine.

1.3.3 Back Emf in a Linear DC Machine

Figure 1.12 shows the linear DC machine where the back emf it generates is now computed. The magnetic field is constant and points into the page, that is, $\vec{\mathbf{B}} = -B\hat{\mathbf{z}}$, where $B > 0$. The magnetic force on the bar is $\vec{\mathbf{F}}_{\text{magnetic}} = i\ell B\hat{\mathbf{x}}$. To compute the induced voltage in the loop of the circuit, let $\hat{\mathbf{n}} = \hat{\mathbf{z}}$ be the normal to the surface so that $d\vec{\mathbf{S}} = dxdy\hat{\mathbf{z}}$, where $dS = dxdy$.

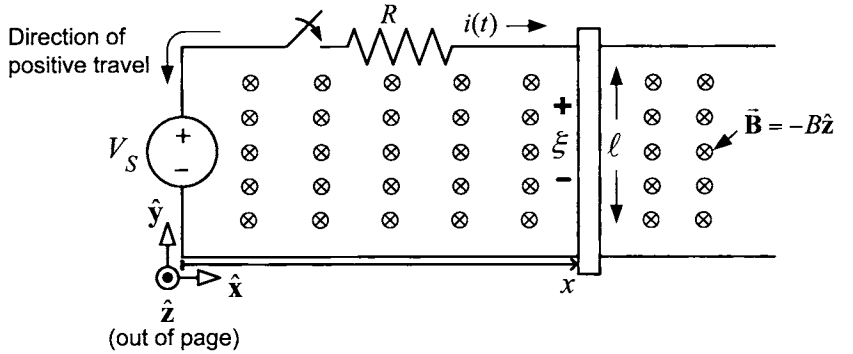


FIGURE 1.12. With $d\vec{\mathbf{S}} = dxdy\hat{\mathbf{z}}$, the direction of positive travel around the flux surface is in the counterclockwise direction.

Then

$$\phi = \int_S \vec{\mathbf{B}} \cdot d\vec{\mathbf{S}} = \int_0^{\ell}\int_0^{x} (-B\hat{\mathbf{z}}) \cdot (dxdy\hat{\mathbf{z}}) = \int_0^{\ell}\int_0^{x} -Bdxdy = -B\ell x.$$

The induced (back) emf is therefore given by

$$\xi = -d\phi/dt = -d(-B\ell x)/dt = B\ell v.$$

In the flux computation, the normal for the surface was taken to be in $+\hat{\mathbf{z}}$ direction. By putting together the differential flux surfaces $d\vec{\mathbf{S}}$ in a fashion

www.EngineeringEBooksPdf.com

similar to Figure 1.11, the positive direction of travel around the surface is counterclockwise around the loop as indicated in Figure 1.12. Here the sign conventions for source voltage V_S and the back emf ξ are opposite so that, as the back emf $\xi = B\ell v > 0$, it is *opposing* the applied source voltage V_S.

Remark $\phi = -B\ell x$ is the flux in the circuit due to the *external* magnetic field $\vec{\mathbf{B}} = -B\hat{\mathbf{z}}$. There is also a flux $\psi = Li$ due to the current i in the circuit. For this example, the inductance is small and one just sets $L = 0$.

Electromechanical Energy Conversion

As the back emf $\xi = Blv$ opposes the current i, electrical power is being absorbed by this back emf. Specifically, the electrical power absorbed by the back emf is $i\xi = iB\ell v$ while the mechanical power produced is $F_{\text{magnetic}}v = i\ell Bv$. That is, the electrical power absorbed by the back emf reappears as mechanical power, as it must by conservation of energy. Another way to view this is to note that $V_S i$ is the electrical power delivered by the source and, as $V_S - B\ell v = Ri$, one may write

$$V_S i = Ri^2 + i(B\ell v) = Ri^2 + F_{\text{magnetic}}v.$$

In words, the power from the source $V_S i$ is dissipated as heat in the resistance R while the rest is converted into mechanical power.

Equations of Motion for the Linear DC Machine

The equations of motion for the bar in the linear DC machine are now derived. With the inductance L of the circuit loop taken to be zero, m_ℓ the mass of the bar, f the coefficient of viscous friction, it follows that

$$\begin{aligned} V_S - B\ell v &= Ri \\ m_\ell \frac{dv}{dt} &= i\ell B - fv. \end{aligned}$$

Eliminating the current i, one obtains

$$m_\ell \frac{d^2x}{dt^2} = \ell B(V_S - B\ell v)/R - fv = -\left(\frac{B^2\ell^2}{R} + f\right)\frac{dx}{dt} + \frac{\ell B}{R}V_S$$

or

$$m_\ell \frac{d^2x}{dt^2} + \left(\frac{B^2\ell^2}{R} + f\right)\frac{dx}{dt} = \frac{\ell B}{R}V_S.$$

This is the equation of motion for the bar with V_S as the control input and the position x at the measured output.

1.3.4 Back Emf in the Single-Loop Motor

The back emf induced in the single loop motor by the external magnetic field of the permanent magnet is now computed. To do so, consider the

www.EngineeringEBooksPdf.com

flux surface for the rotor loop shown in Figure 1.13. The surface is a half-cylinder of radius $\ell_2/2$ and length ℓ_1 with the rotor loop as its boundary. The cylindrical surface is in the air gap, where the magnetic field is known to be radially directed and constant in magnitude, that is,

$$\vec{\mathbf{B}} = \begin{cases} +B\hat{\mathbf{r}} & \text{for } 0 < \theta < \pi \\ -B\hat{\mathbf{r}} & \text{for } \pi < \theta < 2\pi. \end{cases} \tag{1.1}$$

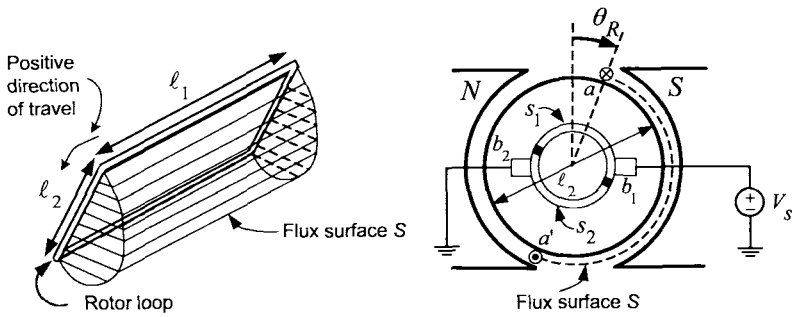


FIGURE 1.13. Flux surface for the single loop motor.

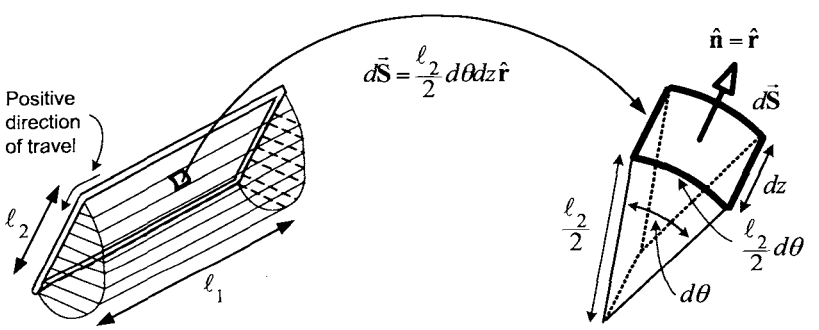


FIGURE 1.14. Surface element vector for the flux surface of Figure 1.13. The positive direction of travel around this surface is indicated by the curved arrow.

On the cylindrical part of the surface, the surface element is chosen as

$$d\vec{\mathbf{S}} = (\ell_2/2) d\theta dz \hat{\mathbf{r}}$$

which is directed outward from the axis of the cylinder as illustrated in Figure 1.14. The corresponding direction of positive travel is also indicated in Figure 1.14. On the two ends (half-disks) of the cylindrical surface, the $\vec{\mathbf{B}}$ field is quite weak making the flux through these two half-disks negligible.

www.EngineeringEBooksPdf.com

Then, neglecting the flux through the two ends of the surface, the flux $\phi(\theta_R)$ for $0 < \theta_R < \pi$ is given by

$$\begin{aligned}
\phi(\theta_R) &= \int_S \vec{\mathbf{B}} \cdot d\vec{\mathbf{S}} \\
&= \int_0^{\ell_1} \int_{\theta=\theta_R}^{\theta=\pi} (B\hat{\mathbf{r}}) \cdot (\frac{\ell_2}{2} d\theta dz \hat{\mathbf{r}}) + \int_0^{\ell_1} \int_{\theta=\pi}^{\theta=\pi+\theta_R} (-B\hat{\mathbf{r}}) \cdot (\frac{\ell_2}{2} d\theta dz \hat{\mathbf{r}}) \\
&= \int_0^{\ell_1} \int_{\theta=\theta_R}^{\theta=\pi} B\frac{\ell_2}{2} d\theta dz + \int_0^{\ell_1} \int_{\theta=\pi}^{\theta=\pi+\theta_R} -B\frac{\ell_2}{2} d\theta dz \\
&= \frac{\ell_1 \ell_2 B}{2}(\pi - \theta_R) - \frac{\ell_1 \ell_2 B}{2}\theta_R \\
&= -\ell_1 \ell_2 B \left(\theta_R - \frac{\pi}{2}\right). \qquad (1.2)
\end{aligned}$$

This derivation is based on the fact that the $\vec{\mathbf{B}}$ field is directed radially outward over the length $(\ell_2/2)(\pi - \theta_R)$ and radially inward over the length $(\ell_2/2)\theta_R$ (see Figure 1.13). In problem 7, the reader is asked to show that

$$\phi(\theta_R) = -\ell_1 \ell_2 B \left(\theta_R - \pi/2 - \pi\right) \text{ for } \pi < \theta_R < 2\pi. \qquad (1.3)$$

A plot of the flux versus the rotor angle θ_R is given in Figure 1.15.

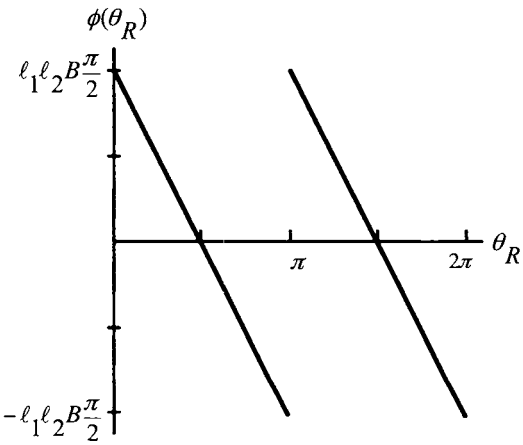


FIGURE 1.15. The rotor flux $\phi(\theta_R)$ due to the external magnetic field vs. θ_R.

Equations (1.2) and (1.3) may be combined into one expression as[5]

$$\phi(\theta_R) = -\ell_1 \ell_2 B \left(\theta_R \bmod \pi - \frac{\pi}{2}\right) \qquad (1.4)$$

[5] $\theta_R \bmod \pi$ is the remainder after θ_R is divided by π. For example, $\theta_R = 5\pi/2 = 4 \times \pi + \pi/2$ so that $5\pi/2 \bmod \pi = \pi/2$.

www.EngineeringEBooksPdf.com

which is a correct expression for any angle θ_R. By (1.2) and (1.3), the induced emf in the rotor loop is calculated as

$$\xi = -\frac{d\phi}{dt} = (\ell_1 \ell_2 B)\frac{d\theta_R}{dt} = K_b \omega_R$$

where $K_b \triangleq \ell_1 \ell_2 B$ is called the back emf constant.

The total emf in the rotor loop due to the voltage source V_S and external magnetic field is $V_S - K_b\omega_R$. How does one know to subtract ξ from the applied voltage V_S? As shown in Figure 1.14, the positive direction of travel around the loop is in *opposition* to V_S, so that if $\xi > 0$, it is opposing the applied voltage V_S. The standard terminology is to call $\xi \triangleq K_b\omega_R$ the *back emf* of the motor.

1.3.5 *Self-Induced Emf in the Single-Loop Motor*

The computation of the flux in the rotor loop produced by its own (armature) *current* is now done. To do so, consider the flux surface shown in Figure 1.16.

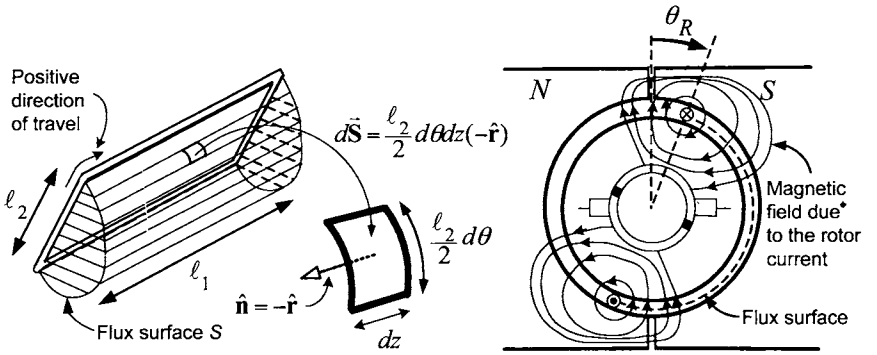


FIGURE 1.16. Computation of the inductance of the rotor loop. The surface element vector is $d\vec{\mathbf{S}} = -r_R d\theta dz\hat{\mathbf{r}}$ with a resulting positive direction of travel as indicated by the curved arrow. This direction coincides with the direction of positive current, that is, $i > 0$.

With reference to Figure 1.16, note that the magnetic field on the flux surface *due to the armature current* has the form

$$\vec{\mathbf{B}}(r_R, \theta - \theta_R, i) = iK(r_R, \theta - \theta_R)\,(-\hat{\mathbf{r}})$$

where

$$\begin{aligned} K(r_R, \theta - \theta_R) &> 0 \qquad \text{for } 0 \le \theta - \theta_R \le \pi \\ K(r_R, \theta - \theta_R) &< 0 \qquad \text{for } \pi \le \theta - \theta_R \le 2\pi. \end{aligned}$$

www.EngineeringEBooksPdf.com

The exact expression for $K(r_R, \theta - \theta_R)$ is not easy to compute, but it is not needed for the analysis here. Rather, the point is that with $i > 0$, the magnetic field $\vec{\mathbf{B}}(r_R, \theta - \theta_R, i)$ due to the current in the rotor loop is radially in on the flux surface shown in Figure 1.16, that is, for $\theta_R \leq \theta \leq \theta_R + \pi$. For convenience, the surface element is chosen to be $d\vec{\mathbf{S}} = r_R d\theta dz(-\hat{\mathbf{r}})$ so that positive direction of travel around the surface coincides with the positive direction of the current i in the loop. The flux ψ in the rotor loop is then computed as[6]

$$\begin{aligned}
\psi(i) &= \int_S \vec{\mathbf{B}} \cdot d\vec{\mathbf{S}} = \int_{\theta_R}^{\theta_R+\pi} \int_0^{\ell_1} iK(r_R, \theta - \theta_R)\,(-\hat{\mathbf{r}}) \cdot (-r_R d\theta dz \hat{\mathbf{r}}) \\
&= i \int_{\theta_R}^{\theta_R+\pi} \int_0^{\ell_1} K(r_R, \theta - \theta_R) r_R d\theta dz \\
&= Li
\end{aligned}$$

where

$$L \triangleq \int_{\theta_R}^{\theta_R+\pi} \int_0^{\ell_1} K(r_R, \theta - \theta_R) r_R d\theta dz > 0. \tag{1.5}$$

This last equation just says the flux in the loop (due to the current in the loop) is proportional to the current i in the loop. The proportionality constant L is the called the *inductance* of the loop.[7] If $-d\psi/dt = -Ldi/dt > 0$, then the induced emf will force current into the page $\otimes$ on side a and out of the page $\odot$ of side a' in Figure 1.16. That is, this induced emf has the same sign convention as the armature current i and the source voltage V_S.

With the rotor locked at some angle θ_R so that the external magnetic field cannot induce an emf in the rotor loop, the equation describing the current i in the rotor loop is given by Kirchhoff's voltage law

$$V_S - Ri - L\frac{di}{dt} = 0$$

or

$$V_S = Ri + L\frac{di}{dt}.$$

Here R is the resistance of the loop and V_S is the source voltage applied to the loop. The loop and its equivalent circuit are shown in Figure 1.17.

---

[6] The notation ψ is used to distinguish this flux from the flux ϕ in the loop due to the *external* permanent magnet. However, the total flux using an inward normal would be $\psi - \phi$ as the *outward* normal was used to compute ϕ in Section 1.3.4.

[7] It appears from equation (1.5) and Figure 1.16 that L can vary with θ_R. However, in an actual motor, there are loops spread evenly around the complete periphery of the rotor and, due to symmetry, the total self-inductance does not depend on θ_R.

www.EngineeringEBooksPdf.com

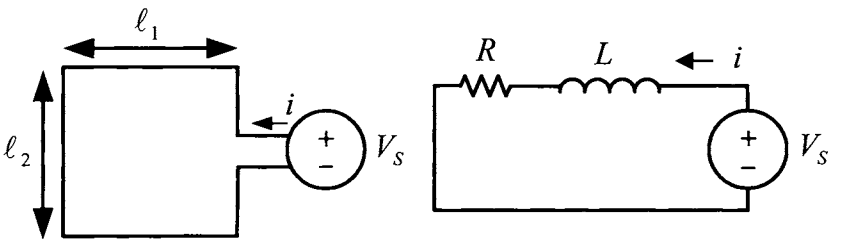


FIGURE 1.17. Left: Rotor loop. Right: Equivalent circuit.

The reader should convince himself/herself that Lenz's law holds as it must. For example, suppose a voltage $V_S > 0$ is applied to the loop resulting in both $i > 0$ and $di/dt > 0$, that is, the flux $\psi = Li$ is positive and increasing. The induced voltage is $-Ldi/dt < 0$ and opposes the current i producing the increasing flux $\psi = Li$. In this circumstance, the voltage source V_S is forcing the current i against this induced voltage $-Ldi/dt$ and the power absorbed by the induced voltage is $-iLdi/dt = -d\left(\frac{1}{2}Li^2\right)/dt$. This power is stored in the energy $\frac{1}{2}Li^2$ of the magnetic field surrounding the loop.

Arcing Between the Commutator and Brushes

Suppose the single-loop motor is rotating at constant speed ω_0 with a constant current i_0 in the rotating loop. Let L be the inductance of the loop. Now, every half-turn, the current in the loop reverses direction as shown in Figures 1.8(b)–(d). During this commutation, the current in the loop goes from i_0 to 0 to $-i_0$ (or vice versa) with a corresponding change in the loop's flux given by $\Delta\psi = L(-i_0) - Li_0 = -2Li_0$. By Faraday's law, the self-induced emf is then $-\Delta\psi/\Delta t = 2Li_0/\Delta t$ where Δt is the time for the current to change direction. Note that this time Δt decreases as the motor speed increases, so that, even if L is small, the induced emf in the loop (due to the reversal of current in the loop) can be quite large at high motor speeds. Large electric fields are produced by the induced voltage Ldi/dt when the loop is shorted which in turn ionizes the surrounding air. As the free electrons collide and recombine with the ionized air, light is given off and seen as arcing or sparking. These large voltages which cause the arcing between the slip rings and the brushes can damage the brushes as well as produce unwanted transient currents in the armature circuit.

1.4 Dynamic Equations of the DC Motor

Based on the simple single-loop DC motor analyzed above, the complete set of equations for a DC motor can be found. The total emf (voltage) in

www.EngineeringEBooksPdf.com

the loop due to the voltage source V_S, the external permanent magnet and the changing current i in the rotor loop is

$$V_S - K_b\omega_R - L\frac{di}{dt}.$$

This voltage goes into building up the current in the loop against the loop's resistance, that is,

$$V_S - K_b\omega_R - L\frac{di}{dt} = Ri$$

or

$$L\frac{di}{dt} = -Ri - K_b\omega_R + V_S.$$

This relationship is often illustrated by the equivalent circuit given in Figure 1.18. Recall that the torque τ_m on the loop due to the external magnetic field acting on the current in the loop is

$$\tau_m = K_T i$$

where $K_T \triangleq \ell_1\ell_2 B$ is called the torque constant. By connecting a shaft and gears to one end of the loop, this motor torque can be used to do work (lift weight, etc.). Let $-f\omega_R$ model the friction torque (due to the brushes, bearings, etc.) where f is the coefficient of viscous friction and let τ_L be the load torque (e.g., due to a weight being lifted).

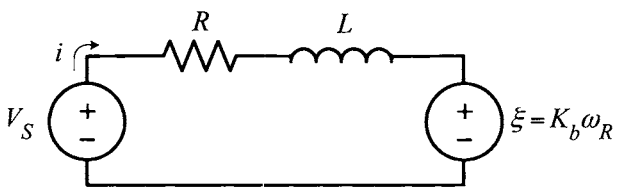


FIGURE 1.18. Equivalent circuit of the armature electrical dynamics.

Then, by Newton's law,

$$\tau_m - \tau_L - f\omega_R = J\frac{d\omega_R}{dt}$$

where J is the moment of inertia of the rotor (See the appendix of this chapter). The system of equations characterizing the DC motor is then

$$\begin{aligned} L\frac{di}{dt} &= -Ri - K_b\omega_R + V_S \\ J\frac{d\omega_R}{dt} &= K_T i - f\omega_R - \tau_L \\ \frac{d\theta_R}{dt} &= \omega_R. \end{aligned} \tag{1.6}$$

www.EngineeringEBooksPdf.com

A picture of a DC motor servo system and its associated schematic is shown in Figure 1.19. In the schematic, R is the resistance of the rotor loop, L is the inductance of the rotor loop, $\xi = K_b\omega_R$ is the back emf, $\tau_m = K_T i$ is the motor torque, J is the rotor moment of inertia, and f is the coefficient of viscous friction. The positive directions for τ_m, θ_R, and τ_L are indicated by the curved arrows. The fact that the curved arrow for τ_L is opposite to that of τ_m just means that if the load torque is positive then it opposes a positive motor torque τ_m.

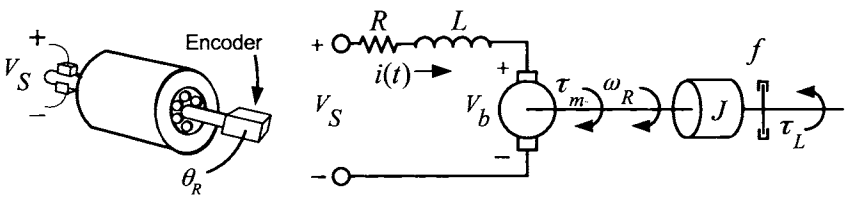


FIGURE 1.19. DC motor drawing and schematic.

Electromechanical Energy Conversion

The mechanical power produced by the DC motor is $\tau_m\omega_R = K_T i\omega_R = i\ell_1\ell_2 B\omega_R$ while the electrical power absorbed by the back emf is $i\xi = iK_b\omega_R = i\ell_1\ell_2 B\omega_R$. The fact that $K_T = K_b = \ell_1\ell_2 B$ must be for conservation of energy to hold. That is, the electrical power absorbed by the back emf equals (is converted to) the mechanical power produced. Another way to view this energy conversion is to write the electrical equation as

$$V_S = Ri + L\frac{di}{dt} + \xi.$$

The power out of the voltage source $V_S(t)$ is given by

$$\begin{aligned} V_S(t)i(t) &= Ri^2(t) + Li\frac{di}{dt} + iK_b\omega_R \\ &= Ri^2 + \frac{d}{dt}\left(\frac{1}{2}Li^2\right) + K_T i\omega_R \\ &= Ri^2 + \frac{d}{dt}\left(\frac{1}{2}Li^2\right) + \tau_m\omega_R. \end{aligned}$$

Thus the power $V_S(t)i(t)$ delivered by the source goes into heat loss in the resistance R, into stored magnetic energy in the inductance L of the loop and the amount $i\xi$ goes into the mechanical energy $\tau_m\omega_R$.

Remark *Voltage and Current Limits*

The amount of voltage V_S that may be applied to the input terminals T_1, T_2 of the motor is limited by capabilities of the amplifier supplying the voltage, that is, $|V_S| \leq V_{\max}$. Let $V_c(t)$ be the voltage commanded to the

www.EngineeringEBooksPdf.com

amplifier, then the actual voltage V_S out of the amplifier to the motor is limited by $V_{\max}$ as illustrated in Figure 1.20.

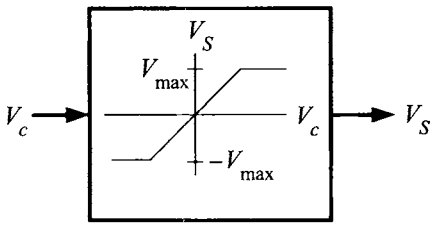


FIGURE 1.20. Saturation model of an amplifier.

In addition, there is a limit to the amount of current the rotating loop can handle before overheating or causing problems with commutation as previously mentioned. Typically there are two current limits (ratings), the *continuous* current limit $I_{\max\_\text{cont}}$ and the *peak* current limit $I_{\max\_\text{peak}}$. The continuous current limit $I_{\max\_\text{cont}}$ is the amount of current the motor can handle if left in use indefinitely. That is, the amount of heat dissipated in the rotor windings due to ohmic losses is equal to the amount of heat taken away by thermal conduction through the brushes and thermal convection with the air so as to be in a thermal equilibrium. The peak current limit $I_{\max\_\text{peak}}$ is the amount of current the motor can handle for short periods of time (typically only a few seconds).

1.5 Microscopic Viewpoint

Additional insight into the back emf ξ is found by calculating it from a microscopic point of view using the ideas given in Ref. [34] (page 887). To illustrate this approach, the back emf in the linear DC machine is recomputed from the microscopic point of view. To proceed, recall that the magnetic force on a charged particle q is $\vec{\mathbf{F}}_{\text{magnetic}} = q\vec{\mathbf{v}} \times \vec{\mathbf{B}}$, where $\vec{\mathbf{v}}$ is the velocity of the charge (see Ref. [34], page 816).

Example *A Linear DC Machine*

In this example, the linear DC machine is reanalyzed from the microscopic point of view. As before, $\vec{\mathbf{B}} = -B\hat{\mathbf{z}}$ where $B > 0$. Suppose the motor (bar) is moving to the right with a constant speed v_m. Each charge q in the sliding bar has total velocity $\vec{\mathbf{v}} = v_m\hat{\mathbf{x}} - v_d\hat{\mathbf{y}}$, where v_d is the drift speed of the charges down the wire. The magnetic force on the charge q is

$$\vec{\mathbf{F}}_{\text{magnetic}} = q\vec{\mathbf{v}} \times \vec{\mathbf{B}} = q(v_m\hat{\mathbf{x}} - v_d\hat{\mathbf{y}}) \times (-B\hat{\mathbf{z}}) = qv_mB\hat{\mathbf{y}} + qv_dB\hat{\mathbf{x}}.$$

www.EngineeringEBooksPdf.com

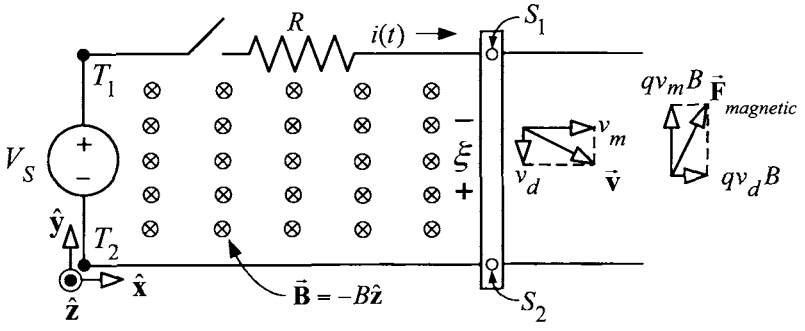


FIGURE 1.21. Linear DC machine.

Now, the component of force $qv_dB\hat{\mathbf{x}}$ perpendicular to the bar causes the bar to move to the right and the component $qv_mB\hat{\mathbf{y}}$ along the bar opposes the current flow. The source voltage V_S sets up an electric field $\vec{\mathbf{E}}_S$ in the bar to overcome the magnetic force $qv_mB\hat{\mathbf{y}}$ so as to make the current flow (setup the drift velocity v_d of the charge carriers against the resistance of the bar). In more detail, with T_1 and T_2 the upper and lower terminals of the source voltage, respectively, and S_1 and S_2 the upper and lower sliding contact points, respectively, the source voltage is given as

$$V_S = \int_{T_1-S_1-S_2-T_2} \vec{\mathbf{E}}_S \cdot d\vec{\ell}.$$

The quantity $q\vec{\mathbf{E}}_S$ is the force on each charge carrier and qV_S is the energy given to the charge carrier by the source voltage as the charge goes around the loop. There is also a component of the magnetic force on the charge carrier that opposes the electric field $\vec{\mathbf{E}}_S$. The energy per unit charge ξ that the magnetic force takes from the charge carrier as it goes down the bar from S_1 to S_2 is given by

$$\begin{aligned}\xi &= \frac{1}{q}\int_{S_1}^{S_2} \vec{\mathbf{F}}_{\text{magnetic}} \cdot d\vec{\ell} = \frac{1}{q}\int_{S_1}^{S_2} q(\vec{\mathbf{v}}\times\vec{\mathbf{B}}) \cdot d\vec{\ell} = \int_0^{\ell} (v_dB\hat{\mathbf{x}}+v_mB\hat{\mathbf{y}}) \cdot (-d\ell\hat{\mathbf{y}}) \\ &= -v_mB\ell.\end{aligned}$$

The fact that ξ is *negative* just indicates that the magnetic force is taking energy out of the charge carrier as it goes down the bar from S_1 to S_2. (Note: The sign convention for ξ shown in Figure 1.21 is reversed from that of Figure 1.12.) This energy per unit charge ξ taken from each charge carrier by the magnetic force as it goes around the loop is called the induced emf. The voltage V_S was computed by integrating $\vec{\mathbf{E}}_S$ in the *clockwise* direction $T_1-S_1-S_2-T_2$ around the loop, and ξ by integrating $\vec{\mathbf{v}}\times\vec{\mathbf{B}}$ also in the

www.EngineeringEBooksPdf.com

clockwise direction down the bar from S_1 to S_2; that is, they both have the same sign convention. This is in contrast to the macroscopic case where V_S and ξ had opposite sign conventions resulting in $\xi = v_m B\ell$ being positive. However, the same (physical) result occurs as in the macroscopic case.

In general, the emf in a loop is defined as the integral of the force per unit charge around the loop. The total emf is the sum of the source voltage and the induced emf. This total emf goes into producing the current, that is,

$$V_S + \xi = V_S - v_m \ell B = Ri$$

where an identical equation was found in the macroscopic case using Faraday's law. The *total* magnetic force on all the charge carriers in the bar in the $\hat{\mathbf{x}}$ direction is given by

$$q(NS\ell)v_d B\hat{\mathbf{x}}$$

where N is the number of charge carriers/volume and S is the cross sectional area of the sliding bar. That is, $NS\ell$ is the total number of charge carriers in the sliding bar each experiencing the force $qv_d B\hat{\mathbf{x}}$. As illustrated in Figure 1.22, in a time Δt, the charges in the volume $NS(v_d \Delta t)$ have moved along the conductor past the point P in Figure 1.22.

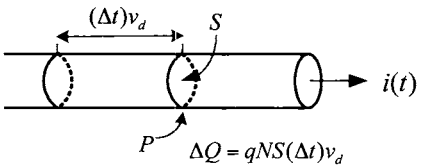


FIGURE 1.22. In the time Δt, the amount of charge $\Delta Q = qNS(v_d \Delta t)$ has moved past the point P resulting in the current $i = \Delta Q/\Delta t = qNSv_d$ in the bar.

That is, the amount of charge $\Delta Q = qNS(v_d \Delta t)$ has moved past the point P in the time Δt resulting in the current $i = \Delta Q/\Delta t = qNSv_d$ in the conductor. Consequently, the total magnetic force on the bar may be rewritten as

$$q(NS\ell)v_d B\hat{\mathbf{x}} = (qNSv_d)\ell B\hat{\mathbf{x}} = i\ell B\hat{\mathbf{x}}$$

which is identical to the expression derived from the macroscopic point of view.

www.EngineeringEBooksPdf.com

1.5.1 *Microscopic Viewpoint of the Single-Loop DC Motor*

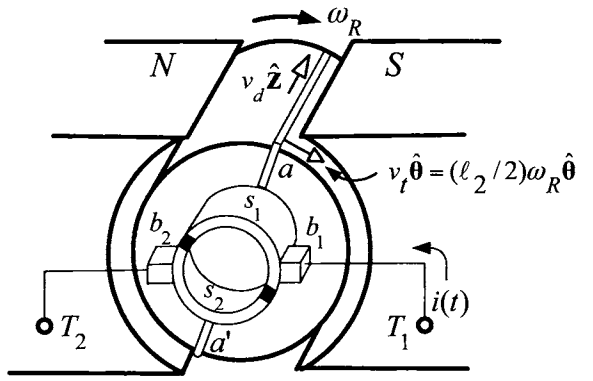


FIGURE 1.23. Single loop DC motor. Adapted from Ref. [21].

The back emf in the single-loop DC motor of Figure 1.23 is now computed from the microscopic point of view. With the loop rotating at the angular speed ω_R, the velocity of the charge carriers that make up the current is given by

$$\vec{\mathbf{v}} = \begin{cases} v_t\hat{\boldsymbol{\theta}} + v_d\hat{\mathbf{z}} & \text{for side } a \\ v_t\hat{\boldsymbol{\theta}} - v_d\hat{\mathbf{z}} & \text{for side } a' \end{cases}$$

where v_d is the drift speed of the charge carriers along the wire and $v_t = (\ell_2/2)\omega_R$ is the tangential velocity due to the rotating loop. Recall that the drift speed has the same sign as the current, that is, $v_d > 0$ for $i > 0$. Also recall that the angular velocity is written as $\vec{\boldsymbol{\omega}}_R = \omega_R\hat{\mathbf{z}}$ where $\hat{\mathbf{z}}$ is the axis the motor is turning about. The magnetic force per unit charge $\vec{\mathbf{F}}_{\text{magnetic}}/q$ on the charge carriers on the axial sides of the loop is

$$\vec{\mathbf{F}}_{\text{magnetic}}/q = \vec{\mathbf{v}}\times\vec{\mathbf{B}}$$

where

$$\vec{\mathbf{v}}\times\vec{\mathbf{B}} = \begin{cases} (v_t\hat{\boldsymbol{\theta}}+v_d\hat{\mathbf{z}}) \times (+B)\hat{\mathbf{r}} = -v_tB\hat{\mathbf{z}}+v_dB\hat{\boldsymbol{\theta}} & \text{for side } a \\ (v_t\hat{\boldsymbol{\theta}}-v_d\hat{\mathbf{z}}) \times (-B)\hat{\mathbf{r}} = +v_tB\hat{\mathbf{z}}+v_dB\hat{\boldsymbol{\theta}} & \text{for side } a' \end{cases}$$

or

$$\vec{\mathbf{v}}\times\vec{\mathbf{B}} = \begin{cases} v_dB\hat{\boldsymbol{\theta}} - \omega_R(\ell_2/2)B\hat{\mathbf{z}} & \text{for side } a \\ v_dB\hat{\boldsymbol{\theta}} + \omega_R(\ell_2/2)B\hat{\mathbf{z}} & \text{for side } a'. \end{cases}$$

The component $v_dB\hat{\boldsymbol{\theta}}$ is what produces the torque. In more detail, with N the number of charge carriers/unit volume, S the cross-sectional area of the wire loop, and ℓ_1 the axial length of the loop, the quantity $NS\ell_1$ is the total number of charge carriers of each side of the loop and the current

www.EngineeringEBooksPdf.com

due to the movement of these charges is $i = qNSv_d$ (see Figure 1.22). The total tangential forces on the axial sides of the rotor loop are given by

$$\begin{aligned}\vec{\mathbf{F}}_{\text{side } a} &= (qNS\ell_1)v_d B\hat{\boldsymbol{\theta}} = i(t)\ell_1 B\hat{\boldsymbol{\theta}} \\ \vec{\mathbf{F}}_{\text{side } a'} &= (qNS\ell_1)v_d B\hat{\boldsymbol{\theta}} = i(t)\ell_1 B\hat{\boldsymbol{\theta}}.\end{aligned}$$

The torque is then

$$\vec{\boldsymbol{\tau}} = \frac{\ell_2}{2}\hat{\mathbf{r}}\times\vec{\mathbf{F}}_{\text{side } a} + \frac{\ell_2}{2}\hat{\mathbf{r}}\times\vec{\mathbf{F}}_{\text{side } a'} = 2(\frac{\ell_2}{2}\hat{\mathbf{r}}) \times (i\ell_1 B\hat{\boldsymbol{\theta}}) = i\ell_1\ell_2 B\hat{\mathbf{z}}$$

which is the same result as in the macroscopic case.

It is now shown that the $\hat{\mathbf{z}}$ component of the magnetic force produces the back emf. The $\hat{\mathbf{z}}$ component of $\vec{\mathbf{F}}_{\text{magnetic}}$, that is, along the axial sides of the loop, is given by

$$(\vec{\mathbf{F}}_{\text{magnetic}}/q)_z\hat{\mathbf{z}} = \begin{cases} -\omega_R(\ell_2/2)B\hat{\mathbf{z}} & \text{for side } a \\ +\omega_R(\ell_2/2)B\hat{\mathbf{z}} & \text{for side } a'. \end{cases}$$

As shown in Figure 1.23, this component of the magnetic force per unit charge $(\vec{\mathbf{F}}_{\text{magnetic}}/q)_z$ opposes the electric field $\vec{\mathbf{E}}_S$ set up in the loop by the applied armature voltage V_S. The relationship between V_S and $\vec{\mathbf{E}}_S$ is

$$V_S = \int_{T_1}^{T_2} \vec{\mathbf{E}}_S \cdot d\vec{\boldsymbol{\ell}}$$

where

$$d\vec{\boldsymbol{\ell}} = \begin{cases} +d\ell\hat{\mathbf{z}} & \text{for side } a \\ -d\ell\hat{\mathbf{z}} & \text{for side } a'. \end{cases}$$

Then, with ξ denoting the integral of the magnetic force per unit charge from T_1 to T_2, one has

$$\begin{aligned}\xi &\triangleq \int_{T_1}^{T_2} (\vec{\mathbf{F}}_{\text{magnetic}}/q) \cdot d\vec{\boldsymbol{\ell}} \\ &= \int_{\text{side } a} (-\omega_R(\ell_2/2)B\hat{\mathbf{z}}) \cdot (d\ell\hat{\mathbf{z}}) + \int_{\text{side } a'} (\omega_R(\ell_2/2)B\hat{\mathbf{z}}) \cdot (-d\ell\hat{\mathbf{z}}) \\ &= \int_{\ell=0}^{\ell=\ell_1} -\omega_R(\ell_2/2)Bd\ell + \int_{\ell=0}^{\ell=\ell_1} -\omega_R(\ell_2/2)Bd\ell \\ &= -\omega_R(\ell_2/2)B\ell_1 - \omega_R(\ell_2/2)B\ell_1 \\ &= -\ell_1\ell_2 B\omega_R.\end{aligned}$$

In this example, the (back) emf ξ is due to the magnetic force while V_S is due to the electric field set up by the voltage source. As the induced emf ξ and the source voltage V_S have the same sign convention, the minus sign

www.EngineeringEBooksPdf.com

in the expression for ξ shows that it opposes the applied armature voltage V_S. The total emf (voltage) in the loop is

$$V_S + \xi = V_S - \ell_1 \ell_2 B \omega_R.$$

Finally, the equation governing the current in the rotor loop is

$$L\frac{di}{dt} + Ri = V_S - \ell_1 \ell_2 B \omega_R.$$

This is the same physical result as shown in the macroscopic case using Faraday's law. However, here the induced emf $\xi = -\ell_1 \ell_2 B \omega_R$ is negative because it was chosen to have the same sign convention as V_S (i.e., both V_S and ξ are positive going from T_1 to T_2). This is in contrast to the macroscopic case in which they had opposite sign conventions so that $\xi = \ell_1 \ell_2 B \omega_R$ was positive, but still opposed V_S.

Remark *Voltage and Emf*

The *electromotive force* or *emf* between two points in a circuit is the integral of the total force per unit charge along the circuit between those two points.[8] The force per unit charge can be due to an electric field, a magnetic field or both. The term voltage (drop) was originally reserved for the integral of the *electric field* between the two points. However, this distinction is usually not made and the two terms (voltage and emf) are used interchangeably.

1.5.2 Drift Speed

Above, it was shown that the drift speed of the charge carriers making up the current is given by $v_d(t) = i(t)/(qNS)$. As explained in Ref. [34] (page 781), this motion (drift speed) of the charges in the conductor is caused by the electric field setup in the conductor by the voltage source and/or induced emfs in the conducting circuit. This electric field is pushing the charges along the conductor against the internal resistance of the conductor. In metals, the outer valence electrons are free to move about the lattice of the metal and are called *conduction electrons*. For example, in copper there is one valence electron per atom and the other 28 electrons remain bound to the copper nucleus. Consequently, as there are 8.4×10^{22} atoms/cm^3 in copper, there are $N = 8.4 \times 10^{22}$ electrons/cm^3 that can move freely within the copper lattice to make up the current in the wire. To consider a simple numerical example, let $i = 10$ A, $S = 0.1$ cm^2 so that with $q = 1.6 \times 10^{-19}$ coulomb/electron, the corresponding drift speed is

$$\begin{aligned} v_d &= \frac{i(t)}{qNS} = \frac{10 \text{ A}}{(1.6 \times 10^{-19} \frac{\text{coulomb}}{\text{electron}})(8.4 \times 10^{22} \frac{\text{electrons}}{\text{cm}^3})(0.1 \text{ cm}^2)} \\ &= 0.74 \text{ cm/sec.} \end{aligned}$$

[8] Note that the electromotive force is *not* a force, but rather an energy per unit charge.

www.EngineeringEBooksPdf.com

That is, it takes $1/(0.74 \text{ cm/sec}) = 1.35$ sec for the charge carrier to travel one centimeter. However, it should be noted that when a voltage/emf is applied to a circuit, the corresponding electric field is setup around the circuit at a speed close to the speed of light. This is analogous to applying pressure to a long tube of water. The pressure wave is transmitted down the tube rapidly (at the speed of sound in water) while the water itself moves much slower [34].

1.6 Tachometer for a DC Machine*[9]

A tachometer is a device for measuring the speed of a DC motor by putting out a voltage proportional to the motor's speed. A tachometer for the simple linear DC machine is considered first.

1.6.1 Tachometer for the Linear DC Machine

Figure 1.24 shows a tachometer added to the linear DC machine. The magnetic field in the DC motor is $\vec{\mathbf{B}}_1 = -B_1\hat{\mathbf{z}}$ with $B_1 > 0$ while in the tachometer it is $\vec{\mathbf{B}}_2 = -B_2\hat{\mathbf{z}}$ with $B_2 > 0$.

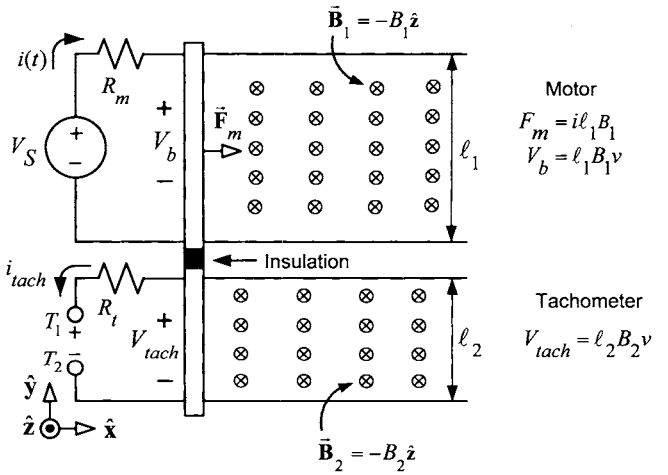


FIGURE 1.24. DC tachometer (generator).

The two bars are rigidly connected together by the insulating material. The motor force (the magnetic force on the upper bar) is $F_m = i\ell_1 B_1$, and

[9]Sections marked with an asterisk (*) may be skipped without loss of continuity.

www.EngineeringEBooksPdf.com

the induced (back) emf in the motor is $\xi = V_b = B_1\ell_1 v$, where v is the speed of the motor (bar).

The induced (back) emf in the tachometer is given by $\xi = V_{tach} = B_2\ell_2 v$ so that by measuring the voltage between the terminals T_1 and T_2, the speed v of the motor can be computed. Note that the tachometer and motor have the same physical structure. In fact, the tachometer is nothing more than a generator putting out a voltage proportional to the speed.

1.6.2 Tachometer for the Single-Loop DC Motor

A tachometer for the single loop DC motor is constructed by attaching another loop to the shaft and rotating it an external magnetic field to act as a DC generator. That is, the changing flux in the tachometer loop produces (generates) an induced emf according to Faraday's law and this emf is proportional to the shaft's speed. To see this, consider Figure 1.25, where a motor loop is driven by a voltage V_S and, attached to the same shaft, is a second loop called a tachometer. Both loops rotate in an external radial magnetic field which is not shown in Figure 1.25, but is shown for the tachometer loop in Figure 1.26. It is important to point out that no voltage is applied to the terminals T_1 and T_2 of the tachometer as was the case for the motor. Instead, the voltage V_{tach} between the terminals T_1 and T_2 of the tachometer is measured (this voltage is proportional to the motor speed ω_R).

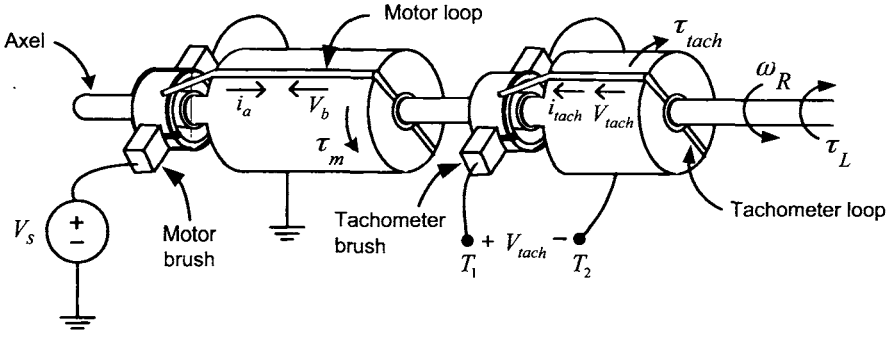


FIGURE 1.25. Single loop motor and tachometer. Drawn by Sharon Katz.

Specifically, in the same way the back emf was computed for the DC motor, one can calculate the flux in the loop of the tachometer due to the

www.EngineeringEBooksPdf.com

external magnetic field. This computation is (see Figure 1.26)

$$\begin{aligned}
\phi &= \int_S \vec{\mathbf{B}} \cdot d\vec{\mathbf{S}} \\
&= \int_0^{\ell_1} \int_{\theta_R}^{\pi} (B\hat{\mathbf{r}}) \cdot (\frac{\ell_2}{2} d\theta dz \hat{\mathbf{r}}) + \int_0^{\ell_1} \int_{\pi}^{\pi+\theta_R} (-B\hat{\mathbf{r}}) \cdot (\frac{\ell_2}{2} d\theta dz \hat{\mathbf{r}}) \\
&= \int_0^{\ell_1} \int_{\theta_R}^{\pi} B\frac{\ell_2}{2} d\theta dz + \int_0^{\ell_1} \int_{\pi}^{\pi+\theta_R} -B\frac{\ell_2}{2} d\theta dz \\
&= (\ell_1 \ell_2 B/2)(\pi - \theta_R) - (\ell_1 \ell_2 B/2)\theta_R \\
&= -\ell_1 \ell_2 B\theta_R + (\ell_1 \ell_2 B/2)\pi.
\end{aligned}$$

The induced emf is then

$$V_{\text{tach}} = -d\phi/dt = (\ell_1 \ell_2 B) d\theta_R/dt = K_{b\_\text{tach}} \omega_R$$

where $K_{b\_\text{tach}} = \ell_1 \ell_2 B$ is a constant depending on the dimensions of the tachometer rotor and the strength of the external magnetic field of the tachometer. This shows that the voltage between the terminals T_1 and T_2 is proportional to the angular speed and therefore can be used to measure the speed.

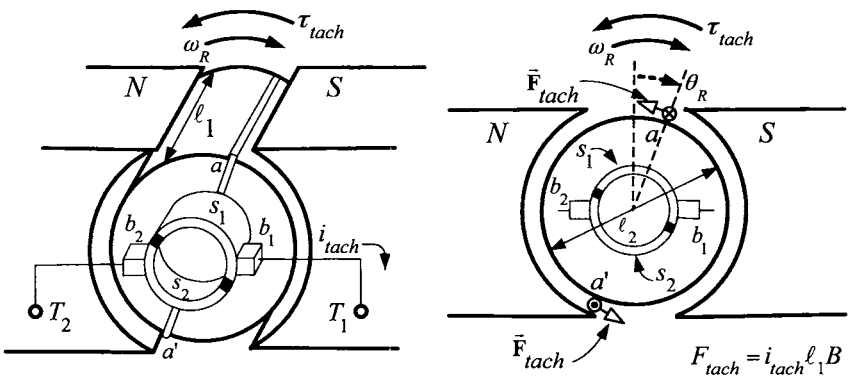


FIGURE 1.26. Cutaway view of the DC tachometer. From *Electromagnetic and Electromechanical Machines,* 3rd edition, L. W. Matsch and J. Derald Morgan, 1986. Reprinted by permisson of John Wiley & Sons.

1.7 The Multiloop DC Motor*

The above single loop motor of Figure 1.5 was used to illustrate the basic Physics of the DC motor. However, it is not a practical motor. The first thing that must be done is to add more loops to extract more torque from

www.EngineeringEBooksPdf.com

the machine. Further, in the single-loop motor, the magnetic field produced by the current in the *rotor* is an external magnetic field acting on the field windings. As the loop rotates, this magnetic field results in a changing flux in the field windings, which in turn induces an emf in the field windings. This emf is referred to as the *armature reaction* and makes it difficult to maintain a constant field current. (The term armature refers to the rotating current loop, and reaction refers to the induced emf in the field windings produced by the rotor current.) The problem of armature reaction can be alleviated by adding more loops to the motor.

1.7.1 Increased Torque Production

Figure 1.27 below shows the addition of several loops to the motor with each loop similar in form to the loop in Figure 1.5. As shown in the figure, there are now eight slots in the rotor with two loops placed in each pair of slots that are 180° apart for a total of eight loops.

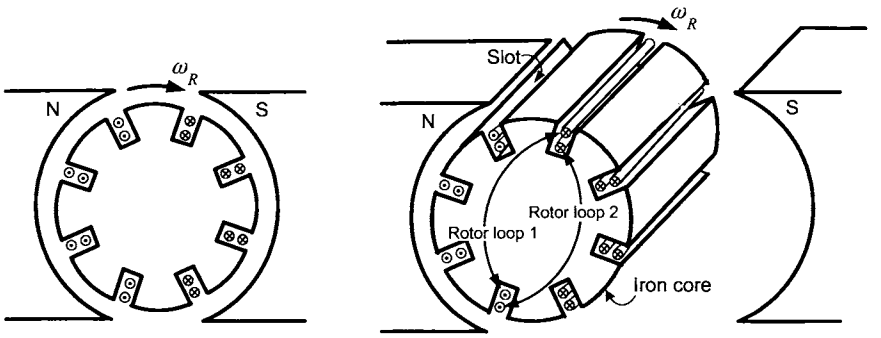


FIGURE 1.27. A multiloop armature for a DC motor.

The torque on the rotor is now $\tau_m = n\ell_1\ell_2 Bi$, where $n = 8$ is the number of rotor loops and B is the strength of the radial magnetic field in the air gap produced by the external magnetic field. Of course, some method must be found to ensure the current in each loop is reversed every half-turn so that (for positive torque) all the loop sides under the south pole face will have their current going into the page $\otimes$ and all the loop sides under the north pole face will have their current coming out of the page $\odot$. This process is referred to as *commutation* and is considered next.

1.7.2 Commutation of the Armature Current

As seen in Figure 1.27, as a rotor loop rotates clockwise past the vertical position, the current in the top side of the loop must change direction from

www.EngineeringEBooksPdf.com

coming out of the page to going into the page. That is, each rotor loop must have the current in it reversed every half-turn. This is done using a commutator which is illustrated in Figure 1.28 for the rotor shown in Figure 1.27. The commutator for this rotor consists of 8 copper segments (labeled a–h in 1.30(a)) which are separated by insulating material. By connecting each of the ends of the rotor loops of Figure 1.27 to the appropriate copper segments of the commutator, the current will be reversed every half-turn as it rotates past the vertical. To explain all of this, consider Figure 1.30(a), which shows explicitly how the ends of the rotor loops are connected to the segments of the commutator. The eight rotor loops of Figure 1.27 are labeled as $1-1'$,..., $8-8'$ in Figure 1.30(a) with the ends of each such loop electrically connected (soldered) to a particular pair of commutator segments. For example, the ends of loop $1-1'$ are connected to commutator segments a and b, respectively. The commutator and rotor loops all rotate together rigidly while the two brushes (labeled b_1 and b_2) remain stationary. The brushes are typically made of a carbon material and are mechanically pressed against the commutator surface, making electrical contact.[10] That is, as the commutator rotates, the particular segment that is rubbing against the brush makes electrical contact.

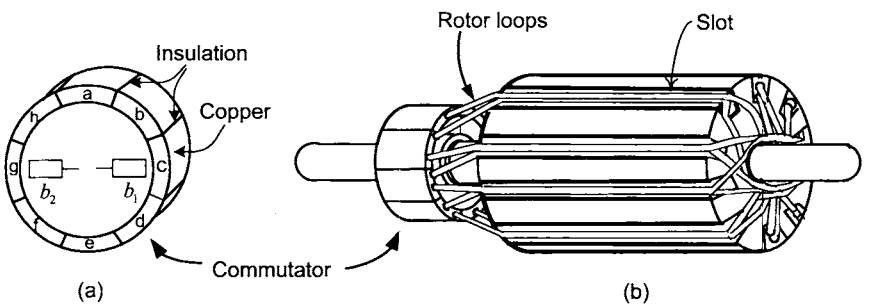


FIGURE 1.28. Commutator for the rotor in Figure 1.27.

Figure 1.29 is a photograph of the rotor of an actual DC motor with a tachometer.

[10] The figure shows a gap between the brushes and the commuator, but this was done for illustration and there is no gap in reality. Also, for illustrative purposes, the brushes are shown inside the commutator when in fact they are normally pressed against the commutator from the outside.

www.EngineeringEBooksPdf.com

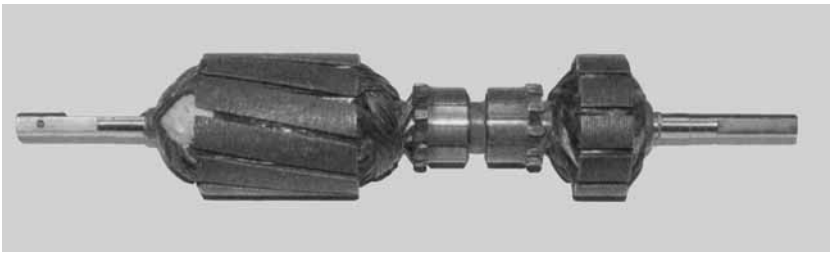


FIGURE 1.29. Photo of the rotor of a DC motor (left) and its tachometer (right). Note that the slots for the windings of the DC motor are skewed (see problem 9). Photo courtesy of Professor J. D. Birdwell of the University of Tennessee.

As previously explained, to obtain positive torque, it must be that whenever a side of a loop is under a south pole face, the current must be into the page ($\otimes$) and the other side of the loop, which is under the north pole face, must have its current out of the page ($\odot$). When the loop side rotates from being under one pole face to the other pole face, the current in that loop must be reversed (commutated). The mechanism of how this connection between the armature loops, the commutator and the brushes can reverse the current in each rotor loop every half turn is now explained.

With reference to Figure 1.30(a), the armature current i enters brush b_1 and into commutator segment c. By symmetry, half of this armature current (i.e., $i/2$) goes through loop $3{-}3'$ into commutator segment d, then through loop $4{-}4'$ into commutator segment e, then through loop $5{-}5'$ into commutator segment f, then through loop $6{-}6'$ into commutator segment g, and, finally, out through brush b_2. This path (circuit) of the current is denoted in **bold**. Similarly, there is a parallel path for the other half of the current armature current. Specifically, the other half of the armature current $i/2$ goes through loop $2'{-}2$ into commutator segment b, then through loop $1'{-}1$ into commutator segment a, then through loop $8'{-}8$ into commutator segment h, then into loop $7'{-}7$ into commutator segment g, and finally, out through brush b_2. This path (circuit) is denoted without bold. So, for the rotor in the position shown in Figure 1.30(a), there are two parallel circuits from b_1 to b_2 each made up of four loops connected in series and each circuit carries half of the armature current. The sides of the loops under the south pole face have their current into the page while the other side of these loops (which are under the north pole face) have their current out of the page so that positive torque is produced.

The sides of the loops in Figure 1.30(a) are 45° apart. Figure 1.30(b) shows the rotor turned $45°/2$ with respect to Figure 1.30(a). In this case, brush b_1 shorts the two commutator segment b and c together while the brush b_2 shorts together the two commutator segments f and g. The ends of loop $2{-}2'$ are connected to commutator segments b and c (which are now shorted together) so that the current in this loop is now zero. Similarly,

www.EngineeringEBooksPdf.com

the ends of loop $6-6'$ are connected to commutator segments f and g and the current in this loop is also zero. For the remaining loops, $i/2$ goes through loop $3-3'$ into commutator segment d, then through loop $4-4'$ into commutator segment e, then into loop $5-5'$ into commutator segment f, and finally, out brush b_2. These loops are denoted in **bold** in the figure. Similarly, $i/2$ goes through loop $1-1'$ into commutator segment a, then through loop $8'-8$ into commutator segment h, then into loop $7'-7$ into commutator segment g, and finally out brush b_2.

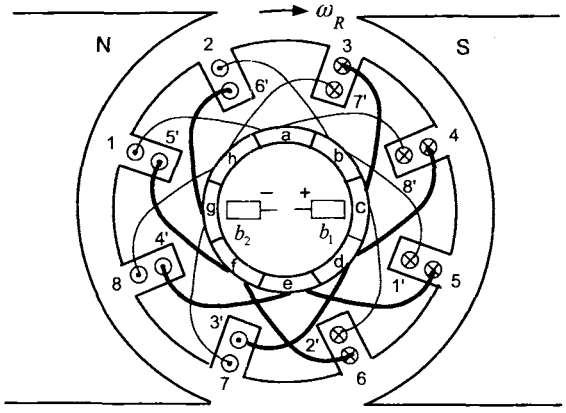


FIGURE 1.30. (a). Rotor loops and commutator for 4 sets of rotor loops. Brushes remained fixed in space, that is, they do not rotate. From *Electric Machinery Fundamentals,* 2nd edition by S. J. Chapman, McGraw-Hill 1991. Reproduced with permission of McGraw-Hill Companies.

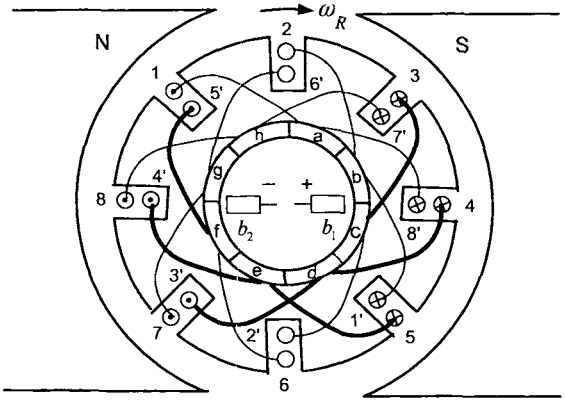


Figure 1.30(b). Rotor turned $45°/2$ with respect to Figure 1.30(a). Adapted from Chapman [19].

www.EngineeringEBooksPdf.com

The motor continues to rotate and consider it now after it has moved additional $45°/2$ so that it has the position shown in Figure 1.30(c). In this case, the current enters brush b_1 and into commutator segment b. By symmetry, half the current $i/2$ goes through loop $2-2'$ into commutator segment c, then through loop $3-3'$ into commutator segment d, then through loop $4-4'$ into commutator segment e, then through loop $5-5'$ into commutator segment f, and finally out through brush b_2. This path (circuit) of the current is denoted in **bold**. Similarly, the other half of the current goes through loop $1'-1$ into commutator segment a then through loop $8'-8$ into commutator segment h then through loop $7'-7$ into commutator segment g then into loop $6'-6$ into commutator segment f and finally, out through brush b_2. This path (circuit) is denoted without using bold.

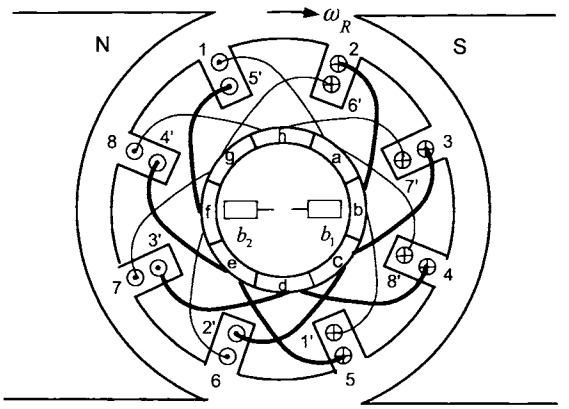


Figure 1.30(c). Rotor turned 45° with respect to Figure 1.30(a). Adapted from Chapman [19].

As the sequence of figures 1.30(a)–(c) show, the current in loops $2-2'$ and $6-6'$ were reversed as these two loops rotated past the vertical position. In summary, there are two parallel paths, each consisting of four loops, and when any loop goes to the vertical position, the current in that loop is reversed. In this way, all sides of the loop under the south pole have their current going into the page and all sides under the north pole have their current coming out of the page for positive torque production.

Remark The scheme for current commutation presented here is from [19]. However, there are many other schemes and the reader is referred to Refs. [19], [21], [24], and [26] for an introduction to other schemes. See Ref. [24] for a discussion of how commutation is often carried out in small PM DC motors.

www.EngineeringEBooksPdf.com

Stator Iron Construction

A more realistic depiction of the stator for a (single pole pair) permanent magnet DC motor is shown in Figure 1.31. The radial magnetic field in the air gap is produced by the two semicircular-shaped permanent magnets.

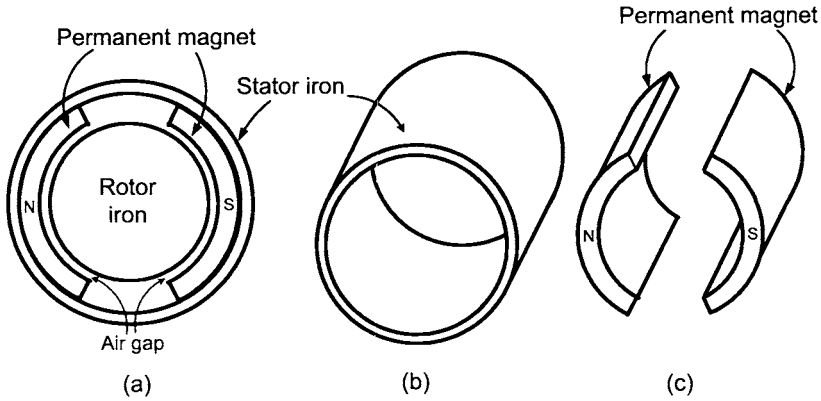


FIGURE 1.31. (a) Stator of a PM DC motor. (b) Stator iron. (c) Stator permanent magnet.

In the case where the DC motor has a field winding, a more realistic depiction of the stator iron (single pole pair) is shown in Figure 1.32 (compare with Figure 1.7).

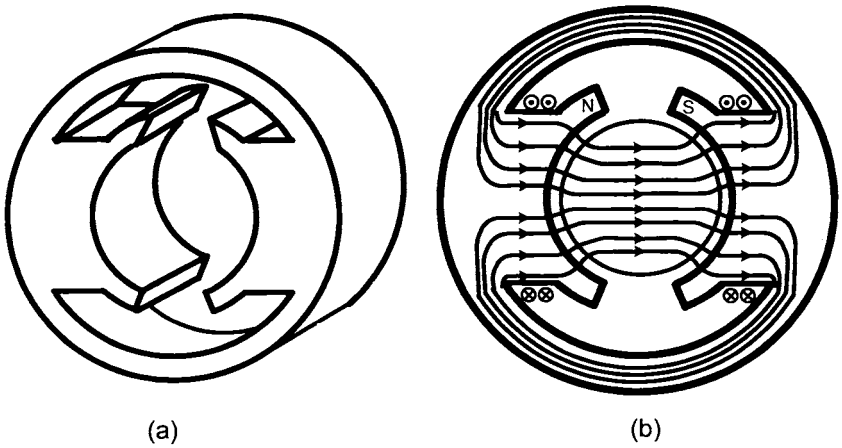


FIGURE 1.32. (a) Stator iron for a wound field DC motor. (b) Cross-sectional view of the stator iron with the field windings.

www.EngineeringEBooksPdf.com

1.7.3 Armature Reaction

Figure 1.33 shows current in a field winding which is used to magnetize the iron in a fashion similar to that shown in Figure 1.7. Closed curves are drawn in Figure 1.33 to show the magnetic field distribution in the iron and air gap due to just the field current. Note that the magnetic field tends to be in the horizontal direction as it goes inside the field windings. Figure 1.34 shows the magnetic field distribution in the iron and air gap due to just the armature current. By having many equally spaced loops on the rotor, the magnetic field distribution due to the armature current will be as shown in Figure 1.34 for *any* rotor position. Note that this magnetic field tends to be vertical in the iron core inside the field windings (the field windings are not shown in Figure 1.34). In other words, in the stator iron core within the field windings, the magnetic field due to the armature current is perpendicular to the flux surfaces of the field windings. As a result, any changing magnetic field due to a changing armature current will not induce voltages inside the field windings. *Armature reaction* refers to the voltage induced in the field winding by the magnetic field of the armature current. (This is undesirable as such a voltage would cause the current in the field winding to change, and therefore not be constant as the analysis up to this point has assumed.) The symmetric placement of rotor loops around the periphery of the rotor essentially eliminates the armature reaction.

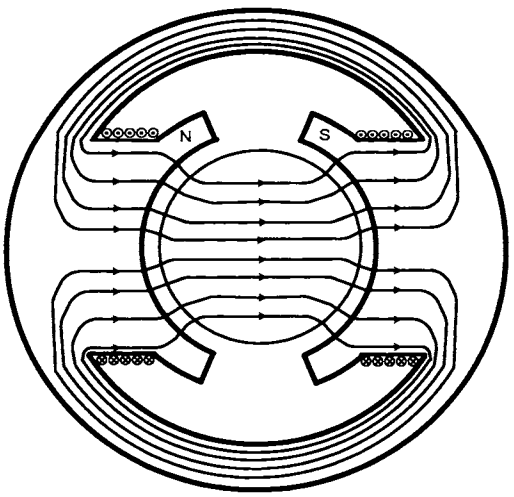


FIGURE 1.33. Magnetic field due to the field current. Adapted from Ref. [23].

www.EngineeringEBooksPdf.com

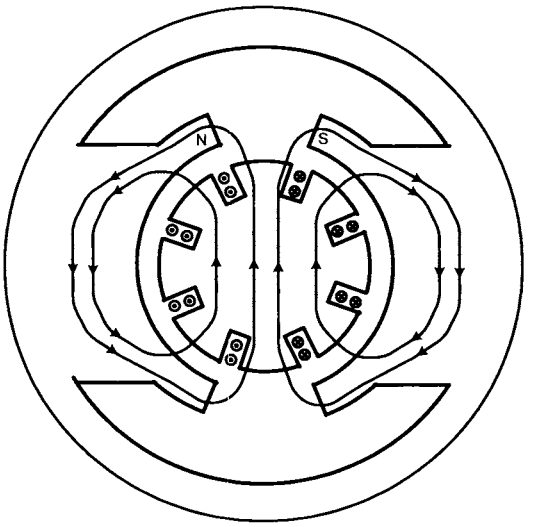


FIGURE 1.34. Magnetic field distribution due to the armature current. Adapted from Ref. [23].

Finally, Figure 1.35 shows the sum of the two magnetic fields.

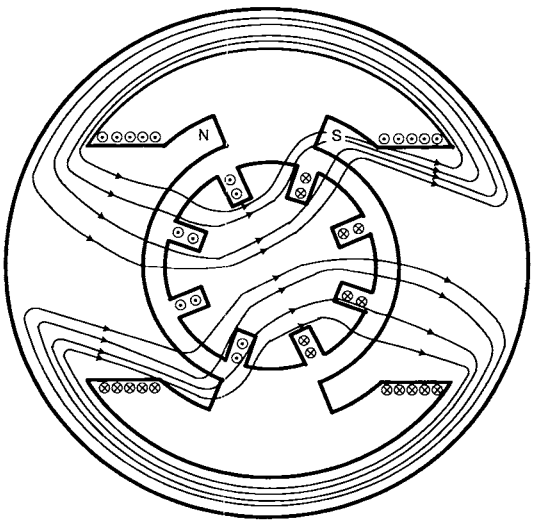


FIGURE 1.35. Magnetic field due to field and armature currents. Adapted from Ref. [23].

www.EngineeringEBooksPdf.com

1.7.4 *Field Flux Linkage and the Air Gap Magnetic Field*

In the separately excited DC motor of Figure 1.36, it is convenient to have an expression relating the radial magnetic field B in the air gap to the total flux in the field windings.

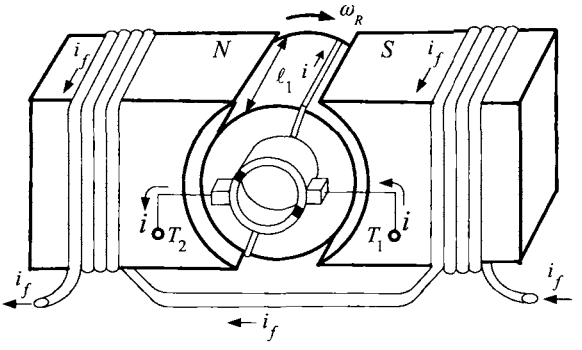


FIGURE 1.36. Separately excited DC motor. Adapted from Ref. [21].

The magnetic field lines are shown in Figure 1.4. Figure 1.37 shows a closed flux surface which is now used to derive a relationship between the radial magnetic field B in the air gap and the field flux linkage λ_f.

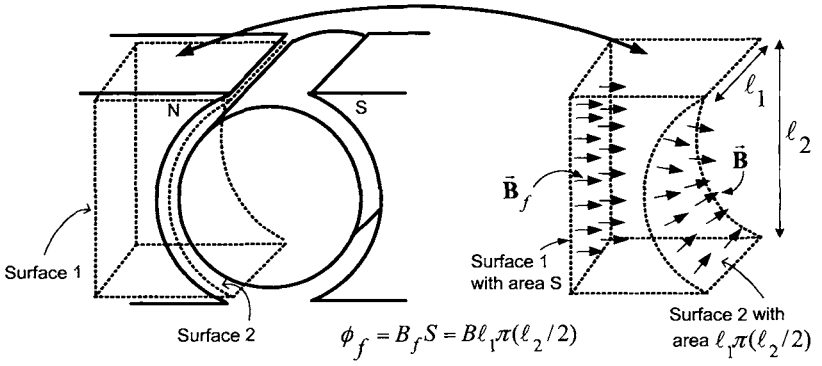


FIGURE 1.37. The flux through surface 1 is $B_f S$ and the flux through surface 2 is $\ell_1\pi(\ell_2/2)B$. To a good approximation, these two fluxes are equal.

The field flux *linkage* λ_f is defined by

$$\lambda_f(i_f) = N_f\phi_f = N_f S B_f(i_f)$$

where N_f is the total number of field windings, S is the cross-sectional area of the iron core of the field winding and $B_f(i_f)$ is the magnetic field

www.EngineeringEBooksPdf.com

produced *inside the magnetic material* of the field circuit due to the field current i_f. With this definition of flux linkage, the total induced emf in the field windings produced by a changing B_f is given by

$$\xi_{\text{fieldwinding}} = -\frac{d\lambda_f(i_f)}{dt} = -N_f\frac{d\phi_f}{dt}.$$

With the two flux surfaces shown in Figure 1.37, it turns out that *conservation of flux*[11] implies the flux through the surface 1 in the iron core equals the flux through the half cylindrical surface 2 in the air gap. That is,

$$\phi_f = SB_f(i_f) = \ell_1\pi(\ell_2/2)B(i_f)$$

where $\ell_2/2$ is the radius of the rotor, ℓ_1 is the axial length of the rotor and $B(i_f)$ is the radial magnetic field *in the air gap* due to the field current i_f. Consequently,

$$B(i_f) = \frac{SB_f(i_f)}{\pi\ell_1\ell_2/2} = \frac{\lambda_f(i_f)}{N_f\pi\ell_1\ell_2/2}$$

is an expression for the radial magnetic field $B(i_f)$ *in the air gap* in terms of the flux linkage $\lambda_f(i_f) = N_f\ell_1\ell_2B_f(i_f)$ in the field windings.

1.7.5 Armature Flux Due to the External Magnetic Field

In what follows, the multiloop motor of Figure 1.30 is considered in which the armature circuit consists of two parallel circuits each having n loops. Let θ_R be referenced relative to loop $1{-}1'$ so that $\theta_R = 0$ corresponds to loop $1{-}1'$ being vertical. (Recall in Figure 1.5 that $\theta_R = 0$ corresponded to loop $a{-}a'$ being vertical.) For the single loop motor, the flux $\phi_{sl}(i_f, \theta_R)$ in the loop $1{-}1'$ of the rotor due to the external magnetic field $B(i_f)$ is

$$\phi_{sl}(i_f, \theta_R) = -\ell_1\ell_2B(i_f)(\theta_R \bmod \pi - \pi/2).$$

In general, let $\theta_k = 0$ correspond to loop $k{-}k'$ being vertical so that the position of the kth rotor loop may be written as

$$\theta_k = \theta_R + (k-1)\pi/n \qquad \text{for } k = 1, ..., n$$

where n is the number of loops connected in series in each parallel circuit ($n = 4$ in Figure 1.30). The flux in the kth rotor loop is [see equation (1.4)]

$$\begin{aligned}\phi_k(i_f, \theta_R) &= -\ell_1\ell_2B(i_f)\left(\theta_k \bmod \pi - \frac{\pi}{2}\right)\\ &= -\ell_1\ell_2B(i_f)\left(\left\{\theta_R + (k-1)\frac{\pi}{n}\right\} \bmod \pi - \frac{\pi}{2}\right).\end{aligned}$$

[11] See problem 6 and Chapter 3.

www.EngineeringEBooksPdf.com

The total flux linkage $\lambda(i_f, \theta_R)$ in the n rotor loops is then

$$\begin{aligned}\lambda(i_f, \theta_R) &= \sum_{k=1}^{n} \phi_k(i_f, \theta_R) \\ &= -\sum_{k=1}^{n} \ell_1 \ell_2 B(i_f) \left(\left\{ \theta_R + (k-1)\frac{\pi}{n} \right\} \bmod \pi - \frac{\pi}{2} \right). \quad (1.7)\end{aligned}$$

In Figures 1.30(a)–(c), *each* of the two parallel sets of n rotor loops has the flux linkage $\lambda(i_f, \theta_R)$ in it.

Recall that the sign convention for the fluxes $\phi_k(i_f, \theta_R)$ is such that if $-d\phi_k(i_f, \theta_R)/dt > 0$, then it is acting in the direction opposite to positive current flow, that is, its sign convention is opposite to that of applied voltage V_S. As a consequence, the sum

$$V_S - \left(-\frac{d\lambda(i_f, \theta_R)}{dt} \right) = V_S + \frac{d\lambda(i_f, \theta_R)}{dt}$$

is the total emf in the loop due to the applied voltage and the external magnetic field.

For $n = 4$, the flux linkage $\lambda(i_f, \theta_R)$ is plotted as a function of the rotor position θ_R in Figure 1.38. Note that $\partial\lambda(i_f, \theta_R)/\partial\theta_R = -n\ell_1\ell_2 B(i_f)$ which is proportional to the number of rotor loops n and to the strength of the external magnetic field strength $B(i_f)$ in the air gap.

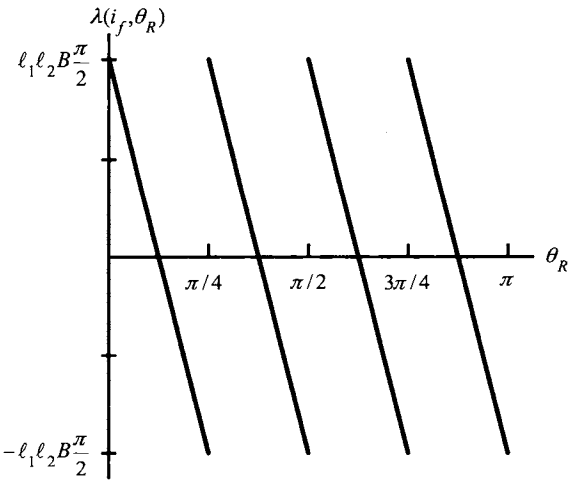


FIGURE 1.38. Flux linkage $\lambda(i_f, \theta_R)$ versus θ_R in radians with $n = 4$ sets of rotor loops and $0 \le \theta_R \le \pi$. The slope is $\partial\lambda(i_f, \theta_R)/\partial\theta_R = -n\ell_1\ell_2 B(i_f)$.

www.EngineeringEBooksPdf.com

In the case of a permanent magnet stator, the armature flux linkage is simply given by

$$\begin{aligned}\lambda(\theta_R) &= \sum_{k=1}^{n} \phi_k(\theta_R) \\ &= -\sum_{k=1}^{n} \ell_1 \ell_2 B\left(\left\{\theta_R + (k-1)\frac{\pi}{n}\right\} \bmod \pi - \frac{\pi}{2}\right) \qquad (1.8)\end{aligned}$$

where $B > 0$ is the strength of the radial magnetic field in the air gap produced by the permanent magnet of the stator.

1.7.6 Equations of the PM DC Motor

In the multiloop motor considered here, the armature circuit consists of two parallel circuits each having n loops. That is, there are a total of $2n$ loops on the rotor as each of the two parallel circuits has a loop at the same location on the rotor. Let L denote the total inductance of the n rotor loops making up either of the two parallel circuits. Then, if a current $i/2$ is in each parallel circuit, each circuit will have a flux linkage of $Li/2$ due to its current and an *additional* flux linkage of $Li/2$ due to the current in the other circuit. This is simply because the two sets of parallel loops (windings) are wound around the rotor core together so that they can be considered to be perfectly (magnetically) coupled.

The total flux linkage in the n loops making up either of the parallel circuits is now computed. To proceed, let i be the current into the armature so that $i/2$ is the current in the n loops of each parallel circuit. The quantity $Li/2$ is the flux linkage due to the current $i/2$ in the loops and an additional flux linkage of $Li/2$ is produced in these same loops by the current $i/2$ in the *other* parallel circuit for a total flux of Li. By equation (1.8), $\lambda(\theta_R)$ is the flux linkage in the n loops due to the *external* magnetic field produced by the permanent magnet of the stator. Recall that the sign convention for the induced emf $-d\lambda(\theta_R)/dt$ is opposite to that of $-d(Li)/dt$. Specifically (see Section 1.3.5), the normal to the flux surface was taken to be *radially in* to compute the flux Li while in Section 1.3.4 the surface normal was taken to be *radially out* to compute the flux $\lambda(\theta_R)$. Simply writing $-\lambda(\theta_R)$ then gives the flux due to the external magnetic field with the surface normal radially in and the induced voltages by both of these changing fluxes will then have the same sign convention as the applied armature voltage. Using the same sign convention as the applied armature voltage V_S, the total flux linkage in each parallel circuit of the armature may be written as

$$Li - \lambda(\theta_R).$$

Let R_1 denote the resistance of the n loops connected in series making up either of the two parallel circuits. The equation describing the electrical

www.EngineeringEBooksPdf.com

dynamics of the current in each of the parallel circuits is found by applying Kirchhoff's voltage law to obtain

$$-\frac{d}{dt}\Big(Li - \lambda(\theta_R)\Big) - R_1 i/2 + V_S = 0$$

where V_S is the applied voltage to the armature. Finally, defining $R \triangleq R_1/2$, the equation describing the electrical dynamics of the armature circuit is

$$L\frac{di}{dt} = -Ri + \frac{d\lambda(\theta_R)}{dt} + V_S. \tag{1.9}$$

The quantity $d\lambda(\theta_R)/dt$ can be expanded to obtain

$$\frac{d\lambda(\theta_R)}{dt} = \frac{\partial\lambda(\theta_R)}{\partial\theta_R}\omega_R = -n\ell_1\ell_2 B\omega_R = -K_b\omega_R \tag{1.10}$$

where $K_b \triangleq n\ell_1\ell_2 B$.

Each loop carries the current $i/2$ so that the torque produced by the two sides of each loop is $2\,(\ell_2/2)\,(i/2)\ell_1 B$. As there are $2n$ loops, the total torque is

$$\tau_m = 2n\ell_1\ell_2 B(i/2) = n\ell_1\ell_2 Bi = K_T i \tag{1.11}$$

where $K_T \triangleq n\ell_1\ell_2 B = K_b$. Finally, using (1.9) and (1.11), the complete set of equations for the PM DC motor is then

$$L\frac{di}{dt} = -Ri - K_b\omega_R + V_S \tag{1.12}$$

$$J\frac{d\omega_R}{dt} = K_T i - f\omega_R - \tau_L \tag{1.13}$$

$$\frac{d\theta_R}{dt} = \omega_R \tag{1.14}$$

where V_S is the applied armature voltage, τ_L is the load torque on the motor, f is the coefficient of viscous friction and J is the rotor's moment of inertia.

1.7.7 Equations of the Separately Excited DC Motor

The separately excited DC motor has an additional equation compared to the PM DC motor which describes the flux/current in the field winding. Similar to the case of the PM DC motor, the total flux linkage in either parallel circuit of the armature windings is given by

$$Li - \lambda(i_f, \theta_R)$$

where $\lambda(i_f, \theta_R)$ now depends on i_f as given by (1.7), and L is the inductance the n loops connected in series making up either parallel circuit. Again, R_1 denotes the resistance of either circuit and Kirchhoff's voltage law gives

$$-\frac{d}{dt}\Big(Li - \lambda(i_f, \theta_R)\Big) - R_1 i/2 + V_S = 0$$

www.EngineeringEBooksPdf.com

where V_S is the applied voltage to the armature. Finally, defining $R \triangleq R_1/2$, the equation describing the electrical dynamics of the armature circuit is

$$L\frac{di}{dt} = -Ri + \frac{d\lambda(i_f, \theta_R)}{dt} + V_S. \tag{1.15}$$

The quantity $d\lambda(i_f, \theta_R)/dt$ can be expanded to obtain

$$\frac{d\lambda(i_f, \theta_R)}{dt} = \frac{\partial \lambda}{\partial i_f}\frac{di_f}{dt} + \frac{\partial \lambda}{\partial \theta_R}\omega_R = \frac{\partial \lambda}{\partial i_f}\frac{di_f}{dt} - n\ell_1\ell_2 B(i_f)\omega_R. \tag{1.16}$$

Here $B(i_f)$ is the strength of the radial magnetic field *in the air gap* produced by the current in the field windings. The flux linkage in the field windings is $\lambda_f(i_f) = N_f S B_f(i_f)$ where $B_f(i_f)$ is the magnetic field strength *in the iron core* of the field, N_f is the number of field windings, and S is the cross sectional area of this iron core. The flux $SB_f(i_f)$ in each of the field windings goes through the air gap and, by conservation of flux (see Section 1.7.4), $SB_f(i_f) = \ell_1(\pi\ell_2/2)B(i_f)$ so that the radial magnetic field in the air gap produced by the field current is

$$B(i_f) = \frac{N_f}{N_f}\frac{SB_f(i_f)}{\pi\ell_1\ell_2/2} = \frac{\lambda_f(i_f)}{N_f\pi\ell_1\ell_2/2}.$$

Consequently,

$$n\ell_1\ell_2 B(i_f) = n\ell_1\ell_2\frac{\lambda_f(i_f)}{N_f\pi\ell_1\ell_2/2} = K_m\lambda_f(i_f)$$

where

$$K_m \triangleq \frac{2}{\pi}\frac{n}{N_f}.$$

As a result, equation (1.16) may be rewritten as

$$\frac{d\lambda(i_f, \theta_R)}{dt} = \frac{\partial \lambda}{\partial i_f}\frac{di_f}{dt} - K_m\lambda_f(i_f)\omega_R. \tag{1.17}$$

Each loop carries the current $i/2$ so that the torque produced on each of the two sides of the loop is $2\,(\ell_2/2)\,(i/2)\ell_1 B(i_f)$. As there are $2n$ loops, the total torque is

$$\tau_m = 2n\ell_1\ell_2 B(i_f)(i/2) = n\ell_1\ell_2 B(i_f)i = K_m\lambda_f(i_f)i \tag{1.18}$$

using the above expressions for K_m and $\lambda_f(i_f)$. Finally, using (1.15), (1.16), and (1.18), the mathematical model of the separately excited DC motor is given by

$$L\frac{di}{dt} = -Ri + \frac{\partial \lambda}{\partial i_f}\frac{di_f}{dt} - K_m\lambda_f(i_f)\omega_R + V_S \tag{1.19}$$

$$J\frac{d\omega_R}{dt} = K_m\lambda_f(i_f)i - \tau_L \tag{1.20}$$

$$\frac{d\lambda_f(i_f)}{dt} = -R_f i_f + V_f \tag{1.21}$$

www.EngineeringEBooksPdf.com

where V_f is the applied voltage to the field, R_f is the resistance of the field winding, τ_L is the load torque on the motor and J is the rotor's moment of inertia.

If the iron in the field is not in saturation, then one may write

$$\lambda_f(i_f) = L_f i_f$$

and the dynamic model simplifies to

$$L\frac{di}{dt} = -Ri + \frac{\partial \lambda}{\partial i_f}\frac{di_f}{dt} - K_m L_f i_f \omega_R + V_S \tag{1.22}$$

$$J\frac{d\omega_R}{dt} = K_m L_f i_f i - \tau_L \tag{1.23}$$

$$L_f\frac{di_f}{dt} = -R_f i_f + V_f. \tag{1.24}$$

Under normal operating conditions, the term $\frac{\partial \lambda}{\partial i_f}\frac{di_f}{dt}$ is typically negligible and the model then reduces to[12]

$$L\frac{di}{dt} = -Ri - K_m L_f i_f \omega_R + V_S \tag{1.25}$$

$$J\frac{d\omega_R}{dt} = K_m L_f i_f i - \tau_L \tag{1.26}$$

$$L_f\frac{di_f}{dt} = -R_f i_f + V_f. \tag{1.27}$$

A typical mode of operation is to use the field voltage V_f to hold the field current i_f constant at some value. Then the field flux is of course constant and $L_f di_f/dt = 0$. However, in the first equation (1.19) (or 1.25), it is seen that the back emf is $-K_m\lambda_f\omega_R$ (or $-K_m L_f i_f \omega_R$) which increases in proportion to the speed. The input voltage V_S must be at least large enough to overcome the back emf in order to maintain the armature current. To have the motor achieve higher speeds within the voltage limit $|V_S| \leq V_{\max}$, *field weakening* is employed. This is accomplished by using the input voltage V_f to decrease the field flux $\lambda_f = L_f i_f$ at higher speeds usually according to a flux reference of the form

$$\lambda_{ref} = \begin{cases} \lambda_{f0} & |\omega_R| \leq \omega_{base} \\ \lambda_{f0}\dfrac{\omega_{base}}{|\omega_R|} & |\omega_R| \geq \omega_{base}. \end{cases} \tag{1.28}$$

This is illustrated in Figure 1.39. For $\omega > \omega_{base}$, field weakening results in the back emf $-K_m\lambda_f\omega_R = -K_m\lambda_{f0}\frac{\omega_{base}}{|\omega_R|}\omega_R = -K_m\lambda_{f0}\omega_{base}\text{sign}(\omega_R)$ being constant. The trade-off is that the torque $K_m\lambda_f i = K_m\lambda_{f0}\frac{\omega_{base}}{|\omega_R|}i$ is now

[12] It will be seen later that field-oriented control of an induction motor results in a mathematical model of the induction motor that looks similar to these equations!

www.EngineeringEBooksPdf.com

less for the same armature current i due to the decrease in the field flux linkage λ_f. If the armature resistance is negligible and i_f is constant, then the *base speed* ω_{base} is defined to be the speed satisfying $K_m \lambda_f \omega_{base} = V_{\max}$. Otherwise, the base speed is chosen to be somewhat smaller to account for the Ri and $\frac{\partial \lambda}{\partial i_f}\frac{di_f}{dt}$ voltage drops [see equation (1.19)].

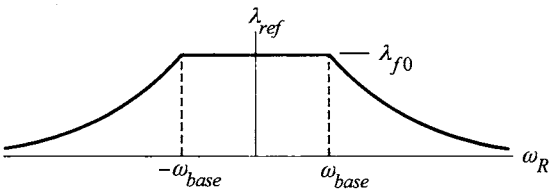


FIGURE 1.39. Flux reference for field weakening.

Appendices

Rotational Dynamics

The equations of motion of a rigid body that is constrained to rotate about a fixed axis are reviewed here briefly. Consider a cylinder which is constrained to rotate about a fixed axis as shown below.

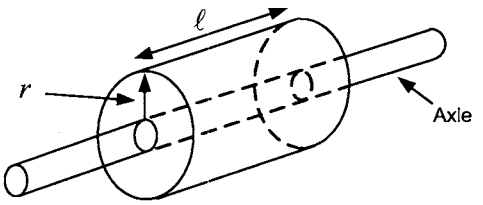


FIGURE 1.40. Cylinder constrained to rotate about a fixed axis.

The approach here is to obtain the equations of motion of the cylinder by first computing obtaining an expression for its kinetic energy. To do so, denote the angular speed of the cylinder by ω and the mass density of the material making up the cylinder by ρ. Then consider the cylinder to be made up of n small pieces of material Δm_i where the ith piece has mass

$$\Delta m_i = \rho r \Delta\theta \Delta\ell \Delta r.$$

This is illustrated in Figure 1.41.

www.EngineeringEBooksPdf.com

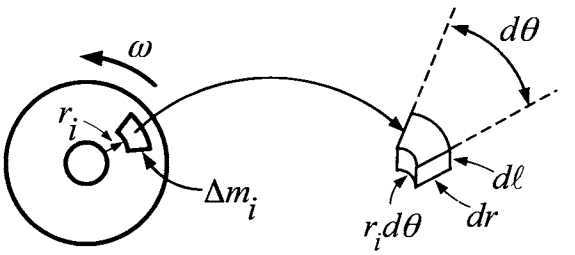


FIGURE 1.41. Cylinder is considered to be made up of small masses Δm_i. Drawn by Sharon Katz.

Each piece of mass Δm_i is rotating at the same angular speed ω so that the *linear* speed of Δm_i is $v_i = r_i\omega$ where r_i is the distance of Δm_i from the axis of rotation. The kinetic energy KE_i of Δm_i is given by

$$KE_i = \frac{1}{2}\Delta m_i v_i^2 = \frac{1}{2}\Delta m_i (r_i\omega)^2 .$$

The total kinetic energy is then

$$KE = \sum_{i=1}^{n} (KE)_i = \sum_{i=1}^{n} \frac{1}{2}\Delta m_i v_i^2 = \sum_{i=1}^{n} \frac{1}{2}\Delta m_i (r_i\omega)^2 = \frac{1}{2}\omega^2 \sum_{i=1}^{n} \Delta m_i r_i^2.$$

Dividing the cylinder into finer and finer pieces so that $n \to \infty$ and $\Delta m_i \to 0$, the sum

$$\sum_{i=1}^{n} \Delta m_i r_i^2$$

becomes the integral

$$J = \iiint_{cylinder} r^2 dm.$$

The quantity J is called the *moment of inertia* and the kinetic energy of the cylinder may now be written as

$$KE = \frac{1}{2}J\omega^2.$$

Assuming the axle radius is zero, the moment of inertia of the cylinder is computed to be

$$J = \int_0^R \int_0^\ell \int_0^{2\pi} r^2 \rho r d\theta d\ell dr = \frac{1}{2}(\pi R^2 \ell \rho) R^2 = \frac{1}{2} M R^2$$

where M is the total mass of the cylinder.

The above expression for the kinetic energy is now used to derive a relationship between torque and angular acceleration. Recall from elementary

www.EngineeringEBooksPdf.com

mechanics that the work done on a mass by an external force equals the change in its kinetic energy. In particular, consider an external force $\vec{\mathbf{F}}$ acting on the cylinder as shown in Figure 1.42.

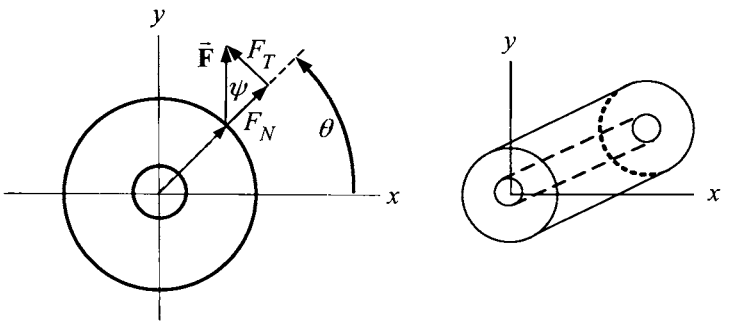


FIGURE 1.42. Force $\vec{\mathbf{F}}$ applied to the cylinder is resolved into a normal and tangential component. Drawn by Sharon Katz.

The cylinder is on an axle and therefore constrained to rotate about the z axis. Figure 1.42 shows the force $\vec{\mathbf{F}}$ applied to the cylinder at the position (r, θ) (in polar coordinates) resolved into a tangential component F_T and a normal component F_N so that $\vec{\mathbf{F}} = F_N\hat{\mathbf{r}} + F_T\hat{\boldsymbol{\theta}}$. The torque is defined as

$$\vec{\boldsymbol{\tau}} \triangleq \vec{\mathbf{r}} \times \vec{\mathbf{F}} = r\hat{\mathbf{r}} \times \left(F_N\hat{\mathbf{r}} + F_T\hat{\boldsymbol{\theta}}\right) = rF_T\hat{\mathbf{z}} = rF\sin(\psi)\hat{\mathbf{z}} \qquad (1.29)$$

where ψ is the angle between $\vec{\mathbf{r}}$ and $\vec{\mathbf{F}}$. (By definition, the magnitude of the cross product $\vec{\mathbf{r}} \times \vec{\mathbf{F}}$ is defined as $rF\sin(\psi)$ and the direction of $\vec{\mathbf{r}} \times \vec{\mathbf{F}}$ is perpendicular to both $\vec{\mathbf{r}}$ and $\vec{\mathbf{F}}$ along the axis of rotation determined by the right hand rule[13]). As $F_T = F\sin(\psi)$ is the tangential component, the torque may be rewritten as

$$\vec{\boldsymbol{\tau}} = \tau\hat{\mathbf{z}} = rF_T\hat{\mathbf{z}}$$

or, in scalar form, as

$$\tau = rF_T.$$

The motivation for the definition of torque as given by (1.29) is that it is the cause of *rotational* motion. Specifically, the rotational motion about an axis is caused by the applied tangential force F_T and the further away from the axis of rotation that the tangential force F_T is applied, the easier it is to get rotational motion. That is, the torque (cause of rotational motion)

[13]Using your right hand, curl your fingers in the direction from the first vector $\vec{\mathbf{r}}$ to the second vecotor $\vec{\mathbf{F}}$. Then your thumb points in the direction of $\vec{\mathbf{r}} \times \vec{\mathbf{F}}$.

www.EngineeringEBooksPdf.com

increases if either r or F_T increases which corresponds to one's experience (e.g., opening doors).

To summarize, $\vec{\boldsymbol{\tau}}$ is a vector pointing along the axis of rotation and the magnitude is given by

$$|\vec{\boldsymbol{\tau}}| = |\tau| = |rF_T|\,.$$

(Recall that the angular velocity vector $\vec{\boldsymbol{\omega}} = \omega\hat{\mathbf{z}}$ also points along the axis of rotation where ω is the angular speed.)

With $d\vec{\mathbf{s}} \triangleq ds\hat{\boldsymbol{\theta}} = rd\theta\hat{\boldsymbol{\theta}}$, the change in work done on the cylinder by the external force $\vec{\mathbf{F}}$ is

$$dW = \vec{\mathbf{F}} \cdot d\vec{\mathbf{s}} = F_T r d\theta = \tau d\theta$$

where $\tau \triangleq rF_T$. Dividing by dt, the power (rate of work) delivered to the cylinder is given by

$$\frac{dW}{dt} = \tau\frac{d\theta}{dt} = \tau\omega.$$

As the rate of work done equals the rate of change of kinetic energy, it follows that

$$\frac{dW}{dt} = \frac{d}{dt}\left(\frac{1}{2}J\omega^2\right) = \tau\frac{d\theta}{dt}$$

or

$$J\omega\frac{d\omega}{dt} = \tau\omega.$$

This gives the fundamental relationship between torque and angular acceleration:

$$\tau = J\frac{d\omega}{dt}.$$

That is, the applied torque equal the moment of inertia times the angular acceleration. This is the basic equation for rigid body rotational dynamics.

Viscous Rotational Friction

Almost always there are frictional forces, and therefore, frictional torques acting between the axle and the bearings.[14] This is illustrated in Figure 1.43.

[14] An interesting exception are magnetic bearings where the axel is levitated by magnetic fields so that there is no mechanical contact.

www.EngineeringEBooksPdf.com

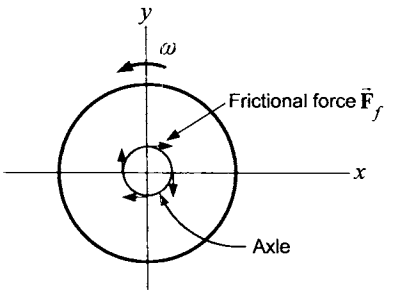


FIGURE 1.43. Viscous friction torque.

Often the frictional force is proportional to the angular speed and this model of friction is called *viscous friction* which is expressed mathematically as

$$\vec{\tau} = -f\vec{\omega} = -f\omega\hat{\mathbf{z}}$$

or, in scalar form,

$$\tau = -f\omega$$

where $f > 0$ is the *coefficient of viscous friction.*

Sign Convention for Torque

Suppose the axis of rotation is along the z axis. Recall that the definition of torque is

$$\vec{\tau} \triangleq \vec{\mathbf{r}} \times \vec{\mathbf{F}} = rF\sin(\psi)\hat{\mathbf{z}} = rF_T\hat{\mathbf{z}}$$

where ψ is the angle between $\vec{\mathbf{r}}$ and $\vec{\mathbf{F}}$. The magnitude of the cross product $\vec{\mathbf{r}} \times \vec{\mathbf{F}}$ is $rF\sin(\psi)$ and the direction of $\vec{\mathbf{r}} \times \vec{\mathbf{F}}$ is perpendicular to both $\vec{\mathbf{r}}$ and $\vec{\mathbf{F}}$ along the z axis. In engineering applications, the systems are designed so that the applied force is tangential to the rotational motion, i.e., $\psi = \pi/2$, $F = F_T$, and

$$\vec{\tau} \triangleq \tau\hat{\mathbf{z}} = rF\hat{\mathbf{z}}.$$

If $\tau = rF > 0$ then the torque will cause the cylinder to rotate around the z axis in the direction indicated by the curved arrow. On the other hand, if $\tau = rF < 0$ then the torque will cause the cylinder to rotate around the z axis in the direction *opposite* to that indicated by the curved arrow. Typically in engineering texts, the sign convention for torque is indicated by a curved arrow as shown in Figure 1.44. (Physics texts prefer to write $\vec{\tau} \triangleq \tau\hat{\mathbf{z}}$.)

www.EngineeringEBooksPdf.com

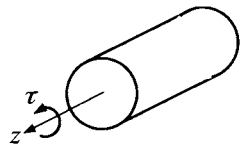


FIGURE 1.44. Sign convention for torque.

Gears

Using the elementary rigid body dynamics developed in the previous appendix, the model of a two gear system illustrated in Figure 1.45 below is now developed.

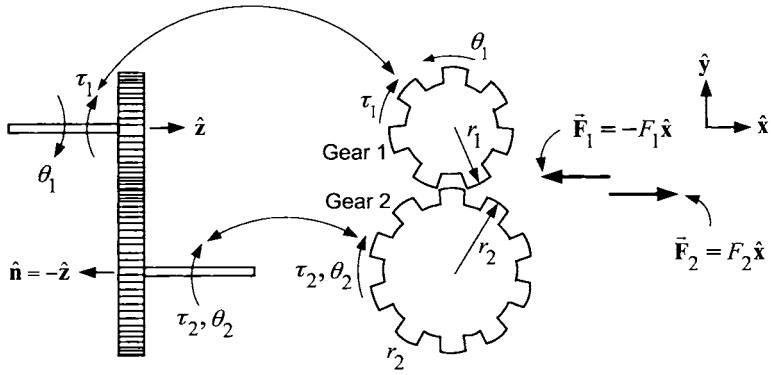


FIGURE 1.45. Two gear system. Drawn by Sharon Katz.

This presentation is from that given in Professor Ogata's book [37]. In Figure 1.45,

τ_1 is the torque exerted on gear 1 by gear 2.
F_1 is the force exerted on gear 1 by gear 2.
τ_2 is the torque exerted on gear 2 by gear 1.
F_2 is the force exerted on gear 2 by gear 1.
θ_1 is the angle rotated by gear 1.
θ_2 is the angle rotated by gear 2.
n_1 is the number of teeth on gear 1.
n_2 is the number of teeth on gear 2.
r_1 is the radius of gear 1.
r_2 is the radius of gear 2.

Let $\vec{\mathbf{F}}_1 \triangleq F_1(-\hat{\mathbf{x}})$ so that if $F_1 > 0$, the force is in the $-\hat{\mathbf{x}}$ direction as shown in Figure 1.45. Also, let $\vec{\mathbf{r}}_1 \triangleq r_1(-\hat{\mathbf{y}})$ so that $\vec{\boldsymbol{\tau}}_1 = \vec{\mathbf{r}}_1 \times \vec{\mathbf{F}}_1 =$

www.EngineeringEBooksPdf.com

$r_1F_1(-\hat{\mathbf{y}}) \times (-\hat{\mathbf{x}}) = r_1F_1(-\hat{\mathbf{z}}) = r_1F_1\hat{\mathbf{n}}$. That is, $\vec{\boldsymbol{\tau}}_1 = \tau_1\hat{\mathbf{n}}$ where $\tau_1 = r_1F_1$ and $\hat{\mathbf{n}} \triangleq -\hat{\mathbf{z}}$ is a unit vector. Similarly, let $\vec{\mathbf{F}}_2 \triangleq F_2\hat{\mathbf{x}}$ so that if $F_2 > 0$, the force is in the $\hat{\mathbf{x}}$ direction. Writing $\vec{\mathbf{r}}_2 \triangleq r_2\hat{\mathbf{y}}$ it follows that $\vec{\boldsymbol{\tau}}_2 = \vec{\mathbf{r}}_2 \times \vec{\mathbf{F}}_2 = r_2F_2(-\hat{\mathbf{z}}) = -\tau_2\hat{\mathbf{z}} = \tau_2\hat{\mathbf{n}}$ with $\tau_2 = r_2F_2$. The reason that $\vec{\mathbf{r}}_1, \vec{\boldsymbol{\tau}}_1, \vec{\mathbf{F}}_1$ are referred to the basis vectors $-\hat{\mathbf{x}}, -\hat{\mathbf{y}}, -\hat{\mathbf{z}}$ while $\vec{\mathbf{r}}_2, \vec{\boldsymbol{\tau}}_2, \vec{\mathbf{F}}_2$ are referred to the basis vectors $\hat{\mathbf{x}}, \hat{\mathbf{y}}, \hat{\mathbf{z}}$ is so that there will no minus signs in the gear relationships to be derived below.

Algebraic Relationships Between Two Gears

There are three important algebraic relationships between the gears.

1. The gears have different radii, but the teeth on each gear are the same size so that they will mesh together properly. Consequently, the number of teeth on the surface of gears is proportional to the radius of the gears so that, for example, if $r_2 = 2r_1$, then $n_2 = 2n_1$. In general,
$$\frac{r_2}{r_1} = \frac{n_2}{n_1}.$$

2. By Newton's third law, the forces $\vec{\mathbf{F}}_1 = F_1(-\hat{\mathbf{x}}), \vec{\mathbf{F}}_2 \triangleq F_2\hat{\mathbf{x}}$ are equal in magnitude, but opposite in direction so that $F_2 = -(-F_1) = F_1$. Thus, as $\tau_1 = r_1F_1$ and $\tau_2 = r_2F_2$ it follows that
$$\frac{\tau_2}{\tau_1} = \frac{r_2}{r_1}.$$

3. As the teeth on each gear are meshed together at the point of contact, the distance traveled along the surface of the gears is the same. In other words, $\theta_1r_1 = \theta_2r_2$ or
$$\frac{\theta_2}{\theta_1} = \frac{r_1}{r_2}$$

The first two algebraic relationships can be summarized as

$$\frac{\tau_2}{\tau_1} = \frac{r_2}{r_1} = \frac{n_2}{n_1}$$

and these ratios are easily remembered by thinking of gear 2 as larger in radius than gear 1. Then the number of teeth on gear 2 must also be larger (because its circumference is larger) and the torque on gear 2 is also larger (because its radius is larger).

The last algebraic relationship is summarized as

$$\frac{r_1}{r_2} = \frac{\theta_2}{\theta_1} = \frac{\omega_2}{\omega_1}$$

but it is more easily remembered by writing $\theta_1r_1 = \theta_2r_2$ which just states the distance traveled along the surface of each gear is the same as they are meshed together.

www.EngineeringEBooksPdf.com

Dynamic Relationship Between Two Gears

Consider the two gear system shown in Figure 1.46 below. The motor torque τ_m acts on gear 1 and the torque τ_L is a load torque acting on gear 2.

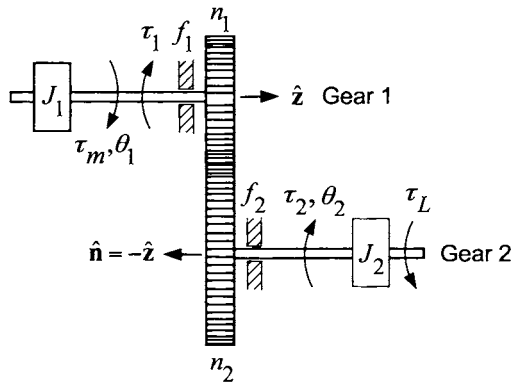


FIGURE 1.46. Dynamic equations for a two gear system. Drawn by Sharon Katz.

In Figure 1.46,

J_1 is the moment of inertia of the motor shaft.
J_2 is the moment of inertia of the output shaft.
f_1 is the viscous friction coefficient of the motor shaft.
f_2 is the viscous friction coefficient of the output shaft.
θ_1 is the angle rotated by gear 1.
θ_2 is the angle rotated by gear 2.
ω_1 is the angular speed of gear 1.
ω_2 is the angular speed of gear 2.
τ_1 is the torque exerted on gear 1 by gear 2.
τ_2 is the torque exerted on gear 2 by gear 1.

The sign conventions for the torques $\tau_m, \tau_1, \tau_2, \tau_L$ are indicated in Figure 1.46. In particular, if $\tau_m > 0, \tau_1 > 0$ then they oppose each other and similarly, if $\tau_2 > 0, \tau_L > 0$ then these two torques oppose each other. A load torque is illustrated in Figure 1.47 in which the load torque on gear 2 is $\tau_L = r_2 mg$ with r_2 the radius of the pick up reel (gear 2).

www.EngineeringEBooksPdf.com

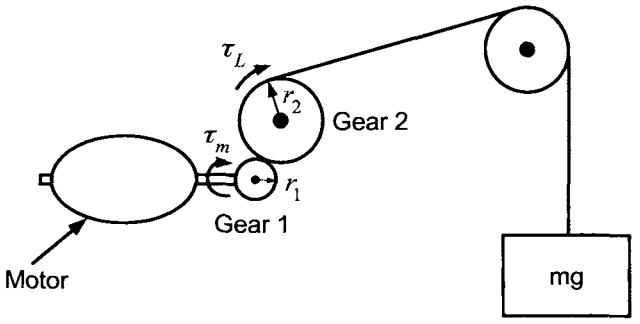


FIGURE 1.47. Illustration of load torque. Drawn by Sharon Katz.

The above development is now put together to write down differential equations that characterize the dynamic behavior of the gears. Recall that the fundamental equation of rigid body dynamics is given by

$$\tau = J\frac{d\omega}{dt}$$

where τ is the *total* torque on the rigid body, J is the moment of inertia of the rigid body and $d\omega/dt$ is its angular acceleration about the fixed axis of rotation. Applying this relationship, the equations of motion for the two gears are then

$$\begin{aligned} \tau_m - \tau_1 - f_1\omega_1 &= J_1\frac{d\omega_1}{dt} \\ \tau_2 - \tau_L - f_2\omega_2 &= J_2\frac{d\omega_2}{dt}. \end{aligned} \tag{1.30}$$

Typically, the input (motor) torque τ_m is known and, the output position θ_2 and speed ω_2 are measured. Consequently, the variables τ_1, τ_2, ω_1 need to be eliminated which is done as follows:

$$\begin{aligned} \tau_2 &= \frac{n_2}{n_1}\tau_1 \\ &= \frac{n_2}{n_1}\left(\tau_m - f_1\omega_1 - J_1\frac{d\omega_1}{dt}\right) \\ &= \frac{n_2}{n_1}\left(\tau_m - f_1\left(\frac{n_2}{n_1}\omega_2\right) - J_1\frac{d}{dt}\left(\frac{n_2}{n_1}\omega_2\right)\right) \\ &= \frac{n_2}{n_1}\tau_m - \left(\frac{n_2}{n_1}\right)^2 f_1\omega_2 - \left(\frac{n_2}{n_1}\right)^2 J_1\frac{d\omega_2}{dt}. \end{aligned} \tag{1.31}$$

Substituting this expression for τ_2 into the second equation of (1.30) results in

$$\frac{n_2}{n_1}\tau_m - \left(\frac{n_2}{n_1}\right)^2 f_1\omega_2 - \left(\frac{n_2}{n_1}\right)^2 J_1\frac{d\omega_2}{dt} - \tau_L - f_2\omega_2 = J_2\frac{d\omega_2}{dt}$$

www.EngineeringEBooksPdf.com

Rearranging, the desired result is

$$\frac{n_2}{n_1}\tau_m = \Big(J_2 + (n_2/n_1)^2 J_1\Big)\frac{d\omega_2}{dt} + \Big(f_2 + (n_2/n_1)^2 f_1\Big)\omega_2 + \tau_L. \quad (1.32)$$

Let $n = n_2/n_1$ denote the *gear ratio*, $J \triangleq J_2 + n^2 J_1$ denote the total inertia *reflected to output shaft* and $f \triangleq f_2 + n^2 f_1$ denote the total viscous friction coefficient *reflected to the output shaft*, equation (1.32) can be written succinctly as

$$n\tau_m = J\frac{d\omega_2}{dt} + f\omega_2 + \tau_L. \quad (1.33)$$

The net effect of the gears is to increase the motor torque from τ_m on the motor shaft to $n\tau_m$ on the output shaft, to add the quantity $n^2 J_1$ to the inertia of the output shaft and to add $n^2 f_1$ to the viscous friction coefficient of the output shaft.

Remark

Everything could have been referred to the motor shaft instead of the output (load) shaft. To do so, simply substitute $\omega_2 = (n_1/n_2)\omega_1$ into (1.32) to obtain

$$\frac{n_2}{n_1}\tau_m = \left(J_2 + \left(\frac{n_2}{n_1}\right)^2 J_1\right)\frac{d\left(\frac{n_1}{n_2}\omega_1\right)}{dt} + \left(f_2 + \left(\frac{n_2}{n_1}\right)^2 f_1\right)\left(\frac{n_1}{n_2}\omega_1\right) + \tau_L$$

Multiply both sides by n_1/n_2 results in

$$\tau_m = \left(J_2 + \left(\frac{n_2}{n_1}\right)^2 J_1\right)\left(\frac{n_1}{n_2}\right)^2\frac{d\omega_1}{dt} + \left(f_2 + \left(\frac{n_2}{n_1}\right)^2 f_1\right)\left(\frac{n_2}{n_1}\right)^2\omega_1 + \frac{n_1}{n_2}\tau_L$$

or, finally, the desired form is

$$\tau_m = \left(\left(\frac{n_1}{n_2}\right)^2 J_2 + J_1\right)\frac{d\omega_1}{dt} + \left(\left(\frac{n_1}{n_2}\right)^2 f_2 + f_1\right)\omega_1 + \frac{n_1}{n_2}\tau_L. \quad (1.34)$$

In this formulation, the load torque on the input shaft is *reduced* by n_1/n_2 from that on the output shaft, and $(n_1/n_2)^2 J_2$ has been added to the inertia of the motor shaft and $(n_1/n_2)^2 f_2$ has been added to the viscous friction coefficient of the motor shaft.

www.EngineeringEBooksPdf.com

Problems

Faraday's Law and Induced Electromotive Force (emf)

Problem 1 Faraday's Law

Consider Figure 1.48 where a magnet is moving up *into a square planar loop of copper wire.*

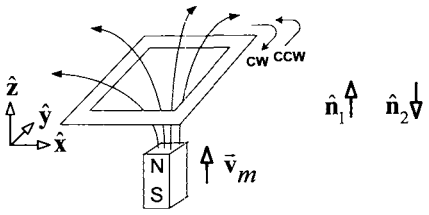


FIGURE 1.48. Induced emf in a loop due to a moving magnet.

(a) Using the normal $\hat{\mathbf{n}}_1$*, is the flux in the loop produced by the magnet increasing or decreasing?*

(b) Using the normal $\hat{\mathbf{n}}_1$*, what is the direction of positive travel around the surface whose boundary is the loop (clockwise or counterclockwise)?*

(c) What is the direction of the induced current in Figure 1.48 (clockwise or counterclockwise)? Does the induced current produce a change in the flux in the loop that opposes the change in flux produced by the magnet?

(d) Using the normal $\hat{\mathbf{n}}_2$*, is the flux increasing or decreasing?*

(e) Using the normal $\hat{\mathbf{n}}_2$*, what is the direction of positive travel around the surface whose boundary is the loop (clockwise or counterclockwise)?*

(f) What is the direction of the induced current in Figure 1.48 (clockwise or counterclockwise)? Does the induced current produce a change in the flux in the loop that opposes the change in flux produced by the magnet?

Problem 2 Faraday's Law

Consider Figure 1.49 where a magnet is moving down *away from a square planar loop of copper wire.*

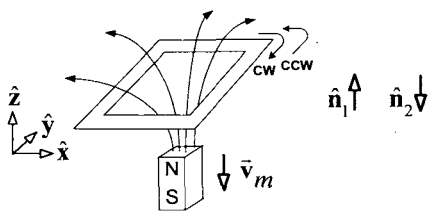


FIGURE 1.49. Induced emf in a loop due to a moving magnet.

www.EngineeringEBooksPdf.com

(a) Using the normal $\hat{\mathbf{n}}_1$, is the flux in the loop produced by the magnet increasing or decreasing?

(b) Using the normal $\hat{\mathbf{n}}_1$, what is the direction of positive travel around the surface whose boundary is the loop (clockwise or counterclockwise)?

(c) What is the direction of the induced current in Figure 1.49 (clockwise or counterclockwise)? Does the induced current produce a change in the flux in the loop that opposes the change of flux produced by the magnet?

(d) Using the normal $\hat{\mathbf{n}}_2$, is the flux increasing or decreasing?

(e) Using the normal $\hat{\mathbf{n}}_2$, what is the direction of positive travel around the surface whose boundary is the loop (clockwise or counterclockwise)?

(f) What is the direction of the induced current in Figure 1.49 (clockwise or counterclockwise)? Does the induced current produce a change in the flux in the loop that opposes the change of flux produced by the magnet?

Problem 3 The Linear DC Motor

Consider the simple linear DC motor of Figure 1.3. Take the normal to the surface enclosed by the loop taken to be $\hat{\mathbf{n}} = -\hat{\mathbf{z}}$.

(a) What is the flux through the surface?

(b) What is the direction of positive travel around this flux surface?

(c) What is the induced emf ξ in the loop in terms of B, ℓ and the speed v of the bar?

(d) Do V_S and ξ have the same sign convention? Explain why ξ is now negative. With R the resistance of the circuit and the inductance $L = 0$, write down the differential equations for the current i in the machine and the speed v of the bar.

Problem 4 The Linear DC Motor

Consider the simple linear motor in Figure 1.50 where the magnetic field $\vec{\mathbf{B}} = B\hat{\mathbf{z}}$ $(B > 0)$ is up out of the page.

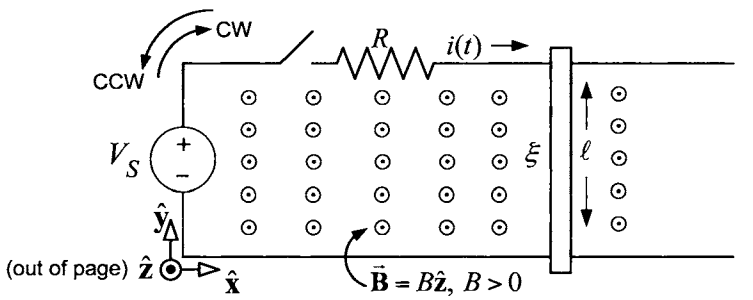


FIGURE 1.50. Linear DC machine with $\vec{\mathbf{B}} = B\hat{\mathbf{z}}$, $B > 0$.

Closing the switch causes a current to flow in the wire loop.

(a) What is the magnetic force $\vec{\mathbf{F}}_{magnetic}$ on the sliding bar in terms of B, i, and ℓ? Give both the magnitude and direction of $\vec{\mathbf{F}}_{magnetic}$.

www.EngineeringEBooksPdf.com

(b) Take the normal to the surface enclosed by the loop to be $\hat{\mathbf{n}} = \hat{\mathbf{z}}$. *What is the flux through the surface?*

(c) What is the induced emf ξ *in the loop in terms of* B, ℓ, *and the speed* v *of the bar?*

(d) What is the sign convention for the induced emf ξ *drop around the loop? (That is, if* $\xi > 0$, *would it act to push current in the clockwise or counterclockwise direction?)*

(e) Do V_S *and* ξ *have the same sign convention? Draw* $+$ *and* $-$ *signs above and below* ξ *to indicate the sign convention for* ξ.

Problem 5 Back Emf in the Single-Loop Motor

Consider the single loop motor with the flux surface as indicated in Figure 1.51. A voltage source connected to the brushes is forcing current down side a $(\otimes)$ *and up side* a' $(\odot)$.

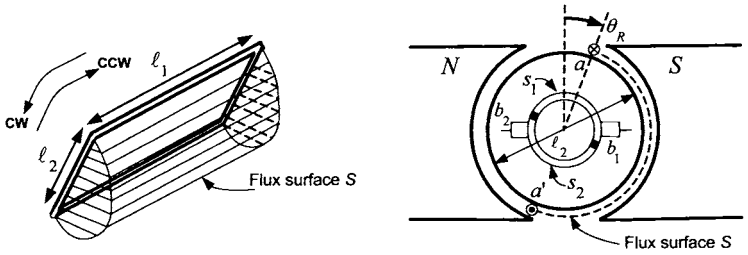


FIGURE 1.51. Computing the flux with $\hat{\mathbf{n}} = -\hat{\mathbf{r}}$.

(a) With the motor at the angular position θ_R *shown, that is, with* $0 < \theta_R < \pi$, *and using the* inward *normal* $(\hat{\mathbf{n}} = -\hat{\mathbf{r}})$, *compute the flux through the surface in terms of the magnitude* B *of the radial magnetic field in the air gap, the axial length* ℓ_1 *of the motor, the diameter* ℓ_2 *of the motor and the angle* θ_R *of the rotor.*

(b) What is the positive direction of travel around the flux surface $\mathcal{S}$ *(CW or CCW)?*

(c) What is the emf ξ *induced in the rotor loop? What is the sign convention for the induced emf* ξ *drop around the loop? (That is, if* $\xi > 0$, *would it act to push current in CW direction or the CCW direction?) Do* V_S *and* ξ *have the same sign convention? Explain why* ξ *is now negative. Draw an equivalent circuit of the form in Figure 1.18 for the rotor loop current.*

Problem 6 Gauss's Law and Conservation of Flux

The flux surface in Figure 1.13 was chosen as the half-cylindrical surface with two half disks at either end because the B *field is known on the cylindrical surface being given by equation (1.1) and can be taken to be zero on the two half disks. If the flux surface had been taken to be a flat planar surface with the rectangular loop as its boundary, then it would not be clear*

www.EngineeringEBooksPdf.com

how to compute the flux on this surface as the B field there is unknown. Show, using Gauss's law

$$\phi = \oint_S \vec{\mathbf{B}} \cdot d\vec{\mathbf{S}} \equiv 0,$$

that both surfaces give the same flux. In general, by Gauss's law, one can compute the flux using any surface as long as its boundary is the loop.

Problem 7 Flux in the Single-Loop DC Motor

Figure 1.52 shows the rotor loop with $\pi < \theta_R < 2\pi$.

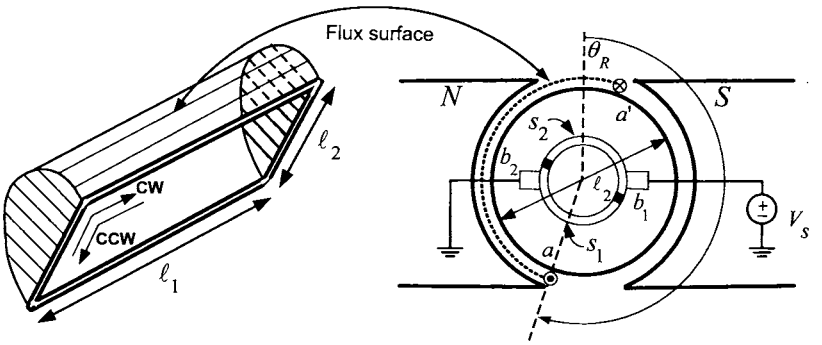


FIGURE 1.52. Rotor loop where $\pi < \theta_R < 2\pi$.

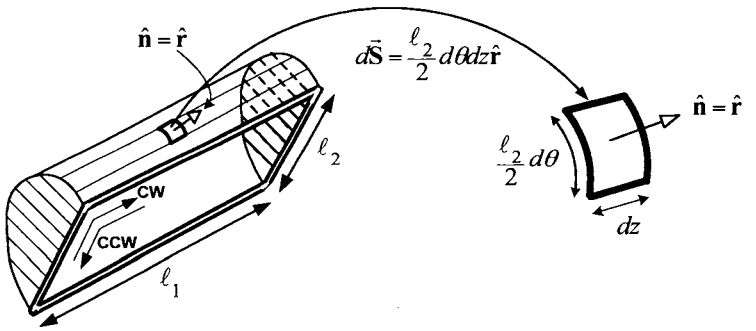


FIGURE 1.53. Flux surface with the normal radially out.

(a) Using the flux surface shown in Figure 1.53 with $d\vec{\mathbf{S}} = (\ell_2/2)d\theta dz\hat{\mathbf{r}}$, *show that* $\phi(\theta_R) = (\theta_R - \pi/2 - \pi)\,\ell_1\ell_2 B$ *for* $\pi < \theta_R < 2\pi$. *Plot* $\phi(\theta_R)$ *for* $0 < \theta_R < 2\pi$ *(note that* $\phi(\theta_R)$ *for* $0 < \theta_R < \pi$ *is computed in the text). Compute the back emf* ξ *and give its sign convention, that is, if* $\xi = -d\phi(\theta_R)/dt > 0$, *will it force current in the CW or the CCW direction?*

www.EngineeringEBooksPdf.com

Do ξ and V_S have the same sign convention? (Yes! Explain!) Draw an equivalent circuit diagram of the form of Figure 1.18 to illustrate the sign convention.

(b) Using the flux surface shown in Figure 1.54 with $d\vec{\mathbf{S}} = (\ell_2/2)d\theta dz\,(-\hat{\mathbf{r}})$, show that $\phi(\theta_R) = -(\theta_R - \pi/2 - \pi)\,\ell_1\ell_2 B$ for $\pi < \theta_R < 2\pi$.

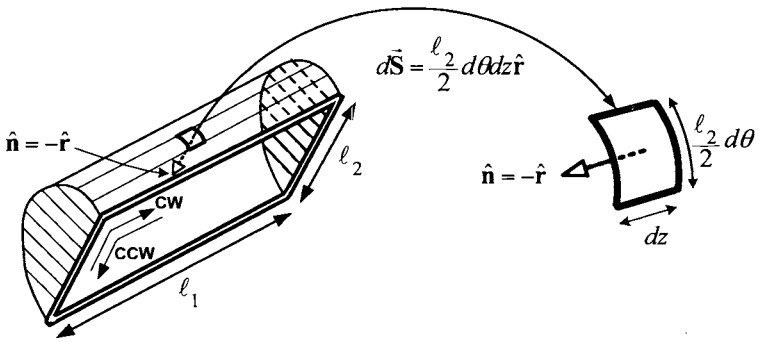


FIGURE 1.54. Flux surface with the normal radially in.

Compute the back emf and give its sign convention, that is, if $-d\phi(\theta_R)/dt > 0$ will it force current in the CW or the CCW direction. Do ξ and V_S have the same sign convention? (No, they are opposite! Explain!) Draw an equivalent circuit diagram of the form of Figure 1.18 to illustrate the sign convention.

(c) Note that in part (b) the normal to the flux surface is taken to be radially in while with $0 < \theta_R < \pi$ it was taken to be radially out (see Figure 1.14). Explain why reversing the normal of the flux surface each half turn in this way results in an equivalent circuit of the form shown in Figure 1.18 which is valid for all rotor angular positions

Hint: Note that the + side of V_S is now electrically connected to side a' of the loop through brush b_1, while when $0 < \theta_R < \pi$ in Figure 1.14, the + side of V_S was electrically connected to side a of the loop through brush b_1. That is, the sign convention for V_S in the loop changes every half-turn. Thus it is also necessary to change the sign convention for the flux and therefore for ξ every half-turn in order that the sign conventions for V_S and ξ have the same relationship to each other for all θ_R.

(d) Show by taking $d\vec{\mathbf{S}} = (\ell_2/2)d\theta dz\hat{\mathbf{r}}$ for $0 < \theta_R < \pi$ and $d\vec{\mathbf{S}} = (\ell_2/2)d\theta dz\,(-\hat{\mathbf{r}})$ for $\pi < \theta_R < 2\pi$, that $\phi(\theta_R) = -(\theta_R \bmod \pi - \pi/2)\,\ell_1\ell_2 B$ for all θ_R and that $\xi = -d\phi(\theta_R)/dt$ has the sign convention given in Figure 1.18 for all θ_R. Verify that the plot of $\phi(\theta_R)$ in Figure 1.15 is correct.

www.EngineeringEBooksPdf.com

Problem 8 Simulation of the DC Motor

Let $V_{max} = 40$ *V,* $I_{max} = 5$ *A,* $K_b = K_T = 0.07$ *V/rad/sec (= N-m/A),* $J = 6 \times 10^{-5}$ *kg-m*^{2}*,* $R = 2$ *ohms,* $L = 2$ *mH, and* $f = 0.0004$ *N-m/rad/sec. Develop a simulation of the DC motor that includes the motor model given by (1.6) and a voltage saturation model of the amplifier as illustrated in Figure 1.20. Put a step input of* $V_S(t) = 10$ *V into the motor and plot out (a)* $\theta(t)$*, (b)* $\omega(t)$*, (c)* $i(t)$*, and (d)* $V_S(t)$*.*

Multiloop Motor

Problem 9 Skewing of the Rotor Sides

Figure 1.29 shows the sides of the rotor loops for the motor (but not the tachometer!) are not straight in the axial direction, but instead are skewed. Can you think of a reason why this is done?

Problem 10 Neutral Plane and Brush Shifting

In the commutation scheme for the multiloop motor, it was shown that when a rotor loop was perpendicular to the brushes, the current in the loop was shorted out (brought to zero). Consequently, it is highly desirable that the total induced voltage in that loop be as close to zero as possible to prevent arcing. Figure 1.35 shows the total *B field distribution in the DC machine. If the armature current were zero, then the field would be horizontal as in Figure 1.33. At very high armature currents (e.g., in large machines used in heavy industry), the field is skewed as shown in Figure 1.35. The neutral plane is the plane cutting through the axis of the rotor for which the* total *B field is perpendicular to the plane. Let* $\psi_k(i, i_f, \theta_R)$ *be the total flux in the* kth *rotor loop due to* both *the field current and the armature current.*

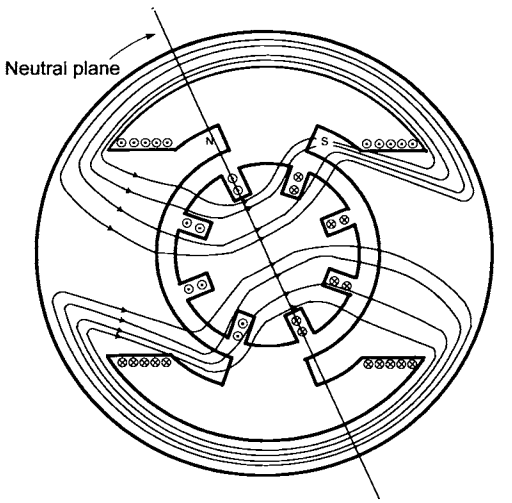


FIGURE 1.55. Magnetic field due to both the field and armature currents.

www.EngineeringEBooksPdf.com

(a) Explain why $\psi_k(i, i_f, \theta_R)$ is a maximum (or minimum) as a function of the rotor position θ_R when the kth *loop coincides with the neutral plane, or equivalently, why $-\partial\psi_k(i, i_f, \theta_R)/\partial\theta_R = 0$ when the* kth *loop coincides with the neutral plane. (This is seen more easily if one takes the flux surface to be the plane of the loop rather than the cylindrical surface.)*

(b) As explained in Section 1.7.2, the current in a rotor loop is commutated when the plane of the loop is perpendicular to the line containing the two brushes. Consider the situation in which the brushes of Figure 1.30(a) are rotated counterclockwise (shifted) so that the plane *of the loop undergoing commutation is coincident with the neutral plane as shown in Figure 1.56. (After the brushes are rotated, they are held fixed at that position.)*

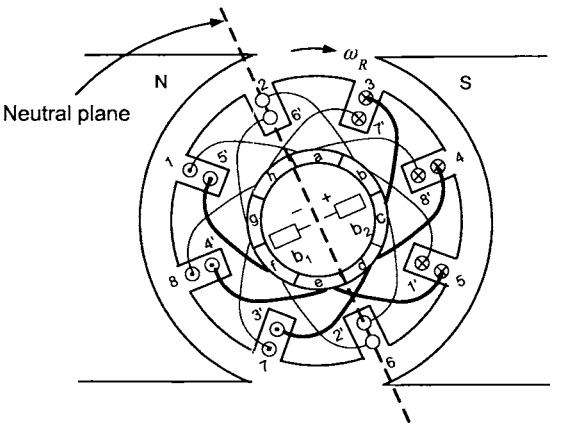


FIGURE 1.56. Rotating the brushes so that commutation in the loop occurs when the loop is aligned with the neutral plane.

Show then that the induced voltage in the kth *loop when it undergoes commutation is*

$$-\frac{d\psi_k(i, i_f, \theta_R)}{dt} = -\frac{\partial\psi_k(i, i_f, \theta_R)}{\partial i}\frac{di}{dt} - \frac{\partial\psi_k(i, i_f, \theta_R)}{\partial i_f}\frac{di_f}{dt}$$

(c) Explain why shifting the brushes alleviates arcing.

(d) Does the amount that the brushes are to be rotated depend on the amount of armature current?

Problem 11 Flux in the Multiloop Motor

With $\lambda(\theta_R)$ given by (1.8) and $n = 4$, write a program to plot $\lambda(\theta_R)/(\ell_1\ell_2 B)$ versus θ_R to obtain a figure similar to that of Figure 1.38.

www.EngineeringEBooksPdf.com

Separately Excited, Series and Shunt DC Machines

Problem 12 Conservation of Energy in the Separately Excited DC Motor

Using the equations (1.19), (1.20) and (1.21) of the separately excited DC motor show that energy conservations holds. Give a physical interpretation to the various expressions.

Problem 13 Series DC Motor [1]

Consider a separately excited DC motor in which the terminal T_1 *of the armature is connected to the terminal* T_2' *of the field circuit and a single voltage source is applied between the two remaining terminals* T_1' *and* T_2. *This configuration is referred to as a* series DC motor *and is illustrated in Figure 1.57. This type of connection is often used when the motor is employed as a traction drive, that is, for subways, trolley cars, and so on. An equivalent circuit for the series DC motor is given in Figure 1.58 where* $\lambda_f(i_f) = L_f i_f$ *is used.*

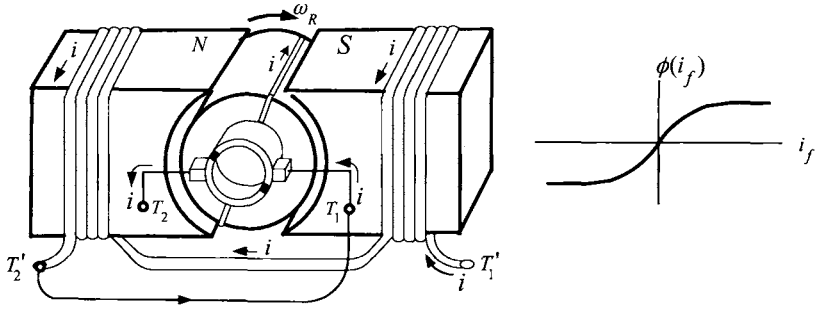


FIGURE 1.57. Series-connected DC motor. Adapted from Ref. [21].

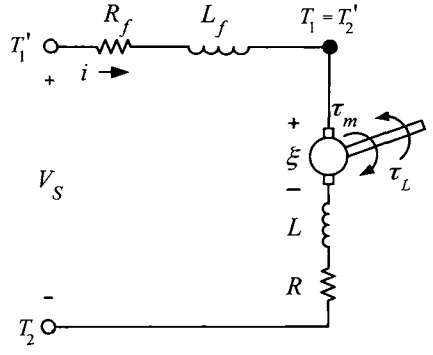


FIGURE 1.58. Equivalent circuit for a series DC motor.

www.EngineeringEBooksPdf.com

(a) Starting from the model (1.22), (1.23), (1.24) of the separately excited DC motor, derive the set of differential equations that characterize the series connected DC motor.

(b) Show that the torque cannot change sign, i.e., it is always positive or always negative.

(c) What must be done to change the sign of the torque?

Problem 14 Shunt DC Motor [3]

Consider a separately excited DC motor in which the terminal T_1 of the armature is connected to the terminal T_1' of the field circuit and similarly, the other two terminals T_2, T_2' are connected together as indicated in Figure 1.59. This configuration is referred to as a shunt DC motor *for which an equivalent circuit is shown in Figure 1.60. The resistance R_{adj} is an adjustable resistance added in series with the field winding and aids in the control of the motor.*

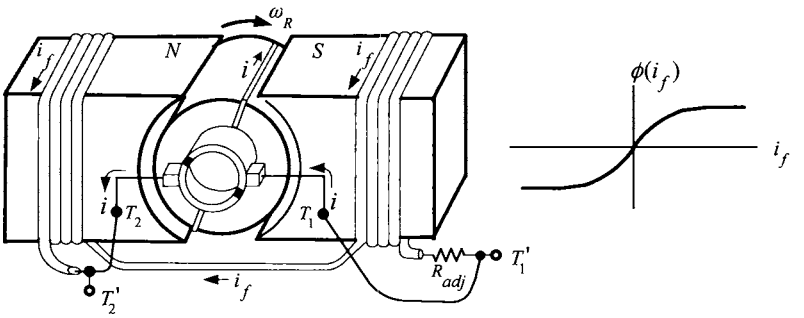


FIGURE 1.59. Shunt connected DC motor. Adapted from Ref. [21].

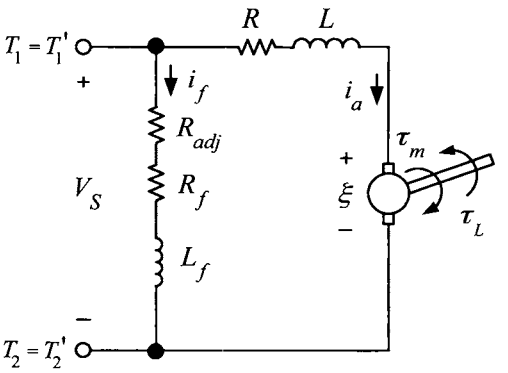


FIGURE 1.60. Equivalent circuit for a shunt DC motor.

www.EngineeringEBooksPdf.com

Let $\lambda(i_f) = L_f i_f$ and using the model (1.22), (1.23), (1.24) of the separately excited DC motor, derive the complete set of equations that characterize the shunt DC motor.

Simple AC Generators

Problem 15 A Three-Phase Generator [38]

Consider a simplified model of a three-phase generator shown in Figures 1.61 and 1.62.

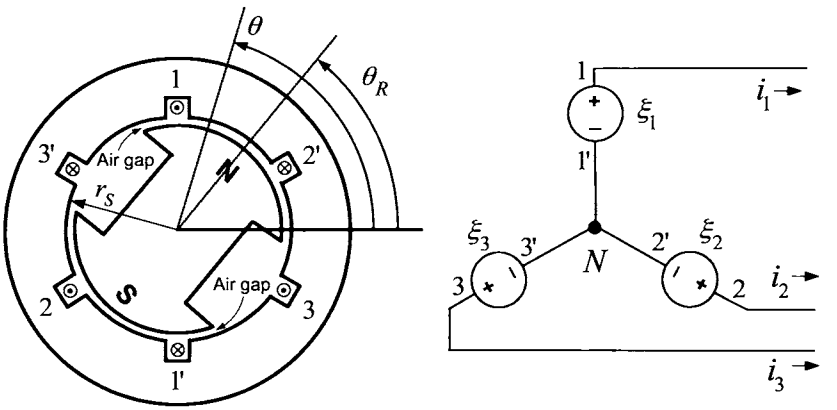


FIGURE 1.61. Simplified three-phase permanent magnet generator.

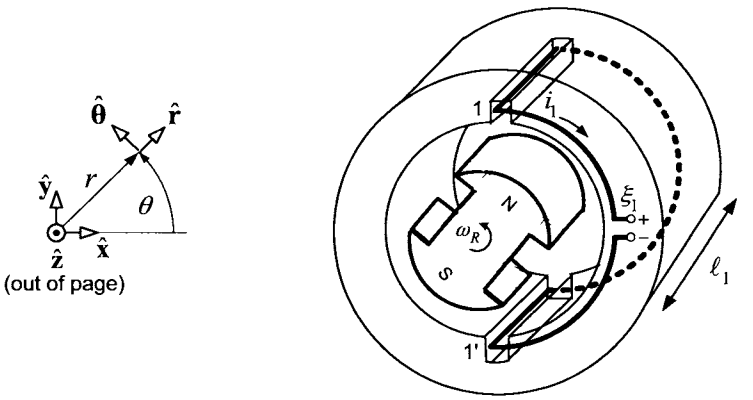


FIGURE 1.62. Half-cylindrical-shaped winding of phase 1.

The rotor consists of a two-pole (one north and one south) permanent magnet with the pole faces shaped so that the radial magnetic field in the

www.EngineeringEBooksPdf.com

air gap due to the rotor's permanent magnet is given by

$$\vec{\mathbf{B}}(r,\theta) = B_{R\max}\frac{r_S}{r}\cos(\theta-\theta_R)\hat{\mathbf{r}}$$

where $B_{R\max} > 0, r_S = \ell_2/2 + g$ *is the radius of the inside surface of the stator iron and* θ, θ_R *are defined as in Figure 1.61. One of the stator phases (consisting of a single loop) is shown in Figure 1.62 where the rotor and stator sizes are distorted for expository reasons.*

(a) Using a half-cylinder flux surface whose boundary is the stator loop and whose surface normal is $\hat{\mathbf{n}} = \hat{\mathbf{r}}$*, compute the flux* ϕ_1 *in stator loop 1 and the voltage* $\xi_1 = -d\phi_1/dt$ *induced in this loop.*

(b) Also, compute the fluxes ϕ_2, ϕ_3 *and the induced voltages* ξ_2, ξ_3 *in phases 2 and 3, respectively.*

(c) With the ends $1', 2', 3'$ *tied together (called the neutral point), show that if the machine is rotating at constant angular speed* ω_R*, this results in a three-phase generator producing three sinusoidal voltages which are identical except being* $120°$ *out of phase with each other.*

(d) It is shown in Chapters 4 *and* 5 *that the magnetic field due to the rotating permanent magnet rotor produces an* axial electrical field *in the air gap given by*

$$\vec{\mathbf{E}}_R(\theta-\theta_R) = \omega_R B_{R\max} r_S \cos(\theta-\theta_R)\,\hat{\mathbf{z}}.$$

Show that

$$\xi_1 = \int_{1'}^{1} \vec{\mathbf{E}}_R(\theta-\theta_R)\cdot d\vec{\ell}.$$

Problem 16 A Two-Phase Four-Pole Generator

To introduce a two-phase four-pole *generator, consider first Figure 1.63(a), which shows a two-phase* two-pole *generator. Its rotor is a two-pole (one north and one south) permanent magnet whose pole faces are shaped so that the radial air gap magnetic field is given by*

$$\vec{\mathbf{B}}(r,\theta) = B_{R\max}\frac{r_S}{r}\cos(\theta-\theta_R)\hat{\mathbf{r}}$$

where $B_{R\max} > 0, r_S = \ell_2/2 + g$ *is the radius of the inside surface of the stator iron, and* θ, θ_R *are defined as in Figure 1.63(a). The stator phases are wound in a similar fashion to those of problem 15, and the voltages induced in the stator phases are computed similarly.*

www.EngineeringEBooksPdf.com

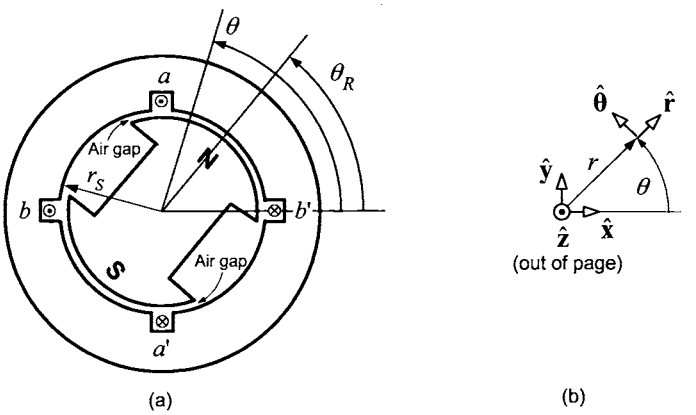


FIGURE 1.63. (a) A two-phase two-pole machine. (b) Polar coordinate system.

Now consider a two-phase four-pole *generator illustrated in Figure 1.64(a). The rotor is a* four-pole *(two north poles and two south poles) permanent magnet whose pole faces are shaped so that the radial air gap magnetic field is given by*

$$\vec{\mathbf{B}}(r,\theta) = B_{R\max}\frac{r_S}{r}\cos\left(n_p(\theta-\theta_R)\right)\hat{\mathbf{r}}.$$

Here $B_{R\max} > 0$, $r_S = \ell_2/2 + g$ *is the radius of the inside surface of the stator iron,* θ_R *is defined as in Figure 1.64(a), and* n_p $(= 2$ *in Figure 1.64) is the number of* pole pairs. *Figure 1.64(c) is a perspective view showing how phase a is wound while Figure 1.64(d) is a cross-sectional view of the same phase.*

(a) Using an outward normal for the flux surface ($\hat{\mathbf{n}} = \hat{\mathbf{r}}$)*, compute the flux linkage* λ_a *in phase a due to the permanent magnet rotor. (The flux linkage is the sum of the fluxes in the two loops* $\mathrm{a_1}$–$\mathrm{a_1'}$ *and* $\mathrm{a_2}$–$\mathrm{a_2'}$ *making up phase a.)*

(b) Does the positive direction of travel around each of the two flux surfaces of phase a coincide with the positive direction of current?

(c) Compute the voltage ξ_a *induced in phase a by the permanent magnet rotor.*

(d) Using the expression for ξ_a *in phase a from part (c), and the fact that phase b is rotated* $\pi/(2n_p)$ *radians from phase a, give the expression for* ξ_b.

(e) It is shown in Chapters 4 *and* 5 *that the magnetic field due to the rotating permanent magnet rotor produces an* axial electrical field *in the air gap given by*

$$\vec{\mathbf{E}}_R\left(\theta-\theta_R\right) = \omega_R B_{R\max} r_S \cos\left(n_p(\theta-\theta_R)\right)\hat{\mathbf{z}}.$$

www.EngineeringEBooksPdf.com

Show that

$$\xi_a = \int_{a'}^{a} \vec{\mathbf{E}}_R(\theta - \theta_R) \cdot d\vec{\ell}.$$

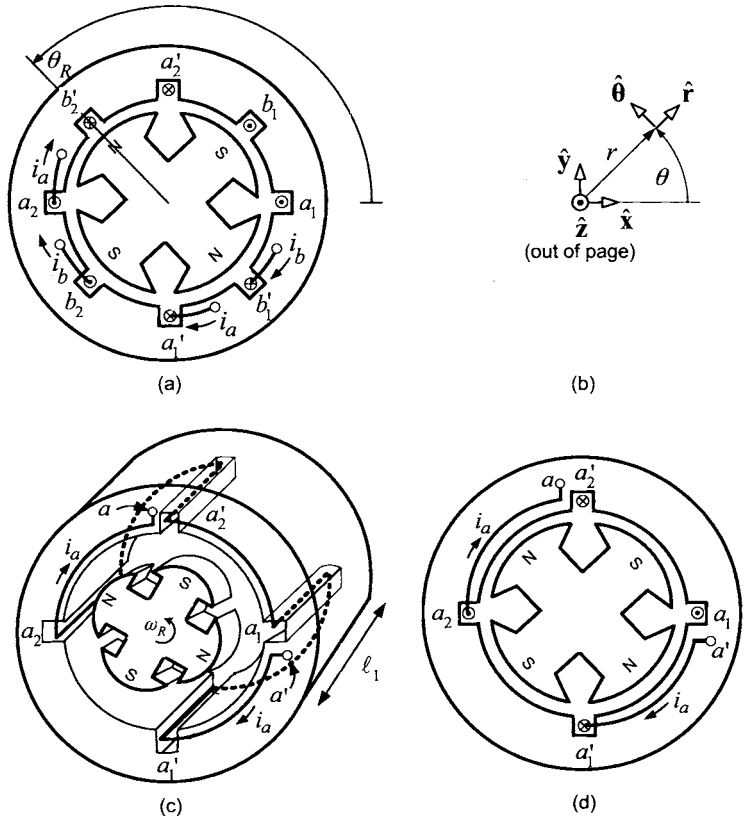


FIGURE 1.64. (a) A two-phase four-pole machine. (b) Polar coordinate system. (c) A perspective view of the phase a winding. (d) Cross-sectional view of the phase a winding.

Problem 17 Generator/Motor

Do problem 6 in Chapter 5. (The background in this chapter is sufficient to work this problem!)

www.EngineeringEBooksPdf.com

This Page Intentionally Left Blank

www.EngineeringEBooksPdf.com

2

Feedback Control

The DC motor model developed in the previous chapter is used to illustrate basic control techniques. The techniques developed here will be straightforwardly generalized for the AC motor case.

2.1 Model of a DC Motor Servo System

A DC motor servo (positioning) system typically consists of a DC motor, amplifier and sensors for position and current measurements. The interest here is to understand how to model this system for control purposes. Recall the dynamic equations of the DC motor given as

$$\begin{aligned} L\frac{di}{dt} &= -Ri(t) - K_b\omega(t) + v(t) \\ J\frac{d\omega}{dt} &= -f\omega(t) + K_T i(t) - \tau_L(t) \\ \frac{d\theta}{dt} &= \omega(t) \end{aligned} \tag{2.1}$$

where, in this chapter, θ and ω replace θ_R and ω_R, respectively. Also, $-f\omega$ models the viscous friction torque on the motor due to both the bearings and to the brushes rubbing against the commutator. The voltage v is commanded to the motor through a power amplifier. The amplifier is limited in how much voltage it can actually put out. This limit is denoted by $V_{\max}$ in Figure 2.1.

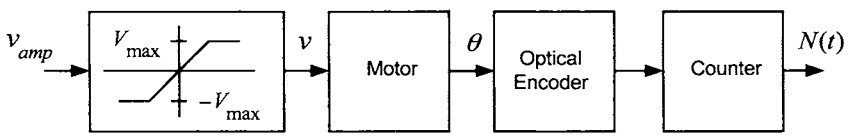


FIGURE 2.1. Open-loop DC motor.

A common position sensor used in industry is an optical encoder, which is illustrated in Figure 2.2(a) [39]. As shown, the optical encoder consists of a set of windows spaced equally around a circular disk with a light source shining through the window when it is aligned with the source. A detector puts out a high voltage when there is light and a low voltage otherwise.

www.EngineeringEBooksPdf.com

For the setup of Figure 2.2(a), there are 12 windows (lines or slots) so that for every complete revolution of the circular disk (i.e., of the motor), there will be 12 pulses. Using digital electronic circuitry, one can detect a pulse going high or low so that in one revolution with 12 pulses, there will be a total of 24 times that a pulse went either high or low. Note that each time a pulse goes high or low, the motor has rotated $2\pi/24$ or $360°/24 = 15°$. By simply counting the number N of rising and falling edges of the pulse, one can obtain the position of the rotor to within 15°.

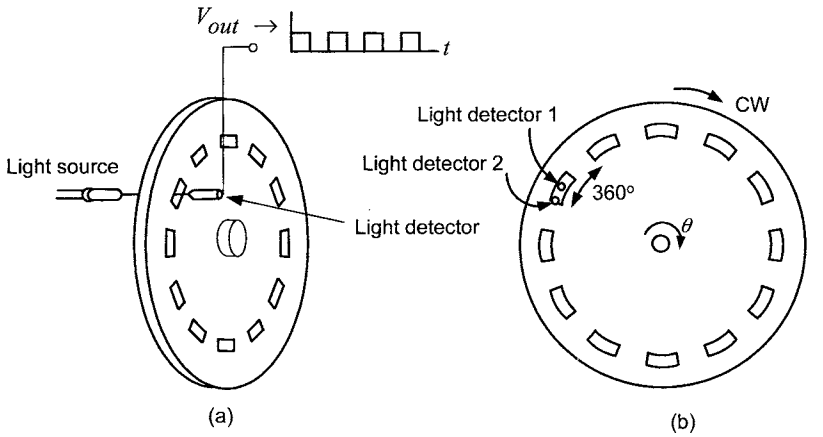


FIGURE 2.2. Schematic diagram of an optical encoder. (a) Encoder disk with 12 windows. Reprinted with permission from *Mechatronics: An Integrated Approach* by Clarence W. deSilva, Copyright CRC Press, Boca Raton, Florida [40]. (b) A second light detector added 90° from the first one in order to detect the direction of rotation.

In order to detect the direction of rotation, two light detectors are used as shown in Figure 2.2(b). In detail, the length of the windows is the same as the length of the distance between windows. The two light detectors are placed a distance of 1/2 of a window length apart. One period of the voltage waveform coming out of the light detector corresponds to the distance from the beginning of one window to the next and this cycle of the voltage waveform is considered to be 360° [see Figure 2.2(b)]. Consequently, the two light detectors are considered to be 90° apart and are said to be in *quadrature*.

Figure 2.3(a) shows the voltage waveforms out of the two light detectors when the rotor is turning *clockwise*. Note that the voltage of light detector 1 is 90° (1/4 cycle) behind that of light detector 2; that is, the voltage from light detector 2 goes high first and then a quarter of a cycle later, the voltage from light detector 1 goes high. However, if the rotor is turning *counterclockwise*, then the voltage of light detector 2 is 90° behind that

www.EngineeringEBooksPdf.com

of light detector 1 as shown in Figure 2.3(b). Consequently, the encoder electronics detects the relative phase of the two light detector voltage signals and uses it to determine whether the rising or falling edges of a pulse should increase the count (clockwise motion) or decrease the count (counterclockwise motion). For example, one could monitor light detector 2. If light detector1 goes high before light detector 2 goes low as in Figure 2.3(a), then the motion is clockwise. Otherwise, if light detector 1 goes low before light detector 2 goes low as in Figure 2.3(b), the motion is counterclockwise.

If an optical encoder has N_w windows (lines/slots), then there are $2N_w$ rising and falling edges per revolution giving a resolution of $2\pi/(2N_w)$ radians. Problem 4 shows how using the output of both light detectors, a resolution of $2\pi/(4N_w)$ radians is achieved. So, for example, with $N_w = 500$, the resolution of the encoder is $2\pi/2000$ radians or $360°/2000 = 0.18°$.

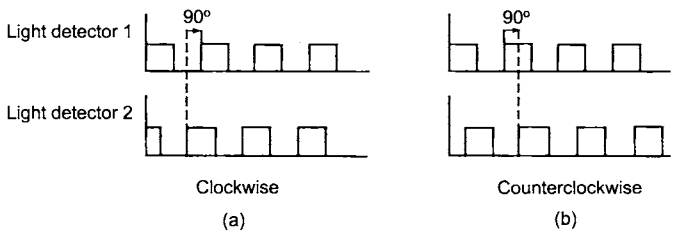


FIGURE 2.3. (a) Detector outputs for clockwise rotation. (b) Detector outputs for counterclockwise rotation.

Figure 2.4 shows a plot of the position $\theta(t)$ and the corresponding encoder

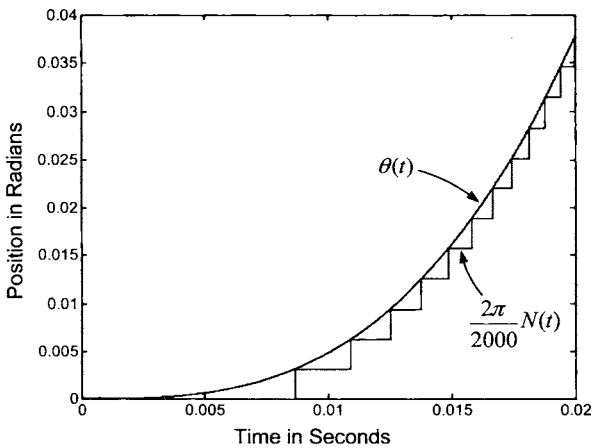


FIGURE 2.4. Plot of $\theta(t)$ and the encoder output $(2\pi/2000)N(t)$.

www.EngineeringEBooksPdf.com

output $(2\pi/2000)N(t)$. Due to the way the encoder works, if $\theta(t)$ is increasing, the position output of the encoder is always less than or equal to the actual position.

Current Command

The input to the motor is the voltage v. However, from the above equations, the torque equation is $Jd\omega/dt = -f\omega + K_T i - \tau_L$, where the motor torque $K_T i$ is proportional to the current. Thus, it would be convenient if the current was the input since one could easily specify the motor's torque by specifying the current. Typically, to get around the fact that the voltage is the input, one designs an inner current control loop that allows direct current command. That is, the voltage is forced by a controller to go to whatever value necessary to obtain the desired current. To understand how this is done, consider the equations (2.1) in the Laplace domain given by

$$\begin{aligned} i(s) &= \frac{-K_b\omega(s) + V(s)}{sL + R} \\ \omega(s) &= \frac{K_T i(s) - \tau_L(s)}{sJ + f} \\ \theta(s) &= \frac{1}{s}\omega(s). \end{aligned}$$

These algebraic relationships are illustrated in the block diagram shown in Figure 2.5.

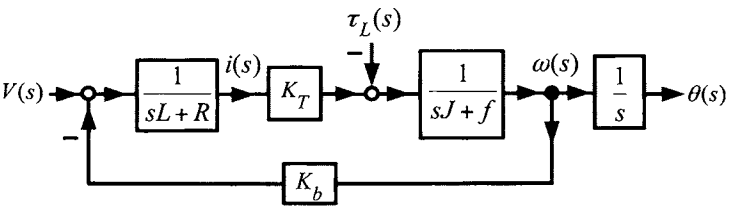


FIGURE 2.5. Block diagram of a DC motor.

Often the approximation that $L = 0$ is made to simplify the analysis of the system. However, a standard approach in industry is to put the amplifier into a *current command* mode which results in making the effect of L negligible. To do so, the current is fed back (typically using analog electronics) through a proportional controller as shown in Figure 2.6.

www.EngineeringEBooksPdf.com

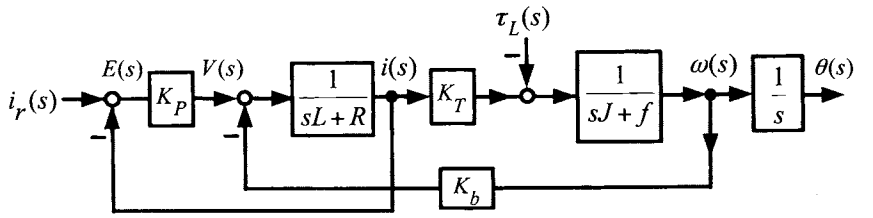


FIGURE 2.6. DC motor with an inner current control loop.

Here, $i_r(s)$ is the Laplace transform of the reference current, $i(s)$ is the Laplace transform of the actual current in the motor, and $K_P > 0$ is a proportional gain. The transfer function $G(s) = \omega(s)/i_r(s)$ is easily found using the block diagram reduction method. In order to do so, note that this block diagram is equivalent to that of Figure 2.7.

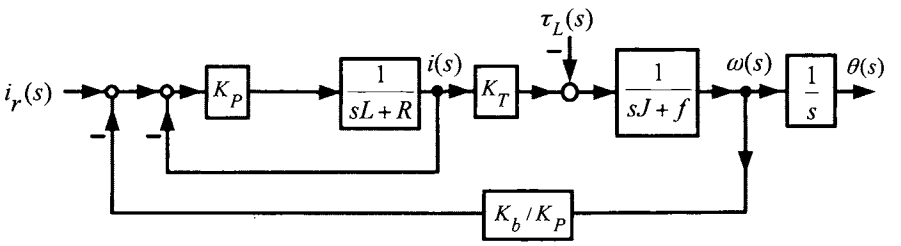


FIGURE 2.7. Equivalent block diagram.

The block diagram of Figure 2.7 is then easily seen to simplify to that of Figure 2.8.

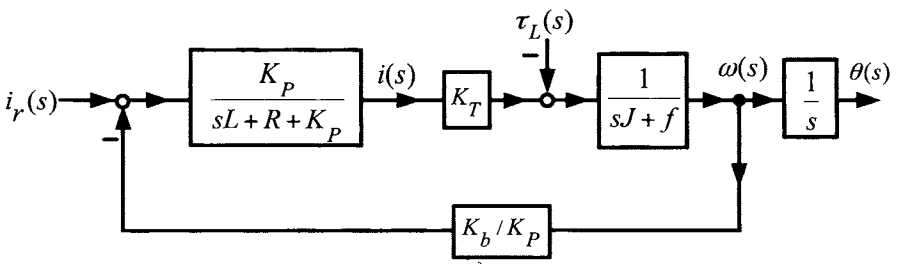


FIGURE 2.8. Simplified block diagram.

www.EngineeringEBooksPdf.com

As a result, with $\tau_L(s) \equiv 0$,

$$\begin{aligned} G(s) &\triangleq \omega(s)/i_r(s) \\ &= \frac{K_P K_T}{(sL+R+K_P)(sJ+f)+K_T K_b} \\ &= \frac{K_T}{(\frac{sL+R}{K_P}+1)(sJ+f)+K_T K_b/K_P}. \end{aligned}$$

Using high-gain feedback, that is, letting $K_P \to \infty$, $G(s)$ reduces to

$$G(s) = \omega(s)/i_r(s) = \frac{K_T}{(sJ+f)}. \tag{2.2}$$

In other words, if the gain K_P can be made large enough, the actual current $i(t)$ can be forced to track $i_r(t)$ quite fast. However, note that one cannot make the gain K_P arbitrarily large. This is easily seen by noting that the voltage commanded into the amplifier is

$$v(t) = K_P(i_r(t) - i(t))$$

which, for large gains K_P, could be greater than $V_{\max}$, causing the amplifier to saturate.

In summary, with a good current controller, the voltage $v(t)$ is automatically adjusted to force $i(t) \to i_r(t)$ fast enough that the reference (commanded) current $i_r(t)$ can be considered to be equal to the actual motor current $i(t)$. That is, for all practical purposes, the dynamics from $i_r(t)$ to $i(t)$ can be neglected allowing one to consider the input $i_r(t)$ as equal to the motor current $i(t)$. The following reduced-order system can then be used to design the controller:

$$\begin{aligned} \frac{d\omega}{dt} &= (K_T/J)i_r(t) - (f/J)\omega(t) - \tau_L/J \\ \frac{d\theta}{dt} &= \omega. \end{aligned}$$

The corresponding block diagram of the reduced-order system is shown in Figure 2.9.

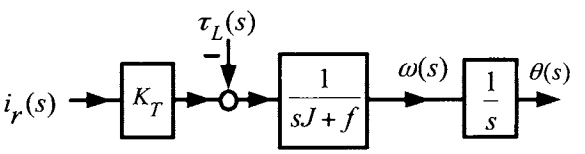


FIGURE 2.9. Reduced-order model of a DC motor.

www.EngineeringEBooksPdf.com

Speed Controller

Using the reduced-order model, it is straightforward to design a simple proportional speed controller as illustrated in Figure 2.10.

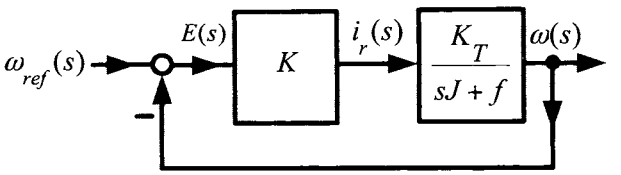


FIGURE 2.10. Simple speed controller for a DC motor.

From the block diagram of Figure 2.10, it follows that

$$\begin{aligned}\omega(s)/\omega_{ref}(s) &= \frac{KK_T/(sJ+f)}{1+KK_T/(sJ+f)} = \frac{KK_T/J}{s+(f+K_TK)/J} \\ &\approx \frac{KK_T/J}{s+K_TK/J} \\ &= \frac{1}{\tau_m s+1}\end{aligned}$$

where $\tau_m \triangleq \dfrac{1}{K_TK/J}$ and $f << K_TK$ were used. This is an example of the classical approach to control and is described in more detail in the Appendix of this chapter. However, in this chapter, the state-space approach to feedback control is pursued.

2.2 Speed Estimation

Typically, in a DC motor drive system, the current, voltage, and position are available by direct measurement. However, the speed is not usually measured directly. In this section, two approaches to estimating the speed are given.

2.2.1 Backward Difference Estimation of Speed

The optical encoder gives the position measurement, but not the speed of the motor. However, one can use this measurement to deduce the speed. The most straightforward way is to compute the *backward difference* of the position and divide by the sample period, that is,

$$\hat{\omega}_{bd}(kT) \triangleq \frac{2\pi}{2000}\left(\frac{N(kT)-N(kT-T)}{T}\right)$$

www.EngineeringEBooksPdf.com

where T is the time between samples and $N(kT)$ is the optical encoder count at time kT.

The error in estimating the speed by differentiation of the position measurements can be found as follows: At any discrete time $kT, N(kT)$ is in error by at most one encoder count. In particular, $N(kT)$ can be only too small by at most one encoder count ($N(kT)$ is never too large because of the way the encoder works). Thus, with $\theta(kT)$ the true position of the motor in radians,

$$\theta(kT) = \frac{2\pi}{2000}N(kT) + \frac{2\pi}{2000}e(kT)$$

where $e(kT)$ represents the *positive fractional* count that the encoder cannot sense; that is, $0 \leq e(kT) < 1$ for all k. Then, the speed may be written as

$$\begin{aligned}\omega(kT) &= \left(\frac{\theta(kT) - \theta(kT-T)}{T}\right) \\ &= \frac{2\pi}{2000}\left(\frac{N(kT) - N(kT-T)}{T}\right) + \frac{2\pi}{2000}\left(\frac{e(kT) - e(kT-T)}{T}\right)\end{aligned}$$

where, as $0 \leq e(kT) \leq 1$ and $0 \leq e((k-1)T) \leq 1$, it follows that $|e(kT) - e(kT-T)| \leq 1$.

It is now straightforward to compute a bound on the error in estimating the speed. As the speed estimate is given by

$$\hat{\omega}_{bd}(kT) = \frac{2\pi}{2000}\left(\frac{N(kT) - N(kT-T)}{T}\right)$$

and the difference $e(kT) - e(kT-T)$ is bounded by ± 1,

$$|\text{Error in } \hat{\omega}_{bd}(kT)| = \frac{2\pi}{2000}\left|\frac{e(kT) - e(kT-T)}{T}\right| \leq \frac{2\pi}{2000}\frac{1}{T}.$$

As the sampling rate increases (T gets smaller), the error gets larger. Of course, as the sampling rate decreases, the approximation

$$\omega(kT) \approx \left(\frac{\theta(kT) - \theta(kT-T)}{T}\right)$$

becomes less and less valid. The choice of T is a trade-off between the error and the accuracy of the finite difference in approximating the derivative. One way to decrease this error would be to use an encoder with higher resolution. Such encoders are typically more expensive and cannot operate at higher speeds (as the speed increases, a large number of pulses are coming in so fast that the pulse detection circuitry cannot keep up).

Figure 2.11 is a plot of the speed estimated by the backward difference method. In this example, the sample period is $T = 0.5$ msec and the encoder

www.EngineeringEBooksPdf.com

has a resolution of $2\pi/2000$ so that error bound is $(2\pi/2000)/T = 6.28$ radians/sec.

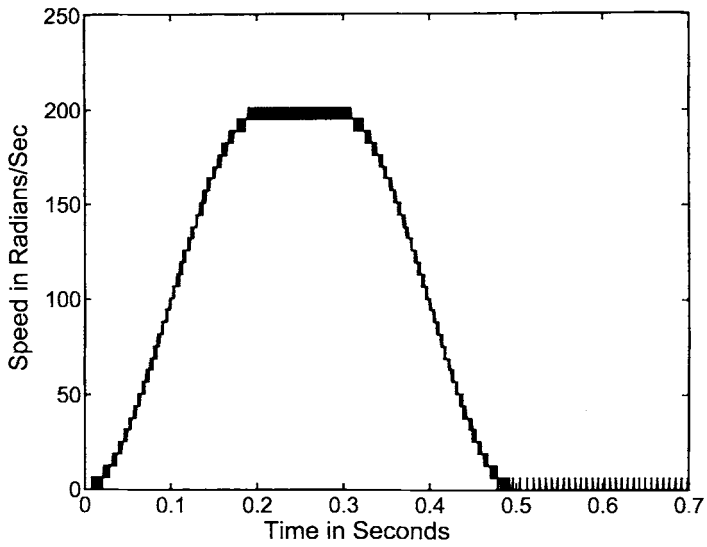


FIGURE 2.11. Plot of the speed computed using the backward difference. The error bound in this example is $(2\pi/2000)/(0.0005) = 6.28$ radians/sec.

2.2.2 *Estimation of Speed Using an Observer*

The differentiation of the position output from the optical encoder can result in a low-resolution, noisy estimate of the speed. Here a different approach is considered. With $\tau_L = 0$ (the case $\tau_L \neq 0$ is explored in problem 13), the system equations for the DC motor are

$$\begin{aligned} \frac{d\theta}{dt} &= \omega \\ \frac{d\omega}{dt} &= -(f/J)\omega + (K_T/J)i(t). \end{aligned} \tag{2.3}$$

Now, consider an *observer* defined by

$$\begin{aligned} \frac{d\hat{\theta}}{dt} &= \hat{\omega} + \ell_1(\theta - \hat{\theta}) \\ \frac{d\hat{\omega}}{dt} &= (K_T/J)i(t) - (f/J)\hat{\omega} + \ell_2(\theta - \hat{\theta}) \end{aligned} \tag{2.4}$$

www.EngineeringEBooksPdf.com

where $\theta(t) = (2\pi/2000)N(t)$ is the (discretized) position measurement from the encoder and $\hat{\theta}, \hat{\omega}$ are the *estimates* of the position and speed, respectively. If ℓ_1, ℓ_2 are chosen correctly, the solution $\hat{\omega}$ to (2.4) gives a good estimate of the speed. To motivate this approach, let $\ell_1 = 0$ and $\ell_2 = 0$ so that (2.4) becomes

$$\begin{aligned} \frac{d\hat{\theta}}{dt} &= \hat{\omega} \\ \frac{d\hat{\omega}}{dt} &= (K_T/J)i(t) - (f/J)\hat{\omega} \end{aligned} \tag{2.5}$$

and thus (2.5) is just a real-time *simulation* of the motor. That is, the actual current in the motor is sampled and brought into a computer processor, the equations (2.5) are integrated in *realtime* by the microprocessor (initialized with the same values of speed and position as the actual motor) and the solution $\hat{\omega}$ is then used as the estimate of the speed. However, there are problems with using (2.5) to estimate the speed. If there is any disturbance that causes the actual motor speed to change, then $\hat{\omega}$ will no longer be correct as such a disturbance is *not* modeled in (2.5) and thus $\hat{\omega}$ will not change to respond to it. After a disturbance has acted on the motor (e.g., suppose the motor shaft is bumped at some time $t = t_d$), its effect can be mathematically modeled as a change of initial conditions for equations (2.3). That is, the motor is described by the system of equations (2.3), but the initial condition $\omega(t_d+)$ is unknown ($\theta(t_d+)$ is measured and thus known at t_d). This is where the error term $\theta - \hat{\theta}$ in (2.4) becomes so important. For example, suppose $\hat{\omega} < \omega$ for a period of time resulting in $\hat{\theta} < \theta$ (as $\hat{\theta}$ is computed by integrating $\hat{\omega}$). Then, with $\ell_2 > 0$, the error term $\ell_2(\theta - \hat{\theta}) > 0$ will cause $\hat{\omega}$ to increase in (2.4) reducing the error $\omega - \hat{\omega}$.

A mathematical argument is now presented to show that, by choosing the gains ℓ_1, ℓ_2 appropriately, the estimate $\hat{\omega}(t)$ from (2.4) can be made to converge to $\omega(t)$ as fast as desired *without* knowledge of the initial condition for ω. To this end, let

$$\begin{aligned} e_1(t) &= \theta(t) - \hat{\theta}(t) \\ e_2(t) &= \omega(t) - \hat{\omega}(t) \end{aligned}$$

so that the dynamic equations for $e_1(t)$ and $e_2(t)$ are found by simply subtracting (2.4) from (2.3) to get

$$\begin{aligned} \frac{de_1}{dt} &= e_2 - \ell_1 e_1 \\ \frac{de_2}{dt} &= -(f/J)e_2 - \ell_2 e_1 \end{aligned} \tag{2.6}$$

www.EngineeringEBooksPdf.com

Notice that the motor torque terms $(K_T/J)i(t)$ in (2.3) and (2.4) canceled each other out.

This system of differential equations can be solved by computing the Laplace transform of (2.6) to obtain

$$\begin{aligned} sE_1(s) - e_1(0) &= E_2(s) - \ell_1 E_1(s) \\ sE_2(s) - e_2(0) &= -(f/J)E_2(s) - \ell_2 E_1(s). \end{aligned}$$

In matrix notation, this is written as

$$\begin{bmatrix} s+\ell_1 & -1 \\ \ell_2 & s+f/J \end{bmatrix} \begin{bmatrix} E_1(s) \\ E_2(s) \end{bmatrix} = \begin{bmatrix} e_1(0) \\ e_2(0) \end{bmatrix}.$$

Multiplying both sides of this matrix equation on the left by the inverse of the 2×2 matrix gives

$$\begin{bmatrix} E_1(s) \\ E_2(s) \end{bmatrix} = \frac{1}{s^2 + (\ell_1 + f/J)s + \ell_2 + \ell_1(f/J)} \begin{bmatrix} s+f/J & 1 \\ -\ell_2 & s+\ell_1 \end{bmatrix} \begin{bmatrix} e_1(0) \\ e_2(0) \end{bmatrix}.$$

In particular,

$$E_2(s) = \frac{-\ell_2 e_1(0) + (s+\ell_1)e_2(0)}{s^2 + (\ell_1 + f/J)s + \ell_2 + \ell_1(f/J)}.$$

It is required that $\omega(t) - \hat{\omega}(t) = e_2(t) = \mathcal{L}^{-1}(E_2(s)) \to 0$ as $t \to \infty$ for any values of $e_1(0)$ and $e_2(0)$. To do this, choose ℓ_1 and ℓ_2 so that

$$\begin{aligned} s^2 + (\ell_1 + f/J)s + \ell_2 + \ell_1(f/J) &= (s+p_1)(s+p_2) \\ &= s^2 + (p_1+p_2)s + p_1 p_2 \end{aligned}$$

with $p_1 > 0, p_2 > 0$. That is, choose

$$\begin{aligned} \ell_1 &= p_1 + p_2 - f/J \\ \ell_2 &= p_1 p_2 - \ell_1(f/J). \end{aligned}$$

Then

$$\begin{aligned} E_2(s) &= \frac{-\ell_2 e_1(0) + (s+\ell_1)e_2(0)}{(s+p_1)(s+p_2)} \\ &= \frac{A}{(s+p_1)} + \frac{B}{(s+p_2)} \end{aligned}$$

so that

$$e_2(t) = Ae^{-p_1 t} + Be^{-p_2 t} \to 0$$

as $t \to \infty$ for any $e_1(0) = \theta(0) - \hat{\theta}(0)$ and $e_2(0) = \omega(0) - \hat{\omega}(0)$.

Remark The importance of the error term in the observer equations should be understood. Note that one would typically know that the initial

www.EngineeringEBooksPdf.com

speed is zero and the initial position is also known (it is measured) so that $e_1(0) = \theta(0) - \hat{\theta}(0) = 0$ and $e_2(0) = \omega(0) - \hat{\omega}(0) = 0$. Consequently, even with $\ell_1 = \ell_2 = 0$, the solution to (2.6) would be $e_1(t) = e_2(t) \equiv 0$. However, in practice if the observer was implemented with the gains equal to zero, it would not work. For example, there could be a torque disturbance acting on the motor for a short period of time. Specifically, let

$$\tau_L(t) = \begin{cases} \tau_{L0} & \text{for } t_1 \leq t \leq t_2 \\ 0 & \text{otherwise.} \end{cases}$$

Then, the second equation of (2.3) is

$$\frac{d\omega}{dt} = -(f/J)\omega + (K_T/J)i(t) - \tau_L(t)/J.$$

During the time this disturbance torque acts on the motor, the observer's speed estimate given by (2.4) will diverge from the true value since the observer equations (2.4) do not have this disturbance modeled. However, after the disturbance has quit acting on the motor at time t_2, the observers equation are again valid and the error term $e_1(t) = \theta(t) - \hat{\theta}(t)$ will force the estimate $\hat{\omega}(t) \to \omega(t)$. That is, at time t_2, the motor and observer are correctly given by (2.3) and (2.4), respectively. Thus, the error system is correctly given by (2.5) with the "initial condition" $\hat{\omega}(t_2)$ at time t_2 *unknown*. As shown above, in spite of $\hat{\omega}(t_2)$ being unknown, the error $e_2(t) = \omega(t) - \hat{\omega}(t) \to 0$ if the gains ℓ_1, ℓ_2 are chosen properly.

Discretization of the Observer Equations

Using a simple Euler integration routine, the observer equations (2.4) may be implemented in discrete time as

$$\begin{aligned} \hat{\theta}\left((k+1)T\right) &= \hat{\theta}\left(kT\right) + T\hat{\omega}(kT) + T\ell_1 e_1(kT) \\ \hat{\omega}\left((k+1)T\right) &= \hat{\omega}\left(kT\right) - T(f/J)\hat{\omega}(kT) + T(K_T/J)i(kT) + T\ell_2 e_1(kT). \end{aligned} \tag{2.7}$$

However, the trapezoidal method described in Section 2.7.9 provides a more accurate method of numerical integration for a given sample period T.

2.3 Trajectory Generation

In this section, a simple way to generate a position and speed reference for a point-to-point move is developed. Assuming the load torque is zero, the

www.EngineeringEBooksPdf.com

equations for the position and speed of the motor are

$$\begin{aligned} \frac{d\theta}{dt} &= \omega \\ \frac{d\omega}{dt} &= -(f/J)\omega + (K_T/J)i_r. \end{aligned} \tag{2.8}$$

For a point-to-point move, it is required that the position reference trajectory $\theta_{ref}(t)$ satisfy $\theta_{ref}(0) = 0$ and $\theta_{ref}(t_f) = \theta_f$ where t_f is the final time and θ_f is the final desired position, that is, going from the "point" 0 to the "point" θ_f. There are many ways to do this, but consider the simple symmetric trajectory shown in Figure 2.12.

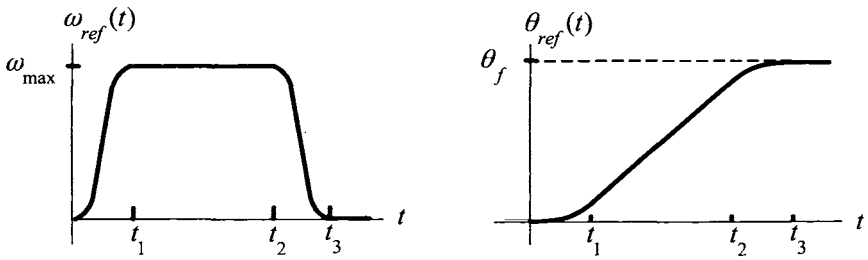


FIGURE 2.12. Reference speed and position profiles.

In order to have a smooth trajectory, that is, the acceleration reference is a continuous function of time, it is required that

$$\begin{aligned} \omega_{ref}(0) &= 0 & \dot{\omega}_{ref}(0) &= 0 \\ \omega_{ref}(t_1) &= \omega_{\max} & \dot{\omega}_{ref}(t_1) &= 0 \\ \omega_{ref}(t) &= \omega_{\max} & t_1 \le t &\le t_2 \\ \omega_{ref}(t_2) &= \omega_{\max} & \dot{\omega}_{ref}(t_2) &= 0 \\ \omega_{ref}(t_3) &= 0 & \dot{\omega}_{ref}(t_3) &= 0. \end{aligned}$$

It is also required that $t_3 - t_2 = t_1$ (i.e., $t_3 = t_1 + t_2$) so that the time required to decelerate the motor is the same as the amount of time to accelerate it. The speed reference is made symmetric by setting

$$\omega_{ref}(t) = \omega_{ref}(t_3 - t)$$

for $t_2 \le t \le t_3$. As the final position is to be θ_{ref}, the following must also hold:

$$\int_0^{t_f} \omega_{ref}(\tau)d\tau = \theta_f.$$

There are still many ways to define a reference trajectory and still satisfy all these conditions. To be specific, consider a polynomial reference trajectory given by

$$\omega_{ref}(t) = c_1 t^2 + c_2 t^3 \quad \text{for } 0 \le t \le t_1$$

www.EngineeringEBooksPdf.com

which clearly satisfies $\omega_{ref}(0) = 0, \dot{\omega}_{ref}(0) = 0$. The conditions at t_1 become

$$\begin{aligned} \omega_{ref}(t_1) &= c_1 t_1^2 + c_2 t_1^3 = \omega_{\max} \\ \dot{\omega}_{ref}(t_1) &= 2c_1 t_1 + 3c_2 t_1^2 = 0 \end{aligned}$$

or

$$\begin{bmatrix} t_1^2 & t_1^3 \\ 2t_1 & 3t_1^2 \end{bmatrix} \begin{bmatrix} c_1 \\ c_2 \end{bmatrix} = \begin{bmatrix} \omega_{\max} \\ 0 \end{bmatrix}.$$

This has the unique solution

$$\begin{bmatrix} c_1 \\ c_2 \end{bmatrix} = \frac{1}{t_1^4} \begin{bmatrix} 3t_1^2 & -t_1^3 \\ -2t_1 & t_1^2 \end{bmatrix} \begin{bmatrix} \omega_{\max} \\ 0 \end{bmatrix} = \begin{bmatrix} +3\omega_{\max}/t_1^2 \\ -2\omega_{\max}/t_1^3 \end{bmatrix}.$$

The distance traveled at time t_1 is then

$$\begin{aligned} \theta_{ref}(t_1) &= \int_0^{t_1} \omega_{ref}(\tau) d\tau = c_1 t_1^3/3 + c_2 t_1^4/4 = \frac{3\omega_{\max}}{t_1^2}\frac{t_1^3}{3} - \frac{2\omega_{\max}}{t_1^3}\frac{t_1^4}{4} \\ &= \frac{\omega_{\max} t_1}{2}. \end{aligned}$$

The speed reference trajectory is

$$\omega_{ref}(t) = \begin{cases} c_1 t^2 + c_2 t^3 & 0 \le t \le t_1 \\ \omega_{\max} & t_1 \le t \le t_2 \\ c_1(t_3 - t)^2 + c_2(t_3 - t)^3 & t_2 \le t \le t_3. \end{cases}$$

As the total distance traveled at time t_3 must be θ_f, it follows that

$$\begin{aligned} \theta_f &= \int_0^{t_3} \omega_{ref}(\tau) d\tau = 2\theta_{ref}(t_1) + \omega_{\max}(t_2 - t_1) \\ &= 2\frac{\omega_{\max} t_1}{2} + \omega_{\max}(t_2 - t_1) \\ &= \omega_{\max} t_2. \end{aligned}$$

This then puts a constraint on the choices of $\omega_{\max}$ and t_2. For example, if θ_f is specified, then $\omega_{\max} = \theta_f / t_2$.

The position reference is just the integral of the speed reference. Consequently,

$$\theta_{ref}(t) = \begin{cases} c_1 t^3/3 + c_2 t^4/4 & 0 \le t \le t_1 \\ \omega_{\max} t_1/2 + \omega_{\max}(t - t_1) & t_1 \le t \le t_2 \\ \omega_{\max} t_2 - c_1(t_3 - t)^3/3 - c_2(t_3 - t)^4/4 & t_2 \le t \le t_3. \end{cases}$$

Finally, the reference acceleration is just the derivative of the speed reference given by

$$\alpha_{ref}(t) = \begin{cases} 2c_1 t + 3c_2 t^2 & 0 \le t \le t_1 \\ 0 & t_1 \le t \le t_2 \\ -2c_1(t_3 - t) - 3c_2(t_3 - t)^2 & t_2 \le t \le t_3. \end{cases}$$

www.EngineeringEBooksPdf.com

The corresponding current reference i_{ref} is then found setting ω equal ω_{ref} in (2.8) and solving for the current to obtain

$$i_{ref}(t) \triangleq \frac{J\alpha_{ref}(t) + f\omega_{ref}(t)}{K_T}.$$

By design, the acceleration, speed, and position references are continuous functions of time. Figure 2.13 is a plot of the acceleration reference $\alpha_{ref}(t)$ and the jerk reference $j_{ref} \triangleq d\alpha_{ref}/dt$, where it is seen that j_{ref} is not continuous at $t = 0, t_1, t_2$, and t_3. In the figure

$$\begin{aligned} \alpha_{\max} &= (3/2)\omega_{\max}/t_1 \\ j_{\max} &= -6\omega_{\max}/t_1^2. \end{aligned}$$

Problem 17 considers a trajectory design for which the jerk is continuous.

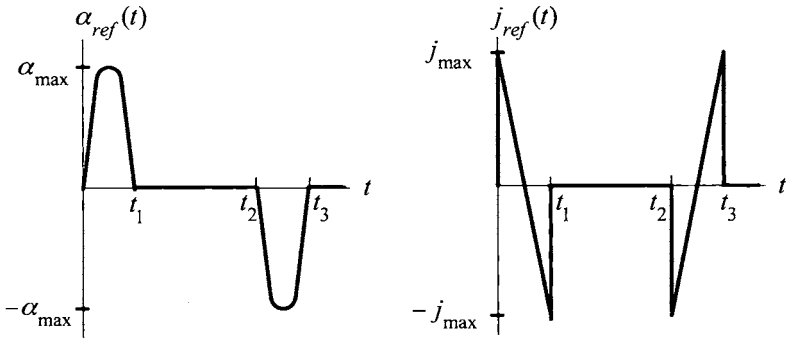


FIGURE 2.13. Left: α_{ref} versus time. Right: j_{ref} versus time.

Specifying a Reference Trajectory

A typical scenario is that θ_f is given and that one chooses t_1 and t_2 with $t_1 < t_2$. Then t_3 and $\omega_{\max}$ are specified by $t_3 = t_2 + t_1$ and $\omega_{\max} = \theta_f/t_1$, respectively. This results in a mechanical reference trajectory

$$\Big(\theta_{ref}(t), \omega_{ref}(t), \alpha_{ref}(t), j_{ref}(t)\Big).$$

The electrical reference trajectory is then determined by

$$\begin{aligned} i_{ref}(t) &\triangleq \frac{J\alpha_{ref}(t) + f\omega_{ref}(t)}{K_T} \\ v_{ref}(t) &\triangleq L\frac{di_{ref}(t)}{dt} + Ri_{ref}(t) + K_b\omega_{ref}(t). \end{aligned}$$

How does one choose t_1, t_2? One typically wants to rotate the motor as fast as possible and therefore chooses t_1 and t_2 to be small. However, the

www.EngineeringEBooksPdf.com

smaller the values of t_1 and t_2, the larger the peak values of $\omega_{ref}(t), \alpha_{ref}(t)$ and therefore the peak values of $i_{ref}(t)$ and $v_{ref}(t)$. It is then a little trial and error to choose values for t_1 and t_2 and check that $|i_{ref}| \leq I_{\max}$, $|v_{ref}| \leq V_{\max}$.

2.4 Design of a State Feedback Tracking Controller

Assuming current command, a *state-space* model of the DC motor is

$$\begin{aligned} \frac{d\theta}{dt} &= \omega \\ \frac{d\omega}{dt} &= (K_T/J)i_r - (f/J)\omega - \tau_L/J \end{aligned} \tag{2.9}$$

where the *state variables* are θ, ω, the *input* is i_r and the *disturbance* is τ_L. The terminology "state-space" model refers to having a system of first-order differential equations, that is, a first-order derivative on one side of the equation and a (possibly) nonlinear function of the state variables, inputs, and disturbances on the other side of the equation.

The reference trajectory and reference input are chosen to satisfy

$$\begin{aligned} \frac{d\theta_{ref}}{dt} &= \omega_{ref} \\ \frac{d\omega_{ref}}{dt} &= (K_T/J)i_{ref} - (f/J)\omega_{ref}. \end{aligned} \tag{2.10}$$

Define

$$\begin{aligned} e_1(t) &= \theta_{ref}(t) - \theta(t) \\ e_2(t) &= \omega_{ref}(t) - \omega(t) \end{aligned}$$

so that subtracting (2.9) from (2.10) results in the error system

$$\begin{aligned} \frac{de_1}{dt} &= e_2 \\ \frac{de_2}{dt} &= -(f/J)e_2 + \tau_L/J + w \end{aligned} \tag{2.11}$$

with

$$w \triangleq \frac{K_T}{J}(i_{ref} - i_r). \tag{2.12}$$

www.EngineeringEBooksPdf.com

Here, i_r is the input the control engineer is free to specify. However, the approach here is to specify w such that $e_1(t) \to 0$ and $e_2(t) \to 0$ as $t \to \infty$. Then i_r is chosen so that (2.12) holds. Specifically, w is specified by

$$w = -\left(K_0 \int_0^t e_1(\tau)d\tau + K_1 e_1(t) + K_2 e_2(t)\right) \tag{2.13}$$

which results in accurate tracking of the trajectory (2.10) provided that the gains are chosen appropriately. By (2.12), this then requires choosing the input i_r as

$$i_r = i_{ref} + \frac{J}{K_T}\left(K_0 \int_0^t e_1(\tau)d\tau + K_1 e_1(t) + K_2 e_2(t)\right). \tag{2.14}$$

To find the gains, define

$$e_0(t) \triangleq \int_0^t e_1(\tau)d\tau$$

so that with the state feedback (2.13) and the system (2.11), one may write

$$\begin{aligned} \frac{de_0}{dt} &= e_1 \\ \frac{de_1}{dt} &= e_2 \\ \frac{de_2}{dt} &= -(f/J)e_2 - K_0 e_0 - K_1 e_1 - K_2 e_2 + \tau_L/J. \end{aligned} \tag{2.15}$$

To solve (2.15), its Laplace transform is computed as

$$\begin{aligned} sE_0(s) - e_0(0) &= E_1(s) \\ sE_1(s) - e_1(0) &= E_2(s) \\ sE_2(s) - e_2(0) &= -K_0 E_0(s) - K_1 E_1(s) - (K_2 + f/J)\, E_2(s) + \tau_L(s)/J. \end{aligned}$$

In matrix notation, one has

$$\begin{bmatrix} s & -1 & 0 \\ 0 & s & -1 \\ K_0 & K_1 & s + f/J + K_2 \end{bmatrix} \begin{bmatrix} E_0(s) \\ E_1(s) \\ E_2(s) \end{bmatrix} = \begin{bmatrix} e_0(0) \\ e_1(0) \\ e_2(0) \end{bmatrix} + \begin{bmatrix} 0 \\ 0 \\ \tau_L(s)/J \end{bmatrix} \tag{2.16}$$

where the inverse of the 3×3 matrix on the left-hand side of (2.16) is given by

$$\frac{1}{s^3 + (K_2 + f/J)\, s^2 + K_1 s + K_0} \times \begin{bmatrix} s^2 + (K_2 + f/J)\, s + K_1 & s + K_2 + f/J & 1 \\ -K_0 & s^2 + (K_2 + f/J)\, s & s \\ -K_0 s & -(K_1 s + K_0) & s^2 \end{bmatrix}.$$

www.EngineeringEBooksPdf.com

Let $\tau_L = 0$ (the case $\tau_L \neq 0$ is explored in problems 21 and 22). Multiplying both sides of (2.16) on the left by this inverse matrix, the Laplace transform of the state variables are found to be

$$\begin{aligned} E_0(s) &= \frac{\left(s^2 + (K_2 + f/J)\, s + K_1\right) e_0(0) + (s + K_2 + f/J)\, e_1(0) + e_2(0)}{s^3 + (K_2 + f/J)\, s^2 + K_1 s + K_0} \\ E_1(s) &= \frac{-K_0 e_0(0) + \left(s^2 + (K_2 + f/J)\, s\right) e_1(0) + s e_2(0)}{s^3 + (K_2 + f/J)\, s^2 + K_1 s + K_0} \\ E_2(s) &= \frac{-K_0 s e_0(0) - (K_1 s + K_0)\, e_1(0) + s^2 e_2(0)}{s^3 + (K_2 + f/J)\, s^2 + K_1 s + K_0}. \end{aligned} \tag{2.17}$$

Note that all three Laplace transforms have the same denominator given by $s^3 + (K_2 + f/J)\, s^2 + K_1 s + K_0$. This is the *characteristic equation* of the system. Using the gains K_0, K_1, and K_2, the roots of the characteristic equation may be assigned to any desired values. For example, let

$$\begin{aligned} a(s) &= (s + r_1)(s + r_2)(s + r_3) \\ &= s^3 + (r_1 + r_2 + r_3)s^2 + (r_1 r_2 + r_1 r_3 + r_2 r_3)s + r_1 r_2 r_3 \end{aligned}$$

be the desired characteristic polynomial and then choose the gains as

$$\begin{aligned} K_2 &= r_1 + r_2 + r_3 - f/J \\ K_1 &= r_1 r_2 + r_1 r_3 + r_2 r_3 \\ K_0 &= r_1 r_2 r_3. \end{aligned} \tag{2.18}$$

With this choice of gains, the closed-loop poles are $p_1 = -r_1$, $p_2 = -r_2$, and $p_3 = -r_3$. Assuming these poles are distinct, $E_1(s)$ in (2.17) becomes

$$\begin{aligned} E_1(s) &= \frac{-K_0 e_0(0) + \left(s^2 + (K_2 + f/J)\, s\right) e_1(0) + s e_2(0)}{(s + r_1)(s + r_2)(s + r_3)} \\ &= \frac{A}{s + r_1} + \frac{B}{s + r_2} + \frac{C}{s + r_3} \end{aligned}$$

where A, B, and C are constants. The inverse Laplace transform of $E_1(s)$ is then

$$e_1(t) = Ae^{-r_1 t} + Be^{-r_2 t} + Ce^{-r_3 t} \to 0$$

as $t \to \infty$. The further the closed-loop poles are in the left-half plane, the faster $e_1(t) \to 0$ and thus, the faster $\theta(t) \to \theta_{ref}(t)$. However, note that the further in the left-half plane the closed-loop poles are chosen, the larger r_1, r_2, and r_3 and, thus, the larger the gains K_0, K_1 and K_2. The difficulty with choosing large values for the feedback gains is that the resulting feedback

$$i_r = i_{ref} + \frac{J}{K_T}\left(K_0 \int_0^t e_1(\tau)d\tau + K_1 e_1(t) + K_2 e_2(t)\right)$$

www.EngineeringEBooksPdf.com

can be quite large and saturate the amplifier,[1] even if the errors e_0, e_1, and e_2 are small. The complete system is illustrated in the block diagram of 2.14.

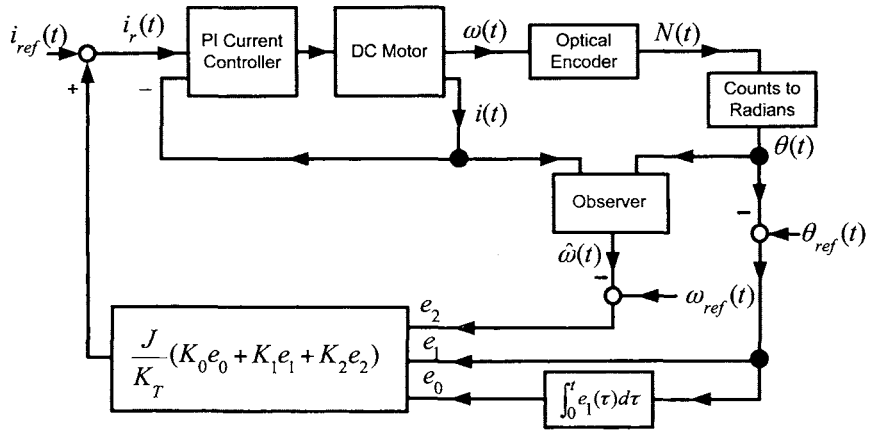


FIGURE 2.14. Block diagram for the state-space controller.

Note that if the desired characteristic equation had been of the form

$$a(s) = (s + r_1)(s^2 + 2\zeta\omega_n s + \omega_n^2)$$

where $0 < \zeta < 1, \omega_n > 0$, then it is again easy to find the corresponding gains. It is up to the control engineer to choose the closed-loop pole locations, or equivalently, the gains. Typically, if the poles are not far enough in the left-half plane, the response is too slow. On the other hand, if the poles are chosen too far in the left-half plane, the amplifier might saturate due to the large value of the gains. This procedure of varying the location of the closed-loop poles by varying the gains is referred to as "tuning the system".

The control designer also must choose the observer poles $-p_1, -p_2$. One typically wants $\hat{\omega}(t) \to \omega(t)$ much faster than the rate at which $\omega_{ref}(t) - \hat{\omega}(t) \to 0$. This is simply because one wants the estimate $\hat{\omega}(t)$ to close to the value $\omega(t)$ so that feeding back $K_1(\omega_{ref}(t) - \hat{\omega}(t))$ will be essentially the same as feeding back $K_1(\omega_{ref}(t) - \omega(t))$. In practice, the observer poles $-p_i$ are taken to be 5–10 times further in the left-half plane than the controller poles $-r_i$.

[1] That is, a current which is larger than the amplifier can produce would be commanded to the amplifier. The voltage output of the amplifier will increase (in order to increase the current) until it reaches the maximum possible value $V_{\max}$ and then it will saturate at this maximum value.

www.EngineeringEBooksPdf.com

2.5 Nested Loop Control Structure*

A nested loop control structure is shown in Figure 2.15. This controller has two nested[2] PID (*proportional, integral plus derivative*) control loops and is common in industrial applications. Part of its popularity is due to the simplicity in tuning (adjusting) the gains of the controller. Specifically, with the position loop gains set to zero, the gains $K_{\omega P}$ and $K_{\omega I}$ of the speed loop can be tuned first online until a satisfactory speed response is obtained.[3] With these values set, the gains $K_{\theta P}$ and $K_{\theta I}$ of the position loops are then tuned until a satisfactory position response is obtained. The signal denoted as $\bar{\omega}_{ref}$ (the output of the position loop) is referred to as the "speed reference" since this would be the speed reference if the position loop was removed.[4]

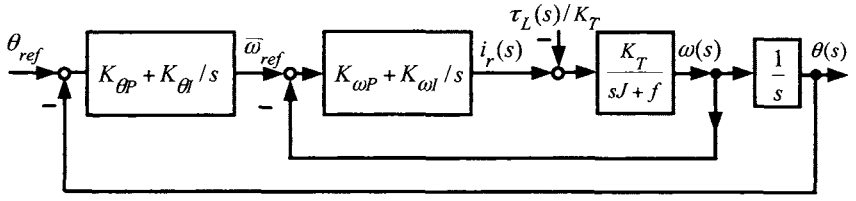


FIGURE 2.15. Nested loop control structure. The gains of the speed loop are tuned first and then the gains of the position loop are tuned.

Taking the transfer function of the system equations

$$\begin{aligned} \frac{d\omega}{dt} &= \frac{K_T}{J} i_r - \frac{f}{J}\omega - \frac{\tau_L}{J} \\ \frac{d\theta}{dt} &= \omega \end{aligned}$$

gives

$$\begin{aligned} \omega(s) &= G_m(s)\left(i_r(s) - \frac{\tau_L(s)}{K_T}\right) \\ \theta(s) &= \frac{1}{s}\omega(s) \end{aligned}$$

where

$$G_m(s) \triangleq \frac{K_T/J}{s + f/J}. \tag{2.19}$$

[2] The terminology "nested" just refers to one of the loops being inside the other.

[3] That is, the response from $\bar{\omega}_{ref}(t) \to \omega(t)$.

[4] However, if the position loop is intact, then there is no guarantee that $\bar{\omega}_{ref}$ (defined as the output of the position loop) equals $\omega_{ref} \triangleq d\theta_{ref}/dt$.

www.EngineeringEBooksPdf.com

To simplify the discussion, let $K_{\omega I} = 0$ (see problem 24) and substitute

$$i_r(s) = K_{\omega P}\left(\bar{\omega}_{ref}(s) - \omega(s)\right)$$

into the previous expression for $\omega(s)$ to obtain

$$\omega(s) = G_m(s)\left(K_{\omega P}\left(\bar{\omega}_{ref}(s) - \omega(s)\right)\right) - G_m(s)\frac{\tau_L(s)}{K_T}. \tag{2.20}$$

The output $\omega(s)$ in terms of the transfer functions from $\bar{\omega}_{ref}(s)$ to $\theta(s)$ and $\tau_L(s)$ to $\theta(s)$ is then

$$\omega(s) = \frac{K_{\omega P}G_m(s)}{1 + K_{\omega P}G_m(s)}\bar{\omega}_{ref}(s) - \frac{G_m(s)}{1 + K_{\omega P}G_m(s)}\frac{\tau_L(s)}{K_T}. \tag{2.21}$$

The position output is then simply

$$\theta(s) = \frac{1}{s}\frac{K_{\omega P}G_m(s)}{1 + K_{\omega P}G_m(s)}\bar{\omega}_{ref}(s) - \frac{1}{s}\frac{G_m(s)}{1 + K_{\omega P}G_m(s)}\frac{\tau_L(s)}{K_T}.$$

With $E(s) \triangleq \theta_{ref}(s) - \theta(s)$ and $\bar{\omega}_{ref}(s) = \left(\frac{K_{\theta P}s + K_{\theta I}}{s}\right)E(s)$, it follows that

$$\begin{aligned} E(s) &\triangleq \theta_{ref}(s) - \theta(s) \\ &= \theta_{ref}(s) - \left(\frac{1}{s}\frac{K_{\omega P}G_m(s)}{1 + K_{\omega P}G_m(s)}\frac{K_{\theta P}s + K_{\theta I}}{s}E(s)\right. \\ &\quad \left. -\frac{1}{s}\frac{G_m(s)}{1 + K_{\omega P}G_m(s)}\frac{\tau_L(s)}{K_T}\right) \end{aligned}$$

or

$$\begin{aligned} E(s) \triangleq\ & \frac{1}{1 + \frac{1}{s}\frac{K_{\omega P}G_m(s)}{1 + K_{\omega P}G_m(s)}\left(\frac{K_{\theta P}s + K_{\theta I}}{s}\right)}\theta_{ref}(s) \\ & + \frac{1}{1 + \frac{1}{s}\frac{K_{\omega P}G_m(s)}{1 + K_{\omega P}G_m(s)}\left(\frac{K_{\theta P}s + K_{\theta I}}{s}\right)}\frac{1}{s}\frac{G_m(s)}{1 + K_{\omega P}G_m(s)}\frac{\tau_L(s)}{K_T}. \end{aligned}$$

Then as

$$\frac{K_{\omega P}G_m(s)}{1 + K_{\omega P}G_m(s)} = \frac{K_{\omega P}K_T/J}{s + f/J + K_{\omega P}K_T/J}$$

one may write $E(s) = G_1(s)\theta_{ref}(s) + G_2(s)\tau_L(s)$, where

$$\begin{aligned} G_1(s) &\triangleq \frac{1}{1 + \frac{1}{s}\frac{K_{\omega P}K_T/J}{s + f/J + K_{\omega P}K_T/J}\left(\frac{K_{\theta P}s + K_{\theta I}}{s}\right)} \\ &= \frac{s^2\left(s + f/J + K_{\omega P}K_T/J\right)}{s^2\left(s + f/J + K_{\omega P}K_T/J\right) + K_{\omega P}K_T/J\left(K_{\theta P}s + K_{\theta I}\right)} \\ &= \frac{s^2\left(s + f/J + K_{\omega P}K_T/J\right)}{s^3 + s^2\left(f/J + K_{\omega P}K_T/J\right) + \left(K_{\theta P}K_{\omega P}K_T/J\right)s + K_{\theta I}K_{\omega P}K_T/J} \end{aligned}$$

www.EngineeringEBooksPdf.com

and

$$
\begin{aligned}
G_2(s) &\triangleq \frac{1}{1+\frac{1}{s}\frac{K_{\omega P}G_m(s)}{1+K_{\omega P}G_m(s)}\left(\frac{K_{\theta P}s+K_{\theta I}}{s}\right)}\frac{1}{s}\frac{G_m(s)}{1+K_{\omega P}G_m(s)}\frac{1}{K_T} \\
&= \frac{1}{1+\frac{1}{s}\frac{K_{\omega P}K_T/J}{(s+f/J+K_{\omega P}K_T/J)}\left(\frac{K_{\theta P}s+K_{\theta I}}{s}\right)}\frac{1}{s}\frac{K_T/J}{s+f/J+K_{\omega P}K_T/J}\frac{1}{K_T} \\
&= \frac{s^2}{s^2\left(s+f/J+K_{\omega P}K_T/J\right)+\left(K_{\omega P}K_T/J\right)\left(K_{\theta P}s+K_{\theta I}\right)}\frac{1}{s}\frac{1}{J} \\
&= \frac{s/J}{s^3+s^2\left(f/J+K_{\omega P}K_T/J\right)+\left(K_{\theta P}K_{\omega P}K_T/J\right)s+K_{\theta I}K_{\omega P}K_T/J}.
\end{aligned}
$$

Both $G_1(s)$ and $G_2(s)$ have the same denominator (characteristic polynomial) given by

$$s^3+s^2\left(f/J+K_{\omega P}K_T/J\right)+\left(K_{\theta P}K_{\omega P}K_T/J\right)s+K_{\theta I}K_{\omega P}K_T/J.$$

Suppose it is desired to have the closed-loop poles at $-r_1, -r_2$, and $-r_3$ with $r_1 > 0, r_2 > 0, r_3 > 0$. The closed-loop characteristic polynomial is then of the form

$$(s+r_1)(s+r_2)(s+r_3) = s^3+(r_1+r_2+r_3)s^2+(r_1r_2+r_1r_3+r_2r_3)s+r_1r_2r_3.$$

This requires setting

$$
\begin{aligned}
f/J+K_{\omega P}K_T/J &= r_1+r_2+r_3 \\
K_{\theta P}K_{\omega P}K_T/J &= r_1r_2+r_1r_3+r_2r_3 \\
K_{\theta I}K_{\omega P}K_T/J &= r_1r_2r_3.
\end{aligned}
\tag{2.22}
$$

Solving (2.22) for the gains gives

$$
\begin{aligned}
K_{\omega P} &= \frac{r_1+r_2+r_3-f/J}{K_T/J} \\
K_{\theta P} &= \frac{r_1r_2+r_1r_3+r_2r_3}{K_{\omega P}K_T/J} \\
K_{\theta I} &= \frac{r_1r_2r_3}{K_{\omega P}K_T/J}.
\end{aligned}
\tag{2.23}
$$

With this choice of gains,[5] the error becomes

$$
\begin{aligned}
E(s) &= E_1(s)+E_2(s) \\
&= \frac{s^2\left(s+f/J+K_{\omega P}K_T/J\right)}{(s+r_1)(s+r_2)(s+r_3)}\theta_{ref}(s)+\frac{s/J}{(s+r_1)(s+r_2)(s+r_3)}\tau_L(s).
\end{aligned}
\tag{2.24}
$$

[5] However, as noted in the beginning of this section, the gains for this controller are not usually chosen according to (2.23). Rather, $K_{\omega P}$ is varied until a satisfactory speed response is obtained. With $K_{\omega P}$ fixed at this value, the gains $K_{\theta P}$ and $K_{\theta I}$ are varied until the position response is satisfactory.

www.EngineeringEBooksPdf.com

The objective here is to have $e(t) = \mathcal{L}^{-1}\{E(s)\} \to 0$ as $t \to \infty$. To study this, expressions for $\theta_{ref}(s)$ and $\tau_L(s)$ are needed. To proceed, consider a trajectory where it is desired to have the motor rotate from $\theta(0) = 0$ to $\theta(t_f) = \theta_f$. A reference trajectory to do this is given in Figure 2.16. The position reference $\theta_{ref}(t)$ is given by

$$\theta_{ref}(t) =$$

$$\begin{cases} \dfrac{\omega_{\max}}{2t_1}t^2 & 0 \le t \le t_1 \\ \omega_{\max}t_1/2 + \omega_{\max}(t - t_1) & t_1 \le t \le t_2 \\ \omega_{\max}t_1/2 + \omega_{\max}(t_2 - t_1) + \dfrac{\omega_{\max}t_1^2}{2t_1} - \dfrac{\omega_{\max}}{2t_1}(t_f - t)^2 & t_2 \le t \le t_f \\ \omega_{\max}t_2 & t \ge t_f \end{cases} \tag{2.25}$$

where $\omega_{\max} = \theta_f/t_2$ and $t_f \triangleq t_2 + t_1$. The corresponding speed reference $\omega_{ref}(t)$ is given by

$$\omega_{ref}(t) = \begin{cases} \dfrac{\omega_{\max}}{t_1}t & 0 \le t \le t_1 \\ \omega_{\max} & t_1 \le t \le t_2 \\ \dfrac{\omega_{\max}}{t_1}(t_f - t) & t_2 \le t \le t_f \\ 0 & t \ge t_f \end{cases} \tag{2.26}$$

and is shown in Figure 2.16(b).

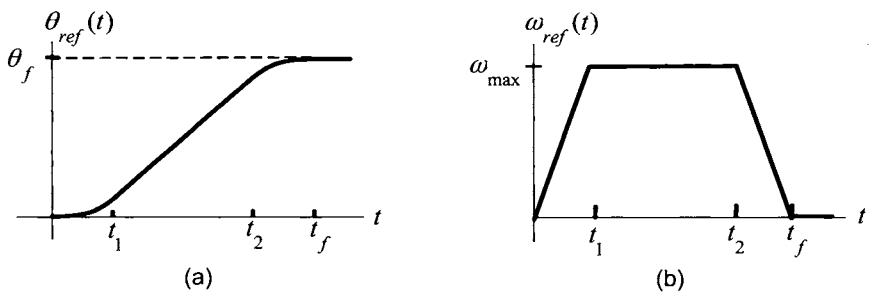


FIGURE 2.16. (a) Position reference. (b) Speed reference.

www.EngineeringEBooksPdf.com

The expression for $\theta_{ref}(t)$ can also be obtained by simply integrating the speed reference $\omega_{ref}(t) \triangleq d\theta_{ref}(t)/dt$. Note that although $\omega_{ref}(t)$ is continuous, $\alpha_{ref}(t) = d\omega_{ref}(t)/dt$ is not and $j_{ref}(t) = d\alpha_{ref}(t)/dt$ has impulses at $t = 0, t_1, t_2, t_f$. The various components of $\theta_{ref}(t)$ have Laplace transforms given by [$u_s(t)$ is the unit step function]

$$\begin{aligned}
\mathcal{L}\left\{\omega_{\max}\frac{t^2}{2t_1}u_s(t)\right\} &= \frac{\omega_{\max}}{t_1}\frac{1}{s^3} \\
\mathcal{L}\left\{\left(\omega_{\max}\frac{t_1}{2}+\omega_{\max}(t-t_1)\right)u_s(t)\right\} &= -\omega_{\max}\frac{t_1}{2}\frac{1}{s}+\omega_{\max}\frac{1}{s^2} \\
\mathcal{L}\left\{\left(\omega_{\max}t_2-\omega_{\max}\frac{(t_f-t)^2}{2t_1}\right)u_s(t)\right\} &= \omega_{\max}t_2\frac{1}{s} \\
&\quad -\omega_{\max}\left(\frac{t_f^2}{2t_1}\frac{1}{s}-\frac{t_f}{t_1}\frac{1}{s^2}+\frac{1}{t_1}\frac{1}{s^3}\right. \\
\mathcal{L}\{\omega_{\max}t_2u_s(t)\} &= \omega_{\max}t_2\frac{1}{s}.
\end{aligned}$$

Finally, the Laplace transform of a *constant* load torque $\tau_L(t) = \tau_{L0}u_s(t)$ acting on the motor is

$$\mathcal{L}\{\tau_L(t)\} = \frac{\tau_{L0}}{s}.$$

The interest here is to analyze the system for tracking and disturbance rejection, that is, to see if it can track $\theta_{ref}(t)$ while a constant load disturbance τ_{L0} acts on the motor.

From the above Laplace transform expressions, $\theta_{ref}(s)$ and $\tau_L(s)$ are of the form (more precisely, see problem 26)

$$\begin{aligned}
\theta_{ref}(s) &= \frac{A}{s}+\frac{B}{s^2}+\frac{C}{s^3} \\
\tau_L(s) &= \tau_{L0}\frac{1}{s}.
\end{aligned}$$

for some constants A, B, and C. Substituting into the above expression for

www.EngineeringEBooksPdf.com

$E(s)$ gives

$$\begin{aligned} E(s) &= E_1(s) + E_2(s) \\ &= \frac{s^2\,(s + f/J + K_{\omega P}K_T/J)}{(s+r_1)(s+r_2)(s+r_3)}\left(\frac{A}{s} + \frac{B}{s^2} + \frac{C}{s^3}\right) \\ &\quad + \frac{s}{(s+r_1)(s+r_2)(s+r_3)}\frac{1}{J}\frac{\tau_{L0}}{s} \\ &= \frac{s + f/J + K_{\omega P}K_T/J}{(s+r_1)(s+r_2)(s+r_3)}\left(As + B + \frac{C}{s}\right) \\ &\quad + \frac{1}{(s+r_1)(s+r_2)(s+r_3)}\frac{\tau_{L0}}{J} \\ &= \frac{c_1}{s+r_1} + \frac{c_2}{s+r_2} + \frac{c_3}{s+r_3} + \frac{c_4}{s} + \frac{d_1}{s+r_1} + \frac{d_2}{s+r_2} + \frac{d_3}{s+r_3} \end{aligned}$$

where

$$\begin{aligned} c_4 &= \lim_{s\to 0} sE_1(s) = \frac{f/J + K_{\omega P}K_T/J}{r_1 r_2 r_3}C \\ &= \frac{r_1 + r_2 + r_3}{r_1 r_2 r_3}C \neq 0 \text{ if } C \neq 0. \end{aligned}$$

Note that $C \neq 0$ if there is a parabolic term in the input (i.e., $t^2/2$). However, if r_1, r_2 and r_3 are large so that the closed-loop poles are far in the left-half plane, then c_4 will be small. In the time domain,

$$\begin{aligned} e(t) &= c_1 e^{-r_1 t} + c_2 e^{-r_2 t} + c_3 e^{-r_3 t} + c_4 u_s(t) + d_1 e^{-r_1 t} + d_2 e^{-r_2 t} + d_3 e^{-r_3 t} \\ &\to c_4 \text{ as } t \to \infty. \end{aligned}$$

This control structure cannot track parabolic type inputs (i.e., $t^2/2$) with zero steady-state error, but if the poles are far enough in the left-half plane, then it will track such an input for all *practical* purposes. Thus good tracking of the reference input with a constant load torque on the motor can be obtained if the poles can be put far enough in the left-half plane (i.e., if the gains can be chosen large enough without causing the amplifier to saturate).

Using the state space approach, it was shown that *any* reference trajectory of the form $\theta_{ref}(t), \omega_{ref}(t) = d\theta_{ref}(t)/dt, \alpha_{ref}(t) = d\omega_{ref}(t)/dt$ with reference input $i_{ref}(t) = (J\alpha_{ref}(t) + f\omega_{ref}(t))/K_T$ can be tracked with zero steady-state error even with a constant load torque acting on the motor. Recall that the reference trajectory used for the state feedback controller had a *continuous* acceleration and the corresponding position reference had the polynomial terms $t^3/3$ and $t^4/4$ with Laplace transforms $2/s^4, 6/s^5$, respectively. The PID nested loop controller above cannot track this reference profile with zero steady-state error.

Another important comparison with the state feedback controller is that of setting the gains. The relationship between the feedback gains and the

www.EngineeringEBooksPdf.com

coefficients of the desired closed-loop characteristic polynomial is always linear in the case of the state feedback controller as illustrated in (2.18). However, in the case of the feedback structure of Figure 2.15, the relationship between the gains and the closed-loop poles is nonlinear [see equation (2.22) and problem 23]. Though (2.22) was readily solvable for the gains, higher-order systems will not be (see problems 24 and 27).

2.6 Identification of the DC Motor Parameters*

Recall the mathematical model of the DC motor given by

$$\begin{aligned} L\frac{di}{dt} &= -Ri(t) - K_b\omega(t) + v(t) \\ J\frac{d\omega}{dt} &= -f\omega(t) + K_T i(t) \\ \frac{d\theta}{dt} &= \omega(t). \end{aligned} \tag{2.27}$$

In order to design a controller based on these equations, the values of the motor parameters $L, R, K_b = K_T, J$, and f need to be found. This can be done by an experiment in which a voltage is commanded into the amplifier of the motor and the measured data $v(t), i(t)$, and $\omega(t)$ is then used to determine the parameters. To understand how this is accomplished, the first two equations above are rewritten as

$$\begin{bmatrix} di/dt & i(t) & \omega(t) & 0 & 0 \\ 0 & 0 & -i(t) & d\omega/dt & \omega(t) \end{bmatrix} \begin{bmatrix} L \\ R \\ K_T \\ J \\ f \end{bmatrix} = \begin{bmatrix} v(t) \\ 0 \end{bmatrix}. \tag{2.28}$$

This is a system of two linear algebraic equations in the unknowns L, R, K_T, J and f. The coefficients of this system of linear equations are found from the measured/calculated data $\theta(t), \omega(t), d\omega/dt, i(t), di/dt, v$.

If the model of the motor is precisely given by (2.27) and the quantities $\theta(t), i(t)$, and $v(t)$ can be measured exactly along with the derivatives $d\theta/dt, d\omega/dt$, and di/dt computed exactly, then equation (2.28) must hold for all time t. Let $\omega(nT)$ denote the speed at time nT, $i(nT)$ denote the current at time nT, $di(nT)/dt$ the derivative of the current at time nT,

www.EngineeringEBooksPdf.com

and so on. Define

$$W(nT) \triangleq \begin{bmatrix} \frac{di}{dt}(nT) & i(nT) & \omega(nT) & 0 & 0 \\ 0 & 0 & -i(nT) & \frac{d\omega}{dt}(nT) & \omega(nT) \end{bmatrix} \in \mathbb{R}^{2\times 5}$$

$$y(nT) \triangleq \begin{bmatrix} v(nT) \\ 0 \end{bmatrix} \in \mathbb{R}^2$$

$$K \triangleq \begin{bmatrix} L \\ R \\ K_T \\ J \\ f \end{bmatrix} \in \mathbb{R}^5$$

so that equation (2.28) above may be written in the form

$$W(nT)K = y(nT). \tag{2.29}$$

W is referred to as the *regressor* matrix. The desire here is to find the constant vector K that satisfies this for all n! To do so, multiply both sides of (2.29) by $W^T(nT)$ to obtain

$$W^T(nT)W(nT)K = W^T(nT)y(nT) \tag{2.30}$$

where

$$\begin{aligned} &W^T(nT)W(nT) \\ &= \begin{bmatrix} \frac{di(nT)}{dt} & 0 \\ i(nT) & 0 \\ \omega(nT) & -i(nT) \\ 0 & \frac{d\omega(nT)}{dt} \\ 0 & \omega(nT) \end{bmatrix} \begin{bmatrix} \frac{di(nT)}{dt} & i(nT) & \omega(nT) & 0 & 0 \\ 0 & 0 & -i(nT) & \frac{d\omega(nT)}{dt} & \omega(nT) \end{bmatrix} \\ &= \begin{bmatrix} (di/dt)^2 & idi/dt & \omega di/dt & 0 & 0 \\ idi/dt & i^2 & \omega i & 0 & 0 \\ \omega di/dt & \omega i & \omega^2 + i^2 & -id\omega/dt & -\omega i \\ 0 & 0 & -id\omega/dt & (d\omega/dt)^2 & \omega d\omega/dt \\ 0 & 0 & -\omega i & \omega d\omega/dt & \omega^2 \end{bmatrix} \Bigg| \, t = nT \end{aligned} \tag{2.31}$$

www.EngineeringEBooksPdf.com

and

$$W^T(nT)y(nT) = \begin{bmatrix} di(nT)/dt & 0 \\ i(nT) & 0 \\ \omega(nT) & -i(nT) \\ 0 & d\omega(nT)/dt \\ 0 & \omega(nT) \end{bmatrix} \begin{bmatrix} v(nT) \\ 0 \end{bmatrix}$$
$$= \begin{bmatrix} v(nT)di(nT)/dt \\ v(nT)i(nT) \\ v(nT)\omega(nT) \\ 0 \\ 0 \end{bmatrix}.$$

Note that $W^T(nT)W(nT) \in \mathbb{R}^{5\times 5}$; that is, it is a square matrix. It would then be convenient if it were possible to multiply both sides of (2.30) by $\left(W^T(nT)W(nT)\right)^{-1}$ to solve for K. However, $W^T(nT)W(nT)$ is *never* invertible! To see this, note that if one multiplies the first row of $W^T(nT)W(nT)$ by $-i(n)$, the second row by $di(nT)/dt$ and adds them, the result is zero. That is,

$$\begin{bmatrix} -i(nT) & di(nT)/dt & 0 & 0 & 0 \end{bmatrix} W^T(nT)W(nT) \equiv \begin{bmatrix} 0 & 0 & 0 & 0 & 0 \end{bmatrix}. \tag{2.32}$$

Now, if $W^T(n)W(nT)$ were invertible, one could multiply both sides of (2.32) by this inverse to obtain

$$\begin{bmatrix} -i(nT) & di(nT)/dt & 0 & 0 & 0 \end{bmatrix} W^T(n)W(nT)\left(W^T(nT)W(nT)\right)^{-1}$$
$$= \begin{bmatrix} 0 & 0 & 0 & 0 & 0 \end{bmatrix}\left(W^T(n)W(nT)\right)^{-1}$$

or

$$\begin{bmatrix} -i(nT) & di(nT)/dt & 0 & 0 & 0 \end{bmatrix} = \begin{bmatrix} 0 & 0 & 0 & 0 & 0 \end{bmatrix}$$

which is a contradiction, as the current does not have to be zero.

Something else has to be done. As equation (2.30) must hold for all n with K a fixed parameter vector, sum up equation (2.30) for N time instants to obtain

$$\left(\sum_{n=1}^{N} W^T(nT)W(nT)\right)K = \sum_{n=1}^{N} W^T(nT)y(nT) \tag{2.33}$$

Define

$$\begin{aligned} R_W &\triangleq \sum_{n=1}^{N} W^T(nT)W(nT) \in \mathbb{R}^{5\times 5} \\ R_{Wy} &\triangleq \sum_{n=1}^{N} W^T(nT)y(nT) \in \mathbb{R}^{5\times 1} \end{aligned} \tag{2.34}$$

www.EngineeringEBooksPdf.com

Then rewrite (2.33) as

$$R_W K = R_{Wy}. \tag{2.35}$$

Suppose the matrix sum $R_W \triangleq \sum_{n=1}^{N} W^T(nT)W(nT)$ is invertible, then multiply both sides of (2.35) by $R_W^{-1} \triangleq \left(\sum_{n=1}^{N} W^T(nT)W(nT)\right)^{-1}$ to obtain K as

$$K = R_W^{-1} R_{Wy}. \tag{2.36}$$

The key to this method is making sure R_W is invertible. This requires choosing a suitable input to the motor, that is, any arbitrary input will not work. For example, suppose $v(t) \equiv 0$ so that $i(t) \equiv 0$ and thus $\omega(t) \equiv 0$. In this case, $W(nT) \equiv 0$ for all n so that $R_W \triangleq \sum_{n=1}^{N} W^T(nT)W(nT) \equiv 0$ and is therefore *not* invertible. As a less trivial example, suppose $i(t) = i_0$ is constant. Then, equation (2.31) shows that the first row of $W^T(nT)W(nT)$ is identically zero for all n and therefore, the first row of R_W is identically zero for all n so that R_W is *not* invertible. Finally, if an experiment was performed where $\omega(t) \equiv \omega_0$ is constant, then the fourth row of R_W is identically zero and thus again, R_W is *not* invertible. It is up to the control engineer to design an input so that the invertibility condition holds. If such an input results in R_W being invertible, then one says the system has been *sufficiently excited.*

2.6.1 *Least-Squares Approximation*

The above analysis was based on the equation $W(nT)K = y(nT)$ being true for all n. However, in the "real-world" that engineers work, this is never true. The model (2.27) is not an exact description of the motor (i.e., it was derived assuming ideal magnetic materials, etc.), the voltage $v(t)$, current $i(t)$ and position $\theta(t)$ cannot be measured perfectly, and the derivatives $\omega(t) = d\theta/dt, d\omega/dt$, and di/dt cannot be computed exactly. Thus, there will not be a parameter vector K that satisfies $W(nT)K = y(nT)$ for all n. One can still run an experiment and collect the data $v(t), i(t)$, and $\theta(t)$ to compute R_W and R_{Wy}, and thus determine

$$\hat{K} = R_W^{-1} R_{Wy}.$$

The key question is then "How well does $\hat{K} = R_W^{-1} R_{Wy}$ satisfy $W(nT)K = y(nT)$ for all n?" To answer this question, let

$$W(nT) \triangleq \begin{bmatrix} di(nT)/dt & i(nT) & \omega(nT) & 0 & 0 \\ 0 & 0 & -i(nT) & d\omega(nT)/dt & \omega(nT) \end{bmatrix} \in \mathbb{R}^{2\times 5}$$

$$y(nT) \triangleq \begin{bmatrix} v(nT) \\ 0 \end{bmatrix} \in \mathbb{R}^2$$

and define the error

$$e(nT) \triangleq y(nT) - W(nT)K \in \mathbb{R}^2.$$

www.EngineeringEBooksPdf.com

The problem is then one of finding the value of K that makes this difference as small as possible for all n. Specifically, the goal is to find the value of K that minimizes the squared error given by

$$\begin{aligned} E^2(K) &\triangleq \sum_{n=1}^{N} (y(nT) - W(nT)K)^T (y(nT) - W(nT)K) \\ &= \sum_{n=1}^{N} (y(nT) - \hat{y}(nT))^T (y(nT) - \hat{y}(nT)) \\ &= \sum_{n=1}^{N} (y_1(nT) - \hat{y}_1(nT))^2 + (y_2(nT) - \hat{y}_2(nT))^2 \\ &= \sum_{n=1}^{N} \left(e_1(nT)^2 + e_2(nT)^2\right) \end{aligned}$$

where $e_1(nT) \triangleq y_1(nT) - \hat{y}_1(nT), e_2(nT) \triangleq y_2(nT) - \hat{y}_2(nT)$.

In the jargon of identification theory, $y(nT)$ is considered the *output* while $\hat{y}(nT) = W(nT)K$ is the *predicted output* based on K as the estimate of the parameters. Consequently,

$$e(nT) \triangleq y(nT) - W(nT)K = y(nT) - \hat{y}(nT) \in \mathbb{R}^2$$

is the *error* and

$$E^2(K) \triangleq \sum_{n=1}^{N} (y(nT) - W(nT)K)^T (y(nT) - W(nT)K) \tag{2.37}$$

is the total *squared error*. If a K can be found that minimizes equation (2.37), it is referred to as the *least-squares* estimate.

It is now shown that there is a unique solution and it equals $R_W^{-1} R_{Wy}$. To do so, expand equation (2.37) above to obtain [recall the matrix fact $(AB)^T = B^T A^T$]

$$\begin{aligned} E^2(K) = \sum_{n=1}^{N} \Big(& y^T(nT)y(nT) - y^T(nT)W(nT)K - K^T W^T(nT)y(nT) \\ & + K^T W^T(nT)W(nT)K \Big) \\ = \sum_{n=1}^{N} & y^T(nT)y(nT) - \left(\sum_{n=1}^{N} y^T(nT)W(nT)\right)K \\ & - K^T \left(\sum_{n=1}^{N} W^T(nT)y(nT)\right) + K^T \left(\sum_{n=1}^{N} W^T(nT)W(nT)\right)K. \end{aligned}$$

www.EngineeringEBooksPdf.com

Adding to the definitions given in (2.34), define

$$\begin{aligned} R_{yW} &\triangleq \sum_{n=1}^{N} y^T(nT)W(nT) \in \mathbb{R}^{1\times 5} \\ R_y &\triangleq \sum_{n=1}^{N} y^T(nT)y(nT) \in \mathbb{R} \end{aligned}$$

where it is clear that $R_{yW} = R_{Wy}^T$. Then $E^2(K)$ is written compactly as

$$\begin{aligned} E^2(K) &= R_y - R_{yW}K - K^T R_{Wy} + K^T R_W K \\ &= R_y - R_{yW}R_W^{-1}R_{Wy} + \left(K - R_W^{-1}R_{Wy}\right)^T R_W \left(K - R_W^{-1}R_{Wy}\right). \end{aligned} \tag{2.38}$$

For a fixed N, the matrices R_y, R_{yW}, R_{Wy}, and R_W are constant and do not depend K. Also, R_W is a *symmetric positive semidefinite* matrix.

Digression [41] A matrix Q is *symmetric* if $Q^T = Q$. A symmetric matrix $Q \in \mathbb{R}^{m\times m}$ is *positive semidefinite* if for all $x \in \mathbb{R}^m$, $x^TQx \geq 0$. Further, Q is *positive definite* if $x^TQx \geq 0$ for all $x \in \mathbb{R}^m$ *and* $x^TQx = 0$ if and only if x is the zero vector (i.e., $x = 0$).

For example, let

$$Q_1 = \begin{bmatrix} 1 & 0 \\ 0 & 2 \end{bmatrix}$$

and note that $Q_1 = Q_1^T$. Also,

$$x^TQ_1x = \begin{bmatrix} x_1 & x_2 \end{bmatrix}^T \begin{bmatrix} 1 & 0 \\ 0 & 2 \end{bmatrix} \begin{bmatrix} x_1 \\ x_2 \end{bmatrix} = x_1^2 + 2x_2^2 \geq 0$$

for all $x \in \mathbb{R}^2$ and the only way it can equal zero is if $x_1 = 0, x_2 = 0$. That is, Q_1 is positive definite.

As another example, let

$$Q_1 = \begin{bmatrix} 0 & 0 \\ 0 & 2 \end{bmatrix}$$

and note that $Q_2 = Q_2^T$. Also,

$$x^TQ_2x = \begin{bmatrix} x_1 & x_2 \end{bmatrix}^T \begin{bmatrix} 0 & 0 \\ 0 & 2 \end{bmatrix} \begin{bmatrix} x_1 \\ x_2 \end{bmatrix} = 2x_2^2 \geq 0$$

for all $x \in \mathbb{R}^2$. Thus Q_2 is positive semidefinite. However, in this case, the nonzero vector $x = \begin{bmatrix} 1 & 0 \end{bmatrix}^T$ makes $x^TQ_2x = 0$; that is, Q_2 is not positive definite.

www.EngineeringEBooksPdf.com

As a final example, let

$$Q_3 = \begin{bmatrix} -1 & 0 \\ 0 & 2 \end{bmatrix}$$

and note that $Q_3 = Q_3^T$. Also,

$$x^T Q_3 x = \begin{bmatrix} x_1 & x_2 \end{bmatrix}^T \begin{bmatrix} -1 & 0 \\ 0 & 2 \end{bmatrix} \begin{bmatrix} x_1 \\ x_2 \end{bmatrix} = -x_1^2 + 2x_2^2$$

In this case, $x^T Q_3 x$ can be positive (e.g., $x = [0\ 1]^T$) or negative (e.g., $x = [1\ 0]^T$) depending on the chosen value of the vector x. Consequently, Q_3 is neither positive definite nor positive semidefinite.

■

To show that R_W is positive semidefinite, for any $x \in \mathbb{R}^5$, it follows that

$$\begin{aligned} x^T W^T(nT) W(nT) x &= (W(nT)x)^T (W(nT)x) = z^T(nT) z(nT) \\ &= z_1^2(nT) + z_2^2(nT) \geq 0 \end{aligned}$$

where $z(nT) \triangleq W(nT)x \in \mathbb{R}^2$. Thus,

$$\begin{aligned} x^T R_W x &= x^T \left(\sum_{n=1}^{N} W^T(nT) W(nT) \right) x \\ &= \sum_{n=1}^{N} x^T W^T(nT) W(nT) x \geq 0. \end{aligned}$$

The control engineer will design the experiment, that is, the specification of $v(t)$ and $i(t)$, so that R_W is invertible. It turns out that if a symmetric, positive semidefinite matrix is also *invertible*, then it must be positive definite. Consequently, R_W is then positive definite so that second term in (2.38) satisfies .

$$\left(K - R_W^{-1} R_{Wy}\right)^T R_W \left(K - R_W^{-1} R_{Wy}\right) \geq 0$$

for all $K \in \mathbb{R}^5$. This equals zero if and only if

$$K - R_W^{-1} R_{Wy} = \begin{bmatrix} 0 & 0 & 0 & 0 & 0 \end{bmatrix}^T.$$

That is, by inspection of equation (2.38), $E^2(K)$ is minimized for $K = \hat{K} = R_W^{-1} R_{Wy}$! Thus, choosing $K = \hat{K} = R_W^{-1} R_{Wy}$ results in the *least*-squared error. The " ˆ " in $\hat{K}$ is used to denote an *estimate* of K. However, the least squares estimate is an *optimal* estimate as it *minimizes* the least-squares error. Then the convention is to use an asterisk $*$ to denote an optimal estimate and so $K^* \triangleq R_W^{-1} R_{Wy}$ is now used.

www.EngineeringEBooksPdf.com

2.6.2 Error Index

How good is the least-squares estimate? Well, the exact value of K is not known so the error between the "exact" value of the parameter vector and its estimate (i.e., $K - K^*$) is unknown. However, an indication of how good the estimate K^* is can be found by comparing it to a given (and thus known) value of K. Specifically, if $K = 0$, then the squared error is $E(0) = R_y$ as seen by putting $K = 0$ in equation (2.38) above. Using the least-squares estimate K^*, that is, setting $K = K^* \triangleq R_W^{-1} R_{Wy}$ in equation (2.38), the error is given by

$$E^2(K)_{|K=K^* \triangleq R_W^{-1} R_{Wy}} = R_y - R_{yW} R_W^{-1} R_{Wy}.$$

This is called the *residual* error; that is, it is the total squared error after using the value of K that minimizes the squared error. As R_W is positive definite, it turns out that its inverse R_W^{-1} must also be positive definite. Further, $R_{yW} \in \mathbb{R}^{1\times 5}, R_{Wy} \in \mathbb{R}^{5\times 1}$ with $R_{yW} = R_{Wy}^T$, it follows that $R_{yW} R_W^{-1} R_{Wy} \geq 0$ so that $E^2(K^*) = R_y - R_{yW} R_W^{-1} R_{Wy} \leq R_y = E^2(0)$. As a result, the quantity

$$\frac{E^2(K^*)}{E^2(0)} = \frac{R_y - R_{yW} R_W^{-1} R_{Wy}}{R_y} \leq 1.$$

The ratio $E^2(K^*)/E^2(0)$ is a measure of the minimum squared error relative to the squared error obtained from taking the parameter vector K to be the zero vector. By taking the square root, a measure of the relative error rather than squared error is obtained. This motivates the definition of the so-called *error index* as

$$\text{Error Index} \triangleq \sqrt{\frac{E^2(K^*)}{E^2(0)}} = \sqrt{\frac{R_y - R_{yW} R_W^{-1} R_{Wy}}{R_y}} \leq 1.$$

Note that if the error index is close to 1, then the estimate is not much better than taking all the parameter values equal to zero! Thus, the error index must be much less than one for the estimate to be of any value. If the error index is close to one, then one would suspect that the original model of the system is incorrect.

2.6.3 Parametric Error Indices

In addition to the overall error index, it is important to know how sensitive the error is to each parameter. That is, does a change δK_i in the ith parameter K_i produce a large or small change in $E^2(K)$? A small change indicates that the parameter estimate could vary greatly without a large change in the residual error. Thus, the accuracy of the parameter estimate

www.EngineeringEBooksPdf.com

of K_i would be in doubt.[6] On the other hand, a large change indicates that the residual error is very sensitive to changes in the parameter K_i so that such a parameter estimate may be considered more accurate.

In addressing the issue of sensitivity of the full parametric vector K^* to errors, the method in Ref. [42] is considered. If follows from (2.38) that K^* satisfies

$$\left.\frac{\partial E^2(K)}{\partial K}\right|_{K=K^*} = \left. 2R_W \left(K - R_W^{-1} R_{Wy}\right)\right|_{K=K^*} = 0 \tag{2.39}$$

so that, in particular,

$$\left.\frac{\partial E^2(K)}{\partial K_i}\right|_{K=K^*} = 0. \tag{2.40}$$

Therefore, it is not possible to use the derivative $\partial E^2(K)/\partial K_i\big|_{K=K^*}$ of the residual error as a measure of how sensitive the error is with respect to K_i as it is always zero.

An alternative is to define δK as the variation in K such that the increase of error is equal to the residual error $E^2(K^*)$ itself. To explain, recall that

$$\begin{aligned} E^2(K^* + \delta K) &= R_y - 2R_{Wy}^T (K^* + \delta K) + (K^* + \delta K)^T R_W (K^* + \delta K) \\ &= E^2(K^*) + \delta K^T R_W \delta K. \end{aligned} \tag{2.41}$$

The δK's that lead to a doubling of the residual error satisfy

$$\delta K^T R_W \delta K = E^2(K^*). \tag{2.42}$$

This is illustrated in Figure 2.17.

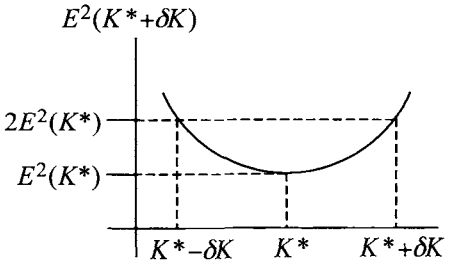


FIGURE 2.17. Illustrating the choice of δK that doubles the minimum mean square error.

The points $\delta K \in \mathbb{R}^5$ that satisfy (8.116) define an *ellipsoid* as illustrated in Figure 2.18.

[6] In other words, if $K_i + \delta K_i$ produces essentially the same value of $E^2(K)$ as K_i, then one is not sure if $K_i + \delta K_i$ or K_i is the better estimate.

www.EngineeringEBooksPdf.com

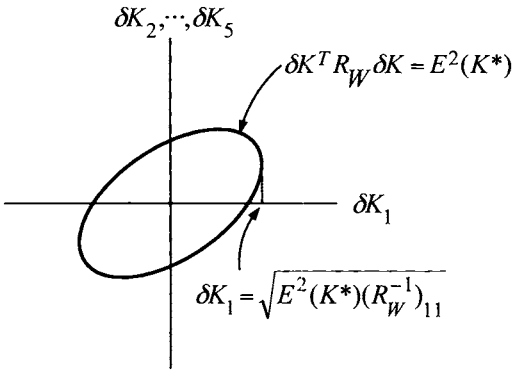


FIGURE 2.18. $\delta K_1 = \sqrt{E^2(K^*)(R_W)_{11}}$ is the largest value of δK_1 that is on the ellipsoid $\delta K^T R_W \delta K = E^2(K^*)$. This is defined as the *parametric error index* for K_1.

Define the *parametric error index* associated to the parameter K_i as the *maximum* value of δK_i such that (8.116) is satisfied. That is, δK_i is the solution to a constrained maximization problem that requires maximizing the quantity

$$\delta K_i$$

subject to the constraint

$$\delta K^T R_W \delta K = E^2(K^*).$$

This is simply the largest possible value for δK_i that would result in $E^2(K^* + \delta K) = 2E^2(K^*)$. This constrained optimization problem can be solved as an unconstrained maximization problem with the help of Lagrange multipliers. To do so, let (see Ref. [42])

$$C(\delta K, \lambda) \triangleq \delta K_i + \lambda\Big(E^2(K^*) - \delta K^T R_W \delta K\Big) \tag{2.43}$$

with respect to δK and λ. To fix ideas, let $i = 1$, and successively differentiate (2.43) with respect to $\delta K_1, \ldots, \delta K_5, \lambda$ so that at the maximum point

www.EngineeringEBooksPdf.com

of (2.43), it follows that

$$\begin{aligned}
\frac{\partial C(\delta K,\lambda)}{\partial \delta K_1} &= 1 - 2\lambda\begin{bmatrix} 1 & 0 & 0 & 0 & 0 \end{bmatrix} R_W \delta K = 0 \\
\frac{\partial C(\delta K,\lambda)}{\partial \delta K_2} &= -2\lambda\begin{bmatrix} 0 & 1 & 0 & 0 & 0 \end{bmatrix} R_W \delta K = 0 \\
\frac{\partial C(\delta K,\lambda)}{\partial \delta K_3} &= -2\lambda\begin{bmatrix} 0 & 0 & 1 & 0 & 0 \end{bmatrix} R_W \delta K = 0 \\
\frac{\partial C(\delta K,\lambda)}{\partial \delta K_4} &= -2\lambda\begin{bmatrix} 0 & 0 & 0 & 1 & 0 \end{bmatrix} R_W \delta K = 0 \\
\frac{\partial C(\delta K,\lambda)}{\partial \delta K_5} &= -2\lambda\begin{bmatrix} 0 & 0 & 0 & 0 & 1 \end{bmatrix} R_{Ww} \delta K = 0 \\
\frac{\partial C(\delta K,\lambda)}{\partial \lambda} &= E^2(K^*) - \delta K^T R_W \delta K = 0.
\end{aligned}$$

This can then be rewritten as

$$\begin{bmatrix} 1 \\ 0 \\ 0 \\ 0 \\ 0 \end{bmatrix} - 2\lambda R_W \delta K = \begin{bmatrix} 0 \\ 0 \\ 0 \\ 0 \\ 0 \end{bmatrix} \tag{2.44}$$

Solving for δK gives

$$\delta K = \frac{1}{2\lambda} R_W^{-1} \begin{bmatrix} 1 \\ 0 \\ 0 \\ 0 \\ 0 \end{bmatrix}. \tag{2.45}$$

To compute λ, multiply both sides of (2.44) by δK^T to obtain

$$\delta K_1 = 2\lambda \delta K^T R_W \delta K = 2\lambda E^2(K^*)$$

and rearranging results in

$$2\lambda = \delta K_1 / E^2(K^*).$$

Substitute this expression for 2λ back into (2.45) to obtain

$$\delta K = \frac{E^2(K^*)}{\delta K_1} R_W^{-1} \begin{bmatrix} 1 \\ 0 \\ 0 \\ 0 \\ 0 \end{bmatrix} \tag{2.46}$$

www.EngineeringEBooksPdf.com

With $\left(R_W^{-1}\right)_{11}$ denoting the $(1,1)$ element of the matrix R_W^{-1}, the first row of (2.46) gives

$$\delta K_1 = \frac{E^2(K^*)}{\delta K_1}\left(R_W^{-1}\right)_{11}$$

or

$$\delta K_1 = \sqrt{E^2(K^*)(R_W^{-1})_{11}}$$

where the + sign was chosen to maximize δK_1. In general (see Ref. [42])

$$\delta K_i = \sqrt{E^2(K^*)(R_W^{-1})_{ii}}. \tag{2.47}$$

The parametric error index δK_i indicates the maximum amount by which K_i, the ith component of K, could vary without causing more than a doubling of the residual error. A large parametric error index indicates that the parameter estimate could vary greatly without a large change in the residual error and thus making the accuracy of the parameter estimates suspect. On the other hand, a small parametric error indicates that the residual error is very sensitive to the changes in the parameter estimates and that the parameter estimates may be considered to be more accurate. In any case, the error indices should not be considered as actual errors, but rather as orders of magnitude of the errors to be expected, to guide the identification process and to warn about unreliable results.

The choice of a parametric error index as corresponding to a doubling of the residual error is arbitrary. A different level of residual error would lead to a scaling of all the components of the parametric error index by a common factor.

www.EngineeringEBooksPdf.com

2.7 Filtering of Noisy Signals*

This section gives a concise discussion of the various ideas in the area of signals and systems that are needed to analyze/process data for implementation of identification and control algorithms. This material is covered in any basic "signals and systems" book such as references [43][44][45].

Recall that the identification algorithm required computing derivatives of the measured data. However, these measured signals typically contain high-frequency low-amplitude noise and the differentiation of such a signal amplifies the noise! That is, a measured signal $m(t)$ is often of the form $m(t) = s(t) + n(t)$, where $s(t)$ is the signal of interest and $n(t)$ is high-frequency low-amplitude noise. For example, Figure 2.19 is a plot of the simulated position measurement of a motor as given by an optical encoder. This signal $m(t) = (2\pi/2000)\,N(t)$ is the measured signal and appears to be right on top of the true signal $s(t) = \theta(t)$.

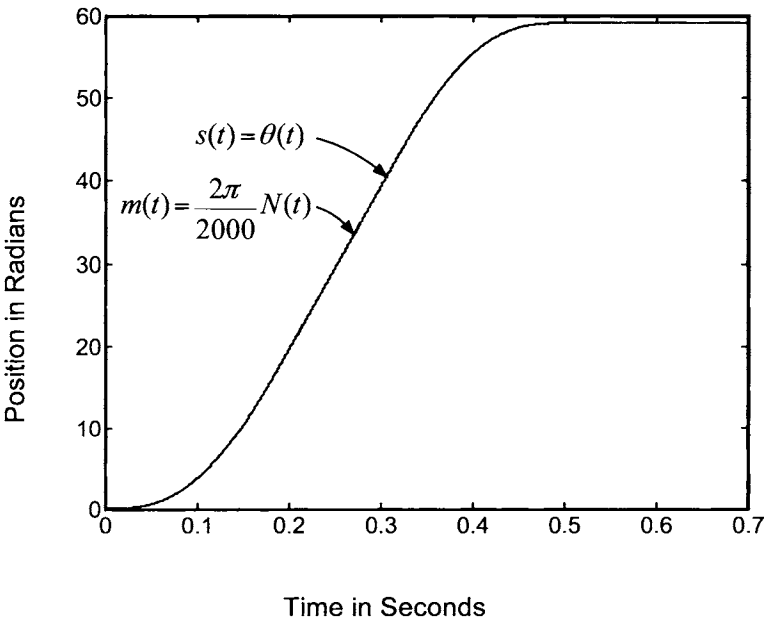


FIGURE 2.19. $\theta(t)$ and the encoder output $(2\pi/2000)N(t)$ in radians versus time in seconds.

Figure 2.20 is a magnification of Figure 2.19 clearly illustrating the discrete nature of the encoder output. The smooth curve $s(t) = \theta(t)$ is the "actual" position of the motor from the simulation and again the measured signal is $m(t) = (2\pi/2000)N(t)$.

www.EngineeringEBooksPdf.com

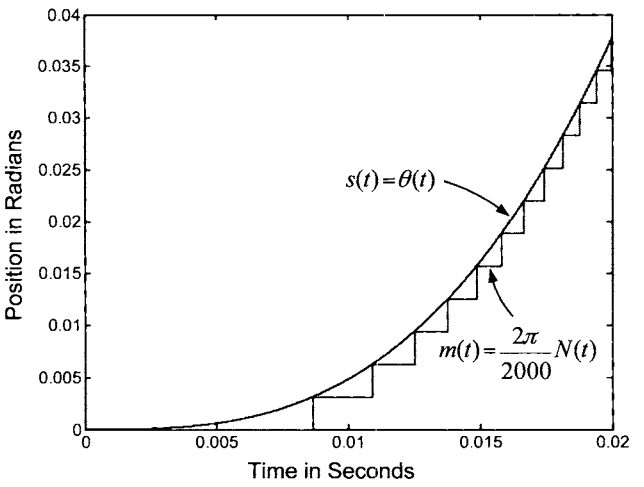


FIGURE 2.20. $\theta(t)$ and the encoder output $(2\pi/2000)N(t)$ in radians vs. time in seconds. Magnification of Figure 2.19.

As this "data set" is from a simulation, the true signal $s(t)$ is known and thus one can calculate the noise $n(t)$ as $n(t) = m(t) - s(t) = (2\pi/2000)N(t) - \theta(t)$, so that $m(t) = s(t) + n(t)$. Figure 2.21 is a plot of the noise $n(t) = (2\pi/2000)N(t) - \theta(t)$, where it is seen that $0 \leq n(t) \leq 3.14 \times 10^{-3}$ radians, that is, it is quite small.

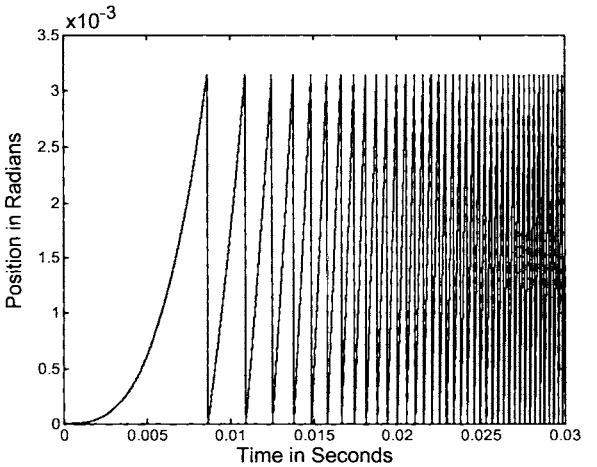


FIGURE 2.21. Position error/noise computed as $n(t) = (2\pi/2000)N(t) - \theta(t)$. The encoder error is bounded by $2\pi/2000 = 3.14 \times 10^{-3}$ radians.

www.EngineeringEBooksPdf.com

To obtain an estimate of $\dot{s}(t)$, the measured signal $m(t) = s(t) + n(t)$ can be numerically differentiated to obtain

$$\frac{s(t) - s(t-T) + n(t) - n(t-T)}{T} = \dot{s}(t) + \dot{n}(t).$$

However, as the difference $n(t) - n(t-T)$ may be of the same order (or higher) of magnitude as $s(t) - s(t-T)$, it follows that $n(t)$ can be of the same order of magnitude as $s(t)$. Going back to the encoder example of Section 2.2, the encoder resolution (error) is $2\pi/2000$ radians where 2000 is the number of counts per revolution so that the noise (error) in the position measurement is bounded by $2\pi/2000$. Computing the speed by numerically differentiating the encoder output results in a tight error bound given by

$$\frac{2\pi}{2000T}$$

where T is the sample period. The sample period T is usually small (on the order of a millisecond) so that $1/T$ is large showing that differentiation amplifies the noise. This is illustrated in Figure 2.22 which was found by differentiating $m(t) = (2\pi/2000)N(t)$ from Figure 2.19 with $T = 0.5$ msec.

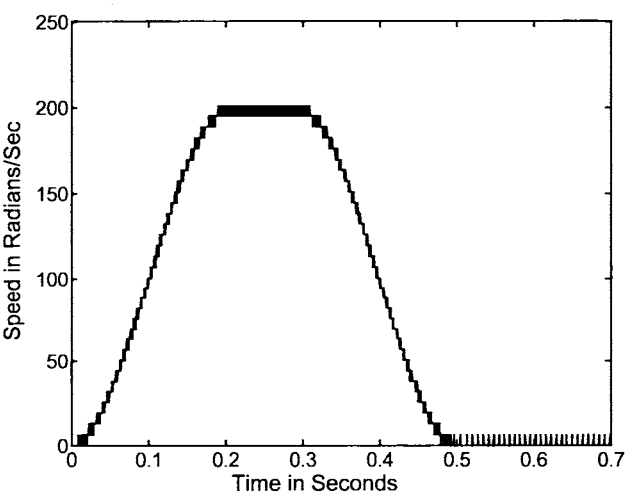


FIGURE 2.22. Estimated angular speed in rads/sec versus time in seconds. Here ω is estimated as $(\theta(nT) - \theta((n-1)T))/T$ with $T = 0.5$ msec resulting in a speed error bound of $\frac{2\pi}{2000T} = 6.28$ radians/sec.

A common way to remove additive high frequency noise is to use a low-pass filter that works as long as the signal $s(t)$ has a much lower

www.EngineeringEBooksPdf.com

frequency content than the noise $n(t)$. For example, let $s(t) = \sin(10t)$ and $n(t) = 0.01\sin(1000t)$ so that $m(t) = s(t) + n(t)$ is the measured signal. Then $\dot{m}(t) = \dot{s}(t) + \dot{n}(t) = 10\cos(10t) + 10\cos(1000t)$. Although $|n(t)| \ll |s(t)|$, the differentiated noise $\dot{n}(t)$ is of the same order of magnitude as the differentiated signal $\dot{s}(t)$. However, by setting the cutoff of the low-pass filter at (say) 100 rad/sec, then $s(t)$ will make it through the filter essentially unchanged and $n(t)$ will be filtered out. Before going into detail of how to design such a filter, some basic facts about filtering are reviewed.

2.7.1 Filter Representations

Let $m(t)$ be the input to the filter and $y(t)$ the output. There are three useful ways to characterize (represent) a causal filter:

(1) Impulse response $g(t)$ so that $y(t) = \int_{-\infty}^{t} g(t-\tau)m(\tau)d\tau$.

(2) Transfer function $G(s)$ so that $Y(s) = G(s)M(s)$
where $Y(s) = \int_0^\infty e^{-st}y(t)dt, G(s) = \int_0^\infty e^{-st}g(t)dt, M(s) = \int_0^\infty e^{-st}m(t)dt$.

(3) Differential equation $\dot{x}(t) = Ax(t) + bm(t), y(t) = cx(t) + dm(t)$
where $x \in \mathbb{R}^n, y \in \mathbb{R}, m \in \mathbb{R}, A \in \mathbb{R}^{n\times n}, b \in \mathbb{R}^n, c \in \mathbb{R}^{1\times n}$.

Example
Consider an impulse response given by

$$g(t) = \begin{cases} e^{-at} & t \geq 0 \\ 0 & t < 0. \end{cases}$$

In terms of $g(t)$, the filter is given by the convolution integral

$$y(t) = \int_{-\infty}^{t} g(t-\tau)m(\tau)d\tau = \int_{-\infty}^{t} e^{-a(t-\tau)}m(\tau)d\tau.$$

The corresponding transfer function is

$$\begin{aligned} G(s) &= \int_0^\infty e^{-st}e^{-at}dt = \frac{1}{s+a} \\ Y(s) &= \frac{1}{s+a}M(s). \end{aligned}$$

The state space (differential equation) representation is

$$\begin{aligned} \dot{x}(t) &= -ax(t) + m(t) \\ y(t) &= x(t). \end{aligned}$$

www.EngineeringEBooksPdf.com

2.7.2 Causality

A more general representation of a linear filter is $y(t) = \int_{-\infty}^{\infty} g(t-\tau)m(\tau)d\tau$. However, recall that for a filter to be causal, the output $y(t)$ of the filter can only depend on the input $m(\tau)$ up to time t, that is, on $m(\tau)$ for $-\infty < \tau < t$. As a consequence of this causality requirement, in the representation $y(t) = \int_{-\infty}^{\infty} g(t-\tau)m(\tau)d\tau$, it follows that $g(t) \equiv 0$ for $t < 0$. If this were not the case, then for some $\tau > t$ (i.e., $t - \tau < 0$), $g(t-\tau)$ would not be zero and $g(t-\tau)m(\tau)d\tau$ would be the contribution of the *input* at time $\tau > t$ to the output response $y(t)$ at time t! Consequently, a causal filter may be written as $y(t) = \int_{-\infty}^{\infty} g(t-\tau)m(\tau)d\tau = \int_{-\infty}^{t} g(t-\tau)m(\tau)d\tau$ as $g(t-\tau) = 0$ for $\tau > t$.

As just explained, the impulse response model provides a simple way of characterizing the causality of a filter. The differential equation representation provides the means of actually *implementing* a filter as will be shown below. On the other hand, the transfer function representation is particularly easy to work with as it allows one to just do algebraic manipulations as opposed to working with a differential equation or a convolution integral. It is also quite useful for filter design and specification as is shown in the next section.

2.7.3 Frequency Response

Consider a filter represented as $y(t) = \int_{-\infty}^{\infty} g(t-\tau)m(\tau)d\tau$ with an input given by $m(t) = e^{st}$ for $-\infty < t < \infty$ and $s = \sigma + j\omega$ is *constant*. Then, the response is given by

$$\begin{aligned} y(t) &= \int_{-\infty}^{\infty} g(t-\tau)e^{s\tau}d\tau = \int_{-\infty}^{\infty} g(t-\tau)e^{-s(t-\tau)}e^{st}d\tau \\ &= e^{st}\int_{-\infty}^{\infty} g(t-\tau)e^{-s(t-\tau)}d\tau = e^{st}\int_{-\infty}^{\infty} g(u)e^{-su}du \\ &= e^{st}\int_{0}^{\infty} g(u)e^{-su}du \\ &= G(s)e^{st}. \end{aligned}$$

In particular, if $s = j\omega$ so that $m(t) = e^{j\omega t} = \cos(\omega t) + j\sin(\omega t)$,

$$\begin{aligned} y(t) &= G(j\omega)e^{j\omega t} = |G(j\omega)|\, e^{j\angle G(j\omega)}e^{j\omega t} \\ &= |G(j\omega)|\left(\cos(\omega t + \angle G(j\omega)) + j\sin(\omega t + \angle G(j\omega))\right). \end{aligned}$$

Considering just the real part, the input $m(t) = \cos(\omega t)$ for $-\infty < t < \infty$ results in the output $y(t) = |G(j\omega)|\cos(\omega t + \angle G(j\omega))$ for $-\infty < t < \infty$.

www.EngineeringEBooksPdf.com

2.7.4 *Low-Pass Filters with Linear Phase*

Suppose for a given *bandwidth* specification ω_b, one is able to design a filter $G(j\omega)$ such that its magnitude response satisfies

$$\begin{aligned} |G(j\omega)| &\leq 1 \qquad \text{for all } \omega \\ |G(j\omega)| &\approx 1 \qquad \text{for } 0 \leq \omega \leq \omega_b < \omega_c \\ &\approx 0 \qquad \text{for } \omega \geq 2\omega_c \end{aligned}$$

where ω_c is referred to as the *cutoff frequency* (see Figure 2.23). Further, suppose the phase response of the filter has the property that

$$\angle G(j\omega) \approx -\gamma\omega \text{ for } 0 \leq \omega \leq \omega_b \qquad \text{where } \gamma > 0.$$

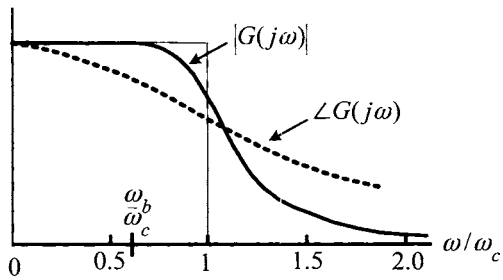


FIGURE 2.23. Magnitude and phase of a low-pass filter.

Then, if the input to this filter is $m(t) = \cos(\omega t)$ with $\omega \leq \omega_b$, the output is given by

$$\begin{aligned} y(t) &= |G(j\omega)| \cos(\omega t + \angle G(j\omega)) \\ &\approx \cos(\omega t - \gamma\omega) \\ &= \cos(\omega(t - \gamma)) \end{aligned}$$

that is, the output is the same as the input except delayed by the time γ. Carrying this idea further, consider the input $m(t) = A_1 \cos(\omega_1 t) + A_2 \cos(\omega_2 t)$ where $\omega_1 < \omega_2 \leq \omega_b < \omega_c$. Then, the corresponding output is

$$\begin{aligned} y(t) &= |G(j\omega_1)| A_1 \cos(\omega_1 t + \angle G(j\omega_1)) + |G(j\omega_2)| A_2 \cos(\omega_2 t + \angle G(j\omega_2)) \\ &\approx A_1 \cos(\omega_1(t - \gamma)) + A_2 \cos(\omega_2(t - \gamma)) \\ &= m(t - \gamma). \end{aligned}$$

Again, the output of the filter is the same as the input except delayed by the time γ.

The usual application of a low-pass filter is to the following situation: There is a signal $s(t)$ with high-frequency additive noise $n(t)$ corrupting it.

www.EngineeringEBooksPdf.com

That is, the signal measured is $m(t) = s(t)+n(t)$ and the desire is to extract the signal $s(t)$ from $m(t)$. For example, let $s(t) = A_1 \cos(\omega_1 t)+A_2 \cos(\omega_2 t)$, $n(t) = N_0 \cos(\omega_N t)$ with $\omega_1 < \omega_2 << \omega_N$ and $m(t) = s(t) + n(t)$. Suppose a low-pass linear-phase filter can be found (as described above) with $\omega_1 < \omega_2 \leq \omega_b < \omega_c << \omega_N$. Then the output of the filter is given by

$$\begin{aligned} y(t) &= |G(j\omega_1)|\, A_1 \cos(\omega_1 t + \angle G(j\omega_1)) + |G(j\omega_2)|\, A_2 \cos(\omega_2 t + \angle G(j\omega_2)) \\ &\quad + |G(j\omega_N)|\, N_0 \cos(\omega_N t + \angle G(j\omega_N)) \\ &\approx A_1 \cos(\omega_1 (t-\gamma)) + A_2 \cos(\omega_2 (t-\gamma)) \\ &= s(t-\gamma) \end{aligned} \tag{2.48}$$

as $|G(j\omega_N)| \approx 0$. The desired signal has been extracted from the noise, but it is delayed by γ seconds.

2.7.5 *Distortion*

The magnitude specification of the filter as $|G(j\omega)| \approx 1$ for $0 \leq \omega \leq \omega_b < \omega_c$ and $|G(j\omega)| \approx 0$ for $\omega \geq 2\omega_c$ is necessary to remove the high-frequency noise. The angle specification of $\angle G(j\omega) \approx -\gamma\omega$ for $0 \leq \omega \leq \omega_b < \omega_c$, $\gamma > 0$ (linear phase) is required to prevent distortion of the signal. That is, suppose $G(j\omega)$ did not have linear phase so that $\angle G(j\omega_1) \approx -\gamma_1\omega_1, \angle G(j\omega_2) \approx -\gamma_2\omega_2$ with $\gamma_1 \neq \gamma_2$, then with $m(t) = A_1 \cos(\omega_1 t) + A_2 \cos(\omega_2 t) + N_0 \cos(\omega_N t)$ applied to the filter, the output would be

$$\begin{aligned} y(t) &= |G(j\omega_1)|\, A_1 \cos(\omega_1 t + \angle G(j\omega_1)) + |G(j\omega_2)|\, A_2 \cos(\omega_2 t + \angle G(j\omega_2)) \\ &\quad + |G(j\omega_N)|\, N_0 \cos(\omega_N t + \angle G(j\omega_N)) \\ &\approx A_1 \cos(\omega_1 (t-\gamma_1)) + A_2 \cos(\omega_2 (t-\gamma_2)) \\ &\neq s(t-\gamma) \end{aligned}$$

for some $\gamma > 0$. That is, *distortion* in the signal results since the output of the filter is not an exact (delayed) reproduction of the desired signal.

2.7.6 *Low-Pass Filtering of High-Frequency Noise*

Now consider an arbitrary signal $s(t)$ where the measured signal is given by $m(t) = s(t) + n(t)$ and the noise $n(t)$ is assumed to have a much higher frequency content than $s(t)$. To understand the filter's effect on these signals, Fourier transform theory is used. The Fourier transforms of these signals

www.EngineeringEBooksPdf.com

are

$$\begin{aligned} M(j\omega) &= \int_{-\infty}^{+\infty} e^{-j\omega t} m(t)dt \\ S(j\omega) &= \int_{-\infty}^{+\infty} e^{-j\omega t} s(t)dt \\ N(j\omega) &= \int_{-\infty}^{+\infty} e^{-j\omega t} n(t)dt. \end{aligned}$$

where $M(j\omega) = S(j\omega) + N(j\omega)$. Their inverse Fourier transforms are given by

$$\begin{aligned} m(t) &= \frac{1}{2\pi}\int_{-\infty}^{+\infty} e^{j\omega t} M(j\omega)d\omega \\ s(t) &= \frac{1}{2\pi}\int_{-\infty}^{+\infty} e^{j\omega t} S(j\omega)d\omega \\ n(t) &= \frac{1}{2\pi}\int_{-\infty}^{+\infty} e^{j\omega t} N(j\omega)d\omega. \end{aligned}$$

Recall that $\frac{1}{2\pi}M(j\omega)d\omega$ is interpreted as the frequency content of $m(t)$ between ω and $\omega + d\omega$. As shown in (2.48), when $\frac{1}{2\pi}e^{j\omega t}M(j\omega)d\omega$ is passed through the filter, the output is $\frac{1}{2\pi}e^{j\omega t}G(j\omega)M(j\omega)d\omega$. Consequently, when $m(t)$ is input to the filter, the output $y(t)$ of the filter is given by

$$\begin{aligned} y(t) &= \frac{1}{2\pi}\int_{-\infty}^{+\infty} e^{j\omega t} G(j\omega)M(j\omega)d\omega \\ &= \frac{1}{2\pi}\int_{-\infty}^{+\infty} e^{j\omega t} G(j\omega)S(j\omega)d\omega + \frac{1}{2\pi}\int_{-\infty}^{+\infty} e^{j\omega t} G(j\omega)N(j\omega)d\omega. \end{aligned}$$

As explained above, to have a low-pass filter remove the noise, the frequency content of $n(t)$ must be much higher than that of $s(t)$. Thus, assuming that

www.EngineeringEBooksPdf.com

$S(j\omega) \approx 0$ for $|\omega| > \omega_b$ and $|N(j\omega)| \approx 0$ for $|\omega| < 2\omega_c$,

$$\begin{aligned}
y(t) &= \frac{1}{2\pi}\int_{-\infty}^{\infty} e^{j\omega t}G(j\omega)S(j\omega)d\omega + \frac{1}{2\pi}\int_{-\infty}^{\infty} e^{j\omega t}G(j\omega)N(j\omega)d\omega \\
&= \frac{1}{2\pi}\int_{-\omega_b}^{+\omega_b} e^{j\omega t}G(j\omega)S(j\omega)d\omega + \frac{1}{2\pi}\int_{-\infty}^{-2\omega_c} e^{j\omega t}G(j\omega)N(j\omega)d\omega \\
&\quad + \frac{1}{2\pi}\int_{2\omega_c}^{\infty} e^{j\omega t}G(j\omega)N(j\omega)d\omega \text{ (as } |N(j\omega)| \approx 0 \text{ for } |\omega| < 2\omega_c) \\
&= \frac{1}{2\pi}\int_{-\omega_b}^{+\omega_b} e^{j\omega t}G(j\omega)S(j\omega)d\omega \text{ as } |G(j\omega)| \approx 0 \text{ for } |\omega| > 2\omega_c \\
&= \frac{1}{2\pi}\int_{-\omega_b}^{+\omega_b} e^{j\omega(t-\gamma)}S(j\omega)d\omega \quad \left(\begin{array}{c}\text{as } G(j\omega) = |G(j\omega)|\, e^{j\angle G(j\omega)} \\ \approx 1e^{-j\gamma\omega} \text{ for } |\omega| \le \omega_b\end{array}\right) \\
&= \frac{1}{2\pi}\int_{-\infty}^{+\infty} e^{j\omega(t-\gamma)}S(j\omega)d\omega \text{ as } S(j\omega) \approx 0 \text{ for } |\omega| > \omega_b \\
&= s(t-\gamma).
\end{aligned}$$

The effect of passing $m(t)$ through the filter is to reproduce $s(t)$, that is, remove the noise from $m(t)$ delayed by γ seconds.

Remark

The "ideal" low-pass filter is specified by

$$G(j\omega) = \begin{cases} 1 & \text{for } |\omega| < \omega_c \\ 0 & \text{for } |\omega| > \omega_c. \end{cases}$$

That is, the frequency content of a signal below ω_c passes through unaffected while the frequency content of the signal above ω_c is removed. However, the ideal filter is neither causal nor stable (see problem 34).

2.7.7 Butterworth Filters

The class of filters known as *Butterworth Filters* have, to a good approximation, the two necessary properties; that is, the magnitude response has the low-pass characteristic along with a linear-phase. Below are the magnitude (Figure 2.24) and phase plots (Figure 2.25) for Butterworth filters of orders $n = 1, 2, 4, 6, 8, 10$, where ω_c denotes the filter cutoff frequency.

www.EngineeringEBooksPdf.com

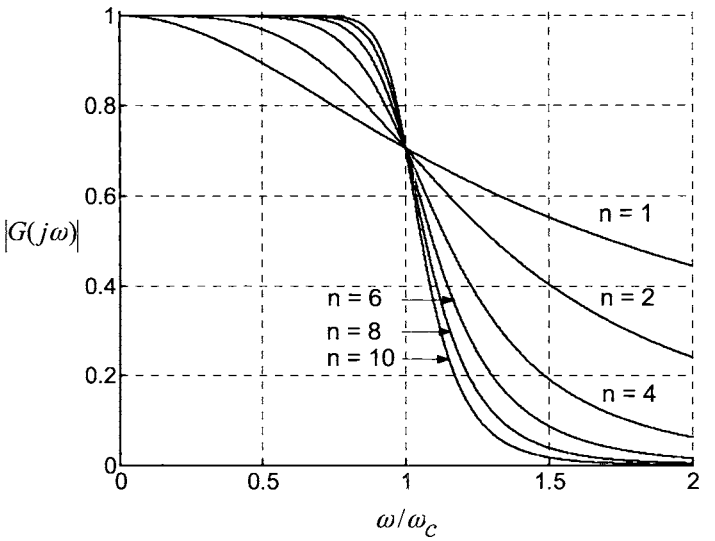


FIGURE 2.24. Plots of the magnitude versus ω/ω_c for Butterworth filters of order $n = 1, 2, 4, 6, 8, 10$.

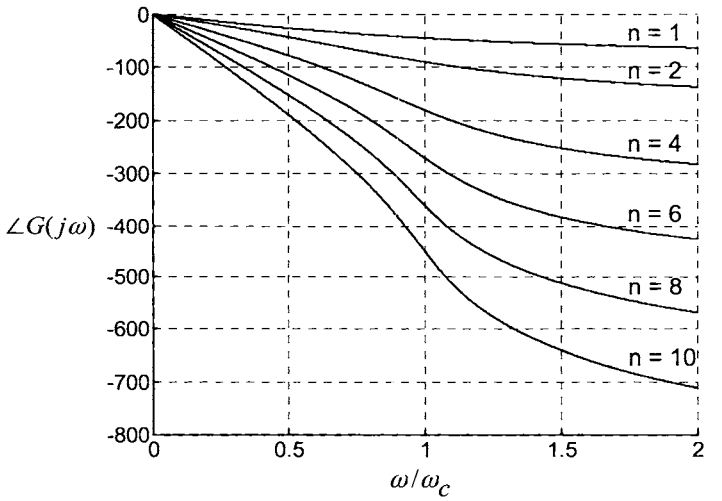


FIGURE 2.25. Plots of the phase in degrees versus ω/ω_c for Butterworth filters of order $n = 1, 2, 4, 6, 8, 10$.

www.EngineeringEBooksPdf.com

Note that for Butterworth filters of order $n = 4$ or greater,

$$\begin{aligned} |G_n(j\omega)| &\approx 1 \qquad \text{for } 0 \le \omega \le \omega_b = 0.6\omega_c \\ &\approx 0 \qquad \text{for } \omega \ge 2\omega_c \end{aligned}$$

and

$$\angle G_n(j\omega) \approx -\gamma_n \omega \text{ for } 0 \le \omega \le \omega_b = 0.6\omega_c$$

where the delays $\gamma_n = m_n/\omega_c$ ($m_n \triangleq$ the slope of the $\angle G_n(j\omega)$ vs. ω/ω_c) are monotonically increasing. In other words, $\gamma_1 < \gamma_2 < \gamma_4 < \gamma_6 < \gamma_8 < \gamma_{10}$ so that the time delay increases as the order of the filter increases.

Let's consider the specific example of a third-order Butterworth filter given by

$$\begin{aligned} G_3(s) &= \frac{1}{(s/\omega_c + 1)\left((s/\omega_c)^2 + s/\omega_c + 1\right)} \\ &= \frac{\omega_c^3}{(s+\omega_c)(s^2 + \omega_c s + \omega_c^2)}. \end{aligned}$$

Note that $|G_3(j\omega)|_{\omega=0} = 1$ and $|G_3(j\omega)|_{\omega=\omega_c} = 1/\sqrt{2}$. By direct computation (tedious!), one can verify that $d^k |G_3(j\omega)| / d\omega^k \,|_{\omega=0} = 0$ for $k = 1, 2, 3, 4, 5$ and $d^6 |G_3(j\omega)| / d\omega^6 \,|_{\omega=0} = -(1/2)(6!)$. The third-order Butterworth filter is the only third-order, causal, rational (i.e., ratio of two polynomials) filter that has its first five derivatives zero at $\omega = 0$. For this reason, the Butterworth filter is known as being *maximally flat*. In general, if $G_n(j\omega)$ denotes an nth-order Butterworth filter, then $d^k |G_n(j\omega)| / d\omega^k_{|\omega=0} = 0$ for $k = 1, 2, 3, 4, 5, ..., 2n-1$ and
$d^{2n} |G_n(j\omega)| / d\omega^{2n} \,|_{\omega=0} = -(1/2)(2n!)$.

2.7.8 *Implementation of the Filter*

To actually implement the filter, a differential equation representation of the filter is used. For a transfer function of the form

$$G(s) = \frac{b_1 s^2 + b_2 s + b_3}{s^3 + a_1 s^2 + a_2 s + a_3},$$

a state space representation (called the control canonical form) is given by

$$\begin{aligned} \dot{x}(t) &= \begin{bmatrix} 0 & 1 & 0 \\ 0 & 0 & 1 \\ -a_3 & -a_2 & -a_1 \end{bmatrix} x(t) + \begin{bmatrix} 0 \\ 0 \\ 1 \end{bmatrix} m(t) \\ y(t) &= \begin{bmatrix} b_3 & b_2 & b_1 \end{bmatrix} x(t) \end{aligned}$$

which may be written in a more compact form as

$$\begin{aligned} \dot{x}(t) &= Ax(t) + bm(t) \\ y(t) &= cx(t) \end{aligned}$$

www.EngineeringEBooksPdf.com

where

$$A = \begin{bmatrix} 0 & 1 & 0 \\ 0 & 0 & 1 \\ -a_3 & -a_2 & -a_1 \end{bmatrix}, \; b = \begin{bmatrix} 0 \\ 0 \\ 1 \end{bmatrix}, \; c = \begin{bmatrix} b_3 & b_2 & b_1 \end{bmatrix}.$$

The characteristic polynomial of the system is given by

$$\begin{aligned} \det(sI - A) &= \det \begin{bmatrix} s & -1 & 0 \\ 0 & s & -1 \\ a_3 & a_2 & s + a_1 \end{bmatrix} \\ &= s \begin{vmatrix} s & -1 \\ a_2 & s + a_1 \end{vmatrix} - (-1) \begin{vmatrix} 0 & -1 \\ a_3 & s + a_1 \end{vmatrix} + 0 \begin{vmatrix} 0 & s \\ a_3 & a_2 \end{vmatrix} \\ &= s^3 + a_1 s^2 + a_2 s + a_3 \end{aligned}$$

and the transfer function is computed as

$$\begin{aligned} Y(s) &= G(s) = c(sI - A)^{-1} b \\ &= \begin{bmatrix} b_3 & b_2 & b_1 \end{bmatrix} \begin{bmatrix} s & -1 & 0 \\ 0 & s & -1 \\ a_3 & a_2 & s + a_1 \end{bmatrix}^{-1} \begin{bmatrix} 0 \\ 0 \\ 1 \end{bmatrix} \\ &= \begin{bmatrix} b_3 & b_2 & b_1 \end{bmatrix} \frac{\begin{bmatrix} \times & \times & 1 \\ \times & \times & s \\ \times & \times & s^2 \end{bmatrix}}{s^3 + a_1 s^2 + a_2 s + a_3} \begin{bmatrix} 0 \\ 0 \\ 1 \end{bmatrix} \\ &= \frac{b_1 s^2 + b_2 s + b_3}{s^3 + a_1 s^2 + a_2 s + a_3} \end{aligned}$$

where the "×" means the specific value of each of these elements is not needed. For the third-order Butterworth filter given by

$$\begin{aligned} G_3(s) &= \frac{\omega_c^3}{(s + \omega_c)(s^2 + \omega_c s + \omega_c^2)} \\ &= \frac{\omega_c^3}{s^3 + 2\omega_c s^2 + 2\omega_c^2 s + \omega_c^3} \end{aligned}$$

direct computation shows that a state-space representation is given by

$$\begin{aligned} \dot{x}(t) &= \begin{bmatrix} 0 & 1 & 0 \\ 0 & 0 & 1 \\ -\omega_c^3 & -2\omega_c^2 & -2\omega_c \end{bmatrix} x(t) + \begin{bmatrix} 0 \\ 0 \\ 1 \end{bmatrix} m(t) \\ y(t) &= \begin{bmatrix} \omega_c^3 & 0 & 0 \end{bmatrix} x(t). \end{aligned} \tag{2.49}$$

www.EngineeringEBooksPdf.com

2.7.9 *Discretization of Differential Equations*

In order to implement a filter on a computer, the continuous time differential equation representing the filter must be discretized, that is, put into a discrete-time equivalent. There are many ways to do this, but only the trapezoidal method (also known as the bilinear transformation) is discussed here.

Consider $\dot{y}(t) = m(t)$ or $y(t) = \int_0^t m(\tau)d\tau$ and let the sample period be T. The trapezoidal method of integration uses the average value of the integrand over the sample period to compute the area under the curve. This is illustrated in Figure 2.26.

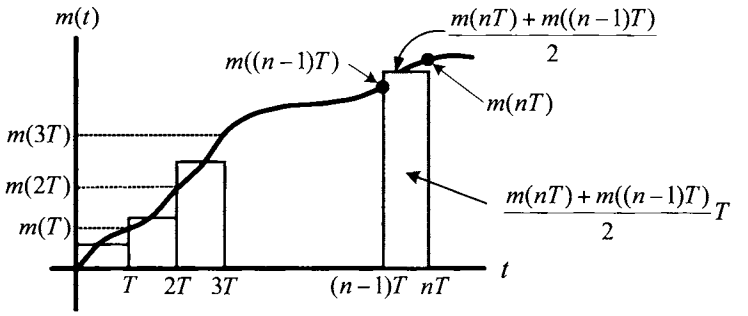


FIGURE 2.26. Trapezoidal method of integration.

Denote the area under the curve $m(t)$ at time nT by $y(nT)$. The average value of $m(t)$ between the times $(n-1)T$ and nT is $\frac{m(nT)+m((n-1)T)}{2}$ so that the approximate area under the curve in this same time period is $\frac{m(nT)+m((n-1)T)}{2}T$. Thus, one can (approximately) find the area under $m(t)$ at any time nT as

$$y(nT) = y((n-1)T) + \frac{m(nT) + m((n-1)T)}{2}T. \tag{2.50}$$

Let

$$\begin{aligned} Y(z) &= \sum_{n=0}^{\infty} y(nT)z^{-n} \\ M(z) &= \sum_{n=0}^{\infty} m(nT)z^{-n} \end{aligned}$$

be the z transform of $\{Y(nT)\}$ and $\{M(nT)\}$, respectively. Take the z

www.EngineeringEBooksPdf.com

transform of (2.50) to obtain

$$\sum_{n=0}^{\infty} y(nT)z^{-n} = z^{-1}\sum_{n=0}^{\infty} y((n-1)T)z^{-(n-1)} + \frac{T}{2}\left(\sum_{n=0}^{\infty} m(nT)z^{-n} + z^{-1}\sum_{n=0}^{\infty} m((n-1)T)z^{-(n-1)}\right).$$

Note that with $y(-1) = 0$,

$$\begin{aligned}\sum_{n=0}^{\infty} y((n-1)T)z^{-(n-1)} &= \sum_{n=1}^{\infty} y((n-1)T)z^{-(n-1)} \\ &= \sum_{k=0}^{\infty} y(kT)z^{-k} \\ &= Y(z).\end{aligned}$$

Similarly, with $m(-1) = 0$, $\sum_{n=0}^{\infty} m((n-1)T)z^{-(n-1)} = M(z)$ so that

$$Y(z) = z^{-1}Y(z) + \frac{T}{2}\left(M(z) + z^{-1}M(z)\right)$$

or

$$\frac{Y(z)}{M(z)} = \frac{T}{2}\frac{1+z^{-1}}{1-z^{-1}}$$

where the right-hand side is known as the *bilinear transformation.* The general case is now considered where the state-space representation

$$\dot{x}(t) = Ax(t) + bm(t)$$

of the filter is used. To numerically integrate this differential equation, the trapezoidal integration algorithm is used as follows:

$$\begin{aligned}x(nT) &= x((n-1)T) + T\frac{\dot{x}(nT) + \dot{x}((n-1)T)}{2} \\ &= x((n-1)T) \\ &\quad + \frac{T}{2}\left(Ax(nT) + bm(nT) + Ax((n-1)T) + bm((n-1)T)\right).\end{aligned}$$

Take the z transform of both sides to obtain

$$X(z) = z^{-1}X(z) + \frac{T}{2}\left(AX(z) + Az^{-1}X(z)\right) + \frac{T}{2}\left(bM(z) + bz^{-1}M(z)\right)$$

or

$$\begin{aligned}(1-z^{-1})X(z) - \frac{T}{2}(1+z^{-1})AX(z) &= \frac{T}{2}(1+z^{-1})bM(z) \\ \frac{2}{T}\frac{1-z^{-1}}{1+z^{-1}}X(z) - AX(z) &= bM(z) \\ \left(\left(\frac{2}{T}\frac{1-z^{-1}}{1+z^{-1}}\right)I - A\right)X(z) &= bM(z).\end{aligned}$$

www.EngineeringEBooksPdf.com

Then, as $Y(z) = cX(z)$,

$$H(z) \triangleq \frac{Y(z)}{M(z)} = c\left(\left(\frac{2}{T}\frac{1-z^{-1}}{1+z^{-1}}\right)I - A\right)^{-1}b.$$

The remarkable result is that the discrete-time transfer function is found by simply evaluating the *continuous-time* transfer function $G(s) = c(sI - A)^{-1}b$ at $s = \frac{2}{T}\frac{1-z^{-1}}{1+z^{-1}}$!

Going back to the third-order Butterworth filter

$$G_3(s) = \frac{\omega_c^3}{s^3 + 2\omega_c s^2 + 2\omega_c^2 s + \omega_c^3},$$

the discrete-time transfer function for this filter (corresponding to integrating the differential equation (2.49) using the trapezoidal approximation) is given by

$$\begin{aligned} H(z) &= G(s)\,|_{s=\frac{2}{T}\frac{1-z^{-1}}{1+z^{-1}}} \\ &= \frac{\omega_c^3}{s^3 + 2\omega_c s^2 + 2\omega_c^2 s + \omega_c^3}\,|_{s=\frac{2}{T}\frac{1-z^{-1}}{1+z^{-1}}} \\ &= \frac{b_1 + b_2 z^{-1} + b_3 z^{-2} + b_4 z^{-3}}{a_1 + a_2 z^{-1} + a_3 z^{-2} + a_4 z^{-3}} \end{aligned}$$

where

$$\begin{aligned} b_1 &= \omega_c^3 T^3, b_2 = 3\omega_c^3 T^3, b_3 = 3\omega_c^3 T^3, b_4 = \omega_c^3 T^3 \\ a_1 &= \omega_c^3 T^3 + 4\omega_c^2 T^2 + 8\omega_c T + 8 \\ a_2 &= 3\omega_c^3 T^3 + 4\omega_c^2 T^2 - 8\omega_c T - 24 \\ a_3 &= 3\omega_c^3 T^3 - 4\omega_c^2 T^2 - 8\omega_c T + 24 \\ a_4 &= \omega_c^3 T^3 - 4\omega_c^2 T^2 + 8\omega_c T - 8. \end{aligned} \tag{2.51}$$

Usually, the filter coefficients are normalized so that leading coefficient in the denominator is 1. The coefficients are then given by $a_1' = 1$, $a_2' = a_2/a_1$, $a_3' = a_3/a_1$, $a_4' = a_4/a_1$, $b_1' = b_1/a_1$, $b_2' = b_2/a_1$, $b_3' = b_3/a_1$, $b_4' = b_4/a_1$.

In order to implement this discrete-time filter, it needs to be reformulated as a discrete-time difference equation. This can be done either as a input-output difference equation or as a state-space difference equation. Both of these representations are considered in the next section.

2.7.10 Digital Filtering

A general second-order digital filter may be represented in input-output form as ($a_1 = 1$)

$$\begin{aligned} y(nT) =& b_1 m(nT) + b_2 m((n-1)T) + b_3 m((n-2)T) \\ &- a_2 y((n-1)T) - a_3 y((n-2)T) \end{aligned} \tag{2.52}$$

www.EngineeringEBooksPdf.com

That is, to get the output of the filter at time nT, one needs to know the current input $m(nT)$, have stored the previous two inputs $m((n-1)T)$, $m((n-2)T)$ and outputs $y((n-1)T), y((n-2)T)$, and then carry out the calculation. Rewrite (2.52) as

$$y(nT) + a_2 y((n-1)T) + a_3 y((n-2)T) = b_1 m(nT)) + b_2 m((n-1)T + b_3 m((n-2)T). \qquad (2.53)$$

To compute the discrete transfer function, multiply both sides by z and sum from $n = 0$ to $n = \infty$ to obtain

$$\begin{aligned}\sum_{n=0}^{\infty} y(nT)z^{-n} &+ a_2 z^{-1} \sum_{n=0}^{\infty} y((n-1)T)z^{-(n-1)} \\ &+ a_3 z^{-2} \sum_{n=0}^{\infty} y((n-2)T)z^{-(n-2)} \\ &= b_1 \sum_{n=0}^{\infty} m(nT)z^{-n} + b_2 z^{-1} \sum_{n=0}^{\infty} m((n-1)T)z^{-(n-1)} \\ &+ b_3 z^{-2} \sum_{n=0}^{\infty} m((n-2)T)z^{-(n-2)}.\end{aligned}$$

Let $Y(z) = \sum_{n=0}^{\infty} y(nT)z^{-n}$ so that with $y(-1) = 0$ it follows that

$$\sum_{n=0}^{\infty} y((n-1)T)z^{-(n-1)} = \sum_{n=1}^{\infty} y((n-1)T)z^{-(n-1)} = \sum_{k=0}^{\infty} y((k)T)z^{-k} = Y(z).$$

In addition, if $y(-2) = 0$, it then follows that $Y(z) = \sum_{n=0}^{\infty} y((n-2)T)z^{-(n-2)}$. Similarly, with $m(-1) = m(-2) = 0$, it follows that

$$\begin{aligned}M(z) &= \sum_{n=0}^{\infty} m(nT)z^{-n} = z^{-1} \sum_{n=0}^{\infty} m((n-1)T)z^{-(n-1)} \\ &= z^{-2} \sum_{n=0}^{\infty} m((n-2)T)z^{-(n-2)},\end{aligned}$$

Using these expressions, (2.53) becomes

$$Y(z) = a_2 z^{-1} Y(z) + a_3 z^{-2} Y(z) = b_1 M(z) + b_2 z^{-1} M(z) + b_3 z^{-2} M(z)$$

or

$$H(z) = \frac{b_1 + b_2 z^{-1} + b_3 z^{-2}}{1 + a_2 z^{-1} + a_3 z^{-2}}. \qquad (2.54)$$

Thus, the filter represented by this transfer function may be implemented on a computer using the difference equation (2.52).

www.EngineeringEBooksPdf.com

Example Consider the computation of speed by differentiation of position:

$$\omega_{bd}(nT) = \frac{\theta(nT) - \theta((n-1)T)}{T}$$

Let $m(nT) = \theta(nT)$ and $y(nT) = \omega(nT)$ so that this becomes

$$y(nT) = \frac{1}{T}m(nT) - \frac{1}{T}m((n-1)T)$$

that is, $b_1 = 1/T, b_2 = -1/T, a_1 = 1, a_2 = 0$. The transfer function is given by

$$\frac{Y(z)}{M(z)} = \frac{b_1 + b_2 z^{-1}}{1}.$$

2.7.11 State-Space Representation

Consider a third-order discrete-time transfer function of the form

$$\begin{aligned} H(z) &= \frac{Y(z)}{M(z)} = \frac{b_0 + b_1 z^{-1} + b_2 z^{-2} + b_3 z^{-3}}{1 + a_1 z^{-1} + a_2 z^{-2} + a_3 z^{-3}} \\ &= \frac{b_0 z^3 + b_1 z^2 + b_2 z + b_3}{z^3 + a_1 z^2 + a_2 z + a_3} = \frac{b_0\left(z^3 + a_1 z^2 + a_2 z + a_3\right)}{z^3 + a_1 z^2 + a_2 z + a_3} \\ &\quad + \frac{(b_1 - b_0 a_1)z^2 + (b_2 - b_0 a_2)z + (b_3 - b_0 a_3)}{z^3 + a_1 z^2 + a_2 z + a_3} \\ &= b_0 + \frac{(b_1 - b_0 a_1)z^2 + (b_2 - b_0 a_2)z + (b_3 - b_0 a_3)}{z^3 + a_1 z^2 + a_2 z + a_3}. \end{aligned} \tag{2.55}$$

With

$$\begin{aligned} A &= \begin{bmatrix} 0 & 1 & 0 \\ 0 & 0 & 1 \\ -a_3 & -a_2 & -a_1 \end{bmatrix}, \quad b = \begin{bmatrix} 0 \\ 0 \\ 1 \end{bmatrix} \\ c &= \begin{bmatrix} b_3 - b_0 a_3 & b_2 - b_0 a_2 & b_1 - b_0 a_1 \end{bmatrix} \\ d &= b_0 \end{aligned}$$

a state-space realization of this transfer function is given by

$$\begin{aligned} x\left((n+1)T\right) &= Ax(nT) + bm(nT),\ x(nT) \in \mathbb{R}^3 \\ y(nT) &= cx(nT) + dm(nT),\ y(nT) \in \mathbb{R}. \end{aligned} \tag{2.56}$$

To see this, the z transform of (2.56) is now computed to obtain the transfer function. Proceeding, let

$$X(z) = \sum_{n=0}^{\infty} x(nT)z^{-n} \in \mathbb{R}^3$$

www.EngineeringEBooksPdf.com

and note that

$$\begin{aligned}\sum_{n=0}^{\infty} x\left((n+1)T\right) z^{-n} &= z\sum_{n=0}^{\infty} x\left((n+1)T\right) z^{-(n+1)} \\ &= z\left(\sum_{n=-1}^{\infty} x\left((n+1)T\right) z^{-(n+1)} - x(0)\right) \\ &= z\left(\sum_{k=0}^{\infty} x(kT) z^{-k} - x(0)\right) \\ &= zX(z) - zx(0).\end{aligned}$$

Thus, taking the z transform of (2.56) results in

$$zX(z) - zx(0) = AX(z) + bM(z).$$

Solve for $X(z)$ to obtain

$$X(z) = (zI - A)^{-1} bM(z) + (zI - A)^{-1} zx(0)$$

or

$$Y(z) = cX(z) + dM(z) = \left(c(zI - A)^{-1} b + d\right) M(z) + z(zI - A)^{-1} x(0).$$

With $x(0) = 0$, the transfer function is

$$\frac{Y(z)}{M(z)} = c(zI - A)^{-1} b + d$$

where

$$\begin{aligned}&c(zI - A)^{-1} b + d \\ &= \begin{bmatrix} b_3 - b_0 a_3 & b_2 - b_0 a_2 & b_1 - b_0 a_1 \end{bmatrix} \begin{bmatrix} z & -1 & 0 \\ 0 & z & -1 \\ a_3 & a_2 & z + a_1 \end{bmatrix}^{-1} \begin{bmatrix} 0 \\ 0 \\ 1 \end{bmatrix} + b_0 \\ &= \begin{bmatrix} b_3 - b_0 a_3 & b_2 - b_0 a_2 & b_1 - b_0 a_1 \end{bmatrix} \frac{\begin{bmatrix} \times & \times & 1 \\ \times & \times & z \\ \times & \times & z^2 \end{bmatrix} \begin{bmatrix} 0 \\ 0 \\ 1 \end{bmatrix}}{z^3 + a_1 z^2 + a_2 z + a_3} + b_0\end{aligned}$$

www.EngineeringEBooksPdf.com

where the "×" denotes values that do not affect the final result. Simplifying, this becomes

$$\begin{aligned} c(zI-A)^{-1}b+d &= \frac{(b_1-b_0a_1)z^2+(b_2-b_0a_2)z+(b_3-b_0a_3)}{z^3+a_1z^2+a_2z+a_3}+b_0 \\ &= \frac{b_0\left(z^3+a_1z^2+a_2z+a_3\right)}{z^3+a_1z^2+a_2z+a_3} \\ &\quad + \frac{(b_1-b_0a_1)z^2+(b_2-b_0a_2)z+(b_3-b_0a_3)}{z^3+a_1z^2+a_2z+a_3} \\ &= \frac{b_0z^3+b_1z^2+b_2z+b_3}{z^3+a_1z^2+a_2z+a_3} \\ &= \frac{b_0+b_1z^{-1}+b_2z^{-2}+b_3z^{-3}}{1+a_1z^{-1}+a_2z^{-2}+a_3z^{-3}}. \end{aligned}$$

In summary, the state-space representation (2.56) can used to implement the digital filter (2.55) in real time on a computer.

2.7.12 Noncausal Filtering

It has been shown how to use a Butterworth filter to realize a filter with low-pass magnitude characteristics and a linear phase. One can get around the problem of requiring a linear phase by filtering the signal twice in an appropriate manner as is now described.

Let $m(t) = s(t) + n(t)$ be the input to a filter whose transfer function is $G(s)$ and let the output be $y(t)$ so that $y(t) = \int_{-\infty}^{t} g(t-\tau)m(\tau)d\tau$. Also, let T_f be a large final time such that $[0, T_f]$ contains the period of time over which the signal $s(t)$ is nonzero. The plots of $m(t), s(t)$ and $y(t)$ are given below in Figure 2.27. Note that the filtered signal $y(t)$ is shifted to the right from $s(t)$ corresponding to a time delay. Next, let $y_b(t) \triangleq y(T_f - t)$ (the subscript b stands for backwards) and then pass this signal through $G(s)$ once again and call the output $y_{ffb}(t)$ (the ff stands for *filter-filter*, i.e., double filtering). Finally, let $y_{ff}(t) \triangleq y_{ffb}(T_f - t)$. Figure 2.28 illustrates these different signals.

It is now shown that $y_{ff}(t)$ is a good estimate of $s(t)$. To explain how this double filtering works, the transfer function from m to y is now computed. The filter may be represented as a convolution or in the s domain as

$$\begin{aligned} y(t) &= \int_0^t g(t-\tau)m(\tau)d\tau \\ Y(s) &= G(s)M(s) \end{aligned}$$

where $G(j\omega) = |G(j\omega)|\, e^{j\angle G(j\omega)}$.

www.EngineeringEBooksPdf.com

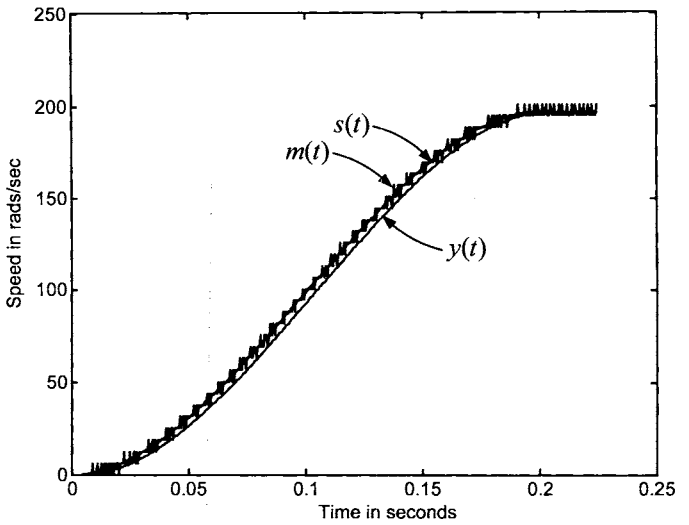


FIGURE 2.27. $m(t) = (\theta(nT) - \theta((n-1)T))/T$ with $T = 0.5$ msec is the measured speed. $s(t)$ is the "true" speed from a simulation and $y(t)$ is the filtered version of $m(t)$. Note that $y(t)$ is delayed with respect to $s(t)$.

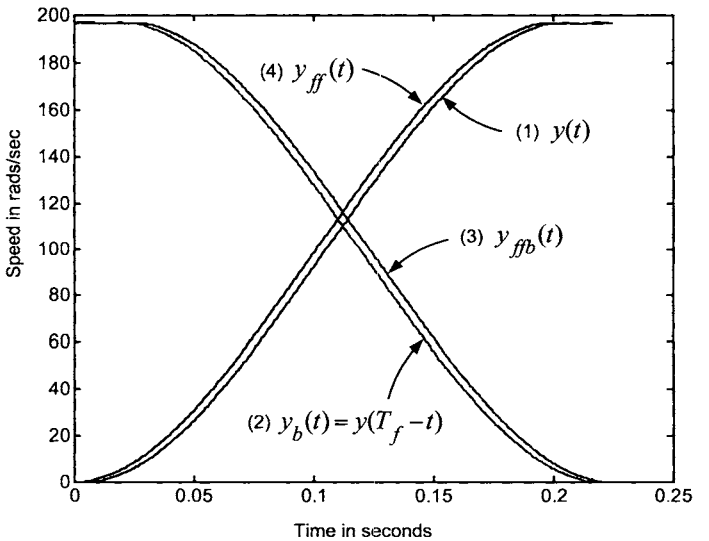


FIGURE 2.28. $y(t), y_b(t) - y(T_f - t), y_{ffb}(t), y_{ff}(t)$ versus t.

www.EngineeringEBooksPdf.com

Then from the convolution representation

$$y_{ffb}(t) = \int_0^t g(t-\tau)y_b(\tau)d\tau = \int_0^t g(t-\tau)y(T_f-\tau)d\tau$$

it follows that

$$Y_{ffb}(s) = G(s)Y_b(s)$$

where[7]

$$\begin{aligned} Y_b(s) &= \int_0^{T_f} e^{-st}y(T_f-t)dt = -\int_{T_f}^0 e^{-s(T_f-u)}y(u)du \\ &= e^{-sT_f}\int_0^{T_f} e^{-(-s)u}y(u)du \\ &= e^{-sT_f}Y(-s) \\ &= e^{-sT_f}G(-s)M(-s). \end{aligned}$$

Thus,

$$Y_{ffb}(s) = G(s)Y_b(s) = e^{-sT_f}G(s)G(-s)M(-s).$$

Then, with

$$y_{ff}(t) = y_{ffb}(T_f-t)$$

it follows that[8]

$$\begin{aligned} Y_{ff}(s) &= e^{-sT_f}Y_{ffb}(-s) = e^{-sT_f}\left(e^{sT_f}G(-s)G(s)M(s)\right) \\ &= G(-s)G(s)M(s) \end{aligned}$$

or

$$Y_{ff}(j\omega) = G(-j\omega)G(j\omega)M(j\omega).$$

As

$$\begin{aligned} G(j\omega) &= |G(j\omega)|\,e^{j\angle G(j\omega)} \\ G(-j\omega) &= |G(-j\omega)|\,e^{j\angle G(-j\omega)} = |G(j\omega)|\,e^{-j\angle G(j\omega)} \end{aligned}$$

it follows that

$$\begin{aligned} Y_{ff}(j\omega) &= G(-j\omega)G(j\omega)M(j\omega) \\ &= |G(j\omega)|\,e^{-j\angle G(j\omega)}\,|G(j\omega)|\,e^{j\angle G(j\omega)}M(j\omega) \\ &= |G(j\omega)|^2\,M(j\omega). \end{aligned}$$

That is, there is no phase shift from $m(t)$ to $y_{ff}(t)$ and thus no distortion. Of course, this filter is noncausal as all of the data $m(t)$ must be collected before the computations can be done.

---

[7] Recall that by assumption $y(t) = 0$ for $t < 0$ and $t > T_f$, which implies $y(T_f - t) = 0$ for $t < 0$ and $t > T_f$.

[8] If $\mathcal{L}\{x(t)\} = X(s)$, then $\mathcal{L}\{x(-t)\} = X(-s)$ and $\mathcal{L}\{x(t-t_0)\} = e^{-t_0 s}X(s)$ so that $\mathcal{L}\{x(-(t-t_0))\} = e^{-t_0 s}\mathcal{L}\{x(-t)\} = e^{-t_0 s}X(-s)$.

www.EngineeringEBooksPdf.com

Appendix - Classical Feedback Control

Tracking and Disturbance Rejection

In order to explain the ideas of tracking and disturbance rejection, consider the block diagram of Figure 2.9 which is redrawn in a standard form in Figure 2.29.

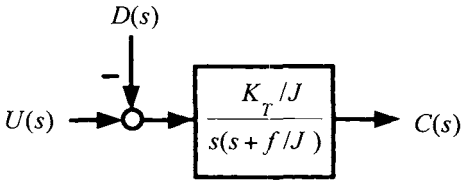


FIGURE 2.29. DC motor block diagram.

In Figure 2.29 $U(s) \triangleq i_r(s), C(s) \triangleq \theta(s)$, and $D(s) \triangleq \tau_L(s)/K_T$. Note that, though this system is mathematically equivalent to the system of Figure 2.9, there is not a one-to-one physical equivalence. Specifically, the disturbance $D(s) = \tau_L(s)/K_T$ has the units of amperes, which is consistent with the above drawing, as it is being subtracted from the input *current* $U(s) = i_r(s)$. This is not to say that the load is a current, but rather, if a current given by $-\tau_L/K_T$ is input to the motor, then the effect on the output position $c(t)$ is the same as the actual load torque.

A block diagram for a simple proportional control system for the motor is given in Figure 2.30, where $R(s) \triangleq \theta_{ref}(s)$ is the reference input and $G_m(s) \triangleq \dfrac{K_T/J}{s\,(s + f/J)}$

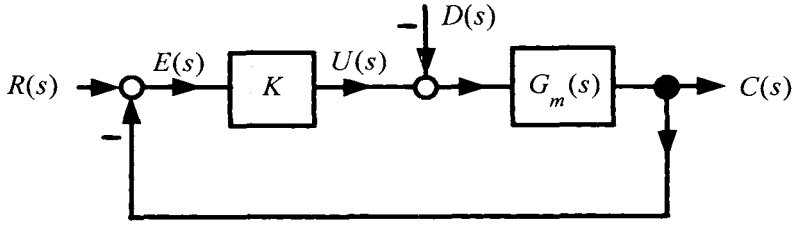


FIGURE 2.30. Simple proportional control system.

A sensor is used to feed back the motor position to obtain the error signal

$$E(s) \triangleq R(s) - C(s).$$

www.EngineeringEBooksPdf.com

A simple proportional controller is specified by

$$U(s) = KE(s)$$

that is, the current commanded to the motor $[U(s) = i_r(s)]$ is proportional to the difference between the reference (desired) position and the actual position.

The simple proportional controller is often replaced by a more general controller (compensator) specified by a transfer function $G_c(s) = b_c(s)/a_c(s)$ where the subscript "c" stands for controller (or compensator). In fact, the whole point of automatic control theory is to provide a methodology on how to specify $G_c(s)$. A general block diagram form for a control system is given in Figure 2.31.

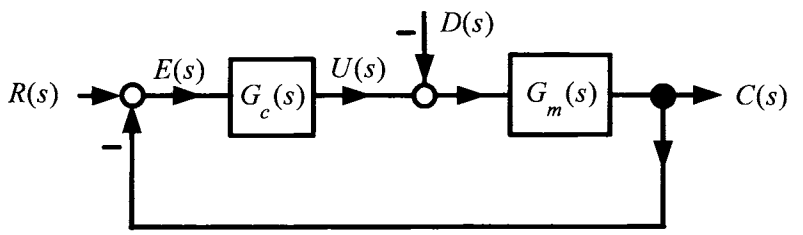


FIGURE 2.31. Standard block diagram of a control system.

To obtain a convenient expression for the transfer function from $R(s)$ and $D(s)$ to the output $C(s)$, compute

$$C(s) = (G_c(s)E(s) - D(s))\,G_m(s) = (G_c(s)\,(R(s) - C(s)) - D(s))\,G_m(s).$$

This is rearranged to obtain

$$C(s)\,(1 + G_c(s)G_m(s)) = G_c(s)G_m(s)R(s) - D(s)G_m(s)$$

or

$$C(s) = \frac{G_c(s)G_m(s)}{1 + G_c(s)G_m(s)}R(s) - \frac{G_m(s)}{1 + G_c(s)G_m(s)}D(s). \tag{2.57}$$

The error $E(s)$ is given by

$$E(s) = R(s) - C(s) = \frac{1}{1 + G_c(s)G_m(s)}R(s) + \frac{G_m(s)}{1 + G_c(s)G_m(s)}D(s). \tag{2.58}$$

Typically, the compensator $G_c(s)$ is chosen to achieve two objectives:

1. *Tracking* If the reference position is set as $r(t) = 30°$ $(R(s) = 30°/s)$, then it is required that $c(t) \to 30°$ as $t \to \infty$, i.e., the output must track the input

www.EngineeringEBooksPdf.com

2. *Disturbance Rejection* If the reference position is set as $r(t) = 30°$, then it is required that $c(t) \to 30°$ as $t \to \infty$ despite any load on the motor. For example, if a robot arm is to move 30°, it must do so no matter how much weight it is carrying.

PID Control of a Simple DC Servo Motor

The ideas of tracking and disturbance rejection are now illustrated through a series of simple examples. This is done by considering a fixed physical system given by $G_m(s) = \dfrac{1}{s(s+1)}$, which could be the model of a DC servo motor system. Various controllers are considered for both tracking and disturbance rejection.

Tracking Control

A simple proportional controller given by $G_c(s) = K$ is considered first.

Example *Tracking a step input*

Consider the unity feedback system control system of Figure 2.32 where $G_m(s) = \dfrac{1}{s(s+1)}$, $D(s) = 0$ and a constant gain controller.

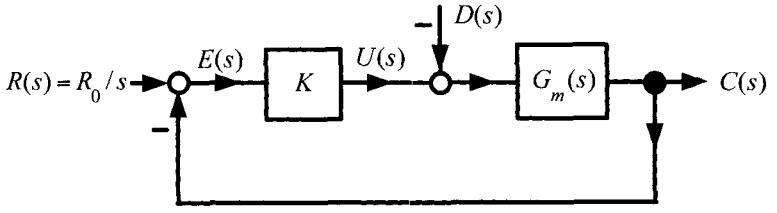


FIGURE 2.32. Tracking a step input.

The output and error transfer functions are, respectively,

$$\begin{aligned} C(s) &= \frac{KG_m(s)}{1 + KG_m(s)} R(s) \\ E(s) &= \frac{1}{1 + KG_m(s)} R(s). \end{aligned}$$

Suppose the objective is to track a step input. Let $u_s(t)$ denote the unit step function and let $r(t) = R_0 u_s(t)$ so that $R(s) = R_0/s$. The objective is to force the error $e(t) \to 0$ as $t \to \infty$ as this means that $c(t) \to R_0$. Evaluating $E(s)$, one obtains

$$E(s) = \frac{1}{1 + K\dfrac{1}{s(s+1)}} \frac{R_0}{s} = \frac{s(s+1)}{s(s+1) + K} \frac{R_0}{s} = \frac{s+1}{s^2 + s + K} R_0.$$

www.EngineeringEBooksPdf.com

Note that the poles of the forward open-loop transfer function $KG_m(s) = K\dfrac{1}{s(s+1)}$ reappear in the numerator of $E(s)$ after clearing the fractions in the denominator. In particular, the "s" in $K\dfrac{1}{s(s+1)}$ cancelled the "s" in the denominator of $R(s)$. For $K > 0$, $s^2 + s + K$ is a stable polynomial so that $sE(s) = \dfrac{s(s+1)}{s^2+s+K}R_0$ is stable. By the final value theorem,

$$e(\infty) = \lim_{s\to 0} sE(s) = \lim_{s\to 0} s\frac{s(s+1)}{s(s+1)+K}\frac{R_0}{s} = 0.$$

Where does stability come in? Let $K = 1$ so that

$$\begin{aligned} s^2+s+1 &= \left(s-\left(-1/2+j\sqrt{3}/2\right)\right)\left(s-\left(-1/2-j\sqrt{3}/2\right)\right) \\ &= (s-p_1)(s-p_2) \end{aligned}$$

with $p_1 = -1/2 + j\sqrt{3}/2$ and $p_2 = p_1^* = -1/2 - j\sqrt{3}/2$. Then a partial fraction expansion of $E(s)$ gives

$$E(s) = \frac{s(s+1)}{s(s+1)+K}\frac{R_0}{s} = \frac{s+1}{(s-p_1)(s-p_2)}R_0 = \frac{\beta}{(s-p_1)} + \frac{\beta^*}{(s-p_2)}$$

where $\beta = \beta_1 + j\beta_2 = |\beta|\, e^{j\angle\beta}$ and $|\beta|^2 = \beta_1^2 + \beta_2^2, \angle\beta = \tan^{-1}(\beta_2/\beta_1)$.

In the time domain,

$$\begin{aligned} e(t) &= \beta e^{p_1 t} + \beta^* e^{p_2 t} \\ &= |\beta|\, e^{j\angle\beta} e^{-(1/2)t + j(\sqrt{3}/2)t} + |\beta|\, e^{-j\angle\beta} e^{-(1/2)t - j(\sqrt{3}/2)t} \\ &= 2\,|\beta|\, e^{-(1/2)t}\cos\left((\sqrt{3}/2)t + \angle\beta\right) \to 0 \text{ as } t \to \infty. \end{aligned}$$

Recall that the poles of the closed-loop transfer function determine the form of the transient response. As the closed-loop poles p_1 and p_2 are in the open left-half plane (LHP), the transients die out. The real part of the closed-loop poles ($\mathrm{Re}\{p_1\} = \mathrm{Re}\{p_2\} = -1/2$) determine how fast the transient $e(t)$ dies out and typically one chooses the amplifier gain K such that the poles of the closed-loop system are as far as possible in the LHP.

Example *Tracking a ramp input*

Consider the same system as in the previous example, but let the input be a ramp function. Specifically, the input is given by $r(t) = \omega_0 t$ where ω_0 is a constant ($R(s) = \omega_0/s^2$) and $D(s) = 0$. The error $E(s)$ is then

$$E(s) = \frac{1}{1+K\dfrac{1}{s(s+1)}}\frac{\omega_0}{s^2} = \frac{s(s+1)}{s(s+1)+K}\frac{\omega_0}{s^2} = \frac{s+1}{s^2+s+K}\frac{\omega_0}{s}.$$

www.EngineeringEBooksPdf.com

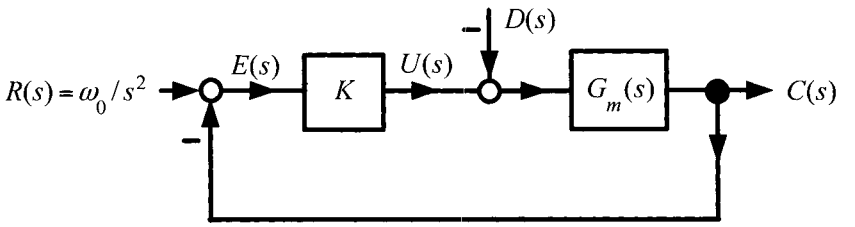


FIGURE 2.33. Tracking a ramp input.

Note again that the pole at $s = 0$ of $KG_m(s)$ cancelled one of the poles at $s = 0$ of $R(s)$. As $s^2 + s + K$ is stable for $K > 0$, $sE(s) = \dfrac{s+1}{s^2+s+K}\omega_0$ is stable. By the final value theorem,

$$e(\infty) = \lim_{s\to 0} sE(s) = \lim_{s\to 0} \frac{s+1}{s(s+1)+K}\omega_0 = \frac{\omega_0}{K}.$$

Consequently, asymptotic tracking is not achieved as $e(t)$ does not go to 0 as $t \to \infty$. However, the motor does follow the input with a finite error which can be made small if K can be made large.

Where does stability come in? Let $K = 1$ so that $p_i = \left(-1 \pm j\sqrt{3}\right)/2$ and

$$\begin{aligned} E(s) &= \frac{s(s+1)}{s(s+1)+K}\frac{\omega_0}{s^2} = \frac{s+1}{s(s-p_1)(s-p_2)}\omega_0 \\ &= \frac{A}{s} + \frac{\beta}{(s-p_1)} + \frac{\beta^*}{(s-p_2)} \\ &= \frac{\omega_0}{s} + \frac{\beta}{(s-p_1)} + \frac{\beta^*}{(s-p_2)} \end{aligned}$$

for some complex constant β and $\omega_0 = \lim_{s\to 0} sE(s)$. Then

$$e(t) = \omega_0 u_s(t) + \beta e^{p_1 t} + \beta^* e^{p_2 t} \to \omega_0$$

as $t \to \infty$, as the poles are in the open left-half plane ($\mathrm{Re}(p_1) = \mathrm{Re}\,(p_2) < 0$). Again, as the closed-loop poles are in the left-half plane, the transients die out.

The simple proportional controller is not adequate to track a ramp input $r(t) = \omega_0 t$ with zero steady-state error. The answer to achieving zero steady-state error for this system lies in considering a different controller!

Example *Integral Controller*

Consider the controller $G_c(s) = K/s$; that is, an integrator.

www.EngineeringEBooksPdf.com

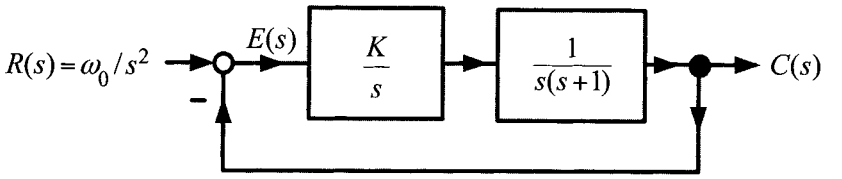


FIGURE 2.34. An integral controller.

Then

$$E(s) = \frac{1}{1+\frac{K}{s}\frac{1}{s(s+1)}}\frac{\omega_0}{s^2} = \frac{s^2(s+1)}{s^2(s+1)+K}\frac{\omega_0}{s^2} = \frac{s+1}{s^3+s^2+K}\omega_0.$$

where note that the denominator (poles) of $\frac{K}{s}\frac{1}{s(s+1)}$ reappeared in the numerator of $E(s)$ after clearing fractions. As a consequence, the s^2 in the denominator of the forward open-loop transfer function $\frac{K}{s}\frac{1}{s(s+1)}$ is in the numerator of $E(s)$ and cancels the s^2 in the denominator of $R(s)$. If s^3+s^2+K were stable, then by the final value theorem,

$$e(\infty) = \lim_{s\to 0} sE(s) = \lim_{s\to 0} s\frac{s+1}{s^3+s^2+K}\omega_0 = 0.$$

The difficulty here is that $s^3+s^2+K = s^3+s^2+0s+K$ is never stable for any value of K as a necessary condition for stability is that all the coefficients of the closed-loop characteristic polynomial be positive. To emphasize the stability aspect, let $K=1$ for which s^3+s^2+1 has roots $-1.47, 0.23\pm j0.79$. The error response is found by doing a partial fraction expansion of $E(s)$ as

$$\begin{aligned} E(s) &= \frac{s+1}{(s+1.47)(s-0.23-j0.79)(s-0.23+j0.79)}\omega_0 \\ &= \frac{A}{s+1.47}+\frac{\beta}{s-0.23-j0.79}+\frac{\beta^*}{s-0.23+j0.79} \end{aligned}$$

for some complex constant β. The time response then has the form

$$\begin{aligned} e(t) &= Ae^{-1.47t}+\beta e^{0.23t}e^{j0.79t}+\beta^* e^{0.23t}e^{-j0.79t} \\ &= Ae^{-1.47t}+2\,|\beta|\,e^{0.23t}\cos(0.79t+\angle\beta). \end{aligned}$$

The error $e(t)$ does not go to zero due to the unstable closed-loop poles at $-0.23\pm j0.79$. Remember, the fact that $lim_{s\to 0}\ sE(s)=0$ says nothing about the steady-state error unless $sE(s)$ is stable!

www.EngineeringEBooksPdf.com

As this example demonstrates, the difficult problem is not in getting $\lim_{s\to 0} sE(s) = 0$, but instead, it is in making the closed-loop system stable. As shown above, a constant gain (proportional) controller will give closed-loop stability, but not $lim_{s\to 0}\ sE(s) = 0$. On the other hand, an integral controller gives $lim_{s\to 0} sE(s) = 0$, but not closed-loop stability. Let's combine the two and see if that will work. Specifically, let

$$G_c(s) = K\frac{s+\alpha}{s} = K + \frac{\alpha K}{s}.$$

This is called a proportional (K) plus integral ($\alpha K/s$) compensator or PI compensator.

Example *PI controller*

Again, consider the same system as in the previous examples, except use a PI compensator.

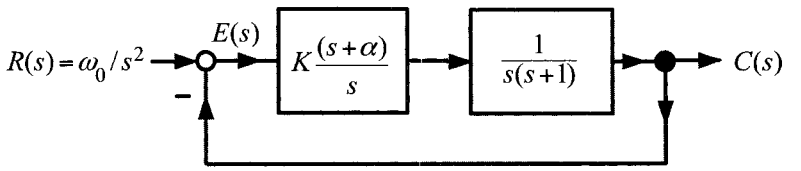


FIGURE 2.35. A proportional plus integral (PI) controller.

From the block diagram, the error $E(s)$ is seen to be given by

$$\begin{aligned} E(s) &= \frac{1}{1 + K\frac{s+\alpha}{s}\frac{1}{s(s+1)}} R(s) = \frac{s^2(s+1)}{s^2(s+1) + K(s+\alpha)}\frac{\omega_0}{s^2} \\ &= \frac{s+1}{s^3 + s^2 + Ks + \alpha K}\omega_0. \end{aligned}$$

Again note that denominator of the open-loop system $K\frac{s+\alpha}{s}\frac{1}{s(s+1)}$ reappears in the numerator of $E(s)$. Consequently, the factor of s^2 in the denominator of $G_c(s)G_m(s)$ cancels the "s" in the denominator of $R(s)$. Then, *if* $s^3 + s^2 + Ks + \alpha K$ is stable, the final value theorem gives

$$e(\infty) = \lim_{s\to 0} sE(s) = \lim_{s\to 0} s\frac{s+1}{s^3 + s^2 + Ks + \alpha K}\omega_0 = 0.$$

To check stability of $s^3 + s^2 + Ks + \alpha K$, the Routh test is used [37][46][47]. The Routh table is

s^3	1	K
s^2	1	αK
s	$K - \alpha K$	0
s^0	αK	

www.EngineeringEBooksPdf.com

The first column is positive if and only if $\alpha K > 0$ and $K - \alpha K = K(1-\alpha) > 0$ or

$$K > 0 \text{ and } 0 < \alpha < 1.$$

For example, with $K = 1$ and $\alpha = 1/2$, the closed-loop characteristic equation is

$$s^3 + s^2 + s + 1/2 = (s + 0.65)(s + 0.176 - j0.861)(s + 0.176 + j0.861).$$

Then, letting $r = -0.65, p_i = -0.176 \pm j0.861$, the partial fraction expansion of $E(s)$ gives

$$E(s) = \frac{s+1}{(s-r)(s-p_1)(s-p_2)}\omega_0 = \frac{A}{s-r} + \frac{\beta}{s-p_1} + \frac{\beta^*}{s-p_2}.$$

The corresponding time response is then

$$\begin{aligned} e(t) &= Ae^{-0.65t} + \beta e^{-0.176t}e^{j0.861t} + \beta^* e^{-0.176t}e^{-j0.861t} \\ &= Ae^{-0.65t} + 2\,|\beta|\, e^{-0.176t}\cos(0.861t + \angle\beta) \to 0 \text{ as } t \to \infty. \end{aligned}$$

In general, adding integrators to the compensator tends to destabilize the closed-loop system while adding a proportional (constant gain) compensator tends to stabilize the closed-loop system. In the above example, an integrator is added to obtain zero steady-state error and the proportional compensator is added to make the closed-loop system stable.

Disturbance Rejection

Consider now the problem of having the motor to rotate R_0 radians with an external load acting on it (Figure 2.37 illustrates such cases).

Example *Constant Load Torque with a Proportional Controller*
Consider the control system in the block diagram below. Let

$$G_m(s) = \frac{1}{s(s+1)}$$

and let the disturbance be the constant load torque

$$\tau_L(t) = \tau_0 u_s(t)$$

so that $D(s) = \dfrac{\tau_L(s)}{K_T} = \dfrac{\tau_0}{K_T}\dfrac{1}{s}$.

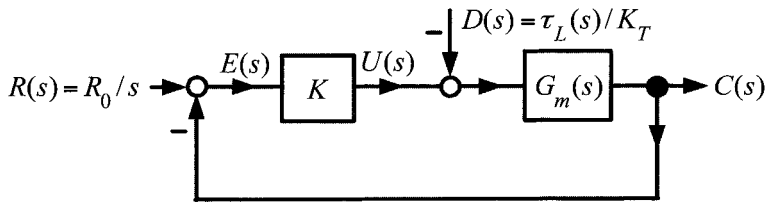


FIGURE 2.36. A proportional controller with a load acting on the system.

www.EngineeringEBooksPdf.com

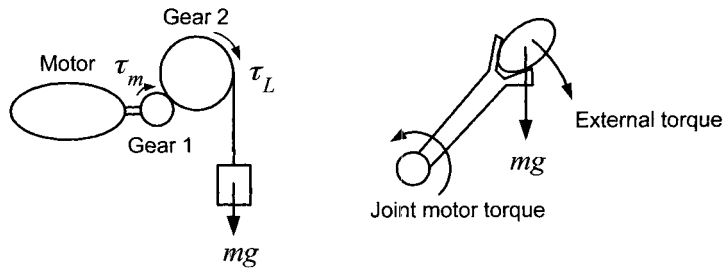


FIGURE 2.37. Examples of torque loads on DC motors.

It was shown in (2.58) that $E(s) = E_R(s) + E_D(s)$ where

$$E_R(s) \triangleq \frac{1}{1 + KG_m(s)} R(s)$$

and

$$E_D(s) \triangleq \frac{G_m(s)}{1 + KG_m(s)} D(s).$$

It was also shown that $\mathcal{L}^{-1}\{E_R(s)\} = e_R(t) \to 0$ as long as $K > 0$. The interest here is disturbance rejection, that is, whether or not $e_D(t) = \mathcal{L}^{-1}\{E_D(s)\} \to 0$ as $t \to \infty$. The Laplace transform of $e_D(t)$ is

$$E_D(s) = \frac{G_m(s)}{1 + KG_m(s)} D(s) = \frac{\dfrac{1}{s(s+1)}}{1 + K\dfrac{1}{s(s+1)}} \frac{\tau_L(s)}{K_T} = \frac{1}{s^2 + s + K} \frac{\tau_L(s)}{K_T}.$$

In words, $E_D(s)$ is the error in the position response due to the load torque. With a constant load torque $\tau_L(s) = \tau_0/s$ and, as $s^2 + s + K$ is stable for $K > 0$, the final position error due to the load torque is

$$e_D(\infty) = \lim_{s \to 0} s \frac{1}{s^2 + s + K} \frac{\tau_0}{K_T} \frac{1}{s} = \frac{\tau_0}{KK_T}.$$

The error

$$r(t) - c(t) = e(t) = e_R(t) + e_D(t) \to e_R(\infty) + e_D(\infty) = 0 + \frac{\tau_0}{KK_T}$$

as $t \to \infty$. Rearranging, the steady-state output is

$$c(\infty) = r(\infty) - e(\infty) = R_0 - \frac{\tau_0}{KK_T}.$$

The conclusion here is that the final output position depends on the value of the load torque τ_0. This is usually not acceptable as typically the load

www.EngineeringEBooksPdf.com

torque is unknown and it is important to precisely position the motor regardless of the load.[9] As is now shown, a PI controller can achieve zero steady-state error for this system even with unknown constant load torques acting on the system.

Example *Constant Load Torque with a PI Controller*

Let $G_c(s) = K_p + K_I/s = K\dfrac{s+\alpha}{s}$ where $K_p = K$ and $K_I = \alpha K$.

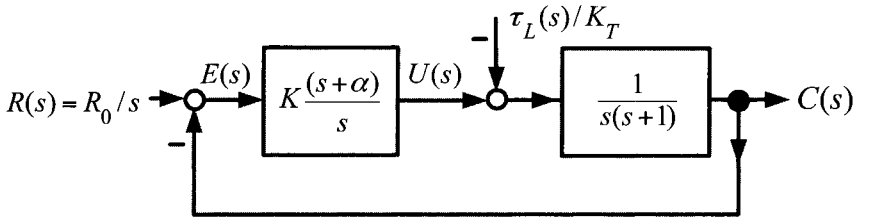


FIGURE 2.38. PI controller for disturbance rejection.

The error due to the disturbance is calculated as

$$\begin{aligned} E_D(s) &= \frac{G_m(s)}{1+G_c(s)G_m(s)}D(s) = \frac{\dfrac{1}{s(s+1)}}{1+K\dfrac{s+\alpha}{s}\dfrac{1}{s(s+1)}}\frac{\tau_0}{K_T}\frac{1}{s} \\ &= \frac{s}{s^2(s+1)+K(s+\alpha)}\frac{\tau_0}{K_T}\frac{1}{s} = \frac{1}{s^3+s^2+Ks+\alpha K}\frac{\tau_0}{K_T}. \end{aligned}$$

Note that, in contrast to the tracking case, only the denominator of $G_c(s)$ (i.e., s) reappears in the numerator after clearing the fractions in $E_D(s)$. This "s" cancels the $1/s$ in $\tau_L(s)$. Now, by the Routh test, $s^3+s^2+Ks+\alpha K$ is stable for $K > 0$ and $0 < \alpha < 1$, and so $sE_D(s)$ is also stable. Again, by the final value theorem,

$$e_D(\infty) = \lim_{s\to 0} sE_D(s) = \lim_{s\to 0} s\frac{1}{s^3+s^2+Ks+\alpha K}\frac{\tau_0}{K_T} = 0.$$

Consequently, the load torque τ_0 has no effect on the final position.

Interpretation of the PI Controller

For the system of Figure 2.38, it was shown that K and α can be chosen so that the closed-loop system is stable and $e(\infty) = \lim_{s\to 0} sE(s) = 0$. $U(s) = i_r(s)$ is the input current to the motor and is given by

$$U(s) = K\frac{s+\alpha}{s}E(s) = KE(s) + \frac{\alpha K}{s}E(s).$$

[9] Note that if the gain K can be made large, then the disturbance term $\tau_0/(K_T K)$ perhaps could be made negligible.

www.EngineeringEBooksPdf.com

In the time domain,

$$u(t) = Ke(t) + \alpha K \int_0^t e(t)dt.$$

The limiting value of $u(t)$ is

$$u(\infty) = \lim_{s \to 0} sU(s) = \alpha K E(0)$$

which is due only to the output of the integrator. With $R(s) = R_0/s$ and $\tau_L(s) = \tau_0/s$, the error is given by

$$E(s) = \frac{s^2(s+1)}{s^3 + s^2 + Ks + \alpha K} \frac{R_0}{s} + \frac{s}{s^2(s+1) + K(s+\alpha)} \frac{\tau_0}{K_T} \frac{1}{s}$$

and, therefore, $E(0) = \tau_0/(\alpha K K_T)$. Consequently, $u(\infty) = \tau_0/K_T$ which shows that the output of the integrator goes to exactly the value needed to cancel the load disturbance.

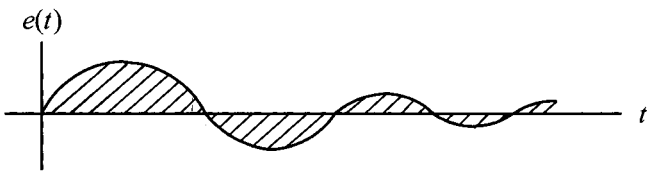


FIGURE 2.39. The error $e(t) \to 0$. The shaded area is $\int_0^\infty e(t)dt$ and $u(\infty) = \alpha K \int_0^\infty e(t)dt = \tau_0/K_T$.

Summary of the PI Controller for a DC Servo

It has been shown that the controller $G_c(s) = K(s+\alpha)/s$ with $K > 0$ and $0 < \alpha < 1$, will force the motor with transfer function $G_m(s) = \dfrac{1}{s(s+1)}$ to track inputs of the form $r(t) = R_0 + \omega_0 t$ with zero steady-state error in spite of any constant load disturbances. The control system designer then wants to choose K and α so that the closed-loop poles are far in the left-half plane in order have the transients die out quickly. Remember, the closed-loop poles determine the transient response! Recall from (2.57) and (2.58) that

$$\begin{aligned} C(s) &= \frac{G_c(s)G_m(s)}{1 + G_c(s)G_m(s)} R(s) - \frac{G_m(s)}{1 + G_c(s)G_m(s)} \frac{\tau_L(s)}{K_T} \\ E(s) &= \frac{1}{1 + G_c(s)G_m(s)} R(s) + \frac{G_m(s)}{1 + G_c(s)G_m(s)} \frac{\tau_L(s)}{K_T}. \end{aligned}$$

Evaluating the error $E(s)$ gives

$$E(s) = \frac{s^2(s+1)}{s^3 + s^2 + Ks + \alpha K} \left(\frac{R_0}{s} + \frac{\omega_0}{s^2} \right) + \frac{K_L s}{s^3 + s^2 + Ks + \alpha K} \frac{\tau_0}{K_T} \frac{1}{s}.$$

www.EngineeringEBooksPdf.com

The gains K and α are chosen so that the poles of the closed-loop characteristic polynomial

$$s^3 + s^2 + Ks + \alpha K = (s - r)(s - p_1)(s - p_2)$$

satisfy $r < 0, \mathrm{Re}(p_1) = \mathrm{Re}(p_2) < 0$. The error $E(s)$ is then

$$E(s) = \frac{(s+1)(R_0 s + \omega_0)}{(s-r)(s-p_1)(s-p_2)} + \frac{1}{(s-r)(s-p_1)(s-p_2)} \frac{\tau_0}{K_T}$$

or, in the time domain,

$$e(t) = Ae^{rt} + Be^{p_1 t} + B^* e^{p_2 t} + (Ce^{rt} + De^{p_1 t} + D^* e^{p_2 t}) K_L \tau_0$$

so that

$$e(t) \to 0 \text{ as } t \to \infty$$

as $r < 0, \mathrm{Re}(p_1) = \mathrm{Re}(p_2) < 0$.

Proportional Plus Integral Plus Derivative (PID) Control

A proportional plus integral plus derivative (PID) controller is defined by

$$G_c(s) = (K_P + K_I/s + K_D s) = \frac{K_D s^2 + K_P s + K_I}{s}$$

or, in the time domain,

$$v_a(t) = Ke(t) + \alpha K \int_0^t e(t)dt + K_D \frac{de}{dt}.$$

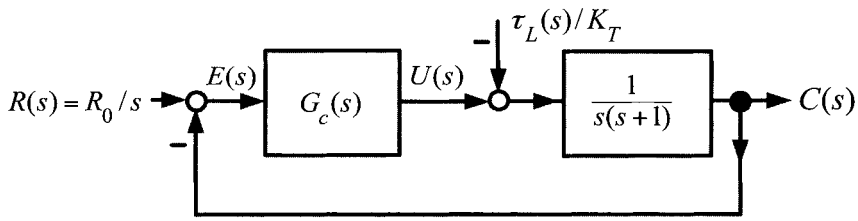


FIGURE 2.40. A proportional plus integral plus derivative controller.

The advantages of Proportional plus Integral (PI) controllers of the form $K_P + K_I/s$ has been discussed. The derivative control term $K_D s$ is used to force the transients to die out faster. That is, as will be shown below, the term $K_D s$ allows the control designer to put the closed-loop poles further in the left-half plane. However, before this is done, some practical issues concerning the derivative controller $K_D s$ are considered.

www.EngineeringEBooksPdf.com

Practical Problem with Derivative Controllers

Differentiation of a signal with noise amplifies the noise!! Most signals contain a high-frequency low-amplitude noise. For example, a DC power supply takes a 60-Hz AC signal and rectifies it into a DC voltage. Due to this process (Full-Wave Rectification) there is a small amplitude 120 Hz signal (i.e., noise) added onto the DC output.

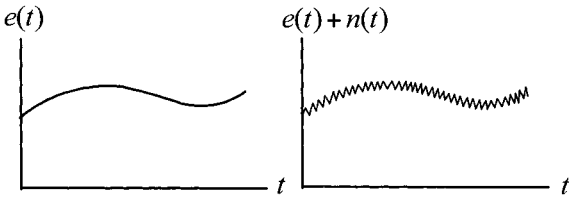


FIGURE 2.41. Left: Error signal. Right: Error signal containing high-frequency low-amplitude noise.

If one measures the error signal $e(t)$, the signal $e(t) + n(t)$ is actually obtained where $n(t)$ is a noise term. Numerically differentiating this signal gives the approximation

$$\dot{e}(t) + \dot{n}(t) \cong \frac{e(t) - e(t - \Delta t) + n(t) - n(t - \Delta t)}{\Delta t}.$$

As the difference $n(t) - n(t - \Delta t)$ may be of the same order (or higher) of magnitude as $e(t) - e(t - \Delta t)$, it follows that $\dot{n}(t)$ can be of the same order of magnitude as $\dot{e}(t)$. For example, let this noise[10] be given by $n(t) = 0.01\sin(2\pi(120t)) = 0.01\sin(754t)$. Thus, even though $n(t)$ is quite small, $\dot{n}(t) = 7.54\sin(754t)$ is large and can swamp out the value of $e(t)$.

Practical Implementation of Derivative Feedback for DC Motors

Consider the control structure shown in Figure 2.42. Using a tachometer, a direct measurement of the speed $\omega(t)$ is obtained which is then used as a feedback signal. K_t is an adjustable gain set by the control system designer. Note that, in contrast to the general PID controller structure originally introduced above, the tachometer is feeding back only the derivative of the output $\dot{c}(t)$ not the derivative of the error $\dot{e}(t)$.

[10] This could be a model for the noise on the DC bus of an amplifier when it uses a full-wave rectifier to convert the 120-Hz AC outlet to DC.

www.EngineeringEBooksPdf.com

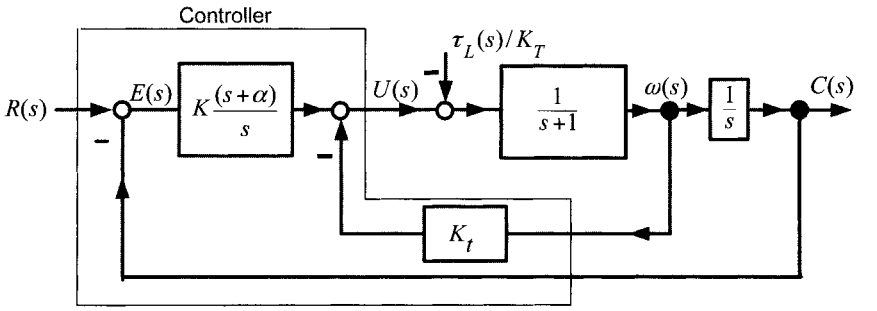


FIGURE 2.42. Implementation of a derivative controller using a tachometer.

To compute the transfer functions from $R(s)$ and $D(s)$ to the error $E(s)$, the block diagram of Figure 2.42 is reduces to

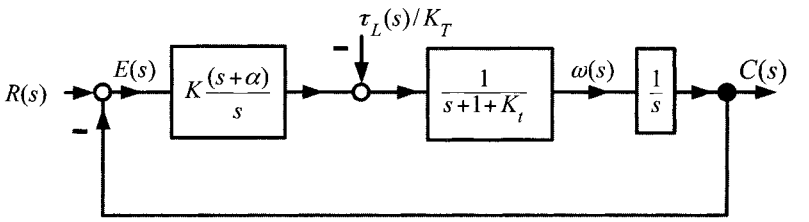


FIGURE 2.43. Block diagram reduction of Figure 2.42.

Thus $E(s) = E_R(s) + E_D(s)$ where

$$E_R(s) = \frac{1}{1 + K\dfrac{s+\alpha}{s}\dfrac{1}{s+1+K_t}\dfrac{1}{s}} R(s)$$
$$= \frac{s^2(s+1+K_t)}{s^3 + (1+K_t)s^2 + Ks + \alpha K} R(s)$$

and

$$E_D(s) = \frac{\dfrac{1}{s+1+K_t}\dfrac{1}{s}}{1 + K\dfrac{s+\alpha}{s}\dfrac{1}{s+1+K_t}\dfrac{1}{s}} D(s)$$
$$= \frac{s}{s^3 + (1+K_t)s^2 + Ks + \alpha K} D(s).$$

As the parameters K_t, K, and α are chosen by the control engineer, the coefficients of the closed-loop characteristic polynomial $s^3 + (1+K_t)s^2 + Ks + \alpha K$ may be chosen arbitrarily. In other words, the location of the

www.EngineeringEBooksPdf.com

closed-loop poles can be placed anywhere in the left-half plane by the control system designer.

In summary, a PID controller for a DC servomotor allows one to achieve tracking of step and ramp inputs, and rejection of constant load torque disturbances, with the closed-loop poles placed in any desired location. Typically, one desires the closed-loop poles to be as far in the left-half plane as possible so that the transients die out quickly. However, this typically means the control gains must be quite large. To see this, consider the above DC servomotor with tachometer feedback. As derived above, the error $E_R(s)$ is given by

$$E_R(s) = \frac{s^2(s+1+K_t)}{s^3+(1+K_t)s^2+Ks+\alpha K} R(s).$$

Suppose it is desired to put the closed-loop poles at $-10, -10+j10$ and $-10-j10$. Set

$$\begin{aligned} s^3+(1+K_t)s^2+Ks+\alpha K &= (s+10)(s-(-10+j10))(s-(-10-j10)) \\ &= (s+10)(s^2+20s+200) \\ &= s^3+30s^2+400s+2000. \end{aligned}$$

That is, $1+K_t = 30$ or $K_t = 29, K = 400$, and $\alpha K = 2000$ or $\alpha = 5$.

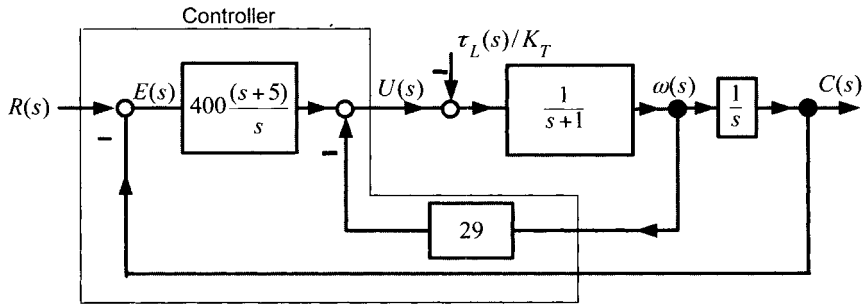


FIGURE 2.44. Example of a PID controller design.

At $t = 0^+$, $c(0^+) = 0, \omega(0^+) = 0$.Then, $e(0^+) = r(0^+) - c(0^+) = R_0$, where $r(t) = R_0 u_s(t)$. The input at $t = 0^+$ is then given by

$$u(0^+) = 400e(0^+) + 2000\int_0^{0^+} e(t)dt - 29\omega(0^+) = 400R_0.$$

This shows that right after the reference input $r(t) = R_0 u_s(t)$ is applied, the output of the controller (the current commanded to the motor amplifier) is $400R_0$ amperes. In particular, if $R_0 = 1$ radian, then the amplifier is

www.EngineeringEBooksPdf.com

required to put out 400 A which would most certainly be beyond the limit of the amplifier. The point here is that, in practice, one cannot place the closed-loop poles arbitrarily, but is limited by physical constraints such as the amplifier limits. These physical constraints were not included in the model on which the design was based.

General Theory of Tracking and Disturbance Rejection

With the above examples as background, a general approach to tracking and disturbance rejection in now presented. First, some definitions are required.

Definition *Type Number of a System*

Let

$$G(s) = \frac{b(s)}{s^j \bar{a}(s)}$$

where $\bar{a}(0) \neq 0$. Then $G(s)$ is said to be a type j systems which simply means it has j poles at the origin.

Examples

$$G(s) = \frac{1}{s^2} \qquad \text{Type 2} \quad \bar{a}(s) = 1$$

$$G(s) = \frac{1}{s(s+1)^2} \qquad \text{Type 1} \quad \bar{a}(s) = (s+1)^2$$

$$G(s) = \frac{1}{(s+2)} \qquad \text{Type 0} \quad \bar{a}(s) = (s+2)$$

$$G(s) = \frac{s+1}{s(s^2+2s+2)} \qquad \text{Type 1} \quad \bar{a}(s) = s^2 + 2s + 2$$

Definition *Type Number of an Input*

If the input to a system $R(s)$ has j poles at the origin (i.e., at $s = 0$) and the rest of the poles of $R(s)$ are stable, then $R(s)$ is said to be a type j input.

www.EngineeringEBooksPdf.com

Examples

$R(s) = \dfrac{1}{s}$ Type 1

$R(s) = \dfrac{1}{s^2}$ Type 2

$R(s) = \dfrac{1}{s^j}$ Type j

$R(s) = \dfrac{1}{s(s+2)}$ Type 1

$R(s) = \dfrac{1}{s(s-2)}$ Type number not assigned (unstable pole at 2)

Remark Consider $R(s) = \dfrac{1}{s(s+2)} = \dfrac{1}{2}\dfrac{1}{s} - \dfrac{1}{2}\dfrac{1}{s+2}$, so that $r(t) = 1/2 - (1/2)e^{-2t}$. To asymptotically track this $r(t)$, the output signal $c(t)$ must just go to $1/2$ as $t \to \infty$ as $-(1/2)e^{-2t}$ dies out. However, if $R(s) = \dfrac{1}{s(s-2)} = -\dfrac{1}{2}\dfrac{1}{s} + \dfrac{1}{2}\dfrac{1}{s-2}$, then $r(t) = -1/2 + (1/2)e^{2t}$ so that $c(t)$ must asymptotically got to $-1/2+(1/2)e^{2t}$ as $t \to \infty$ in order to track the input.

Consider now the general tracking and disturbance rejection problem as setup in the block diagram of Figure 2.45.

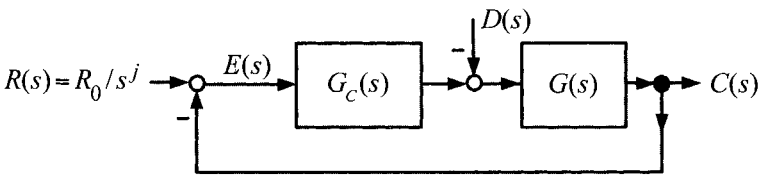


FIGURE 2.45. Block diagram for tracking a type j input.

Let $G_c(s) = Kb_c(s)/a_c(s)$ and $G(s) = b(s)/a(s)$ be the transfer functions of the controller and plant (physical system), respectively. First, the disturbance is taken to be zero and the asymptotic tracking of type j inputs is considered. Then the asymptotic rejection of type j disturbances is addressed.

Theorem *Tracking with Zero Steady-State Error*

Let $R(s) = R_0/s^j$ be a type j input so $r(t) = \dfrac{R_0 t^{j-1}}{(j-1)!}$ and with $D(s) \equiv 0$, the error $e(t)$ satisfies

$$\lim_{t\to\infty} e(t) = \lim_{t\to\infty} (r(t) - c(t)) = 0$$

www.EngineeringEBooksPdf.com

if and only if the closed-loop system is stable; that is, the roots of

$$a_c(s)a(s) + Kb_c(s)b(s) = 0$$

are in the open left-half plane *and* the type number of the forward open-loop transfer function $G_c(s)G(s)$ is j or greater.

Remark The input is $R(s) = R/s^j$, and the second condition says that the forward open-loop transfer function $G_c(s)G(s)$ must also contain at least a factor of $1/s^j$

Proof

(if) Assume that the conditions hold. To show that $e(t) \to 0$ as $t \to \infty$, consider the error $E(s)$ given by

$$\begin{aligned} E(s) &= \frac{1}{1 + G_c(s)G(s)} R(s) = \frac{1}{1 + K\dfrac{b_c(s)}{a_c(s)}\dfrac{b(s)}{a(s)}} \frac{R_0}{s^j} \\ &= \frac{a_c(s)a(s)}{a_c(s)a(s) + Kb_c(s)b(s)} \frac{R_0}{s^j}. \end{aligned}$$

By hypothesis, $G_c(s)G(s)$ is at least type j, so that $a_c(s)a(s) = s^j\bar{a}(s)$. Using this expression, the s^j terms cancel resulting in

$$E(s) = \frac{\bar{a}(s)}{a_c(s)a(s) + Kb_c(s)b(s)} R_0.$$

Also, by hypothesis, the roots of the closed-loop characteristic polynomial

$$a_c(s)a(s) + Kb_c(s)b(s) = (s - p_1) \cdots (s - p_n)$$

satisfy $\mathrm{Re}(p_i) < 0$ for $i = 1, ...n$. A partial fraction expansion[11] of $E(s)$ then gives

$$E(s) = \frac{\bar{a}(s)}{(s - p_1) \cdots (s - p_n)} R_0 = \frac{A_1}{s - p_1} + \frac{A_2}{s - p_2} + \cdots + \frac{A_n}{s - p_n}$$

or, in the time domain,

$$e(t) = A_1 e^{p_1 t} + \cdots A_n e^{p_n t}.$$

As $\mathrm{Re}(p_i) < 0$ for $i = 1, ..., n$, $e(t) \to 0$ as $t \to \infty$.

(only if) Here it must be shown that if $e(t) \to 0$ as $t \to \infty$, then

$$a_c(s)a(s) = s^j\bar{a}(s)$$

[11] This is assuming the poles are distinct. If they are not, the proof is easily modified with the same final result.

www.EngineeringEBooksPdf.com

where $\bar{a}(s)$ is a polynomial and the closed-loop characteristic polynomial is stable, that is,

$$a_c(s)a(s) + Kb_c(s)b(s) = (s - p_1)\cdots(s - p_n)$$

satisfies $\mathrm{Re}(p_i) < 0$ for $i = 1, ..., n$. Proceeding, the error $e(t)$ is the inverse Laplace transform of

$$E(s) = \frac{a_c(s)a(s)}{a_c(s)a(s) + Kb_c(s)b(s)} \frac{R_0}{s^j}. \tag{2.59}$$

Computing $e(t)$ using a partial fraction expansion of $E(s)$, it is clear that $e(t) \to 0$ as $t \to \infty$ only if $E(s)$ is asymptotically stable; that is, $E(s)$ must have all of its poles in the open left-half plane. Now, by equation (2.59), $E(s)$ will have j poles at the origin (unstable) due to the input $R(s) = R_0/s^j$ unless $a_c(s)a(s) = s^j\bar{a}(s)$. It is given that $e(t) \to 0$ as $t \to \infty$, so it follows that $a_c(s)a(s)$ *must* contain a factor s^j. Thus, $E(s)$ is of the form

$$E(s) = \frac{\bar{a}(s)}{a_c(s)a(s) + Kb_c(s)b(s)} R_0.$$

Further, by doing a partial-fraction expansion of this last expression for $E(s)$, it is seen that $\mathrm{Re}(p_i) < 0$ for $i = 1, ..., n$ in order that $e(t) \to 0$ as $t \to \infty$.

Consider now the disturbance rejection problem. The block diagram below illustrates the setup.

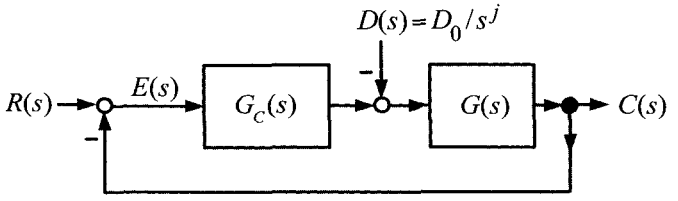


FIGURE 2.46. Block diagram with a type j disturbance.

As before, $G(s) = b(s)/a(s)$ and $G_c(s) = Kb_c(s)/a_c(s)$. The error $E(s)$ is then

$$E(s) = \frac{1}{1 + G_c(s)G(s)} R(s) + \frac{G(s)}{1 + G_c(s)G(s)} D(s).$$

www.EngineeringEBooksPdf.com

The error $E_D(s)$ due to the disturbance is

$$E_D(s) = \frac{G(s)}{1+G_c(s)G(s)}D(s) = \frac{K\dfrac{b(s)}{a(s)}}{1+K\dfrac{b_c(s)}{a_c(s)}\dfrac{b(s)}{a(s)}}D(s)$$

$$= \frac{a_c(s)b(s)}{a_c(s)a(s)+Kb_c(s)b(s)}D(s).$$

Consider a type j disturbance $D(s) = D_0/s^j$ and denote $e(t) = \mathcal{L}^{-1}\{E_D(s)\}$. The following theorem shows how such a disturbance signal can be rejected asymptotically.

Theorem *Disturbance Rejection with Zero Steady-State Error*

The error $e_D(t)$ satisfies

$$\lim_{t\to\infty} e_D(t) = 0$$

if and only if the closed-loop system is stable; that is, the roots of

$$a_c(s)a(s) + Kb_c(s)b(s) = 0$$

are all in the open left-half plane *and* the type number of the compensator transfer function $G_c(s)$ is j or greater.

Remark In contrast to the tracking problem where $G_c(s)G(s)$ must be type j, the compensator $G_c(s)$ *by itself* must contain at least the factor $1/s^j$.

Proof

By the above,

$$E_D(s) = \frac{a_c(s)b(s)}{a_c(s)a(s)+Kb_c(s)b(s)}\frac{D_0}{s^j}.$$

It is assumed here that $b(0) \neq 0$ which is true of most physical systems.[12] Thus $a_c(s)$ must have a factor of s^j to cancel the denominator of $D(s)$ in order to achieve zero steady-state error. With $a_c(s) = s^j\bar{a}(s)$, it follows that

$$E_D(s) = \frac{\bar{a}(s)b(s)}{(s-p_1)\cdots(s-p_n)}D_0 = \frac{A_1}{s-p_1} + \frac{A_2}{s-p_2} + \cdots + \frac{A_n}{s-p_n}.$$

The time response

$$e_D(t) = A_1e^{p_1t} + \cdots + A_ne^{p_nt} \to 0$$

as $t \to \infty$ if and only if $\mathrm{Re}(p_i) < 0$ for $i = 1, ..., n$. ■

[12] If $b(s) = s^k\bar{b}(s), \bar{b}(0) \neq 0$, then $G_c(s)$ need only be type $j-k$ so that $a_c(s)b(s) = s^{j-k}\bar{a}_c(s)s^k\bar{b}(s) = \bar{a}_c(s)\bar{b}(s)$.

www.EngineeringEBooksPdf.com

Internal Model Principle

The proofs of the tracking and disturbance rejection theorems suggest how one can achieve the same results with more general types of reference and disturbance signals. This is illustrated in the following example and is known as the *internal model principle.*

Example *Tracking a Sinusoid*

Consider a sinusoidal input given by $r(t) = R_0 \sin(t)$ or $R(s) = \dfrac{R_0}{s^2+1}$. Let $G(s) = \dfrac{1}{s(s+1)}$ and the problem is to design a compensator so that the output (asymptotically) tracks the input signal. The block diagram of the system is shown in Figure 2.47.

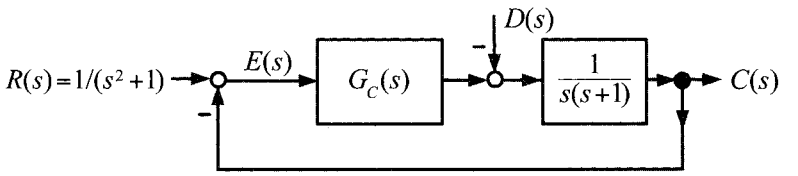


FIGURE 2.47. Ilustrating the internal model principle by tracking a sinusoidal input.

Consider the compensator

$$G_c(s) = K\frac{s+\alpha}{s^2+1}$$

which was chosen to have a denominator that was the *same* as that of the input. The reason for this is clear when the error $E(s)$ is computed as

$$\begin{aligned} E(s) &= \frac{1}{1+G_c(s)G(s)}R(s) \\ &= \frac{1}{1+K\dfrac{s+\alpha}{s^2+1}\dfrac{1}{s(s+1)}}\frac{R_0}{s^2+1} \\ &= \frac{s(s+1)(s^2+1)}{s^4+s^3+s^2+(K+1)s+\alpha K}\frac{R_0}{s^2+1} \\ &= \frac{s(s+1)}{s^4+s^3+s^2+(K+1)s+\alpha K}R_0. \end{aligned}$$

That is, the factor s^2+1 in the denominator of $G_c(s)$ reappears in the numerator of $E(s)$ to cancel the factor s^2+1 in the denominator of $R(s)$. Then $e(t) \to 0$ if the closed-loop characteristic polynomial is stable. The

www.EngineeringEBooksPdf.com

Routh table for $s^4 + s^3 + s^2 + (K+1)s + \alpha K$ is

$$\begin{array}{lll} s^4 & 1 & 1 \quad \alpha K \\ s^3 & 1 & K+1 \quad 0 \\ s^2 & \dfrac{1-(K+1)}{1} = -K & \alpha K \quad 0 \\ s & \dfrac{-K(K+1)-\alpha K}{-K} = \dfrac{K(K+1+\alpha K)}{K} & 0 \\ 1 & \alpha K & \end{array}$$

Stability requires $-K > 0, K+1+\alpha > 0$ and $\alpha K > 0$ or

$$K < 0, \quad -(K+\alpha) < 1, \quad \alpha < 0.$$

For example, choose $\alpha = -0.25$ and $K = -0.6$ so that the closed-loop characteristic polynomial is $s^4 + s^3 + s^2 + 0.4s + 0.15$ which has roots $-0.17 \pm j0.63, -0.33 \pm j0.49$. The error response is

$$e(t) = 4.7e^{-0.17t}\sin(0.63t + 0.37) - 4.1e^{-0.33t}\sin(0.49t + 0.4) \to 0$$

as $t \to \infty$. Note, however, the transients die out slowly.

Remark General procedures exist that allow one to design a compensator that asymptotically tracks any given input signal and, at the same time, arbitrarily place the closed-loop poles in the open left-half plane. The reader is referred to Refs. [47][48][49][50] for this theory.

This example and the previous results can be summarized as the *Internal Model Principle*. This just says that in order to (asymptotically) track a given reference signal, the forward open-loop transfer function $G_c(s)G(s)$ must contain the same *unstable* poles as the reference signal and the closed-loop system must be stable. (The terminology "internal model" refers to the poles of the transfer function as they determine the form of the time response of a transfer function model.)

Similarly, in order to achieve (asymptotic) steady-state rejection of a given disturbance signal, the forward open-loop controller (compensator) $G_c(s)$ must (by itself) contain the same unstable poles as the disturbance signal along with the closed-loop system being stable.

www.EngineeringEBooksPdf.com

Problems

PI Current Controller for a DC Motor

Problem 1 Simulation of the DC Motor

Let $V_{max} = 40$ V, $I_{max} = 5$ A, $K_b = K_T = 0.07$ V/rad/sec (= N-m/A), $J = 6 \times 10^{-5}$ kg-m^2, $R = 2$ ohms, $L = 2$ mH, and $f = 0.0004$ N-m/rad/sec. Develop a simulation of the DC motor that includes the motor and amplifier (with saturation) as well as an encoder with 2000 pulses/rev. Put a step input of $v(t) = 10$ V into the motor and plot out (a) $\theta(t) = \frac{2\pi}{2000} N(t)$ ($N(t)$ is the encoder output), (b) $\omega(t)$, (c) $i(t)$, and (d) $v(t)$. Also, zoom in on $\theta(t)$ to show the staircase waveform similar to that shown in Figure 2.4. (Hint: If it does not show a staircase waveform, then the step size in the simulator's integration algorithm may be too large.)

Problem 2 Load-Torque Transfer Function

(a) Compute the transfer function from $\tau_L(s)$ to $\theta(s)$ in Figure 2.5.

(b) Compute the transfer function from $\tau_L(s)$ to $\theta(s)$ in Figure 2.6. What does it reduce to as $K_P \to \infty$?

Problem 3 Transfer Function $i(s)/i_r(s)$

With $\tau_L(s) = 0$ in Figure 2.6, find the transfer function $i(s)/i_r(s)$. What does it reduce to as $K_p \to \infty$?

Problem 4 Encoder Resolution

It was shown that if there are N_w windows (lines/slots) equally spaced around the encoder disk (wheel), then there are N_w pulses per revolution so that there are $2N_w$ rising and falling edges of the output signal. With the length of the windows the same as the length between the window, the resolution of the encoder is then $2\pi/(2N_w)$ radians. A second light detector is added to determine the direction of rotation. Show that by using the outputs of both light detectors, a resolution of $2\pi/(4N_w)$ radians can be achieved. Hint: Add the two waveforms of Figure 2.3(a) [or Figure 2.3(b)] and show that there is a rising or falling edge every $2\pi/(4N_w)$ radians.

Problem 5 Load-Torque Transfer Function

(a) Find the transfer function from $\tau_L(s)$ to $\theta(s)$ in Figure 2.6.

(b) What does it reduce to as $K_P \to \infty$?

Problem 6 High-Gain Current Control

Consider a PI current controller given by $K_P + K_I/s = K_P(s + \alpha)/s$ where $K_I = \alpha K_P$. This is illustrated in the block diagram given in Figure 2.48.

(a) Using the block diagram reduction method, find $G(s) = \omega(s)/i_r(s)$. Let $K_P \to \infty$ and show that $G(s) = \omega(s)/i_r(s) \to K_T/(sJ + f)$.

(b) With $\tau_L(s) = 0$ in Figure 2.48, find the transfer function $i(s)/i_r(s)$. What does it reduce to as $K_p \to \infty$?

www.EngineeringEBooksPdf.com

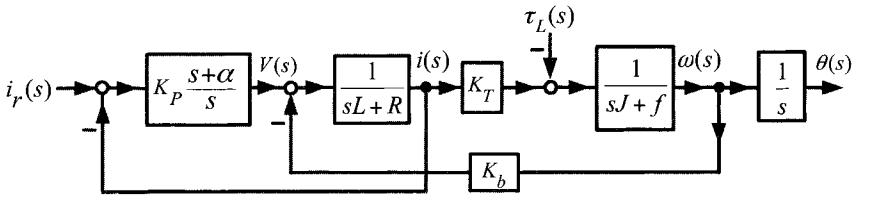


FIGURE 2.48. PI current controller.

Problem 7 Amplifier Saturation

With $i(t) = i_0$ constant and $\tau_L = 0$, find the steady-state values of the speed $\omega(\infty)$ and voltage $v(\infty)$ in terms of i_0 and the motor parameters. With $i_0 = 1$ A, $V_{max} = 40$ V and the values of the motor parameters in problem 1, can this steady-state speed be achieved? Explain. Redo this exercise with $i_0 = 4$ A. Note: You can easily answer this question using the original state space equations:

$$\begin{aligned} L\frac{di}{dt} &= -Ri(t) - K_b\omega(t) + v(t) \\ J\frac{d\omega}{dt} &= -f\omega(t) + K_T i(t) \\ \frac{d\theta}{dt} &= \omega(t). \end{aligned}$$

Problem 8 PI Current Controller

Add the PI current controller to the DC motor simulation of problem 1. Also, add a saturation block to the input of the PI current controller that limits the command current $i_r(t)$ between $\pm I_{max}$. Let $i_r(t)$ be a square wave current reference where one period is specified by

$$i_r(t) = \begin{cases} +I_1 & 0 \le t \le 0.25 \\ -I_1 & 0.25 \le t \le 0.50. \end{cases}$$

Try $I_1 = 0.1$ A and $I_1 = 1.0$ A in a simulation. Plot (a) $i(t)$ and $i_r(t)$ on the same plot and (b) $i_r(t) - i(t)$ on a separate plot. How well does $i(t)$ respond to step changes in $i_r(t)$?

Problem 9 Current Controller Tracking

With the parameter values as given in problem 1, this motor is capable of turning 180° in 0.065 sec (i.e., 65 msec). Consequently, the current controller must respond significantly faster than this if $i(t)$ is to be considered as the input, that is, if the dynamics $i_r(t) \to i(t)$ are to be neglected. To test the current controller under these conditions, consider $i(t) = i_0 \sin(t/T)$ with $i_0 = 1$ A, $T = 2\pi/\left(65 \times 10^{-3}\right)$ sec in the simulation. How well does $i(t)$ track this reference? Use your "best" controller design (i.e., your choice of K_P and α) and plot $i_r(t)$ and $i(t)$ on the same graph. Also plot out $v(t)$ to

www.EngineeringEBooksPdf.com

show it does not saturate. If you have problems with saturation, reduce your gains until you can achieve "good" tracking without exceeding the voltage limits.

Problem 10 Proportional Speed Control

Find the error transfer function $E(s)/\omega_{ref}(s)$ for the system in Figure 2.10.

(a) With $e(t) = \mathcal{L}^{-1}\{E(s)\}$ and $\omega_{ref}(s) = \omega_0/s$, show that the steady-state error $e(\infty) \approx (f/KK_T)\omega_0$ for K large.

(b) Using the parameter values given in problem 1 and K chosen such that $KK_T/J = 100$, compute $e(t) = \mathcal{L}^{-1}\{E(s)\}$ with $\omega_{ref}(t) = 100\sin\left(\frac{2\pi}{0.2}t\right)$.

Estimating the Motor Speed

Problem 11 Backward Difference Speed Estimator

(a) Simulate the backward difference method of computing speed with $T = 0.0002$ sec ($f_s = 5000$). Let $i_r = 1$ A and plot $\omega(kT)$ and $\hat{\omega}_{bd}(kT)$. What are some of the problems with this way of measuring speed? Repeat with $i_r = 0.5\sin((2\pi/0.2)\,t)$.

(b) With $i_r = 1$ A, use the output of a simulation to plot the speed and speed error to show it is bounded by $(2\pi/2000)/T$ when using the backward difference approximation to compute the speed. Do this for $T = 0.001$ sec and $T = 0.0002$ sec.

Problem 12 Recovery from a Load-Torque Disturbance

Add the load torque disturbance

$$\tau_L(t) = \begin{cases} 0 & 0.0 \le t \le 0.5 \\ \tau_{L0} & 0.5 \le t \le 0.6 \\ 0 & 0.6 \le t \end{cases}$$

to the torque equation of simulation of the DC motor. Run the simulation with $i_r = 1$ A and $\tau_{L0} = 0.035$ N-m. Plot $\hat{\omega}(kT), \hat{\omega}_{bd}(kT)$ and $\omega(kT)$ on the same graph. Redo this with $\ell_1 = 0, \ell_2 = 0$. Do you see a difference?

Problem 13 Speed and Load-Torque Estimator

(a) Consider the modification of the speed observer to estimate any constant (or, slowly varying) load-torque. That is, consider the situation where there is an unknown constant *load torque acting on the motor. This may be modeled as*

$$\begin{aligned} \frac{d\theta}{dt} &= \omega \\ \frac{d\omega}{dt} &= (K_T/J)i - (f/J)\omega - \tau_L/J \\ \frac{d(\tau_L/J)}{dt} &= 0 \end{aligned}$$

www.EngineeringEBooksPdf.com

Let a speed and load-torque estimator be given by

$$\begin{aligned} \frac{d\hat{\theta}}{dt} &= \hat{\omega} + \ell_1(\theta - \hat{\theta}) \\ \frac{d\hat{\omega}}{dt} &= (K_T/J)i - \hat{\tau}_L/J - (f/J)\hat{\omega} + \ell_2(\theta - \hat{\theta}) \\ \frac{d(\hat{\tau}_L/J)}{dt} &= 0 + \ell_3(\theta - \hat{\theta}). \end{aligned}$$

Define the estimation errors to be $e_1 = \theta - \hat{\theta}, e_2 = \omega - \hat{\omega}$ *and* $e_3 = \tau_L/J - \hat{\tau}_L/J$. *Subtract the above sets of equations to the find the system of equations describing the dynamics of observer error* $e(t) = (e_1(t), e_2(t), e_3(t))$. *Find* $E_1(s), E_2(s)$, *and* $E_3(s)$ *and show that the observer gains* ℓ_1, ℓ_2, *and* ℓ_3 *can be chosen so that* $e_2(t) \to 0$, $e_3(t) \to 0$ *as* $t \to \infty$ *but that* $e_1(t) \not\to 0$.

(b) Add the load-torque disturbance

$$\tau_L(t) = \begin{cases} 0 & 0.0 \le t \le 0.5 \\ \tau_{L0} & 0.5 \le t \le 1.0 \end{cases}$$

to the torque equation of simulation of the DC motor. Run the simulation with $i_r = 1$ *A and* $\tau_{L0} = 0.035$ *N-m. Plot* $\hat{\omega}(kT), \hat{\omega}_{bd}(kT)$, *and* $\omega(kT)$ *on the same graph. Redo this with* $\ell_1 = 0, \ell_2 = 0, \ell_3 = 0$. *Do you see a difference?*

Problem 14 Speed Observer Versus Backward Differentiation

Implement the observer (2.7) in the DC motor simulation and compare it with the calculation $\hat{\omega}_{bd}(kT) \triangleq \frac{2\pi}{2000}\left(\frac{N(kT) - N(kT-T)}{T}\right)$. *Specifically, let* $i_r = 0.1$ *A,* $\omega(0) = \hat{\omega}(0) = 0$ *and plot* $\omega(kT)$ *and its estimates* $\hat{\omega}(kT), \hat{\omega}_{bd}(kT)$. *You need to choose values for* ℓ_1 *and* ℓ_2*! Repeat with* $i_r = 0.5 \sin((2\pi/0.2)\, t)$.

Problem 15 Position Cannot Be Estimated from Speed Measurements

Suppose a tachometer is available to measure speed, but there is no position measurement. Can the position be estimated from the speed measurements? Well, the answer is no. An easy way to understand this is to realize that $\theta(t) = \theta(0) + \int_0^t \omega(\tau)d\tau$, *but that* $\frac{d}{dt}\left(c + \int_0^t \omega(\tau)d\tau\right) = \omega(t)$ *for* any *constant c. That is, there are an infinite number of position signals with the same speed signal. Consequently, the speed signal does not contain enough information to obtain an estimate for the position. From the point of view of observer theory, consider a position estimator given by*

$$\begin{aligned} \frac{d\hat{\theta}}{dt} &= \hat{\omega} + \ell_1(\omega - \hat{\omega}) \\ \frac{d\hat{\omega}}{dt} &= (K_T/J)i - (f/J)\hat{\omega} + \ell_2(\omega - \hat{\omega}). \end{aligned}$$

Show that ℓ_1, ℓ_2 *cannot be chosen so that* $\hat{\theta} \to \theta$.

www.EngineeringEBooksPdf.com

Problem 16 Discretization of the Observer Equations

Discretize the speed observer equations

$$\begin{aligned} \frac{d\hat{\theta}}{dt} &= \hat{\omega} + \ell_1(\theta - \hat{\theta}) \\ \frac{d\hat{\omega}}{dt} &= (K_T/J)i - (f/J)\hat{\omega} + \ell_2(\theta - \hat{\theta}) \end{aligned}$$

using the trapezoidal *method of integration.*

Trajectory Generation

Problem 17 Trajectory Design

Design a trajectory that also has a continuous jerk rate, that is, a trajectory that satisfies

$$\begin{array}{lll} \omega_{ref}(0) = 0 & \dot{\omega}_{ref}(0) = 0 & \ddot{\omega}_{ref}(0) = 0 \\ \omega_{ref}(t_1) = \omega_{max} & \dot{\omega}_{ref}(t_1) = 0 & \ddot{\omega}_{ref}(t_1) = 0 \\ \omega_{ref}(t) = \omega_{max} & for & t_1 \le t \le t_2 \\ \omega_{ref}(t_2) = \omega_{max} & \dot{\omega}_{ref}(t_2) = 0 & \ddot{\omega}_{ref}(t_2) = 0 \\ \omega_{ref}(t_3) = 0 & \dot{\omega}_{ref}(t_3) = 0 & \ddot{\omega}_{ref}(t_3) = 0 \end{array}$$

Design of a State Feedback Tracking Controller

Problem 18 Simulation of a Fast Point-to-Point Move

Implement the complete state feedback controller of Figure 2.14 in continuous time using the parameter values of problem 1. Specifically, use the speed observer given in equation (2.4), the feedback controller given in equation (2.14) and the trajectory generator of Section 2.3. Be sure to have a saturation block for the current commanded into the PI current controller and for the voltage out of the amplifier. Design a trajectory such that the motor turns $\theta_f = \pi$ radians in under 70 msec (by choosing the time t_1 to reach maximum speed and the time t_2 to begin decelerating) and does not violate the voltage or current constraints. Find the control gains K_0, K_1 and K_2 (by choosing r_1, r_2, r_3) and the observer gains ℓ_1, ℓ_2 (by choosing p_1, p_2) to track the trajectory. Plot (a) $\theta(t), \theta_{ref}(t)$, (b) $\hat{\omega}(t), \omega(t), \omega_{ref}(t)$, (c) $i_r(t), i_{ref}(t)$, (d) $\theta_{ref}(t) - \theta(t)$, (e) $\omega_{ref}(t) - \hat{\omega}(t)$, (g) $i_r(t) - i(t)$.

Problem 19 Simulation Study of Feedback

In order to understand the importance of the controller and reference inputs, carry out the following simulation runs using the simulation setup of problem 18 except in the trajectory generator, use $\theta_f = 30$ radians, $\omega_{max} = 100$ rads/sec, and $t_1 = 0.2$ and run the simulation for 0.6 sec.

(a) With $K_0 = 0, K_1 = 0, K_2 = 0$, $\omega(0) = 0, \theta(0) = 0, \tau_L = 0$ run the simulation with $i_r = i_{ref}$ and plot $\theta(t), \theta_{ref}(t), \hat{\omega}(t), \omega(t), \omega_{ref}(t), i_r(t)$, $i_{ref}(t)$ as well as $\theta_{ref}(t) - \theta(t), \omega(t) - \hat{\omega}(t), \omega_{ref}(t) - \omega(t), i_r(t) - i(t)$. This is referred to as running the system open-loop.

www.EngineeringEBooksPdf.com

(b) Redo (a) with $\omega(0) = 0, \theta(0) = 0.1, \tau_L = 0$.

(c) Redo (a) with $\omega(0) = 5, \theta(0) = 0, \tau_L = 0$.

(d) Redo (a) with $\omega(0) = 0, \theta(0) = 0$, $\tau_L = 0.035$ *N-m.*

(e) With $r_1 = 100, r_2 = 100, r_3 = 100$ *find the corresponding gains* K_0, K_1, K_2 *using given by equation (2.18). Run the simulation with these gains for the following cases:*

(i) Set $\omega(0) = 0, \theta(0) = 0$ *and* $\tau_L = 0$.

(ii) Set $\omega(0) = 0, \theta(0) = 0.1$ *and* $\tau_L = 0$.

(iii) Set $\omega(0) = 0, \theta(0) = 0$ *and* $\tau_L = 0.035$ *N-m.*

For each case, plot $\theta(t), \theta_{ref}(t), \hat{\omega}(t), \omega(t), \omega_{ref}(t), i_r(t), i_{ref}(t)$ *as well as* $\theta_{ref}(t) - \theta(t), \omega(t) - \hat{\omega}(t), \omega_{ref}(t) - \omega(t), i_r(t) - i(t)$.

(f) Remove the integrator term in the feedback expression (2.13) (or (2.14)) to study its effect. That is, substitute $w = K_1 e_1(t) + K_2 e_2(t)$ *for* w *into (2.11) and choose the gains as* $K_2 = r_1 + r_2 - f/J$, $K_1 = r_1 r_2$ *so that the closed-loop characteristic equation is then* $(s + r_1)(s + r_2)$. *With* $r_1 = 100, r_2 = 100$, *redo cases (i), (ii) and (iii) of part (e).*

Problem 20 Final Value Theorem

Let $E(s) = n(s)/d(s)$ *with* $\deg\{n(s)\} < \deg\{d(s)\}$ *and* $e(t) \triangleq \mathcal{L}^{-1}\{E(s)\}$. *The final value theorem says*

If $sE(s)$ *is* stable, *then*

$$e(\infty) = \lim_{s \to 0} sE(s).$$

(a) Let

$$E(s) = \frac{1}{s(s+1)(s+2)}$$

and compute the final value two ways: (1) Do a partial fraction expansion to compute the inverse Laplace transform $e(t)$ *and let* $t \to \infty$ *and (2) Use the final value theorem.*

(b) Let

$$E(s) = \frac{1}{s(s-1)(s+2)}$$

and do a partial fraction expansion to compute the inverse Laplace transform $e(t)$ *and let* $t \to \infty$. *How does this compare with computing* $\lim_{s \to 0} sE(s)$*? Explain.*

(c) Let

$$E(s) = \frac{n(s)}{d(s)}$$

where $\deg\{n(s)\} < \deg\{d(s)\}$. *Prove the final value theorem by doing a partial fraction expansion of* $E(s)$. *To simplify the presentation of the partial fraction expansion, assume that the poles of* $E(s)$ *are distinct, that is,* $d(s)$ *has no repeated roots. [Hint: Note then that* $\lim_{s \to 0} sE(s)$ *is the coefficient of the* $1/s$ *term in the partial fraction expansion of* $E(s)$.*]*

www.EngineeringEBooksPdf.com

Problem 21 State Feedback with a Constant Load Torque

(a) For the case where $\tau_L \neq 0$, give the appropriately modified version of (2.17). Also, with $\tau_L(s) = \tau_{L0}/s$, find the steady-state values $e_0(\infty), e_1(\infty)$, and $e_2(\infty)$ using the final-value theorem. With the constant load-torque disturbance acting on the motor, explain why the steady-state error in speed and position are both zero, that is, $e_2(\infty) = 0$ and $e_1(\infty) = 0$, but that $e_0(\infty) \neq 0$. With

$$i_{fb}(t) \triangleq \frac{J}{K_T}\left(K_0 \int_0^t e_1(\tau)d\tau + K_1 e_1(t) + K_2 e_2(t)\right)$$

Show that $i_{fb}(\infty) = \tau_{L0}/K_T$ and give an interpretation to this value.

(b) Consider state feedback control, but now without *the integrator feedback. That is, consider the system [compare with (2.15)]*

$$\begin{aligned} \frac{de_1}{dt} &= e_2 \\ \frac{de_2}{dt} &= -(f/J)e_2 - K_1 e_1 - K_2 e_2 + \tau_L/J. \end{aligned}$$

With $\tau_L(s) = \tau_{L0}/s$, find $E_1(s)$ and $E_2(s)$. Show that $e_2(t) \to 0$, but $e_1(t) \not\to 0$ as $t \to \infty$. Comparing with your solution to part (a), what can you conclude about using integrator feedback?

Problem 22 State Feedback with a Ramp Load Torque

With $\tau_L(s) = \tau_{L0}/s^2$, that is, $\tau_L(t) = \tau_{L0}t$, find $e_0(\infty)$, $e_1(\infty)$, $e_2(\infty)$. Explain your answers.

Problem 23 State Feedback Design with Voltage as Input

Design a state feedback voltage controller for the DC motor based on the model

$$\begin{aligned} \frac{di}{dt} &= -(R/L)i(t) - (K_b/L)\omega(t) + v(t)/L \\ \frac{d\omega}{dt} &= -(f/J)\omega(t) + (K_T/J)i(t) - \tau_L(t)/J \\ \frac{d\theta}{dt} &= \omega(t). \end{aligned}$$

The reference trajectory satisfies

$$\begin{aligned} \frac{di_{ref}}{dt} &= -(R/L)i_{ref}(t) - (K_b/L)\omega_{ref}(t) + v_{ref}(t)/L \\ \frac{d\omega_{ref}}{dt} &= -(f/J)\omega_{ref}(t) + (K_T/J)i_{ref}(t) \\ \frac{d\theta_{ref}}{dt} &= \omega_{ref}(t). \end{aligned}$$

www.EngineeringEBooksPdf.com

Let

$$\begin{aligned} e_1(t) &= \theta_{ref}(t) - \theta(t) \\ e_2(t) &= \omega_{ref}(t) - \omega(t) \\ e_3(t) &= i_{ref}(t) - i(t) \\ u(t) &= (v_{ref}(t) - v(t))/L \end{aligned}$$

and consider a controller of the form

$$u = -\left(K_0 \int_0^t e_1(\tau)d\tau + K_1 e_1(t) + K_2 e_2(t) + K_3 e_3(t)\right).$$

With $\tau_L(t) = \tau_{L0} u_s(t)$, *for* $i = 0, 1, 2, 3$ *compute* $E_i(s)$ *and* $e_i(\infty)$. *In particular, does the steady-state position error* $e_1(t)$ *go to zero as* $t \to \infty$?

Nested Loop Controllers

Problem 24 Nested PI Controllers

Consider the PID nested loop controller given in Figure 2.49.

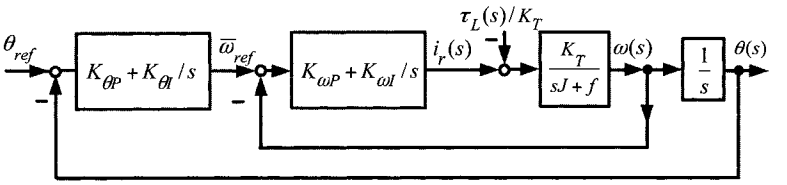


FIGURE 2.49. Control structure where the gains of the speed loop are tuned first and then the gains of the position loops are tuned. The speed reference $\bar{\omega}_{ref}$ is the output of the position loop rather than the stored value of $\omega_{ref} = d\theta_{ref}/dt$.

(a) With $\theta_{ref}(t) = \left(t^2/2\right) u_s(t)$ $(\theta_{ref}(s) = 1/s^3)$, $\tau_L \equiv 0$ *and* $K_{\omega I} = 0$, *can the other gains be chosen so that steady-state error is zero for this type of input? Explain by computing* $E(s)/\theta_{ref}(s)$ *with* $\tau_L \equiv 0$ *and* $K_{\omega I} = 0$.

(b) With $\theta_{ref}(t) \equiv 0, \tau_L(t) = \tau_0 t$ $(\tau_L(s) = \tau_0/s^2)$ *and* $K_{\omega I} \neq 0$, *can the gains be chosen such that steady-state error is zero for this type of load torque disturbance? Explain by computing* $E(s)/\theta_{ref}(s)$ *with* $\theta_{ref}(t) \equiv 0$. *How does your answer change if* $K_{\omega I} = 0$?

(c) With $\tau_L \equiv 0$, *can this controller track* $\theta_{ref}(t) = \cos(\omega_0 t)$ *or, equivalently,* $\theta_{ref}(s) = \omega_0/\left(s^2 + \omega_0^2\right)$ *with zero steady-state error? Explain.*

(d) Repeat (a), (b), and (c) with $K_{\omega I} \neq 0$.

Problem 25 Simulation of the Nested Loop Controller

Do a simulation of the complete system (i.e., motor, controller, and trajectory) given in problem 24. Use the same motor parameters as in problem 1. Take $\theta_f = \pi$ *radians and find the control gains* $K_{\theta P}, K_{\theta I}, K_{\omega P}$

www.EngineeringEBooksPdf.com

($K_{\omega I} = 0$), ω_{max}, and t_1 for the trajectory (2.25) such that the motor turns π radians as fast as possible without violating the voltage or current constraints. Plot (a) $\theta(t), \theta_{ref}(t)$, (b) $\hat{\omega}(t), \omega(t), \omega_{ref}(t)$, (c) $i_r(t), i_{ref}(t)$, (d) $\theta_{ref}(t) - \theta(t)$, (e) $\omega(t) - \hat{\omega}(t)$, (f) $\omega_{ref}(t) - \omega(t)$, (g) $i_r(t) - i(t)$. Compare with problem 18. In particular, can this move be carried out in under 70 msec?

Problem 26 Laplace Transform of the Reference Trajectory

The reference trajectory given in (2.25) can be rewritten as (u_s is the unit step function)

$$\begin{aligned}\theta_{ref}(t) &= \omega_{max}\frac{t^2}{2t_1}\left(u_s(t) - u_s(t-t_1)\right) \\ &\quad + \left(\omega_{max}\frac{t_1}{2} + \omega_{max}(t-t_1)\right)\left(u_s(t-t_1) - u_s(t-t_2)\right) \\ &\quad + \left(\omega_{max}t_2 - \omega_{max}\frac{(t_f-t)^2}{2t_1}\right)\left(u_s(t-t_2) - u_s(t-t_f)\right) \\ &\quad + \omega_{max}t_2 u_s(t-t_f)\end{aligned}$$

where $\omega_{max} = \theta_f/t_2$ to ensure $\theta_{ref}(t_f) = \theta_f$.

Show that the Laplace transform of $\theta_{ref}(t)$ is given by

$$\begin{aligned}\mathcal{L}\{\theta_{ref}(t)\} &= \frac{\omega_{max}}{t_1}\frac{1}{s^3} - \left(\frac{\omega_{max}t_1}{2}\frac{1}{s} + \omega_{max}\frac{1}{s^2} + \frac{\omega_{max}}{t_1}\frac{1}{s^3}\right)e^{-t_1 s} \\ &+ \left(\frac{\omega_{max}t_1}{2}\frac{1}{s} + \frac{\omega_{max}}{s^2}\right)e^{-t_1 s} - \left(\left(-\frac{\omega_{max}t_1}{2} + \omega_{max}t_2\right)\frac{1}{s} + \frac{\omega_{max}}{s^2}\right)e^{-t_2 s} \\ &+ \left(\left(\omega_{max}t_2 - \frac{\omega_{max}(t_2-t_f)^2}{2t_1}\right)\frac{1}{s} - \frac{\omega_{max}(t_2-t_f)}{t_1}\frac{1}{s^2} - \frac{\omega_{max}}{t_1}\frac{1}{s^3}\right)e^{-t_2 s} \\ &- \left(\omega_{max}t_2\frac{1}{s} - \frac{\omega_{max}}{t_1}\frac{1}{s^3}\right)e^{-t_f s} + \omega_{max}t_2\frac{1}{s}e^{-t_f s}.\end{aligned}$$

Explain why the presence of the terms $e^{-t_1 s}, e^{-t_2 s}$, and $e^{-t_f s}$ does not affect the analysis of the steady-state error given in the text.

Problem 27 Nested Loop Control Structure With Voltage Input

In this problem, the PI current loop of the amplifier is included in the analysis of a nested loop controller for a DC motor. The PI current controller in Figure 2.50 can be equivalently considered a torque controller as $\tau = K_T i$. First, both the speed and position loops are opened in order to tune (choose) the torque (current) controller gains. After tuning the gains for this controller, the gains of the speed controller are tuned with the input to the torque controller being the output of the speed controller. Finally, the gains of the position loop are tuned with the input to the speed controller being the output of the position controller. Use the full motor model (2.1) in the analysis below.

www.EngineeringEBooksPdf.com

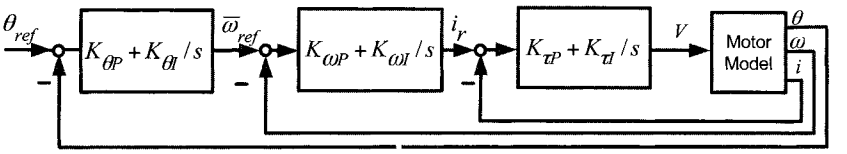


FIGURE 2.50. The gains of the torque (current) loop are tuned first. Next the gains of the speed loop are tuned and finally the gains of the position loop are tuned.

(a) Find the transfer functions $G_1(s), G_2(s)$ such that the error $E(s) = G_1(s)\theta_{ref}(s) + G_2(s)\tau_L(s)$.

(b) Can the gains be chosen to arbitrarily place the closed-loop poles?

(c) What kinds of inputs can be tracked? In particular, what is the largest power n such that

$$\theta_{ref}(t) = \frac{t^{n-1}}{(n-1)!}u_s(t)$$

or, equivalently,

$$\theta_{ref}(s) = \mathcal{L}\left\{\frac{t^{n-1}}{(n-1)!}u_s(t)\right\} = 1/s^n$$

can be tracked with zero steady-state error? What is the largest value of n if it is only required to have constant steady-state error?

(d) What kinds of disturbances can be rejected? That is, with

$$\tau_L(t) = \tau_{L0}\left(t^{m-1}/(m-1)!\right)u_s(t)$$

or

$$\mathcal{L}\left\{\frac{t^{m-1}}{(m-1)!}u_s(t)\right\} = 1/s^m,$$

what is the largest value of m such that there is no steady-state error due to this disturbance?

Identification of the Motor Parameters

Problem 28 Identification of the Motor Parameters

With a PI current controller implemented, run the DC motor simulation with the current reference given by

$$i_r(t) = \begin{cases} 2.5\sin\left(\dfrac{2\pi}{0.1}t\right) & \text{for } 0 \le t \le 0.5 \\ 2.5\sin\left(\dfrac{2\pi}{0.05}t\right) & \text{for } 0.5 \le t \le 1. \end{cases}$$

www.EngineeringEBooksPdf.com

Store $\theta(nT)$ in counts (from the encoder model), $i(nT)$ and $v(nT)$ with a sample period of $T = 0.001$ sec.

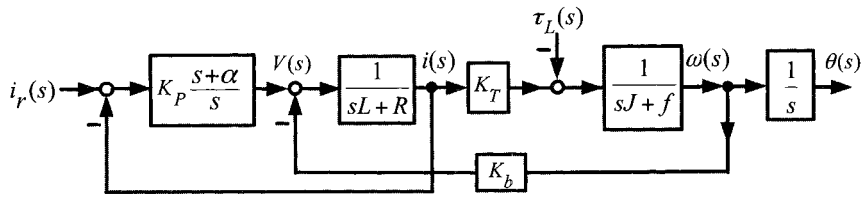


FIGURE 2.51. Block diagram of an open-loop DC motor with a current-command controller.

(a) Save the "data" from the simulation into a file. Using this "data set", write a program to implement the least-squares identification algorithm given in the text. It will be necessary to compute $\omega = d\theta/dt, d\omega/dt$ and di/dt using the "data" from the simulation. Due to the encoder resolution, $d\theta/dt$ and $d\omega/dt$ are noisy and di/dt is also noisy. It will be necessary to filter these computed quantities. Show the double filtering method (e.g., the `filtfilt` *command in* MATLAB*) with a second order Butterworth filter will work with an appropriate choice of the cutoff frequency. Compare your parameter estimates to the actual values in the simulation. Be sure to compute the error index and the parametric error indices of your estimates.*

(b) Do the identification of the parameters using "ideal" data by saving $d\theta/dt, d\omega/dt$ and di/dt from the simulation (rather than computing them offline) and show that this results in almost perfect agreement with the parameter values in the simulation. Compute the error index and the parametric error indices for this case. This is a way to check your identification program for errors.

Problem 29 Insufficient Excitation

Redo problem 28 with $i_r = i_0$ where $i_0 = 2.5$ A. Does the identification procedure work? Explain why or why not.

Problem 30 Completing the Square

Show that equation (2.38) is true.

Problem 31 Matrix Transpose Property

Show by direct computation that

$$\left(y^T(nT)W(nT)\right)^T = W^T(nT)y(nT).$$

Use this to show that $R_{yW} = R_{Wy}^T$.

Problem 32 Parametric Error Indices [42]

www.EngineeringEBooksPdf.com

Choose

$$C(\delta K, \lambda) \triangleq (\delta K_i)^2 + \lambda \left(E^2(K^*) - \delta K^T R_w \delta K \right)$$

and show that one still obtains

$$\delta K_i = \sqrt{E^2(K^*)(R_w^{-1})_{ii}}.$$

for the maximum.

Filtering of Noisy Signals

Problem 33 Transfer Functions

(a) Starting from the representation $y(t) = \int_{-\infty}^{t} g(t-\tau)m(\tau)d\tau$, *take the Laplace transform of both sides to show that* $Y(s) = G(s)M(s)$.

(b) Starting from the representation $\dot{x}(t) = Ax(t) + bm(t)$, $y(t) = cx(t) + dm(t)$ *show that* $G(s) = c(sI - A)^{-1}b$, *where* $A \in \mathbb{R}^{n\times n}, b \in \mathbb{R}^n, c \in \mathbb{R}^{1\times n}$.

Problem 34 Ideal Filters

Consider a unit impulse response given by

$$h(t) \triangleq \frac{\sin(\omega_c t)}{\pi t}$$

so with input $m(t)$, *the output* $y(t)$ *is defined to be*

$$y(t) = \int_{-\infty}^{\infty} h(\tau)m(t-\tau)d\tau.$$

This integral is defined as the Cauchy principal value, that is,

$$y(t) = \int_{-\infty}^{\infty} h(\tau)m(t-\tau)d\tau \triangleq \lim_{T\to\infty} \int_{-T}^{T} h(\tau)m(t-\tau)d\tau.$$

(a) With $m(t) = \cos(\omega t)$, *compute* $y(t) = h(t) * \cos(\omega t)$ *directly by evaluating*

$$y(t) = \lim_{T\to\infty} \int_{-T}^{T} \frac{\sin(\omega_c \tau)}{\pi\tau} \cos(\omega(t-\tau))d\tau$$

to show

$$y(t) = \lim_{T\to\infty} \int_{-T}^{T} \frac{\sin(\omega_c \tau)}{\pi\tau} \cos\left(\omega(t-\tau)\right) dt = \begin{cases} \cos(\omega t) & \text{for } |\omega| < \omega_c \\ \frac{1}{2}\cos(\omega t) & \text{for } \omega = \omega_c \\ 0 & \text{for } |\omega| > \omega_c. \end{cases}$$

This is the reason it is called an ideal filter as it passes any frequency below ω_c *unchanged and any frequency above* ω_c *is zeroed out.*

Why is it necessary to use the Cauchy principal value in the definition of the integral?

www.EngineeringEBooksPdf.com

(b) Compute the Fourier transform of $h(t)$ in the Cauchy principal value sense, that is, show

$$H(j\omega) = \mathfrak{F}\left\{\frac{\sin(\omega_c t)}{\pi t}\right\} \triangleq \lim_{T\to\infty} \int_{-T}^{T} e^{-j\omega t}\frac{\sin(\omega_c \tau)}{\pi\tau}dt = \begin{cases} 1 & \text{for } |\omega| < \omega_c \\ \frac{1}{2} & \text{for } \omega = \omega_c \\ 0 & \text{for } |\omega| > \omega_c. \end{cases}$$

(c) Is this filter causal? Show why or why not.
(d) Is this filter stable? Hint: Consider the input signal

$$m(t) = m_1(t)m_2(t).$$

where $m_1(t)$ is a periodic function with period $2\pi/\omega_c$ specified on one period by

$$m_1(t) = \begin{cases} -1 & \text{for } 0 \le t \le \pi/\omega_c \\ 1 & \text{for } \pi/\omega_c < t \le 2\pi/\omega_c \end{cases}$$

and $m_2(t)$ is defined by

$$m_2(t) = \begin{cases} -1 & \text{for } t \ge 0 \\ 1 & \text{for } t < 0. \end{cases}$$

This input signal is bounded as $|m(t)| = 1$. Compute the response to this input at time $t = 0$; that is, evaluate

$$y(t) = \lim_{T\to\infty} \int_{-T}^{T} \frac{\sin(\omega_c \tau)}{\pi\tau} m(t-\tau)d\tau$$

for $t = 0$ to obtain

$$y(0) = \int_{-\infty}^{\infty} \left|\frac{\sin(\omega_c \tau)}{\pi\tau}\right| d\tau = \infty.$$

(e) Evaluate the inverse Fourier transform of $H(j\omega)$ from part (b) as

$$h(t) = \frac{1}{2\pi}\int_{-\infty}^{\infty} e^{j\omega t}H(j\omega)d\omega$$

to get back $h(t) = \sin(\omega_c t)/(\pi t)$.

Problem 35 Butterworth Filters

For the third-order Butterworth filter, find the value of γ_n that best approximates $\angle G_n(j\omega) \approx -\gamma_n\omega$. For what range of values of ω is this approximation a good one?

Problem 36 Butterworth Filters from MATLAB

(a) With $\omega_c = 2\pi f_c$, $f_c = 100$ Hz and $T = 1/5000$ sec, explicitly compute the coefficients of a third-order Butterworth filter using (2.51).

www.EngineeringEBooksPdf.com

(b) In MATLAB, *use the* `butter` *command to design a third-order Butterworth filter with a cutoff frequency of* 100 *Hz and a sample rate of* 5000 *Hz. That is, use the command* `[b,a] = butter(3,fc/(fs/2))` *and* MATLAB *will return two vectors of the form* `b = [b1 b2 b3 b4 ]` *and* `a = [1 a2 a3 a4 ]` *which contain the coefficients of the filter.*

(c) Compare the coefficients obtained from MATLAB *with those obtained from the above design. Are they the same? Do you need to normalize the coefficients obtained using (2.51)?*

Recall that the cutoff frequency in MATLAB *is specified as* $f_{cmatlab} = f_c/(f_s/2)$ *where* $f_s = 5000$ *Hz. The* MATLAB *command is then* `[a,b] = butter(3,100/2500)`.

Problem 37 The `filter` Command in MATLAB

(a) Use the MATLAB *command* `butter` *to design a third-order Butterworth filter with* $f_s = 5000$ *Hz and* $f_c = 100$ *Hz* ($\omega_c = 2\pi \times 100$ *rads/sec). That is, use the command* `[b,a] = butter(3,fc/(fs/2))` *and* MATLAB *will return two vectors of the form* `b = [b1 b2 b3 b4 ]` *and* `a = [1 a2 a3 a4 ]` *which contain the coefficients of the filter.*

(b) Write a MATLAB *program to implement the state space equations (2.56) from* $n = 0$ *to* $n = N$ *using the coefficients given in part (a). With* $T = 1/f_s$, *run your program on some particular input data file* $\{m(nT)\}$ *with* $x(0) = 0$ *and plot out the response* $y(nT)$ *versus time* nT.

(c) Using the filter designed in part (a) and the MATLAB *command* `filter` *to filter the same input file used in part (b), that is,* `y2 = filter(b,a,m)`. *Plot* $y_2(nT)$ *versus time* nT. *Compare* y *from part (b) to* y_2.

Problem 38 Signal Flow Diagrams

Consider the second-order discrete-time transfer function

$$H(z) = \frac{Y(z)}{M(z)} = \frac{b_0 + b_1 z^{-1} + b_2 z^{-2}}{1 + a_1 z^{-1} + a_2 z^{-2}} = \frac{b_0 z^2 + b_1 z + b_2}{z^2 + a_1 z + a_2}$$

(a) A signal flow diagram for this system is shown in Figure 2.52. Find the transfer function $Y(z)/M(z)$ *from the signal flow (block) diagram. Give a discrete-time state space realization of the transfer function based on the signal flow diagram.*

www.EngineeringEBooksPdf.com

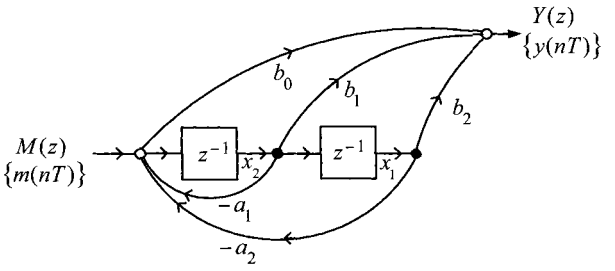


FIGURE 2.52. Signal flow diagram for a second-order filter.

(b) Show that the signal flow (block) diagram in Figure 2.53 is equivalent to the one in part (a) by finding a discrete-time state space realization based on the signal flow diagram and then computing the transfer function $Y(z)/M(z)$ from the state space realization.

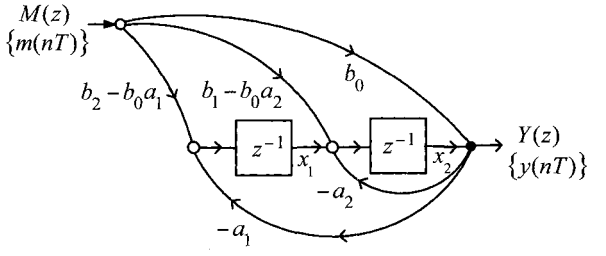


FIGURE 2.53. Equivalent signal flow diagram for a second-order filter.

Problem 39 How the `filtfilt` Command is Implemented

(a) Use the MATLAB *command* `butter` *(i.e.,* `[b,a]=butter[3,`w_n`]`*, where $w_n = f_c/(f_s/2)$) to design a third-order Butterworth filter with $f_s = 5000$ Hz and $f_c = 100$ Hz ($\omega_c = 2\pi \times 100$ rads/sec). Write a* MATLAB *program to implement this filter using the state space equations (2.56) (from $n = 0$ to $n = N$) and the coefficients given by the* `butter` *command. Run your program on some particular input data file $\{m(nT)\}$ with $x(0) = 0$ and plot out the response $y(nT)$ versus time nT. Store the final value of x, that is, $x(NT)$.*

(b) Take the output $\{y(nT), n = 0, ..., N\}$ of the filter in part (a), and compute $\{y_b(nT), n = 0, ..., N\} \triangleq \{y((N-n)T), n = 0, ..., N\}$. Use this as input to the (state space) filter designed in part (a), except initialize *the filter with the final conditions $x(NT)$ found in part (a). Let $\{y_{ffb}(nT), n = 0, ..., N\}$ be the output of this second filtering process and finally compute $\{y_{ff}(nT), n = 0, ..., N\} \triangleq \{y_{ffb}((N-n)T), n = 0, ..., N\}$. Plot $y_{ff}(nT)$ for $n = 0, ..., N$ versus time nT.*

www.EngineeringEBooksPdf.com

(c) Compare the output $y_{ff}(nT)$ from part (b) with the output using the MATLAB *command* `filtfilt` *as* $\mathtt{y}_{ff2} \triangleq \mathtt{filtfilt[b,a,m]}$, *where* `[b,a]= butter[3,`$w_n$`]` *with* $w_n = f_c/(f_s/2) = 100/(5000/2)$. *(They should be the same!)*

Control of Separately Excited, Series and Shunt DC motors

Problem 40 Armature Control of a Separately Excited DC Motor [2][51]

Recall from the previous chapter, the full mathematical model for the separately excited DC motor is

$$\begin{aligned} L\frac{di}{dt} &= -Ri + \frac{\partial \lambda}{\partial i_f}\frac{di_f}{dt} - K_m\lambda_f(i_f)\omega_r + v \\ J\frac{d\omega}{dt} &= K_m\lambda_f(i_f)i - \tau_L \\ \frac{d\lambda_f(i_f)}{dt} &= -R_f i_f + v_f \end{aligned}$$

where $\lambda(i_f, \theta)$ is the flux linkage in the armature loops due to the field current i_f and $\lambda_f(i_f)$ is the flux linkage in the field windings due to the field current i_f.

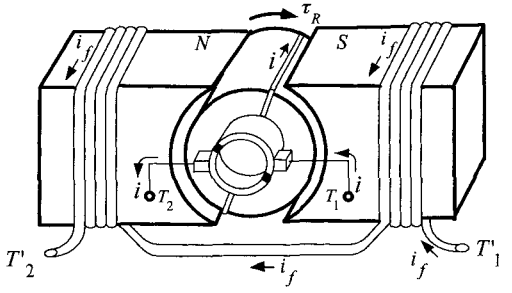


FIGURE 2.54. DC motor with a field winding.

In normal operation of a separately excited DC motor, di_f/dt varies slowly and the $\frac{\partial \lambda}{\partial i_f}\frac{di_f}{dt}$ term is often neglected. With $\lambda_f(i_f) = f(i_f)$ the saturation (magnetization) curve for the field flux linkage so that $i_f = f^{-1}(\lambda_f)$, the model written in terms of the state variables (i, ω, λ_f) be-

www.EngineeringEBooksPdf.com

comes[13]

$$\begin{aligned} L\frac{di}{dt} &= -Ri - K_m\lambda_f\omega + v \\ J\frac{d\omega}{dt} &= K_m\lambda_f i - \tau_L \\ \frac{d\lambda_f}{dt} &= -R_f f^{-1}(\lambda_f) + v_f. \end{aligned}$$

Interestingly, it will be shown in a later chapter that a field-oriented control of an induction motor results in a model of this form! With $x_1 = i, x_2 = \lambda_f, x_3 = \omega, u_1 = v/L$ *and* $u_2 = v_f$, *the model becomes*

$$\begin{aligned} \frac{dx_1}{dt} &= -\frac{R}{L}x_1 - \frac{K_m}{L}x_2x_3 + u_1 \\ \frac{dx_2}{dt} &= -R_f f^{-1}(x_2) + u_2 \\ \frac{dx_3}{dt} &= \frac{K_m}{J}x_2x_1 - \frac{\tau_L}{J}. \end{aligned}$$

(a) Show that the nonlinear transformation

$$\begin{aligned} z_1 &= x_3 \\ z_2 &= (K_m/J)x_2x_1 \\ z_3 &= x_2 \end{aligned}$$

results in the system being equivalent to

$$\begin{aligned} \frac{dz_1}{dt} &= z_2 - \tau_L/J \\ \frac{dz_2}{dt} &= g(x) + u_1(K_m/J)x_2 + (K_m/J)x_1u_2 \\ \frac{dz_3}{dt} &= -R_f f^{-1}(x_2) + u_2 \end{aligned}$$

where $g(x) \triangleq -\frac{RK_m}{JL}x_1x_2 - \frac{K_mR_f}{J}f^{-1}(x_2)x_2 - \frac{K_m^2}{JL}x_2^2x_3$.

(b) Show that the nonlinear feedback

$$\begin{bmatrix} u_1 \\ u_2 \end{bmatrix} = \begin{bmatrix} (K_m/J)x_2 & (K_m/J)x_1 \\ 0 & 1 \end{bmatrix}^{-1} \times \left(- \begin{bmatrix} g(x) \\ -R_f f^{-1}(x_2) \end{bmatrix} + \begin{bmatrix} v_1 \\ v_2 \end{bmatrix} \right)$$

[13] In the case that there is no magnetic saturation, $\lambda_f(i_f) = L_f i_f$ so that $i_f = \lambda_f/L_f$.

www.EngineeringEBooksPdf.com

results in the linear *system*

$$\begin{aligned} \frac{dz_1}{dt} &= z_2 - \tau_L/J \\ \frac{dz_2}{dt} &= v_1 \\ \frac{dz_3}{dt} &= v_2. \end{aligned}$$

This is referred to as exact linearization *or* feedback linearization.

(c) Show that if the load torque is constant, *then choosing*

$$\begin{aligned} v_1 &= -K_0 \int_0^t (z_1 - \omega_{ref})dt - K_1(z_1 - \omega_{ref}) - K_2\,(z_2 - \alpha_{ref}) + \frac{d}{dt}\alpha_{ref} \\ v_2 &= -K_f(z_3 - \lambda_{f\_ref}) + d\lambda_{f\_ref}/dt \end{aligned}$$

with the gains chosen appropriately results in $z_1 \to \omega_{ref}$ *and* $z_3 \to \lambda_{f\_ref}$.

(d) Draw a block diagram for the complete (i.e., nonlinear and linear feedback) control system.

Remarks: *If position control is desired, one simply appends* $dz_0/dt = z_1$ *to the system where* $z_0 = \theta$. *The feedback is singular only if* $x_2 = \lambda_f = 0$. *However, one chooses the input* v_2 *to ensure* $\lambda_f > 0$. *The importance of this approach is that the control of the speed through the input* v_1 *is decoupled from the control of the flux* ($z_2 = x_2 = \lambda_f$) *through the input* v_2. *The linear control techniques of this chapter are directly applicable to this linear model.*

Problem 41 Field Control of a Separately Excited DC Motor [51][52]

Another approach to controlling a separately excited DC motor is the so-called method of field control. *In this approach the armature voltage is held constant while the field voltage is varied to control the speed. This is often used in large DC drives (e.g., rolling mills) since the armature circuit can require* 2000-3000 *A and* 250 *V while the field circuit may require only* 20 *A. Consequently, it is of great economic advantage to use an amplifier that only has to handle the* 20 *A of the field circuit together with a large generator at constant voltage to produce the armature current. A mathematical model for a field controlled motor model in terms of the state variables* (i, ω, λ_f) *is then*

$$\begin{aligned} L\frac{di}{dt} &= -Ri - K_m\lambda_f\omega + V_{a0} \\ J\frac{d\omega}{dt} &= K_m\lambda_f i - \tau_L \\ \frac{d\lambda_f}{dt} &= -R_f f^{-1}(\lambda_f) + v_f \end{aligned}$$

where V_{a0} *is* constant *(typically the output of a generator).*

www.EngineeringEBooksPdf.com

(a) Consider the nonlinear transformation [52]

$$\begin{aligned} z_1 &= \left(Li^2 + J\omega^2\right)/2 \\ z_2 &= i\left(-Ri - K_m\lambda_f\omega + V_{a0}\right) + \omega K_m\lambda_f i = -Ri^2 + iV_{a0} \\ z_3 &= \left(-2Ri + V_{a0}\right)\left(-Ri - K_m\lambda_f\omega + V_{a0}\right)/L \end{aligned}$$

and show that the system equations become

$$\begin{aligned} \frac{dz_1}{dt} &= z_2 \\ \frac{dz_2}{dt} &= z_3 - \tau_L/J \\ \frac{dz_3}{dt} &= f(i,\omega,\lambda_f) + g(i,\omega,\lambda_f)v_f. \end{aligned}$$

Here $f(i,\omega,\lambda_f), g(i,\omega,\lambda_f)$ are nonlinear functions of the state (i,ω,λ_f). Show that application of the feedback

$$v_f = \left(-f(i,\omega,\lambda_f) + u_f\right)/g(i,\omega,\lambda_f)$$

results in a linear system. This is referred to as exact linearization *or a* feedback linearization *controller.*

(b) When is $g(i,\omega,\lambda_f)$ singular (i.e., when does $g(i,\omega,\lambda_f) = 0$)? Can this singularity be avoided in normal operation of the motor?

(c) Show how to pick the gains of the controller

$$\begin{aligned} u_f = &-K_0\int_0^t (z_1 - z_{1ref})dt - K_1(z_1 - z_{1ref}) - K_2\left(z_2 - z_{2ref}\right) \\ &-K_3\left(z_3 - z_{3ref}\right) + dz_{3ref}/dt \end{aligned}$$

such that $z_1 - z_{1ref} \to 0$ with a constant load torque.

(d) What are some practical problems with this approach to controlling the machine? (Hint: How does one choose $z_{1ref}, z_{2ref}, z_{3ref}$ so that $\omega \to \omega_{ref}$?)

Problem 42 Series Connected DC Motor [2][51][53][54]

A DC motor in which the field circuit is connected in series with the armature circuit is referred to as a series DC *motor. This connection is shown in the equivalent circuit of the series DC motor shown in Figure 2.55 and is typically used in applications that require high torque at low speed such as traction drives (e.g., subway trains) [2]. Comparing with the separately excited motor of Figure 2.54, it is seen that the terminal T_2' is connected to the terminal T_1 with the voltage v applied between terminals T_1' and T_2. The resistor R_p put in parallel with the field circuit is switched in at higher speeds to achieve field weakening (see problem 43).*

www.EngineeringEBooksPdf.com

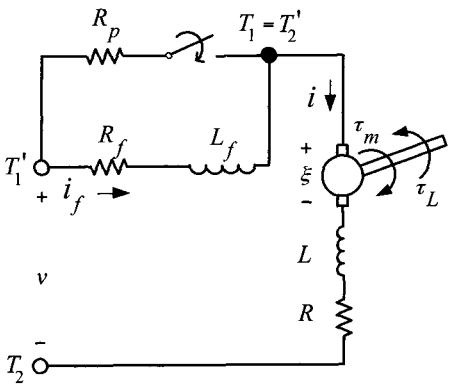


FIGURE 2.55. Equivalent circuit for a series DC motor.

With the switch for R_P open, the equations describing electrical circuit of the field and armature winding is

$$-\frac{d\left(Li - \lambda(i,\theta) + \lambda_f(i)\right)}{dt} - (R_f + R)\, i + v = 0.$$

Using the fact that $\partial\lambda(i_f,\theta)/\partial\theta = -K_m\lambda_f(i_f)$ and that the torque is given by $K_m\lambda_f(i_f)i$, the equations of the series connected DC motor are then

$$\begin{aligned}\frac{d\left(Li + \lambda_f(i)\right)}{dt} &= -(R_f + R)\, i + \frac{\partial\lambda}{\partial i_f}\frac{di_f}{dt} - K_m\lambda_f(i)\omega + v \\ J\frac{d\omega}{dt} &= K_m\lambda_f(i)i - \tau_L.\end{aligned}$$

In the case of the series winding, the armature flux Li can be neglected compared to the field flux $\lambda_f(i)$. Also $\dfrac{\partial\lambda}{\partial i_f}\dfrac{di_f}{dt}$ is neglected to obtain

$$\begin{aligned}\frac{d\lambda_f(i)}{dt} &= -(R_f + R)\, i - K_m\lambda_f(i)\omega + v \\ J\frac{d\omega}{dt} &= K_m\lambda_f(i)i - \tau_L.\end{aligned}$$

(In the case of no magnetic saturation in the field winding $\lambda_f(i) = L_f i$.)

(a) Show that the nonlinear transformation

$$\begin{aligned}z_1 &= \omega \\ z_2 &= (K_m/J)\lambda_f(i)i\end{aligned}$$

gives

$$\begin{aligned}\frac{dz_1}{dt} &= z_2 \\ \frac{dz_2}{dt} &= f(i,\omega) + g(i,\omega)v - \tau_L/J.\end{aligned}$$

www.EngineeringEBooksPdf.com

What are the expressions for $f(i,\omega), g(i,\omega)$?

(b) When is $g(i,\omega)$ *singular? Can this be avoided in normal operation? Show that the nonlinear feedback*

$$v_f = \frac{-f(i,\omega) + u}{g(i,\omega)}$$

results in the linear system

$$\begin{aligned} \frac{dz_1}{dt} &= z_2 \\ \frac{dz_2}{dt} &= u - \tau_L/J. \end{aligned}$$

This is called a feedback linearizing *controller or an* exact linearization *controller.*

(c) Show how to choose the gains for the controller

$$u = K_0 \int_0^t (\omega_{ref}(\tau) - \omega(\tau)d\tau + K_1 (\omega_{ref} - \omega) + K_2(\alpha_{ref} - \alpha) + \frac{d}{dt}\alpha_{ref}$$

so that $\omega_{ref} - \omega \to 0$ *with a constant load torque.*

(d) Draw a complete block diagram of the system including the nonlinear and linear feedback.

Problem 43 Field Weakening Control for a Series DC Motor [2][53]

Consider the series connected DC motor described in problem 42 running at high speed with the switch closed and $\lambda_f > 0$. *The current in the field winding is now less that the armature current* $(i_f < i_a)$ *so that the field flux linkage* $\lambda_f(i_f)$ *and therefore the back emf* $K_m\lambda_f(i_f)\omega$ *is now less than it would have been carrying full armature current. Consequently, this provides a way to achieve higher speeds than otherwise without having the back emf exceed the voltage limit. This is referred to as field weakening as the field flux linkage* $\lambda_f(i_f)$ *is now "weakened" compared to the value* $\lambda_f(i)$ *with full armature current.*

(a) Using the state variables (i, λ_f, ω), *derive a nonlinear state space model of the system.*

(b) Let $L = 0$ *and use the equation for the current* i *(setting* $Ldi/dt = 0$*) to solve for* $i = (v + R_p i_f - K_m\lambda_f\omega)/(R + R_p)$. *Use this to write a second order state space model in terms of the state variables* (λ_f, ω).

(c) Consider an input-output linearization controller of the form $v = -R_p i_f + K_m\lambda_f\omega + u(R + R_p)/(K_m\lambda_f/J)$ *where* u *is a new input. Explain how to control the speed and why the flux must satisfy* $0 < c_1 < \lambda_f < c_2$, *that is, it must be bounded from below and above.*

www.EngineeringEBooksPdf.com

Problem 44 Speed and Load-Torque Observer for the Series DC Motor [51][53][54]

An estimator for the speed and load torque of a series DC motor can be constructed using only a measurement of the current. To see this, consider the equations of the series DC motor with $L = 0$

$$\begin{aligned} \frac{d\lambda_f}{dt} &= -(R_f + R)i - K_m\lambda_f\omega + v \\ J\frac{d\omega}{dt} &= K_m\lambda_f i - \tau_L. \end{aligned}$$

Model the load torque as an unknown constant so that the equation

$$\frac{d(\tau_L/J)}{dt} = 0$$

is appended to the system.

(a) Show that the nonlinear change of coordinates

$$\begin{aligned} z_1 &= \ln(\lambda_f) \\ z_2 &= \omega \\ z_3 &= \tau_L/J \end{aligned}$$

results in

$$\begin{aligned} \dot{z} &= Az + h(i_a, i_f, \lambda_f, V) \\ y &= cz \end{aligned}$$

where

$$z = \begin{bmatrix} z_1 \\ z_2 \\ z_3 \end{bmatrix}, \; A = \begin{bmatrix} 0 & -K_m & 0 \\ 0 & 0 & -1 \\ 0 & 0 & 0 \end{bmatrix}, \; c = \begin{bmatrix} 1 & 0 & 0 \end{bmatrix}$$

and

$$h(i, i_f, \lambda_f, v) = \begin{bmatrix} (-R_f i_f - Ri + v)/\lambda_f \\ (K_m/J)\lambda_f i \\ 0 \end{bmatrix}.$$

(b) Show that the gain vector $\ell = \begin{bmatrix} \ell_1 & \ell_2 & \ell_3 \end{bmatrix}^T$ *can be chosen so that the observer defined by*

$$\begin{aligned} d\hat{z}/dt &= A\hat{z} + h(i, i_f, \lambda_f, v) + \ell(y - \hat{y}) \\ \hat{y} &= c\hat{z} \end{aligned}$$

results in $\hat{z} \to z$ *and, in particular,* $\hat{\omega} \to \omega$ *and* $\hat{\tau}_L/J \to \tau_L/J$.

(c) Is there a practical problem with using such an observer? Explain. (Hint: When is $h(i, i_f, \lambda_f, v)$ *singular?)*

www.EngineeringEBooksPdf.com

Problem 45 Speed and Load-Torque Observer for the Field-Weakened Series DC Motor [53]

Consider the state space model using the state variables (i, λ_f, ω) *as developed in problem 43. Add the first two equations together with* $L = 0$ *to show that*

$$\begin{aligned} \frac{d\lambda_f}{dt} &= -R_f i_f - Ri - K_m \lambda_f \omega + v \\ J\frac{d\omega}{dt} &= K_m \lambda_f i - \tau_L. \end{aligned}$$

Similar to the construction in problem 44, show that a speed and load-torque observer can be designed.

Problem 46 Shunt-Connected DC Machine [51][55]

A shunt-connected DC motor is one in which the armature and field circuits are connected in parallel. Specifically, using the separately excited DC motor of Figure 2.54, one adds an adjustable resistance R_{adj} *to the field circuit and then ties together terminals* T_1 *and* T_1' *as well as the terminals* T_2 *and* T_2' *resulting in the equivalent circuit shown in Figure 2.56.*

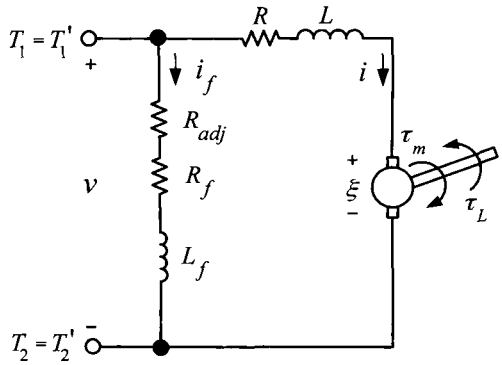


FIGURE 2.56. Equivalent circuit for a shunt DC motor.

The mathematical model is found to be

$$\begin{aligned} L\frac{di}{dt} &= -Ri - K_m \lambda_f \omega + v \\ \frac{d\lambda_f}{dt} &= -R_F f^{-1}(\lambda_f) + v \\ J\frac{d\omega}{dt} &= K_m \lambda_f i - \tau_L \end{aligned}$$

where $R_F = R_f + R_{adj}$. *As in the case of the series DC motor, the armature inductance is negligible so that setting* $L = 0$ *and* $i = (v - K_m \lambda_f \omega)/R$

www.EngineeringEBooksPdf.com

results in the reduced-order system

$$\begin{aligned}\frac{d\lambda_f}{dt} &= -R_F f^{-1}(\lambda_f) + v \\ \frac{d\omega}{dt} &= -\frac{K_m^2}{JR}\lambda_f^2\omega + \frac{K_m}{JR}\lambda_f v - \frac{\tau_L}{J}.\end{aligned}$$

(a) Show that the nonlinear transformation [where $g(\lambda_f) \triangleq f^{-1}(\lambda_f) = i_f$*]*

$$\begin{aligned}z_1 &= \omega - \frac{K_m}{2JR}\lambda_f^2 \\ z_2 &= -\frac{K_m^2}{JR}\lambda_f^2\omega + \frac{R_F K_m}{JR}\lambda_f g(\lambda_f).\end{aligned}$$

results in the system dynamics

$$\begin{aligned}\frac{dz_1}{dt} &= z_2 \\ \frac{dz_2}{dt} &= \alpha(\omega, \lambda_f) + \beta(\omega, \lambda_f)v - \frac{\tau_L}{J}.\end{aligned}$$

Show that application of the feedback

$$v = \frac{-\alpha(\omega, \lambda_f) + u}{\beta(\omega, \lambda_f)}$$

results in a linear system. This is called a feedback linearizing controller.

(b) Compute the expressions for $\alpha(\omega, \lambda_f), \beta(\omega, \lambda_f)$ *for the special case of linear magnetics, that is,* $\lambda_f \triangleq L_f i_f$*. In particular, show that*

$$\beta(\omega, \lambda_f) \triangleq \frac{K_m \lambda_f}{JR}\left(\frac{2R_F}{L_f} - 2K_m\omega - \frac{K_m^2}{JR}\lambda_f^2\right).$$

It turns out that the condition $\beta(\omega, \lambda_f) \neq 0$ *is satisfied for a region of the state space for which one would operate such a motor [55].*

(c) Show how to pick the gains of the controller

$$u_f = -K_0 \int_0^t (z_1 - z_{1ref})dt - K_1(z_1 - z_{1ref}) - K_2(z_2 - z_{2ref}) + \frac{dz_{2ref}}{dt}$$

such that $z_1 - z_{1ref} \to 0$ *with a constant load torque.*

(d) What are some practical problems with this approach to controlling the machine? (Hint: How does one choose z_{1ref}, z_{2ref} *so that* $\omega \to \omega_{ref}$*?)*

Problem 47 Input-Output Linearization of a Shunt DC Motor [51][55]

An alternative to the feedback linearizing controller for the shunt DC motor (see problem 46) is an input-output linearization *controller.*

www.EngineeringEBooksPdf.com

(a) Show that applying the feedback

$$v = \frac{(K_m^2/JR)\lambda_f^2\omega + u}{(K_m/JR)\lambda_f}$$

to the mathematical model in problem 46 results in the system

$$\begin{aligned} \frac{d\lambda_f}{dt} &= -R_F f^{-1}(\lambda_f) + K_m\lambda_f\omega + \frac{JR}{K_m\lambda_f}u \\ \frac{d\omega}{dt} &= u - \tau_L/J \end{aligned}$$

which is still a nonlinear system. The controller is nonsingular for $\lambda_f > 0$.

(b) The stability of the first equation, the so-called zero dynamics, *can be ascertained by multiplying it through by* λ_f *to obtain*

$$\begin{aligned} \frac{d\lambda_f^2}{dt} &= -R\lambda_f f^{-1}(\lambda_f) - K_m\lambda_f^2\omega + \frac{JR}{K_m}u \\ &= -\left(\frac{R}{L_f} - K_m\omega\right)\lambda_f^2 + \frac{JR}{K_m}u \end{aligned}$$

where the second line assumes linear magnetics. Show that λ_f *is bounded if* u *is bounded and* $\omega < \omega_{max} \triangleq R/(K_m L_f)$. *(Note that the adjustable resistor allows the designer to accommodate any specified maximum speed.)*

(c) Show how to pick the gains of the controller

$$u = -K_0\int_0^t(\omega - \omega_{ref})dt - K_1(\omega - \omega_{ref}) + \frac{d\omega_{ref}}{dt}$$

such that $\omega - \omega_{ref} \to 0$ *with a constant load torque.*

www.EngineeringEBooksPdf.com

This Page Intentionally Left Blank

www.EngineeringEBooksPdf.com

3

Magnetic Fields and Materials

The goal of this chapter is to present a concise, but relatively complete, introduction to the modeling of magnetic materials. The magnetic *intensity* field $\vec{\mathbf{H}}$ is introduced as way to modify Ampère's law $\oint \vec{\mathbf{B}} \cdot d\vec{\ell} = \mu_0 i_{\text{enclosed}}$ so that it is valid in the presence of magnetic materials. The difference between the magnetic *intensity* field $\vec{\mathbf{H}}$ and the magnetic *induction* field $\vec{\mathbf{B}}$ is explained. It is shown that $\vec{\mathbf{B}} = \mu_0 \vec{\mathbf{H}}$ in air while in ideal magnetic materials $\vec{\mathbf{H}} \equiv \mathbf{0}$ with $\vec{\mathbf{B}} \neq \mathbf{0}$. The distinction between "soft" and "hard" magnetic materials is explained.

3.1 Introduction

In this introductory section, an attempt is made to review the basic concepts of magnetic fields. Magnetic materials include iron (Fe), cobalt (Co), and nickel (Ni). All magnetic fields are produced by the motion of charged particles. The concern here will be with those magnetic fields setup by the flow (motion) of currents in wires and those due to the spin (motion) of electrons in the atoms making up magnetic materials. A common way one is introduced to magnetic fields is in the form of magnetic materials such as iron. That is, pieces of iron can be magnetized so that they attract or repel one another depending on their orientation with respect to each other. In Figure 3.1, the familiar bar magnet is shown.

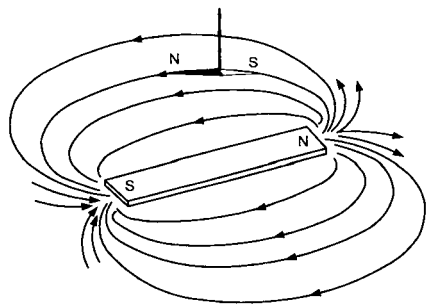


FIGURE 3.1. The direction of the compass needle specifies the direction of the magnetic field. From Figure 11-1 of *PSSC Physics*, 7th edition, by Haber-Schaim, Dodge, Gardner, and Shore, published by Kendall/Hunt, 1991.

www.EngineeringEBooksPdf.com

The curves shown in the figure are drawn to show the *direction* of the magnetic field. As shown in the figure, the direction of the magnetic field is simply defined to be the direction that a small compass needle (which is just another bar magnet) points. That is, the large bar magnet exerts a force/torque on the compass needle such that in equilibrium it is aligned in a particular direction which is taken by definition to be the direction of the magnetic field at that point.

Figures 3.2 through 3.7 show some simple experiments to demonstrate the direction of the magnetic fields produced by currents and magnetic materials. In these experiments, small iron filings (i.e., compass needles!) are uniformly spread over a piece of smooth paper so that when a magnetic field is applied, the iron filings will align themselves with the direction of the magnetic field. Of course, the field must be strong enough to make the filings turn against the friction force of the paper. In Figure 3.2, the magnetic field of a long straight wire carrying a current is seen to consist of concentric circles around the wire.

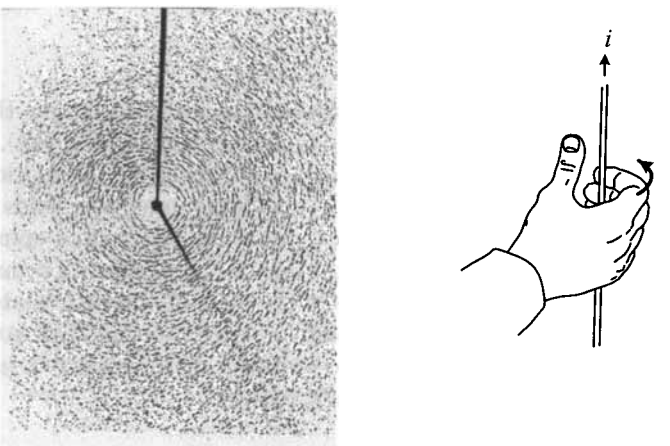


FIGURE 3.2. Magnetic field lines of a long straight wire carrying a current. Near the wire, concentric circles of iron filings are visible. At right is an illustration of the right-hand rule for the direction of the magnetic field lines around a wire carrying a current. From Figures 11-2(b) and 11-8, respectively, of *PSSC Physics*, 7th edition, by Haber-Schaim, Dodge, Gardner, and Shore, published by Kendall/Hunt, 1991.

Close to the wire where the magnetic field is strong, the concentric circles following the magnetic field are visible. However, as the distance from the wire increases, the magnetic field weakens to the point that it cannot align the iron filings against the friction forces of the paper.

Figure 3.2 also illustrates the right-hand rule for the direction of the magnetic field due to current in a wire. Simply, one puts their right thumb

www.EngineeringEBooksPdf.com

along the wire in the direction of the current and the fingers curl around the wire in the direction of the magnetic field.

Figure 3.3 shows another view of Figure 3.2 along with a simple drawing to illustrate the magnetic field lines.

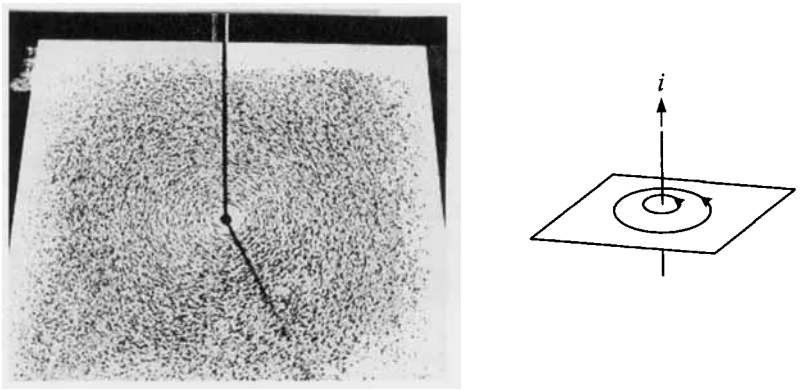


FIGURE 3.3. Iron filing experimental view and drawing of the magnetic field lines produced by a long straight wire carrying a current. From Figures 11-5 and 11-6(a) of *PSSC Physics*, 7th edition, by Haber-Schaim, Dodge, Gardner, and Shore, published by Kendall/Hunt, 1991.

In Figure 3.4, the magnetic field due to a loop carrying a current is shown along with a drawing illustrating the magnetic field lines.

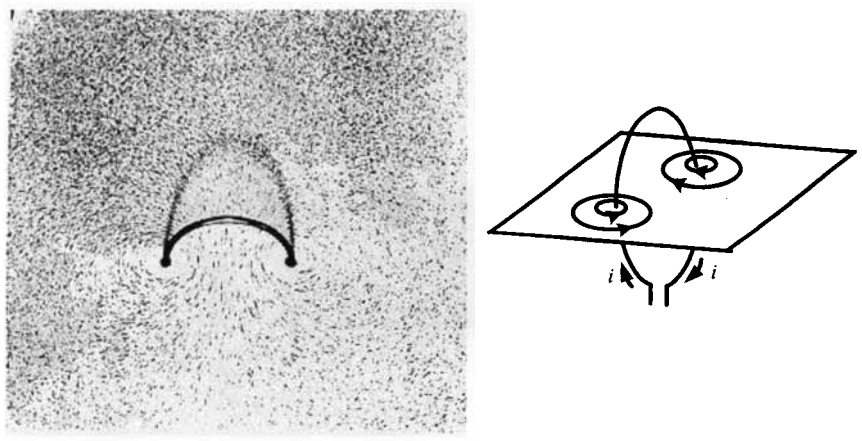


FIGURE 3.4. Iron filing experimental view and drawing of the magnetic field lines produced by a loop of wire carrying a current. From Figure 11-2(c) of *PSSC Physics*, 7th edition, by Haber-Schaim, Dodge, Gardner, and Shore, published by Kendall/Hunt, 1991.

www.EngineeringEBooksPdf.com

Figure 3.5 depicts the magnetic field produced by a coil of wire carrying a current. Such a coil is referred to as a *solenoid*. Notice that inside the solenoid, the field follows straight lines and then flares out at the ends. Figure 3.6 is another experimental example of a tightly wound short solenoid.

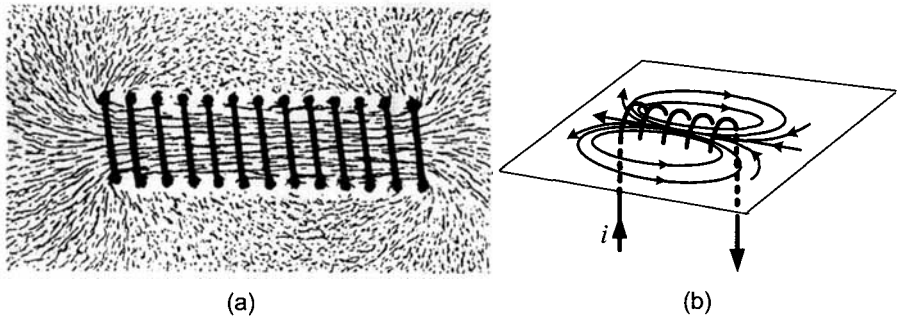


FIGURE 3.5. (a) Experimental view of the magnetic field lines of a solenoid using iron filings. Reprinted from Figure 43 of *Textbook of Physics*, R. Kronig, Editor, Pergamon Press, 1959 with permission from Elsevier. (b) Drawing of the magnetic field lines produced by a coil of wire carrying a current. From Figure 11-6(c) of *PSSC Physics*, 7th edition, by Haber-Schaim, Dodge, Gardner, and Shore, published by Kendall/Hunt, 1991.

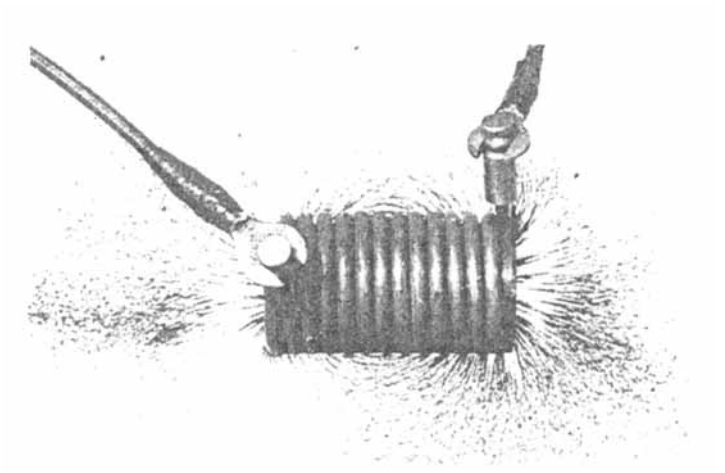


FIGURE 3.6. Experimental view of the magnetic field lines of a tightly wound solenoid using iron filings. From *An Introduction to Electrical Machines and Transformers*, 2nd edition, G. McPherson and R. D. Laramore, 1990. Reprinted by permisson of John Wiley & Sons.

www.EngineeringEBooksPdf.com

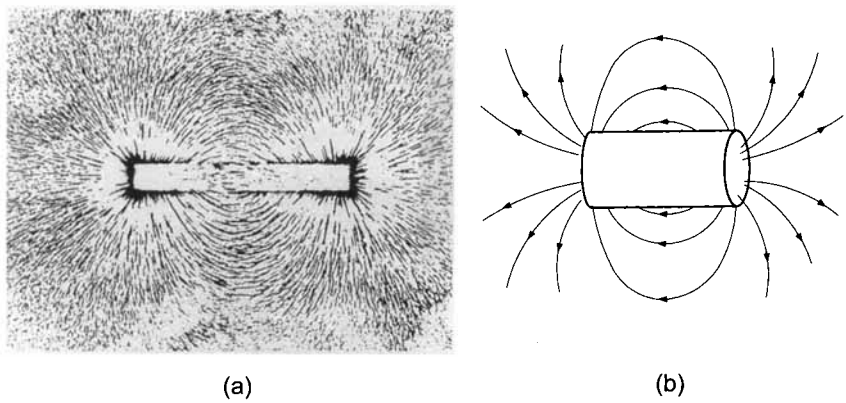


FIGURE 3.7. Experimental view of the magnetic field lines of a cylindrical bar magnet using iron filings. From Figure 11-2(b) of *PSSC Physics*, 7th edition, by Haber-Schaim, Dodge, Gardner, and Shore, published by Kendall/Hunt, 1991. (b) Drawing of the magnetic field produced by a cylindrical-shaped bar magnet.

Figure 3.7 shows the magnetic field of a cylindrical-shaped bar magnet along with a drawing illustrating the magnetic field lines. Note that the magnetic field lines are similar in shape to the air-filled solenoid coil of Figure 3.5. Figures 3.8(a) and 3.8(b) compare the magnetic field lines of an air filled coil with that of an iron core coil. The magnetic field lines of the coil with the iron core are drawn closer together to illustrate that its magnetic field is much stronger than that of the air filed coil due to the iron. In other words, for the same current in the coil, an iron core coil results in a much stronger magnetic field.

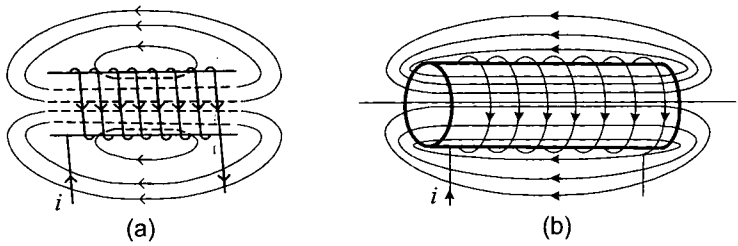


FIGURE 3.8. (a) Coil with air core. (b) Coil with iron core. From *Electric Machines: Dynamics and Steady State* by G. J. Thaler and M. L. Wilcox, 1966. Reprinted by permission of John Wiley & Sons.

Figure 3.9 illustrates the important property of iron that it can be used to make the magnetic field lines follow a specific path. In this case, the current in the coil magnetizes the iron making a strong magnetic field inside the

www.EngineeringEBooksPdf.com

iron that follows the path of the iron to the air gap. If the air gap is small, the strength of the magnetic field there is approximately the same as in the iron.

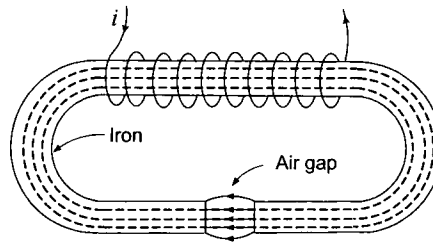


FIGURE 3.9. Iron core with air gap. From *Electric Machines: Dynamics and Steady State* by G. J. Thaler and M. L. Wilcox, 1966. Reprinted by permission of John Wiley & Sons.

An experimental verification of the setup in Figure 3.9 is the photograph in Figure 3.10. Note that the magnetic field does not actually stay confined to the iron core and air gap. However, the large number of iron filings oriented by the magnetic field in and around the air gap compared to those oriented outside the iron core indicates that the magnetic field is much stronger in the core and air gap.

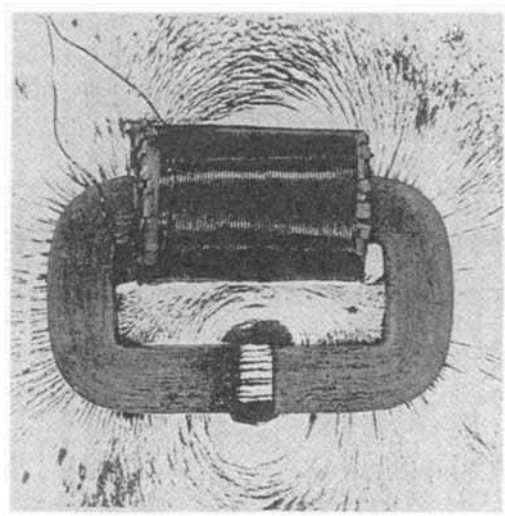


FIGURE 3.10. Experimental verification of the magnetic field produced by the setup of Figure 3.9. From *An Introduction to Electrical Machines and Transformers*, 2nd edition, G. McPherson and R. D. Laramore, 1990. Reprinted by permisson of John Wiley & Sons.

www.EngineeringEBooksPdf.com

An experimental verification of the magnetic field lines of a horseshoe magnet is given in Figure 3.11(a).

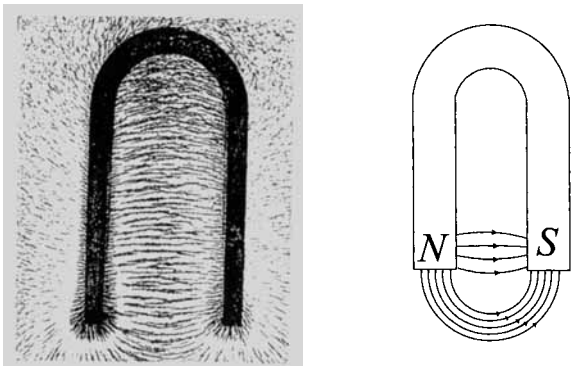


FIGURE 3.11. Magnetic field lines of a horseshoe magnet using iron filings. From *PSSC Physics*, 7th edition, by Haber-Schaim, Dodge, Gardner, and Shore, published by Kendall/Hunt, 1991. (b) Drawing illustrating the magnetic field lines of a horseshoe magnet.

Remark Normally a solenoidal coil is tightly wound so that there is no space between successive turns as shown in Figure 3.10. It was loosely wound in Figure 3.5 so that the orientation of the iron filings inside the coil could be shown. In Figure 3.5, the field outside the coil is too weak to align the iron filings against the friction of the paper, but the direction in this region is indicated in the drawing.

3.2 The Magnetic Field $\vec{\mathbf{B}}$ and Gauss's Law

Before going into the details of modeling magnetic material, the definition of the magnetic field is reviewed along with the concept of conservation of flux.

Recall that the direction of the magnetic field is defined to be the direction that a small compass needle points. The magnitude of the magnetic field is defined in terms of the forces it produces. Magnetism was discovered because naturally occurring magnets (e.g., the earth) exerted forces on each other. In 1819, the Danish physicist Hans Ørsted discovered that magnets can also exert forces on currents in wires and that currents in wires produces magnetic fields. This is illustrated in Figure 3.12, where a wire carrying a current is placed in a magnetic field. The conducting wire is oriented so that it is *perpendicular* to the magnetic field. The experimentally determined rule for determining the direction of the force is shown

www.EngineeringEBooksPdf.com

in the figure as another right-hand rule. Specifically, extend the fingers of the right hand in the direction of the magnetic field and the thumb in the direction of the current. Then the force is in the direction up out of the palm. Another experimental fact is that if the wire was placed *parallel* to the magnetic field, one finds that there is no force. That is, only the component of the magnetic field perpendicular to the current produces a force.

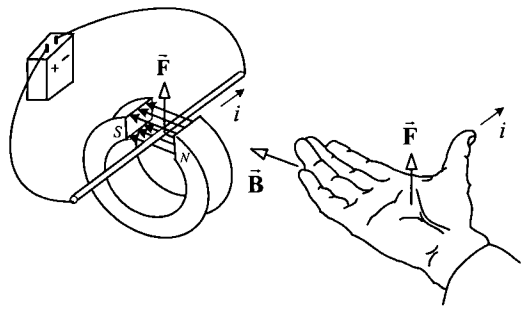


FIGURE 3.12. Direction of the magnetic force on currents. From Figure 11-3 of *PSSC Physics*, 7th edition, by Haber-Schaim, Dodge, Gardner, and Shore, published by Kendall/Hunt, 1991.

It is exactly this force phenomena that is used to define the magnetic field strength. In more detail, consider the experimental setup shown in Figure 3.13 which consists of an air-core solenoid coil carrying a current that produces a nearly constant magnetic field $\vec{\mathbf{B}}$ inside the coil in the direction shown. A wire is strung along a rectangular shaped pivot of width ℓ carrying a current i as shown in the figure. Only the part of the wire of length ℓ at the back end of the rectangular shaped pivot experiences a force since the other two sides are parallel to the field and thus experience no force. One then measures the force $\vec{\mathbf{F}}$. Experimentally, one finds that the force is proportional to the current i in the wire, i.e., if the current is doubled, then the force is doubled. Also, the force is proportional to the length of wire perpendicular to the field. That is, if the width was decreased to $\ell/2$, then one would find that the force is decreased by $1/2$ also. Consequently, one needs to divide out the length of the wire and current in the wire to find the intrinsic quantity producing the force. This leads to the following definition of the magnetic field.

www.EngineeringEBooksPdf.com

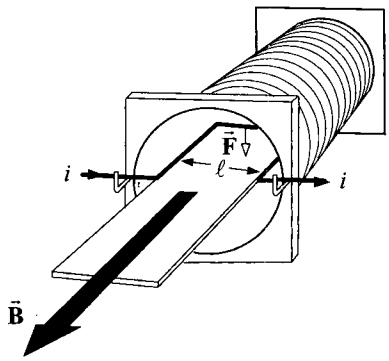


FIGURE 3.13. Apparatus to measure the magnetic field by the force it produces. From Figure 11-12 of *PSSC Physics*, 7th edition, by Haber-Schaim, Dodge, Gardner, and Shore, published by Kendall/Hunt, 1991.

Definition of the Magnetic Induction Field $\vec{\mathbf{B}}$

1. The *direction* of the magnetic field $\vec{\mathbf{B}}$ is defined by the direction a small compass needle points.

2. The *magnitude* $B \triangleq \left|\vec{\mathbf{B}}\right|$ of the magnetic field $\vec{\mathbf{B}}$ is defined by

$$B \triangleq \frac{F}{\ell i}$$

where F is the force on the conductor of length ℓ carrying the current i. Here, the length of wire ℓ carrying the current i is assumed to be perpendicular to the direction of $\vec{\mathbf{B}}$.

3. The units of the magnetic field are

$$\text{tesla} \triangleq \frac{\text{N}}{\text{m-A}} = \frac{\text{weber}}{\text{m}^2} = 10^4 \text{ gauss.}$$

Magnetic Force Law

As stated above, magnetic fields were discovered because of the forces they produce and this phenomena is used to define the magnetic field. The experiments with magnetic forces and the definition of the magnetic field can be turned around to obtain the magnetic force law. To repeat, the force on the current carrying wire is proportional to the *component* of $\vec{\mathbf{B}}$ perpendicular to the wire. One defines a vector $\vec{\ell}$ whose magnitude is the length ℓ of the wire in the magnetic field and its direction is that of the positive current flow in the wire. Then, the magnetic force on a wire of length ℓ carrying a current i in a magnetic field $\vec{\mathbf{B}}$ is given by

$$\vec{\mathbf{F}} = i\vec{\ell} \times \vec{\mathbf{B}}.$$

www.EngineeringEBooksPdf.com

Let θ denote the angle between $\vec{\ell}$ and $\vec{\mathbf{B}}$ as shown in Figure 3.14. The magnitude of the force $F = |\vec{\mathbf{F}}|$ may be written as

$$F = i\ell B \sin(\theta) = i\ell B_\perp$$

where $B_\perp = B\sin(\theta)$ is just the component of $\vec{\mathbf{B}}$ perpendicular to the wire.

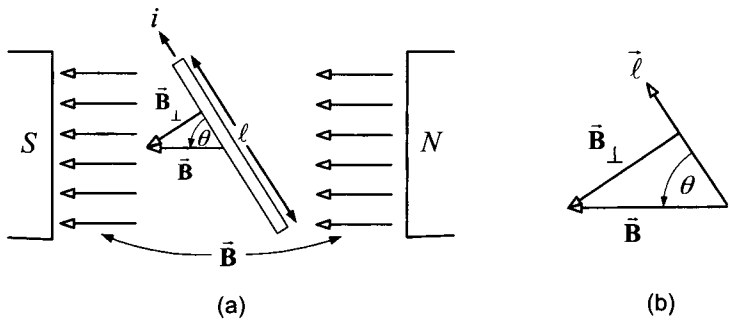


FIGURE 3.14. $F = i\ell B\sin(\theta) = i\ell B_\perp$.

3.2.1 Conservation of Flux

One of Maxwell's equations is that integral of the flux over a closed surface is zero, that is,

$$\oint_S \vec{\mathbf{B}} \cdot d\vec{\mathbf{S}} \equiv 0.$$

This fundamental property of magnetic fields is referred to as Gauss's law for magnetic fields or as the *conservation of flux*. To explain the notion of conservation of flux, consider the *closed* surface S shown in Figure 3.15 consisting of two disk-shaped ends connected by the tube-shaped surface.

The two disk-shaped surfaces making up the closed surface S are denoted by S_1 and S_2, respectively, while the tube-shaped surface is denoted by S_3. This particular surface S was purposely chosen so that on the surface S_3 the magnetic field $\vec{\mathbf{B}}$ points along the surface S_3 resulting in $\vec{\mathbf{B}} \cdot d\vec{\mathbf{S}} \equiv 0$ there. At all points of the surface S, let $d\vec{\mathbf{S}}$ be the outward normal to the surface. Then, by Gauss's law, it follows that

$$\oint_S \vec{\mathbf{B}} \cdot d\vec{\mathbf{S}} = \int_{S_1} \vec{\mathbf{B}} \cdot d\vec{\mathbf{S}} + \int_{S_2} \vec{\mathbf{B}} \cdot d\vec{\mathbf{S}} + \int_{S_3} \vec{\mathbf{B}} \cdot d\vec{\mathbf{S}} \equiv 0$$

or

$$\int_{S_1} \vec{\mathbf{B}} \cdot d\vec{\mathbf{S}} + \int_{S_2} \vec{\mathbf{B}} \cdot d\vec{\mathbf{S}} \equiv 0$$

as $\vec{\mathbf{B}} \cdot d\vec{\mathbf{S}} \equiv 0$ on S_3.

www.EngineeringEBooksPdf.com

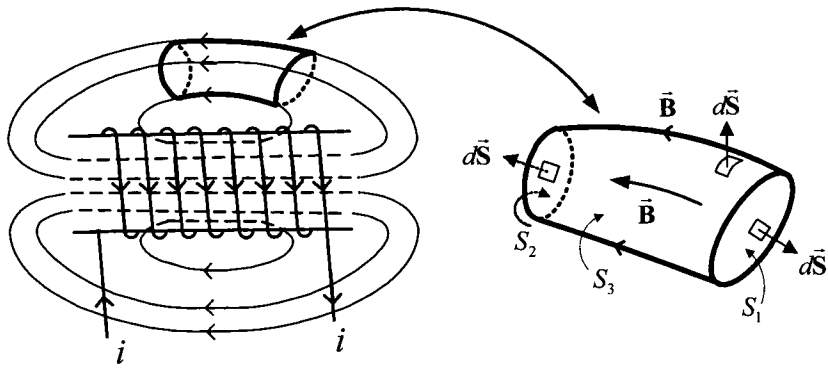


FIGURE 3.15. Conservation of flux in a flux tube.

Then

$$\phi_{S_2} = \int_{S_2} \vec{\mathbf{B}} \cdot d\vec{\mathbf{S}} = -\int_{S_1} \vec{\mathbf{B}} \cdot d\vec{\mathbf{S}} = \int_{S_1} \vec{\mathbf{B}} \cdot d\vec{\mathbf{S}}' = \phi_{S_1} \tag{3.1}$$

where

$$d\vec{\mathbf{S}}' \triangleq -d\vec{\mathbf{S}}$$

is the *inward* normal to the closed surface S on S_1. Equation (3.1) shows that the flux ϕ_{S_1} through surface S_1 *equals* the flux ϕ_{S_2} through the surface S_2 if their surface normals are chosen as above. The volume enclosed by S_1, S_2, S_3 is called a *flux tube* and is characterized by $\vec{\mathbf{B}} \cdot d\vec{\mathbf{S}} \equiv 0$ on the tube shaped part of the surface S_3. This results in the flux through S_1 equaling that through S_2 and is simply a consequence of conservation of flux applied to this closed surface.

In the above derivation, it was crucial that the flux through S_3 was zero. Magnetic materials provide the capability of being able to approximately construct such a situation, that is, of being able to (approximately) direct the magnetic field. This is illustrated in Figure 3.16, where a coil has been wrapped around an iron core containing an air gap. The point here is that the axially directed magnetic field inside the coil produced by the current and magnetized iron follows along the path of the iron to the air gap. That is, to a reasonable approximation, the magnetic material keeps the magnetic field inside the magnetic material following the path of the material. As a result, the tube-shaped surface of the magnetic material in Figure 3.16 forms a surface for which for which $\vec{\mathbf{B}} \cdot d\vec{\mathbf{S}} = \mathbf{0}$[1] so that the magnetic flux through any cross section of the iron tube is approximately

[1] It turns out that there will always be some $\vec{\mathbf{B}}$ field leaving the tube-shaped outer surface of the iron (leakage). However, by magnetizing the material as shown in the figure, the main $\vec{\mathbf{B}}$ field strength goes around to the air gap and the part that leaves the tube-shaped outer surface of the iron is much weaker.

www.EngineeringEBooksPdf.com

the same throughout the tube and in particular at the air gap. As the figure shows, the magnetic field spreads out across the air gap, but this spreading can be kept small by keeping the air gap small. In summary, magnetic materials give the capability to create a magnetic field/flux at one location and transport it to another location where it can be used, for example, to produce a force on a wire carrying a current. However, it is important to note that all of this is only approximately true in that the magnetic field does not stay completely within the material so that the field/flux is actually weaker at the air gap than the field/flux in the coil.

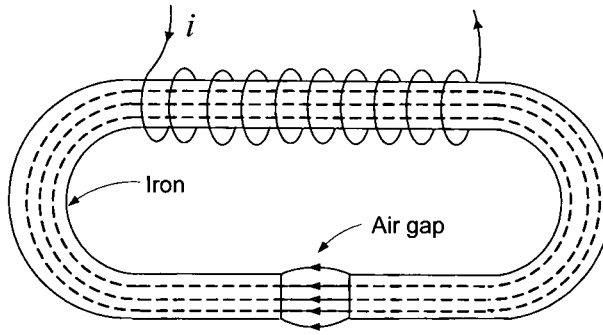


FIGURE 3.16. Creating and directing a magnetic field. From *Electric Machines: Dynamics and Steady State* by G. J. Thaler and M. L. Wilcox, 1966. Reprinted by permission of John Wiley & Sons.

Continuity of the Normal Component of $\vec{\mathbf{B}}$

As another application of Gauss's flux law $\oint_S \vec{\mathbf{B}} \cdot d\vec{\mathbf{S}} \equiv 0$, it is now shown that at the interface (boundary) between air and magnetic material, the normal (perpendicular) component of $\vec{\mathbf{B}}$ to the surface is *continuous* across the boundary. Figure 3.17 shows a piece of magnetic material and a closed cylindrical-shaped surface, of which half is inside the magnetic material and the other half in the air. Let $\vec{\mathbf{B}}_1 = B_{1x}\hat{\mathbf{x}} + B_{1y}\hat{\mathbf{y}} + B_{1z}\hat{\mathbf{z}}$ denote the magnetic field on the surface S_1 in the air and $\vec{\mathbf{B}}_2 = B_{2x}\hat{\mathbf{x}} + B_{2y}\hat{\mathbf{y}} + B_{2z}\hat{\mathbf{z}}$ denote the magnetic field on the surface S_2 just inside the magnetic material. Note that coordinate system has been chosen so that the normal component to the surface is the z component of the field. The conservation of flux $\oint_S \vec{\mathbf{B}} \cdot d\vec{\mathbf{S}} \equiv 0$ is then applied to the closed cylindrical surface S shown in Figure 3.17 consisting of the four pieces S_1 (disk-shaped in air with area πr^2), S_2 (disk-shaped in the magnetic material with area πr^2), S_3 (cylindrical-shaped in air with area $2\pi r(h/2)$), and S_4 (cylindrical-shaped in the magnetic material with area $2\pi r(h/2)$).

www.EngineeringEBooksPdf.com

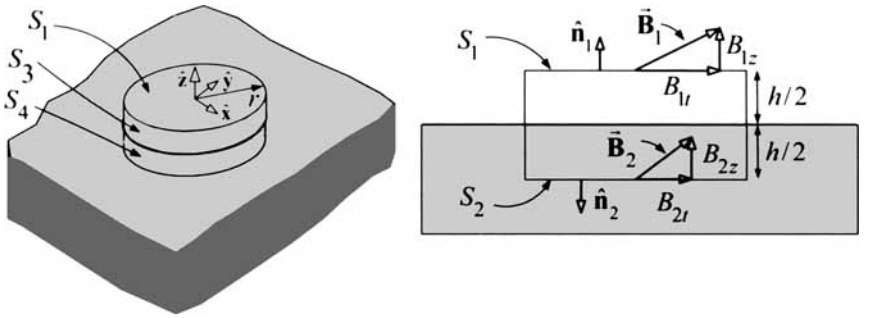


FIGURE 3.17. (a) Closed cylindrical surface at the interface of air and magnetic material (b) Cross-sectional view of the flux surface. As $h \to 0$, $\vec{\mathbf{B}}_1$ is just above the surface and $\vec{\mathbf{B}}_2$ is just below the surface.

It follows that

$$\oint_S \vec{\mathbf{B}} \cdot d\vec{\mathbf{S}} = \int_{S_1} \vec{\mathbf{B}} \cdot d\vec{\mathbf{S}} + \int_{S_2} \vec{\mathbf{B}} \cdot d\vec{\mathbf{S}} + \int_{S_3} \vec{\mathbf{B}} \cdot d\vec{\mathbf{S}} + \int_{S_4} \vec{\mathbf{B}} \cdot d\vec{\mathbf{S}} \equiv 0.$$

With r finite, but small, let the length h of the cylinder go to zero with the consequence that the area of sides S_3 and S_4 go to zero, and the disk-shaped sides S_1 and S_2 are just above and just below the air-magnetic material interface, respectively. Letting $h \to 0$, it follows that

$$\int_{S_1} \vec{\mathbf{B}} \cdot d\vec{\mathbf{S}} + \int_{S_2} \vec{\mathbf{B}} \cdot d\vec{\mathbf{S}} \equiv 0.$$

Evaluating these integrals results in

$$\int_{S_1} \vec{\mathbf{B}}_1 \cdot d\vec{\mathbf{S}} = \int_{S_1} (B_{1z}\hat{\mathbf{z}}) \cdot (dS\hat{\mathbf{z}}) = B_{1z}\pi r^2$$

$$\int_{S_2} \vec{\mathbf{B}}_2 \cdot d\vec{\mathbf{S}} = \int_{S_2} (B_{2z}\hat{\mathbf{z}}) \cdot (-dS\hat{\mathbf{z}}) = -B_{2z}\pi r^2$$

so that

$$B_{1z} = B_{2z}.$$

That is, the component of $\vec{\mathbf{B}}$ perpendicular to the surface is *continuous* across the surface.

As an example, consider Figure 3.18 [from Figure 3.19(a)] showing the magnetic fields due to a cylindrical-shaped permanent magnet. For reference, use a cylindrical coordinate system whose origin is at the center of the magnet with the z axis pointing up along the axis of the magnet. Note that on the cylindrical side of the magnet, the tangential component (z

www.EngineeringEBooksPdf.com

component) of $\vec{\mathbf{B}}$ is *not* continuous. In particular, consider the point P in Figure 3.18 where just inside the surface of the magnet, the tangential component of $\vec{\mathbf{B}}$ is up ($+\hat{\mathbf{z}}$ direction) while just outside the surface, it is down ($-\hat{\mathbf{z}}$ direction). However, the normal component ($\hat{\mathbf{r}}$ direction) must be the same on both sides of the surface by Gauss's law.

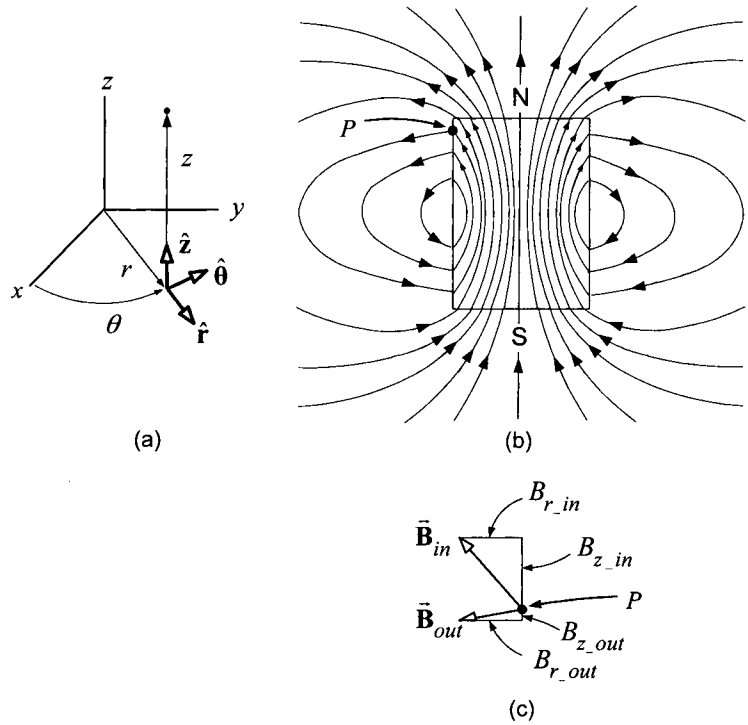


FIGURE 3.18. (a) Cylindrical coordinate system for the magnet. (b) Magnetic field lines for a cylindrical-shaped magnet. At the point P, the normal component ($\hat{\mathbf{r}}$ direction) is continuous while the tangential component ($\hat{\mathbf{z}}$ direction) is not. Adapted from Figure 37-4 of Ref. [34]. (c) $\vec{\mathbf{B}}_{in}$ and $\vec{\mathbf{B}}_{out}$ are, respectively, the magnetic field just inside and just outside the surface at the point P. Note that $B_{r\_in} = B_{r\_out}$, but $B_{z\_in} \neq B_{z\_out}$.

3.3 Modeling Magnetic Materials

Figures 3.19(a) and 3.19(b) compare the magnetic field lines of a cylindrical shaped bar magnet and a cylindrical-shaped air-filled solenoid coil, respectively. The interesting and important observation here is that the magnetic field outside the bar magnet has the *same* shape as that of the coil of wire carrying a current. This leads one to conjecture that the magnetic field

www.EngineeringEBooksPdf.com

inside the bar magnet of Figure 3.19(a) follows straight lines as they do inside the coil of Figure 3.19(b). Perhaps one can picture the bar magnet as having some kind of "bound" current which goes around its periphery producing the bar magnet's field analogous to the current in the coil of the air filled solenoid.

Pursuing this conjecture, consider an iron atom in the bar magnet as a small current loop as in Figure 3.20. That is, the motion of the electrons in the individual iron atoms are considered to be equivalent to a current loop as drawn in Figure 3.20(a). As illustrated in Figures 3.20(a) and 3.20(b), inside the material, the current in the adjacent sides of neighboring loops go in opposite directions so that their effects cancel. However, the part of the loops on the surface of the material have no corresponding neighboring loop to cancel and the net effect is a current around the periphery of the magnetic material as illustrated in Figure 3.20(c). This is a so-called *bound* current, since an individual electron does not go around the surface of the magnet, but stays with the particular iron atom. It is only the net effect of all the current loops being aligned that results in a current around the surface of the bar magnet. This is in contrast to *free* currents associated with current flow in copper conductors where individual electrons actually move down the wire through the crystal lattice of the copper.

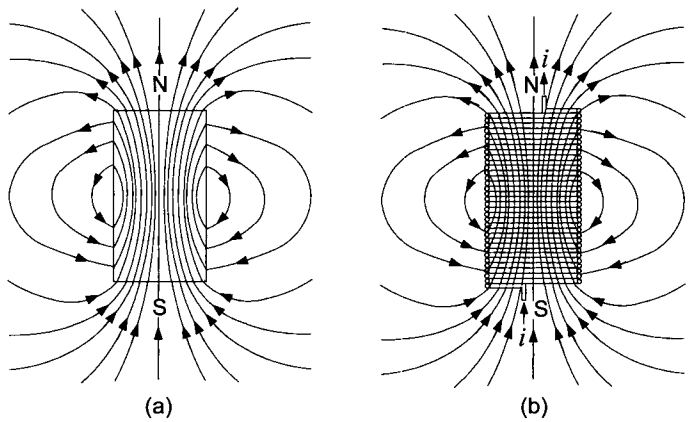


FIGURE 3.19. (a) Magnetic field lines for a bar magnet. (b) Magnetic field lines for a short air-filled solenoid coil. From *Physics*, 2nd edition, by D. Halliday and R. Resnick, 1962. Reprinted by permission of John Wiley & Sons.

To reiterate, the point here is that in *magnetic* materials, the motion (spin) of the electrons in the atoms are able to align themselves as shown in Figure 3.20 so that the current loops are all in the same plane with the currents circulating clockwise. This is in contrast to *nonmagnetic* materials where the current loops are at *random* orientations with respect to each

www.EngineeringEBooksPdf.com

other and are unable to align themselves so their net effect cancels.

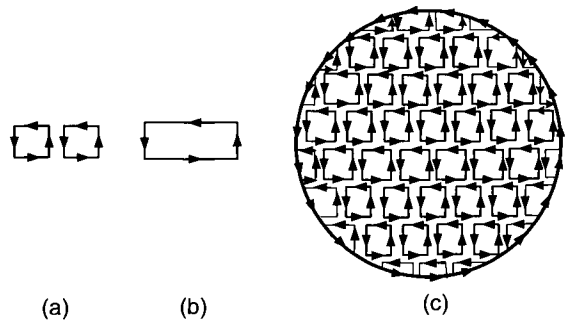


FIGURE 3.20. Viewing the atoms of magnetic materials as current loops which are able to align themselves. From *PSSC Physcis*, 7th edition, by Haber-Schaim, Dodge, Gardner, and Shore, published by Kendall/Hunt, 1991.

Figure 3.21 again illustrates this idea of representing the magnetic material by current loops which results in an equivalent bound current i_b going around the periphery of the cylinder.

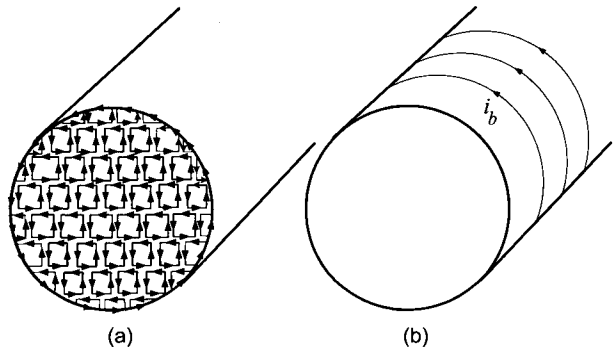


FIGURE 3.21. (a) View of magnetic material consisting of aligned dipole moments. (b) Magnetic material represented by an equivalent bound current i_b going around the periphery of the cylinder that produces the same magnetic field as the magnetic material. This interpretation is motivated by Figure 3.20.

3.3.1 Magnetic Dipole Moments

To develop a mathematical model to go along with the pictures in Figures 3.20 and 3.21, the concept of a magnetic dipole moment is reviewed. Consider a small planar loop of area S with a current i going around the loop such as illustrated in Figure 3.22. The scalar magnetic moment is defined

www.EngineeringEBooksPdf.com

to be

$$m \triangleq iS.$$

The direction of the magnetic moment is taken to be normal to the loop. A *unique* normal $\hat{\mathbf{n}}$ is specified by direction of the current using the right-hand rule. That is, curl the fingers of the right-hand around the loop in the direction of positive current flow and the normal $\hat{\mathbf{n}}$ is defined to be the direction of the extended thumb. Putting this all together, the *magnetic moment* vector is defined as

$$\vec{\mathbf{m}} \triangleq iS\hat{\mathbf{n}}$$

where $\hat{\mathbf{n}}$ is a unit normal to the loop determined by the right-hand rule. Magnetic material (such as iron) is now pictured by modeling the atoms as magnetic moments which are able to *align* themselves in the same direction. As shown in Figure 3.21, the net effect is then a (bound) surface current that produces the external magnetic field analogous to a current-carrying coil with air inside.

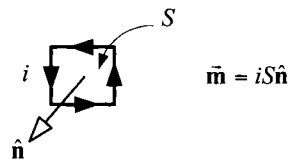


FIGURE 3.22. Small current loop as a magnetic dipole momentt. S is the area of the loop, i is the current in the loop and $\hat{\mathbf{n}}$ is the normal to the loop given by the right-hand rule. The dipole moment is $\vec{\mathbf{m}} \triangleq iS\hat{\mathbf{n}}$.

The model of the iron atom as a magnetic dipole moment will be used to construct a macroscopic picture of the magnetic properties of iron. However, the magnetic property of iron (ferromagnetism) is only explained through Quantum Mechanics. Quoting from Melvin Schwartz [35] "*Iron has two remarkable atomic properties that have far-reaching consequences with respect to its macroscopic magnetic behavior. First, 4 of the 26 electrons in an isolated atom of iron have their intrinsic angular momenta lined up. Second, within solid iron, there are very strong quantum-mechanical forces tending to make the intrinsic angular momenta of neighboring atoms line up. This results in domains of macroscopic size having net magnetizations corresponding to about two aligned electron moments per atom on the average. Applying a magnetic field causes those domains, which are aligned in the same direction as the field, to grow until the iron finally reaches a saturated state of magnetization. Typically, saturation occurs at fields in the neighborhood of 10,000 to 20,000 gauss. Needless to say, removal of the applied field does not lead to complete randomization of the domains. The*

www.EngineeringEBooksPdf.com

residual magnetization can be quite large, as in the case of special permanent magnetic alloys, or it can be quite small, as in the case of soft iron. These phenomena are characteristic of ferromagnetism."

3.3.2 The Magnetization $\vec{\mathbf{M}}$ and Ampère's Law

The picture adopted here for iron and other magnetic materials is one in which they consist of small current loops with a magnetic dipole moment associated with each one as illustrated in Figure 3.21. It is emphasized that one could model any material with such current loops, but that in the case of magnetic materials, the loops (dipole moments) align themselves when an external magnetic field is applied. This alignment of the current loops can be viewed as a net bound current which goes around the surface and produces a magnetic field.[2] Nonmagnetic materials have their dipole moments in random orientations with respect to each other and are not able to align to produce any significant magnetic field even under the presence of an external magnetic field. Consequently, there is no net bound surface current or magnetic field. When an external magnetic field is applied to a magnetic dipole moment (loop of current), the moment tends to align itself with the external field. This is illustrated in Figure 3.23, which shows two current loops whose normals $\hat{\mathbf{n}}$ are not aligned with the external magnetic field $\vec{\mathbf{B}}$. In Figure 3.23(a), the forces $\vec{\mathbf{F}}_1$,$\vec{\mathbf{F}}_2$ provide a torque $\vec{\tau}$ to align the dipole moment (i.e., the normal $\hat{\mathbf{n}}$ to the surface of the loop) with the direction of the external field $\vec{\mathbf{B}}$. Similarly, in 3.23(b) the forces $\vec{\mathbf{F}}_3$,$\vec{\mathbf{F}}_4$ provide a torque $\vec{\tau}$ to align the dipole moment with the direction of the external field $\vec{\mathbf{B}}$.

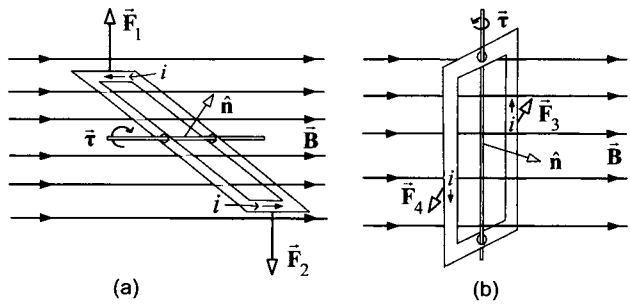


FIGURE 3.23. Magnetic dipole in an external magnetic field. (a) Dipole tilted vertically. (b) Dipole tilted laterally.

[2]This ability of materials such as iron to align their magnetic moments together to form domains which grow and align in the same direction as an externally applied magnetic field is succesfully explained only by quantum mechanics.

www.EngineeringEBooksPdf.com

As a specific example of this viewpoint, consider the magnetic circuit of Figure 3.16. Here the current in the coil magnetizes the iron, that is, causes the dipole moments of the iron atoms to align themselves with the (external) magnetic field produced by the coil current. This results in a much larger magnetic field in the iron than that which would be produced by the current in the coil alone.

The Magnetization Vector $\vec{\mathbf{M}}$

Define the *magnetization* vector $\vec{\mathbf{M}}$ as follows: At any arbitrary point (x', y', z') inside the magnetic material (see Figure 3.24) define

$$\vec{\mathbf{m}}(x', y', z') \triangleq \text{Average magnetic dipole moment of the atoms in a neighborhood of the point } (x', y', z').$$

$$N_m \triangleq \text{Number of atoms (e.g., iron) per unit volume.}$$

Then, the magnetization $\vec{\mathbf{M}}(x', y', z')$ is defined as

$$\vec{\mathbf{M}}(x', y', z') \triangleq N_m \vec{\mathbf{m}}(x', y', z').$$

The magnitude $M = |\vec{\mathbf{M}}|$ of the magnetization vector is simply the magnetic dipole moment per unit volume. The fundamental issue here is to determine the magnetic field $\vec{\mathbf{B}}(x, y, z)$ at the point (x, y, z) outside the material due to the magnetization $\vec{\mathbf{M}}(x', y', z')$ at the point (x', y', z') inside the material. To do so, it is necessary to relate the magnetization vector $\vec{\mathbf{M}}(x', y', z')$ to the magnetic field it produces. First, Ampère's law is reviewed as it is the Maxwell equation that relates currents to magnetic fields.

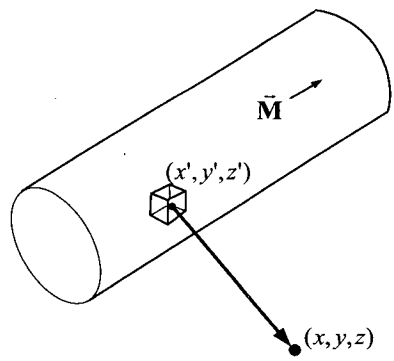


FIGURE 3.24. Magnetic field produced by magnetic material. How does one compute $\vec{\mathbf{B}}$ at (x, y, z) due to $\vec{\mathbf{M}}$ at (x', y', z')?

www.EngineeringEBooksPdf.com

Ampère's Law

When magnetic materials are *not* present, Ampère's law is

$$\oint_C \vec{\mathbf{B}} \cdot d\vec{\ell} = \mu_0 i_{\text{enclosed}}$$

where i_{enclosed} is the current enclosed by the path C.

Some examples are now given to recall how Ampère's law is used to determine the magnetic field from currents.

Example *Long Straight Wire*

Consider a long straight wire carrying a current as in Figure 3.25(a).

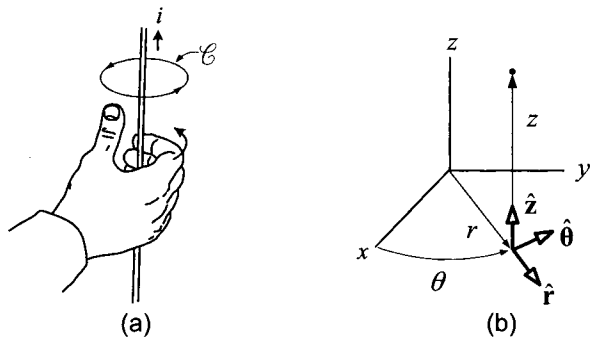


FIGURE 3.25. Sign convention in Ampère's law for positive current through a closed curve C. From *PSSC Physics*, 7th edition, by Haber-Schaim, Dodge, Gardner, and Shore, published by Kendall/Hunt, 1991.

This figure shows a closed curve C with a direction of *positive travel* for going around the curve indicated as well as a direction for *positive current* in the wire. For Ampère's law to apply, these two sign conventions must be related to each other by another right-hand rule. Specifically, as shown in Figure 3.25(a), if one takes their right hand and curls the fingers in the positive direction of travel around the curve, then the thumb points in the positive direction of current through the surface *enclosed* by this curve.

Ampère's law is now used to compute the magnetic field due to a current in a long straight wire. A cylindrical coordinate system whose z axis is along the wire is appropriate for the geometry of this problem [see Figure 3.25(b)]. To proceed, first note that due to symmetry, the $\vec{\mathbf{B}}$ field cannot depend on the axial position z nor the azimuthal position θ so that

$$\vec{\mathbf{B}} = B_r(r)\hat{\mathbf{r}} + B_\theta(r)\hat{\boldsymbol{\theta}} + B_z(r)\hat{\mathbf{z}}.$$

To find the azimuthal component $B_\theta(r)$, apply Ampère's law to the closed

www.EngineeringEBooksPdf.com

curve C in Figure 3.25(b) to obtain

$$\oint_C \vec{\mathbf{B}} \cdot d\vec{\boldsymbol{\ell}} = \int_0^{2\pi} \left(B_\theta \hat{\boldsymbol{\theta}}\right) \cdot \left(r d\theta \hat{\boldsymbol{\theta}}\right) = \int_0^{2\pi} B_\theta r d\theta = 2\pi r B_\theta = \mu_0 i$$

or,

$$B_\theta(r) = \frac{\mu_0 i}{2\pi r}.$$

In problem 3, using Gauss's law for $\vec{\mathbf{B}}$, the reader is asked to show that $B_r(r) \equiv 0$.

It is now shown that $B_z(r) \equiv 0$. To do so, apply Ampère's law to the curve C shown in Figure 3.26, to obtain

$$\begin{aligned}
\oint_C \vec{\mathbf{B}} \cdot d\vec{\boldsymbol{\ell}} &= \mu_0 i_{\text{enclosed}} \\
\int_1^2 \vec{\mathbf{B}} \cdot d\vec{\boldsymbol{\ell}} + \int_2^3 \vec{\mathbf{B}} \cdot d\vec{\boldsymbol{\ell}} + \int_3^4 \vec{\mathbf{B}} \cdot d\vec{\boldsymbol{\ell}} + \int_4^1 \vec{\mathbf{B}} \cdot d\vec{\boldsymbol{\ell}} &= 0 \\
\int_1^2 (B_z(r_1)\hat{\mathbf{z}}) \cdot (dh\hat{\mathbf{z}}) + \int_3^4 (B_z(r_2)\hat{\mathbf{z}}) \cdot (-dh\hat{\mathbf{z}}) &= 0 \\
B_z(r_1)h - B_z(r_2)h &= 0 \\
B_z(r_1) &= B_z(r_2)
\end{aligned}$$

where the fact that $\int_2^3 \vec{\mathbf{B}} \cdot d\vec{\boldsymbol{\ell}} + \int_4^1 \vec{\mathbf{B}} \cdot d\vec{\boldsymbol{\ell}} = 0$ was used.

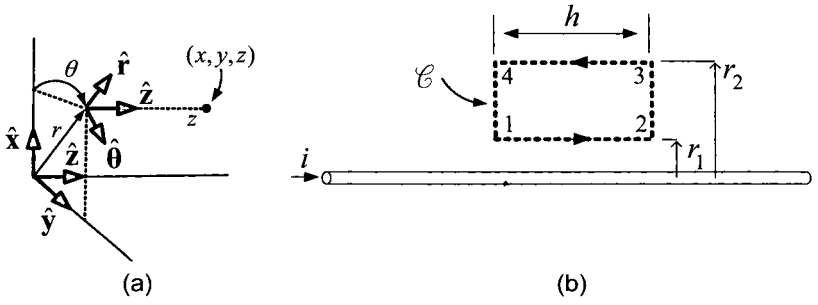


FIGURE 3.26. (a) Cylindrical coordinate system. (b) Long straight wire carrying a current.

That is, the z component of $\vec{\mathbf{B}}$ is constant. However, as one goes to infinity in the radial direction ($r \to \infty$), the magnetic field will be zero as one is infinitely far from the source i of the magnetic field. Consequently, B_z must be zero at infinity and, as it is constant, it must equal zero everywhere. Thus, the form of the magnetic field of an infinitely long straight wire reduces to

$$\vec{\mathbf{B}}(r, \theta, z) = \frac{\mu_0 i}{2\pi r} \hat{\boldsymbol{\theta}}.$$

www.EngineeringEBooksPdf.com

Example *Ideal Infinitely Long Solenoid* [34]

Recall that a solenoid coil is a long wire which is wrapped in a close-packed helix-shaped coil where the length of the coil is very long compared to its diameter. An ideal solenoid is one in which the helix is infinitely long with no spacing between coils as shown in Figure 3.27.

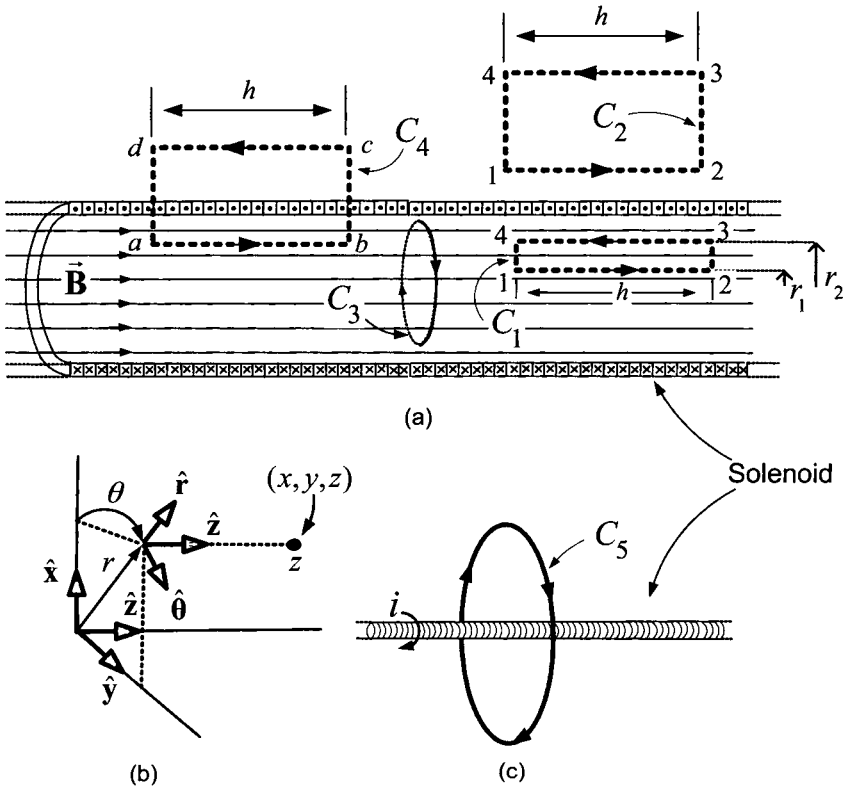


FIGURE 3.27. Infinitely long coil with an air core. (a) Curves C_1, C_2, C_3, and C_4 for applying Ampère's law. (b) Cylindrical coordinate system. (c) Curve C_5 for applying Ampère's law.

In this example, a current is put through the wire and the goal is to compute the magnetic field inside and outside the coil. In this case of an ideal solenoid coil, the magnetic field can be computed using symmetry arguments and Ampère's law. To do so, Figure 3.27 shows five closed curves C_1, C_2, C_3, C_4 and C_5 that are used to apply Ampère's law to compute $\vec{\mathbf{B}}$. Figure 3.27(b) shows a cylindrical coordinate system chosen for the solenoid.

Proceeding, first note that due to symmetry, the $\vec{\mathbf{B}}$ field cannot depend

www.EngineeringEBooksPdf.com

on the axial position z nor on the azimuthal angle θ so that

$$\vec{\mathbf{B}} = B_r(r)\hat{\mathbf{r}} + B_\theta(r)\hat{\boldsymbol{\theta}} + B_z(r)\hat{\mathbf{z}}.$$

The reader is asked in problem 4 to show using Gauss's law for $\vec{\mathbf{B}}$ that $B_r(r) \equiv 0$. To compute B_z inside the solenoid, Ampère's law is applied to the curve C_1 (side *1–2* is a radial distance r_1 from the center of the coil and side *3–4* is a radial distance r_2 from the center of the coil) and one obtains

$$\begin{aligned}
\oint_{C_1} \vec{\mathbf{B}} \cdot d\vec{\boldsymbol{\ell}} &= \mu_0 i_{\text{enclosed}} \\
\int_1^2 \vec{\mathbf{B}} \cdot d\vec{\boldsymbol{\ell}} + \int_2^3 \vec{\mathbf{B}} \cdot d\vec{\boldsymbol{\ell}} + \int_3^4 \vec{\mathbf{B}} \cdot d\vec{\boldsymbol{\ell}} + \int_4^1 \vec{\mathbf{B}} \cdot d\vec{\boldsymbol{\ell}} &= \mu_0 i_{\text{enclosed}} \\
B_z(r_1)h - B_z(r_2)h &= 0 \\
B_z(r_1) &= B_z(r_2)
\end{aligned}$$

where the fact that $\int_2^3 \vec{\mathbf{B}} \cdot d\vec{\boldsymbol{\ell}} + \int_4^1 \vec{\mathbf{B}} \cdot d\vec{\boldsymbol{\ell}} = 0$ was used. Thus, $B_z = B_{z\text{inside}}$ is *constant* inside the solenoid. Similarly, applying Ampère's law to the curve C_2, one finds that $B_z = B_{z\text{outside}}$ is also *constant* outside the solenoid. As one goes to infinity in the radial direction ($r \to \infty$), the magnetic field will be zero as one is infinitely far from the source i of the magnetic field. Consequently, $B_{z\text{outside}}$ must be equal to zero.

Applying Ampère's law to the curves C_3 and C_5, the reader can show that $B_\theta(r) \equiv 0$ inside the solenoid and $B_\theta(r) = \mu_0 i/(2\pi r)$ outside the cylinder (see problem 5). Thus,

$$\vec{\mathbf{B}} = \begin{cases} B_{z\text{inside}}\hat{\mathbf{z}} & \text{inside the solenoid} \\ \dfrac{\mu_0 i}{2\pi r}\hat{\boldsymbol{\theta}} & \text{outside the solenoid.} \end{cases}$$

Finally, to determine $B_{z\text{inside}}$ in terms of the solenoid current i, consider the curve C_4. Let n be the number of coil turns per unit length and i be the current in the coil, so that in the length h of the coil, the current nhi is going through the curve *abcda* in Figure 3.27(a). Applying Ampère's law to the curve C_4, one obtains

$$\begin{aligned}
\oint_{C_4} \vec{\mathbf{B}} \cdot d\vec{\boldsymbol{\ell}} &= \mu_0 i_{\text{enclosed}} \\
\int_a^b \vec{\mathbf{B}} \cdot d\vec{\boldsymbol{\ell}} &= \mu_0 i_{\text{enclosed}} \\
B_{z\text{inside}}h &= \mu_0 nhi \\
B_{z\text{inside}} &= \mu_0 ni.
\end{aligned}$$

The final expression for the magnetic field is given by

$$\vec{\mathbf{B}}(r,\theta,z) = \begin{cases} \mu_0 ni\hat{\mathbf{z}} & \text{inside the solenoid} \\ \dfrac{\mu_0 i}{2\pi r}\hat{\boldsymbol{\theta}} & \text{outside the solenoid.} \end{cases}$$

www.EngineeringEBooksPdf.com

This expression is consistent with the iron filings experiment of Figure 3.5 which shows the field inside the solenoid is along the axis and outside the solenoid the field is weaker (by a factor of $\frac{n}{2\pi r}$) compared to the field inside.

The quantity $\lambda = ni$ is the surface current (on the surface defined by the coil) per unit length of the coil going around it in the azimuthal ($\hat{\theta}$) direction. It is referred to as the *surface current density* and, for an infinitely long solenoid, $B = \mu_0 \lambda$ inside.

Example *Toroidal Solenoid*

A toroidal solenoidal coil with an air core is shown in Figure 3.28. It has an inside radius of r_1, an outside radius of r_2 and a core diameter of d. Figure 3.28(b) shows an iron filing experiment of the lines of $\vec{\mathbf{B}}$ of an air filled toroidal solenoid. The toroid does not possess as much symmetry as the previous examples making the complete derivation of the magnetic field everywhere more difficult. However, it turns out that outside of the toroid, the magnetic field is quite weak. Inside the toroid, the reader is asked to show that the magnetic field is only nonzero in the azimuthal direction (see problem 6).

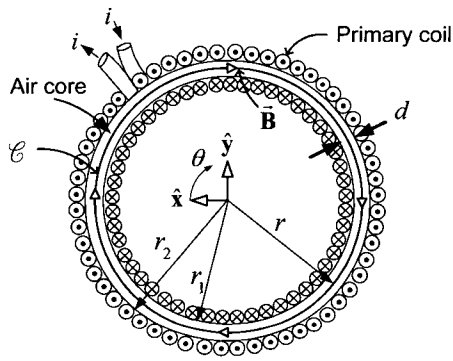


FIGURE 3.28. (a) Cross-sectional view of a toroidal coil with an air core. Adapted from [34]. (b) Experimental verification of the lines of $\vec{\mathbf{B}}$ for a loosely wound toroid with an air core. Reprinted from Figure 44 of *Textbook of Physics*, R. Kronig, Editor, Pergamon Press, 1959 with permission from Elsevier.

Let i denote the current in the toroid wire and n denote the number of loops (turns) per unit length along the radius r_1 of the toroid so that $2\pi r_1 n$ the total number of loops wound around the toroid. Application of

www.EngineeringEBooksPdf.com

Ampère's law to the circular curve C at radius r gives

$$\begin{aligned} \oint_C \vec{\mathbf{B}} \cdot d\vec{\ell} &= \mu_0 i_{\text{enclosed}} \\ B_\theta 2\pi r &= \mu_0 2\pi r_1 n i \\ B_\theta(r) &= \frac{r_1}{r}\mu_0 n i. \end{aligned}$$

This is valid for $r_1 < r < r_2$ and, if $d = r_2 - r_1 << r_1$, then $r_1/r \approx 1$ and $B \approx \mu_0 ni$ inside the toroid just as in the case of the long straight solenoid.

Remark

In the examples in this chapter using a toroid, it will always be assumed that $d = r_2 - r_1 << r_1$ so that the approximation $r_1/r \approx 1$ is valid.

3.3.3 Relating $\vec{\mathbf{B}}$ to $\vec{\mathbf{M}}$

Using Ampère's law, it was shown in the previous example that $B \approx \mu_0 ni$ in an air core toroidal coil. It is now shown how this relationship can be *experimentally* verified. To do so, a secondary coil is wrapped around the toroid as shown in Figure 3.29 to carry out the experiment.

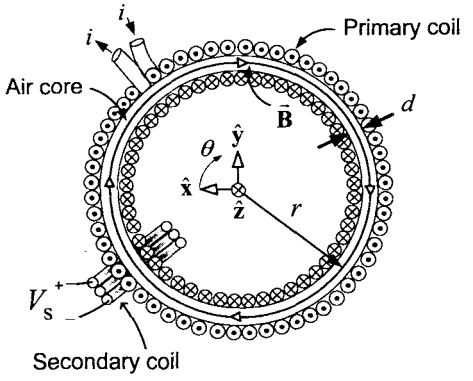


FIGURE 3.29. Experimental setup for determining $\vec{\mathbf{B}}$ versus i in an *air-filled* toroid. Adapted from [34].

The secondary coil is used to measure $\vec{\mathbf{B}} = B\hat{\boldsymbol{\theta}}$ inside the toroid as follows:[3] With N_s the number of turns in the secondary coil, $S = \pi(d/2)^2$ the cross sectional area of the toroidal coil, the flux linkage λ_s through the secondary coil is

$$\lambda_s = N_s B(t) S$$

[3]The subscript θ on B_θ has now been dropped without confusion because the other components of the magnetic field are insignificant (see problem 6).

www.EngineeringEBooksPdf.com

where, as it is assumed that $d = r_2 - r_1 << r_1$, B is taken to be constant across the cross section S of the toroid as well as in the azimuthal direction. Now, by Faraday's law, the voltage induced in the secondary coil is given by

$$V_s = -\frac{d\lambda_s}{dt} = -\frac{d}{dt}\left(N_s B(t) S\right) = -N_s S \frac{dB(t)}{dt}$$

so that

$$B(t) = -\frac{1}{N_s S}\int_0^t V_s(\tau)d\tau. \tag{3.2}$$

By measuring the current $i(t)$ in the primary windings and the voltage $V_s(t)$ between the terminals of the secondary coil, the magnetic field B inside the toroid can be found as a function of the current i. That is, one would ramp up the primary current $i(t)$ from 0 to some $I_{\max}$ as in Figure 3.30(a), while at the same time measure/store the secondary voltage $V_s(t)$ (see Figure 3.30(b). $B(t)$ is then computed using (3.2) as in Figure 3.30(c) and one then plots B versus i as in Figure 3.30(d). In this case in which the toroid is air filled, these measurements simply verify that $B \approx \mu_0 ni$.

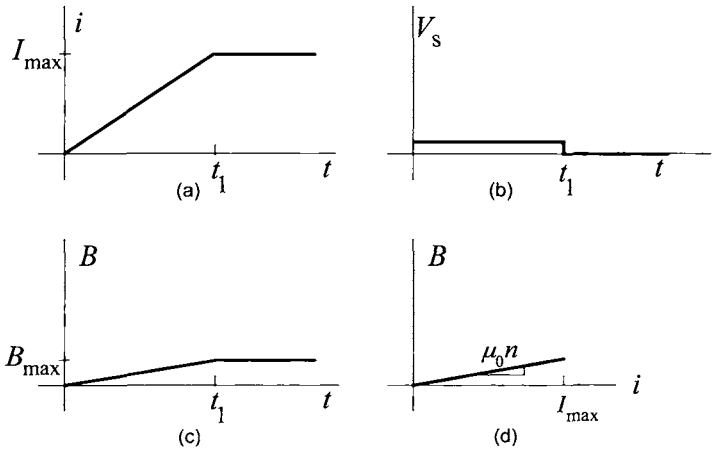


FIGURE 3.30. (a) Current in primary winding. (b) Voltage measured in secondary winding. (c) Magnetic field inside the toroid versus time calculated according to equation (3.2). (d) Magnetic field plotted versus the primary current (slope $\approx \mu_0 n$).

This *same* experimental setup can also be used to measure the magnetic field inside the toroidal coil when it has an *iron* core. The experiment is now repeated, but with the toroid filled with an iron core as shown in Figure 3.31. Of course, there is then a *non zero* magnetization $\vec{\mathbf{M}}$ in the iron core.

www.EngineeringEBooksPdf.com

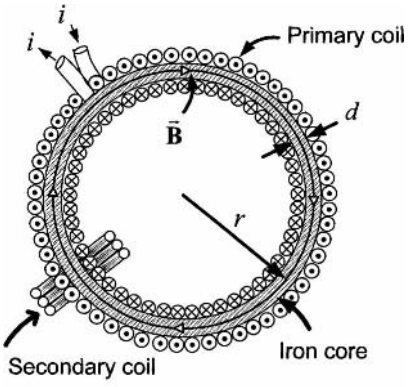


FIGURE 3.31. Iron-filled toroid with secondary coil. Adapted from [34].

The magnetic field strength B inside the toroid is computed as a function of the current i just as before. In this case, the primary current is as shown in Figure 3.32(a) and is the same as in Figure 3.30(a).

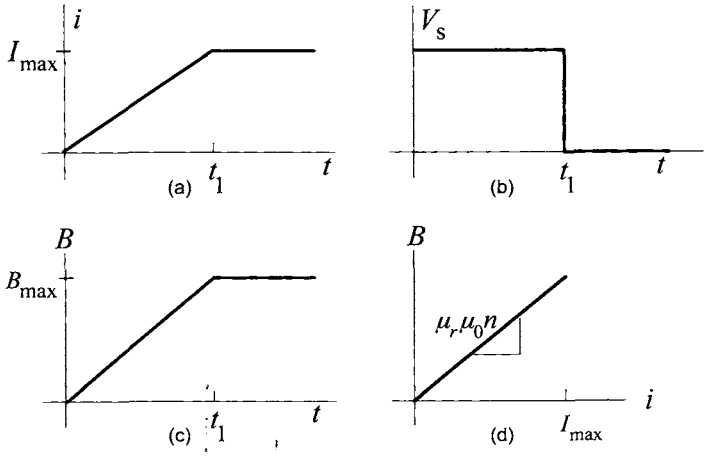


FIGURE 3.32. (a) Current in primary winding. (b) Voltage measured in secondary winding. (c) Magnetic field inside the toroid calculated according to (3.2). (d) Magnetic field plotted versus the primary current (slope $\approx \mu_r\mu_0 ni$).

Again, the voltage induced in the secondary winding is measured [see 3.32(b)] and is now much greater in value than the measured voltage in the case of the air filled toroid. The magnetic field B is again found by integrating the voltage $V_s(t)$ in the secondary coil according to equation (3.2) and is shown in Figure 3.32(c). Finally, the magnetic field B is plotted versus the primary current i as shown in Figure 3.32(d). In this case, with

www.EngineeringEBooksPdf.com

the toroid filled with magnetic material, the slope is greater by a factor μ_r than that of Figure 3.30(d). The factor μ_r is called the *relative permeability* and is typically on the order of 1000. Rewrite B in the iron core

$$B = B_0 + B_M \tag{3.3}$$

where $B_0 = \mu_0 ni$ denotes the magnetic field when no magnetic material is present and B_M represents the additional strength in the magnetic field due to the magnetic material. The strength B of the magnetic field in the toroid is then plotted versus $B_0 = \mu_0 ni$ (rather than i) resulting in a curve of the form shown in Figure 3.33. The slope of the straight line part of the curve is then the relative permeability μ_r so that $B = \mu_r B_0 = \mu_r \mu_0 ni$ for $i \leq i_{\text{sat}}$. If one continues to increase the current above some current level i_{sat}, B no longer increases at the rate $\mu_r \mu_0 n$, but only as $\mu_0 n$.

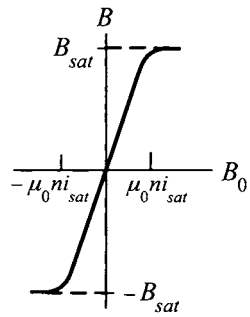


FIGURE 3.33. B versus B_0.

Again, the important point here is that the field B_M is typically on the order of a 1000 times greater than B_0 in good magnetic materials (i.e., $\mu_r > 1000$). This is, of course, the reason magnetic materials are used! This phenomena can be pictured as the magnetic field inside the toroid produced by the current i aligns (magnetizes) the magnetic dipoles moments [see Figures 3.21 and 3.23)] of the iron so that they produce a magnetic field that adds to that produced by the current. As the current in the wire of the toroid is increased, more magnetic dipoles are aligned increasing the B field more. As a result, the magnetic field due to the current and magnetic material is much larger (on the order of a thousand times) than that produced by just the current. As the current increases to a level i_{sat}, all of the dipole moments of the iron atoms are aligned so that increasing the current beyond this level does not result in a large increase in the magnetic field as it did below this level of current.

Reiterating, for the same current in the toroidal coil, the one filled with magnetic material will have a $\vec{\mathbf{B}}$ field that is typically more than a 1000 times that of the coil with only air inside. As will be described shortly, the

www.EngineeringEBooksPdf.com

quantity $H \triangleq B_0/\mu_0 = ni$ is the *magnetic field intensity* and $M \triangleq B_M/\mu_0$ turns out to be the *magnetization* so that

$$B = B_0 + B_M = \mu_0 H + \mu_0 M$$

where $H << M$ as $B_0 << B_M$. Consequently, in soft[4] magnetic materials, one can take $H = 0$ as a reasonable approximation. In other words, in such magnetic materials, the B field is primarily due to the magnetization (alignment of the magnetic dipoles) of the magnetic material rather than the current that magnetizes the magnetic material.

3.4 The Magnetic Intensity Field Vector $\vec{\mathbf{H}}$

Here the definition of the *magnetic intensity* vector $\vec{\mathbf{H}}$ is given in terms of the *magnetization* vector $\vec{\mathbf{M}}$ (defined in Section 3.3.2) and the *magnetic induction* vector $\vec{\mathbf{B}}$. To proceed, consider the toroid in Figure 3.34 which shows a toroid with an iron core 3.34(a) and redrawn in 3.34(b) with the iron core replaced by an equivalent coil carrying the bound current i_b.

Ampère's law must be modified to account for magnetic materials. Recall that when the iron core was not present inside the toroid, Ampère's law showed that $B \approx \mu_0 ni$. However, when the iron core was present, experiments showed that the B field was on the order of a 1000 times greater. The discussion concerning Figure 3.21 showed that the magnetization (dipole moment per unit volume) can be pictured as an equivalent bound current going around the surface of the toroidal core. Following Ref. [34], consider the modification to Ampère's law as

$$\oint_C \vec{\mathbf{B}} \cdot d\vec{\boldsymbol{\ell}} = \mu_0 \left(i_{\text{enclosed}} + i_{M\text{enclosed}} \right) \tag{3.4}$$

where $i_{M\text{enclosed}}$ is the equivalent *bound* current enclosed by the curve C (see Figure 3.34).

As before, it is assumed the core diameter $d = r_2 - r_1 << r_1$ so that $r_1 \approx r \approx r_2$ is valid. With n_b the number of loops/coils per unit length of the *equivalent* coil in Figure 3.34(b), $i_{M\text{enclosed}} = 2\pi r_1 n_b i_b$. The next step is to relate this bound current to the magnetization M. To do so, define the *surface current density*

$$\lambda_M \triangleq \frac{i_{M\text{enclosed}}}{2\pi r_1} = n_b i_b$$

and is simply the (average) amount of bound current per unit length around the toroid coil coming out of (or going into) the page.

---

[4] For now, consider a "soft" magnetic material to be one that has a B versus B_0 curve similar to that of Figure 3.33 and whose slope is orders of magnitude greater than one.

www.EngineeringEBooksPdf.com

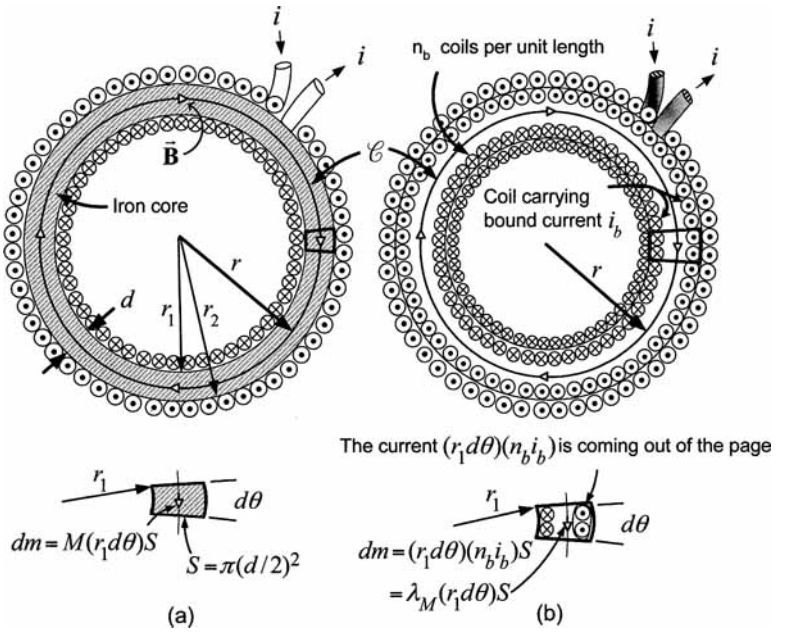


FIGURE 3.34. (a) Toroidal coil with an iron core. Adapted from [34]. (b) Iron core replaced with an equivalent coil carrying the bound current i_b. The bound current produces the same magnetic field as the magnetized iron in Figure 3.34(a).

This is analogous to $\lambda = ni$ being the *free* current in the wire per unit length around the circumference of the toroid. As shown in Section 3.3.1, the magnetic dipole moment is the product of the current around a loop times the area of the loop. The amount of bound current going around the periphery of the toroid between θ and $\theta + d\theta$ is $\lambda_M(r_1 d\theta)$ and, with $S = \pi(d/2)^2$ the cross-sectional area of the toroid, it follows that the magnetic dipole moment dm due to the bound surface current density λ_M in the volume between θ and $\theta + d\theta$ is

$$dm = \lambda_M(r_1 d\theta)S.$$

However, by definition, the magnetization M is the amount of magnetic dipole moment per unit volume, so that the magnetic dipole moment dm in the volume between θ and $\theta + d\theta$ is also given by

$$dm = M(r_1 d\theta)S$$

which results in

$$\lambda_M = M.$$

That is, in this example, the surface current density λ_M is equal to the

www.EngineeringEBooksPdf.com

magnetization M of the iron material. As a result,

$$i_{M\text{enclosed}} = \lambda_M 2\pi r = M2\pi r = \oint_C \left(M\hat{\boldsymbol{\theta}}\right) \cdot \left(rd\theta\hat{\boldsymbol{\theta}}\right) = \oint_C \vec{\mathbf{M}} \cdot d\vec{\boldsymbol{\ell}}.$$

Equation (3.4) therefore becomes

$$\oint_C \vec{\mathbf{B}} \cdot d\vec{\boldsymbol{\ell}} = \mu_0 \left(i_{\text{enclosed}} + \oint_C \vec{\mathbf{M}} \cdot d\vec{\boldsymbol{\ell}} \right).$$

Rearranging this equation gives

$$\oint_C \left(\frac{\vec{\mathbf{B}} - \mu_0 \vec{\mathbf{M}}}{\mu_0} \right) \cdot d\vec{\boldsymbol{\ell}} = i_{\text{enclosed}}.$$

This leads to the definition of the *magnetic intensity* field $\vec{\mathbf{H}}$ given by

$$\vec{\mathbf{H}} \triangleq \frac{\vec{\mathbf{B}}}{\mu_0} - \vec{\mathbf{M}}.$$

Ampère's law in its most general form is then

$$\oint_C \vec{\mathbf{H}} \cdot d\vec{\boldsymbol{\ell}} = i_{\text{free}} \tag{3.5}$$

where $i_{\text{free}} = i_{\text{enclosed}}$ represents the enclosed *free* current in the wire in contrast to the *bound* current in the magnetic material. Both $\vec{\mathbf{B}}$ and $\vec{\mathbf{M}}$ were defined in terms of physical phenomena. However, $\vec{\mathbf{H}}$ is defined as the difference between $\vec{\mathbf{B}}/\mu_0$ and $\vec{\mathbf{M}}$ which does not lend itself to a physical interpretation. It is simply defined as a quantity whose line integral around a closed curve depends only on the free current through the curve. The next section shows how $\vec{\mathbf{B}}$ and $\vec{\mathbf{H}}$ can be related experimentally.

3.4.1 The B–H Curve

With the definition $\vec{\mathbf{H}} \triangleq \vec{\mathbf{B}}/\mu_0 - \vec{\mathbf{M}}$, Ampère's law was modified to

$$\oint_C \vec{\mathbf{H}} \cdot d\vec{\boldsymbol{\ell}} = i_{\text{free}}.$$

Ampère's law can be used to calculate $\vec{\mathbf{H}}$, but $\vec{\mathbf{B}}$ is the desired quantity as it produces forces on currents and magnetic materials. As $\vec{\mathbf{M}}$ is typically not known, one cannot compute $\vec{\mathbf{B}}$ from the definition of $\vec{\mathbf{H}}$. As a consequence, empirical/experimental methods are used to relate $\vec{\mathbf{B}}$ and $\vec{\mathbf{H}}$. The empirical method to determine this relationship is typically done using the toroidal coil setup of the previous section. Specifically, consider the setup of Figure 3.31 in which the initial magnetization is zero (this can be done by heating

www.EngineeringEBooksPdf.com

up the iron core so that the magnetic dipole moments become randomly oriented with respect to each other). Application of Ampère's law gives[5]

$$\begin{aligned} \oint_C \vec{\mathbf{H}} \cdot d\vec{\ell} &= i_{\text{free}} \\ H 2\pi r &= 2\pi r_1 ni \\ H &= \frac{r_1}{r} ni \approx ni \end{aligned}$$

so that $H = B_0/\mu_0$ as in equation (3.3). Equation (3.2) given by

$$B(t) = -\frac{1}{N_s S} \int_0^t V_s(\tau) d\tau$$

is again used to find the value of B as a function of $H = ni$ resulting in the so-called $B - H$ curve as shown in Figure 3.35(a). This is now considered in more detail. (Note that as $H = ni$, one can specify the value of H by simply specifying the current i.)

First, the current i is increased from 0 to $I_{\max}$ so that H goes from 0 to $H_{\max} = nI_{\max}$ along the curve a–b in Figure 3.35(a), where $H_{\max} = 100 \frac{\text{ampere-turn}}{\text{meter}}$. As the current is increased, the voltage V_s in the secondary coil is measured and B is calculated according to (3.2). Plotting B versus H one obtains the curve a–b shown in Figure 3.35(a). Along the curve a–b, $H > 0, B > 0$, and $M > 0$.

Next, H (or equivalently i) is decreased from $H_{\max}$ to 0. Again, B is computed according to (3.2), resulting in the curve b–c shown in Figure 3.35(a). At the point c, $B > 0$ with $H = 0$ and therefore $i = 0$, that is, there is a magnetic field in the core without any current in the coil. In words, the toroidal is core is permanently magnetized. The corresponding value of the magnetic field is denoted B_r and is called the *remanence* or *retentivity*. Along the curve b–c, $H > 0, B > 0$, and $M > 0$.

In the next step, H is made negative by putting negative current in the coil ($i < 0$), and B decreases along the curve c–d where at the point d, the magnetic field strength is zero in the core ($B = 0$). The magnetic field produced by the (negative) current in the coil is canceling the magnetic field produced by the aligned dipoles of the magnetic material. At this point, $H = -H_c$ where $H_c > 0$ is called the *coercive force* or *coercivity*.[6] Along the curve c–d, $H < 0, B > 0$, and $M > 0$.

Continuing, H is decreased even more (i.e., $i < 0$ is decreased more) resulting in the magnetic dipoles of the material realigning in the opposite

[5] By definition $\vec{\mathbf{H}} \triangleq \vec{\mathbf{B}}/\mu_0 - \vec{\mathbf{M}}$ and on physcial grounds $\vec{\mathbf{B}}$ and $\vec{\mathbf{M}}$ point in the same direction which in this case is the $\hat{\boldsymbol{\theta}}$ direction inside the toroid. Consequently, $\vec{\mathbf{H}}$ will also be in the $\hat{\boldsymbol{\theta}}$ direction and may be written in the form $\vec{\mathbf{H}} = H\hat{\boldsymbol{\theta}}$.

[6] H_c is not a force so "coercive force" is not a good name. The value of H_c depends on the particular B-H loop that the system is going through.

www.EngineeringEBooksPdf.com

direction to add to the magnetic field produced by the current in the coil (see path d–e). At the point e where $H = -H_{\max} = -100\frac{\text{ampere-turn}}{\text{meter}}$, the value of B is the negative of that given at the point b. Along the curve d–e, $H < 0, B < 0$, and $M < 0$.

Finally, in a similar fashion, H is brought from $-H_{\max}$ to 0 to $H_{\max}$ and the plot of B versus H follows the curve e–f–g–b.

In summary, letting H vary from $H_{\max}$ to 0 to $-H_{\max}$ and then from $-H_{\max}$ to 0 back to $H_{\max}$, the plot of B versus H follows the curve b–c–d–e–f–g–b. This is called the *hysteresis loop*. If the hysteresis loop of the iron is quite thin, it is considered to be "soft" iron as in Figure 3.35(b) while if the hysteresis loop is quite thick, then it is considered to be "hard" iron as in Figure 3.35(a).

In the case of soft iron magnetic material such as Figure 3.35(b), the hysteresis loop is thin enough that it can be approximated by a single curve lying only in the first and third quadrants.

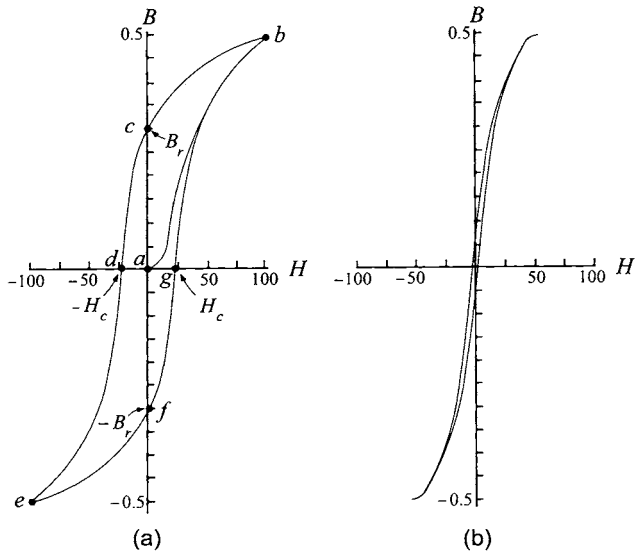


FIGURE 3.35. B versus H curve. (a) Hysteresis curve for a "hard" magnetic material. (b) Hysteresis curve for a "soft" magnetic material.

Figure 3.36 shows experimentally determined B–H curves for the two soft magnetic materials M-19 29-gauge steel and a soft steel iron casting where, as B is an odd function of H, only the first quadrant need be given. Note that at smaller values of H, the B–H curves in Figure 3.36 are approximately linear.

Remark Figure 3.33 would correspond to a soft magnetic material in which the hysteresis can be ignored.

www.EngineeringEBooksPdf.com

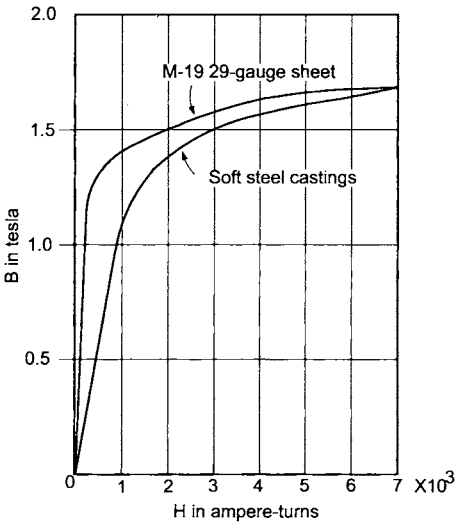


FIGURE 3.36. B (tesla) versus H (ampere-turns) curves for two different soft magnetic materials. From *An Introduction to Electrical Machines and Transformers*, 2nd edition, G. McPherson and R. D. Laramore, 1990. Reprinted by permisson of John Wiley & Sons.

Example

Consider the experimental B versus H curves for two different soft iron materials as given in Figure 3.36. As $\vec{\mathbf{B}}$ and $\vec{\mathbf{M}}$ (and therefore $\vec{\mathbf{H}}$) tend to point in the *same* direction in soft iron, the relationship

$$\vec{\mathbf{B}} = \mu_0 \vec{\mathbf{H}} + \mu_0 \vec{\mathbf{M}}$$

may be written approximately as

$$\vec{\mathbf{B}} = \mu_r \mu_0 \vec{\mathbf{H}}$$

or

$$B = \mu_r \mu_0 H$$

where μ_r is that empirically determined number that makes this equation valid. For example, using the soft steel casting material with i chosen in the primary coil of the toroidal solenoid so that $H = 1000$ ampere-turns, the data curve in Figure 3.36 gives $B = 1.2$ tesla. Thus,

$$\mu_r = \frac{B}{\mu_0 H} = \frac{1.2}{(4\pi \times 10^{-7}) \times 1000} = 955.$$

The important observation from this numerical example is that μ_r is quite large. In a coil carrying a current i with an *air core*,

$$B_{\text{inside}} = \mu_0 H_{\text{inside}} = \mu_0 n i$$

www.EngineeringEBooksPdf.com

while in an identical coil carrying the same current i with an *iron core*,

$$B_{\text{inside}} = \mu_r \mu_0 H_{\text{inside}} = \mu_r \mu_0 ni.$$

The H field is the *same* in both coils as the current is the same in each coil. However, as μ_r is on the order of 1000, the magnetic field B in the coil with the iron core is much larger. The terminology "ideal" soft magnetic material is one in which $\mu_r = \infty$ while a "good" magnetic material just means μ_r is very large.

3.4.2 Computing $\vec{\mathbf{B}}$ and $\vec{\mathbf{H}}$ in Magnetic Circuits

Based on the previous sections, a simple procedure is now given that gives an accurate enough computation of $\vec{\mathbf{B}}$ and $\vec{\mathbf{H}}$ for modeling the magnetic circuits of electric machines. To start with a simple example, consider the toroidal coil with an iron core shown in Figure 3.37 in which a small air gap of length g has been cut out.

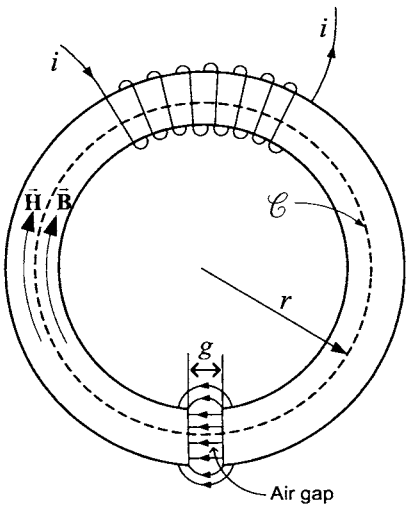


FIGURE 3.37. Coil wrapped around a torus with an air gap. From *Electric Machines: Dynamics and Steady State* by G. J. Thaler and M. L. Wilcox, 1966. Reprinted by permission of John Wiley & Sons.

Ampère's law

$$\oint_C \vec{\mathbf{H}} \cdot d\vec{\boldsymbol{\ell}} = i_{\text{free}}$$

is applied to a circular curve C of radius r in Figure 3.37. In the magnetic material, $\vec{\mathbf{B}} = B_m \hat{\boldsymbol{\theta}}$ while in the air gap $\vec{\mathbf{B}} = B_a \hat{\boldsymbol{\theta}}$. Though azimuthal symmetry does not hold because of the air gap, it turns out that if the air

www.EngineeringEBooksPdf.com

gap is small, it is still approximately true that B_m has a constant value as a function of the azimuthal angle θ in the magnetic material and, similarly, B_a is constant as a function of θ in the air gap. Further, with the standing assumption that the diameter of the core is much smaller than the inner radius of the toroidal coil, B_m and B_a are essentially constant across the cross section of the core. In the same way, $\vec{\mathbf{M}} = M\hat{\boldsymbol{\theta}}$ is constant as a function of θ in the iron core while it is, of course, zero in the air gap. Thus H_m and H_a are also approximately constant as functions of θ and over the cross-sectional area of the core. With N the total number of coil turns, Ampère's law applied to the circular curve C of radius r in Figure 3.37 gives

$$H_m(2\pi r - g) + H_a g = Ni \tag{3.6}$$

with

$$\begin{aligned} B_m &= \mu_0 H_m + \mu_0 M = \mu_r \mu_0 H_m \text{ (from the measured } B\text{–}H \text{ curve)} \\ B_a &= \mu_0 H_a. \end{aligned}$$

It is assumed that the air gap is small enough that B_a is essentially constant across it. Recall that by Gauss's law for $\vec{\mathbf{B}}$, $B_m = B_a$ *at the air-iron interface.* As B_m is approximately constant in the iron and B_a is constant in the air gap, $B_m = B_a$. Thus,

$$\mu_0 H_a = B_a = B_m = \mu_r \mu_0 H_m$$

or

$$H_m = \frac{H_a}{\mu_r}.$$

Again, in good magnetic materials, μ_r is greater than 1000 so that H_m is more than a thousand times smaller than H_a. Consequently, one often takes $H_m = 0$ in good magnetic materials. In this case, taking $H_m = 0$ in (3.6) leads to

$$H_a g = Ni$$

so that

$$B_a = \mu_0 H_a = \frac{\mu_0 Ni}{g} \qquad (H_m = 0). \tag{3.7}$$

This last expression is important because it gives us the magnetic field in air gap in terms of known quantities. The value of B in the air gap is the important quantity since, for example, a current carrying wire can be run through the air gap and the value of B will determine how much force can be exerted on the wire.

It is important to note that to use the approximation $H_m = 0$, one must check that $2\pi r - g$ is not too large. For example, with $\mu_r = 1000$, if $2\pi r - g$ is a thousand times longer than g, then

$$H_m(2\pi r - g) + H_a g = \frac{H_a}{1000} 1000g + H_a g = 2H_a g = Ni$$

www.EngineeringEBooksPdf.com

or

$$B_a = \mu_0 H_a = \frac{\mu_0 N i}{2g}$$

This large error (a factor of 2) in the calculation of the magnetic field in the air gap due to the fact that $H_m(2\pi r - g)$ is not negligible. However, if the designer of this magnetic circuit made sure that $2\pi r - g = 100g$, then

$$\begin{aligned} H_m(2\pi r - g) + H_a g &= \frac{H_a}{1000} 100g + H_a g \\ &= 1.1 H_a g \end{aligned}$$

resulting in

$$B_a = \mu_0 H_a = \frac{\mu_0 N i}{1.1g}.$$

which is not much different from (3.7) where $H_m = 0$ was assumed.

In summary, B in the air gap is the fundamental quantity of interest as it is the field that can produce forces on currents in wires placed in the air gap, or can induce voltages in wire loops, and so on. Here, Ampère's law

$$\oint_C \vec{\mathbf{H}} \cdot d\vec{\ell} = i_{\text{free}}$$

was used to find a relation between H_m (H in the magnetic material) and H_a (H in the air gap). The free currents (currents in the wires) are known or easily measured. Assuming that the magnetic paths in the iron are not too long, one can use the approximation that $H_m = 0$ in the magnetic material. Then, H_a can be found in the air gap from Ampère's law which in turn is used to obtain the magnetic field *in the air gap* from $B_a = \mu_0 H_a$.

Example (Adapted from Chapman [19])

Following Chapman [19], Figure 3.38 shows a setup to produce the radial magnetic field in the air gap of a separately excited DC motor. The objective here is to determine the strength of the field B in the air gap in terms of the current i_f in the field coil. Ampère's law gives

$$H_m \ell + H_a g + H_m \ell_2 + H_a g = N i_f \tag{3.8}$$

where ℓ is the length of the path in the field iron, ℓ_1 is the length of the rotor, ℓ_2 is the diameter of the rotor iron, and g is the air gap length. Here $N = 200$, $\ell = 0.5$ m, $g = 5 \times 10^{-4}$ m, $\ell_1 = 2.4 \times 10^{-2}$ m, $\ell_2 = 5 \times 10^{-2}$ m, and $S = \ell_1 \ell_2 = 12 \times 10^{-4}$ m^2. Equation (3.8) is an approximation as it is being assumed that H_m is constant in magnitude everywhere inside the magnetic material and that it follows the path of the iron.

www.EngineeringEBooksPdf.com

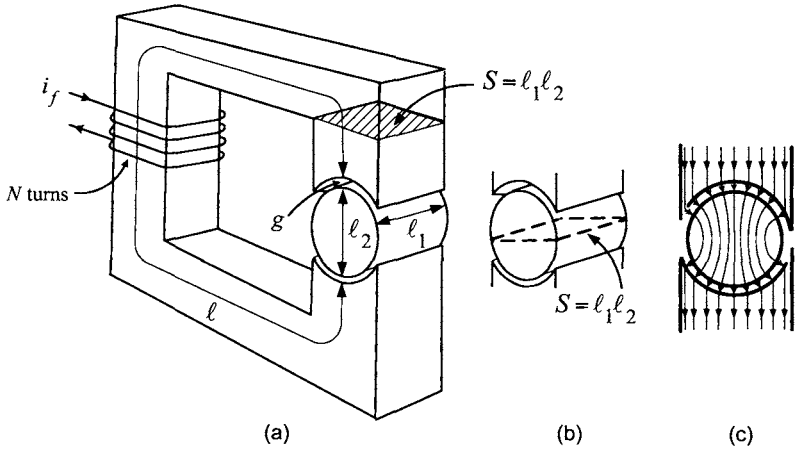


FIGURE 3.38. Magnetic circuit for producing the magnetic field in the air gap of a DC motor. Figure 3.38(a) from *Electric Machinery Fundamentals* by S. J. Chapman, 2nd edition, 1991, McGraw-Hill. Reproduced by permission of McGraw-Hill Companies.

Assuming ideal magnetic material so that H_m is taken to be zero inside the magnetic material,

$$B_a = \mu_0 H_a = \frac{\mu_0 N i_f}{2g} = K_f i_f.$$

Evaluating,

$$B_a = \frac{(4\pi \times 10^{-7}) \times 200}{2 \times 5 \times 10^{-4} \text{ m}} i_f = 0.25 i_f \text{ tesla}$$

where 1 weber/m^2 = 1 tesla.

Example (Chapman [19])

The previous example is redone without setting $H_m = 0$ in the magnetic material. It is still assumed that H_m is constant in magnitude everywhere inside the magnetic material and that it follows the path of the iron. Suppose that for the iron used in the rotor and the core of the field winding, the relative permeability is $\mu_r = 2000$ so that $B_m = \mu_r \mu_0 H_m$. As before, $N = 200$, $\ell = 0.5$ m, $g = 5 \times 10^{-4}$ m, $\ell_1 = 2.4 \times 10^{-2}$ m, $\ell_2 = 5 \times 10^{-2}$ m, and $S = \ell_1 \ell_2 = 12 \times 10^{-4}$ m^2. The path $\ell + \ell_2 = 55$ cm is 550 times longer than the path $2g = 0.1$ cm in the air gap. From Ampère's law

$$H_m \ell + H_a g + H_m \ell_2 + H_a g = N i_f. \tag{3.9}$$

The problem here is that this is only one equation with two unknowns H_m, H_a. However, another relation is found by making use of the assumption (approximation) that the flux ϕ in the cross-section of the magnetic

www.EngineeringEBooksPdf.com

circuit is constant. That is, it is assumed that the magnetic material essentially keeps the magnetic field either in the core itself or within the air gap in the radial direction. This assumption is usually stated as saying the magnetic circuit has no (flux) *leakage*. In the iron core of the field,

$$\phi = B_m S = \mu_r \mu_0 H_m S$$

where $S = \ell_1 \ell_2$ is the core cross sectional area and B_m is constant in the cross-section. Then

$$H_m \ell = \frac{H_m \ell}{\phi}\phi = \frac{H_m \ell}{\mu_r \mu_0 H_m S}\phi = \frac{\ell}{\mu_r \mu_0 S}\phi = R_c \phi.$$

Here R_c is called the *reluctance* of the core path and it has been used to relate H_m to the flux ϕ. Evaluating this expression for R_c gives

$$R_c = \frac{\ell}{\mu_r \mu_0 S} = \frac{50 \times 10^{-2} \text{ m}}{(2000)(4\pi \times 10^{-7})(12 \times 10^{-4} \text{ m}^2)} = 166 \times 10^3 \frac{\text{A-turns}}{\text{Wb}}.$$

Because of the cylindrical shape of the rotor core and conservation of flux, B_m (and therefore $H_m = \mu_r \mu_0 B_m$) is not constant as one goes through the rotor [see Figure 3.38(c)]. Specifically, $B_{mR} S_R = B_m S$ where $S_R = \pi(\ell_2/2)\ell_1$ is the surface area of the top (or bottom) side of the rotor core, B_{mR} is the magnetic field at the surface of the rotor core and $B_m S$ is the flux computed in the middle of the core [which has the same cross section as the field core as indicated in Figure 3.38(b)]. By conservation of flux, H_m in the rotor core has a minimum value at the (inside) surface of the rotor iron and a maximum value in the middle of the rotor on the surface S in Figure 3.38(b). The maximum value of H_m in the middle of the core is used because it leads to a larger value for the reluctance of the core and therefore a more conservative (higher) estimate of the current needed to set up a specified magnetic field in the air gap. So, with H_m taken as its value in the middle of the core on the surface S in Figure 3.38(b), in the rotor iron

$$H_m \ell_2 = \frac{H_m \ell_2}{\phi}\phi = \frac{H_m \ell_2}{\mu_r \mu_0 H_m S}\phi = \frac{\ell_2}{\mu_r \mu_0 S}\phi = R_r \phi.$$

Evaluating the expression for R_r gives

$$R_r = \frac{\ell_2}{\mu_r \mu_0 S_r} = \frac{5 \times 10^{-2} \text{ m}}{(2000)(4\pi \times 10^{-7})(12 \times 10^{-4} \text{ m}^2)} = 16.6 \times 10^3 \frac{\text{A-turns}}{\text{Wb}}.$$

The flux in the air gap is $B_a S_g = \mu_0 H_a S_g$ where $S_g = \pi(\ell_2/2 + g/2)\ell_1 = 19.0 \text{ cm}^2$ is the surface area of the top (bottom) stator side of the air gap. Further this flux is equal to the flux $\phi = B_m S = \mu_r \mu_0 H_m S$ in the iron core. It then follows that

$$H_a g = \frac{H_a g}{\phi}\phi = \frac{H_a g}{\mu_0 H_a S_g}\phi = \frac{g}{\mu_0 S_g}\phi = R_g \phi.$$

www.EngineeringEBooksPdf.com

Then

$$R_g = \frac{g}{\mu_0 S_g} = \frac{0.05 \times 10^{-2} \text{ m}}{(4\pi \times 10^{-7})(19.0 \times 10^{-4} \text{ m}^2)} = 209.4 \times 10^3 \frac{\text{A-turns}}{\text{Wb}}.$$

With this information, equation (3.9) may be rewritten as

$$(R_c + R_r + 2R_g)\,\phi = Ni_f$$

which evaluates to

$$(166 + 16.6 + 2(209.4)) \times 10^3 \phi = 601.4 \times 10^3 \phi = Ni_f.$$

Solving for ϕ, one obtains

$$\phi = 3.3 \times 10^{-4} i_f \text{ Wb}.$$

The magnetic field in the air gap is then

$$B_a = \frac{\phi}{S_g} = \frac{3.3 \times 10^{-4}}{19.0 \times 10^{-4}} i_f = 0.17 i_f \frac{\text{Wb}}{\text{m}^2}$$

which is significantly less than the $0.25 i_f$ Wb/m^2 found assuming $H_m = 0$. However, suppose that the magnetic circuit is redesigned so that $\ell = 10$ cm instead of 50 cm. Then

$$\begin{aligned} R_c &= \frac{\ell}{\mu_r \mu_0 S} = \frac{5 \times 10^{-2} \text{ m}}{(2000)(4\pi \times 10^{-7})(12 \times 10^{-4} \text{ m}^2)} \\ &= 33.2 \times 10^3 \frac{\text{A-turns}}{\text{Wb}} \end{aligned}$$

and equation (3.9) reduces to

$$(R_c + R_r + 2R_g)\,\phi = Ni_f$$

and evaluates to

$$\Big(33.2 + 16.6 + 2(209.4)\Big) \times 10^3 \phi = 468.6 \times 10^3 \phi = Ni_f.$$

The flux is then

$$\phi = 4.23 \times 10^{-4} i_f \text{ Wb}$$

resulting in the magnetic field in the air gap being

$$B_a = \frac{\phi}{S_g} = \frac{4.23 \times 10^{-4}}{19.0 \times 10^{-4}} i_f = 0.22 i_f \frac{\text{Wb}}{\text{m}^2}$$

which is much closer to $0.25 i_f$ Wb/m^2.

www.EngineeringEBooksPdf.com

The point of this example is that taking $H_m = 0$ in magnetic materials and then using Ampère's law to find B_a in the air gap depends on the proper design of the magnetic circuit. Machine designers spend a great deal of effort trying to make the reluctance in the magnetic material as small as possible by making the path length small, the cross sectional area large and using highly permeable magnetic material (i.e., μ_r large). Figure 3.38 is not a practical design for the stator iron of a DC motor. Figures 1.31 and 1.32 of Chapter 1 depict actual stator iron cores for a DC motor. It will be assumed in all that follows that good machine designs have resulted in making the approximation $H_m = 0$ valid.

3.4.3 $\vec{\mathbf{B}}$ *is Normal to the Surface of Soft Magnetic Material*

It is now shown that $\vec{\mathbf{B}}$ is normal (perpendicular) to the surface at an air/magnetic-material interface under two assumptions: (1) The magnetic material is assumed to be ideal (soft) magnetic material so that $\mu_r = \infty$, or equivalently, $H = 0$. (2) There are no current carrying wires on the surface.

For example, it is not true for toroids as wire is wrapped around surface of the magnetic material. Also, typically $H \neq 0$ inside a permanent magnet.

Consider the closed rectangular-shaped curve C in Figure 3.39 for which half is in the air and the other half is in the magnetic material.

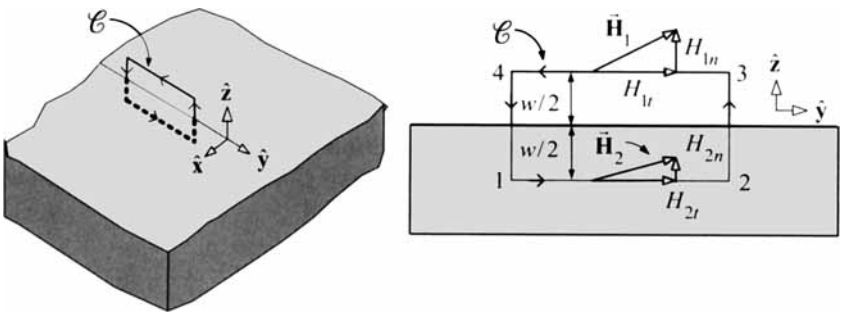


FIGURE 3.39. Closed rectangular-shaped curve enclosing the air and magnetic material. As $w \to 0$, $\vec{\mathbf{H}}_1$ is just above the surface and $\vec{\mathbf{H}}_2$ is just below the surface.

Ampère's law is applied to the rectangular-shaped curve C, which in this instance is given by

$$\oint_C \vec{\mathbf{H}} \cdot d\vec{\ell} = 0 \tag{3.10}$$

as there is no free current, that is, no wires on the surface carrying current. With $\vec{\mathbf{H}}(x, y, z) = H_x\hat{\mathbf{x}} + H_y\hat{\mathbf{y}} + H_z\hat{\mathbf{z}}$ and the coordinate system defined as

www.EngineeringEBooksPdf.com

shown in Figure 3.39, it is seen that $H_z\hat{\mathbf{z}}$ is the part of $\vec{\mathbf{H}}$ normal to the surface while $H_x\hat{\mathbf{x}} + H_y\hat{\mathbf{y}}$ is the tangential component to the surface.

Expanding (3.10) results in

$$\oint_C \vec{\mathbf{H}} \cdot d\vec{\ell} = \int_1^2 \vec{\mathbf{H}} \cdot d\vec{\ell} + \int_2^3 \vec{\mathbf{H}} \cdot d\vec{\ell} + \int_3^4 \vec{\mathbf{H}} \cdot d\vec{\ell} + \int_4^1 \vec{\mathbf{H}} \cdot d\vec{\ell} = 0 \quad (3.11)$$

where side 1–2 is in the magnetic material and side 3–4 is in the air. Sides 2–3 and 4–1 are short segments of length w going between the air and magnetic material. The interest here is in the tangential component of $\vec{\mathbf{H}}$ just above and just below the surface. Making the rectangular curve C very thin ($w \to 0$) so that the lengths of sides 2–3 and 4–1 go to zero, equation (3.11) reduces to

$$\int_1^2 \vec{\mathbf{H}} \cdot d\vec{\ell} + \int_3^4 \vec{\mathbf{H}} \cdot d\vec{\ell} = 0 \quad (3.12)$$

as $w \to 0$. Also, as

$$d\vec{\ell} = \begin{cases} d\ell\hat{\mathbf{y}} & \text{side } 1\text{–}2 \\ -d\ell\hat{\mathbf{y}} & \text{side } 3\text{–}4 \end{cases}$$

it follows that

$$\int_1^2 (H_{1x}\hat{\mathbf{x}} + H_{1y}\hat{\mathbf{y}} + H_{1z}\hat{\mathbf{z}}) \cdot (d\ell\hat{\mathbf{y}}) + \int_3^4 (H_{2x}\hat{\mathbf{x}} + H_{2y}\hat{\mathbf{y}} + H_{2z}\hat{\mathbf{z}}) \cdot (-d\ell\hat{\mathbf{y}})$$
$$= H_{1y}\ell_1 - H_{2y}\ell_1 = 0$$

or

$$H_{2y} = H_{1y}.$$

But $H_{2y} = 0$ in ideal soft magnetic materials so that $H_{1y} = 0$. Similarly, one can show that $H_{1x} = 0$ by taking a curve C that is in the x–z plane. That is, at the surface of the magnetic material

$$\vec{\mathbf{H}}_1(x, y, z) = H_{1z}\hat{\mathbf{z}}$$

and, as this is in the air,

$$\vec{\mathbf{B}}_1 = \mu_0\vec{\mathbf{H}}_1 = \mu_0 H_{1z}\hat{\mathbf{z}}$$

so that $\vec{\mathbf{B}}$ is normal to the surface.

Remark

The magnetic circuit of Figure 3.10 has a soft iron core. Note that the lines of $\vec{\mathbf{B}}$ are perpendicular at the surface of the iron core, but not at the coil surface. Figures 3.7 and 3.11 of the bar and horseshoe magnets, respectively, are permanent (hard) magnets for which the above assumptions do not necessarily hold (in particular, $\vec{\mathbf{H}} = 0$ is not usually true in permanent magnets). For example, note that $\vec{\mathbf{B}}$ is *not* perpendicular to the surface of the cylindrical *permanent* magnet shown in Figure 3.18.

www.EngineeringEBooksPdf.com

3.5 Permanent Magnets*

Consider the cylindrical-shaped permanent magnet in Figure 3.40 where there is no free current.

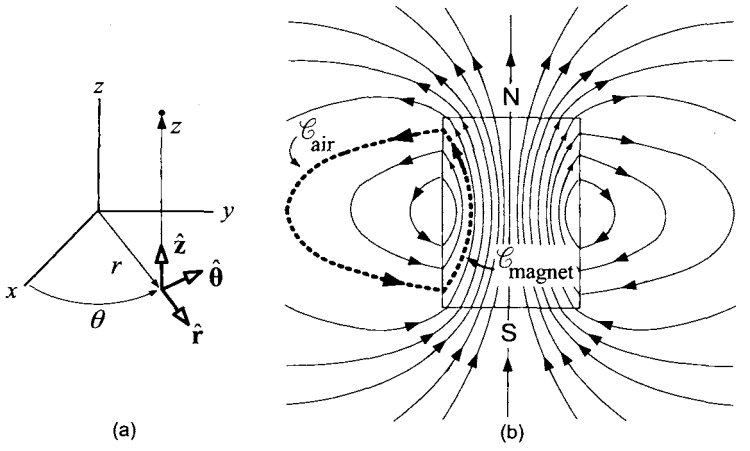


FIGURE 3.40. (a) Cylindrical coordinate system for the bar magnet. (b) Magnetic field lines $\vec{\mathbf{B}}$ around a cylindrical-shaped permanent magnet. Adapted from Figures 37-4(a) and 37-4(b) of Ref. [34].

Ampère's law applied to the path C in the figure gives

$$\oint_C \vec{\mathbf{H}} \cdot d\vec{\ell} = \int_{C_{\text{air}}} \vec{\mathbf{H}} \cdot d\vec{\ell} + \int_{C_{\text{magnet}}} \vec{\mathbf{H}} \cdot d\vec{\ell} = 0$$

where $d\vec{\ell} = dr\hat{\mathbf{r}} + rd\theta\hat{\boldsymbol{\theta}} + dz\hat{\mathbf{z}}$ and the curve has been decomposed into its part in the air and its part in the magnet. As $\vec{\mathbf{H}} = \vec{\mathbf{B}}/\mu_0$ in the air,

$$\int_{C_{\text{air}}} \vec{\mathbf{H}} \cdot d\vec{\ell} > 0.$$

Consequently,

$$\int_{C_{\text{magnet}}} \vec{\mathbf{H}} \cdot d\vec{\ell} < 0$$

in order that $\oint_C \vec{\mathbf{H}} \cdot d\vec{\ell} = 0$. Note that the path C was chosen to follow the closed curve of one of the magnetic lines of $\vec{\mathbf{B}}$. As a result,

$$\oint_C \vec{\mathbf{H}} \cdot d\vec{\ell} = \oint_C \left(H_r\hat{\mathbf{r}} + H_\theta\hat{\boldsymbol{\theta}} + H_z\hat{\mathbf{z}}\right) \cdot d\vec{\ell} = \oint_C (H_r\hat{\mathbf{r}} + H_z\hat{\mathbf{z}}) \cdot d\vec{\ell}$$

www.EngineeringEBooksPdf.com

as the $\hat{\boldsymbol{\theta}}$ component of $d\vec{\boldsymbol{\ell}}$ is zero. Thus

$$\int_{C_{\text{air}}} (H_r\hat{\mathbf{r}} + H_z\hat{\mathbf{z}}) \cdot d\vec{\boldsymbol{\ell}} + \int_{C_{\text{magnet}}} (H_r\hat{\mathbf{r}} + H_z\hat{\mathbf{z}}) \cdot d\vec{\boldsymbol{\ell}} = 0. \tag{3.13}$$

Figure 3.40 shows that on C_{air}, $d\vec{\boldsymbol{\ell}}$ and $\vec{\mathbf{H}} = \vec{\mathbf{B}}/\mu_0$ point in the same direction so that the first integral in (3.13) must be positive. As a result, the second integral in (3.13) must be negative meaning that on C_{magnet}, the component of $\vec{\mathbf{H}}$ tangent to the curve C_{magnet} points opposite to $d\vec{\boldsymbol{\ell}}$. In other words, in Figure 3.40, $\vec{\mathbf{H}}$ must be pointing *downwards* inside the magnet while $\vec{\mathbf{B}}$ is pointing *upwards* inside the magnet. Physically, the z components of $\vec{\mathbf{B}}$ and $\vec{\mathbf{M}}$ are in the $+\hat{\mathbf{z}}$ direction inside the magnet which means that $M_z > B_z/\mu_0$ as $H_z = B_z/\mu_0 - M_z < 0$. This is in contrast to the air-filled solenoid coil shown in Figure 3.19(b) where $\vec{\mathbf{B}}$ and $\vec{\mathbf{H}}$ point in the *same* direction inside the coil and $\oint_C \vec{\mathbf{H}} \cdot d\vec{\boldsymbol{\ell}} = i_{\text{free}} \neq 0$ as there is free current on the surface of the solenoid going through the closed curve C. Consequently, in the case of the permanent magnet, the magnetic material is operating in the *second* quadrant of the B–H curve ($B > 0, H < 0$) at some point *strictly* between points c and d in Figure 3.35(a) while the air-filled solenoid is operating in the *first* quadrant ($B > 0, H > 0$), at some point strictly between points b and c in Figure 3.35(a). How can this be understood? Consider a process to make a cylindrical magnet as shown in Figure 3.41. To begin, take an iron alloy such as carbon steel (used for permanent magnets) and make it into an oblong shape closed solid as shown in Figure 3.41(a). Note that the straight segments are already "cut out" and will become the cylindrical magnets. Wire is wrapped around this iron core (like a toroid) and the current applied to the winding to magnetize the iron as shown in Figure 3.41(b). Assuming that the core diameter is small compared to the overall length of the core, it is a reasonable approximation to assume that $\vec{\mathbf{B}}$ and $\vec{\mathbf{H}}$ are constant in magnitude over the cross section of the core and that they follow the closed path around the core. As a result,

$$H(2\ell_1 + 2\ell_2) = ni \tag{3.14}$$

where H is the magnitude of $\vec{\mathbf{H}}$ in the core, ℓ_1 is the length of each cylinder and ℓ_2 is the length of each end piece. Using the setup shown in Figure 3.41(b), the current is increased up to the saturation point of the core (point b in Figure 3.42) and then it is brought back down to zero (point c in Figure 3.42). At this point, the magnet is operating at the point c of the B–H curve so that $H = 0$ as $i = 0$ from equation (3.14). The winding is now removed and this does not affect the B–H relationship in the magnetic material of the core as $i = 0$. At each point of the core,

$$\vec{\mathbf{H}} = \frac{\vec{\mathbf{B}}}{\mu_0} - \vec{\mathbf{M}} = 0 \tag{3.15}$$

www.EngineeringEBooksPdf.com

that is,

$$\vec{\mathbf{B}} = \mu_0 \vec{\mathbf{M}} \quad \text{or} \quad B = \mu_0 M. \tag{3.16}$$

Recall this same result was shown for the toroidal cylindrical core where $B = \mu_0 \lambda_m = \mu_0 M$ with $\lambda_m = M$ an equivalent (bound) surface current density going around core periphery due to the magnetization M (magnetic dipole moment per unit volume).

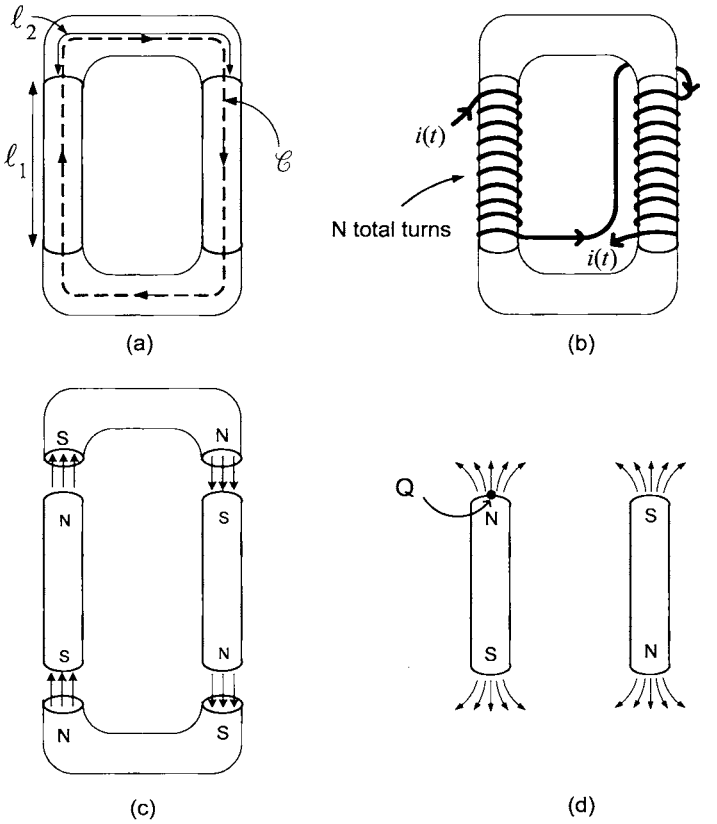


FIGURE 3.41. (a) Oblong shaped iron core with two cylinders cut out. (b) Winding wrapped around the core to magnetize the iron. (c) Current is brought to zero, windings removed and the end pieces removed in the direction shown. (d) Two cylindrical-shaped permanent magnets.

Next, as shown in Figure 3.41(c), the two end pieces of the iron core are pulled away in the direction shown. By pulling apart the end pieces in this manner, the magnetization M in each of the remaining cylindrical cores stays pretty much the same, i.e., the magnetic dipoles of the iron tend to stay aligned. However, with the end pieces removed, one would

www.EngineeringEBooksPdf.com

not expect equation (3.15), or equivalently (3.16), to remain valid for the remaining cylindrical cores. For example, consider the point Q at the end of the cylinder shown in Figure 3.41(d), where now there is only air above the surface instead of magnetic material as before. The B field at any point of the material is due to the magnetic field produced by *all* of the iron atoms in the material, especially those atoms that are close by. Even with the iron uniformly magnetized with the same constant strength M everywhere, at the ends of the cylinder such as the point Q, one would expect that B is reduced (on the order of a factor of 2) as there is only air on one side of the surface rather than magnetized iron as before. Consequently,

$$H = \frac{B}{\mu_0} - M < 0$$

as the value of B at the point Q is reduced after removing the two end pieces even if M remains the same.

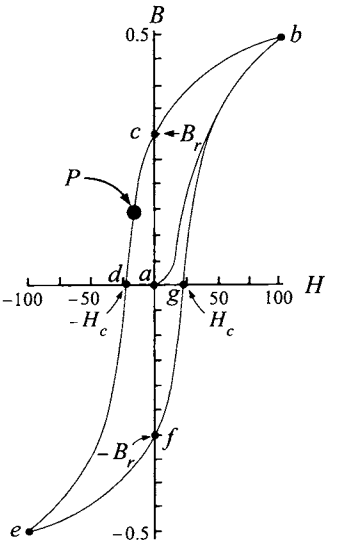


FIGURE 3.42. B versus H curve. Inside the permanent magnet, the material is operating at a point in the second quadrant such as P.

Reiterating, if the magnetization M in the core remains constant and equal to its value before the two end pieces were removed, the H field is now negative in the two cylindrical bar magnets because B is reduced in strength due to the two end pieces being removed. Consequently, as the two end pieces are removed, the operating point for the magnetic material of the two cylindrical magnets moves down the B–H curve from c to a new point (say) P. The closer one is to either end of the cylindrical magnets, the

www.EngineeringEBooksPdf.com

farther down the curve the operating point goes into the second quadrant. On the other hand, at the center of the cylindrical magnets, the operating point is closer to point c and would be exactly at point c if the cylindrical piece was infinitely long.

3.5.1 Hysteresis Loss

Consider a steady-state situation of going around the B–H curve of Figure 3.35(a). That is, after an initial magnetization of the material so that the (B, H) coordinates are at the point b with $i = I_{\max}$, the current is decreased to 0 bringing the system to point c where $H = 0$, then the current is brought down to the point where the B field is zero putting the system at d, and next the current is brought down to $-I_{\max}$ so the system is at e. Going from b to e represents 1/2 of the B–H cycle as indicated in Figure 3.43(a).

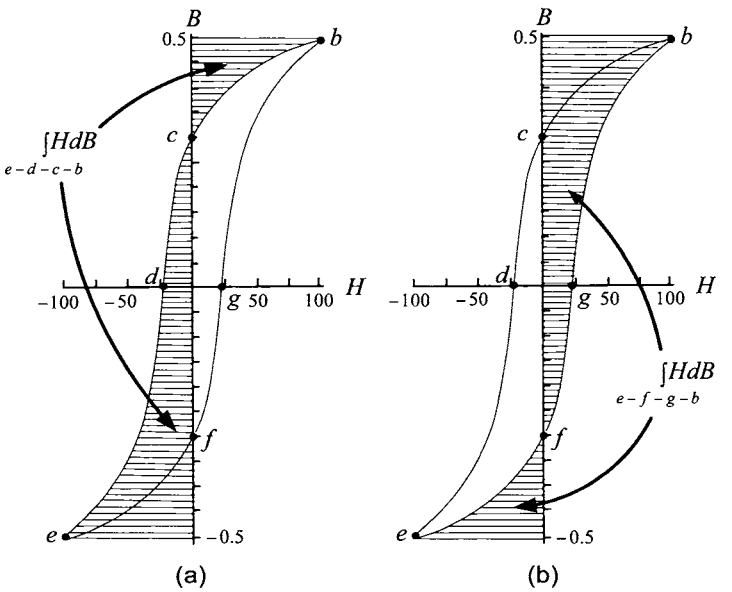


FIGURE 3.43. (a) $\int_{\text{e–d–c–b}} HdB$. (b) $\int_{\text{e–f–g–b}} HdB$.

The other half is similar. That is, the current is brought back to 0 to put the system at f, next it is increased so that the B field is again zero and the system is at g and finally the current is brought back up to $I_{\max}$ so that the system is back at b (see Figure 3.43(b)).

At any time t, the flux linkage in the primary windings wound around the toroid core is $\lambda(t) = N\phi(t) = NB(t)S$ where N is the total number of primary windings, S is the cross-sectional area of the core and B is the

www.EngineeringEBooksPdf.com

magnetic field in the core. Further, at any time t, $H(t) = Ni(t)/(2\pi r)$ where r is a radius inside the toroid. Suppose that one goes through this complete cycle $b{-}c{-}d{-}e{-}f{-}g{-}b$ in the time T. Then the energy from the source which is providing the current to the coil is given by

$$\begin{aligned} E_{\text{one cycle}} &= \int_{t_1}^{t_1+T} i\dot{\lambda}dt = \int_{t_1}^{t_1+T} \frac{2\pi r H(t)}{N} NS\frac{dB}{dt}dt \\ &= 2\pi r S \int_{t_1}^{t_1+T} H(t)\frac{dB}{dt}dt \end{aligned}$$

By a change of variables, this becomes

$$E_{\text{one cycle}} = V \oint_{\text{b}-\text{c}-\text{d}-\text{e}-\text{f}-\text{g}-\text{b}} HdB$$

where $V = 2\pi r S$ is the volume of the core. In the first half period $T/2$, the energy provided by the source is

$$E_{\text{First half-cycle/unit volume}} = \int_{\text{b}-\text{c}-\text{d}-\text{e}} HdB = -\int_{\text{e}-\text{d}-\text{c}-\text{b}} HdB$$

where $\int_{\text{e}-\text{d}-\text{c}-\text{b}} HdB$ is the area indicated in Figure 3.43(a). Similarly,

$$E_{\text{Second half-cycle/unit volume}} = \int_{\text{e}-\text{f}-\text{g}-\text{b}} HdB$$

which is the area indicated in Figure 3.43(b). The total energy absorbed per cycle is then

$$E_{\text{cycle/unit-volume}} = \int_{\text{e}-\text{f}-\text{g}-\text{b}} HdB - \int_{\text{e}-\text{d}-\text{c}-\text{b}} HdB = \oint_{\text{b}-\text{c}-\text{d}-\text{e}-\text{f}-\text{g}-\text{b}} HdB$$

which is just the area inside the $B{-}H$ curve. This is the energy required for each cycle to magnetize (align the dipole moments of) the iron along the $B{-}H$ curve (i.e., rotate the magnetic dipole moments 360°).

As an example, consider the iron core inside the rotor of a DC motor which is constantly being magnetized and demagnetized as it rotates by the external magnetic field. For example, the point P in Figure 3.44 corresponds to the point b in Figure 3.35. After the iron core rotates clockwise 90 degrees, the magnetic material at point P corresponds to the point d in Figure 3.43. After rotating another 90 degrees, the magnetic material at point P corresponds to point e in Figure 3.43, and so on. That is, the magnetic material at each point in the core is going through a complete cycle of the $B{-}H$ curve each time the core rotates 360 degrees. In this application, it is important that the core be made of soft magnetic material with a very narrow $B{-}H$ loop so that the hysteresis loss is small.

www.EngineeringEBooksPdf.com

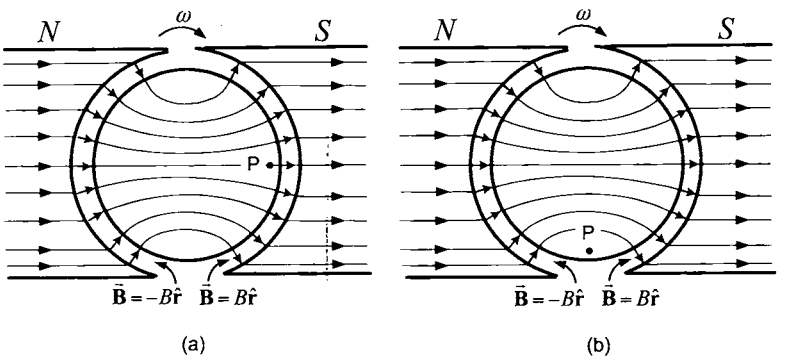


FIGURE 3.44. The magnetic material of the rotor goes through the $B-H$ curve as it rotates.

3.5.2 Common Magnetic Materials

Both soft and hard magnetic materials are used in electric machines. Soft magnetic materials are used as a core structure on which the turns (windings) of the motor are wound (e.g., such as the field circuit of a separately excited DC motor). In such an application, the copper wire of the field winding is wrapped around soft magnetic material, which then results in a much larger radial magnetic field in the air gap than if nonmagnetic material was used. The most common material for the core in an electric machine is an iron-silicon alloy (silicon steel) which contains between 1% and 4% silicon [56]. The relative permeability μ_r of silicon steel ranges from 400 to 800 [56][7] which seems low compared to the gauge steel and iron casting steel of Figure 3.36. However, its low, good mechanical strength and a high Curie Point[8] of 740° C makes it an attractive material [56] and provides a challenge to the machine designer to have short paths for the magnetic field in the iron. It turns out that by special processing, some 4% silicon steels can have a relative permeability 5.5 times greater than the 800 quoted above, that is, up to 4400 [56].

Small permanent magnet synchronous machines often use rare-earth cobalt alloys for the hard magnetic material which has a rather high cost [56]. As a consequence, it is usually bonded to the surface of rotor which is made of soft magnetic material. The rare-earth cobalt alloys have a remanent (permanent) magnetic field between 0.75 and 1.1 tesla, are very hard to demagnetize and have a high Curie temperature [56].

---

[7]Reference [56] gives the permeability range as 5 to 10 kilogauss/oersted $= 0.5 \times 10^4$ to 1.0×10^4 gauss/(10^3ampere/meter) $= 0.5 \times 10^{-3}$ to 1.0×10^{-3} telsa/(ampere/meter). The relative permeability is found by dividing through by $\mu_0 = 4\pi \times 10^{-7}$ henry/meter giving 400 to 800.

[8]This is the temperature at which the material loses it magnetic properties.

www.EngineeringEBooksPdf.com

Problems

Problem 1 Azimuthal Magnetic Field of a Circular Current Loop

Consider the circular current loop shown in Figure 3.45. Using symmetry arguments and Ampère's law, show that the azimuthal component $B_\theta \hat{\boldsymbol{\theta}}$ *of* $\vec{\mathbf{B}}$ *must be zero everywhere.*

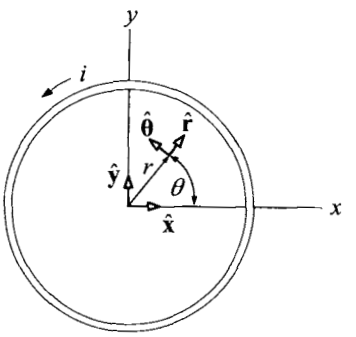


FIGURE 3.45. Circular loop carrying the current i.

Problem 2 Ampère's Law [35]

(a) Figure 3.46 shows a long straight conductor carrying a current I*. The current is uniformly distributed across the cross section so that the current* i *enclosed within a circle of radius* r *is*

$$i = \begin{cases} I\dfrac{r^2}{R^2} & \text{for } 0 \le r \le R \\ I & \text{for } r > R. \end{cases}$$

Use Ampère's law to find the magnetic field B *inside the conductor.*

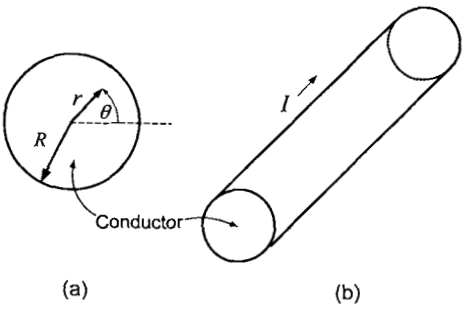


FIGURE 3.46. Long straight wire. (a) Cross-sectional view. (b) Perspective view.

www.EngineeringEBooksPdf.com

(b) A cylindrical conductor with an off axis cylindrical hole carries a total current I. Find the magnetic field in the cylindrical hole. [Hint: Use part (a) and superposition.]

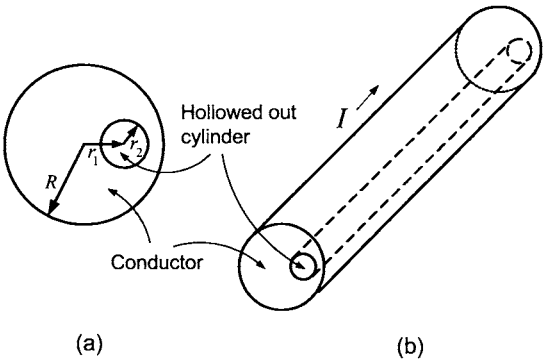


FIGURE 3.47. Conductor with a hollowed cylindrical core. (a) Cross-sectional view. (b) Perspective view.

Problem 3 Radial Magnetic Field of a Long Straight Wire

Apply conservation of flux to the cylindrical-shaped flux surface shown in Figure 3.48 to show that $B_r(r) \equiv 0$ for an infinitely long straight wire. Denote by R the radii of the disk-shaped surfaces S_1, S_2 and let ℓ denote the length of the cylindrical-shaped surface S_3.

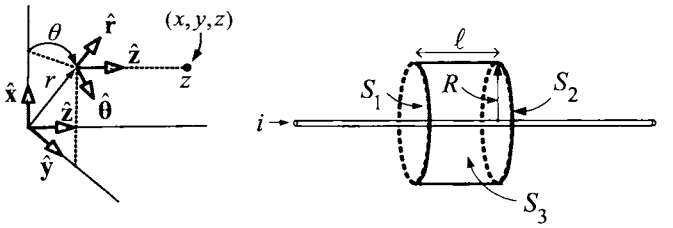


FIGURE 3.48. Closed flux surface used to show $B_r \equiv 0$ around an infinitely long straight wire carrying a current.

Problem 4 Radial Magnetic Field of an Ideal Solenoid

Use some symmetry arguments when applying Gauss's law to the closed surface shown in Figure 3.49 whose sides are S_1, S_2, and S_3 to show that the radial component of $\vec{\mathbf{B}}$ must be zero inside *an infinitely long solenoidal coil. Denote by R the radii of the disk-shaped surfaces S_1 and S_2, and let ℓ denote the length of the cylindrical-shaped surface S_3.*

Using a similar argument, show that the radial component of $\vec{\mathbf{B}}$ outside *of an infinitely long solenoidal coil must also be zero.*

www.EngineeringEBooksPdf.com

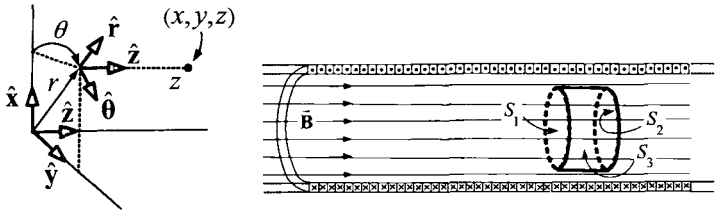


FIGURE 3.49. Using Gauss's law to show $B_r \equiv 0$ inside an ideal solenoid.

Problem 5 Azimuthal Magnetic Field of an Ideal Solenoid

Apply Ampère's law to the curves C_3, C_5 of Figure 3.27 to show that $B_\theta(r) \equiv 0$ inside the solenoid and $B_\theta(r) = \mu_0 i/(2\pi r)$ outside the cylinder.

Problem 6 Magnetic Field in an Ideal Toroidal Coil

(a) In Figure 3.50, apply Ampère's law to the circular curve C and Gauss's law to the closed surface S whose sides are S_1, S_2, and S_3 to show that $\vec{\mathbf{B}}$ only has a nonzero azimuthal component inside *the toroidal coil, that is, the lines of B are concentric circles inside the toroid coil. (Hint: Let $\vec{\mathbf{B}} = B_\rho\hat{\boldsymbol{\rho}} + B_\varphi\hat{\boldsymbol{\varphi}} + B_\theta\hat{\boldsymbol{\theta}}$ using the "toroidal" coordinate system of Figure 3.50 and show that $B_\rho = B_\varphi = 0$.)*

(b) Show that the azimuthal component of $\vec{\mathbf{B}}$ must be zero outside *the toroidal coil.*

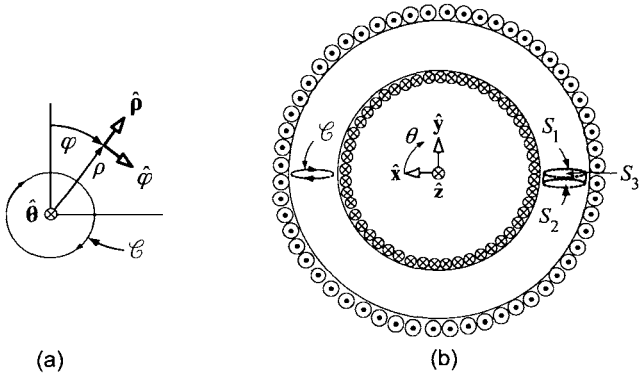


FIGURE 3.50. (a) "Toroidal" coordinate system. $\hat{\boldsymbol{\theta}}$ is into the page. (b) Curve and surface for Ampère's and Gauss's law, respectively, to show that $B_\rho = B_\varphi = 0$.

Problem 7 Equations of the Ideal Transformer from Ampère's Law

Consider an ideal transformer in Figure 3.51 consisting of two sets of turns wound on a single iron core. Assuming ideal soft magnetic material ($H = 0$ in the iron), N_1 turns in phase 1, and N_2 turns in phase 2, apply

www.EngineeringEBooksPdf.com

Ampère's law to a closed path C in the core of the iron to show that

$$i_1 = -\frac{N_2}{N_1} i_2.$$

Use this result and conservation of power $v_1 i_1 + v_2 i_2 = 0$ (assuming there are no losses) to show that

$$v_1 = \frac{N_1}{N_2} v_2.$$

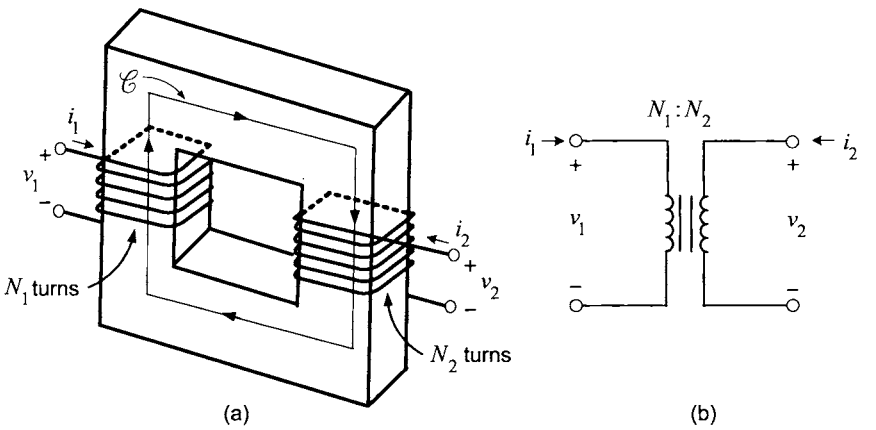


FIGURE 3.51. Derivation of the ideal transformer equation using Ampère's law. Adapted from Figure 20.12 of Kassakian et al. [57].

Problem 8 Equations of the Ideal Transformer from Faraday's Law

Consider an ideal transformer as shown in Figure 3.52 consisting of two sets of turns wound on a single iron core. Assume ideal soft magnetic material ($H = 0$ in the iron), N_1 turns in phase 1 and N_2 turns in phase 2. Let ϕ be the flux in any cross section of the iron core.

(a) Compute ϕ using the normal $\hat{\mathbf{n}}_1$ in the turns of phase 1, that is,

$$\phi = \int_S \vec{\mathbf{B}} \cdot d\vec{\mathbf{S}}$$

with $d\vec{\mathbf{S}} = dS\hat{\mathbf{n}}_1$ and the corresponding flux linkage $\lambda_1 = N_1\phi$. What is the sign convention for the induced voltage $-d\lambda_1/dt$? That is, if

$$-\frac{d\lambda_1}{dt} > 0,$$

will it attempt to force current in the positive direction of i_1 or the negative direction?

www.EngineeringEBooksPdf.com

(b) Use Gauss's law with the iron core defining a flux tube to explain why ϕ, as computed in part (a), can also be computed using the normal $\hat{\mathbf{n}}_2$ to obtain the same value.

(c) Use the fact that by Faraday's law, $v_1 = -d\lambda_1/dt, v_2 = -d\lambda_2/dt$ to show that

$$v_1 = \frac{N_1}{N_2} v_2.$$

(d) Use this result and $v_1 i_1 + v_2 i_2 = 0$ (assuming there are no losses) to show that

$$i_1 = -\frac{N_2}{N_1} i_2.$$

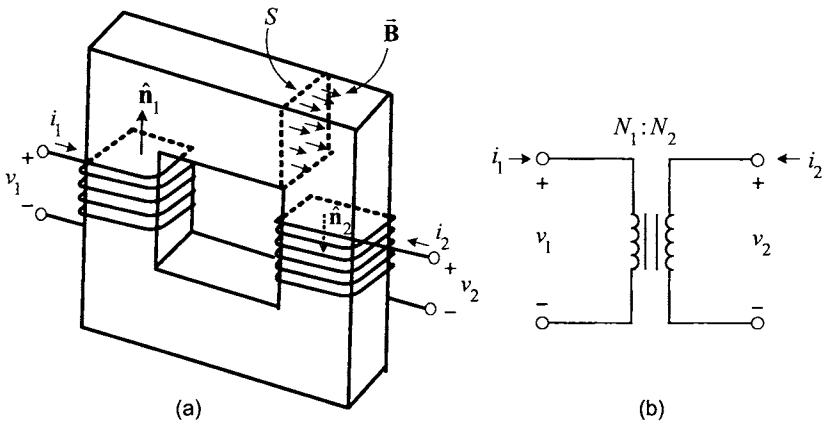


FIGURE 3.52. Derivation of the ideal transformer equations using Faraday's law. Adapted from Figure 20.12 of Kassakian et al. [57].

Problem 9 Magnetizing Inductance in the Transformer Model [25][57]

Consider the transformer in Figure 3.53 to be non ideal in the sense that H is not zero in the iron; that is, assume that μ_r is large, but finite. It is still assumed that the magnetic fields B and H are confined to the core, follow the path of the core, and are constant in magnitude in the core.

(a) With a current in phase 1, but phase 2 open-circuited, apply Ampère's law to the curve C and use this to show that the magnetic field in the core is given by

$$B = \mu_r \mu_0 H = \frac{\mu_r \mu_0}{\ell_c} N_1 i_m \text{ (phase 2 open-circuited)} \qquad (3.17)$$

where i_m is the current in phase 1 with phase 2 open circuited, ℓ_c is the length of the path C and μ_r is the relative permeability of the iron in the core. Of course the length ℓ_c is different in value for different paths. For this

www.EngineeringEBooksPdf.com

approximate analysis, one just takes ℓ_c to be some average length around the core.

(b) Show that the flux ϕ in the core is given by

$$\phi = \frac{\mu_r \mu_0 S}{\ell_c} N_1 i_m. \tag{3.18}$$

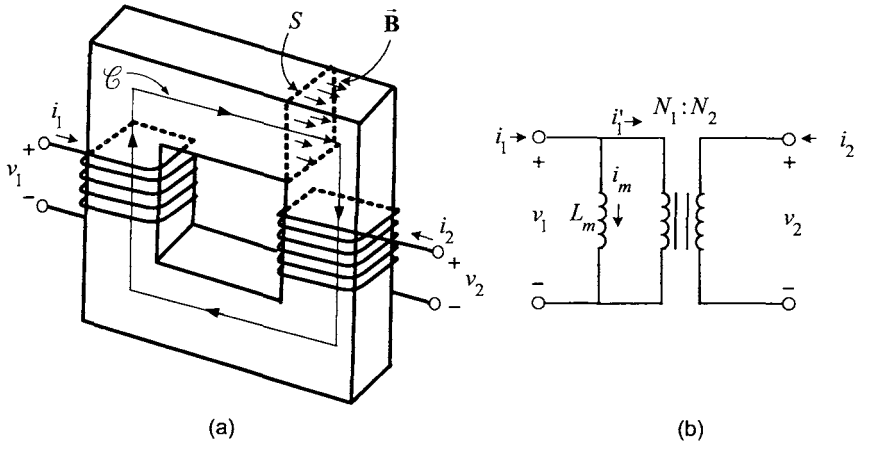


FIGURE 3.53. Magnetizing inductance L_m for a transformer.

By the assumption that the magnetic fields B and H are confined to the core and follow the path of the core, this flux is the same everywhere in the core. The flux linkage in phase 1 is

$$\lambda_1 = N_1 \phi = \frac{\mu_r \mu_0 S}{\ell_c} N_1^2 i_m = L_m i_m.$$

This current i_m (with phase 2 open-circuited) is called the magnetizing current *and is the current required to produce the magnetic field B (by aligning/magnetizing the dipole moments of the iron atoms) given in equation (3.17) and the corresponding flux ϕ in the core as given in equation (3.18). $L_m \triangleq \mu_r \mu_0 N_1^2 S/\ell_c$ is called the* magnetizing inductance *and the equivalent circuit for a transformer with a finite μ_r is shown in Figure 3.53(b).*

(c) By Faraday's law, the flux in the iron core and the applied voltage are related by

$$-\frac{d}{dt}\lambda_1 = -\frac{d}{dt} N_1 \phi = v_1$$

or

$$\phi = \frac{1}{N_1} \int_0^t v_1(\tau) d\tau.$$

www.EngineeringEBooksPdf.com

That is, the flux ϕ in the core is completely determined by the applied voltage to the phase. Consider now that phase 2 has a load (e.g., a resistor) attached to it so i_2 is nonzero and apply the same voltage as before to phase 1. Explain why the total flux is now

$$\phi = \frac{\mu_r \mu_0 S}{\ell_c} (N_1 i_1 + N_2 i_2) .$$

(d) Decompose the current i_1 as $i_1 = i_m + i_1'$ where i_m is the (magnetizing) current with phase 2 open and i_1' is the additional current in phase 1 when phase 2 is not an open circuit. The flux can then be written as

$$\phi = \frac{\mu_r \mu_0 S}{\ell_c} (N_1 i_m + N_1 i_1' + N_2 i_2)$$

As the flux depends only on the applied voltage v_1, explain why

$$N_1 i_1' + N_2 i_2 \equiv 0$$

is always true.

(e) Explain why it is still true with finite μ_r that

$$v_2 = \frac{N_2}{N_1} v_1 .$$

(f) Show that in an ideal transformer, the flux $\phi \equiv 0$. How does this affect the derivation in problem 8?

Remark *The effect of finite μ_r in a transformer is accounted for in the equivalent circuit model by the addition of an inductor with inductance L_m in parallel with the ideal transformer. Note that as $\mu_r \to \infty$, $L_m \to \infty$, that is, it becomes an infinite impedance and the circuit reduces to the ideal case with $i_1 = i_1'$. Note that in the ideal transformer with phase 2 open, applying a voltage v_1 to phase 1 would result in i_1 also being zero; that is, phase 1 would behave as open circuit due to the magnetic coupling of the two phases. In this nonideal case with phase 2 open, after applying a voltage v_1, there is a nonzero current i_m in phase 1 which satisfies $v_1 = L_m di_m/dt$.*

Problem 10 $B-H$ Curve

Explain how a transformer can be used to experimentally determine the $B-H$ curve of its iron core, i.e., the core is never perfectly ideal soft magnetic material and therefore has a hysteresis curve to be measured.

Problem 11 Magnetic Force [35]

Consider the electromagnetic crane drawn in Figure 3.54. Figure 3.54(a) shows the movable piece a distance x below the electromagnet. The current in the wire magnetizes the iron core it is wrapped about to produce a magnetic field which crosses the air gaps to magnetize the movable piece attracting it to the electromagnet. Let the iron have permeability μ_r, the

www.EngineeringEBooksPdf.com

cross section have area $S = \ell_1\ell_2$, *the number of turns of the coil be* N, *the path length of the closed curve* C *in Figure 3.54(a) be* $\ell + 2x$ *and* ℓ *in Figure 3.54(b). It is assumed that* B *and* H *are both constant in the iron and (a different) constant in the air gap and that these fields are contained within the iron and air gaps. Compute the force of the electromagnet on the moveable piece by doing the following:*

(a) Use Ampère's law to compute the magnetic field B *in the core (which is equal to the magnetic field strength in the air gap for small* x*) as a function of the current* i *in the winding.*

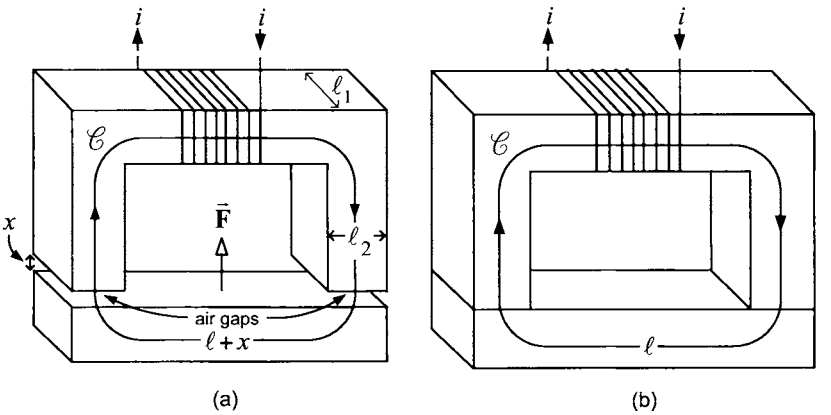


FIGURE 3.54. Electromagnet exerting a force on a rectangular-shaped iron block.

(b) Use the answer of part (a) to show that the flux linkage of the winding is

$$\lambda = N\phi = NBS = \frac{NS\mu_0}{(\ell/\mu_r + 2x)} i = L(x)i$$

where

$$L(x) \triangleq \frac{NS\mu_0}{(\ell/\mu_r + 2x)}.$$

(c) With x *held constant, compute the energy* W *required to bring the current from* 0 *to* I*; that is, compute*

$$W(x, I) = \int_0^t i\frac{d\lambda}{dt} = \int_0^I id\lambda.$$

This energy from the source current is stored as magnetic energy in the iron core and the air gaps.

(d) With the current held constant at I*, if the moveable piece moves by the force of attraction from* x *to* 0 *(so the change in position is* $-x$*), the energy goes from* $W(x, I)$ *to* $W(0, I)$*. The change in energy equals the work*

www.EngineeringEBooksPdf.com

done, that is, with x small

$$\left(F\Big|_{x=0} \right) \times (-x) = W(x, I) - W(0, I).$$

Use this to show that the force of attraction at $x = 0$ in Figure 3.54(b) is

$$F\Big|_{x=0} = -\frac{\partial W(x, I)}{\partial x}\Bigg|_{I \text{ constant}}$$

(e) With the bar at the location x and the current in the winding given by i, explain why the force is given by

$$F(x, i) = -\frac{\partial W(x, i)}{\partial x}$$

even if the current is changing in time. That is, holding the current constant was only required for the derivation of the expression for the force. (Note that the notation "I constant" in $-\frac{\partial W(x,I)}{\partial x}\Big|_{I \text{ constant}}$ is redundant as the partial derivative $\partial/\partial x$ means to take the derivative with the other variable held constant.)

Problem 12 Relative Permeability

Consider a permanent magnet which is placed in another (external) magnetic field. Explain that, as far as this external magnetic field's effect on the permanent magnet, one can take $\mu_r = 1$ in the permanent magnet.

www.EngineeringEBooksPdf.com

Part II

AC Machine Theory

www.EngineeringEBooksPdf.com

With the preliminary material presented in the first three chapters, the remaining chapters cover the modeling and control of AC machines. However, before embarking on this odyssey, an elementary notion of how AC machines operate is first presented. This will hopefully help the reader to understand the overall picture as he/she goes through the detailed analysis in the remaining chapters.

Induction Motor

The goal here is to give an elementary idea of how an induction motor works. First, the construction of a simple two-phase machine is described. This is followed by explaining how a radially directed rotating magnetic field is set up in the air gap by the stator currents and how this rotating field induces currents in the rotor loops. Finally, it is described how this same rotating magnetic field produces torque of on the current it induces.

Construction of the Induction Motor

To begin, the construction of a simplistic model of a two-phase induction motor is described.

Figure II.1(a) shows a half-cylindrical-shaped loop, which is wound around a cylindrical-shaped iron core, and denoted as loop a. A second identical loop, denoted as loop b, is then wound 90 degrees from loop a as shown in Figure II.1(b). The currents in loops a and b are denoted as i_{Ra}, i_{Rb}, respectively. The two loops are electrically isolated.

In Figure II.1, the notation $\odot$ means that if $i > 0$, the current is coming *out* of the page while $\otimes$ means that if $i > 0$, then the current is going *into* the page.

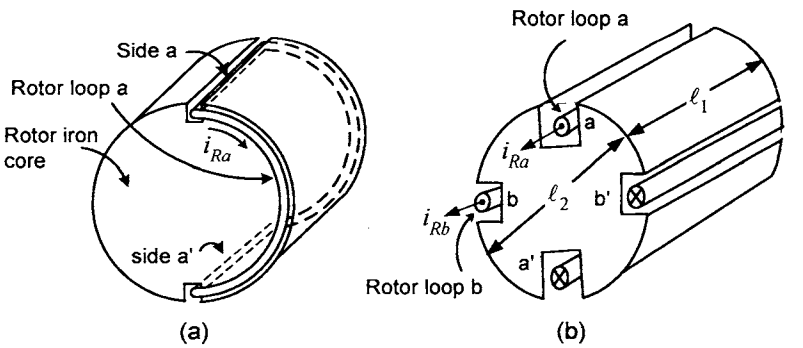


Figure II.1. Rotor of an induction motor.

The stator is constructed similarly. Figure II.2(a) shows stator loop a

www.EngineeringEBooksPdf.com

that has a half-cylindrical shape and is wound on the inside surface of the stator iron. However, as shown in Figure II.2(a), it also has a voltage source connected. Similarly, Figure II.2(b) shows that stator loop b is identical in form to stator loop a, but is wound 90 degrees from loop a. The applied voltages are denoted as u_{Sa}, u_{Sb} and the corresponding currents are denoted as i_{Sa}, i_{Sb}, respectively. These two loops are electrically isolated.

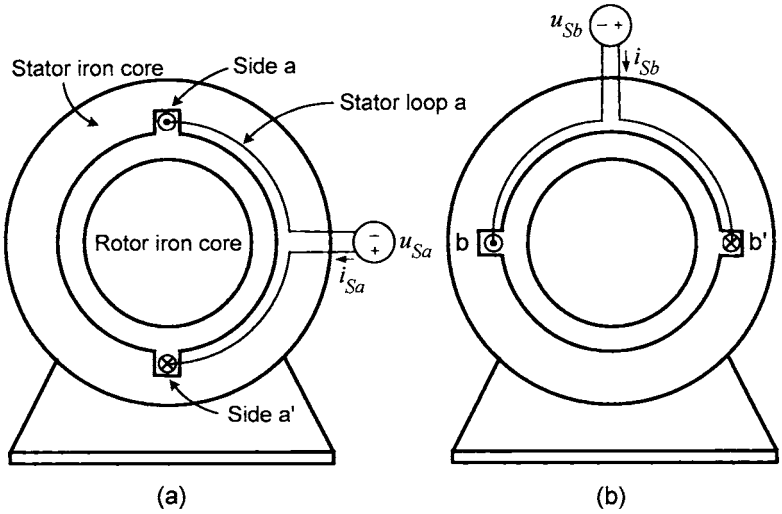


Figure II.2. Induction motor stator. (a) Stator loop a. (b) Stator loop b.

Combining Figures II.1 and II.2, a simple two-phase induction motor is illustrated in Figure II.3. The position of the rotor is located by a line perpendicular to rotor loop a as shown in Figure II.3.

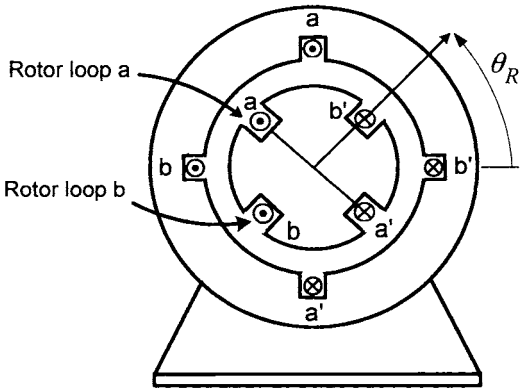


Figure II.3. Cross-sectional view of a simple two-phase induction motor.

www.EngineeringEBooksPdf.com

Rotating Magnetic Field

Figure II.4(a) shows that the magnetic field in the air gap produced by $i_{Sa} > 0$ (with $i_{Sb} = 0$) is radially out on the right-hand side and radially in on the left-hand side. Figure II.4(b) shows that the directions are simply reversed for $i_{Sa} < 0$.

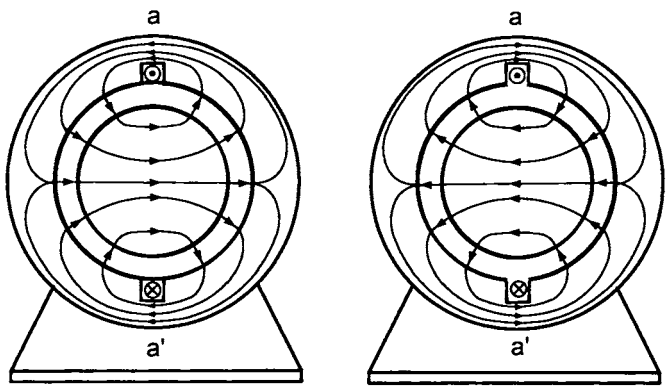


Figure II.4. Magnetic field distribution produced by i_{Sa}.

Similarly, Figure II.5(a) shows that the magnetic field in the air gap produced by $i_{Sb} > 0$ (with $i_{Sa} = 0$) is radially out on the top-half side of the air gap and radially in on the bottom-half side of the air gap. The directions are simply reversed for $i_{Sb} < 0$.

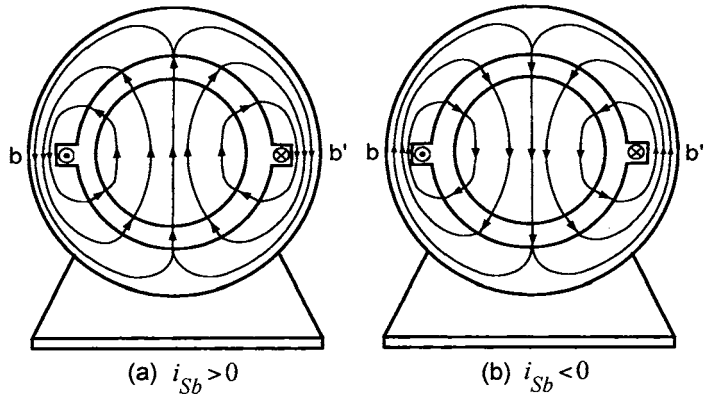


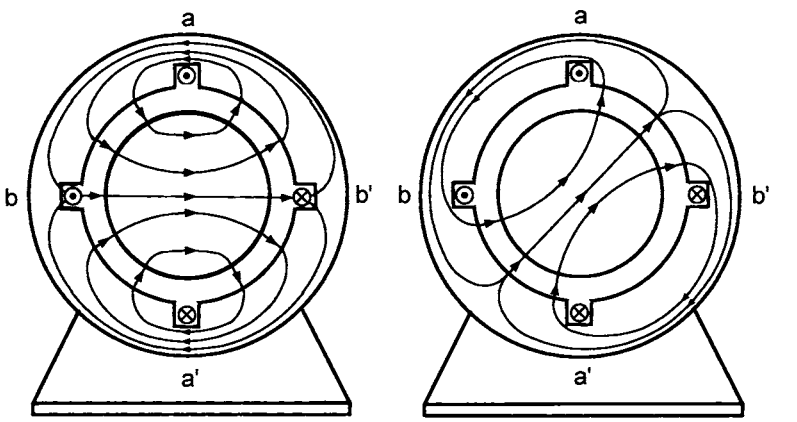
Figure II.5. Magnetic field distribution produced by i_{Sb}.

www.EngineeringEBooksPdf.com

Combing the magnetic fields of stator loops a and b, a *rotating* magnetic field is created in the air gap by choosing

$$i_{Sa} = I_S \cos(\omega_S t), i_{Sb} = I_S \sin(\omega_S t).$$

This is illustrated in Figure II.6, which shows the total magnetic field $\vec{\mathbf{B}}_S$ due to both i_{Sa} and i_{Sb}.



(a) $\omega_S t = 0$
$i_{Sa} = I_S, i_{Sb} = 0$

(b) $\omega_S t = \pi/4$
$i_{Sa} = I_S/\sqrt{2}, i_{Sb} = I_S/\sqrt{2}$

(c) $\omega_S t = \pi/2$
$i_{Sa} = 0, i_{Sb} = I_S$

(d) $\omega_S t = 3\pi/4$
$i_{Sa} = -I_S/\sqrt{2}, i_{Sb} = -I_S/\sqrt{2}$

Figure II.6. Rotating magnetic field.

www.EngineeringEBooksPdf.com

Induced Rotor Currents

The rotating magnetic field $\vec{B}_S$ produced by the stator currents produces a changing flux in each of the rotor phases. By Faraday's law, voltages and hence currents, are produced in the rotor phases. This is illustrated in Figure II.7 showing the rotation of the stator magnetic field past rotor loop a (rotor loop b is not shown for clarity). As it rotates past rotor loop a, the changing flux in the loop produces an emf, which in turn produces the current i_{Ra}.

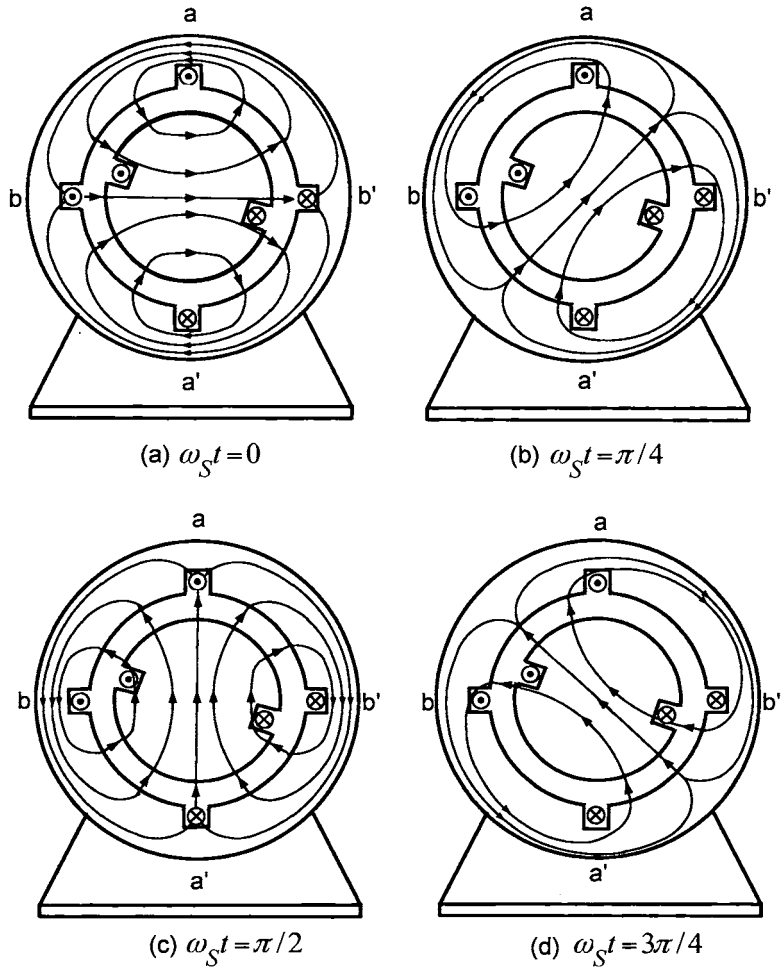


Figure II.7. The changing flux in rotor phase a due to the rotating magnetic field of the stator. Rotor phase b is not shown.

www.EngineeringEBooksPdf.com

Torque

Recall that from the magnetic force law, the force on side a of rotor loop a is given by

$$F_{\text{side a}} = i_{Ra}\ell_1 B_S$$

where ℓ_1 is the length of the rotor. By the right-hand rule, this force has the direction shown in Figure II.8. The torque on this rotor loop is then

$$\tau_{\text{side a}} = (\ell_2/2) i_{Ra}\ell_1 B_S$$

where $\ell_2/2$ is the radius of the rotor. Similarly, the forces on sides a', b, and b' can be computed and are shown in Figure II.8. With the currents in the rotor phases as shown in Figure II.8, the magnetic force law shows that the sides of each rotor loop have a tangential force pushing the rotor in the counterclockwise direction.[1] That is, there is a torque on the rotor, causing it to turn.

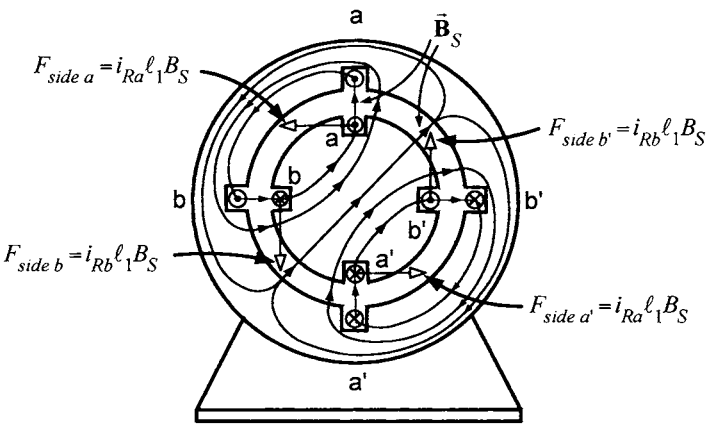


Figure II.8. Torque in an induction motor.

Slip

ω_S is the angular speed of the stator's rotating magnetic field and ω_R is the rotor speed. The slip speed is defined as

$$\omega_{slip} \triangleq \omega_S - \omega_R.$$

It turns out that positive torque production requires $\omega_S > \omega_R$, while to obtain negative torque $\omega_S < \omega_R$ and no torque is produced if $\omega_S = \omega_R$.

[1] That the currents in the rotor loops are in the directions indicated in the figure can only be proven using the analysis developed in later chapters.

www.EngineeringEBooksPdf.com

That is, $\omega_{slip} \triangleq \omega_S - \omega_R \neq 0$ when producing torque. The induction motor is said to operate *asynchronously* since the rotor angular speed ω_R is not the same as the angular speed ω_S ($\omega_S \neq \omega_R$) of the stator's rotating magnetic field when producing torque. The fact that the slip must be nonzero to get torque is easily explained. Consider the situation shown in Figure II.9 where $\omega_{slip} = 0$ or $\omega_S = \omega_R$. As Figure II.9 shows, the flux in the rotor loop does not change and consequently there is no induced voltage nor current in the rotor loop and, therefore, no torque is produced.

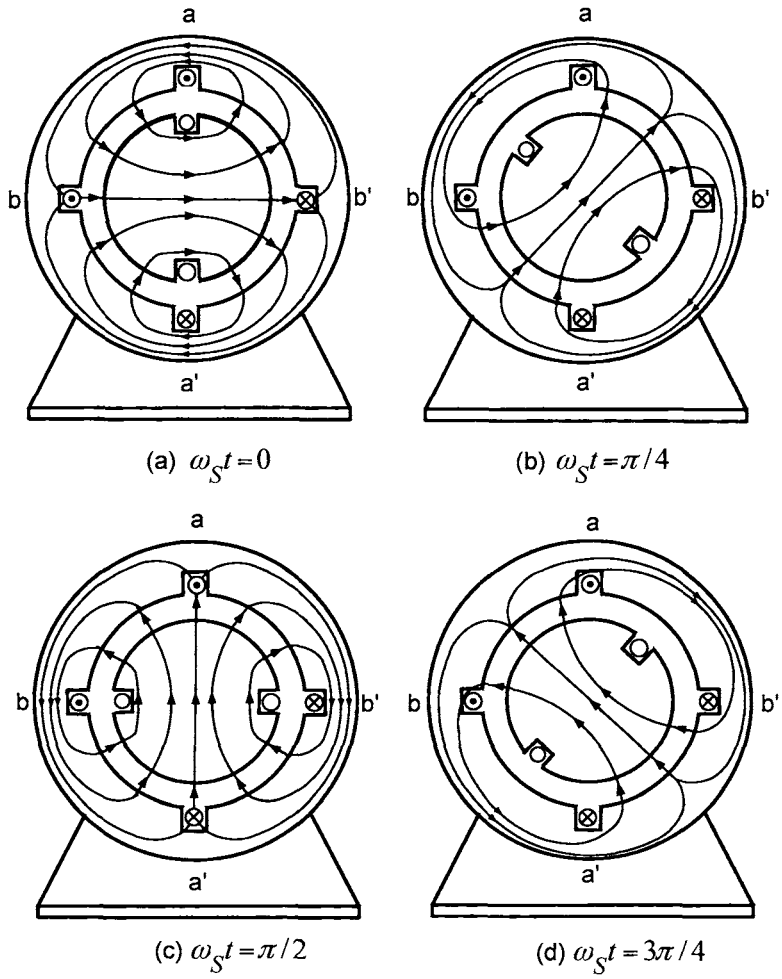


Figure II.9. No changing flux in the rotor loop if $\omega_S = \omega_R$. (Rotor loop b not shown for clarity.)

www.EngineeringEBooksPdf.com

Summary

Summarizing, the induction motor works as follows:

- A rotating radially directed magnetic field $\vec{\mathbf{B}}_S$ is set up in the air gap between the rotor and stator iron by the stator currents i_{Sa}, i_{Sb}.
- This rotating magnetic field produces a changing flux in the rotor loops (phases).
- By Faraday's law, voltages, and hence currents, are induced in the rotor loops.
- This *same* magnetic field $\vec{\mathbf{B}}_S$ that induced the currents in the rotor loops produces a torque on them.

Permanent Magnet Synchronous Motor

The principle of operation of a synchronous machine is illustrated in Figure II.10, which shows two permanent magnets rotating on different axles. The "stator" permanent magnet is rotated at angular speed ω_S by mechanically turning it on its axle. As it rotates, its north end attracts the south end of the rotor permanent magnet to turn it on its axle. Consequently, they rotate together at the same speed (i.e., $\omega_R = \omega_S$) so that their speeds are *synchronized.*

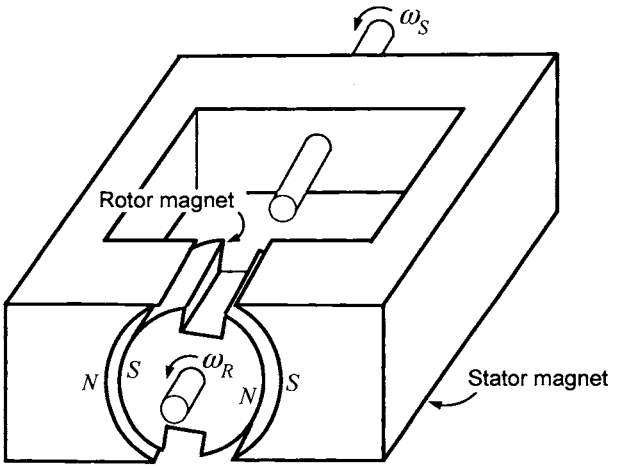


Figure II.10. Two permanent magnets rotating on different axles.

It was shown above that the stator of an induction motor can produce a rotating magnetic field. To make a synchronous motor, one simply removes the rotor from the induction motor and replaces it with a permanent magnet rotor as shown in Figure II.11. As in the case of the induction motor, the stator currents i_{Sa}, i_{Sb} produce a rotating magnetic field. This rotating

www.EngineeringEBooksPdf.com

magnetic field then pulls the rotor magnet along with it at the same angular speed. That is, $\omega_S = \omega_R$ so that the rotor itself and the stator magnetic field rotate together *synchronously.*

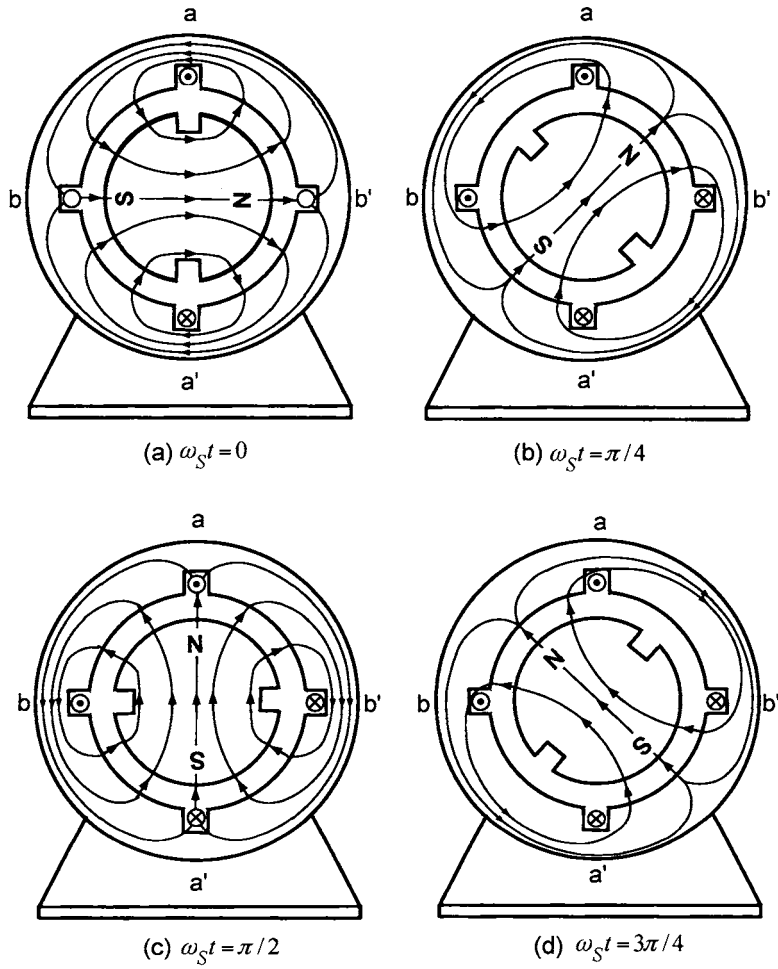


Figure II.11. The permanent magnet rotor is pulled by the rotating magnetic field of the stator. (a) $i_{Sa} = I_S$, $i_{Sb} = 0$. (b) $i_{Sa} = I_S/\sqrt{2}$, $i_{Sb} = I_S/\sqrt{2}$. (c) $i_{Sa} = 0$, $i_{Sb} = I_S$. (d) $i_{Sa} = -I_S/\sqrt{2}$, $i_{Sb} = I_S/\sqrt{2}$.

www.EngineeringEBooksPdf.com

4

Rotating Magnetic Fields

The production of a rotating radially directed magnetic field in the air gap by the stator currents is fundamental to the operation of both induction motors and synchronous motors. Using the assumption of ideal magnetic materials (i.e., materials where $\vec{\mathbf{H}} = \mathbf{0}$), expressions for the radial magnetic field distribution in the air gap of AC machines due to the currents in the stator phases are found. Specifically, a two-phase machine is considered. It is shown that if the stator phases are sinusoidally wound and 90° apart from each other and, with the stator currents given by $i_{Sa} = I_S \cos(\omega_S t)$ and $i_{Sa} = I_S \cos(\omega_S t)$, the result is a rotating radial magnetic field that is sinusoidally distributed in space. Finally, expressions for the azimuthal magnetic field as well as the axial electric field in the air gap are also found.

4.1 Distributed Windings

Before embarking on how a rotating magnetic field is produced, the geometric structure of the windings (loops/turns) on the rotor and stator iron are described. To do so, consider Figure 4.1(a), which shows a cylindrical iron rotor core with six slots in it. A single length of wire is wound around the core forming three rotor loops to make up a phase winding. The top three slots are at $\theta = \pi/3$, $\theta = \pi/2$, and $\theta = 2\pi/3$, and the bottom three slots are at $\theta = 4\pi/3$, $\theta = 3\pi/2$, and $\theta = 5\pi/3$.

In more detail, starting with a single wire, the first loop of the phase is wound starting in the bottom leftmost slot at the point a in Figure 4.1(a) and then follows a semicircular path in the counterclockwise direction to the rightmost top slot. From there, the wire goes down the length of the cylinder to the back side and then follows another semicircular path in the clockwise direction to the back side of the leftmost bottom slot. Next, the wire is brought up the length of the iron to the front side to the point b in the figure. The wire from point a to point b makes up the first *loop* (or *turn* or *winding*) of the phase. Continuing, the wire is extended to point c to start the second loop. As shown in Figure 4.1(b), the second loop goes from point c to point d, making a half-cylindrical-shaped loop in the top and bottom slots. Finally, the wire is extended from point d to point e to start the third loop. The third loop goes from point e to point f as shown in Figure 4.1(c). As stated above, the single piece of wire (consisting of three loops in this example) is referred to as a *phase winding* or simply *phase*.

www.EngineeringEBooksPdf.com

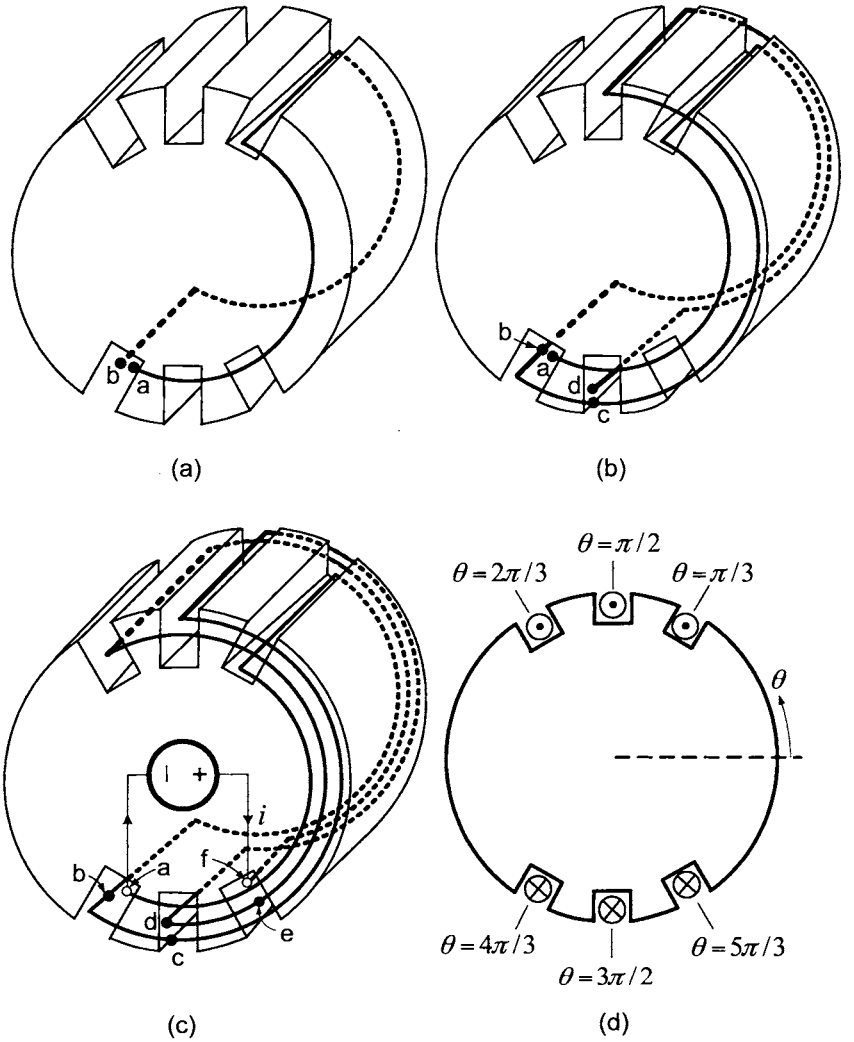


FIGURE 4.1. Distributed phase winding consisting of three loops. (a) First loop of the phase winding from a to b. (b) Second loop of the phase winding from c to d. (c) Third loop of the phase winding from e to f. (d) Cross-sectional view of the rotor phase winding. All three of these half-cylindrical surfaces have the same radii. They are drawn with different radii in the figure so that the reader can tell them apart. Drawn by Bret Wilfong.

This is called a *distributed* phase winding because the loops making up the phase winding are not all in a single pair of slots, but rather, they are distributed over three pairs of slots. The semi-circular sides of each loop are referred to as *end turns*.

www.EngineeringEBooksPdf.com

Figure 4.1(c) shows that the two ends of the phase (points a and f) are connected to a voltage source, which, if positive, will force current up out of the top sides of the loop and down the bottom side of the loops. This sign convention for the current is also illustrated in Figure 4.1(d), which is a cross section of the rotor. The cross-sectional view of Figure 4.1(d) is the standard way to represent a phase winding. Figure 4.3(a) shows a cross-sectional view of a single phase similar to Figure 4.1(d) except that two loops are now wound in the middle slots rather than just one loop as in Figure 4.1(b).

Figure 4.2 illustrates how electrical power can be brought into the rotor of 4.1. The slip rings 1 and 2 are made of conducting material and are rigidly connected to the rotor. As the rotor turns, they make sliding contact with (slip against) the brushes b_1 and b_2, which are fixed in space. Slip ring 1 is also electrically connected to a wire conductor that goes through slip ring 2 (and is electrically isolated from slip ring 2) and is connected to point f in Figure 4.1(c). Slip ring 1 is electrically connected to a wire conductor which is connected to point a in Figure 4.1(c). In this way, voltage and current can be supplied to the rotor from an outside power source.

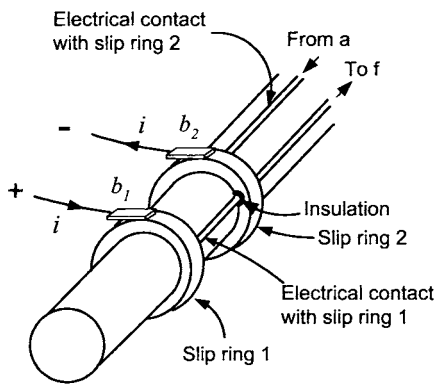


FIGURE 4.2. A set of brushes and slip rings can be used to bring electrical power to the rotor winding.

A distributed *stator* phase winding is wound in similar fashion as the distributed rotor winding of Figure 4.1. In the case of the stator winding, the loops of the phase are wound on the *inside* surface of the stator as shown in Figure 4.3(b). The simple single stator phase of Figure 4.3(b) consists of four turns (loops/windings). Specifically, this phase winding is made by winding a single wire around the inside of the stator iron once at $\theta = \pi/3$ (with the other side of the loop at $4\pi/3$), then twice at $\theta = \pi/2$ (with the other side of the loop at $3\pi/2$), and finally once more at $\theta = 2\pi/3$ (with the other side at $5\pi/3$). The radial air gap distance is denoted as g and an

www.EngineeringEBooksPdf.com

arbitrary point is located using the polar coordinates (r, θ) as shown.

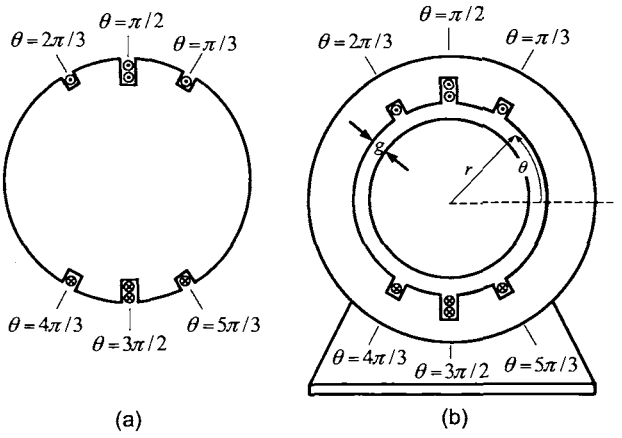


FIGURE 4.3. (a) Distributed rotor phase winding with two loops in the middle slot. (b) Distributed stator phase winding with two loops in the middle slots.

There are other ways to distribute the windings of a phase such as shown in Figure 4.4. Figure 4.4(a) shows a distributed rotor phase winding with one side of a loop at $\theta = \pi/6$ (the other side of the loop at $7\pi/6$), two loop sides at $\theta = \pi/3$ (with the other sides at $4\pi/3$), three loop sides at $\theta = \pi/2$ (with the other sides at $3\pi/2$), two loops at $\theta = 2\pi/3$ (with the other sides at $5\pi/3$) and one loop side at $\theta = 5\pi/6$ (with the other side at $11\pi/6$). Figure 4.4(b) shows a similar winding on the stator.

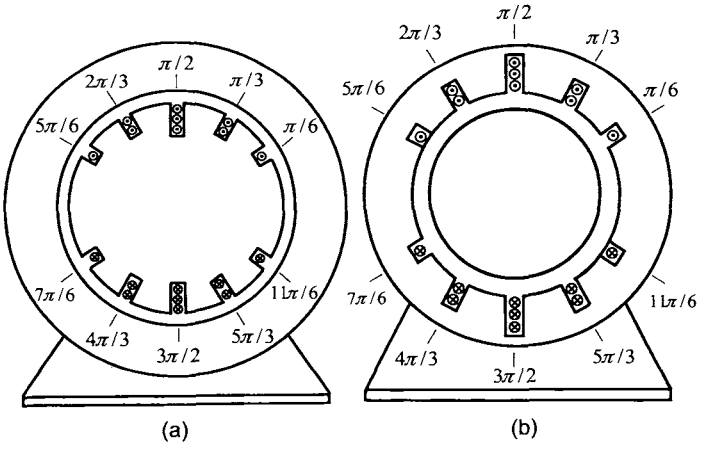


FIGURE 4.4. (a) Distributed rotor winding. (b) Distributed stator winding.

www.EngineeringEBooksPdf.com

4.2 Approximate Sinusoidally Distributed $\vec{\mathbf{B}}$ Field

The goal here is to compute the radial magnetic field $\vec{\mathbf{B}}$ established *in the air gap* by the current in a distributed winding. To do so, Ampère's law $\oint \vec{\mathbf{H}} \cdot d\vec{\ell} = i_{\text{enclosed}}$ is the key tool that is used. However, to obtain a nice elegant expression for the magnetic field $\vec{\mathbf{B}}$ using Ampère's law, an additional assumption is required. This assumption is that the wires loops in a phase winding have an *infinitesimal* cross-sectional area; that is, the wire has length, but its cross-sectional area is infinitesimal. To emphasize this, Figure 4.3(a) is redrawn in Figure 4.5(a) to indicate that the wire has no width. The two $\odot$ are drawn at the top middle slot while only one $\odot$ is drawn at either side to indicate that the middle slot has twice as many windings (loops) as either of the other two slots. Similarly, the stator winding of Figure 4.3(b) is redrawn in Figure 4.5(b).

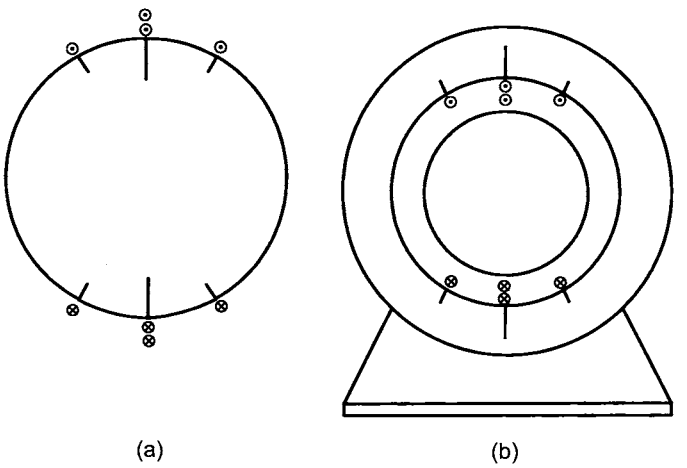


FIGURE 4.5. (a) This is Figure 4.3(a) redrawn to show that the wire has no width. (b) This is Figure 4.3(b) redrawn to show that the wire has no width.

However, even Figure 4.5 does not quite capture what it means for the wire to have a cross-sectional area that is infinitesimal in size because the slots should not have any depth. So, Figure 4.5 is redrawn in Figure 4.6 to illustrate that the depth of the slots are also infinitesimal.

To be consistent with the literature, Figures 4.1(d), 4.3, and 4.4 will be used for illustration, but it is to be understood that the standing assumption is that the wires loops in a phase winding have an *infinitesimally* small cross-sectional area so that the reader should think of Figure 4.6 in the derivations that follow.

www.EngineeringEBooksPdf.com

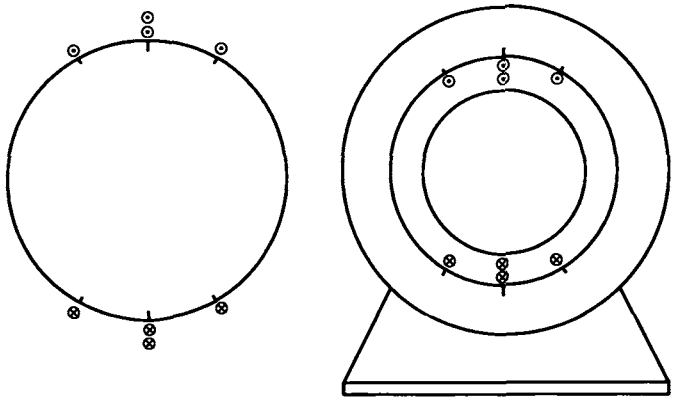


FIGURE 4.6. This is Figures 4.5(a) and 4.5(b) redrawn to show the slots have no depth.

The problem of computing the radial magnetic field established *in the air gap* by the current in a distributed winding is now considered. To fix ideas, the distributed winding shown in Figure 4.3(b) [or equivalently, Figure 4.6(b)] is used. This winding is redrawn in Figure 4.7 where it is now denoted as phase a and the current in it is denoted as i_{Sa}.

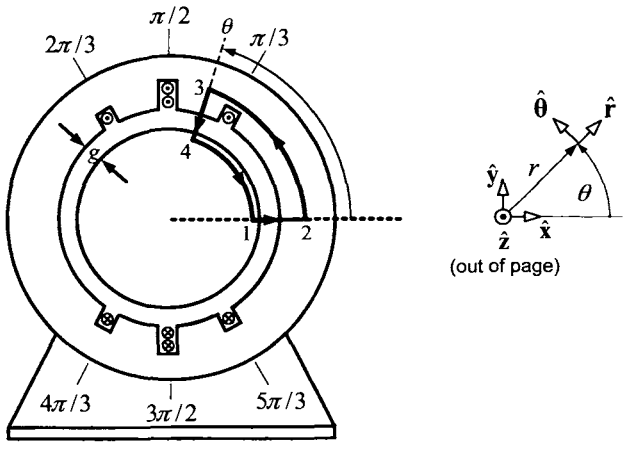


FIGURE 4.7. Use of Ampère's law to determine the radial magnetic field in the airgap due to the current i_{Sa} in stator phase a.

To compute the radial magnetic field $\vec{\mathbf{B}}_{Sa}$ in the air gap produced by i_{Sa}, Ampère's law $\oint \vec{\mathbf{H}} \cdot d\vec{\ell} = i_{\text{enclosed}}$ is applied to the closed path 1–2–3–4–1

www.EngineeringEBooksPdf.com

shown in Figure 4.7. The assumption that the wire has an infinitesimal cross section means that the sides of the copper loops lie just at the inside surface of the stator iron. In particular, this assumption allows one to take the points $1, 2, 3, 4$ on the path to all be just inside the magnetic material at the air gap/iron interface and still have the closed-path $1{-}2{-}3{-}4{-}1$ enclose any current in the loop sides between 0 and θ. Further, computing $\int \vec{\mathbf{H}} \cdot d\vec{\boldsymbol{\ell}}$ across any (infinitesimally thin) wire is then equal to zero.[1] With $\vec{\mathbf{H}} \equiv 0$ in the iron and g the air gap length, it follows that

$$\begin{aligned}
\int_1^2 \vec{\mathbf{H}}_{Sa} \cdot d\vec{\boldsymbol{\ell}} + \int_2^3 \vec{\mathbf{H}}_{Sa} \cdot d\vec{\boldsymbol{\ell}} + \int_3^4 \vec{\mathbf{H}}_{Sa} \cdot d\vec{\boldsymbol{\ell}} + \int_4^1 \vec{\mathbf{H}}_{Sa} \cdot d\vec{\boldsymbol{\ell}} &= i_{\text{enclosed}} \\
\int_1^2 \vec{\mathbf{H}}_{Sa} \cdot d\vec{\boldsymbol{\ell}} + \int_3^4 \vec{\mathbf{H}}_{Sa} \cdot d\vec{\boldsymbol{\ell}} &= i_{\text{enclosed}} \\
\int_1^2 H_{Sa}(0)\hat{\mathbf{r}} \cdot d\ell\hat{\mathbf{r}} + \int_3^4 H_{Sa}(\theta)\hat{\mathbf{r}} \cdot (-d\ell\hat{\mathbf{r}}) &= i_{\text{enclosed}} \\
gH_{Sa}(0) - gH_{Sa}(\theta) &= i_{\text{enclosed}}.
\end{aligned} \tag{4.1}$$

In this derivation, it was assumed that H_{Sa} is constant across the air gap, that is, H_{Sa} does not depend on the radial distance r in the air gap. The enclosed current i_{enclosed} between 0 and θ inside the curve $1{-}2{-}3{-}4{-}1$ of Figure 4.7 is given by

$$i_{\text{enclosed}} = \begin{cases}
0 & \text{for} \quad 0 \leq \theta \leq \pi/3 \\
i_{Sa} & \text{for} \quad \pi/3 \leq \theta \leq \pi/2 \\
3i_{Sa} & \text{for} \quad \pi/2 \leq \theta \leq 2\pi/3 \\
4i_{Sa} & \text{for} \quad 2\pi/3 \leq \theta \leq 4\pi/3 \\
3i_{Sa} & \text{for} \quad 4\pi/3 \leq \theta \leq 3\pi/2 \\
i_{Sa} & \text{for} \quad 3\pi/2 \leq \theta \leq 5\pi/3 \\
0 & \text{for} \quad 5\pi/3 \leq \theta \leq 2\pi
\end{cases}$$

and is plotted in Figure 4.8.

[1] This assumption does not appear to be realistic especially in the above figure. Copper is not a magnetic material so $\vec{\mathbf{H}} \neq 0$ inside. The assumption of an "infinitesimal cross section" for the wire allows one to still take $\int \vec{\mathbf{H}} \cdot d\vec{\boldsymbol{\ell}} = 0$ across the wire as its cross-sectional area is infinitesmal. Although on the face of it this assumption may not seem reasonable, it does lead to a model that is not only reasonable, but quite good. Again, the reader is encouraged to think of Figure 4.6(b) in this derivation and all that follow.

www.EngineeringEBooksPdf.com

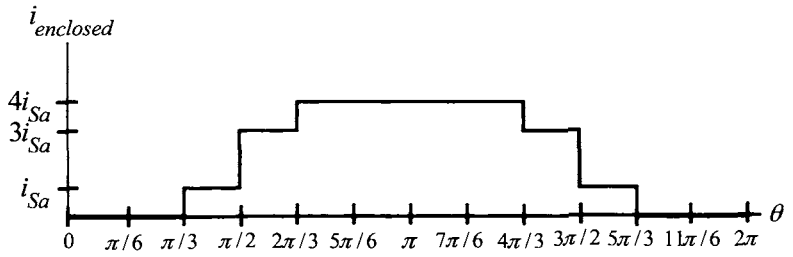


FIGURE 4.8. $i_{enclosed}$ versus θ.

The magnetic intensity is then

$$H_{Sa}(\theta) = H_{Sa}(0) - \frac{i_{\text{enclosed}}(\theta)}{g}$$

where $H_{Sa}(0)$ on the right-hand side must still be determined.

To compute $H_{Sa}(0)$, the conservation of flux law is used. Consider a *closed* cylindrical flux surface whose cylindrical surface is in the air gap and whose disk shaped ends just contain the rotor iron as shown in Figure 4.9. Since this surface is in air, $\vec{\mathbf{B}}_{Sa} = \mu_0 \vec{\mathbf{H}}_{Sa}$ on the surface. On the disk-shaped surfaces at the each end of the cylinder, $\vec{\mathbf{B}}_{Sa} = 0$, while on the cylindrical-shaped part of the surface, $\vec{\mathbf{B}}_{Sa} = B_{Sa}\hat{\mathbf{r}} = \mu_0 \left(H_{Sa}(0) - i_{\text{enclosed}}(\theta)/g\right)\hat{\mathbf{r}}$. Conservation of flux gives

$$\oint \vec{\mathbf{B}} \cdot d\vec{\mathbf{S}} = \int_0^{\ell_1} \int_0^{2\pi} (B_{Sa}(\theta)\hat{\mathbf{r}}) \cdot (r d\theta dz \hat{\mathbf{r}}) = r\ell_1 \int_0^{2\pi} B_{Sa}(\theta) d\theta = 0$$

or, substituting in the above expression for $B_{Sa}(\theta)$, one finds

$$\int_0^{2\pi} \left(\mu_0 H_{Sa}(0) - \mu_0 \frac{i_{\text{enclosed}}(\theta)}{g}\right) d\theta = 0.$$

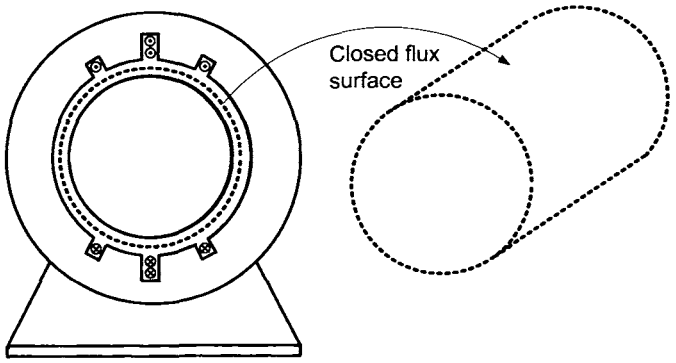


FIGURE 4.9. A closed flux surface in the air gap which contains the rotor.

www.EngineeringEBooksPdf.com

Rearranging

$$\begin{aligned} H_{Sa}(0) &= \int_0^{2\pi} \frac{i_{\text{enclosed}}(\theta)}{2\pi g} d\theta \\ &= \frac{1}{2\pi g}\left(i_{Sa}\frac{\pi}{6} + 3i_{Sa}\frac{\pi}{6} + 4i_{Sa}\frac{2\pi}{3} + 3i_{Sa}\frac{\pi}{6} + i_{Sa}\frac{\pi}{6}\right) \\ &= \frac{2i_{Sa}}{g}. \end{aligned}$$

So

$$\vec{\mathbf{B}}_{Sa} = B_{Sa}(\theta)\hat{\mathbf{r}} = \mu_0\left(\frac{2i_{Sa}}{g} - \frac{i_{\text{enclosed}}(\theta)}{g}\right)\hat{\mathbf{r}}. \tag{4.2}$$

$B_{Sa}(\theta)$ versus θ is plotted in Figure 4.10.

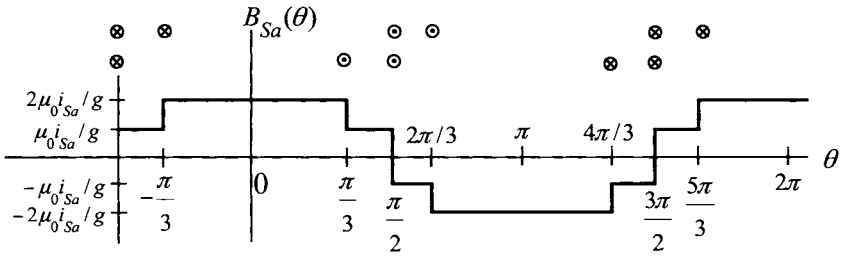


FIGURE 4.10. Magnetic field $B_{Sa}(\theta)$ versus θ due to the current in phase a of a two-phase machine.

Expanding $B_{Sa}(\theta)$ in a Fourier series, one obtains (see problem 3)

$$\begin{aligned} B_{Sa}(\theta) &= \mu_0 \frac{i_{Sa}}{g}\frac{4}{\pi} \times \sum_{k=1,3,5,\ldots}^{\infty} \frac{\left(1+\cos(\frac{k\pi}{6})\right)}{k} \sin\left(k(\theta+\frac{\pi}{2})\right) \\ &= \mu_0 \frac{i_{Sa}}{g}\frac{4}{\pi}\left(\frac{2+\sqrt{3}}{2}\sin\left(\theta+\frac{\pi}{2}\right) + \frac{1}{3}\sin\left(3(\theta+\frac{\pi}{2})\right)\right. \\ &\quad \left. + \frac{1-\sqrt{3}/2}{5}\sin\left(5(\theta+\frac{\pi}{2})\right) + \frac{1-\sqrt{3}/2}{7}\sin\left(7(\theta+\frac{\pi}{2})\right) + \cdots\right) \\ &= \mu_0 \frac{i_{Sa}}{g}\frac{4}{\pi}\left(1.866\cos(\theta) - 0.333\cos 3(\theta) + 0.0268\cos(5\theta)\right. \\ &\quad \left. - 0.0191\cos(7\theta) + \cdots\right). \end{aligned} \tag{4.3}$$

To a first approximation, the radial magnetic field distribution $B_{Sa}(\theta)$ may be approximated by its first harmonic as

$$\vec{\mathbf{B}}_{Sa}(\theta) = B_{Sa}(\theta)\hat{\mathbf{r}} \approx 1.866\mu_0 \frac{i_{Sa}}{g}\frac{4}{\pi}\cos(\theta)\hat{\mathbf{r}} \tag{4.4}$$

www.EngineeringEBooksPdf.com

which is a sinusoidal distribution in θ.

A similar procedure can be applied to the stator winding in Figure 4.4(b), resulting in a radial magnetic field distribution in the air gap as given in Figure 4.11 (see problem 4).

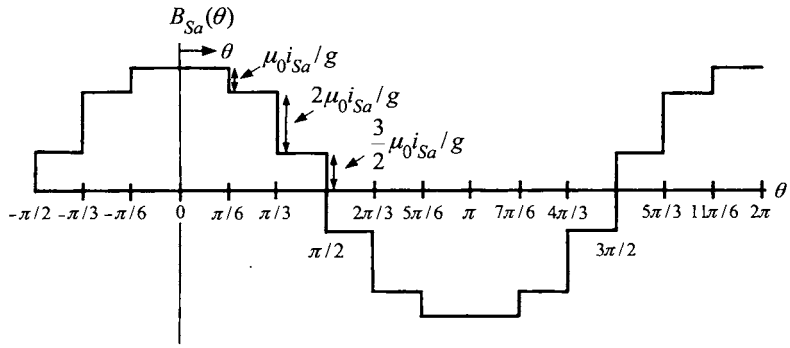


FIGURE 4.11. Radial magnetic field $B_{Sa}(\theta)$ in the air gap for the distributed winding of Figure 4.4(b).

4.2.1 Conservation of Flux and $1/r$ Dependence

Consider the closed flux surface in the air gap shown in Figure 4.12. This closed surface is composed of two concentric cylindrical-shaped surfaces S_1 and S_2 and four other planar sides S_3, S_4, S_5, and S_6 as illustrated in Figure 4.12. The surface normal on the closed surface is given by

$$d\vec{\mathbf{S}} = \begin{cases} -r_1 d\theta dz\hat{\mathbf{r}} & \text{for} \quad S_1 \\ r_2 d\theta dz\hat{\mathbf{r}} & \text{for} \quad S_2 \\ dr dz\hat{\boldsymbol{\theta}} & \text{for} \quad S_3 \\ r d\theta dr\hat{\mathbf{z}} & \text{for} \quad S_4 \\ -dr dz\hat{\boldsymbol{\theta}} & \text{for} \quad S_5 \\ -r d\theta dr\hat{\mathbf{z}} & \text{for} \quad S_6 \end{cases}$$

As $\vec{\mathbf{B}}$ is taken to have only a radial component, $\vec{\mathbf{B}} \cdot d\vec{\mathbf{S}} = 0$ on the surfaces S_3, S_4, S_5, S_6 as $\vec{\mathbf{B}}$ is perpendicular (normal) to $d\vec{\mathbf{S}}$ on these surfaces. Consequently, $\int_{S_3} \vec{\mathbf{B}} \cdot d\vec{\mathbf{S}} = \int_{S_4} \vec{\mathbf{B}} \cdot d\vec{\mathbf{S}} = \int_{S_5} \vec{\mathbf{B}} \cdot d\vec{\mathbf{S}} = \int_{S_6} \vec{\mathbf{B}} \cdot d\vec{\mathbf{S}} = 0$. In this

www.EngineeringEBooksPdf.com

case, conservation of flux gives

$$\oint \vec{\mathbf{B}} \cdot d\vec{\mathbf{S}} = \int_{S_1} \vec{\mathbf{B}} \cdot d\vec{\mathbf{S}} + \int_{S_2} \vec{\mathbf{B}} \cdot d\vec{\mathbf{S}} = 0$$

$$\int_0^{\ell_1} \int_{\theta_1}^{\theta_2} (B_{Sa}(\theta)\hat{\mathbf{r}}) \cdot (r_1 d\theta dz(-\hat{\mathbf{r}})) + \int_0^{\ell_1} \int_{\theta_1}^{\theta_2} (B_{Sa}(\theta)\hat{\mathbf{r}}) \cdot (r_2 d\theta dz\hat{\mathbf{r}}) = 0 \tag{4.5}$$

$$-\ell_1 r_1 \int_{\theta_1}^{\theta_2} B_{Sa}(\theta)d\theta + \ell_1 r_2 \int_{\theta_1}^{\theta_2} B_{Sa}(\theta)d\theta = 0$$

$$\ell_1 (r_2 - r_1) \int_{\theta_1}^{\theta_2} B_{Sa}(\theta)d\theta = 0$$

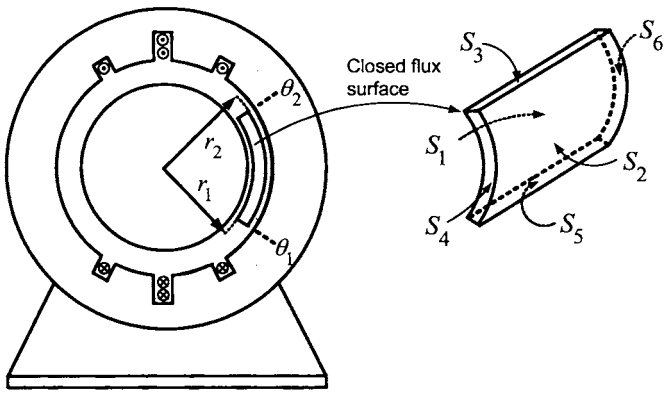


FIGURE 4.12. Closed flux surface to show the $1/r$ dependence of the magnetic field in the air gap.

As $r_1 \neq r_2$, conservation of flux does not hold. The problem here is that the magnetic field B_{Sa} was assumed to be constant as a function of r across the air gap in deriving (4.2) [and therefore, in deriving (4.3) and (4.4)] when in fact it must vary as $1/r$ to satisfy the conservation of flux law. That is, with r_R the radius of the rotor, replace $B_{Sa}(\theta)$ by $B_{Sa}(r,\theta) \triangleq \frac{r_R}{r} B_{Sa}(\theta)$ in (4.5) and $\oint \vec{\mathbf{B}} \cdot d\vec{\mathbf{S}} \equiv 0$ will then hold. The expression for the magnetic field is now

$$\vec{\mathbf{B}}_{Sa}(r,\theta) = B_{Sa}(r,\theta)\hat{\mathbf{r}} = \mu_0 \frac{r_R}{r}\left(\frac{2i_{Sa}}{g} - \frac{i_{\text{enclosed}}(\theta)}{g}\right)\hat{\mathbf{r}}. \tag{4.6}$$

Similarly, the expressions (4.3) and (4.4) are multiplied by the factor r_R/r.

The air gap g is assumed to be small so that

$$\frac{r_R}{r} \approx 1 \text{ for } r_R \leq r \leq r_S = r_R + g.$$

www.EngineeringEBooksPdf.com

Consequently, the factor r_R/r does not really change the value of the magnetic field in the air gap.[2] However, it is straightforward to see that this expression for $\vec{\mathbf{B}}_{Sa}(r,\theta)$ satisfies conservation of flux for the closed surface given in Figure 4.12 (see problems 5 and 17).

4.2.2 Magnetic Field Distribution Due to the Stator Currents

Consider a second stator phase, denoted as phase b, which is rotated 90° from phase a as drawn in Figure 4.13.

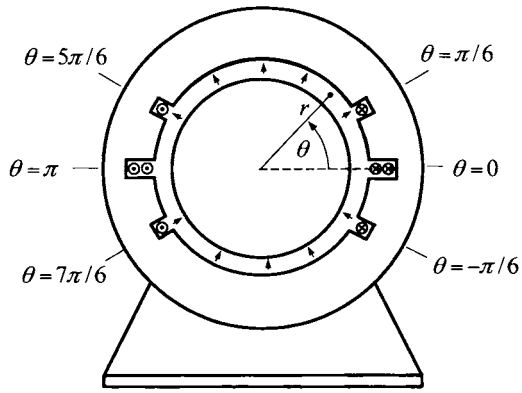


FIGURE 4.13. Phase b windings carrying the current i_{Sb}.

A similar argument to that given for phase a shows that the magnetic field $\vec{\mathbf{B}}_{Sb}$ due to the current i_{Sb} in phase b is found by replacing i_{Sa} by i_{Sb} and θ by $\theta - \pi/2$ to obtain

$$\begin{aligned}\vec{\mathbf{B}}_{Sb}(r,\theta) &= B_{Sb}(r,\theta)\hat{\mathbf{r}} = \mu_0 \frac{i_{Sb}}{g}\frac{r_R}{r}\frac{4}{\pi}\sum_{k=1,3,5,\ldots}^{\infty}\frac{(1+\cos(k\pi/6)}{k}\sin(k\theta) \\ &\approx 1.866\mu_0\frac{i_{Sb}}{g}\frac{r_R}{r}\frac{4}{\pi}\sin(\theta)\hat{\mathbf{r}}.\end{aligned}$$

In summary, the first harmonic approximation for $\vec{\mathbf{B}}_{Sa}(r,\theta)$ and $\vec{\mathbf{B}}_{Sb}(r,\theta)$ are

$$\vec{\mathbf{B}}_{Sa}(r,\theta) = B_{Sa}(r,\theta)\hat{\mathbf{r}} \approx 1.866\mu_0\frac{i_{Sa}}{g}\frac{4}{\pi}\frac{r_R}{r}\cos(\theta)\hat{\mathbf{r}}$$

$$\vec{\mathbf{B}}_{Sb}(r,\theta) = B_{Sb}(r,\theta)\hat{\mathbf{r}} \approx 1.866\mu_0\frac{i_{Sb}}{g}\frac{4}{\pi}\frac{r_R}{r}\sin(\theta)\hat{\mathbf{r}}.$$

[2]It would have been just as valid to use r_S/r where r_S is the inside radius of the stator, or a value $r_0, r_R < r_0 < r_S$ satisfying $\int_{r_R}^{r_S}(r_0/r_R)dr = g$ (see problem 11).

www.EngineeringEBooksPdf.com

4.3 Sinusoidally Wound Phases

In the previous section, the higher-order terms in the expression for the radial magnetic field in the air gap were ignored. In this section, the concept of a sinusoidally wound phase is explained, and it is shown that the higher-order harmonic terms in the Fourier series expansion of $\vec{\mathbf{B}}_{Sa}, \vec{\mathbf{B}}_{Sb}$ are *identically* zero. A sinusoidally wound rotor phase is first described as the corresponding figures are easier to draw in order to get the point across. Next, sinusoidally wound stator phases are described and an expression for the corresponding sinusoidally distributed magnetic fields produced in the air gap by the phase currents are then derived.

4.3.1 Sinusoidally Wound Rotor Phase

To construct a *sinusoidally* wound rotor phase, a single strand of wire is wrapped around the axial length of a cylindrical core of iron, making coil-loops or *turns* according to a *sinusoidal turns density* given by

$$N_{Ra}(\theta - \theta_R) = \frac{N_R}{2}\sin(\theta - \theta_R) \text{ for } \theta_R < \theta < \pi + \theta_R$$

where θ_R is the rotor position. That is, this specifies that the number of the loops (turns) wrapped around the rotor iron core between θ and $\theta + d\theta$ is $N_{Ra}(\theta - \theta_R)d\theta$ [see Figure 4.14(a)].

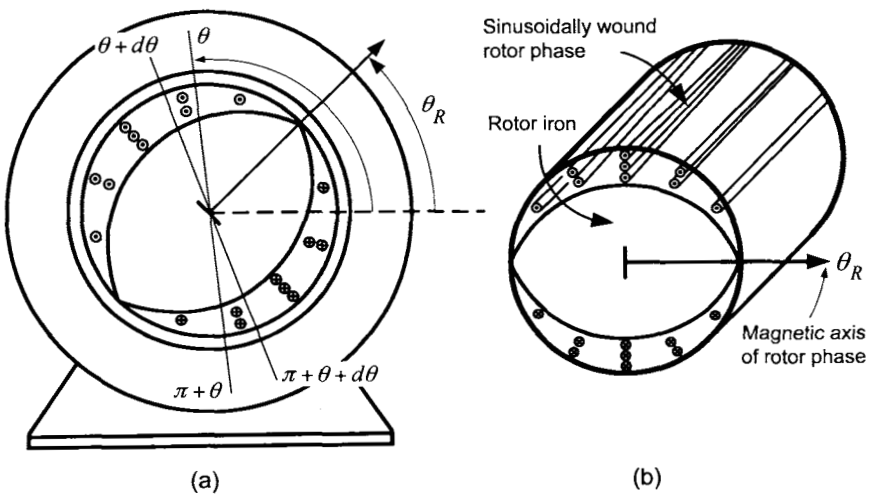


FIGURE 4.14. Sinusoidally wound rotor phase. The number of loops/turns wound between θ and $\theta + d\theta$ is $N_{Ra}(\theta - \theta_R)d\theta$ with the other side of these loops between $\pi + \theta$ and $\pi + \theta + d\theta$. The sine curve envelope drawn around the windings is used to indicate a sinusoidally wound phase. Although not drawn to show this, the cross-sectional area of the sinusoidally wound phase is taken to be infinitesimal.

www.EngineeringEBooksPdf.com

Consequently, the total number of turns wrapped around the rotor core is then $\int_{\theta_R}^{\theta_R+\pi} N_{Ra}(\theta-\theta_R)d\theta = N_R$. Figure 4.14(a) shows how a sinusoidally wound rotor is indicated schematically. In comparison with Figure 4.4, the slots have been removed in Figure 4.14(a), showing only the loops which are now enclosed in a *sine* curve envelope. This is a standard representation to denote a sinusoidal winding and is also adopted here [3][24].

4.3.2 Sinusoidally Wound Stator Phases

As in the case of the rotor phase, a sinusoidally wound stator phase is constructed by wrapping a single strand of wire around the inside surface of the stator iron to make coil loops or *turns*. For stator phase a, the number of the coil loops at any angle θ is specified by the *sinusoidal turns density*

$$N_{Sa}(\theta) = \frac{N_S}{2}\sin(\theta) \text{ for } 0 < \theta < \pi \tag{4.7}$$

that is, $N_{Sa}(\theta)d\theta$ is the number of turns between θ and $\theta + d\theta$. The total number of turns wrapped around the inside surface of the stator core is $\int_0^{\pi} N_{Sa}(\theta)d\theta = N_S$. This is illustrated in Figure 4.15.[3] The top side of this winding, where positive current is out of the page, is denoted as side a while the bottom side of the winding, where positive current is into the page, is denoted as side a'.

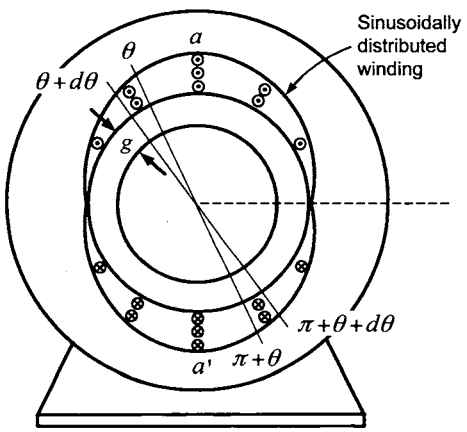


FIGURE 4.15. Sinusoidally wound stator phase a. The number of loops wound between θ and $\theta + d\theta$ is $N_{Sa}(\theta)d\theta$ with the other side of these loops between $\pi+\theta$ and $\pi + \theta + d\theta$.

[3]The figure shows a single phase wound such that there is one loop at $\pi/6$, two loops at $\pi/3$, three loops at $\pi/2$, two loops at $2\pi/3$, and one loop at $5\pi/6$ (see problem 4, where such a winding is analyzed). However, again following Refs. [3] and [24], the sine curve envelope of these loops is used to indicate that it is *sinusoidally* wound.

www.EngineeringEBooksPdf.com

Similarly, stator phase b consists of a separate sinusoidally wound wire identical in structure to phase a except it is rotated 90° with respect to phase a [see Figure 4.17(b)]. The turns density for phase b is therefore

$$N_{Sb}(\theta) = \frac{N_S}{2}\sin(\theta - \pi/2) \quad \text{for } \pi/2 < \theta < 3\pi/2. \tag{4.8}$$

The number of turns between θ and $\theta + d\theta$ is $N_{Sb}(\theta)d\theta = (N_S/2)\sin(\theta - \pi/2)d\theta$ and the total number of turns making up stator phase b is

$$\int_{\pi/2}^{3\pi/2} N_{Sb}(\theta)d\theta = N_S.$$

Remark Though Figures 4.14 and 4.15 are not drawn to show this, the cross-sectional area of a sinusoidally distributed winding is modeled as being infinitesimal.

4.4 Sinusoidally Distributed Magnetic Fields

Sinusoidally distributed windings (turns density) are used because the current in such a winding produces a sinusoidally distributed (in θ) radial magnetic field in the air gap. This is now explained.

The objective here is to determine the radial magnetic field $\vec{\mathbf{B}}_{Sa}$ established *in the air gap* by the current i_{Sa} in the sinusoidally distributed winding of phase a. To do so, Ampère's law $\oint \vec{\mathbf{H}} \cdot d\vec{\ell} = i_{\text{enclosed}}$ is applied to the closed-path 1–2–3–4–1 indicated in Figure 4.16 to obtain

$$\begin{aligned} \oint \vec{\mathbf{H}}_{Sa} \cdot d\vec{\ell} &= \int_0^{\theta} i_{Sa}(N_S/2)\sin(\theta')d\theta' \\ \int_1^2 \vec{\mathbf{H}}_{Sa} \cdot d\vec{\ell} + \int_3^4 \vec{\mathbf{H}}_{Sa} \cdot d\vec{\ell} &= \int_0^{\theta} i_{Sa}(N_S/2)\sin(\theta')d\theta'. \end{aligned}$$

Evaluating, this becomes

$$\int_{\ell=0}^{\ell=g} H_{Sa}(i_{Sa},0)\hat{\mathbf{r}} \cdot (d\ell\hat{\mathbf{r}}) + \int_{\ell=0}^{\ell=g} H_{Sa}(i_{Sa},\theta)\hat{\mathbf{r}} \cdot (-d\ell\hat{\mathbf{r}}) = -i_{Sa}\frac{N_S}{2}\cos(\theta) + i_{Sa}\frac{N_S}{2}$$

or

$$H_{Sa}(i_{Sa},0)g - H_{Sa}(i_{Sa},\theta)g = -i_{Sa}\frac{N_S}{2}\cos(\theta) + i_{Sa}\frac{N_S}{2} \tag{4.9}$$

where it was assumed that $\vec{\mathbf{H}}_{Sa}$ is *constant* across the air gap. Rearranging,

$$H_{Sa}(i_{Sa},\theta) = i_{Sa}\frac{N_S}{2g}\cos(\theta) + H_{Sa}(i_{Sa},0) - i_{Sa}\frac{N_S}{2g}.$$

www.EngineeringEBooksPdf.com

In this equation, both $H_{Sa}(i_{Sa}, \theta)$ and $H_{Sa}(i_{Sa}, 0)$ are unknown. The conservation of flux law $\oint_S \vec{\mathbf{B}} \cdot d\vec{\mathbf{S}} = 0$ can be used to determine $H_{Sa}(i_{Sa}, 0)$. To do so, consider a closed surface S that contains the rotor core as shown in Figure 4.16. The cylindrical part of the surface S is in the air gap and has radius r_R so that it just contains the rotor core. The two disk-shaped ends of the surface S are considered to have zero flux through them as $\vec{\mathbf{B}}$ is essentially zero there.

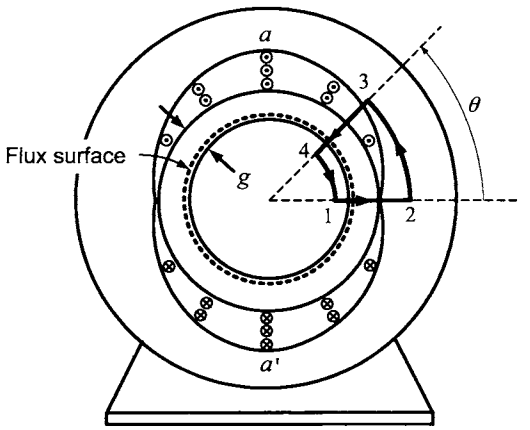


FIGURE 4.16. Use of Ampère's law and Gauss's law to determine the air gap radial magnetic field due to i_{Sa}.

Then

$$\begin{aligned}\oint_S \vec{\mathbf{B}}_{Sa} \cdot d\vec{\mathbf{S}} &= \int_0^{\ell_1} \int_0^{2\pi} B_{Sa}(i_{Sa}, \theta)\hat{\mathbf{r}} \cdot (r_R d\theta dz \hat{\mathbf{r}}) \\ &= \ell_1 r_R \int_0^{2\pi} B_{Sa}(i_{Sa}, \theta) d\theta \\ &= 0.\end{aligned}$$

Now $B_{Sa}(i_{Sa}, \theta) = \mu_0 H_{Sa}(i_{Sa}, \theta)$ as the flux surface is in the air gap. Thus,

$$\begin{aligned}\int_0^{2\pi} B_{Sa}(i_{Sa}, \theta) d\theta &= \int_0^{2\pi} \mu_0 \left(i_{Sa} \frac{N_S}{2g} \cos(\theta) + H_{Sa}(i_{Sa}, 0) - i_{Sa} \frac{N_S}{2g} \right) d\theta \\ &= 2\pi\mu_0 \left(H_{Sa}(i_{Sa}, 0) - i_{Sa} \frac{N_S}{2g} \right) \\ &= 0\end{aligned}$$

or

$$H_{Sa}(i_{Sa}, 0) = i_{Sa} \frac{N_S}{2g}.$$

www.EngineeringEBooksPdf.com

It then follows that

$$\begin{aligned} H_{Sa}(i_{Sa},\theta) &= \frac{N_S}{2g} i_{Sa}\cos(\theta) \\ B_{Sa}(i_{Sa},\theta) &= \frac{\mu_0 N_S}{2g} i_{Sa}\cos(\theta). \end{aligned} \tag{4.10}$$

In applying Ampère's law, it was assumed that $\vec{\mathbf{B}} = \mu_0\vec{\mathbf{H}}$ was constant across the air gap in the radial direction, that is, $\vec{\mathbf{B}}$ did not depend on the cylindrical coordinate r. However, in order to satisfy the conservation of flux $\oint_S \vec{\mathbf{B}} \cdot d\vec{\mathbf{S}} = 0$ in the air gap for a closed surface such as the one in Figure 4.12, it is necessary that $\vec{\mathbf{B}}$ decrease as $1/r$ in the air gap. Therefore, the expressions for H_{Sa}, B_{Sa} are modified by the factor r_R/r so that conservation of flux holds in the air gap.[4] Finally then, the magnetic field $\vec{\mathbf{B}}_{Sa}$ *in the air gap* due to i_{Sa} is given by

$$\vec{\mathbf{B}}_{Sa}(i_{Sa},r,\theta) = \frac{\mu_0 N_S r_R}{2g}\frac{i_{Sa}\cos(\theta)}{r}\hat{\mathbf{r}}.$$

Similarly, for stator phase b which is also sinusoidally wound, but rotated 90° counterclockwise from phase a, the magnetic field $\vec{\mathbf{B}}_{Sb}$ *in the air gap* due to i_{Sb} is given by

$$\begin{aligned} \vec{\mathbf{B}}_{Sb}(i_{Sb},r,\theta) &= \frac{\mu_0 N_S r_R}{2g}\frac{i_{Sb}\cos(\theta-\pi/2)}{r}\hat{\mathbf{r}} \\ &= \frac{\mu_0 N_S r_R}{2g}\frac{i_{Sb}\sin(\theta)}{r}\hat{\mathbf{r}}. \end{aligned}$$

Figure 4.17(a) shows the magnetic field lines due to the current i_{Sa} in phase a (drawn with $i_{Sa} > 0$) while Figure 4.17(b) shows the magnetic field lines due to i_{Sb} in phase b (drawn with $i_{Sb} > 0$). The sinusoidal windings have resulted in sinusoidally distributed radial magnetic fields in the air gap produced by the stator currents.

[4] See problem 11 for a discussion how Ampère's law changes when the factor r_R/r is added.

www.EngineeringEBooksPdf.com

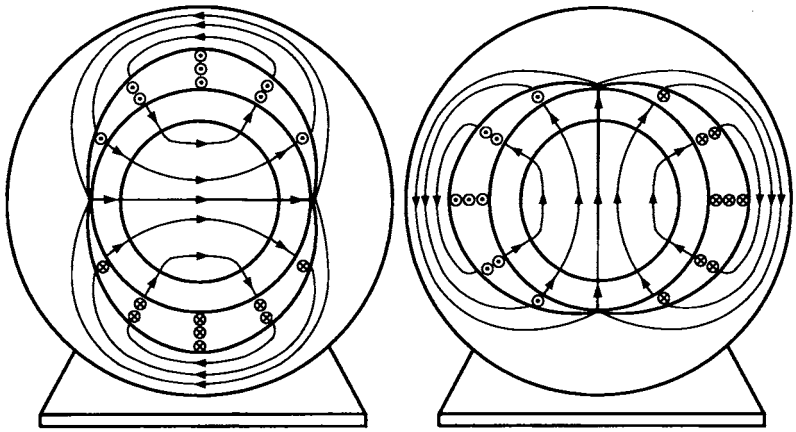


FIGURE 4.17. (a) Magnetic field lines due to the current i_{Sa} in the sinusoidally distributed winding of phase a. (b) Magnetic field lines due to the current i_{Sb} in the sinusoidally distributed winding of phase b.

4.4.1 Sinusoidally Distributed Rotating Magnetic Field

The total magnetic field in the air gap due to the current in both stator phases is then

$$\begin{aligned}\vec{\mathbf{B}}_S(i_{Sa}, i_{Sb}, r, \theta) &= \vec{\mathbf{B}}_{Sa}(i_{Sa}, r, \theta) + \vec{\mathbf{B}}_{Sb}(i_{Sb}, r, \theta) \\ &= \frac{\mu_0 r_R N_S}{2g} \frac{1}{r} \Big(i_{Sa} \cos(\theta) + i_{Sb} \sin(\theta) \Big) \hat{\mathbf{r}}. \quad (4.11)\end{aligned}$$

With $i_{Sa}(t) = I_S \cos(\omega_S t)$ and $i_{Sb}(t) = I_S \sin(\omega_S t)$, the expression (4.11) simplifies to

$$\begin{aligned}\vec{\mathbf{B}}_S(r, \theta, t) &= \frac{\mu_0 r_R N_S I_S}{2g} \frac{1}{r} \Big(\cos(\omega_S t) \cos(\theta) + \sin(\omega_S t) \sin(\theta) \Big) \hat{\mathbf{r}} \\ &= \frac{\mu_0 r_R N_S I_S}{2g} \frac{1}{r} \cos(\theta - \omega_S t) \hat{\mathbf{r}} \\ &= \frac{\mu_0 r_R N_S I_S}{2g} \frac{1}{r} \cos\Big(\theta - \theta_S(t) \Big) \hat{\mathbf{r}} \quad (4.12)\end{aligned}$$

where $\theta_S(t) \triangleq \omega_S t$.

Equation (4.12) is the mathematical representation of a *rotating magnetic field* which rotates at the angular (electrical) frequency ω_S and is illustrated in Figure 4.18. Note that the magnetic field has a fixed distribution *with respect* to θ_S. The angle θ_S is referred to as the *magnetic axis* of the rotating magnetic field.

www.EngineeringEBooksPdf.com

Remark In Figure 4.18, the sinusoidally distributed stator windings are drawn with four loops in the sine curve envelope rather than with nine loops as in Figure 4.17. This is done for clarity of presentation. The reader should always assume that the sine curve envelope implies that the winding densities for phases a and b are given by (4.7) and (4.8), respectively.

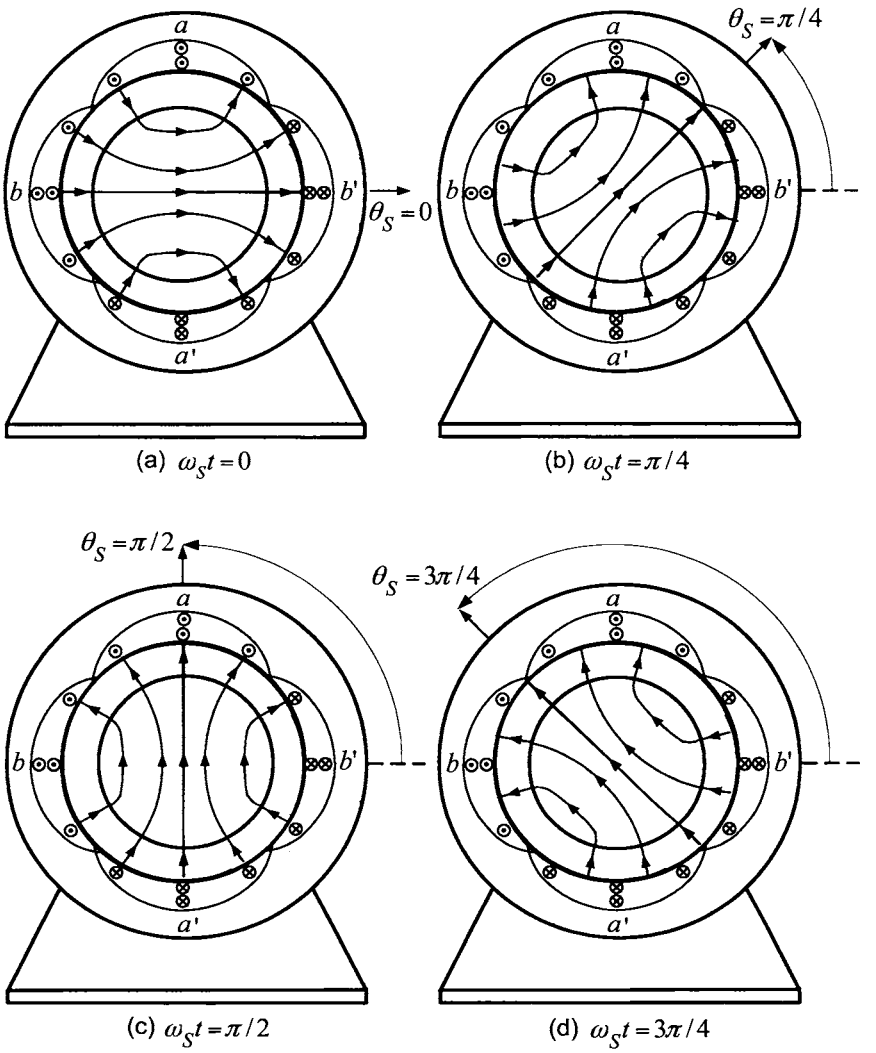


FIGURE 4.18. Sinusoidally distributed rotating radial magnetic field in the air gap. (For convenience, the magnetic field lines inside the stator iron are not drawn.)

www.EngineeringEBooksPdf.com

4.5 Magnetomotive Force (mmf)

The magnetomotive force (mmf) is defined to be $\Im \triangleq \oint \vec{\mathbf{H}} \cdot d\vec{\boldsymbol{\ell}}$, that is, the integral of $\vec{\mathbf{H}}$ around a *closed* curve. Of course, by Ampère's law,

$$\Im = \oint \vec{\mathbf{H}} \cdot d\vec{\boldsymbol{\ell}} = i_{\text{enclosed}}.$$

Instead of the path used in Figure 4.16, consider applying Ampère's law to the path 1–2–3–4–1 in Figure 4.19 .

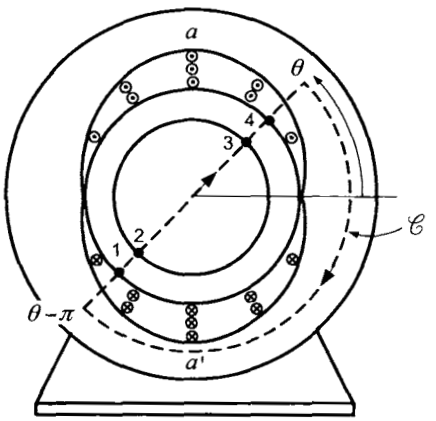


FIGURE 4.19. Sinusoidally wound stator phase.

Now $\vec{\mathbf{H}} = 0$ on the paths 2–3 and 4–1. By symmetry, $\vec{\mathbf{H}}(\theta - \pi) = -\vec{\mathbf{H}}(\theta)$ and, as $d\vec{\boldsymbol{\ell}} = d\ell(-\hat{\mathbf{r}})$ on the path 1–2 while $d\vec{\boldsymbol{\ell}} = d\ell\hat{\mathbf{r}}$ on the path 3–4, it follows that $\int_3^4 \vec{\mathbf{H}} \cdot d\vec{\boldsymbol{\ell}} = \int_1^2 \vec{\mathbf{H}} \cdot d\vec{\boldsymbol{\ell}}$ and so

$$\Im \triangleq \oint \vec{\mathbf{H}} \cdot d\vec{\boldsymbol{\ell}} = 2\int_3^4 \vec{\mathbf{H}} \cdot d\vec{\boldsymbol{\ell}} = 2\int_3^4 (H(\theta)\hat{\mathbf{r}}) \cdot (d\ell\hat{\mathbf{r}}) = 2H(\theta)g.$$

In Figure 4.19 the path is traversed in the clockwise direction in contrast to the path in Figure 4.16 which is traversed in the counterclockwise direction. Consequently, in the application of Ampère's law, the current is now considered positive if it is into the page rather than out of the page. The enclosed current for the path 1–2–3–4–1 is therefore

$$i_{\text{enclosed}} = -\int_{\theta-\pi}^{\theta} i_{Sa}(N_S/2)\sin(\theta')d\theta' = i_{Sa}N_S\cos(\theta).$$

www.EngineeringEBooksPdf.com

Ampère's law $\oint \vec{\mathbf{H}} \cdot d\vec{\boldsymbol{\ell}} = i_{\text{enclosed}}$ then gives

$$\Im \triangleq \oint \vec{\mathbf{H}} \cdot d\vec{\boldsymbol{\ell}} = i_{Sa} N_S \cos(\theta)$$

or

$$\Im(\theta) = 2H(\theta)g = i_{Sa} N_S \cos(\theta).$$

The interpretation is that the mmf $\Im(\theta) = i_{Sa} N_S \cos(\theta)$ which is produced by the current is "dropped" across the air gap in the amount of $\Im_1(\theta) = H(\theta)g$ across each of the two diametrically opposite sides of the air gap. Then one works with the mmf $\Im$ and refers to an "mmf wave" $\Im_1(\theta) = H(\theta)g$ set up in the air gap, and so on (see, e.g., Refs. [5][19][21][24][26][58]). In contrast, a different emphasis (but with the same results) has been taken here. Specifically, Ampère's law is used to find $\vec{\mathbf{H}}$ in the air gap by computing the mmf and using $\vec{\mathbf{H}} \equiv 0$ in the iron. Then $\vec{\mathbf{B}}$ in the air gap is found simply from $\vec{\mathbf{B}} = \mu_0 \vec{\mathbf{H}}$. In other words, the mmf is only used as a device to compute the magnetic induction field $\vec{\mathbf{B}}$ in the air gap. After this is accomplished, the $\vec{\mathbf{B}}$ field is used exclusively because it is the quantity that produces forces on currents and voltages in coil loops, that is, it is directly related to the physical phenomena. This is perhaps better said in the following quotation from Melvin Schwartz, a 1988 Noble Laureate in Physics:[5]

... we must interject a small bit of philosophy. It is customary to call $\vec{\mathbf{B}}$ *the magnetic induction and* $\vec{\mathbf{H}}$ *the magnetic field strength. We reject this custom inasmuch as* $\vec{\mathbf{B}}$ *is the truly fundamental field and* $\vec{\mathbf{H}}$ *is a subsidiary artifact. We shall call* $\vec{\mathbf{B}}$ *the magnetic field and leave the reader to deal with* $\vec{\mathbf{H}}$ *as he pleases.*

Remark

In this and the previous sections, only the radial component (i.e., in the $\hat{\mathbf{r}}$ direction) of $\vec{\mathbf{B}}$ in the air gap was found. However, Figures 3.2–3.5 indicate that one would expect that an azimuthal component (i.e., in the $\hat{\boldsymbol{\theta}}$ direction) of $\vec{\mathbf{B}}$ would also be present in the air gap. This is indeed the case and it is derived in (the optional) Section 4.6. Only the radial component of $\vec{\mathbf{B}}$ contributes to the machine torque and produces emfs in the windings of the machine, which is the reason that one need only consider this component to derive the mathematical models of AC machines.

[5] See M. Schwartz [35], page 156.

www.EngineeringEBooksPdf.com

4.6 Flux Linkage

The notion of flux $\phi = \int_S \vec{\mathbf{B}} \cdot d\vec{\mathbf{S}}$ is defined for a surface whose boundary is a simple closed curve. After computing the flux, Faraday's law $\xi = -d\phi/dt$ is then used to compute the induced emf (voltage) in the loop. However, phase windings are usually comprised of many windings which are also distributed and one wants to compute the total emf induced in the phase winding. It has been found that the notion of *flux linkage* can be used to do this in a convenient fashion.

To show how flux linkage is used in AC machines, consider Figure 4.20 which shows three loops wound on the inside surface of a stator iron. That is, a single piece of wire is wound around the inside surface where one loop is placed in a slot at $\theta = \pi/3$ (the other side of the loop is in the slot at $\theta = \pi/3 - \pi$) then a second loop is wound at $\theta = \pi/2$ with its other side at $\theta = 3\pi/2$) and finally a third loop is wound at $\theta = 2\pi/3$ (with its other side at $\theta = 5\pi/3$). The flux surface for each loop is taken to coincide with the loop itself as shown in Figure 4.20(b). As this figure shows, the first loop/surface is the path from a to b, the second loop/surface is the path from c to d and the third loop is the path from e to $f = a'$. One end of the wire is labeled a and the other a' and the objective here is to calculate the total emf $\xi_{a-a'}$ induced in the wire by the rotating permanent magnet rotor.

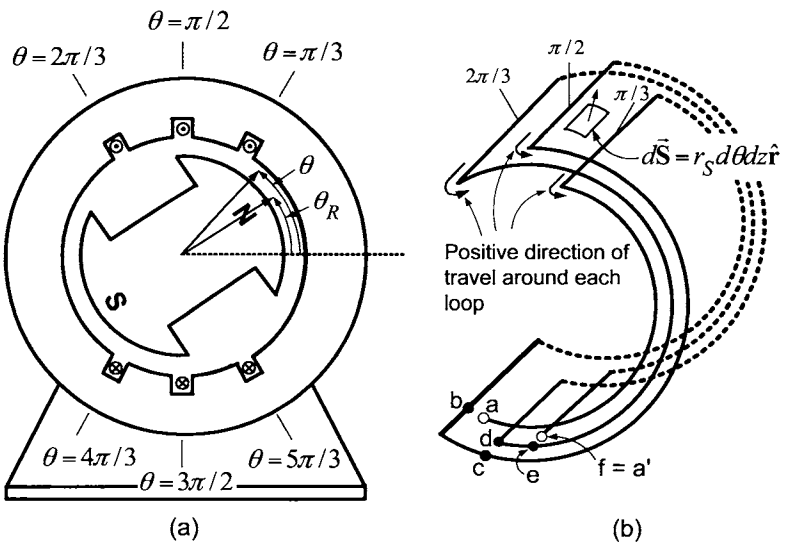


FIGURE 4.20. (a) Distributed winding for stator phase a with a permanent magnet rotor. (b) The flux surfaces for each stator loop.

www.EngineeringEBooksPdf.com

As before, if the current in the stator winding is positive, the symbol $\odot$ means that it is coming out of the page and the symbol $\otimes$ means that it is going into the page. Here it is assumed that the permanent magnet produces a radial magnetic field in the air gap given by

$$\vec{\mathbf{B}}_R(\theta - \theta_R) = B_{\max}\frac{r_R}{r}\cos(\theta - \theta_R)\hat{\mathbf{r}}$$

where r_R is the radius of the rotor, (r, θ) are the polar coordinates of an arbitrary location in the air gap and θ_R is the rotor angle defined by the center line (magnetic axis) of the rotor's north pole [see Figure 4.20(a)]. This rotor magnet produces a flux in each loop and, for any given rotor position θ_R, this flux is different in the loop at $\theta = \pi/3$, the loop at $\pi/2$, and the loop at $2\pi/3$. Further, if the rotor is moving, then it is producing a changing flux in each of the three loops and therefore, by Faraday's law, this changing flux will produce an emf in each of the three loops. Of course, at any point in time, the emfs will be different in each of the three loops.

To compute these emfs, let

$$d\vec{\mathbf{S}} = r_S d\theta dz\hat{\mathbf{r}} \tag{4.13}$$

where r_S is the radius of the inside surface of the stator iron. Note that with this choice of $d\vec{\mathbf{S}}$, the positive direction of travel around the loop coincides with the positive direction chosen for the current in that loop [see Figure 4.20(b)]. On the inside surface of the rotor, $r = r_S$ so that the flux in the loop whose sides are in the slots at $\theta = \pi/3$ and $\theta = \pi/3 - \pi$ is

$$\begin{aligned}
\phi_{\pi/3} &= \int_{\substack{\text{Loop from} \\ \pi/3-\pi \text{ to } \pi/3}} \vec{\mathbf{B}}_R \cdot d\vec{\mathbf{S}} \\
&= \int_0^{\ell_1}\int_{\theta=\pi/3-\pi}^{\theta=\pi/3} B_{\max}\frac{r_R}{r_S}\cos(\theta - \theta_R)\hat{\mathbf{r}}\cdot(r_S d\theta dz\hat{\mathbf{r}}) \\
&= \ell_1 r_R\int_{\theta=\pi/3-\pi}^{\theta=\pi/3} B_{\max}\cos(\theta - \theta_R)d\theta \\
&= \ell_1 r_R B_{\max}\sin(\theta - \theta_R)d\theta\Big|_{\theta=\pi/3-\pi}^{\theta=\pi/3} \\
&= 2\ell_1 r_R B_{\max}\sin(\pi/3 - \theta_R).
\end{aligned}$$

Then the emf induced in this loop by the magnetic field of the permanent magnet is

$$\xi_{\pi/3} = -\frac{d\phi_{\pi/3}}{dt} = 2\ell_1 r_R B_{\max}\omega_R\cos(\theta_R - \pi/3)$$

where $\omega_R \triangleq d\theta_R/dt$. If $\xi_{\pi/3} > 0$, this emf will force current to go in the positive direction of travel around the loop which coincides with the positive direction of current in that loop.

www.EngineeringEBooksPdf.com

Again using the outward normal so that $d\vec{\mathbf{S}}$ is still given by equation (4.13) as before, the flux in the loop between $-\pi/2$ to $\pi/2$ is

$$\phi_{\pi/2} = \int_{\substack{\text{Loop from} \\ -\pi/2 \text{ to } \pi/2}} \vec{\mathbf{B}}_R \cdot d\vec{\mathbf{S}} = 2\ell_1 r_R B_{\max} \sin(\pi/2 - \theta_R)$$

and the induced emf in the loop is

$$\xi_{\pi/2} = -\frac{d\phi_{\pi/2}}{dt} = 2\ell_1 r_R B_{\max} \omega_R \cos(\theta_R - \pi/2).$$

If $\xi_{\pi/2} > 0$, it will force current to go in the positive direction of travel around the loop which also coincides with the positive direction of current in that loop.

Finally, with $d\vec{\mathbf{S}}$ given by (4.13) once more,

$$\phi_{2\pi/3} = \int_{\substack{\text{Loop from} \\ 2\pi/3-\pi \text{ to } 2\pi/3}} \vec{\mathbf{B}}_R \cdot d\vec{\mathbf{S}} = 2\ell_1 r_R B_{\max} \sin(2\pi/3 - \theta_R)$$

and

$$\xi_{2\pi/3} = -\frac{d\phi_{2\pi/3}}{dt} = 2\ell_1 r_R B_{\max} \omega_R \cos(\theta_R - 2\pi/3).$$

Again, if $\xi_{2\pi/3} > 0$, it will force current to go in the positive direction of travel around the loop coinciding with the positive direction of current in that loop.

All three loops are connected in series to make up the phase winding and the sign convention for positive travel around each loop was chosen to coincide with the positive direction of current in the phase as illustrated in Figure 4.20(b). That is, the induced emfs in the loops are all in series in the phase winding and, as they all have the *same* sign convention, they can be added up to obtain the total emf in the phase winding. As a result, the total voltage induced in the phase is

$$\begin{aligned} \xi_{a-a'} &= \xi_{\pi/3} + \xi_{\pi/2} + \xi_{2\pi/3} = 2\ell_1 r_R B_{\max} \omega_R \cos(\theta_R - \pi/3) \\ &\quad + 2\ell_1 r_R B_{\max} \omega_R \cos(\theta_R - \pi/2) + 2\ell_1 r_R B_{\max} \omega_R \cos(\theta_R - 2\pi/3) \\ &= \left(1 + \sqrt{3}\right) 2\ell_1 r_R B_{\max} \omega_R \sin(\theta_R). \end{aligned}$$

However, consider

$$\begin{aligned} \xi_{a-a'} &= \xi_{\pi/3} + \xi_{\pi/2} + \xi_{2\pi/3} \\ &= -\left(\frac{d\phi_{\pi/3}}{dt} + \frac{d\phi_{\pi/2}}{dt} + \frac{d\phi_{2\pi/3}}{dt}\right) \\ &= -\frac{d}{dt}\left(\phi_{\pi/3} + \phi_{\pi/2} + \phi_{2\pi/3}\right) \\ &= -\frac{d}{dt}\lambda_{a-a'} \end{aligned}$$

www.EngineeringEBooksPdf.com

where

$$\begin{aligned}\lambda_{a-a'} &\triangleq \phi_{\pi/3} + \phi_{\pi/2} + \phi_{2\pi/3} \\ &= 2\ell_1 r_R B_{\max} \sin(\pi/3 - \theta_R) + 2\ell_1 r_R B_{\max} \sin(\pi/2 - \theta_R) \\ &\quad +2\ell_1 r_R B_{\max} \sin(2\pi/3 - \theta_R) \\ &= \left(1 + \sqrt{3}\right) 2\ell_1 r_R B_{\max} \cos(\theta_R)\end{aligned}$$

is defined as the total *flux linkage* in phase a–a'. Then the total induced emf $\xi_{a-a'}$ in the phase a–a' is

$$\xi_{a-a'} = -\frac{d\lambda_{a-a'}}{dt} = \left(1 + \sqrt{3}\right) 2\ell_1 r_R B_{\max} \omega_R \sin(\theta_R).$$

The point here is that one can first sum the fluxes in all the loops of a phase winding (i.e., compute the flux linkage), and then apply Faraday's law to the resulting flux linkage to obtain the total emf in the phase winding. However, as done above, care must be taken to ensure that the flux in each loop is computed in a consistent fashion so that the resulting emfs all have the same sign convention and therefore add up to give the total emf in the phase winding.

4.7 Azimuthal Magnetic Field in the Air Gap*

It was shown above that the radial magnetic field $\vec{\mathbf{B}}_{Sa}$ at a point (r, θ) in the air gap due to the current i_{Sa} in phase a is given by ($r_R = \ell_2/2$)

$$\vec{\mathbf{B}}_{Sa}(i_{Sa}, r, \theta) = \frac{\mu_0 r_R N_S}{2gr} i_{Sa} \cos(\theta) \hat{\mathbf{r}} \tag{4.14}$$

where $\hat{\mathbf{r}}$ is a unit vector in the radial direction and g is the radial length of the air gap. However, there *has* to be a component of the magnetic field in the $\hat{\boldsymbol{\theta}}$ direction (azimuthal component) as is now shown by applying Ampère's law to the curve 1–2–3–4–1 shown in Figure 4.21. By Ampère's law,

$$\oint_{1-2-3-4-1} \vec{\mathbf{H}}_{Sa} \cdot d\vec{\ell} = \int_1^2 \vec{\mathbf{H}}_{Sa} \cdot d\vec{\ell} = \int_{\theta_1}^{\theta_2} (-i_{Sa}) \frac{N_S}{2} \sin(\theta) d\theta$$

as sides 2–3, 3–4, and 4–1 are inside the magnetic material[6] where $\vec{\mathbf{H}} \equiv \mathbf{0}$ and side 1–2 is in the air gap just along the inside surface of the stator. Note

[6] Remember that the cross-sectional area of the windings is modeleded as being infinitesimal.

www.EngineeringEBooksPdf.com

that for closed curve $1{-}2{-}3{-}4{-}1$ with $0 \leq \theta_1 \leq \theta_2 \leq \pi$, the minus sign is used with the current (i.e., $-i_{Sa}$). This is because the path $1{-}2{-}3{-}4{-}1$ is traversed in the clockwise direction so that Ampère's law assumes that positive current is *into* the page ($\otimes$) while $i_{Sa} > 0$ means the current is *out* of the page ($\odot$).

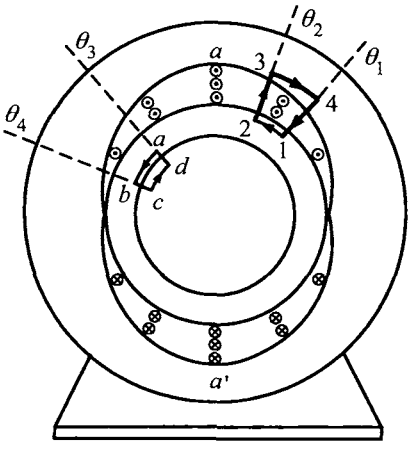


FIGURE 4.21. Closed curves for determining the *azimuthal* component $B_{Sa\theta}$ of the magnetic field produced by i_{Sa} in the air gap using Ampère's law.

With $r_S = r_R + g$, on the path $1{-}2$ the differential line element is $d\vec{\boldsymbol{\ell}} = r_S d\theta \hat{\boldsymbol{\theta}}$ so that the integral $\int_1^2 \vec{\mathbf{H}}_{Sa} \cdot d\vec{\boldsymbol{\ell}}$ evaluates to

$$\int_{\theta_1}^{\theta_2} (H_{Sa\theta}\hat{\boldsymbol{\theta}}) \cdot (r_S d\theta \hat{\boldsymbol{\theta}}) = -\int_{\theta_1}^{\theta_2} i_{Sa} \frac{N_S}{2} \sin(\theta) d\theta$$

for $0 \leq \theta_1 \leq \theta \leq \theta_2 \leq \pi$. This must hold for *any* θ_1, θ_2 which implies that

$$H_{Sa\theta}(i_{Sa}, r_S, \theta) = -\frac{N_S}{2r_S} i_{Sa} \sin(\theta)$$

for $0 \leq \theta \leq \pi$. For $\pi \leq \theta_1 \leq \theta \leq \theta_2 \leq 2\pi$, the turns density is $(N_S/2)\,|\sin(\theta)| = -(N_S/2)\sin(\theta)$. However, for this range of θ, $i_{Sa} > 0$ means that the current is *into* the page so that a similar argument shows that

$$H_{Sa\theta}(i_{Sa}, r_S, \theta) = -\frac{N_S}{2r_S} i_{Sa} \sin(\theta)$$

for $\pi \leq \theta \leq 2\pi$. Combining,

$$B_{Sa\theta}(i_{Sa}, r_S, \theta) = -\frac{\mu_0 N_S}{2r_S} i_{Sa} \sin(\theta)$$

www.EngineeringEBooksPdf.com

for $0 \leq \theta \leq 2\pi$. This is the *tangential* magnetic field at the inside surface of the stator (i.e., at $r = r_S$). To compute the azimuthal component of $B_{Sa\theta}$ at the surface of the rotor, that is, $B_{Sa\theta}(i_{Sa}, r_R, \theta)$, Ampère's law is applied to the closed path a–b–c–d–a in Figure 4.21. Specifically,

$$\oint_{a\text{-}b\text{-}c\text{-}d\text{-}a} \vec{\mathbf{H}}_{Sa} \cdot d\vec{\boldsymbol{\ell}} = \int_a^b \vec{\mathbf{H}}_{Sa} \cdot d\vec{\boldsymbol{\ell}} = \int_{\theta_3}^{\theta_4} H_{Sa\theta}(i_{Sa}, r_R, \theta) r_R d\theta \equiv 0$$

as the path does not enclose any current. (The sides b–c,c–d and d–a are inside the magnetic material of the rotor where $\vec{\mathbf{H}} \equiv 0$ and the path a–b is just on the surface of the rotor in the air gap.) As θ_3, θ_4 are arbitrary, it follows that

$$\begin{aligned} H_{Sa\theta}(i_{Sa}, r_R, \theta) &\equiv 0 \\ B_{Sa\theta}(i_{Sa}, r_R, \theta) &\equiv 0. \end{aligned}$$

The azimuthal component of the magnetic field in the air gap at the *surface* of both the stator and rotor has now been found. To find $\vec{\mathbf{B}}_S$ inside the air gap, let the tangential (azimuthal) component of $\vec{\mathbf{B}}_S$ be of the form

$$B_{Sa\theta}(i_{Sa}, r_S, \theta)\hat{\boldsymbol{\theta}} = -\alpha(r)\frac{\mu_0 N_S}{2r_S} i_{Sa} \sin(\theta)\hat{\boldsymbol{\theta}} \tag{4.15}$$

where

$$\begin{aligned} \alpha(r_S) &= 1 \\ \alpha(r_R) &= 0 \end{aligned} \tag{4.16}$$

as $\alpha(r)$ must satisfy (9.75) in order for (4.15) to hold at the rotor and stator surfaces.

Before the expression for $\alpha(r)$ is derived, it is first shown that the radial component of $\vec{\mathbf{B}}_{Sa}$ given in (4.14) must be modified to account for the azimuthal magnetic field. To see this, recall that Gauss's equation requires that the divergence of $\vec{\mathbf{B}}$ be identically zero. With $\vec{\mathbf{B}} = B_r\hat{\mathbf{r}} + B_\theta\hat{\boldsymbol{\theta}} + B_z\hat{\mathbf{z}}$, the divergence in cylindrical coordinates is given by

$$\nabla \cdot \vec{\mathbf{B}} = \frac{1}{r}\frac{\partial}{\partial r}(rB_r) + \frac{1}{r}\frac{\partial B_\theta}{\partial \theta} + \frac{\partial B_z}{\partial z} \equiv 0.$$

Consider $\vec{\mathbf{B}}_{Sa}$ of the form

$$\begin{aligned} \vec{\mathbf{B}}_{Sa} &= B_{Sar}\hat{\mathbf{r}} + B_{Sa\theta}\hat{\boldsymbol{\theta}} \\ &= B_{Sar}\hat{\mathbf{r}} - \alpha(r)\frac{\mu_0 N_S}{2r_S} i_{Sa} \sin(\theta)\hat{\boldsymbol{\theta}}. \end{aligned}$$

Taking the divergence of this expression results in

$$\frac{1}{r}\frac{\partial}{\partial r}(rB_{Sar}) - \frac{1}{r}\alpha(r)\frac{\mu_0 N_S}{2r_S} i_{Sa}\frac{\partial}{\partial \theta}\sin(\theta) \equiv 0$$

www.EngineeringEBooksPdf.com

or

$$\frac{\partial}{\partial r}(rB_{Sar}) = \alpha(r)\frac{\mu_0 N_S}{2r_S} i_{Sa}\cos(\theta).$$

Integrating with respect to r, one obtains

$$rB_{Sar} = \frac{\mu_0 N_S}{2r_S} i_{Sa}\cos(\theta)\int_{r_R}^{r}\alpha(r')dr' + f(\theta)$$

where $f(\theta)$ is a "constant of integration". Taking it to be

$$f(\theta) = \frac{\mu_0 r_R N_S}{2g} i_{Sa}\cos(\theta)$$

gives

$$\frac{f(\theta)}{r} = \frac{\mu_0 r_R N_S}{2gr} i_{Sa}\cos(\theta)$$

which is the original expression for the radial component of $\vec{\mathbf{B}}_{Sa}$ given in (4.14). Thus, the radial component of $\vec{\mathbf{B}}_{Sa}$ is now given by

$$B_{Sar} = \frac{\mu_0 r_R N_S}{2g} i_{Sa}\frac{\cos(\theta)}{r}\left(1 + \frac{g}{r_S r_R}\int_{r_R}^{r}\alpha(r')dr'\right).$$

At the rotor surface, this expression for B_{Sar} is the same as that given by (4.14) with $r = r_R$. Consequently, the torque on the rotor will not change due to this change in the radial component of $\vec{\mathbf{B}}$. It is shown below that $0 \leq \int_{r_R}^{r}\alpha(r')dr' \leq g/2$ for small air gaps so that the change in the radial component is bounded by

$$\frac{g^2}{2r_S r_R} << 1$$

so that it is indeed a small effect.

Summarizing,

$$\begin{aligned}\vec{\mathbf{B}}_{Sa} &= \frac{\mu_0 r_R N_S}{2g} i_{Sa}\frac{\cos(\theta)}{r}\left(1 + \frac{g}{r_S r_R}\int_{r_R}^{r}\alpha(r')dr'\right)\hat{\mathbf{r}} \\ &\quad - \frac{\mu_0 r_R N_S}{2g}\frac{g}{r_S r_R}\alpha(r) i_{Sa}\sin(\theta)\hat{\boldsymbol{\theta}} \end{aligned} \tag{4.17}$$

with

$$\begin{aligned}\alpha(r_S) &= 1 \\ \alpha(r_R) &= 0.\end{aligned}$$

Figure 4.22 indicates the distribution of the azimuthal magnetic field with $i_{Sa} > 0$. Note that the field strength decreases as one moves along the radial direction from the stator side of the air gap to the rotor side. It also decreases as one moves in the θ direction from $\pm\pi/2$ to 0 or π.

www.EngineeringEBooksPdf.com

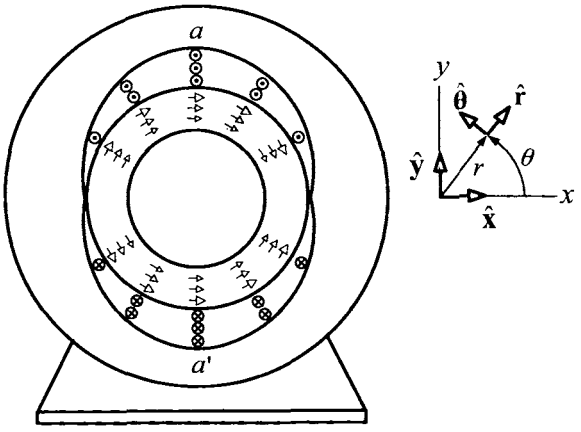


FIGURE 4.22. Distribution of azimuthal magnetic field $B_{Sa\theta}\hat{\boldsymbol{\theta}}$ in the air gap.

Determination of $\alpha(r)$

To determine $\alpha(r)$ for $r_R < r < r_S$, Ampère's law in differential form $\nabla \times \vec{\mathbf{H}} = \vec{\mathbf{J}}_{\text{free}}$ is used. In the air gap, there are no currents so $\nabla \times \vec{\mathbf{H}} = \mathbf{0}$, nor is there any magnetic material so that $\vec{\mathbf{B}} = \mu_0 \vec{\mathbf{H}}$. Consequently, Ampère's law in the air gap is simply

$$\nabla \times \vec{\mathbf{B}} = \mathbf{0}.$$

In cylindrical coordinates, this becomes

$$\begin{aligned} \nabla \times \vec{\mathbf{B}} &= \left(\frac{1}{r}\frac{\partial B_z}{\partial \theta} - \frac{\partial B_\theta}{\partial z}\right)\hat{\mathbf{r}} + \left(\frac{\partial B_r}{\partial z} - \frac{\partial B_z}{\partial r}\right)\hat{\boldsymbol{\theta}} + \frac{1}{r}\left(\frac{\partial}{\partial r}(rB_\theta) - \frac{\partial B_r}{\partial \theta}\right)\hat{\mathbf{z}} \\ &= \mathbf{0}. \end{aligned}$$

By the assumed cylindrical symmetry, $B_{Saz} \equiv 0$ and $B_{Sar}, B_{Sa\theta}$ do not depend on the coordinate z, so that one need only satisfy the z component of $\nabla \times \vec{\mathbf{B}} = \mathbf{0}$, that is,

$$\frac{\partial}{\partial r}(rB_{Sa\theta}) = \frac{\partial B_{Sar}}{\partial \theta}.$$

This becomes

$$-\frac{g}{r_S r_R}\frac{\partial}{\partial r}\left(r\alpha(r)\right) i_{Sa}\sin(\theta) = -i_{Sa}\frac{\sin(\theta)}{r}\left(1 + \frac{g}{r_S r_R}\int_{r_R}^{r}\alpha(r')dr'\right).$$

www.EngineeringEBooksPdf.com

Canceling terms and expanding, this reduces to

$$\begin{aligned}\frac{g}{r_S r_R}\frac{d}{dr}\left(r\alpha(r)\right) &= \frac{1}{r}\left(1+\frac{g}{r_S r_R}\int_{r_R}^{r}\alpha(r')dr'\right)\\ \frac{d}{dr}(r\alpha) &= \frac{1}{r}\frac{r_S r_R}{g}+\frac{\int_{r_R}^{r}\alpha(r')dr'}{r}\\ r\alpha+r^2\frac{d\alpha}{dr} &= \frac{r_S r_R}{g}+\int_{r_R}^{r}\alpha(r')dr'.\end{aligned}$$

Differentiating this last expression with respect to r and rearranging, the differential equation

$$\alpha+r\frac{d\alpha}{dr}+2r\frac{d\alpha}{dr}+r^2\frac{d^2\alpha}{dr^2}=\alpha$$

is obtained, or

$$\frac{d^2\alpha}{dr^2}+\frac{3}{r}\frac{d\alpha}{dr}=0.$$

Solving this differential equation for $d\alpha/dr$ results in

$$\frac{d\alpha}{dr}=c_1 e^{-\int_{r_R}^{r}(3/r')dr'}=c_1 e^{-3\ln(r/r_R)}$$

and therefore

$$\alpha(r)=c_1\int_{r_R}^{r}e^{-3\ln(r'/r_R)}dr'+c_2. \tag{4.18}$$

The condition $\alpha(r_R)=0$ forces $c_2=0$ and $\alpha(r_S)=1$ requires that

$$c_1=\frac{1}{\int_{r_R}^{r_S}e^{-3\ln(r'/r_R)}dr'}\approx\frac{1}{g}.$$

This approximation follows from the assumption of a small air gap as

$$\ln(r/r_R)\approx\ln(1)=0 \quad \text{for } r_R<r<r_S \tag{4.19}$$

so that

$$\int_{r_R}^{r_S}e^{-3\ln(r'/r_R)}dr'\approx\int_{r_R}^{r_S}1dr'=r_S-r_R=g.$$

Substitution of $c_1=1/g, c_2=0$ into (4.18) and invoking the approximation (4.19) gives

$$\begin{aligned}\alpha(r) &= \frac{1}{g}\int_{r_R}^{r}e^{-3\ln(r'/r_R)}dr'\\ &\approx \frac{1}{g}\int_{r_R}^{r}1dr'\\ &= \frac{r-r_R}{g}.\end{aligned}$$

In other words, $\alpha(r)$ is approximately a linear function of r in the air gap. Such a linear dependence is pointed out by C. B. Gray [5].

www.EngineeringEBooksPdf.com

4.7.1 *Electric Field* $\vec{\mathbf{E}}_{Sa}$

The axial electric field produced by the magnetic field $\vec{\mathbf{B}}_{Sa}$ is now computed. Recall that the magnetic field is given by

$$\begin{aligned}\vec{\mathbf{B}}_{Sa} &= \frac{\mu_0 \ell_2 N_S}{4g} i_{Sa} \frac{\cos(\theta)}{r} \left(1 + \frac{g}{r_S r_R} \int_{r_R}^{r} \alpha(r')dr'\right)\hat{\mathbf{r}} \\ &\quad - \frac{\mu_0 \ell_2 N_S}{4g} \frac{g}{r_S r_R} \alpha(r) i_{Sa} \sin(\theta)\hat{\boldsymbol{\theta}}.\end{aligned}$$

The electric field induced by this changing magnetic field is found by solving

$$\nabla \times \vec{\mathbf{E}}_{Sa} = -\frac{\partial \vec{\mathbf{B}}_{Sa}}{\partial t}. \tag{4.20}$$

In cylindrical coordinates, the curl of $\vec{\mathbf{E}}$ is given by

$$\nabla \times \vec{\mathbf{E}} = \left(\frac{1}{r}\frac{\partial E_z}{\partial \theta} - \frac{\partial E_\theta}{\partial z}\right)\hat{\mathbf{r}} + \left(\frac{\partial E_r}{\partial z} - \frac{\partial E_z}{\partial r}\right)\hat{\boldsymbol{\theta}} + \frac{1}{r}\left(\frac{\partial}{\partial r}(rE_\theta) - \frac{\partial E_r}{\partial \theta}\right)\hat{\mathbf{z}}.$$

By the usual symmetry assumptions

$$\frac{\partial E_{Sa\theta}}{\partial z} = 0, \quad \frac{\partial E_{Sar}}{\partial z} = 0 \tag{4.21}$$

and, as the z component of $\vec{\mathbf{B}}_{Sa}$ is zero (i.e., $B_{Saz} \equiv 0$), it follows that

$$\frac{\partial}{\partial r}(rE_{Sa\theta}) - \frac{\partial E_{Sar}}{\partial \theta} \equiv 0. \tag{4.22}$$

Then (4.20) reduces to

$$\nabla \times \vec{\mathbf{E}}_{Sa} = \frac{1}{r}\frac{\partial E_{Saz}}{\partial \theta}\hat{\mathbf{r}} - \frac{\partial E_{Saz}}{\partial r}\hat{\boldsymbol{\theta}} = -\frac{\partial B_{Sar}}{\partial t}\hat{\mathbf{r}} - \frac{\partial B_{Sa\theta}}{\partial t}\hat{\boldsymbol{\theta}}. \tag{4.23}$$

The simplest solution is one of the form

$$\vec{\mathbf{E}}_{Sa} = E_{Saz}\hat{\mathbf{z}},$$

that is, where $E_{Sar} = E_{Sa\theta} \equiv 0$ so that the conditions (4.21) and (4.22) are automatically satisfied.

Solving equation (4.23), one obtains

$$\begin{aligned}\vec{\mathbf{E}}_{Sa} &= E_{Saz}\hat{\mathbf{z}} = -\frac{\mu_0 r_R N_S}{2g}\frac{di_{Sa}}{dt}\sin(\theta)\left(1 + \frac{g}{r_S r_R}\int_{r_R}^{r}\alpha(r')dr'\right)\hat{\mathbf{z}} \\ &\approx -\frac{\mu_0 r_R N_S}{2g}\frac{di_{Sa}}{dt}\sin(\theta)\left(1 + \frac{(r-r_R)^2}{2r_S r_R}\right)\hat{\mathbf{z}} \\ &\approx -\frac{\mu_0 r_R N_S}{2g}\frac{di_{Sa}}{dt}\sin(\theta)\hat{\mathbf{z}}.\end{aligned}$$

www.EngineeringEBooksPdf.com

4.7.2 The Magnetic and Electric Fields $\vec{\mathbf{B}}_{Sa}, \vec{\mathbf{E}}_{Sa}, \vec{\mathbf{B}}_{Sb}, \vec{\mathbf{E}}_{Sb}$

The magnetic and electric fields due to the current in phase b are found from their corresponding expressions for phase a by simply replacing θ by $\theta - \pi/2$.

In summary, given two sinusoidally distributed stator windings a and b wound 90 degrees apart, the magnetic and electric fields in the air gap produced by the phase currents i_{Sa}, i_{Sb} in the phase a and b, respectively, are given by

$$\begin{aligned}
\vec{\mathbf{B}}_{Sa} &= \frac{\mu_0 \ell_2 N_S}{4g} i_{Sa} \frac{\cos(\theta)}{r} \left(1 + \frac{g}{r_S r_R} \int_{r_R}^{r} \alpha(r')dr'\right)\hat{\mathbf{r}} \\
&\quad - \frac{\mu_0 \ell_2 N_S}{4g} \frac{g}{r_S r_R} \alpha(r) i_{Sa} \sin(\theta)\hat{\boldsymbol{\theta}} \\
\vec{\mathbf{E}}_{Sa} &= E_{Saz}\hat{\mathbf{z}} = -\frac{\mu_0 r_R N_S}{2g} \frac{di_{Sa}}{dt} \sin(\theta) \left(1 + \frac{g}{r_S r_R} \int_{r_R}^{r} \alpha(r')dr'\right)\hat{\mathbf{z}}
\end{aligned} \tag{4.24}$$

and

$$\begin{aligned}
\vec{\mathbf{B}}_{Sb} &= \frac{\mu_0 r_R N_S}{2g} i_{Sb} \frac{\sin(\theta)}{r} \left(1 + \frac{g}{r_S r_R} \int_{r_R}^{r} \alpha(r')dr'\right)\hat{\mathbf{r}} \\
&\quad + \frac{\mu_0 r_R N_S}{2g} \frac{g}{r_S r_R} \alpha(r) i_{Sb} \cos(\theta)\hat{\boldsymbol{\theta}} \\
\vec{\mathbf{E}}_{Sb} &= E_{Sbz}\hat{\mathbf{z}} = \frac{\mu_0 r_R N_S}{2g} \frac{di_{Sb}}{dt} \cos(\theta) \left(1 + \frac{g}{r_S r_R} \int_{r_R}^{r} \alpha(r')dr'\right)\hat{\mathbf{z}}.
\end{aligned} \tag{4.25}$$

With $i_{Sa}(t) = I_S \cos(\omega_S t)$, $i_{Sb}(t) = I_S \sin(\omega_S t)$ and $\alpha \equiv 0$, the expressions (4.24) and (4.25) simplify to

$$\begin{aligned}
\vec{\mathbf{B}}_S(r, \theta, t) &= \frac{\mu_0 r_R N_S I_S}{2g} \frac{1}{r} \cos(\theta - \omega_S t)\hat{\mathbf{r}} \\
\vec{\mathbf{E}}_S(\theta, t) &= \omega_S \frac{\mu_0 r_R N_S I_S}{2g} \cos(\theta - \omega_S t)\hat{\mathbf{z}}.
\end{aligned} \tag{4.26}$$

Remark

Note that at $r = r_R$, the expressions for the electric and magnetic fields given by (4.24) and (4.25) reduce to their approximate values (i.e., taking $\alpha \equiv 0$). Consequently, the induced emfs in the rotor loops are not affected by neglecting the azimuthal magnetic fields.

www.EngineeringEBooksPdf.com

Problems

Problem 1 A Two-Phase Stator with Single-Loop Windings

(a) Consider the simple single-loop stator phase shown in Figure 4.23. Show that in the air gap, the magnetic intensity $H(\theta)$ in the radial direction satisfies

$$H(\theta) = \begin{cases} H_1 & for \quad -\pi/2 < \theta < \pi/2 \\ H_2 & for \quad +\pi/2 < \theta < 3\pi/2 \end{cases}$$

where H_1, H_2 are constants and assuming H is constant as a function of r across the air gap. (Hint: Apply Ampère's law to the path $a-b-c-d-a$ to show that $H(\theta) = H_1$ for $-\pi/2 < \theta < \pi/2$, etc.).

(b) Applying Ampère's law to the path $1-2-3-4-1$ in Figure 4.23(a) along with a symmetry argument to show that $H_2 = -H_1$.

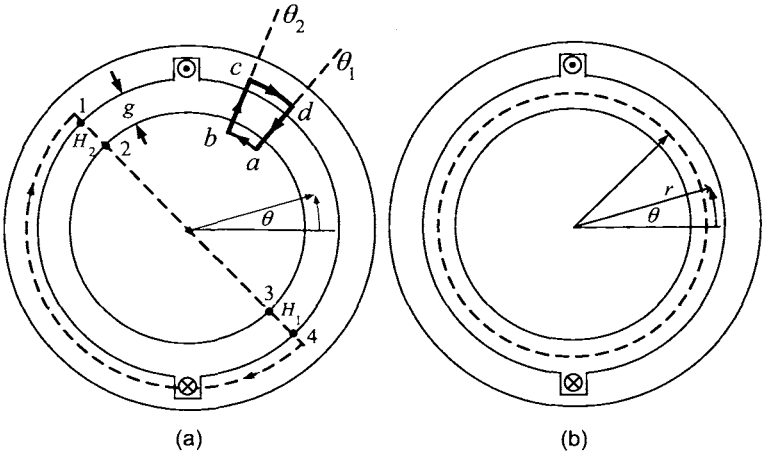


FIGURE 4.23. Single-loop stator phase. (a) Paths for Ampère's law. (b) Flux surface in the air gap. The closed flux surface completely contains the rotor.

(c) Alternatively, rather than using Ampère's law as in part (b), use Gauss's law applied to the surface shown in Figure 4.23(b) to obtain $H_2 = -H_1$.

(d) Give an explicit expression for $\vec{\mathbf{B}}$ in the air gap as a function of θ in terms of the current i in the winding and the air gap length g. Recall that $\vec{\mathbf{B}} = \mu_0 \vec{\mathbf{H}}$ in the air gap. This is said to be a uniformly *distributed magnetic field in θ.*

(e) Show that by multiplying the answer for $\vec{\mathbf{B}}$ in part (d) by r_R/r results in the magnetic field satisfying Gauss's law for closed surfaces in the air gap as in Figure 4.12.

(f) Consider a simple two-phase machine as in Figure 4.24.

www.EngineeringEBooksPdf.com

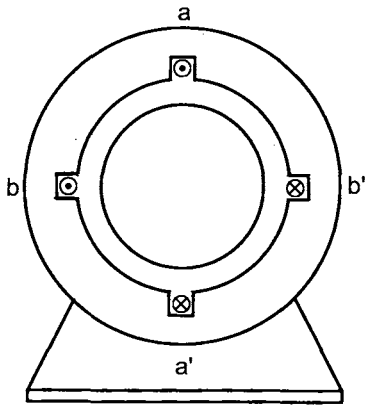


FIGURE 4.24. Simple two-phase machine.

Let the phase currents i_{Sa}, i_{Sb} be periodic with period T as given in Figure 4.25. Show that the magnetic axis of the stator's magnetic field can assume only four angular positions. What are they? In particular, plot the radial air-gap magnetic field for $0 \leq \theta \leq 2\pi$ at $t = 0, T/4, T/2,$ and $3T/4$.

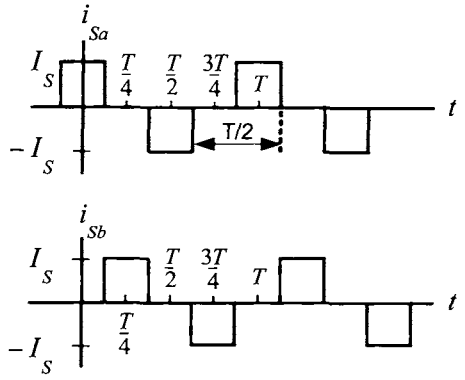


FIGURE 4.25. Periodic square-wave currents.

(g) Repeat part (f) where the phase currents i_{Sa}, i_{Sb} are again periodic with period T with their waveforms as given in Figure 4.26. Show that the magnetic axis of the stator's magnetic field can assume only four angular positions. What are they? In particular, plot the radial air-gap magnetic field for $0 \leq \theta \leq 2\pi$ at $t = T/8, 3T/8, 5T/8,$ and $7T/8$.

www.EngineeringEBooksPdf.com

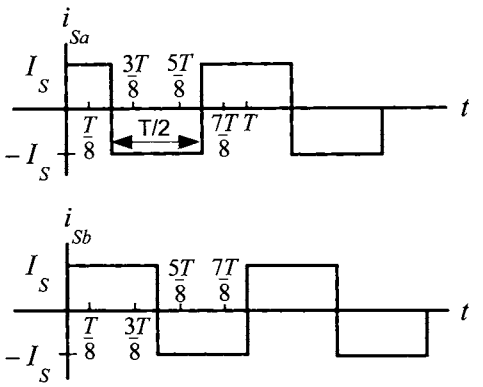


FIGURE 4.26. Periodic square-wave phase currents.

Problem 2 Fourier Series Expansion

Consider the function $F'(\theta')$ shown in Figure 4.27.

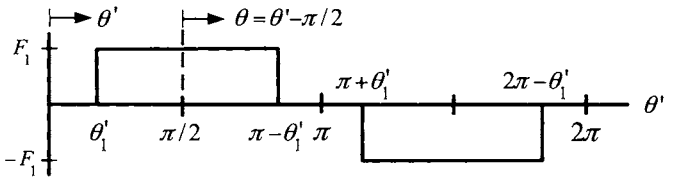


FIGURE 4.27. $F'(\theta')$ versus θ'.

(a) Show that the Fourier series expansion of this function is

$$F'(\theta') = \frac{4}{\pi} F_1 \times \sum_{k=1,3,5,\ldots}^{\infty} \frac{1}{k} \cos(k\theta'_1) \sin(k\theta'). \tag{4.27}$$

(b) With respect to the angle $\theta \triangleq \theta' - \pi/2$, show that (4.27) becomes

$$F(\theta) \triangleq F'(\theta + \pi/2) = \frac{4}{\pi} \times \sum_{k=1,3,5,\ldots}^{\infty} F_1 \frac{1}{k} \cos(k\theta'_1) \sin(k(\theta + \pi/2)).$$

(c) Use the result of part (b) to show that the Fourier series expansion of the function in Figure 4.28 is

$$F(\theta) = \frac{4}{\pi} \sum_{k=1,3,5,\cdots}^{\infty} \frac{1}{k} \left(F_1 \cos(k\theta'_1) + F_2 \cos(k\theta'_2) + F_3 \cos(k\theta'_3) \right) \sin\left(k\left(\theta + \frac{\pi}{2} \right) \right).$$

www.EngineeringEBooksPdf.com

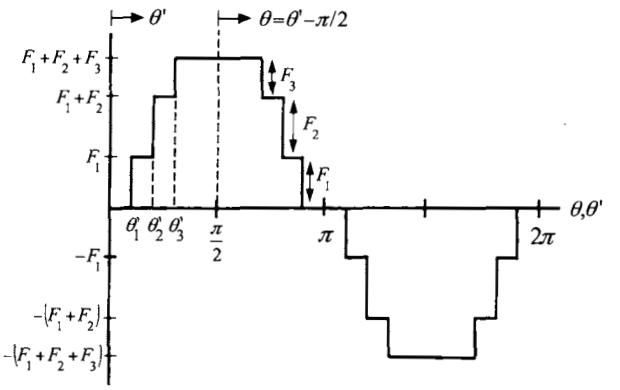


FIGURE 4.28. $F(\theta), F'(\theta')$.

(d) Show that

$$\sin\left(k(\theta+\pi/2)\right) = \begin{cases} \cos(k\theta) & \text{for} \quad k = 6m-1 \text{ where } m = 1,2,\ldots \\ -\cos(k\theta) & \text{for} \quad k = 6m+1 \text{ where } m = 1,2,\ldots \end{cases}$$

Problem 3 Two-Level Approximate Sinusoidal Winding

Apply the results of problem 2 (with $F_3 = 0$ or $\theta_3 = \pi/2$) to derive the Fourier expansion given in equation (4.3).

Problem 4 Three-Level Approximate Sinusoidal Winding

Consider the approximate sinusoidal winding of Figure 4.29(a) in which a single phase is wound such that there is one loop at $\pi/6$, two loops at $\pi/3$, three loops at $\pi/2$, two loops at $2\pi/3$, and one loop at $5\pi/6$.

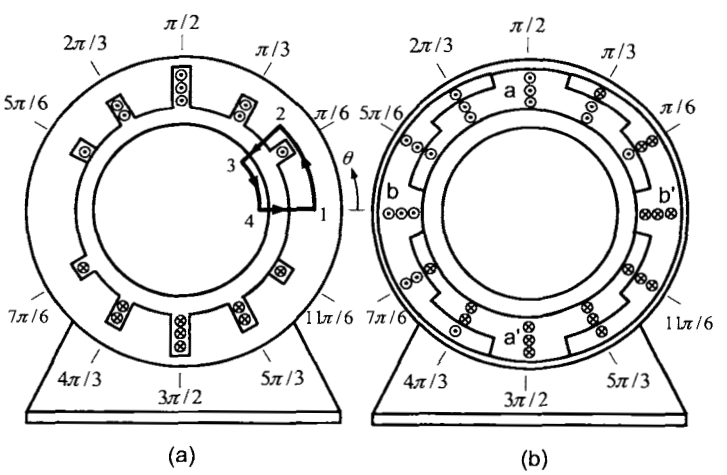


FIGURE 4.29. Approximately sinusoidally wound two-phase stator.

www.EngineeringEBooksPdf.com

(a) Find the enclosed current $i_{enclosed}$ between 0 and θ for $0 \leq \theta \leq 2\pi$.

(b) Assuming $\vec{\mathbf{H}}$ is constant across the air gap and the windings/loops have an infinitesimal cross section, show that a straightforward application of Ampère's law gives $H_{Sa}(\theta) = H_{Sa}(0) - i_{enclosed}(\theta)/g$. Use conservation of flux to find $H_{Sa}(0)$. Show that $B_{Sa}(\theta) = \mu_0 H_{Sa}(\theta)$ is given by the plot in Figure 4.11.

(c) With $B_{Sa}(r,\theta) = \mu_0(r_R/r)H_{Sa}(\theta)$ as given in Figure 4.11, use the results of problem 2 to show that the Fourier series expansion of $B_{Sa}(r,\theta)$ in θ is

$$B_{Sa}(r,\theta) = \mu_0 \frac{i_{Sa}}{g}\frac{4}{\pi}\frac{r_R}{r}$$
$$\times \sum_{k=1,3,5,\ldots}^{\infty} \frac{1}{k}\left(\frac{3}{2}\cos(0) + 2\cos(k\pi/6) + \cos(k\pi/3)\right)\sin(k(\theta+\pi/2) \quad (4.28)$$

(d) Let b_k be the coefficient of $\sin(k(\theta+\pi/2)$ in the Fourier expansion of $B_{Sa}(r,\theta)/\left(\mu_0\frac{i_{Sa}}{g}\frac{r_R}{r}\right)$ in equation (4.28) and let a_k be the coefficient of $\sin(k(\theta+\pi/2)$ in the Fourier expansion of $B_{Sa}(\theta)/(\mu_0 i_{Sa}/g)$ in equation (4.3). With $a_{\max} = \max_{k=1,\ldots,15}\{a_k\}, b_{\max} = \max_{k=1,\ldots,15}\{b_k\}$, plot the relative harmonic content $a_k/a_{\max}$ and $b_k/b_{\max}$ as a function of k for $k = 1, 2, \ldots, 15$ on separate figures. Note that $a_{\max} = a_1, b_{\max} = b_1$; that is, the maximum is achieved at the fundamental for both expansions. Compute b_1/a_1.

(e) Finally, plot $a_k/a_{\max} - b_k/b_{\max}$ for $k = 1, 2, 3, \ldots, 15$. What is the value of this difference for $k = 5, 7, 11, 13$? What is this difference for $k = 3, 9, 15$?

Comments: Note the reduction in relative harmonic content is only for the triplen harmonics. Also, the fact that $b_1 = 2a_1$ means that, for the same phase current, the number of turns in this (three-level) approximate sinusoidal winding results in doubling the strength of the magnetic field in the air gap compared to the approximate sinusoidal winding with only two levels.

(f) Consider using the winding of Figure 4.29(a) in a two-phase machine as shown in Figure 4.29(b). Use the solution of part (c) to write down the expression for the radial magnetic field in the air gap due to the current i_{Sb} in stator phase b.

Problem 5 Gauss's Law

Show that the expression [see equation (4.6)]

$$\vec{\mathbf{B}}_{Sa}(r,\theta) = B_{Sa}(r,\theta)\hat{\mathbf{r}} = \mu_0\frac{r_R}{r}\left(\frac{2i_{Sa}}{g} - \frac{i_{enclosed}(\theta)}{g}\right)\hat{\mathbf{r}}$$

for the magnetic field due to the current in an approximate sinusoidal winding satisfies $\oint \vec{\mathbf{B}} \cdot d\vec{\mathbf{S}} = 0$ for the flux surface given in Figure 4.12.

www.EngineeringEBooksPdf.com

Problem 6 Three-Phase Stator and Spatial Harmonics

Figure 4.30(a) shows a machine with both a three-phase stator and a three-phase rotor. Figure 4.30(b) gives more detail of stator phase $1'-1$ where it is shown that one side of a loop is wound at $\pi/3$ (the other side at $4\pi/3$), two loop sides are wound at $\pi/2$ (the other two sides at $3\pi/2$), and, finally, one side of a loop is wound at $2\pi/3$ (the other side at $5\pi/3$).

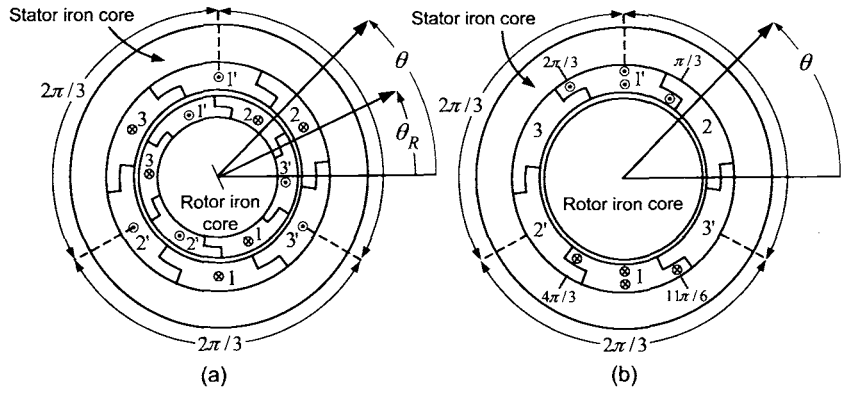


FIGURE 4.30. (a) Three-phase stator and rotor. (b) Three-phase stator with an iron core rotor. Windings shown for stator phase a only.

With the assumptions that the conductors have an infinitesimal cross section, the iron has infinite permeability (i.e., $\vec{\mathbf{H}} = 0$ in the iron), and the air gap is small, Ampère's law was used to show that the radial magnetic field in the air gap produced by the current i_{S1} in phase $1'-1$ is given by [see equation (4.3)]

$$B_{S_1}(i_{S1},\theta) = \mu_0 \frac{i_{S1}}{g}\frac{4}{\pi} \times \sum_{k=1,3,5,\ldots}^{\infty} \frac{\left(1+\cos(\frac{k\pi}{6})\right)}{k} \sin\Big(k(\theta+\frac{\pi}{2})\Big)$$

Let $B_{S_1}(i_{S1},r,\theta) \triangleq (r_R/r)\, B_{S_1}(i_{S1},\theta)$ and similarly for $B_{S_2}(i_{S2},r,\theta)$ and $B_{S_3}(i_{S3},r,\theta)$ so that

$$B_{S_1}(i_{S1},r,\theta) = \mu_0 \frac{i_{S1}}{g}\frac{4}{\pi}\frac{r_R}{r} \times \sum_{k=1,3,5,\ldots}^{\infty} \frac{\left(1+\cos(\frac{k\pi}{6})\right)}{k} \sin\Big(k(\theta+\frac{\pi}{2})\Big)$$

$$B_{S_2}(i_{S2},r,\theta) = \mu_0 \frac{i_{S2}}{g}\frac{4}{\pi}\frac{r_R}{r} \times \sum_{k=1,3,5,\ldots}^{\infty} \frac{\left(1+\cos(\frac{k\pi}{6})\right)}{k} \sin\Big(k(\theta-\frac{2\pi}{3}+\frac{\pi}{2})\Big)$$

$$B_{S_3}(i_{S3},r,\theta) = \mu_0 \frac{i_{S3}}{g}\frac{4}{\pi}\frac{r_R}{r} \times \sum_{k=1,3,5,\ldots}^{\infty} \frac{\left(1+\cos(\frac{k\pi}{6})\right)}{k} \sin\Big(k(\theta-\frac{4\pi}{3}+\frac{\pi}{2})\Big).$$

www.EngineeringEBooksPdf.com

(a) With the currents balanced, i.e., $i_{S1} + i_{S2} + i_{S3} \equiv 0$, *show that in the Fourier expansion of the total radial magnetic field*

$$\vec{\mathbf{B}}_S = \vec{\mathbf{B}}_{S_1} + \vec{\mathbf{B}}_{S_2} + \vec{\mathbf{B}}_{S_3}$$

the triplen harmonics are zero. (The triplen harmonics are the harmonic terms of order k *with* $k = 3m, m = 1, 2, \ldots$*)*

(b) Explain why the phase winding of Figure 4.3(b) is really more suited for a three-phase machine rather than a two phase machine. What about the winding of Figure 4.29 (see problem 4)?

(c) Let

$$i_{S1} = I_S \cos(\omega_S t), i_{S2} = I_S \cos(\omega_S t - 2\pi/3), i_{S3} = I_S \cos(\omega_S t - 4\pi/3)$$

in the above expressions for the magnetic fields. Show that the 5*th harmonic component of* $\vec{\mathbf{B}}_S$ *given by*

$$\vec{\mathbf{B}}_{S5}(r, \theta, t) \triangleq \vec{\mathbf{B}}_{S_15}(i_{S1}, r, \theta) + \vec{\mathbf{B}}_{S_25}(i_{S2}, r, \theta) + \vec{\mathbf{B}}_{S_35}(i_{S3}, r, \theta)$$

is a rotating magnetic field in the clockwise (negative) direction at angular speed $-\omega_S/5$. *(Here* $\vec{\mathbf{B}}_{S_15}$ *is the* $k = 5$ *term in the above Fourier series expansion of* $\vec{\mathbf{B}}_{S_1}$*, etc.)*

(d) Repeat part (c) for the 7*th harmonic* $\vec{\mathbf{B}}_{S7}(r, \theta, t)$ *of* $\vec{\mathbf{B}}_S$. *What direction does it rotate? At what angular speed?*

Problem 7 Self-Inductance of a Distributed Winding

Consider the stator phase winding shown in Figure 4.3(b) and redrawn in Figure 4.31. The radial magnetic field due to the current in the phase is shown in Figure 4.10.

(a) Using flux surfaces similar to those of Figure 4.20, compute the total flux linkage in the stator phase winding due to the current in the phase.

(b) What is the self-inductance of the stator phase?

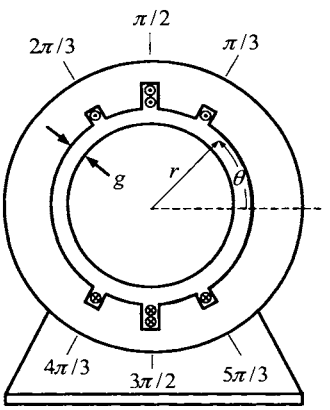


FIGURE 4.31. Computation of the self-inductance of a distributed winding.

www.EngineeringEBooksPdf.com

Problem 8 Flux Linkage

Figure 4.32 shows a motor with a permanent magnet rotor which has a single stator phase wound as in Figure 4.3(b). Let the magnetic field in the air gap due to the permanent magnet rotor be given by

$$\vec{\mathbf{B}}_R(\theta - \theta_R) = B_{max}\frac{r_R}{r}\cos(\theta - \theta_R)\hat{\mathbf{r}}.$$

(a) Compute the flux in each loop and the total flux linkage in the stator phase.

(b) Find an expression for the emf induced in the stator phase by the PM rotor.

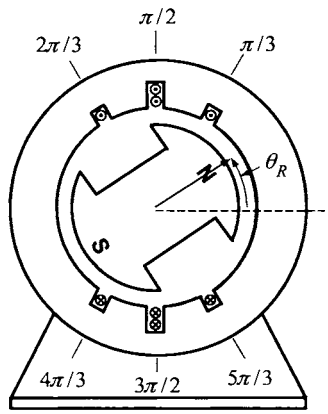


FIGURE 4.32. A motor with a PM rotor and a single rotor phase.

Problem 9 A Two-Phase Machine [4]

Consider a machine with two stator phases wound as shown in Figure 4.33. That is, phase a has one turn at $\pi/4$ (with its other side at $5\pi/4$), two turns at $5\pi/12$ (with the other sides at $17\pi/12$), and so on. Let the current in phase a be denoted as i_{Sa} and the current in phase b be denoted as i_{Sb}.

(a) Compute the radial magnetic field $\vec{\mathbf{B}}_{Sa}$ in the air gap due to the current i_{Sa} in phase a. Express it as a Fourier series.

(b) Compute the flux linkage in phase a due to $\vec{\mathbf{B}}_{Sa}$.

(c) Compute the flux linkage in phase b due to $\vec{\mathbf{B}}_{Sa}$.

(d) Compute the Fourier series expansion of the expression for the magnetic field in part (a).

(e) Compute the ratio of the fundamental of the magnetic field given in part (d) to the fundamental of the magnetic field whose Fourier series is given in equation (4.3) for the winding of Figure 4.7. Also, compute the ratio of the 3rd harmonic to the 1st harmonic for the magnetic field given in part (d) and then compare it to the corresponding ratio for the magnetic

www.EngineeringEBooksPdf.com

field of equation (4.3). Is the winding of Figure 4.33 or the winding of Figure 4.7 better suited for a two phase machine? Explain.

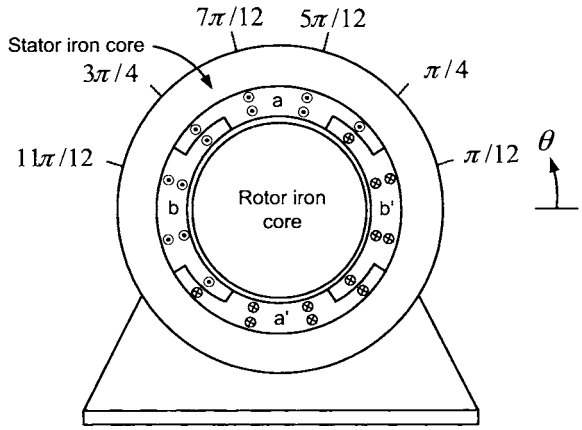


FIGURE 4.33. Stator phases for a single pole pair two-phase machine.

Problem 10 Uniformly Distributed Winding

Consider a machine with a three-phase stator and a rotor of soft iron as shown in Figure 4.34. There are three sets of windings which are uniformly wound on the inside surface of the stator. By uniformly *wound, it is meant that the number of turns between θ and $\theta+d\theta$ is constant independent of the angle θ. Phase 1 with current i_{S1} has its turns uniformly wound between $\pi/3$ and $2\pi/3$ on one side of the stator's inside surface and between $4\pi/3$ and $5\pi/3$ on the other side of the stator. Similarly, phase 2 with current i_{S2} has its turns uniformly wound between π and $4\pi/3$, and between 0 and $\pi/3$. Phase 3 with current i_{S3} has its turns uniformly wound between $2\pi/3$ and π, and between $5\pi/3$ and 2π.*

Let the turns density for stator phase 1 be given by

$$N_{S1}(\theta) = \begin{cases} \dfrac{N_S}{\pi/3} & \text{for} \quad \dfrac{\pi}{3} \le \theta \le \dfrac{2\pi}{3} \\ \dfrac{N_S}{\pi/3} & \text{for} \quad \dfrac{4\pi}{3} \le \theta \le \dfrac{5\pi}{3} \\ 0 & \text{elsewhere.} \end{cases}$$

The total number of windings (turns or loops) making up phase 1 is then

$$\int_{\pi/3}^{2\pi/3} \frac{N_S}{\pi/3} d\theta = N_S.$$

Compute the radial magnetic field $\vec{\mathbf{B}}_{S1}$ in the air gap produced by the current i_{S1} in phase 1.

www.EngineeringEBooksPdf.com

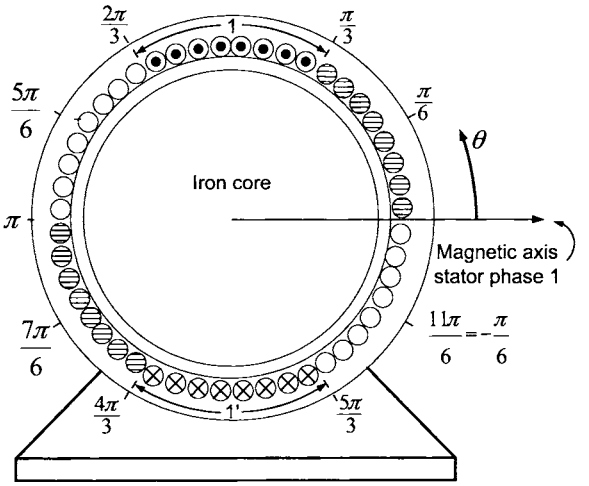


FIGURE 4.34. Uniformly distributed windings.

Problem 11 Modifying Ampère's Law to Account for a r_0/r Dependence

This problem considers how Ampère's law changes when H_{Sa} is assumed to have a factor of the form r_0/r so that conservation of flux holds. Specifically, in Ampère's law as given by equation (4.9), replace $H_{Sa}(i_{Sa}, \theta)$ by

$$H_{Sa}(i_{Sa}, r, \theta) \triangleq (r_0/r) H_{Sa}(i_{Sa}, \theta) \tag{4.29}$$

to obtain

$$\int_{r=r_R}^{r=r_S} H_{Sa}(i_{Sa}, r, 0)\hat{\mathbf{r}} \cdot (dr\hat{\mathbf{r}}) + \int_{r=r_R}^{r=r_S} H_{Sa}(i_{Sa}, r, \theta)\hat{\mathbf{r}} \cdot (-dr\hat{\mathbf{r}})$$
$$= -\frac{N_S i_{Sa}}{2}\cos(\theta) + \frac{N_S i_{Sa}}{2}. \tag{4.30}$$

(a) Show that for the expression

$$\vec{\mathbf{H}}_{Sa}(i_{Sa}, r, \theta) = \frac{N_S}{2g}\frac{r_0}{r} i_{Sa}\cos(\theta)\hat{\mathbf{r}}$$

to still work out the same way as before, that is, for (4.30) to reduce to

$$H_{Sa}(i_{Sa}, r_0, 0)g - H_{Sa}(i_{Sa}, r_0, \theta)g = -i_{Sa}\frac{N_S}{2}\cos(\theta) + i_{Sa}\frac{N_S}{2},$$

then r_0 must be chosen such that $\int_{r=r_R}^{r=r_S} r_0/r dr = g$.

(b) Show that there is an r_0 with $r_R < r_0 < r_S$ such that $\int_{r=r_R}^{r=r_S} r_0/r dr = g$ holds.

(c) Show that (4.30) holds approximately with H_{Sa} given by (4.29) if $r_0 = r_R$ (or $r_0 = r_S$) and $g << r_R$.

www.EngineeringEBooksPdf.com

Problem 12 Three-Phase, Four-Pole, 36-Slot Stator

Consider a three-phase, four-pole, 36-slot stator as shown in Figure 4.35. The figure illustrates the slots in which the wire making up phase 1 *is wound with the (angular) location of the windings as indicated in the figure. Denote the current in this phase as* i_{S1}.

(a) Assuming that the cross-sectional area of the slots is infinitesimal, compute the radial magnetic field B_{S1} *in the air gap produced by* i_{S1} *and plot it as a function of* θ.

(b) Compute the Fourier series expansion of the radial air-gap magnetic field B_{S1} *found in part (a).*

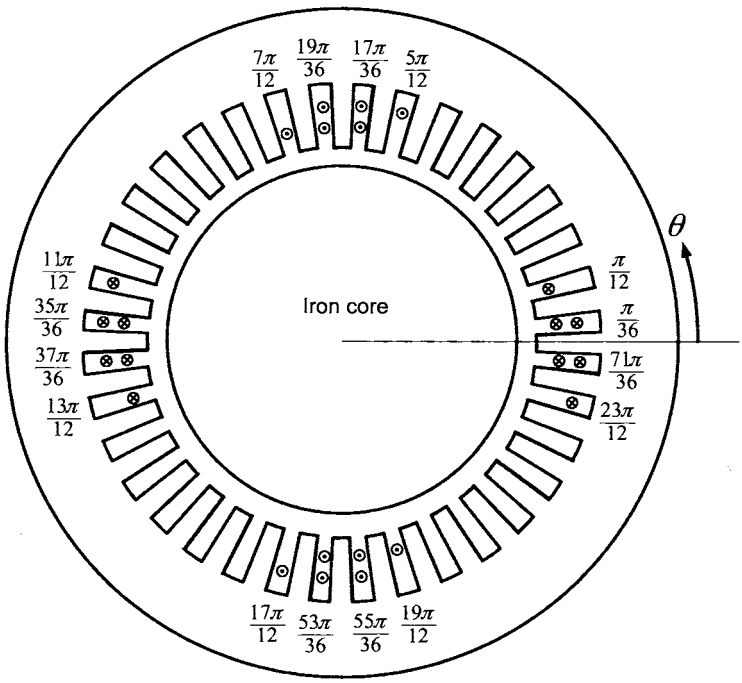


FIGURE 4.35. A three-phase, four-pole, 36-slot stator. Only the winding of stator phase 1 is shown.

www.EngineeringEBooksPdf.com

Problem 13 Three-Phase Six-Pole Permanent Magnet Machine

Figure 4.36 shows a three-phase, six-pole machine with a permanent magnet rotor. Take $\theta_R = 0$ *for the rotor in the position as drawn. Let the magnetic field in the air gap due to the permanent magnet rotor be given by*

$$\vec{\mathbf{B}}_R(r,\theta) = B_{R\max}\frac{r_R}{r}\cos\Big(n_p(\theta-\theta_R)\Big)$$

where n_p *is the number of pole pairs that in this case is* $n_p = 3$. *Phase* 1 *of the stator consists of connecting the three single-loop windings* $a_1 - a_1'$, $a_2 - a_2'$, *and* $a_3 - a_3'$ *in series as shown. Each winding encloses a cylindrical-shaped surface spanning* $\pi/3$ *radians (or* $60°$*).*

(a) Compute the flux linkage λ_{S1} *in the phase winding* 1 *due to the magnetic field of the rotor as a function of the rotor position* θ_R.

(b) Compute the induced voltage in the phase winding 1 *due to the magnetic field of the rotor as a function of the rotor position* θ_R *and the rotor speed* ω_R.

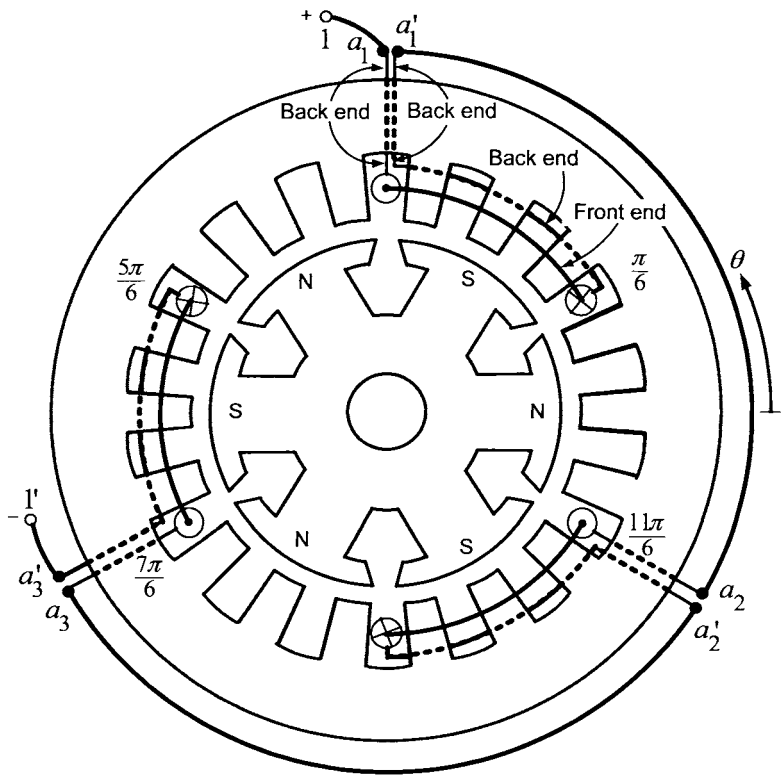


FIGURE 4.36. A three-phase, six-pole permanent magnet machine.

www.EngineeringEBooksPdf.com

Problem 14 Flux Linkage in a Phase Winding with Short-Pitched Turns

Figure 4.37 shows a motor with a PM rotor and a single stator phase whose turns are short-pitched. By "short-pitched" is meant that each turn does not span 180° *degrees, but rather less than* 180° *such as in this problem where they span only* 150°. *The first loop has axial sides* a_1 *and* a_1', *the second loop has axial sides* a_2 *and* a_2', *and so on. Let the magnetic field in the air gap due to the permanent magnet rotor be given by*

$$\vec{\mathbf{B}}_R(\theta - \theta_R) = B_{max}\frac{r_R}{r}\cos(\theta - \theta_R)\hat{\mathbf{r}}.$$

In order to illustrate the windings of a short-pitched phase, Figure 4.38 shows the slots of a cylindrical rotor iron core being wound with four short-pitched turns. The short-pitched windings of the stator phase of Figure 4.37 are wound similarly.

(a) Compute the flux in each loop using a surface normal for whose direction is chosen so that the positive direction of travel around the surface coincides with the direction of positive current flow as given in Figure 4.37.

(b) Compute the flux linkage in the stator phase produced the rotor's magnetic field.

(c) Using Faraday's law, compute the induced emf in the stator phase due to the rotor's magnetic field.

(d) How do the answers to parts (a), (b), and (c) compare to the corresponding values for the full-pitch wound stator of problem 8?

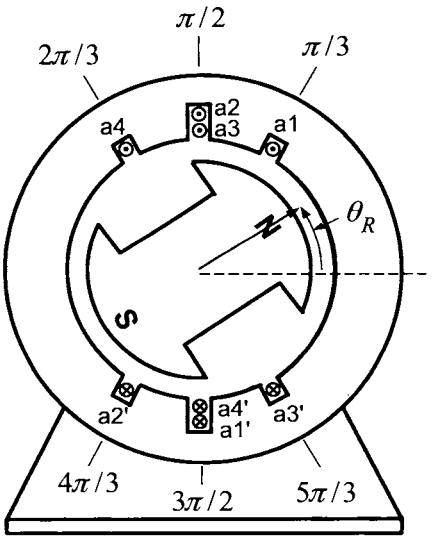


FIGURE 4.37. A short-pitched stator winding.

www.EngineeringEBooksPdf.com

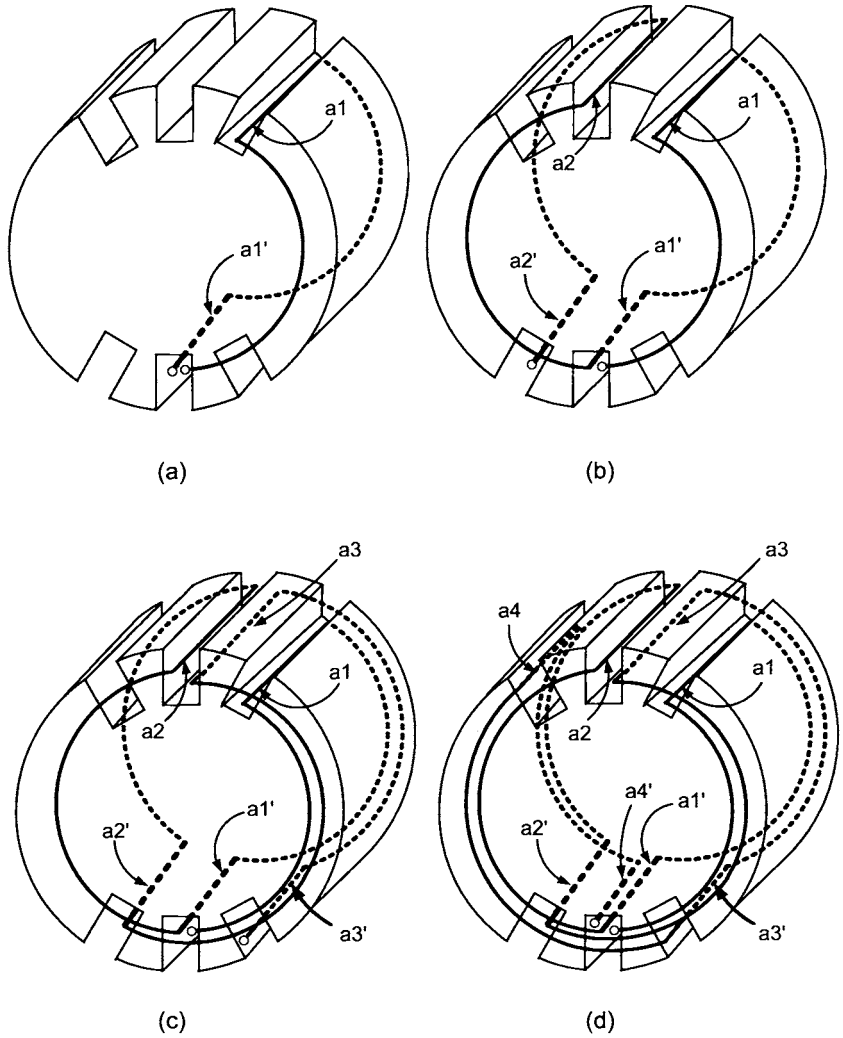


FIGURE 4.38. Illustration of winding a distributed rotor phase with short-pitched windings. (a) First loop with axial sides a_1 and a_1'. (b) Second loop with axial sides a_2 and a_2'. (c) Third loop with axial sides a_3 and a_3'. (d) Fourth loop with axial sides a_4 and a_4'.

www.EngineeringEBooksPdf.com

Problem 15 Self-Inductance of a Short-Pitched Phase Winding

Figure 4.39 shows a single stator phase with short-pitched windings (see problem 14 for an explanation of short-pitched windings).

(a) Explain why the radial magnetic field is identical to that drawn in Figure 4.10.

(b) Compute the flux in each loop due to the current in that loop and then the total flux linkage. To ensure that the induced emfs in each loop have the same sign conventions, choose a flux surface normal whose positive direction of travel around the surface coincides with the positive direction of current.

(c) What is the self-inductance of the stator phase? How does it compare with the self-inductance of the stator phase in problem 7?

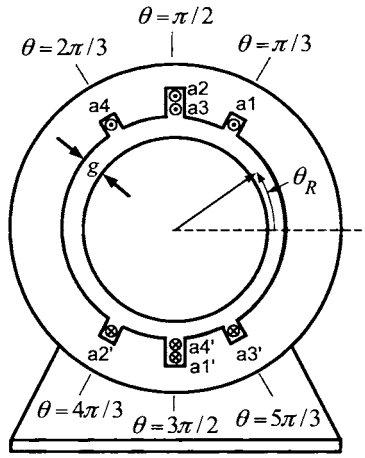


FIGURE 4.39. Self-inductance for a distributed phase winding with fractional pitch turns.

Problem 16 "Long-Pitched" Phase Winding

Consider Figure 4.39 where now each winding loop spans $7\pi/6$ radians (210°) rather than $5\pi/6$ radians (150°) as in Figure 4.38.

(a) Explain why the radial magnetic field is identical to that drawn in Figure 4.10.

(b) Compute the flux in each loop due to the current in that loop and then the total flux linkage. To ensure that the induced emfs in each loop have the same sign conventions, choose a flux surface normal whose positive direction of travel around the surface coincides with the positive direction of current. Without any computation, use Gauss's law for $\vec{\mathbf{B}}$ to show the result must be the same as part (b) of problem 15. Consequently, the inductance of this winding must be the same as that given in part (c) of problem 15.

www.EngineeringEBooksPdf.com

Problem 17 Divergence of the Magnetic Field

Recall that the divergence of a vector field $\vec{\mathbf{W}}(r,\theta,z)$ *in cylindrical coordinates is given by*

$$\nabla \cdot \vec{\mathbf{W}} = \frac{1}{r}\frac{\partial}{\partial r}(rW_r) + \frac{1}{r}\frac{\partial W_\theta}{\partial \theta} + \frac{\partial W_z}{\partial z}$$

where $\vec{\mathbf{W}} = W_r\hat{\mathbf{r}} + W_\theta\hat{\boldsymbol{\theta}} + W_z\hat{\mathbf{z}}$. *Also, recall that the divergence theorem says that*

$$\oint_S \vec{\mathbf{W}} \cdot d\vec{\mathbf{S}} = \iiint_V \nabla \cdot \vec{\mathbf{W}}\, dV$$

where S *is the closed surface that encloses the volume* V.

With

$$\vec{\mathbf{B}}_{Sa} = B_{Sa}(r,\theta)\hat{\mathbf{r}} = \mu_0 \frac{r_R}{r}\left(\frac{2i_{Sa}}{g} - \frac{i_{enclosed}(\theta)}{g}\right)\hat{\mathbf{r}}$$

in the air gap of an approximately sinusoidally wound stator phase, show that $\nabla \cdot \vec{\mathbf{B}}_{Sa} \equiv 0$.

Problem 18 Azimuthal Magnetic Field

Use the expression (4.24) for the radial magnetic field to explicitly show that

$$\oint_S \vec{\mathbf{B}}_{Sa} \cdot d\vec{\mathbf{S}} = 0$$

for the closed surface shown in Figure 4.40 with $r_R \le r_1 < r_2 \le r_S$.

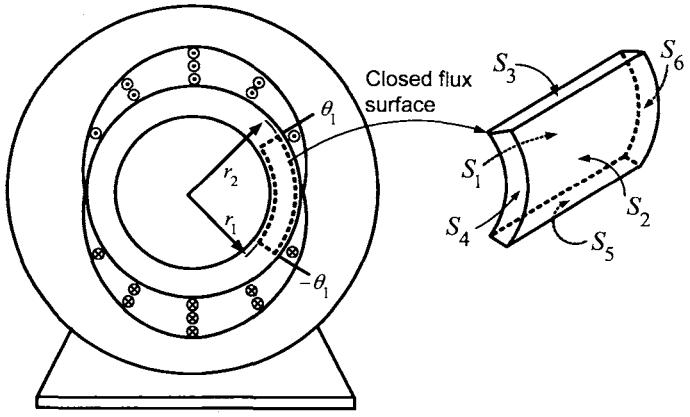


FIGURE 4.40. Gauss's law in the air gap with a nonzero azimuthal magnetic field.

www.EngineeringEBooksPdf.com

5

The Physics of AC Machines

The goal here is to present the operation of both the induction and synchronous machines using basic concepts in physics. In particular, Faraday's law of induction and the Lorentz force/magnetic force law will be used to analyze the physical basis of operation of these machines [34].

5.1 Rotating Magnetic Field

Assuming ideal magnetic material, that is, $\vec{\mathbf{H}} \equiv 0$ in the iron, and that the stator phases are sinusoidally wound, Ampère's law ($\oint \vec{\mathbf{H}} \cdot d\vec{\boldsymbol{\ell}} = i_{enclosed}$) was used to show that the magnetic field $\vec{\mathbf{B}}_{Sa}$ at any point (r, θ) in the air gap due to the current i_{Sa} in phase a is given by

$$\vec{\mathbf{B}}_{Sa}(i_{Sa}, r, \theta) = \frac{\mu_0 \ell_2 N_S}{4gr} i_{Sa} \cos(\theta) \hat{\mathbf{r}}.$$

Here $\hat{\mathbf{r}}$ is a unit vector in the radial direction, $r_R = \ell_2/2$ is the radius of the rotor and g is the radial length of the air gap. The magnetic field distribution of $\vec{\mathbf{B}}_{Sa}$ is illustrated in Figure 5.1.

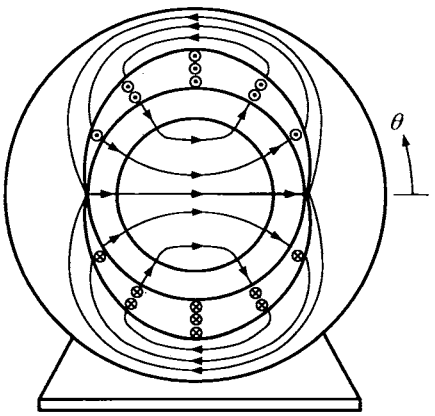


FIGURE 5.1. Radial air-gap magnetic field due to phase current i_{Sa} in a sinusoidally wound stator.

Similarly, the magnetic field $\vec{\mathbf{B}}_{Sb}$ at the point (r, θ) in the air gap due to

www.EngineeringEBooksPdf.com

the current i_{Sb} in phase b is given by

$$\begin{aligned}\vec{\mathbf{B}}_{Sb}(i_{Sb}, r, \theta) &= \frac{\mu_0 \ell_2 N_S}{4gr} i_{Sb} \cos(\theta - \pi/2)\hat{\mathbf{r}} \\ &= \frac{\mu_0 \ell_2 N_S}{4gr} i_{Sb} \sin(\theta)\hat{\mathbf{r}}.\end{aligned}$$

The magnetic field distribution of $\vec{\mathbf{B}}_{Sb}$ is illustrated in Figure 5.2.

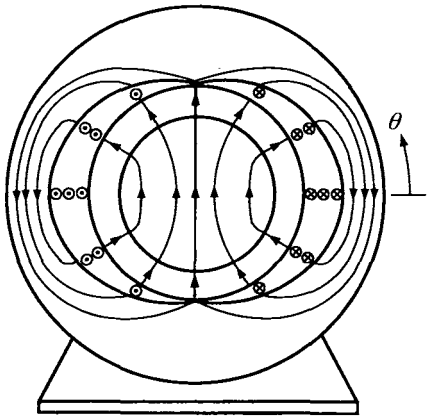


FIGURE 5.2. Radial air-gap magnetic field due to phase current i_{Sb} in a sinusoidally wound stator.

The total magnetic field in the air gap due to the current in both stator phases is then

$$\begin{aligned}\vec{\mathbf{B}}_S(i_{Sa}, i_{Sb}, r, \theta) &= \vec{\mathbf{B}}_{Sa}(i_{Sa}, r, \theta) + \vec{\mathbf{B}}_{Sb}(i_{Sb}, r, \theta) \\ &= \frac{\mu_0 \ell_2 N_S}{4gr} \left(i_{Sa} \cos(\theta) + i_{Sb} \sin(\theta)\right)\hat{\mathbf{r}}. \qquad (5.1)\end{aligned}$$

With $i_{Sa}(t) = I_S \cos(\omega_S t)$, $i_{Sb}(t) = I_S \sin(\omega_S t)$, (5.1) simplifies to

$$\begin{aligned}\vec{\mathbf{B}}_S &= \frac{\mu_0 \ell_2 N_S I_S}{4gr} \left(\cos(\omega_S t)\cos(\theta) + \sin(\omega_S t)\sin(\theta)\right)\hat{\mathbf{r}} \\ &= \frac{\mu_0 \ell_2 N_S I_S}{4gr} \cos(\theta - \omega_S t)\hat{\mathbf{r}} \\ &= \frac{\mu_0 \ell_2 N_S I_S}{4gr} \cos(\theta - \theta_S(t))\hat{\mathbf{r}} \qquad (5.2)\end{aligned}$$

where $\theta_S(t) \triangleq \omega_S t$. This is a *rotating magnetic field* rotating at the electrical frequency ω_S and is illustrated in Figure 5.3. The center line of this rotating magnetic field is referred to as its *magnetic axis* and is located at $\theta_S(t) \triangleq \omega_S t$.

www.EngineeringEBooksPdf.com

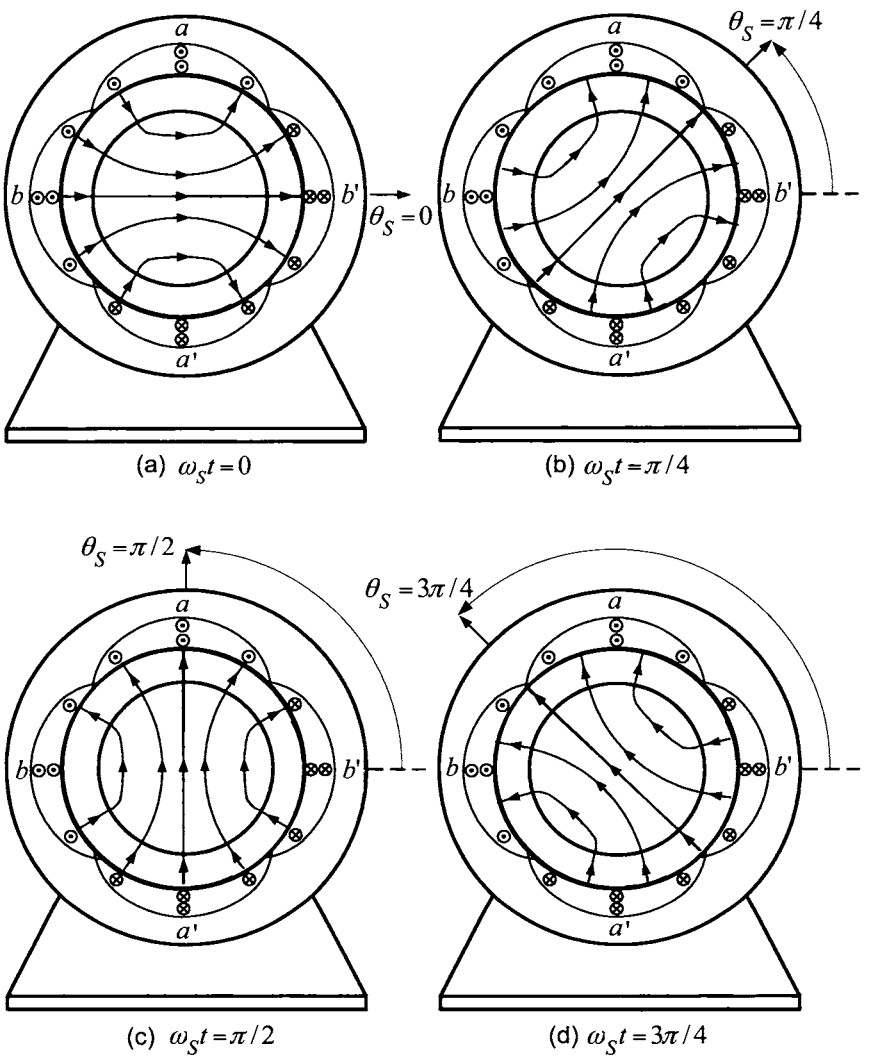


FIGURE 5.3. Sinusoidally distributed rotating radial magnetic field in the air gap. (For convenience, the magnetic field lines are not drawn in the stator iron.)

www.EngineeringEBooksPdf.com

5.2 The Physics of the Induction Machine

In this section, a simple two-phase induction motor is analyzed in order to understand the elementary Physics which characterizes its operation.

The stator consists of two sinusoidally wound phases 90° apart as described in the previous section. Figure 5.4 shows a loop wound around the surface of the rotor iron denoted as phase a (or simply loop a) and its two axial sides as a and a', respectively.

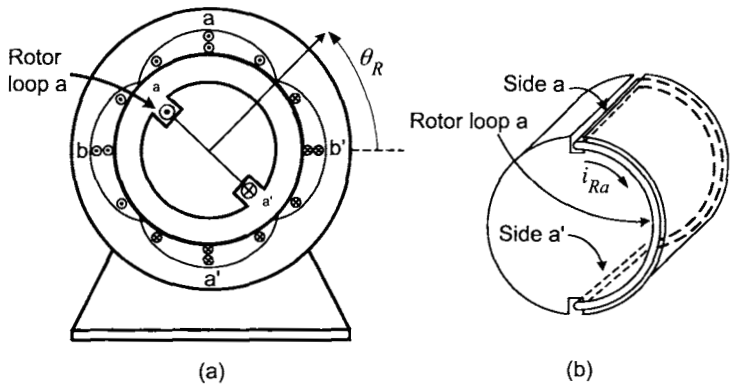


FIGURE 5.4. A single rotor loop and the chosen positive direction of current.

Similarly, a second loop is wound around the rotor iron 90° from (and electrically isolated from) loop a and is denoted as phase b or simply, loop b. This results in the simple two phase machine illustrated in Figure 5.5.

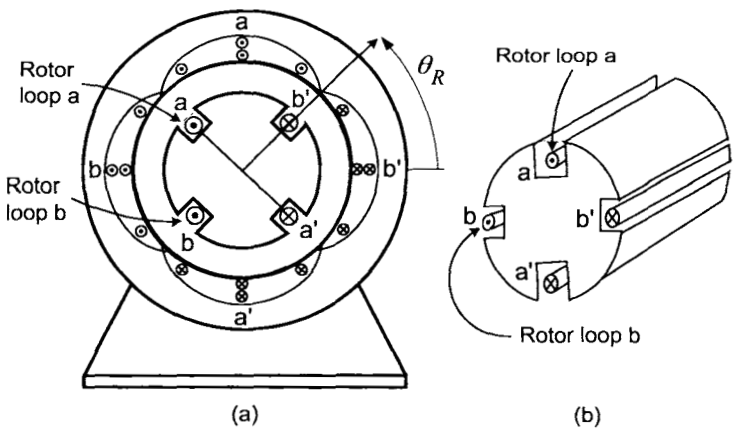


FIGURE 5.5. Basic motor with two single-loop rotor phases a and b.

www.EngineeringEBooksPdf.com

As above, $\theta_S(t) = \omega_S t$ denotes the angular position of the magnetic axis of the rotating magnetic field produced by the stator currents, $\theta_R(t)$ denotes the angular position of the rotor defined as the normal to rotor loop a [see Figure 5.4(a) or 5.5(a)] and (r, θ) denotes the polar coordinates of an arbitrary point in the air gap. In the remainder of this chapter, it will assumed that the rotor is turning at constant angular speed ω_R with $\theta_R(t) = \omega_R t$.

5.2.1 *Induced Emfs in the Rotor Loops*

The rotating magnetic field $\vec{\mathbf{B}}_S$ produces a changing flux in the rotor loops so that an *electromotive force (emf)* is induced in each rotor loop according to Faraday's law. To compute the induced emf in rotor phase a, consider a flux surface for rotor loop a consisting of a half-cylinder lying in the air gap whose boundary is the rotor loop itself. This is illustrated in Figure 5.6 where only rotor loop a is shown for clarity.

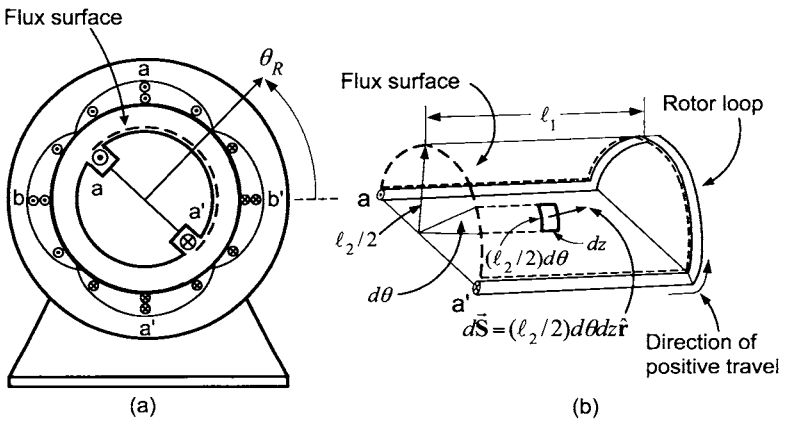


FIGURE 5.6. (a) Flux surface for the rotor winding. (b) Surface element $d\vec{\mathbf{S}}$ and direction of positive travel around the flux surface. (For clarity, only rotor loop a is shown.)

With $d\vec{\mathbf{S}} = (\ell_2/2)d\theta dz\hat{\mathbf{r}}$, the direction of positive travel is indicated in Figure 5.6(b), and it is the same as the direction chosen for positive current flow in the loop. The *flux* λ_{Ra} in rotor loop a due to the stator magnetic

www.EngineeringEBooksPdf.com

field $\vec{\mathbf{B}}_S$ is calculated as follows:

$$\begin{aligned}
\lambda_{Ra} &= \int_S \vec{\mathbf{B}}_S \cdot d\vec{\mathbf{S}} \\
&= \int_{z=0}^{z=\ell_1} \int_{\theta_R(t)-\pi/2}^{\theta_R(t)+\pi/2} \frac{\mu_0 \ell_2 N_S I_S}{4gr} \Big|_{r=\ell_2/2} \cos(\theta - \theta_S(t))\hat{\mathbf{r}} \cdot ((\ell_2/2)d\theta dz\hat{\mathbf{r}}) \\
&= \frac{\mu_0 \ell_1 \ell_2 N_S I_S}{4g} \sin(\theta - \theta_S(t)) \Big|_{\theta_R(t)-\pi/2}^{\theta_R(t)+\pi/2} \\
&= \frac{\mu_0 \ell_1 \ell_2 N_S I_S}{2g} \cos\Big(\theta_S(t) - \theta_R(t)\Big).
\end{aligned}$$

By Faraday's law, the induced *electromotive force* or *emf* in rotor loop a is given by

$$\begin{aligned}
\xi_{Ra} &= -\frac{d\lambda_{Ra}}{dt} \\
&= -\frac{d}{dt} \frac{\mu_0 \ell_1 \ell_2 N_S I_S}{2g} \cos\Big(\theta_S(t) - \theta_R(t)\Big) \\
&= \frac{\mu_0 \ell_1 \ell_2 N_S I_S}{2g} (\omega_S - \omega_R) \sin\Big((\omega_S - \omega_R)t\Big) \qquad (5.3)
\end{aligned}$$

where $\omega_R = d\theta_R/dt$. The current i_{Ra} in phase a is then found by solving

$$L_R \frac{di_{Ra}}{dt} = -R_R i_{Ra} + \xi_{Ra}$$

where L_R and R_R are, respectively, the inductance and resistance of the rotor phases. Neglecting the inductance[1] (i.e., set $L_R = 0$), the current in phase a produced by the emf is then

$$i_{Ra}(t) = \xi_{Ra}/R_R. \qquad (5.4)$$

[1] See problem 2 for the analysis when $L_R > 0$.

www.EngineeringEBooksPdf.com

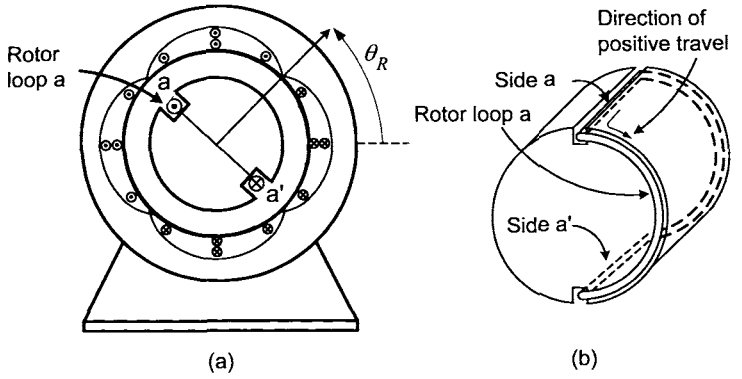


FIGURE 5.7. Induced rotor current i_{Ra} produced by ξ_{Ra}. (Rotor loop b is not shown for clarity.)

Similarly, the flux λ_{Rb}, the induced emf ξ_{Rb}, and the current i_{Rb} in rotor loop b are computed. The flux λ_{Rb} in rotor loop b due to $\vec{\mathbf{B}}_S$ is given by

$$\begin{aligned}
\lambda_{Rb} &= \int_S \vec{\mathbf{B}}_S \cdot d\vec{\mathbf{S}} \\
&= \int_{z=0}^{z=\ell_1} \int_{\theta_R(t)}^{\theta_R(t)+\pi} \frac{\mu_0 \ell_2 N_S I_S}{4gr}\Big|_{r=\ell_2/2} \cos\left(\theta - \theta_S(t)\right) \hat{\mathbf{r}} \cdot \left((\ell_2/2) dz d\theta \hat{\mathbf{r}}\right) \\
&= \frac{\mu_0 \ell_1 \ell_2 N_S I_S}{4g} \sin\left(\theta - \theta_S(t)\right) \Big|_{\theta_R(t)}^{\theta_R(t)+\pi} \\
&= \frac{\mu_0 \ell_1 \ell_2 N_S I_S}{2g} \sin\left(\theta_S(t) - \theta_R(t)\right).
\end{aligned}$$

The induced *emf* in rotor loop b is then

$$\begin{aligned}
\xi_{Rb}(t) &= -\frac{d\lambda_{Rb}}{dt} \\
&= -\frac{\mu_0 \ell_1 \ell_2 N_S I_S}{2g} (\omega_S - \omega_R) \cos\Big((\omega_S - \omega_R)t\Big)
\end{aligned}$$

where $\omega_R = d\theta_R/dt$. Again, neglecting the inductance of rotor phase b, this emf produces a current i_{Rb} in rotor loop b given by

$$i_{Rb}(t) = \xi_{Rb}(t)/R_R. \tag{5.5}$$

5.2.2 *Magnetic Forces and Torques on the Rotor*

The rotating magnetic field $\vec{\mathbf{B}}_S$ produced by the stator currents produces a magnetic force on the rotor currents it induced. The magnetic force on the

www.EngineeringEBooksPdf.com

rotor and the resulting torque are now computed. Recall that the magnetic force law is simply $\vec{\mathbf{F}}_{magnetic} = i\vec{\boldsymbol{\ell}} \times \vec{\mathbf{B}}$, where $\ell = |\,\vec{\boldsymbol{\ell}}\,|$ is the length of the conductor in the magnetic field, and $\vec{\boldsymbol{\ell}}$ points in the direction of positive current flow. Thus, the magnitude of the force is $F_{magnetic} = i\ell B_{\perp}$ where $B_{\perp}$ is the magnetic field strength perpendicular to the conductor. The magnetic force law is now applied to *side a* of rotor loop a, which is located at $\theta = \theta_R + \pi/2$ [see Figure 5.8(a)]. To do so, recall the symbol $\odot$ means that if $i_{Ra} > 0$, the current is coming out of the page so $\vec{\boldsymbol{\ell}} = \ell_1 \hat{\mathbf{z}}$ on side a, and compute

$$\begin{aligned}
\vec{\mathbf{F}}_{side-a} &= i_{Ra}\vec{\boldsymbol{\ell}} \times \vec{\mathbf{B}}_S \\
&= i_{Ra}\ell_1 \hat{\mathbf{z}} \times \frac{\mu_0 \ell_2 N_S I_S}{4gr}|_{r=\ell_2/2} \cos(\theta - \theta_S)_{|\theta=\theta_R+\pi/2}\,\hat{\mathbf{r}} \\
&= i_{Ra}\frac{\mu_0 \ell_1 N_S I_S}{2g}\sin(\theta_S - \theta_R)\hat{\boldsymbol{\theta}}.
\end{aligned}$$

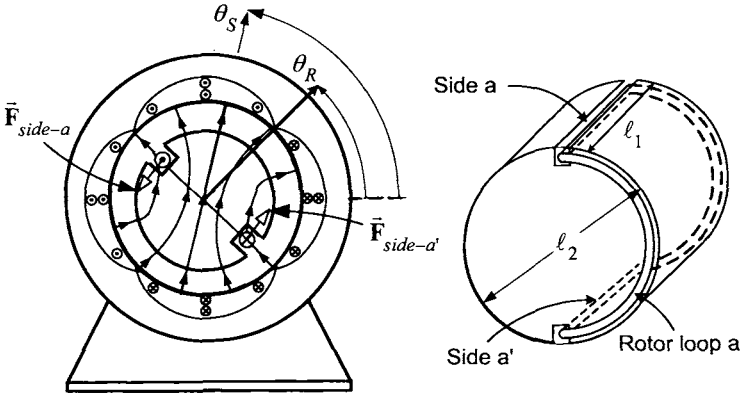


FIGURE 5.8. The torque τ_{Ra} on rotor loop a due to i_{Ra} and $\vec{\mathbf{B}}_S$.

The torque produced by this force is then

$$\begin{aligned}
\vec{\boldsymbol{\tau}}_{side-a} &= \vec{\mathbf{r}} \times \vec{\mathbf{F}}_{side-a} \\
&= (\ell_2/2)\hat{\mathbf{r}} \times i_{Ra}\frac{\mu_0 \ell_1 N_S I_S}{2g}\sin(\theta_S - \theta_R)\hat{\boldsymbol{\theta}} \\
&= \frac{\mu_0 \ell_1 \ell_2 N_S I_S}{4g} i_{Ra}\sin(\theta_S - \theta_R)\hat{\mathbf{z}}.
\end{aligned}$$

Similarly, the magnetic force law is applied to *side* a' of rotor loop a, which is located at $\theta_R - \pi/2$. Recalling the symbol $\otimes$ means that if $i_{Ra} > 0$, the

www.EngineeringEBooksPdf.com

current is going into the page so that $\vec{\boldsymbol{\ell}} = -\ell_1 \hat{\mathbf{z}}$ for side a'; it follows that

$$\begin{aligned}
\vec{\mathbf{F}}_{side-a'} &= i_{Ra}\vec{\boldsymbol{\ell}} \times \vec{\mathbf{B}}_S \\
&= i_{Ra}(-\ell_1 \hat{\mathbf{z}}) \times \frac{\mu_0 \ell_2 N_S I_S}{4gr}\Big|_{r=\ell_2/2} \cos(\theta - \theta_S)_{|\theta=\theta_R-\pi/2}\,\hat{\mathbf{r}} \\
&= i_{Ra}\frac{\mu_0 \ell_1 N_S I_S}{2g}\sin(\theta_S - \theta_R)\hat{\boldsymbol{\theta}}.
\end{aligned}$$

The *torque* produced by this force on side a' is then

$$\begin{aligned}
\vec{\boldsymbol{\tau}}_{side-a'} &= (\ell_2/2)\hat{\mathbf{r}} \times \vec{\mathbf{F}}_{side-a'} \\
&= \frac{\mu_0 \ell_1 \ell_2 N_S I_S}{4g} i_{Ra} \sin\Big((\omega_S - \omega_R)t\Big)\hat{\mathbf{z}} \\
&= \vec{\boldsymbol{\tau}}_{side-a}.
\end{aligned}$$

The total torque $\vec{\boldsymbol{\tau}}_{Ra} = \tau_{Ra}\hat{\mathbf{z}}$ on rotor phase a is simply

$$\tau_{Ra} = \tau_{side-a} + \tau_{side-a'} = \frac{\mu_0 \ell_1 \ell_2 N_S I_S}{2g} i_{Ra} \sin\Big((\omega_S - \omega_R)t\Big). \qquad (5.6)$$

Recall that

$$i_{Ra}(t) = \xi_{Ra}(t)/R_R = \frac{\mu_0 \ell_1 \ell_2 N_S I_S}{2g}\frac{1}{R_R}(\omega_S - \omega_R)\sin\Big((\omega_S - \omega_R)t\Big).$$

Using this expression, the total torque on rotor phase a may be rewritten as

$$\tau_{Ra} = \left(\frac{\mu_0 \ell_1 \ell_2 N_S I_S}{2g}\right)^2 \frac{1}{R_R}(\omega_S - \omega_R)\sin^2\Big((\omega_S - \omega_R)t\Big). \qquad (5.7)$$

Similarly, for rotor phase b

$$\begin{aligned}
\vec{\mathbf{F}}_{side-b} &= i_{Rb}\vec{\boldsymbol{\ell}} \times \vec{\mathbf{B}}_S \\
&= i_{Rb}\ell_1 \hat{\mathbf{z}} \times \frac{\mu_0 \ell_2 N_S I_S}{4gr}\Big|_{r=\ell_2/2} \cos(\theta - \theta_S)_{|\theta=\theta_R+\pi}\,\hat{\mathbf{r}} \\
&= -i_{Rb}\frac{\mu_0 \ell_1 N_S I_S}{2g}\cos(\theta_S - \theta_R)\hat{\boldsymbol{\theta}}
\end{aligned}$$

and, as in the case of loop a, $\vec{\mathbf{F}}_{side-b'} = \vec{\mathbf{F}}_{side-b}$. It then follows that the total torque on rotor phase b is

$$\begin{aligned}
\tau_{Rb} &= \tau_{side-b} + \tau_{side-b'} \\
&= 2\tau_{side-b} \\
&= -\frac{\mu_0 \ell_1 \ell_2 N_S I_S}{2g} i_{Rb} \cos\Big((\omega_S - \omega_R)t\Big).
\end{aligned}$$

www.EngineeringEBooksPdf.com

Further, as

$$i_{Rb}(t) = \xi_{Rb}(t)/R_R = -\frac{\mu_0 \ell_1 \ell_2 N_S I_S}{2g}(\omega_S - \omega_R)\cos\Big((\omega_S - \omega_R)t\Big)/R_R$$

the torque on rotor loop b may be rewritten as

$$\tau_{Rb} = \left(\frac{\mu_0 \ell_1 \ell_2 N_S I_S}{2g}\right)^2 \frac{1}{R_R}(\omega_S - \omega_R)\cos^2\Big((\omega_S - \omega_R)t\Big). \tag{5.8}$$

Combining equations (5.7) and (5.8), the *total torque* τ_R is given by

$$\tau_R = \tau_{Ra} + \tau_{Rb} = \left(\frac{\mu_0 \ell_1 \ell_2 N_S I_S}{2g}\right)^2 \frac{1}{R_R}(\omega_S - \omega_R). \tag{5.9}$$

For a constant angular frequency ω_S and a constant angular rotor speed ω_R, the torque is constant.

5.2.3 *Slip Speed*

The stator currents are given by $i_{Sa}(t) = I_S \cos(\omega_S t)$, $i_{Sb}(t) = I_S \sin(\omega_S t)$ and, neglecting the inductance of the rotor phases, equation (5.9) shows that the torque on the rotor is proportional to the *difference* between the angular speed ω_S of the rotating stator magnetic field and the rotor speed ω_R, that is,

$$\tau_R = \left(\frac{\mu_0 \ell_1 \ell_2 N_S I_S}{2g}\right)^2 \frac{1}{R_R}(\omega_S - \omega_R).$$

This difference is called the *slip speed* ω_{slip}, that is,

$$\omega_{slip} \triangleq \omega_S - \omega_R.$$

In particular, if the slip speed is zero, there is *no* torque. The reason is simply that if the slip speed is zero, then the rotating stator magnetic field and the rotor are rotating at the *same* angular rate with the result that the fluxes in the rotor loops are *constant*. As the rate of change of these fluxes is zero, Faraday's law tells us that neither voltages nor currents are induced in the rotor and, without rotor currents, there can be no magnetic force/torque on the rotor. In order to produce torque in an induction machine, the rotor shaft and the stator's magnetic field do not rotate together at the same rate, that is, they are not synchronized. It is for this reason that the induction motor is referred to as an *asynchronous* machine.

5.3 The Physics of the Synchronous Machine

In this section, the physics of the synchronous motor is described where both the salient and nonsalient machines are considered. A *salient* rotor is

www.EngineeringEBooksPdf.com

one in which the rotor is not cylindrically shaped so that air gap does not have a uniform thickness. A *nonsalient* machine is one which is *not* salient meaning it does have a cylindrical rotor with a uniform or constant air-gap thickness.

5.3.1 *Two-Phase Synchronous Motor with a Sinusoidally Wound Rotor*

A synchronous machine with a sinusoidally wound rotor (also referred to as a nonsalient machine) is considered first. The rotor consists of a single sinusoidally wound phase of wire while the stator is constructed identically to that of the induction motor as illustrated in Figure 5.9. The rotor construction, torque production and energy conversion for this synchronous machine is now described.

Sinusoidally Wound Rotor

Consider a synchronous machine where the stator consists of two sinusoidally wound phases which are 90° apart as shown in Figure 5.9(a). Let the rotor consist of a cylindrical core of iron on which a single phase with a sinusoidal turns density has been wound as illustrated in Figure 5.9(b). That is, the turns density of the single-phase rotor winding is given by

$$N_{RF}(\theta - \theta_R) = \frac{N_F}{2} |\sin(\theta - \theta_R)|$$

where N_F is the total number of windings in the phase.

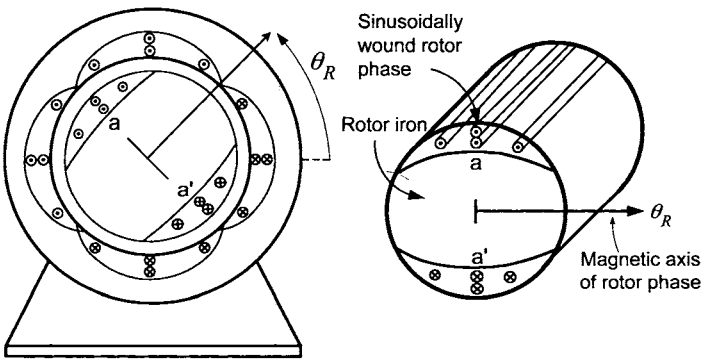


FIGURE 5.9. Single-phase sinusoidally wound rotor.

The single-phase winding on the rotor is usually referred to as the *field* winding and hence the subscript "F". The radial magnetic field in the air-gap due to the rotor current i_F in the sinusoidally wound rotor is (see

www.EngineeringEBooksPdf.com

problem 7)

$$\vec{\mathbf{B}}_R = B_R\hat{\mathbf{r}} = \frac{\mu_0 \ell_2 N_F i_F}{4gr}\cos(\theta - \theta_R)\hat{\mathbf{r}} \tag{5.10}$$

For this machine to operate as a synchronous machine, the rotor must be carrying a *constant current*, that is, $i_F = I_F$ with I_F constant. Again, the subscript "F" is used to denote the rotor current as the *field* current where the term "field" refers to the current being constant. The rotor position is taken to be aligned with the magnetic axis of the rotor as shown in Figure 5.9. Furthermore, as the rotor current is constant, the rotor can be viewed simply as a magnet that rotates at angular speed $\omega_R = d\theta_R/dt$. Figure 5.10 illustrates the radial magnetic field in air gap produced by a constant current I_F in a sinusoidally wound rotor phase.

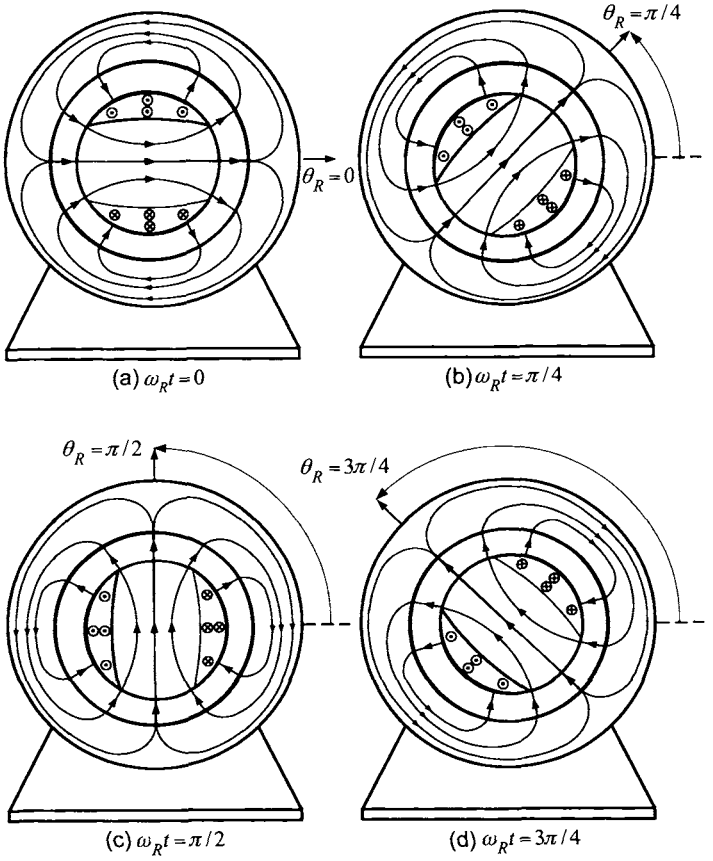


FIGURE 5.10. Magnetic field lines produced by a sinusoidally distributed rotor winding carrying a constant current $i_F = I_F$. (The stator windings are not drawn for clarity.)

www.EngineeringEBooksPdf.com

To describe the Physics of this machine, consider the motor to be in steady-state operation. By this it is meant that the stator magnetic field $\vec{\mathbf{B}}_S$ and the rotor are rotating at the *same* angular speed (i.e., $\omega_R = \omega_S$), which is the origin of the term *synchronous*. As shown below, with the magnetic axis of $\vec{\mathbf{B}}_S$ given by $\theta_S(t) = \omega_S t$, the rotor position in steady state is written as $\theta_R(t) = \omega_S t - \delta$, where $\delta > 0$ is a constant angle whose value will be shown to depend on how much load (i.e., external torque, friction, etc.) there is on the motor.

Magnetic Forces/Torques

The magnetic field in the air-gap due to the stator currents is given by

$$\vec{\mathbf{B}}_S(i_{Sa}, i_{Sb}, r, \theta) = \frac{\mu_0 \ell_2 N_S}{4gr} \left(i_{Sa}\cos(\theta) + i_{Sb}\sin(\theta)\right)\hat{\mathbf{r}}. \tag{5.11}$$

With the rotor field current $i_F(t) = I_F$ constant, the magnetic field in the air gap due to this constant rotor current is

$$\vec{\mathbf{B}}_R = \frac{\mu_0 \ell_2 N_F I_F}{4gr} \cos(\theta - \theta_R)\hat{\mathbf{r}} \tag{5.12}$$

where θ_R is the rotor position which is aligned with the magnetic axis of the rotor.

The same procedure used to compute the torque produced by the induction motor could also be used. That is, one uses the expression (5.11) for $\vec{\mathbf{B}}_S$ to compute the torque this magnetic field produces on the current in the sinusoidally wound rotor phase. This is explored in problem 9. However, a different approach is taken here that will also work in the case of both a permanent magnet rotor and a salient rotor (see problem 8).

By Newton's third law, the magnetic forces on the rotor currents produced by the rotating stator magnetic field is the *negative* of the forces on the stator currents produced by rotor's magnetic field. The approach here is to compute the torque $\vec{\boldsymbol{\tau}}_S$ exerted on the currents in the sinusoidally wound stator phases by the rotor's magnetic field. Then the rotor torque $\vec{\boldsymbol{\tau}}_R$ is found by $\vec{\boldsymbol{\tau}}_R = -\vec{\boldsymbol{\tau}}_S$.

To proceed, consider Figure 5.11 where at any position θ on the stator, the number of axial sides of stator phase a between θ and $\theta + d\theta$ is $(N_S/2)\,|\sin(\theta)|\,d\theta$. Thus, the total amount of current in the axial sides of stator phase a between θ and $\theta + d\theta$ is $i_{Sa}(N_S/2)\,|\sin(\theta)|\,d\theta$. Using the magnetic force law, the incremental force $d\vec{\mathbf{F}}_{Sa}$ on the currents in the windings of stator phase a between θ and $\theta + d\theta$ is given by

$$d\vec{\mathbf{F}}_{Sa} = \begin{cases} i_{Sa}(t)\dfrac{N_S}{2}\,|\sin(\theta)|\,d\theta(+\ell_1\hat{\mathbf{z}}) \times \vec{\mathbf{B}}_R & 0 \le \theta \le \pi \\ \\ i_{Sa}(t)\dfrac{N_S}{2}\,|\sin(\theta)|\,d\theta(-\ell_1\hat{\mathbf{z}}) \times \vec{\mathbf{B}}_R & \pi \le \theta \le 2\pi. \end{cases}$$

www.EngineeringEBooksPdf.com

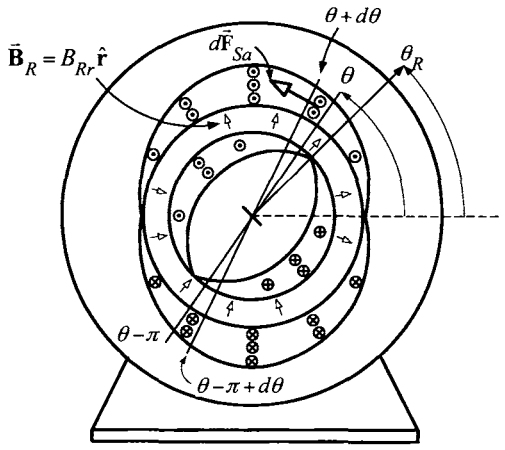


FIGURE 5.11. Computation of force/torque on stator phase a due to the rotor's magnetic field. Stator phase b is not shown for clarity.

As $\sin(\theta)$ is positive in the interval $0 \leq \theta \leq \pi$ and $|\sin(\theta)| = -\sin(\theta)$ in the interval $\pi \leq \theta \leq 2\pi$, the incremental force for $0 \leq \theta \leq 2\pi$ may be rewritten compactly as

$$\begin{aligned} d\vec{\mathbf{F}}_{Sa} &= \left(i_{Sa}(t)\frac{N_S}{2}\sin(\theta)d\theta\right)(\ell_1\hat{\mathbf{z}}) \times \vec{\mathbf{B}}_R \\ &= \left(i_{Sa}(t)\frac{N_S}{2}\sin(\theta)d\theta\right)(\ell_1\hat{\mathbf{z}}) \times \frac{\mu_0\ell_2 N_F I_F}{4gr}|_{r=r_S}\cos(\theta-\theta_R)\hat{\mathbf{r}} \\ &= \frac{\mu_0\ell_1\ell_2 N_S N_F I_F}{8gr_S} i_{Sa}(t)\sin(\theta)\cos(\theta-\theta_R)d\theta\hat{\mathbf{z}} \times \hat{\mathbf{r}} \\ &= \frac{\mu_0\ell_1\ell_2 N_S N_F I_F}{8gr_S} i_{Sa}(t)\sin(\theta)\cos(\theta-\theta_R)d\theta\hat{\boldsymbol{\theta}} \end{aligned}$$

where $r_S = \ell_2/2 + g$ is the inside radius of the stator. Then, the incremental torque on these windings of phase a is given by

$$\begin{aligned} d\vec{\boldsymbol{\tau}}_{Sa} &= (r_S\hat{\mathbf{r}}) \times d\vec{\mathbf{F}}_{Sa} \\ &= r_S\hat{\mathbf{r}} \times \left(\frac{\mu_0\ell_1\ell_2 N_S N_F I_F}{8gr_S} i_{Sa}(t)\sin(\theta)\cos(\theta-\theta_R)d\theta\right)\hat{\boldsymbol{\theta}} \\ &= \frac{\mu_0\ell_1\ell_2 N_S N_F I_F}{8g} i_{Sa}(t)\sin(\theta)\cos(\theta-\theta_R)d\theta\hat{\mathbf{z}}. \end{aligned}$$

www.EngineeringEBooksPdf.com

The total torque on stator phase a is then

$$\begin{aligned}\vec{\tau}_{Sa}(i_{Sa},\theta_R) &= \int_0^{2\pi} \frac{\mu_0 \ell_1 \ell_2 N_S N_F I_F}{8g} i_{Sa}(t)\sin(\theta)\cos(\theta-\theta_R)d\theta\hat{\mathbf{z}} \\ &= \frac{\mu_0 \ell_1 \ell_2 N_S N_F I_F}{8g} i_{Sa}(t)\int_0^{2\pi} \sin(\theta)\Big(\cos(\theta)\cos(\theta_R) \\ &\quad + \sin(\theta)\sin(\theta_R)\Big)\,d\theta\hat{\mathbf{z}} \\ &= \frac{\mu_0 \ell_1 \ell_2 N_S N_F I_F}{8g} i_{Sa}(t)\sin(\theta_R)\int_0^{2\pi} \sin^2(\theta)d\theta\hat{\mathbf{z}} \\ &= \frac{\mu_0 \pi \ell_1 \ell_2 N_S N_F I_F}{8g} i_{Sa}(t)\sin(\theta_R)\hat{\mathbf{z}}.\end{aligned}$$

Similarly, with $N_{Sb}(\theta)d\theta = (N_S/2)\,|\sin(\theta-\pi/2)|\,d\theta$ the number of axial sides of the windings of stator phase b between θ and $\theta+d\theta$, the incremental force $d\vec{\mathbf{F}}_{Sb}$ on the current in these windings for $0 \le \theta \le 2\pi$ is given by[2]

$$\begin{aligned}d\vec{\mathbf{F}}_{Sb} &= \left(i_{Sb}(t)\frac{N_S}{2}\sin(\theta-\pi/2)d\theta\right)(\ell_1\hat{\mathbf{z}}) \times \vec{\mathbf{B}}_R \\ &= \left(i_{Sb}(t)\frac{N_S}{2}\sin(\theta-\pi/2)d\theta\right)(\ell_1\hat{\mathbf{z}}) \times \frac{\mu_0 \ell_2 N_F I_F}{4gr}|_{r=r_S}\cos(\theta-\theta_R)\hat{\mathbf{r}} \\ &= \frac{\mu_0 \ell_1 \ell_2 N_S N_F I_F}{8gr_S} i_{Sb}(t)\sin(\theta-\pi/2)\cos(\theta-\theta_R)d\theta\hat{\mathbf{z}} \times \hat{\mathbf{r}} \\ &= -\frac{\mu_0 \ell_1 \ell_2 N_S N_F I_F}{8gr_S} i_{Sb}(t)\cos(\theta)\cos(\theta-\theta_R)d\theta\hat{\boldsymbol{\theta}}.\end{aligned}$$

Thus, the incremental torque on phase b of the stator is given by

$$\begin{aligned}d\vec{\tau}_{Sb} &= (r_S\hat{\mathbf{r}}) \times d\vec{\mathbf{F}}_{Sb} \\ &= (r_S\hat{\mathbf{r}}) \times \left(-\frac{\mu_0 \ell_1 \ell_2 N_S N_F I_F}{8gr_S} i_{Sb}(t)\cos(\theta)\cos(\theta-\theta_R)d\theta\right)\hat{\boldsymbol{\theta}} \\ &= -\frac{\mu_0 \ell_1 \ell_2 N_S N_F I_F}{8g} i_{Sb}(t)\cos(\theta)\cos(\theta-\theta_R)d\theta\hat{\mathbf{z}}.\end{aligned}$$

[2]Note that $(N_S/2)\,|\sin(\theta-\pi/2)| = (N_S/2)\sin(\theta-\pi/2)$ for $\pi/2 \le \theta \le 3\pi/2$ and $(N_S/2)\,|\sin(\theta-\pi/2)| = -(N_S/2)\sin(\theta-\pi/2)$ for $-\pi/2 \le \theta \le \pi/2$.

www.EngineeringEBooksPdf.com

The total torque on stator phase b is then

$$\begin{aligned}
\vec{\tau}_{Sb}(i_{Sb},\theta_R) &= \int_0^{2\pi} -\frac{\mu_0\ell_1\ell_2 N_S N_F I_F}{8g} i_{Sb}(t)\cos(\theta)\cos(\theta-\theta_R)d\theta\hat{\mathbf{z}} \\
&= -\frac{\mu_0\ell_1\ell_2 N_S N_F I_F}{8g} i_{Sb}(t)\int_0^{2\pi}\cos(\theta)\Big(\cos(\theta)\cos(\theta_R) \\
&\quad +\sin(\theta)\sin(\theta_R)\Big)d\theta\hat{\mathbf{z}} \\
&= -\frac{\mu_0\ell_1\ell_2 N_S N_F I_F}{8g} i_{Sb}(t)\cos(\theta_R)\int_0^{2\pi}\cos^2(\theta)d\theta\hat{\mathbf{z}} \\
&= -\frac{\mu_0\pi\ell_1\ell_2 N_S N_F I_F}{8g} i_{Sb}(t)\cos(\theta_R)\hat{\mathbf{z}}.
\end{aligned}$$

The total torque exerted on the stator by the rotor is then

$$\begin{aligned}
\vec{\tau}_S &= \vec{\tau}_{Sa}+\vec{\tau}_{Sb} \\
&= \frac{\mu_0\pi\ell_1\ell_2 N_S N_F I_F}{8g}\left(i_{Sa}(t)\sin(\theta_R)-i_{Sb}(t)\cos(\theta_R)\right)\hat{\mathbf{z}}.
\end{aligned}$$

Consequently, $\vec{\tau}_R = -\vec{\tau}_S$ is the torque exerted on the rotor by the stator and is given by

$$\vec{\tau}_R = \frac{\mu_0\pi\ell_1\ell_2 N_S N_F I_F}{8g}\left(-i_{Sa}(t)\sin(\theta_R)+i_{Sb}(t)\cos(\theta_R)\right)\hat{\mathbf{z}}.$$

Define

$$\begin{aligned}
B_{R\max} &\triangleq \frac{\mu_0\ell_2 N_F I_F}{4gr}\Big|_{r=\ell_2/2} = \frac{\mu_0 N_F I_F}{2g} \\
V_{\text{airgap}} &\triangleq 2\pi(\ell_2/2)\ell_1 g = \pi\ell_1\ell_2 g
\end{aligned}$$

where $B_{R\max}$ is the maximum values of the rotor's magnetic field at the surface of the rotor[3] and V_{airgap} is the volume of the air gap (assuming g is small). The torque is now rewritten as

$$\tau_R = V_{\text{airgap}} B_{R\max}\frac{N_S}{4g}\left(-i_{Sa}(t)\sin(\theta_R)+i_{Sb}(t)\cos(\theta_R)\right)$$

and the dynamic equation describing the motion of the rotor is then

$$J\frac{d\omega_R}{dt} = V_{\text{airgap}} B_{R\max}\frac{N_S}{4g}\left(-i_{Sa}(t)\sin(\theta_R)+i_{Sb}(t)\cos(\theta_R)\right)-\tau_L.$$

To obtain an expression for this torque in steady state, set

$$i_{Sa}(t) = I_S\cos(\omega_S t) = I_S\cos(\theta_S), i_{Sb}(t) = I_S\sin(\omega_S t) = I_S\sin(\theta_S)$$

[3] See equation (5.12).

www.EngineeringEBooksPdf.com

where $\theta_S(t) = \omega_S t$ so that

$$\begin{aligned}\tau_R &= V_{\text{airgap}} B_{R\max} \frac{N_S I_S}{4g} (\cos(\theta_S)\sin(\theta_R) - \sin(\theta_S)\cos(\theta_R)) \\ &= V_{\text{airgap}} B_{R\max} \frac{N_S I_S}{4g} \sin(\theta_S - \theta_R) \\ &= V_{\text{airgap}} \frac{B_{R\max} B_{S\max}}{2\mu_0} \sin(\theta_S - \theta_R).\end{aligned}$$

Here

$$B_{S\max} \triangleq \frac{\mu_0 \ell_2 N_S I_S}{4gr} \Big|_{r=\ell_2/2} = \frac{\mu_0 N_S I_S}{2g}$$

is the maximum value of the rotating stator magnetic field at the surface of the rotor [see equation (5.2)]. With

$$\begin{aligned}\theta_S(t) &= \omega_S t \\ \theta_R(t) &= \omega_R t - \delta,\end{aligned}$$

it follows that

$$\sin(\theta_S - \theta_R) = \sin(\omega_S t - (\omega_R t - \delta)) = \sin((\omega_S - \omega_R)t + \delta)).$$

Thus, the only way to obtain *constant* torque is with the stator's magnetic field and the rotor rotating at the same constant angular speed (i.e., $\omega_S = \omega_R$). In other words, the stator's rotating magnetic field $\vec{\mathbf{B}}_S$ and the rotor must be rotating *synchronously*. In this case, the expression for the torque simplifies to

$$\tau_R = V_{\text{airgap}} \frac{B_{R\max} B_{S\max}}{2\mu_0} \sin(\delta). \tag{5.13}$$

This last expression leads to a simple picture for the synchronous motor. That is, the stator currents set up a rotating "stator magnet" which pulls along the "rotor magnet" (see Figure II.10). The torque on the "rotor magnet" is proportional to the maximum value of the magnetic field of the rotating "stator magnet", the maximum value of the magnetic field of the "rotor magnet", and the sine of the angle between them.

5.3.2 Emfs and Energy Conversion

The flux linkage in stator phase a due to the rotor's magnetic field $\vec{\mathbf{B}}_R$ is now found in order to compute the induced emf in this phase. Recall that for $0 \le \theta \le \pi$, the number of turns (loops) in stator phase a between θ and $\theta + d\theta$ is $(N_S/2)\sin(\theta)d\theta$. As the cross-sectional area of the wire is assumed negligible, the flux through each of these loops/turns is the same.

www.EngineeringEBooksPdf.com

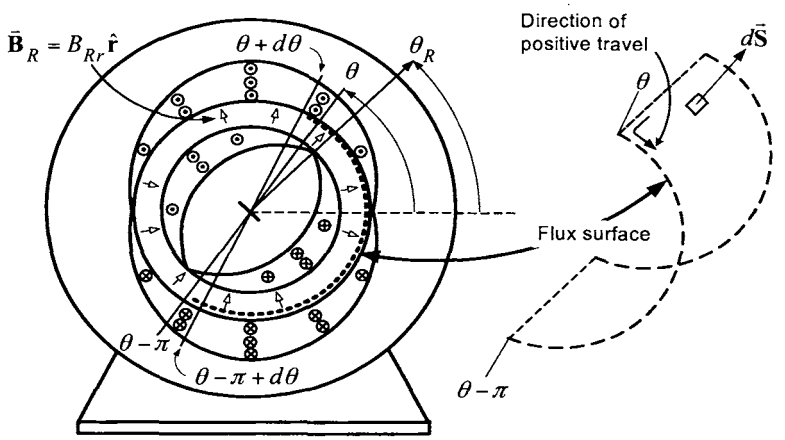


FIGURE 5.12. Computation of the flux in a turn of stator phase a located between θ and $\theta + d\theta$. All the loops between θ and $\theta + d\theta$ have the same flux as the cross-sectional area of the wire is assumed infinitesimal. The normal for the flux surface is taken to be $\hat{\mathbf{n}} = \hat{\mathbf{r}}$. Stator phase b is not shown for clarity.

Denoting the flux in each stator turn/loop between θ and $\theta + d\theta$ by $\phi_{Sa}(\theta)$, this flux is computed as

$$\begin{aligned}
\phi_{Sa}(\theta) &\triangleq \int_{\substack{\text{A single loop of stator} \\ \text{phase } a \text{ at the angle } \theta}} \vec{\mathbf{B}}_R \cdot d\vec{\mathbf{S}} \\
&= \int_{\theta'=\theta-\pi}^{\theta'=\theta} \int_{z=0}^{z=\ell_1} \left(\frac{\mu_0 N_F \ell_2 I_F}{4 g r_S} \cos(\theta' - \theta_R(t)) \hat{\mathbf{r}} \right) \cdot \left(r_S d\theta' dz\, \hat{\mathbf{r}} \right) \\
&= \int_{\theta'=\theta-\pi}^{\theta'=\theta} \frac{\mu_0 N_F \ell_1 \ell_2 I_F}{4g} \cos(\theta' - \theta_R(t)) d\theta' \\
&= \frac{\ell_1 \ell_2}{2} \frac{\mu_0 N_F I_F}{2g} \left(\sin(\theta - \theta_R) - \sin(\theta - \pi - \theta_R) \right) \\
&= \ell_1 \ell_2 B_{R\max} \sin(\theta - \theta_R) \qquad (5.14)
\end{aligned}$$

where $B_{R\max} = (\mu_0 N_F I_F)/(2g)$.

As there are $(N_S/2)\sin(\theta)d\theta$ turns/loops of stator phase a between θ and $\theta + d\theta$ each containing the flux $\phi_{Sa}(\theta)$, the total flux linkage λ_{Sa} in all the windings making up stator phase a due to the *rotor's* magnetic field is

www.EngineeringEBooksPdf.com

given by

$$\begin{aligned}
\lambda_{Sa}(\theta_R) &\triangleq \int_{\theta=0}^{\theta=\pi} \phi_{Sa}(\theta)\frac{N_S}{2}\sin(\theta)d\theta \\
&= \int_0^{\pi} \ell_1\ell_2 B_{R\max}\sin(\theta-\theta_R)\frac{N_S}{2}\sin(\theta)d\theta \\
&= \ell_1\ell_2 B_{R\max}\frac{N_S}{2}\int_0^{\pi}\sin(\theta)\sin(\theta-\theta_R)d\theta \\
&= \ell_1\ell_2 B_{R\max}\frac{N_S}{2}\frac{\pi}{2}\cos(\theta_R) \\
&= \pi\ell_1\ell_2 g B_{R\max}\frac{N_S}{4g}\cos(\theta_R) \\
&= V_{\text{airgap}} B_{R\max}\frac{N_S}{4g}\cos(\theta_R) \qquad (5.15)
\end{aligned}$$

where $V_{\text{airgap}} \triangleq \pi\ell_1\ell_2 g$. Similarly, denote by $\phi_{Sb}(\theta)$ the flux in windings/turns of stator phase b between θ and $\theta+d\theta$ due to the rotor's magnetic field. It follows that

$$\begin{aligned}
\phi_{Sb}(\theta) &\triangleq \int_{\substack{\text{A single loop of stator}\\ \text{phase } b \text{ at the angle } \theta}} \vec{\mathbf{B}}_R \cdot d\vec{\mathbf{S}} \\
&= \int_{\theta'=\theta-\pi}^{\theta'=\theta}\int_{z=0}^{z=\ell_1}\left(\frac{\mu_0 N_F \ell_2 I_F}{4g r_S}\cos(\theta'-\theta_R(t))\hat{\mathbf{r}}\right)\cdot\left(r_S d\theta' dz\hat{\mathbf{r}}\right) \\
&= \ell_1\ell_2\frac{\mu_0 N_F I_F}{2g}\sin(\theta-\theta_R) \\
&= \ell_1\ell_2 B_{R\max}\sin(\theta-\theta_R). \qquad (5.16)
\end{aligned}$$

The total flux linkage in stator phase b is then

$$\begin{aligned}
\lambda_{Sb}(\theta_R) &= \int_{\theta=\pi/2}^{\theta=3\pi/2}\phi_{Sb}(\theta)\frac{N_S}{2}\sin(\theta-\pi/2)d\theta \\
&= \int_{\pi/2}^{3\pi/2}\ell_1\ell_2 B_{R\max}\sin(\theta-\theta_R)\frac{N_S}{2}\sin(\theta-\pi/2)d\theta \\
&= -\ell_1\ell_2 B_{R\max}\frac{N_S}{2}\int_{\pi/2}^{3\pi/2}\cos(\theta)\sin(\theta-\theta_R)d\theta \\
&= -\ell_1\ell_2 B_{R\max}\frac{N_S}{2}\left(-\frac{\pi}{2}\sin(\theta_R)\right) \\
&= V_{\text{airgap}} B_{R\max}\frac{N_S}{4g}\sin(\theta_R). \qquad (5.17)
\end{aligned}$$

The quantities λ_{Sa} and λ_{Sb} denote the flux linkages in the stator phases

www.EngineeringEBooksPdf.com

due to the *rotor's* magnetic field.[4] By Faraday's law, the emf's induced in the stator phases due to the rotor's magnetic field (i.e., the *back emfs* in the stator phases) are then

$$\begin{aligned} \xi_{Sa} &= -d\lambda_{Sa}/dt = +V_{\text{airgap}} B_{R\max} \frac{N_S}{4g} \sin(\theta_R) \frac{d\theta_R}{dt} \\ \xi_{Sb} &= -d\lambda_{Sb}/dt = -V_{\text{airgap}} B_{R\max} \frac{N_S}{4g} \cos(\theta_R) \frac{d\theta_R}{dt}. \end{aligned} \tag{5.18}$$

As the normal $\hat{\mathbf{n}} = \hat{\mathbf{r}}$ was chosen for the flux surface to compute (5.14) and therefore for all the loops in (5.15), the induced emf ξ_{Sa} in phase a has the same sign convention as that chosen for the phase current i_{Sa}. Similarly, the induced emf ξ_{Sb} in phase b has the same sign convention as the phase current i_{Sb}.

The electrical power absorbed by the emfs ξ_{Sa}, ξ_{Sb} is

$$\begin{aligned} P_{\text{elec}} &= i_{Sa}(t)\xi_{Sa}(t) + i_{Sb}(t)\xi_{Sb}(t) \\ &= V_{\text{airgap}} B_{R\max} \frac{N_S}{4g} \left(i_{Sa}(t)\sin(\theta_R) - i_{Sb}(t)\cos(\theta_R)\right)\omega_R \\ &= V_{\text{airgap}} B_{R\max} \frac{N_S I_S}{4g} \left(\cos(\omega_S t)\sin(\theta_R) - \sin(\omega_S t)\cos(\theta_R)\right)\omega_R \\ &= V_{\text{airgap}} B_{R\max} B_{S\max} \frac{1}{2\mu_0} \omega_R \sin(\theta_R - \omega_S t) \\ &= \frac{V_{\text{airgap}}}{2\mu_0} B_{S\max} B_{R\max} \omega_R \sin\Big(\underbrace{(\omega_R - \omega_S)t - \delta}\Big) \\ &= -\frac{B_{S\max} B_{R\max}}{2\mu_0} V_{\text{airgap}} \omega_R \sin(\delta) \end{aligned}$$

where the motor is now assumed to be in steady state so that $\theta_S = \omega_S t$, $\theta_R = \omega_R t - \delta$ with $\omega_S = \omega_R$. By the torque equation (5.13), the mechanical power produced is

$$P_{\text{mech}} = \tau_R \omega_R = \frac{B_{S\max} B_{R\max}}{2\mu_0} V_{\text{airgap}} \sin(\delta)\omega_R$$

so that

$$P_{\text{elec}} + P_{\text{mech}} = 0.$$

That is, the electrical power absorbed in the stator phases reappears as the mechanical power of the motor.

---

[4] Note that as $V_{\text{airgap}} B_{R\max} \frac{N_s}{4g} = \pi \ell_1 \ell_2 g \frac{\mu_0 N_F I_F}{2g} \frac{N_s}{4g} = (\mu_0 \pi \ell_1 \ell_2 N_S N_R / 8g) I_F$, these flux linkages may also be written in the form $\lambda_{Sa}(\theta_R) = M I_F \cos(\theta_R), \lambda_{Sb}(\theta_R) = M I_F \sin(\theta_R)$ where, $M \triangleq (\mu_0 \pi \ell_1 \ell_2 N_S N_R / 8g)$ is called the *coefficient of mutual inductance.*

www.EngineeringEBooksPdf.com

5.3.3 *Synchronous Motor with a Salient Rotor*

To actually produce a rotor winding for a machine that is sinusoidally wound is more expensive than other types of windings. In the case of the synchronous motor, one can eliminate the need for a sinusoidally wound rotor. Recall that in the above analysis of the synchronous machine, the important fact was that the magnetic field of the rotor was sinusoidally distributed in $\theta - \theta_R$. It is now shown that by putting a *uniformly* wound coil on the rotor and shaping the pole faces of the rotor appropriately, a sinusoidally distributed magnetic field in the air gap can be produced.

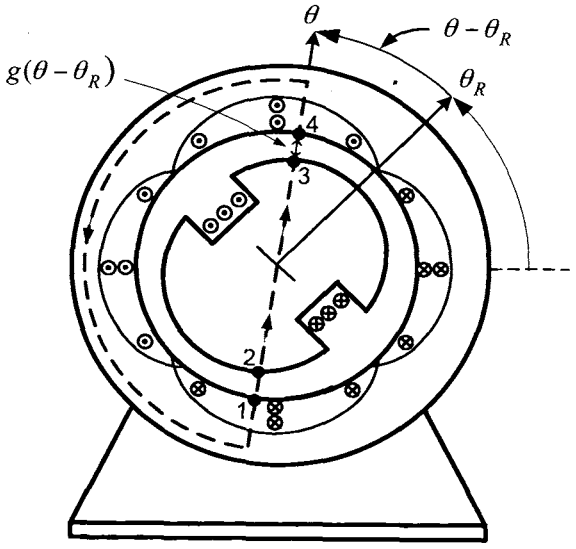


FIGURE 5.13. Synchronous motor with a salient rotor.

To do so, consider Figure 5.13 where the rotor iron is now wrapped with a standard coil with N_F turns and the pole faces have been shaped so that the air gap is no longer uniform, but instead given by

$$g(\theta - \theta_R) \triangleq \frac{g_0}{\cos(\theta - \theta_R)} = g_0 \sec(\theta - \theta_R) \tag{5.19}$$

where g_0 is the minimum air-gap distance. (Obviously, this can only be done approximately as $\cos(\theta - \theta_R) = 0$ for $\theta = \theta_R \pm \pi/2$.) To determine the magnetic field $\vec{\mathbf{B}}_R$ in the air gap due to the rotor, Ampère's law is applied

www.EngineeringEBooksPdf.com

to the path 1–2–3–4–1 above to obtain[5]

$$\int_1^2 \vec{\mathbf{H}} \cdot d\vec{\ell} + \int_3^4 \vec{\mathbf{H}} \cdot d\vec{\ell} = N_F i_F \tag{5.20}$$

where the standard assumption that $\vec{\mathbf{H}} \equiv 0$ in the magnetic material has been used. As

$$d\vec{\ell} = \begin{cases} +dr\hat{\mathbf{r}} & \text{for path } 1\text{–}2 \\ -dr\hat{\mathbf{r}} & \text{for path } 3\text{–}4 \end{cases}$$

equation (5.20) reduces to ($\vec{\mathbf{H}} = H_r\hat{\mathbf{r}}$)

$$H_r(\theta)g(\theta - \theta_R) - H_r(\theta + \pi)g(\theta - \theta_R) = N_F i_F. \tag{5.21}$$

By symmetry, the radial component must satisfy $H_r(\theta) = -H_r(\theta \pm \pi)$ so that (5.21) becomes

$$2H_r(\theta)g(\theta - \theta_R) = N_F i_F.$$

Finally,

$$H_r(\theta) = \frac{N_F i_F}{2g(\theta - \theta_R)} = \frac{N_F i_F}{2g_0}\cos(\theta - \theta_R).$$

Finally, this is multiplied by both μ_0 and r_R/r (to satisfy conservation of flux in the air gap) to obtain

$$\vec{\mathbf{B}}_R(\theta - \theta_R) = \frac{\mu_0 N_F I_F}{2g_0}\frac{r_R}{r}\cos(\theta - \theta_R)\hat{\mathbf{r}}.$$

By shaping the pole faces of the rotor according to equation (5.19), it was found this salient rotor produced the *same* magnetic field in the air gap as a sinusoidally wound rotor. However, as one moves away from the (salient) rotors' magnetic axis, the air gap is no longer small so that the assumptions about the magnetic field due to the rotor current being constant and radially directed across the air gap are less valid. On the other hand, with either a salient or sinusoidally wound rotor, the magnetic field strength of the rotor is quite weak as one moves away from the magnetic axis so that these portions do not contribute significantly to the torque. (The same can be said of the strength of the stator's magnetic field as one moves away from its magnetic axis.) As the angle between the stator's and rotor's magnetic axis is usually small, the region where the assumptions

[5] Only those paths that do not go through the field coil are being considered. At those angles θ corresponding to going through the field coil, it will turn out that the $\vec{\mathbf{B}}$ field due to the current in the coil is weak and can be neglected.

As before, it is assumed that the stator windings have an infinitesimal cross section so that $\int \vec{\mathbf{H}} \cdot d\vec{\ell} = 0$ across the winding because $d\vec{\ell} = 0$.

www.EngineeringEBooksPdf.com

are violated do not contribute significantly to the torque lending credence to the above analysis.

Remark With $r_R = \ell_2/2$, the expression for $\vec{\mathbf{B}}_S$ in (5.11) can be written as

$$\vec{\mathbf{B}}_S(i_{Sa}, i_{Sb}, r, \theta) = \frac{\mu_0 r_R N_S}{2gr} \Big(i_{Sa} \cos(\theta) + i_{Sb} \sin(\theta) \Big) \hat{\mathbf{r}}.$$

and was derived assuming a uniform air gap. If a salient rotor as in Figure 5.13 is used, then this assumption no longer holds. However, to a reasonable approximation, one can use (5.11) with $g = g_1 > g_0$, that is, some average value g_1 of the air gap length. Further, as the rotor no longer has a circular cross section, one can take $r_R = r_S - g_1$ as an average radius of the rotor.

5.3.4 Armature and Field Windings

Recall that the rotor of a DC motor was referred to as the *armature* winding. This terminology is used to indicate that the current in this winding is alternating current (AC) as every half-turn the commutator and brushes reverse the direction of the current in any given rotor loop. For a synchronous or induction motor, the stator windings carry AC current (in normal operation) so the stator windings are referred to as the armature (see Woodson and Melcher [20], page 121). Further, recall that the stator winding of a separately excited DC motor is called the *field* winding and this terminology is used to indicate that it normally carries a DC current to establish a *constant magnetic field* in the air gap that produces torque on the current in the rotor windings. Similarly, on a wound rotor synchronous machine, the rotor winding is called the *field* winding because it normally operates with a DC current to establish a *constant magnetic field* in the air gap. (This magnetic field is constant for someone rotating with the rotor.)

5.4 Microscopic Viewpoint of AC Machines*

The microscopic viewpoint of the Physics of AC machines is described in this section. This is analogous to the microscopic viewpoint of DC machines given in Chapter 1. The analysis is first done from the point of view of a stationary coordinate system and then from the point of view of a coordinate system rotating with the stator's magnetic field.

www.EngineeringEBooksPdf.com

5.4.1 *Rotating Axial Electric Field Due to the Stator Currents*

Recall from equation (5.2) that the rotating magnetic field in the air gap produced by the stator currents is

$$\begin{aligned}\vec{\mathbf{B}}_S(r,\theta,t) &= B_{Sr}(r,\theta,t)\hat{\mathbf{r}} \\ &= \frac{\mu_0 \ell_2 N_S I_S}{4gr}\cos(\theta-\omega_S t)\hat{\mathbf{r}}. \end{aligned} \tag{5.22}$$

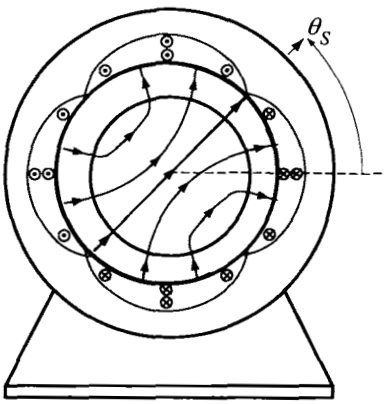


FIGURE 5.14. Rotating magnetic field $\vec{\mathbf{B}}_S$.

In Chapter 4 [see equation (4.26)], it was shown that the axial electric field produced by $\vec{\mathbf{B}}_S$ in equation (5.22) according to

$$\nabla \times \vec{\mathbf{E}}_S = -\frac{\partial \vec{\mathbf{B}}_S}{\partial t}$$

is

$$\vec{\mathbf{E}}_S(\theta,t) = E_{Sz}(\theta,t)\hat{\mathbf{z}} = \frac{\mu_0 \ell_2 N_S I_S}{4g}\omega_S \cos(\theta-\omega_S t)\hat{\mathbf{z}}. \tag{5.23}$$

This axially directed rotating electric field $\vec{\mathbf{E}}_S(\theta,t)$ is illustrated in Figure 5.15. For $\theta_S - \pi/2 \le \theta \le \theta_S + \pi/2$, the electric field is into the page ($\otimes$) while for $\theta_S + \pi/2 \le \theta \le \theta_S + 3\pi/2$, the electric field is out of the page ($\odot$).

www.EngineeringEBooksPdf.com

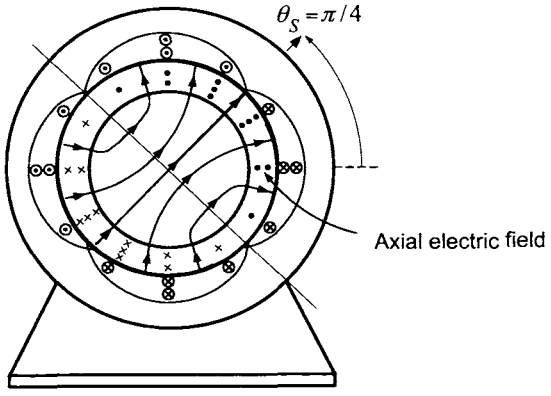


FIGURE 5.15. Rotating axial electric field $\vec{\mathbf{E}}_S = E_{Sz}(\theta, t)\hat{\mathbf{z}}$ induced by the rotating magnetic field $\vec{\mathbf{B}}_S = B_{Sr}(\theta, t)\hat{\mathbf{r}}$.

5.4.2 *Induction Machine in the Stationary Coordinate System*

Consider the setup of Figure 5.16.

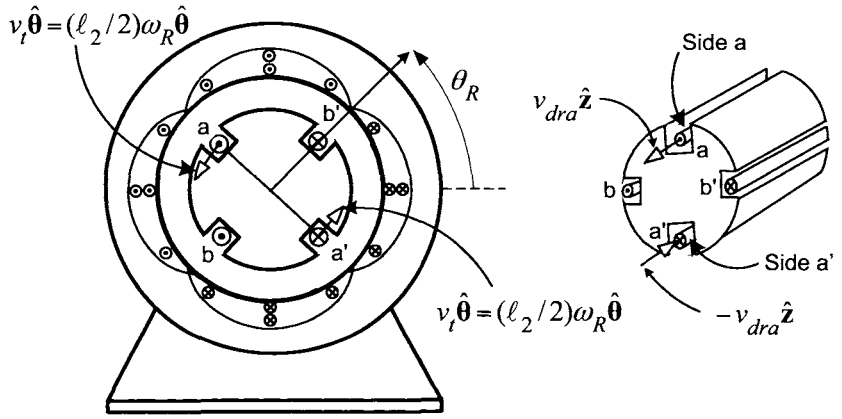


FIGURE 5.16. Simple induction motor with two single-loop rotor phases.

The axial electric field $\vec{\mathbf{E}}_S$ produces a force on charge carriers in the rotor loops. However, the *total* force on a charge carrier in a rotor loop is due to *both* the electric and magnetic fields as given by the Lorentz expression

$$\vec{\mathbf{F}} = q\vec{\mathbf{E}}_S + q\vec{\mathbf{v}} \times \vec{\mathbf{B}}_S$$

www.EngineeringEBooksPdf.com

where

$$\begin{aligned}\vec{\mathbf{B}}_S(r,\theta,t) &= B_{Sr}(r,\theta,t)\hat{\mathbf{r}} = (\mu_0 \ell_2 N_S I_S/4gr)\cos(\theta - \omega_S t)\hat{\mathbf{r}} \\ \vec{\mathbf{E}}_S(\theta,t) &= E_{Sz}(\theta,t)\hat{\mathbf{z}} = \frac{\mu_0 \ell_2 N_S I_S}{4g}\omega_S \cos(\theta - \omega_S t)\hat{\mathbf{z}}.\end{aligned} \tag{5.24}$$

To compute $\vec{\mathbf{v}}\times\vec{\mathbf{B}}_S$, let v_{dra} be the (drift) speed of the charge carriers (which make up the current) along rotor loop a. The speed v_{dra} being positive means that the current is positive; that is, coming out of the page $\odot$ on side a and into the page $\otimes$ on side a'. Then, with $v_t = (\ell_2/2)\omega_R$, the speed of the charge carriers in the $\hat{\boldsymbol{\theta}}$ direction, the *total* velocity of the charge carriers along the axial sides of rotor loop a is

$$\vec{\mathbf{v}} = \begin{cases} +v_{dra}\hat{\mathbf{z}} + v_t\hat{\boldsymbol{\theta}} & \text{for side } a \\ -v_{dra}\hat{\mathbf{z}} + v_t\hat{\boldsymbol{\theta}} & \text{for side } a'. \end{cases}$$

The magnetic force per unit charge on the charge carriers on the axial sides of rotor loop a is given by

$$\vec{\mathbf{v}} \times \vec{\mathbf{B}}_S =$$

$$\begin{cases} +v_{dra}B_{Sr}(\ell_2/2,\theta_R+\pi/2,t)\hat{\boldsymbol{\theta}} - v_t B_{Sr}(\ell_2/2,\theta_R+\pi/2,t)\hat{\mathbf{z}} & \text{for side } a \\ -v_{dra}B_{Sr}(\ell_2/2,\theta_R-\pi/2,t)\hat{\boldsymbol{\theta}} - v_t B_{Sr}(\ell_2/2,\theta_R-\pi/2,t)\hat{\mathbf{z}} & \text{for side } a'. \end{cases}$$

Using equation (5.24), it follows that for side a

$$\begin{aligned} B_{Sr}(\ell_2/2,\theta_R+\pi/2,t)\hat{\mathbf{r}} &= \frac{\mu_0 N_S I_S}{2g}\cos(\theta_R+\pi/2-\omega_S t)\hat{\mathbf{r}} \\ &= \frac{\mu_0 N_S I_S}{2g}\sin(\omega_S t - \theta_R)\hat{\mathbf{r}}. \end{aligned}$$

Similarly, on side a'

$$\begin{aligned} B_{Sr}(\ell_2/2,\theta_R-\pi/2,t)\hat{\mathbf{r}} &= \frac{\mu_0 N_S I_S}{2g}\cos(\theta_R-\pi/2-\omega_S t)\hat{\mathbf{r}} \\ &= -\frac{\mu_0 N_S I_S}{2g}\sin(\omega_S t - \theta_R)\hat{\mathbf{r}}. \end{aligned}$$

With $v_t = (\ell_2/2)\omega_R$ and $\theta_R = \omega_R t$, the magnetic force per unit charge in rotor loop a may now be written as

$$\vec{\mathbf{v}}\times\vec{\mathbf{B}}_S =$$

$$\begin{cases} v_{dra}\frac{\mu_0 N_S I_S}{2g}\sin(\omega_S t-\omega_R t)\hat{\boldsymbol{\theta}} - \omega_R\frac{\mu_0 \ell_2 N_S I_S}{4g}\sin(\omega_S t-\omega_R t)\hat{\mathbf{z}} & \text{for side } a \\ v_{dra}\frac{\mu_0 N_S I_S}{2g}\sin(\omega_S t-\omega_R t)\hat{\boldsymbol{\theta}} + \omega_R\frac{\mu_0 \ell_2 N_S I_S}{4g}\sin(\omega_S t-\omega_R t)\hat{\mathbf{z}} & \text{for side } a'. \end{cases} \tag{5.25}$$

www.EngineeringEBooksPdf.com

Next, the electric field $\vec{\mathbf{E}}_S$ in rotor loop a is given by

$$\vec{\mathbf{E}}_S = \begin{cases} E_{Sz}(\theta_R + \pi/2, t)\hat{\mathbf{z}} & \text{for side } a \\ E_{Sz}(\theta_R - \pi/2, t)\hat{\mathbf{z}} & \text{for side } a'. \end{cases}$$

Using (5.24) and $\theta_R(t) = \omega_R t$, this becomes for side a

$$\begin{aligned} \vec{\mathbf{E}}_S &= \frac{\mu_0 \ell_2 N_S I_S}{4g} \omega_S \cos(\omega_R t + \pi/2 - \omega_S t)\hat{\mathbf{z}} \\ &= \frac{\mu_0 \ell_2 N_S I_S}{4g} \omega_S \sin(\omega_S t - \omega_R t)\hat{\mathbf{z}} \end{aligned} \tag{5.26}$$

and for side a'

$$\begin{aligned} \vec{\mathbf{E}}_S &= \frac{\mu_0 \ell_2 N_S I_S}{4g} \omega_S \cos(\omega_R t - \pi/2 - \omega_S t)\hat{\mathbf{z}} \\ &= -\frac{\mu_0 \ell_2 N_S I_S}{4g} \omega_S \sin(\omega_S t - \omega_R t)\hat{\mathbf{z}}. \end{aligned} \tag{5.27}$$

The total force per unit charge $\vec{\mathbf{F}}/q = \vec{\mathbf{E}}_S + \vec{\mathbf{v}} \times \vec{\mathbf{B}}_S$ on side a is then

$$\begin{aligned} \vec{\mathbf{F}}_{\text{side } a}/q = \frac{\mu_0 \ell_2 N_S I_S}{4g} \omega_S \sin(\omega_S t - \omega_R t)\hat{\mathbf{z}} + v_{dra} \frac{\mu_0 N_S I_S}{2g} \\ \times \sin(\omega_S t - \omega_R t)\hat{\boldsymbol{\theta}} - \omega_R \frac{\mu_0 \ell_2 N_S I_S}{4g} \sin(\omega_S t - \omega_R t)\hat{\mathbf{z}} \end{aligned} \tag{5.28}$$

and for side a' it is given by

$$\begin{aligned} \vec{\mathbf{F}}_{\text{side } a'}/q = -\frac{\mu_0 \ell_2 N_S I_S}{4g} \omega_S \sin(\omega_S t - \omega_R t)\hat{\mathbf{z}} + v_{dra} \frac{\mu_0 N_S I_S}{2g} \\ \times \sin(\omega_S t - \omega_R t)\hat{\boldsymbol{\theta}} + \omega_R \frac{\mu_0 \ell_2 N_S I_S}{4g} \sin(\omega_S t - \omega_R t)\hat{\mathbf{z}}. \end{aligned} \tag{5.29}$$

These last two expressions simplify to

$$\begin{aligned} \vec{\mathbf{F}}_{\text{side } a}/q &= v_{dra} \frac{\mu_0 N_S I_S}{2g} \sin\left((\omega_S - \omega_R)t\right)\hat{\boldsymbol{\theta}} \\ &\quad + \frac{\mu_0 \ell_2 N_S I_S}{4g} (\omega_S - \omega_R) \sin\left((\omega_S - \omega_R)t\right)\hat{\mathbf{z}} \end{aligned} \tag{5.30}$$

and

$$\begin{aligned} \vec{\mathbf{F}}_{\text{side } a'}/q &= v_{dra} \frac{\mu_0 N_S I_S}{2g} \sin\left((\omega_S - \omega_R)t\right)\hat{\boldsymbol{\theta}} \\ &\quad - \frac{\mu_0 \ell_2 N_S I_S}{4g} (\omega_S - \omega_R) \sin\left((\omega_S - \omega_R)t\right)\hat{\mathbf{z}}. \end{aligned} \tag{5.31}$$

The component in $\hat{\boldsymbol{\theta}}$ direction (tangential to the rotor motion) is what produces the torque. With N the number of charge carriers per unit volume

www.EngineeringEBooksPdf.com

in the conductor of rotor phase a, S the cross-sectional area of the loop, it follows that $qNS\ell_1$ is the total number of charge carriers on each axial side of the loop. Therefore, the total tangential magnetic force on these charge carriers is

$$\vec{\mathbf{F}}_{\hat{\boldsymbol{\theta}}} = qNS\ell_1 v_{dra} \frac{\mu_0 N_S I_S}{2g} \sin\left((\omega_S - \omega_R)t\right)\hat{\boldsymbol{\theta}}.$$

Recalling that $i_{Ra} = qNSv_{dra}$ is the rotor current and computing the torque according to $(\ell_2/2)\hat{\mathbf{r}} \times \vec{\mathbf{F}}_{\hat{\boldsymbol{\theta}}}$, the total torque on rotor loop a is

$$\begin{aligned}
\vec{\boldsymbol{\tau}}_{Ra} &= \tau_{Ra}\hat{\mathbf{z}} \\
&= \left((\ell_2/2)\hat{\mathbf{r}} \times \vec{\mathbf{F}}_{\hat{\boldsymbol{\theta}}}\right)_{side-a} + \left((\ell_2/2)\hat{\mathbf{r}} \times \vec{\mathbf{F}}_{\hat{\boldsymbol{\theta}}}\right)_{side-a'} \\
&= 2i_{Ra}\ell_1 \frac{\mu_0 N_S I_S}{2g} \sin((\omega_S - \omega_R)t)\,(\ell_2/2)\hat{\mathbf{r}} \times \hat{\boldsymbol{\theta}} \\
&= i_{Ra} \frac{\mu_0 \ell_1 \ell_2 N_S I_S}{2g} \sin((\omega_S - \omega_R)t)\hat{\mathbf{z}}. \qquad (5.32)
\end{aligned}$$

To evaluate the torque, the current i_{Ra} must be computed. The current in the rotor loop is produced by the total emf in the loop. Note that the electric field $\vec{\mathbf{E}}_S = E_{Sz}\hat{\mathbf{z}}$ induced by the stator's rotating magnetic field is pushing charge out of side a and into side a', and it is being opposed by the axial magnetic force $(\vec{\mathbf{v}} \times \vec{\mathbf{B}}_S)_z\hat{\mathbf{z}}$ as equation (5.28) shows. For example, on side a, the electric field

$$E_{Sz}\hat{\mathbf{z}} = \frac{\mu_0 \ell_2 N_S I_S}{4g} \omega_S \sin((\omega_S - \omega_R)t)\hat{\mathbf{z}}$$

is opposed by the z component of the magnetic force per unit charge

$$(\vec{\mathbf{v}} \times \vec{\mathbf{B}}_S)_z\hat{\mathbf{z}} = -\frac{\mu_0 \ell_2 N_S I_S}{4g} \omega_R \sin((\omega_S - \omega_R)t)\hat{\mathbf{z}}.$$

It follows by (5.30) and (5.31) that the total *axial* or z component of the force per unit charge is

$$(\vec{\mathbf{F}}/q)_z = \begin{cases} \dfrac{\mu_0 \ell_2 N_S I_S}{4g}(\omega_S - \omega_R)\sin((\omega_S - \omega_R)t)\,\hat{\mathbf{z}} & \text{side } a \\ -\dfrac{\mu_0 \ell_2 N_S I_S}{4g}(\omega_S - \omega_R)\sin((\omega_S - \omega_R)t)\,\hat{\mathbf{z}} & \text{side } a'. \end{cases} \qquad (5.33)$$

Thus *electromotive force* or *emf* in the rotor loop is simply the integral of the force per unit charge around the loop, that is,

$$\begin{aligned}
\xi_{Ra} &\triangleq \oint_{\text{rotor loop } a} (\vec{\mathbf{F}}/q) \cdot d\vec{\boldsymbol{\ell}} \\
&= \oint_{\text{rotor loop } a} (\vec{\mathbf{E}}_S + \vec{\mathbf{v}} \times \vec{\mathbf{B}}_S) \cdot d\vec{\boldsymbol{\ell}}
\end{aligned}$$

www.EngineeringEBooksPdf.com

where

$$d\vec{\ell} = \begin{cases} +dz\hat{\mathbf{z}} & \text{for side } a \\ -dz\hat{\mathbf{z}} & \text{for side } a'. \end{cases}$$

As $d\vec{\ell}$ is aligned with $\pm\hat{\mathbf{z}}$, only the axial component $(\vec{\mathbf{F}}/q)_z$ given in equation (5.33) contributes to the emf.

Evaluating the line integral, the induced emf in rotor phase a is given by

$$\xi_{Ra} = \frac{\mu_0 \ell_1 \ell_2 N_S I_S}{2g}(\omega_S - \omega_R)\sin((\omega_S - \omega_R)t) \tag{5.34}$$

which is the same as in the macroscopic case. Neglecting the rotor inductance so that $i_{Ra} = \xi_{Ra}/R_R$, the torque on rotor loop a is

$$\tau_{Ra} = \frac{1}{R_R}\left(\frac{\mu_0 \ell_1 \ell_2 N_S I_S}{2g}\right)^2 (\omega_S - \omega_R)\sin^2\Big((\omega_S - \omega_R)t\Big). \tag{5.35}$$

A similar analysis shows that

$$\tau_{Rb} = \frac{1}{R_R}\left(\frac{\mu_0 \ell_1 \ell_2 N_S I_S}{2g}\right)^2 (\omega_S - \omega_R)\cos^2\Big((\omega_S - \omega_R)t\Big). \tag{5.36}$$

Rotor Torque Computed from Microscopic Point of View

Adding equations (5.35) and (5.36), the total torque on the rotor is

$$\tau = \tau_{Ra} + \tau_{Rb} = \left(\frac{\mu_0 \ell_1 \ell_2 N_S I_S}{2g}\right)^2 \frac{1}{R_R}(\omega_S - \omega_R)$$

which is the same expression as that computed in the macroscopic case.

Electromechanical Energy Conversion

Define the voltage in rotor loop a produced by the stator electric field $\vec{\mathbf{E}}_S$ as

$$V_{Ra} \triangleq \oint_{\text{rotor loop } a} \vec{\mathbf{E}}_S \cdot d\vec{\ell} = \frac{\mu_0 \ell_1 \ell_2 N_S I_S}{2g}\omega_S \sin\Big((\omega_S - \omega_R)t\Big). \tag{5.37}$$

For example, if the rotor was locked so that $\omega_R = 0$ in (5.37), then this would be the total emf in the rotor loop as can be seen by setting $\omega_R = 0$ in (5.34). However, due to the rotor's motion ($\omega_R \neq 0$), there is an axial (z component) magnetic force per unit charge. Define the "back emf" ζ_{Ra} as the integral of the axial magnetic force per unit charge around the rotor

www.EngineeringEBooksPdf.com

loop, that is,

$$\begin{aligned}\zeta_{Ra} &\triangleq \oint_{\text{rotor loop } a} (\vec{\mathbf{v}}\times\vec{\mathbf{B}}_S)_z \cdot d\vec{\ell} \\ &= \int_0^{\ell_1} \left(-\omega_R \frac{\mu_0 \ell_2 N_S I_S}{4g} \sin(\omega_S t - \omega_R t)\hat{\mathbf{z}}\right) \cdot (d\ell\hat{\mathbf{z}}) \\ &\quad + \int_0^{\ell_1} \left(\omega_R \frac{\mu_0 \ell_2 N_S I_S}{4g} \sin(\omega_S t - \omega_R t)\hat{\mathbf{z}}\right) \cdot (-d\ell\hat{\mathbf{z}}) \\ &= -\frac{\mu_0 \ell_1 \ell_2 N_S I_S}{2g} \omega_R \sin((\omega_S - \omega_R)t)\,. \end{aligned} \tag{5.38}$$

In summary, the total emf ξ_{Ra} in rotor loop a may be written as

$$\begin{aligned}\xi_{Ra} &= \oint_{\text{rotor loop } a} (\vec{\mathbf{E}}_S + \vec{\mathbf{v}}\times\vec{\mathbf{B}}_S) \cdot d\vec{\ell} = V_{Ra} + \zeta_{Ra} \\ &= \frac{\mu_0 \ell_1 \ell_2 N_S I_S}{2g} (\omega_S - \omega_R) \sin((\omega_S - \omega_R)t) \end{aligned} \tag{5.39}$$

where V_{Ra} is the voltage produced in the rotor loop by the induced electric field $\vec{\mathbf{E}}_S$ and ζ_{Ra} is the back emf produced by the axial magnetic force per unit charge $\vec{\mathbf{v}}\times\vec{\mathbf{B}}_S$. By direct substitution using equations (5.32) and (5.38), it is easy to see that

$$\tau_{Ra}\omega_R + i_{Ra}\zeta_{Ra} = 0.$$

Here $\tau_{Ra}\omega_R$ is the mechanical power produced on rotor loop a while $i_{Ra}\zeta_{Ra}$ is the electrical power absorbed by the back emf. That is, if $\tau_{Ra}\omega_R > 0$ so that mechanical power is being produced, then $i_{Ra}\zeta_{Ra} < 0$ is the electrical power being absorbed by back emf in rotor loop a. Another interesting point is that

$$i_{Ra}V_{Ra}$$

is the total electrical power into rotor loop a from the stator, that is,

$$i_{Ra}V_{Ra} = i_{Ra}\xi_{Ra} - i_{Ra}\zeta_{Ra} = i_{Ra}\xi_{Ra} + \tau_{Ra}\omega_R.$$

In other words, the total power $i_{Ra}V_{Ra}$ into rotor loop a is converted into the electrical power $i_{Ra}\xi_{Ra}$ (ultimately dissipated as heat in the rotor resistance) and into the mechanical power $\tau_{Ra}\omega_R$ ($= -i_{Ra}\zeta_{Ra}$). Similar remarks hold for rotor loop b.

www.EngineeringEBooksPdf.com

5.4.3 *Faraday's Law and the Integral of the Force per Unit Charge*

In this subsection, it is shown that Faraday's law gives the same emf as integrating the force per unit charge around the loop, that is,

$$\xi = -\frac{d}{dt}\left(\int_S \vec{\mathbf{B}} \cdot d\vec{\mathbf{S}}\right) = \oint_C (\vec{\mathbf{E}} + \vec{\mathbf{v}} \times \vec{\mathbf{B}}) \cdot d\vec{\ell}. \tag{5.40}$$

In equation (5.3), ξ_{Ra} was computed using $\xi_{Ra} = -\frac{d}{dt}\left(\int_S \vec{\mathbf{B}} \cdot d\vec{\mathbf{S}}\right)$ while in equation (5.39), it was computed using $\xi_{Ra} = \oint_C (\vec{\mathbf{E}}_S + \vec{\mathbf{v}} \times \vec{\mathbf{B}}_S) \cdot d\vec{\ell}$ and both methods gave the same result. The objective here is to show that this is true in general.

To show that (5.40) is true in general, let S be a surface whose boundary is the closed loop C in a region of space with an electric field $\vec{\mathbf{E}}$ and a magnetic field $\vec{\mathbf{B}}$. The line integral of the force per unit charge gives

$$\begin{aligned}\oint_C (\vec{\mathbf{E}} + \vec{\mathbf{v}} \times \vec{\mathbf{B}}) \cdot d\vec{\ell} &= \oint_S \left(\nabla \times \vec{\mathbf{E}}\right) \cdot d\vec{\mathbf{S}} + \oint_C \left(\vec{\mathbf{v}} \times \vec{\mathbf{B}}\right) \cdot d\vec{\ell} \\ &= \oint_S \left(-\frac{\partial \vec{\mathbf{B}}}{\partial t}\right) \cdot d\vec{\mathbf{S}} + \oint_C \left(\vec{\mathbf{v}} \times \vec{\mathbf{B}}\right) \cdot d\vec{\ell}\end{aligned}$$

where Stokes theorem

$$\oint_C \vec{\mathbf{E}} \cdot d\vec{\ell} = \oint_S \left(\nabla \times \vec{\mathbf{E}}\right) \cdot d\vec{\mathbf{S}}$$

and Faraday's law in differential form

$$\nabla \times \vec{\mathbf{E}} = -\frac{\partial \vec{\mathbf{B}}}{\partial t}$$

were used [35][36]. Using the fact that

$$\oint_S \left(-\frac{\partial \vec{\mathbf{B}}}{\partial t}\right) \cdot d\vec{\mathbf{S}} = -\frac{\partial}{\partial t} \oint_S \vec{\mathbf{B}} \cdot d\vec{\mathbf{S}}$$

and the vector identity

$$\left(\vec{\mathbf{v}} \times \vec{\mathbf{B}}\right) \cdot d\vec{\ell} = -\vec{\mathbf{B}} \cdot \left(\vec{\mathbf{v}} \times d\vec{\ell}\right)$$

this reduces to

$$\begin{aligned}\oint_C (\vec{\mathbf{E}} + \vec{\mathbf{v}} \times \vec{\mathbf{B}}) \cdot d\vec{\ell} &= -\frac{\partial}{\partial t} \oint_S \vec{\mathbf{B}} \cdot d\vec{\mathbf{S}} + \oint_C \left(\vec{\mathbf{v}} \times \vec{\mathbf{B}}\right) \cdot d\vec{\ell} \\ &= -\frac{\partial}{\partial t} \oint_S \vec{\mathbf{B}} \cdot d\vec{\mathbf{S}} - \oint_C \vec{\mathbf{B}} \cdot \left(\vec{\mathbf{v}} \times d\vec{\ell}\right). \end{aligned} \tag{5.41}$$

www.EngineeringEBooksPdf.com

Now $\vec{\mathbf{v}}$ is the velocity of the charge carriers in the loop C and note that if the loop itself is not moving, then $\vec{\mathbf{v}}$ is in the same direction as $d\vec{\boldsymbol{\ell}}$ so that $\vec{\mathbf{v}} \times d\vec{\boldsymbol{\ell}} = 0$. In general, with γ the angle between $\vec{\mathbf{v}}$ and $d\vec{\boldsymbol{\ell}}$,

$$| \vec{\mathbf{v}} \times d\vec{\boldsymbol{\ell}} | = v \sin(\gamma) d\ell = v_\perp d\ell$$

where $v_\perp = v\sin(\gamma)$ is the velocity component perpendicular to $d\vec{\boldsymbol{\ell}}$. The quantity $| \vec{\mathbf{v}} \times d\vec{\boldsymbol{\ell}} |$ represents a *change* in the flux surface as is now explained.

To fix ideas, consider a single loop on the rotor of a motor as shown in Figure 5.17.

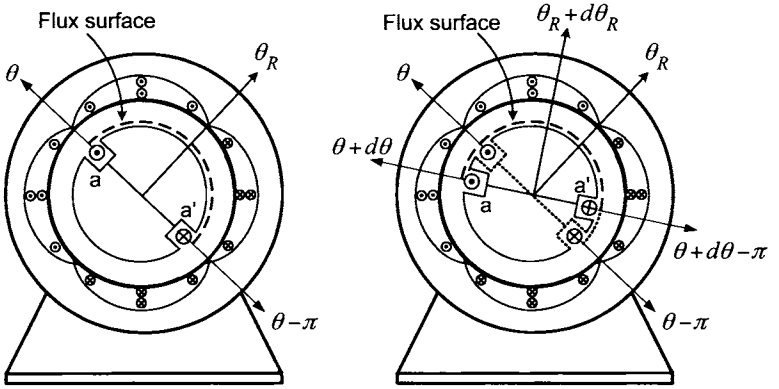


FIGURE 5.17. (a) Flux surface on a moving loop with side a at θ. (b) Loop rotates with side a going from θ to $\theta + d\theta$.

Consider that in the time dt, side a of the loop rotates from $\theta = \theta_R + \pi/2$ to $\theta + d\theta = \theta_R + \pi/2 + d\theta_R$ (with side a' going from $\theta - \pi$ to $\theta + d\theta - \pi$, $d\theta/dt = \omega_R$). With $\vec{\mathbf{B}}$ denoting the magnetic field produced by the stator currents, the quantity

$$\begin{aligned}
dt \oint_C \vec{\mathbf{B}} \cdot \left(\vec{\mathbf{v}} \times d\vec{\boldsymbol{\ell}} \right) &= dt \int_{\text{side } a} B_r(r_R, \theta, t)\hat{\mathbf{r}} \cdot \left(\frac{\ell_2}{2}\omega_R \hat{\boldsymbol{\theta}} \times d\ell \hat{\mathbf{z}} \right) \\
&\quad + dt \int_{\text{side } a'} B_r(r_R, \theta - \pi, t)\hat{\mathbf{r}} \cdot \left(\frac{\ell_2}{2}\omega_R \hat{\boldsymbol{\theta}} \times (-d\ell)\hat{\mathbf{z}} \right) \\
&= \int_{\text{side } a} B_r(r_R, \theta, t)\hat{\mathbf{r}} \cdot \left(\omega_R dt \frac{\ell_2}{2} d\ell \hat{\mathbf{r}} \right) \\
&\quad + \int_{\text{side } a'} B_r(r_R, \theta - \pi, t)\hat{\mathbf{r}} \cdot \left(-\omega_R dt \frac{\ell_2}{2} d\ell \hat{\mathbf{r}} \right) \\
&= \int_{\text{side } a} \left(B_r(r_R, \theta, t)\frac{\ell_2}{2}\omega_R dt \right) d\ell + \int_{\text{side } a'} \left(-B_r(r_R, \theta - \pi, t)\frac{\ell_2}{2}\omega_R dt \right) d\ell \\
&= B_r(r_R, \theta, t)\ell_1 \frac{\ell_2}{2} d\theta - B_r(r_R, \theta - \pi, t)\ell_1 \frac{\ell_2}{2} d\theta
\end{aligned}$$

www.EngineeringEBooksPdf.com

where $d\theta = \omega_R dt$ was used in the last line. Then $B_r(r_R, \theta, t)\ell_1(\ell_2/2)d\theta$ is the additional flux due to the surface area change as side a moved from θ to $\theta + d\theta$ while $-B_r(r_R, \theta - \pi, t)\ell_1(\ell_2/2)d\theta$ is the decrease in flux due to the surface area change as side a' moved from $\theta - \pi$ to $\theta + d\theta - \pi$. That is, the quantity

$$dt \oint_C \left(\vec{\mathbf{v}} \times d\vec{\boldsymbol{\ell}}\right) \cdot \vec{\mathbf{B}} = B_r(r_R, \theta, t)\ell_1 \frac{\ell_2}{2} d\theta - B_r(r_R, \theta - \pi, t)\ell_1 \frac{\ell_2}{2} d\theta \quad (5.42)$$

is the *change in flux* $d\phi$ in the rotor loop due to the rotation of the loop through the angle $d\theta$. In more detail,

$$\phi(\theta, t) \triangleq \oint_S \vec{\mathbf{B}} \cdot d\vec{\mathbf{S}} = \int_{\theta-\pi}^{\theta} \int_0^{\ell_1} B_r(r_R, \theta', t)(\ell_2/2)d\theta'$$

so that

$$\begin{aligned} \frac{d\phi}{dt} &= \frac{\partial \phi(\theta, t)}{\partial t} + \frac{\partial \phi(\theta, t)}{\partial \theta}\frac{d\theta}{dt} \\ &= \frac{\partial \phi(\theta, t)}{\partial t} + \frac{\partial}{\partial \theta}\left(\int_{\theta-\pi}^{\theta} \int_0^{\ell_1} B_r(r_R, \theta', t)(\ell_2/2)d\theta'\right)\frac{d\theta}{dt} \\ &= \frac{\partial}{\partial t}\oint_S \vec{\mathbf{B}} \cdot d\vec{\mathbf{S}} + \left(B_r(r_R, \theta, t)\ell_1 \frac{\ell_2}{2} - B_r(r_R, \theta - \pi, t)\ell_1 \frac{\ell_2}{2}\right)\frac{d\theta}{dt} \end{aligned}$$

where the Liebniz rule for differentiation was used. Consequently, by comparison with (5.42), it follows that

$$\oint_C \left(\vec{\mathbf{v}} \times d\vec{\boldsymbol{\ell}}\right) \cdot \vec{\mathbf{B}} = \frac{\partial \phi(\theta, t)}{\partial \theta}\frac{d\theta}{dt}$$

is the rate of change of flux due to the motion of the loop while

$$\frac{\partial}{\partial t}\oint_S \vec{\mathbf{B}} \cdot d\vec{\mathbf{S}} = \frac{\partial \phi(\theta, t)}{\partial t}$$

is the rate of change of flux due to the time-varying magnetic field $\vec{\mathbf{B}}$. By Faraday's law, the induced voltage in the loop is given by

$$\begin{aligned} \xi &= -\frac{d\phi}{dt} = -\frac{\partial \phi(\theta, t)}{\partial t} - \frac{\partial \phi(\theta, t)}{\partial \theta}\frac{d\theta}{dt} = -\frac{\partial}{\partial t}\oint_S \vec{\mathbf{B}} \cdot d\vec{\mathbf{S}} - \oint_C \left(\vec{\mathbf{v}} \times d\vec{\boldsymbol{\ell}}\right) \cdot \vec{\mathbf{B}} \\ &= \oint_C (\vec{\mathbf{E}} + \vec{\mathbf{v}} \times \vec{\mathbf{B}}) \cdot d\vec{\boldsymbol{\ell}} \end{aligned}$$

where (5.41) was used.

www.EngineeringEBooksPdf.com

5.4.4 *Induction Machine in the Synchronous Coordinate System*

Up to this point, the electric and magnetic fields have been viewed from the reference frame of the stator. Often in electric machine theory, concepts are discussed from the point of view of a *rotating* reference frame such as that of the stator's rotating magnetic field which rotates at angular speed ω_S or that of the rotor which rotates at angular speed ω_R. It turns out that the electric and magnetic fields *change* from one moving coordinate system to another. To understand the changes, the microscopic viewpoint is repeated in a coordinate system that rotates with the rotating magnetic field produced by the stator currents. (Problem 17 considers the microscopic point of view in the rotor coordinate system.)

Figure 5.18 shows the rotating stator magnetic field $\vec{\mathbf{B}}_S$. The observer is face down and rotates with the stator magnetic field.

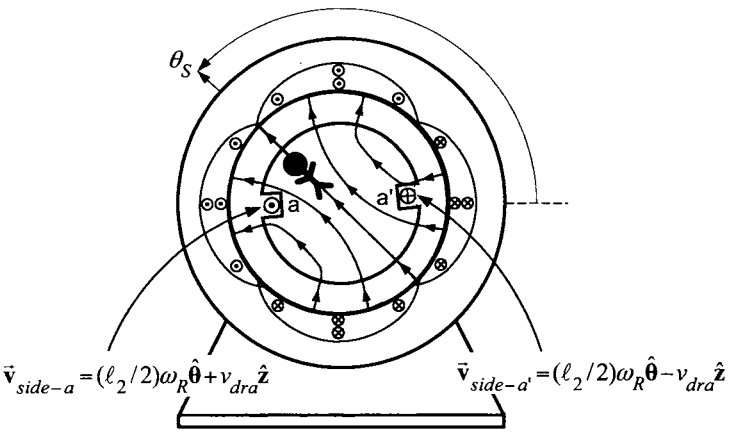


FIGURE 5.18. An observer in the synchronous coordinate system that rotates with $\vec{\mathbf{B}}_S$. The rotating magnetic field produced by the stator currents has angular speed ω_S while the rotor has angular speed ω_R.

In any given reference/coordinate system, the Lorentz force on a charge carrier is given by

$$\vec{\mathbf{F}} = q\left(\vec{\mathbf{E}} + \vec{\mathbf{v}}\times\vec{\mathbf{B}}\right)$$

where $\vec{\mathbf{E}}$ and $\vec{\mathbf{B}}$ are the electric and magnetic fields measured in the particular reference/coordinate system and $\vec{\mathbf{v}}$ is the velocity of the charge carrier as measured in the same coordinate system.

Recall that, in the coordinate system fixed to stator, the electric and magnetic fields in the air gap of the motor produced by the stator currents

www.EngineeringEBooksPdf.com

are

$$\begin{aligned}\vec{\mathbf{E}}_S(\theta,t) &= E_{Sz}(\theta,t)\hat{\mathbf{z}} = \frac{\mu_0 \ell_2 N_S I_S}{4g}\omega_S \cos(\theta-\omega_S t)\hat{\mathbf{z}} \\ \vec{\mathbf{B}}_S(r,\theta,t) &= B_{Sr}(r,\theta,t)\hat{\mathbf{r}} = \frac{\mu_0 \ell_2 N_S I_S}{4gr}\cos(\theta-\omega_S t)\hat{\mathbf{r}}\end{aligned} \tag{5.43}$$

and the velocity of the charge carriers in the axial sides of rotor loop a is

$$\vec{\mathbf{v}}_{Ra} = \begin{cases} v_{dra}\hat{\mathbf{z}} + v_t\hat{\boldsymbol{\theta}} & \text{side } a \\ -v_{dra}\hat{\mathbf{z}} + v_t\hat{\boldsymbol{\theta}} & \text{side } a' \end{cases}$$

where $v_t = (\ell_2/2)\omega_R$.

Consider a jump into a coordinate system moving (rotating) with the magnetic field $\vec{\mathbf{B}}_S$, that is, a coordinate system that rotates at angular speed ω_S. This referred to as the *synchronous coordinate* coordinate system and is denoted here as the primed ($'$) coordinate system. How do the above electric and magnetic fields transform (change) when one goes to the rotating (primed) coordinate system? Consider Figure 5.19 depicting two coordinate systems in which the primed ($'$) coordinate system has velocity $\vec{\mathbf{v}}' = v'\hat{\mathbf{y}}$ with respect to the unprimed coordinate system. According to the Special Theory of Relativity [35][36], the fields transform according to

$$\begin{aligned}\vec{\mathbf{E}}'_{||} &= \vec{\mathbf{E}}_{||} & \vec{\mathbf{B}}'_{||} &= \vec{\mathbf{B}}_{||} \\ \vec{\mathbf{E}}'_{\perp} &= \gamma\left(\vec{\mathbf{E}}_{\perp} + \vec{\mathbf{v}}'\times\vec{\mathbf{B}}_{\perp}\right) & \vec{\mathbf{B}}'_{\perp} &= \gamma\left(\vec{\mathbf{B}}_{\perp} + (v'/c^2)\times\vec{\mathbf{E}}_{\perp}\right)\end{aligned}$$

where $\gamma \triangleq 1/\sqrt{1-(v'/c)^2}$, c is the speed of light, $v' = |\vec{\mathbf{v}}'|$, $\vec{\mathbf{E}}_{||}$ and $\vec{\mathbf{B}}_{||}$ are, respectively, the electric and magnetic fields parallel to the motion (i.e., in the y direction in Figure 5.19) and finally, $\vec{\mathbf{E}}_{\perp}$ and $\vec{\mathbf{B}}_{\perp}$ are, respectively, the electric and magnetic fields perpendicular to the motion (i.e., in an x-z plane of Figure 5.19). Similar comments apply to $\vec{\mathbf{E}}'_{||}$, $\vec{\mathbf{B}}'_{||}$, $\vec{\mathbf{E}}'_{\perp}$, and $\vec{\mathbf{B}}'_{\perp}$.

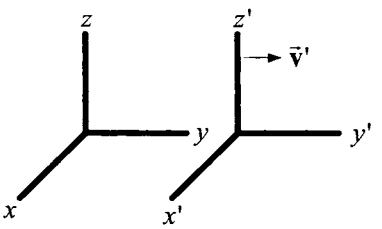


FIGURE 5.19. Two coordinate systems moving with respect to one another.

www.EngineeringEBooksPdf.com

For the application to electric machines where $(v'/c)^2 \ll 1$, it follows that $\gamma = 1$ can be used as an excellent approximation and the above transformation reduces to

$$\begin{aligned} \vec{\mathbf{E}}'_{||} &= \vec{\mathbf{E}}_{||} & \vec{\mathbf{B}}'_{||} &= \vec{\mathbf{B}}_{||} \\ \vec{\mathbf{E}}'_{\perp} &= \vec{\mathbf{E}}_{\perp} + \vec{\mathbf{v}}' \times \vec{\mathbf{B}}_{\perp} & \vec{\mathbf{B}}'_{\perp} &= \vec{\mathbf{B}}_{\perp}. \end{aligned} \tag{5.44}$$

Returning to the induction motor and the rotating coordinate system of the stator magnetic field, the coordinate transformation from the stationary coordinate system (unprimed) to the rotating coordinate system (primed) of the rotating stator magnetic field is

$$\begin{bmatrix} x' \\ y' \\ z' \end{bmatrix} = \begin{bmatrix} \cos(\omega_S t) & \sin(\omega_S t) & 0 \\ -\sin(\omega_S t) & \cos(\omega_S t) & 0 \\ 0 & 0 & 1 \end{bmatrix} \begin{bmatrix} x \\ y \\ z \end{bmatrix}.$$

In cylindrical coordinates, the transformation is simply

$$\begin{aligned} r' &= r \\ \theta' &= \theta - \omega_S t \\ z' &= z. \end{aligned}$$

Remark Note that a *stationary* point (r', θ') in this rotating coordinate system has velocity $\vec{\mathbf{v}} = r'\omega_S \hat{\boldsymbol{\theta}}$ in the (original unprimed) stator coordinate system. Note also that in this rotating coordinate system, the rotor's angular speed ω'_R is given by $\omega'_R = -(\omega_S - \omega_R) < 0$. This is simply a consequence of the fact that the coordinate system rotating with the stator magnetic field is rotating *faster* than the rotor.

The first step is to find the electric and magnetic fields in this rotating coordinate system. For the induction motor, the fields perpendicular and parallel to the motion are given by

$$\begin{aligned} \vec{\mathbf{E}}_{\perp} &= \vec{\mathbf{E}}_S \\ \vec{\mathbf{E}}_{||} &= \mathbf{0} \\ \vec{\mathbf{B}}_{\perp} &= \vec{\mathbf{B}}_S \\ \vec{\mathbf{B}}_{||} &= \mathbf{0} \end{aligned}$$

where $\vec{\mathbf{E}}_S$ and $\vec{\mathbf{B}}_S$ are given in (5.43). At the surface of the rotor, the new coordinate system has velocity $\vec{\mathbf{v}}' = (\ell_2/2)\omega_S \hat{\boldsymbol{\theta}}$ with respect to the original coordinate system so that the electric and magnetic fields in the rotating

www.EngineeringEBooksPdf.com

coordinate system are given by

$$\begin{aligned}\vec{\mathbf{E}}'_S &= \vec{\mathbf{E}}_S + \vec{\mathbf{v}}' \times \vec{\mathbf{B}}_S = E_{Sz}(\theta,t)\hat{\mathbf{z}} + (\ell_2/2)\omega_S\hat{\boldsymbol{\theta}} \times B_{Sr}\hat{\mathbf{r}} \\ &= \frac{\mu_0\ell_2 N_S I_S}{4g}\omega_S \cos(\theta - \omega_S t)\hat{\mathbf{z}} - (\ell_2/2)\omega_S \frac{\mu_0\ell_2 N_S I_S}{4g(\ell_2/2)} \cos(\theta - \omega_S t)\hat{\mathbf{z}} \\ &= 0\end{aligned}$$

$$\vec{\mathbf{B}}'_S = B'_{Sr}(r',\theta')\hat{\mathbf{r}} = \vec{\mathbf{B}}_{S|_{r=r',\theta=\theta'+\omega_S t}} = \frac{\mu_0\ell_2 N_S I_S}{4gr'}\cos(\theta')\hat{\mathbf{r}}.$$

The fact that the axial electric field in the rotating coordinate system is zero could have been anticipated. That is, to an observer in the rotating coordinate system, the magnetic field is given by $\vec{\mathbf{B}}'_S = (\mu_0\ell_2 N_S I_S/4gr')\cos(\theta')\hat{\mathbf{r}}$ which is *static* in time. Faraday's law $\nabla \times \vec{\mathbf{E}}'_S = -\partial\vec{\mathbf{B}}'_S/\partial t = 0$ then gives $\vec{\mathbf{E}}'_S = \mathbf{0}$ as the solution.

In the rotating coordinate system, the Lorentz force on the charge carriers in rotor loop a is

$$\vec{\mathbf{F}}' = q(\vec{\mathbf{E}}'_S + \vec{\mathbf{v}}'_{Ra} \times \vec{\mathbf{B}}'_S) = q\vec{\mathbf{v}}'_{Ra} \times \vec{\mathbf{B}}'_S$$

where, with $\omega'_R = -(\omega_S - \omega_R)$,

$$\vec{\mathbf{v}}'_{Ra} = \begin{cases} (\ell_2/2)\omega'_R\hat{\boldsymbol{\theta}} + v_{dra}\hat{\mathbf{z}} & \text{side } a \\ (\ell_2/2)\omega'_R\hat{\boldsymbol{\theta}} - v_{dra}\hat{\mathbf{z}} & \text{side } a' \end{cases}$$

is the total velocity of the charge carriers in the axial sides of rotor loop a with respect to the *rotating* coordinate system.

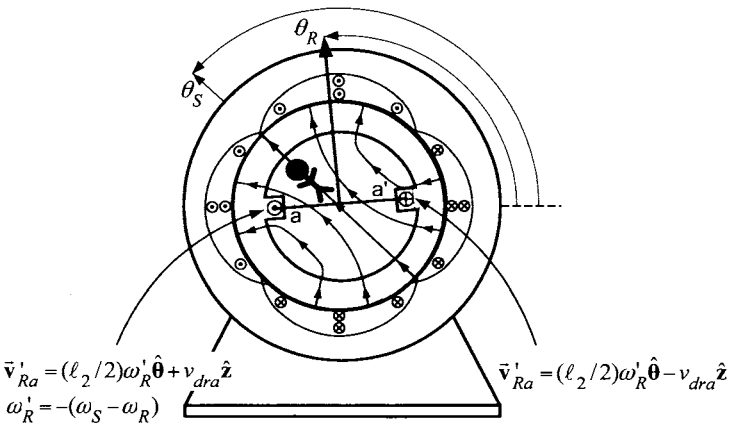


FIGURE 5.20. In the synchronous coordinate system, the rotor has angular speed $\omega'_R\hat{\boldsymbol{\theta}} = -(\omega_S - \omega_R)\hat{\boldsymbol{\theta}}$. Rotor loop b is not drawn for clarity.

www.EngineeringEBooksPdf.com

Then, with $\vec{\mathbf{B}}'_S = \vec{\mathbf{B}}_S = B_{Sr}\hat{\mathbf{r}}$, $\theta' = \theta_R + \pi/2 - \omega_S t = \omega'_R t + \pi/2$ on side a of the rotor and $\theta' = \theta_R - \pi/2 - \omega_S t = \omega'_R t - \pi/2$ on side a' of the rotor,

$$\vec{\mathbf{v}}'_{Ra}\times\vec{\mathbf{B}}'_S =$$
$$\begin{cases} +v_{dra}B_{Sr}(\ell_2/2,\omega'_R t+\pi/2)\hat{\boldsymbol{\theta}} - (\ell_2/2)\omega'_R B_{Sr}(\ell_2/2,\omega'_R t+\pi/2)\hat{\mathbf{z}} & \text{side } a \\ -v_{dra}B_{Sr}(\ell_2/2,\omega'_R t-\pi/2)\hat{\boldsymbol{\theta}} - (\ell_2/2)\omega'_R B_{Sr}(\ell_2/2,\omega'_R t-\pi/2)\hat{\mathbf{z}} & \text{side } a'. \end{cases}$$

Substituting in the expressions

$$B_{Sr}(\ell_2/2,\omega'_R t+\pi/2) = \frac{\mu_0\ell_2 N_S I_S}{4g(\ell_2/2)}\cos(\omega'_R t+\pi/2) = -\frac{\mu_0 N_S I_S}{2g}\sin(\omega'_R t)$$

$$B_{Sr}(\ell_2/2,\omega'_R t-\pi/2) = \frac{\mu_0\ell_2 N_S I_S}{4g(\ell_2/2)}\cos(\omega'_R t-\pi/2) = +\frac{\mu_0 N_S I_S}{2g}\sin(\omega'_R t)$$

results in

$$\begin{aligned} \vec{\mathbf{F}}'_{\text{side } a}/q &= \vec{\mathbf{v}}'_{Ra}\times\vec{\mathbf{B}}'_S \\ &= -v_{dra}\frac{\mu_0 N_S I_S}{2g}\sin(\omega'_R t)\hat{\boldsymbol{\theta}} + (\ell_2/2)\omega'_R\frac{\mu_0 N_S I_S}{2g}\sin(\omega'_R t)\hat{\mathbf{z}} \end{aligned}$$

$$\begin{aligned} \vec{\mathbf{F}}'_{\text{side } a'}/q &= \vec{\mathbf{v}}'_{Ra}\times\vec{\mathbf{B}}'_S \\ &= -v_{dra}\frac{\mu_0 N_S I_S}{2g}\sin(\omega'_R t)\hat{\boldsymbol{\theta}} - (\ell_2/2)\omega'_R\frac{\mu_0 N_S I_S}{2g}\sin(\omega'_R t)\hat{\mathbf{z}}. \end{aligned}$$

With $\omega'_R = -(\omega_S - \omega_R)$, it is seen that the force per unit charge $\vec{\mathbf{F}}'/q = \vec{\mathbf{v}}'_{Ra}\times\vec{\mathbf{B}}'_S$ in this coordinate system equals that obtained in the original coordinates system given in (5.30). This is as it must be since the forces in the two coordinate systems must be equal by the principle of relativity (both Newton's and Einstein's).

The total torque on rotor loop a is then

$$\begin{aligned} \vec{\boldsymbol{\tau}}'_{Ra} &= 2(qNS\ell_1)(-v_{dra})\frac{\mu_0 N_S I_S}{2g}\sin(\omega'_R t)(\ell_2/2)(\hat{\mathbf{r}}\times\hat{\boldsymbol{\theta}}) \\ &= -i_{Ra}\frac{\mu_0\ell_1\ell_2 N_S I_S}{2g}\sin(\omega'_R t)\hat{\mathbf{z}} \end{aligned}$$

where $i_{Ra} = qNSv_{dra}$. Note that, as $\omega'_R = -(\omega_S - \omega_R)$, we may rewrite this as

$$\tau'_{Ra} = i_{Ra}\frac{\mu_0\ell_1\ell_2 N_S I_S}{2g}\sin\Big((\omega_S - \omega_R)t\Big)$$

which is the same expression as in (5.6) and (5.32).

Of course, there is a similar expression for the torque on rotor loop b given by

$$\vec{\boldsymbol{\tau}}'_{Rb} = i_{Rb}\frac{\mu_0\ell_1\ell_2 N_S I_S}{2g}\cos(\omega'_R t)\hat{\mathbf{z}} = i_{Rb}\frac{\mu_0\ell_1\ell_2 N_S I_S}{2g}\cos\Big((\omega_S - \omega_R)t\Big)\hat{\mathbf{z}}.$$

www.EngineeringEBooksPdf.com

It has been shown that the axial magnetic force per unit charge is given by

$$\left(\vec{\mathbf{v}}'_{Ra}\times\vec{\mathbf{B}}'_S\right)_z = \begin{cases} +\omega'_R\dfrac{\mu_0\ell_2 N_S I_S}{4g}\sin(\omega'_R t)\hat{\mathbf{z}} & \text{for side } a \\ -\omega'_R\dfrac{\mu_0\ell_2 N_S I_S}{4g}\sin(\omega'_R t)\hat{\mathbf{z}} & \text{for side } a' \end{cases}$$

and, as the electric field $\vec{\mathbf{E}}'_S = \mathbf{0}$, this is also the total axial force per unit charge $(\vec{\mathbf{F}}/q)_z$. As a result, with

$$d\vec{\ell} = \begin{cases} dz\hat{\mathbf{z}} & \text{for side } a \\ -dz\hat{\mathbf{z}} & \text{for side } a' \end{cases}$$

the emf induced in rotor loop a is simply

$$\begin{aligned} \xi'_{Ra} &= \oint_{\text{rotor loop } a} (\vec{\mathbf{F}}/q)_z \cdot d\vec{\ell} = \ell_1\omega'_R\frac{\mu_0\ell_2 N_S I_S}{2g}\sin(\omega'_R t) \\ &= (\omega_S-\omega_R)\frac{\mu_0\ell_1\ell_2 N_S I_S}{2g}\sin((\omega_S-\omega_R)t). \end{aligned} \tag{5.45}$$

Similarly,

$$\begin{aligned} \xi'_{Rb} &= \omega'_R\frac{\mu_0\ell_1\ell_2 N_S I_S}{2g}\cos(\omega'_R t) \\ &= -(\omega_S-\omega_R)\frac{\mu_0\ell_1\ell_2 N_S I_S}{2g}\cos((\omega_S-\omega_R)t). \end{aligned} \tag{5.46}$$

Then, with

$$i_{Ra} = \xi'_{Ra}/R_R \tag{5.47}$$

$$i_{Rb} = \xi'_{Rb}/R_R \tag{5.48}$$

the total torque on the rotor in the primed coordinate system is given by

$$\begin{aligned} \tau' &= \tau'_{Ra}+\tau'_{Rb} = -\omega'_R\left(\frac{\mu_0\ell_1\ell_2 N_S I_S}{2g}\right)^2\frac{1}{R_R} \\ &= \frac{1}{R_R}\left(\frac{\mu_0\ell_1\ell_2 N_S I_S}{2g}\right)^2(\omega_S-\omega_R). \end{aligned}$$

This is the same as the expression (5.9) derived in the stationary coordinate system.

Electromechanical Energy Conversion

It has been shown that, to the observer in Figure 5.20 in the rotating coordinate system, the torque is given by

$$\tau' = -\omega'_R\left(\frac{\mu_0\ell_1\ell_2 N_S I_S}{2g}\right)^2\frac{1}{R_R} > 0$$

www.EngineeringEBooksPdf.com

However, to this same observer, the angular speed of the rotor is

$$\omega'_R = -(\omega_S - \omega_R) < 0$$

so that power delivered to the rotor is

$$\tau'\omega'_R = -(\omega_S - \omega_R)^2 \left(\frac{\mu_0 \ell_1 \ell_2 N_S I_S}{2g}\right)^2 \frac{1}{R_R} < 0.$$

That is, in the rotating coordinate system of the stator magnetic field (Figure 5.20), the tangential velocity of the rotor loop is in the $-\hat{\boldsymbol{\theta}}$ direction while the above torque is pushing the rotor in the $+\hat{\boldsymbol{\theta}}$ direction. The torque is *slowing* the rotor down from the point of view of the observer *in* the rotating coordinate system of Figure 5.20 and thus taking out mechanical power! Where is this mechanical power going? From the point of view of someone in the rotating coordinate system, this mechanical energy is being converted into electrical power in the rotor. That is, the electric power produced is

$$i_{Ra}\xi'_{Ra} + i_{Rb}\xi'_{Rb} = (\omega_S - \omega_R)^2 \left(\frac{\mu_0 \ell_1 \ell_2 N_S I_S}{2g}\right)^2 \frac{1}{R_R}$$

which is easily verified by substitution of the expressions (5.45), (5.46), (5.47), and (5.48) for the emfs and currents. In summary, to someone in the rotating coordinate system, the induction machine looks like a *generator* rather than a motor.

Magnetic Force and Work

Recall, in the rotating coordinate system of Figure 5.20, the electric field $\vec{\mathbf{E}}'_S = \mathbf{0}$ so that the magnetic force per unit charge on the axial sides of the rotor is then

$$\vec{\mathbf{F}}'/q = \vec{\mathbf{E}}'_S + \vec{\mathbf{v}}'_{Ra} \times \vec{\mathbf{B}}'_S = \vec{\mathbf{v}}'_{Ra} \times \vec{\mathbf{B}}'_S$$

where

$$\vec{\mathbf{v}}'_{Ra} = \begin{cases} (\ell_2/2)\omega'_R\hat{\boldsymbol{\theta}} + v_{dra}\hat{\mathbf{z}} & \text{side } a \\ (\ell_2/2)\omega'_R\hat{\boldsymbol{\theta}} - v_{dra}\hat{\mathbf{z}} & \text{side } a'. \end{cases}$$

Explicitly,

$$\vec{\mathbf{v}}'_{Ra} \times \vec{\mathbf{B}}'_S = \begin{cases} -v_{dra}\dfrac{\mu_0 N_S I_S}{2g}\sin(\omega'_R t)\hat{\boldsymbol{\theta}} + \omega'_R \dfrac{\mu_0 \ell_2 N_S I_S}{4g}\sin(\omega'_R t)\hat{\mathbf{z}} & \text{side } a \\ -v_{dra}\dfrac{\mu_0 N_S I_S}{2g}\sin(\omega'_R t)\hat{\boldsymbol{\theta}} - \omega'_R \dfrac{\mu_0 \ell_2 N_S I_S}{4g}\sin(\omega'_R t)\hat{\mathbf{z}} & \text{side } a'. \end{cases}$$

The power per unit charge done by the (purely) magnetic force $\vec{\mathbf{F}}' = q(\vec{\mathbf{v}}'_{Ra} \times \vec{\mathbf{B}}'_S)$ is then

$$(\vec{\mathbf{F}}'/q) \cdot \vec{\mathbf{v}}'_{Ra} = (\vec{\mathbf{v}}'_{Ra} \times \vec{\mathbf{B}}'_S) \cdot \vec{\mathbf{v}}'_{Ra} \equiv \mathbf{0}$$

www.EngineeringEBooksPdf.com

as it must, since the magnetic force on a moving charge is always orthogonal to the velocity of the charge and thus cannot change the energy of the charge carriers. How is the energy transfer in the rotating coordinate system accomplished from mechanical to electrical? Consider another observer in the rotating coordinate system as shown in Figure 5.21(a).

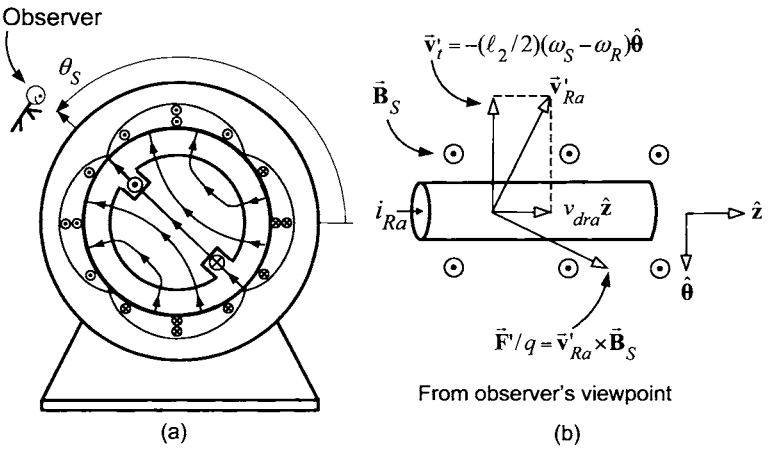


FIGURE 5.21. (a) View by an observer in the synchronous coordinate system. (b) The magnetic force on the rotor loop from the observer's point of view.

The observer is still rotating with the stator magnetic field at angular speed ω_S. The magnetic force opposes the rotor angular velocity and produces the current in the rotor as seen in Figure 5.21(b). From the point of view of the rotating coordinate system, the magnetic force is the mechanism which converts the mechanical (kinetic) energy into electrical energy while not adding any energy (i.e., doing any work). In more detail, the power delivered by the magnetic force on the two sides of rotor loop a is

$$
\begin{aligned}
&2(qNS\ell_1)\vec{F}' \cdot \vec{v}'_{Ra} = 2(qNS\ell_1)(\vec{v}'_{Ra} \times \vec{B}'_S) \cdot \vec{v}'_{Ra} \\
&= 2(qNS\ell_1)\left(-v_{dra}\frac{\mu_0 N_S I_S}{2g}\sin(\omega'_R t)\hat{\theta} + \omega'_R \frac{\mu_0 \ell_2 N_S I_S}{4g}\sin(\omega'_R t)\hat{z}\right) \\
&\quad \cdot \left((\ell_2/2)\omega'_R\hat{\theta} + v_{dra}\hat{z}\right) \\
&= 2\left(-qNS\ell_1 v_{dra}\frac{\mu_0 N_S I_S}{2g}\sin(\omega'_R t)\hat{\theta}\right) \cdot \left((\ell_2/2)\omega'_R\hat{\theta}\right) \\
&\quad + 2\left(\omega'_R \frac{\mu_0 \ell_2 N_S I_S}{4g}\sin(\omega'_R t)\hat{z}\right) \cdot \left(qNS\ell_1 v_{dra}\hat{z}\right)
\end{aligned}
$$

www.EngineeringEBooksPdf.com

Rearranging the right hand side of this last equations gives

$$2(qNS\ell_1)\vec{\mathbf{F}}' \cdot \vec{\mathbf{v}}'_{Ra} = -\left(i_{Ra}\frac{\mu_0\ell_1\ell_2 N_S I_S}{2g}\sin(\omega'_R t)\right)\omega'_R\hat{\boldsymbol{\theta}}\cdot\hat{\boldsymbol{\theta}} + \left(\omega'_R\frac{\mu_0\ell_1\ell_2 N_S I_S}{2g}\sin(\omega'_R t)\right)i_{Ra}\hat{\mathbf{z}}\cdot\hat{\mathbf{z}}. \qquad (5.49)$$

However

$$\vec{\mathbf{F}}' \cdot \vec{\mathbf{v}}'_{Ra} = q(\vec{\mathbf{v}}'_{Ra} \times \vec{\mathbf{B}}'_S)\cdot\vec{\mathbf{v}}'_{Ra} \equiv 0$$

as the magnetic force on a charged particle is always perpendicular to its velocity. The coefficient of $\hat{\boldsymbol{\theta}}\cdot\hat{\boldsymbol{\theta}}$ in (5.49) is $\tau'_{Ra}\omega'_R$ - the mechanical power, while the coefficient of $\hat{\mathbf{z}}\cdot\hat{\mathbf{z}}$ is $\xi'_{Ra}i_{Ra}$ - the electrical power in rotor loop a. As these terms are equal in magnitude, but opposite in sign, it is seen that the magnetic force just converts the mechanical energy to electrical energy, but does not add any energy.

5.4.5 Synchronous Machine

The microscopic viewpoint of the synchronous machine is explored in problems 18 and 19 at the end of the chapter.

5.5 Steady-State Analysis of a Squirrel Cage Induction Motor*

Consider the two-loop induction motor of Figure 5.22 where, as before, $\theta_S(t) = \omega_S t$ denotes the angular position of the magnetic axis of the rotating magnetic field produced by the stator currents, $\theta_R(t) = \omega_R t$ denotes the angular position of the rotor defined as the magnetic axis of rotor loop a (the magnetic axis of rotor loop b is at $\theta_R(t) + \pi/2$), and θ denotes an arbitrary angular position in the air gap.

In order to obtain more torque, additional pairs of loops (each pair $\pi/2$ apart) are placed around the complete periphery of the rotor. For example, Figure 5.23 shows a cross section of a rotor with six rotor loops $a_1{-}a'_1$, $a_2{-}a'_2$, $a_3{-}a'_3$, $b_1{-}b'_1$, $b_2{-}b'_2$, and $b_3{-}b'_3$, which are considered as the three *pairs* of rotor loops $\{a_1{-}a'_1, b_1{-}b'_1\}$, $\{a_2{-}a'_2, b_2{-}b'_2\}$, and $\{a_3{-}a'_3, b_3{-}b'_3\}$. In general, the ith rotor loop pair is located by the center line (magnetic axis) of its rotor loop a which is $\theta_{R_i} = \theta_R + \frac{\pi}{2}\frac{i-1}{N_R}$ for $i = 1, ..., N_R$, where N_R is the number of *pairs* of rotor loops.[6] Phase a of

[6] Each loop has four sides. The term *rotor bar* refers to the sides of a loop which go along the length of the rotor. The other two sides of the loop are referred to as the *end turns*. Consequently, there are two rotor bars per loop and so each pair of loops has four rotor bars. With N_R the number of pairs of *loops*, there are then $4N_R$ rotor bars around the periphery of the rotor.

www.EngineeringEBooksPdf.com

the first rotor loop pair ($i = 1$) is arbitrarily chosen to be the one whose magnetic axis is used to reference the rotor position θ_R. The induced emfs, the currents, and the resulting torque in each pair of loops are now computed, and then the total torque is found by summing the torques on each rotor loop pair.

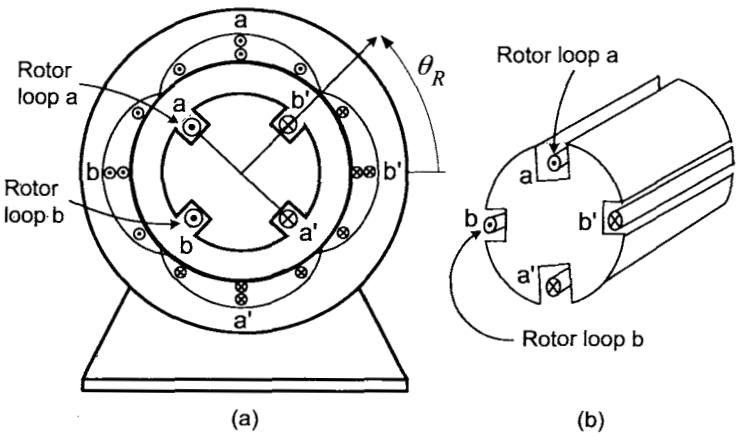


FIGURE 5.22. Induction motor with two single-loop rotor phases a and b.

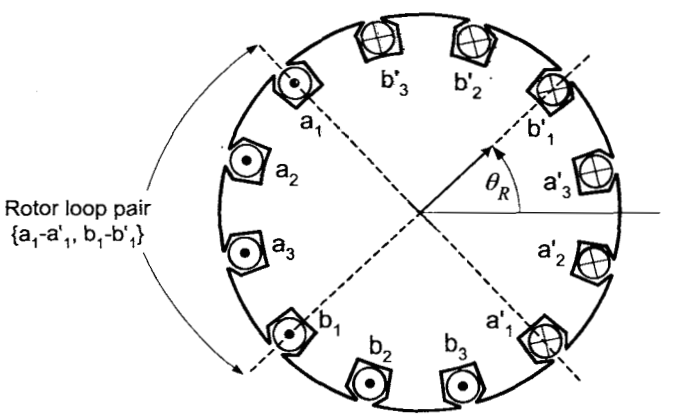


FIGURE 5.23. Rotor with six rotor loops $a_1{-}a_1'$, $a_2{-}a_2'$, $a_3{-}a_3'$, $b_1{-}b_1'$, $b_2{-}b_2'$, and $b_3{-}b_3'$ considered as three pairs of loops $\{a_1{-}a_1', b_1{-}b_1'\}$, $\{a_2{-}a_2', b_2{-}b_2'\}$, and $\{a_3{-}a_3', b_3{-}b_3'\}$. In this figure, there are $N_R = 3$ pairs of rotor loops and θ_R is chosen to coincide with the magnetic axis of rotor loop $a_1{-}a_1'$.

www.EngineeringEBooksPdf.com

5.5.1 *Rotor Fluxes, Emfs, and Currents*

The *flux* λ_{Ra_i} in phase a of the ith rotor loop pair due to the stator magnetic field $\vec{\mathbf{B}}_S$ is calculated as $\left(\theta_{R_i} = \theta_R + \frac{\pi}{2}\frac{i-1}{N_R}\right)$

$$\begin{aligned}
\lambda_{Ra_i} &= \int_{S_{a_i}} \vec{\mathbf{B}}_S \cdot d\vec{\mathbf{S}} \\
&= \int_{\theta_{R_i}-\pi/2}^{\theta_{R_i}+\pi/2} \frac{\mu_0 \ell_2 N_S I_S}{4gr}|_{r=\ell_2/2} \cos(\theta - \theta_S)\hat{\mathbf{r}} \cdot (\ell_1(\ell_2/2)d\theta\hat{\mathbf{r}}) \\
&= \frac{\mu_0 \ell_1 \ell_2 N_S I_S}{4g} \sin(\theta - \theta_S)\Big|_{\theta_{R_i}-\pi/2}^{\theta_{R_i}+\pi/2} \\
&= \frac{\mu_0 \ell_1 \ell_2 N_S I_S}{2g} \cos\left(\theta_S - \left(\theta_R + \frac{\pi}{2}\frac{i-1}{n}\right)\right). \qquad (5.50)
\end{aligned}$$

By Faraday's law, the induced *electromotive force* (*emf*) in phase a of ith rotor loop pair is given by

$$\begin{aligned}
\xi_{Ra_i} &= -\frac{d\lambda_{Ra_i}}{dt} = -\frac{d}{dt}\frac{\mu_0 \ell_1 \ell_2 N_S I_S}{2g}\cos(\theta_S - \theta_{R_i}) \\
&= \frac{\mu_0 \ell_1 \ell_2 N_S I_S}{2g}(\omega_S - \omega_R)\sin\left(\theta_S - \left(\theta_R + \frac{\pi}{2}\frac{i-1}{n}\right)\right) \qquad (5.51)
\end{aligned}$$

where $\omega_R = d\theta_R/dt$.

Similarly, the flux λ_{Rb_i} in phase b of the ith rotor loop pair is

$$\lambda_{Rb_i} = \int_{S_{b_i}} \vec{\mathbf{B}}_S \cdot d\vec{\mathbf{S}} = \frac{\mu_0 \ell_1 \ell_2 N_S I_S}{2g}\sin\left(\theta_S - \left(\theta_R + \frac{\pi}{2}\frac{i-1}{N_R}\right)\right)$$

and the corresponding induced *emf* ξ_{Rb_i} is

$$\xi_{Rb_i} = -\frac{d\lambda_{Rb_i}}{dt} = -\frac{\mu_0 \ell_1 \ell_2 N_S I_S}{2g}(\omega_S - \omega_R)\cos\left(\theta_S - \left(\theta_R + \frac{\pi}{2}\frac{i-1}{N_R}\right)\right) \qquad (5.52)$$

where $\omega_R = d\theta_R/dt$. Assuming each rotor loop has an inductance L_R and resistance R_R, the equations describing the current dynamics are

$$L_R\frac{di_{Ra_i}}{dt} + R_R i_{Ra_i} = \xi_{Ra_i},$$

$$\xi_{Ra_i} = \frac{\mu_0 \ell_1 \ell_2 N_S I_S}{2g}(\omega_S - \omega_R)\sin\left((\omega_S - \omega_R)t - \frac{\pi}{2}\frac{i-1}{N_R}\right)$$

and

$$L_R\frac{di_{Rb_i}}{dt} + R_R i_{Rb_i} = \xi_{Rb_i},$$

$$\xi_{Rb_i} = -\frac{\mu_0 \ell_1 \ell_2 N_S I_S}{2g}(\omega_S - \omega_R)\cos\left((\omega_S - \omega_R)t - \frac{\pi}{2}\frac{i-1}{N_R}\right).$$

www.EngineeringEBooksPdf.com

A system of the form

$$L\frac{di}{dt} + Ri = A\cos(\omega t + \varphi)$$

with $R/L > 0$ is a stable linear time-invariant system so that its steady-state solution is given by

$$i_{ss}(t) = |G(j\omega)|\, A\cos\left(\omega t + \varphi + \angle G(j\omega)\right) \quad \text{where } G(j\omega) = \frac{1}{R + j\omega L}.$$

So, for $i = 1, ..., N_R$, the *steady-state* solutions for the currents in the ith rotor loop pair are given by

$$\begin{aligned} i_{RaSS_i} &= \frac{(\omega_S - \omega_R)}{\sqrt{(\omega_S - \omega_R)^2 L_R^2 + R_R^2}} \frac{\mu_0 \ell_1 \ell_2 N_S I_S}{2g} \\ &\quad \times \sin\left((\omega_S - \omega_R)t - \frac{\pi}{2}\frac{i-1}{N_R} + \tan^{-1}\left(\frac{(\omega_S - \omega_R)L_R}{R_R}\right)\right) \\ i_{RbSS_i} &= -\frac{(\omega_S - \omega_R)}{\sqrt{(\omega_S - \omega_R)^2 L_R^2 + R_R^2}} \frac{\mu_0 \ell_1 \ell_2 N_S I_S}{2g} \\ &\quad \times \cos\left((\omega_S - \omega_R)t - \frac{\pi}{2}\frac{i-1}{N_R} + \tan^{-1}\left(\frac{(\omega_S - \omega_R)L_R}{R_R}\right)\right). \end{aligned} \tag{5.53}$$

5.5.2 *Rotor Torque*

As previously explained, the rotating magnetic field produced by the stator currents produces a magnetic force on the rotor currents it induced. The magnetic force law is simply $\vec{\mathbf{F}}_{magnetic} = i\vec{\boldsymbol{\ell}} \times \vec{\mathbf{B}}$, where $\ell = |\,\vec{\boldsymbol{\ell}}\,|$ is the length of the conductor in the magnetic field, and $\vec{\boldsymbol{\ell}}$ points in the direction of positive current flow. Recalling that $\odot$ means that if $i_{Ra_i} > 0$, the current is coming out of the page, it follows that $\vec{\boldsymbol{\ell}} = \ell_1 \hat{\mathbf{z}}$ on side a_i and $\vec{\boldsymbol{\ell}} = -\ell_1 \hat{\mathbf{z}}$ on side a_i'. Along with the fact that $\vec{\mathbf{B}}_S(r, \theta + \pi) = -\vec{\mathbf{B}}_S(r, \theta)$, it was shown that the force on each side of the loop is equal (i.e., $\vec{\mathbf{F}}_{a_i} = \vec{\mathbf{F}}_{a_i'}$). Applying the magnetic force law to loop a_i of the ith rotor loop pair, the torque is computed as

$$\vec{\boldsymbol{\tau}}_{a_i} = 2\vec{\mathbf{r}} \times \vec{\mathbf{F}}_{a_i} = 2(\ell_2/2)\hat{\mathbf{r}} \times \vec{\mathbf{F}}_{a_i}$$

where

$$\begin{aligned} \vec{\mathbf{F}}_{a_i} &= i_{Ra_i}\vec{\boldsymbol{\ell}} \times \vec{\mathbf{B}}_S \\ &= i_{Ra_i}\ell_1 \hat{\mathbf{z}} \times \frac{\mu_0 \ell_2 N_S I_S}{4gr}\Big|_{r=\ell_2/2} \cos(\theta - \theta_S)\Big|_{\theta = \theta_{R_i} + \pi/2} \hat{\mathbf{r}} \\ &= i_{Ra_i}\frac{\mu_0 \ell_1 N_S I_S}{2g} \sin(\theta_S - \theta_{R_i})\hat{\boldsymbol{\theta}}. \end{aligned}$$

www.EngineeringEBooksPdf.com

The torque is then

$$\vec{\tau}_{a_i} = \frac{\mu_0 \ell_1 \ell_2 N_S I_S}{2g} i_{Ra_i} \sin(\theta_S - \theta_{R_i}) \hat{\mathbf{z}}. \tag{5.54}$$

Similarly,

$$\vec{\tau}_{b_i} = 2\vec{\mathbf{r}} \times \vec{\mathbf{F}}_{b_i} = 2(\ell_2/2)\hat{\mathbf{r}} \times \vec{\mathbf{F}}_{b_i}$$

where

$$\begin{aligned} \vec{\mathbf{F}}_{b_i} &= i_{Rb_i} \vec{\boldsymbol{\ell}} \times \vec{\mathbf{B}}_S \\ &= i_{Rb_i} \ell_1 \hat{\mathbf{z}} \times \frac{\mu_0 \ell_2 N_S I_S}{4gr} |_{r=\ell_2/2} \cos(\theta - \theta_S)_{|\theta=\theta_{R_i}+\pi} \hat{\mathbf{r}} \\ &= -i_{Rb_i} \frac{\mu_0 \ell_1 N_S I_S}{2g} \cos(\theta_S - \theta_{R_i}) \hat{\boldsymbol{\theta}}. \end{aligned}$$

The torque $\vec{\tau}_{b_i}$ becomes

$$\vec{\tau}_{b_i} = -\frac{\mu_0 \ell_1 \ell_2 N_S I_S}{2g} i_{Rb_i} \cos(\theta_S - \theta_{R_i}) \hat{\mathbf{z}}.$$

Letting

$$I_R \triangleq \frac{(\omega_S - \omega_R)}{\sqrt{(\omega_S - \omega_R)^2 L_R^2 + R_R^2}} \frac{\mu_0 \ell_1 \ell_2 N_S I_S}{2g} \tag{5.55}$$

in (5.53) and substituting (5.53) into equation (5.54), the total torque on loop $a_i - a_i'$ of the ith rotor loop pair becomes

$$\begin{aligned} \tau_{Ra_i} &= \frac{\mu_0 \ell_1 \ell_2 N_S I_S}{2g} i_{RaSS_i} \sin\left((\omega_S - \omega_R)t - \frac{\pi}{2}\frac{i-1}{N_R}\right) \\ &= \frac{\mu_0 \ell_1 \ell_2 N_S I_S}{2g} I_R \sin\left((\omega_S - \omega_R)t - \frac{\pi}{2}\frac{i-1}{N_R} + \tan^{-1}\left(\frac{(\omega_S - \omega_R)L_R}{R_R}\right)\right) \\ &\quad \times \sin\left((\omega_S - \omega_R)t - \frac{\pi}{2}\frac{i-1}{N_R}\right) \end{aligned}$$

Similarly, the total torque on loop $b_i - b_i'$ of the ith rotor loop pair is

$$\begin{aligned} \tau_{Rb_i} &= -\frac{\mu_0 \ell_1 \ell_2 N_S I_S}{2g} i_{RbSS_i} \cos\left((\omega_S - \omega_R)t - \frac{\pi}{2}\frac{i-1}{N_R}\right) \\ &= \frac{\mu_0 \ell_1 \ell_2 N_S I_S}{2g} I_R \cos\left((\omega_S - \omega_R)t - \frac{\pi}{2}\frac{i-1}{N_R} + \tan^{-1}\left(\frac{(\omega_S - \omega_R)L_R}{R_R}\right)\right) \\ &\quad \times \cos\left((\omega_S - \omega_R)t - \frac{\pi}{2}\frac{i-1}{N_R}\right). \end{aligned}$$

Using the trigonometric identity $\sin(x)\sin(y) + \cos(x)\cos(y) = \cos(x - y)$ to combine the above results, the *total torque* τ_{R_i} on the ith rotor loop *pair* is given by

www.EngineeringEBooksPdf.com

$$\tau_{R_i} = \tau_{Ra_i} + \tau_{Rb_i} = \frac{\mu_0 \ell_1 \ell_2 N_S I_S}{2g} I_R \cos\left(\tan^{-1}\left(\frac{(\omega_S - \omega_R)L_R}{R_R}\right)\right).$$

This can be put in a more illuminating form by noting that

$$\cos\left(\tan^{-1}\left(\frac{(\omega_S - \omega_R)L_R}{R_R}\right)\right) = \frac{1}{\sqrt{\left(\frac{(\omega_S - \omega_R)L_R}{R_R}\right)^2 + 1}}$$

and substituting back the expression (5.55) for I_R, the torque can be written as

$$\begin{aligned}
\tau_{R_i} &= \frac{\mu_0 \ell_1 \ell_2 N_S I_S}{2g} I_R \cos\left(\tan^{-1}\left(\frac{(\omega_S - \omega_R)L_R}{R_R}\right)\right) \\
&= \left(\frac{\mu_0 \ell_1 \ell_2 N_S I_S}{2g}\right)^2 \frac{(\omega_S - \omega_R)}{\sqrt{(\omega_S - \omega_R)^2 L_R^2 + R_R^2}} \frac{1}{\sqrt{\left(\frac{(\omega_S - \omega_R)L_R}{R_R}\right)^2 + 1}} \\
&= \left(\frac{\mu_0 \ell_1 \ell_2 N_S I_S}{2g}\right)^2 \frac{1}{L_R} \frac{\frac{(\omega_S - \omega_R)L_R}{R_R}}{\left(\frac{(\omega_S - \omega_R)L_R}{R_R}\right)^2 + 1} \\
&= \left(\frac{\mu_0 \ell_1 \ell_2 N_S I_S}{2g}\right)^2 \frac{1}{L_R} \frac{1}{2} \frac{2}{S/s_p + s_p/S}
\end{aligned}$$

where

$$S \triangleq \frac{\omega_S - \omega_R}{\omega_S} \text{ and } s_p \triangleq \frac{R_R}{\omega_S L_R}.$$

The quantity $S \triangleq \frac{\omega_S - \omega_R}{\omega_S}$ is the *normalized slip*.[7] It is straightforward to show that $\frac{2}{S/s_p + s_p/S}$ has a maximum value of 1 for $S = s_p$ and a minimum value of -1 for $S = -s_p$ so that the torque achieves its maximum (minimum) at $S = s_p (S = -s_p)$.

This derivation shows that, in steady state, each pair of rotor loops has the same torque on it. Consequently, the total torque on the N_R pairs of

[7] Later the quantity $S_p \triangleq \frac{R_R}{\sigma \omega_S L_R}$ will be defined as the *pull out slip* so that $s_p \triangleq \frac{R_R}{\omega_S L_R} = \sigma S_p$ where σ is the so-called *leakage parameter* (also defined later). For the reader familiar with the torque-slip curve of an induction motor, the quantity s_p rather than the pull out slip S_p occurs because impressed currents are used here rather than impressed voltages (see problem 25 of Chapter 7).

www.EngineeringEBooksPdf.com

loops is

$$\begin{aligned}\tau_R &= \sum_{i=1}^{N_R} \tau_{Ri} = \frac{N_R}{2L_R}\left(\frac{\mu_0 \ell_1 \ell_2 N_S I_S}{2g}\right)^2 \frac{2}{S/s_p + s_p/S} \\ &= \tau_p \frac{2}{S/s_p + s_p/S}\end{aligned}$$

where

$$\tau_p \triangleq \frac{N_R}{2L_R}\left(\frac{\mu_0 \ell_1 \ell_2 N_S I_S}{2g}\right)^2.$$

For $|S| \ll s_p$, this reduces to

$$\begin{aligned}\tau_R &\approx k(\omega_S - \omega_R) \\ k &\triangleq \frac{N_R}{R_R}\left(\frac{\mu_0 \ell_1 \ell_2 N_S I_S}{2g}\right)^2.\end{aligned}$$

The analysis was done assuming that each rotor loop was electrically isolated from any other rotor loop. The most common rotor for an induction motor is the *squirrel cage rotor* shown in Figure 5.24. It is simply a set of conducting bars around the periphery of the rotor iron that are connected to conducting end rings at each end. This is in contrast to the rotor of Figure 5.5 where loop $a-a'$ is electrically isolated from loop $b-b'$.

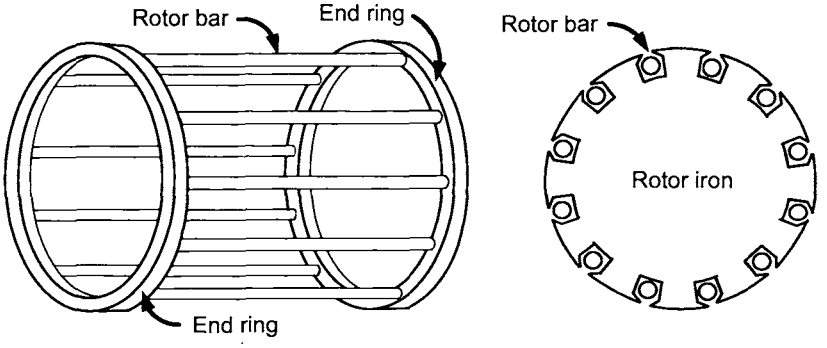


FIGURE 5.24. Squirrel cage rotor.

However, assuming the emf drop across each rotor bar remains the same as in the case when the rotor loops are electrically isolated, the above analysis still applies.[8] That is, consider the squirrel cage to be made up of loops consisting of two rotor bars that are on diametrically opposite sides

[8]This argument is perhaps more convincing from the microscopic point of view. It is shown in an optional section of this chapter that the rotating magnetic field $\vec{\mathbf{B}}_S(r,\theta,t) =$

www.EngineeringEBooksPdf.com

of the rotor. The flux in each loop depends on the rotor position so that the induced emf in each rotor loop is different. In particular, as one goes from one rotor bar to the next, the emf drop across their lengths are different even though they are connected in parallel. This can be visualized as shown in Figure 5.25 which shows the induced emfs $\xi_{b'_1}$, $\xi_{b'_2}$, $\xi_{b'_3}$, ξ_{a_1}, ξ_{a_2}, ξ_{a_3}, ξ_{b_1}, ξ_{b_2}, ξ_{b_3}, $\xi_{a'_1}$, $\xi_{a'_2}$, $\xi_{a'_3}$ in each rotor bar being in series with the resistance $R_R/2$ of each rotor bar.

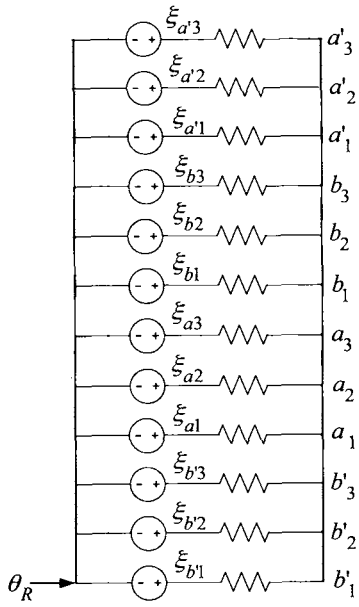


FIGURE 5.25. Equivalent circuit of a squirrel cage rotor. The rotor bars are annotated as in Figure 5.23. Each bar has resistance $R_R/2$ so that the total resistance in a loop consisting of diametrically opposite bars is R_R.

For example, in the two rotor bars a_1, a'_1 (which are on diametrically opposite sides of the rotor), the voltage in the rotor loop made up from

---

$B_r(r,\theta,t)\hat{\mathbf{r}} = \frac{\mu_0 \ell_2 N_S I_S}{4gr}\cos(\theta - \omega_S t)\hat{\mathbf{r}}$ in the air gap produced by the stator currents induces an axial electric field in the air gap (according to $\nabla \times \vec{\mathbf{E}}_S = -\partial \vec{\mathbf{B}}_S/\partial t$) given by $\vec{\mathbf{E}}_S(\theta,t) = E_z(\theta,t)\hat{\mathbf{z}} = \frac{\mu_0 \ell_2 N_S I_S}{4g}\omega_S \cos(\theta - \omega_S t)\hat{\mathbf{z}}$ (see Figure 5.15). The voltage drop across the ith rotor bar produced by this electric field is then $\int_0^{\ell_1} \left(\vec{\mathbf{E}}_S(\theta,t)\Big|_{\theta=\theta_R+\varphi_i} \right) \cdot d\vec{\boldsymbol{\ell}}$ where $\varphi_i = \frac{\pi}{2}\frac{i-1}{N_R}$. One then argues that, as this depends only on the stator quantities, this voltage drop is the same whether or not the rotor bars are electrically connected (shorted) at their ends. The total emf in each bar is this voltage drop plus the back emf $\int_0^{\ell_1} \left(\vec{\mathbf{v}} \times \vec{\mathbf{B}}_S(\theta,t)\Big|_{\theta=\theta_R+\varphi_i} \right) \cdot d\vec{\boldsymbol{\ell}}$ in each rotor bar ($|\vec{\mathbf{v}}| = v = r_R\omega$).

www.EngineeringEBooksPdf.com

these two sides is[9] $\xi_{a_1} - \xi_{a_1'} = 2\xi_{a_1}$ and this loop has resistance R_R. This emf $\xi_{Ra_1} \triangleq \xi_{a_1} - \xi_{a_1'} = 2\xi_{a_1}$ equals the emf given in equation (5.51) with $i = 1$. Note from Figure 5.23 that the rotor angle θ_R locates the rotor bar b_1' as is also indicated in Figure 5.25.

5.5.3 *Rotor Magnetic Field*

As equation (5.53) shows, the current in the rotor bars of the squirrel cage rotor differs from bar to bar (loop to loop) while the current in each phase of a *sinusoidally wound* rotor loop is the same. Of course, in the squirrel cage rotor, it is arbitrary what is called a phase a loop and what is called a phase b loop. It is more convenient to speak of a current distribution on the surface of the rotor (i.e., in the rotor bars). With $\varphi_i = \frac{\pi}{2}\frac{i-1}{N_R}$, the ith rotor bar is located at $\theta_R(t)+\varphi_i = \omega_R t + \frac{\pi}{2}\frac{i-1}{N_R}$. Combining the expressions (5.53) above for the rotor currents, the steady-state current distribution in the $4N_R$ rotor bars distributed around the periphery of the rotor can be found. Specifically, with I_R given by (5.55), the two equations (5.53) are combined to show that the rotor current in the ith bar at $\theta_R(t) + \varphi_i$ is[10]

$$\begin{aligned} i_{RSS}(t,\varphi_i) &= I_R \sin\left(\theta_S(t) - (\theta_R(t)+\varphi_i) + \tan^{-1}\left(\frac{(\omega_S-\omega_R)L_R}{R_R}\right)\right) \\ \theta_R(t)+\varphi_i &= \omega_R t + \frac{\pi}{2}\frac{i-1}{N_R} \quad \text{for } i = 1,...,4N_R \\ \theta_S(t) &= \omega_S t. \end{aligned} \tag{5.56}$$

Applying Ampère's law $\oint \vec{\mathbf{H}}_R \cdot d\vec{\ell} = i_{\text{enclosed}}$ to the closed curve 1–2–3–4–1 in Figure 5.26, the radial magnetic field $B_R(\theta)$ in the air gap due to this rotor current distribution can be found. To do so, first note that for N_R large, the discrete angles $\varphi_i = \frac{\pi}{2}\frac{i-1}{N_R}$ locating the individual rotor bars can be approximated by a continuous angle φ with a continuous current distribution $i_{RSS}(t,\varphi)$. Specifically, the incremental angle from one rotor bar to the next is $d\varphi = \frac{\pi}{2}\frac{1}{N_R}$ so that the enclosed current may be written as

$$\begin{aligned} i_{\text{enclosed}}(\theta) &= \sum_{\varphi_i=\theta-\theta_R}^{\varphi_i=\theta-\theta_R+\pi} i_{RSS}(t,\varphi_i) = \frac{2N_R}{\pi}\left(\sum_{\varphi_i=\theta-\theta_R}^{\varphi_i=\theta-\theta_R+\pi} i_{RSS}(t,\varphi_i)d\varphi\right) \\ &\approx \frac{2N_R}{\pi}\int_{\varphi=\theta-\theta_R}^{\varphi=\theta-\theta_R+\pi} i_{RSS}(t,\varphi)d\varphi \end{aligned}$$

[9] By symmetry, diametrically opposite sides of the rotor have emfs which are opposite in sign, but equal in magnitude.

[10] As $i = 1,...,4N_R$, the angles φ_i go from $\varphi_1 = 0$ to $\varphi_{4N_R} = \frac{\pi}{2}\frac{4N_R-1}{N_R} = 2\pi - \frac{\pi}{2}\frac{1}{N_R}$.

www.EngineeringEBooksPdf.com

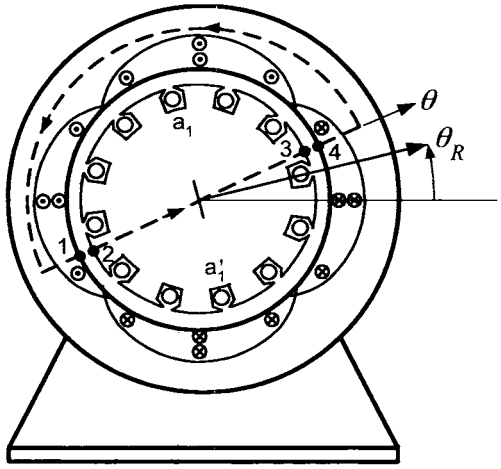


FIGURE 5.26. Path for Ampère's law to compute $\vec{\mathbf{B}}_R$ in the air gap.

where the summation has been approximated by the integral. Ampère's law gives

$$2H_R(\theta)g = i_{\text{enclosed}}(\theta)$$

or

$$H_R(\theta) = \frac{i_{\text{enclosed}}(\theta)}{2g}.$$

The expression (5.56) is substituted for $i_{RSS}(t,\varphi)$ to evaluate $i_{\text{enclosed}}(\theta)$ as

$$\begin{aligned} i_{\text{enclosed}}(\theta) &= \frac{2N_R}{\pi}\int_{\varphi=\theta-\theta_R}^{\varphi=\theta-\theta_R+\pi} i_{RSS}(\varphi)d\varphi \\ &= -\frac{2N_R}{\pi}I_R\cos\Big(\theta_S(t) - (\theta_R(t)+\varphi) + \tan^{-1}\Big(\frac{(\omega_S-\omega_R)L_R}{R_R}\Big)\Big)\Big|_{\varphi=\theta-\theta_R}^{\varphi=\theta-\theta_R+\pi} \\ &= \frac{4}{\pi}N_R I_R\cos\Big(\theta_S(t) - \theta + \tan^{-1}\Big(\frac{(\omega_S-\omega_R)L_R}{R_R}\Big)\Big). \end{aligned}$$

The radial magnetic field due to the rotor currents is then

$$\begin{aligned} \vec{\mathbf{B}}_R(\theta,t) &= B_R(\theta,t)\hat{\mathbf{r}} \\ &= \mu_0 H_R(\theta)\hat{\mathbf{r}} \\ &= \frac{4}{\pi}\frac{\mu_0 N_R I_R}{2g}\cos\Big(\theta - \big(\theta_S(t) + \varphi_R\big)\Big)\hat{\mathbf{r}} \end{aligned}$$

www.EngineeringEBooksPdf.com

where

$$I_R \triangleq \frac{(\omega_S - \omega_R)}{\sqrt{(\omega_S - \omega_R)^2 L_R^2 + R_R^2}} \frac{\mu_0 \ell_1 \ell_2 N_S I_S}{2g}$$
$$\varphi_R \triangleq \tan^{-1}\left(\frac{(\omega_S - \omega_R)L_R}{R_R}\right).$$

In chapter 8, it will be shown that the steady-state rotor currents in a *sinusoidally wound* rotor induction motor will produce a rotating magnetic field given by

$$\vec{\mathbf{B}}_R(\theta, t) = \frac{\mu_0 N_R I_{R_{\text{wound}}}}{2g} \cos(\theta - (\omega_S t + \varphi_{R_{\text{wound}}}))\hat{\mathbf{r}}$$

The only difference in the *form* of these expressions is the factor of $4/\pi$. However, the values of the rotor current $I_{R_{\text{wound}}}$ and the phase angle $\varphi_{R_{\text{wound}}}$ are in general different as they depend on the $L_{R_{\text{wound}}}, R_{R_{\text{wound}}}$ which have different values in a squirrel cage rotor.

5.5.4 *Comparison with a Sinusoidally Wound Rotor*

It is quite interesting to note that in the squirrel cage rotor, the effective rotor time constant is still L_R/R_R, that is, the time constant due to just a *single* loop. (By "effective" is meant that this is the ratio that appears in the expression for the quantity $s_p = R_R/(\omega_S L_R)$ used in the above expression for the steady-state torque.) A small value for the time constant $T_R = L_R/R_R$ is usually desired since the value of s_p is then large, making $\tau \approx k(\omega_S - \omega_R)$ for a large range of slip speeds. Assuming ideal magnetic material and a small air gap, it is straightforward to show that $L_R = \pi\mu_0\ell_1\ell_2/(4g)$ for each loop of the rotor. Consequently, the time constant is $T_R = L_R/R_R = \pi\mu_0\ell_1\ell_2/(4gR_R)$ where R_R is the resistance of the single loop.

This is in contrast to a sinusoidally wound rotor induction motor (discussed in a later chapter) where the rotor loops of each phase are connected in series resulting in $L_{R_{\text{wound}}} = \pi\mu_0\ell_1\ell_2 N_R^2/(8g)$ (N_R is the total number of loops in a sinusoidally wound rotor phase) and $R_{R_{\text{wound}}}$ is the sum of the resistances of each loop in the rotor ($R_{R_{\text{wound}}} = N_R R_1$ with R_1 the resistance in each loop). The time constant is then $T_{R_{wound}} = L_{R_{\text{wound}}}/R_{R_{\text{wound}}} = \pi\mu_0\ell_1\ell_2 N_R/(8gR_1)$). The ratio of these two time constants is $T_{R_{wound}}/T_{R_{squirrel}} = N_R/2$ showing that for a squirrel cage rotor with the same number of loops as the wound rotor, the effective time constant can be significantly smaller.

To compare the torque of the two motors, consider the steady-state torque produced by a sinusoidally wound two-phase induction motor. It is shown in Chapter 7 (or see Chapter 10 of [1]) that the expression for this

www.EngineeringEBooksPdf.com

torque is given by ($|\underline{I}_S| = I_S/\sqrt{2}$, $|\underline{I}_R| = I_{R_{\text{wound}}}/\sqrt{2}$)[11]

$$\begin{aligned}\tau_{\text{wound rotor}} &= M\,\text{Im}\{\underline{I}_S\underline{I}_R^*\},\\ &= M\,\text{Im}\left\{\underline{I}_S\left(-\frac{j\omega_S M}{R_R/S + j\omega_S L_R}\underline{I}_S\right)^*\right\}\end{aligned}$$

With $S_p \triangleq \dfrac{R_{R_{\text{wound}}}}{\sigma\omega_S L_{R_{\text{wound}}}}$ and $s_p \triangleq \sigma S_p = \dfrac{R_{R_{\text{wound}}}}{\omega_S L_{R_{\text{wound}}}}$ this becomes

$$\tau_{\text{wound rotor}} = \frac{I_S^2}{2}M\,\text{Im}\left\{\frac{\dfrac{j\omega_S MS}{R_R}\,1+\dfrac{jS}{\sigma S_p}}{1-\dfrac{jS}{\sigma S_p}\,1+\dfrac{jS}{\sigma S_p}}\right\}.$$

Rearranging, this becomes

$$\begin{aligned}\tau_{\text{wound rotor}} &= \frac{I_S^2}{2}M\,\text{Im}\left\{\frac{\dfrac{j\omega_S MR_R}{S}\left(1+\dfrac{jS}{s_p}\right)}{1+(S/s_p)^2}\right\}\\ &= \frac{I_S^2}{2}M\frac{\omega_S MS/R_{R_{\text{wound}}}}{1+(S/s_p)^2}\\ &= \frac{1}{4L_R}M^2I_S^2\frac{2}{s_p/S+S/s_p}.\end{aligned}$$

Finally, using

$$M = \frac{\mu_0\pi\ell_1\ell_2N_SN_R}{8g} = \left(\frac{\pi N_R}{4}\right)\left(\frac{\mu_0\ell_1\ell_2N_S}{g}\right)$$

it follows that

$$\begin{aligned}\tau_{\text{wound rotor}} &= \frac{1}{4L_R}\left(\frac{\pi N_R}{4}\right)^2\left(\frac{\mu_0\ell_1\ell_2N_SI_S}{g}\right)^2\frac{2}{s_p/S+S/s_p}\\ &= \frac{N_R}{2}\left(\frac{\pi}{4}\right)^2\frac{N_R}{2L_R}\left(\frac{\mu_0\ell_1\ell_2N_SI_S}{g}\right)^2\frac{2}{s_p/S+S/s_p}.\end{aligned}$$

In *form*, this differs from the squirrel cage case by the factor $\dfrac{N_R}{2}\left(\dfrac{\pi}{4}\right)^2$. However, also note that $s_p \triangleq \dfrac{R_{R_{\text{wound}}}}{\omega_S L_{R_{\text{wound}}}}$ has a different value than that of the squirrel cage rotor.

---

[11] The magnitude of the currents are written in the (nonstandard) form $|\underline{I}_S| = I_S/\sqrt{2}$, $|\underline{I}_R| = I_{R_{\text{wound}}}/\sqrt{2}$ so that $I_S, I_{R_{\text{wound}}}$ are peak values (rather than rms values) to facilitate a comparison with the squirrel cage rotor torque.

www.EngineeringEBooksPdf.com

Problems

Problem 1 Solutions to Linear Time-Invariant Systems

Consider the linear time-invariant system specified by

$$\frac{d^3y}{dt^3} + a_2\frac{d^2y}{dt^2} + a_1\frac{dy}{dt} + a_0 y = b_2\frac{d^2u}{dt^2} + b_1\frac{du}{dt} + b_0 u. \tag{5.57}$$

The transfer function $G(s)$ of this system is

$$G(s) = \frac{b(s)}{a(s)} = \frac{b_2 s^2 + b_1 s + b_0}{s^3 + a_2 s^2 + a_1 s + a_0}.$$

(a) Show that if

$$u(t) \triangleq U_0 e^{j\omega t} = U_0(\cos(\omega t) + j\sin(\omega t))$$

then

$$y_p(t) = U_0\,|G(j\omega)|\,e^{j(\omega t + \angle G(j\omega))}$$

is a (particular) solution to the differential equation (5.57).

(b) Show that if

$$u(t) \triangleq \mathrm{Re}\left\{U_0 e^{j\omega t}\right\} = U_0\cos(\omega t),$$

then

$$y_p(t) = U_0\,|G(j\omega)|\cos(\omega t + \angle G(j\omega))$$

is a particular solution to the differential equation (5.57).

(c) Let

$$a(s) = s^3 + a_2 s^2 + a_1 s + a_0 = (s - p_1)(s - p_2)(s - p_3)$$

so that p_1, p_2, p_3 are the poles of $G(s)$. To simplify the discussion, assume the p_i are distinct.

With $u(t) \equiv 0$ and arbitrary initial conditions $y(0), y'(0), y''(0)$, show that the solution to (5.57) has the form $y(t) = A_1 e^{p_1 t} + A_2 e^{p_2 t} + A_3 e^{p_3 t}$.

Next, show that the complete *solution to the differential equation (5.57) with arbitrary initial conditions $y(0), y'(0), y''(0)$ and input $u(t) = U_0\cos(\omega t)$ is*

$$y(t) = U_0\,|G(j\omega)|\cos(\omega t + \angle G(j\omega)) + A_1 e^{p_1 t} + A_2 e^{p_2 t} + A_3 e^{p_3 t}$$

where the A_i are the unique *solution to*

$$\begin{bmatrix} y(0) \\ y'(0) \\ y''(0) \end{bmatrix} = \begin{bmatrix} y_p(0) \\ y_p'(0) \\ y_p''(0) \end{bmatrix} + \begin{bmatrix} 1 & 1 & 1 \\ p_1 & p_2 & p_3 \\ p_1^2 & p_2^2 & p_3^2 \end{bmatrix} \begin{bmatrix} A_1 \\ A_2 \\ A_3 \end{bmatrix}.$$

(d) Show that the steady-state solution of the differential equation (5.57) equals $y_p(t)$ if and only if $\mathrm{Re}\{p_i\} < 0$ for $i = 1, 2, 3$.

(e) Show that the steady-state solution to $dy/dt + ay = u(t)$ with $a > 0$ and $u(t) = U_0\cos(\omega_0 t)$ is $y_{SS}(t) = U_0\,|G(j\omega)|\cos(\omega t + \angle G(j\omega))$ with $G(s) = 1/(s + a)$.

www.EngineeringEBooksPdf.com

The Physics of the Induction Machine

Problem 2 Torque Versus Slip for the Induction Motor

The expressions for the rotor currents in equations (5.4) and (5.5) were found neglecting the rotor loop inductance. Assuming the rotor speed is constant and the currents are in sinusoidal steady-state, find an expression for these currents when the rotor loops have resistance R_R and *an inductance* L_R. *Modify the corresponding expression for the torque given in (5.9) to show that it now has the form*

$$\tau = \left(\frac{\mu_0 \ell_1 \ell_2 N_S I_S}{2g}\right)^2 \frac{1}{2L_R} \frac{2}{S/s_p + s_p/S}$$

where $S \triangleq \dfrac{\omega_S - \omega_R}{\omega_S}$ *is the* normalized slip *and* $s_p \triangleq \dfrac{R_R}{\omega_S L_R}$. *The* pull-out slip *is defined by* $S_p \triangleq \dfrac{R_R}{\sigma \omega_S L_R} = s_p/\sigma$ *where* σ *is the so-called leakage factor (see Chapter 6).*

Finally, sketch the torque as a function of the normalized slip $S \triangleq (\omega_S - \omega_R)/\omega_S$.

Problem 3 Induction Motor under Load

In problem 2 it is shown that the torque produced by a two-phase induction motor with two rotor loops $\pi/2$ *radians apart and nonzero rotor inductance* L_R *is given by*

$$\tau = \left(\frac{\mu_0 \ell_1 \ell_2 N_S I_S}{2g}\right)^2 \frac{1}{2L_R} \frac{2}{s_p/S + S/s_p} = \tau_p \frac{2}{s_p/S + S/s_p} \tag{5.58}$$

where

$$\begin{aligned} S &\triangleq \frac{\omega_S - \omega_R}{\omega_S} \\ \tau_p &\triangleq \left(\frac{\mu_0 \ell_1 \ell_2 N_S I_S}{2g}\right)^2 \frac{1}{2L_R} \\ s_p &\triangleq \frac{R_R}{\omega_S L_R}. \end{aligned}$$

A plot of τ/τ_p *versus* S/s_p *is given in Figure 5.27. A typical rotor for an induction motor has more than two loops on it. The squirrel cage rotor for an induction motor is shown in Figure 5.28 with a cross-sectional view of the rotor given in Figure 5.28(b). This shows a rotor consisting of* 6 *rotor loops (*12 *sides) that can be viewed as three sets of* 2 *rotor loops. Each set consists of two rotor loops* $\pi/2$ *radians apart.*

www.EngineeringEBooksPdf.com

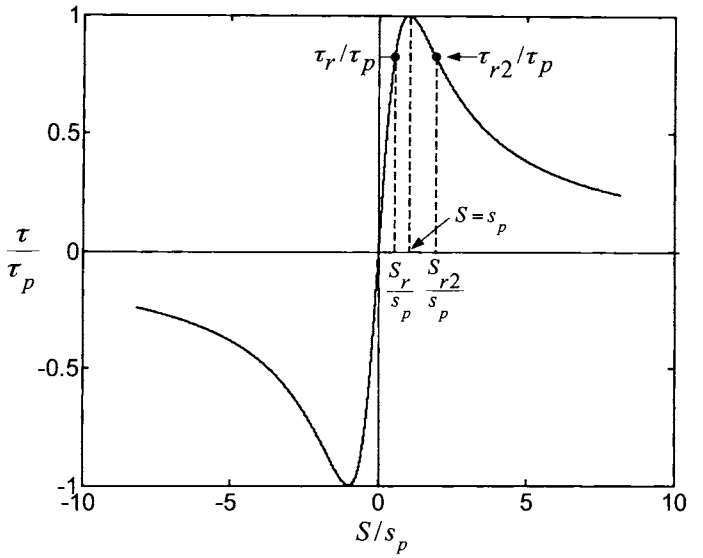


FIGURE 5.27. Normalized torque versus normalized slip.

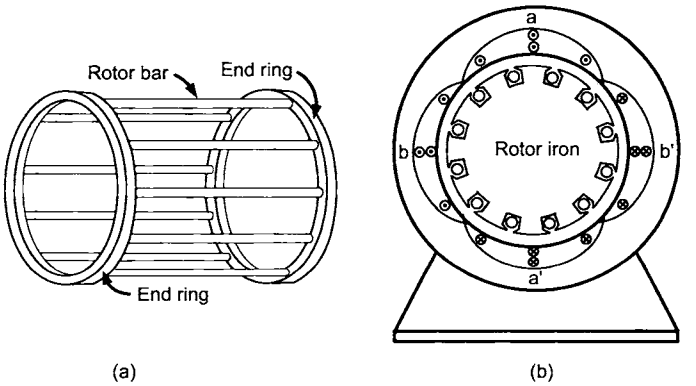


FIGURE 5.28. (a) Squirrel cage rotor for an induction motor. (b) Cross-sectional view.

(a) With the rotor of Figure 5.28(b), explain why the expression (5.58) for the steady-state torque needs to be multiplied by three to obtain the torque of the motor in Figure 5.28(b).

(b) Suppose the induction motor has a load on it and is producing the torque τ_r that is, it is operating at the point $(S_r/s_p, \tau_r/\tau_p)$ shown in Figure 5.27. Next, suppose an additional load is put on the motor so that the total

www.EngineeringEBooksPdf.com

load torque τ_L now satisfies $\tau_r < \tau_L < \tau_p$. After the additional load is put on the motor:

Will the speed increase or decrease?

Will the normalized slip increase or decrease?

Will the motor torque increase to handle the increased load?

(c) Repeat part (b), but with the motor initially operating at $(S_{r2}/s_p, \tau_{r2}/\tau_p)$.

(d) Suppose the induction motor is turned off (no currents applied to the stator phases) so that $\omega_R = 0$, but it has a load torque $\tau_L = \tau_r$ on it (the same τ_r as in Figure 5.27). Suppose further that $s_p = 0.2$ and that currents of frequency ω_S are now applied to the stator phases. Just after applying the stator currents, answer the following:

What is the value of S/s_p ?

Mark on Figure 5.27 the operating point of the motor.

Can the motor start with the load torque $\tau_L = \tau_r$ on it? Explain.

Problem 4 Torque

In developing the expression (5.6) for the torque on a rotor loop of an induction motor, why wasn't the magnetic force on the two semicircular ends of the rotor loop considered (see Figure 5.8)?

Problem 5 Simple Induction Machine with Three-Phases

Figure 5.29 shows a three phase stator with a rotor iron core.

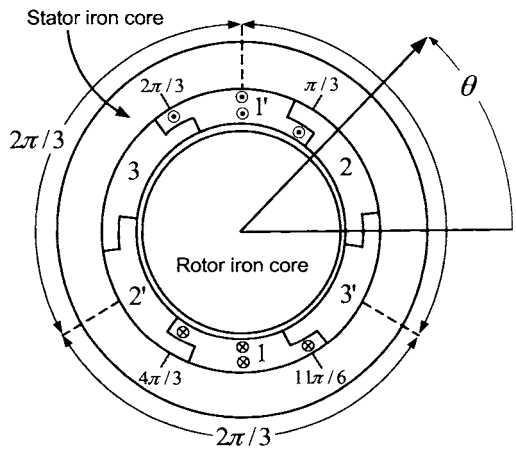


FIGURE 5.29. Three-phase stator. Currents are only shown for phase 1.

Phase 1 is identical to phase a in a two phase stator. The magnetic field in the air gap due to the current i_{S1} in phase 1 is then

$$\vec{\mathbf{B}}_{S1}(i_{S1}, r, \theta) = \frac{\mu_0 \ell_2 N_S}{4gr} i_{S1} \cos(\theta)\hat{\mathbf{r}}.$$

www.EngineeringEBooksPdf.com

Phase 2 is wound the same way as phase 1 except that is rotated $2\pi/3$ radians with respect to phase 1. The third phase is also wound the same way as phases 1 and 2, but rotated another $2\pi/3$ radians with respect to phase 2. The magnetic field in the air gap due to the current i_{S2} in phase 2 is then

$$\vec{\mathbf{B}}_{S2}(i_{S2}, r, \theta) = \frac{\mu_0 \ell_2 N_S}{4gr} i_{S2} \cos(\theta - 2\pi/3)\hat{\mathbf{r}}$$

and the magnetic field in the air gap due to the current i_{S3} in phase 3 is then

$$\vec{\mathbf{B}}_{S3}(i_{S3}, r, \theta) = \frac{\mu_0 \ell_2 N_S}{4gr} i_{S3} \cos(\theta - 4\pi/3)\hat{\mathbf{r}}.$$

Let the currents be given by

$$\begin{aligned} i_{S1} &= I_S \cos(\omega_S t) \\ i_{S2} &= I_S \cos(\omega_S t - 2\pi/3) \\ i_{S3} &= I_S \cos(\omega_S t - 4\pi/3). \end{aligned}$$

(a) Show that the total magnetic in the air gap may be written as

$$\vec{\mathbf{B}}_S = \vec{\mathbf{B}}_{S1} + \vec{\mathbf{B}}_{S2} + \vec{\mathbf{B}}_{S3} = \frac{\mu_0 \ell_2 N_S I_S}{4gr} \frac{3}{2} \cos(\theta - \omega_S t)\hat{\mathbf{r}}.$$

(b) Is this a sinusoidally distributed magnetic field?
(c) With two rotor loops $\pi/2$ radians apart, what changes (if any) are required to analyze this three-phase induction machine compared to the two-phase induction machine in this chapter?

Problem 6 A PM-Generator/Induction-Motor Machine (motivated by [27])

In this problem, a rather strange type of machine is analyzed. Figure 5.30 shows a permanent magnet rotating inside a hollowed out core of soft iron. (This setup is the reverse of that for the DC motor in Chapter 1, where the rotating part is made of soft iron and the external stationary part is soft iron.) By properly designing the permanent magnet, it can be assumed that the magnetic field in the air gap is given by

$$\vec{\mathbf{B}}_S = B_S \hat{\mathbf{r}} = B_{Smax} \frac{r_R}{r} \cos(\theta - \theta_S)\hat{\mathbf{r}} \tag{5.59}$$

where θ is an arbitrary angular location in the air gap and θ_S locates the north end (magnetic axis) of the permanent magnet as shown in Figure 5.30 (The subscript "S" is used because this magnetic field will take the place of the stator magnetic field discussed in the text.). Figures 5.30(b)–(d) illustrate the radial magnetic field due to the permanent magnet as it rotates from 0 to $\pi/2$ to π.

www.EngineeringEBooksPdf.com

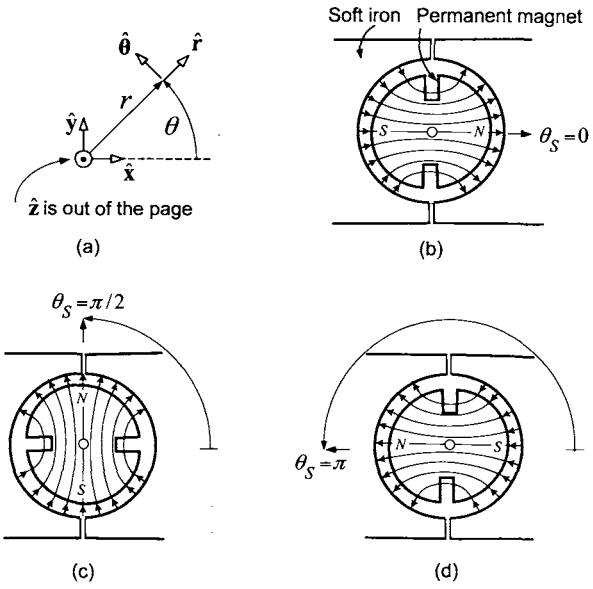


FIGURE 5.30. A permanent magnet rotating inside a hollowed out core of soft iron.

The next part of the construction is to put a conducting loop in the air gap. This is illustrated in Figure 5.31(a), which shows a half-cylindrical-shaped loop placed in the air gap.

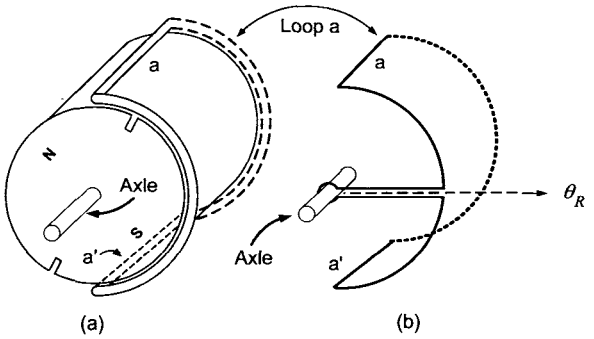


FIGURE 5.31. (a) Loop in the air gap which rotates about the axle independent of the rotating permanent magnet. (b) Illustrating how the loop is mechanically supported so that it can rotate independent of the permanent magnet.

However, this loop is not *attached to the permanent magnet; rather, it rotates independently of the permanent magnet on the same axle. Figure*

www.EngineeringEBooksPdf.com

5.31(b) illustrates how the loop is mechanically supported so that it can rotate on the axle independent of the permanent magnet. This loop is referred to as rotor loop $a-a'$ (or rotor phase a) and its position is located by the angle θ_R which is fixed to the loop half way between sides a and a' as shown in Figure 5.31(b). To complete the description of the construction of this motor, a second rotor loop is added to the system as shown in Figure 5.32. This loop is denoted rotor loop $b-b'$ (or rotor phase b) and is rotated 90° with respect to loop $a-a'$. As shown in Figure 5.32(b), a brace is put between the two loops so that they are rigidly held 90° apart. The brace and axle are non conducting so that the two loops are electrically isolated. The pair of loops rotate together on the axle independent of the permanent magnet. This completes the construction of the machine.

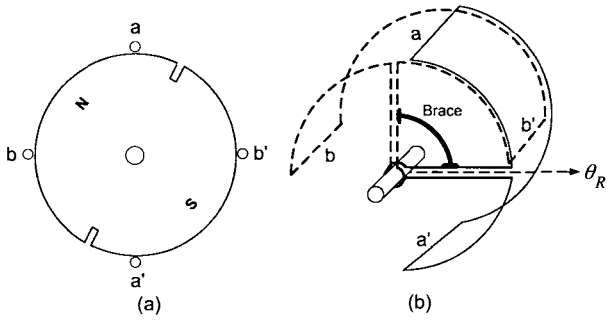


FIGURE 5.32. Two cylindrical rotor loops mechanically held together 90° apart, which rotate together on the axle independently of the rotating permanent magnet.

(a) Let $\theta_S(t) = \omega_S t$ so that the permanent magnet is rotating with constant angular speed ω_S by some external mechanical force. Consequently, a rotating radially directed magnetic field is setup in the air gap of the machine. Compute the fluxes in the two rotor loops due to the rotating magnetic field $\vec{\mathbf{B}}_S$.

(b) With R_R the resistance of a rotor loop and L_R the inductance of the rotor loop, compute the sinusoidal steady-state currents i_{RaSS} and i_{RbSS} in the two rotor loops. Assume the rotor has constant angular velocity ω_R where $0 < \omega_R < \omega_S$.

(c) Compute the torques τ_{Ra} and τ_{Rb} on the two rotor loops due to the magnetic field $\vec{\mathbf{B}}_S$ acting on the current in the rotor sides a, a', b, b' in terms of $i_{Ra}, i_{Rb}, \ell_1, \ell_2, B_{Smax}, \omega_S$ and ω_R.

(d) Substitute the expressions for the currents from part (b) into the expressions for the torques in part (c) and show that the resulting expression has the same form as that derived in problem 2.

www.EngineeringEBooksPdf.com

Synchronous Machines

Problem 7 Magnetic Field of a Sinusoidally Wound Rotor

Using Ampère's law, derive the expression given in equation (5.10) for the radial magnetic field in the air gap due to the current in the rotor windings. Assume ideal magnetic material and, that the rotor and stator windings have cross-sectional areas that are infinitesimal.

Problem 8 Mathematical Model of a PM Synchronous Motor

Consider a two phase permanent magnet synchronous motor. This is constructed like the wound rotor in Figure 5.33, but the rotor is replaced by a permanent magnet *as shown. Let the magnetic field due to the permanent magnet rotor be given by*

$$\vec{\mathbf{B}}_R = B_R(r,\theta)\hat{\mathbf{r}} = B_{R\max}\frac{r_R}{r}\cos(\theta-\theta_R)\hat{\mathbf{r}}$$

and derive the mathematical model of the PM synchronous motor.

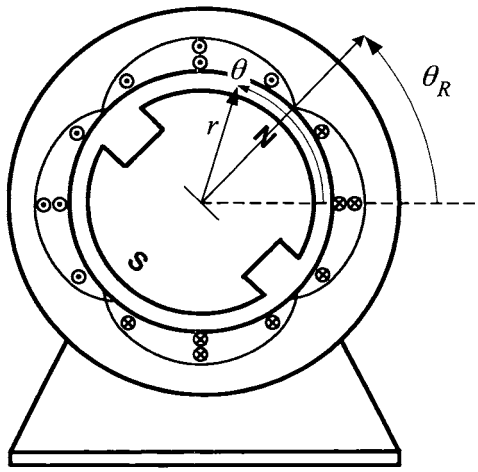


FIGURE 5.33. Two-phase permanent magnet synchronous motor.

Problem 9 Synchronous Motor with a Sinusoidally Wound Rotor

Consider a synchronous motor with a sinusoidally wound rotor as in Figure 5.9. An analytical expression for the torque produced by this motor was derived in the text. However, this expression can also be derived by considering the magnetic force due to the stator magnetic field $\vec{\mathbf{B}}_S$ *acting on the currents in the rotor windings. This problem outlines such an approach.*

(a) Using the magnetic force law, show that the incremental magnetic force $d\vec{\mathbf{F}}_R$ *due to* $\vec{\mathbf{B}}_S$ *acting on the rotor current in the windings of the*

www.EngineeringEBooksPdf.com

rotor between θ and $\theta + d\theta$ is given by

$$d\vec{\mathbf{F}}_R = \begin{cases} I_F \dfrac{N_F}{2} |\sin(\theta - \theta_R)| d\theta (+\ell_1 \hat{\mathbf{z}}) \times \vec{\mathbf{B}}_S & \theta_R \le \theta \le \theta_R + \pi \\ I_F \dfrac{N_F}{2} |\sin(\theta - \theta_R)| d\theta (-\ell_1 \hat{\mathbf{z}}) \times \vec{\mathbf{B}}_S & \theta_R + \pi \le \theta \le \theta_R + 2\pi \end{cases}$$

or, more simply, for $\theta_R \le \theta \le \theta_R + 2\pi$

$$\begin{aligned} d\vec{\mathbf{F}}_R &= I_F \frac{N_F}{2} \sin(\theta - \theta_R) d\theta (+\ell_1 \hat{\mathbf{z}}) \times \vec{\mathbf{B}}_S \\ &= I_F \frac{N_F}{2} \sin(\theta - \theta_R) d\theta (+\ell_1 \hat{\mathbf{z}}) \times \frac{\mu_0 N_S I_S}{2g} \cos(\theta - \theta_S) \hat{\mathbf{r}} \\ &= \frac{\mu_0 \ell_1 N_S N_F I_S I_F}{4g} \sin(\theta - \theta_R) \cos(\theta - \theta_S) d\theta \hat{\boldsymbol{\theta}}. \end{aligned}$$

(b) Integrate the incremental torque $d\vec{\boldsymbol{\tau}}_R$

$$\begin{aligned} d\vec{\boldsymbol{\tau}}_R &= (\ell_2/2)\hat{\mathbf{r}} \times d\vec{\mathbf{F}}_R \\ &= \frac{\mu_0 \ell_1 \ell_2 N_S N_F I_S I_F}{8g} \sin(\theta - \theta_R) \cos(\theta - \theta_S) d\theta \hat{\mathbf{z}} \end{aligned}$$

over the rotor windings to obtain the total torque $\vec{\boldsymbol{\tau}}_R$ on the rotor.

(c) Assume the motor is in steady-state with $\theta_S = \omega_S t, \theta_R = \omega_R t - \delta$ and $\omega_S = \omega_R$. With

$$\begin{aligned} B_{R\max} &\triangleq \frac{\mu_0 \ell_2 N_F I_F}{4gr} |_{r=\ell_2/2} = \frac{\mu_0 N_F I_F}{2g} \\ V_{airgap} &\triangleq 2\pi(\ell_2/2)\ell_1 g = \pi \ell_1 \ell_2 g \\ B_{S\max} &\triangleq \frac{\mu_0 \ell_2 N_S I_S}{4gr} |_{r=\ell_2/2} = \frac{\mu_0 N_S I_S}{2g} \end{aligned}$$

show that the answer to part (b) reduces to the expression given in (5.13).

Problem 10 Synchronous Motor with a Salient Rotor

Consider a synchronous machine with two sinusoidally wound stator phases and a salient *rotor as in Figure 5.13 of Section 5.3.3. Let $i_{Sa} = I_S \cos(\omega_S t)$, $i_{Sb} = I_S \sin(\omega_S t)$ be the stator currents and $i_F(t) = I_F =$ constant so that the magnetic fields in the air gap are*

$$\begin{aligned} \vec{\mathbf{B}}_S &= \frac{\mu_0 N_S I_S}{2g_1} \frac{r_R}{r} \cos(\theta - \theta_S) \hat{\mathbf{r}} \\ \vec{\mathbf{B}}_R &= \frac{\mu_0 N_F I_F}{2g_0} \frac{r_R}{r} \cos(\theta - \theta_R) \hat{\mathbf{r}} \end{aligned}$$

where $\theta_S(t) = \omega_S t$ denotes angular position of the magnetic axis of the stator magnetic field and $\theta_R(t) = \omega_R t - \delta$ denotes the angular position of

www.EngineeringEBooksPdf.com

the rotor which is taken to coincide with the rotor's magnetic axis. Here g_1 *is the average air gap length* ($g_1 > g_0$) *and, as the rotor's cross section is not circular, let* $r_R \triangleq r_S - g_1$ *(see the remark in Section 5.3.3).*

(a) Compute the torque τ_S *on the stator phases due to the rotor's magnetic field* $\vec{\mathbf{B}}_R$ *acting on the stator currents* i_{Sa}, i_{Sb}. *Use this to find* τ_R. *Is there anything that has to be done different here than in the sinusoidally wound rotor case? Explain why or why not.*

(b) Compute the induced emf's ξ_{Sa} *and* ξ_{Sb} *in the stator phases due to the rotor's magnetic field* $\vec{\mathbf{B}}_R$. *Is there anything that has to be done different here than in the sinusoidally-wound rotor case? Explain why or why not.*

(c) Compute the power absorbed in the stator by these induced emf's and show it equals the negative of the mechanical power produced by the motor. Is there anything that has to be done different here than in the sinusoidally wound rotor case? Explain why or why not.

(d) Is it possible (in a nice analytic fashion) to find the motor's torque directly by computing the torque on the rotor due to the magnetic field $\vec{\mathbf{B}}_S$ *acting on the rotor current? Explain why or why not.*

Problem 11 Emf in the Rotor Winding of a Synchronous Machine

Consider a synchronous motor with a sinusoidally wound rotor as in Figure 5.9. This problem outlines how to derive an expression for the flux and induced emf in the rotor winding produced by the stator magnetic field.

(a) Compute the flux linkage λ_R *in the rotor loops due to the stator magnetic field* $\vec{\mathbf{B}}_S$; *that is, with*

$$\vec{\mathbf{B}}_S(i_{Sa}, i_{Sb}, r, \theta) = \frac{\mu_0 \ell_2 N_S}{4gr} \left(i_{Sa}\cos(\theta) + i_{Sb}\sin(\theta)\right)\hat{\mathbf{r}}$$

compute

$$\lambda_R = \int_{\substack{All\ loops\ of \\ the\ rotor}} \vec{\mathbf{B}}_S \cdot d\vec{\mathbf{S}}.$$

(b) Compute the emf induced in the windings, that is,

$$\xi_R = -\frac{d\lambda_R}{dt}.$$

(c) Let $i_{Sa}(t) = I_S\cos(\omega_S t)$, $i_{Sb}(t) = I_S\sin(\omega_S t)$, $\theta_S = \omega_S t$, $\theta_R = \omega_R t - \delta$ *with* $\omega_S = \omega_R$ *and show that in this case*

$$\xi_R = -\frac{d\lambda_R}{dt} \equiv 0.$$

Explain why.

www.EngineeringEBooksPdf.com

Microscopic Viewpoint of Electric Machines

Problem 12 Linear Motor in a Coordinate System Attached to the Bar

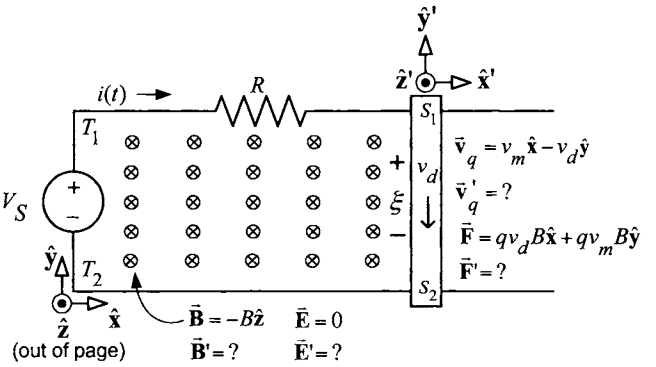


FIGURE 5.34. Linear DC machine. The primed coordinate system is attached to the sliding bar and moves at velocity $v_m\hat{\mathbf{x}}$ with respect to the unprimed coordinate system attached to the rails.

In chapter 1, *the linear DC machine was analyzed from the microscopic point of view in a stationary coordinate system of the rails. In the stationary coordinate system,* $\vec{\mathbf{B}} = -B\hat{\mathbf{z}}$, $\vec{\mathbf{E}} = 0$ ($B > 0$ *and* $\vec{\mathbf{E}}$ *denotes the electric field in the air surrounding the linear motor; there is another electric field* $\vec{\mathbf{E}}_S$ *in the wire setup by the source voltage* V_S*). In this coordinate system, the bar moves in the* $+\hat{\mathbf{x}}$ *direction with a constant speed* v_m *and each charge* q *in the sliding bar has total velocity* $\vec{\mathbf{v}}_q = v_m\hat{\mathbf{x}} - v_d\hat{\mathbf{y}}$ *where* v_d *is the drift speed. Consider the primed (′) coordinate system shown in Figure 5.34 which is attached to the sliding bar. Redo the analysis from the point of view of this coordinate system. Specifically,*

(a) Compute the electric $\vec{\mathbf{E}}'$ *and magnetic* $\vec{\mathbf{B}}'$ *fields in the reference frame of the moving bar using the transformation (5.44).*

(b) Find the velocity $\vec{\mathbf{v}}_q'$ *of the charge carriers in the sliding bar.*

(c) Find the magnetic force per unit charge $\vec{\mathbf{v}}_q' \times \vec{\mathbf{B}}'$ *on the charge carriers in sliding bar.*

(d) Compute the Lorentz force per unit charge $\vec{\mathbf{F}}'/q \triangleq \vec{\mathbf{E}}' + \vec{\mathbf{v}}_q' \times \vec{\mathbf{B}}'$ *on charge carriers in the sliding bar due to the external electric and magnetic fields. What part of this force is canceled out by* $\vec{\mathbf{E}}_S$*? What is the resulting total force on the sliding bar?*

(e) In this coordinate system, what is the "back electric field" and "back emf"? Show that conservation of energy holds; that is, the energy absorbed by the back emf reappears as mechanical power out.

(f) In the coordinate system of the sliding bar, what is the flux in the loop of the linear motor. Use Faraday's law to compute the emf ξ_{bar} *induced in*

www.EngineeringEBooksPdf.com

loop of the linear motor. Neglecting the inductance, compute the current as $i_b = \xi_{bar}/R$ *where* R *is the resistance of the bar. What is the net force on the bar in this coordinate system?*

Problem 13 Linear Motor in a Coordinate System with Velocity $v_c < v_m$

Repeat problem 12 for the case where the coordinate system is moving at speed v_c*, where* $v_c < v_m$*.*

Problem 14 Linear Motor in a Coordinate System with Velocity $v_c > v_m$

Repeat problem 12 for the case where the coordinate system is moving at speed v_c*, where* $v_c > v_m$*.*

Problem 15 Stator Electric Field

In the derivation of the stator electric field $\vec{\mathbf{E}}_S(\theta, t)$ *in the air gap due to the rotating stator magnetic field, the "constant of integration" was set to zero so that* $\vec{\mathbf{E}}_S(\theta, t)$ *is given by equation (5.23)*

$$\vec{\mathbf{E}}_S(\theta, t) = E_{Sz}(\theta, t)\hat{\mathbf{z}} = \frac{\mu_0 \ell_2 N_S I_S}{4g}\omega_S \cos(\theta - \omega_S t)\hat{\mathbf{z}}.$$

Note that $\vec{\mathbf{E}}_S(\theta, t)$ *is a maximum at* $\theta = \omega_S t$*, a minimum at* $\theta = \omega_S t + \pi$ *and zero at* $\theta = \omega_S t \pm \pi/2$*. Similarly, the stator magnetic field*

$$\vec{\mathbf{B}}_S(r, \theta, t) = \frac{\mu_0 \ell_2 N_S I_S}{4gr} \cos(\theta - \omega_S t)\hat{\mathbf{r}}$$

is a maximum at $\theta = \omega_S t$*, a minimum at* $\theta = \omega_S t + \pi$ *and zero at* $\theta = \omega_S t \pm \pi/2$*.*

(a) Consider a locked rotor, that is, the rotor is constrained so that it cannot move. Show that the induced emf in a rotor loop is zero at a time t *when one side of the loop is located at* $\theta = \omega_S t + \pi/2$ *(so the other side of the loop is located at* $\theta = \omega_S t - \pi/2$*), that is, when the flux through the loop is maximum or minimum (see Figure 5.15).*

(b) With the rotor locked (i.e., $\omega_R = 0$*), the induced emf is equal to*

$$\xi_{Ra} = V_{Ra} \triangleq \oint_{\text{rotor loop } a} \vec{\mathbf{E}}_S \cdot d\vec{\ell}.$$

Use this to explain why the stator electric field $\vec{\mathbf{E}}_S(\theta, t)$ *must be zero for* $\theta = \omega_S t \pm \pi/2$*, or equivalently, why must the "constant of integration" be zero (see Figure 5.15).*

Problem 16 Induction Motor in the Synchronous Coordinate System

Rederive the emf $\xi'_{Ra} = -d\lambda'_{Ra}/dt$ *given in equation (5.45) by computing the* flux λ'_{Ra} *in rotor loop a due to the stator magnetic field* $\vec{\mathbf{B}}'_S$*. That is,*

www.EngineeringEBooksPdf.com

show that

$$\lambda'_{Ra} = \int_S \vec{\mathbf{B}}'_S \cdot d\vec{\mathbf{S}} = \int_{\theta'=-\omega_R t-\pi/2}^{\theta'=-\omega_R t+\pi/2} \frac{\mu_0 \ell_2 N_S I_S}{4gr} \Big|_{r=\ell_2/2} \cos(\theta')\hat{\mathbf{r}}\cdot\ell_1(\ell_2/2)d\theta'\hat{\mathbf{r}}$$
$$= \frac{\mu_0 \ell_1 \ell_2 N_S I_S}{4g} \cos(-\omega'_R t).$$

Problem 17 Induction Motor in the Rotor Coordinate System

Consider the simple induction motor analyzed in the text. That is, a machine whose stator consists of two sinusoidally wound phases 90° apart and whose rotor consists of two electrically isolated loops also 90° apart. This problem outlines the Physics of the motor from a coordinate system attached to the rotor of the motor; that is, it rotates at an angular speed ω_R with respect to the stator. Denote this rotor *coordinate system as the primed (′) coordinate system and,* in this coordinate system, *do the following:*

(a) Compute the electric $\vec{\mathbf{E}}'_S$ and magnetic $\vec{\mathbf{B}}'_S$ fields in the air gap from the electric and magnetic fields $\vec{\mathbf{E}}_S$ and $\vec{\mathbf{B}}_S$ in the stator coordinate system.

(b) Find the velocity $\vec{\mathbf{v}}'_{Ra}$ of the charge carriers on the axial sides of rotor phase/loop a (note that in this coordinate system $\omega'_R = 0$).

(c) Find the magnetic force per unit charge $\vec{\mathbf{v}}'_{Ra} \times \vec{\mathbf{B}}'_S$ on the charge carriers in the axial sides of rotor phase a.

(d) Compute the torque τ'_{Ra} on the rotor loop.

(e) Compute the emf ξ'_{Ra} induced in rotor loop a by computing the rate of change of the flux in the loop. Neglecting the rotor inductance, compute the current as $i_{Ra} = \xi'_{Ra}/R_R$.

(f) Compute the voltage $V'_{Ra} = \oint_{\text{rotor loop a}} \vec{\mathbf{E}}'_S \cdot d\vec{\boldsymbol{\ell}}$ in rotor loop a produced by the axial electric field $\vec{\mathbf{E}}'_S$.

(g) Compute the back emf ζ'_{Ra} by integrating the axial magnetic force per unit charge around rotor loop a. Show that $\xi'_{Ra} = V'_{Ra} + \zeta'_{Ra}$.

(h) Find the corresponding quantities $\vec{\mathbf{v}}'_{Rb}$, $\vec{\mathbf{v}}'_{Rb} \times \vec{\mathbf{B}}'_S$, τ'_{Rb}, ξ'_{Rb}, i_{Rb}, V'_{Rb}, and ζ'_{Rb} for rotor phase b.

(i) Show that conservation of energy holds in this coordinate system; that is,

$$i_{Ra}V'_{Ra} + i_{Rb}V'_{Rb} = (i_{Ra}\xi'_{Ra} + i_{Rb}\xi'_{Rb}) - (i_{Ra}\zeta'_{Ra} + i_{Rb}\zeta'_{Rb})$$

where $-(i_{Ra}\zeta'_{Ra} + i_{Rb}\zeta'_{Rb}) = (\tau'_{Ra} + \tau'_{Rb})\omega'_R$ so that the power absorbed by the back emf is converted into mechanical power.

Problem 18 Synchronous Machine in the Stationary Coordinate System

Consider a synchronous motor with a sinusoidally wound rotor to be in steady state so $i_F = I_F =$ constant, $i_{Sa} = I_S \cos(\omega_S t), i_{Sb} = I_S \sin(\omega_S t)$, $\omega_R = \omega_S$, $\theta_S = \omega_S t$ and $\theta_R = \omega_R t - \delta$. The stator of this machine is identical to that of an induction motor so that the electric and magnetic

www.EngineeringEBooksPdf.com

fields in the air gap due to the stator currents are given by

$$\begin{aligned}\vec{\mathbf{E}}_S(\theta,t) &= E_{Sz}(\theta,t)\hat{\mathbf{z}} = \frac{\mu_0 \ell_2 N_S I_S}{4g}\omega_S \cos(\theta-\omega_S t)\hat{\mathbf{z}} \\ \vec{\mathbf{B}}_S(r,\theta,t) &= B_{Sr}(\theta,t)\hat{\mathbf{r}} = \frac{\mu_0 \ell_2 N_S I_S}{4gr}\cos(\theta-\omega_S t)\hat{\mathbf{r}}.\end{aligned}$$

The sinusoidally wound rotor phase has a winding density $(N_F/2)\,|\sin(\theta-\theta_R)|$ *with the constant current* I_F *in it so that the rotor magnetic field in the air gap is*

$$\vec{\mathbf{B}}_R = \frac{\mu_0 \ell_2 N_F I_F}{4gr}\cos(\theta-\theta_R)\hat{\mathbf{r}}.$$

Redo the Physics of the synchronous motor from the microscopic point of view by doing the following:

(a) Find the velocity $\vec{\mathbf{v}}_F$ *of the charge carriers on the axial sides of the rotor phase (field winding).*

(b) Find the magnetic force per unit charge $\vec{\mathbf{v}}_F \times \vec{\mathbf{B}}_S$ *on the charge carriers in the axial sides of the rotor phase.*

(c) Find the Lorentz force per unit charge $\vec{\mathbf{F}}/q \triangleq \vec{\mathbf{E}}_S + \vec{\mathbf{v}}_F \times \vec{\mathbf{B}}_S$ *on the charge carriers in the axial sides of the rotor phase.*

(d) Compute the emf $V_F = \oint_{All\ rotor\ loops} \left(\vec{\mathbf{F}}/q\right)\cdot d\vec{\boldsymbol{\ell}}$ *in the rotor windings/loops produced by the Lorentz force* $\vec{\mathbf{F}}/q$*. Can you explain your answer?*

(e) Compute the torque τ_R *on the rotor loop using the magnetic force per unit charge in the* $\hat{\boldsymbol{\theta}}$ *direction.*

(f) Use Faraday's law in differential form $\nabla \times \vec{\mathbf{E}}_R = -\partial\vec{\mathbf{B}}_R/\partial t$ *to find* $\vec{\mathbf{E}}_R$ *in the air gap.*

(g) In the macroscopic approach, it was shown in (5.18) that

$$\begin{aligned}\xi_{Sa} &= -d\lambda_{Sa}/dt \\ \xi_{Sb} &= -d\lambda_{Sb}/dt.\end{aligned}$$

Show that the expressions for the emf's induced in the stator windings by the rotor's magnetic field can also be found by computing

$$\begin{aligned}\xi_{Sa} &= \oint_{\substack{All\ loops\ of\\ stator\ phase\ a}} \vec{\mathbf{E}}_R \cdot d\vec{\boldsymbol{\ell}} \\ \xi_{Sb} &= \oint_{\substack{All\ loops\ of\\ stator\ phase\ b}} \vec{\mathbf{E}}_R \cdot d\vec{\boldsymbol{\ell}}.\end{aligned}$$

Why isn't it necessary to include the magnetic force per unit charge $\vec{\mathbf{v}}_{Sa} \times \vec{\mathbf{B}}_R$ *term in the computation of* ξ_{Sa} *and* ξ_{Sb}*? (*$\vec{\mathbf{v}}_{Sa}$ *is the velocity of charge carriers in the windings of stator phase a.)*

www.EngineeringEBooksPdf.com

(h) Show that

$$-\frac{d\left(L_S i_{Sa}\right)}{dt} = \oint_{\substack{All\ loops\ of \\ stator\ phase\ a}} \vec{\mathbf{E}}_S \cdot d\vec{\boldsymbol{\ell}}$$

$$-\frac{d\left(L_S i_{Sb}\right)}{dt} = \oint_{\substack{All\ loops\ of \\ stator\ phase\ b}} \vec{\mathbf{E}}_S \cdot d\vec{\boldsymbol{\ell}}.$$

That is, compute the line integrals on the right-hand side and show that they are of the form given on the left-hand side with $L_S \triangleq \frac{\mu_0 \ell_1 \ell_2 \pi}{8g} N_S^2$. *(It can be shown that* $L_S i_{Sa}$ *is the flux in stator phase a due to the stator magnetic field* $\vec{\mathbf{B}}_S$*). Why isn't it necessary to include the magnetic force per unit charge* $\vec{\mathbf{v}}_{Sa} \times \vec{\mathbf{B}}_S$ *term in the computation of the line integrals?*

(i) Given that $L_S i_{Sa}$ *is the flux in stator phase a due to the stator magnetic field* $\vec{\mathbf{B}}_S$ *and the answers to the previous parts of this problem, show that the* total *voltage/emf induced in the stator phases may be written as*

$$-\frac{d\left(\lambda_{Sa} + L_S i_{Sa}\right)}{dt} = \oint_{\substack{All\ loops\ of \\ stator\ phase\ a}} \left(\vec{\mathbf{E}}_R + \vec{\mathbf{E}}_S\right) \cdot d\vec{\boldsymbol{\ell}}$$

$$-\frac{d\left(\lambda_{Sb} + L_S i_{Sb}\right)}{dt} = \oint_{\substack{All\ loops\ of \\ stator\ phase\ b}} \left(\vec{\mathbf{E}}_R + \vec{\mathbf{E}}_S\right) \cdot d\vec{\boldsymbol{\ell}}.$$

(j) Show that power is conserved; that is,

$$i_{Sa}(t)\xi_{Sa}(t) + i_{Sb}(t)\xi_{Sb}(t) = -\tau_R \omega_R.$$

Problem 19 Synchronous Machine in the Rotor Coordinate System

Consider a synchronous motor with a sinusoidally wound rotor. With the motor in steady state ($\omega_R = \omega_S$)*, consider a coordinate system attached to the rotor so that it is rotating at synchronous speed; that is, it rotates at the angular speed* $\omega_R = \omega_S$ *with respect to the stator. Further, let the coordinate system be aligned with the rotor so that in cylindrical coordinates,*

$$\begin{aligned} r' &= r \\ \theta' &= \theta - \omega_R t \\ z' &= z \end{aligned}$$

where (r, θ, z) *are the cylindrical coordinates in the stationary coordinate system of the stator and* (r', θ', z') *are the cylindrical coordinates in the rotating coordinate system of the rotor. This* rotor *coordinate system is referred to as the primed* $(')$ *coordinate system;* in this coordinate system, *do the following:*

www.EngineeringEBooksPdf.com

(a) Compute the electric $\vec{\mathbf{E}}'_S$ *and magnetic* $\vec{\mathbf{B}}'_S$ *fields in the air gap from the electric and magnetic fields* $\vec{\mathbf{E}}_S, \vec{\mathbf{B}}_S$ *in the stator coordinate system.*

(b) Compute the electric $\vec{\mathbf{E}}'_R$ *and magnetic* $\vec{\mathbf{B}}'_R$ *fields in the air gap from the electric and magnetic fields* $\vec{\mathbf{E}}_R, \vec{\mathbf{B}}_R$ *in the stator coordinate system.*

(c) Find the velocity $\vec{\mathbf{v}}'_F$ *of the charge carriers on the axial sides of the (field) rotor windings (note that in this coordinate system* $\omega'_R = 0$*).*

(d) Find the magnetic force per unit charge $\vec{\mathbf{v}}'_F \times \vec{\mathbf{B}}'_S$ *on the charge carriers in the axial sides of the rotor.*

(e) Compute the torque τ_R *on the rotor loop.*

(f) Compute the back emf ξ'_{Sa} *induced in stator phase a by computing the rate of change of the flux due to* $\vec{\mathbf{B}}'_R$ *in that phase. Similarly, compute* ξ'_{Sb} *in stator phase b.*

(g) Find the velocity $\vec{\mathbf{v}}'_{Sa}$ *of the charge carriers on the axial sides of the stator phase a. Note that the stator windings are rotating with angular speed* $-\omega_R$ *with respect to the rotor. Similarly, find* $\vec{\mathbf{v}}'_{Sb}$*.*

(h) Show that the back emf in stator phase a can also be computed as

$$\xi'_{Sa} = \oint_{rotor\ loops} \left(\vec{\mathbf{E}}'_R + \vec{\mathbf{v}}'_{Sa} \times \vec{\mathbf{B}}'_R\right) \cdot d\vec{\boldsymbol{\ell}}$$

Similarly, find ξ'_{Sb}*.*

(i) Compute the rotor emf $V_F = \oint_{rotor\ loops} \left(\vec{\mathbf{E}}'_S + \vec{\mathbf{v}}'_F \times \vec{\mathbf{B}}'_S\right) \cdot d\vec{\boldsymbol{\ell}}$

in the rotor loops produced by the stator fields $\vec{\mathbf{E}}'_S, \vec{\mathbf{B}}'_S$*.*

(j) Using the $\hat{\boldsymbol{\theta}}$ *component of* $\vec{\mathbf{v}}'_{Sa} \times \vec{\mathbf{B}}'_R$*, compute the torque* τ_{Sa} *exerted on the stator by the rotor. Similarly, compute* τ_{Sb}*. Is* $\tau_R = -(\tau_{Sa} + \tau_{Sb})$*?*

(k) In this coordinate system, $\omega'_R = 0$ *so that no mechanical power is being given to the rotor. Show that conservation of energy holds in this coordinate system, i.e.,* $i_{Sa}\xi'_{Sa} + i_{Sb}\xi'_{Sb} = -(\tau_{Sa} + \tau_{Sb})\omega'_S$ *where* $\omega'_S = -\omega_S$*. From the point of view of this coordinate system, is the machine acting as a motor or generator?*

Problem 20 Emfs in Full-Pitched and Short-Pitched Windings

Figure 5.35 shows a motor with a permanent magnet rotor which has a single stator phase with full-pitched turns, that is, wound with each loop spanning π *radians [see Figures 4.1 and 4.3(b) of Chapter 4]. Let the magnetic field in the air gap due to the permanent magnet rotor be given by*

$$\vec{\mathbf{B}}_R(\theta - \theta_R) = B_{max}\frac{r_R}{r}\cos(\theta - \theta_R)\hat{\mathbf{r}}.$$

(a) Let $\theta_R(t) = \omega_R t$ *and compute the axial electric field* $\vec{\mathbf{E}}_R = E_{Rz}\hat{\mathbf{z}}$ *induced in the air gap by the time varying magnetic field.*

(b) Using the expression derived for the axial electric field in part (a) to compute the emf induced in the stator phase by the PM rotor.

www.EngineeringEBooksPdf.com

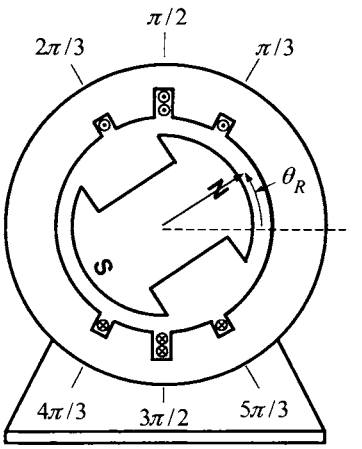


FIGURE 5.35. A machine with a PM rotor and a single stator phase.

(c) Suppose that the stator in part (b) now consists of short-pitched turns as indicated in Figure 5.36. That is, each turn spans only 150° *rather than* 180° *as in part (b). (See problem 14 of Chapter* 4 *for a more detailed explanation of short-pitched turns.)*

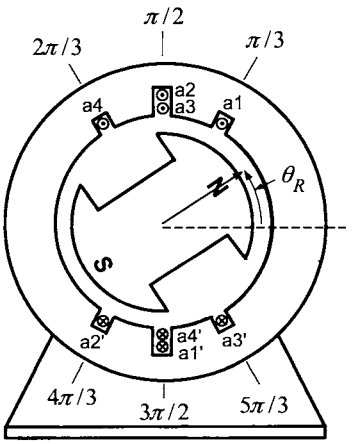


FIGURE 5.36. A motor with a PM rotor and a single stator phase whose turns are short-pitched.

Without any computation, explain why the induced emf in this short-pitched winding must be the same as in the full-pitched winding of part (b).

www.EngineeringEBooksPdf.com

6

Mathematical Models of AC Machines

In this chapter, the mathematical models of the induction and synchronous machines are derived. The derivations in this chapter will be based on a two-phase machine. In Chapter 7 three-phase machines are considered, and it is shown there that any balanced three-phase induction or synchronous machine has a two-phase equivalent model identical in form to its two-phase counterpart. The models derived in this chapter are standard throughout the literature and form the basis for deriving control algorithms.

The symmetric, two-pole (single pole-pair), two-phase machine shown in Figure 6.1 is used for the derivations that follow. The stator of this machine is constructed with a hollow cylindrical shell of iron wrapped with two sets of sinusoidally wound phases, each with a total of N_S turns and 90° apart. These stator windings are denoted as phases a and b, respectively, carrying the currents i_{Sa} and i_{Sb}, respectively. Stator phase a is connected to a voltage source u_{Sa}, while stator phase b is connected to a voltage source u_{Sb}. The resistance of the windings of the two phases are assumed to be identical and equal to R_S.

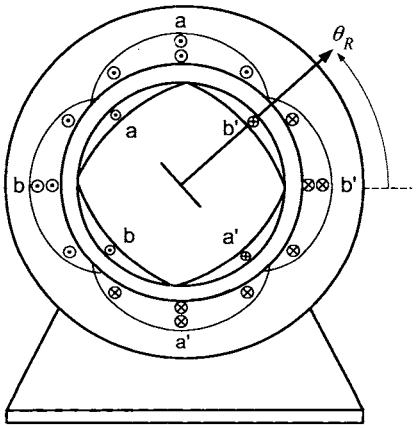


FIGURE 6.1. Representation of a two-phase sinusoidally wound machine.

The rotor consists of a cylindrical core of iron with two sinusoidally wound phases each with a total of N_R turns and 90° apart. These phases are denoted a and b as indicated in Figure 6.1. The currents in the rotor

www.EngineeringEBooksPdf.com

phases are denoted as i_{Ra} and i_{Rb}, respectively and the resistance of each of the rotor phase windings is denoted as R_R. At this point, no assumption is made on whether or not the ends of the rotor phases are shorted or connected to voltage sources. The rotor is located with respect to the stator by the magnetic axis of rotor phase a as shown in Figure 6.1.

The currents in the phases of the machine establish magnetic fields and these magnetic fields in turn produce fluxes in the windings of all four of the machine's phases. In order to obtain a mathematical model of an AC machine, an expression for the total flux linkage in each of the stator and rotor phases due to the currents i_{Sa}, i_{Sb}, i_{Ra}, and i_{Rb} must be found. However, before these flux linkages can be computed, an expression for the magnetic field $\vec{\mathbf{B}}_R(i_{Ra}, i_{Rb}, r, \theta)$ in the air gap produced by the rotor currents is required. An expression for the magnetic field $\vec{\mathbf{B}}_S(i_{Sa}, i_{Sb}, r, \theta)$ in the air gap produced by the stator currents was derived in Chapter 4. Also, the concept of leakage is explained and the expressions for the magnetic fields $\vec{\mathbf{B}}_S, \vec{\mathbf{B}}_R$ are modified to account for it. The modified expressions for the magnetic fields $\vec{\mathbf{B}}_S$ and $\vec{\mathbf{B}}_R$ are then used to compute the flux linkage in each phase of the machine.

6.1 The Magnetic Field $\vec{\mathbf{B}}_R(i_{Ra}, i_{Rb}, r, \theta - \theta_R)$

The radial magnetic field $\vec{\mathbf{B}}_{Ra}$ established *in the air gap* by the current i_{Ra} in the sinusoidally distributed winding of rotor phase a is now computed. The winding/turns density of rotor phase a is $(N_R/2)\,|\sin(\theta - \theta_R)|$ so that the number of turns between θ and $\theta + d\theta$ is $(N_R/2)\,|\sin(\theta - \theta_R)|\,d\theta$. To proceed, Ampère's law $\oint \vec{\mathbf{H}} \cdot d\vec{\ell} = i_{enclosed}$ (with $\vec{\mathbf{H}} \equiv 0$ in the magnetic material) is applied to the closed path 1–2–3–4–1 drawn in Figure 6.2 to obtain

$$\int_4^1 \vec{\mathbf{H}}_{Ra} \cdot d\vec{\ell} + \int_2^3 \vec{\mathbf{H}}_{Ra} \cdot d\vec{\ell} = \int_{\theta' = \theta_R}^{\theta' = \theta} i_{Ra} \frac{N_R}{2} \sin(\theta' - \theta_R) d\theta'.$$

Evaluating gives

$$\int_{\ell=0}^{\ell=g} H_{Ra}(i_{Ra}, \theta_R)\hat{\mathbf{r}} \cdot (d\ell\hat{\mathbf{r}}) + \int_{\ell=0}^{\ell=g} H_{Ra}(i_{Ra}, \theta)\hat{\mathbf{r}} \cdot (-d\ell\hat{\mathbf{r}}) = -i_{Ra}\frac{N_R}{2}\cos(\theta - \theta_R) + i_{Ra}\frac{N_R}{2}$$

or

$$H_{Ra}(i_{Ra}, \theta_R)g - H_{Ra}(i_{Ra}, \theta)g = -i_{Ra}\frac{N_R}{2}\cos(\theta - \theta_R) + i_{Ra}\frac{N_R}{2}.$$

www.EngineeringEBooksPdf.com

It was assumed that $\vec{\mathbf{H}}_{Ra}$ is *constant* across the air gap. Rearranging gives

$$H_{Ra}(i_{Ra},\theta) = i_{Ra}\frac{N_R}{2g}\cos(\theta-\theta_R) + H_{Ra}(i_{Ra},\theta_R) - i_{Ra}\frac{N_R}{2g} \tag{6.1}$$

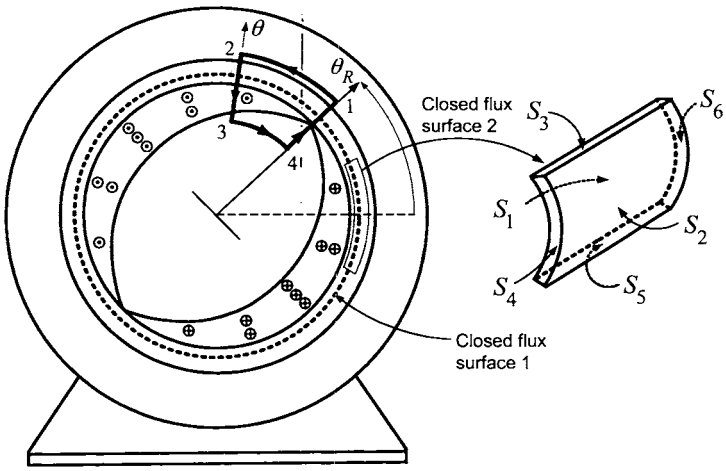


FIGURE 6.2. Use of Ampère's and Gauss's laws to determine B_{Ra} in the air gap due to i_{Ra}. (Rotor phase b is not shown for clarity.)

In this equation, both $H_{Ra}(i_{Ra},\theta), H_{Ra}(i_{Ra},\theta_R)$ are unknown. As in the case of the magnetic field produced by the stator currents, conservation of flux $\oint_S \vec{\mathbf{B}}\cdot d\vec{\mathbf{S}} = 0$ is applied to the closed surface 1 which encloses the rotor (see the dashed circle in Figure 6.2 around the rotor iron) to show that $H_{Ra}(i_{Ra},\theta_R) = i_{Ra}(N_R/2g)$. Then,

$$\begin{aligned} H_{Ra}(i_{Ra},\theta) &= \frac{N_R}{2g} i_{Ra}\cos(\theta-\theta_R) \\ B_{Ra}(i_{Ra},\theta) &= \frac{\mu_0 N_R}{2g} i_{Ra}\cos(\theta-\theta_R). \end{aligned} \tag{6.2}$$

In applying Ampère's law, it was assumed that $\vec{\mathbf{B}}_{Ra} = \mu_0\vec{\mathbf{H}}_{Ra}$ was constant across the air gap in the radial direction, that is, $\vec{\mathbf{B}}_{Ra}$ does not depend on the cylindrical coordinate r. However, as shown in Chapter 4 for the stator magnetic field, in order that $\vec{\mathbf{B}}_{Ra}$ satisfy the conservation of flux for the closed flux surface 2 shown in Figure 6.2 whose sides are $S_1, S_2, S_3, S_3, S_4, S_5$, and S_6, equation (6.2) is modified by setting

$$\vec{\mathbf{B}}_{Ra}(i_{Ra},r,\theta-\theta_R) = B_{Ra}(i_{Ra},r,\theta-\theta_R)\hat{\mathbf{r}} \triangleq \frac{\mu_0 N_R}{2g}\frac{r_R}{r} i_{Ra}\cos(\theta-\theta_R)\hat{\mathbf{r}} \tag{6.3}$$

www.EngineeringEBooksPdf.com

where r_R is the rotor radius.[1]

Similarly, the magnetic field $\vec{\mathbf{B}}_{Rb}$ established in the air gap by the sinusoidally wound rotor phase b (rotated 90° with respect to rotor phase a) carrying the current i_{Rb} is given by

$$\begin{aligned}\vec{\mathbf{B}}_{Rb}(i_{Rb}, r, \theta - \theta_R) &= B_{Rb}(i_{Rb}, r, \theta - \theta_R)\hat{\mathbf{r}} \\ &= \frac{\mu_0 N_R}{2g}\frac{r_R}{r} i_{Rb}\cos(\theta - \pi/2 - \theta_R)\hat{\mathbf{r}} \\ &= \frac{\mu_0 N_R}{2g}\frac{r_R}{r} i_{Rb}\sin(\theta - \theta_R)\hat{\mathbf{r}}. \qquad (6.4)\end{aligned}$$

In summary, the magnetic fields due to the stator and rotor currents are

$$\begin{aligned}\vec{\mathbf{B}}_S(i_{Sa}, i_{Sb}, r, \theta) &= \vec{\mathbf{B}}_{Sa}(i_{Sa}, r, \theta) + \vec{\mathbf{B}}_{Sb}(i_{Sb}, r, \theta) \\ &= \frac{\mu_0 r_R N_S}{2g}\frac{1}{r}\left(i_{Sa}\cos(\theta) + i_{Sb}\sin(\theta)\right)\hat{\mathbf{r}} \qquad (6.5)\end{aligned}$$

and

$$\begin{aligned}\vec{\mathbf{B}}_R(i_{Ra}, i_{Rb}, r, \theta - \theta_R) &= \vec{\mathbf{B}}_{Ra}(i_{Ra}, r, \theta - \theta_R) + \vec{\mathbf{B}}_{Rb}(i_{Rb}, r, \theta - \theta_R) \\ &= \frac{\mu_0 N_R r_R}{2g}\frac{1}{r}\left(i_{Ra}\cos(\theta - \theta_R) + i_{Rb}\sin(\theta - \theta_R)\right)\hat{\mathbf{r}}. \qquad (6.6)\end{aligned}$$

respectively.

6.2 Leakage

Consider Figure 6.3, which shows a single-phase distributed winding on the rotor. It has been assumed up to now that the magnetic field produced by the rotor current is *radially* directed in the air gap so that only the surfaces S_1 and S_2 in Figure 6.3 have nonzero flux. With this assumption and along with the (outward) surface element vectors to the closed surface of Figure 6.3 given by

$$d\vec{\mathbf{S}} = \begin{cases} -r_R d\theta dz\hat{\mathbf{r}} & \text{on } S_1 \\ r_S d\theta dz\hat{\mathbf{r}} & \text{on } S_2 \\ drdz\hat{\boldsymbol{\theta}} & \text{on } S_3 \\ rd\theta dr\hat{\mathbf{z}} & \text{on } S_4 \\ -drdz\hat{\boldsymbol{\theta}} & \text{on } S_5 \\ -rd\theta dr\hat{\mathbf{z}} & \text{on } S_6, \end{cases}$$

[1] It is now easy to see that $\oint_S \vec{\mathbf{B}}_{Ra} \cdot d\vec{\mathbf{S}} = 0$ for *any* closed surface in the air gap. Ampere's law will also continue to hold for $g << r_R$ using the approximation $\int_{\ell=0}^{\ell=g} r_R/(r_R + \ell)\, d\ell \approx g$.

www.EngineeringEBooksPdf.com

it was shown that conservation of flux $\oint_S \vec{\mathbf{B}}_R \cdot d\vec{\mathbf{S}} = 0$ required a $1/r$ dependence by the magnetic field in the air gap (see Chapter 4). That is, up to now, it has been assumed that $\vec{\mathbf{B}}_R \cdot d\vec{\mathbf{S}} \equiv 0$ on the surfaces S_3, S_4, S_5, and S_6 so that the radial magnetic field $\vec{\mathbf{B}}_R$ must decrease as $1/r$ going from S_1 to S_2 in order to satisfy conservation of flux. However, in a real machine, the slots have finite dimensions, the air gap is of finite size and there are end effects at either end of the rotor. As a consequence, the magnetic field does have components in the azimuthal $\hat{\boldsymbol{\theta}}$ direction and axial $\hat{\mathbf{z}}$ direction in addition to the radial direction $\hat{\mathbf{r}}$ so that the surfaces S_3, S_4, S_5, and S_6 also have nonzero flux.

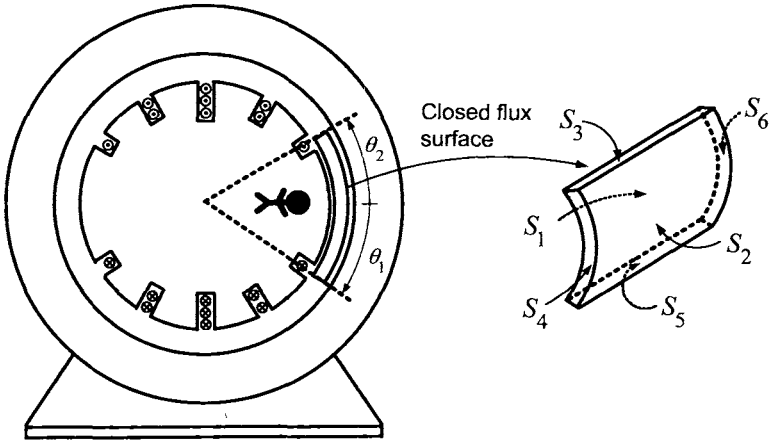


FIGURE 6.3. Closed flux surface to illustrate flux leakage. With the assumption of no leakage, only the surfaces S_1, S_2 have nonzero flux. With leakage, all six surfaces have nonzero flux through them.

To see how this affects the radial magnetic field, Figure 6.4 shows an enlargement of the cross section of Figure 6.3 from the point of view of the observer in Figure 6.3 looking *into* the page. In Figure 6.4, the lines of the magnetic field $\vec{\mathbf{B}}_R$ produced by the rotor currents are shown. At the slot openings, there is no iron so that in this vicinity the magnetic field tends to circle around the rotor winding rather than go across the air gap. Even away from the slots, the magnetic field spreads out from the radial direction due to the finite length of the air gap and the finite (axial) length of the machine. What this all means is that the average radial $\vec{\mathbf{B}}_R$ field on the surface S_2 actually decreases a little more than $1/r$. This now considered in more detail.

www.EngineeringEBooksPdf.com

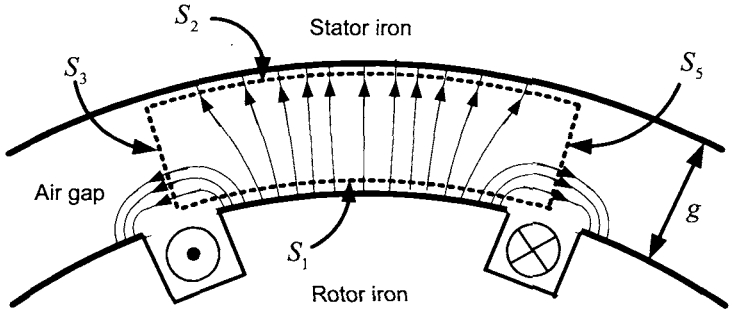


FIGURE 6.4. Cross-sectional view of the flux surface in Figure 6.3. The rotor magnetic field $\vec{\mathbf{B}}_R$ is perpendicular at the surface of the rotor and then spreads out in both the azimuthal and axial directions so the flux it produces at the inside surface of the stator is less that at the surface of the rotor.

To simplify the discussion, it is now assumed that there is no spreading in axial (z) direction so that $\int_{S_4} \vec{\mathbf{B}}_R \cdot d\vec{\mathbf{S}} = \int_{S_6} \vec{\mathbf{B}}_R \cdot d\vec{\mathbf{S}} = 0$. Using an outward normal, $\oint \vec{\mathbf{B}}_R \cdot d\vec{\mathbf{S}} = 0$ is computed on the closed surface shown in Figures 6.3 and 6.4 to obtain

$$\oint \vec{\mathbf{B}}_R \cdot d\vec{\mathbf{S}} = \int_{S_1} \vec{\mathbf{B}}_R \cdot d\vec{\mathbf{S}} + \int_{S_2} \vec{\mathbf{B}}_R \cdot d\vec{\mathbf{S}} + \int_{S_3} \vec{\mathbf{B}}_R \cdot d\vec{\mathbf{S}} + \int_{S_5} \vec{\mathbf{B}}_R \cdot d\vec{\mathbf{S}} = 0.$$

Rearranging, this becomes

$$\int_{S_1} \vec{\mathbf{B}}_R \cdot \left(-d\vec{\mathbf{S}}\right) = \int_{S_2} \vec{\mathbf{B}}_R \cdot d\vec{\mathbf{S}} + \int_{S_3} \vec{\mathbf{B}}_R \cdot d\vec{\mathbf{S}} + \int_{S_5} \vec{\mathbf{B}}_R \cdot d\vec{\mathbf{S}}$$

or

$$\int_{S_1} B_R(r_R, \theta, t)\hat{\mathbf{r}} \cdot (r_R d\theta dz \hat{\mathbf{r}}) = \int_{S_2} B_R(r_S, \theta, t)\hat{\mathbf{r}} \cdot (r_S d\theta dz \hat{\mathbf{r}}) + \int_{S_3} \vec{\mathbf{B}}_R \cdot d\vec{\mathbf{S}} + \int_{S_5} \vec{\mathbf{B}}_R \cdot d\vec{\mathbf{S}}. \qquad (6.7)$$

The surface S_1 is just at the surface of the rotor and the surface element vector $-d\vec{\mathbf{S}} = r_R d\theta dz \hat{\mathbf{r}}$ points in the positive radial direction on the surface S_1. If there was no spreading, then $\int_{S_1} B_R(r_R, \theta, t)\hat{\mathbf{r}} \cdot (r_R d\theta dz \hat{\mathbf{r}}) = \int_{S_2} B_R(r_S, \theta, t)\hat{\mathbf{r}} \cdot (r_S d\theta dz \hat{\mathbf{r}})$; that is, if both surfaces use the normal $\hat{\mathbf{r}}$, then the flux through S_1 equals the flux through S_2. However, the magnetic field does spread out in azimuthal direction and the fluxes through the surfaces S_2, S_3, and S_5 are then all *positive*. In this case, the radial $\vec{\mathbf{B}}_R$ field on the surface S_2 must be less on average than it was when it was assumed there was no flux through the surfaces S_3 and S_5. This is simply because the flux $\int_{S_1} B_R(r_R, \theta, t)\hat{\mathbf{r}} \cdot (r_R d\theta dz \hat{\mathbf{r}})$ on the left-hand side of (6.7) stays the same

www.EngineeringEBooksPdf.com

whether or not there is spreading[2] and is always equal to the sum of the fluxes on the right-hand side of (6.7).

To model this effect, a parameter κ, with $0 < \kappa < 1$, is introduced so that on the *stator side* of the air gap, the *rotor* magnetic field is given by

$$\vec{\mathbf{B}}_R(i_{Ra}, i_{Rb}, r, \theta - \theta_R)\Big|_{r=r_S} = \kappa \frac{\mu_0 N_R}{2g} \frac{r_R}{r_S} \left(i_{Ra}\cos(\theta - \theta_R) + i_{Rb}\sin(\theta - \theta_R)\right)\hat{\mathbf{r}}.$$

That is, the rotor radial $\vec{\mathbf{B}}_R$ field decreases to $\kappa r_R/r_S$ (rather than just r_R/r_S) in going from the surface of the rotor to the inside surface of the stator. The parameter κ is referred to as a *global coupling factor* [1].

Similarly, on the *rotor* side of the air gap, the *stator* magnetic field is given by

$$\vec{\mathbf{B}}_S(i_{Sa}, i_{Sb}, r, \theta)\Big|_{r=r_R} = \kappa \frac{\mu_0 N_S}{2g} \frac{r_R}{r_R} \left(i_{Sa}\cos(\theta) + i_{Sb}\sin(\theta)\right)\hat{\mathbf{r}}$$

so that the radial dependence of the stator $\vec{\mathbf{B}}_S$ field increases from r_R/r_S to only $\kappa r_R/r_R$ (rather than $r_R/r_R = 1$) in going from the inside surface of the stator to the surface of the rotor. The above example is not the only source of leakage,[3] but all such effects can be modeled for the purposes here by a single parameter κ.

In summary, the coupling factor κ is included in the expression for $\vec{\mathbf{B}}_R$ on the *stator side* of the air gap to account for $\vec{\mathbf{B}}_R$ decreasing at a rate slightly less than $1/r$ (due to leakage) going across the air gap to the stator side. Similarly, κ is included in the expression for $\vec{\mathbf{B}}_S$ on the *rotor side* of the air gap to account for leakage effect going across the air gap.

It may seem rather inconsistent with the development of the mathematical model of the machine to now add in this leakage effect. That is, up to this point, ideal magnetic materials have been assumed, the air gap length has been assumed to be small, and the cross sections of the windings/slots have been assumed to be negligible. However, it will be seen shortly that this leakage factor will be essential to obtain a realistic model.

---

[2] As iron is a good magnetic material, $\vec{\mathbf{B}}_R$ is perpendicular at both the surface of the rotor iron and the stator iron.

[3] For example, a similar analysis can be done to account for the leakage through S_4 and S_6.

www.EngineeringEBooksPdf.com

6.3 Flux Linkages in AC Machines

Expressions for the flux linkages in both the rotor and stator windings are now computed.

6.3.1 Flux Linkages in the Stator Phases

The computation of the total flux linkage in the sinusoidally wound stator phase a is now considered. The flux in stator phase a is due to the magnetic fields produced by both the stator currents i_{Sa} and i_{Sb}, and the rotor currents i_{Ra} and i_{Rb}. That is,

$$\lambda_{Sa}(i_{Ra}, i_{Rb}, i_{Sa}, i_{Sb}, \theta_R) \triangleq \int_{\substack{\text{All loops of} \\ \text{stator phase } a}} (\vec{\mathbf{B}}_S + \vec{\mathbf{B}}_R) \cdot d\vec{\mathbf{S}}.$$

This computation is carried out in two parts by separately considering the flux linkage due to the stator currents and then the flux linkage due to the rotor currents. That is,

$$\lambda_{Sa}(0, 0, i_{Sa}, i_{Sb}, \theta_R) \triangleq \int_{\substack{\text{All loops of} \\ \text{stator phase } a}} \vec{\mathbf{B}}_S \cdot d\vec{\mathbf{S}}$$

and

$$\lambda_{Sa}(i_{Ra}, i_{Rb}, 0, 0, \theta_R) \triangleq \int_{\substack{\text{All loops of} \\ \text{stator phase } a}} \vec{\mathbf{B}}_R \cdot d\vec{\mathbf{S}}$$

so that

$$\lambda_{Sa}(i_{Ra}, i_{Rb}, i_{Sa}, i_{Sb}, \theta_R) = \lambda_{Sa}(0, 0, i_{Sa}, i_{Sb}, \theta_R) + \lambda_{Sa}(i_{Ra}, i_{Rb}, 0, 0, \theta_R).$$

Stator Flux Linkage Produced by the Stator Currents

Consider a single turn (loop) of stator phase a at the angular position θ with $0 \leq \theta \leq \pi$, that is, one side of the loop is at θ and the other side is at $\theta - \pi$. Choose the flux surface S for this single turn to lie just inside the air gap next to the stator surface as shown in Figure 6.5.

www.EngineeringEBooksPdf.com

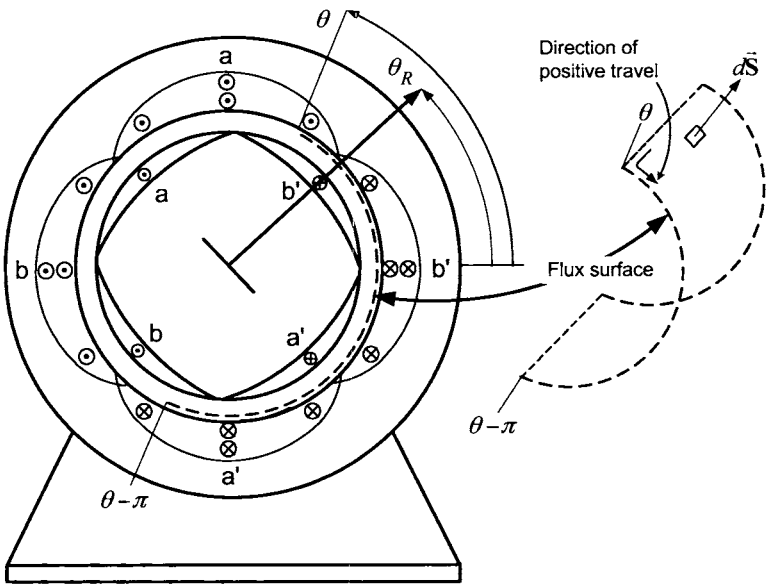


FIGURE 6.5. Surface to compute the flux in a single turn of stator phase a produced by $\vec{\mathbf{B}}_S$.

To compute the flux through the surface, the surface element vector $d\vec{\mathbf{S}} = r_S d\theta' dz\hat{\mathbf{r}}$ is chosen. The flux $\phi_{Sa}(i_{Sa}, i_{Sb}, \theta)$ in each turn of stator phase a at the angular position θ of the stator is then given by

$$
\begin{aligned}
&\phi_{Sa}(i_{Sa}, i_{Sb}, \theta) \\
&\quad \triangleq \int_{\theta'=\theta-\pi}^{\theta'=\theta} \int_{z=0}^{z=\ell_1} \frac{\mu_0 r_R N_S}{2g} \frac{1}{r_S} \Big(i_{Sa}\cos(\theta') + i_{Sb}\sin(\theta') \Big) \hat{\mathbf{r}} \cdot (r_S d\theta' dz\hat{\mathbf{r}}) \\
&\quad = \frac{\mu_0 r_R \ell_1 N_S}{2g} \int_{\theta'=\theta-\pi}^{\theta'=\theta} \Big(i_{Sa}\cos(\theta') + i_{Sb}\sin(\theta') \Big)\, d\theta' \\
&\quad = \frac{\mu_0 r_R \ell_1 N_S}{2g} \Big(i_{Sa}\sin(\theta') - i_{Sb}\cos(\theta') \Big) \Big|_{\theta'=\theta-\pi}^{\theta'=\theta} \\
&\quad = \frac{\mu_0 r_R \ell_1 N_S}{2g} \Big(i_{Sa} \Big(\sin(\theta) - \sin(\theta-\pi) \Big) - i_{Sb} \Big(\cos(\theta) - \cos(\theta-\pi) \Big) \Big) \\
&\quad = \frac{\mu_0 r_R \ell_1 N_S}{g} \Big(i_{Sa}\sin(\theta) - i_{Sb}\cos(\theta) \Big) . \qquad (6.8)
\end{aligned}
$$

Remark Note that by taking the flux surface normal to be $d\vec{\mathbf{S}} = r_S d\theta' dz\hat{\mathbf{r}}$, the positive direction of travel around the turns of stator phase a at the angular position θ is out of the page on side a and into the page on side a'; that is, it is the same direction as positive current flow in stator phase a. If $-d\phi_{Sa}/dt > 0$, then this emf will push current in the same direction

www.EngineeringEBooksPdf.com

as that chosen for the direction of positive current.

Between the angular positions θ and $\theta + d\theta$ of stator phase a there are $(N_S/2)\sin(\theta)d\theta$ turns each having the flux (6.8) in them. The flux *linkage* in the turns of phase a between θ and $\theta + d\theta$ is then

$$\begin{aligned} d\lambda_{Sa} &\triangleq \phi_{Sa}(i_{Sa}, i_{Sb}, \theta)(N_S/2)\sin(\theta)d\theta \\ &= \frac{\mu_0 r_R \ell_1 N_S}{g}\left(i_{Sa}\sin(\theta) - i_{Sb}\cos(\theta)\right)\frac{N_S}{2}\sin(\theta)d\theta. \end{aligned} \tag{6.9}$$

To obtain the flux linkage in all the turns of stator phase a, simply integrate (6.9) as θ varies from 0 to π, that is,

$$\begin{aligned} \lambda_{Sa}(0,0,i_{Sa},i_{Sb},\theta_R) &= \int_{\substack{\text{All loops of}\\ \text{stator phase } a}} \vec{\mathbf{B}}_S \cdot d\vec{\mathbf{S}} \\ &= \int_{\theta=0}^{\theta=\pi} \frac{\mu_0 r_R \ell_1 N_S}{g}\left(i_{Sa}\sin(\theta) - i_{Sb}\cos(\theta)\right)\frac{N_S}{2}\sin(\theta)d\theta \\ &= \frac{\mu_0 r_R \ell_1 N_S^2}{2g}\int_{\theta=0}^{\theta=\pi}\left(i_{Sa}\sin^2(\theta) - i_{Sb}\cos(\theta)\sin(\theta)\right)d\theta \\ &= \frac{\mu_0 r_R \ell_1 N_S^2}{2g} i_{Sa}\frac{\pi}{2} \\ &= L_S i_{Sa} \end{aligned} \tag{6.10}$$

where

$$L_S \triangleq \frac{\mu_0 r_R \ell_1 \pi N_S^2}{4g} = \frac{\mu_0 \ell_1 \ell_2 \pi}{8g} N_S^2.$$

Note that for this two-phase machine, the magnetic field produced by the current i_{Sb} in phase b does not produce any net flux linkage in phase a. Similarly,

$$\begin{aligned} \lambda_{Sb}(0,0,i_{Sa},i_{Sb},\theta_R) &= \int_{\substack{\text{All loops of}\\ \text{stator phase } b}} \vec{\mathbf{B}}_S \cdot d\vec{\mathbf{S}} \\ &= \frac{\mu_0 r_R \ell_1 \pi N_S^2}{4g} i_{Sb} \\ &= L_S i_{Sb}. \end{aligned} \tag{6.11}$$

www.EngineeringEBooksPdf.com

Stator Flux Linkage Produced by the Rotor Currents

The flux linkage in stator phase a due to magnetic field produced by the rotor currents is now computed from

$$\lambda_{Sa}(i_{Ra}, i_{Rb}, 0, 0, \theta_R) \triangleq \int_{\substack{\text{All loops of} \\ \text{stator phase } a}} \vec{\mathbf{B}}_R \cdot d\vec{\mathbf{S}}.$$

The flux surface of Figure 6.5 is also used for this computation. With $d\vec{\mathbf{S}} = r_S d\theta' dz \hat{\mathbf{r}}$ as the surface element vector, the flux $\phi_{Sa}(i_{Ra}, i_{Rb}, \theta - \theta_R)$ in each turn of stator phase a at the angular position θ of the stator due to the magnetic field $\vec{\mathbf{B}}_R$ is

$$\begin{aligned}
\phi_{Sa}(i_{Ra}, i_{Rb}, \theta - \theta_R) &\triangleq \int_{\theta'=\theta-\pi}^{\theta'=\theta} \int_{z=0}^{z=\ell_1} \kappa \frac{\mu_0 N_R r_R}{2g} \frac{1}{r_S} \Big(i_{Ra} \cos(\theta' - \theta_R) \\
&\qquad + i_{Rb} \sin(\theta' - \theta_R) \hat{\mathbf{r}} \cdot (r_S d\theta' dz \hat{\mathbf{r}}) \Big) \\
&= \kappa \frac{\mu_0 r_R \ell_1 N_R}{2g} \int_{\theta'=\theta-\pi}^{\theta'=\theta} \Big(i_{Ra} \cos(\theta' - \theta_R) + i_{Rb} \sin(\theta' - \theta_R) \Big) d\theta' \\
&= \kappa \frac{\mu_0 r_R \ell_1 N_R}{g} \Big(i_{Ra} \sin(\theta - \theta_R) - i_{Rb} \cos(\theta - \theta_R) \Big). \qquad (6.12)
\end{aligned}$$

Note that the factor κ has been included as the rotor's magnetic field is being evaluated on the stator side of the air gap. Between the angular positions θ and $\theta + d\theta$, there are $(N_S/2)\sin(\theta)d\theta$ turns, each having the flux (6.12) in them due to $\vec{\mathbf{B}}_R$. The flux linkage $d\lambda_{Sa}$ in the turns of stator phase a between θ and $\theta + d\theta$ produced by the rotor's magnetic field is then

$$\begin{aligned}
d\lambda_{Sa} &= \phi_{Sa}(i_{Ra}, i_{Rb}, \theta - \theta_R) \frac{N_S}{2} \sin(\theta) d\theta \qquad (6.13) \\
&= \kappa \frac{\mu_0 r_R \ell_1 N_R N_S}{2g} \Big(i_{Ra} \sin(\theta - \theta_R) - i_{Rb} \cos(\theta - \theta_R) \Big) \sin(\theta) d\theta.
\end{aligned}$$

To obtain the total flux linkage due to the rotor's magnetic field in all the

www.EngineeringEBooksPdf.com

turns of stator phase a, integrate (6.13) as θ varies from 0 to π to obtain

$$\begin{aligned}
\lambda_{Sa}(i_{Ra}, i_{Rb}, 0, 0, \theta_R) &= \int_{\substack{\text{All loops of} \\ \text{stator phase } a}} \vec{\mathbf{B}}_R \cdot d\vec{\mathbf{S}} \\
&= \int_{\theta=0}^{\theta=\pi} \kappa \frac{\mu_0 r_R \ell_1 N_S N_R}{2g} \left(i_{Ra} \sin(\theta - \theta_R) - i_{Rb} \cos(\theta - \theta_R)\right) \sin(\theta) d\theta \\
&= \kappa \frac{\mu_0 r_R \ell_1 N_S N_R}{2g} \left(i_{Ra} \int_{\theta=0}^{\theta=\pi} \Big(\sin(\theta)\cos(\theta_R) - \cos(\theta)\sin(\theta_R)\Big) \sin(\theta) d\theta \right. \\
&\quad \left. - i_{Rb} \int_{\theta=0}^{\theta=\pi} \left(\cos(\theta)\cos(\theta_R) + \sin(\theta)\sin(\theta_R)\right) \sin(\theta) d\theta \right) \\
&= \kappa \frac{\mu_0 r_R \ell_1 N_S N_R}{2g} \int_{\theta=0}^{\theta=\pi} \Big(i_{Ra} \sin^2(\theta)\cos(\theta_R) - i_{Rb} \sin^2(\theta) \sin\theta_R) \Big) d\theta \\
&= M\Big(i_{Ra}\cos(\theta_R) - i_{Rb}\sin(\theta_R)\Big) \qquad (6.14)
\end{aligned}$$

where

$$M \triangleq \kappa \frac{\mu_0 \pi r_R \ell_1 N_S N_R}{4g} = \kappa \frac{\mu_0 \pi \ell_1 \ell_2 N_S N_R}{8g}.$$

Similarly,

$$\begin{aligned}
\lambda_{Sb}(i_{Ra}, i_{Rb}, , 0, 0, \theta_R) &= \int_{\substack{\text{All loops of} \\ \text{stator phase } b}} \vec{\mathbf{B}}_R \cdot d\vec{\mathbf{S}} \\
&= M\Big(i_{Ra}\sin(\theta_R) + i_{Rb}\cos(\theta_R)\Big). \qquad (6.15)
\end{aligned}$$

Total Flux Linkage in the Stator Phases

Combining (6.10), (6.11), (6.14), and (6.15), the total flux linkage in each of the stator phases is then

$$\begin{aligned}
\lambda_{Sa}(i_{Ra}, i_{Rb}, i_{Sa}, i_{Sb}, \theta_R) &= \int_{\substack{\text{All loops of} \\ \text{stator phase } a}} (\vec{\mathbf{B}}_S + \vec{\mathbf{B}}_R) \cdot d\vec{\mathbf{S}} \\
&= L_S i_{Sa} + M\Big(i_{Ra}\cos(\theta_R) - i_{Rb}\sin(\theta_R)\Big) \qquad (6.16) \\
\lambda_{Sb}(i_{Ra}, i_{Rb}, i_{Sa}, i_{Sb}, \theta_R) &= \int_{\substack{\text{All loops of} \\ \text{stator phase } b}} (\vec{\mathbf{B}}_S + \vec{\mathbf{B}}_R) \cdot d\vec{\mathbf{S}} \\
&= L_S i_{Sb} + M\Big(i_{Ra}\sin(\theta_R) + i_{Rb}\cos(\theta_R)\Big).
\end{aligned}$$

www.EngineeringEBooksPdf.com

6.3.2 *Flux Linkages in the Rotor Phases*

The flux linkages in the two sinusoidally wound phases of the rotor are computed according to

$$\lambda_{Ra}(i_{Ra}, i_{Rb}, i_{Sa}, i_{Sb}, \theta_R) \triangleq \int_{\substack{\text{All loops of} \\ \text{rotor phase } a}} (\vec{\mathbf{B}}_S + \vec{\mathbf{B}}_R) \cdot d\vec{\mathbf{S}}$$

$$\lambda_{Rb}(i_{Ra}, i_{Rb}, i_{Sa}, i_{Sb}, \theta_R) \triangleq \int_{\substack{\text{All loops of} \\ \text{rotor phase } b}} (\vec{\mathbf{B}}_S + \vec{\mathbf{B}}_R) \cdot d\vec{\mathbf{S}}.$$

Starting with rotor phase a and, as in the case of the stator flux linkages, this computation is done in two parts as

$$\lambda_{Ra}(0, 0, i_{Sa}, i_{Sb}, \theta_R) \triangleq \int_{\substack{\text{All loops of} \\ \text{rotor phase } a}} \vec{\mathbf{B}}_S \cdot d\vec{\mathbf{S}}$$

and

$$\lambda_{Ra}(i_{Ra}, i_{Rb}, 0, 0, \theta_R) \triangleq \int_{\substack{\text{All loops of} \\ \text{rotor phase } a}} \vec{\mathbf{B}}_R \cdot d\vec{\mathbf{S}}.$$

The total flux linkage is then

$$\lambda_{Ra}(i_{Ra}, i_{Rb}, i_{Sa}, i_{Sb}, \theta_R) = \lambda_{Ra}(0, 0, i_{Sa}, i_{Sb}, \theta_R) + \lambda_{Ra}(i_{Ra}, i_{Rb}, 0, 0, \theta_R).$$

Rotor Flux Linkage Produced by the Stator Currents

The flux in the rotor phase due to the magnetic field established by the stator currents is given by

$$\lambda_{Ra}(0, 0, i_{Sa}, i_{Sb}, \theta_R) \triangleq \int_{\substack{\text{All loops of} \\ \text{rotor phase } a}} \vec{\mathbf{B}}_S \cdot d\vec{\mathbf{S}}.$$

To do this computation, consider a single turn (loop) of the rotor phase at the angular position θ with $0 \leq \theta - \theta_R \leq \pi$ so that one side of the rotor loop is at θ and the other side is at $\theta - \pi$. The flux surface S is chosen to lie just inside the air gap as shown in Figure 6.6.

www.EngineeringEBooksPdf.com

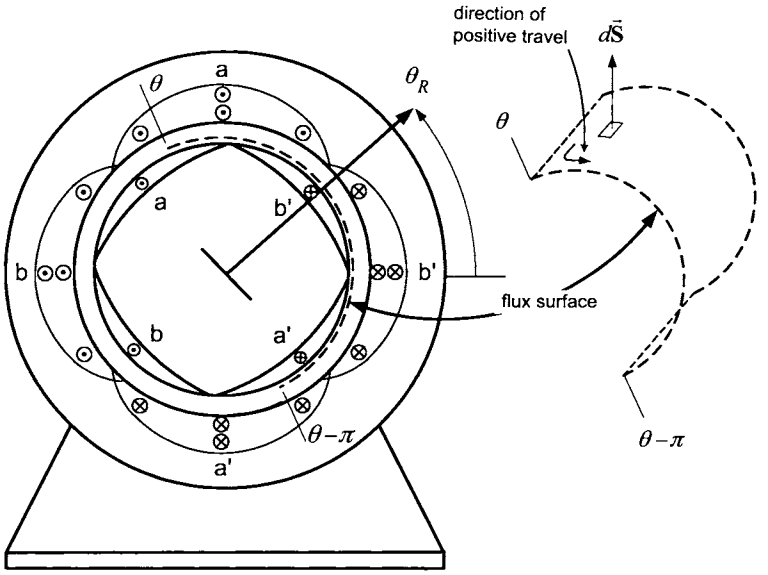


FIGURE 6.6. Surface to compute the flux in a single turn of rotor phase a produced by $\vec{\mathbf{B}}_S$.

On the flux surface, the surface element vector is chosen as $d\vec{\mathbf{S}} = r_R d\theta' dz\hat{\mathbf{r}}$. The flux $\phi_{Ra}(i_{Sa}, i_{Sb}, \theta)$ in each turn of rotor phase a at the angular position θ of the rotor is given by

$$\begin{aligned}
&\phi_{Ra}(i_{Sa}, i_{Sb}, \theta) \\
&= \int_{\theta'=\theta-\pi}^{\theta'=\theta} \int_{z=0}^{z=\ell_1} \kappa \frac{\mu_0 r_R N_S}{2g} \frac{1}{r_R} \Big(i_{Sa}\cos(\theta') + i_{Sb}\sin(\theta') \Big) \hat{\mathbf{r}} \cdot (r_R d\theta' dz\hat{\mathbf{r}}) \\
&= \kappa \frac{\mu_0 r_R \ell_1 N_S}{2g} \int_{\theta'=\theta-\pi}^{\theta'=\theta} \Big(i_{Sa}\cos(\theta') + i_{Sb}\sin(\theta') \Big) d\theta' \\
&= \kappa \frac{\mu_0 r_R \ell_1 N_S}{2g} \Big(i_{Sa}\sin(\theta') - i_{Sb}\cos(\theta') \Big) \Big|_{\theta'=\theta-\pi}^{\theta'=\theta} \\
&= \kappa \frac{\mu_0 r_R \ell_1 N_S}{2g} \Big(i_{Sa}(\sin(\theta) - \sin(\theta-\pi)) - i_{Sb}(\cos(\theta) - \cos(\theta-\pi) \Big) \\
&= \kappa \frac{\mu_0 r_R \ell_1 N_S}{g} \Big(i_{Sa}\sin(\theta) - i_{Sb}\cos(\theta) \Big) . \qquad (6.17)
\end{aligned}$$

Remarks Note that the factor κ has been included as the rotor's magnetic field is being evaluated on the stator side of the air gap. Also, note that by taking the flux surface normal to be $d\vec{\mathbf{S}} = r_R d\theta' dz\hat{\mathbf{r}}$, the positive direction of travel around the turns of rotor phase a at the angular position θ is out of the page on side a and into the page on side a'; that is, it coincides with the direction chosen for positive current flow in rotor phase a.

www.EngineeringEBooksPdf.com

Between the angular positions θ and $\theta + d\theta$, there are $(N_R/2)\sin(\theta - \theta_R)d\theta$ turns each having the flux (6.17) in them. The flux linkage $d\lambda_{Ra}$ in the turns of phase a between θ and $\theta + d\theta$ produced by the stator's magnetic field is then

$$\begin{aligned} d\lambda_{Ra} &\triangleq \phi_{Ra}(i_{Sa}, i_{Sb}, \theta)\frac{N_R}{2}\sin(\theta - \theta_R)d\theta \\ &= \kappa\frac{\mu_0 r_R \ell_1 N_S N_R}{2g}\left(i_{Sa}\sin(\theta) - i_{Sb}\cos(\theta)\right)\sin(\theta - \theta_R)d\theta. \end{aligned} \tag{6.18}$$

To obtain the flux linkage in all the turns of rotor phase a, (6.18) is integrated between $\theta = \theta_R$ and $\theta = \theta_R + \pi$, that is,

$$\begin{aligned} \lambda_{Ra}(0, 0, i_{Sa}, i_{Sb}, \theta_R) &= \int_{\substack{\text{All loops of} \\ \text{rotor phase } a}} \vec{\mathbf{B}}_S \cdot d\vec{\mathbf{S}} \\ &= \int_{\theta=\theta_R}^{\theta=\theta_R+\pi} \kappa\frac{\mu_0 r_R \ell_1 N_S N_R}{2g}\left(i_{Sa}\sin(\theta) - i_{Sb}\cos(\theta)\right)\sin(\theta - \theta_R)d\theta \\ &= \kappa\frac{\mu_0 r_R \ell_1 N_S N_R}{2g}\int_{\theta=\theta_R}^{\theta=\theta_R+\pi}\Big(i_{Sa}\sin(\theta - \theta_R + \theta_R)\sin(\theta - \theta_R) \\ &\quad - i_{Sb}\cos(\theta - \theta_R + \theta_R)\sin(\theta - \theta_R)\Big)\,d\theta \\ &= \kappa\frac{\mu_0 r_R \ell_1 N_S N_R}{2g} \\ &\quad \times \int_{\theta=\theta_R}^{\theta=\theta_R+\pi}\Big(i_{Sa}\sin^2(\theta - \theta_R)\cos(\theta_R) + i_{Sa}\cos(\theta - \theta_R)\sin(\theta_R)\sin(\theta - \theta_R) \\ &\quad - i_{Sb}\cos(\theta - \theta_R)\cos(\theta_R)\sin(\theta - \theta_R) + i_{Sb}\sin^2(\theta - \theta_R)\sin(\theta_R)\Big)d\theta \\ &= \kappa\frac{\mu_0 r_R \ell_1 N_S N_R}{2g}\left(i_{Sa}\frac{\pi}{2}\cos(\theta_R) + \frac{\pi}{2}i_{Sb}\sin(\theta_R)\right) \\ &= M\Big(i_{Sa}\cos(\theta_R) + i_{Sb}\sin(\theta_R)\Big) \end{aligned} \tag{6.19}$$

where, as before,

$$M \triangleq \kappa\frac{\mu_0 \pi r_R \ell_1 N_S N_R}{4g} = \kappa\frac{\mu_0 \pi \ell_1 \ell_2 N_S N_R}{8g}.$$

Similarly,

$$\begin{aligned} \lambda_{Rb}(0, 0, i_{Sa}, i_{Sb}, \theta_R) &\triangleq \int_{\substack{\text{All loops of} \\ \text{rotor phase } b}} \vec{\mathbf{B}}_S \cdot d\vec{\mathbf{S}} \\ &= M\Big(-i_{Sa}\sin(\theta_R) + i_{Sb}\cos(\theta_R)\Big). \end{aligned} \tag{6.20}$$

www.EngineeringEBooksPdf.com

Rotor Flux Linkage Produced by the Rotor Currents

The flux linkage in the rotor phases due to the magnetic field produced by the rotor currents is now computed. Consider a single turn (loop) of rotor phase a at the angular position θ with $0 \leq \theta - \theta_R \leq \pi$ and the same flux surface drawn in Figure 6.6.

To compute flux through the surface, $d\vec{\mathbf{S}} = r_R d\theta' dz\hat{\mathbf{r}}$ is chosen as the surface element vector. The flux $\phi_{Ra}(i_{Ra}, i_{Rb}, \theta - \theta_R)$ in each turn of rotor phase a at the angular position θ of the rotor is given by

$$\begin{aligned}
&\phi_{Ra}(i_{Ra}, i_{Rb}, \theta - \theta_R) \\
&\quad \triangleq \int_{\theta'=\theta-\pi}^{\theta'=\theta} \int_{z=0}^{z=\ell_1} \frac{\mu_0 r_R N_R}{2g} \frac{1}{r_R} \Big(i_{Ra} \cos(\theta' - \theta_R) + i_{Rb} \sin(\theta' - \theta_R) \Big) \hat{\mathbf{r}} \\
&\qquad \cdot \Big(r_R d\theta' dz \hat{\mathbf{r}} \Big) \\
&\quad = \frac{\mu_0 r_R \ell_1 N_R}{2g} \int_{\theta'=\theta-\pi}^{\theta'=\theta} \Big(i_{Ra} \cos(\theta' - \theta_R) + i_{Rb} \sin(\theta' - \theta_R) \Big) d\theta' \\
&\quad = \frac{\mu_0 r_R \ell_1 N_R}{2g} \Big(i_{Ra} \sin(\theta' - \theta_R) - i_{Rb} \cos(\theta' - \theta_R) \Big|_{\theta'=\theta-\pi}^{\theta'=\theta} \\
&\quad = \frac{\mu_0 r_R \ell_1 N_R}{2g} \left(i_{Ra} (\sin(\theta - \theta_R) - \sin(\theta - \theta_R - \pi)) \right. \\
&\qquad \left. - i_{Rb} (\cos(\theta - \theta_R) - \cos(\theta - \theta_R - \pi)) \right) \\
&\quad = \frac{\mu_0 r_R \ell_1 N_R}{g} \Big(i_{Ra} \sin(\theta - \theta_R) - i_{Rb} \cos(\theta - \theta_R) \Big).
\end{aligned} \tag{6.21}$$

Remark Again, by taking the flux surface normal to be $d\vec{\mathbf{S}} = r_R d\theta' dz\hat{\mathbf{r}}$, the positive direction of travel around the turns of rotor phase a at the angular position θ is out of the page on side a of the rotor phase and into the page on side a' of the rotor phase coinciding with the direction chosen for positive current flow in rotor phase a.

Between the angular positions θ and $\theta + d\theta$, there are $(N_R/2)\sin(\theta - \theta_R)d\theta$ turns, each having the flux (6.21) in them. The flux linkage in the turns of phase a between θ and $\theta + d\theta$ is then

$$\begin{aligned}
d\lambda_{Ra} &\triangleq \phi_{Ra}(i_{Ra}, i_{Rb}, \theta - \theta_R) \frac{N_R}{2} \sin(\theta - \theta_R) d\theta \\
&= \frac{\mu_0 r_R \ell_1 N_R^2}{2g} (i_{Ra} \sin(\theta - \theta_R) - i_{Rb} \cos(\theta - \theta_R)) \sin(\theta - \theta_R) d\theta.
\end{aligned} \tag{6.22}$$

To obtain the flux linkage in all the turns of stator phase a, (6.22) is inte-

www.EngineeringEBooksPdf.com

grated from $\theta = \theta_R$ to $\theta = \theta_R + \pi$, that is,

$$\lambda_{Ra}(i_{Ra}, i_{Rb}, 0, 0, \theta_R) = \int_{\substack{\text{All loops of} \\ \text{rotor phase } a}} \vec{\mathbf{B}}_R \cdot d\vec{\mathbf{S}}$$

$$= \int_{\theta=\theta_R}^{\theta=\theta_R+\pi} \frac{\mu_0 r_R \ell_1 N_R^2}{2g} \left(i_{Ra} \sin(\theta - \theta_R) - i_{Rb} \cos(\theta - \theta_R)\right) \sin(\theta - \theta_R) d\theta$$

$$= \frac{\mu_0 r_R \ell_1 N_R^2}{2g} \int_{\theta=\theta_R}^{\theta=\theta_R+\pi} \left(i_{Ra} \sin^2(\theta - \theta_R) - i_{Rb} \cos(\theta - \theta_R) \sin(\theta - \theta_R)\right) d\theta$$

$$= \frac{\mu_0 r_R \ell_1 N_R^2}{2g} i_{Ra} \frac{\pi}{2}$$

$$= L_R i_{Ra} \tag{6.23}$$

where

$$L_R \triangleq \frac{\mu_0 r_R \ell_1 \pi N_R^2}{4g} = \frac{\mu_0 \ell_1 \ell_2 \pi}{8g} N_R^2.$$

Note that for this particular two-phase system, the magnetic field produced by the current i_{Rb} in rotor phase b does not produce any net flux linkage in rotor phase a. Similarly,

$$\lambda_{Rb}(i_{Ra}, i_{Rb}, 0, 0, \theta_R) = \int_{\substack{\text{All loops of} \\ \text{rotor phase } b}} \vec{\mathbf{B}}_R \cdot d\vec{\mathbf{S}} = L_R i_{Rb}. \tag{6.24}$$

Total Flux Linkage in the Rotor Phases

Combining the expressions (6.19), (6.20), (6.23), and (6.24), the total flux in the sinusoidally wound rotor phases due to both the stator and rotor magnetic fields is then

$$\begin{aligned} \lambda_{Ra}(i_{Ra}, i_{Rb}, i_{Sa}, i_{Sb}, \theta_R) &= \int_{\substack{\text{All loops of} \\ \text{rotor phase } a}} (\vec{\mathbf{B}}_S + \vec{\mathbf{B}}_R) \cdot d\vec{\mathbf{S}} \\ &= L_R i_{Ra} + M\Big(i_{Sa} \cos(\theta_R) + i_{Sb} \sin(\theta_R)\Big) \end{aligned} \tag{6.25}$$

$$\begin{aligned} \lambda_{Rb}(i_{Ra}, i_{Rb}, i_{Sa}, i_{Sb}, \theta_R) &= \int_{\substack{\text{All loops of} \\ \text{rotor phase } b}} (\vec{\mathbf{B}}_S + \vec{\mathbf{B}}_R) \cdot d\vec{\mathbf{S}} \\ &= L_R i_{Rb} + M\Big(-i_{Sa} \sin(\theta_R) + i_{Sb} \cos(\theta_R)\Big). \end{aligned}$$

www.EngineeringEBooksPdf.com

6.4 Torque Production in AC Machines

The stator currents establish a radial magnetic field in the air gap. The torque produced by this magnetic field on the currents in the sinusoidally wound rotor phases is now computed. In order to carry out this computation, a more convenient way of representing the stator and rotor magnetic fields is now used following Refs. [1] and [2].

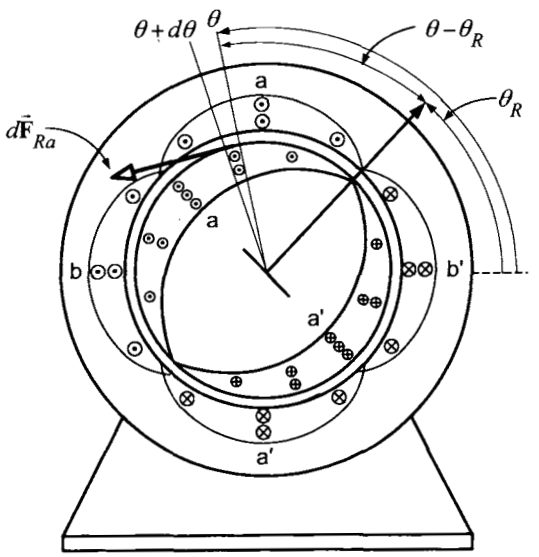


FIGURE 6.7. Computation of the torque on the current i_{Ra} in rotor phase a produced by $\vec{\mathbf{B}}_S$. Rotor phase b not shown for clarity.

The magnetic field at an arbitrary angle θ in the air-gap due to the stator currents is

$$\vec{\mathbf{B}}_S(i_{Sa},\, i_{Sb},\, \theta) = \frac{\mu_0 r_R N_S}{2gr_R}\Big(i_{Sa}(t)\cos(\theta) + \; i_{Sb}(t)\sin(\theta)\Big)\hat{\mathbf{r}}.$$

Let $i_S(t) \triangleq \sqrt{i_{Sa}^2(t) + i_{Sb}^2(t)}$, $\xi(t) \triangleq \tan^{-1}\left(i_{Sb}(t)/i_{Sa}(t)\right)$ so that $\vec{\mathbf{B}}_S$ may be rewritten as

$$\begin{aligned}\vec{\mathbf{B}}_S &= \frac{\mu_0 \ell_2 N_S}{4gr} i_S(t)\Big(\cos(\xi)\cos(\theta) + \; \sin(\xi)\sin(\theta)\Big)\hat{\mathbf{r}} \\ &= \frac{\mu_0 \ell_2 N_S}{4gr} i_S(t)\cos(\theta-\xi)\hat{\mathbf{r}}. \qquad (6.26)\end{aligned}$$

Similarly, the magnetic field at the angle θ in the air gap due to the rotor currents is

$$\vec{\mathbf{B}}_R(i_{Ra},\, i_{Rb},\, \theta{-}\theta_R) = \frac{\mu_0 \ell_2 N_R}{4gr}\Big(i_{Ra}(t)\cos(\theta-\theta_R) + \; i_{Rb}(t)\sin(\theta-\theta_R)\Big)\hat{\mathbf{r}}.$$

www.EngineeringEBooksPdf.com

Let $i_R(t) \triangleq \sqrt{i_{Ra}^2(t) + i_{Rb}^2(t)}$, $\zeta(t) \triangleq \tan^{-1}(i_{Rb}(t)/i_{Ra}(t))$ so that $\vec{\mathbf{B}}_R$ may be rewritten as

$$\begin{aligned}\vec{\mathbf{B}}_R &= \frac{\mu_0 \ell_2 N_R}{4gr} i_R(t) \Big(\cos(\zeta)\cos(\theta - \theta_R) + \sin(\zeta)\sin(\theta - \theta_R)\Big)\hat{\mathbf{r}} \\ &= \frac{\mu_0 \ell_2 N_R}{4gr} i_R(t)\cos(\theta - \theta_R - \zeta)\hat{\mathbf{r}}. \qquad (6.27)\end{aligned}$$

The torque $\vec{\tau}_R$ produced by a two-phase machine is now computed. This is done by computing the force on the rotor current loops due to the magnetic field established by the stator currents. Referring to Figure 6.7, the differential magnetic force $d\vec{\mathbf{F}}_{Ra}$ produced on the loops of rotor phase a between θ and $\theta + d\theta$ by $\vec{\mathbf{B}}_S = B_S\hat{\mathbf{r}} = \kappa\dfrac{\mu_0 r_R N_S}{2gr_R} i_S(t)\cos(\theta - \xi)\hat{\mathbf{r}}$ is[4]

$$d\vec{\mathbf{F}}_{Ra} = \begin{cases} i_{Ra}(t)\dfrac{N_R}{2}\sin(\theta - \theta_R)d\theta(+\ell_1\hat{\mathbf{z}}) \times B_S\hat{\mathbf{r}}, & \theta_R \le \theta \le \theta_R + \pi \\ \\ i_{Ra}(t)\dfrac{N_R}{2}|\sin(\theta - \theta_R)|d\theta(-\ell_1\hat{\mathbf{z}}) \times B_S\hat{\mathbf{r}}, & \theta_R + \pi \le \theta \le \theta_R + 2\pi \end{cases}$$

where $(N_R/2)|\sin(\theta - \theta_R)|d\theta$ is the number of axial sides of rotor phase a between θ and $\theta + d\theta$, each carrying the current $i_{Ra}(t)$. As $\sin(\theta - \theta_R) \le 0$ for $\theta_R + \pi \le \theta \le \theta_R + 2\pi$, it follows that $|\sin(\theta - \theta_R)| = -\sin(\theta - \theta_R)$ for $\theta_R + \pi \le \theta \le \theta_R + 2\pi$ so that $d\vec{\mathbf{F}}_{Ra}$ can be written more compactly as

$$\begin{aligned} d\vec{\mathbf{F}}_{Ra} &= i_{Ra}(t)\frac{N_R}{2}\sin(\theta - \theta_R)d\theta\ell_1\hat{\mathbf{z}} \times B_S\hat{\mathbf{r}} \\ &= i_{Ra}(t)\frac{N_R}{2}\sin(\theta - \theta_R)\ell_1 B_S d\theta\hat{\boldsymbol{\theta}} \\ &= i_{Ra}(t)\frac{N_R}{2}\sin(\theta - \theta_R)\ell_1\kappa\frac{\mu_0 r_R N_S}{2gr_R} i_S(t)\cos(\theta - \xi)d\theta\hat{\boldsymbol{\theta}} \\ &= \kappa\frac{\mu_0 \ell_1 N_S N_R}{4g} i_{Ra}(t) i_S(t)\sin(\theta - \theta_R)\cos(\theta - \xi)d\theta\hat{\boldsymbol{\theta}} \end{aligned}$$

for $\theta_R \le \theta \le \theta_R + 2\pi$. The differential torque $d\vec{\tau}_{Ra}$ is then given by

$$\begin{aligned} d\vec{\tau}_{Ra} &= (\ell_2/2)\hat{\mathbf{r}} \times d\vec{\mathbf{F}}_{Ra} \\ &= (\ell_2/2)\frac{\mu_0 \ell_1 N_S N_R}{4g} i_{Ra}(t) i_S(t)\sin(\theta - \theta_R)\cos(\theta - \xi)d\theta\hat{\mathbf{r}} \times \hat{\boldsymbol{\theta}} \\ &= \kappa\frac{\mu_0 \ell_1 \ell_2 N_S N_R}{8g} i_{Ra}(t) i_S(t)\sin(\theta - \theta_R)\cos(\theta - \xi)d\theta\hat{\mathbf{z}} \\ &= \frac{M}{\pi} i_{Ra}(t) i_S(t)\sin(\theta - \theta_R)\cos(\theta - \xi)d\theta\hat{\mathbf{z}} \\ &= \frac{M}{\pi} i_{Ra}(t) i_S(t)\frac{1}{2}\left(\sin(2\theta - \theta_R - \xi) + \sin(\xi - \theta_R)\right)d\theta\hat{\mathbf{z}} \end{aligned}$$

[4] Note that the leakage factor κ has been included as this is the stator magnetic field on the rotor side of the air gap.

www.EngineeringEBooksPdf.com

where $M = \kappa\mu_0\pi\ell_1\ell_2 N_S N_R/(8g)$ is the coefficient of mutual inductance as previously defined. The torque on rotor phase a is then

$$\begin{aligned}
\vec{\tau}_{Ra} &= \int_0^{2\pi} d\vec{\tau}_{Ra} \\
&= \int_0^{2\pi} \frac{M}{2\pi} i_{Ra}(t) i_S(t) \Big(\sin(2\theta - \theta_R - \xi) + \sin(\xi - \theta_R)\Big)\, d\theta \hat{\mathbf{z}} \\
&= M i_{Ra}(t) i_S(t) \sin(\xi - \theta_R)\hat{\mathbf{z}} \\
&= M i_{Ra}(t) i_S(t) \Big(\sin(\xi)\cos(\theta_R) - \sin(\theta_R)\cos(\xi)\Big)\hat{\mathbf{z}} \\
&= M i_{Ra}(t) \Big(i_{Sb}(t)\cos(\theta_R) - i_{Sa}(t)\sin(\theta_R)\Big)\hat{\mathbf{z}}.
\end{aligned}$$

Similarly,

$$d\vec{\mathbf{F}}_{Rb} = \begin{cases} i_{Rb}(t)\dfrac{N_R}{2}\sin(\theta - \pi/2 - \theta_R)d\theta(\ell_1\hat{\mathbf{z}}) \times B_S\hat{\mathbf{r}}, & \theta_R + \dfrac{\pi}{2} \le \theta \le \theta_R + \dfrac{3\pi}{2} \\ i_{Rb}(t)\dfrac{N_R}{2}\left|\sin(\theta - \pi/2 - \theta_R)\right| d\theta(-\ell_1\hat{\mathbf{z}}) \times B_S\hat{\mathbf{r}}, & \theta_R - \dfrac{\pi}{2} \le \theta \le \theta_R + \dfrac{\pi}{2} \end{cases}$$

Again, as $\sin(\theta - \pi/2 - \theta_R) < 0$ for $\theta_R - \pi/2 \le \theta \le \theta_R + \pi/2$, $\left|\sin(\theta - \frac{\pi}{2} - \theta_R)\right|$ $= -\sin(\theta - \pi/2 - \theta_R)$ for $\theta_R - \pi/2 \le \theta \le \theta_R + \pi/2 < 0$, the expression for the force $d\vec{\mathbf{F}}_{Rb}$ may be written more compactly for $\theta_R \le \theta \le \theta_R + 2\pi$ as

$$\begin{aligned}
d\vec{\mathbf{F}}_{Rb} &= i_{Rb}(t)\frac{N_R}{2}\sin(\theta - \pi/2 - \theta_R)d\theta(\ell_1\hat{\mathbf{z}}) \times (B_S\hat{\mathbf{r}}) \\
&= i_{Rb}(t)\frac{N_R}{2}\sin(\theta - \pi/2 - \theta_R)\ell_1 B_S d\theta\hat{\boldsymbol{\theta}} \\
&= -i_{Rb}(t)\frac{N_R}{2}\cos(\theta - \theta_R)\ell_1\kappa\frac{\mu_0 r_R N_S}{2gr_R} i_S(t)\cos(\theta - \xi)d\theta\hat{\boldsymbol{\theta}} \\
&= -\kappa\frac{\mu_0\ell_1 N_S N_R}{4g} i_{Rb}(t) i_S(t)\cos(\theta - \theta_R)\cos(\theta - \xi)d\theta\hat{\boldsymbol{\theta}}.
\end{aligned}$$

The differential torque $d\vec{\tau}_{Rb}$ is then given by

$$\begin{aligned}
d\vec{\tau}_{Rb} &= (\ell_2/2)\hat{\mathbf{r}} \times d\vec{\mathbf{F}}_{Rb} \\
&= -(\ell_2/2)\kappa\frac{\mu_0\ell_1 N_S N_R}{4g} i_{Rb}(t) i_S(t)\cos(\theta - \theta_R)\cos(\theta - \xi)d\theta\hat{\mathbf{r}} \times \hat{\boldsymbol{\theta}} \\
&= -\kappa\frac{\mu_0\ell_1\ell_2 N_S N_R}{8g} i_{Rb}(t) i_S(t)\cos(\theta - \theta_R)\cos(\theta - \xi)d\theta\hat{\mathbf{z}} \\
&= -\frac{M}{\pi} i_{Rb}(t) i_S(t)\cos(\theta - \theta_R)\cos(\theta - \xi)d\theta\hat{\mathbf{z}} \\
&= -\frac{M}{\pi} i_{Rb}(t) i_S(t)\frac{1}{2}\left(\cos(2\theta - \theta_R - \xi) + \cos(\xi - \theta_R)\right)d\theta\hat{\mathbf{z}}.
\end{aligned}$$

www.EngineeringEBooksPdf.com

The torque on rotor phase b is then

$$\begin{aligned}
\vec{\tau}_{Rb} &= \int_0^{2\pi} d\vec{\tau}_{Rb} \\
&= -\int_0^{2\pi} \frac{M}{2\pi} i_{Rb}(t) i_S(t) \left(\cos(2\theta - \theta_R - \xi) + \cos(\xi - \theta_R)\right) d\theta \hat{\mathbf{z}} \\
&= -M i_{Rb}(t) i_S(t) \cos(\xi - \theta_R) \hat{\mathbf{z}} \\
&= -M i_{Rb}(t) i_S(t) \Big(\cos(\xi)\cos(\theta_R) + \sin(\xi)\sin(\theta_R)\Big) \hat{\mathbf{z}} \\
&= -M i_{Rb}(t) \Big(i_{Sa}(t)\cos(\theta_R) + i_{Sb}(t)\sin(\theta_R)\Big) \hat{\mathbf{z}}.
\end{aligned}$$

The total torque on the rotor is then

$$\begin{aligned}
\tau_R &= \tau_{Ra} + \tau_{Rb} \\
&= M\Big(-i_{Ra}(t) i_{Sa}(t)\sin(\theta_R) + i_{Ra}(t) i_{Sb}(t)\cos(\theta_R) \\
&\qquad - i_{Rb}(t) i_{Sa}(t)\cos(\theta_R) - i_{Rb}(t) i_{Sb}(t)\sin(\theta_R)\Big). \qquad (6.28)
\end{aligned}$$

Remark The assumption that the stator and rotor turns have negligible cross-sectional area was still in effect in the above derivation of the torque on the rotor. However, in a real motor, the windings are only approximately sinusoidally wound and this is accomplished by putting the turns in *slots* as explained in Chapter 4. In this case, it is pointed out by G. R. Slemon (see Section 3.4 of Ref. [32]) as well as by W. Leonhard (see p. 173 of Ref. [2]) that the magnetic forces are actually acting on the slides of rotor slots where the magnetic field enters the rotor iron. In the idealized model here, the slots do not exist and the forces/torques can be computed as described above. Further, the resulting mathematical model of the machine derived under these idealized assumptions will be shown to be a very good dynamic model of the machine (see Chapter 8).

6.5 Mathematical Model of a Sinusoidally Wound Induction Machine

The hard work of computing the expressions for the flux linkages in the phases of an AC machine as well as for the rotor torque has been completed. The analysis is now specialized to an induction motor which is illustrated in Figure 6.8. This figure is the same as Figure 6.1 except now it is explicitly assumed that the two ends of each rotor phase are shorted together, that is, there are no voltage sources for the rotor phases. With the rotor phases

www.EngineeringEBooksPdf.com

shorted, the expressions for the phase flux linkages and rotor torque are used to derive the nonlinear differential equation model of a two-phase sinusoidally wound induction motor.

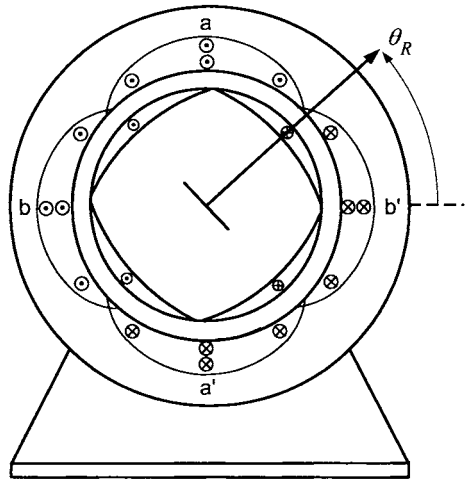


FIGURE 6.8. A symmetric sinusoidally wound two-phase induction machine.

By (6.16) and (6.25), the flux linkages in the stator and rotor phases in terms of the currents and rotor position are

$$\begin{aligned}
\lambda_{Sa}(i_{Ra}, i_{Rb}, i_{Sa}, i_{Sb}, \theta_R) &= L_S i_{Sa} + M\Big(+i_{Ra}\cos(\theta_R) - i_{Rb}\sin(\theta_R)\Big) \\
\lambda_{Sb}(i_{Ra}, i_{Rb}, i_{Sa}, i_{Sb}, \theta_R) &= L_S i_{Sb} + M\Big(+i_{Ra}\sin(\theta_R) + i_{Rb}\cos(\theta_R)\Big) \\
\lambda_{Ra}(i_{Ra}, i_{Rb}, i_{Sa}, i_{Sb}, \theta_R) &= L_R i_{Ra} + M\Big(+i_{Sa}\cos(\theta_R) + i_{Sb}\sin(\theta_R)\Big) \\
\lambda_{Rb}(i_{Ra}, i_{Rb}, i_{Sa}, i_{Sb}, \theta_R) &= L_R i_{Rb} + M\Big(-i_{Sa}\sin(\theta_R) + i_{Sb}\cos(\theta_R)\Big).
\end{aligned} \tag{6.29}$$

By Faraday's and Ohm's laws, the equations describing the electrical dynamics of this system are

$$\begin{aligned}
-\frac{d\lambda_{Sa}}{dt} - R_S i_{Sa} + u_{Sa} &= 0 \\
-\frac{d\lambda_{Sb}}{dt} - R_S i_{Sb} + u_{Sb} &= 0 \\
-\frac{d\lambda_{Ra}}{dt} - R_R i_{Ra} &= 0 \\
-\frac{d\lambda_{Rb}}{dt} - R_R i_{Rb} &= 0.
\end{aligned}$$

www.EngineeringEBooksPdf.com

Explicitly, this is

$$\begin{aligned}
L_S\frac{d}{dt}i_{Sa} + M\frac{d}{dt}\Big(+i_{Ra}\cos(\theta_R) - i_{Rb}\sin(\theta_R)\Big) + R_S i_{Sa} &= u_{Sa}\\
L_S\frac{d}{dt}i_{Sb} + M\frac{d}{dt}\Big(+i_{Ra}\sin(\theta_R) + i_{Rb}\cos(\theta_R)\Big) + R_S i_{Sb} &= u_{Sb}\\
L_R\frac{d}{dt}i_{Ra} + M\frac{d}{dt}\Big(+i_{Sa}\cos(\theta_R) + i_{Sb}\sin(\theta_R)\Big) + R_R i_{Ra} &= 0\\
L_R\frac{d}{dt}i_{Rb} + M\frac{d}{dt}\Big(-i_{Sa}\sin(\theta_R) + i_{Sb}\cos(\theta_R)\Big) + R_R i_{Rb} &= 0.
\end{aligned} \tag{6.30}$$

By equation (6.28), the torque produced by this machine is given by

$$\begin{aligned}
\tau_R = M\Big(&-i_{Ra}(t)i_{Sa}(t)\sin(\theta_R) + i_{Ra}(t)i_{Sb}(t)\cos(\theta_R)\\
&- i_{Rb}(t)i_{Sa}(t)\cos(\theta_R) - i_{Rb}(t)i_{Sb}(t)\sin(\theta_R)\Big)
\end{aligned} \tag{6.31}$$

so that, with τ_L the load torque, the mechanical equations are simply

$$\begin{aligned}
J\frac{d\omega_R}{dt} &= \tau_R - \tau_L\\
\frac{d\theta_R}{dt} &= \omega_R.
\end{aligned} \tag{6.32}$$

Equations (6.30), (6.31), and (6.32) are the set of nonlinear differential equations characterizing a two-phase sinusoidally wound induction motor.

A *space vector* representation of the equations of the induction motor is given in problem 5 (see also problem 6).

6.6 Total Leakage Factor

The leakage factor is defined as

$$\sigma = 1 - \frac{M^2}{L_S L_R}$$

Substituting the expressions

$$\begin{aligned}
L_R &= \frac{\mu_0 \ell_1 \ell_2 \pi}{8g} N_R^2\\
L_S &= \frac{\mu_0 \ell_1 \ell_2 \pi}{8g} N_S^2\\
M &= \frac{\kappa \mu_0 \pi \ell_1 \ell_2 N_S N_R}{8g}
\end{aligned}$$

www.EngineeringEBooksPdf.com

results in

$$\sigma = 1 - \kappa^2.$$

Note that if $\kappa = 1$, corresponding to no spreading of the magnetic field as one goes across the air gap, then $\sigma = 0$. However, in a practical motor $\sigma > 0$. As pointed out in Ref. [2], σ typically varies from 0.05 for low leakage machines up 0.20.

6.7 The Squirrel Cage Rotor

The above mathematical model of the induction motor was derived assuming sinusoidally wound rotor phases. However, the most commonly used induction motor has a squirrel cage rotor which is illustrated in Figure 6.9.

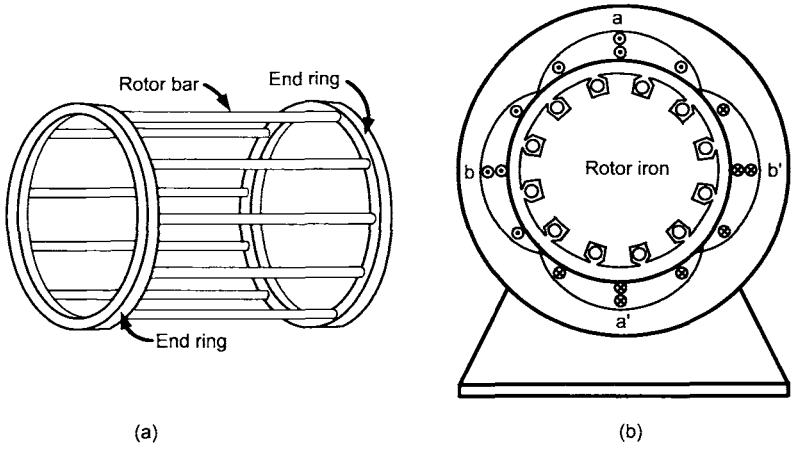


FIGURE 6.9. (a) Squirrel cage rotor for an induction motor. (b) Cross-sectional view of the squirrel cage embedded in the rotor iron core.

It is standard practice to use the same mathematical model given in (6.30) and (6.31) for the induction motor with a squirrel cage rotor. In this case, the rotor currents i_{Ra} and i_{Rb} as well as the parameters R_R and L_R must be given a different interpretation. There is actually a different current in each rotor bar of the squirrel cage and these together make up a current distribution around the periphery of the rotor (see the discussion of the squirrel cage rotor in Chapter 5). The parameters R_R and L_R in the model can be interpreted as those values that best fit the mathematical model (6.30), (6.31), and (6.32) to that of an actual squirrel cage motor. For example, in Stephan et al. [42] and Wang et al. [59] the parameters of the model (6.30), (6.31), and (6.32) were identified based on data from a squirrel cage motor using a least-squares algorithm. The simulated response

www.EngineeringEBooksPdf.com

of the system $(\omega_R, i_{Sa}, i_{Sb})$ based on the model (6.30), (6.31), and (6.32) using these parameters values was shown to be quite close to the actual measured response of the squirrel cage motor [42][59]. The parameter values determined in this manner are then interpreted as those values that best fit the model (6.30), (6.31), and (6.32) to the squirrel cage motor data in the least-squares sense. See Chapter 8 where it is shown how to use the least-squares method to identify the induction motor parameters.

6.8 Induction Machine With Multiple Pole Pairs

It is left to problem 10 at the end of this chapter to show that if the machine has n_p pole pairs, then the expressions for the flux linkages are modified to

$$\begin{aligned}
\lambda_{Sa} &= L_S i_{Sa} + M\Big(i_{Ra}\cos(n_p\theta_R) - i_{Rb}\sin(n_p\theta_R)\Big) \\
\lambda_{Sb} &= L_S i_{Sb} + M\Big(i_{Ra}\sin(n_p\theta_R) + i_{Rb}\cos(n_p\theta_R)\Big) \\
\lambda_{Ra} &= L_R i_{Ra} + M\Big(+i_{Sa}\cos(n_p\theta_R) + i_{Sb}\sin(n_p\theta_R)\Big) \\
\lambda_{Rb} &= L_R i_{Rb} + M\Big(-i_{Sa}\sin(n_p\theta_R) + i_{Sb}\cos(n_p\theta_R)\Big)
\end{aligned} \tag{6.33}$$

where

$$L_S \triangleq \frac{\mu_0\pi\ell_1\ell_2 N_S^2}{8g},\ L_R \triangleq \frac{\mu_0\pi\ell_1\ell_2 N_R^2}{8g},\ M \triangleq \frac{\kappa\mu_0\pi\ell_1\ell_2 N_S N_R}{8g}.$$

Here N_S, and N_R are the number of stator and rotor windings, respectively, *per pole pair*. The total number of windings in a stator phase is $n_p N_S$ and $n_p N_R$ is the total number of windings in a rotor phase. The dynamic equations are

$$\begin{aligned}
u_{Sa} &= R_S i_{Sa} + \frac{d}{dt}\Big(L_S i_{Sa} + M\Big(i_{Ra}\cos(n_p\theta_R) - i_{Rb}\sin(n_p\theta_R)\Big)\Big) \\
u_{Sb} &= R_S i_{Sb} + \frac{d}{dt}\Big(L_S i_{Sb} + M\Big(i_{Ra}\sin(n_p\theta_R) + i_{Rb}\cos(n_p\theta_R)\Big)\Big) \\
0 &= R_R i_{Ra} + \frac{d}{dt}\Big(L_R i_{Ra} + M\Big(+i_{Sa}\cos(n_p\theta_R) + i_{Sb}\sin(n_p\theta_R)\Big)\Big) \\
0 &= R_R i_{Rb} + \frac{d}{dt}\Big(L_R i_{Rb} + M\Big(-i_{Sa}\sin(n_p\theta_R) + i_{Sb}\cos(n_p\theta_R)\Big)\Big) \\
J\frac{d\omega_R}{dt} &= n_p M\Big(i_{Sb}(i_{Ra}\cos(n_p\theta_R) - i_{Rb}\sin(n_p\theta_R) \\
&\qquad - i_{Sa}(i_{Ra}\sin(n_p\theta_R) + i_{Rb}\cos(n_p\theta_R))\Big) - \tau_L \\
\frac{d\theta_R}{dt} &= \omega_R.
\end{aligned} \tag{6.34}$$

www.EngineeringEBooksPdf.com

Consider two induction machines which are identical in all aspects except that one has only a single pole pair (i.e., $n_p = 1$) while the other has $n_p > 1$. That is, each has the same geometrical construction (ℓ_1, ℓ_2, and g are the same), the same number N_S of stator windings *per pole pair*, the same number of rotor windings N_R *per pole pair*, and the same current ratings. Then the torque output of the machine with n_p pole pairs will have a torque output that is a factor n_p *greater* than the single pole pair machine. This is clear from considering the coefficient $n_p M$ in the torque expression (6.34). However, the n_p pole pair machine has n_p more turns/windings in each phase than a single pole pair machine.

6.9 Mathematical Model of a Wound Rotor Synchronous Machine

The mathematical model of a wound rotor synchronous machine is straightforwardly derived from the expressions for the phase flux linkages and rotor torque derived above. Figure 6.10 shows the synchronous motor to be modeled which differs from Figure 6.1 in that there is only one rotor phase and this rotor phase is explicitly assumed to have a voltage source.

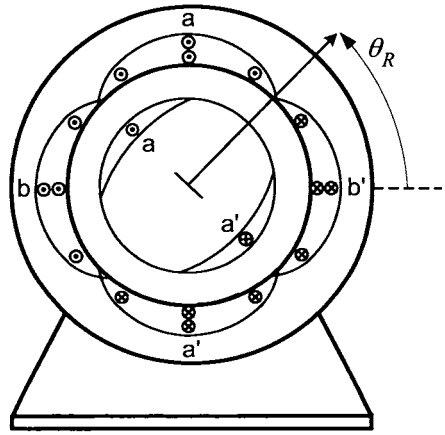


FIGURE 6.10. A symmetric two-phase synchronous machine with a sinusoidally wound rotor phase. The two stator phases have voltage sources u_{Sa} and u_{Sb}, respectively, and the single rotor phase has voltage source u_F.

The terminology for the synchronous machine changes to the rotor phase being referred to as the *field winding*; its current is called the *field current* i_F, the flux linkage in its windings is called the *field flux (linkage)* λ_F, and the voltage source u_F applied to the phase winding is called the *field* source.

www.EngineeringEBooksPdf.com

Recall that the term "field" refers to the fact that during normal operation, i_F and λ_F are constant, which is the case for a synchronous machine. The flux linkages in this machine are found by simply setting $i_{Ra} = i_F$ and $i_{Rb} \equiv 0$ in (6.16) and (6.25) to obtain

$$\begin{aligned} \lambda_{Sa}(i_F, i_{Sa}, i_{Sb}, \theta_R) &= L_S i_{Sa} + M i_F \cos(\theta_R) \\ \lambda_{Sb}(i_f, i_{Sa}, i_{Sb}, \theta_R) &= L_S i_{Sb} + M i_F \sin(\theta_R) \\ \lambda_F(i_F, i_{Sa}, i_{Sb}, \theta_R) &= L_F i_F + M\left(i_{Sa}\cos(\theta_R) + i_{Sb}\sin(\theta_R)\right) \end{aligned} \tag{6.35}$$

where $L_F \triangleq L_R$. With R_S the resistance of each stator phase and R_F the resistance of the field winding (rotor phase), Faraday's and Ohm's laws give

$$\begin{aligned} -\frac{d\lambda_{Sa}}{dt} - R_S i_{Sa} + u_{Sa} &= 0 \\ -\frac{d\lambda_{Sb}}{dt} - R_S i_{Sb} + u_{Sb} &= 0 \\ -\frac{d\lambda_F}{dt} - R_F i_F + u_F &= 0 \end{aligned} \tag{6.36}$$

where u_F is the voltage source for the field (rotor) winding.

Setting $i_{Ra} = i_F$ and $i_{Rb} \equiv 0$ in equation (6.28), the torque produced by this machine is

$$\tau_R = M i_F\Big(-i_{Sa}\sin(\theta_R) + i_{Sb}\cos(\theta_R)\Big). \tag{6.37}$$

Combining these equations together, a nonlinear differential equation model of a two-phase synchronous motor with a sinusoidally wound rotor is

$$\begin{aligned} -\frac{d}{dt}\Big(L_S i_{Sa} + M i_F\cos(\theta_R)\Big) - R_S i_{Sa} + u_{Sa} &= 0 \\ -\frac{d}{dt}\Big(L_S i_{Sb} + M i_F\sin(\theta_R)\Big) - R_S i_{Sb} + u_{Sb} &= 0 \\ -\frac{d}{dt}\Big(L_F i_F + M\left(i_{Sa}\cos(\theta_R) + i_{Sb}\sin(\theta_R)\right)\Big) - R_F i_F + u_F &= 0 \\ M i_F\Big(-i_{Sa}\sin(\theta_R) + i_{Sb}\cos(\theta_R)\Big) - \tau_L &= J\frac{d\omega_R}{dt} \\ \frac{d\theta_R}{dt} &= \omega_R \end{aligned} \tag{6.38}$$

where τ_L is the load torque.

In a synchronous machine, the rotor current is often chosen be constant, that is,

$$i_F = I_F.$$

This can be done by choosing the voltage u_F in the field winding according to

$$u_F = K_P(I_F - i_F) + K_I\int_0^t (I_F - i_F)dt.$$

www.EngineeringEBooksPdf.com

The mathematical model of a two-phase synchronous motor with a sinusoidally wound rotor with constant field current then reduces to

$$\begin{aligned} L_S\frac{di_{Sa}}{dt} &= -R_S i_{Sa} + MI_F \sin(\theta_R)\omega_R + u_{Sa} \\ L_S\frac{di_{Sb}}{dt} &= -R_S i_{Sb} - MI_F \cos(\theta_R)\omega_R + u_{Sb} \\ J\frac{d\omega_R}{dt} &= MI_F\Big(-i_{Sa}\sin(\theta_R) + i_{Sb}\cos(\theta_R)\Big) - \tau_L \\ \frac{d\theta_R}{dt} &= \omega_R. \end{aligned} \tag{6.39}$$

6.10 Mathematical Model of a PM Synchronous Machine

Consider the case of a two-phase permanent magnet machine with the permanent magnet of the rotor designed to produce a sinusoidally distributed radially directed magnetic field in the air gap (see Figure 6.11). That is,

$$\vec{\mathbf{B}}_R(r, \theta - \theta_R) = B_m \frac{r_R}{r}\cos(\theta - \theta_R)\hat{\mathbf{r}}.$$

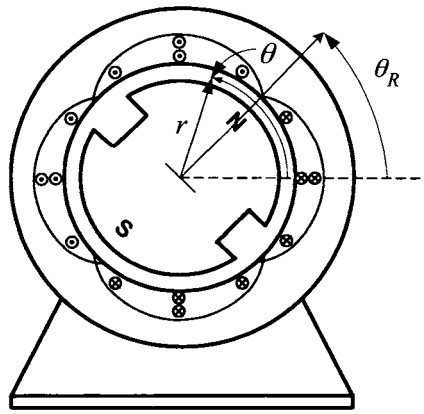


FIGURE 6.11. Two-phase permanent magnet synchronous machine.

This is essentially the same situation as a wound rotor synchronous machine with a constant field current. It is straightforward to show that its model

www.EngineeringEBooksPdf.com

has the same form as (6.39) given by (see problem 11)

$$\begin{aligned} L_S\frac{di_{Sa}}{dt} &= -R_S i_{Sa} + K_m \sin(\theta_R)\omega_R + u_{Sa} \\ L_S\frac{di_{Sb}}{dt} &= -R_S i_{Sb} - K_m \cos(\theta_R)\omega_R + u_{Sb} \\ J\frac{d\omega_R}{dt} &= K_m\Big(-i_{Sa}\sin(\theta_R) + i_{Sb}\cos(\theta_R)\Big) - \tau_L \\ \frac{d\theta_R}{dt} &= \omega_R. \end{aligned} \tag{6.40}$$

6.11 The Stator and Rotor Magnetic Fields of an Induction Machine Rotate Synchronously*

Recall the radial magnetic field in the air gap produced by the stator currents is given by

$$\vec{\mathbf{B}}_S(i_{Sa}, i_{Sb}, r, \theta) = \frac{\mu_0 r_R N_S}{2g}\frac{1}{r}\left(i_{Sa}\cos(\theta) + i_{Sb}\sin(\theta)\right)\hat{\mathbf{r}} \tag{6.41}$$

while the radial magnetic field in the air gap produced by the rotor currents is given by

$$\vec{\mathbf{B}}_R(i_{Ra}, i_{Rb}, r, \theta - \theta_R) = \frac{\mu_0 r_R N_R}{2g}\frac{1}{r}\left(i_{Ra}\cos(\theta - \theta_R) + i_{Rb}\sin(\theta - \theta_R)\right)\hat{\mathbf{r}}. \tag{6.42}$$

Applying the voltages

$$\begin{aligned} u_{Sa} &= U_S\cos(\omega_S t) \\ u_{Sb} &= U_S\sin(\omega_S t) \end{aligned}$$

to the stator phases, a steady-state solution for the currents and rotor position has the form

$$\begin{aligned} i_{Sa} &= I_S\cos(\omega_S t + \phi_S) \\ i_{Sb} &= I_S\sin(\omega_S t + \phi_S) \\ i_{Ra} &= I_R\cos((\omega_S - \omega_R)t + \phi_R) \\ i_{Rb} &= I_R\sin((\omega_S - \omega_R)t + \phi_R) \\ \theta_R &= \omega_R t. \end{aligned} \tag{6.43}$$

Problem 9 outlines the derivation of these expressions to show that the phase angles ϕ_S, ϕ_R are functions of the stator frequency ω_S and the normalized slip $(\omega_S - \omega_R)/\omega_S$; thus they are *constant* in steady state. Substituting the expressions (6.43) into (6.41), the steady-state stator magnetic

www.EngineeringEBooksPdf.com

field may be written as

$$\vec{\mathbf{B}}_S(r,\theta,t) = \frac{\mu_0 r_R N_S I_S}{2g}\frac{1}{r}\cos(\theta-(\omega_S t+\phi_S))\hat{\mathbf{r}}$$

where at the angular position $\theta_{B_S}(t) \triangleq \omega_S t + \phi_S$, $\vec{\mathbf{B}}_S$ has its maximum magnitude. Denote $\theta_{B_S}(t)$ as the *magnetic axis* of $\vec{\mathbf{B}}_S$ and note that the magnetic field distribution of $\vec{\mathbf{B}}_S$ is fixed relative to $\theta_{B_S}(t)$; that is, $\vec{\mathbf{B}}_S$ is a "magnet" that rotates at the angular rate ω_S. Similarly, substituting the expressions (6.43) into (6.42), the steady-state rotor magnetic field may then be written as

$$\begin{aligned}
\vec{\mathbf{B}}_R(r,\theta,t) &= \frac{\mu_0 r_R N_R I_R}{2g}\frac{1}{r}\Big(\cos((\omega_S-\omega_R)t+\phi_R)\cos(\theta-\omega_R t) \\
&\quad +\sin((\omega_S-\omega_R)t+\phi_R)\sin(\theta-\omega_R t)\Big)\hat{\mathbf{r}} \\
&= \frac{\mu_0 r_R N_R I_R}{2g}\frac{1}{r}\cos\Big(\theta-\omega_R t-\Big((\omega_S-\omega_R)t+\phi_R\Big)\Big)\hat{\mathbf{r}} \\
&= \frac{\mu_0 r_R N_R I_R}{2g}\frac{1}{r}\cos\Big(\theta-(\omega_S t+\phi_R)\Big)\hat{\mathbf{r}}
\end{aligned}$$

where at the angular position $\theta_{B_R}(t) \triangleq \omega_S t + \phi_R$, $\vec{\mathbf{B}}_R$ has its maximum magnitude. Denote $\theta_{B_R}(t)$ as the *magnetic axis* of $\vec{\mathbf{B}}_R$ and note that the magnetic field distribution of $\vec{\mathbf{B}}_R$ is fixed relative to $\theta_{B_R}(t)$; that is, $\vec{\mathbf{B}}_R$ is also a "magnet" that rotates at the angular rate ω_S.

Both of these magnetic fields rotate at the angular rate ω_S, with the angle between the two "magnets" being $\theta_{B_S}(t)-\theta_{B_R}(t) = \phi_S - \phi_R$ which is *constant*; that is, the two *magnetic fields* rotate synchronously together! Another way to view this is to note that by (6.43) the currents i_{Sa} and i_{Sb} have angular frequency ω_S and produce a magnetic field rotating at the angular speed ω_S. Also, equations (6.43) show that rotor currents i_{Ra} and i_{Rb} have angular frequency $\omega_S-\omega_R$ and thus produce a magnetic field that rotates at angular speed $\omega_S-\omega_R$ *with respect to the rotor*. However, the rotor is moving at angular speed ω_R so that the magnetic field produced by the rotor currents is rotating at angular speed $\omega_S-\omega_R+\omega_R = \omega_S$ *with respect to the stator*. Again, both fields rotate at the same angular speed ω_S.

Substituting the expressions (6.43) for the steady-state currents and $\theta_R(t)$ into equation (6.31) results in the steady-state torque being given by (see problem 9)

$$\begin{aligned}
\tau_R &= M I_S I_R \sin(\phi_S-\phi_R) \\
&= g 2\pi(\ell_1/2)\ell_2 \frac{1}{2\mu_0}\left(\kappa\frac{\mu_0 N_S I_S}{2g}\right)\left(\frac{\mu_0 N_R I_R}{2g}\right)\sin(\phi_S-\phi_R) \\
&= V_{\text{airgap}}\frac{1}{2\mu_0}B_{S\max}B_{R\max}\sin(\phi_S-\phi_R)
\end{aligned}$$

www.EngineeringEBooksPdf.com

where $M = \kappa\mu_0\pi\ell_1\ell_2 N_S N_R/(8g)$, $B_{S\max} \triangleq \kappa\mu_0 N_S I_S/(2g)$ and $B_{R\max} \triangleq \mu_0 N_R I_R/(2g)$ are the maximum values of the stator and rotor magnetic fields, respectively, at the surface of the rotor, and $V_{\text{airgap}} = g2\pi(\ell_1/2)\ell_2$ is the approximate volume of the air gap for g small. This expression shows that the torque is proportional to the maximum strength of the stator and rotor magnetic fields and to the sine of the angle between them.[5]

Finally, the steady-state condition requires $Jd\omega_R/dt \equiv 0$ so that the load-torque τ_L must be such that it satisfies

$$MI_S I_R \sin(\phi_S - \phi_R) - \tau_L = 0.$$

6.12 Torque, Energy, and Co-energy*

In this section it is shown how the torque of an AC machine can be derived from conservation of energy. The analysis is carried out for the two-phase induction motor while the synchronous machine is considered in problem 19.

6.12.1 Magnetic Field Energy

The equations describing the electrical dynamics of a two-phase induction motor are

$$\begin{aligned} -\frac{d\lambda_{Sa}}{dt} - R_S i_{Sa} + u_{Sa} &= 0 \\ -\frac{d\lambda_{Sb}}{dt} - R_S i_{Sb} + u_{Sb} &= 0 \\ -\frac{d\lambda_{Ra}}{dt} - R_R i_{Ra} + u_{Ra} &= 0 \\ -\frac{d\lambda_{Rb}}{dt} - R_R i_{Rb} + u_{Rb} &= 0 \end{aligned} \tag{6.44}$$

where the flux linkages are given by ($n_p = 1$)

$$\begin{aligned} \lambda_{Sa}(i_{Ra}, i_{Rb}, i_{Sa}, i_{Sb}, \theta_R) &= L_S i_{Sa} + M(+i_{Ra}\cos(\theta_R) - i_{Rb}\sin(\theta_R)) \\ \lambda_{Sb}(i_{Ra}, i_{Rb}, i_{Sa}, i_{Sb}, \theta_R) &= L_S i_{Sb} + M(+i_{Ra}\sin(\theta_R) + i_{Rb}\cos(\theta_R)) \\ \lambda_{Ra}(i_{Ra}, i_{Rb}, i_{Sa}, i_{Sb}, \theta_R) &= L_R i_{Ra} + M(+i_{Sa}\cos(\theta_R) + i_{Sb}\sin(\theta_R)) \\ \lambda_{Rb}(i_{Ra}, i_{Rb}, i_{Sa}, i_{Sb}, \theta_R) &= L_R i_{Rb} + M(-i_{Sa}\sin(\theta_R) + i_{Sb}\cos(\theta_R)). \end{aligned} \tag{6.45}$$

[5] There is an expression identical in form for the torque of a synchronous motor!

www.EngineeringEBooksPdf.com

Of course, normally $u_{Ra} \equiv 0, u_{Rb} \equiv 0$. Substituting these expressions for the flux linkages into the system equations (6.44), it follows that

$$\begin{aligned}
L_S\frac{d}{dt}i_{Sa} + M\frac{d}{dt}\left(+i_{Ra}\cos(\theta_R) - i_{Rb}\sin(\theta_R)\right) + R_S i_{Sa} &= u_{Sa}\\
L_S\frac{d}{dt}i_{Sb} + M\frac{d}{dt}\left(+i_{Ra}\sin(\theta_R) + i_{Rb}\cos(\theta_R)\right) + R_S i_{Sb} &= u_{Sb}\\
L_R\frac{d}{dt}i_{Ra} + M\frac{d}{dt}\left(+i_{Sa}\cos(\theta_R) + i_{Sb}\sin(\theta_R)\right) + R_R i_{Ra} &= u_{Ra}\\
L_R\frac{d}{dt}i_{Rb} + M\frac{d}{dt}\left(-i_{Sa}\sin(\theta_R) + i_{Sb}\cos(\theta_R)\right) + R_R i_{Rb} &= u_{Rb}.
\end{aligned} \tag{6.46}$$

In order to calculate the energy stored in the magnetic field of the induction machine (that is, the magnetic field in the stator/rotor iron as well as in the air gap), the rotor is locked and voltage is applied to the phases. Using the system (6.44), the power delivered to each of the phases is given by

$$\begin{aligned}
i_{Sa}u_{Sa} &= R_S i_{Sa}^2 + i_{Sa}\frac{d\lambda_{Sa}}{dt}\\
i_{Sb}u_{Sb} &= R_S i_{Sb}^2 + i_{Sb}\frac{d\lambda_{Sb}}{dt}\\
i_{Ra}u_{Ra} &= R_R i_{Ra}^2 + i_{Ra}\frac{d\lambda_{Ra}}{dt}\\
i_{Rb}u_{Rb} &= R_R i_{Rb}^2 + i_{Rb}\frac{d\lambda_{Rb}}{dt}
\end{aligned} \tag{6.47}$$

Substituting the expressions (6.45) for the flux linkages into (6.47) and adding up the resulting four equations one obtains (see problem 17)

$$\begin{aligned}
i_{Sa}u_{Sa}+i_{Sb}u_{Sb} + i_{Ra}u_{Ra} + i_{Rb}u_{Rb} &= R_S(i_{Sa}^2 + i_{Sb}^2) + R_R(i_{Ra}^2 + i_{Rb}^2)\\
&+ \frac{d}{dt}\left(\frac{1}{2}L_S(i_{Sa}^2 + i_{Sb}^2) + \frac{1}{2}L_R(i_{Ra}^2 + i_{Rb}^2)\right)\\
&+ \frac{d}{dt}\left(Mi_{Sa}\left(+i_{Ra}\cos(\theta_R) - i_{Rb}\sin(\theta_R)\right)\right)\Big|_{\theta_R \text{ constant}}\\
&+ \frac{d}{dt}\left(Mi_{Sb}\left(+i_{Ra}\sin(\theta_R) + i_{Rb}\cos(\theta_R)\right)\right)\Big|_{\theta_R \text{ constant}}.
\end{aligned} \tag{6.48}$$

Defining the magnetic field energy W_{field} as

$$\begin{aligned}
W_{\text{field}}(i_{Sa}, i_{Sb}, i_{Ra}, i_{Rb}, \theta_R) \triangleq{}& \frac{1}{2}L_S(i_{Sa}^2 + i_{Sb}^2) + \frac{1}{2}L_R(i_{Ra}^2 + i_{Rb}^2)\\
&+ Mi_{Sa}\left(+i_{Ra}\cos(\theta_R) - i_{Rb}\sin(\theta_R)\right)\\
&+ Mi_{Sb}\left(+i_{Ra}\sin(\theta_R) + i_{Rb}\cos(\theta_R)\right)
\end{aligned} \tag{6.49}$$

www.EngineeringEBooksPdf.com

equation (6.48) may be rewritten as

$$i_{Sa}u_{Sa} + i_{Sb}u_{Sb} + i_{Ra}u_{Ra} + i_{Rb}u_{Rb} = R_S(i_{Sa}^2 + i_{Sb}^2) + R_R(i_{Ra}^2 + i_{Rb}^2) + \frac{d}{dt}W_{\text{field}}\Big|_{\theta_R \text{ constant}}$$

Here

$$\frac{d}{dt}W_{\text{field}} = \frac{\partial W_{\text{field}}}{\partial i_{Sa}}\frac{di_{Sa}}{dt} + \frac{\partial W_{\text{field}}}{\partial i_{Sb}}\frac{di_{Sb}}{dt} + \frac{\partial W_{\text{field}}}{\partial i_{Ra}}\frac{di_{Ra}}{dt} + \frac{\partial W_{\text{field}}}{\partial i_{Rb}}\frac{di_{Rb}}{dt} + \frac{\partial W_{\text{field}}}{\partial \theta_R}\frac{d\theta_R}{dt}$$

$$\frac{d}{dt}W_{\text{field}}\Big|_{\theta_R \text{ constant}} = \frac{\partial W_{\text{field}}}{\partial i_{Sa}}\frac{di_{Sa}}{dt} + \frac{\partial W_{\text{field}}}{\partial i_{Sb}}\frac{di_{Sb}}{dt} + \frac{\partial W_{\text{field}}}{\partial i_{Ra}}\frac{di_{Ra}}{dt} + \frac{\partial W_{\text{field}}}{\partial i_{Rb}}\frac{di_{Rb}}{dt}.$$

The quantity $W_{\text{field}}(i_{Sa}, i_{Sb}, i_{Ra}, i_{Rb}, \theta_R)$ is the energy stored in the magnetic field established in the stator/rotor iron[6] and in the air gap by the phase currents. (This was derived in the same way that one derives the expression $Li^2/2$ for the energy in a standard inductor.) Defining

$$W_{\text{ohmic loss}} = \int_0^t \left(R_S(i_{Sa}^2 + i_{Sb}^2) + R_R(i_{Ra}^2 + i_{Rb}^2)\right) dt$$

$$W_{\text{electrical}} = \int_0^t (i_{Sa}u_{Sa} + i_{Sb}u_{Sb} + i_{Ra}u_{Ra} + i_{Rb}u_{Rb})\, dt$$

it then follows that

$$W_{\text{electrical}} = W_{\text{field}} + W_{\text{ohmic loss}}.$$

This is simply an energy conservation equation. It says that, with the rotor locked, the energy supplied by the voltage sources u_{Sa}, u_{Sb}, u_{Ra}, and u_{Rb} goes into magnetic field energy W_{field} and into the heat energy $W_{\text{ohmic loss}}$ dissipated in the resistance of the windings.

The expression (6.49) for the field energy is valid whether or not the rotor is moving. This is because if the rotor is at the angle θ_R and the currents in the phases are i_{Sa}, i_{Sb}, i_{Ra}, and i_{Rb}, then the magnetic field at each point of the motor (i.e., in the stator/rotor iron and in the air

[6] Actually, as the iron is assumed to have infinite permeability ($\mu_r = \infty$), the stored energy is all in the air gap. This is simply because electromagnetic theory allows one to write the stored field energy as $W_{\text{field}} = (1/2)\int_{\substack{\text{rotor and}\\ \text{stator iron}}} (B^2/(\mu_0\mu_r))\, dV + (1/2)\int_{\text{air gap}} (B^2/\mu_0)\, dV = (1/2)\int_{\text{air gap}} (B^2/\mu_0)\, dV$ as $\mu_r = \infty$.

www.EngineeringEBooksPdf.com

gap) is the same whether or not the rotor is moving. In other words, the stored magnetic energy depends only on $(i_{Sa}, i_{Sb}, i_{Ra}, i_{Rb}, \theta_R)$ and not on ω_R. The derivation was carried out with the rotor locked so that it could be concluded that the applied power went only into the field energy and ohmic losses (i.e., not into mechanical power) in deriving the expression (6.49) for the magnetic field energy.

6.12.2 Computing Torque From the Field Energy

In order to derive an expression for the torque in terms of the stored energy, the rotor is unlocked and allowed to move under the torque produced by the magnetic forces. Multiplying the first equation of (6.46) by i_{Sa}, the second by i_{Sb}, the third by i_{Ra}, and the fourth by i_{Rb} and adding them together give $(\omega_R = d\theta_R/dt \neq 0)$

$$i_{Sa}u_{Sa} + i_{Sb}u_{Sb} + i_{Ra}u_{Ra} + i_{Rb}u_{Rb} = \frac{d}{dt}W_{\text{field}}\Big|_{\theta_R \text{ constant}} + 2\frac{\partial W_{\text{field}}}{\partial \theta_R}\frac{d\theta_R}{dt} + R_S(i_{Sa}^2 + i_{Sb}^2) + R_R(i_{Ra}^2 + i_{Rb}^2). \tag{6.50}$$

The reader is asked to verify this expression in problem 18. The term $2(\partial W_{\text{field}}/\partial\theta_R)d\theta_R/dt$ is an additional term describing power being absorbed from the sources when there is rotor movement. As

$$dW_{\text{field}}/dt = dW_{\text{field}}/dt|_{\theta_R \text{ constant}} + (\partial W_{\text{field}}/\partial\theta_R)(d\theta_R/dt),$$

equation (6.50) may be rewritten as

$$i_{Sa}u_{Sa} + i_{Sb}u_{Sb} + i_{Ra}u_{Ra} + i_{Rb}u_{Rb} = \frac{d}{dt}W_{\text{field}} + \frac{\partial W_{\text{field}}}{\partial \theta_R}\frac{d\theta_R}{dt} + R_S(i_{Sa}^2 + i_{Sb}^2) + R_R(i_{Ra}^2 + i_{Rb}^2). \tag{6.51}$$

Integrating both sides with respect to time t gives the conservation of energy equation

$$W_{\text{electrical}} = W_{\text{field}} + \int_0^t \frac{\partial W_{\text{field}}}{\partial \theta_R}\omega_R dt + W_{\text{ohmic loss}}.$$

The electrical power supplied by the source goes into the magnetic field energy, heat losses in the phase windings and another term given by

$$\int_0^t \frac{\partial W_{\text{field}}}{\partial \theta_R}\omega_R dt.$$

The only other energy conversion is mechanical energy. Consequently, this term represents the energy from the supply converted into mechanical work.

www.EngineeringEBooksPdf.com

The mechanical power $\tau_R \omega_R$ is therefore given by $\tau_R \omega_R = (\partial W_{\text{field}}/\partial \theta_R)\,\omega_R$ so that the torque produced by the machine is[7]

$$\tau_R = \frac{\partial W_{\text{field}}}{\partial \theta_R}. \tag{6.52}$$

Using the expression (6.49) for W_{field} results in

$$\begin{aligned} \tau_R &= M\Big(-i_{Ra}(t)i_{Sa}(t)\sin(\theta_R) + i_{Ra}(t)i_{Sb}(t)\cos(\theta_R) \\ &\quad -i_{Rb}(t)i_{Sa}(t)\cos(\theta_R) - i_{Rb}(t)i_{Sb}(t)\sin(\theta_R)\Big) \end{aligned}$$

which is the same expression as in equation (6.31) derived previously.

6.12.3 Computing Torque From the Co-energy

The above analysis was done assuming linear magnetics for the two-phase induction motor. A more general approach is now given that does not assume linear magnetics.

Recall the electrical dynamics of the two-phase induction motor can be written as

$$\begin{aligned} u_{Sa} - R_S i_{Sa} &= \frac{d\lambda_{Sa}}{dt} \\ u_{Sb} - R_S i_{Sb} &= \frac{d\lambda_{Sb}}{dt} \\ u_{Ra} - R_R i_{Ra} &= \frac{d\lambda_{Ra}}{dt} \\ u_{Rb} - R_R i_{Rb} &= \frac{d\lambda_{Rb}}{dt}. \end{aligned} \tag{6.53}$$

These equations are very general in the sense that they hold even in the case of magnetic saturation in the rotor or stator iron.[8] Define a new set of voltages $e_{Sa} \triangleq u_{Sa} - R_S i_{Sa}$, $e_{Sb} \triangleq u_{Sb} - R_S i_{Sb}$, $e_{Ra} \triangleq u_{Ra} - R_R i_{Ra}$, and $e_{Rb} \triangleq u_{Rb} - R_R i_{Rb}$ and consider these voltages as the *inputs* to the phase windings. In this way, the power loss to ohmic heating of the phase windings can be considered as part of the power supply and not the machine. The power delivered to the phases is then $i_{Sa}e_{Sa} + i_{Sb}e_{Sb} + i_{Ra}e_{Ra} + i_{Rb}e_{Rb}$ and, using (6.53), the basic equation for conservation of power may be written

[7] This derivation assumed that (6.45) held, that is, that magnetic saturation was not present. This result does not hold if magnetic saturation is present. A more general result that holds in the presence of magnetic saturation is given in the next subsection.

[8] However, the expressions (6.45) are valid only for the linear magnetics case, that is, no magnetic saturation.

www.EngineeringEBooksPdf.com

as

$$\begin{aligned} i_{Sa}e_{Sa} + i_{Sb}e_{Sb} + i_{Ra}e_{Ra} + i_{Rb}e_{Rb} &= i_{Sa}\frac{d\lambda_{Sa}}{dt} + i_{Sb}\frac{d\lambda_{Sb}}{dt} + i_{Ra}\frac{d\lambda_{Ra}}{dt} \\ &\quad + i_{Rb}\frac{d\lambda_{Rb}}{dt} \\ &= \frac{d}{dt}W_{\text{field}}(i_{Sa}, i_{Sb}, i_{Ra}, i_{Rb}, \theta_R) \\ &\quad + \tau_R\frac{d\theta_R}{dt}. \end{aligned} \tag{6.54}$$

This equation just says that the power provided to the phases by the voltage sources equals the rate of change of the field energy and the mechanical power produced. This expression is perfectly general in that it holds in the case of magnetic saturation. However, it does assume that an expression for the field energy $W_{\text{field}}(i_{Sa}, i_{Sb}, i_{Ra}, i_{Rb}, \theta_R)$ in terms of the phase currents and rotor position has been found.[9]

Now,

$$\begin{aligned} \frac{d}{dt}W_{\text{field}} &= \frac{\partial W_{\text{field}}}{\partial i_{Sa}}\frac{di_{Sa}}{dt} + \frac{\partial W_{\text{field}}}{\partial i_{Sb}}\frac{di_{Sb}}{dt} + \frac{\partial W_{\text{field}}}{\partial i_{Ra}}\frac{di_{Ra}}{dt} + \frac{\partial W_{\text{field}}}{\partial i_{Rb}}\frac{di_{Rb}}{dt} \\ &\quad + \frac{\partial W_{\text{field}}}{\partial \theta_R}\frac{d\theta_R}{dt} \end{aligned} \tag{6.55}$$

and, with $\lambda = \lambda(i_{Sa}, i_{Sb}, i_{Ra}, i_{Rb}, \theta_R)$,

$$\frac{d\lambda}{dt} = \frac{\partial\lambda}{\partial i_{Sa}}\frac{di_{Sa}}{dt} + \frac{\partial\lambda}{\partial i_{Sb}}\frac{di_{Sb}}{dt} + \frac{\partial\lambda}{\partial i_{Ra}}\frac{di_{Ra}}{dt} + \frac{\partial\lambda}{\partial i_{Rb}}\frac{di_{Rb}}{dt} + \frac{\partial\lambda}{\partial\theta_R}\frac{d\theta_R}{dt}$$

where λ stands for $\lambda_{Sa}, \lambda_{Sb}, \lambda_{Ra}$, and λ_{Rb} (see the footnote[10]). Equation (6.54) holds for all $i_{Sa}, i_{Sb}, i_{Ra}, i_{Rb}$, and θ_R and their derivatives di_{Sa}/dt, di_{Sb}/dt, di_{Ra}/dt, di_{Rb}/dt, and $d\theta_R/dt$. The next step is to substitute the derivative of the flux linkages into left-hand side of (6.54) and the derivative

---

[9] The expression (6.49) is valid only for the linear magnetics case. To determine the field energy in the general case, one would lock the rotor so that $i_{Sa}e_{Sa} + i_{Sb}e_{Sb} + i_{Ra}e_{Ra} + i_{Rb}e_{Rb} = \frac{d}{dt}W_{\text{field}}(i_{Sa}, i_{Sb}, i_{Ra}, i_{Rb}, \theta_R)$ holds. Then one would try to integrate this expression to obtain W_{field}. Though the left-hand side is known, such a calculation would typically require numerical techniques in the presence of magnetic saturation. The "Achilles heel" in this approach is trying to find the field energy W_{field}.

[10] In the case of linear magnetics, the expressions (6.45) would be used. However, in the case of magnetic saturation, one proceeds as follows: For each phase, integrate $\lambda(t) = \int_0^t (u - Ri)dt$ to compute the phase flux as the currents i_{Sa}, i_{Sb}, i_{Ra}, and i_{Rb} are varied between $-I_{\max}$ and $I_{\max}$, and the rotor position is varied for $0 \le \theta_R \le \frac{2\pi}{n_p}$. This then gives the phase flux as a function of $i_{Sa}, i_{Sb}, i_{Ra}, i_{Rb}$, and θ_R.

www.EngineeringEBooksPdf.com

of the field energy (6.55) into the right-hand side of (6.54). This results in

$$\begin{aligned}
&\left(i_{Sa}\frac{\partial\lambda_{Sa}}{\partial i_{Sa}}+i_{Sb}\frac{\partial\lambda_{Sb}}{\partial i_{Sa}}+i_{Ra}\frac{\partial\lambda_{Ra}}{\partial i_{Sa}}+i_{Rb}\frac{\partial\lambda_{Rb}}{\partial i_{Sa}}\right)\frac{di_{Sa}}{dt}\\
&\quad+\left(i_{Sa}\frac{\partial\lambda_{Sb}}{\partial i_{Sb}}+i_{Sb}\frac{\partial\lambda_{Sb}}{\partial i_{Sb}}+i_{Ra}\frac{\partial\lambda_{Ra}}{\partial i_{Sb}}+i_{Rb}\frac{\partial\lambda_{Rb}}{\partial i_{Sb}}\right)\frac{di_{Sb}}{dt}\\
&\quad+\left(i_{Sa}\frac{\partial\lambda_{Ra}}{\partial i_{Ra}}+i_{Sb}\frac{\partial\lambda_{Sb}}{\partial i_{Ra}}+i_{Ra}\frac{\partial\lambda_{Ra}}{\partial i_{Ra}}+i_{Rb}\frac{\partial\lambda_{Rb}}{\partial i_{Ra}}\right)\frac{di_{Ra}}{dt}\\
&\quad+\left(i_{Sa}\frac{\partial\lambda_{Rb}}{\partial i_{Rb}}+i_{Sb}\frac{\partial\lambda_{Sb}}{\partial i_{Rb}}+i_{Ra}\frac{\partial\lambda_{Ra}}{\partial i_{Rb}}+i_{Rb}\frac{\partial\lambda_{Rb}}{\partial i_{Rb}}\right)\frac{di_{Rb}}{dt}\\
&\quad+\left(i_{Sa}\frac{\partial\lambda_{Sa}}{\partial\theta_R}+i_{Sb}\frac{\partial\lambda_{Sb}}{\partial\theta_R}+i_{Ra}\frac{\partial\lambda_{Ra}}{\partial\theta_R}+i_{Rb}\frac{\partial\lambda_{Rb}}{\partial\theta_R}\right)\frac{d\theta_R}{dt}\\
&=\frac{\partial W_{\text{field}}}{\partial i_{Sa}}\frac{di_{Sa}}{dt}+\frac{\partial W_{\text{field}}}{\partial i_{Sb}}\frac{di_{Sb}}{dt}+\frac{\partial W_{\text{field}}}{\partial i_{Ra}}\frac{di_{Ra}}{dt}+\frac{\partial W_{\text{field}}}{\partial i_{Rb}}\frac{di_{Rb}}{dt}\\
&\quad+\frac{\partial W_{\text{field}}}{\partial\theta_R}\frac{d\theta_R}{dt}+\tau_R\frac{d\theta_R}{dt}.
\end{aligned}\tag{6.56}$$

Given any set of values for i_{Sa}, i_{Sb}, i_{Ra}, i_{Rb}, and θ_R, by proper choice of u_{Sa},u_{Sb}, u_{Ra}, u_{Rb}, and τ_L, the derivatives di_{Sa}/dt, di_{Sb}/dt, di_{Ra}/dt, di_{Rb}/dt, and $d\theta_R/dt$ can be arbitrarily chosen (see problem 20). Therefore, the only way that (6.56) can be satisfied for any such values of di_{Sa}/dt, di_{Sb}/dt, di_{Ra}/dt, di_{Rb}/dt, and $d\theta_R/dt$ is that the coefficients of these derivatives in (6.56) must be equal for all time, that is,

$$\begin{aligned}
i_{Sa}\frac{\partial\lambda_{Sa}}{\partial i_{Sa}}+i_{Sb}\frac{\partial\lambda_{Sb}}{\partial i_{Sa}}+i_{Ra}\frac{\partial\lambda_{Ra}}{\partial i_{Sa}}+i_{Rb}\frac{\partial\lambda_{Rb}}{\partial i_{Sa}} &= \frac{\partial W_{\text{field}}}{\partial i_{Sa}}\\
i_{Sa}\frac{\partial\lambda_{Sb}}{\partial i_{Sb}}+i_{Sb}\frac{\partial\lambda_{Sb}}{\partial i_{Sb}}+i_{Ra}\frac{\partial\lambda_{Ra}}{\partial i_{Sb}}+i_{Rb}\frac{\partial\lambda_{Rb}}{\partial i_{Sb}} &= \frac{\partial W_{\text{field}}}{\partial i_{Sb}}\\
i_{Sa}\frac{\partial\lambda_{Ra}}{\partial i_{Ra}}+i_{Sb}\frac{\partial\lambda_{Sb}}{\partial i_{Ra}}+i_{Ra}\frac{\partial\lambda_{Ra}}{\partial i_{Ra}}+i_{Rb}\frac{\partial\lambda_{Rb}}{\partial i_{Ra}} &= \frac{\partial W_{\text{field}}}{\partial i_{Ra}}\\
i_{Sa}\frac{\partial\lambda_{Rb}}{\partial i_{Rb}}+i_{Sb}\frac{\partial\lambda_{Sb}}{\partial i_{Rb}}+i_{Ra}\frac{\partial\lambda_{Ra}}{\partial i_{Rb}}+i_{Rb}\frac{\partial\lambda_{Rb}}{\partial i_{Rb}} &= \frac{\partial W_{\text{field}}}{\partial i_{Rb}}\\
i_{Sa}\frac{\partial\lambda_{Sa}}{\partial\theta_R}+i_{Sb}\frac{\partial\lambda_{Sb}}{\partial\theta_R}+i_{Ra}\frac{\partial\lambda_{Ra}}{\partial\theta_R}+i_{Rb}\frac{\partial\lambda_{Rb}}{\partial\theta_R} &= \frac{\partial W_{\text{field}}}{\partial\theta_R}+\tau_R.
\end{aligned}\tag{6.57}$$

In particular, the last expression shows that

$$\tau_R=i_{Sa}\frac{\partial\lambda_{Sa}}{\partial\theta_R}+i_{Sb}\frac{\partial\lambda_{Sb}}{\partial\theta_R}+i_{Ra}\frac{\partial\lambda_{Ra}}{\partial\theta_R}+i_{Rb}\frac{\partial\lambda_{Rb}}{\partial\theta_R}-\frac{\partial W_{\text{field}}}{\partial\theta_R}.$$

Finally, making the definition of *co-energy* as

$$W_{\text{co-energy}}\triangleq i_{Sa}\lambda_{Sa}+i_{Sb}\lambda_{Sb}+i_{Ra}\lambda_{Ra}+i_{Rb}\lambda_{Rb}-W_{\text{field}},\tag{6.58}$$

it follows that the torque may be written as

$$\tau_R=\frac{\partial W_{\text{co-energy}}}{\partial\theta_R}.\tag{6.59}$$

www.EngineeringEBooksPdf.com

This derivation assumed that all of the phases had voltage inputs. However, the expression for torque (6.59) still holds even if the rotor phases are shorted. That is, the expression (6.59) is true for any set of inputs, so it must be true for $u_{Ra} = u_{Rb} \equiv 0$.

The co-energy (6.58) does not have any physical significance and only represents a convenient mathematical quantity for computing the torque.

The reader is asked in problem 15 to show that, in the case of linear magnetics, the expression for W_{field} given in (6.49) equals the expression for $W_{\text{co-energy}}$ given in (6.58).

www.EngineeringEBooksPdf.com

Problems

Torque Production in AC Machines

Problem 1 Torque on the Stator Winding

Use the expression (6.27) for radial magnetic field in the air gap due to the rotor currents and compute the total torque $\vec{\tau}_S$ it produces on the currents in the stator windings. In particular, show that $\vec{\tau}_S = -\vec{\tau}_R$.

Problem 2 $\vec{\mathbf{B}}_R$ Cannot Produce Torque on the Rotor

(a) Using the expression (6.6) [or (6.27)] for the radial magnetic field in the air gap produced by the rotor currents, show by direct computation that the total torque this magnetic field produces on the rotor *currents is zero.*

(b) Similarly, using the expression (6.5) [or (6.26)] for the radial magnetic field in the air gap produced by the stator currents, show by direct computation that the torque this magnetic field produces on the stator *currents is zero.*

(c) Explain why these two results must be true from basic principles of Physics.

Problem 3 The Induction Motor as a Transformer

Using the flux linkage equations (6.45), show that [$\sigma = 1 - M^2/(L_S L_R)$]

$$\begin{aligned}
\sigma L_S L_R i_{Sa} &= L_R \lambda_{Sa} - M(+\lambda_{Ra}\cos(\theta_R) - \lambda_{Rb}\sin(\theta_R)) \\
\sigma L_S L_R i_{Sb} &= L_R \lambda_{Sb} - M(+\lambda_{Ra}\sin(\theta_R) + \lambda_{Rb}\cos(\theta_R)) \\
\sigma L_S L_R i_{Ra} &= L_S \lambda_{Ra} - M(+\lambda_{Sa}\cos(\theta_R) + \lambda_{Sb}\sin(\theta_R)) \\
\sigma L_S L_R i_{Rb} &= L_S \lambda_{Rb} - M(-\lambda_{Sa}\sin(\theta_R) + \lambda_{Sb}\cos(\theta_R)).
\end{aligned}$$

If $\sigma = 0$, find an expression for the rotor flux linkages in terms of the stator flux linkages. Use this expression to show that, with the rotor locked at some angle θ_R, the induction motor (with a sinusoidally wound rotor) is a (two-input two-output) transformer with a turns ratio of either $(M/L_S)\cos(\theta_R) = (N_R/N_S)\cos(\theta_R)$ or $(M/L_S)\sin(\theta_R) = (N_R/N_S)\sin(\theta_R)$ from a stator winding to a rotor winding. In particular, find $\lambda_{Ra}/\lambda_{Sa}$ and $\lambda_{Rb}/\lambda_{Sb}$ for $\theta_R = 0$.

What if one had a squirrel cage induction motor rather than a sinusoidally wound rotor induction motor?

Mathematical Models of an Induction Machine

Problem 4 State-Space Model of the Induction Motor

Starting from the mathematical model (6.30) and (6.31), derive a state space model for the two-phase induction motor where the state variables are $i_{Sa}, i_{Sb}, i_{Ra}, i_{Rb}, \omega$, and θ. (See problem 6 for a simpler, but equivalent, model.)

www.EngineeringEBooksPdf.com

Problem 5 Space Vector Model of the Induction Motor (Leonhard [1])

Let $\underline{i}_S \triangleq i_{Sa} + ji_{Sb}$, $\underline{i}_R \triangleq i_{Ra} + ji_{Rb}$, $\underline{u}_S \triangleq u_{Sa} + ju_{Sb}$ *and show that the equations of the induction motor (6.34) may be written succinctly as*

$$\begin{aligned} R_S\underline{i}_S + L_S\frac{d}{dt}\underline{i}_S + M\frac{d}{dt}\left(\underline{i}_R e^{jn_p\theta_R}\right) &= \underline{u}_S \\ R_R i_R + L_R\frac{d}{dt}\underline{i}_R + M\frac{d}{dt}\left(\underline{i}_S e^{-jn_p\theta_R}\right) &= 0 \\ n_p M \mathrm{Im}\left\{\underline{i}_S(\underline{i}_R e^{jn_p\theta_R})^*\right\} - \tau_L &= J\frac{d\omega_R}{dt} \end{aligned}$$

where $Im\{\cdot\}$ *denotes the* imaginary *part and* $*$ *denotes complex conjugate. This is known as the* space vector *representation.*

Problem 6 A Standard Model of the Induction Motor

The model (6.34) of the induction motor (or its equivalent space vector representation given in problem 5) is quite complicated. By doing a change of variables, a simpler, but equivalent model can be found. In particular, a model can found where the explicit dependency on θ_R *[i.e., the* $\sin(n_p\theta_R)$ *and* $\cos(n_p\theta_R)$ *terms] can be eliminated. To do so, define new (fictitious) flux linkages as*

$$\underline{\psi}_R \triangleq \psi_{Ra} + j\psi_{Rb} \triangleq \underline{\lambda}_R e^{jn_p\theta_R} = L_R\underline{i}_R e^{jn_p\theta_R} + M\underline{i}_S$$

(a) Make this substitution into the representation given in problem 5 to show that the system of equations for the induction motor may be rewritten in the space vector form as

$$\begin{aligned} \frac{d}{dt}\underline{\psi}_R &= \left(-\frac{1}{T_R} + jn_p\omega_R\right)\underline{\psi}_R + \frac{M}{T_R}\underline{i}_S \\ \underline{u}_S &= \frac{M}{L_R}\frac{d}{dt}\underline{\psi}_R + \sigma L_S\frac{d}{dt}\underline{i}_S + R_S\underline{i}_S \\ \frac{d\omega_R}{dt} &= \mu\,\mathrm{Im}\left\{\underline{i}_S(\underline{\psi}_R)^*\right\} - \frac{\tau_L}{J} \end{aligned}$$

where $\mu \triangleq n_p M/(JL_R)$, $\sigma \triangleq 1 - M^2/L_S L_R$ *is the leakage factor, and* $T_R \triangleq L_R/R_R$ *is the rotor time constant. This model is often seen in the literature.*

(b) Equate real and imaginary parts in part (a) to write the model as five differential equations.

(c) Use the answer in part (b) to find a state space model of the motor with state variables $i_{Sa}, i_{Sb}, \psi_{Ra}, \psi_{Rb}$, *and* ω_R.

Remark *This problem illustrates the power of the space vector representation as the manipulations of the equations are all done with (complex) scalar quantities rather than dealing with vectors and matrices. The representations in parts (a) and (b) are standard forms seen in the literature.*

www.EngineeringEBooksPdf.com

Often the real and imaginary parts of $\psi_{Ra} + j\psi_{Rb}$ are referred to as the "rotor fluxes", but the actual rotor flux linkages are the real and imaginary parts of $\underline{\lambda}_R = (\psi_{Ra} + j\psi_{Rb})\, e^{-jn_p\theta_R}$.

Problem 7 Simulation of an Induction Motor

(a) Using the state-space model derived in problem 6(c), simulate a two-phase induction motor. Set the parameters as $R_R = 3.9\ \Omega$, $R_S = 1.7\ \Omega$, $L_R = 0.014\ H$, $L_S = 0.014\ H$, $M = 0.0117\ H$, $J = 0.00011\ kg\text{-}m^2$, $f = 0\ N\text{-}m/rad/sec$, $n_p = 3$, $\omega_S = (2\pi)60\ rad/sec$, $V = V_{max} = 60\ V$ (peak), $I_{max} = 12\ A$, $\tau_L = 0$. Let $u_{Sa} = V\cos(\omega_S t)$, $u_{Sb} = V\sin(\omega_S t)$ and plot (a) i_{Sa} and i_{Sb}, (b) i_{Ra} and i_{Rb}, and (c) ω. Run the simulation long enough (about 0.5 sec) so that the speed ω_R goes to a constant steady-state value. Notice that at steady-state (constant) speed, the rotor currents are zero. Give a physical *explanation as to why this happens.*

(b) Rerun the simulation with a load torque of $\tau_L = 0.2\ N\text{-}m$ acting on the system after *it has reached steady-state (synchronous) speed. Be sure to run the simulation until the motor speed has reached its new (lower) steady-state speed. Note that the steady-state rotor currents are no longer zero. Why?*

(c) What happens if $\tau_L = 0.5\ N\text{-}m$ is used? Note that the frequency of the rotor currents increases as the load-torque increases. Give a physical *explanation to why this happens.*

Problem 8 Induction Motor Model in Terms of the Flux Linkages

With λ_{Sa} and λ_{Sb} the total flux linkage in stator phases a and b, respectively, define

$$\underline{\lambda}_S \triangleq \lambda_{Sa} + j\lambda_{Sb} \triangleq L_S\underline{i}_S + M\underline{i}_R e^{+jn_p\theta_R}.$$

Similarly, let λ_{Ra} and λ_{Rb} be the total flux linkage in rotor phases a and b, respectively, and define

$$\underline{\lambda}_R \triangleq \lambda_{Ra} + j\lambda_{Rb} \triangleq L_R\underline{i}_R + M\underline{i}_S e^{-jn_p\theta_R}.$$

(a) Show that the electrical equations of the induction motor may be written as

$$\begin{aligned} R_S\underline{i}_S + \frac{d}{dt}\underline{\lambda}_S &= \underline{u}_S \\ R_R\underline{i}_R + \frac{d}{dt}\underline{\lambda}_R &= 0. \end{aligned}$$

(b) Using the fact that

$$\begin{bmatrix} \underline{i}_S \\ \underline{i}_R e^{+jn_p\theta_R} \end{bmatrix} = \frac{1}{L_S L_R - M^2} \begin{bmatrix} +L_R & -M \\ -M & +L_S \end{bmatrix} \begin{bmatrix} \underline{\lambda}_S \\ \underline{\lambda}_R e^{+jn_p\theta_R} \end{bmatrix}$$

www.EngineeringEBooksPdf.com

show that

$$\begin{aligned}
\frac{R_S}{L_S L_R - M^2}\left(L_R\underline{\lambda}_S - M\underline{\lambda}_R e^{+jn_p\theta_R}\right) + \frac{d}{dt}\underline{\lambda}_S &= \underline{u}_S \\
\frac{R_R}{L_S L_R - M^2}\left(-M\underline{\lambda}_S e^{-jn_p\theta_R} + L_S\underline{\lambda}_R\right) + \frac{d}{dt}\underline{\lambda}_R &= 0 \\
\frac{M}{L_S L_R - M^2}\,\mathrm{Im}\{\underline{\lambda}_S(\underline{\lambda}_R e^{+jn_p\theta_R})^*\} - \tau_L &= J\frac{d\omega_R}{dt} \\
\frac{d\theta_R}{dt} &= \omega_R
\end{aligned}$$

is a representation of the induction motor in terms of the variables $\underline{\lambda}_S \triangleq \lambda_{Sa} + j\lambda_{Sb}, \underline{\lambda}_R \triangleq \lambda_{Ra} + j\lambda_{Rb}, \omega_R$, *and* θ_R.

(c) By equating real and imaginary parts of the answer to part (b), find a state space representation of the induction motor in terms of the state variables $\lambda_{Sa}, \lambda_{Sb}, \lambda_{Ra}, \lambda_{Rb}, \omega_R$, *and* θ_R.

Problem 9 Steady-State Solution of the Induction Motor Equations [1]

Use the space vector formulation given in problem 5 to find a sinusoidal steady-state solution to the induction motor equations. In particular, try a solution of the form

$$\begin{aligned}
\underline{u}_S &= u_{Sa} + ju_{Sb} = U_S\cos(\omega_S t + \phi_{Us}) + jU_S\sin(\omega_S t + \phi_{Us}) \\
&= U_S e^{j\phi_{Us}} e^{j\omega_S t} = \underline{U}_S e^{j\omega_S t}
\end{aligned}$$

$$\begin{aligned}
\underline{i}_S &= i_{Sa} + ji_{Sb} = I_S\cos(\omega_S t + \phi_S) + jI_S\sin(\omega_S t + \phi_S) \\
&= I_S e^{j\phi_S} e^{j\omega_S t} = \underline{I}_S e^{j\omega_S t}
\end{aligned}$$

$$\begin{aligned}
\underline{i}_R &= i_{Ra} + ji_{Rb} = I_R\cos\left((\omega_S - \omega_R)t + \phi_R\right) + jI_R\sin\left((\omega_S - \omega_R)t + \phi_R\right) \\
&= I_R e^{j\phi_R} e^{j(\omega_S - \omega_R)t} = \underline{I}_R e^{j(\omega_S - \omega_R)t}
\end{aligned}$$

$$\theta_R(t) = \omega_R t$$

where the stator electrical frequency ω_S, *rotor speed* ω_R *and* $\underline{U}_S = U_S e^{j\phi_{Us}}$ *are assumed to be known and constant. The stator and rotor current phasors given by* $\underline{I}_S \triangleq I_S e^{j\phi_S}$ *and* $\underline{I}_R \triangleq I_R e^{j\phi_R}$ *are to be determined; that is, the unknowns are* I_S, ϕ_S, I_R, *and* ϕ_R.

(a) Substitute these expressions into the space vector representation of the induction motor equations to obtain

$$\begin{aligned}
(R_S + j\omega_S L_S)\,\underline{I}_S + j\omega_S M\underline{I}_R &= \underline{U}_S \\
(R_R + j(\omega_S - \omega_R)L_R)\,\underline{I}_R + j(\omega_S - \omega_R)M\underline{I}_S &= 0 \\
M\,\mathrm{Im}\{\underline{I}_S(\underline{I}_R)^*\} - \tau_L &= 0.
\end{aligned}$$

www.EngineeringEBooksPdf.com

With the normalized slip speed defined by $S \triangleq (\omega_S - \omega_R)/\omega_S$, *it follows that*

$$\begin{bmatrix} \underline{I}_S \\ \underline{I}_R \end{bmatrix} = \frac{1}{\det} \begin{bmatrix} R_R/S + j\omega_S L_R & -j\omega_S M \\ -j\omega_S M & R_S + j\omega_S L_S \end{bmatrix} \begin{bmatrix} \underline{U}_S \\ 0 \end{bmatrix}$$

where

$$\det \triangleq (R_S + j\omega_S L_S)\,(\frac{R_R}{S} + j\omega_S L_R) - (j\omega_S M)^2\,.$$

(b) Use these expressions to compute I_S, ϕ_S, I_R, ϕ_R, *and* $\tau = M\,\mathrm{Im}\{\underline{I}_S(\underline{I}_R)^*\} = MI_SI_R\sin(\phi_S - \phi_R)$ *as functions of the stator frequency* ω_S *and the normalized slip* S.

(c) Using the parameter values given in problem 7, write a program to plot $\tau = MI_SI_R\sin(\phi_S - \phi_R)$ *for a fixed* $\omega_S = 2\pi * 60$ *as* S *varies from* 0 *to* 20.

Problem 10 Model of an Induction Motor with Multiple Pole Pairs

Consider a two-phase motor with n_p *pole pairs. With* $n_p = 2$, *Figure 6.12(a) shows stator phase a and Figure 6.12(b) shows stator phase b.*

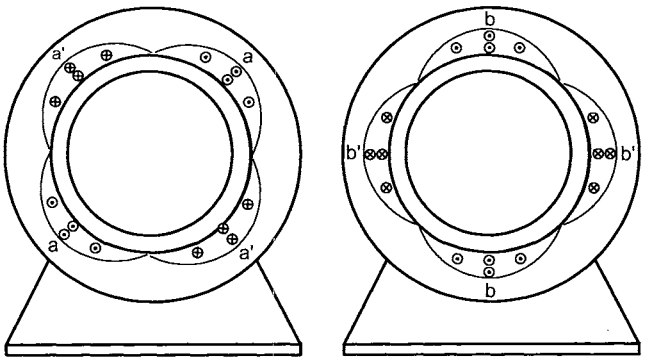


FIGURE 6.12. (a) Sinusoidally wound stator phase a with $n_p = 2$ and turns density $N_{Sa}(\theta) = (n_pN_S/2)\,|\sin(n_p\theta)|$. (b) Sinusoidally wound stator phase b with $n_p = 2$ and turns density $N_{Sb}(\theta) = (n_pN_S/2)\,|\sin(n_p(\theta - \pi/2))|\,.$

The sinusoidal turns density *for the windings of each phase are given by*

$$\begin{aligned} N_{Sa}(\theta) &= \frac{n_pN_S}{2}\,|\sin(n_p\theta)| \\ N_{Sb}(\theta) &= \frac{n_pN_S}{2}\,|\sin(n_p(\theta - \pi/2))| \\ N_{Ra}(\theta) &= \frac{n_pN_R}{2}\,|\sin(n_p(\theta - \theta_R))| \\ N_{Rb}(\theta) &= \frac{n_pN_R}{2}\,|\sin(n_p(\theta - \theta_R - \pi/2))|\,. \end{aligned}$$

www.EngineeringEBooksPdf.com

For example, the first pole pair of stator phase a is made up of the turns for $-\pi/n_p < \theta < \pi/n_p$, *the second pole pair of stator phase a is made up of the turns for* $\pi/n_p < \theta < 3\pi/n_p$, *and so on. The total number of turns making up the first pole pair is* $\int_0^{\pi/n_p} N_{Sa}(\theta)d\theta = N_S$. *As there are* n_p *pole pairs, the total number of turns in phase a is* $n_p N_S$; *that is,* N_S *is the number of turns in phase a per pole pair.*

(a) Explain why Ampère's law $\oint \vec{\mathbf{H}} \cdot d\vec{\boldsymbol{\ell}} = i_{enclosed}$ *applied to the closed path* 1–2–3–4–1 *indicated in Figure 6.13 is*

$$\oint_{1-2-3-4-1} \vec{\mathbf{H}}_{Sa} \cdot d\vec{\boldsymbol{\ell}} = \int_0^{\theta} i_{Sa} \frac{n_p N_S}{2} \sin(n_p \theta')d\theta' \tag{6.60}$$

for any *angle* θ.

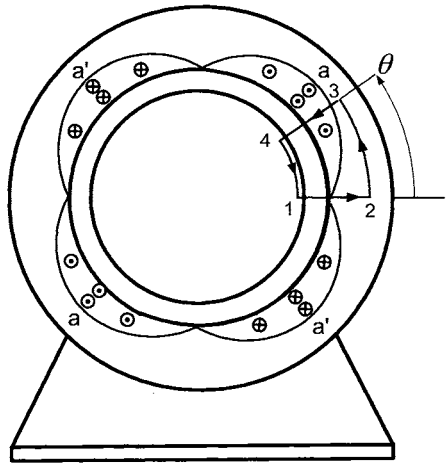


FIGURE 6.13. Use of Ampère's law to determine the air gap radial magnetic field produced by i_{Sa} in a n_p pole-pair machine.

Show that equation (6.60) leads to

$$B_{Sa}(i_{Sa}, \theta) = \frac{\mu_0 N_S}{2g} i_{Sa} \cos(n_p \theta). \tag{6.61}$$

(b) Show that conservation of flux will hold in the air gap if this expression is modified by including the factor r_R/r *to obtain*

$$\vec{\mathbf{B}}_{Sa}(i_{Sa}, r, \theta) = \frac{\mu_0 N_S}{2g} \frac{r_R}{r} i_{Sa} \cos(n_p \theta)\hat{\mathbf{r}}.$$

www.EngineeringEBooksPdf.com

(c) Show that

$$\begin{aligned}\vec{\mathbf{B}}_S(i_{Sa}, i_{Sb}, r, \theta) &= \vec{\mathbf{B}}_{Sa}(i_{Sa}, r, \theta) + \vec{\mathbf{B}}_{Sb}(i_{Sb}, r, \theta) \\ &= \frac{\mu_0 N_S}{2g}\frac{r_R}{r}\left(i_{Sa}\cos(n_p\theta) + i_{Sb}\sin(n_p\theta)\right)\hat{\mathbf{r}} \\ \vec{\mathbf{B}}_R(i_{Ra}, i_{Rb}, r, \theta - \theta_R) &= \vec{\mathbf{B}}_{Ra}(i_{Ra}, r, \theta - \theta_R) + \vec{\mathbf{B}}_{Rb}(i_{Rb}, r, \theta - \theta_R) \\ &= \frac{\mu_0 N_R}{2g}\frac{r_R}{r} \\ &\quad \times \Big(i_{Ra}\cos\left(n_p(\theta - \theta_R)\right) + i_{Rb}\sin\left(n_p(\theta - \theta_R)\right)\Big)\hat{\mathbf{r}}.\end{aligned}$$

(d) Show that

$$\begin{aligned}\lambda_{Sa}(i_{Ra}, i_{Rb}, i_{Sa}, i_{Sb}, \theta_R) &\triangleq \int_{\substack{All\ loops\ of \\ stator\ phase\ a}} (\vec{\mathbf{B}}_S + \vec{\mathbf{B}}_R)\cdot d\vec{\mathbf{S}} \\ &= L_S i_{Sa} + M\Big(i_{Ra}\cos(n_p\theta_R) - i_{Rb}\sin(n_p\theta_R)\Big) \\ \lambda_{Sb}(i_{Ra}, i_{Rb}, i_{Sa}, i_{Sb}, \theta_R) &= \int_{\substack{All\ loops\ of \\ stator\ phase\ b}} (\vec{\mathbf{B}}_S + \vec{\mathbf{B}}_R)\cdot d\vec{\mathbf{S}} \\ &= L_S i_{Sb} + M\Big(i_{Ra}\sin(n_p\theta_R) + i_{Rb}\cos(n_p\theta_R)\Big)\end{aligned}$$

$$\begin{aligned}\lambda_{Ra}(i_{Ra}, i_{Rb}, i_{Sa}, i_{Sb}, \theta_R) &= \int_{\substack{All\ loops\ of \\ rotor\ phase\ a}} (\vec{\mathbf{B}}_S + \vec{\mathbf{B}}_R)\cdot d\vec{\mathbf{S}} \\ &= L_R i_{Ra} + M\Big(i_{Sa}\cos(n_p\theta_R) + i_{Sb}\sin(n_p\theta_R)\Big) \\ \lambda_{Rb}(i_{Ra}, i_{Rb}, i_{Sa}, i_{Sb}, \theta_R) &= \int_{\substack{All\ loops\ of \\ rotor\ phase\ b}} (\vec{\mathbf{B}}_S + \vec{\mathbf{B}}_R)\cdot d\vec{\mathbf{S}} \\ &= L_R i_{Rb} + M\Big(-i_{Sa}\sin(n_p\theta_R) + i_{Sb}\cos(n_p\theta_R)\Big)\end{aligned}$$

$$\begin{aligned}\tau_R &= n_p M\Big(-i_{Ra}(t)i_{Sa}(t)\sin(n_p\theta_R) + i_{Ra}(t)i_{Sb}(t)\cos(n_p\theta_R) \\ &\quad - i_{Rb}(t)i_{Sa}(t)\cos(n_p\theta_R) - i_{Rb}(t)i_{Sb}(t)\sin(n_p\theta_R)\Big)\end{aligned}$$

where $L_S = \dfrac{\mu_0\ell_1\ell_2\pi}{8g}N_S^2$, $L_R = \dfrac{\mu_0\ell_1\ell_2\pi}{8g}N_R^2$, $M = \kappa\dfrac{\mu_0\pi\ell_1\ell_2}{8g}N_S N_R$.

www.EngineeringEBooksPdf.com

Mathematical Model of a Two-Phase Synchronous Machine

Problem 11 Mathematical Model of a PM Synchronous Machine

Consider a two-phase synchronous machine in which the rotor consists of a permanent magnet which produces a sinusoidally distributed radial magnetic field in the air gap given by

$$\vec{\mathbf{B}}_R(r, \theta - \theta_R) = B_m \frac{r_R}{r} \cos(\theta - \theta_R)\hat{\mathbf{r}}.$$

At $r = r_S$ this is written as

$$\vec{\mathbf{B}}_R(r_S, \theta - \theta_R) = \kappa B_m \frac{r_R}{r_S} \cos(\theta - \theta_R)\hat{\mathbf{r}}$$

where the coupling factor κ is included to account for leakage.

The stator is identical to the wound rotor synchronous motor, that is, it has two sinusoidally wound phases 90° apart with voltage sources u_{Sa} and u_{Sb}. The radial magnetic field in the air gap due to the stator currents is then given by (6.5).

(a) Show that the flux linkages in the stator phases have the form

$$\begin{aligned} \lambda_{Sa}(t) &= L_S i_{Sa}(t) + K_m \cos(\theta_R) \\ \lambda_{Sb}(t) &= L_S i_{Sb}(t) + K_m \sin(\theta_R) \end{aligned}$$

and compute explicit expressions for L_S and K_m in terms of $\mu_0, \kappa, \ell_1, \ell_2, N_S$, B_m, and g.

(b) Find the torque $\vec{\boldsymbol{\tau}}_S$ on the currents in the stator windings produced by $\vec{\mathbf{B}}_R(r_S, \theta - \theta_R)$. Then compute the torque on the rotor as $\vec{\boldsymbol{\tau}}_R = -\vec{\boldsymbol{\tau}}_S$.

(c) Give the complete set of equations characterizing a two-phase permanent magnet synchronous machine and show that it has the form (6.40).

Problem 12 Wound Rotor Synchronous Machine with Multiple Pole Pairs

Using the multiple-pole-pair model of a two-phase sinusoidally wound induction motor (see problem 10), show that it can be used directly to derive the multiple-pole-pair model of a two-phase sinusoidally wound synchronous motor. Specifically, show

$$\begin{aligned} \lambda_{Sa}(i_F, i_{Sa}, i_{Sb}, \theta_R) &= L_S i_{Sa} + M i_F \cos(n_p \theta_R) \\ \lambda_{Sb}(i_F, i_{Sa}, i_{Sb}, \theta_R) &= L_S i_{Sb} + M i_F \sin(n_p \theta_R) \\ \lambda_F(i_F, i_{Sa}, i_{Sb}, \theta_R) &= L_F i_{Fa} + M(i_{Sa} \cos(n_p \theta_R) + i_{Sb} \sin(n_p \theta_R)) \\ \tau_R &= n_p M i_F \left(-i_{Sa} \sin(n_p \theta_R) + i_{Sb} \cos(n_p \theta_R)\right) \end{aligned}$$

where $L_S = \dfrac{\mu_0 \ell_1 \ell_2 \pi}{8g} N_S^2, L_F = \dfrac{\mu_0 \ell_1 \ell_2 \pi}{8g} N_F^2$, and $M = \kappa \dfrac{\mu_0 \pi \ell_1 \ell_2}{8g} N_S N_F$. N_S is the number of winding per pole pair in each of the stator phases and N_F is the number of turns in the field winding. Use these expressions to deduce the dynamic equations of this machine.

www.EngineeringEBooksPdf.com

Problem 13 State-Space Model of a Wound Rotor Synchronous Machine

For the synchronous machine model of problem 12 [see also (6.38)], note that the relationship between the currents and the flux linkages may be written as

$$\begin{bmatrix} \lambda_{Sa} \\ \lambda_{Sb} \\ \lambda_F \end{bmatrix} \triangleq \begin{bmatrix} L_S & 0 & M\cos(n_p\theta_R) \\ 0 & L_S & M\sin(n_p\theta_R) \\ M\cos(n_p\theta_R) & M\sin(n_p\theta_R) & L_F \end{bmatrix} \begin{bmatrix} i_{Sa} \\ i_{Sb} \\ i_F \end{bmatrix}.$$

With $\Lambda(n_p\theta_R)$ denoting the 3×3 matrix on the right-hand side, it follows that

$$\begin{bmatrix} i_{Sa} \\ i_{Sb} \\ i_F \end{bmatrix} = \Lambda^{-1}(n_p\theta_R) \begin{bmatrix} \lambda_{Sa} \\ \lambda_{Sb} \\ \lambda_F \end{bmatrix}$$

where, with $\sigma \triangleq 1 - M^2/L_S L_F$,

$$\Lambda^{-1}(n_p\theta_R) = \frac{1}{\sigma L_S^2 L_F} \times$$

$$\begin{bmatrix} L_S L_F - M^2\sin^2(n_p\theta_R) & M^2\sin(n_p\theta_R)\cos(n_p\theta_R) & -L_S M\cos(n_p\theta_R) \\ M^2\sin(n_p\theta_R)\cos(n_p\theta_R) & L_S L_F - M^2\cos^2(n_p\theta_R) & -L_S M\sin(n_p\theta_R) \\ -L_S M\cos(n_p\theta_R) & -L_S M\sin(n_p\theta_R) & L_S^2 \end{bmatrix}.$$

(a) Use these relationships to find a state-space representation of the synchronous motor in terms of the flux linkages $\lambda_{Sa}, \lambda_{Sb}$, and λ_F. Be sure to include the torque equation.

(b) Use these relationships to find a state-space representation of the synchronous motor in terms of the currents i_{Sa}, i_{Sb}, and i_F. Be sure to include the torque equation.

Problem 14 DQ State-Space Model of a Synchronous Machine

For the synchronous machine model of Problem 12 [see also (6.38)], consider a change of coordinates to the so-called direct-quadrature *(dq) reference frame defined by*

$$\begin{bmatrix} u_d \\ u_q \\ u_F \end{bmatrix} \triangleq \begin{bmatrix} \cos(n_p\theta_R) & \sin(n_p\theta_R) & 0 \\ -\sin(n_p\theta_R) & \cos(n_p\theta_R) & 0 \\ 0 & 0 & 1 \end{bmatrix} \begin{bmatrix} u_{Sa} \\ u_{Sb} \\ u_F \end{bmatrix}$$

$$\begin{bmatrix} i_d \\ i_q \\ i_F \end{bmatrix} \triangleq \begin{bmatrix} \cos(n_p\theta_R) & \sin(n_p\theta_R) & 0 \\ -\sin(n_p\theta_R) & \cos(n_p\theta_R) & 0 \\ 0 & 0 & 1 \end{bmatrix} \begin{bmatrix} i_{Sa} \\ i_{Sb} \\ i_F \end{bmatrix}$$

$$\begin{bmatrix} \lambda_d \\ \lambda_q \\ \lambda_F \end{bmatrix} \triangleq \begin{bmatrix} \cos(n_p\theta_R) & \sin(n_p\theta_R) & 0 \\ -\sin(n_p\theta_R) & \cos(n_p\theta_R) & 0 \\ 0 & 0 & 1 \end{bmatrix} \begin{bmatrix} \lambda_{Sa} \\ \lambda_{Sb} \\ \lambda_F \end{bmatrix}.$$

www.EngineeringEBooksPdf.com

(a) Show that

$$\begin{bmatrix} \lambda_d \\ \lambda_q \\ \lambda_F \end{bmatrix} = \begin{bmatrix} L_S & 0 & M \\ 0 & L_S & 0 \\ M & 0 & L_F \end{bmatrix} \begin{bmatrix} i_d \\ i_q \\ i_F \end{bmatrix}.$$

(b) Show that

$$\begin{bmatrix} i_d \\ i_q \\ i_F \end{bmatrix} = \frac{1}{\sigma L_S L_F} \begin{bmatrix} L_F & 0 & -M \\ 0 & \sigma L_F & 0 \\ -M & 0 & L_S \end{bmatrix} \begin{bmatrix} \lambda_d \\ \lambda_q \\ \lambda_F \end{bmatrix}.$$

(c) Use the expressions from parts (a) and (b) to show that

$$\begin{aligned} \frac{d\lambda_d}{dt} &= n_p\omega\lambda_q - R_S i_d + u_d \\ \frac{d\lambda_q}{dt} &= -n_p\omega\lambda_d - R_S i_q + u_q \\ \frac{d\lambda_F}{dt} &= -R_F i_F + u_F \\ J\frac{d\omega_R}{dt} &= M i_F i_q - \tau_L \end{aligned}$$

and so

$$\frac{d}{dt}\begin{bmatrix} L_S & 0 & M \\ 0 & L_S & 0 \\ M & 0 & L_F \end{bmatrix}\begin{bmatrix} i_d \\ i_q \\ i_F \end{bmatrix} = \begin{bmatrix} -R_S & n_p\omega L_S & 0 \\ -n_p\omega L_S & -R_S & -n_p\omega M \\ 0 & 0 & R_F \end{bmatrix}\begin{bmatrix} i_d \\ i_q \\ i_F \end{bmatrix} + \begin{bmatrix} u_d \\ u_q \\ u_F \end{bmatrix}.$$

(d) Show that

$$\frac{d}{dt}\begin{bmatrix} i_d \\ i_q \\ i_F \end{bmatrix} = \frac{1}{\sigma}\begin{bmatrix} -R_S/L_S & n_p\omega & -M/L_S \\ -\sigma n_p\omega & -\sigma R_S/L_S & -n_p\omega\sigma M/L_S \\ -MR_S/L_S L_F & -n_p\omega M/L_F & R_F/L_F \end{bmatrix}\begin{bmatrix} i_d \\ i_q \\ i_F \end{bmatrix} + \frac{1}{\sigma L_S L_F}\begin{bmatrix} L_F & 0 & -M \\ 0 & \sigma L_F & 0 \\ -M & 0 & L_S \end{bmatrix}\begin{bmatrix} u_d \\ u_q \\ u_F \end{bmatrix}$$

$$J\frac{d\omega_R}{dt} = M i_F i_q - \tau_L$$

where

$$\sigma \triangleq 1 - \frac{M^2}{L_S L_F}.$$

www.EngineeringEBooksPdf.com

Magnetic Field Energy, Co-energy and Torque

Problem 15 Co-energy

The co-energy is defined by

$$W_{co\text{-}energy} \triangleq i_{Sa}\lambda_{Sa} + i_{Sb}\lambda_{Sb} + i_{Ra}\lambda_{Ra} + i_{Rb}\lambda_{Rb} - W_{field}.$$

The expression for the field energy given in equation (6.49) is valid if magnetic saturation is not *present. In this case, show that* $W_{co\text{-}energy} = W_{field}$ *and consequently, either (6.52) or (6.59) is valid for computing the torque. (The co-energy is* not *equal to the magnetic field energy when magnetic saturation is present in the iron.)*

Problem 16 Co-energy

Inverting the flux linkage equations (6.45) gives $\left(\sigma = 1 - \dfrac{M^2}{L_S L_R}\right)$

$$\begin{aligned}
i_{Sa} &= \frac{1}{\sigma L_S L_R}\Big(L_R\lambda_{Sa} - M\Big(+\lambda_{Ra}\cos(\theta_R) - \lambda_{Rb}\sin(\theta_R)\Big)\Big)\\
i_{Sb} &= \frac{1}{\sigma L_S L_R}\Big(L_R\lambda_{Sb} - M\Big(+\lambda_{Ra}\sin(\theta_R) + \lambda_{Rb}\cos(\theta_R)\Big)\Big)\\
i_{Ra} &= \frac{1}{\sigma L_S L_R}\Big(L_S\lambda_{Ra} - M\Big(+\lambda_{Sa}\cos(\theta_R) + \lambda_{Sb}\sin(\theta_R)\Big)\Big)\\
i_{Rb} &= \frac{1}{\sigma L_S L_R}\Big(L_S\lambda_{Rb} - M\Big(-\lambda_{Sa}\sin(\theta_R) + \lambda_{Sb}\cos(\theta_R)\Big)\Big).
\end{aligned}$$

Use this to find an expression for the field energy and torque in terms of $\lambda_{Sa}, \lambda_{Sb}, \lambda_{Ra}, \lambda_{Rb}$, *and* θ_R.

Problem 17 Co-energy

Verify equation (6.48).

Problem 18 Co-energy

Verify equation (6.50).

Problem 19 Energy, Co-energy, and Torque in Synchronous Machines

Use the equations (6.35) and (6.36) to compute the field energy and the co-energy in a two-phase wound rotor synchronous machine. Use $\tau = \partial W_{field}/\partial\theta_R$ *to obtain an expression for the torque put out by this machine and compare it with the expression (6.37).*

Problem 20 Specifying the Derivatives of the Induction Motor Model

Prove that given any state $i_{Sa}, i_{Sb}, i_{Ra}, i_{Rb}$, *and* θ_R *of the motor, the derivatives* di_{Sa}/dt, di_{Sb}/dt, di_{Ra}/dt, di_{Rb}/dt, *and* $d\theta_R/dt$ *can be arbitrarily chosen by appropriately choosing* $u_{Sa}, u_{Sb}, u_{Ra}, u_{Rb}$, *and* τ_L.

www.EngineeringEBooksPdf.com

This Page Intentionally Left Blank

www.EngineeringEBooksPdf.com

7

Symmetric Balanced Three-Phase AC Machines

The mathematical models of two-phase induction and synchronous machines have been derived. In this chapter, the mathematical models of *three-phase* induction and permanent magnet synchronous machines are developed. From the three-phase models, two-phase equivalent models are derived. A classical steady-state analysis of the induction motor is also presented including the development of an equivalent circuit from the nonlinear differential equation model. Finally, the chapter concludes with a discussion on why power systems are three-phase systems with sinusoidal voltages operating at 60 Hz is presented.

7.1 Mathematical Model of a Three-Phase Induction Motor

A three-phase induction motor model is now developed and its two-phase equivalent model is then derived. Figure 7.1 illustrates how the stator and rotor windings are laid out in a three-phase machine.

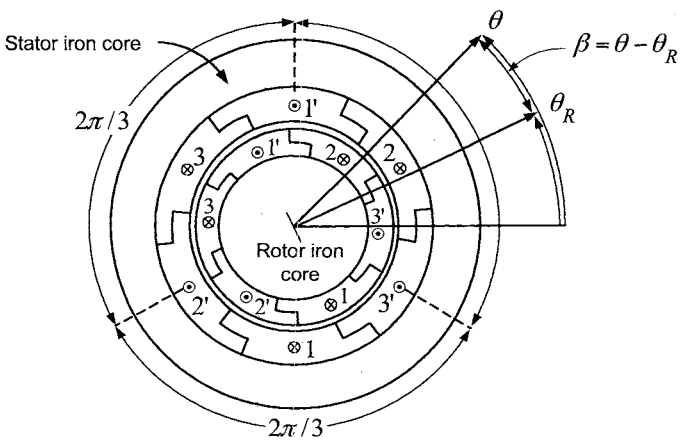


FIGURE 7.1. Cross-sectional view of a three-phase induction motor. The stator phases are $2\pi/3$ radians from each other as are the rotor phases.

www.EngineeringEBooksPdf.com

To explain the winding layout in more detail, Figure 7.2 shows stator phase 1 where it is seen that one side of a loop is wound at $\pi/3$ (the other side at $4\pi/3$), two loop sides are wound at $\pi/2$ (the other two sides at $3\pi/2$), and, finally, one loop side is wound at $2\pi/3$ (the other side at $5\pi/3$).

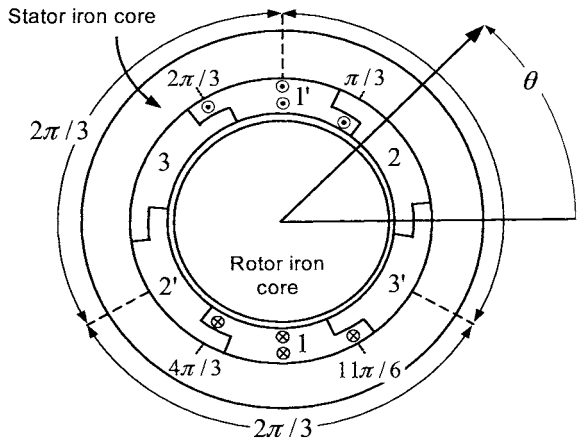


FIGURE 7.2. Cross-sectional view of stator phase 1.

Figures 7.1 and 7.2 show that the loops of the phases are wound in two layers which is a common layout in AC machines. Using Ampère's law,[1] one can straightforwardly compute the radial magnetic field in the air gap. The developed view in Figure 7.3 shows that the resulting radial magnetic field B_{S1} in the air gap due to the current i_{S1} in stator phase 1 is a staircase function that is approximately sinusoidal.

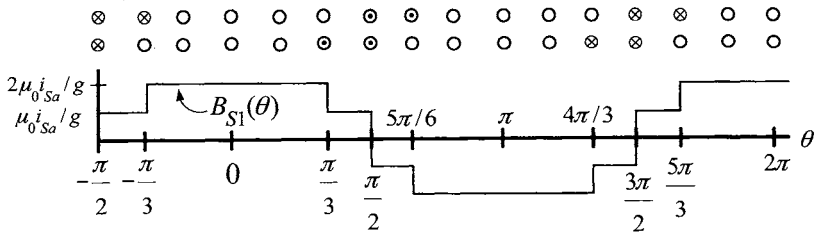


FIGURE 7.3. Developed view of the windings of stator phase 1.

The machine of Figure 7.1 (or Figure 7.2) is referred to as a *symmetric*

[1] Of course, in the use of Ampère's law, it is still assumed that the cross section of the winding is negligible in order to obtain a relatively simple analytical expression for the radial magnetic field in the air gap.

www.EngineeringEBooksPdf.com

machine because the stator phases are identical in structure only rotated $2\pi/3$ radians from each other and similarly for the rotor phases.

In order to obtain a sinusoidally (spatially) distributed magnetic field in the air gap, it will be necessary to assume that the phases are sinusoidally wound. This is now described.

Sinusoidal Windings

Let θ_R denote the rotor position taken to coincide with the magnetic axis of rotor phase 1 as shown in Figure 7.1, θ is an arbitrary angular position in the air gap so that $\beta \triangleq \theta - \theta_R$ represents the same angle with respect to the rotor position.

Now consider the three stator phases to be sinusoidally wound with their stator turns densities given by

$$\begin{aligned} N_{S1}(\theta) &= \frac{N_S}{2}|\sin(\theta)| \\ N_{S2}(\theta) &= \frac{N_S}{2}|\sin(\theta - 2\pi/3)| \\ N_{S3}(\theta) &= \frac{N_S}{2}|\sin(\theta - 4\pi/3)|\,. \end{aligned}$$

Stator phases 1 and 2 are illustrated in Figures 7.4(a) and 7.4(b), respectively.

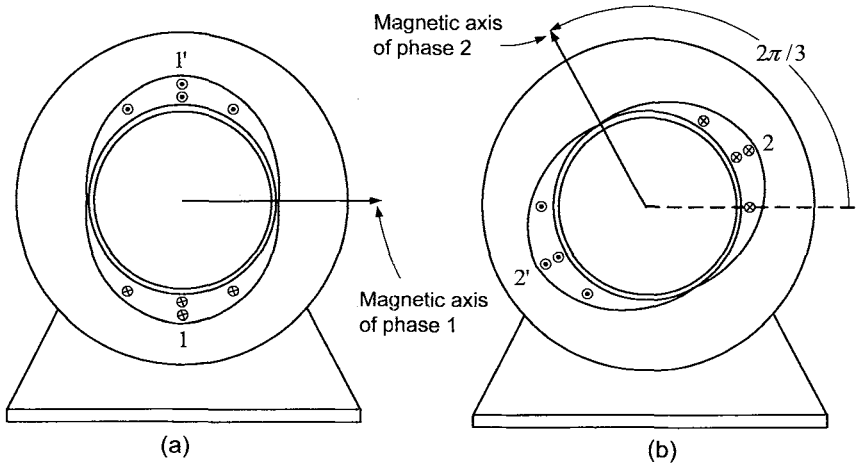


FIGURE 7.4. Sinusoidally wound stator phases. (a) Stator phase 1 windings. (b) Stator phase 2 windings.

www.EngineeringEBooksPdf.com

Similarly, the rotor turns densities are given by

$$\begin{aligned} N_{R1}(\theta - \theta_R) &= \frac{N_R}{2} |\sin(\theta - \theta_R)| \\ N_{R2}(\theta - \theta_R) &= \frac{N_R}{2} |\sin(\theta - \theta_R - 2\pi/3)| \\ N_{R3}(\theta - \theta_R) &= \frac{N_R}{2} |\sin(\theta - \theta_R - 4\pi/3)| . \end{aligned}$$

This is referred to as a symmetric machine as the windings are all identical in construction being shifted by $2\pi/3$ with respect to each other and, similarly, the rotor windings are identical in construction also being shifted by $2\pi/3$ with respect to each other. As illustrated in Figure 7.5, the stator end windings $1', 2'$, and $3'$ are tied together to form the *motor neutral* $\hat{N}$, and the stator end windings $1, 2$, and 3 are connected to the source voltages u_{S1}, u_{S2}, and u_{S3}, respectively. The other end of the source voltages are tied together to form the *source neutral* N. This is called a *wye-connected* motor. Similarly, the rotor end windings $1, 2$, and 3 are shorted (connected) together and the other rotor end windings $1', 2'$, and $3'$ are also shorted together as shown in Figure 7.6. Due to the wye connection of the stator and rotor windings, the neutrals N and $\hat{N}$ in Figures 7.5 and 7.6, respectively, are isolated so that $i_{S1} + i_{S2} + i_{S2} \equiv 0$ and $i_{R1} + i_{R2} + i_{R2} \equiv 0$.

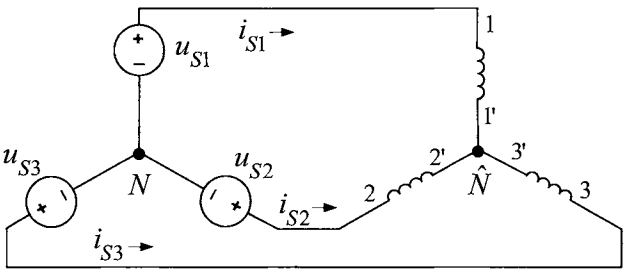


FIGURE 7.5. Wye-connected stator windings.

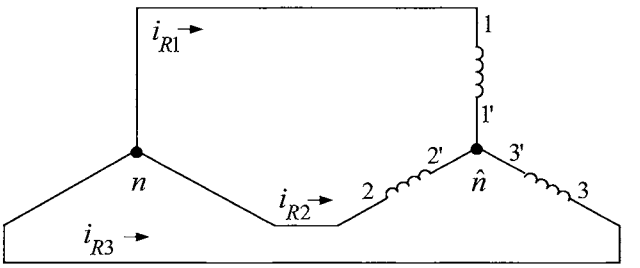


FIGURE 7.6. Wye-connected rotor windings.

www.EngineeringEBooksPdf.com

The stator magnetic field is the vector sum of the fields due to each phase. These fields are

$$\begin{aligned}
\vec{\mathbf{B}}_{S1}(i_{S1}, r, \theta) &= \frac{\mu_0 N_S}{2g}\frac{r_R}{r} i_{S1}\cos(\theta)\hat{\mathbf{r}} \\
\vec{\mathbf{B}}_{S2}(i_{S2}, r, \theta) &= \frac{\mu_0 N_S}{2g}\frac{r_R}{r} i_{S2}\cos(\theta - 2\pi/3)\hat{\mathbf{r}} \\
\vec{\mathbf{B}}_{S3}(i_{S3}, r, \theta) &= \frac{\mu_0 N_S}{2g}\frac{r_R}{r} i_{S3}\cos(\theta - 4\pi/3)\hat{\mathbf{r}}
\end{aligned}$$

so that

$$\begin{aligned}
\vec{\mathbf{B}}_S(i_{S1}, i_{S2}, i_{S3}, r, \theta) &= \frac{\mu_0 N_S}{2g}\frac{r_R}{r}\Big(i_{S1}\cos(\theta) + i_{S2}\cos(\theta - 2\pi/3) \\
&\quad + i_{S3}\cos(\theta - 4\pi/3)\Big)\hat{\mathbf{r}}. \qquad (7.1)
\end{aligned}$$

If the balanced[2] three-phase set of currents

$$\begin{aligned}
i_{S1} &= I_S\cos(\omega_S t) \\
i_{S2} &= I_S\cos(\omega_S t - 2\pi/3) \\
i_{S3} &= I_S\cos(\omega_S t - 4\pi/3)
\end{aligned}$$

are applied to the stator phases, the corresponding stator magnetic field can be written as

$$\begin{aligned}
\vec{\mathbf{B}}_S(I_S, r, \theta, t) &= \frac{\mu_0 N_S I_S}{2g}\frac{r_R}{r}\Big(\cos(\omega_S t)\cos(\theta) + \cos(\omega_S t - \frac{2\pi}{3})\cos(\theta - \frac{2\pi}{3}) \\
&\quad + \cos(\omega_S t - \frac{4\pi}{3})\cos(\theta - 4\pi/3)\Big)\hat{\mathbf{r}} \\
&= \frac{\mu_0 N_S I_S}{2g}\frac{r_R}{r}\frac{3}{2}\cos(\theta - \omega_S t)\hat{\mathbf{r}}.
\end{aligned}$$

That is, with balanced three-phase currents, a radial rotating magnetic field is established in the air gap.

Similarly, the magnetic fields due to the rotor currents are given by

$$\begin{aligned}
\vec{\mathbf{B}}_{R1}(i_{R1}, r, \theta) &= \frac{\mu_0 N_R}{2g}\frac{r_R}{r} i_{R1}\cos(\theta - \theta_R)\hat{\mathbf{r}} \\
\vec{\mathbf{B}}_{R2}(i_{R2}, r, \theta) &= \frac{\mu_0 N_R}{2g}\frac{r_R}{r} i_{R2}\cos(\theta - \theta_R - 2\pi/3)\hat{\mathbf{r}} \\
\vec{\mathbf{B}}_{R3}(i_{R3}, r, \theta) &= \frac{\mu_0 N_R}{2g}\frac{r_R}{r} i_{R3}\cos(\theta - \theta_R - 4\pi/3)\hat{\mathbf{r}}
\end{aligned}$$

[2]Balanced just means $i_{S1} + i_{S2} + i_{S3} \equiv 0$.

www.EngineeringEBooksPdf.com

so that, with $\beta = \theta - \theta_R$,

$$\begin{aligned}
&\vec{\mathbf{B}}_R(i_{R1}, i_{R2}, i_{R3}, r, \beta) \\
&= \frac{\mu_0 N_R}{2g}\frac{r_R}{r}\Big(i_{R1}\cos(\theta - \theta_R) + i_{R2}\cos(\theta - \theta_R - 2\pi/3) \\
&\quad + i_{R3}\cos(\theta - \theta_R - 4\pi/3)\Big)\hat{\mathbf{r}} \\
&= \frac{\mu_0 N_R}{2g}\frac{r_R}{r}\Big(i_{R1}\cos(\beta) + i_{R2}\cos(\beta - 2\pi/3) + i_{R3}\cos(\beta - 4\pi/3)\Big)\hat{\mathbf{r}}.
\end{aligned} \tag{7.2}$$

As explained in the previous chapter, the coupling factor κ is included in the expression for $\vec{\mathbf{B}}_R$ on the *stator side* of the air gap and is included in the expression for $\vec{\mathbf{B}}_S$ on the *rotor side* of the air gap to account for the spreading (leakage) of the magnetic field from the radial direction as one goes across the air gap. That is, with $\vec{\mathbf{B}}_S$ and $\vec{\mathbf{B}}_R$ given by (7.1) and (7.2) respectively, the total radial magnetic field $\vec{\mathbf{B}}$ on the stator side of the air gap is taken as

$$\begin{aligned}
\vec{\mathbf{B}}(i_{S1}, i_{S2}, i_{S3}, i_{R1}, i_{R2}, i_{R3}, r_S, \theta, \theta_R) \triangleq\ & \vec{\mathbf{B}}_S(i_{S1}, i_{S2}, i_{S3}, r_S, \theta) \\
& + \kappa\vec{\mathbf{B}}_R(i_{R1}, i_{R2}, i_{R3}, r_S, \theta - \theta_R).
\end{aligned} \tag{7.3}$$

On the rotor side of the air gap, the total radial magnetic field $\vec{\mathbf{B}}$ is taken as

$$\begin{aligned}
\vec{\mathbf{B}}(i_{S1}, i_{S2}, i_{S3}, i_{R1}, i_{R2}, i_{R3}, r_R, \theta, \theta_R) \triangleq\ & \kappa\vec{\mathbf{B}}_S(i_{S1}, i_{S2}, i_{S3}, r_R, \theta) \\
& + \vec{\mathbf{B}}_R(i_{R1}, i_{R2}, i_{R3}, r_R, \theta - \theta_R)
\end{aligned}$$

or, in terms of $\beta = \theta - \theta_R$ and an abuse of notation,

$$\begin{aligned}
\vec{\mathbf{B}}(i_{S1}, i_{S2}, i_{S3}, i_{R1}, i_{R2}, i_{R3}, r_R, \beta, \theta_R) \triangleq\ & \kappa\vec{\mathbf{B}}_S(i_{S1}, i_{S2}, i_{S3}, r_R, \beta + \theta_R) \\
& + \vec{\mathbf{B}}_R(i_{R1}, i_{R2}, i_{R3}, r_R, \beta).
\end{aligned} \tag{7.4}$$

www.EngineeringEBooksPdf.com

Stator Flux Linkages

Using (7.3) for $\vec{\mathbf{B}}$ on the stator side of the air gap, the stator flux linkages are given by (see problem 1)

$$\begin{aligned}\psi_{S1}(t) &= \int_0^{\pi} \frac{N_S}{2}\sin(\theta) \\ &\quad \times \left(\int_{\theta-\pi}^{\theta} \ell_1 r_S B(i_{S1}, i_{S2}, i_{S3}, i_{R1}, i_{R2}, i_{R3}, r_S, \theta', \theta_R)d\theta'\right)d\theta \\ &= \frac{2}{3}L_S(i_{S1} + i_{S2}\cos(2\pi/3) + i_{S3}\cos(4\pi/3)) \\ &\quad + \frac{2}{3}M\Big(i_{R1}\cos(\theta_R) + i_{R2}\cos(\theta_R + 2\pi/3) + i_{R3}\cos(\theta_R + 4\pi/3)\Big)\end{aligned} \tag{7.5}$$

$$\begin{aligned}\psi_{S2}(t) &= \int_{2\pi/3}^{2\pi/3+\pi} \frac{N_S}{2}\sin(\theta - 2\pi/3) \\ &\quad \times \left(\int_{\theta-\pi}^{\theta} \ell_1 r_S B(i_{S1}, i_{S2}, i_{S3}, i_{R1}, i_{R2}, i_{R3}, r_S, \theta', \theta_R)d\theta'\right)d\theta \\ &= \frac{2}{3}L_S(i_{S1}\cos(2\pi/3) + i_{S2} + i_{S3}\cos(2\pi/3)) \\ &\quad + \frac{2}{3}M\Big(i_{R1}\cos(\theta_R - 2\pi/3) + i_{R2}\cos(\theta_R) + i_{R3}\cos(\theta_R + 2\pi/3)\Big)\end{aligned} \tag{7.6}$$

$$\begin{aligned}\psi_{S3}(t) &= \int_{4\pi/3}^{4\pi/3+\pi} \frac{N_S}{2}\sin(\theta - 4\pi/3) \\ &\quad \times \left(\int_{\theta-\pi}^{\theta} \ell_1 r_S B(i_{S1}, i_{S2}, i_{S3}, i_{R1}, i_{R2}, i_{R3}, r_S, \theta', \theta_R)d\theta'\right)d\theta \\ &= \frac{2}{3}L_S(i_{S1}\cos(4\pi/3) + i_{S2}\cos(2\pi/3) + i_{S3}) \\ &\quad + \frac{2}{3}M\Big(i_{R1}\cos(\theta_R - 4\pi/3) + i_{R2}\cos(\theta_R - 2\pi/3) + i_{R3}\cos(\theta_R)\Big)\end{aligned} \tag{7.7}$$

where

$$\begin{aligned}L_S &\triangleq \frac{3}{2}\frac{\pi\mu_0\ell_1\ell_2 N_S^2}{8g} \\ M &\triangleq \frac{3}{2}\kappa\frac{\pi\mu_0\ell_1\ell_2 N_S N_R}{8g} \\ L_R &\triangleq \frac{3}{2}\frac{\pi\mu_0\ell_1\ell_2 N_R^2}{8g}.\end{aligned} \tag{7.8}$$

www.EngineeringEBooksPdf.com

The reason for the factor 2/3 in equations (7.5), (7.6), and (7.7), and the factor 3/2 in the expressions for L_S, M, and L_R in (7.8) are so that the expressions (7.8) represent the *two-phase equivalent* coefficients of inductances in the two-phase equivalent model as will be shown below. In matrix form, the flux linkages may be written as

$$\begin{bmatrix} \psi_{S1}(t) \\ \psi_{S2}(t) \\ \psi_{S3}(t) \end{bmatrix} = \frac{2}{3}L_S \begin{bmatrix} 1 & \cos(2\pi/3) & \cos(4\pi/3) \\ \cos(2\pi/3) & 1 & \cos(2\pi/3) \\ \cos(4\pi/3) & \cos(-2\pi/3) & 1 \end{bmatrix} \begin{bmatrix} i_{S1}(t) \\ i_{S2}(t) \\ i_{S3}(t) \end{bmatrix}$$
$$+ \frac{2}{3}M \begin{bmatrix} \cos(\theta_R) & \cos(\theta_R + 2\pi/3) & \cos(\theta_R + 4\pi/3) \\ \cos(\theta_R - 2\pi/3) & \cos(\theta_R) & \cos(\theta_R + 2\pi/3) \\ \cos(\theta_R - 4\pi/3) & \cos(\theta_R - 2\pi/3) & \cos(\theta_R) \end{bmatrix} \begin{bmatrix} i_{R1}(t) \\ i_{R2}(t) \\ i_{R3}(t) \end{bmatrix}. \tag{7.9}$$

Note that $\theta_R - 4\pi/3 = \theta_R - 2\pi + 2\pi/3$ so that $\cos(\theta_R - 4\pi/3) = \cos(\theta_R + 2\pi/3)$. With the obvious definitions for the matrices C_1 and $C_2(\theta_R)$, the flux linkages are written more compactly as

$$\begin{bmatrix} \psi_{S1}(t) \\ \psi_{S2}(t) \\ \psi_{S3}(t) \end{bmatrix} = C_1 \begin{bmatrix} i_{S1}(t) \\ i_{S2}(t) \\ i_{S3}(t) \end{bmatrix} + C_2(\theta_R) \begin{bmatrix} i_{R1}(t) \\ i_{R2}(t) \\ i_{R3}(t) \end{bmatrix}. \tag{7.10}$$

Rotor Flux Linkages

Using (7.4) for $\vec{\mathbf{B}}$ on the rotor side of the air gap, the rotor flux linkages are given by (see problem 2)

$$\begin{aligned} \psi_{R1}(t) &= \int_0^{\pi} \frac{N_R}{2} \sin(\beta) \\ &\quad \times \left(\int_{\beta-\pi}^{\beta} \ell_1 r_R B(i_{S1}, i_{S2}, i_{S3}, i_{R1}, i_{R2}, i_{R3}, r_R, \beta', \theta_R) d\beta' \right) d\beta \\ &= \frac{2}{3}L_R(i_{R1} + i_{SR2}\cos(2\pi/3) + i_{R1}\cos(4\pi/3)) \\ &\quad + \frac{2}{3}M\Big(i_{S1}\cos(\theta_R) + i_{S2}\cos(\theta_R - 2\pi/3) + i_{S3}\cos(\theta_R - 4\pi/3)\Big) \end{aligned} \tag{7.11}$$

www.EngineeringEBooksPdf.com

$$\psi_{R2}(t) = \int_{2\pi/3}^{2\pi/3+\pi} \frac{N_R}{2} \sin(\beta - 2\pi/3) \times \left(\int_{\beta-\pi}^{\beta} \ell_1 r_R B(i_{S1}, i_{S2}, i_{S3}, i_{R1}, i_{R2}, i_{R3}, r_R, \beta', \theta_R) d\beta' \right) d\beta$$
$$= \frac{2}{3} L_R (i_{R1} \cos(2\pi/3) + i_{R2} + i_{R3} \cos(2\pi/3)) + \frac{2}{3} M \Big(i_{S1} \cos(\theta_R + 2\pi/3) + i_{S2} \cos(\theta_R) + i_{S3} \cos(\theta_R - 2\pi/3) \Big) \tag{7.12}$$

$$\psi_{R3}(t) = \int_{4\pi/3}^{4\pi/3+\pi} \frac{N_R}{2} \sin(\beta - 4\pi/3) \times \left(\int_{\beta-\pi}^{\beta} \ell_1 r_R B(i_{S1}, i_{S2}, i_{S3}, i_{R1}, i_{R2}, i_{R3}, r_R, \beta', \theta_R) d\beta' \right) d\beta$$
$$= \frac{2}{3} L_R (i_{R1} \cos(4\pi/3) + i_{R2} \cos(2\pi/3) + i_{R3}) + \frac{2}{3} M \Big(i_{S1} \cos(\theta_R + 4\pi/3) + i_{S2} \cos(\theta_R + 2\pi/3) + i_{S3} \cos(\theta_R) \Big) . \tag{7.13}$$

In matrix form, the rotor flux linkages may be written as

$$\begin{bmatrix} \psi_{R1}(t) \\ \psi_{R2}(t) \\ \psi_{R3}(t) \end{bmatrix} = \frac{2}{3} L_R \begin{bmatrix} 1 & \cos(2\pi/3) & \cos(4\pi/3) \\ \cos(2\pi/3) & 1 & \cos(2\pi/3) \\ \cos(4\pi/3) & \cos(2\pi/3) & 1 \end{bmatrix} \begin{bmatrix} i_{R1}(t) \\ i_{R2}(t) \\ i_{R3}(t) \end{bmatrix}$$
$$+ \frac{2}{3} M \begin{bmatrix} \cos(\theta_R) & \cos(\theta_R - 2\pi/3) & \cos(\theta_R - 4\pi/3) \\ \cos(\theta_R + 2\pi/3) & \cos(\theta_R) & \cos(\theta_R - 2\pi/3) \\ \cos(\theta_R + 4\pi/3) & \cos(\theta_R + 2\pi/3) & \cos(\theta_R) \end{bmatrix} \begin{bmatrix} i_{S1}(t) \\ i_{S2}(t) \\ i_{S3}(t) \end{bmatrix} \tag{7.14}$$

or, more compactly,

$$\begin{bmatrix} \psi_{R1}(t) \\ \psi_{R2}(t) \\ \psi_{R3}(t) \end{bmatrix} = C_1 \begin{bmatrix} i_{R1}(t) \\ i_{R2}(t) \\ i_{R3}(t) \end{bmatrix} + C_2(-\theta_R) \begin{bmatrix} i_{S1}(t) \\ i_{S2}(t) \\ i_{S3}(t) \end{bmatrix} \tag{7.15}$$

where C_1 and C_2 are defined as in (7.10).

Balanced Conditions

As described above, the source voltages $u_{S1}(t), u_{S2}(t)$, and $u_{S3}(t)$ are wye connected as are the stator and rotor phases (see Figures 7.5 and 7.6). Consequently, it is always true that

$$i_{S1}(t) + i_{S2}(t) + i_{S3}(t) \equiv 0$$

www.EngineeringEBooksPdf.com

$$i_{R1}(t) + i_{R2}(t) + i_{R3}(t) \equiv 0.$$

The currents are then said to be *balanced* as they sum up to zero.

Using (7.10) and (7.15) it is straightforward to show that the stator and rotor fluxes are always balanced, that is,

$$\begin{aligned} \psi_{S1}(t) + \psi_{S2}(t) + \psi_{S3}(t) &\equiv 0 \\ \psi_{R1}(t) + \psi_{R2}(t) + \psi_{R3}(t) &\equiv 0. \end{aligned}$$

(Note that these two equations hold whether or not the currents are balanced. See problem 4.)

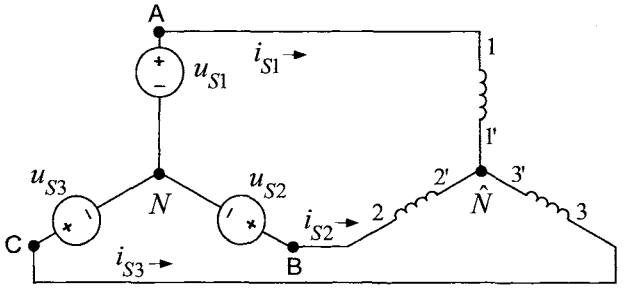


FIGURE 7.7. Wye-connected stator windings.

Referring to Figure 7.7, let $v_{A\hat{N}} = v_A - v_{\hat{N}}$, $v_{B\hat{N}}(t) = v_B - v_{\hat{N}}$, and $v_{C\hat{N}}(t) = v_C - v_{\hat{N}}$ denote the phase to *motor neutral* voltages. Faraday's and Ohm's laws give

$$\begin{aligned} v_{A\hat{N}} &= R_S i_{S1} + \frac{d\psi_{S1}(t)}{dt} \\ v_{B\hat{N}} &= R_S i_{S2} + \frac{d\psi_{S2}(t)}{dt} \\ v_{C\hat{N}} &= R_S i_{S3} + \frac{d\psi_{S3}(t)}{dt}. \end{aligned}$$

Adding these three equations results in

$$\begin{aligned} v_{A\hat{N}} + v_{B\hat{N}} + v_{C\hat{N}} &= R_S\left(i_{S1} + i_{S2} + i_{S3}\right) + \frac{d}{dt}\left(\psi_{S1}(t) + \psi_{S2}(t) + \psi_{S3}(t)\right) \\ &\equiv 0. \end{aligned}$$

That is, the phase to motor neutral voltages are always balanced. However, the voltages that are applied to the motor are the phase to *source neutral* voltages $u_{S1}(t), u_{S2}(t)$, and $u_{S3}(t)$. The next lemma relates the motor voltages $v_{A\hat{N}}, v_{B\hat{N}}$, and $v_{C\hat{N}}$ to the source voltages $u_{S1}(t), u_{S2}(t)$, and $u_{S3}(t)$ in terms of the voltage drop $v_{\hat{N}N}$ from the motor neutral to the source neutral.

www.EngineeringEBooksPdf.com

Lemma
Let $v_{\hat{N}N} \triangleq v_{\hat{N}} - v_N$, then

$$v_{\hat{N}N} = \frac{u_{S1}(t) + u_{S2}(t) + u_{S3}(t)}{3}.$$

Proof[3]
Referring to Figure 7.7, write

$$\begin{aligned} u_{S1}(t) &= v_A - v_N = v_{A\hat{N}} + v_{\hat{N}N} \\ u_{S2}(t) &= v_B - v_N = v_{B\hat{N}} + v_{\hat{N}N} \\ u_{S3}(t) &= v_C - v_N = v_{C\hat{N}} + v_{\hat{N}N} \end{aligned}$$

and adding up these three equations, one obtains

$$\begin{aligned} u_{S1}(t) + u_{S2}(t) + u_{S3}(t) &= v_{A\hat{N}} + v_{B\hat{N}}(t) + v_{C\hat{N}}(t) + 3v_{\hat{N}N} \\ &= 3v_{\hat{N}N} \end{aligned}$$

or

$$v_{\hat{N}N} = \frac{u_{S1}(t) + u_{S2}(t) + u_{S3}(t)}{3}.$$

From this result, the following corollary is easily seen to be true.

Corollary
If the source voltages are balanced, that is,

$$u_{S1}(t) + u_{S2}(t) + u_{S3}(t) \equiv 0$$

then

$$v_{\hat{N}N} \equiv 0$$

so that

$$\begin{aligned} u_{S1}(t) &= v_{A\hat{N}} \\ u_{S2}(t) &= v_{B\hat{N}} \\ u_{S3}(t) &= v_{C\hat{N}}. \end{aligned}$$

By the above lemma, it follows that for a wye-connected motor,

$$\begin{aligned} v_{A\hat{N}} &= u_{S1}(t) - v_{\hat{N}N} = R_S i_{S1} + \frac{d\psi_{S1}(t)}{dt} \\ v_{B\hat{N}} &= u_{S2}(t) - v_{\hat{N}N} = R_S i_{S2} + \frac{d\psi_{S2}(t)}{dt} \\ v_{C\hat{N}} &= u_{S3}(t) - v_{\hat{N}N} = R_S i_{S3} + \frac{d\psi_{S3}(t)}{dt} \end{aligned} \tag{7.16}$$

where $v_{\hat{N}N} = 0$ if the source voltages are balanced.

[3] See, for example, Appendix 4.1 of Murphy and Turnbull [9].

www.EngineeringEBooksPdf.com

Three-Phase to Two-Phase Transformation

Define a *three-phase to two-phase* transformation of the voltages by

$$\begin{bmatrix} u_{Sa}(t) \\ u_{Sb}(t) \\ u_{S0}(t) \end{bmatrix} \triangleq \sqrt{\frac{2}{3}} \begin{bmatrix} 1 & \cos(2\pi/3) & \cos(4\pi/3) \\ 0 & \sin(2\pi/3) & \sin(4\pi/3) \\ 1/\sqrt{2} & 1/\sqrt{2} & 1/\sqrt{2} \end{bmatrix} \begin{bmatrix} u_{S1}(t) \\ u_{S2}(t) \\ u_{S3}(t) \end{bmatrix}$$
$$= \sqrt{\frac{2}{3}} \begin{bmatrix} 1 & -1/2 & -1/2 \\ 0 & \sqrt{3}/2 & -\sqrt{3}/2 \\ 1/\sqrt{2} & 1/\sqrt{2} & 1/\sqrt{2} \end{bmatrix} \begin{bmatrix} u_{S1}(t) \\ u_{S2}(t) \\ u_{S3}(t) \end{bmatrix}.$$

If the source voltages are balanced,

$$u_{S0}(t) \triangleq \frac{1}{\sqrt{3}} (u_{S1}(t) + u_{S2}(t) + u_{S3}(t)) \equiv 0.$$

The inverse transformation is given by

$$\begin{bmatrix} u_{S1}(t) \\ u_{S2}(t) \\ u_{S3}(t) \end{bmatrix} = \sqrt{\frac{3}{2}} \begin{bmatrix} 2/3 & 0 & \sqrt{2}/3 \\ -1/3 & 1/\sqrt{3} & \sqrt{2}/3 \\ -1/3 & -1/\sqrt{3} & \sqrt{2}/3 \end{bmatrix} \begin{bmatrix} u_{Sa}(t) \\ u_{Sb}(t) \\ u_{S0}(t) \end{bmatrix}.$$

Denote the *3-2* transformation matrix as Q, that is,

$$Q \triangleq \sqrt{\frac{2}{3}} \begin{bmatrix} 1 & -1/2 & -1/2 \\ 0 & \sqrt{3}/2 & -\sqrt{3}/2 \\ 1/\sqrt{2} & 1/\sqrt{2} & 1/\sqrt{2} \end{bmatrix} \tag{7.17}$$

with inverse

$$Q^{-1} = \sqrt{\frac{3}{2}} \begin{bmatrix} 2/3 & 0 & \sqrt{2}/3 \\ -1/3 & +1/\sqrt{3} & \sqrt{2}/3 \\ -1/3 & -1/\sqrt{3} & \sqrt{2}/3 \end{bmatrix}. \tag{7.18}$$

Q is an *orthogonal* matrix, that is, $Q^{-1} = Q^T$. Define

$$\begin{bmatrix} i_{Sa}(t) \\ i_{Sb}(t) \\ i_{S0}(t) \end{bmatrix} \triangleq Q \begin{bmatrix} i_{S1}(t) \\ i_{S2}(t) \\ i_{S3}(t) \end{bmatrix}, \quad \begin{bmatrix} i_{Ra}(t) \\ i_{Rb}(t) \\ i_{R0}(t) \end{bmatrix} \triangleq Q \begin{bmatrix} i_{R1}(t) \\ i_{R2}(t) \\ i_{R3}(t) \end{bmatrix}$$
$$\begin{bmatrix} \lambda_{Sa}(t) \\ \lambda_{Sb}(t) \\ \lambda_{S0}(t) \end{bmatrix} \triangleq Q \begin{bmatrix} \psi_{S1}(t) \\ \psi_{S2}(t) \\ \psi_{S3}(t) \end{bmatrix}, \quad \begin{bmatrix} \lambda_{Ra}(t) \\ \lambda_{Rb}(t) \\ \lambda_{R0}(t) \end{bmatrix} \triangleq Q \begin{bmatrix} \psi_{R1}(t) \\ \psi_{R2}(t) \\ \psi_{R3}(t) \end{bmatrix}.$$

As shown in problem 4,

$$\lambda_{S0}(t) = \frac{1}{\sqrt{3}} (\psi_{S1}(t) + \psi_{S2}(t) + \psi_{S3}(t)) \equiv 0$$
$$\lambda_{R0}(t) = \frac{1}{\sqrt{3}} (\psi_{R1}(t) + \psi_{R2}(t) + \psi_{R3}(t)) \equiv 0.$$

www.EngineeringEBooksPdf.com

As the phases are wye connected, it follows that

$$\begin{aligned} i_{S0}(t) &= \frac{1}{\sqrt{3}}\left(i_{S1}(t)+i_{S2}(t)+i_{S3}(t)\right)\equiv 0 \\ i_{R0}(t) &= \frac{1}{\sqrt{3}}\left(i_{R1}(t)+i_{R2}(t)+i_{R3}(t)\right)\equiv 0. \end{aligned}$$

Remark If in addition the source voltages are balanced, it also follows that

$$u_{S0}(t)=\frac{1}{\sqrt{3}}\left(u_{S1}(t)+u_{S2}(t)+u_{S3}(t)\right)\equiv 0.$$

That is, when the source voltages are balanced, all of the so-called *zero sequence* quantities $i_{S0}(t), i_{R0}(t), \lambda_{S0}(t), \lambda_{R0}(t)$, and $u_{S0}(t)$ are identically zero under the transformation Q and the original three-phase model consisting of the three phases $1, 2$, and 3 is now reduced to an *equivalent two-phase model* consisting of the phases a and b. This is not surprising as the balanced conditions imply that there are only two independent variables (e.g., if $u_{S1}(t)$ and $u_{S2}(t)$ are given, then $u_{S3}(t) = -\left(u_{S1}(t)+u_{S2}(t)\right)$ is determined).

In the case when the source voltages are not balanced, the phase to neutral voltages of the machine $v_{A\hat{N}}, v_{B\hat{N}}$, and $v_{C\hat{N}}$ transform as

$$\begin{bmatrix} u_{Sa}(t) \\ u_{Sb}(t) \\ u_{S0}(t)-\sqrt{3}v_{\hat{N}N} \end{bmatrix} = \sqrt{\frac{2}{3}} \begin{bmatrix} 1 & -1/2 & -1/2 \\ 0 & \sqrt{3}/2 & -\sqrt{3}/2 \\ 1/\sqrt{2} & 1/\sqrt{2} & 1/\sqrt{2} \end{bmatrix} \begin{bmatrix} u_{S1}(t)-v_{\hat{N}N} \\ u_{S2}(t)-v_{\hat{N}N} \\ u_{S3}(t)-v_{\hat{N}N} \end{bmatrix}.$$

and the dynamic equations for the stator flux linkages (7.16) then transform to

$$\begin{aligned} u_{Sa}(t) &= R_S i_{Sa}+\frac{d\lambda_{Sa}(t)}{dt} \\ u_{Sb}(t) &= R_S i_{Sb}+\frac{d\lambda_{Sb}(t)}{dt} \\ u_{S0}(t)-\sqrt{3}v_{\hat{N}N} &= R_S i_{S0}+\frac{d\lambda_{S0}(t)}{dt}. \end{aligned} \tag{7.19}$$

To find the expressions for the two-phase equivalent flux linkages in terms of the two-phase equivalent currents, recall that

$$\begin{bmatrix} \psi_{S1}(t) \\ \psi_{S2}(t) \\ \psi_{S3}(t) \end{bmatrix} = C_1 \begin{bmatrix} i_{S1}(t) \\ i_{S2}(t) \\ i_{S3}(t) \end{bmatrix} + C_2(\theta_R) \begin{bmatrix} i_{R1}(t) \\ i_{R2}(t) \\ i_{R3}(t) \end{bmatrix}$$

so that

$$\begin{bmatrix} \lambda_{Sa}(t) \\ \lambda_{Sb}(t) \\ \lambda_{S0}(t) \end{bmatrix} = QC_1Q^{-1} \begin{bmatrix} i_{Sa}(t) \\ i_{Sb}(t) \\ i_{S0}(t) \end{bmatrix} + QC_2(\theta_R)Q^{-1} \begin{bmatrix} i_{Ra}(t) \\ i_{Rb}(t) \\ i_{R0}(t) \end{bmatrix}$$

www.EngineeringEBooksPdf.com

$$= \begin{bmatrix} L_S & 0 & 0 \\ 0 & L_S & 0 \\ 0 & 0 & 0 \end{bmatrix} \begin{bmatrix} i_{Sa}(t) \\ i_{Sb}(t) \\ i_{S0}(t) \end{bmatrix} + \begin{bmatrix} M\cos(\theta_R) & -M\sin(\theta_R) & 0 \\ M\sin(\theta_R) & M\cos(\theta_R) & 0 \\ 0 & 0 & 0 \end{bmatrix} \begin{bmatrix} i_{Ra}(t) \\ i_{Rb}(t) \\ i_{R0}(t) \end{bmatrix} \tag{7.20}$$

or

$$\begin{aligned} \lambda_{Sa}(t) &= L_S i_{Sa}(t) + M\Big(i_{Ra}(t)\cos(\theta_R) - i_{Rb}(t)\sin(\theta_R)\Big) \\ \lambda_{Sb}(t) &= L_S i_{Sb}(t) + M\Big(i_{Ra}(t)\sin(\theta_R) + i_{Rb}(t)\cos(\theta_R)\Big) \\ \lambda_{S0} &\equiv 0. \end{aligned} \tag{7.21}$$

Similarly, the rotor flux linkages satisfy the system of equations

$$\begin{aligned} 0 &= R_R i_{R1} + \frac{d\psi_{R1}(t)}{dt} \\ 0 &= R_R i_{R2} + \frac{d\psi_{R2}(t)}{dt} \\ 0 &= R_R i_{R3} + \frac{d\psi_{R3}(t)}{dt} \end{aligned}$$

so that multiplying this system of equations through by Q results in

$$\begin{aligned} 0 &= R_R i_{Ra} + \frac{d\lambda_{Ra}(t)}{dt} \\ 0 &= R_R i_{Rb} + \frac{d\lambda_{Rb}(t)}{dt} \\ 0 &= R_R i_{R0} + \frac{d\lambda_{R0}(t)}{dt} \end{aligned} \tag{7.22}$$

where $i_{R0} \equiv 0, \lambda_{R0}(t) \equiv 0$. Also, as

$$\begin{bmatrix} \psi_{R1}(t) \\ \psi_{R2}(t) \\ \psi_{R3}(t) \end{bmatrix} = C_1 \begin{bmatrix} i_{R1}(t) \\ i_{R2}(t) \\ i_{R3}(t) \end{bmatrix} + C_2(-\theta_R) \begin{bmatrix} i_{S1}(t) \\ i_{S2}(t) \\ i_{S3}(t) \end{bmatrix}$$

it follows that

$$\begin{aligned} \begin{bmatrix} \lambda_{Ra}(t) \\ \lambda_{Rb}(t) \\ \lambda_{R0}(t) \end{bmatrix} &= QC_1Q^{-1} \begin{bmatrix} i_{Ra}(t) \\ i_{Rb}(t) \\ i_{R0}(t) \end{bmatrix} + QC_2(-\theta_R)Q^{-1} \begin{bmatrix} i_{Sa}(t) \\ i_{Sb}(t) \\ i_{S0}(t) \end{bmatrix} \\ &= \begin{bmatrix} L_R & 0 & 0 \\ 0 & L_R & 0 \\ 0 & 0 & 0 \end{bmatrix} \begin{bmatrix} i_{Ra}(t) \\ i_{Rb}(t) \\ i_{R0}(t) \end{bmatrix} \\ &\quad + \begin{bmatrix} M\cos(\theta_R) & M\sin(\theta_R) & 0 \\ -M\sin(\theta_R) & M\cos(\theta_R) & 0 \\ 0 & 0 & 0 \end{bmatrix} \begin{bmatrix} i_{Sa}(t) \\ i_{Sb}(t) \\ i_{S0}(t) \end{bmatrix} \end{aligned} \tag{7.23}$$

www.EngineeringEBooksPdf.com

or

$$\begin{aligned}
\lambda_{Ra}(t) &= L_R i_{Ra}(t) + M\Big(+i_{Sa}(t)\cos(\theta_R) + i_{Sb}(t)\sin(\theta_R)\Big) \\
\lambda_{Rb}(t) &= L_R i_{Rb}(t) + M\Big(-i_{Sa}(t)\sin(\theta_R) + i_{Sb}(t)\cos(\theta_R)\Big) \\
\lambda_{R0} &\equiv 0.
\end{aligned} \tag{7.24}$$

Collecting together equations (7.19), (7.21) and (7.24), the two-phase equivalent equations for the stator and rotor currents of a *wye connected* three-phase motor become

$$\begin{aligned}
u_{Sa} &= L_S\frac{d}{dt}i_{Sa} + M\frac{d}{dt}\Big(+i_{Ra}\cos(\theta_R) - i_{Rb}\sin(\theta_R)\Big) + R_S i_{Sa} \\
u_{Sb} &= L_S\frac{d}{dt}i_{Sb} + M\frac{d}{dt}\Big(+i_{Ra}\sin(\theta_R) + i_{Rb}\cos(\theta_R)\Big) + R_S i_{Sb} \\
u_{S0} &= \sqrt{3}v_{\hat{N}N} \\
0 &= L_R\frac{d}{dt}i_{Ra} + M\frac{d}{dt}\Big(+i_{Sa}\cos(\theta_R) + i_{Sb}\sin(\theta_R)\Big) + R_R i_{Ra} \\
0 &= L_R\frac{d}{dt}i_{Rb} + M\frac{d}{dt}\Big(-i_{Sa}\sin(\theta_R) + i_{Sb}\cos(\theta_R)\Big) + R_R i_{Rb}
\end{aligned} \tag{7.25}$$

where $i_{S0} \equiv 0, i_{R0} \equiv 0$. In what follows, it is now assumed that the voltages are balanced so that $u_{S0} = \sqrt{3}v_{\hat{N}N} \equiv 0$. In this case, there is a one-to-one correspondence between the two-phase variables i_{Sa}, i_{Sb}, i_{Ra}, i_{Rb}, u_{Sa}, and u_{Sb} and the three-phase variables i_{S1}, i_{S2}, i_{S3}, i_{R1}, i_{R2}, i_{R3}, u_{S1}, u_{S2}, and u_{S3}.

Torque

It was shown above that the stator currents established a radial magnetic field in the air gap. The torque produced by this magnetic field on the currents in the sinusoidally wound rotor phases is now computed. Recall that the stator magnetic field in terms of $\beta = \theta - \theta_R$ at $r = r_R$ is given by

$$\begin{aligned}
&\vec{\mathbf{B}}_S(i_{S1}, i_{S2}, i_{S3}, r, \beta, \theta_R)\Big|_{r=r_R} = \kappa\frac{\mu_0 N_S}{2g}\frac{r_R}{r_R}\times \\
&\Big(i_{S1}\cos(\beta+\theta_R) + i_{S2}\cos(\beta+\theta_R - 2\pi/3) + i_{S3}\cos(\beta+\theta_R - 4\pi/3)\Big)\hat{\mathbf{r}}.
\end{aligned}$$

www.EngineeringEBooksPdf.com

The torque is then (see problem 8)

$$\begin{aligned}
\vec{\tau}_{R1} &= \int_{\beta=0}^{2\pi} (r_R\hat{\mathbf{r}}) \times \left(i_{R1}(t)\frac{N_R}{2}\ \sin(\beta)d\beta(+\ell_1\hat{\mathbf{z}}) \times \left(B_{S|_{r=r_R}}\hat{\mathbf{r}}\right)\right) \\
&= \int_{\beta=0}^{2\pi} r_R i_{R1}(t)\frac{\ell_1 N_R}{2}\ \sin(\beta)\left(\kappa\frac{\mu_0 N_S}{2g}\right)\Big(i_{S1}\cos(\beta+\theta_R) \\
&\quad + (i_{S2}\cos(\beta+\theta_R-2\pi/3)+i_{S3}\cos(\beta+\theta_R-4\pi/3))\,d\beta\Big)\hat{\mathbf{z}} \\
&= \kappa\frac{r_R\ell_1\mu_0 N_R N_S}{4g} i_{R1}(t)\left(i_{S1}(-\pi\sin(\theta_R)) + i_{S2}\pi\cos(\theta_R-\frac{\pi}{6})\right. \\
&\quad \left. + i_{S3}(-\pi\cos(\theta_R+\frac{\pi}{6}))\right)\hat{\mathbf{z}} \\
&= \frac{2}{3}Mi_{R1}(t)\left(-i_{S1}\sin(\theta_R) + i_{S2}\cos(\theta_R-\frac{\pi}{6}) - i_{S3}\cos(\theta_R+\frac{\pi}{6})\right)\hat{\mathbf{z}}
\end{aligned} \tag{7.26}$$

where $M \triangleq (3/2)\kappa\pi\mu_0\ell_1\ell_2 N_S N_R/(8g)$. The torque on phase 2 of the rotor is then

$$\begin{aligned}
\vec{\tau}_{R2} &= \int_{\beta=0}^{2\pi} (r_R\hat{\mathbf{r}}) \times \left(i_{R2}(t)\frac{N_R}{2}\sin(\beta-2\pi/3)d\beta(+\ell_1\hat{\mathbf{z}}) \times \left(B_{S|_{r=r_R}}\hat{\mathbf{r}}\right)\right) \\
&= \int_{\beta=0}^{2\pi} r_R i_{R2}(t)\frac{\ell_1 N_R}{2}\sin(\beta-2\pi/3)\left(\kappa\frac{\mu_0 N_S}{2g}\right) \times \Big(i_{S1}\cos(\beta+\theta_R) \\
&\quad + i_{S2}\cos(\beta+\theta_R-2\pi/3)+i_{S3}\cos(\beta+\theta_R-4\pi/3)\Big)\,d\beta\hat{\mathbf{z}} \\
&= \kappa\frac{r_R\ell_1\mu_0 N_R N_S}{4g} i_{R2}(t)\left(i_{S1}(-\pi\cos(\theta_R+\frac{\pi}{6})) + i_{S2}(-\pi\sin(\theta_R))\right. \\
&\quad \left. + i_{S3}\pi\sin(\theta_R+\frac{\pi}{3})\right)\hat{\mathbf{z}} \\
&= \frac{2}{3}Mi_{R2}(t)\left(-i_{S1}\cos(\theta_R+\frac{\pi}{6}) - i_{S2}\sin(\theta_R) + i_{S3}\sin(\theta_R+\frac{\pi}{3})\right)\hat{\mathbf{z}}.
\end{aligned} \tag{7.27}$$

Finally, the torque on phase 3 is computed as

$$\begin{aligned}
\vec{\tau}_{R3} &= \int_{\beta=0}^{2\pi} (r_R\hat{\mathbf{r}}) \times \left(i_{R3}(t)\frac{N_R}{2}\sin(\beta-4\pi/3)d\beta(+\ell_1\hat{\mathbf{z}}) \times \left(B_{S|_{r=r_R}}\hat{\mathbf{r}}\right)\right) \\
&= \int_{\beta=0}^{2\pi} r_R i_{R3}(t)\frac{\ell_1 N_R}{2}\sin(\beta-4\pi/3)\left(\kappa\frac{\mu_0 N_S}{2g}\right) \times \Big(i_{S1}\cos(\beta+\theta_R) \\
&\quad + i_{S2}\cos(\beta+\theta_R-2\pi/3)+i_{S3}\cos(\beta+\theta_R-4\pi/3)\Big)\,d\beta\hat{\mathbf{z}}
\end{aligned}$$

www.EngineeringEBooksPdf.com

$$= \kappa \frac{r_R \ell_1 \mu_0 N_R N_S}{4g} i_{R3}(t) \Big(i_{S1} \pi \cos(\theta_R - \frac{\pi}{6}) + i_{S2} \pi \sin(\theta_R - \frac{\pi}{3}) + i_{S3} (-\pi \sin(\theta_R)) \Big) \hat{\mathbf{z}}$$

$$= \frac{2}{3} M i_{R3}(t) \Big(i_{S1} \cos(\theta_R - \frac{\pi}{6}) + i_{S2} \sin(\theta_R - \frac{\pi}{3}) - i_{S3} \sin(\theta_R) \Big) \hat{\mathbf{z}}. \tag{7.28}$$

The total torque is then

$$\begin{aligned} \tau_R &= \tau_{R1} + \tau_{R2} + \tau_{R3} \\ &= \frac{2}{3} M \Big(i_{R1}(t) \Big(-i_{S1} \sin(\theta_R) + i_{S2} \cos(\theta_R - \frac{\pi}{6}) - i_{S3} \cos(\theta_R + \frac{\pi}{6}) \Big) \\ &\quad + i_{R2}(t) \Big(-i_{S1} \cos(\theta_R + \frac{\pi}{6}) - i_{S2} \sin(\theta_R) + i_{S3} \sin(\theta_R + \frac{\pi}{3}) \Big) \\ &\quad + i_{R3}(t) \Big(i_{S1} \cos(\theta_R - \frac{\pi}{6}) + i_{S2} \sin(\theta_R - \frac{\pi}{3}) - i_{S3} \sin(\theta_R) \Big) \Big). \end{aligned} \tag{7.29}$$

With $i_{S0}(t) \equiv 0, i_{R0}(t) \equiv 0$, substitute

$$\begin{bmatrix} i_{S1}(t) \\ i_{S2}(t) \\ i_{S3}(t) \end{bmatrix} \triangleq Q^{-1} \begin{bmatrix} i_{Sa}(t) \\ i_{Sb}(t) \\ i_{S0}(t) \end{bmatrix} = \sqrt{\frac{3}{2}} \begin{bmatrix} 2/3 & 0 & \sqrt{2}/3 \\ -1/3 & 1/\sqrt{3} & \sqrt{2}/3 \\ -1/3 & -1/\sqrt{3} & \sqrt{2}/3 \end{bmatrix} \begin{bmatrix} i_{Sa}(t) \\ i_{Sb}(t) \\ i_{S0}(t) \end{bmatrix}$$

$$\begin{bmatrix} i_{R1}(t) \\ i_{R2}(t) \\ i_{R3}(t) \end{bmatrix} \triangleq Q^{-1} \begin{bmatrix} i_{Ra}(t) \\ i_{Rb}(t) \\ i_{R0}(t) \end{bmatrix} = \sqrt{\frac{3}{2}} \begin{bmatrix} 2/3 & 0 & \sqrt{2}/3 \\ -1/3 & 1/\sqrt{3} & \sqrt{2}/3 \\ -1/3 & -1/\sqrt{3} & \sqrt{2}/3 \end{bmatrix} \begin{bmatrix} i_{Ra}(t) \\ i_{Rb}(t) \\ i_{R0}(t) \end{bmatrix}$$

into (7.29) to obtain (see problem 10)

$$\begin{aligned} \tau_R &= M \Big(-i_{Ra}(t) i_{Sa}(t) \sin(\theta_R) + i_{Ra}(t) i_{Sb}(t) \cos(\theta_R) \\ &\quad - i_{Rb}(t) i_{Sa}(t) \cos(\theta_R) - i_{Rb}(t) i_{Sb}(t) \sin(\theta_R) \Big). \end{aligned} \tag{7.30}$$

Substituting the two-phase equivalent stator flux linkages (7.21) into (7.19) and the two-phase equivalent rotor flux linkages (7.24) into (7.22) along with torque equation (7.30) gives the following two-phase equivalent

www.EngineeringEBooksPdf.com

mathematical model of a three-phase wye-connected induction motor:

$$\begin{aligned}
u_{Sa} &= L_S\frac{d}{dt}i_{Sa} + M\frac{d}{dt}\Big(+i_{Ra}\cos(\theta_R) - i_{Rb}\sin(\theta_R)\Big) + R_S i_{Sa}\\
u_{Sb} &= L_S\frac{d}{dt}i_{Sb} + M\frac{d}{dt}\Big(+i_{Ra}\sin(\theta_R) + i_{Rb}\cos(\theta_R)\Big) + R_S i_{Sb}\\
0 &= L_R\frac{d}{dt}i_{Ra} + M\frac{d}{dt}\Big(+i_{Sa}\cos(\theta_R) + i_{Sb}\sin(\theta_R)\Big) + R_R i_{Ra}\\
0 &= L_R\frac{d}{dt}i_{Rb} + M\frac{d}{dt}\Big(-i_{Sa}\sin(\theta_R) + i_{Sb}\cos(\theta_R)\Big) + R_R i_{Rb}\\
J\frac{d\omega_R}{dt} &= M\Big(-i_{Ra}(t)i_{Sa}(t)\sin(\theta_R) + i_{Ra}(t)i_{Sb}(t)\cos(\theta_R)\\
&\quad - i_{Rb}(t)i_{Sa}(t)\cos(\theta_R) - i_{Rb}(t)i_{Sb}(t)\sin(\theta_R)\Big) - \tau_L\\
\frac{d\theta_R}{dt} &= \omega_R. \qquad (7.31)
\end{aligned}$$

The system (7.31) may be rewritten using a *space vector* representation as

$$R_S\underline{i}_S + L_S\frac{d}{dt}\underline{i}_S + M\frac{d}{dt}\left(\underline{i}_R e^{j\theta_R}\right) = \underline{u}_S \qquad (7.32)$$

$$R_R\underline{i}_R + L_R\frac{d}{dt}\underline{i}_R + M\frac{d}{dt}\left(\underline{i}_S e^{-j\theta_R}\right) = 0 \qquad (7.33)$$

$$M\,\mathrm{Im}\{\underline{i}_S(\underline{i}_R e^{j\theta_R})^*\} - \tau_L = J\frac{d\omega_R}{dt} \qquad (7.34)$$

$$\frac{d\theta_R}{dt} = \omega_R \qquad (7.35)$$

where $\underline{u}_S \triangleq u_{Sa} + ju_{Sb}$, $\underline{i}_S \triangleq i_{Sa} + ji_{Sb}$, and $\underline{i}_R \triangleq i_{Ra} + ji_{Rb}$ are the space vector form of the two-phase equivalent voltages and currents.

Remarks

The model (7.31) [or, equivalently, (7.32), (7.33), and (7.34)] is identical in form to the model derived for a two-phase motor in Chapter 6.

The parameters L_S, L_R, and M are the two-phase equivalent inductance values for the three-phase machine. As seen from equations (7.5), (7.6), (7.7), (7.11), (7.12), and (7.13), the actual stator, rotor, and mutual coefficients of inductance in the three-phase machine are $2L_S/3$, $2L_R/3$, and $2M/3$, respectively. However, the phase resistances R_S and R_R in the two-phase model are the same as in the three-phase model.

Simulation of the Three-Phase Machine

Figure 7.8 illustrates how the two-phase model is used to simulate a balanced three-phase machine.

www.EngineeringEBooksPdf.com

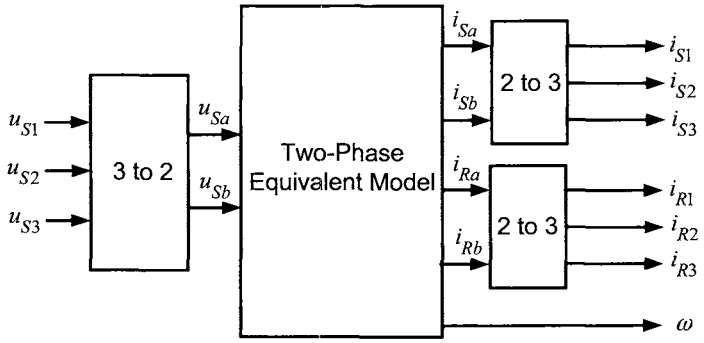


FIGURE 7.8. Block diagram for simulating a three-phase machine using the two-phase equivalent model.

One simply uses the transformation

$$\begin{bmatrix} u_{Sa}(t) \\ u_{Sb}(t) \end{bmatrix} \triangleq \sqrt{\frac{2}{3}} \begin{bmatrix} 1 & -1/2 & -1/2 \\ 0 & \sqrt{3}/2 & -\sqrt{3}/2 \end{bmatrix} \begin{bmatrix} u_{S1}(t) \\ u_{S2}(t) \\ u_{S3}(t) \end{bmatrix}$$

to obtain the voltages $u_{Sa}(t)$ and $u_{Sb}(t)$ which are then applied to the two-phase equivalent simulation model. The currents i_{Sa}, i_{Sb}, i_{Ra}, and i_{Rb} from the simulation are then put through the two-phase to three-phase (2-3) transformation

$$\begin{bmatrix} i_{S1}(t) \\ i_{S2}(t) \\ i_{S3}(t) \end{bmatrix} \triangleq \sqrt{\frac{3}{2}} \begin{bmatrix} 2/3 & 0 \\ -1/3 & 1/\sqrt{3} \\ -1/3 & -1/\sqrt{3} \end{bmatrix} \begin{bmatrix} i_{Sa}(t) \\ i_{Sb}(t) \end{bmatrix}$$

$$\begin{bmatrix} i_{R1}(t) \\ i_{R2}(t) \\ i_{R3}(t) \end{bmatrix} \triangleq \sqrt{\frac{3}{2}} \begin{bmatrix} 2/3 & 0 \\ -1/3 & 1/\sqrt{3} \\ -1/3 & -1/\sqrt{3} \end{bmatrix} \begin{bmatrix} i_{Ra}(t) \\ i_{Rb}(t) \end{bmatrix}$$

to obtain the (balanced) three-phase stator and rotor currents.

Zero Component

The three-phase to two-phase (3 to 2) transformation is given by

$$\begin{bmatrix} u_{Sa}(t) \\ u_{Sb}(t) \\ u_{S0}(t) \end{bmatrix} \triangleq \sqrt{\frac{2}{3}} \begin{bmatrix} 1 & \cos(2\pi/3) & \cos(4\pi/3) \\ 0 & \sin(2\pi/3) & \sin(4\pi/3) \\ 1/\sqrt{2} & 1/\sqrt{2} & 1/\sqrt{2} \end{bmatrix} \begin{bmatrix} u_{S1}(t) \\ u_{S2}(t) \\ u_{S3}(t) \end{bmatrix}. \quad (7.36)$$

Figure 7.9 shows the three magnetic axes s_1, s_2, and s_3 for the stator phases and two orthogonal axes which are denoted a and b, respectively. Note that the s_1, s_2, and s_3 axes are not orthogonal.

www.EngineeringEBooksPdf.com

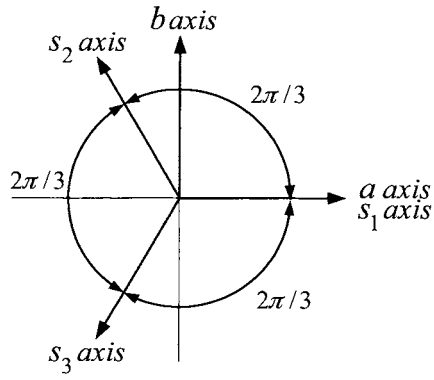


FIGURE 7.9. Magnetic axes for the three-phase and two-phase models.

An interpretation of the 3 to 2 transformation (7.36) is that the elements of the 3-tuple

$$\begin{bmatrix} u_{S1}(t) \\ u_{S2}(t) \\ u_{S3}(t) \end{bmatrix}$$

are the *components* of the vector

$$\vec{\mathbf{u}}_S \triangleq u_{S1}(t)\hat{\mathbf{e}}_{S1} + u_{S2}(t)\hat{\mathbf{e}}_{S2} + u_{S3}(t)\hat{\mathbf{e}}_{S3}$$

with respect to the basis of orthogonal unit vectors

$$\hat{\mathbf{e}}_{S1} = \sqrt{\frac{2}{3}}\begin{bmatrix} 1 \\ 0 \\ 1/\sqrt{2} \end{bmatrix},\ \hat{\mathbf{e}}_{S2} = \sqrt{\frac{2}{3}}\begin{bmatrix} \cos(2\pi/3) \\ \sin(2\pi/3) \\ 1/\sqrt{2} \end{bmatrix},\ \hat{\mathbf{e}}_{S3} = \sqrt{\frac{2}{3}}\begin{bmatrix} \cos(4\pi/3) \\ \sin(4\pi/3) \\ 1/\sqrt{2} \end{bmatrix}$$

while the 3-tuple

$$\begin{bmatrix} u_{Sa}(t) \\ u_{Sb}(t) \\ u_{S0}(t) \end{bmatrix}$$

are the *components* of this *same* vector

$$\vec{\mathbf{u}}_S = u_{Sa}(t)\hat{\mathbf{e}}_{Sa} + u_{Sb}(t)\hat{\mathbf{e}}_{Sb} + u_{S0}\hat{\mathbf{e}}_{S0}$$

with respect to the basis of orthogonal unit vectors

$$\hat{\mathbf{e}}_{Sa} = \begin{bmatrix} 1 \\ 0 \\ 0 \end{bmatrix},\ \hat{\mathbf{e}}_{Sb} = \begin{bmatrix} 0 \\ 1 \\ 0 \end{bmatrix},\ \hat{\mathbf{e}}_{S0} = \begin{bmatrix} 0 \\ 0 \\ 1 \end{bmatrix}$$

The third component u_{S0} is referred to as the *zero component* because in a balanced three-phase system it is zero.

www.EngineeringEBooksPdf.com

Note that the projections of $\hat{\mathbf{e}}_{S1}, \hat{\mathbf{e}}_{S2}$, and $\hat{\mathbf{e}}_{S3}$ onto the ab plane of Figure 7.9 are in the directions of the s_1, s_2, and s_3 axes, respectively, which are not orthogonal.

Remarks The 3 to 2 transformation (7.36) is also referred to as *Clarke's transformation* [6]. The three-phase windings whose magnetic axes are shown in Figure 7.9 are magnetically coupled. For example, a current i_{S1} in phase 1 will produce a net (nonzero) flux linkage in the other two phases. As pointed out by Holtz [60], the 3 to 2 transformation has (mathematically) replaced the magnetically coupled three-phase windings with an equivalent two-phase set of windings whose magnetic axes are orthogonal (in quadrature) and are *not* magnetically coupled. That is, a current i_{Sa} in phase a will not produce a net flux linkage in phase b. Often phase a is referred to as the *direct* or d axis and phase b is referred to as the *quadrature* or q axis. For example, in problem 13, a standard model of the induction is given in space vector form. In that formulation, the notation $(u^S_{Sd}, u^S_{Sq}, i^S_{Sd}, i^S_{Sq}, i^S_{Rd}, i^S_{Rq})$ is often used for the equivalent two-phase variables (the superscript "S" refers to the "stationary frame"). However, in this book, the dq notation is reserved for the *field-oriented* coordinate system (see Chapters 8 and 9) and so the reader must be wary when reading different authors. Further, one also sees the notation $(u_{S\alpha}, u_{S\beta}, i_{S\alpha}, i_{S\beta}, i_{R\alpha}, i_{R\beta})$ and the notation $(u_{Sd}, u_{Sq}, i_{Sd}, i_{Sq}, i_{Rd}, i_{Rq})$ for these same variables.

www.EngineeringEBooksPdf.com

7.2 Steady-State Analysis of the Induction Motor

The objective here is to find steady-state solutions to the mathematical model (7.31) of the induction motor. The space vector representation of the induction motor given by (7.32), (7.33), and (7.34) will be used because it is especially convenient for this analysis. This presentation is from the development in Chapter 10 of Professor Leonhard's book [1][2].

With $\underline{U}_S \triangleq |\underline{U}_S|\, e^{j\angle \underline{U}_S} = U_S e^{j\angle \underline{U}_S}$ a root mean square (rms) phasor[4] for the voltage, a balanced set of three-phase steady-state voltages is specified by

$$\begin{aligned} u_{S1} &= \sqrt{2}U_S \cos(\omega_S t + \angle \underline{U}_S) \\ &= \frac{\sqrt{2}}{2}\left(\underline{U}_S e^{j\omega_S t} + \underline{U}_S^* e^{-j\omega_S t}\right) \\ u_{S2} &= \sqrt{2}U_S \cos(\omega_S t + \angle \underline{U}_S - 2\pi/3) \\ &= \frac{\sqrt{2}}{2}\left(\underline{U}_S e^{j(\omega_S t - 2\pi/3)} + \underline{U}_S^* e^{-j(\omega_S t - 2\pi/3)}\right) \\ u_{S3} &= \sqrt{2}U_S \cos(\omega_S t + \angle \underline{U}_S - 4\pi/3) \\ &= \frac{\sqrt{2}}{2}\left(\underline{U}_S e^{j(\omega_S t - 4\pi/3)} + \underline{U}_S^* e^{-j(\omega_S t - 4\pi/3)}\right). \end{aligned} \tag{7.37}$$

The objective here is to apply these voltages to the motor and find the resulting steady-state currents and torque.

7.2.1 Steady-State Currents and Voltages

The three-phase to two-phase transformation (7.17) can be represented in the space vector form as (see problem 11)

$$\underline{u}_S \triangleq \sqrt{\frac{2}{3}}\left(u_{S1} + u_{S2}e^{j2\pi/3} + u_{S3}e^{j4\pi/3}\right). \tag{7.38}$$

Expanded out, this becomes

$$\begin{aligned} \underline{u}_S &= \sqrt{\frac{2}{3}}\left(u_{S1} + u_{S2}\cos(2\pi/3) + u_{S3}\cos(4\pi/3)\right) \\ &\quad + j\sqrt{\frac{2}{3}}\left(u_{S2}\sin(2\pi/3) + u_{S3}\sin(4\pi/3)\right) \\ &= u_{Sa} + j u_{Sb}. \end{aligned}$$

[4] In this section, $U_S \triangleq |\underline{U}_S|$ is an rms voltage rather than a peak voltage. This is to keep the notation in this section consistent with standard practice.

www.EngineeringEBooksPdf.com

Substituting the expressions (7.37) into (7.38) and using the fact that $1 + e^{j4\pi/3} + e^{j8\pi/3} = 0$ results in

$$\begin{aligned}
\underline{u}_S &= \frac{1}{\sqrt{3}}\left(\underline{U}_S e^{j\omega_S t} + \underline{U}_S^* e^{-j\omega_S t}\right) \\
&\quad + \frac{1}{\sqrt{3}}\left(\underline{U}_S e^{j(\omega_S t - 2\pi/3)} + \underline{U}_S^* e^{-j(\omega_S t - 2\pi/3)}\right) e^{j2\pi/3} \\
&\quad + \frac{1}{\sqrt{3}}\left(\underline{U}_S e^{j(\omega_S t - 4\pi/3)} + \underline{U}_S^* e^{-j(\omega_S t - 4\pi/3)}\right) e^{j4\pi/3} \\
&= \sqrt{3}\underline{U}_S e^{j\omega_S t}.
\end{aligned}$$

This is the voltage to be applied to the induction motor model (7.32), (7.33), and (7.34).

The approach taken here is to look for a solution consisting of a balanced set of three-phase stator currents. With $\underline{I}_S \triangleq |\underline{I}_S|\, e^{j\angle \underline{I}_S} = I_S e^{j\angle \underline{I}_S}$ an rms current phasor, the stator currents take the form

$$\begin{aligned}
i_{S1} &= \sqrt{2} I_S \cos(\omega_S t + \angle \underline{I}_S) \\
&= \frac{\sqrt{2}}{2}\left(\underline{I}_S e^{j\omega_S t} + \underline{I}_S^* e^{-j\omega_S t}\right) \\
i_{S2} &= \sqrt{2} I_S \cos(\omega_S t + \angle \underline{I}_S - 2\pi/3) \\
&= \frac{\sqrt{2}}{2}\left(\underline{I}_S e^{j(\omega_S t - 2\pi/3)} + \underline{I}_S^* e^{-j(\omega_S t - 2\pi/3)}\right) \\
i_{S3} &= \sqrt{2} I_S \cos(\omega_S t + \angle \underline{I}_S - 4\pi/3) \\
&= \frac{\sqrt{2}}{2}\left(\underline{I}_S e^{j(\omega_S t - 4\pi/3)} + \underline{I}_S^* e^{-j(\omega_S t - 4\pi/3)}\right)
\end{aligned}$$

where the three-phase to two-phase transformation results in

$$\underline{i}_S = \sqrt{\frac{2}{3}}\left(i_{S1} + i_{S2} e^{j2\pi/3} + i_{S3} e^{j4\pi/3}\right) = \sqrt{3}\underline{I}_S e^{j\omega_S t}.$$

For the rotor currents, a solution consisting of a balanced set of three-phase rotor currents with angular frequency $\omega_S - \omega_R$ is sought. With $\underline{I}_R = |\underline{I}_R|\, e^{j\angle \underline{I}_R} = I_R e^{j\angle \underline{I}_R}$, the rotor currents take the form

$$\begin{aligned}
i_{R1} &= \frac{\sqrt{2}}{2}\left(\underline{I}_R e^{j(\omega_S - \omega_R)t} + \underline{I}_R^* e^{-j(\omega_S - \omega_R)t}\right) \\
i_{R2} &= \frac{\sqrt{2}}{2}\left(\underline{I}_R e^{j((\omega_S - \omega_R)t - 2\pi/3)} + \underline{I}_R^* e^{-j((\omega_S - \omega_R)t - 2\pi/3)}\right) \\
i_{R3} &= \frac{\sqrt{2}}{2}\left(\underline{I}_R e^{j((\omega_S - \omega_R)t - 4\pi/3)} + \underline{I}_R^* e^{-j((\omega_S - \omega_R)t - 4\pi/3)}\right).
\end{aligned}$$

The three-phase to two-phase transformation of the rotor currents results in

$$\underline{i}_R = \sqrt{\frac{2}{3}}\left(i_{R1} + i_{R2} e^{j2\pi/3} + i_{R3} e^{j4\pi/3}\right) = \sqrt{3}\underline{I}_R e^{j(\omega_S - \omega_R)t}.$$

www.EngineeringEBooksPdf.com

Finally, with $\theta_R(t) = \omega_R t$,

$$\underline{i}_R(t)e^{j\theta_R(t)} = \sqrt{3}\underline{I}_R e^{j\omega_S t}.$$

7.2.2 *Steady-State Equivalent Circuit Model*

The above expressions for the steady-state currents are convenient for developing an equivalent circuit model of the induction motor in steady state. To do so, the expressions $\underline{u}_S = \sqrt{3}\underline{U}_S e^{j\omega_S t}$, $\underline{i}_S = \sqrt{3}\underline{I}_S e^{j\omega_S t}$, $\underline{i}_R = \sqrt{3}\underline{I}_R e^{j(\omega_S - \omega_R)t}$ and $\underline{i}_R e^{j\theta_R(t)} = \sqrt{3}\underline{I}_R e^{j\omega_S t}$ are substituted into (7.32) and (7.33). After canceling out the terms $\sqrt{3}e^{j\omega_S t}$ and $\sqrt{3}e^{j(\omega_S - \omega_R)t}$, one obtains

$$(R_S + j\omega_S L_S)\underline{I}_S + j\omega_S M\underline{I}_R = \underline{U}_S \quad (7.39)$$

$$(R_R + j(\omega_S - \omega_R)L_R)\underline{I}_R + j(\omega_S - \omega_R)M\underline{I}_S = 0. \quad (7.40)$$

With $\omega_{slip} \triangleq \omega_S - \omega_R$, define the normalized slip

$$S = \frac{\omega_{slip}}{\omega_S} = \frac{\omega_S - \omega_R}{\omega_S}.$$

Replace $\omega_{slip} = \omega_S - \omega_R$ by $S\omega_S$ into (7.40) and rearrange to obtain

$$(R_S + j\omega_S L_S)\underline{I}_S + j\omega_S M\underline{I}_R = \underline{U}_S \quad (7.41)$$

$$(R_R/S + j\omega_S L_R)\underline{I}_R + j\omega_S M\underline{I}_S = 0. \quad (7.42)$$

With $L_S = (1+\sigma_S)M, L_R = (1+\sigma_R)M$, equations (7.41) and (7.42) can be rearranged to obtain[5]

$$(R_S + j\omega_S\sigma_S M)\underline{I}_S + j\omega_S M(\underline{I}_S + \underline{I}_R) = \underline{U}_S \quad (7.43)$$

$$(R_R/S + j\omega_S\sigma_R M)\underline{I}_R + j\omega_S M(\underline{I}_S + \underline{I}_R) = 0. \quad (7.44)$$

In this analysis, it was assumed that ω_S, ω_R, and therefore $\omega_{slip} = \omega_S - \omega_R$ are all *constant*. The two algebraic relationships (7.43) and (7.44) may be viewed as the result of applying Kirchhoff's voltage law to the two loops indicated in the *equivalent circuit* of Figure 7.10.

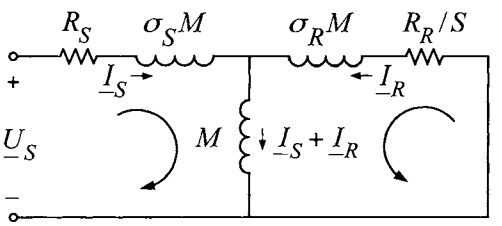


FIGURE 7.10. An equivalent circuit of the induction motor.

[5] Setting $L_S = (1+\sigma_S)M, L_R = (1+\sigma_R)M$ is just saying that L_S and L_R are slightly greater than M. Due to leakage, this is always true as $\sigma = 1 - M^2/(L_S L_R) > 0$.

www.EngineeringEBooksPdf.com

The system (7.41) and (7.42) may be rewritten as

$$\begin{bmatrix} R_S + j\omega_S L_S & j\omega_S M \\ j\omega_S M & R_R/S + j\omega_S L_R \end{bmatrix} \begin{bmatrix} \underline{I}_S \\ \underline{I}_R \end{bmatrix} = \begin{bmatrix} \underline{U}_S \\ 0 \end{bmatrix}. \tag{7.45}$$

Solving for $\underline{I}_S$ and $\underline{I}_R$ gives

$$\begin{bmatrix} \underline{I}_S \\ \underline{I}_R \end{bmatrix} = \frac{1}{(R_S + j\omega_S L_S)(R_R/S + j\omega_S L_R) - (j\omega_S M)^2} \times \begin{bmatrix} R_R/S + j\omega_S L_R & -j\omega_S M \\ -j\omega_S M & R_S + j\omega_S L_S \end{bmatrix} \begin{bmatrix} \underline{U}_S \\ 0 \end{bmatrix}.$$

The input impedance is then

$$\begin{aligned} Z_S &= \frac{\underline{U}_S}{\underline{I}_S} = \frac{(R_S + j\omega_S L_S)(R_R/S + j\omega_S L_R) - (j\omega_S M)^2}{R_R/S + j\omega_S L_R} \\ &= R_S + j\omega_S L_S - \frac{(j\omega_S M)^2}{R_R/S + j\omega_S L_R}. \end{aligned}$$

Using the fact that $M = L_S/(1+\sigma_S) = L_R/(1+\sigma_R)$ and $\sigma = 1 - \dfrac{1}{(1+\sigma_S)(1+\sigma_R)}$, this becomes

$$\begin{aligned} Z_S &= R_S + j\omega_S L_S \left(1 - \frac{\dfrac{S}{R_R} j\omega_S L_R \dfrac{1}{(1+\sigma_S)(1+\sigma_R)}}{1 + \dfrac{j\omega_S L_R S}{R_R}} \right) \\ &= R_S + j\omega_S L_S \left(\frac{1 + \dfrac{j\omega_S L_R S}{R_R} \left(1 - \dfrac{1}{(1+\sigma_S)(1+\sigma_R)} \right)}{1 + \dfrac{j\omega_S L_R S}{R_R}} \right) \\ &= R_S + j\omega_S L_S \left(\frac{1 + \dfrac{j\sigma\omega_S L_R S}{R_R}}{1 + \dfrac{j\omega_S L_R S}{R_R}} \right). \end{aligned}$$

Finally, defining S_p as

$$S_p \triangleq \frac{R_R}{\sigma\omega_S L_R}, \tag{7.46}$$

the input impedance may be written as

$$Z_S = R_S + j\omega_S L_S \left(\frac{1 + \dfrac{jS}{S_p}}{1 + \dfrac{jS}{\sigma S_p}} \right).$$

www.EngineeringEBooksPdf.com

With $R_S = 0$[6], the stator current phasor $\underline{I}_S = \underline{U}_S/Z_S$ becomes

$$\underline{I}_S = \frac{\underline{U}_S}{j\omega_S L_S}\left(\frac{1+\frac{jS}{\sigma S_p}}{1+\frac{jS}{S_p}}\right) \tag{7.47}$$

$$= \underline{I}_{S0}\left(\frac{1+\sigma}{2\sigma} - \frac{1-\sigma}{2\sigma}\frac{1-\frac{jS}{S_p}}{1+\frac{jS}{S_p}}\right)$$

$$= \underline{I}_{S0}\left(\frac{1+\sigma}{2\sigma} - \frac{1-\sigma}{2\sigma}e^{-j2\tan^{-1}(S/S_p)}\right). \tag{7.48}$$

Here $\underline{I}_{S0} \triangleq \underline{U}_S/(j\omega_S L_S)$ is the no-load current phasor, that is, the current phasor when the slip is zero. For convenience, choose $\underline{U}_S = jU_S$ so that $\underline{I}_{S0} = I_{S0} = U_S/(\omega_S L_S)$ is real. Figure 7.11 shows a plot of phasor $\underline{I}_S$ versus S/S_p.

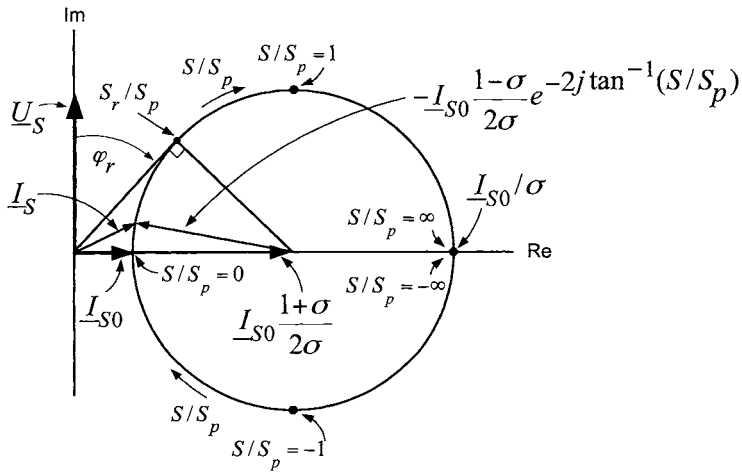


FIGURE 7.11. Circle diagram of the stator current phasor as a function of S/S_p with $R_S = 0$.

As S/S_p varies in the interval $-\infty \leq S/S_p \leqslant \infty$, the tip of the phasor $\underline{I}_S$ traces out a circle so that Figure 7.11 is referred to as the *circle diagram*. As illustrated in the figure, the tip of the phasor $\underline{I}_S$ lies on a

[6]This is primarily done so that the expressions that are now derived for the stator input impedance, power factor, and torque have a nice form.

www.EngineeringEBooksPdf.com

circle whose center is at $\underline{I}_{S0}\frac{1+\sigma}{2\sigma}$ on the real axis and whose radial arm is $-\underline{I}_{S0}\frac{1+\sigma}{2\sigma}e^{-j2\tan^{-1}(S/S_p)}$.

The average power P_{stator} into the stator from the source is

$$P_{\text{stator}} = \frac{1}{2\pi/\omega_S}\int_0^{2\pi/\omega_S}(u_{S1}i_{S1} + u_{S2}i_{S2} + u_{S3}i_{S3})\,dt.$$

Then

$$\frac{1}{2\pi/\omega_S}\int_0^{2\pi/\omega_S} u_{S1}i_{S1}dt = \frac{1}{2\pi/\omega_S}\int_0^{2\pi/\omega_S}\left(\frac{\sqrt{2}}{2}\left(\underline{U}_S e^{j\omega_S t} + \underline{U}_S^* e^{-j\omega_S t}\right)\right) \times \left(\frac{\sqrt{2}}{2}\left(\underline{I}_S e^{j\omega_S t} + \underline{I}_S^* e^{-j\omega_S t}\right)\right) dt$$

$$= \frac{1}{2\pi/\omega_S}\int_0^{2\pi/\omega_S}\frac{1}{2}\left[\underline{U}_S\underline{I}_S^* + \underline{U}_S^*\underline{I}_S + \underline{U}_S\underline{I}_S e^{j2\omega_S t} + \underline{U}_S^*\underline{I}_S^* e^{-j2\omega_S t}\right] dt$$

$$= \frac{1}{2}\left[\underline{U}_S\underline{I}_S^* + \underline{U}_S^*\underline{I}_S\right] = \text{Re}\{\underline{U}_S\underline{I}_S^*\} = U_S I_S\cos(\angle\underline{U}_S - \angle\underline{I}_S)$$

as

$$\text{Re}\{\underline{U}_S\underline{I}_S^*\} = \text{Re}\left\{|\underline{U}_S|\,e^{j\angle\underline{U}_S}\,|\underline{I}_S|\,e^{-j\angle\underline{I}_S}\right\} = |\underline{U}_S|\,|\underline{I}_S|\cos(\angle\underline{U}_S - \angle\underline{I}_S).$$

The angle $\varphi \triangleq \angle\underline{U}_S - \angle\underline{I}_S$ is the angle between the phasors $\underline{U}_S$ and $\underline{I}_S$, and is called the *power factor angle*. Each phase contributes the same average power so that the total electrical power into the stator is

$$P_{\text{stator}} = 3U_S I_S\cos(\varphi)$$

where $\cos(\varphi)$ is the *power factor*. Using equation (7.47), the power factor angle φ is written as a function of S/S_p by

$$\varphi = \angle\underline{U}_S - \angle\underline{I}_S = \frac{\pi}{2} - \left(\tan^{-1}\left(\frac{S}{\sigma S_p}\right) - \tan^{-1}\left(\frac{S}{S_p}\right)\right).$$

The *rated* slip S_r is defined as the value of S that minimizes φ or equivalently, maximizes $\cos(\varphi)$. Solving $d\varphi/dS = 0$ gives

$$S_r = \sqrt{\sigma}S_p. \tag{7.49}$$

Again using equation (7.47), the ratio I_S/I_{S0} may be written as

$$\left(\frac{I_S}{I_{S0}}\right)^2 = \frac{1 + \left(\frac{S}{\sigma S_p}\right)^2}{1 + \left(\frac{S}{S_p}\right)^2}, \quad I_{S0} = \frac{U_S}{\omega_S L_S} \tag{7.50}$$

www.EngineeringEBooksPdf.com

so that at rated slip, the *rated current* is

$$\frac{I_{S_r}}{I_{S0}} = \frac{1}{\sqrt{\sigma}}. \tag{7.51}$$

Also note that it follows from equation (7.50) that

$$\lim_{S\to\infty} \frac{I_S}{I_{S0}} = \frac{1}{\sigma}.$$

A plot of I_S/I_{S0} versus S/S_p is shown in Figure 7.12. At rated slip, the power factor angle is

$$\varphi_r \triangleq \varphi_{|S=S_r} = \pi/2 - \left(\tan^{-1}\left(1/\sqrt{\sigma}\right) - \tan^{-1}\left(\sqrt{\sigma}\right)\right)$$

so that power factor is [see (7.57) below]

$$\cos(\varphi_r) = \frac{1-\sigma}{1+\sigma}. \tag{7.52}$$

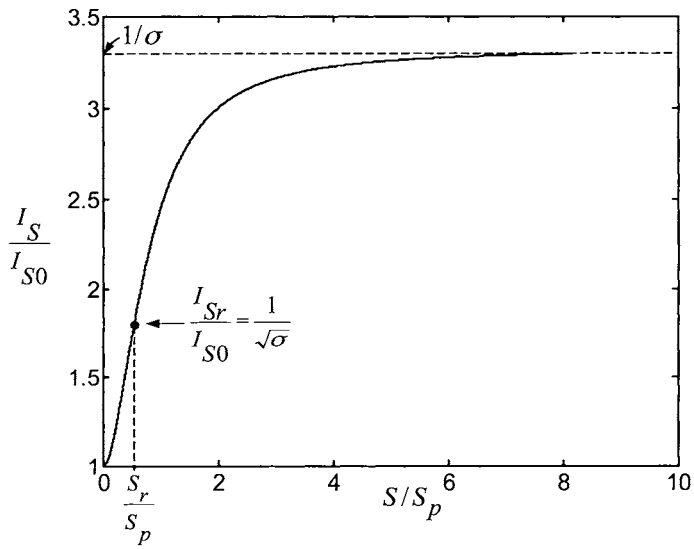


FIGURE 7.12. I_S/I_{S0} versus S/S_p, with $\sigma = 0.3$ and $R_S = 0$.

7.2.3 Rated Conditions

An interpretation to the definition of rated slip and the other corresponding rated variables is as follows: The balanced three-phase sinusoidal input

www.EngineeringEBooksPdf.com

voltages are constant in both magnitude and frequency. If the motor is operating at *rated* slip (done by choosing the appropriate load on the motor), then the power into the motor is

$$3U_S I_{S_r} \cos(\varphi_r) = 3U_S \frac{I_{S0}}{\sqrt{\sigma}} \frac{1-\sigma}{1+\sigma} \tag{7.53}$$

where $I_{S_r} = I_{S0}/\sqrt{\sigma}, \cos(\varphi_r) = (1-\sigma)/(1+\sigma)$ as previously shown. At rated slip, the power factor $\cos(\varphi_r)$ is at its maximum value so that the amount of stator current I_S required to achieve the particular input power level (7.53) is at a minimum. This power goes into mechanical work and losses given by[7]

$$3U_S I_{S_r} \cos(\varphi_r) = \tau_r \omega_R + 3R_R I_R^2.$$

The torque τ_r and speed ω_R under these operating conditions are called the *rated* torque and *rated* speed, respectively. A real motor has the stator current losses $3R_S I_S^2$ so that if motor is operating at rated slip, the amount of stator current required to produce the rated torque is minimized, making this an efficient operating point.

7.2.4 Steady-State Torque

Substituting $\underline{i}_S = \sqrt{3}\underline{I}_S e^{j\omega_S t}$ and $\underline{i}_R(t)e^{j\theta_R(t)} = \sqrt{3}\underline{I}_R e^{j\omega_S t}$ into (7.34) gives

$$\tau = M \operatorname{Im}\{\underline{i}_S(\underline{i}_R e^{j\theta_R})^*\} = 3M \operatorname{Im}\{\underline{I}_S \underline{I}_R^*\}. \tag{7.54}$$

From (7.45), the rotor current phasor is related to the stator current phasor by

$$\underline{I}_R = -\frac{j\omega_S M}{R_R/S + j\omega_S L_R}\underline{I}_S. \tag{7.55}$$

Substituting this into the steady-state torque expression (7.54) gives

$$\begin{aligned}\tau &= 3M \operatorname{Im}\{\underline{I}_S \underline{I}_R^*\} = 3M \operatorname{Im}\left\{\underline{I}_S \left(-\frac{j\omega_S M}{R_R/S + j\omega S L_R}\underline{I}_S\right)^*\right\} \\ &= 3M \operatorname{Im}\left\{\underline{I}_S \frac{j\omega_S M}{R_R/S - j\omega_S L_R}\underline{I}_S^*\right\} = 3MI_S^2 \operatorname{Im}\left\{\frac{\frac{j\omega_S MS}{R_R}}{1 - \frac{j\omega_S L_R S}{R_R}}\right\}.\end{aligned}$$

[7] Recall that this analysis assumes $R_S = 0$. The mechanical losses (friction, windage, etc.) have also been assumed to be zero in this analysis.

www.EngineeringEBooksPdf.com

Recalling that $S_p = \dfrac{R_R}{\sigma\omega_S L_R}$, this becomes

$$\tau = 3MI_S^2 \operatorname{Im}\left\{\frac{\dfrac{j\omega_S MS}{R_R}}{1-\dfrac{jS}{\sigma S_p}}\frac{1+\dfrac{jS}{\sigma S_p}}{1+\dfrac{jS}{\sigma S_p}}\right\} = 3MI_S^2 \operatorname{Im}\left\{\frac{\dfrac{j\omega_S MS}{R_R}\left(1+\dfrac{jS}{\sigma S_p}\right)}{1+\left(\dfrac{S}{\sigma S_p}\right)^2}\right\}$$

$$= 3MI_S^2 \frac{\omega_S MS/R_R}{1+\left(\dfrac{S}{\sigma S_p}\right)^2} = 3M\left(\frac{I_S}{I_{S0}}\right)^2 (I_{S0})^2 \frac{\omega_S MS/R_R}{1+\left(\dfrac{S}{\sigma S_p}\right)^2}.$$

Using (7.50), this simplifies to

$$\begin{aligned}\tau &= 3M\frac{1+\left(\dfrac{S}{\sigma S_p}\right)^2}{1+\left(\dfrac{S}{S_p}\right)^2}\left(\frac{U_S}{\omega_S L_S}\right)^2 \frac{\omega_S MS/R_R}{1+\left(\dfrac{S}{\sigma S_p}\right)^2} \\ &= 3\frac{U_S^2}{\omega_S^2 L_S^2}\frac{\omega_S M^2 S/R_R}{1+\left(\dfrac{S}{S_p}\right)^2} = 3\frac{U_S^2}{\omega_S^2 L_S^2}\frac{S_p/S}{S_p/S+S/S_p}\frac{\omega_S M^2 S}{R_R}.\end{aligned}$$

Rewriting $M^2 = \dfrac{L_S}{(1+\sigma_S)}\dfrac{L_R}{(1+\sigma_R)} = L_S L_R(1-\sigma)$, one obtains

$$\begin{aligned}\tau &= 3\frac{U_S^2}{\omega_S^2 L_S^2}\frac{S_p/S}{S_p/S+S/S_p}L_S(1-\sigma)\frac{\omega_S L_R}{R_R}S \\ &= 3\frac{U_S^2}{\omega_S^2 L_S}\frac{S_p/S}{S_p/S+S/S_p}\frac{(1-\sigma)}{\sigma}\frac{S}{S_p} \\ &= 3\frac{U_S^2}{\omega_S^2 L_S}\frac{1}{S_p/S+S/S_p}\frac{(1-\sigma)}{\sigma}.\end{aligned}$$

Finally,

$$\tau = \frac{3}{2}\frac{(1-\sigma)}{\sigma}\frac{U_S^2}{\omega_S^2 L_S}\frac{2}{S_p/S+S/S_p} = \tau_p\frac{2}{S_p/S+S/S_p} \tag{7.56}$$

where

$$\tau_p \triangleq \frac{3}{2}\frac{(1-\sigma)}{\sigma}\frac{U_S^2}{\omega_S^2 L_S}.$$

This is the well-known *torque-slip* curve for an induction motor and is plotted in Figure 7.13.

www.EngineeringEBooksPdf.com

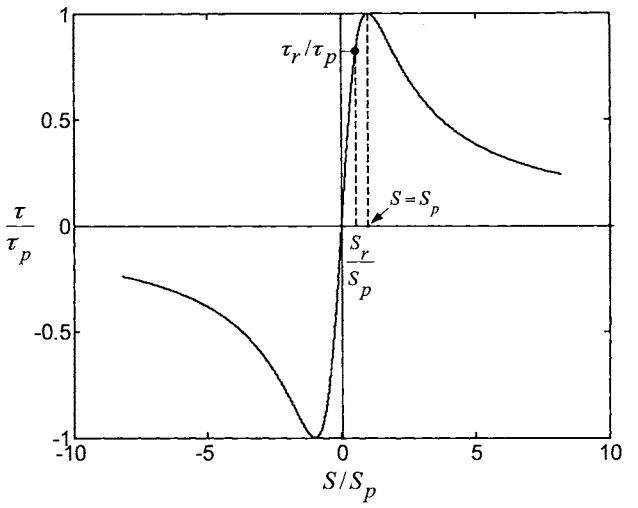


FIGURE 7.13. τ/τ_p versus S/S_p, with $R_S = 0$.

For a fixed U_S and ω_S, the torque is a maximum for $S = S_p$. S_p is called the *pull-out slip* and the corresponding maximum torque τ_p is called the *pull-out torque.* This terminology comes from the fact that for $S > S_p$ the torque *decreases* as the slip increases. Consequently, if the motor is operating at $S = S_p$ (putting out maximum torque) and then more load (load torque) is added, the rotor speed ω_R decreases and the (normalized) slip $S = (\omega_S - \omega_R)/\omega_S$ increases. But in this situation, even less torque is produced so the motor's speed continues to decrease and the motor ultimately comes to a stop. That is, for $S \geq S_p$ the motor is not at a stable operating point. On the other hand, if the motor is operating at a slip $S < S_p$, then putting more load on the motor will decrease the speed, thus increasing the slip, but in this case the torque increases. Consequently, the motor keeps running at a little lower speed, but with the additional load on it. At the rated slip $S_r = \sqrt{\sigma} S_p$, the corresponding rated torque τ_r is defined as

$$\tau_r \triangleq \tau_p \frac{2}{S/S_p + S_p/S}\Big|_{S=S_r} = \tau_p \frac{2}{\sqrt{\sigma} + 1/\sqrt{\sigma}} = \tau_p \frac{2\sqrt{\sigma}}{1+\sigma}.$$

The ratio of the pull-out (or peak) torque τ_p to the rated torque τ_r is then

$$\frac{\tau_r}{\tau_p} = \frac{2\sqrt{\sigma}}{1+\sigma}.$$

This is a measure of the *overload capacity* in that, with the motor normally operating at rated torque, the factor $(1+\sigma)/(2\sqrt{\sigma})$ is how much the torque can be increased before pull-out [2]. It is normally desired to operate the

www.EngineeringEBooksPdf.com

motor at rated slip S_r. That is, one picks ("sizes") the motor so that its rated torque is close to the torque load expected on the motor. Then the motor will put out the required torque while minimizing the stator current and, therefore, the $R_S I_S^2$ losses.

7.2.5 *Steady-State Power Transfer in the Induction Motor*

Recall that the power into the stator is given by

$$P_{\text{stator}} = 3U_S I_S \cos(\varphi)$$

where

$$\begin{aligned}
\frac{I_S}{I_{S0}} &= \sqrt{\frac{1+\left(\dfrac{S}{\sigma S_p}\right)^2}{1+\left(\dfrac{S}{S_p}\right)^2}} \\
I_{S0} &= \frac{U_S}{\omega_S L_S} \\
\varphi &= \angle \underline{U}_S - \angle \underline{I}_S = \frac{\pi}{2} - \left(\tan^{-1}\left(\frac{S}{\sigma S_p}\right) - \tan^{-1}\left(\frac{S}{S_p}\right)\right).
\end{aligned}$$

The power factor may then be written as

$$\begin{aligned}
\cos(\varphi) &= \cos\left(\frac{\pi}{2} - \tan^{-1}\left(\frac{S}{\sigma S_p}\right) + \tan^{-1}\left(\frac{S}{S_p}\right)\right) \\
&= \sin\left(\tan^{-1}\left(\frac{S}{\sigma S_p}\right) - \tan^{-1}\left(\frac{S}{S_p}\right)\right) \\
&= \sin\left(\tan^{-1}\left(\frac{S}{\sigma S_p}\right)\right)\cos\left(\tan^{-1}\left(\frac{S}{S_p}\right)\right) \\
&\quad - \sin\left(\tan^{-1}\left(\frac{S}{S_p}\right)\right)\cos\left(\tan^{-1}\left(\frac{S}{\sigma S_p}\right)\right) \\
&= \frac{\dfrac{S}{\sigma S_p}}{\sqrt{1+\left(\dfrac{S}{\sigma S_p}\right)^2}}\frac{1}{\sqrt{1+\left(\dfrac{S}{S_p}\right)^2}} - \frac{\dfrac{S}{S_p}}{\sqrt{1+\left(\dfrac{S}{S_p}\right)^2}}\frac{1}{\sqrt{1+\left(\dfrac{S}{\sigma S_p}\right)^2}}
\end{aligned}$$

or

$$\cos(\varphi) = \frac{\dfrac{S}{\sigma S_p} - \dfrac{S}{S_p}}{\sqrt{1+\left(\dfrac{S}{\sigma S_p}\right)^2}\sqrt{1+\left(\dfrac{S}{S_p}\right)^2}}. \tag{7.57}$$

www.EngineeringEBooksPdf.com

The power into the stator can now be written as

$$\begin{aligned}
P_{\text{stator}} &= 3U_S I_S \cos(\varphi) \\
&= 3U_S \sqrt{\frac{1+\left(\frac{S}{\sigma S_p}\right)^2}{1+\left(\frac{S}{S_p}\right)^2}} \frac{U_S}{\omega_S L_S} \frac{\frac{S}{\sigma S_p} - \frac{S}{S_p}}{\sqrt{1+\left(\frac{S}{\sigma S_p}\right)^2}\sqrt{1+\left(\frac{S}{S_p}\right)^2}} \\
&= 3\frac{U_S^2}{\omega_S L_S} \frac{\frac{S}{\sigma S_p} - \frac{S}{S_p}}{1+\left(\frac{S}{S_p}\right)^2} \\
&= 3\frac{U_S^2}{\omega_S L_S} \frac{1/\sigma - 1}{\frac{S_p}{S} + \frac{S}{S_p}} \\
&= \frac{3}{2}\frac{U_S^2}{\omega_S L_S} \frac{1-\sigma}{\sigma} \frac{2}{S_p/S + S/S_p} \\
&= \omega_S \tau.
\end{aligned}$$

The mechanical power produced is

$$P_{\text{mech}} = \omega_R \tau$$

and the difference between the power into the stator and the mechanical output power is

$$P_{\text{stator}} - P_{\text{mech}} = (\omega_S - \omega_R)\tau = \omega_S S \tau.$$

Where does this power go? It is now shown that this power is dissipated as heat in the rotor windings, that is, $\omega_S S\tau = 3I_R^2 R_R$. To do so, equation (7.45) is used to obtain

$$\begin{aligned}
I_R^2 &= \frac{\omega_S^2 M^2}{(R_R/S)^2 + \omega_S^2 L_R^2} I_S^2 = \frac{\left(\frac{\omega_S M S}{R_R}\right)^2}{1+\left(\frac{\omega_S L_R S}{R_R}\right)^2} I_S^2 \\
&= \frac{\frac{1}{(1+\sigma_R)(1+\sigma_S)}\left(\frac{\omega_S L_R S}{R_R}\right)\left(\frac{\omega_S L_S S}{R_R}\right)}{1+\left(\frac{S}{\sigma S_p}\right)^2} I_S^2 \\
&= \frac{(1-\sigma)\left(\frac{S}{\sigma S_p}\right)^2 \frac{L_S}{L_R}}{1+\left(\frac{S}{\sigma S_p}\right)^2} I_S^2
\end{aligned}$$

www.EngineeringEBooksPdf.com

Using (7.50) to eliminate I_S^2, this further simplifies to

$$\begin{aligned} I_R^2 &= \frac{(1-\sigma)\left(\frac{S}{\sigma S_p}\right)^2 \frac{L_S}{L_R}}{1+\left(\frac{S}{\sigma S_p}\right)^2} \frac{1+\left(\frac{S}{\sigma S_p}\right)^2}{1+\left(\frac{S}{S_p}\right)^2} \left(\frac{U_S}{\omega_S L_S}\right)^2 \\ &= \frac{(1-\sigma)\left(\frac{S}{\sigma S_p}\right)^2 \frac{L_S}{L_R}}{1+\left(\frac{S}{S_p}\right)^2} \left(\frac{U_S}{\omega_S L_S}\right)^2 \\ &= \frac{U_S^2}{\omega_S^2 L_S} \frac{(1-\sigma)}{\sigma} \frac{\frac{S}{\sigma S_p}}{\frac{S_p}{S}+\frac{S}{S_p}} \frac{1}{L_R} \\ &= \frac{1}{2} \frac{U_S^2}{\omega_S^2 L_S} \frac{(1-\sigma)}{\sigma} \frac{2}{S_p/S+S/S_p} S \frac{\omega_S}{R_R} \end{aligned}$$

where

$$\frac{1}{\sigma S_p L_R} = \frac{1}{\sigma \frac{R_R}{\sigma \omega_S L_R} L_R} = \frac{\omega_S}{R_R}$$

was used. Then

$$3I_R^2 R_R = \left(\frac{3}{2} \frac{U_S^2}{\omega_S^2 L_S} \frac{(1-\sigma)}{\sigma} \frac{2}{S_p/S+S/S_p}\right) S\omega_S = \omega_S S\tau.$$

In summary, it has just been shown that

$$P_{\text{stator}} - P_{\text{mech}} = (\omega_S - \omega_R)\tau = \omega_S S\tau = 3I_R^2 R_R.$$

The mechanical power may be rewritten as

$$P_{\text{mech}} = \omega_R \tau = \frac{\omega_R}{\omega_S S} \omega_S S\tau = \frac{(1-S)\omega_S}{\omega_S S} 3I_R^2 R_R = \frac{1-S}{S} 3I_R^2 R_R$$

so that

$$P_{\text{stator}} = P_{\text{stator}} - P_{\text{mech}} + P_{\text{mech}} = 3I_R^2 R_R + \frac{1-S}{S} 3I_R^2 R_R = 3I_R^2 \frac{R_R}{S}.$$

In words, one can view all of the energy put into the rotor as being dissipated in an "equivalent" resistance of $R_R/S = R_R + (1-S)R_R/S$ where the energy dissipated in R_R are ohmic losses due to the rotor resistance while the energy "dissipated" in $(1-S)R_R/S$ is the mechanical energy produced by the machine (see Figure 7.14).

www.EngineeringEBooksPdf.com

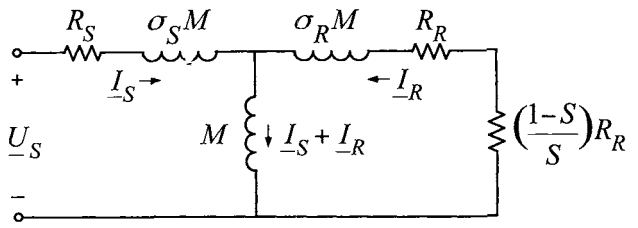


FIGURE 7.14. Mechanical energy represented as a loss in the resistor $(\frac{1-S}{S})R_R$.

Using the expressions (7.50), (7.51), (7.56), and (7.57), the normalized stator current I_S/I_{S_r}, the normalized torque τ/τ_p, and the power factor $\cos(\varphi)$ are plotted versus S/S_p in Figure 7.15.

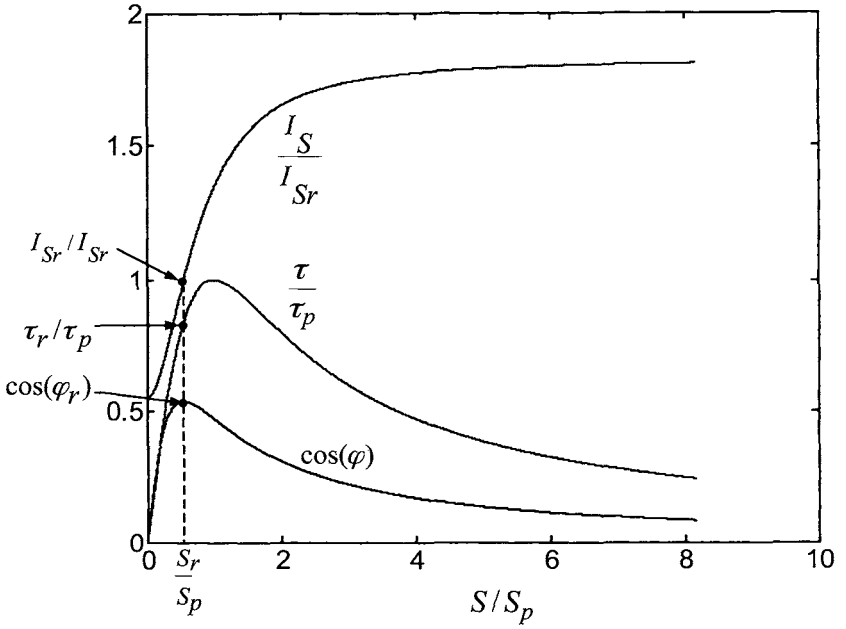


FIGURE 7.15. Plots of $\cos(\varphi)$, τ/τ_r, and I_S/I_{S_r} versus S/S_p with $\sigma = 0.3$, $S_r/S_p = \sqrt{\sigma} = 0.549$, and $\cos(\varphi_r) = (1-\sigma)/(1+\sigma) = 0.537$.

www.EngineeringEBooksPdf.com

Efficiency

The efficiency[8] is defined as

$$\text{Efficiency} \triangleq \frac{P_{\text{mech}}}{P_{\text{stator}}} = \frac{\frac{1-S}{S}3I_R^2R_R}{3I_R^2\frac{R_R}{S}} = 1 - S = \frac{\omega_R}{\omega_S} < 1.$$

The power input to the rotor that is not converted to mechanical power is lost as heat in the rotor windings so it is obviously important to have high efficiency. Consequently, the slip must not be too large and this must be traded off with the amount of torque required since the torque output goes down as the slip is decreased.

Theory Versus Experiment [1][2]

A comparison of the predicted values for the rated slip (7.49), the ratio of the no-load current to the rated current (7.51), the maximum power factor (7.52) and the steady-state torque (7.56) versus their measured values for two motors are reproduced in the tables below from Professor Leonhard's book [1][2]. In the tables, two different 50-Hz motors are used. The first one has two poles ($n_p = 1$) and a corresponding synchronous rotor speed[9] of 50 $\frac{\text{rev}}{\text{sec}} \times 60 \frac{\text{sec}}{\text{min}} \frac{1}{n_p} = 3000$ rev/min. The second motor has eight poles ($n_p = 4$) with a synchronous rotor speed of 50 $\frac{\text{rev}}{\text{sec}} \times 60 \frac{\text{sec}}{\text{min}} \frac{1}{n_p} = 750$ rev/min. The comparison for the two-pole machine (3000 rev/min) with $\sigma = 0.05$ is shown in the table given in Figure 7.16.

Quantity	Predicted Value $\sigma = 0.05$	Actual Value
S_r/S_p	$\sqrt{\sigma} = 0.22$	0.20
I_{S0}/I_{Sr}	$\sqrt{\sigma} = 0.22$	0.30
$\cos(\varphi_r)$	$\frac{1-\sigma}{1+\sigma} = 0.90$	0.90
τ_r/τ_p	$\frac{1+\sigma}{2\sqrt{\sigma}} = 2.35$	2.30

FIGURE 7.16. A table comparing the predicted values of S_r, I_r, φ_r, and τ_r with their measured values for a two-pole machine with $\sigma = 0.05$. From Table 10.2 of *Control of Electrical Drives,* 3rd edition by W. Leonhard, Springer-Verlag, 2001. Reprinted with permission.

[8] Remember that $R_S = 0$ is still assumed.

[9] The synchronous motor speed is the rotor speed with no load and rated frequency applied.

www.EngineeringEBooksPdf.com

The comparison for the eight pole machine (750 rev/min) with $\sigma = 0.10$ is shown in the table given in Figure 7.17.

Quantity	Predicted Value $\sigma = 0.1$	Actual Value
S_r/S_p	$\sqrt{\sigma} = 0.32$	0.30
I_{S0}/I_{Sr}	$\sqrt{\sigma} = 0.32$	0.40
$\cos(\varphi_r)$	$\frac{1-\sigma}{1+\sigma} = 0.82$	0.84
τ_r/τ_p	$\frac{1+\sigma}{2\sqrt{\sigma}} = 1.82$	2.0

FIGURE 7.17. A table comparing the predicted values of S_r, I_r, φ_r, and τ_r with their measured values for an eight pole machine with $\sigma = 0.10$. From Table 10.2 of *Control of Electrical Drives*, 3rd edition by W. Leonhard, Springer-Verlag, 2001. Reprinted with permission.

The predicted values and the measured values are in very good agreement. It is interesting to note that these open-loop characteristics depend only on the leakage parameter σ. This is particularly remarkable as one recalls that in the derivation of the model (7.32)–(7.35), the leakage parameter σ is introduced through the parameter κ ($\sigma = 1 - \kappa^2$) in a pretty much ad hoc manner to account for fact that as the air gap is crossed the magnetic field spreads out in the axial and azimuthal directions. The nonlinear differential equation model (7.31) will be seen to be invaluable for designing feedback controllers for the induction motor, but a more detailed model is needed by machine designers to be able to specify the leakage and therefore the open loop operating characteristics of the machine.

7.3 Mathematical Model of a Three-Phase PM Synchronous Motor

Figure 7.18 shows a sinusoidally wound three-phase synchronous machine with a permanent magnet rotor. The derivation of its mathematical model is now presented. The stator magnetic field is the same as in the case of the induction motor so that it is given by (7.1) which is repeated below.

$$\vec{\mathbf{B}}_S(i_{S1}, i_{S2}, i_{S3}, r, \theta) = \frac{\mu_0 N_S}{2g}\frac{r_R}{r}\Big(i_{S1}\cos(\theta) + i_{S2}\cos(\theta - 2\pi/3) + i_{S3}\cos(\theta - 4\pi/3)\Big)\hat{\mathbf{r}}. \tag{7.58}$$

www.EngineeringEBooksPdf.com

The magnetic field due to the permanent magnet is of the form

$$\vec{\mathbf{B}}_R(r, \theta - \theta_R) = B_m \frac{r_R}{r} \cos(\theta - \theta_R)\hat{\mathbf{r}}.$$

At $r = r_S$ this is written as

$$\vec{\mathbf{B}}_R(r_S, \theta - \theta_R) = \kappa B_m \frac{r_R}{r_S} \cos(\theta - \theta_R)\hat{\mathbf{r}} \tag{7.59}$$

where the coupling factor κ is included to account for leakage. The quantities that are to be computed are the stator flux linkages and the rotor torque. As the rotor has no windings, the torque is computed by finding the torque exerted on the stator windings and then letting $\vec{\boldsymbol{\tau}}_R = -\vec{\boldsymbol{\tau}}_S$. Consequently, the computations can all be done with the value of the total magnetic field at the inside surface of the stator.

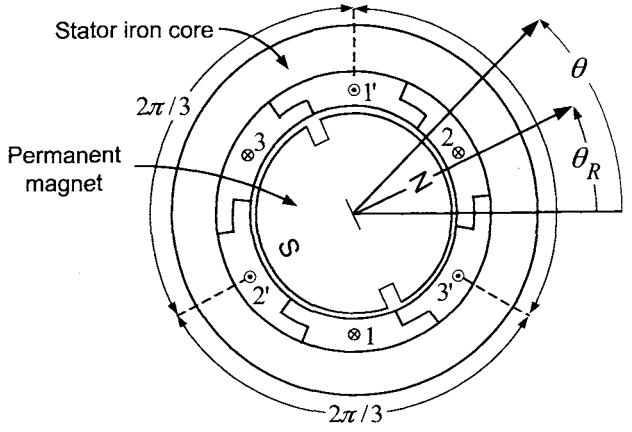


FIGURE 7.18. Three-phase synchronous machine with a permanent magnet rotor.

With $\vec{\mathbf{B}}_S$ and $\vec{\mathbf{B}}_R$ given by (7.58) and (7.59), respectively, the total radial magnetic field $\vec{\mathbf{B}}$ on the stator side of the air gap is

$$\vec{\mathbf{B}}(i_{S1}, i_{S2}, i_{S3}, r_S, \theta, \theta_R) \triangleq \vec{\mathbf{B}}_S(i_{S1}, i_{S2}, i_{S3}, r_S, \theta) + \vec{\mathbf{B}}_R(r_S, \theta - \theta_R). \tag{7.60}$$

www.EngineeringEBooksPdf.com

Stator Flux Linkages

Using (7.60) for $\vec{\mathbf{B}}$ on the stator side of the air gap, the stator flux linkage in stator phase 1 is computed as

$$\begin{aligned}\psi_{S1}(t) &= \int_0^{\pi} \frac{N_S}{2}\sin(\theta) \times \left(\int_{\theta-\pi}^{\theta} \ell_1 r_S B(i_{S1}, i_{S2}, i_{S3}, r_S, \theta', \theta_R) d\theta'\right) d\theta \\ &= \int_0^{\pi} \frac{N_S}{2}\sin(\theta) \times \left(\int_{\theta-\pi}^{\theta} \ell_1 r_S B_S(i_{S1}, i_{S2}, i_{S3}, r_S, \theta') d\theta'\right) d\theta \\ &\quad + \int_0^{\pi} \frac{N_S}{2}\sin(\theta) \times \left(\int_{\theta-\pi}^{\theta} \ell_1 r_S B_R(r_S, \theta' - \theta_R) d\theta'\right) d\theta.\end{aligned}$$

The first integral is the same as in the wound rotor case and the induction motor so that by (7.5) this evaluates to

$$\begin{aligned}&\int_0^{\pi} \frac{N_S}{2}\sin(\theta) \times \left(\int_{\theta-\pi}^{\theta} \ell_1 r_S B_S(i_{S1}, i_{S2}, i_{S3}, r_S, \theta') d\theta'\right) d\theta \\ &\quad = \frac{2}{3} L_S \left(i_{S1} + i_{S2}\cos(2\pi/3) + i_{S3}\cos(4\pi/3)\right)\end{aligned}$$

where

$$L_S = \frac{3}{2}\frac{\pi\mu_0 \ell_1 \ell_2 N_S^2}{8g}. \tag{7.61}$$

The second integral evaluates as

$$\begin{aligned}&\int_0^{\pi} \frac{N_S}{2}\sin(\theta) \left(\int_{\theta-\pi}^{\theta} \kappa B_m \frac{r_R}{r_S}\cos(\theta' - \theta_R)\ell_1 r_S d\theta'\right) d\theta \\ &= \int_0^{\pi} \frac{N_S}{2}\sin(\theta) 2\kappa B_m \frac{r_R}{r_S}\sin(\theta - \theta_R)\ell_1 r_S d\theta \\ &= \kappa \ell_1 r_R B_m N_S \cos(\theta_R)\int_0^{\pi}\sin^2(\theta)d\theta = \kappa\ell_1 r_R B_m N_S\cos(\theta_R)\frac{\pi}{2} \\ &= \kappa\ell_1 r_R B_m N_S \frac{\pi}{2}\cos(\theta_R) \\ &= \sqrt{\frac{2}{3}} K_m \cos(\theta_R)\end{aligned}$$

where

$$K_m \triangleq \sqrt{\frac{3}{2}}\frac{\kappa\pi\ell_1\ell_1 B_m N_S}{4}. \tag{7.62}$$

That is,

$$\psi_{S1}(t) = \frac{2}{3}L_S\left(i_{S1} + i_{S2}\cos(2\pi/3) + i_{S3}\cos(4\pi/3)\right) + \sqrt{\frac{2}{3}}K_m\cos(\theta_R). \tag{7.63}$$

www.EngineeringEBooksPdf.com

Similarly,

$$\psi_{S2}(t)$$
$$= \int_{2\pi/3}^{2\pi/3+\pi} \frac{N_S}{2} \sin(\theta - 2\pi/3) \left(\int_{\theta-\pi}^{\theta} \ell_1 r_S B(i_{S1}, i_{S2}, i_{S3}, r_S, \theta', \theta_R) d\theta' \right) d\theta$$
$$= \frac{2}{3} L_S (i_{S1} \cos(2\pi/3) + i_{S2} + i_{S3} \cos(2\pi/3)) + \sqrt{\frac{2}{3}} K_m \cos(\theta_R - 2\pi/3) \tag{7.64}$$

and

$$\psi_{S3}(t)$$
$$= \int_{4\pi/3}^{4\pi/3+\pi} \frac{N_S}{2} \sin(\theta - 4\pi/3) \left(\int_{\theta-\pi}^{\theta} \ell_1 r_S B(i_{S1}, i_{S2}, i_{S3}, r_S, \theta', \theta_R) d\theta' \right) d\theta$$
$$= \frac{2}{3} L_S (i_{S1} \cos(4\pi/3) + i_{S2} \cos(2\pi/3) + i_{S3}) + \sqrt{\frac{2}{3}} K_m \cos(\theta_R - 4\pi/3). \tag{7.65}$$

The factor $2/3$ in front of L_S and the factor $\sqrt{2/3}$ in front of K_m in equations (7.63), (7.64), and (7.65) are so that the expressions for L_S and K_m are the *two-phase equivalent* coefficient of inductance and back-emf constant, respectively, in the two-phase equivalent model.

In matrix form, the flux linkages may be written as

$$\begin{bmatrix} \psi_{S1}(t) \\ \psi_{S2}(t) \\ \psi_{S3}(t) \end{bmatrix} = \frac{2}{3} L_S \begin{bmatrix} 1 & \cos(2\pi/3) & \cos(4\pi/3) \\ \cos(2\pi/3) & 1 & \cos(2\pi/3) \\ \cos(4\pi/3) & \cos(-2\pi/3) & 1 \end{bmatrix} \begin{bmatrix} i_{S1}(t) \\ i_{S2}(t) \\ i_{S3}(t) \end{bmatrix} + \sqrt{\frac{2}{3}} K_m \begin{bmatrix} \cos(\theta_R) \\ \cos(\theta_R - 2\pi/3) \\ \cos(\theta_R - 4\pi/3) \end{bmatrix}. \tag{7.66}$$

With the obvious definition for matrix C_1, the flux linkages are written more compactly as

$$\begin{bmatrix} \psi_{S1}(t) \\ \psi_{S2}(t) \\ \psi_{S3}(t) \end{bmatrix} = C_1 \begin{bmatrix} i_{S1}(t) \\ i_{S2}(t) \\ i_{S3}(t) \end{bmatrix} + \sqrt{\frac{2}{3}} K_m \begin{bmatrix} \cos(\theta_R) \\ \cos(\theta_R - 2\pi/3) \\ \cos(\theta_R - 4\pi/3) \end{bmatrix}. \tag{7.67}$$

With the stator voltages $u_{S1}(t), u_{S2}(t)$, and $u_{S3}(t)$ assumed to be balanced and R_S the resistance in each stator phase, Faraday's law gives

$$\begin{aligned} u_{S1}(t) &= R_S i_{S1} + \frac{d\psi_{S1}(t)}{dt} \\ u_{S2}(t) &= R_S i_{S2} + \frac{d\psi_{S2}(t)}{dt} \\ u_{S3}(t) &= R_S i_{S3} + \frac{d\psi_{S3}(t)}{dt}. \end{aligned} \tag{7.68}$$

www.EngineeringEBooksPdf.com

Three-Phase to Two-Phase Transformation

The stator voltages are (assumed) balanced and the machine is assumed to be wye-connected so that the stator currents are also balanced. The *three-phase to two-phase* transformation defined by (7.17) is again used to simplify the flux equations by defining

$$\begin{bmatrix} i_{Sa}(t) \\ i_{Sb}(t) \\ i_{S0}(t) \end{bmatrix} \triangleq Q \begin{bmatrix} i_{S1}(t) \\ i_{S2}(t) \\ i_{S3}(t) \end{bmatrix}, \quad \begin{bmatrix} \lambda_{Sa}(t) \\ \lambda_{Sb}(t) \\ \lambda_{S0}(t) \end{bmatrix} \triangleq Q \begin{bmatrix} \psi_{S1}(t) \\ \psi_{S2}(t) \\ \psi_{S3}(t) \end{bmatrix}.$$

where (see problem 4)

$$\begin{aligned} \lambda_{S0}(t) &= \frac{1}{\sqrt{3}}(\psi_{S1}(t) + \psi_{S2}(t) + \psi_{S3}(t)) \equiv 0 \\ i_{S0}(t) &= \frac{1}{\sqrt{3}}(i_{S1}(t) + i_{S2}(t) + i_{S3}(t)) \equiv 0. \end{aligned}$$

The dynamic equations for the stator flux linkages (7.68) then transform to

$$\begin{aligned} u_{Sa}(t) &= R_S i_{Sa} + \frac{d\lambda_{Sa}(t)}{dt} \\ u_{Sb}(t) &= R_S i_{Sb} + \frac{d\lambda_{Sb}(t)}{dt} \\ u_{S0}(t) &= R_S i_{S0} + \frac{d\lambda_{S0}(t)}{dt}. \end{aligned} \tag{7.69}$$

To find the expressions for the two-phase equivalent flux linkages in terms of the two-phase equivalent currents, recall that

$$\begin{bmatrix} \psi_{S1}(t) \\ \psi_{S2}(t) \\ \psi_{S3}(t) \end{bmatrix} = C_1 \begin{bmatrix} i_{S1}(t) \\ i_{S2}(t) \\ i_{S3}(t) \end{bmatrix} + \sqrt{\frac{2}{3}} K_m \begin{bmatrix} \cos(\theta_R) \\ \cos(\theta_R - 2\pi/3) \\ \cos(\theta_R - 4\pi/3) \end{bmatrix}. \tag{7.70}$$

Then

$$\begin{aligned} \begin{bmatrix} \lambda_{Sa}(t) \\ \lambda_{Sb}(t) \\ \lambda_{S0}(t) \end{bmatrix} &= QC_1Q^{-1} \begin{bmatrix} i_{Sa}(t) \\ i_{Sb}(t) \\ i_{S0}(t) \end{bmatrix} + Q\sqrt{\frac{2}{3}} K_m \begin{bmatrix} \cos(\theta_R) \\ \cos(\theta_R - 2\pi/3) \\ \cos(\theta_R - 4\pi/3) \end{bmatrix} \\ &= \begin{bmatrix} L_S & 0 & 0 \\ 0 & L_S & 0 \\ 0 & 0 & 0 \end{bmatrix} \begin{bmatrix} i_{Sa}(t) \\ i_{Sb}(t) \\ i_{S0}(t) \end{bmatrix} + K_m \begin{bmatrix} \cos\theta_R \\ \sin\theta_R \\ 0 \end{bmatrix} \end{aligned} \tag{7.71}$$

or

$$\begin{aligned} \lambda_{Sa}(t) &= L_S i_{Sa}(t) + K_m \cos(\theta_R) \\ \lambda_{Sb}(t) &= L_S i_{Sb}(t) + K_m \sin(\theta_R) \\ \lambda_{S0} &\equiv 0. \end{aligned} \tag{7.72}$$

www.EngineeringEBooksPdf.com

Collecting together equations (7.69) and (7.72), the two-phase equivalent equations for the stator and rotor currents of a *wye connected* three-phase motor become

$$\begin{aligned} u_{Sa} &= L_S \frac{d}{dt} i_{Sa} + K_m \frac{d}{dt} \cos(\theta_R) + R_S i_{Sa} \\ u_{Sb} &= L_S \frac{d}{dt} i_{Sb} + K_m \frac{d}{dt} \sin(\theta_R) + R_S i_{Sb} \\ u_{S0} &= 0 \end{aligned} \tag{7.73}$$

where $i_{S0} \equiv 0$.

Torque

The strategy is to compute the rotor torque $\vec{\tau}_R$ by first determining the torque $\vec{\tau}_S$ that the magnetic field of the rotor's permanent magnet produces on the stator windings and then use $\vec{\tau}_R = -\vec{\tau}_S$. The rotor's magnetic field at the inside surface of the stator is

$$\vec{\mathbf{B}}_R(r_S, \theta - \theta_R) = \kappa B_m \frac{r_R}{r_S} \cos(\theta - \theta_R)\hat{\mathbf{r}}.$$

The torque on stator phase 1 is then computed by

$$\begin{aligned} \vec{\tau}_{S1} &= \int_{\theta=0}^{2\pi} r_S \hat{\mathbf{r}} \times \left(i_{S1}(t) \frac{N_S}{2} \sin(\theta) d\theta (+\ell_1 \hat{\mathbf{z}}) \times \left(B_{R|_{r=r_S}} \hat{\mathbf{r}} \right) \right) \\ &= \int_{\theta=0}^{2\pi} r_S i_{S1}(t) \frac{\ell_1 N_S}{2} \sin(\theta) \left(\kappa B_m \frac{r_R}{r_S} \right) \cos(\theta - \theta_R) d\theta \hat{\mathbf{z}} \\ &= i_{S1}(t) \frac{\kappa B_m \ell_1 r_R N_S}{2} \int_{\theta=0}^{2\pi} \sin(\theta) \cos(\theta - \theta_R) d\theta \hat{\mathbf{z}} \\ &= \kappa \ell_1 r_R B_m N_S \frac{\pi}{2} i_{S1}(t) \sin(\theta_R) \hat{\mathbf{z}} \\ &= \sqrt{\frac{2}{3}} K_m i_{S1}(t) \sin(\theta_R) \hat{\mathbf{z}} \end{aligned} \tag{7.74}$$

where K_m is as given in (7.62).

www.EngineeringEBooksPdf.com

The torque on stator phase 2 of the rotor is then

$$\begin{aligned}
\vec{\tau}_{S2} &= \int_{\theta=0}^{2\pi} r_S\hat{\mathbf{r}} \times \left(i_{S2}(t)\frac{N_S}{2}\sin(\theta - 2\pi/3)d\theta(+\ell_1\hat{\mathbf{z}}) \times \left(B_{R|_{r=r_S}}\hat{\mathbf{r}} \right) \right) \\
&= \int_{\theta=0}^{2\pi} r_S i_{S2}(t)\frac{\ell_1 N_S}{2}\sin(\theta - 2\pi/3)\left(\kappa B_m \frac{r_R}{r_S}\right)\cos(\theta - \theta_R)d\theta\hat{\mathbf{z}} \\
&= i_{S2}(t)\frac{\kappa B_m \ell_1 r_R N_S}{2}\int_{\theta=0}^{2\pi}\sin(\theta - 2\pi/3)\cos(\theta - \theta_R)d\theta\hat{\mathbf{z}} \\
&= i_{S2}(t)\frac{\kappa B_m \ell_1 r_R N_S}{2}\int_{\theta=0}^{2\pi}\frac{1}{2}\left(\sin(2\theta - \frac{2\pi}{3} - \theta_R) + \sin(\theta_R - \frac{2\pi}{3})\right)d\theta\hat{\mathbf{z}} \\
&= \kappa\ell_1 r_R B_m N_S\frac{\pi}{2}i_{S2}(t)\sin(\theta_R - 2\pi/3)\hat{\mathbf{z}} \\
&= \sqrt{\frac{2}{3}}K_m i_{S2}(t)\sin(\theta_R - 2\pi/3)\hat{\mathbf{z}}. \qquad (7.75)
\end{aligned}$$

Finally, the torque on stator phase 3 is computed as

$$\begin{aligned}
\vec{\tau}_{S3} &= \int_{\theta=0}^{2\pi} r_S\hat{\mathbf{r}} \times \left(i_{S3}(t)\frac{N_S}{2}\sin(\theta - 4\pi/3)d\theta(+\ell_1\hat{\mathbf{z}}) \times \left(B_{R|_{r=r_S}}\hat{\mathbf{r}} \right) \right) \\
&= \int_{\theta=0}^{2\pi} r_S i_{S3}(t)\frac{\ell_1 N_S}{2}\sin(\theta - 4\pi/3)\left(\kappa B_m \frac{r_R}{r_S}\right)\cos(\theta - \theta_R)d\theta\hat{\mathbf{z}} \\
&= i_{S3}(t)\frac{\kappa B_m \ell_1 r_R N_S}{2}\int_{\theta=0}^{2\pi}\sin(\theta - 4\pi/3)\cos(\theta - \theta_R)d\theta\hat{\mathbf{z}} \\
&= i_{S3}(t)\frac{\kappa B_m \ell_1 r_R N_S}{2}\int_{\theta=0}^{2\pi}\frac{1}{2}\left(\sin(2\theta - \frac{4\pi}{3} - \theta_R) + \sin(\theta_R - \frac{4\pi}{3})\right)d\theta\hat{\mathbf{z}} \\
&= \kappa\ell_1 r_R B_m N_S\frac{\pi}{2}i_{S3}(t)\sin(\theta_R - 4\pi/3)\hat{\mathbf{z}} \\
&= \sqrt{\frac{2}{3}}K_m i_{S3}(t)\sin(\theta_R - 4\pi/3)\hat{\mathbf{z}}. \qquad (7.76)
\end{aligned}$$

The total torque is then $\tau_S = \tau_{S1} + \tau_{S2} + \tau_{S3}$ or

$$\tau_S = \sqrt{\frac{2}{3}}K_m\Big(i_{S1}\sin(\theta_R) + i_{S2}\sin(\theta_R - 2\pi/3) + i_{S3}\sin(\theta_R - 4\pi/3)\Big). \qquad (7.77)$$

Substitute

$$\begin{bmatrix} i_{S1}(t) \\ i_{S2}(t) \\ i_{S3}(t) \end{bmatrix} \triangleq Q^{-1}\begin{bmatrix} i_{Sa}(t) \\ i_{Sb}(t) \\ i_{S0}(t) \end{bmatrix} = \sqrt{\frac{3}{2}}\begin{bmatrix} 2/3 & 0 & \sqrt{2}/3 \\ -1/3 & 1/\sqrt{3} & \sqrt{2}/3 \\ -1/3 & -1/\sqrt{3} & \sqrt{2}/3 \end{bmatrix}\begin{bmatrix} i_{Sa}(t) \\ i_{Sb}(t) \\ i_{S0}(t) \end{bmatrix}$$

into (7.77) to obtain ($i_{S0}(t) \equiv 0$)

$$\tau_S = K_m\Big(i_{Sa}\sin(\theta_R) - i_{Sb}\cos(\theta_R)\Big). \qquad (7.78)$$

www.EngineeringEBooksPdf.com

The torque on the rotor is then

$$\tau_R = -K_m\Big(i_{Sa}\sin(\theta_R) - i_{Sb}\cos(\theta_R)\Big). \tag{7.79}$$

Substituting the two-phase equivalent stator flux linkages (7.72) into (7.69) along with torque equation (7.79) gives the following two-phase equivalent mathematical model of a three-phase wye-connected permanent magnet synchronous motor

$$\begin{aligned} u_{Sa} &= L_S\frac{di_{Sa}}{dt} + K_m\frac{d}{dt}\cos(\theta_R) + R_S i_{Sa} \\ u_{Sb} &= L_S\frac{di_{Sb}}{dt} + K_m\frac{d}{dt}\sin(\theta_R) + R_S i_{Sb} \\ J\frac{d\omega_R}{dt} &= K_m\Big(i_{Sb}\cos(\theta_R) - i_{Sa}\sin(\theta_R)\Big) - \tau_L \\ \frac{d\theta_R}{dt} &= \omega_R \end{aligned} \tag{7.80}$$

which simplifies to

$$\begin{aligned} L_S\frac{di_{Sa}}{dt} &= -R_S i_{Sa} - K_m\omega_R\sin(\theta_R) + u_{Sa} \\ L_S\frac{di_{Sb}}{dt} &= -R_S i_{Sb} + K_m\omega_R\cos(\theta_R) + u_{Sb} \\ J\frac{d\omega_R}{dt} &= K_m\Big(i_{Sb}\cos(\theta_R) - i_{Sa}\sin(\theta_R)\Big) - \tau_L \\ \frac{d\theta_R}{dt} &= \omega_R. \end{aligned} \tag{7.81}$$

Figure 7.19 is a block diagram for using the two-phase equivalent model to simulate the three-phase model.

Remark

With $L = (2/3)L_S$, and $K = \sqrt{2/3}K_m$ the three-phase flux linkages can be written in a standard three-phase form as

$$\begin{bmatrix} \psi_{S1} \\ \psi_{S2} \\ \psi_{S3} \end{bmatrix} = \begin{bmatrix} L & -L/2 & -L/2 \\ -L/2 & L & -L/2 \\ -L/2 & -L/2 & L \end{bmatrix} \begin{bmatrix} i_{S1} \\ i_{S2} \\ i_{S3} \end{bmatrix} + K\begin{bmatrix} \cos(\theta_R) \\ \cos(\theta_R - 2\pi/3) \\ \cos(\theta_R - 4\pi/3) \end{bmatrix} \tag{7.82}$$

so that

$$\begin{bmatrix} L & -L/2 & -L/2 \\ -L/2 & L & -L/2 \\ -L/2 & -L/2 & L \end{bmatrix} \begin{bmatrix} di_{S1}/dt \\ di_{S2}/dt \\ di_{S3}/dt \end{bmatrix} = K\omega_R\begin{bmatrix} \sin(\theta_R) \\ \sin(\theta_R - 2\pi/3) \\ \sin(\theta_R - 4\pi/3) \end{bmatrix} - R_S\begin{bmatrix} i_{S1} \\ i_{S2} \\ i_{S3} \end{bmatrix} + \begin{bmatrix} u_{S1} \\ u_{S2} \\ u_{S3} \end{bmatrix}. \tag{7.83}$$

www.EngineeringEBooksPdf.com

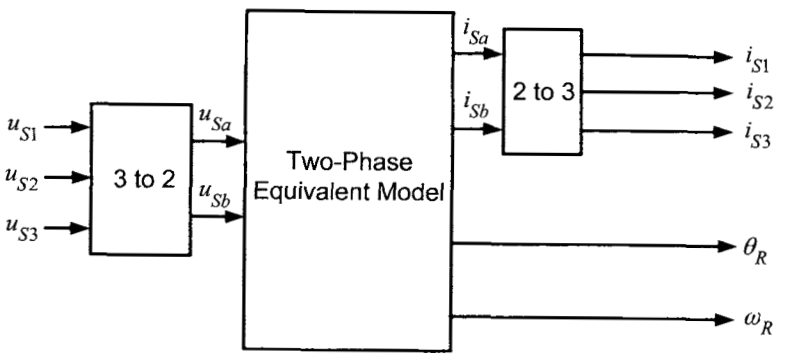


FIGURE 7.19. Three-phase PM motor simulated using a two-phase equivalent model.

The torque is then written as

$$\tau_R = -K\Big(i_{S1}\sin(\theta_R) + i_{S2}\sin(\theta_R - 2\pi/3) + i_{S3}\sin(\theta_R - 4\pi/3)\Big). \tag{7.84}$$

As the currents are balanced ($i_{S1} + i_{S2} + i_{S3} \equiv 0$), equation (7.82) may be rewritten as

$$\begin{bmatrix} \psi_{S1} \\ \psi_{S2} \\ \psi_{S3} \end{bmatrix} = \begin{bmatrix} 3L/2 & 0 & 0 \\ 0 & 3L/2 & 0 \\ 0 & 0 & 3L/2 \end{bmatrix} \begin{bmatrix} i_{S1} \\ i_{S2} \\ i_{S3} \end{bmatrix} + K \begin{bmatrix} \cos(\theta_R) \\ \cos(\theta_R - 2\pi/3) \\ \cos(\theta_R - 4\pi/3) \end{bmatrix} \tag{7.85}$$

and equation (7.83) becomes

$$\begin{bmatrix} di_{S1}/dt \\ di_{S2}/dt \\ di_{S3}/dt \end{bmatrix} = -\frac{2}{3}\frac{R_S}{L}\begin{bmatrix} i_{S1} \\ i_{S2} \\ i_{S3} \end{bmatrix} + \frac{2}{3}\frac{K}{L}\omega_R \begin{bmatrix} \sin(\theta_R) \\ \sin(\theta_R - 2\pi/3) \\ \sin(\theta_R - 4\pi/3) \end{bmatrix} + \frac{2}{3}\frac{1}{L}\begin{bmatrix} u_{S1} \\ u_{S2} \\ u_{S3} \end{bmatrix}. \tag{7.86}$$

www.EngineeringEBooksPdf.com

7.4 Three-Phase, Sinusoidal, 60-Hz Voltages*

Electric machines and power systems have been around for over 100 years. Basic choices in construction and operation of these systems were made along the way. In North America, this has resulted in a power system providing three-phase sinusoidal voltages operating at 60 Hz passing through three-phase transformers to power three-phase induction motors, light buildings, and so on. Why these specific choices? The answer to these questions are given in the book [61] by Laithewaite and Freris and are summarized below.

7.4.1 Why Three-Phase?

Modeling has been done of both two-phase and three-phase AC machines. One could consider a four-phase machine as well. Why are most electric machines three-phase? To answer this question, consider a simple generator shown in Figure 7.20 where a single-phase winding consists of three loops with one of the loops having a side in the slot at $\theta = \pi/3$ (the other side of this loop in the slot at $\theta = 4\pi/3$), another one at $\theta = \pi/2$, and the third one at $\theta = 2\pi/3$.

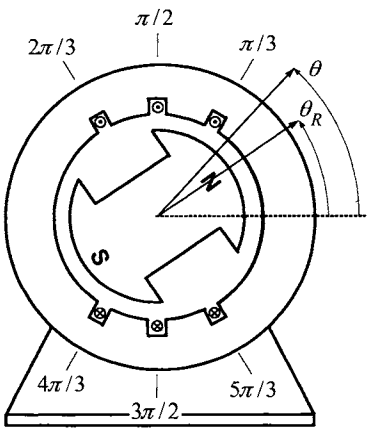


FIGURE 7.20. Computation of the emf in a distributed winding.

Consider the rotor to be a permanent magnet with the magnetic field in the air gap given by

$$\vec{\mathbf{B}}_R(\theta - \theta_R) = B_{\max}\frac{r_R}{r}\cos(\theta - \theta_R)\hat{\mathbf{r}}.$$

With $d\vec{\mathbf{S}} = r_S d\theta d\ell\hat{\mathbf{r}}$ and the rotor moving at a constant angular speed so

www.EngineeringEBooksPdf.com

that $\theta_R = \omega_R t$, the flux in the loop at θ_i is

$$\phi_{\theta_i} = \int_{\substack{\text{Loop from} \\ \theta_i - \pi \text{ to } \theta_i}} \vec{\mathbf{B}}_R \cdot d\vec{\mathbf{S}} = \int_0^{\ell_1} \int_{\theta=\theta_i-\pi}^{\theta=\theta_i} B_{\max} \frac{r_R}{r_S} \cos(\theta - \theta_R) \hat{\mathbf{r}} \cdot (r_S d\theta d\ell \hat{\mathbf{r}})$$
$$= 2\ell_1 r_R B_{\max} \sin(\theta_i - \theta_R).$$

With $\theta_R = \omega_R t$, the corresponding emf is

$$\xi_{\theta_i} = -\frac{d\phi_{\theta_i}}{dt} = V_{\max} \cos(\theta_R - \theta_i) = \text{Re}\{V_{\max} e^{j(\omega_R t - \theta_i)}\}$$

where $V_{\max} \triangleq 2\ell_1 r_R B_{\max} \omega_R$. Denoting the three loops shown in Figure 7.20 as phase 1, the total emf generated in this phase is

$$\begin{aligned} \xi_1 &= V_{\max} \text{Re}\left\{ e^{j(\omega_R t - \pi/3)} + e^{j(\omega_R t - \pi/2)} + e^{j(\omega_R t - 2\pi/3)} \right\} \\ &= V_{\max} \text{Re}\left\{ e^{j\omega_R t} \left(e^{-j\pi/3} + e^{-j\pi/2} + e^{-j2\pi/3} \right) \right\} \\ &= V_{\max}(1 + \sqrt{3}) \cos(\omega_R t - \pi/2) \end{aligned}$$

as $e^{-j\pi/3} + e^{-j\pi/2} + e^{-j2\pi/3} = (1 + \sqrt{3}) e^{-j\pi/2}$.

On the other hand, if all three loops were located in the single pair of slots at $\theta = \pi/2$ and $-\pi/2$, then the generated voltage ζ_1 would be

$$\begin{aligned} \zeta_1 &= 3V_{\max} \text{Re}\left\{ e^{j\omega_R t} e^{-j\pi/2} \right\} \\ &= 3V_{\max} \cos(\omega_R t - \pi/2). \end{aligned}$$

The ratio of these two voltages is then

$$\frac{\xi_1}{\zeta_1} = \frac{1 + \sqrt{3}}{3} = 0.91.$$

That is, by spreading the loops along the inside periphery of the stator, the voltage generated is about 91% of the voltage that would result if all the loops were put in the same slot. Why spread out the windings? A fundamental problem that limits the output power of an electric machine is the amount of heat it generates. So as to not damage the winding insulation by overheating, the amount of heat generated must be limited, and this is directly related to the amount of current in the windings. The addition of a fan on the rotor of the machine greatly enhances the heat transfer (removal) so that much larger currents could be used in the phase windings. (The payoff of being able to have larger currents in the windings greatly outweighs the loss of power due to the drag of the fan.) However, even with a fan, the amount of current in a winding at any location of the stator is still limited. With a current i_S in a phase winding, putting all three loops

www.EngineeringEBooksPdf.com

at one location will generate three times the heat of putting just one loop at the one location. So, if more windings (loops) are desired to obtain a greater generated voltage, they must be distributed around the periphery for cooling (heat transfer) to avoid overheating the insulation.

The above analysis is now generalized to distributing the loops around the complete inner surface of the stator. Reiterating, to obtain more generated voltage out of the machine without overheating it, the loops must be distributed along the inner periphery of the stator.

Single Phase

First consider the case of a *single-phase* machine where N_S stator loops are equally spread around the complete 2π radians of the inner stator surface as shown in Figure 7.21(a).

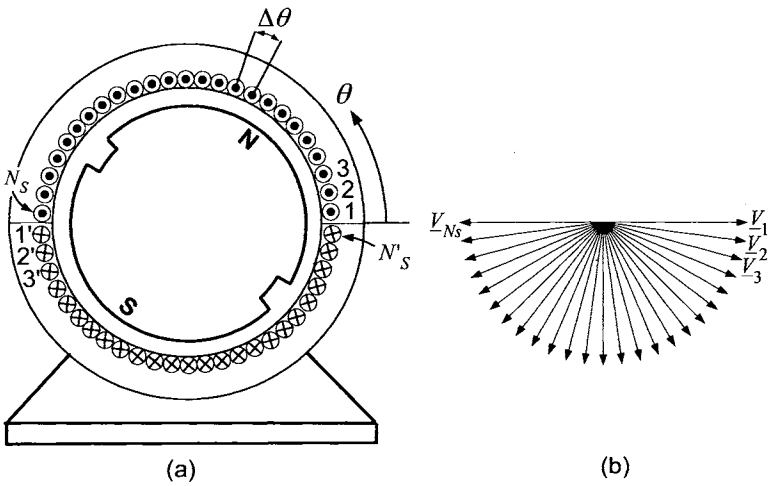


FIGURE 7.21. A single phase machine with a total of N_S turns/loops. (a) The first loop has sides 1, the second loop has sides 2, and so on. with the final loop having sides $N_S - N'_S$. These loops are all electrically connected in series to make up the single-phase winding. (b) The phasors for each loop.

The top sides of the N_S loops are placed in slots on the inside surface of the stator core at

$$\theta_i = (i-1)\Delta\theta \quad \text{for } i = 1, ..., N_S \tag{7.87}$$

where $\Delta\theta = \pi/N_S$ and the other side of each loop is at the diametrically opposite side of the stator. Then the total voltage $\xi_{1\text{ph}}$ generated in this

www.EngineeringEBooksPdf.com

single phase is

$$\begin{aligned}\xi_{1\text{ph}}(t) &= \text{Re}\left\{V_{\max}\left(\sum_{i=1}^{N_S} e^{j(\omega_R t-\theta_i)}\right)\right\} = \text{Re}\left\{\left(\sum_{i=1}^{N_S}\underline{V}_i\right)e^{j\omega_R t}\right\} \\ &= \text{Re}\left\{\underline{\xi}_{1\text{ph}}e^{j\omega_R t}\right\} = \text{Re}\left\{\left|\underline{\xi}_{1\text{ph}}\right|e^{j\angle\underline{\xi}_{1\text{ph}}}e^{j\omega_R t}\right\} \qquad (7.88)\end{aligned}$$

where

$$\underline{V}_i \triangleq V_{\max}e^{-j\theta_i} = V_{\max}e^{-j\left((i-1)\Delta\theta\right)}$$

is the voltage phasor for loop $i-i'$ and

$$\underline{\xi}_{1\text{ph}} \triangleq \sum_{i=1}^{N_S}\underline{V}_i.$$

is the phasor for the total emf generated in the phase.

With N_S large (so $\Delta\theta = \pi/N_S$ is small), the phasors $\underline{V}_i$ in Figure 7.21 put end to end trace out (to a good approximation) a semicircle as illustrated in Figure 7.22 with their sum $\underline{\xi}_{1\text{ph}} = \sum_{i=1}^{N_S}\underline{V}_i$ being the diameter of the semicircle.

On the other hand, if all N_S loops are in the single pair of slots at $\pi/2$ and $3\pi/2$, the generated voltage is ($\underline{V}_1 = V_{\max}$ for the single-phase machine)

$$\zeta_{1\text{ph}}(t) = \text{Re}\left\{\left(N_S\underline{V}_1e^{-j\pi/2}\right)e^{j\omega_R t}\right\} = \text{Re}\left\{\underline{\zeta}_{1\text{ph}}e^{j\omega_R t}\right\}$$

with the magnitude of this voltage phasor given by

$$\left|\underline{\zeta}_{1\text{ph}}\right| = \left|N_S\underline{V}_1\right| = \sum_{i=1}^{N_S}\left|\underline{V}_i\right|.$$

With r the radius of the semicircle, $\left|\underline{\xi}_{1\text{ph}}\right|$ is just the circumferential length πr of the semicircle. It then follows that

$$\begin{aligned}\left|\underline{\xi}_{1\text{ph}}\right| &= \left|\sum_{i=1}^{N_S}\underline{V}_i\right| = 2r \\ \left|\underline{\zeta}_{1\text{ph}}\right| &= \sum_{i=1}^{N_S}\left|\underline{V}_i\right| = \pi r\end{aligned}$$

or

$$\frac{\left|\underline{\xi}_{1\text{ph}}\right|}{\left|\underline{\zeta}_{1\text{ph}}\right|} = \frac{2}{\pi} = 0.636.$$

That is, for a *single-phase* machine, only 63.6% of the voltage is obtained distributing the N_S loops over the inner stator surface compared to being

www.EngineeringEBooksPdf.com

able to put all N_S windings at a single location. However, the distributed winding can carry a much larger current without overheating and damaging the conductor insulation compared to having all the windings concentrated in one pair of slots.

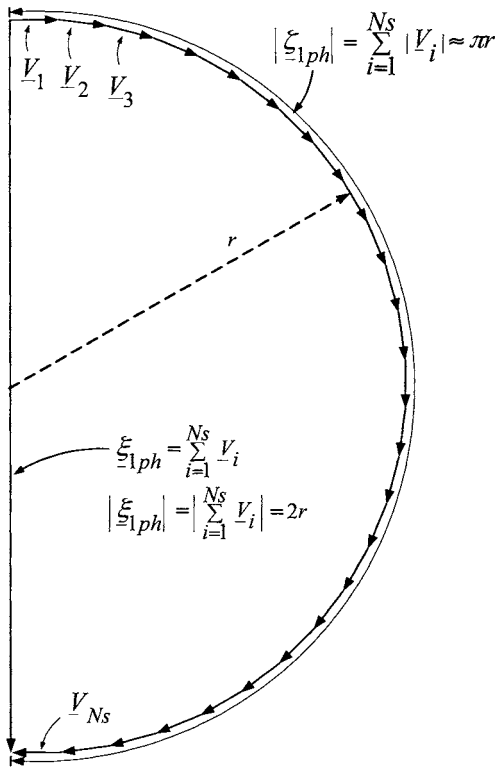


FIGURE 7.22. A geometric representation of the phasor sum $\underline{\boldsymbol{\xi}}_{1\,\mathrm{ph}} = \sum_{i=1}^{N_S} \underline{\mathbf{V}}_i$. The diameter of the semicircle is $\left|\sum_{i=1}^{N_S} \underline{\mathrm{V}}_i\right| = 2r$ while its circumferential length is $\sum_{i=1}^{N_S} |\underline{\mathrm{V}}_i| = \pi r$.

Two Phases

For a two-phase machine with phases 1 and 2, the N_S loops of *each* phase are distributed over only π radians; that is, with $\Delta\theta = \pi/(2N_S)$, the top side of the loops of phase 1 are in the slots at

$$\theta_i = \frac{\pi}{4} + (i-1)\Delta\theta \quad \text{for } i = 1, ..., N_S$$

as shown in Figure 7.23(a).

www.EngineeringEBooksPdf.com

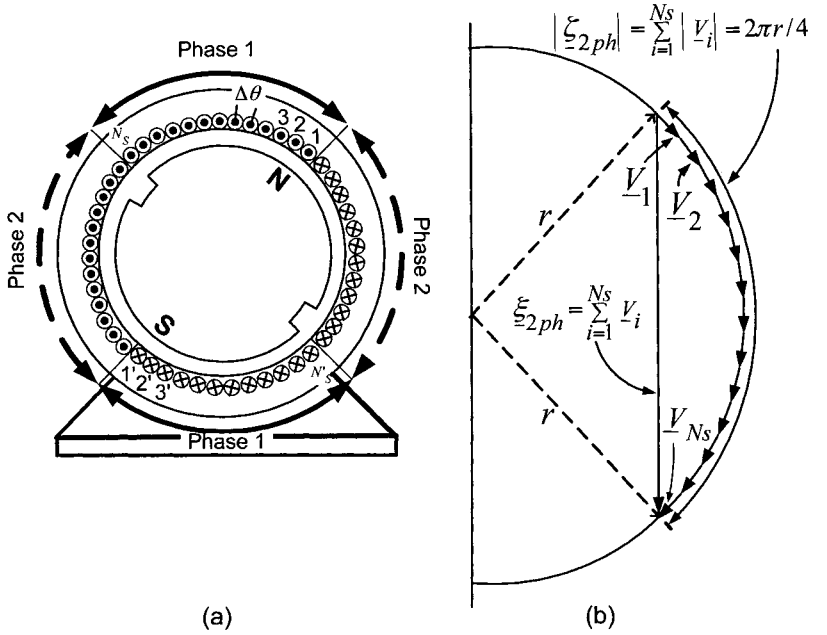


FIGURE 7.23. (a) Distributed two-phase windings. (b) Phasor diagram of the voltages in the loops of phase 1.

In this case, the voltage $\xi_{2\text{ph}}$ generated in this distributed winding is

$$\begin{aligned}\xi_{2\text{ph}}(t) &= \text{Re}\left\{V_{\max}\left(\sum_{i=1}^{N_S} e^{j(\omega_R t-\theta_i)}\right)\right\} = \text{Re}\left\{\left(\sum_{i=1}^{N_S}\underline{V}_i\right)e^{j\omega_R t}\right\} \\ &= \text{Re}\left\{\underline{\boldsymbol{\xi}}_{2\text{ph}}e^{j\omega_R t}\right\} = \text{Re}\left\{\left|\underline{\boldsymbol{\xi}}_{2\text{ph}}\right|e^{j\angle\underline{\boldsymbol{\xi}}_{2\text{ph}}}e^{j\omega_R t}\right\} \qquad (7.89)\end{aligned}$$

where

$$\underline{V}_i \triangleq V_{\max}e^{-j\theta_i} = V_{\max}e^{-j\left((i-1)\Delta\theta\right)}$$

is the voltage phasor for loop $i-i'$ and

$$\underline{\boldsymbol{\xi}}_{2\text{ph}} \triangleq \sum_{i=1}^{N_S}\underline{V}_i$$

is the phasor of the total emf generated in the phase.

With N_S large, the phasors $\underline{V}_i$ put end-to-end trace out a quarter of a circle and their sum $\underline{\boldsymbol{\xi}}_{2\text{ph}} = \sum_{i=1}^{N_S}\underline{V}_i$ is a chord of the circle as illustrated in Figure 7.23(b). The magnitude of this phasor is

$$\left|\underline{\boldsymbol{\xi}}_{2\text{ph}}\right| = \left|\sum_{i=1}^{N_S}\underline{V}_i\right| = \sqrt{2}r$$

www.EngineeringEBooksPdf.com

where r is the radius of the circle.

If all N_S loops are in a single-slot pair at $\pi/2$ and $3\pi/2$, the generated voltage is ($\underline{V}_1 = V_{\max} e^{-j\pi/4}$ for the two-phase machine so that $\underline{V}_1 e^{-j\pi/4} = V_{\max} e^{-j\pi/2}$)

$$\zeta_{2\text{ph}}(t) = \text{Re}\left\{ \left(N_S \underline{V}_1 e^{-j\pi/4} \right) e^{j\omega_R t} \right\} = \text{Re}\left\{ \underline{\zeta}_{2\text{ph}} e^{j\omega_R t} \right\}$$

where the magnitude of this voltage phasor given by

$$\left| \underline{\zeta}_{2\text{ph}} \right| = |N_S \underline{V}_1| = \sum_{i=0}^{N_S} |\underline{V}_i| = \frac{2\pi r}{4}$$

as it is just the circumferential length of the quarter circle. The ratio of the magnitude of these two generated emfs is

$$\frac{\left| \underline{\xi}_{2\text{ph}} \right|}{\left| \underline{\zeta}_{2\text{ph}} \right|} = \frac{2\sqrt{2}}{\pi} = 0.9.$$

Three Phases

For a three-phase motor with phases 1, 2 and 3, the N_S loops of *each* phase are distributed over $2\pi/3$ radians. With $\Delta\theta = \pi/(3N_S)$, the top side of the loops of phase 1 are in the slots at

$$\theta_i = \frac{\pi}{3} + (i-1)\Delta\theta \quad \text{for } i = 1, ..., N_S$$

as illustrated in Figure 7.24. The total voltage $\xi_{3\text{ph}}$ generated in phase 1 is

$$\begin{aligned} \xi_{3\text{ph}}(t) &= \text{Re}\left\{ V_{\max} \left(\sum_{i=1}^{N_S} e^{j(\omega_R t - \theta_i)} \right) \right\} = \text{Re}\left\{ \left(\sum_{i=1}^{N_S} \underline{V}_i \right) e^{j\omega_R t} \right\} \\ &= \text{Re}\left\{ \underline{\xi}_{3\text{ph}} e^{j\omega_R t} \right\} = \text{Re}\left\{ \left| \underline{\xi}_{3\text{ph}} \right| e^{j\angle \underline{\xi}_{3\text{ph}}} e^{j\omega_R t} \right\} \end{aligned} \tag{7.90}$$

where

$$\underline{V}_i \triangleq V_{\max} e^{-j\theta_i} = V_{\max} e^{-j((i-1)\Delta\theta)}$$

is the voltage phasor for loop i–i' and

$$\underline{\xi}_{3\text{ph}} \triangleq \sum_{i=1}^{N_S} \underline{V}_i$$

is the phasor of the total emf generated in the phase.

www.EngineeringEBooksPdf.com

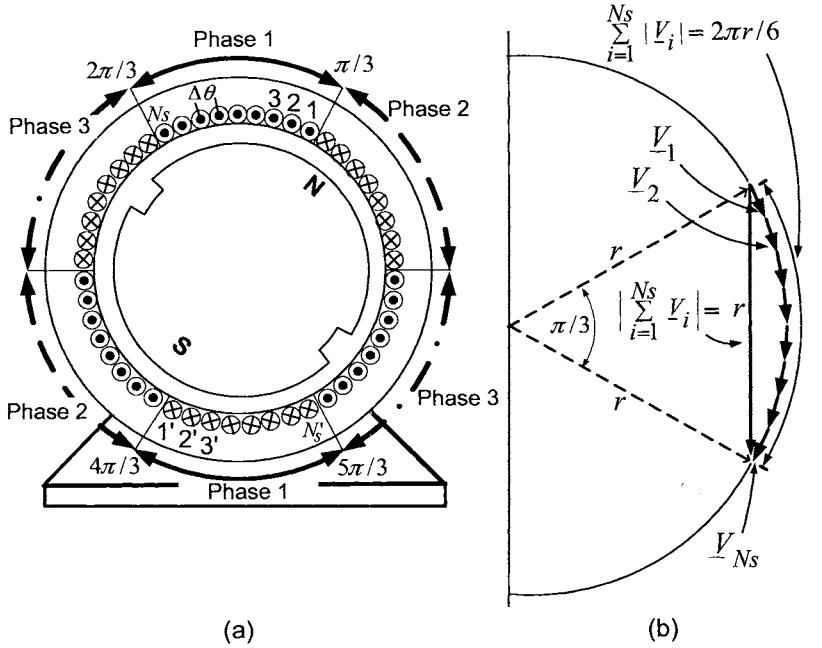


FIGURE 7.24. (a) Distributed three-phase windings. (b) Phasor diagram of the voltages in each loop of phase 1.

With N_S large, the phasors $\underline{V}_i$ put end to end trace out a sixth of a circle and the sum $\underline{\xi}_{3\text{ph}} = \sum_{i=1}^{N_S} \underline{V}_i$ is a chord of this circle as shown in Figure 7.24(b). The magnitude of the phasor $\underline{\xi}_{3\text{ph}}$ is given by

$$\left|\underline{\xi}_{3\text{ph}}\right| = \left|\sum_{i=1}^{N_S} \underline{V}_i\right| = 2r\sin(\pi/6) = r$$

where r is the radius of the circle.

If all N_S loops are in a single-slot pair at $\pi/2$ and $3\pi/2$, the generated voltage $\zeta_{3\text{ph}}(t)$ is given by ($\underline{V}_1 = V_{\max}e^{-j\pi/3}$ for the three-phase machine so that $\underline{V}_1 e^{-j\pi/6} = V_{\max}e^{-j\pi/2}$)

$$\zeta_{3\text{ph}}(t) = \text{Re}\left\{\left(N_S\underline{V}_1 e^{-j\pi/6}\right)e^{j\omega_R t}\right\} = \text{Re}\left\{\underline{\zeta}_{3\text{ph}}e^{j\omega_R t}\right\}$$

where the magnitude of this voltage phasor given by

$$\left|\underline{\zeta}_{3\text{ph}}\right| = |N_S\underline{V}_1| = \sum_{i=0}^{N_S}|\underline{V}_i| = \frac{2\pi r}{6}$$

www.EngineeringEBooksPdf.com

as it is just the circumferential length of the sixth of a circle. The ratio of these generated emfs is

$$\frac{\left|\underline{\xi}_{3\text{ph}}\right|}{\left|\underline{\zeta}_{3\text{ph}}\right|} = \frac{3}{\pi} = 0.955.$$

Four or More Phases

Consider a four-phase machine where the N_S loops of *each* phase are distributed over $\pi/2$ radians, that is, with $\Delta\theta = \pi/(8N_S)$, the top side of the loops of phase 1 are in the slots at

$$\theta_i = \frac{\pi}{2} + (i-1)\Delta\theta \quad \text{for } i = 1, ..., N_S.$$

The ratio of the voltage $\left|\underline{\xi}_{4\text{ph}}\right|$ generated in the distributed windings to the voltage $\left|\underline{\zeta}_{4\text{ph}}\right|$ generated if all the windings are in a single slot is

$$\frac{\left|\underline{\xi}_{4\text{ph}}\right|}{\left|\underline{\zeta}_{4\text{ph}}\right|} \approx \frac{2r\sin(\pi/8)}{\pi r/(4)} = \frac{\sin(\pi/8)}{\pi/8} = 0.975.$$

In general, for a machine with n_{ph} phases, the ratio is given by

$$\frac{\left|\underline{\xi}_{n\text{ph}}\right|}{\left|\underline{\zeta}_{n\text{ph}}\right|} \approx \frac{2r\sin\left(\dfrac{\pi}{2n_{ph}}\right)}{2r\dfrac{\pi}{2n_{ph}}} = \frac{\sin\left(\dfrac{\pi}{2n_{ph}}\right)}{\dfrac{\pi}{2n_{ph}}} \to 1 \text{ as } n_{ph} \to \infty.$$

Finally, for a machine with n_{ph} phases and N_S large, the sum $\sum_{i=1}^{N_S} \underline{V}_i$ from each phase spans a circumferential length of $(1/2)(2\pi r/n_{ph})$, which is approximately $N_S V_{\max}$, that is,

$$\frac{1}{2}\frac{2\pi r}{n_{ph}} \approx N_S V_{\max} \implies 2r \approx \frac{N_S V_{\max}}{\pi/(2n_{ph})}.$$

Comparison

The table below summarizes the results of computing the ratio of the magnitude of the voltage in a distributed winding to that of a concentrated winding when the number of phases is $1, 2, 3$, and 4.

n_{ph}	$\left\|\underline{\xi}_{n\text{ph}}\right\| / \left\|\underline{\zeta}_{n\text{ph}}\right\|$
1	0.636
2	0.900
3	0.955
4	0.975

www.EngineeringEBooksPdf.com

The quantity N_S denotes the total number of loops per phase so that *total* number of loops in a machine with n_{ph} phases is $N_{\text{total}} = n_{ph}N_S$. To make a comparison of the voltage output of machines with different number of phases, it is assumed that the total number of windings N_{total} is the same in each machine. For example, in a three-phase machine, the N_S loops of *each* phase are distributed over $2\pi/3$ radians making full use of the inside stator surface with $N_{total} = 3N_S$. In a three-phase generator, all the available surface area of the inside stator surface is used and the three independent phase voltages coming out of the machine produce 95.5% of the voltage compared to putting all the windings of each phase in a single pair of slots.

A comparison of the machines is done on the basis of the power that can be produced. That is, all things being equal other than the number of phases, how do the number of phases impact the amount of electric power that can be extracted from the machine? The three-phase, two-phase and single-phase machines are now considered in this context.

Let

$$\begin{aligned}
\xi_{S1}(t) &= \text{Re}\left\{\underline{\boldsymbol{\xi}}_{3\text{ph}} e^{j\omega_R t}\right\} \\
\xi_{S2}(t) &= \text{Re}\left\{\underline{\boldsymbol{\xi}}_{3\text{ph}} e^{-j2\pi/3} e^{j\omega_R t}\right\} \\
\xi_{S3}(t) &= \text{Re}\left\{\underline{\boldsymbol{\xi}}_{3\text{ph}} e^{-j4\pi/3} e^{j\omega_R t}\right\}
\end{aligned}$$

be the generated voltages with $\underline{\boldsymbol{\xi}}_{3\text{ph}} = \sum_{i=1}^{N_S} \underline{V}_i$ the sum of the phasors in phase 1.

In a three-phase machine, the generated output power is

$$p_{3\text{phase}} = i_{S1}\xi_{S1} + i_{S2}\xi_{S2} + i_{S3}\xi_{S3}$$

and, in steady state with $\theta_R = \omega_R t$ and a balanced load, the currents constitute a three-phase balanced set of the form

$$\begin{aligned}
i_{S1} &= I\cos(\omega_R t + \angle\underline{\boldsymbol{\xi}}_{3\text{ph}} - \phi_{3\text{ph}}) \\
i_{S2} &= I\cos(\omega_R t - 2\pi/3 + \angle\underline{\boldsymbol{\xi}}_{3\text{ph}} - \phi_{3\text{ph}}) \\
i_{S3} &= I\cos(\omega_R t - 4\pi/3 + \angle\underline{\boldsymbol{\xi}}_{3\text{ph}} - \phi_{3\text{ph}}).
\end{aligned}$$

www.EngineeringEBooksPdf.com

Under these conditions, the output power is constant and equal to

$$\begin{aligned}
p_{3\text{phase}} &= i_{S1}\xi_{S1} + i_{S2}\xi_{S2} + i_{S3}\xi_{S3} \\
&= \frac{\sin(\pi/6)}{\pi/6} N_S V_{\max} I \Big(\cos(\omega_R t + \angle\underline{\boldsymbol{\xi}}_{3\text{ph}})\cos(\omega_R t + \angle\underline{\boldsymbol{\xi}}_{3\text{ph}} - \phi_{3\text{ph}}) \\
&\quad + \cos(\omega_R t + \angle\underline{\boldsymbol{\xi}}_{3\text{ph}} - 2\pi/3)\cos(\omega_R t - 2\pi/3 + \angle\underline{\boldsymbol{\xi}}_{3\text{ph}} - \phi_{3\text{ph}}) \\
&\quad + \cos(\omega_R t + \angle\underline{\boldsymbol{\xi}}_{3\text{ph}} - 4\pi/3)\cos(\omega_R t - 4\pi/3 + \angle\underline{\boldsymbol{\xi}}_{3\text{ph}} - \phi_{3\text{ph}})\Big) \\
&= \frac{3}{2}\frac{\sin(\pi/6)}{\pi/6} N_S V_{\max} I \cos(\phi_{3\text{ph}}) \\
&= (0.955)\,\frac{1}{2} N_{\text{total}} V_{\max} I \cos(\phi_{3\text{ph}})
\end{aligned}$$

where $N_{\text{total}} = 3N_S$ in a three-phase machine.

In a similar fashion, let

$$\begin{aligned}
\xi_{S1}(t) &= \text{Re}\Big\{\underline{\boldsymbol{\xi}}_{2\text{ph}} e^{j\omega_R t}\Big\} \\
\xi_{S2}(t) &= \text{Re}\Big\{\underline{\boldsymbol{\xi}}_{2\text{ph}} e^{-j\pi/2} e^{j\omega_R t}\Big\}
\end{aligned}$$

be the generated voltages in the two-phase machine where $\underline{\boldsymbol{\xi}}_{2\text{ph}} = \sum_{i=1}^{N_S} \underline{V}_i$ is the sum of the voltage phasors of phase 1. It is straightforward to show that the power in a two-phase machine is constant and given by ($N_{\text{total}} = 2N_S$ in a two-phase machine)

$$\begin{aligned}
p_{2\text{phase}} &= i_{S1}\xi_{S1} + i_{S2}\xi_{S2} \\
&= N_S \frac{\sin(\pi/4)}{\pi/4} V_{\max} I \Big(\cos(\omega_R t + \angle\underline{\boldsymbol{\xi}}_{2\text{ph}})\cos(\omega_R t + \angle\underline{\boldsymbol{\xi}}_{2\text{ph}} - \phi_{2\text{ph}}) \\
&\qquad + \cos(\omega_R t + \angle\underline{\boldsymbol{\xi}}_{2\text{ph}} - \frac{\pi}{2})\cos(\omega_R t + \angle\underline{\boldsymbol{\xi}}_{2\text{ph}} - \frac{\pi}{2} - \phi_{2\text{ph}})\Big) \\
&= \frac{1}{2}\frac{\sin(\pi/4)}{\pi/4} N_{\text{total}} V_{\max} I \cos(\phi_{2\text{ph}}) \\
&= (0.9)\,\frac{1}{2} N_{\text{total}} V_{\max} I \cos(\phi_{2\text{ph}}).
\end{aligned}$$

In a *single-phase* generator, there would be N_{total} windings distributed around the inner stator surface. The power is not constant in this case as

$$\begin{aligned}
\xi_{S1}(t) &= \text{Re}\Big\{\underline{\boldsymbol{\xi}}_{1\text{ph}} e^{j\omega_R t}\Big\} \\
i_{S1} &= I\cos(\omega_R t + \angle\underline{\boldsymbol{\xi}}_{1\text{ph}} - \phi_{1\text{ph}})
\end{aligned}$$

www.EngineeringEBooksPdf.com

and

$$\begin{aligned} p_{\text{single-phase}} &= \xi_{S1} i_{S1} \\ &= \left(N_{\text{total}} V_{\max} \cos(\omega_R t + \angle \underline{\boldsymbol{\xi}}_{1\text{ph}})\right)\left(I \cos(\omega_R t + \angle \underline{\boldsymbol{\xi}}_{1\text{ph}} - \phi_{1\text{ph}})\right) \\ &= N_{\text{total}} V_{\max} I \frac{\sin(\pi/2)}{\pi/2} \frac{1}{2}\left(\cos(\phi_{1\text{ph}}) + \cos(2\omega_R t + 2\angle \underline{\boldsymbol{\xi}}_{1\text{ph}} - \phi_{1\text{ph}})\right). \end{aligned}$$

The average power is

$$\begin{aligned} \langle p_{\text{single-phase}} \rangle &\triangleq \frac{1}{2\pi} \int_0^{2\pi} p_{\text{single-phase}}(\omega_R t) d(\omega_R t) \\ &= (0.64) \frac{1}{2} N_{\text{total}} V_{\max} I \cos(\phi_{1\text{ph}}). \end{aligned}$$

For the same-size machine (that is, air gap length, rotor radius, stator radius, axial length, etc.) with the same total number of windings, the same current in the windings and operating at the same power factor (so that $\phi_{1\text{ph}} = \phi_{2\text{ph}} = \phi_{3\text{ph}}$), the single-phase machine can (on average) only generate 0.64/0.955 or 67% of the power of the three-phase system. Similarly, the two-phase machine can only generate 0.9/0.955 (94.2%) of a three-phase system. A three-phase machine can generate 95.5% (0.955) of the power that an ideal machine with an infinite number of phases could produce. Going to a four-phase machine results in a gain of only 2% compared to a three-phase machine (that is, $p_{4\text{phase}} = (0.975/0.955) p_{3\text{phase}} = (1.02) p_{3\text{phase}}$). This analysis shows that a three-phase generator is a good trade-off between complexity (that is, number of phases) and the achievable output power of the machine.

Sinusoidally Wound Stator

The windings in a practical machine can be approximately sinusoidally wound in two layers as illustrated in Figure 7.25 (see also Figures 7.1 and 7.2). As shown previously, the windings are distributed this way so that the radial magnetic field in the air gap produced by the stator currents is (approximately) sinusoidally distributed in space (as is the magnetic field due to the rotor currents). Note that the periphery of the inside surface of the stator has the loops evenly distributed (in two layers) over the complete circumference.

www.EngineeringEBooksPdf.com

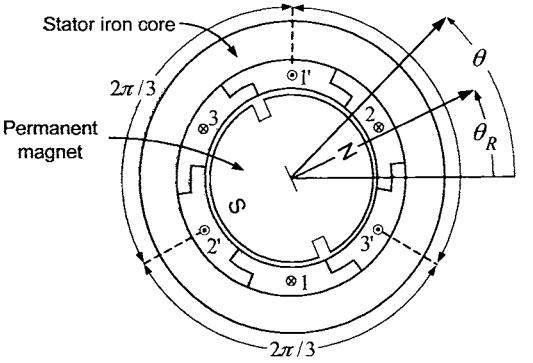


FIGURE 7.25. Three-phase sinusoidally wound PM synchronous motor.

In this case, the voltage produced by phase 1 is (see Figure 7.2)

$$\begin{aligned}\xi_1 &= V_{\max}\,\mathrm{Re}\left\{e^{j(\omega_R t-\pi/3)}+2e^{j(\omega_R t-\pi/2)}+e^{j(\omega_R t-2\pi/3)}\right\}\\ &= V_{\max}\,\mathrm{Re}\left\{e^{j\omega_R t}\left(e^{-j\pi/3}+2e^{-j\pi/2}+e^{-j2\pi/3}\right)\right\}\\ &= V_{\max}(2+\sqrt{3})\cos(\omega_R t-\pi/2)\end{aligned}$$

where $e^{-j\pi/3}+2e^{-j\pi/2}+e^{-j2\pi/3}=(2+\sqrt{3})e^{-j\pi/2}$, $\omega_R \triangleq d\theta_R/dt$, and $V_{\max}\triangleq 2\ell_1 r_R B_{\max}\omega_R$.

This can be compared to the voltage produced by putting all four windings in a single slot where the ratio of the magnitude of these two voltages is $(2+\sqrt{3})/4=0.933$.

On the other hand, if only one layer was used, the four loops would be evenly spread over $2\pi/3$ radians. The resulting voltage would then be ($\Delta\theta=\frac{\pi/3}{4}=\frac{\pi}{12}, \theta_i=\frac{9\pi}{24}+(i-1)\frac{\pi}{12}$ for $i=1,2,3,4$.)

$$\begin{aligned}\xi_1 &= V_{\max}\,\mathrm{Re}\left\{e^{j(\omega_R t-9\pi/24)}+e^{j(\omega_R t-11\pi/24)}+e^{j(\omega_R t-13\pi/24)}\right.\\ &\quad\left.+e^{j(\omega_R t-15\pi/24)}\right\}\\ &= V_{\max}\,\mathrm{Re}\left\{e^{j\omega_R t}\left(e^{-j9\pi/24}+e^{-j11\pi/24}+e^{-j13\pi/24}+e^{-j15\pi/24}\right)\right\}\\ &= V_{\max}\left(\sin(9\pi/24)+\sin(11\pi/24)+\sin(13\pi/24)+\sin(15\pi/24)\right)\\ &\quad\times\cos(\omega_R t-\pi/2)\\ &= 3.83V_{\max}\cos(\omega_R t-\pi/2)\end{aligned}$$

and the ratio would be $3.83/4=0.958$. Though this gives a higher voltage output, this configuration requires 24 slots (one side of a loop in each slot) compared to the one of Figure 7.25 which requires only 12 slots (two loops

www.EngineeringEBooksPdf.com

in each slot). The mechanical integrity of the machine usually favors going with 12 slots as there is more stator iron between the slots in this case.

7.4.2 Why AC?

Why is the power system AC and not DC? A three-phase generator supplies constant power by producing three balanced *sinusoidal* voltages to a balanced three-phase load. Historically, the use of AC power was important for efficient distribution of electric power over long distances. To explain, consider a three-phase generator connected to a balanced three-phase power line which is then connected to a balanced three-phase load. Let the output voltages of the generator be of the form

$$\begin{aligned} v_{S1} &= V\cos(\omega t - \pi/2) \\ v_{S2} &= V\cos(\omega t - \pi/2 - 2\pi/3) \\ v_{S3} &= V\cos(\omega t - \pi/2 - 4\pi/3) \end{aligned}$$

and the corresponding currents are of the form

$$\begin{aligned} i_{S1} &= I\cos(\omega t - \pi/2 - \phi) \\ i_{S2} &= I\cos(\omega t - \pi/2 - 2\pi/3 - \phi) \\ i_{S3} &= I\cos(\omega t - \pi/2 - 4\pi/3 - \phi). \end{aligned}$$

The frequency $\omega = 2\pi f$ is constant at 60 Hz (50 Hz in Europe). Here the quantities I and ϕ depend on the values of the inductances and resistances of the generator, the transmission line, and the load as well as the operating frequency. The power delivered by the generator is then

$$p_{\text{generator}} = v_{S1}i_{S1} + v_{S2}i_{S2} + v_{S3}i_{S3} = \frac{3}{2}VI\cos(\phi).$$

Let the power line have length ℓ and let R denote the resistance per unit length in each phase of the power line so that the average electric power lost in the line is then

$$p_{\text{lost}} = \frac{3}{2}\ell RI^2.$$

The power delivered to the load is then

$$p_{\text{load}} = p_{\text{generator}} - p_{\text{lost}} = \frac{3}{2}VI\cos(\phi) - \frac{3}{2}\ell RI^2$$

For a given total resistance ℓR in the line, one keeps the loss down by delivering the power using as little current as possible. For a given power factor $\cos(\phi)$ (fixed by the impedances of the load and power line), the power delivered $\frac{3}{2}VI\cos(\phi)$ depends on the product VI. The generator is designed to put out a large voltage V (accomplished by putting many

www.EngineeringEBooksPdf.com

turns in each stator slot and having a strong rotor magnetic field[10]) so that the current is (relatively) small and yet the generator still delivers the requisite power needed by the load.[11] However, though the power is efficiently delivered to the load, the voltage is too large to be used by the consumer (industrial or home). As this power is AC, it can be stepped down by a transformer to a level that can be used by the consumer for lighting, running motors, and so on.[12] The induction motor was (and still is) so important because it could be started and run open-loop off of a three-phase AC power supply.[13] (The synchronous motor would not work because it cannot be started by direct connection to a three-phase 60-Hz AC source and can stall out of control quite easily under changing loads when run in open loop.) For these reasons, AC power won out over DC power many years ago. An interesting article on this history is Ref. [62].

7.4.3 Why Sinusoidal Voltages?

The question still remains as to why sinusoids for the voltages. The voltage out of the generator will be periodic as long as the generator is run at constant speed. Why is the rotor iron designed to produce a sinusoidally distributed magnetic field in the air gap resulting in sinusoidal voltages induced in the sinusoidally distributed stator windings? Again, the answer to this question is provided in Laithwaite and Freris [61]. It comes down to the fact that sinusoids are the only signals that can be passed through a stable linear time-invariant system and still be sinusoids. For example, consider the transmission of the power through a transformer. Let the three-phase output voltages of the generator be of the form

$$\begin{aligned} v_{S1} &= V\cos(\omega t) \\ v_{S2} &= V\cos(\omega t - 2\pi/3) \\ v_{S3} &= V\cos(\omega t - 4\pi/3). \end{aligned}$$

---

[10] $V \propto N_{\text{total}} V_{\max} = N_{\text{total}} 2\ell_1 r_R B_{\max} \omega_R$

[11] As pointed out in Ref. [61], it is still a tradeoff in the sense that the higher the voltage adopted, the higher costs in the insulation for the power lines, the higher the transmission towers, the wider the right-of-way for the transmission lines, and so on. This cost must be traded off with the cost due to energy losses in the power line.

[12] Of course, transformers don't work with DC voltages and it was only in the latter part of the 20th century that power elecronics has provided the means to step down DC voltages.

[13] The argument for the DC generation was that the DC motor could be employed by the end user. However, as the voltage could not be large in order to run the DC motor, the transmitted voltages from the DC generator must be (relatively) small. The losses in the power lines delivering this DC power (low voltage and high current) over large distances are so great that a DC power grid would have required building a power station every 2 kilometers or so!

www.EngineeringEBooksPdf.com

Let these voltages be input to a transformer in the power system so that with N_2/N_1 the transformer ratio, the output voltages are then

$$\begin{aligned} v'_{S1} &= \frac{N_2}{N_1} v_{S1} \\ v'_{S2} &= \frac{N_2}{N_1} v_{S2} \\ v'_{S2} &= \frac{N_2}{N_1} v_{S2} \end{aligned}$$

for an *ideal* transformer. The corresponding transfer function of the ideal transformer is then [see Figure 7.26(a)]

$$G_{\text{ideal}}(j\omega) \triangleq \frac{V'_{S1}(j\omega)}{V_{S1}(j\omega)} = \frac{N_2}{N_1}.$$

However, real transformers are not ideal. Figure 7.26(b) shows an equivalent circuit model for a nonideal transformer connected to a resistive load.

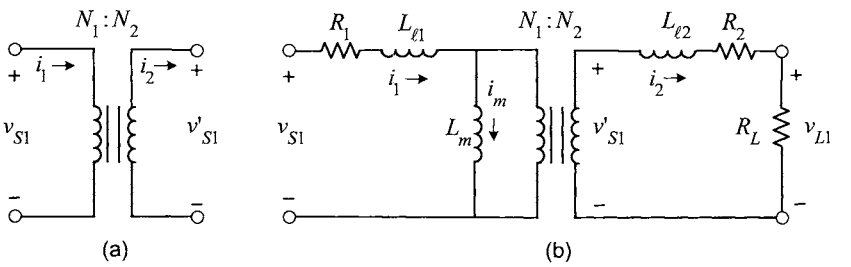


FIGURE 7.26. (a) Ideal transformer. (b) Nonideal transformer whose primary is connected to one phase of a three-phase source and whose secondary is connected to a load.

With

$$\begin{aligned} a_0 &= R_1R_2 + R_1R_L \\ a_1 &= L_{\ell 2}R_1 + L_mR_1n^2 + L_{\ell 1}R_2 + L_mR_2 + L_{\ell 1}R_{\text{load}} + L_mR_L \\ a_2 &= L_{\ell 1}L_{\ell 2} + L_{\ell 2}L_m + L_{\ell 1}L_mn^2 \\ b_1 &= nR_LL_m \\ n &= N_2/N_1 \end{aligned}$$

the transfer function of the nonideal transformer is

$$G(s) \triangleq \frac{V_{L1}(s)}{V_{S1}(s)} = \frac{b_1 s}{a_2 s^2 + a_1 s + a_0}.$$

www.EngineeringEBooksPdf.com

The output voltages are then

$$\begin{aligned} v_{L1}(\omega t) &= |G(j\omega)|\, V \cos\Big(\omega t + \angle G(j\omega)\Big) \\ v_{L2}(\omega t) &= |G(j\omega)|\, V \cos\Big(\omega t - 2\pi/3 + \angle G(j\omega)\Big) \\ v_{L2}(\omega t) &= |G(j\omega)|\, V \cos\Big(\omega t - 4\pi/3 + \angle G(j\omega)\Big) \end{aligned}$$

which is still a balanced three-phase set of sinusoidal voltages! That is, they are sinusoidal voltages of the same form as the input only shifted in phase by $\angle G(j\omega)$ and scaled in amplitude by the factor $|G(j\omega)|$. In particular, a three-phase induction motor is designed to run efficiently off any three-phase set of *sinusoidal* voltages.

Suppose the generator produced a periodic waveform $w_{S1}(\omega t)$ that is not sinusoidal. The waveform $w_{S1}(\omega t)$ can be expanded in a Fourier series as

$$w_{S1}(\omega t) = \sum_{n=1}^{\infty} A_n \cos(n\omega t + \Phi_i)$$

where $A_1 \neq 0$ and $A_n \neq 0$ for some $n \geq 2$ (in the sinusoidal case, $A_n = 0$ for *all* $n \geq 2$). When passed through the (nonideal) transformer, the output voltage will then be

$$w'_{S1}(\omega t) = \sum_{n=1}^{\infty} A_n\, |G(jn\omega)| \cos\Big(n\omega t + \Phi_i + \angle G(jn\omega)\Big).$$

The output waveform is distorted when compared to the input waveform as the different harmonic components ($n = 1, 2, ...$) of the waveform are shifted in phase by different amounts $\angle G(jn\omega)$ and are scaled in amplitude by different amounts $|G(jn\omega)|$. As a result, the output waveform does not have the same shape as the input voltage.

Of course, in addition to transformers, the generated power goes through transmission lines that are effectively modeled by *RLC* circuits and are also stable linear time-invariant systems. As long as the output voltage of the generator is a pure sinusoid, it may pass through any number of such systems and remain a pure sinusoid.

By designing the generator to produce a balanced set of three-phase *sinusoidal* voltages and designing the motors to run off of a balanced set of three-phase *sinusoidal* voltages, the transmission line and the transformer between the two will still output a (stepped-down) balanced three-phase set of *sinusoidal* voltages to provide the right match between the two.

7.4.4 Why 60 Hz?

The use of 60 Hz for the frequency of a power system is trade-off just as all the other choices in a power system [61]. A 10-Hz source would provide

www.EngineeringEBooksPdf.com

too much flicker in electric lights as perceived by the human eye to be of use. However, 50 Hz or 60 Hz is of high enough frequency so that no flicker is perceived. As far as an upper limit in frequency, note that the angle ϕ between the voltage and current increases as the operating frequency increases so that the power factor $\cos(\phi)$ goes down at higher frequency. Further, the upper limit in frequency is also limited by losses and resonance problems. For example, in the iron of electric machines and transformers connected to a power system, the hysteresis losses go up in proportion to the frequency ($p_{\text{hysteresis\_loss}}/\text{volume} = \frac{\omega}{2\pi} \oint_{cycle} HdB$) while the eddy current losses go up in proportion to the *square* of the frequency. Further, the distributed inductances and capacitances in the power line result in a transfer function for the power network that can have resonances at high frequencies, and thus the operating frequency of the power system must be well below any such resonant frequencies. Airplanes typically have a 400-Hz power system, but as the power system is spatially contained, such resonances can be avoided by design. In the case of aircraft, using a power system with higher frequency reduces the amount of iron, and therefore weight, required in transformers, which is obviously important.

Problems

Calculations

Problem 1 Stator Flux Linkages

Carry out the integrations to compute the expressions for the stator flux linkages given in equations (7.5), (7.6), and (7.7).

Problem 2 Rotor Flux Linkages

Carry out the integrations to compute the expressions for the stator flux linkages given in equations (7.11), (7.12), and (7.13).

Problem 3 Balanced Conditions

Show that

$$\begin{aligned} 1 + \cos(2\pi/3) + \cos(4\pi/3) &= 0 \\ \sin(2\pi/3) + \sin(4\pi/3) &= 0 \\ 1 + e^{j2\pi/3} + e^{j4\pi/3} &= 0 \\ \cos(\theta_R) + \cos(\theta_R - 2\pi/3) + \cos(\theta_R - 4\pi/3) &\equiv 0 \\ \cos(\theta_R) + \cos(\theta_R + 2\pi/3) + \cos(\theta_R + 4\pi/3) &\equiv 0 \end{aligned}$$

Problem 4 Balanced Conditions

Using the identities from problem 3, and equations (7.10) and (7.15),

www.EngineeringEBooksPdf.com

show that

$$\begin{aligned}\psi_{S1}(t)+\psi_{S2}(t)+\psi_{S3}(t) &\equiv 0\\ \psi_{R1}(t)+\psi_{R2}(t)+\psi_{R3}(t) &\equiv 0.\end{aligned}$$

Problem 5 Three-Phase to Two-Phase Transformation
Verify equation (7.20).

Problem 6 Three-Phase to Two-Phase Transformation
Verify equation (7.23).

Problem 7 Induction Motor with Unbalanced Voltages
The system of equations (7.25) are valid even if the voltages are not balanced. Explain why the two-phase model (7.31) is no longer an equivalent *model, that is, knowledge of the two-phase variables $i_{Sa}, i_{Sb}, i_{Ra}, i_{Rb}, u_{Sa}, u_{Sb}$, ω, and θ is not enough to determine the three-phase variables $i_{S1}, i_{S2}, i_{S3}, i_{R1}$, $i_{R2}, i_{R3}, u_{S1}, u_{S2}, u_{S3}, \omega$, and θ. What if $u_{S0} = \sqrt{3}v_{\hat{N}N} = (u_{S1}+u_{S2}+u_{S3})/\sqrt{3}$ is known?*
Do the three-phase variables uniquely determine the two-phase variables if the voltages are unbalanced?

Problem 8 Induction Motor Torque
Verify the calculations used to derive the expressions for the phase torques given in equations (7.26), (7.27), and (7.28).

Problem 9 Three-Phase to Two-Phase Transformation
Show that with the three-phase to two-phase transformation given by (7.17), it follows that

$$u_{Sa}(t)i_{Sa}(t)+u_{Sb}(t)i_{Sb}(t)=u_{S1}(t)i_{S1}(t)+u_{S2}(t)i_{S2}(t)+u_{S3}(t)i_{S3}(t).$$

Problem 10 Three-Phase to Two-Phase Transformation
Do the calculations to verify that (7.30) is the correct expression for the two-phase equivalent torque.

Space Vector Induction Motor Models

Problem 11 Space Vector Form of the Three-Phase to Two-Phase Transformation
Defining $\underline{u}_S \triangleq u_{Sa}+ju_{Sb}$, show that the three-phase to two-phase transformation

$$\begin{bmatrix} u_{Sa}(t)\\ u_{Sb}(t)\end{bmatrix} \triangleq \sqrt{\frac{2}{3}}\begin{bmatrix} 1 & -1/2 & -1/2\\ 0 & \sqrt{3}/2 & -\sqrt{3}/2\end{bmatrix}\begin{bmatrix} u_{S1}(t)\\ u_{S2}(t)\\ u_{S3}(t)\end{bmatrix}$$

may be written as

$$\underline{u}_S = u_{Sa}+ju_{Sb}=\sqrt{\frac{2}{3}}\left(u_{S1}+u_{S2}e^{j2\pi/3}+u_{S3}e^{j4\pi/3}\right)$$

www.EngineeringEBooksPdf.com

and similarly for $\underline{i}_S, \underline{i}_R$, *and so on.*

Problem 12 Alternative Definition of the Three-Phase to Two-Phase Transformation [1]

(a) Show that if the three-phase to two-phase transformation is defined by

$$\begin{aligned} \underline{u}_S &= u_{S1} + u_{S2}e^{j2\pi/3} + u_{S3}e^{j4\pi/3} \\ \underline{i}_S &= i_{S1} + i_{S2}e^{j2\pi/3} + i_{S3}e^{j4\pi/3} \\ \vdots &= \vdots \end{aligned}$$

that is, without the factor $\sqrt{2/3}$, *then the equations of the induction motor are given by*

$$\begin{aligned} R_S\underline{i}_S + L_S\frac{d}{dt}\underline{i}_S + M\frac{d}{dt}\left(\underline{i}_R e^{jn_p\theta_R}\right) &= \underline{u}_S \\ R_R\underline{i}_R + L_R\frac{d}{dt}\underline{i}_R + M\frac{d}{dt}\left(\underline{i}_S e^{-jn_p\theta_R}\right) &= 0 \\ \frac{2}{3}n_p M \operatorname{Im}\left\{\underline{i}_S\left(\underline{i}_R e^{jn_p\theta_R}\right)^*\right\} - \tau_L &= J\frac{d\omega_R}{dt}. \end{aligned}$$

(b) With the three-phase to two-phase transformation defined as in part (a), show that

$$u_{Sa}(t)i_{Sa}(t) + u_{Sb}(t)i_{Sb}(t) = \frac{3}{2}\Big(u_{S1}(t)i_{S1}(t) + u_{S2}(t)i_{S2}(t) + u_{S3}(t)i_{S3}(t)\Big).$$

Problem 13 Space Vector Representation of the Induction Motor

(a) Define

$$\underline{i}_r = \underline{i}_{ra} + j\underline{i}_{rb} \triangleq \underline{i}_R e^{jn_p\theta_R}.$$

Show that the system of equations

$$\begin{aligned} R_S\underline{i}_S + L_S\frac{d}{dt}\underline{i}_S + M\frac{d}{dt}\left(\underline{i}_R e^{jn_p\theta_R}\right) &= \underline{u}_S \\ R_R\underline{i}_R + L_R\frac{d}{dt}\underline{i}_R + M\frac{d}{dt}\left(\underline{i}_S e^{-jn_p\theta_R}\right) &= 0 \\ n_p M \operatorname{Im}\left\{\underline{i}_S\left(\underline{i}_R e^{jn_p\theta_R}\right)^*\right\} - \tau_L &= J\frac{d\omega_R}{dt} \end{aligned}$$

may be rewritten as

$$\begin{aligned} R_S\underline{i}_S + L_S\frac{d}{dt}\underline{i}_S + M\frac{d}{dt}\underline{i}_r &= \underline{u}_S \\ R_R\underline{i}_r + \sigma_R M\frac{d}{dt}\underline{i}_r + M\frac{d}{dt}\left(\underline{i}_S + \underline{i}_r\right) - jn_p\omega_R\underline{\psi}_R &= 0 \qquad (7.91) \\ n_p M \operatorname{Im}\left\{\underline{i}_S\left(\underline{i}_r\right)^*\right\} - \tau_L &= J\frac{d\omega_R}{dt} \end{aligned}$$

www.EngineeringEBooksPdf.com

in terms of $\underline{i}_S$ *and* $\underline{i}_r$, *where*

$$\underline{\psi}_R \triangleq L_R \underline{i}_r + M \underline{i}_S.$$

[Note that the model (7.91) has no explicit dependence on θ_R*.]*

(b) With $L_S = (1+\sigma_S)M, L_R = (1+\sigma_R)M$, *and*

$$\begin{aligned} \underline{\lambda}_R &= L_R \underline{i}_R + M \underline{i}_S e^{-jn_p\theta_R} \\ \underline{\psi}_R &= \underline{\lambda}_R e^{jn_p\theta_R} = L_R \underline{i}_r + M \underline{i}_S \end{aligned}$$

show that the electrical equations of part (a) may be illustrated by the "equivalent circuit" of Figure 7.27.

(c) Put the result from part (a) in state space form.

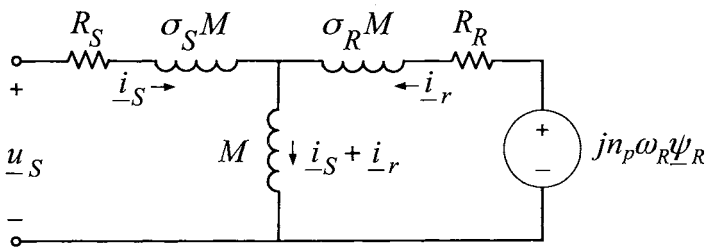


FIGURE 7.27. Circuit representation of the electrical equations of an induction motor.

Remark 1 *The quantity* $\underline{\lambda}_{ag} \triangleq M(\underline{i}_S + \underline{i}_r)$ *is called the* air gap (or magnetizing) flux linkage *(see Lipo and Novotny* [7], *page* 75*). The* air-gap voltage *is then defined as*

$$\underline{v}_{ag} = -\frac{d}{dt}\underline{\lambda}_{ag} = -\frac{d}{dt}M(\underline{i}_S + \underline{i}_r).$$

Remark 2 *The notation* $\underline{u}_S^S = u_{Sd} + ju_{Sq} \triangleq u_{Sa} + ju_{Sb}, \underline{i}_S^S = i_{Sd} + ji_{Sq} \triangleq i_{Sa} + ji_{Sb}$, *and* $\underline{i}_R^S = i_{Rd} + ji_{Rq} \triangleq \underline{i}_{ra} + j\underline{i}_{rb} = \underline{i}_r$ *is often used for the equivalent two-phase model developed in this problem. The superscript "S" refers to the "stationary frame" while the d and q subscripts refer to the direct and quadrature axis, respectively. However, in this book, the dq notation is reserved for the* field oriented *coordinate system (see Chapters* 8 *and* 9*) so the reader must be wary when reading different authors.*

Problem 14 Arbitrary Rotating Reference Frame

(a) Let

$$\begin{aligned} \underline{i}_{S\varphi} &\triangleq \underline{i}_S e^{-j\varphi} \\ \underline{i}_{R\varphi} &\triangleq i_{R\varphi a} + j i_{R\varphi b} \triangleq \underline{i}_R e^{-j(\varphi - n_p\theta_R)} \\ \underline{u}_{S\varphi} &\triangleq \underline{u}_S e^{-j\varphi} \end{aligned}$$

www.EngineeringEBooksPdf.com

where $\varphi(t)$ is an arbitrary *function of time. With $\omega_\varphi \triangleq d\varphi/dt$, show that a space vector representation of the induction motor model*

$$\begin{aligned} R_S\underline{i}_S + L_S\frac{d}{dt}\underline{i}_S + M\frac{d}{dt}\left(\underline{i}_R e^{jn_p\theta_R}\right) &= \underline{u}_S \\ R_R\underline{i}_R + L_R\frac{d}{dt}\underline{i}_R + M\frac{d}{dt}\left(\underline{i}_S e^{-jn_p\theta_R}\right) &= 0 \\ n_pM\,\mathrm{Im}\left\{\underline{i}_S\left(\underline{i}_R e^{jn_p\theta_R}\right)^*\right\} - \tau_L &= J\frac{d\omega_R}{dt} \end{aligned}$$

in terms of $\underline{i}_{S\varphi}$, $\underline{i}_{R\varphi}$ and $\underline{u}_{S\varphi}$ is given by

$$\begin{aligned} \underline{u}_{S\varphi} &= R_S\underline{i}_{S\varphi} + L_S\frac{d}{dt}\underline{i}_{S\varphi} + j\omega_\varphi L_S\underline{i}_{S\varphi} + M\frac{d}{dt}\underline{i}_{R\varphi} + j\omega_\varphi M\underline{i}_{R\varphi} \\ 0 &= R_R\underline{i}_{R\varphi} + L_R\frac{d}{dt}\underline{i}_{R\varphi} + j\left(\omega_\varphi - n_p\omega_R\right)L_R\underline{i}_{R\varphi} + M\frac{d}{dt}\underline{i}_{S\varphi} \\ &\quad + j\left(\omega_\varphi - n_p\omega_R\right)M\underline{i}_{S\varphi} \\ J\frac{d\omega_R}{dt} &= n_pM\,\mathrm{Im}\left\{\underline{i}_{S\varphi}\left(\underline{i}_{R\varphi}\right)^*\right\} - \tau_L. \end{aligned}$$

Common choices for φ are $\varphi = 0$ (the stationary coordinate system; see problem 13), $\varphi = n_p\omega_R$ (the rotor coordinate system), $\varphi = \angle\underline{u}_S$ (the synchronous coordinate system), and $\varphi = \angle\left(\underline{i}_S + (L_R/M)\underline{i}_R e^{jn_p\theta_R}\right) = \angle\underline{\psi}_R$ (the field-oriented coordinate system; see problem 6 of Chapter 6 and problem 4 of Chapter 8).

(b) Put the result from part (a) in state-space form.

Problem 15 Space Vector Model with Leakage on the Rotor Side

(a) Starting from the model (7.91) derived in problem 13, make the change of variables

$$\begin{aligned} \underline{i}'_r &\triangleq \frac{M}{L_S}\underline{i}_r \\ \underline{\psi}'_R &\triangleq \frac{L_S}{M}\underline{\psi}_R = (L_S/M)\left(L_R\underline{i}_r + M\underline{i}_S\right) = L_S\underline{i}_S + (L_S/M)^2L_R\underline{i}'_r \\ &= L_S\left(\underline{i}_S + \underline{i}'_r\right) + \frac{\sigma L_S}{1-\sigma}\underline{i}'_r \\ \underline{\lambda}_S &\triangleq L_S\underline{i}_S + M\underline{i}_r = L_S(\underline{i}_S + \underline{i}'_r). \end{aligned}$$

and show that the model may be rewritten as

$$\begin{aligned} R_S\underline{i}_S + \frac{d}{dt}\underline{\lambda}_S &= \underline{u}_S \\ R'_R\underline{i}'_r + \frac{d}{dt}\underline{\lambda}_S - jn_p\omega\underline{\psi}'_R + L_\sigma\frac{d}{dt}\underline{i}'_r &= 0 \\ \frac{n_pM^2}{L_SL_R}\,\mathrm{Im}\left\{\underline{i}_S(\underline{\psi}'_R)^*\right\} = \frac{n_p}{L_\sigma}\,\mathrm{Im}\left\{\underline{\lambda}_S(\underline{\psi}'_R)^*\right\} &= \tau \end{aligned}$$

www.EngineeringEBooksPdf.com

where

$$\begin{aligned} \sigma &\triangleq 1 - M^2/L_S L_R \\ R'_R &\triangleq (L_S/M)^2 R_R \\ L_\sigma &\triangleq \sigma L_S/(1-\sigma). \end{aligned}$$

(b) Show that an equivalent circuit representation of this model is

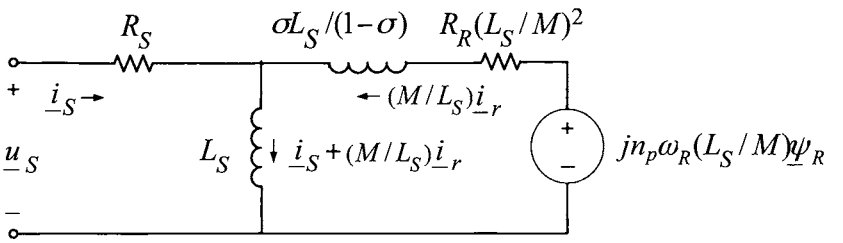


FIGURE 7.28.

where it is noted that there is leakage inductance only on the rotor side.

Problem 16 Space Vector Model with Leakage on the Stator Side

(a) Starting from the model (7.91) derived in problem 13 make the substitutions

$$\begin{aligned} \underline{i}''_r &\triangleq \frac{L_R}{M}\underline{i}_r \\ \underline{\psi}''_R &\triangleq \frac{M}{L_R}\underline{\psi}_R = (M/L_R)\left(L_R\underline{i}_r + M\underline{i}_S\right) = \left(M^2/L_R\right)\underline{i}_S + \left(M^2/L_R\right)L_R\underline{i}''_r \\ &= \left(M^2/L_R\right)\left(\underline{i}_S + \underline{i}''_r\right) \\ \underline{\lambda}_S &\triangleq L_S\underline{i}_S + M\underline{i}_r = L_S\underline{i}_S + \left(M^2/L_R\right)\underline{i}''_r = \sigma L_S\underline{i}_S + \left(M^2/L_R\right)\left(\underline{i}_S + \underline{i}''_r\right) \end{aligned}$$

and show that the model (7.91) may be rewritten as

$$\begin{aligned} R_S\underline{i}_S + \sigma L_S\frac{d}{dt}\underline{i}_S + \frac{d}{dt}\left(M^2/L_R\right)\left(\underline{i}_S + \underline{i}''_r\right) &= \underline{u}_S \\ (M/L_R)^2 R_R\underline{i}''_r + \frac{d}{dt}\left(M^2/L_R\right)\left(\underline{i}_S + \underline{i}''_r\right) - jn_p\omega\left(M/L_R\right)\underline{\psi}_R &= 0 \\ \frac{n_p}{\sigma L_S}\operatorname{Im}\left\{\underline{\lambda}_S(\underline{\psi}''_R)^*\right\} &= \tau. \end{aligned}$$

(b) Show that an equivalent circuit representation of this model is

www.EngineeringEBooksPdf.com

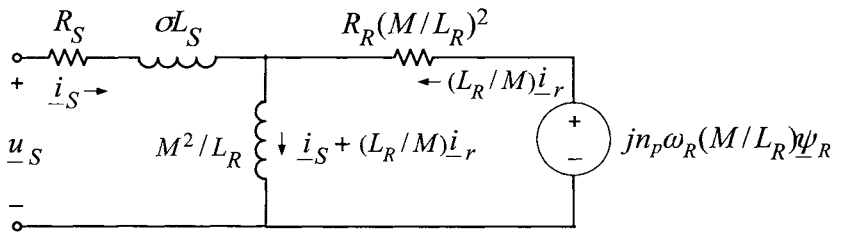


FIGURE 7.29.

where it is noted that there is leakage inductance only on the stator side.

Steady-State Induction Motor Models

Problem 17 Steady-State Solutions of the Induction Motor Equations

(a) Write a program to plot the circle diagram of Figure 7.11.

(b) Write a program to reproduce the plots of Figures 7.12, 7.13, and 7.15.

For the motor parameter values, use $R_R = 3.9\ \Omega$, $R_S = 1.7\ \Omega$, $L_R = 0.014\ H$, $L_S = 0.014\ H$, $M = 0.0117\ H$, $J = 0.00011\ kg\text{-}m^2$, $f = 0\ N\text{-}m/(rad/s)$, $n_p = 3$, $\omega_S = (2\pi)60\ rad/sec$, *and* $U_S = 80\ V$. *However, the analysis assumes the stator resistance is zero so set* $R_S = 0$.

Problem 18 Open-Loop Simulation of a Three-Phase Induction Machine

Let the parameter values of an induction motor be $R_R = 2.1\ \Omega$, $R_S = 1.85\ \Omega$, $L_R = 0.244\ H$, $L_S = 0.244\ H$, $M = 0.225\ H$, $J = 0.0185\ kg\text{-}m^2$, $f = 0\ N\text{-}m/(rad/s)$, $n_p = 3$, $\omega_S = (2\pi)60\ rad/sec$. *With* $V_{max} = 200$ *(peak),* $I_{max} = 10$ *(peak) simulate the open-loop machine based on the two-phase equivalent model as indicated in Figure 7.19 with a 208-V (rms) line-to-line voltage applied. (That is, the phase to neutral peak voltage is* $V_{3ph} = \sqrt{2}\,(208)/\sqrt{3} = 169.8\ V$.)

Problem 19 No-Load and Blocked-Rotor Tests

A standard method of determining the (two-phase equivalent) machine parameters is to use a couple of special tests called the no-load *test and the* blocked-rotor *test. Both of these tests involve applying a balanced three-phase set of sinusoidal voltages to the motor and measuring the resulting steady-state stator currents and stator power. In the no-load test, nothing is attached to the machine and so, after the voltages are applied, the machine quickly goes to steady state in which* $n_p\omega_R = \omega_S$ *(assuming no frictional losses). In this case,* $S = 0$ *and the equivalent circuit of Figure 7.10 reduces to that of Figure 7.30.*

www.EngineeringEBooksPdf.com

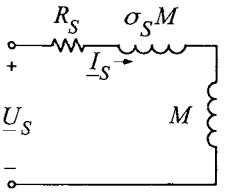


FIGURE 7.30. Equivalent circuit with no load so that $n_p\omega_R = \omega_S \Rightarrow S = 0$.

The blocked-rotor test refers to having the rotor held immobile so that $\omega_R \equiv 0$. *In this case,* $S = 1$ *and the equivalent circuit of Figure 7.10 reduces to that of Figure 7.31(a). Usually, the impedances in the two branches satisfy*

$$j\omega_S M >> j\omega_S \sigma_R M + R_R$$

so that the equivalent circuit reduces to that shown in Figure 7.31(b).

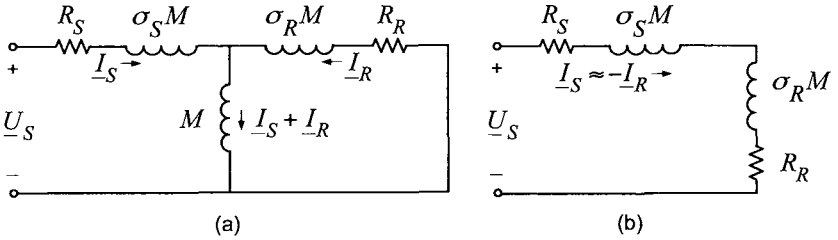


FIGURE 7.31. (a) Equivalent circuit with a locked rotor so that $\omega_R = 0 \Rightarrow S = 1$. (b) Equivalent circuit if $j\omega_S M >> j\omega_S \sigma_R M + R_R$.

(a) Run the simulation of problem 18 with no load. Assume that R_S *is known (perhaps measured using an ohmmeter). Use the steady-state stator voltages and currents to compute* $L_S = (1 + \sigma_S)M$. *(The amplitudes of the voltages and the currents along with the angle between them is needed.) How does this value of* L_S *compare with the actual value in the simulation? That is, what is the percent error?*

(b) Run the simulation of problem 18 with a blocked rotor (if the currents exceed I_{max}, *then reduce the input voltage) and assume that* $\sigma_S = \sigma_R$. *Using the known value of* R_S, *the value of* L_S *from part (a), and the measured stator voltages and currents, compute* $\sigma_S M$ *and* R_R *based on the equivalent circuit of Figure 7.31(b).*

(c) Use the information from parts (a) and (b) to compute M, L_R, *and* $\sigma = 1 - M^2/(L_S L_R)$. *How do they compare with the actual values in the simulation? That is, what is the percent error?*

(d) Repeat parts (a), (b), and (c) with the viscous friction coefficient set to $f = 0.00005$ *rather than* $f = 0$.

www.EngineeringEBooksPdf.com

Problem 20 Induction Generator (M. Bodson [63])

Consider the equivalent circuit of a three-phase induction machine in Figure 7.32.

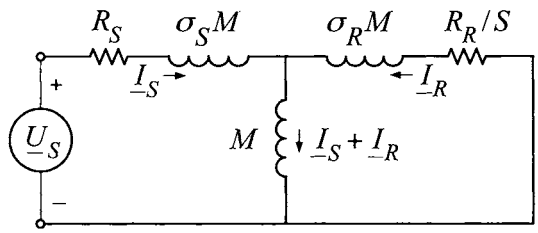


FIGURE 7.32. Equivalent circuit of an induction motor.

(a) Suppose the motor shaft (rotor) is connected to a prime mover (e.g., a windmill) that turns at a constant angular speed $\omega_R > \omega_S$, where ω_S is the angular frequency of the balanced three-phase voltage set applied to the stator terminals (e.g., connect the stator terminals to a three-phase transmission line). Show that the power to the motor is negative; that is, electrical power is being delivered to the source voltage converted from the mechanical power supplied to shaft. (Hint: note that $S < 0$.)

(b) Replace the three-phase power source by a three-phase impedance $Z_S = R + j\omega L$ as indicated schematically in Figure 7.33. The corresponding equivalent circuit is shown in Figure 7.34. Suppose the motor shaft is still connected to a prime mover (e.g., a windmill) that turns at a constant angular speed ω_R. Can there be a steady-state electrical power out of the motor into the impedance Z_S? Explain.

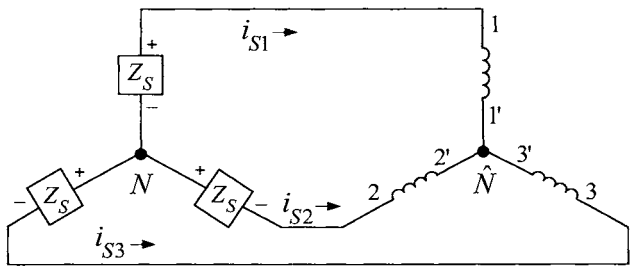


FIGURE 7.33. Stator windings of an induction motor connected to a symmetric three-phase load.

www.EngineeringEBooksPdf.com

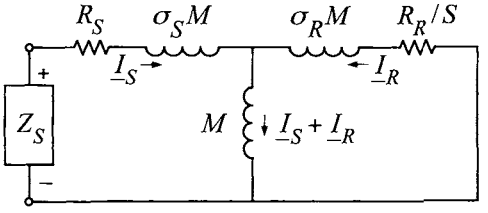


FIGURE 7.34. An equivalent circuit of the induction motor where the source voltage is replaced by a passive load.

Problem 21 Equivalent Circuit With Leakage on the Stator Side [2]

Show that the circuit in Figure 7.35 where the leakage inductance is completely on the stator *side is equivalent to the circuit given in Figure 7.10.*

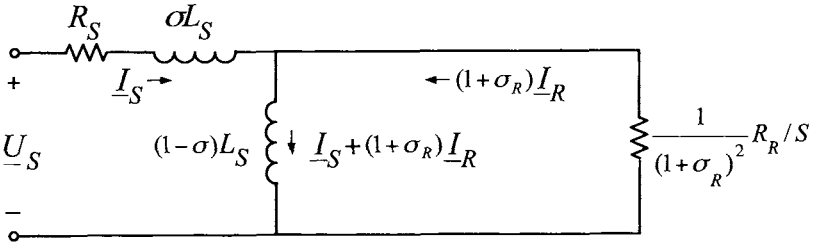


FIGURE 7.35. Equivalent circuit of induction motor with the leakage inductance completely on the stator side.

Problem 22 Equivalent Circuit With Leakage on the Rotor Side [2]

Show that the circuit in Figure 7.36 where the leakage inductance is completely on the rotor *side is equivalent to the circuit given in Figure 7.10.*

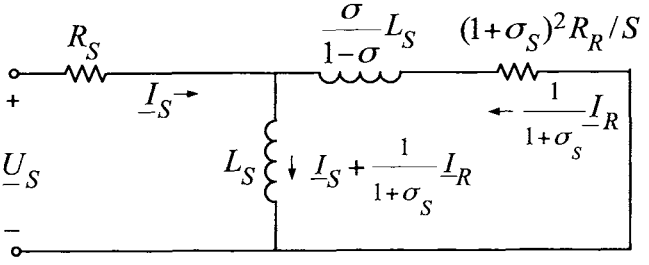


FIGURE 7.36. Equivalent circuit of induction motor with the leakage inductance completely on the rotor side.

www.EngineeringEBooksPdf.com

Problem 23 Constant Speed Induction Machine as a Linear System

(a) Let $\left\{\underline{u}_S^{(1)}, \underline{i}_S^{(1)}, \underline{i}_R^{(1)}\right\}$ *and* $\left\{\underline{u}_S^{(2)}, \underline{i}_S^{(2)}, \underline{i}_R^{(2)}\right\}$ *each be a solution set to*

$$\begin{aligned} R_S\underline{i}_S + L_S\frac{d}{dt}\underline{i}_S + M\frac{d}{dt}\left(\underline{i}_R e^{j\theta_R(t)}\right) &= \underline{u}_S \\ R_R\underline{i}_R + L_R\frac{d}{dt}\underline{i}_R + M\frac{d}{dt}\left(\underline{i}_S e^{-j\theta_R(t)}\right) &= 0 \end{aligned}$$

where $\theta_R(t)$ *is the* same *function of time for both inputs [e.g.,* $\theta_R(t) = \omega_R t$ *with* ω_R *the* same *constant value for both inputs]. Under these conditions, show that the input*

$$\underline{u}_S = \underline{u}_S^{(1)} + \underline{u}_S^{(2)}$$

results in the stator and rotor currents being

$$\begin{aligned} \underline{i}_S &= \underline{i}_S^{(1)} + \underline{i}_S^{(2)} \\ \underline{i}_R &= \underline{i}_R^{(1)} + \underline{i}_R^{(2)}. \end{aligned}$$

(b) Assuming ω_R *is constant and that the inputs are sinusoids so that*

$$\underline{u}_S^{(1)} = \sqrt{2}\underline{U}_S^{(1)} e^{j\omega_{S1}t} = \sqrt{2}\left|\underline{U}_S^{(1)}\right| e^{j\angle\underline{U}_S^{(1)}} e^{j\omega_{S1}t}$$

then the phasor equations (7.39) and (7.40) can be solved for $\underline{I}_S^{(1)}$ *and* $\underline{I}_R^{(1)}$*, resulting in currents of the form*

$$\begin{aligned} \underline{i}_S^{(1)} &= \sqrt{2}\underline{I}_S^{(1)} e^{j\omega_{S1}t} = \sqrt{2}\left|\underline{I}_S^{(1)}\right| e^{j\angle\underline{I}_S^{(1)}} e^{j\omega_{S1}t} \\ \underline{i}_R^{(1)} &= \sqrt{2}\underline{I}_R^{(1)} e^{j(\omega_{S1}-\omega_R)t} = \sqrt{2}\left|\underline{I}_R^{(1)}\right| e^{j\angle\underline{I}_R^{(1)}} e^{j(\omega_{S1}-\omega_R)t}. \end{aligned}$$

Similarly, the input

$$\underline{u}_S^{(2)} = \sqrt{2}\underline{U}_S^{(2)} e^{j\omega_{S2}t} = \sqrt{2}\left|\underline{U}_S^{(2)}\right| e^{j\angle\underline{U}_S^{(2)}} e^{j\omega_{S2}t}$$

results in the stator and rotor currents being given by

$$\begin{aligned} \underline{i}_S^{(2)} &= \sqrt{2}\underline{I}_S^{(2)} e^{j\omega_{S2}t} = \sqrt{2}\left|\underline{I}_S^{(2)}\right| e^{j\angle\underline{I}_S^{(2)}} e^{j\omega_{S2}t} \\ \underline{i}_R^{(2)} &= \sqrt{2}\underline{I}_R^{(2)} e^{j(\omega_{S2}-\omega_R)t} = \sqrt{2}\left|\underline{I}_R^{(2)}\right| e^{j\angle\underline{I}_R^{(2)}} e^{j(\omega_{S2}-\omega_R)t}. \end{aligned}$$

Use the results of part (a) to compute the torque produced by the motor due to the input

$$\underline{u}_S = \underline{u}_S^{(1)} + \underline{u}_S^{(2)} = \sqrt{2}\underline{U}_S^{(1)} e^{j\omega_{S1}t} + \sqrt{2}\underline{U}_S^{(2)} e^{j\omega_{S2}t}. \qquad (7.92)$$

(c) Consider the motor to be two-phase. Assuming $\theta_R = \omega_R t$ *with* ω_R *constant, use*

$$\tau = M\,\mathrm{Im}\{\underline{i}_S(\underline{i}_R e^{j\theta_R})^*\}$$

www.EngineeringEBooksPdf.com

to find an expression for the torque produced by the input (7.92) in terms of the phasors $\left|\underline{I}_S^{(1)}\right|e^{j\angle \underline{I}_S^{(1)}}$, $\left|\underline{I}_R^{(1)}\right|e^{j\angle \underline{I}_R^{(1)}}$, $\left|\underline{I}_S^{(2)}\right|e^{j\angle \underline{I}_S^{(2)}}$, *and* $\left|\underline{I}_R^{(2)}\right|e^{j\angle \underline{I}_R^{(2)}}$. *What is the average torque* τ_{avg} *where* $\tau_{avg} \triangleq \lim_{T\to\infty}(1/T)\int_0^T \tau(t)dt$? *Of course, for* $\omega_{S2} = \omega_{S1}$, *the torque will be constant and equal to its average. Under what* other *conditions is the torque essentially (approximately) constant?*

(d) Assuming $R_S = 0$, *show that the average torque computed in part (c) may be written as*

$$\tau_{avg} = \frac{(1-\sigma)}{\sigma}\frac{U_{S1}^2}{\omega_{S1}^2 L_S}\frac{2}{S_p/S_1 + S_1/S_p} + \frac{(1-\sigma)}{\sigma}\frac{U_{S2}^2}{\omega_{S2}^2 L_S}\frac{2}{S_p/S_2 + S_2/S_p}$$

where

$$S_1 \triangleq \frac{\omega_{S1} - \omega_R}{\omega_{S1}}, \quad S_2 \triangleq \frac{\omega_{S2} - \omega_R}{\omega_{S2}}.$$

(e) Consider the special case with $\omega_{S2} = -\omega_{S1}$ *and*

$$\begin{aligned} \underline{U}_S^{(1)} &= \left|\underline{U}_S^{(1)}\right| e^{j\angle \underline{U}_S^{(1)}} = \frac{U_S}{2} e^{j\angle \underline{U}_S^{(1)}} \\ \underline{U}_S^{(2)} &= \left(\underline{U}_S^{(1)}\right)^* = \frac{U_S}{2} e^{-j\angle \underline{U}_S^{(1)}}. \end{aligned}$$

Show that the inputs to the two-phase motor are of the form

$$\begin{aligned} u_{Sa}(t) &= \sqrt{2}U_S \cos(\omega_S t + \angle \underline{U}_S) \\ u_{Sb}(t) &= 0. \end{aligned}$$

Show that the average torque is given by $(S \triangleq \frac{\omega_S - \omega_R}{\omega_S})$

$$\begin{aligned} \tau_{avg} &= \tau_p \left(\frac{2}{S_p/S + S/S_p} - \frac{2}{S_p/(2-S) + (2-S)/S_p} \right) \\ \tau_p &\triangleq \frac{1}{4}\frac{(1-\sigma)}{\sigma}\frac{U_S^2}{\omega_{S1}^2 L_S}. \end{aligned}$$

Plot τ_{avg}/τ_p *as a function of* S/S_p. *What is the average torque if* $\omega_R = 0$?

Problem 24 Single-Phase Induction Motor with a Shorted Phase

Background: Motors are needed in homes for the compressors used in refrigerators and air conditioners as well as for washing machines, dryers, and so on. A typical home has only a single-phase source available, for example, a 120-V (rms) 60-Hz wall outlet and the (two-phase) induction motor requires two voltage sources 90 degrees out of phase in time. Though the DC machine can run off of a single-phase source, the induction motor is the motor of choice because it is much cheaper. Based on problem 23, this problem outlines how an induction motor can be run using only a single-phase source $u_{Sa} = \sqrt{2}U_S \cos(\omega_S t + \angle \underline{U}_S)$ *with the other stator phase*

www.EngineeringEBooksPdf.com

shorted so that $u_{Sb} = 0$. *(However, the standard way of running a single-phase induction motor is to* open *the second stator phase rather than short it.) Consider a two-phase induction motor with inputs* u_{Sa}, u_{Sb}. *Figure 7.37 illustrates a single-phase induction motor where the same voltage* u_{Sa} *is applied to both phases and phase b has a resistor* R_b *and capacitor* C *added in series in the winding. By part (e) of problem 23, if* $u_{Sa}(t) = \sqrt{2}\,|\underline{U}_S|\cos(\omega_S t + \angle\underline{U}_S)$ *and* $u_{Sb}(t) \equiv 0$ *with* $\omega_R = 0$, *then the average torque is zero. To start the motor, the switch in Figure 7.37 is opened. Denote by* $Z_a(j\omega) = R_S + j\omega L_S$ *and* $Z_b(j\omega) = R_S + R_b + j\omega L_S + 1/(j\omega C)$ *the impedances of the stator windings a and b, respectively, where the effect of the rotor has been neglected. Rewrite the stator phase b impedance as*

$$Z_b(j\omega) = R_S + R_b + j\omega L_S + 1/(j\omega C) = R_S + R_b + j\left(\omega^2 L_S C - 1\right)/(\omega C).$$

Choose $C = \dfrac{1}{(2\pi 60)^2 L_S}$ *so that* $Z_b(j\omega) = R_S + R_b$ *for* $\omega = \omega_S = 60$ *Hz. With* $\omega L_S >> R_S$, *the impedances* $Z_a(j\omega_S)$ *and* $Z_b(j\omega_S)$ *are*

$$\begin{aligned} Z_a(j\omega_S) &\approx j\omega_S L_S \\ Z_b(j\omega_S) &= R_S + R_b. \end{aligned}$$

The corresponding currents in the windings of phases a and b are then

$$\begin{aligned} i_{Sa}(t) &\approx \frac{\sqrt{2}U_S}{\omega_S L_S}\sin(\omega_S t + \angle\underline{U}_S) \\ i_{Sb}(t) &\approx \frac{\sqrt{2}U_S}{R_S + R_b}\cos(\omega_S t + \angle\underline{U}_S). \end{aligned}$$

Finally, design the phase b resistance R_b *such that* $R_S + R_b = \omega_S L_S$ *so that the phase currents are equal amplitude sinusoidal currents and* $\pi/2$ *radians out of phase in time. These currents establish a rotating sinusoidally distributed magnetic field in the air gap just as in the case of the symmetric motor. In reality, the inductance, resistance, and capacitance in the phase windings are not set precisely to these ideal values, but the motor will still start.*[14] *This is called a* capacitor-start *single-phase induction motor.*

[14] Even if the parameter values are set exactly as described, this is still approximate because the effect of the rotor on the stator impedance has been ignored (compare with the equivalent circuit model of the symmetric induction motor).

www.EngineeringEBooksPdf.com

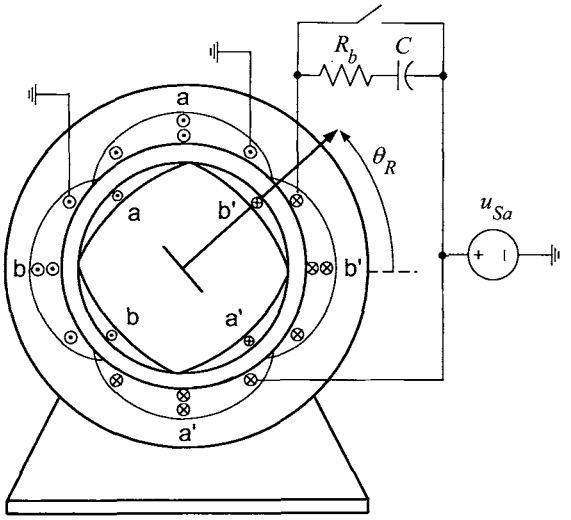


FIGURE 7.37. Capacitor-start single-phase induction motor.

(a) Is open circuiting phase b the same as applying zero voltage to it?

(b) Consider a capacitor-start single-phase induction motor as described above. Suppose that after the motor gets up to speed $\omega_R \approx \omega_S$*, the switch in Figure 7.37 is closed so*

$$\begin{aligned} u_{Sa}(t) &= \sqrt{2}U_S \cos(\omega_S t + \angle \underline{U}_S) \\ u_{Sb}(t) &= 0. \end{aligned}$$

Assuming the rotor speed is essentially constant, it was shown in problem 23(d) that the average torque produced is given by

$$\begin{aligned} \tau_{avg} &= \tau_p \left(\frac{2}{S_p/S + S/S_p} - \frac{2}{S_p/(2-S) + (2-S)/S_p} \right) \\ \tau_p &\triangleq \frac{1}{4} \frac{(1-\sigma)}{\sigma} \frac{U_S^2}{\omega_S^2 L_S} \\ S &\triangleq \frac{\omega_S - \omega_R}{\omega_S}. \end{aligned}$$

Plot τ_{avg}/τ_p *for* $S_p = 0.1, 0.2$ *and* 1*. Based on these plots, explain why* $0 < S_p \ll 1$ *for the single-phase induction motor to work.*

(c) Using the two-phase induction motor model, simulate a single-phase induction motor by applying a 60-Hz, 120-V (rms) source voltage to one phase and 0 V to the other. Set the initial speed to be $\omega_R(0) = \omega_S/n_p$ *where* $\omega_S = 2\pi 60$*. Use the parameter values of* $L_S = 0.157$ *H,* $L_R = 0.157$ *H,* $M = 0.148$ *H,* $R_R = 0.6\ \Omega$*,* $R_S = 2.9\ \Omega$*,* $n_P = 2$*,* $J = 0.01$ *kg-m*^{2}*,* $f = 0$ *N-m/rad/sec, and* $\tau_L = 0.8$ *N-m. Set* $R_S = 0$ *for the calculations, but not*

www.EngineeringEBooksPdf.com

in the simulation. What is the value of S_p and τ_p for this motor? What is the value of S that the machine is operating at?

Problem 25 Torque-Slip Curve with Impressed Stator Currents

Suppose that the motor phases are fed by a three-phase current source rather than a three-phase voltage source. Use (7.47) to obtain U_S^2 in terms of I_S^2 and substitute this expression into (7.56) to show that the expression for the torque-slip curve in terms of the rms stator current I_S is

$$\tau = \frac{3}{2}(1-\sigma)I_S^2 \frac{2}{s_p/S + S/s_p}$$

where $s_p \triangleq \sigma S_p = R_R/(\omega L_R)$.

Problem 26 Maximum Mechanical Power

The steady-state mechanical power is

$$P_{mech} = \tau\omega_R = \tau_p \frac{2}{S_p/S + S/S_p}(1-S)\omega_S.$$

(a) Compute the normalized slip $S_{maxpower}$ corresponding to maximum power *transfer for both motoring and generating.*

(b) For both motoring and generating, compute the power and torque achieved when the normalized slip is at the values found in part (a).

(c) Let $\sigma = 0.05$ and compute the rated slip S_r and maximum power transfer slip $S_{maxpower}$. Which is larger? By approximately how much?

(d) Compute the corresponding power factors when the machine is operating at S_r and $S_{maxpower}$. Which is larger and by how much?

(e) Compute the corresponding efficiencies when the machine is operating at S_r and $S_{maxpower}$. Which is larger and by how much?

(f) Compare operating the motor at S_r and $S_{maxpower}$ in terms of advantages and disadvantages.

Wound Rotor Synchronous Machines

These problems explore the mathematical modeling of wound rotor synchronous machines. For more detailed models of large (wound rotor) synchronous machines, see Krause et al. [4] and Ong [6].

Problem 27 Model of a Wound Rotor Synchronous Machine [1]

A mathematical model of a balanced three-phase wound rotor synchronous motor can be found directly from the induction motor expressions for the flux linkages and torque. The difference in this case is that the rotor currents are held constant in a synchronous machine by a voltage source u_F applied to the rotor windings. In order to keep the rotor currents balanced let

$$\begin{aligned} i_{R1} &= +i_f \\ i_{R2} &= -i_f/2 \\ i_{R3} &= -i_f/2 \end{aligned}$$

www.EngineeringEBooksPdf.com

in equation (7.2) where i_f is nominally constant.

(a) Show that the rotor torque τ_R is given by

$$\tau_R = Mi_f\left(-i_{S1}\sin(\theta_R) - i_{S2}\sin(\theta_R - \frac{2\pi}{3}) - i_{S3}\sin(\theta_R - \frac{4\pi}{3})\right).$$

(b) Show that the flux linkages in the stator phases are given by

$$\begin{bmatrix} \psi_{S1}(t) \\ \psi_{S2}(t) \\ \psi_{S3}(t) \end{bmatrix} = \frac{2}{3}L_S\begin{bmatrix} 1 & \cos(2\pi/3) & \cos(4\pi/3) \\ \cos(-2\pi/3) & 1 & \cos(2\pi/3) \\ \cos(-4\pi/3) & \cos(-2\pi/3) & 1 \end{bmatrix}\begin{bmatrix} i_{S1}(t) \\ i_{S2}(t) \\ i_{S3}(t) \end{bmatrix} + Mi_f\begin{bmatrix} \cos(\theta_R) \\ \cos(\theta_R - 2\pi/3) \\ \cos(\theta_R - 4\pi/3) \end{bmatrix}.$$

(c) Show that an equivalent two-phase model of the wound rotor synchronous machine is given by

$$\begin{aligned} u_{Sa} &= L_S\frac{di_{Sa}}{dt} + M\frac{d}{dt}\left(i_F\cos(\theta_R)\right) + R_S i_{Sa} \\ u_{Sb} &= L_S\frac{di_{Sb}}{dt} + M\frac{d}{dt}\left(i_F\sin(\theta_R)\right) + R_S i_{Sb} \\ u_F &= L_R\frac{di_F}{dt} + M\frac{d}{dt}\left(i_{Sa}\cos(\theta_R) + i_{Sb}\sin(\theta_R)\right) + R_R i_F \\ J\frac{d\omega_R}{dt} &= Mi_F\left(-i_{Sa}\sin(\theta_R) + i_{Sb}\cos(\theta_R)\right) - \tau_L \end{aligned} \tag{7.93}$$

where $u_F \triangleq \sqrt{3/2}u_{R1}, i_F(t) \triangleq \sqrt{3/2}i_f(t)$. A block diagram for simulating a three-phase machine using a two-phase equivalent model is shown in Figure 7.38.

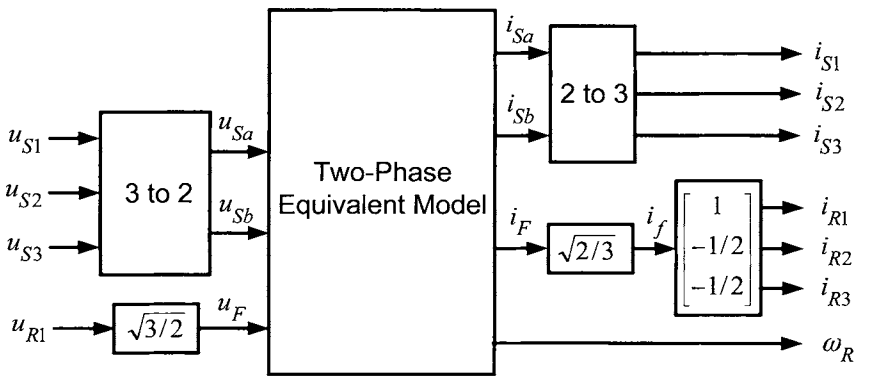


FIGURE 7.38. Using a two-phase equivalent model to simulate a three-phase machine.

www.EngineeringEBooksPdf.com

Problem 28 State-Space Model of a Wound Rotor Synchronous Machine

Develop a state space representation of the wound rotor synchronous motor model (7.93) given in problem (27) using $i_{Sa}, i_{Sb}, i_F, \omega_R$, *and* θ_R *as the state variables and* u_{Sa}, u_{Sb}, *and* u_F *as the inputs.*

Problem 29 DQ model of a Wound Rotor Synchronous Machine

Define

$$\begin{bmatrix} i_d \\ i_q \end{bmatrix} = \begin{bmatrix} \cos(\theta_R) & \sin(\theta_R) \\ -\sin(\theta_R) & \cos(\theta_R) \end{bmatrix} \begin{bmatrix} i_{Sa} \\ i_{Sb} \end{bmatrix}$$

$$\begin{bmatrix} u_d \\ u_q \end{bmatrix} = \begin{bmatrix} \cos(\theta_R) & \sin(\theta_R) \\ -\sin(\theta_R) & \cos(\theta_R) \end{bmatrix} \begin{bmatrix} u_{Sa} \\ u_{Sb} \end{bmatrix}$$

(a) Rewrite the wound rotor synchronous motor model (7.93) given in problem (27) in terms of $i_d, i_q, i_F, \omega_R, \theta_R, u_d, u_q$, *and* u_F.

(b) Develop a state space dq model in terms of the state variables i_d, i_q, i_F, ω_R, *and* θ_R *and the inputs* u_d, u_q, *and* u_F.

Problem 30 Model of a Wound Rotor Synchronous Machine

Modify the approach in problem 27 to rederive the mathematical model of the wound rotor synchronous motor assuming that $i_{R1} = i_f, i_{R2} = 0$, *and* $i_{R3} = 0$. *That is, assume there is only one winding on the rotor.*

www.EngineeringEBooksPdf.com

This Page Intentionally Left Blank

www.EngineeringEBooksPdf.com

8

Induction Motor Control

In this chapter, the methods of field-oriented control and a modification of it known as input-output linearization control are described. These techniques allow one to achieve fast, precise tracking of demanding trajectories using an induction motor. These controllers are based on the nonlinear differential equation model of the induction motor and require (full) state feedback. As measurements of the rotor flux linkages (or, equivalently, the rotor currents) are not usually available, they must be estimated and techniques to do this are also described. Experimental results are presented to demonstrate the effectiveness of these control schemes. The chapter ends with two optional sections. The first describes a systematic procedure to obtain the maximum torque from the machine without violating the voltage or current constraints. The final section presents a nonlinear least-squares approach to identification of the induction motor parameters.

8.1 Dynamic Equations of the Induction Motor

The starting point for the control of the induction motor is the system of nonlinear differential equations which characterize its behavior. As derived previously, the dynamics of a n_p pole-pair two-phase induction motor[1] are given by the system of differential equations

$$\begin{aligned}
u_{Sa} &= R_S i_{Sa} + L_S \frac{d}{dt} i_{Sa} + M \frac{d}{dt}\Big(i_{Ra}\cos(n_p\theta) - i_{Rb}\sin(n_p\theta)\Big) \\
u_{Sb} &= R_S i_{Sb} + L_S \frac{d}{dt} i_{Sb} + M \frac{d}{dt}\Big(i_{Ra}\sin(n_p\theta) + i_{Rb}\cos(n_p\theta)\Big) \\
0 &= R_R i_{Ra} + L_R \frac{d}{dt} i_{Ra} + M \frac{d}{dt}\Big(+i_{Sa}\cos(n_p\theta) + i_{Sb}\sin(n_p\theta)\Big) \\
0 &= R_R i_{Rb} + L_R \frac{d}{dt} i_{Rb} + M \frac{d}{dt}\Big(-i_{Sa}\sin(n_p\theta) + i_{Sb}\cos(n_p\theta)\Big) \\
J\frac{d\omega}{dt} &= n_p M\Big(i_{Sb}\Big(i_{Ra}\cos(n_p\theta) - i_{Rb}\sin(n_p\theta)\Big) \\
&\quad - i_{Sa}\Big(i_{Ra}\sin(n_p\theta) + i_{Rb}\cos(n_p\theta)\Big)\Big) - f\omega - \tau_L \\
\frac{d\theta}{dt} &= \omega
\end{aligned} \tag{8.1}$$

[1] (Or, the two-phase equivalent model of a three phase motor.)

www.EngineeringEBooksPdf.com

with the flux linkages of the motor phases given by

$$\begin{aligned}
\lambda_{Sa} &= L_S i_{Sa} + M\Big(i_{Ra}\cos(n_p\theta) - i_{Rb}\sin(n_p\theta)\Big) \\
\lambda_{Sb} &= L_S i_{Sb} + M\Big(i_{Ra}\sin(n_p\theta) + i_{Rb}\cos(n_p\theta)\Big) \\
\lambda_{Ra} &= L_R i_{Ra} + M\Big(+i_{Sa}\cos(n_p\theta) + i_{Sb}\sin(n_p\theta)\Big) \\
\lambda_{Rb} &= L_R i_{Rb} + M\Big(-i_{Sa}\sin(n_p\theta) + i_{Sb}\cos(n_p\theta)\Big)
\end{aligned} \tag{8.2}$$

where

$$L_S \triangleq \frac{\mu_0 \pi \ell_1 \ell_2 N_S^2}{8g},\ L_R \triangleq \frac{\mu_0 \pi \ell_1 \ell_2 N_R^2}{8g},\ M \triangleq \frac{\kappa \mu_0 \pi \ell_1 \ell_2 N_S N_R}{8g}.$$

Here N_S and N_R are the number of windings per pole-pair of the stator and rotor phases, respectively. The retarding torque produced by the friction in the ball bearings of the machine is modeled here by $-f\omega$, where f is called the *coefficient of viscous friction*. Of course, one could just consider this part of the load torque τ_L. However, as one can typically estimate f at the same time as estimating the motor parameters, $-f\omega$ then represents the "known" load torque and τ_L is then the "unknown" load torque. Also, to simplify the notation, the subscript "R" on θ_R and ω_R has now been dropped as there should be no confusion. As stated above, the mathematical model derived above is that of a sinusoidally wound, two-phase, n_p pole-pair induction motor. Nevertheless, it is standard practice to also use this model for induction motors with *squirrel cage* rotors (see Refs. [42][59] for experimental validation).

8.1.1 The Control Problem

The control problem is to choose u_{Sa} and u_{Sb} in such a way as to force ω and/or θ to track a given reference trajectory. Measurements of i_{Sa}, i_{Sb}, and θ are usually available for feedback control. However, measurements of i_{Ra} and i_{Rb} are typically not available. In fact, the most common type of induction motor is the squirrel cage motor, where rotor currents are distributed on the surface of the rotor making it very impractical to measure the current in each rotor bar. The resulting flux can be measured through the use of Hall sensors placed in the air gap, but such sensors are not economical and diminish the overall reliability of the control system.

The particular set of nonlinear differential equations (8.1) describing the induction motor is complicated and a control strategy is by no means self-evident. The solution lies in finding an *equivalent* set of equations which are simpler in form for which the control design becomes apparent. As a first step toward simplifying the above equations, the dynamic equations are rewritten in terms of some equivalent rotor flux linkages. This results

www.EngineeringEBooksPdf.com

in an equivalent model in which the $\cos(n_p\theta)$ and $\sin(n_p\theta)$ expressions are eliminated. To proceed, define an equivalent set of rotor flux linkages as

$$\begin{bmatrix} \psi_{Ra} \\ \psi_{Rb} \end{bmatrix} = \begin{bmatrix} \cos(n_p\theta) & -\sin(n_p\theta) \\ \sin(n_p\theta) & \cos(n_p\theta) \end{bmatrix} \begin{bmatrix} \lambda_{Ra} \\ \lambda_{Rb} \end{bmatrix}$$

where upon substituting the expressions for the rotor fluxes in (8.2), one obtains

$$\begin{aligned} \psi_{Ra} &= L_R\left(i_{Ra}\cos(n_p\theta) - i_{Rb}\sin(n_p\theta)\right) + Mi_{Sa} \\ \psi_{Rb} &= L_R\left(i_{Ra}\sin(n_p\theta) + i_{Rb}\cos(n_p\theta)\right) + Mi_{Sb}. \end{aligned} \tag{8.3}$$

The model of the induction motor in terms of the state variables ψ_{Ra}, ψ_{Rb}, i_{Sa}, i_{Sb}, and ω is now derived.[2] Using (8.3) to eliminate the rotor currents, the first two equations of (8.1) may be rewritten as

$$\begin{aligned} u_{Sa} &= R_S i_{Sa} + L_S\frac{d}{dt}i_{Sa} + M\frac{d}{dt}(\psi_{Ra} - Mi_{Sa})/L_R \\ u_{Sb} &= R_S i_{Sb} + L_S\frac{d}{dt}i_{Sb} + M\frac{d}{dt}(\psi_{Rb} - Mi_{Sb})/L_R \end{aligned}$$

or

$$\begin{aligned} u_{Sa} &= R_S i_{Sa} + L_S\left(1 - \frac{M^2}{L_R L_S}\right)\frac{d}{dt}i_{Sa} + \frac{M}{L_R}\frac{d}{dt}\psi_{Ra} \\ u_{Sb} &= R_S i_{Sb} + L_S\left(1 - \frac{M^2}{L_R L_S}\right)\frac{d}{dt}i_{Sb} + \frac{M}{L_R}\frac{d}{dt}\psi_{Rb}. \end{aligned}$$

The third and fourth equations of (8.1) can be rewritten as

$$\begin{aligned} \begin{bmatrix} 0 \\ 0 \end{bmatrix} &= \begin{bmatrix} R_R i_{Ra} \\ R_R i_{Rb} \end{bmatrix} + \frac{d}{dt}\left(\begin{bmatrix} \cos(n_p\theta) & \sin(n_p\theta) \\ -\sin(n_p\theta) & \cos(n_p\theta) \end{bmatrix}\right. \\ &\quad \left.\times \begin{bmatrix} L_R\left(\cos(n_p\theta)i_{Ra} - \sin(n_p\theta)i_{Rb}\right) + Mi_{Sa} \\ L_R\left(\sin(n_p\theta)i_{Ra} + \cos(n_p\theta)i_{Rb}\right) + Mi_{Sb} \end{bmatrix}\right) \end{aligned}$$

or, simply

$$\begin{bmatrix} 0 \\ 0 \end{bmatrix} = \begin{bmatrix} R_R i_{Ra} \\ R_R i_{Rb} \end{bmatrix} + \frac{d}{dt}\left(\begin{bmatrix} \cos(n_p\theta) & \sin(n_p\theta) \\ -\sin(n_p\theta) & \cos(n_p\theta) \end{bmatrix}\begin{bmatrix} \psi_{Ra} \\ \psi_{Rb} \end{bmatrix}\right).$$

Expanding,

$$\begin{aligned} \begin{bmatrix} 0 \\ 0 \end{bmatrix} &= \begin{bmatrix} R_R i_{Ra} \\ R_R i_{Rb} \end{bmatrix} + \frac{d}{dt}\left(\begin{bmatrix} \cos(n_p\theta) & \sin(n_p\theta) \\ -\sin(n_p\theta) & \cos(n_p\theta) \end{bmatrix}\right)\begin{bmatrix} \psi_{Ra} \\ \psi_{Rb} \end{bmatrix} \\ &\quad + \begin{bmatrix} \cos(n_p\theta) & \sin(n_p\theta) \\ -\sin(n_p\theta) & \cos(n_p\theta) \end{bmatrix}\frac{d}{dt}\begin{bmatrix} \psi_{Ra} \\ \psi_{Rb} \end{bmatrix} \end{aligned}$$

[2] See problem 2 where this set of equations is rederived in a simpler fashion using the space vector representation.

www.EngineeringEBooksPdf.com

Multiplying both sides on the left by $\begin{bmatrix} \cos(n_p\theta) & -\sin(n_p\theta) \\ \sin(n_p\theta) & \cos(n_p\theta) \end{bmatrix}$ gives

$$\begin{bmatrix} 0 \\ 0 \end{bmatrix} = \begin{bmatrix} \cos(n_p\theta) & -\sin(n_p\theta) \\ \sin(n_p\theta) & \cos(n_p\theta) \end{bmatrix} \begin{bmatrix} R_R i_{Ra} \\ R_R i_{Rb} \end{bmatrix} + \begin{bmatrix} \cos(n_p\theta) & -\sin(n_p\theta) \\ \sin(n_p\theta) & \cos(n_p\theta) \end{bmatrix}$$

$$\times\, n_p\omega \begin{bmatrix} -\sin(n_p\theta) & \cos(n_p\theta) \\ -\cos(n_p\theta) & -\sin(n_p\theta) \end{bmatrix} \begin{bmatrix} \psi_{Ra} \\ \psi_{Rb} \end{bmatrix} + \frac{d}{dt} \begin{bmatrix} \psi_{Ra} \\ \psi_{Rb} \end{bmatrix}$$

which simplifies to

$$\begin{bmatrix} 0 \\ 0 \end{bmatrix} = \begin{bmatrix} (R_R/L_R)(\psi_{Ra} - Mi_{Sa}) \\ (R_R/L_R)(\psi_{Rb} - Mi_{Sb}) \end{bmatrix} - n_p\omega \begin{bmatrix} 0 & -1 \\ 1 & 0 \end{bmatrix} \begin{bmatrix} \psi_{Ra} \\ \psi_{Rb} \end{bmatrix} + \frac{d}{dt} \begin{bmatrix} \psi_{Ra} \\ \psi_{Rb} \end{bmatrix}.$$

Finally, the torque equation becomes

$$\begin{aligned} J\frac{d\omega}{dt} &= n_p M \left(i_{Sb} \frac{\psi_{Ra} - Mi_{Sa}}{L_R} - i_{Sa} \frac{\psi_{Rb} - Mi_{Sb}}{L_R} \right) - f\omega - \tau_L \\ &= n_p \frac{M}{L_R} (i_{Sb}\psi_{Ra} - i_{Sa}\psi_{Rb}) - f\omega - \tau_L. \end{aligned}$$

Collecting these equations together, the dynamic model of the induction motor in terms of the state variables θ, ω, ψ_{Ra}, ψ_{Rb}, i_{Sa}, and i_{Sb} is then

$$\begin{aligned} \frac{d\theta}{dt} &= \omega \\ \frac{d\omega}{dt} &= \frac{n_p M}{JL_R} (i_{Sb}\psi_{Ra} - i_{Sa}\psi_{Rb}) - \frac{f}{J}\omega - \frac{\tau_L}{J} \\ \frac{d\psi_{Ra}}{dt} &= -\frac{R_R}{L_R}\psi_{Ra} - n_p\omega\psi_{Rb} + \frac{MR_R}{L_R} i_{Sa} \\ \frac{d\psi_{Rb}}{dt} &= -\frac{R_R}{L_R}\psi_{Rb} + n_p\omega\psi_{Ra} + \frac{MR_R}{L_R} i_{Sb} \\ u_{Sa} &= R_S i_{Sa} + \sigma L_S \frac{di_{Sa}}{dt} + \frac{M}{L_R}\frac{d\psi_{Ra}}{dt} \\ u_{Sb} &= R_S i_{Sb} + \sigma L_S \frac{di_{Sb}}{dt} + \frac{M}{L_R}\frac{d\psi_{Rb}}{dt} \end{aligned} \tag{8.4}$$

where

$$\sigma \triangleq 1 - \frac{M^2}{L_R L_S}$$

is the *leakage* parameter. Substituting the expressions for $d\psi_{Ra}/dt$ and $d\psi_{Rb}/dt$ from the third and fourth equations of (8.4) into the fifth and sixth equations of (8.4) and rearranging, one obtains the state-space form

www.EngineeringEBooksPdf.com

of the system given by (see Refs. [64][65])

$$\begin{aligned}
\frac{d\theta}{dt} &= \omega \\
\frac{d\omega}{dt} &= \mu\left(i_{Sb}\psi_{Ra} - i_{Sa}\psi_{Rb}\right) - (f/J)\omega - \tau_L/J \\
\frac{d\psi_{Ra}}{dt} &= -\eta\psi_{Ra} - n_p\omega\psi_{Rb} + \eta M i_{Sa} \\
\frac{d\psi_{Rb}}{dt} &= -\eta\psi_{Rb} + n_p\omega\psi_{Ra} + \eta M i_{Sb} \\
\frac{di_{Sa}}{dt} &= \eta\beta\psi_{Ra} + \beta n_p\omega\psi_{Rb} - \gamma i_{Sa} + u_{Sa}/\sigma L_S \\
\frac{di_{Sb}}{dt} &= \eta\beta\psi_{Rb} - \beta n_p\omega\psi_{Ra} - \gamma i_{Sb} + u_{Sb}/\sigma L_S
\end{aligned} \tag{8.5}$$

with

$$\eta \triangleq \frac{R_R}{L_R}, \beta \triangleq \frac{M}{\sigma L_R L_S}, \mu \triangleq \frac{n_p M}{J L_R}, \gamma \triangleq \frac{M^2 R_R}{\sigma L_R^2 L_S} + \frac{R_S}{\sigma L_S}. \tag{8.6}$$

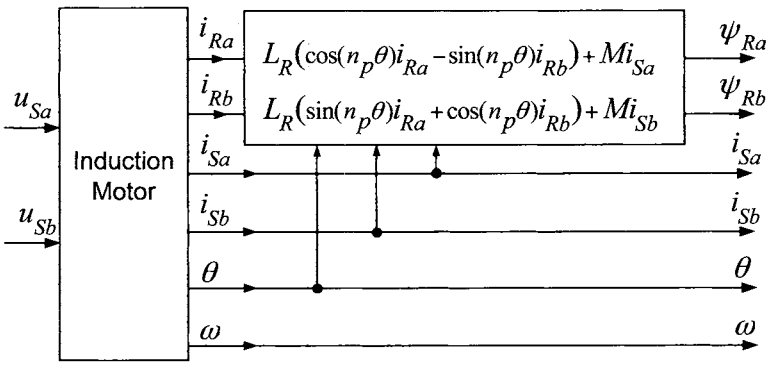


FIGURE 8.1. Block diagram of an equivalent induction motor model.

8.2 Field-Oriented and Input-Output Linearization Control of an Induction Motor

Recall that the fictitious rotor flux linkages ψ_{Ra} and ψ_{Rb} were used in the state-space formulation rather than the actual rotor flux linkages λ_{Ra} and λ_{Rb} in order to eliminate $\cos(\theta_R)$ and $\sin(\theta_R)$ from the mathematical model. However, even with this simplification, it is still not clear how to design a controller. That is, how does one choose u_{Sa} and u_{Sb} in order to control the torque, speed and/or position of the motor? The key idea of field-oriented control is to go to another *coordinate system* or *state variable representation*

www.EngineeringEBooksPdf.com

in which it becomes clear how to design a controller. There is an interesting analogy from mankind's understanding of the motion of the planets around the sun. Before the Polish astronomer Mikołaj Kopernik[3] came along in the 1500s, the view of the solar system was earth-centered; that is, the trajectories of the planets and the sun were described in terms of their motion with respect to the earth. The trajectories were quite complicated from this reference frame since the planets moved back and forth across the night sky while the sun appeared to go completely around the earth. Copernicus pointed out that if one viewed these motions from the sun's point of view, the planetary motions are quite simple. That is, one would jump into a new coordinate system where the sun is the stationary origin of the new coordinates. Then the erratic motions of the planets, as viewed from the earth, are now simple elliptical trajectories around the sun with the sun at one focus of the ellipse. The idea of field-oriented control is the same: Find a new coordinate system where the equations are simple enough that the way to control the system is self-evident.

For field-oriented control, the new coordinate system is a rotating system whose angular position is defined by

$$\rho \triangleq \tan^{-1}\left(\frac{\psi_{Rb}}{\psi_{Ra}}\right).$$

That is, instead of working with $(\psi_{Ra},\ \psi_{Rb})$, one uses the polar coordinate representation $(\rho,\ \psi_d)$ given by (see Ref. [64])

$$\begin{aligned} \rho &= \tan^{-1}\left(\frac{\psi_{Rb}}{\psi_{Ra}}\right) \\ \psi_d &= \sqrt{\psi_{Ra}^2 + \psi_{Rb}^2}. \end{aligned}$$

The phase currents and voltages are then transformed into the new coordinate system as

$$\begin{bmatrix} i_d \\ i_q \end{bmatrix} \triangleq \begin{bmatrix} \cos(\rho) & \sin(\rho) \\ -\sin(\rho) & \cos(\rho) \end{bmatrix} \begin{bmatrix} i_{Sa} \\ i_{Sb} \end{bmatrix} \tag{8.7}$$

$$\begin{bmatrix} u_d \\ u_q \end{bmatrix} \triangleq \begin{bmatrix} \cos(\rho) & \sin(\rho) \\ -\sin(\rho) & \cos(\rho) \end{bmatrix} \begin{bmatrix} u_{Sa} \\ u_{Sb} \end{bmatrix}. \tag{8.8}$$

The quantity ψ_d is referred to as the magnitude of the *rotor field flux* while ρ is the angle of the rotor field flux. This coordinate system is one that is moving (oriented) with this field flux and thus is called the *rotor-flux field-oriented* coordinate system. The currents i_d and i_q are called the direct and quadrature currents, respectively. Similarly, the voltages u_d and u_q are

[3] Better known as Copernicus.

www.EngineeringEBooksPdf.com

called the direct and quadrature voltages, respectively. The rotation matrix used in (8.7) and (8.8) is called the direct quadrature or dq transformation.

A mathematical model of the induction motor in which ω, i_d, i_q, ψ_d, and ρ are the state variables and the inputs are u_d and u_q is now developed. The torque equation is $(\cos(\rho) = \psi_{Ra}/\psi_d, \sin(\rho) = \psi_{Rb}/\psi_d)$

$$\begin{aligned}
\frac{d\omega}{dt} &= \mu(\psi_{Ra} i_{Sb} - \psi_{Rb} i_{Sa}) - (f/J)\omega - \tau_L/J \\
&= \mu\psi_d\,(\psi_{Ra}/\psi_d) i_{Sb} - (\psi_{Rb}/\psi_d) i_{Sa}) - (f/J)\omega - \tau_L/J \\
&= \mu\psi_d\,(-\sin(\rho) i_{Sa} + \cos(\rho) i_{Sb}) - (f/J)\omega - \tau_L/J \\
&= \mu\psi_d i_q - (f/J)\omega - \tau_L/J.
\end{aligned}$$

The equation describing the dynamics of the magnitude of the rotor flux is

$$\begin{aligned}
\frac{d\psi_d}{dt} &= \frac{d}{dt}\sqrt{\psi_{Ra}^2 + \psi_{Rb}^2} \\
&= \frac{1/2}{\sqrt{\psi_{Ra}^2 + \psi_{Rb}^2}}\left(2\psi_{Ra}\frac{d}{dt}\psi_{Ra} + 2\psi_{Rb}\frac{d}{dt}\psi_{Rb}\right) \\
&= \cos(\rho)\,(-\eta\psi_{Ra} - n_p\omega\psi_{Rb} + \eta M i_{Sa}) \\
&\quad + \sin(\rho)\,(-\eta\psi_{Rb} + n_p\omega\psi_{Ra} + \eta M i_{Sb}) \\
&= -\eta\,(\cos(\rho)\psi_{Ra} + \sin(\rho)\psi_{Rb}) + n_p\omega\,(-\cos(\rho)\psi_{Rb} + \sin(\rho)\psi_{Ra}) \\
&\quad + \eta M\,(\cos(\rho) i_{Sa} + \sin(\rho) i_{Sb}) \\
&= -\eta\psi_d + \eta M i_d.
\end{aligned}$$

The rotor flux angle dynamics are then

$$\begin{aligned}
\frac{d\rho}{dt} &= \frac{d}{dt}\tan^{-1}\left(\frac{\psi_{Rb}}{\psi_{Ra}}\right) \\
&= \frac{1}{1 + (\psi_{Rb}/\psi_{Ra})^2}\,\frac{\dot{\psi}_{Rb}\psi_{Ra} - \psi_{Rb}\dot{\psi}_{Ra}}{\psi_{Ra}^2} \\
&= \frac{1}{\psi_{Ra}^2 + \psi_{Rb}^2}\,(\psi_{Ra}(-\eta\psi_{Rb} + n_p\omega\psi_{Ra} + \eta M i_{Sb}) \\
&\quad -\psi_{Rb}(-\eta\psi_{Ra} - n_p\omega\psi_{Rb} + \eta M i_{Sa})) \\
&= \frac{1}{\psi_d^2}\left(n_p\omega(\psi_{Ra}^2 + \psi_{Rb}^2)\right) + \eta M\frac{1}{\psi_d}\left((\psi_{Ra}/\psi_d) i_{Sb} - (\psi_{Rb}/\psi_d) i_{Sa}\right) \\
&= n_p\omega + \eta M\frac{1}{\psi_d}\,(\cos(\rho) i_{Sb} - \sin(\rho) i_{Sa}) \\
&= n_p\omega + \eta M\frac{i_q}{\psi_d}.
\end{aligned}$$

www.EngineeringEBooksPdf.com

The dynamic equation describing the direct current is

$$\begin{aligned}
\frac{di_d}{dt} &= \frac{d}{dt}\left(\cos(\rho)i_{Sa} + \sin(\rho)i_{Sb}\right) \\
&= \left(-\sin(\rho)i_{Sa} + \cos(\rho)i_{Sb}\right)\frac{d\rho}{dt} + \cos(\rho)\frac{di_{Sa}}{dt} + \sin(\rho)\frac{di_{Sb}}{dt} \\
&= i_q\frac{d\rho}{dt} + \cos(\rho)\left(\eta\beta\psi_{Ra} + \beta n_p\omega\psi_{Rb} - \gamma i_{Sa} + \frac{u_{Sa}}{\sigma L_S}\right) \\
&\quad + \sin(\rho)\left(\eta\beta\psi_{Rb} - \beta n_p\omega\psi_{Ra} - \gamma i_{Sb} + \frac{u_{Sb}}{\sigma L_S}\right) \\
&= i_q\left(n_p\omega + \eta M\frac{i_q}{\psi_d}\right) + \eta\beta\left(\cos(\rho)\psi_{Ra} + \sin(\rho)\psi_{Rb}\right) \\
&\quad + n_p\omega\beta\left(\cos(\rho)\psi_{Rb} - \sin(\rho)\psi_{Ra}\right) - \gamma\left(\cos(\rho)i_{Sa} + \sin(\rho)i_{Sb}\right) \\
&\quad + \left(\cos(\rho)u_{Sa} + \sin(\rho)u_{Sb}\right)/\sigma L_S \\
&= i_q n_p\omega + \eta M\frac{i_q^2}{\psi_d} + \eta\beta\psi_d - \gamma i_d + \frac{u_d}{\sigma L_S}.
\end{aligned}$$

The dynamic equation describing the quadrature current is

$$\begin{aligned}
\frac{di_q}{dt} &= \frac{d}{dt}\left(-\sin(\rho)i_{Sa} + \cos(\rho)i_{Sb}\right) \\
&= -\left(\cos(\rho)i_{Sa} + \sin(\rho)i_{Sb}\right)\frac{d\rho}{dt} - \sin(\rho)\frac{di_{Sa}}{dt} + \cos(\rho)\frac{di_{Sb}}{dt} \\
&= -i_d\frac{d\rho}{dt} - \sin(\rho)\left(\eta\beta\psi_{Ra} + \beta n_p\omega\psi_{Rb} - \gamma i_{Sa} + \frac{u_{Sa}}{\sigma L_S}\right) \\
&\quad + \cos(\rho)\left(\eta\beta\psi_{Rb} - \beta n_p\omega\psi_{Ra} - \gamma i_{Sb} + \frac{u_{Sb}}{\sigma L_S}\right) \\
&= -i_d\left(n_p\omega + \eta M i_q/\psi_d\right) + \eta\beta\left(-\sin(\rho)\psi_{Ra} + \cos(\rho)\psi_{Rb}\right) \\
&\quad - n_p\omega\beta\left(\sin(\rho)\psi_{Rb} + \cos(\rho)\psi_{Ra}\right) - \gamma\left(-\sin(\rho)i_{Sa} + \cos(\rho)i_{Sb}\right) \\
&\quad + \left(-\sin(\rho)u_{Sa} + \cos(\rho)u_{Sb}\right)/\sigma L_S \\
&= -i_d n_p\omega - \eta M i_d i_q/\psi_d - n_p\omega\beta\psi_d - \gamma i_q + \frac{u_q}{\sigma L_S}.
\end{aligned}$$

Collecting the above equations together, a state-space model in the field-

www.EngineeringEBooksPdf.com

oriented coordinate system is given by

$$\begin{aligned}
\frac{d\theta}{dt} &= \omega \\
\frac{d\omega}{dt} &= \mu\psi_d i_q - (f/J)\omega - \tau_L/J \\
\frac{d\psi_d}{dt} &= -\eta\psi_d + \eta M i_d \\
\frac{di_d}{dt} &= -\gamma i_d + (\eta M/\sigma L_R L_S)\psi_d + n_p\omega i_q + \eta M i_q^2/\psi_d + u_d/\sigma L_S \\
\frac{di_q}{dt} &= -\gamma i_q - (M/\sigma L_R L_S) n_p\omega\psi_d - n_p\omega i_d - \eta M i_q i_d/\psi_d + u_q/\sigma L_S \\
\frac{d\rho}{dt} &= n_p\omega + \eta M i_q/\psi_d.
\end{aligned} \tag{8.9}$$

This model is now used to develop a very effective method of control. It is first assumed that all of the state-variables θ, ω, ψ_d, i_d, i_q, and ρ are available for feedback. This would mean that one physically measures θ, ω, i_{Sa}, i_{Sb}, i_{Ra}, and i_{Rb} and then uses these measurements to compute ψ_d, i_d, i_q, and ρ in *real time*. In practice, one is rarely able to measure the rotor currents i_{Ra} and i_{Rb}. This problem can be resolved using an *observer* to estimate ρ and ψ_d as will be shown later. Then i_d and i_q can be computed using the estimated value for ρ and the measured stator currents i_{Sa} and i_{Sb}.

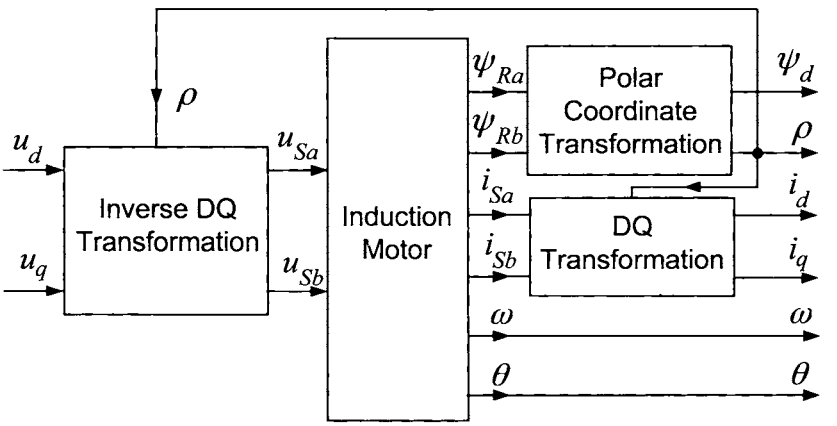


FIGURE 8.2. Transformation to the field-oriented (dq) coordinate system.

8.2.1 *Current-Command Field-Oriented Control*

Note that the electromagnetic torque $\tau = J\mu\psi_d i_q$ is now just proportional to the product of two state variables. However, the differential equations

www.EngineeringEBooksPdf.com

for i_d and i_q still contain quite complicated nonlinearities. One possibility to simplify these current dynamics is to use feedback cancellation; that is, let

$$\begin{aligned} u_d &= -(\sigma L_S)\left(-\gamma i_d + \eta\beta\psi_d + n_p\omega i_q + \eta M i_q^2/\psi_d\right) + (\sigma L_S)v_d \\ u_q &= -(\sigma L_S)\left(-\gamma i_q - \beta n_p\omega\psi_d - n_p\omega i_d - \eta M i_q i_d/\psi_d\right) + (\sigma L_S)v_q \end{aligned} \tag{8.10}$$

so that (8.9) simplifies to

$$\begin{aligned} d\omega/dt &= \mu\psi_d i_q - (f/J)\omega - \tau_L/J \\ d\psi_d/dt &= -\eta\psi_d + \eta M i_d \\ di_d/dt &= v_d \\ di_q/dt &= v_q \\ d\rho/dt &= n_p\omega + \eta M i_q/\psi_d \end{aligned} \tag{8.11}$$

For current-command control, one may choose

$$\begin{aligned} v_d &= K_{dI}\int_0^t (i_{dr} - i_d)dt + K_{dP}(i_{dr} - i_d) \\ v_q &= K_{qI}\int_0^t (i_{qr} - i_q)dt + K_{qP}(i_{qr} - i_q) \end{aligned}$$

and by appropriate choice of the PI gains, $i_d \to i_{dr}$ and $i_q \to i_{qr}$. However, in practice, this is *not* done. To explain, note that in applying the feedback (8.10), there is some uncertainty in the knowledge of the motor parameters and the state variables. The motor parameters R_R and R_S can vary significantly due to ohmic heating while L_R and L_S can also vary due to magnetic saturation. Furthermore, the state variables ρ and ψ_d must be estimated leaving uncertainty not only in their values, but in the currents i_d and i_q as the value of ρ is also needed to estimate them.

Experience has shown that the effect of the nonlinear terms in (8.9) can be eliminated by forcing the system into *current-command* mode using high-gain feedback [66]. That is, one applies the PI current loops

$$\begin{aligned} u_d &= K_{dI}\int_0^t (i_{dr} - i_d)dt + K_{dP}(i_{dr} - i_d) \\ u_q &= K_{qI}\int_0^t (i_{qr} - i_q)dt + K_{qP}(i_{qr} - i_q) \end{aligned} \tag{8.12}$$

directly to (8.9) to force i_d and i_q to track their corresponding references i_{dr} and i_{qr}, respectively. Values of the gains in (8.12) can be found that result in fast responses $i_d \to i_{dr}$ and $i_q \to i_{qr}$ for the currents. Consequently, i_{dr}

www.EngineeringEBooksPdf.com

and i_{qr} can then be considered as the new inputs for the control design where the system equations simplify to (i.e., are approximated as)

$$\frac{d\theta}{dt} = \omega \tag{8.13}$$

$$\frac{d\omega}{dt} = \mu\psi_d i_{qr} - (f/J)\omega - \tau_L/J \tag{8.14}$$

$$\frac{d\psi_d}{dt} = -\eta\psi_d + \eta M i_{dr} \tag{8.15}$$

$$\frac{d\rho}{dt} = n_p\omega + \eta M i_q/\psi_d. \tag{8.16}$$

Remark Note the the subscript "r" is not used on i_q in (8.16). The reason for this is that one is only interested in controlling θ, ω, and ψ_d, but not ρ. However, one must estimate ρ (as well as ψ_d), and this equation will be used for that purpose using the estimated value i_q rather than the reference value i_{qr}.

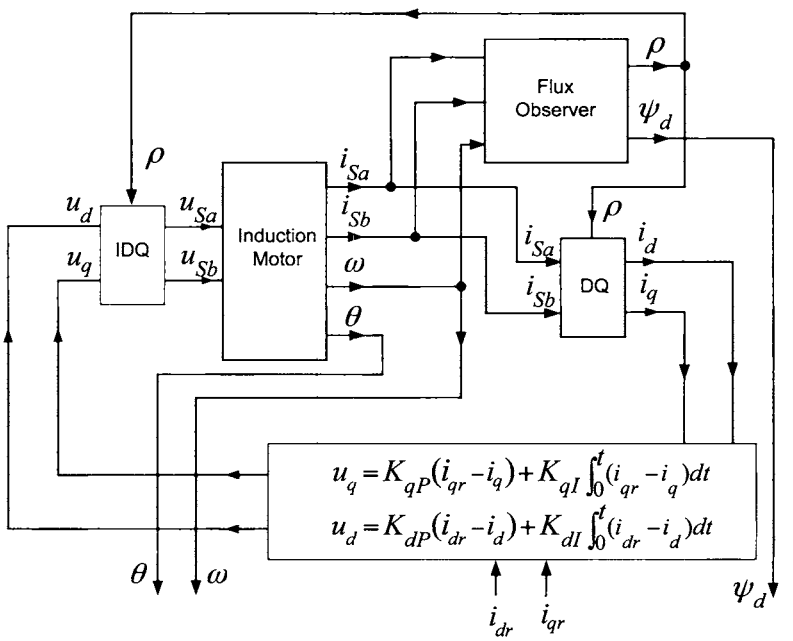


FIGURE 8.3. Block diagram of a current-command field-oriented system model.

A block diagram for the current-command field-oriented system model is given in Figure 8.3. The "Flux Observer" block will be described in Section 8.3.1. For now, the reader should just understand this block to represent an algorithm to compute ρ and ψ_d from measurements of i_{Sa}, i_{Sb}, and ω.

www.EngineeringEBooksPdf.com

Field-oriented control consists of using i_{dr} to force ψ_d to track the *constant* flux reference $\psi_{d0} = Mi_{d0}$. As a consequence, equations (8.13) and (8.14) become

$$\frac{d\theta}{dt} = \omega \tag{8.17}$$

$$\frac{d\omega}{dt} = \mu\psi_{d0}i_{qr} - (f/J)\omega - \tau_L/J \tag{8.18}$$

so that there is now a *linear* relationship between the input i_{qr} and the speed. To complete the control design, let

$$\begin{bmatrix} \theta_{ref}(t) \\ \omega_{ref}(t) \\ \alpha_{ref}(t) \end{bmatrix} = \begin{bmatrix} \theta_{ref}(t) \\ d\theta_{ref}/dt \\ d^2\theta_{ref}/dt^2 \end{bmatrix}$$

be the mechanical reference trajectory the motor is required to track. The control of speed/position is then done through the input i_{qr}. Specifically, choose

$$\begin{aligned} i_{qr} = \Big(& K_0 \int_0^t (\theta_{ref} - \theta)dt + K_1(\theta_{ref} - \theta) + K_2(\omega_{ref} - \omega) \\ & + (f/J)\omega + \alpha_{ref} \Big) / \mu\psi_{d0}. \end{aligned} \tag{8.19}$$

With the proper choice of the gains K_0, K_1, and K_2 (see problem 8), $\theta \to \theta_{ref}$ and $\omega \to \omega_{ref}$ even with a constant load torque τ_L acting on the motor.

The flux ψ_d is regulated to a constant value ψ_{d0} by

$$i_{dr} = K_{\psi I} \int_0^t (\psi_{d0} - \psi_d)dt + K_{\psi P}(\psi_{d0} - \psi_d) + i_{d0}. \tag{8.20}$$

That is, with proper choice of the feedback gains (see problem 7), $\psi_d \to \psi_{d0} = Mi_{d0}$.

A block diagram of this trajectory tracking controller is given in Figure 8.4.

Remarks

The roles of ψ_d and i_q (i_{dr} and i_{qr}) could, in principle, be reversed, but this is not done because the input i_d's (i_{dr}'s) ability to rapidly change ψ_d is limited by the rotor time constant $T_R = 1/\eta = L_R/R_R$, which is not the case for $i_q(i_{qr})$.

www.EngineeringEBooksPdf.com

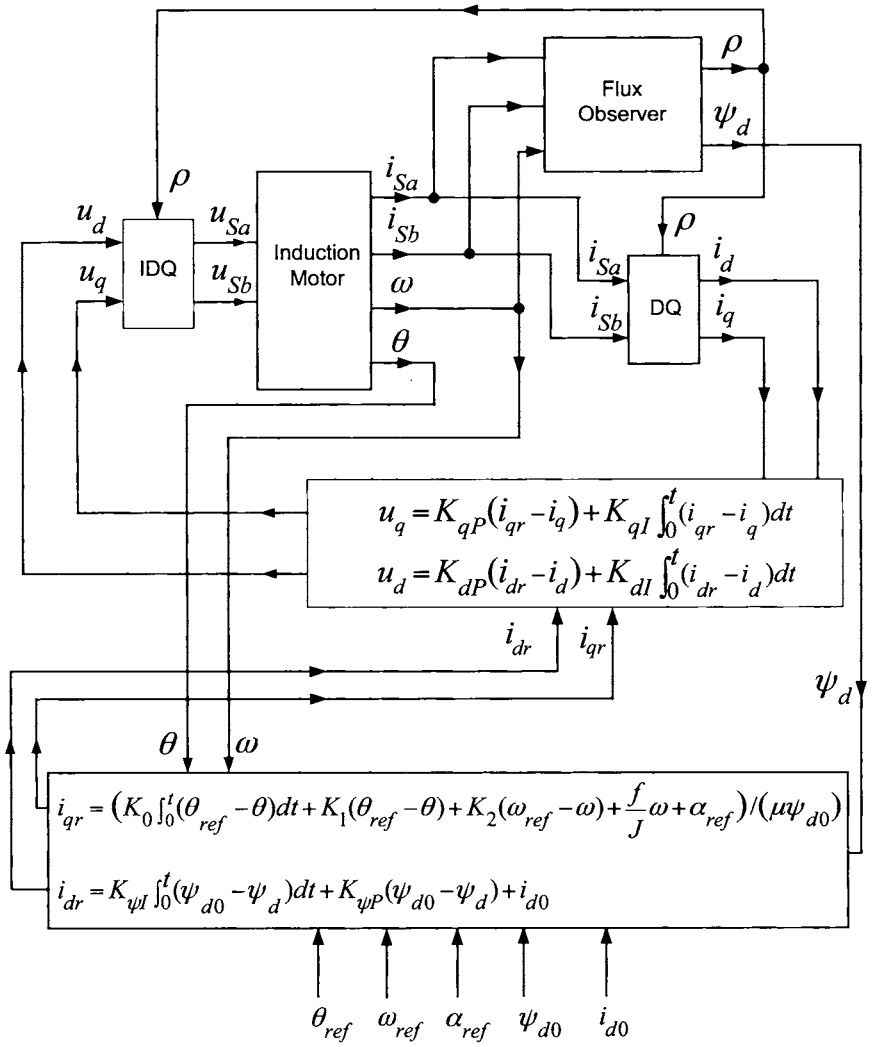


FIGURE 8.4. Block diagram of a trajectory tracking controller using a field-oriented controller.

As ψ_{d0} is constant, one usually incorporates $\mu\psi_{d0}$ directly into the controller gains as

$$i_{qr} = \bar{K}_0 \int_0^t (\theta_{ref} - \theta)dt + \bar{K}_1(\theta_{ref} - \theta) + \bar{K}_2(\omega_{ref} - \omega) - \bar{f}\omega + \bar{\alpha}_{ref} \quad (8.21)$$

where $\bar{K}_0 = K_0/(\mu\psi_{d0})$, $\bar{K}_1 = K_1/(\mu\psi_{d0})$, $\bar{K}_2 = K_2/(\mu\psi_{d0})$, $\bar{f} = f/(J\mu\psi_{d0})$, and $\bar{\alpha}_{ref} = \alpha_{ref}/(\mu\psi_{d0})$.

www.EngineeringEBooksPdf.com

Also, in practice, one typically leaves out the term $\bar{\alpha}_r$ in (8.21) and the term i_{d0} in (8.20) and finds that there is no significant deterioration in tracking if the gains can be chosen large enough.

8.2.2 Experimental Results Using a Field-Oriented Controller

Some experimental results showing the type of servo performance that can be achieved are now presented [67]. The motor is a 6-pole ($n_p = 3$) 1/12-horsepower two-phase induction motor with a squirrel cage rotor that is rated for 2.4 A (continuous) and 60 V. The rest of the hardware (see Figure 8.5) consists of a Motorola $DSP56001$ digital signal processing system for implementation of the control algorithm, two PWM amplifiers (± 80 V and ± 6 A), two analog-to-digital (A/D) converters to sample the stator currents, two digital-to-analog (D/A) converters to command voltage to the amplifiers, an electronic interface boards for the A/Ds and D/As, and a 2000 pulse/rev encoder (resolution of $360°/2000 = 0.18°$) to sense the angular position of the rotor. The PC indicated in Figure 8.5 is used to write, edit, and download the assembly language programs to the DSP which execute the controller algorithms. The parameters were identified using the technique given in Stephan et al. [42] and are $M = 0.0117$ H, $R_R = 3.9$ Ω, $R_S = 1.7$ $\Omega, L_R = 0.014$ H, $L_S = 0.014$ $H, f = 0.00014$ N-m/rad/sec and $J = 0.00011$ kg-m^2. The constant flux reference ψ_{d0} was chosen to be $\psi_{d0} = Mi_{d0} = 0.0117(5.5/\sqrt{2}) = 0.0455$ Wb. (See problem 13 for an explanation of the choice $i_{d0} = 5.5/\sqrt{2}$.)

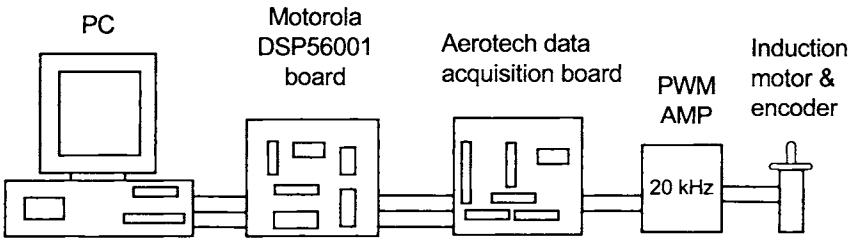


FIGURE 8.5. Hardware setup.

Figure 8.6 is a plot of the measure motor position and its reference trajectory used to carry out the turn. This figure shows the controller was able to turn the motor 180° in 73 msec. The tracking of the motor position to its reference is close enough that they are indistinguishable in Figure 8.6. Their difference in encoder counts is plotted in Figure 8.7 where it is seen that the measured error is less than two counts [$= 2(2\pi/2000) = 0.00314$ radians] for the entire move.

www.EngineeringEBooksPdf.com

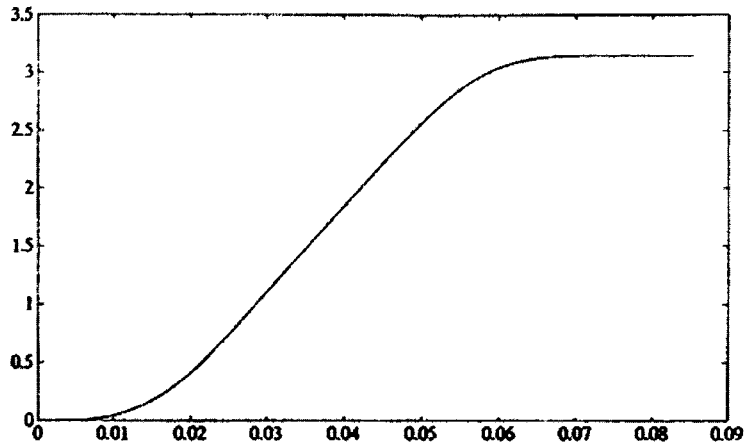


FIGURE 8.6. θ and θ_{ref} in radians versus time in seconds. From Bodson et al. [67], © 2004 IEEE.

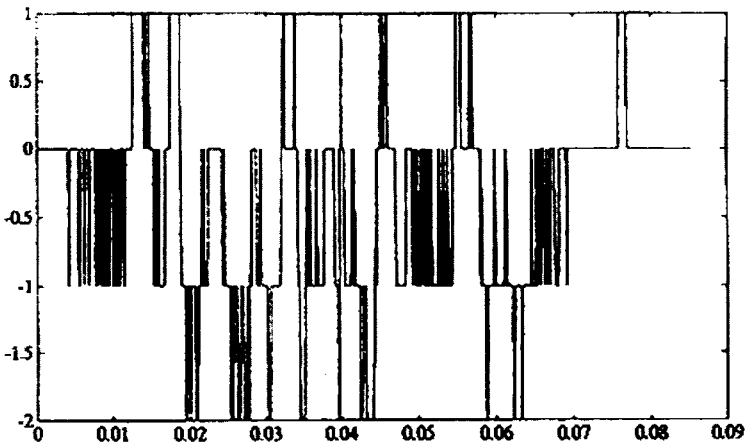


FIGURE 8.7. $\theta_{ref} - \theta$ in encoder counts versus time in seconds. From Bodson et al. [67], © 2004 IEEE.

The corresponding estimated speed and the speed reference are shown in Figure 8.8.

www.EngineeringEBooksPdf.com

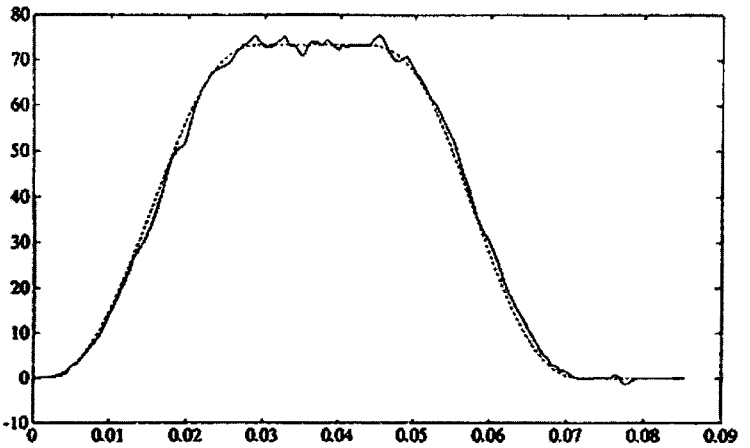


FIGURE 8.8. ω and ω_{ref} in radians/sec versus time in seconds. From Bodson et al. [67], © 2004 IEEE.

Finally, the quadrature current i_q and $i_{qref} = \alpha_{ref}/\psi_{d0}$ are given in Figure 8.9 while the flux ψ_d and its reference $\psi_{dref} = \psi_{d0}$ are given in Figure 8.10.

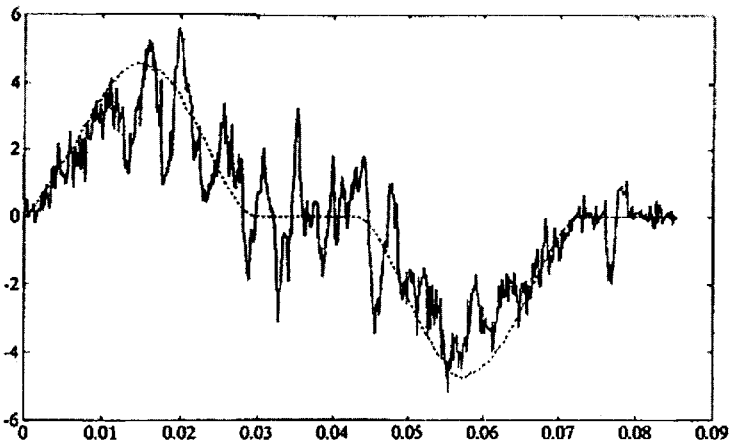


FIGURE 8.9. i_q and i_{qref} in amperes versus time in seconds. From Bodson et al. [67], © 2004 IEEE.

www.EngineeringEBooksPdf.com

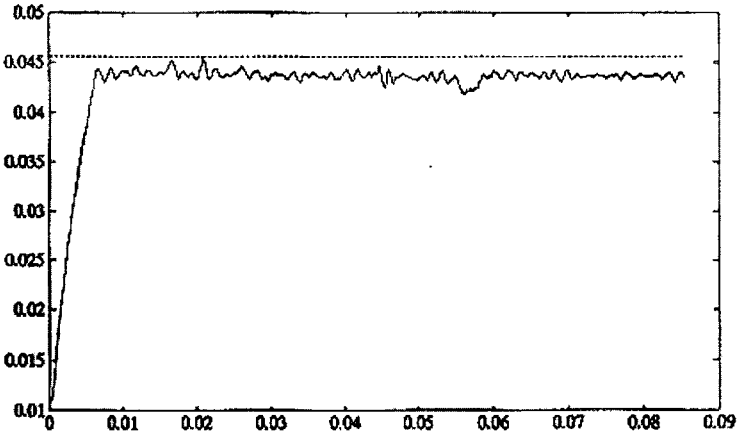


FIGURE 8.10. ψ_d and ψ_{dref} in webers versus time in seconds. From Bodson et al. [67], © 2004 IEEE.

The PI current gains for the tracking error in (8.12) where chosen as $K_{dI} = 740, K_{dP} = 6.4, K_{qI} = 740$, and $K_{qP} = 6.4$. The gains for the trajectory tracking controller in (8.19) were set as

$$\begin{aligned} K_0 &= 1.07 \times 10^6 \\ K_1 &= 7.04 \times 10^5 \\ K_2 &= 1.07 \times 10^3 \end{aligned} \tag{8.22}$$

and the gains for the flux regulator (8.20) were set to

$$\begin{aligned} K_{\psi P} &= 1600 \\ K_{\psi I} &= 23000. \end{aligned} \tag{8.23}$$

8.2.3 Field Weakening

The torque is controlled through the quadrature current i_q. Inspection of the fifth equation in (8.9) reveals that in order to maintain or increase i_q, the voltage u_q must be chosen such that $di_q/dt \geq 0$, that is,

$$\begin{aligned} u_q &\geq \sigma L_S \gamma i_q + M n_p \omega \psi_d / L_R + \sigma L_S n_p \omega i_d + \sigma L_S \eta M i_q i_d / \psi_d \\ &= \left(\frac{M^2}{L_R^2} R_R + R_S \right) i_q + \frac{M}{L_R} n_p \omega \psi_d + \sigma L_S n_p \omega i_d + \sigma L_S \frac{R_R}{L_R} i_q M i_d / \psi_d \end{aligned}$$

www.EngineeringEBooksPdf.com

where (8.6) was used. Consider the machine in steady state so that $\psi_d = Mi_d$ and use the approximation $L_S \approx L_R \approx M$ so that this inequality reduces to

$$u_q \geq (R_R + R_S)\, i_q + n_p \omega \psi_d + \sigma n_p \omega \psi_d + \sigma R_R i_q.$$

At higher speeds, the dominant term on the right-hand side of this inequality is $n_p \omega \psi_d$. When the motor speed reaches a high enough speed, called the *base speed* ω_{base}, the required voltage to maintain the current i_q equals the maximum voltage $V_{\max}$ the amplifier can produce. To get around this problem, the flux ψ_d is decreased at higher speeds. The standard way to choose the flux reference is given by

$$\psi_{dref} = \begin{cases} \psi_{d0} & \text{for} \quad |\omega| < \omega_{base} \\ \psi_{d0}\omega_{base}/|\omega| & \text{for} \quad |\omega| \geq \omega_{base} \end{cases} \tag{8.24}$$

which is plotted versus ω in Figure 8.11.

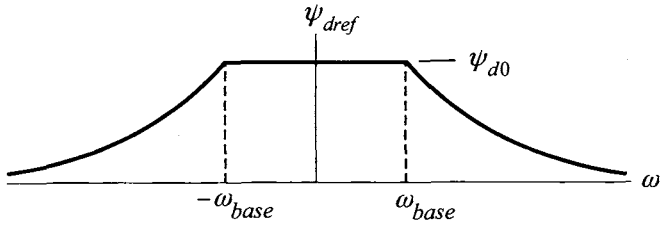


FIGURE 8.11. Flux reference for field weakening.

The direct current i_{dr} is chosen to force ψ_d to track ψ_{dref} specified by (8.24) so that above the base speed ω_{base} the term $n_p \omega \psi_d = n_p \omega_{base} \psi_{d0}$ is constant. This reduction of ψ_d above ω_{base} is referred to as *field weakening*. One way to choose the base speed ω_{base} is to set $n_p \omega_{base} \psi_{d0} = V_{\max}$ or $\omega_{base} = V_{\max}/(n_p \psi_{d0})$, where $V_{\max}$ is the (equivalent two-phase) stator voltage maximum. The trade-off here is that one can have the motor achieve speeds above the base speed, but less torque is produced as $\tau = J\mu\psi_d i_q$ so that for the same i_q, decreasing ψ_d means that less torque is produced.

Another way to formulate the problem of selecting the flux reference is as a static optimization problem. That is, at each constant rotor speed ω, maximize

$$\tau = J\mu\psi_d i_q \tag{8.25}$$

subject to the constraints

$$u_d^2 + u_q^2 \leq V_{\max}^2, i_d^2 + i_q^2 \leq I_{\max}^2. \tag{8.26}$$

Such an approach is given in Section 8.4 based on Refs. [68] and [69].

www.EngineeringEBooksPdf.com

8.2.4 *Input-Output Linearization*

In the above field-oriented control scheme, the speed ω and flux ψ_d are only *asymptotically* decoupled [64]. In other words, the speed equation (8.14) is linear only *after* ψ_d is constant. For high speeds, field weakening (i.e., decreasing ψ_d), is necessary so as not to exceed the stator voltage limit. Since in the field-weakening region, the flux reference varies as a function of the speed, the dynamics of ψ_d then interfere with the dynamics of ω. This coupling of the flux and speed dynamics can be eliminated by considering an *input-output linearizing* controller [64][65][70][71]. Recall the system (8.13)-(8.16) repeated below:

$$\begin{aligned}
\frac{d\theta}{dt} &= \omega \\
\frac{d\omega}{dt} &= \mu\psi_d i_{qr} - (f/J)\omega - \tau_L/J \\
\frac{d\psi_d}{dt} &= -\eta\psi_d + \eta M i_{dr} \\
\frac{d\rho}{dt} &= n_p\omega + \eta M i_q/\psi_d.
\end{aligned}$$

In this model, i_{dr} and i_{qr} are the inputs. Let them now be specified by

$$\begin{aligned}
i_{dr} &= u_1 \\
i_{qr} &= \frac{u_2}{\mu\psi_d}
\end{aligned} \tag{8.27}$$

so that the system becomes

$$\begin{aligned}
d\theta/dt &= \omega \\
d\omega/dt &= u_2 - (f/J)\omega - \tau_L/J \\
d\psi_d/dt &= -\eta\psi_d + \eta M u_1 \\
d\rho/dt &= n_p\omega + \eta M i_q/\psi_d.
\end{aligned} \tag{8.28}$$

The flux dynamics are now decoupled from the speed dynamics. That is, the first three equations of (8.28) may be written as two decoupled linear subsystems

$$d\psi_d/dt = -\eta\psi_d + \eta M u_1 \tag{8.29}$$

and

$$\begin{aligned}
d\theta/dt &= \omega \\
d\omega/dt &= u_2 - (f/J)\omega - \tau_L/J.
\end{aligned} \tag{8.30}$$

The input u_1 is chosen to force the *linear* system (8.29) to track a given flux reference trajectory ψ_{dr}, and the input u_2 is used to force

www.EngineeringEBooksPdf.com

the *linear* system (8.30) to track a given mechanical reference trajectory $(\theta_{ref}(t), \omega_{ref}(t), \alpha_{ref}(t))$. After the input u_2 is specified in order to accomplish the control task, the current reference i_{qr} is then simply chosen to be $i_{qr} = u_2/(\mu\psi_d)$.

As system (8.28) is *linear* from the inputs u_1, u_2 to the outputs ω, ψ, this controller is referred to as an *input-output linearization* controller. However, the overall system (8.28) is still *nonlinear* as the dynamics of ρ are nonlinear. The boundedness (stability) of ρ is guaranteed since it is an angle and reset to 0 every 2π radians.

The new inputs u_1 and u_2 may be chosen as follows:

Let $\psi_{dref}(t)$ be a desired flux reference and choose

$$u_1 = i_{dr} = K_{\psi P}(\psi_{dref} - \psi_d) + K_{\psi I}\int_0^t (\psi_{dref} - \psi_d)dt + i_{dref} \qquad (8.31)$$

where i_{dref} satisfies

$$d\psi_{dref}/dt = -\eta\psi_{dref} + \eta M i_{dref}.$$

With proper choice of the feedback gains $K_{\psi P}$ and $K_{\psi I}$ (see problem 10), $\psi_d \to \psi_{dref}$.

Let $\left(\theta_{ref}(t), \omega_{ref}(t), \alpha_{ref}(t)\right)$ be the mechanical reference trajectory the motor is required to track. Choosing

$$\begin{aligned} u_2 \;=\; & K_0\int_0^t (\theta_{ref} - \theta)dt + K_1(\theta_{ref} - \theta) + K_2(\omega_{ref} - \omega) \\ & + \alpha_{ref} + (f/J)\omega \end{aligned} \qquad (8.32)$$

and along with a proper choice of the gains K_0, K_1, and K_2 (see problem 11) results in $\theta \to \theta_{ref}$ and $\omega \to \omega_{ref}$ even with a constant load torque τ_L acting on the motor. Figure 8.12 is a block diagram of the input–output linearization controller. The "speed observer" block will be described in Section 8.3.2. For now, the reader should understand it to be an algorithm to obtain an estimate $\hat{\omega}$ of the speed ω from knowledge of ψ_d, i_q, and θ.

Voltage Command Input-Output Control

An input-output linearization controller may also be designed for the full-order (voltage command) system model (8.11). Specifically, the transformation

$$\begin{aligned} \omega &\triangleq \omega \\ \alpha &\triangleq \mu\psi_d i_q \\ \psi_d &\triangleq \psi_d \\ \psi_d' &\triangleq -\eta\psi_d + \eta M i_d \\ \rho &\triangleq \rho \end{aligned}$$

www.EngineeringEBooksPdf.com

is applied to (8.11), resulting in

$$\begin{aligned} d\omega/dt &= \alpha - (f/J)\omega - \tau_L/J \\ d\alpha/dt &= \mu\psi_d' i_q + (\mu\psi_d)v_q \\ d\psi_d/dt &= \psi_d' \\ d\psi_d'/dt &= -\eta\psi_d' + (\eta M)v_d \\ d\rho/dt &= n_p\omega + \eta M\alpha/(\mu\psi_d^2). \end{aligned}$$

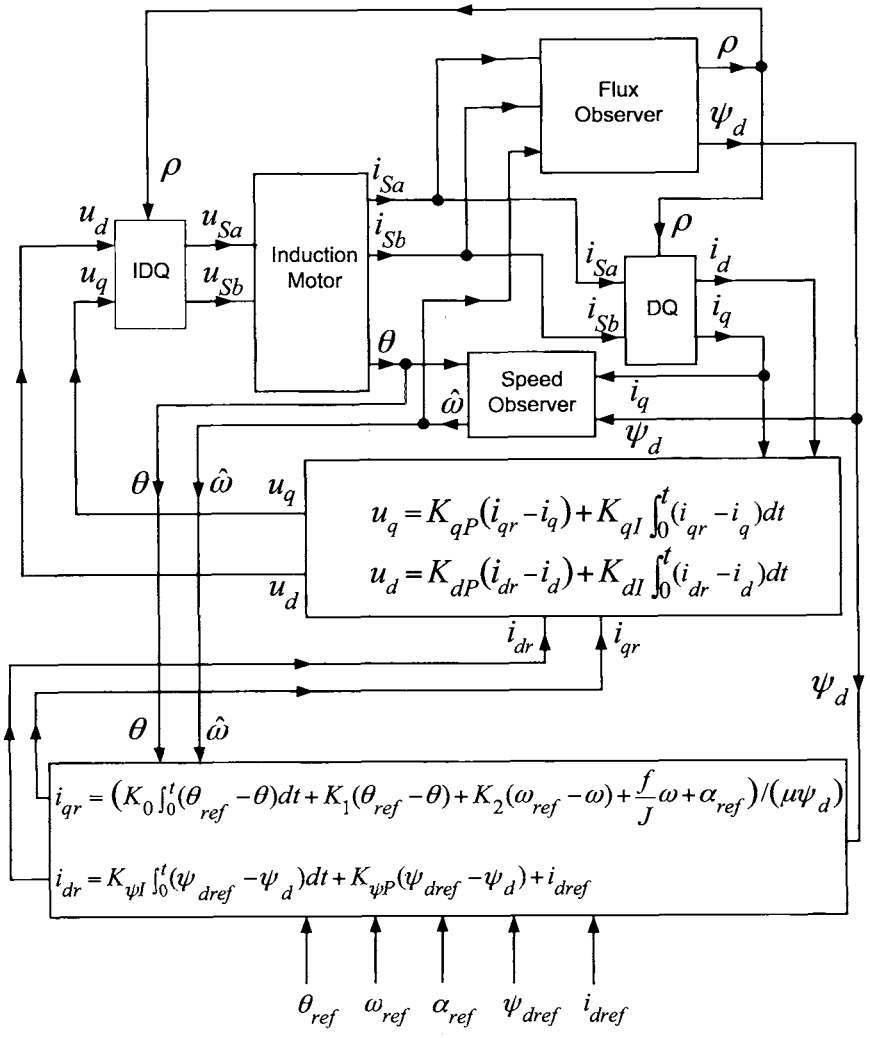


FIGURE 8.12. Block diagram of an input-output linearization controller.

www.EngineeringEBooksPdf.com

With w_d and w_q being two new inputs, application of the feedback

$$\begin{aligned} v_d &= \psi_d'/M + w_d/(\eta M) \\ v_q &= -\mu\psi_d' i_q/(\mu\psi_d) + w_q/(\mu\psi_d) \end{aligned} \tag{8.33}$$

results in the input-output linearized system

$$\begin{aligned} d\omega/dt &= \alpha - (f/J)\omega - \tau_L/J \\ d\alpha/dt &= w_q \\ d\psi_d/dt &= \psi_d' \\ d\psi_d'/dt &= w_d \\ d\rho/dt &= n_p\omega + \eta M \mu\alpha/\psi_d^2. \end{aligned}$$

8.2.5 Experimental Results Using an Input-Output Controller

Some experimental results are now presented to show the increased performance that can be extracted from the motor using an input–output linearization controller [65][69]. The motor and experimental setup is the same as that used for the field-oriented controller.

An experiment requiring a point-to-point position move was carried out in which the motor was brought up to a speed of 8000 rev/min in 0.38 seconds and brought down from 8000 rev/min to 0 rev/min in 0.265 sec (see Figure 8.15). The PI current gains in (8.12) were set at $K_{dI} = 9000, K_{dP} = 15, K_{qI} = 9000$, and $K_{qP} = 15$. The PI gains for the flux tracking controller (8.31) were chosen as $K_{\psi P} = 10,000, K_{\psi I} = 420,000$. The PID gains for the tracking error in (8.32) were chosen as $K_0 = 3.0 \times 10^5, K_1 = 5.5 \times 10^4$, and $K_2 = 125$. The sample rate was 4 kHz.

Figure 8.13 is a plot of the position and its reference where the tracking is close enough that they are indistinguishable in this figure. The difference $\theta_{ref} - \theta$ in encoder counts is given in Figure 8.14. The maximum error is 34 encoder counts.

www.EngineeringEBooksPdf.com

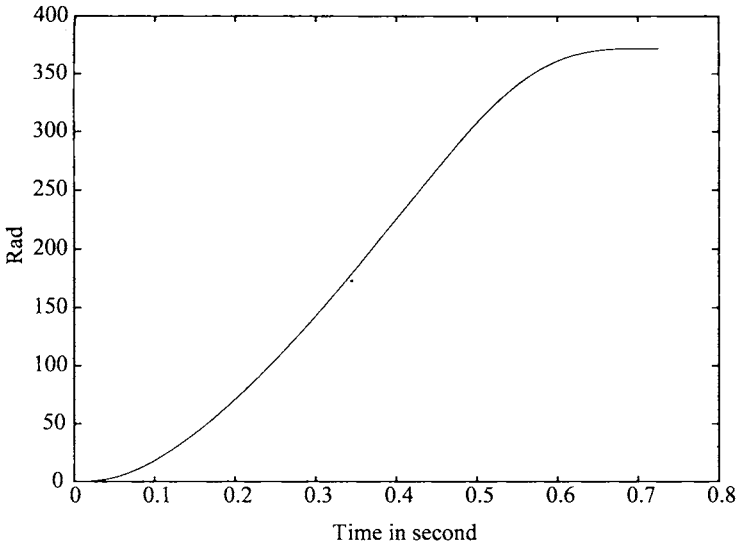


FIGURE 8.13. θ and θ_{ref} in radians versus time in seconds. From Bodson et al. [65], © 2004 IEEE.

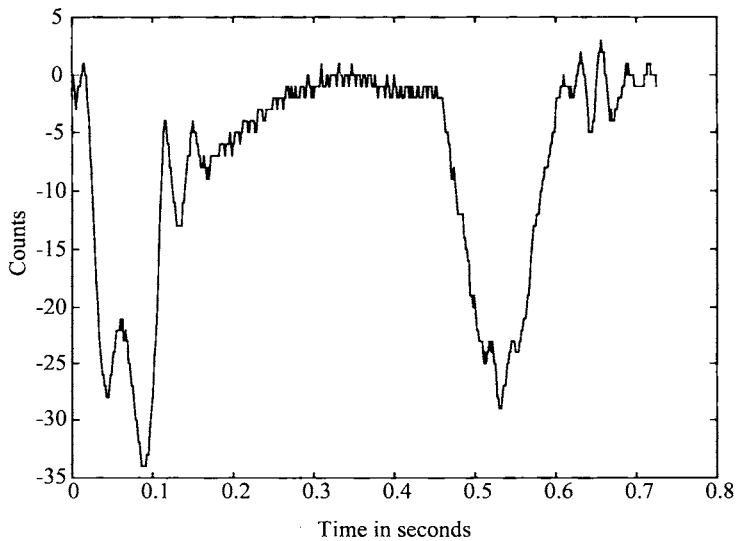


FIGURE 8.14. $\theta_{ref} - \theta$ in encoder counts versus time in seconds. From Bodson et al. [65], © 2004 IEEE.

www.EngineeringEBooksPdf.com

As Figure 8.14 shows, the final position error is zero at the end of the run which is a requirement of a point-to-point move. Comparing with Figure 8.18, it is seen that the maximum position errors occur when either the acceleration or deceleration is at a maximum. This is especially true at about 0.1 sec where, in addition, the jerk ($\triangleq d\alpha/dt$) is discontinuous.

Figure 8.15 is a plot of the estimated speed and the reference speed. Note the excellent speed tracking despite the time-varying flux (see Figure 8.17).

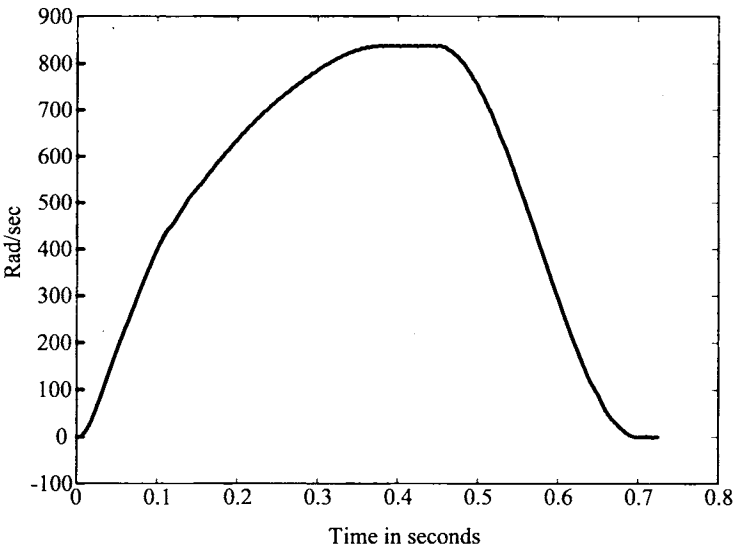


FIGURE 8.15. ω and ω_{ref} in radians/sec versus time in seconds. From Bodson et al. [65], © 2004 IEEE.

Figure 8.16 is a plot of i_q along with its reference $i_{qref} \triangleq \alpha_{ref}/(\mu\psi_{dref})$. Figure 8.17 shows a plot of ψ_{dref} and ψ_d, where ψ_{dref} is the result of solving the static optimization problem of equations (8.25) and (8.26) (see Section 8.4 and Refs. [68][69]). Figures 8.16 and 8.17 indicate that ψ_d and i_q vary significantly, yet the input–output controller forces the resultant torque $\tau = J\mu\psi_d i_q$ to provide smooth tracking of the position and speed as shown in Figures 8.13 and 8.15, respectively.

The dashed line in Figure 8.18 is a plot of the reference torque τ_{ref} ($\alpha_{ref} = \tau_{ref}/J$) corresponding to the position and speed references given in Figures 8.13 and 8.15. The solid line is a plot of the motors' optimum achievable torque by the motor given the voltage and current constraints [i.e., the solution $\tau_{optimum}$ for τ in equations (8.25) and (8.26)]. Note the closeness of the reference to the optimum.

www.EngineeringEBooksPdf.com

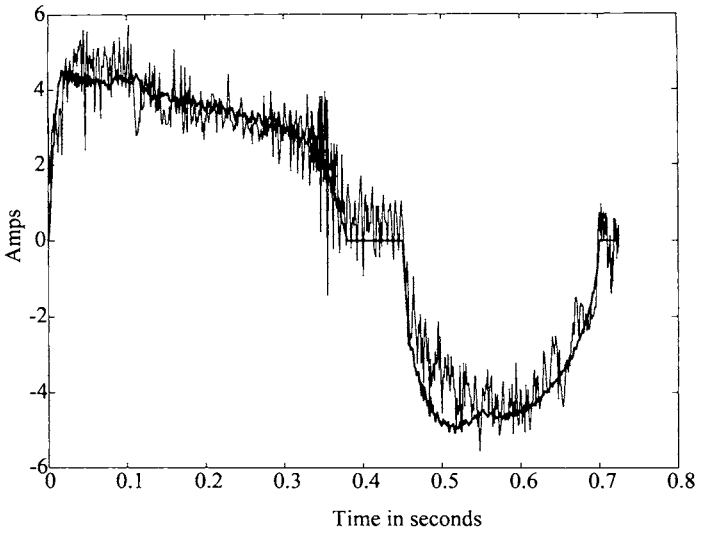


FIGURE 8.16. i_q and i_{qref} in amperes versus time in seconds. From Bodson et al. [65], © 2004 IEEE.

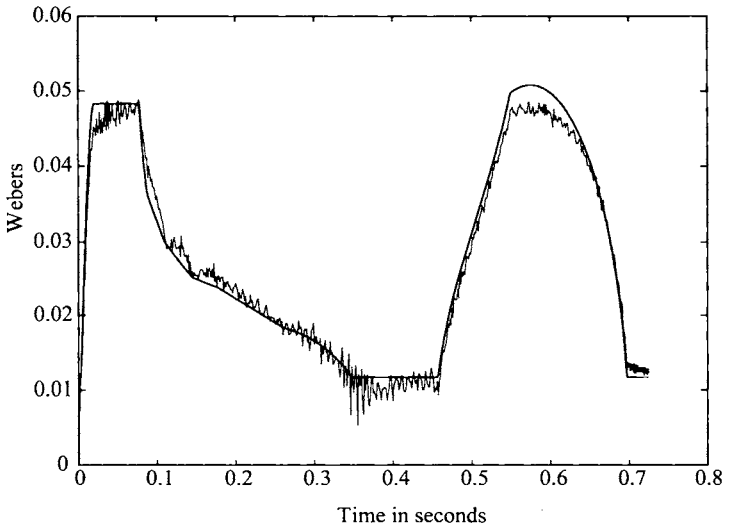


FIGURE 8.17. ψ_d and ψ_{dref} in webers versus time in seconds. From Bodson et al. [65], © 2004 IEEE.

www.EngineeringEBooksPdf.com

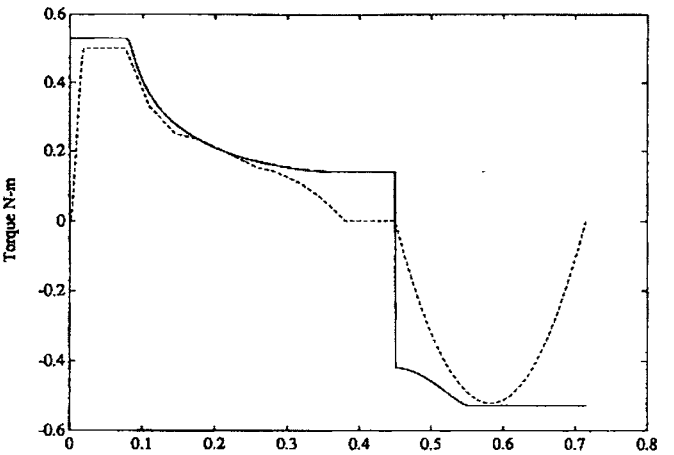


FIGURE 8.18. $\tau_{optimum}$ and τ_{ref} in N-m versus time in seconds. From Bodson et al. [65], © 2004 IEEE.

This high-speed experiment (i.e., the trajectories of Figures 8.13, 8.15, and 8.17) was attempted using a field-oriented controller and was not successful as the phase voltages exceed their limits. That is, the input-output linearization controller was essential for obtaining such high performance.

Remarks This control algorithm depends on the inner PI current control loops working satisfactorily. That is, they must be given sufficient time, as well as sufficient source voltage, to track the current references. As pointed out above, the dominant term in the equation for di_q/dt [fifth equation of (8.9)] is the *back emf* term given by $Mn_p\omega\psi_d/L_R \approx n_p\omega\psi_d$ (see problem 9). When n_p is large, a small change in ω results in a correspondingly large change in the back emf, making it difficult (i.e., takes time) for the PI current controller to overcome this disturbance in order to track the reference i_{qr}. Typically, induction motors do not have a large number of pole pairs; and even if they do (say $n_p = 12$), they are not usually run at high speeds. Consequently, the PI current loops usually perform satisfactorily. On the other hand, permanent magnet stepping (synchronous) motors typically have 50 pole pairs. In that case, the current dynamics must be taken into account (rather than swamped out by high-gain feedback) in order to achieve high performance. That is, for the same trajectory, less source voltage may be needed compared to the current-command input-output controller. (See Ref. [72] where voltage command was essential in achieving high-performance motion control of a 50-pole-pair PM stepper motor.)

www.EngineeringEBooksPdf.com

8.3 Observers

The field-oriented and input-output controllers require the rotor flux linkages in order to implement them. The simplest type of algorithm to estimate them based on observer theory is now presented. Also, when a position sensor is used, a speed sensor is typically *not* available. Instead, one usually numerically differentiates the position measurement to get the speed. However, it is shown how a smoother estimate can be found using a speed observer.

8.3.1 Flux Observer

Recall from (8.4) the dynamic equations of the flux linkages are given by ($\eta = 1/T_R$)

$$\begin{aligned} \frac{d}{dt}\psi_{Ra} &= -\eta\psi_{Ra} - n_p\omega\psi_{Rb} + \eta M i_{Sa} \\ \frac{d}{dt}\psi_{Rb} &= -\eta\psi_{Rb} + n_p\omega\psi_{Ra} + \eta M i_{Sb}. \end{aligned} \tag{8.34}$$

A straightforward way to estimate the fluxes ψ_{Ra} and ψ_{Rb} is to simply implement a *real-time* simulation of the equations (8.34) on the controller processor. That is, the currents i_{Sa} and i_{Sb} are sampled from the motor through analog to digital (A/D) converters, the speed ω is known through a sensor and these quantities are then used to run the following *real-time* simulation of the flux linkage equations

$$\begin{aligned} \frac{d}{dt}\hat{\psi}_{Ra} &= -\eta\hat{\psi}_{Ra} - n_p\omega\hat{\psi}_{Rb} + \eta M i_{Sa} \\ \frac{d}{dt}\hat{\psi}_{Rb} &= -\eta\hat{\psi}_{Rb} + n_p\omega\hat{\psi}_{Ra} + \eta M i_{Sb} \end{aligned} \tag{8.35}$$

on the controller processor. The solutions to these equations are then used as the *estimates* of the fluxes for use in the feedback control algorithm.

Note that for this to work, it is implicitly assumed that (i) the model (8.34) is the correct dynamic model of the flux linkages, (ii) the parameters η and M are known, (iii) the currents and speed are measured precisely, and (iv) the numerical integration of (8.35) is done accurately. Under these conditions, it is now shown that the flux linkage estimates given by the solution to (8.35) will converge to the correct values even if the initial conditions $\psi_{Ra}(0)$ and $\psi_{Rb}(0)$ for (8.35) are *unknown*. This is important because it also implies the observer will work even in the presence of disturbances. For example, suppose at time t_1 there is noise on the measurement of $\omega(t_1)$. Further, at time $t_1 + \delta$, say, the noise is no longer present on

www.EngineeringEBooksPdf.com

the speed measurement. Then, for $t_1 < t < t_1 + \delta$, the speed is measured as $\omega(t) + n(t)$ rather than the correct value of $\omega(t)$. This incorrect measurement is then being used in (8.35) to calculate the estimates $\hat{\psi}_{Ra}(t)$ and $\hat{\psi}_{Rb}(t)$. Consequently, these estimates are now incorrect. However, for $t > t_1 + \delta$, the measured speed is again $\omega(t)$, that is, the correct value. Thus, one can model the situation at time $t = t_1 + \delta$ as (8.35) being the *correct* equations with the initial conditions $\hat{\psi}_{Ra}(t_1 + \delta)$ and $\hat{\psi}_{Rb}(t_1 + \delta)$ being *unknown*. If the estimates from (8.35) converge to the true values irrespective of the initial conditions, the estimator (8.35) is able to recover from disturbances in the measurements.

To show the convergence, subtract (8.35) from (8.34) to obtain error system

$$\begin{aligned} \dot{\varepsilon}_{Ra} &= -\eta\varepsilon_{Ra} - n_p\omega\varepsilon_{Rb} \\ \dot{\varepsilon}_{Rb} &= -\eta\varepsilon_{Rb} + n_p\omega\varepsilon_{Ra} \end{aligned} \tag{8.36}$$

where $\varepsilon_{Ra} \triangleq \psi_{Ra} - \hat{\psi}_{Ra}$, $\varepsilon_{Rb} \triangleq \psi_{Rb} - \hat{\psi}_{Rb}$ are the errors in the estimates.

Consider a (Lyapunov) function defined by

$$\begin{aligned} V(t) &\triangleq \left(\psi_{Ra}(t) - \hat{\psi}_{Ra}(t)\right)^2 + \left(\psi_{Rb}(t) - \hat{\psi}_{Rb}(t)\right)^2 \\ &= \varepsilon_{Ra}^2(t) + \varepsilon_{Rb}^2(t). \end{aligned}$$

If it can be shown $V(t) \to 0$ as $t \to \infty$, then $\hat{\psi}_{Ra}(t) \to \psi_{Ra}(t)$, $\hat{\psi}_{Rb}(t) \to \psi_{Rb}(t)$ as $t \to \infty$. To do this, compute

$$\begin{aligned} dV/dt &= 2\varepsilon_{Ra}\dot{\varepsilon}_{Ra} + 2\varepsilon_{Rb}\dot{\varepsilon}_{Rb} \\ &= 2\varepsilon_{Ra}\left(-\eta\varepsilon_{Ra} - n_p\omega\varepsilon_{Rb}\right) + 2\varepsilon_{Rb}\left(-\eta\varepsilon_{Rb} + n_p\omega\varepsilon_{Ra}\right) \\ &= -2\eta\left(\varepsilon_{Ra}^2 + \varepsilon_{Rb}^2\right) \\ &= -2\eta V. \end{aligned}$$

That is, $dV/dt = -2\eta V$ with solution $V(t) = V(0)e^{-2\eta t}$. Now, $V(0) = \left(\psi_{Ra}(0) - \hat{\psi}_{Ra}(0)\right)^2 + \left(\psi_{Rb}(0) - \hat{\psi}_{Rb}(0)\right)^2$ is unknown, but $V(t) \to 0$ regardless of the value of $V(0)$ and thus $\hat{\psi}_{Ra}(t) \to \psi_{Ra}(t)$, $\hat{\psi}_{Rb}(t) \to \psi_{Rb}(t)$ as $t \to \infty$ independent of the initial conditions used for (8.35).

The nice thing about the development of this observer based on the model (8.34) is that one is able to show that the estimate converges to the actual flux. An equivalent representation of the system (8.34) is its polar coordinate form. That is, defining

$$\begin{aligned} \rho &\triangleq \tan^{-1}\left(\psi_{Rb}/\psi_{Ra}\right) \\ \psi_d &\triangleq \sqrt{\psi_{Ra}^2 + \psi_{Rb}^2} \end{aligned}$$

www.EngineeringEBooksPdf.com

one then defines a flux estimator by

$$\begin{aligned}\frac{d\hat{\rho}}{dt} &= n_p\omega + \eta M \hat{i}_q/\hat{\psi}_d \\ &= n_p\omega + \eta M\Big(-i_{Sa}\sin(\hat{\rho}) + i_{Sb}\cos(\hat{\rho})\Big)/\hat{\psi}_d \\ \frac{d\hat{\psi}_d}{dt} &= -\eta\hat{\psi}_d + \eta M \hat{i}_d \\ &= -\eta\hat{\psi}_d + \eta M\Big(i_{Sa}\cos(\hat{\rho}) + i_{Sb}\sin(\hat{\rho})\Big).\end{aligned} \tag{8.37}$$

As the estimator (8.37) is just the polar coordinate form of (8.35), it follows that its solution will converge to the true values for ρ and ψ_d. The usefulness of the representation (8.37) is that the variables ψ_d, i_d, and i_q vary much slower than variables $\psi_{Ra}(t)$ and $\psi_{Rb}(t)$. For example, if the motor is running at a constant speed, the variables ψ_d, i_d, and i_q are constant no matter how high the speed. In contrast, $\psi_{Ra}(t)$ and $\psi_{Rb}(t)$ vary at the stator frequency, which at high speeds is quite large. This high frequency makes the numerical integration of (8.35) difficult in that a small time step is required.

Remarks

To implement either observer (8.35) or (8.37), η and M must be known. The parameter $\eta = 1/T_R = R_R/L_R$ and the resistance R_R can vary by 100% due to ohmic heating of the rotor windings [2].

8.3.2 Speed Observer

In a position (servo) control system, typically one has a position measurement (e.g., from an optical encoder), but a speed measurement is not available. It is standard practice in industry to compute the speed by a discrete differentiation of the position output (backward difference) from the optical encoder as

$$\hat{\omega}_{bd}(kT) = \frac{\theta(kT) - \theta((k-1)T)}{T} \tag{8.38}$$

where T is the sample period. The difference $\theta(kT) - \theta((k-1)T)$ can be in error by no more than one count so that, using a 2000 pulse/rev encoder, the error in this estimate of the speed is tightly bounded by $(2\pi/2000)/T$. This noise is particularly significant at high sample rates and moderate to low speeds as less encoder counts are detected per sample period than at higher speeds. For example, in the experiment presented in Section 8.2.2 where the motor is turned 180° in 73 msec, the top speed of the motor was less than 75 rad/sec and a sample rate of 8 kHz was required. In this circumstance, the error bound on the speed computed by differentiation

www.EngineeringEBooksPdf.com

is $(2\pi/2000)8000 = 25.13$ rad/sec. This is shown in Figure 8.19. However, this noise (the difference $\omega - \hat{\omega}_{bd}$) has a high frequency, and for the most part the machine responds to the average value of $\hat{\omega}_{bd}$ over several time steps, which is close to the actual value.

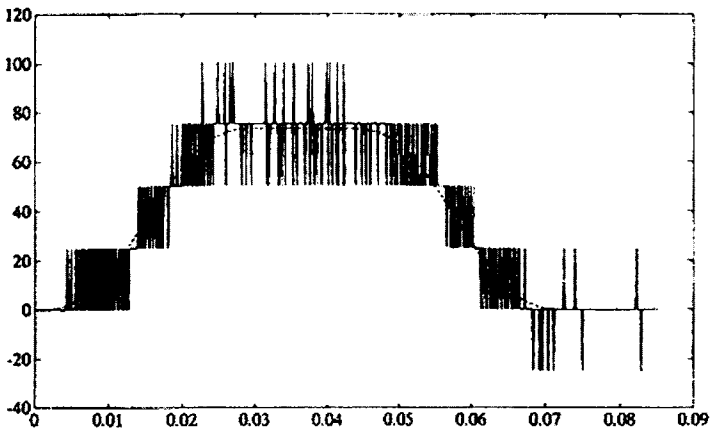


FIGURE 8.19. $\hat{\omega}_{bd}$ and ω_{ref} in radians/sec versus time in seconds. From Bodson et al. [67], © 2004 IEEE.

The speed estimate used to obtain Figure 8.8 (repeated in Figure 8.20) of Section 8.2.2 is much smoother and was computed using an observer.

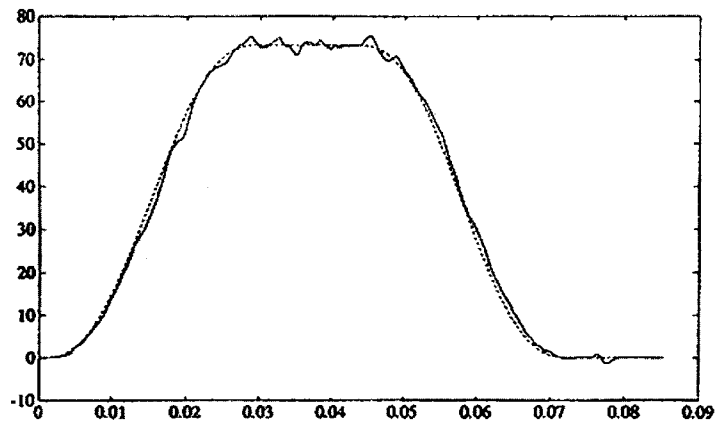


FIGURE 8.20. $\hat{\omega}$ and ω_{ref} in radians/sec versus time in seconds. From Bodson et al. [67], © 2004 IEEE.

www.EngineeringEBooksPdf.com

This approach is now described. In the field-oriented coordinates, the equation governing the speed in an induction motor is given by

$$\begin{aligned} \frac{d\theta}{dt} &= \omega \\ \frac{d\omega}{dt} &= \mu\psi_d i_q - (f/J)\omega \end{aligned} \tag{8.39}$$

The quantities ψ_d and i_q are not known, but can be estimated as shown above. Thus, consider an observer defined by

$$\begin{aligned} \frac{d\hat{\theta}}{dt} &= \hat{\omega} + \ell_1(\theta - \hat{\theta}) \\ \frac{d\hat{\omega}}{dt} &= \mu\hat{\psi}_d\hat{i}_q - (f/J)\hat{\omega} + \ell_2(\theta - \hat{\theta}). \end{aligned} \tag{8.40}$$

Assuming that $\hat{\psi}_d\hat{i}_q \to \psi_d i_q$ fast enough so that there are essentially equal, one subtracts (8.40) from (8.39) to obtain the error system

$$\begin{aligned} \frac{de_1}{dt} &= e_2 - \ell_1 e_1 \\ \frac{de_2}{dt} &= -(f/J)e_2 - \ell_2 e_1 \end{aligned} \tag{8.41}$$

where $e_1 = \theta - \hat{\theta}$ and $e_2 = \omega - \hat{\omega}$. The characteristic polynomial for the error system is then

$$\det\left(s\begin{bmatrix} 1 & 0 \\ 0 & 1 \end{bmatrix} - \begin{bmatrix} -\ell_1 & 1 \\ -\ell_2 & -f/J \end{bmatrix}\right) = s^2 + (\ell_1 + f/J)s + \ell_2 + \ell_1(f/J).$$

Choosing

$$\begin{aligned} \ell_1 &= r_1 + r_2 - f/J \\ \ell_2 &= r_1 r_2 - \ell_1(f/J) \end{aligned}$$

puts the roots of the characteristic polynomial at $-r_1$ and $-r_2$. It turns out in practice that this estimate of ω is much better than plain differentiation of the position [67]. This estimate is then used for the speed feedback and in the flux observer (8.37).

With the gains set as $\ell_1 = 1.8 \times 10^3$ and $\ell_2 = 8 \times 10^5$, the result of using the speed observer (8.40) is given in Figure 8.20. This same observer (with the same gain settings) was also used to obtain the speed estimate for the input output linearization controller in Figure 8.15. This approach to estimating ω can be modified to account for a load torque on the motor (see problem 25). A disadvantage of a speed observer is that the machine parameters must be known accurately [$\mu, f/J$ for (8.40) and $\eta = 1/T_R, M$ for the flux observer] while the backward difference estimator (8.38) is independent of the machine parameters.

www.EngineeringEBooksPdf.com

Remark The flux estimator (8.37) and speed estimator (8.40) are coupled; that is, to estimate the flux and speed, it is required to integrate the fourth-order system given by

$$\begin{aligned}
\frac{d\hat{\rho}}{dt} &= n_p\hat{\omega} + \eta M(-i_{Sa}\sin(\hat{\rho}) + i_{Sb}\cos(\hat{\rho}))/\hat{\psi}_d \\
\frac{d\hat{\psi}_d}{dt} &= -\eta\hat{\psi}_d + \eta M(i_{Sa}\cos(\hat{\rho}) + i_{Sb}\sin(\hat{\rho})) \\
\frac{d\hat{\theta}}{dt} &= \hat{\omega} + \ell_1(\theta - \hat{\theta}) \\
\frac{d\hat{\omega}}{dt} &= \mu\hat{\psi}_d(-i_{Sa}\sin(\hat{\rho}) + i_{Sb}\cos(\hat{\rho})) - (f/J)\hat{\omega} + \ell_2(\theta - \hat{\theta})
\end{aligned}$$

where i_{Sa}, i_{Sb} and θ are the measured "inputs" to this observer.

8.3.3 *Verghese–Sanders Flux Observer**

Using the observer (8.35), it was shown that the magnitude of the error $V(t) = (\psi_{Ra}(t) - \hat{\psi}_{Ra}(t))^2 + (\psi_{Rb}(t) - \hat{\psi}_{Rb}(t))^2$ went to zero exponentially as $V(t) = V(0)e^{-2\eta t}$. For example, with $L_R = 0.085$ Henries and $R_R = 0.8$ ohms, $\eta = 9.4$ so that $V(t) = V(0)e^{-2(9.4)t} = V(0)e^{-t/.05}$ and the error dies out after four time constants or $4 \times 0.05 = 0.2$ sec. It is usually preferable to force the error to go to zero *arbitrarily* fast rather than just as $e^{-2\eta t}$.

An ingenious approach has been given by Verghese and Sanders [73] that allows one to specify an *arbitrary* rate of convergence for the flux estimator. This was done by first observing that the four electrical equations in (8.4) may be broken up into two subsystems consisting of the flux *system model*

$$\begin{aligned}
\frac{d}{dt}\psi_{Ra} &= -\frac{R_R}{L_R}\psi_{Ra} - n_p\omega\psi_{Rb} + \frac{MR_R}{L_R}i_{Sa} \\
\frac{d}{dt}\psi_{Rb} &= -\frac{R_R}{L_R}\psi_{Rb} + n_p\omega\psi_{Ra} + \frac{MR_R}{L_R}i_{Sb}
\end{aligned} \tag{8.42}$$

and the voltage *measurement model*

$$\begin{aligned}
u_{Sa} &= R_S i_{Sa} + \sigma L_S\frac{di_{Sa}}{dt} + \frac{M}{L_R}\frac{d\psi_{Ra}}{dt} \\
u_{Sb} &= R_S i_{Sb} + \sigma L_S\frac{di_{Sb}}{dt} + \frac{M}{L_R}\frac{d\psi_{Rb}}{dt}.
\end{aligned} \tag{8.43}$$

The insight given by this decomposition is that a measurement of the voltages (assuming the currents and their derivatives are known) provides an estimate of the *derivative* of the flux linkages by equation (8.43), which

www.EngineeringEBooksPdf.com

in turn can then be used to force the flux error to zero arbitrarily fast. Specifically, consider the estimator based on (8.42) defined by

$$\begin{aligned}\frac{d}{dt}\hat{\psi}_{Ra} &= -\frac{R_R}{L_R}\hat{\psi}_{Ra} - n_p\omega\hat{\psi}_{Rb} + \frac{MR_R}{L_R}i_{Sa} + k(\hat{u}_{Sa} - u_{Sa}) \\ \frac{d}{dt}\hat{\psi}_{Rb} &= -\frac{R_R}{L_R}\hat{\psi}_{Rb} + n_p\omega\hat{\psi}_{Ra} + \frac{MR_R}{L_R}i_{Sb} + k(\hat{u}_{Sb} - u_{Sb})\end{aligned} \tag{8.44}$$

with the *predicted measurements* $\hat{u}_{Sa}$ and $\hat{u}_{Sb}$ given by

$$\begin{aligned}\hat{u}_{Sa} &= R_S i_{Sa} + \sigma L_S\frac{di_{Sa}}{dt} + \frac{M}{L_R}\frac{d\hat{\psi}_{Ra}}{dt} \\ \hat{u}_{Sb} &= R_S i_{Sb} + \sigma L_S\frac{di_{Sb}}{dt} + \frac{M}{L_R}\frac{d\hat{\psi}_{Rb}}{dt}.\end{aligned} \tag{8.45}$$

These expressions for $\hat{u}_{Sa}$ and $\hat{u}_{Sb}$ (8.45) are then substituted into (8.44) and, after some rearrangement, result in the flux estimator given by

$$\begin{aligned}\frac{d}{dt}\hat{\psi}_{Ra} &= \frac{1}{1-k\frac{M}{L_R}}\left(-\frac{R_R}{L_R}\hat{\psi}_{Ra} - n_p\omega\hat{\psi}_{Rb} + \frac{MR_R}{L_R}i_{Sa}\right. \\ &\quad \left. + k(R_S i_{Sa} + \sigma L_S\frac{di_{Sa}}{dt} - u_{Sa})\right) \\ \frac{d}{dt}\hat{\psi}_{Rb} &= \frac{1}{1-k\frac{M}{L_R}}\left(-\frac{R_R}{L_R}\hat{\psi}_{Rb} + n_p\omega\hat{\psi}_{Ra} + \frac{MR_R}{L_R}i_{Sb}\right. \\ &\quad \left. + k(R_S i_{Sb} + \sigma L_S\frac{di_{Sb}}{dt} - u_{Sb})\right).\end{aligned} \tag{8.46}$$

The idea here is that the system (8.46) is implemented in real time using the measured voltages u_{Sa} and u_{Sb} and currents i_{Sa} and i_{Sb}, the measured speed ω, and the motor parameter values. The solutions $\hat{\psi}_{Ra}$ and $\hat{\psi}_{Rb}$ are then used as the estimate of the state variables ψ_{Ra} and ψ_{Rb}.

To show that the estimator (8.46) works (i.e., $\hat{\psi}_{Ra} \to \psi_{Ra}, \hat{\psi}_{Rb} \to \psi_{Rb}$ if the gain k is chosen correctly), subtract (8.42) from (8.44) to obtain the error system

$$\begin{aligned}\frac{de_{Ra}}{dt} &= -\eta e_{Ra} - n_p\omega e_{Rb} + k(\hat{u}_{Sa} - u_{Sa}) \\ \frac{de_{Rb}}{dt} &= -\eta e_{Rb} + n_p\omega e_{Ra} + k(\hat{u}_{Sb} - u_{Sb}).\end{aligned} \tag{8.47}$$

www.EngineeringEBooksPdf.com

where $e_{Ra} \triangleq \hat{\psi}_{Ra} - \psi_{Ra}, e_{Rb} \triangleq \hat{\psi}_{Rb} - \psi_{Rb}$.

Using (8.43) and (8.45), this is rewritten as

$$\begin{aligned} \frac{de_{Ra}}{dt} &= -\eta e_{Ra} - n_p \omega e_{Rb} + \frac{kM}{L_R}\frac{de_{Ra}}{dt} \\ \frac{de_{Rb}}{dt} &= -\eta e_{Rb} + n_p \omega e_{Ra} + \frac{kM}{L_R}\frac{de_{Rb}}{dt} \end{aligned} \tag{8.48}$$

or

$$\begin{aligned} \frac{de_{Ra}}{dt} &= \frac{1}{1-k(M/L_R)}\left(-\eta e_{Ra} - n_p \omega e_{Rb}\right) \\ \frac{de_{Rb}}{dt} &= \frac{1}{1-k(M/L_R)}\left(-\eta e_{Rb} + n_p \omega e_{Ra}\right). \end{aligned} \tag{8.49}$$

Use of the (Lyapunov) function

$$V(e_{Ra}, e_{Rb}) \triangleq \left(e_{Ra}^2 + e_{Rb}^2\right)/2 \tag{8.50}$$

with the error system (8.49) results in

$$\begin{aligned} \frac{dV}{dt} &= e_{Ra}\frac{de_{Ra}}{dt} + e_{Rb}\frac{de_{Rb}}{dt} \\ &= \frac{1}{1-k(M/L_R)}\left(e_{Ra}(-\eta e_{Ra} - n_p \omega e_{Rb}) + e_{Rb}(-\eta e_{Rb} + n_p \omega e_{Ra})\right) \\ &= -\frac{\eta}{1-k(M/L_R)}\left(e_{Ra}^2 + e_{Rb}^2\right) \\ &= -\frac{2\eta}{1-k(M/L_R)}V. \end{aligned}$$

Clearly then,

$$V(t) = V(0)e^{-\left(\frac{2\eta}{1-kM/L_R}\right)t}$$

which can be made to go to zero arbitrarily fast by choosing the gain k close to (but less than) L_R/M. Note that by choosing $k > L_R/M$, the estimation error actually diverges. However, as $L_R = (1+\sigma_R)M$ where $\sigma_R > 0$ is a small leakage constant [1], it is always true that $L_R/M > 1$. Consequently, by choosing $k \leq 1$, one is assured of avoiding this problem.

The estimator (8.46) requires the derivative of the current to implement it. This can be avoided using the method as described in Ref. [73]. Specifically, (8.45) is substituted into (8.44) and rearranged by bringing all of the

www.EngineeringEBooksPdf.com

terms with derivatives to the left-hand side, resulting in

$$\begin{aligned}\left(1-k\frac{M}{L_R}\right)\frac{d\hat{\psi}_{Ra}}{dt}-k\sigma L_S\frac{di_{Sa}}{dt} &= -\frac{R_R}{L_R}\hat{\psi}_{Ra}-n_p\omega\hat{\psi}_{Rb}+\frac{MR_R}{L_R}i_{Sa}\\ &\quad +k\Big(R_Si_{Sa}-u_{Sa}\Big)\\ \left(1-k\frac{M}{L_R}\right)\frac{d\hat{\psi}_{Rb}}{dt}-k\sigma L_S\frac{di_{Sb}}{dt} &= -\frac{R_R}{L_R}\hat{\psi}_{Rb}+n_p\omega\hat{\psi}_{Ra}+\frac{MR_R}{L_R}i_{Sb}\\ &\quad +k\Big(R_Si_{Sb}-u_{Sb}\Big).\end{aligned} \tag{8.51}$$

Defining the auxiliary variables

$$\begin{aligned}\hat{z}_1 &= \left(1-k\frac{M}{L_R}\right)\hat{\psi}_{Ra}-k\sigma L_Si_{Sa}\\ \hat{z}_2 &= \left(1-k\frac{M}{L_R}\right)\hat{\psi}_{Rb}-k\sigma L_Si_{Sb}\end{aligned}$$

with inverse

$$\begin{aligned}\hat{\psi}_{Ra} &= \Big(\hat{z}_1+k\sigma L_Si_{Sa}\Big)\Big/\left(1-k\frac{M}{L_R}\right)\\ \hat{\psi}_{Rb} &= \Big(\hat{z}_2+k\sigma L_Si_{Sb}\Big)\Big/\left(1-k\frac{M}{L_R}\right)\end{aligned} \tag{8.52}$$

the system (8.51) has the form

$$\begin{aligned}\frac{d\hat{z}_1}{dt} &= f_1(\hat{z}_1,\hat{z}_2,\omega,i_{Sa},i_{Sb},u_{Sa})\\ \frac{d\hat{z}_2}{dt} &= f_2(\hat{z}_1,\hat{z}_2,\omega,i_{Sa},i_{Sb},u_{Sb})\end{aligned} \tag{8.53}$$

where f_1 and f_2 are simply the right-hand sides of (8.51) after substituting the expressions for $\hat{\psi}_{Ra}$ and $\hat{\psi}_{Rb}$ in terms of $\hat{z}_1$ and $\hat{z}_2$ from (8.52). The real-time solutions to (8.53) are then substituted into (8.52) to obtain the flux estimates.

Remarks As before, there are numerical issues to consider. In this case, the system (8.53) is driven by the stator currents which vary at the electrical frequency $\omega_S=\omega_{slip}+n_p\omega$ which can be quite large. This necessitates a small step size to accurately carry out the numerical integration of (8.53). An appropriate way to handle this issue is given in Ref. [73] (see problem 22).

www.EngineeringEBooksPdf.com

As in any model-based scheme, these estimates are sensitive to parameter error. In this case, the significant parameter is the rotor time constant $T_R = 1/\eta$ as its value can vary as the rotor windings heat up or cool down. An analysis of this sensitivity is also given in [73]. A generalization of this observer is the Martin–Rouchon observer Refs. [74][75] outlined in problem 27.

8.4 Optimal Field Weakening*

In Section 8.2.3, field weakening was introduced as means to achieve higher speeds without violating the stator voltage constraints with the trade off being that the available torque is less. In that approach, the reference for the (magnitude of the) flux linkage was specified by (8.24). In this section, the general problem of extracting the maximum torque from an induction motor without violating the voltage or current constraints is addressed systematically. There has been considerable work in this area including the approaches in Refs. [71][76][77][78][79][80]. Here the approach in Refs. [68][69] is presented. The field-oriented model of the motor as given in (8.9) is used as a starting point and, in order to obtain a tractable solution, the problem is formulated with the machine in steady state. Specifically, consider the following formulation:

Maximize the steady-state torque ($J\mu = n_p M/L_R$)

$$\frac{n_p M}{L_R}\psi_d i_q$$

subject to the constraints

$$\begin{aligned} u_d^2 + u_q^2 &\leq V_{\max}^2 \\ i_d^2 + i_q^2 &\leq I_{\max}^2. \end{aligned}$$

Remark The actual physical constraints are

$$\begin{aligned} |u_{Sa}| &\leq V_{\max}, \quad |u_{Sb}| \leq V_{\max} \\ |i_{Sa}| &\leq V_{\max}, \quad |i_{Sb}| \leq V_{\max}. \end{aligned}$$

However, at constant rotor speed in steady state, the voltages and currents have the form

$$\begin{aligned} u_{Sa} &= V\cos(\omega_S t + \phi) \\ u_{Sb} &= V\cos(\omega_S t + \phi) \\ i_{Sa} &= I\cos(\omega_S t + \varphi) \\ i_{Sb} &= I\cos(\omega_S t + \varphi) \end{aligned}$$

www.EngineeringEBooksPdf.com

where ω_S is the stator electrical frequency. As a consequence,

$$\begin{aligned} V^2 &= u_{Sa}^2 + u_{Sb}^2 = u_d^2 + u_q^2 \leq V_{\max}^2 \\ I^2 &= i_{Sa}^2 + i_{Sb}^2 = i_d^2 + i_q^2 \leq I_{\max}^2 \end{aligned}$$

so that in steady state the conditions are equivalent.

To proceed with the solution of the torque optimization problem, the system of equations (8.9) are written in steady state as

$$0 = \mu\psi_d i_q - (f/J)\omega - \tau_L/J \tag{8.54}$$

$$0 = -\psi_d + Mi_d \tag{8.55}$$

$$0 = -\left(\frac{M^2 R_R}{L_R^2} + R_S\right) i_d + \frac{\eta M}{L_R}\psi_d + \sigma L_S n_p \omega i_q + \sigma L_S M \frac{i_q^2}{T_R \psi_d} + u_d \tag{8.56}$$

$$0 = -\left(\frac{M^2 R_R}{L_R^2} + R_S\right) i_q - n_p \omega \psi_d \frac{M}{L_R} - \sigma L_S n_p \omega i_d - \sigma L_S M \frac{i_q i_d}{T_R \psi_d} + u_q \tag{8.57}$$

$$\frac{d\rho}{dt} = n_p\omega + Mi_q/(T_R\psi_d) = \text{ constant.} \tag{8.58}$$

Using $T_S \triangleq L_S/R_S$, $\psi_d = Mi_d$, and making the substitution $\sigma = 1 - M^2/(L_S L_R)$ into (8.57) results in (8.56) and (8.57) simplifying to

$$\frac{u_d}{R_S} = i_d - \sigma T_S i_q \left(n_p\omega + \frac{i_q}{T_R i_d}\right) \tag{8.59}$$

$$\frac{u_q}{R_S} = i_q + T_S i_d \left(n_p\omega + \frac{i_q}{T_R i_d}\right). \tag{8.60}$$

8.4.1 Torque Optimization Under Current Constraints

In the case of only the current constraint being active, the problem reduces to maximizing

$$\tau = \frac{n_p M}{L_R}\psi_d i_q = \frac{n_p M^2}{L_R} i_d i_q \tag{8.61}$$

subject to the constraint

$$i_d^2 + i_q^2 = I^2 \leq I_{\max}^2.$$

Defining

$$\delta = i_q/i_d$$

the expression for the torque may be rewritten as

$$\tau = \frac{n_p M^2}{L_R}\delta i_d^2 = \frac{n_p M^2}{L_R} I^2 \frac{\delta}{1+\delta^2}. \tag{8.62}$$

www.EngineeringEBooksPdf.com

Optimizing (max or min) the torque requires $I = I_{\max}$. Also, solving $\partial\tau/\partial\delta = 0$ gives $\delta = \pm 1$ and checking $\partial^2\tau/\partial\delta^2$ at $\delta = \pm 1$ results in the maximum torque for $I = I_{\max}$ and $\delta = 1$ ($i_d = I_{\max}/\sqrt{2}$) and the minimum torque for $I = I_{\max}$ and $\delta = -1$ ($i_d = -I_{\max}/\sqrt{2}$).

8.4.2 Torque Optimization Under Voltage Constraints

In the case of only the voltage constraint being active, the problem reduces to maximizing

$$\tau = \frac{n_p M}{L_R}\psi_d i_q = \frac{n_p M^2}{L_R} i_d i_q \tag{8.63}$$

subject to the constraint

$$u_d^2 + u_q^2 = V^2 \leq V_{\max}^2.$$

Again letting $\delta = i_q/i_d$ and using (8.59) and (8.60), the square of the voltage V^2 may be written as

$$\begin{aligned}\frac{V^2}{R_S^2} &= \frac{u_d^2 + u_q^2}{R_S^2} \\ &= \left(i_d - \sigma T_S i_q\left(n_p\omega + \frac{i_q}{T_R i_d}\right)\right)^2 + \left(i_q + T_S i_d\left(n_p\omega + \frac{i_q}{T_R i_d}\right)\right)^2 \\ &= i_d^2\left(\left(1 - \sigma T_S\delta(n_p\omega + \delta/T_R)\right)^2 + \left(\delta + T_S\left(n_p\omega + \delta/T_R\right)\right)^2\right)\end{aligned} \tag{8.64}$$

and the torque is then rewritten as

$$\begin{aligned}\tau &= \frac{n_p M^2}{L_R}\delta i_d^2 \\ &= \frac{n_p M^2}{L_R R_S^2} V^2 \frac{\delta}{\left(1 - \sigma T_S\delta\left(n_p\omega + \delta/T_R\right)\right)^2 + \left(\delta + T_S\left(n_p\omega + \delta/T_R\right)\right)^2}.\end{aligned} \tag{8.65}$$

Remark

This expression for the torque is comparable to the standard torque-slip equation for the torque. Specifically, with $\omega_S = n_p\omega + \delta/T_R$ the electrical frequency, $S_p = 1/(\sigma\omega_S T_R)$ the normalized pull-out slip, and $S = (\omega_S - n_p\omega)/\omega_S = (\delta/T_R)/\omega_S$ the normalized slip, this last expression for the torque reduces to (letting $R_S \to 0$)

$$\tau = n_p\frac{3}{2}\frac{1-\sigma}{\sigma}\frac{U_S^2}{\omega_S^2 L_S}\frac{2}{S/S_p + S_p/S} \tag{8.66}$$

where $U_S \triangleq \sqrt{2/3}\left(V/\sqrt{2}\right)$ (see problem 31). ($V/\sqrt{2}$ is the two-phase equivalent rms voltage so that $\sqrt{2/3}\left(V/\sqrt{2}\right)$ is the line-to-neutral rms voltage

www.EngineeringEBooksPdf.com

in the three-phase machine.) The expression (8.65) gives the torque as a function of the slip ($\delta/T_R = \omega_S - n_p\omega$) with the *rotor speed* ω held constant while the expression (8.66) gives the torque as function of the (normalized) slip with the *electrical frequency* ω_S held constant.

■

The denominator of (8.65) is always positive so that $\tau > 0$ for $\delta > 0$ and $\tau < 0$ for $\delta < 0$. As the torque (8.65) is proportional to V^2, the optimum torque is achieved choosing δ to optimize (8.65) with $V = V_{\max}$. To compute the maxima and minima of τ with respect to δ, one sets

$$\frac{\partial \tau}{\partial \delta} = \frac{n_p M^2}{L_R R_S^2} V^2 \frac{p(\delta)}{\left(\left(1 - \sigma T_S \delta \left(n_p\omega + \delta/T_R\right)\right)^2 + \left(\delta + T_S\left(n_p\omega + \delta/T_R\right)\right)^2 \right)^2} = 0 \tag{8.67}$$

where

$$\begin{aligned} p(\delta) = &-3\sigma^2 \left(\frac{T_S}{T_R}\right)^2 \delta^4 - 4\sigma^2 \left(\frac{T_S}{T_R}\right) \left(T_S n_p \omega\right) \delta^3 \\ &+ \left(2\sigma \left(\frac{T_S}{T_R}\right) - \sigma^2 (T_S n_p \omega)^2 - \left(1 + \left(\frac{T_S}{T_R}\right)\right)^2\right) \delta^2 \\ &+ 0 \cdot \delta + 1 + \left(T_S n_p \omega\right)^2 . \end{aligned} \tag{8.68}$$

The solutions to $p(\delta)$ give the values of δ corresponding to local maxima and minima. Let δ_0 be a solution to $p(\delta) = 0$. The second derivative at such a δ_0 is given by

$$\left.\frac{\partial^2 \tau}{\partial \delta^2}\right|_{\delta_0} = \frac{n_p M^2}{L_R R_S^2} V^2 \times \frac{p'(\delta_0)}{\left(\left(1 - \sigma T_S \delta \left(n_p\omega + \delta_0/T_R\right)\right)^2 + \left(\delta_0 + T_S\left(n_p\omega + \delta_0/T_R\right)\right)^2 \right)^2} \tag{8.69}$$

www.EngineeringEBooksPdf.com

where

$$\begin{aligned} p'(\delta) &= -12\sigma^2\left(\frac{T_S}{T_R}\right)^2\delta^3 - 12\sigma^2\left(\frac{T_S}{T_R}\right)(T_S n_p\omega)\,\delta^2 \\ &\quad + 2\left(2\sigma\left(\frac{T_S}{T_R}\right) - \sigma^2(T_S n_p\omega)^2 - \left(1+\left(\frac{T_S}{T_R}\right)\right)^2\right)\delta \\ &= -\delta\left(12\sigma^2\left(\frac{T_S}{T_R}\right)^2\delta^2 + 12\sigma^2\left(\frac{T_S}{T_R}\right)^2(T_R n_p\omega)\,\delta\right. \\ &\quad \left. + 2 + 4(1-\sigma)\left(\frac{T_S}{T_R}\right) + 2\left(\frac{T_S}{T_R}\right)^2 + 2\sigma^2\left(\frac{T_S}{T_R}\right)^2(T_R n_p\omega)^2\right). \end{aligned} \tag{8.70}$$

The sign of $p'(\delta_0)$ determines whether or not δ_0 corresponds to a local minima or a local maxima.

Example 1 To study equation (8.68), consider an induction machine with parameter values $n_p = 3, R_S = 1.7$ ohms, $L_S = 0.014$ H, $R_R = 3.9$ ohms, $L_R = 0.014$ H, $M = 0.0117$ H, $V_{\max} = 80$ V, $I_{\max} = 6$ A, $J = 1.1 \times 10^{-4}$ kg-m^2 and $f = 1.4 \times 10^{-4}$ N-m/rad/sec. Figure 8.21 is a plot of the four roots of $p(\delta) = 0$ as the speed ω varies from 0 to 8000 rpm. In this example motor, only two of the roots are real in this speed range.

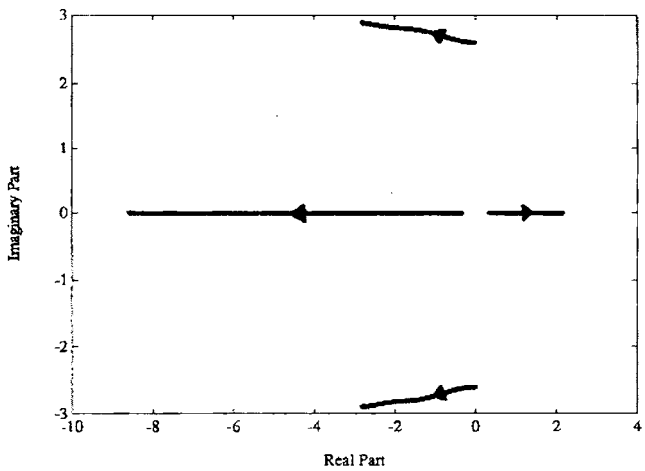


FIGURE 8.21. The four roots of $p(\delta) = 0$ for $0 \le \omega \le 8000$ rpm. From Bodson et al. [69], © 2004 IEEE.

www.EngineeringEBooksPdf.com

Solutions of $p(\delta) = 0$

The polynomial $p(\delta)$ is fourth order in δ and our interest here is to determine which of the roots optimizes the torque. For $\omega \geq 0$ and constant, there are two cases to consider: $\tau > 0$ and $\tau < 0$.

$\boldsymbol{\tau > 0}$: The first case is $\tau > 0$ so that the machine is motoring. In this case $\delta > 0$ as both i_d and i_q are positive. The Routh–Hurwitz test [37][81][46] (see problem 32) implies that $p(\delta) = 0$ has exactly one positive root for all $\omega \geq 0$. Furthermore, for any $\delta > 0$, it follows by equation (8.70) that $\partial^2\tau/\partial\delta^2 < 0$ so this unique positive root corresponds to a global maximum. In Figure 8.21, this unique positive root starts out at approximately 0.323 for $\omega = 0$ and ends at approximately 2.2 for $\omega = 800$ rpm. The asymptotic value of this root is found by dividing (8.68) by $\sigma^2(T_S/T_R)^2(T_S n_p\omega)^2$ and letting $\omega \to \infty$ where it is seen that $p(\delta)/\left(\sigma^2(T_S/T_R)^2(T_S n_p\omega)^2\right) \to (T_R/T_S)^2\left(-\delta^2 + 1/\sigma^2\right)$ and the positive root goes to $1/\sigma$ ($= 3.33$ in Figure 8.21). Further, as $\omega \to \infty$,

$$\tau(\delta) \to \tau(1/\sigma) = \left(n_p M^2/L_R R_S^2\right) V^2/\left(2\sigma(T_S n_p \omega_R)^2\right).$$

$\boldsymbol{\tau < 0}$: The second case is $\tau < 0$ so that the induction machine is generating. In this case, the minimum of τ is sought (i.e., maximizing $|\tau|$ with $\tau < 0$) so that δ is negative with $i_q > 0$ and $i_d < 0$. As $p(\delta)$ is fourth order, it has four roots of which exactly one root is in the right-half plane. The remaining three roots all have negative real parts of which there are two possibilities. Either there are three real negative roots (two local minima and a local maximum) or there is one real negative root (single global minimum) and a complex conjugate pair with negative real parts.

First consider the solutions of (8.68) for ω small. In general, equation (8.68) has a unique negative root for sufficiently small speeds. To see this, let $\omega = 0$ in (8.68) to obtain

$$p(\delta) = -3\sigma^2\left(\frac{T_S}{T_R}\right)^2\delta^4 + \left(2\sigma\left(\frac{T_S}{T_R}\right) - \left(1 + \left(\frac{T_S}{T_R}\right)\right)^2\right)\delta^2 + 1 = 0.$$

Then with

$$a \triangleq 3\sigma^2\left(\frac{T_S}{T_R}\right)^2,\ b \triangleq \left(\frac{T_S}{T_R}\right)^2 + 2(1-\sigma)\left(\frac{T_S}{T_R}\right) + 1,\ c \triangleq -1$$

the quadratic formula gives

$$\delta^2 = \frac{-b \pm \sqrt{b^2 - 4ac}}{2a} \tag{8.71}$$

where $-4ac > 0$ so that $\sqrt{b^2 - 4ac} > b$. Consequently, one must choose the

www.EngineeringEBooksPdf.com

+ sign in (8.71) for δ^2 to be positive. Doing so, let

$$\delta_{pos} \triangleq \sqrt{\frac{-b+\sqrt{b^2-4ac}}{2a}} \tag{8.72}$$

$$\delta_{neg} \triangleq -\sqrt{\frac{-b+\sqrt{b^2-4ac}}{2a}} \tag{8.73}$$

be the (unique) positive and negative roots, respectively, of (8.68) for $\omega = 0$. Note that $\delta_{pos} = 0.323$ in Figure 8.21.

At high enough speeds, there are always two local minima. To see this, rewrite (8.68) as

$$\begin{aligned} p(\delta) = &-3\sigma^2\left(\frac{T_S}{T_R}\right)^2\delta^4 - 4\sigma^2\left(\frac{T_S}{T_R}\right)^2(T_R n_p\omega)\,\delta^3 \\ &+\left(1+2(1-\sigma)\left(\frac{T_S}{T_R}\right)+\left(\frac{T_S}{T_R}\right)^2+\sigma^2\left(\frac{T_S}{T_R}\right)^2(T_R n_p\omega)^2\right)\delta^2 \\ &+0\cdot\delta+1+\left(\frac{T_S}{T_R}\right)^2(T_R n_p\omega)^2 . \end{aligned} \tag{8.74}$$

It is now shown that one of the roots $\delta \to -T_R n_p\omega$ as $\omega \to \infty$. To do so, let $x \triangleq \delta/(T_R n_p\omega)$ in (8.74) and divide through by $-3\sigma^2\left(\frac{T_S}{T_R}\right)^2(T_R n_p\omega)^4$ to obtain

$$x^4+\frac{4}{3}x^3+\frac{1}{3}x^2 = -\frac{1+2(1-\sigma)\left(\frac{T_S}{T_R}\right)+\left(\frac{T_S}{T_R}\right)^2-1-\left(\frac{T_S}{T_R}\right)^2(T_R n_p\omega)^2}{3\sigma^2\left(\frac{T_S}{T_R}\right)^2(T_R n_p\omega)^4}. \tag{8.75}$$

Equation (8.75) shows that $x = -1$ is a solution as $\omega \to \infty$; that is, $-T_R n_p\omega$ is an asymptotic solution to $p(\delta) = 0$ for large ω. Substitution of $\delta = -T_R n_p\omega$ into (8.69) shows that $\partial^2\tau/\partial\delta^2\big|_{\delta=-T_R n_p\omega} > 0$ and thus corresponds to a minimum. Also, $\tau(-T_R n_p\omega) \to \left(n_p M^2/L_R R_S^2\right)V^2/\left(T_R n_p\omega_R\right)$ as $\omega \to \infty$. The other negative root corresponding to a local minimum is found by dividing (8.68) through by $\sigma^2\left(T_S/T_R\right)^2(T_R n_p\omega)^2$ and letting $\omega \to \infty$ to find $\delta \to -1/\sigma$. Again using (8.69), it is seen that this root does indeed correspond to a local minimum where

$$\tau(-1/\sigma) \to -\frac{\left(n_p M^2/L_R R_S^2\right)V^2}{2\sigma\left(T_S n_p\omega_R\right)^2}$$

as $\omega \to \infty$. Comparing the expressions for the torque at the two minima, it is seen that for ω sufficiently large, $\tau(-T_R n_p\omega) < \tau(-1/\sigma)$. As a consequence, $-1/\sigma$ corresponds to an asymptotic local minimum while $-T_R n_p\omega$

www.EngineeringEBooksPdf.com

corresponds to the asymptotic global minimum for the torque. In general, at sufficiently high speeds, the complex conjugate pair of roots must come together so that there are three negative real roots corresponding to the two minima and one local maximum. (From specific examples, it appears that the δ corresponding to the global minimum is the negative root that starts δ_{neg} for $\omega = 0$ and remains real and negative throughout the speed range.)

For the specific motor example used in Figure 8.21, there is a unique negative root for the speed range $0 \leq \omega \leq 8000$ rpm, that is, throughout the speed rating of the motor. However, it was shown above that if the speed is large enough, the complex conjugate pair of roots eventually come together.

Example 2 Consider a motor with the parameter values $n_p = 3, R_S = 1.85$ ohms, $L_S = 0.244$ H, $R_R = 2.1$ ohms, $L_R = 0.244$ H, $M = 0.224$ H, $V_{\max} = 225$ V, and $I_{\max} = 15$ A. Using these parameter values, Figure 8.22 is a plot of $\tau(\delta)$ versus δ for the fixed motor speed $\omega = 200$ radians/sec. The torque is a maximum (motoring) at $\delta_{\max} = 5.7$, but for generating, there is a global minimum at $\delta_a = -69$, a local minimum at $\delta_b = -8.8$, and a local maximum at $\delta_c = -20.8$.

Remark For future reference, the values of δ_1^{vc} and δ_2^{vc} in Figure 8.22 are where $V = V_{\max}, I = I_{\max}$. In particular, for $\delta_1^{vc} < \delta < \delta_2^{vc}$, it turns out that $I > I_{\max}$; for δ outside of this interval, it happens that $I \leq I_{\max}$. This will be shown below.

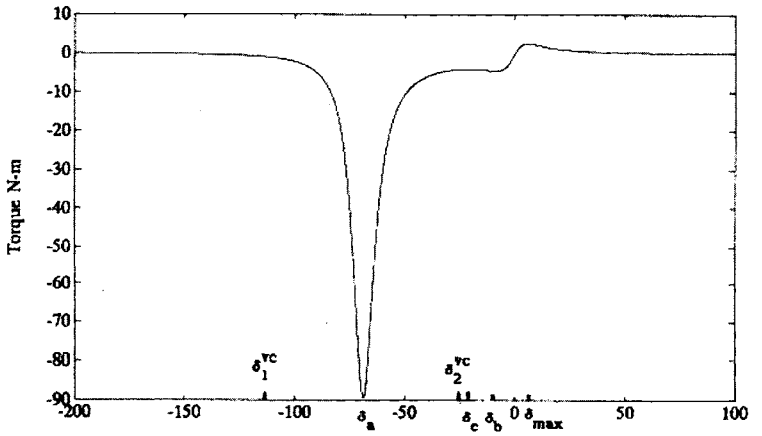


FIGURE 8.22. $\tau(\delta)$ in N-m versus δ for $\omega = 200$ rad/sec. At δ_1^{vc} and δ_2^{vc}, both constraints are encountered (i.e., $V = V_{\max}$ and $I = I_{\max}$). The torque $\tau(\delta)$ has a global minimum at δ_a, a relative minimum at δ_b, and a relative maximum at δ_c. From Bodson et al. [69], © 2004 IEEE.

www.EngineeringEBooksPdf.com

Numerical Solution of $p(\delta) = 0$

The complete set of solutions to (8.68) can be found with a Newton–Raphsor technique provided it is initialized properly. A closed-form approximate solution for δ can be found if the slip $\omega_{slip} = i_q/(T_R i_d) = \delta/T_R$ is small (in magnitude) compared to the stator frequency $\omega_S = n_p\omega + i_q/(T_R i_d)$; that is, $\omega_S \approx n_p\omega$ so that (8.59) and (8.60) become

$$\frac{u_d}{R_S} = i_d - \sigma T_S i_q n_p \omega \tag{8.76}$$

$$\frac{u_q}{R_S} = i_q + T_S i_d n_p \omega \tag{8.77}$$

$$\tau(\delta) = \frac{n_p M^2}{L_R R_S^2} V^2 \frac{}{(1 - \sigma T_S \delta n_p \omega)^2 + (\delta + T_S n_p \omega)^2}. \tag{8.78}$$

Setting $\partial\tau/\partial\delta = 0$ gives

$$\delta^2 = \frac{1 + (T_S \delta n_p \omega)^2}{1 + (\sigma T_S \delta n_p \omega)^2}$$

or

$$\delta = \pm\sqrt{\frac{1 + (T_S \delta n_p \omega)^2}{1 + (\sigma T_S \delta n_p \omega)^2}}. \tag{8.79}$$

At higher speeds for which $\sigma T_S \delta n_p \omega >> 1$, this reduces further to $\delta^2 = 1/\sigma^2$. As shown above, $\delta = 1/\sigma$ corresponds to the global maximum for the torque $\tau > 0$ while the solution $\delta = -1/\sigma$ corresponds to a local minimum for the torque $\tau < 0$. Also, as shown above, $\delta = -T_R n_p \omega$ is the asymptotic solution for the global minimum. [Note that the slip in this case is $\omega_{slip} = \delta/T_R = -n_p\omega$ which is not small in magnitude and, therefore, the equations (8.76)–(8.78) do not hold.]

To proceed with the numerical solution of (8.68), the global maximum is found by initializing the Newton–Raphson algorithm with the positive square root of (8.79). In the numerical examples given here, five iterations were sufficient to obtain a solution in the speed range $0 \le \omega \le 8000$ rpm. To obtain the global minimum, the Newton–Raphson algorithm is initialized with δ_{neg} [see equation (8.73)] for speeds below 1 rad/sec and by $-T_R n_p \omega$ for all higher speeds. In the numerical examples here, this initialization resulted in a solution after five iterations in the speed range $0 \le \omega \le 8000$ rpm.

Remark It is straightforward to show that the problem just considered of choosing $\delta = i_q/i_d$ to maximize the torque $\tau = (n_p M^2/L_R) i_d i_q$ subject to the voltage constraint $u_d^2 + u_q^2 = V^2 \le V_{\max}^2$ is equivalent to minimizing the voltage $u_d^2 + u_q^2 = V^2$ subject to the constant torque constraint $\tau = (n_p M^2/L_R) i_d i_q = \text{constant}$.

www.EngineeringEBooksPdf.com

8.4.3 *Torque Optimization Under Voltage and Current Constraints*

The previous two subsections considered the problem of obtaining the optimum torque from an induction machine without violating the current and voltage constraints, respectively. At low speeds the back emf of the machine is small and the inrush of current results encountering the current limits. At high speeds, the back emf is dominates and one encounters the voltage limits. Between these limiting cases, it is not surprising that one would encounter both voltage and current limits simultaneously. This is now considered.

To proceed, rewrite (8.65) for the torque as

$$\tau(\delta) = \frac{n_p M^2}{L_R} V^2 Q(\delta, \omega)$$

$$Q(\delta, \omega) \triangleq \frac{\delta / R_S^2}{\left(1 - \sigma T_S \delta \left(n_p \omega + \delta / T_R\right)\right)^2 + \left(\delta + T_S \left(n_p \omega + \delta / T_R\right)\right)^2}. \quad (8.80)$$

Recall by equation (8.62) that the torque can also be written as

$$\tau(\delta) = \frac{n_p M^2}{L_R} I^2 \frac{\delta}{1 + \delta^2}. \quad (8.81)$$

Equation (8.80) was convenient when operating at the voltage constraint while equation (8.81) was convenient when operating at the current constraint. Under both constraints, the optimization problem is formulated as follows: Given

$$\tau(\delta) = \frac{n_p M^2}{L_R} I^2 \frac{\delta}{1 + \delta^2} = \frac{n_p M^2}{L_R} V^2 Q(\delta, \omega), \quad (8.82)$$

for each fixed speed ω, find the value of δ that optimizes the torque (maximum for motoring or minimum for generating) with $V^2 \leq V_{\max}^2$ and $I^2 \leq I_{\max}^2$. As V^2 and I^2 appear linearly in (8.82), the optimal torque must occur with $V^2 = V_{\max}^2$, or $I^2 = I_{\max}^2$, or both. It has been shown in Section 8.4.2 that for a fixed voltage magnitude V the torque is optimized for some δ satisfying $\partial Q(\delta, \omega)/\partial \delta = 0$, while for a fixed current magnitude I the torque is optimized for $\delta = \pm 1$. For each fixed ω, let $\delta_{opt}(\omega)$ denote the value of δ that optimizes the torque under both voltage and current constraints. Then at each such fixed speed, one of the following three cases must hold:

Case I $I^2 = I_{\max}^2$ and $V^2 < V_{\max}^2 \implies \delta_{opt} = \pm 1$

Case II $V^2 = V_{\max}^2$ and $I^2 < I_{\max}^2 \implies \partial Q(\delta_{opt}, \omega)/\partial \delta = 0$

Case III $I^2 = I_{\max}^2$ and $V^2 = V_{\max}^2 \implies I_{\max}^2 \frac{\delta_{opt}}{1 + \delta_{opt}^2} = V_{\max}^2 Q(\delta_{opt}, \omega)$

www.EngineeringEBooksPdf.com

Generating Mode

The following algorithm is then used to obtain δ_{opt} and $\tau(\delta_{opt})$ for generator mode.

1. Let $\delta_1 = -1$ and compute τ_1, V_1 according to

$$\tau_1 \triangleq \frac{n_p M^2}{L_R} I_{\max}^2 \frac{\delta_1}{1+\delta_1^2}$$
$$V_1 \triangleq \frac{\tau_1}{\frac{n_p M^2}{L_R} Q(\delta_1, \omega)}.$$

   If $V_1 > V_{\max}$, then τ_1 is not the minimum torque and proceed to step 2. Otherwise, store the pair (δ_1, τ_1) as a possible optimum pair $(\delta_{opt}, \tau_{opt})$ and then proceed to step 2.

2. Solve $\partial Q(\delta, \omega)/\partial\delta = 0$ for its roots as explained in Section 8.4.2. There are then two possible subcases (a) and (b):

   (a) One real negative root δ_a (the other two complex conjugate roots). In this case, compute

$$\tau_2 \triangleq \frac{n_p M^2}{L_R} V_{\max}^2 Q(\delta_a, \omega)$$
$$I_a^2 \triangleq \frac{\tau_2}{(n_p M^2/L_R)} \frac{1+\delta_a^2}{\delta_a}.$$

   If $I_a > I_{\max}$, then go to step 3 as this solution violates the current constraint. Otherwise, store the pair (δ_a, τ_2) as a possible candidate for $(\delta_{opt}, \tau_{opt})$ and proceed to step 3.

   (b) Three real negative roots denoted as δ_a, δ_b, and δ_c. In this case, let δ_a correspond to the global minimum, δ_b correspond to the local minimum, and δ_c correspond to the local maximum (see Figure 8.22). Next compute

$$\tau_a \triangleq \frac{n_p M^2}{L_R} V_{\max}^2 Q(\delta_a, \omega), I_a^2 \triangleq \frac{\tau_a}{(n_p M^2/L_R)} \frac{1+\delta_a^2}{\delta_a}$$
$$\tau_b \triangleq \frac{n_p M^2}{L_R} V_{\max}^2 Q(\delta_b, \omega), I_b^2 \triangleq \frac{\tau_b}{(n_p M^2/L_R)} \frac{1+\delta_b^2}{\delta_b}$$

   If $I_a < I_{\max}$, then store (δ_a, τ_a) as a possible candidate for $(\delta_{opt}, \tau_{opt})$ and proceed to step 3. Otherwise, check if $I_b < I_{\max}$ is satisfied. If so, then store (δ_b, τ_b) as a possible candidate for $(\delta_{opt}, \tau_{opt})$ and proceed to step 3. If not, just proceed to step 3.

www.EngineeringEBooksPdf.com

3. Solve
$$\frac{n_p M^2}{L_R} I_{\max}^2 \frac{\delta}{1+\delta^2} = \frac{n_p M^2}{L_R} V_{\max}^2 Q(\delta, \omega)$$
and let δ_3 denote the value corresponding to the minimum torque and denote the minimum torque as τ_3. Store (δ_3, τ_3) as a possible candidate for $(\delta_{opt}, \tau_{opt})$.

4. Choose τ_{opt} as the minimum value of the torque from steps 1, 2, and 3 and δ_{opt} as the corresponding value of δ.

Motoring Mode

The algorithm is similar, but simpler, in the motoring mode.

1. Let $\delta_1 = 1$ and compute τ_1, V_1 according to
$$\begin{aligned} \tau_1 &\triangleq \frac{n_p M^2}{L_R} I_{\max}^2 \frac{\delta_1}{1+\delta_1^2} \\ V_1 &\triangleq \frac{\tau_1}{\frac{n_p M^2}{L_R} Q(\delta_1, \omega)}. \end{aligned}$$
If $V_1 > V_{\max}$, then τ_1 is not the maximum torque and proceed to step 2. Otherwise, store the pair (δ_1, τ_1) as a possible optimum pair $(\delta_{opt}, \tau_{opt})$ and also proceed to step 2.

2. Solve $\partial Q(\delta, \omega)/\partial \delta = 0$ for its roots as explained in Section 8.4.2. Let the unique positive root be denoted as δ_a and compute
$$\begin{aligned} \tau_2 &\triangleq \frac{n_p M^2}{L_R} V_{\max}^2 Q(\delta_a, \omega) \\ I_a^2 &\triangleq \frac{\tau_2}{(n_p M^2/L_R)} \frac{1+\delta_a^2}{\delta_a}. \end{aligned}$$
If $I_a > I_{\max}$, then go to step 3 as this solution violates the constraint. Otherwise, store the pair (δ_a, τ_2) as a possible candidate for $(\delta_{opt}, \tau_{opt})$ and then proceed to step 3.

3. Solve
$$\frac{n_p M^2}{L_R} I_{\max}^2 \frac{\delta}{1+\delta^2} = \frac{n_p M^2}{L_R} V_{\max}^2 Q(\delta, \omega)$$
and let δ_3 denote the value corresponding to the maximum torque and denote the maximum torque as τ_3. Store (δ_3, τ_3) as a possible candidate for $(\delta_{opt}, \tau_{opt})$.

4. Choose τ_{opt} as the maximum value of the torque from steps 1, 2, and 3 and δ_{opt} as the corresponding value of δ.

www.EngineeringEBooksPdf.com

Remark If the induction machine is operating in the generating mode, step 2 above can lead to interesting solutions when the machine is at both the current and voltage limits. For example, in step 2 of the generating mode, for either subcase (a) or (b), the global minimum at δ_a will typically result in $I^2 > I_{\max}^2$. However, in subcase (b), the local minimum at δ_b (found under the voltage constraint only) can turn out to be the global minimum when the current constraint is also taken into account. This is in fact the situation depicted in Figure 8.22. Specifically, at $\omega = 200$ rads/sec, step 1 violates the voltage constraint while for step 2 the *global* minimum at $\delta_a = -69$ violates the current constraint (it can be shown that for $\delta_1^{vc} < \delta < \delta_2^{vc}$, $I > I_{\max}$). The local minimum at $\delta_b = -8.8$ producing the torque $\tau(\delta_b) = -4.4$ N-m does not violate the current constraint, that is,

$$I_b^2(\delta_b) \triangleq \left(\tau(\delta_b)/\left(n_p M^2/L_R\right)\right)\left(1+\delta_b^2\right)/\delta_b < I_{\max}^2.$$

Going on to step 3 of the algorithm, one solves $I_{\max}^2\delta/\left(1+\delta^2\right) = V_{\max}^2 Q(\delta,\omega)$ for its real roots to obtain $\delta_1^{vc} = -22.9, \tau\left(\delta_1^{vc}\right) = -4.06$ N-m and $\delta_2^{vc} = -116.4, \tau(\delta_2^{vc}) = -0.8$ N-m which are indicated in Figure 8.22 (the other two roots are complex conjugates). Consequently, $\delta_{opt} = \delta_b = -8.8$ produces the global minimum torque of $\tau_{opt} = -4.4$ N-m.

Numerical Solution of $I_{\max}^2\delta/\left(1+\delta^2\right) = V_{\max}^2 Q(\delta,\omega)$

Step 3 of the algorithm requires solving $I_{\max}^2\delta/\left(1+\delta^2\right) = V_{\max}^2 Q(\delta,\omega)$ for δ with ω fixed. This is rewritten as a polynomial in δ by

$$\begin{aligned}\frac{V_{\max}^2}{R_S^2 I_{\max}^2}\left(1+\delta^2\right) &= \sigma^2\left(\frac{T_S}{T_R}\right)^2\delta^4 + 2\sigma^2\left(\frac{T_S}{T_R}\right)^2 T_R n_p\omega\delta^3 \\ &+ \left(1+2(1-\sigma)\left(\frac{T_S}{T_R}\right)+\left(\frac{T_S}{T_R}\right)^2+\sigma^2\left(\frac{T_S}{T_R}\right)^2(T_R n_p\omega)^2\right)\delta^2 \\ &+ \left(2(1-\sigma)\left(\frac{T_S}{T_R}\right)+2\left(\frac{T_S}{T_R}\right)^2\right)T_R n_p\omega\delta + 1 + \left(\frac{T_S}{T_R}\right)^2(T_R n_p\omega)^2. \quad (8.83)\end{aligned}$$

This equation does not lend itself to as complete an analysis as (8.68) because the coefficient of δ in (8.83) is not zero as was the case for (8.68). The four roots of (8.83) are plotted in Figure 8.23. Upon computing the values of the torque corresponding to these values of δ, it turns out the positive real root between 1 and 1.5 in Figure 8.23 is the root corresponding to the (global) maximum torque for speeds between 2940 rpm and 3330 rpm. Similarly, the negative real root which is approximately between -1 and -2 in Figure 8.23 corresponds to the (global) minimum torque (i.e., $\max|\tau|, \tau < 0$) for speeds greater than 5410 rpm. These two sets of roots are easily found using the Newton–Raphson method and initializing it with $\delta = 1$ and $\delta = -1$ for the maximum and the minimum torques, respectively.

www.EngineeringEBooksPdf.com

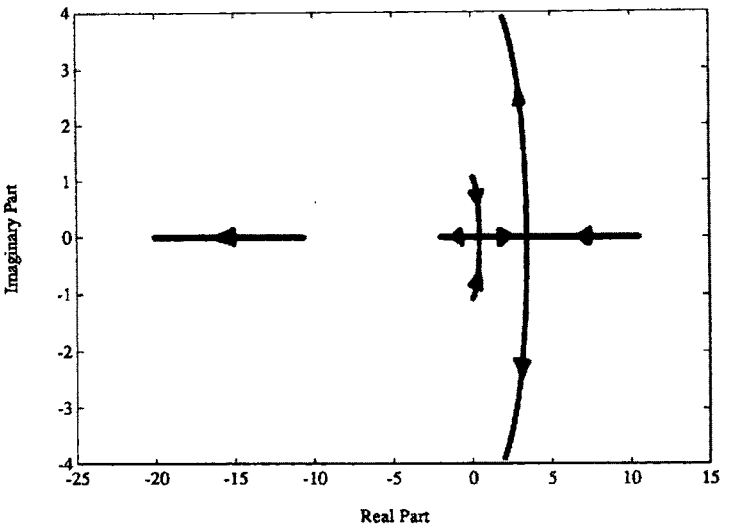


FIGURE 8.23. The four roots of $I_{\max}^2\delta/\left(1+\delta^2\right) = V_{\max}^2 Q(\delta,\omega)$ for $0 \leq \omega \leq 8000$ rpm. From Bodson et al. [69], © 2004 IEEE.

Base Speed

For low enough speeds, the machine is operating at the current limit to achieve optimum torque. The *base speed* ω_{base} can be defined as the speed where the flux linkage magnitude ψ_d is first decreased to avoid the voltage limit. Using the above analysis, a natural procedure to determine this base speed is possible as follows. Below the base speed, where $\delta = \delta_1$ with $\delta_1 = 1$ for motoring and $\delta_1 = -1$ for generating, the torque is given by

$$\tau\left(\delta_1\right) = \frac{n_p M^2}{L_R} I_{\max}^2 \frac{\delta_1}{1+\delta_1^2} = \frac{n_p M^2}{L_R} \frac{I_{\max}^2}{2} \delta_1.$$

The voltage required to achieve this torque is then

$$\begin{aligned} V^2 &= \frac{\tau\left(\delta_1\right)}{\frac{n_p M^2}{L_R} Q\left(\delta_1,\omega\right)} \\ &= \frac{n_p M^2}{L_R} \frac{I_{\max}^2}{2} \delta_1 \frac{\left(1-\sigma T_S \delta_1 (n_p\omega + \delta_1/T_R)\right)^2 + \left(\delta_1 + T_S\left(n_p\omega + \delta_1/T_R\right)\right)^2}{\frac{n_p M^2}{L_R} \frac{\delta_1}{R_S^2}} \\ &= \frac{R_S^2 I_{\max}^2}{2} \left(\left(1-\sigma T_S \delta_1 \left(n_p\omega + \delta_1/T_R\right)\right)^2 + \left(\delta_1 + T_S\left(n_p\omega + \delta_1/T_R\right)\right)^2\right). \end{aligned} \tag{8.84}$$

www.EngineeringEBooksPdf.com

To satisfy the voltage constraint, the condition $V^2 \leq V_{\max}^2$ must hold. To compute the maximum speed for which this holds, set $V^2 = V_{\max}^2$ in (8.84) and rearrange to obtain

$$\begin{aligned} 2\frac{V_{\max}^2}{R_S^2 I_{\max}^2} &= \delta_1^2 + 2(1-\sigma)\frac{T_S}{T_R}\delta_1^2 + \frac{T_S^2}{T_R^2}\delta_1^2\left(1+\sigma^2\delta_1^2\right) + \omega^2 T_S^2 n_p^2\left(1+\sigma^2\delta_1^2\right) \\ &\quad + \omega 2 T_S \delta_1 n_p\left(1-\sigma+\frac{T_S}{T_R}\left(1+\sigma^2\delta_1^2\right)\right) + 1. \end{aligned}$$

Using the fact that $\delta_1^2 = 1$, this simplifies to

$$\begin{aligned} 0 = {} & \omega^2 T_S^2 n_p^2\left(1+\sigma^2\right) + \omega 2 T_S \delta_1 n_p\left(1-\sigma+\frac{T_S}{T_R}\left(1+\sigma^2\right)\right) \\ & + 1 + 2(1-\sigma)\frac{T_S}{T_R} + \frac{T_S^2}{T_R^2}\left(1+\sigma^2\right) + 1 - 2\frac{V_{\max}^2}{R_S^2 I_{\max}^2}. \end{aligned} \tag{8.85}$$

In a practical motor, $V_{\max}^2 >> R_S^2 I_{\max}^2$ so that

$$1+2(1-\sigma)\frac{T_S}{T_R}+\frac{T_S^2}{T_R^2}\left(1+\sigma^2\right)+1-2\frac{V_{\max}^2}{R_S^2 I_{\max}^2} \approx 1+\left(1+\frac{T_S}{T_R}\right)^2-2\frac{V_{\max}^2}{R_S^2 I_{\max}^2} < 0. \tag{8.86}$$

That is, the constant term of (8.85) is negative. The coefficient of ω is positive for $\delta_1 = 1$ and negative for $\delta_1 = -1$. Using these facts, it follows using the Routh–Hurwitz stability test (see problem 33) that (8.86) has exactly one positive root each for $\delta_1 = 1$ and for $\delta_1 = -1$. For the motor parameter values used in Figure 8.21, the positive solution of (8.86) for $\delta_1 = 1$ is $\omega_{base} = 2990$ rpm (motoring) and the positive solution of (8.86) for $\delta_1 = -1$ is $\omega_{base} = 5410$ rpm (generating). These speeds can be seen in Figure 8.24.

Numerical Results

Here the motor used in example 1 (page 532 above) is analyzed in terms of the optimum torque it can produce. Its parameter values are $n_p = 3, R_S = 1.7$ ohms, $L_S = 0.014$ H, $R_R = 3.9$ ohms, $L_R = 0.014$ H, $M = 0.0117$ H, $V_{\max} = 80$ V, $I_{\max} = 6$ A, $J = 1.1 \times 10^{-4}$ kg-m^2 and $f = 1.4 \times 10^{-4}$ N-m/rad/sec. Using the above algorithm, the maximum and minimum torques were computed and are shown in Figure 8.24 versus ω with the corresponding δ versus ω shown in Figure 8.25.

www.EngineeringEBooksPdf.com

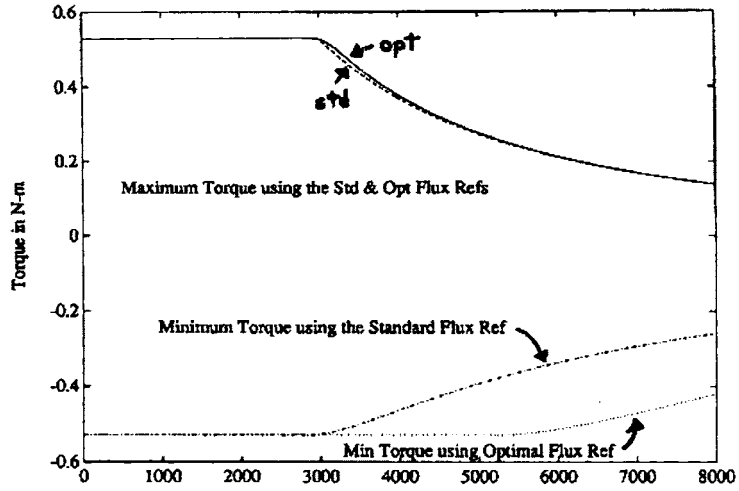


FIGURE 8.24. Maximum and minimum torque achievable versus ω (in rpm) for both optimal and standard field weakening. For the optimal field weakening, ω_{base} = 2990 rpm for motoring and ω_{base} = 5410 rpm for generating. From Bodson et al. [69], © 2004 IEEE.

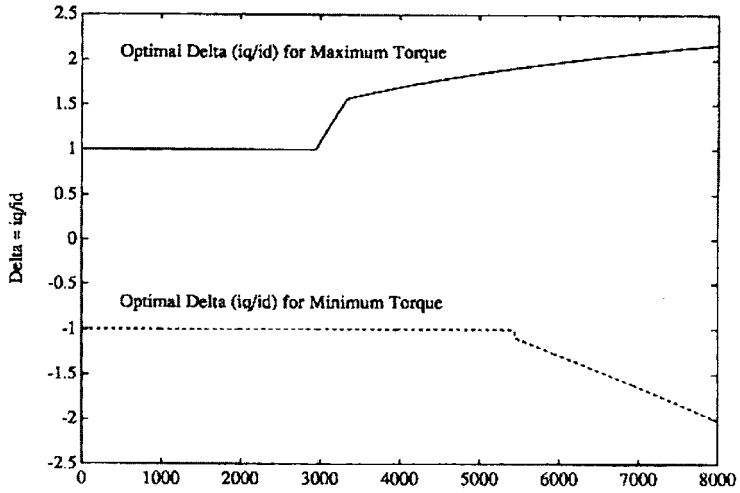


FIGURE 8.25. δ versus ω in rpm corresponding to the maximum and minimum torque. From Bodson et al. [69], © 2004 IEEE.

www.EngineeringEBooksPdf.com

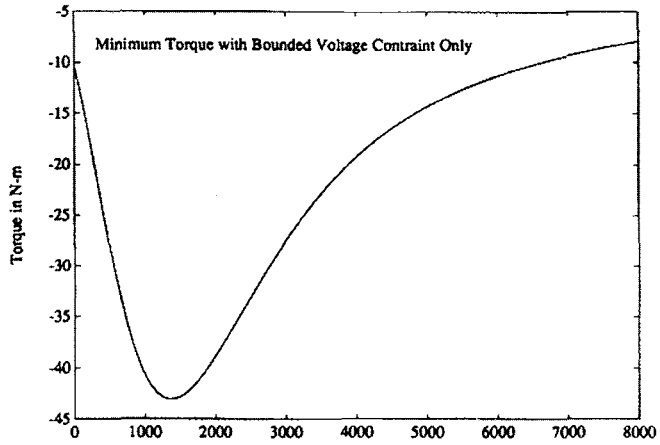


FIGURE 8.26. Minimum torque versus ω in rpm under just the voltage contraint. From Bodson et al. [69], © 2004 IEEE.

The maximum torque is limited by the current constraint up to a speed of 2990 rpm and by the voltage constraint for speeds above 3330 rpm. There is a small speed range from 2990 rpm to 3330 rpm where both the voltage and current constraints are encountered. This last observation is more clearly illustrated in Figure 8.25. For the minimum torque, Figure 8.24 shows it is determined by the current constraint up to 5410 rpm and then by both the voltage and current constraints for all higher speeds. In other words, the minimum torque under just the voltage constraint alone is never achieved because it requires too much current. This is demonstrated vividly by Figure 8.26, which is a plot of the minimum torque achievable with only the voltage constraint and no current constraint. Comparing with Figure 8.24, it is clear that the current limits prevent these large negative torques from ever being achieved.

Comparison with Standard Field Weakening

Recall that the standard approach to field weakening is to choose the flux as

$$\psi_{dref}(\omega) = \begin{cases} \psi_{d0} & \text{for} \quad |\omega| < \omega_{base} \\ \psi_{d0}\omega_{base}/|\omega| & \text{for} \quad |\omega| \geq \omega_{base} \end{cases} \tag{8.87}$$

where $\psi_{d0} = Mi_{d0}$. For the machine of example 1 (page 532 above), the direct current reference is chosen as $i_{d0} = 6/\sqrt{2}$ A to make the torque using the flux reference (8.87) equal to that of the optimal torque (i.e., choosing $\delta = 1$ so that $i_d = i_q = I_{\max}/\sqrt{2}$) below the base speed. The base speed is chosen as $\omega_{base} = 2990$ rpm (≈ 300 rads/sec) so as to coincide with the

www.EngineeringEBooksPdf.com

speed at which the maximum possible torque achievable starts to decrease (see Figure 8.24).

To provide a fair comparison of the two approaches to field weakening, it is necessary to determine the maximum torque that can be delivered under the standard field weakening approach without violating the constraints. The motor torque is $J\mu\psi_d i_q$ and, as the flux is determined by (8.87) at any constant speed, the optimum torque in this situation is determined by optimizing i_q subject to the voltage and current constraints. To proceed, in (8.64) set $V = V_{\max}, i_d(\omega) = \psi_{dref}(\omega)/M$ with $\psi_{dref}(\omega)$ given by (8.87) and compute its roots. With $\delta_{\max}$ the maximum real root of (8.64), the maximum i_q subject to the voltage constraint is simply $\delta_{\max} i_d$. Similarly, with $\delta_{\min}$ the minimum real root of (8.64), the minimum i_q subject to the voltage constraint is $\delta_{\min} i_d$. To account for the current constraint, one just takes the values of i_q as just explained and tests if $|i_q| \leq I_{q\max} \triangleq \sqrt{I_{\max}^2 - i_d(\omega)}$. If $|i_q| \leq I_{q\max}$ then i_q is left unchanged and it is at its optimum value. Otherwise, i_q is set to $\pm I_{q\max}$ where the $+$ is taken if $i_q > 0$ and the $-$ sign is taken if $i_q < 0$. Figure 8.24 shows the maximum and minimum torques computed using the standard flux reference. It is interesting to note that this maximum torque is essentially the same as that produced by the optimum torque *provided* that i_{d0} and ω_{base} are chosen as in the optimum torque case.

The Optimal Flux Reference

The algorithm above for computing $\delta = i_q/i_d$ to achieve the optimum torque under both voltage and current constraints was derived assuming constant speed. However, achieving the optimum torque is of particular interest in high-performance applications where the speed varies greatly. Here it is shown that the algorithm is indeed applicable to such applications due to the fact that the electrical dynamics of a machine are typically much faster than the mechanical dynamics. Figure 8.24 shows that the torque optimization will have a significant advantage during deceleration. In fact, the flux and current references used for the input output controller of Section 8.2.4 were developed using the algorithm of this section. The speed trajectory of Figure 8.15 shows the motor goes from 0 rpm to 8000 rpm in 0.38 seconds and from 8000 rpm to 0 rpm in only 0.265 seconds. The corresponding position reference trajectory is given in Figure 8.13. For the speed reference trajectory of Figure 8.15 the corresponding optimum achievable torque τ_{opt} is shown as the solid curve in Figure 8.18 while the dashed curve is the torque reference τ_{ref}. Note that the torque reference is close to the optimum reference throughout most of the speed range. The quadrature current reference is chosen as

$$i_{qref} \triangleq \frac{\tau_{ref}}{J\mu\psi_{dref}}$$

www.EngineeringEBooksPdf.com

where, as stated above, τ_{ref} is the dashed curve in Figure 8.18. The direct current reference is then specified as

$$i_{ref}(\omega) = \frac{i_{qref}}{\delta(\omega_{ref})} = \frac{\tau_{ref}}{J\mu\delta(\omega_{ref})\psi_{dref}}$$

where $\delta(\omega_{ref})$ is the optimal i_q/i_d to optimize the torque and is shown in Figure 8.27.

This derivation has been done under the assumption of constant speed so that choosing $\psi_{dref} = Mi_{ref}$ would be consistent with this assumption. However, while the currents can be changed relatively fast, the flux may take time to build up. As a consequence, the flux reference is chosen as the solution to

$$\begin{aligned}\frac{d\psi_{dref}}{dt} &= -\frac{1}{T_R}\psi_{dref} + \frac{M}{T_R}i_{dref} \\ &= -\frac{1}{T_R}\psi_{dref} + \frac{M}{J\mu T_R}\frac{\tau_{ref}}{\delta(\omega_{ref})\psi_{dref}}.\end{aligned}$$

Figure 8.28 is a plot of the commanded voltage to the amplifier where it is noted that the it stays quite close to the 80-V limit as the motor goes from 0 rpm to 8000 rpm.

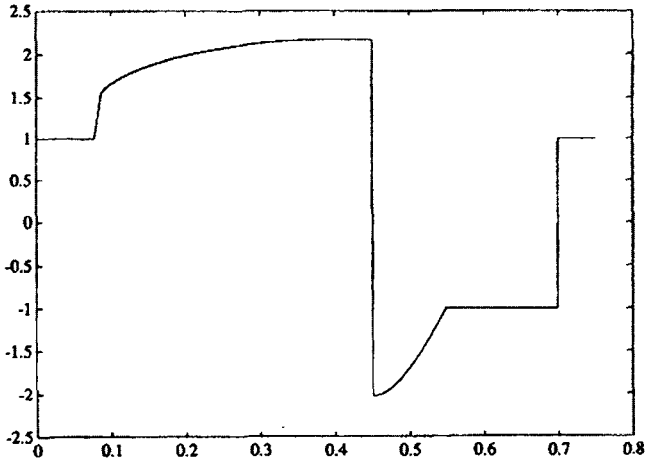


FIGURE 8.27. Optimal $\delta(\omega_{ref}(t)) = i_q/i_d$ versus time for the speed trajectory of Figure 8.15. From Bodson et al. [69], © 2004 IEEE.

www.EngineeringEBooksPdf.com

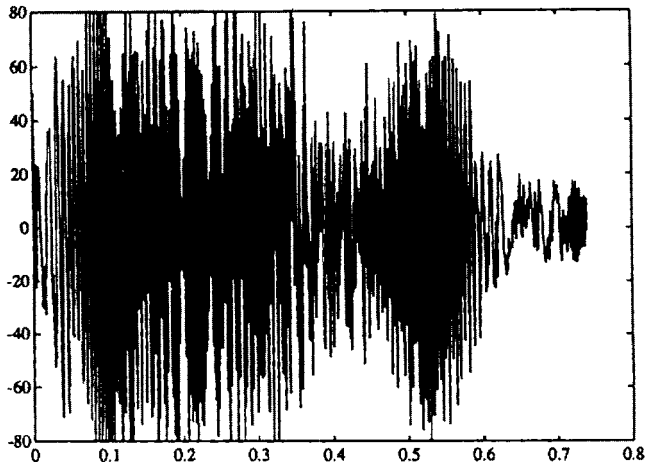


FIGURE 8.28. u_{Sa} versus time. From Bodson et al. [69], © 2004 IEEE.

Figure 8.29 shows the phase current i_{Sa} versus time.

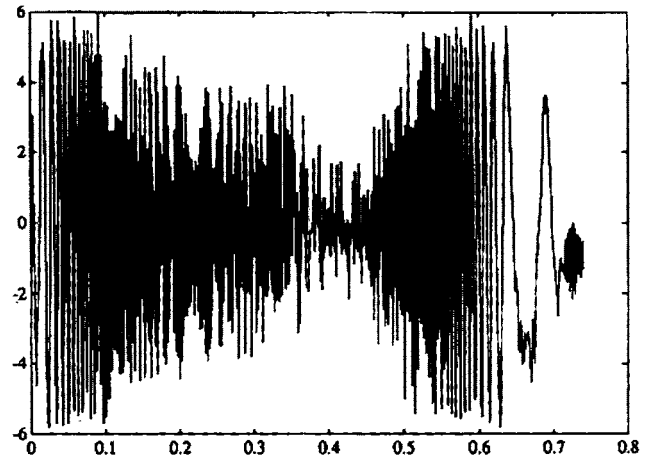


FIGURE 8.29. i_{Sa} versus time. From Bodson et al. [69], © 2004 IEEE.

The flux reference ψ_{dref} and the (estimated) flux ψ_d are shown in Figure 8.17. The position reference and measured position are shown in Figure 8.13 with the position error given in Figure 8.14 in encoder counts. This shows that the position error for the last 100 samples is less than one encoder

www.EngineeringEBooksPdf.com

count verifying that the motor comes into the final position to a complete stop.

The generalization of this approach to the situation in which the main magnetic path of the machine undergoes significant saturation has been considered in [82][83][84].

8.5 Identification of the Induction Motor Parameters*

The induction motor parameters are the mutual inductance M, the stator inductance L_S, the rotor inductance L_R, the stator resistance R_S, the rotor resistance R_R, the inertia of the rotor J and the load torque τ_L. Standard methods for the estimation of induction motor parameters include the locked rotor test, the no-load test, and the standstill frequency response test (see problem 19 of Chapter 7). In Ref. [85], an automatic procedure is described in which a sequence of such tests is performed, each designed to isolate and measure a specific parameter. The method is applied for the automatic tuning (self-commissioning) of an induction motor drive. In Ref. [86], another procedure is described, based primarily on the identification of the motor transfer function at standstill. The model is then refined to account for magnetic saturation and adaptation is included to compensate for the effects of heating. However, these approaches cannot be used online, that is, during normal operation of the machine. This is a disadvantage as some of the parameters do vary during operation. For example, field-oriented control requires knowledge of the rotor time constant $T_R = L_R/R_R$ in order to estimate the rotor flux linkages and R_R varies significantly due to ohmic heating. Based on the work in Refs. [42][59][87], a method for identifying the parameters of the induction motor that can be implemented *online* is now described. To proceed, recall the state-space model (8.5) of the induction motor given by

$$\begin{aligned}
\frac{d\omega}{dt} &= \frac{n_p M}{J L_R}\left(i_{Sb}\psi_{Ra} - i_{Sa}\psi_{Rb}\right) - \frac{\tau_L}{J} \\
\frac{d\psi_{Ra}}{dt} &= -\frac{1}{T_R}\psi_{Ra} - n_p\omega\psi_{Rb} + \frac{M}{T_R}i_{Sa} \\
\frac{d\psi_{Rb}}{dt} &= -\frac{1}{T_R}\psi_{Rb} + n_p\omega\psi_{Ra} + \frac{M}{T_R}i_{Sb} \\
\frac{di_{Sa}}{dt} &= \frac{\beta}{T_R}\psi_{Ra} + \beta n_p\omega\psi_{Rb} - \gamma i_{Sa} + \frac{1}{\sigma L_S}u_{Sa} \\
\frac{di_{Sb}}{dt} &= \frac{\beta}{T_R}\psi_{Rb} - \beta n_p\omega\psi_{Ra} - \gamma i_{Sb} + \frac{1}{\sigma L_S}u_{Sb}
\end{aligned} \tag{8.88}$$

www.EngineeringEBooksPdf.com

where again

$$T_R = L_R/R_R, \qquad \sigma = 1 - M^2/(L_S L_R)$$
$$\beta = M/(\sigma L_S L_R), \qquad \gamma = R_S/(\sigma L_S) + M^2 R_R/(\sigma L_S L_R^2)$$

have been used to simplify the expressions. This model is then transformed into a coordinate system attached to the rotor where, for example, the current variables are transformed according to

$$\begin{bmatrix} i_{Sx} \\ i_{Sy} \end{bmatrix} = \begin{bmatrix} \cos(n_p\theta) & \sin(n_p\theta) \\ -\sin(n_p\theta) & \cos(n_p\theta) \end{bmatrix} \begin{bmatrix} i_{Sa} \\ i_{Sb} \end{bmatrix}. \tag{8.89}$$

An advantage of this transformation is that the signals in the moving frame (i.e., the (x, y) frame) typically vary slower than those in the (a, b) frame (they vary at the slip frequency rather than at the stator frequency). At the same time, the transformation does not depend on any unknown parameter in contrast to the field-oriented dq transformation. The stator voltages and the rotor flux linkages are transformed as the currents resulting in the following model [87]:

$$\frac{di_{Sx}}{dt} = \frac{1}{\sigma L_S}u_{Sx} - \gamma i_{Sx} + \frac{\beta}{T_R}\psi_{Rx} + n_p\beta\omega\psi_{Ry} + n_p\omega i_{Sy} \tag{8.90}$$

$$\frac{di_{Sy}}{dt} = \frac{1}{\sigma L_S}u_{Sy} - \gamma i_{Sy} + \frac{\beta}{T_R}\psi_{Ry} - n_p\beta\omega\psi_{Rx} - n_p\omega i_{Sx} \tag{8.91}$$

$$\frac{d\psi_{Rx}}{dt} = \frac{M}{T_R}i_{Sx} - \frac{1}{T_R}\psi_{Rx} \tag{8.92}$$

$$\frac{d\psi_{Ry}}{dt} = \frac{M}{T_R}i_{Sy} - \frac{1}{T_R}\psi_{Ry} \tag{8.93}$$

$$\frac{d\omega}{dt} = \frac{n_p M}{J L_R}(i_{Sy}\psi_{Rx} - i_{Sx}\psi_{Ry}) - \frac{\tau_L}{J}. \tag{8.94}$$

8.5.1 *Linear Overparameterized Model*

Measurements of the stator currents i_{Sa} and i_{Sb} and voltages u_{Sa} and u_{Sb} as well as the position θ of the rotor are assumed to be available (velocity may then be reconstructed from position measurements). However, the rotor flux linkages ψ_{Rx} and ψ_{Ry} are not assumed to be measured. Standard methods for parameter estimation are based on equalities where known signals depend *linearly* on unknown parameters. However, the induction motor model described above does not fit in this category unless the rotor flux linkages are measured. The first step is to eliminate the fluxes ψ_{Rx} and ψ_{Ry} and their derivatives $d\psi_{Rx}/dt$ and $d\psi_{Ry}/dt$. The four equations (8.90), (8.91), (8.92), (8.93) can be used to solve for ψ_{Rx}, ψ_{Ry}, $d\psi_{Rx}/dt$, and $d\psi_{Ry}/dt$, but one is left without another independent equation(s) to set up a regressor system for the identification algorithm (see Chapter 2).

www.EngineeringEBooksPdf.com

A new set of independent equations are found by differentiating equations (8.90) and (8.91) to obtain

$$\frac{1}{\sigma L_s}\frac{du_{Sx}}{dt} = \frac{d^2 i_{Sx}}{dt^2} + \gamma\frac{di_{Sx}}{dt} - \frac{\beta}{T_R}\frac{d\psi_{Rx}}{dt} - n_p\beta\omega\frac{d\psi_{Ry}}{dt} - n_p\beta\psi_{Ry}\frac{d\omega}{dt} - n_p\omega\frac{di_{Sy}}{dt} - n_p i_{Sy}\frac{d\omega}{dt} \tag{8.95}$$

$$\frac{1}{\sigma L_s}\frac{du_{Sy}}{dt} = \frac{d^2 i_{Sy}}{dt^2} + \gamma\frac{di_{Sy}}{dt} - \frac{\beta}{T_R}\frac{d\psi_{Ry}}{dt} + n_p\beta\omega\frac{d\psi_{Rx}}{dt} + n_p\beta\psi_{Rx}\frac{d\omega}{dt} + n_p\omega\frac{di_{Sx}}{dt} + n_p i_{Sx}\frac{d\omega}{dt}. \tag{8.96}$$

Next, equations (8.90), (8.91), (8.92), and (8.93) are solved for ψ_{Rx}, ψ_{Ry}, $d\psi_{Rx}/dt$, and $d\psi_{Ry}/dt$ and substituted into equations (8.95) and (8.96) to obtain

$$\begin{aligned} 0 = &-\frac{d^2 i_{Sx}}{dt^2} + \frac{di_{Sy}}{dt}n_p\omega + \frac{1}{\sigma L_S}\frac{du_{Sx}}{dt} - (\gamma + \frac{1}{T_R})\frac{di_{Sx}}{dt} - i_{Sx}(-\frac{\beta M}{T_R^2} + \frac{\gamma}{T_R}) \\ &+ i_{Sy}n_p\omega(\frac{1}{T_R} + \frac{\beta M}{T_R}) + \frac{u_{Sx}}{\sigma L_S T_R} + n_p\frac{d\omega}{dt}i_{Sy} - n_p\frac{d\omega}{dt}\frac{1}{\sigma L_S(1 + n_p^2\omega^2 T_R^2)} \\ &\times \Big(-\sigma L_S T_R\frac{di_{Sy}}{dt} - \gamma i_{Sy}\sigma L_S T_R - i_{Sx}n_p\omega\sigma L_S T_R - \frac{di_{Sx}}{dt}n_p\omega\sigma L_S T_R^2 \\ &- \gamma i_{Sx}n_p\omega\sigma L_S T_R^2 + i_{Sy}n_p^2\omega^2\sigma L_S T_R^2 + n_p\omega T_R^2 u_{Sx} + T_R u_{Sy}\Big) \end{aligned} \tag{8.97}$$

and

$$\begin{aligned} 0 = &-\frac{d^2 i_{Sy}}{dt^2} - \frac{di_{Sx}}{dt}n_p\omega + \frac{1}{\sigma L_S}\frac{du_{Sy}}{dt} - (\gamma + \frac{1}{T_R})\frac{di_{Sy}}{dt} - i_{Sy}(-\frac{\beta M}{T_R^2} + \frac{\gamma}{T_R}) \\ &- i_{Sx}n_p\omega(\frac{1}{T_R} + \frac{\beta M}{T_R}) + \frac{u_{Sy}}{\sigma L_S T_R} - n_p\frac{d\omega}{dt}i_{Sx} + n_p\frac{d\omega}{dt}\frac{1}{\sigma L_S(1 + n_p^2\omega^2 T_R^2)} \\ &\times \Big(-\sigma L_S T_R\frac{di_{Sx}}{dt} - \gamma i_{Sx}\sigma L_S T_R + i_{Sy}n_p\omega\sigma L_S T_R + \frac{di_{Sy}}{dt}n_p\omega\sigma L_S T_R^2 \\ &+ \gamma i_{Sy}n_p\omega\sigma L_S T_R^2 + i_{Sx}n_p^2\omega^2\sigma L_S T_R^2 - n_p\omega T_R^2 u_{Sy} + T_R u_{Sx}\Big). \end{aligned} \tag{8.98}$$

The set of equations (8.97) and (8.98) may be rewritten in regressor form as

$$y(t) = W(t)K \tag{8.99}$$

where $y \in \mathbb{R}^2, W \in \mathbb{R}^{2\times 15}$, and $K \in \mathbb{R}^{15}$ are given by

$$K \triangleq \Big[\ \gamma \quad \beta M \quad \frac{1}{\sigma L_S} \quad \frac{\beta M}{T_R^2} \quad \frac{1}{T_R} \quad \frac{\gamma}{T_R} \quad \frac{\beta M}{T_R} \quad T_R \quad \gamma T_R \quad \beta M T_R \quad T_R^2 \quad \gamma T_R^2 \quad \frac{T_R^2}{\sigma L_S} \quad \frac{1}{\sigma L_S T_R} \quad \frac{T_R}{\sigma L_S}\ \Big]^T$$

www.EngineeringEBooksPdf.com

$$W(t) \triangleq \left[\begin{array}{cccccc} -\frac{di_{Sx}}{dt} & n_p^2\omega^2 i_{Sx} & \frac{du_{Sx}}{dt} & i_{Sx} & n_p\omega i_{Sy} - \frac{di_{Sx}}{dt} & -i_{Sx} \\ -\frac{di_{Sy}}{dt} & n_p^2\omega^2 i_{Sy} & \frac{du_{Sy}}{dt} & i_{Sy} & -n_p\omega i_{Sx} - \frac{di_{Sy}}{dt} & -i_{Sy} \end{array} \right.$$

$$\begin{array}{cc} n_p\omega i_{Sy} & -n_p^2\omega^2\frac{di_{Sx}}{dt} + n_p^3\omega^3 i_{Sy} + \frac{d\omega}{dt}\left(n_p\frac{di_{Sy}}{dt} + n_p^2\omega i_{Sx}\right) \\ -n_p\omega i_{Sx} & -n_p^2\omega^2\frac{di_{Sy}}{dt} - n_p^3\omega^3 i_{Sx} + \frac{d\omega}{dt}\left(-n_p\frac{di_{Sx}}{dt} + n_p^2\omega i_{Sy}\right) \end{array}$$

$$\begin{array}{cc} n_p i_{Sy}\frac{d\omega}{dt} - n_p^2\omega^2 i_{Sx} & n_p^3\omega^3 i_{Sy} \\ -n_p i_{Sx}\frac{d\omega}{dt} - n_p^2\omega^2 i_{Sy} & -n_p^3\omega^3 i_{Sx} \end{array}$$

$$\begin{array}{cc} n_p^2(\omega\frac{di_{Sx}}{dt}\frac{d\omega}{dt} - \omega^2\frac{d^2 i_{Sx}}{dt^2}) + n_p^3\omega^3\frac{di_{Sy}}{dt} & n_p^2(\omega i_{Sx}\frac{d\omega}{dt} - \omega^2\frac{di_{Sx}}{dt}) \\ n_p^2(\omega\frac{di_{Sy}}{dt}\frac{d\omega}{dt} - \omega^2\frac{d^2 i_{Sy}}{dt^2}) - n_p^3\omega^3\frac{di_{Sx}}{dt} & n_p^2(\omega i_{Sy}\frac{d\omega}{dt} - \omega^2\frac{di_{Sy}}{dt}) \end{array}$$

$$\left. \begin{array}{cc} n_p^2(\omega^2\frac{du_{Sx}}{dt} - u_{Sx}\omega\frac{d\omega}{dt}) & u_{Sx} \quad n_p^2\omega^2 u_{Sx} - n_p u_{Sy}\frac{d\omega}{dt} \\ n_p^2(\omega^2\frac{du_{Sy}}{dt} - u_{Sy}\omega\frac{d\omega}{dt}) & u_{Sy} \quad n_p^2\omega^2 u_{Sy} + n_p u_{Sx}\frac{d\omega}{dt} \end{array} \right]$$

and

$$y(t) \triangleq \left[\begin{array}{c} \frac{d^2 i_{Sx}}{dt^2} - n_p i_{Sy}\frac{d\omega}{dt} - n_p\omega\frac{di_{Sy}}{dt} \\ \frac{d^2 i_{Sy}}{dt^2} + n_p i_{Sx}\frac{d\omega}{dt} + n_p\omega\frac{di_{Sx}}{dt} \end{array} \right].$$

The system (8.99) is linear in the parameters. However, this system is *over-parameterized*, meaning that the components K_i of the parameter vector K are *not* independent of each other. The relationship between the parameters is

$$\begin{array}{rcl} K_1 & = & K_6K_8, K_2 = K_4K_8^2, K_3 = K_8K_{14}, K_5 = 1/K_8, \\ K_7 & = & K_4K_8, K_9 = K_6K_8^2, K_{10} = K_4K_8^3, K_{11} = K_8^2, \\ K_{12} & = & K_6K_8^3, K_{13} = K_{14}K_8^3, K_{15} = K_{14}K_8^2 \end{array} \tag{8.100}$$

so that only the four parameters K_4, K_6, K_8, and K_{14} are independent. If the parameter vector is computed according to $K = R_W^{-1}R_{Wy} \in \mathbb{R}^{15}$ as in Chapter 2, one would find out that the problem is numerically *ill-conditioned*. This means that small changes in the data matrices R_W and R_{Wy} will lead to large changes in the computed value for $K \in \mathbb{R}^{15}$ and therefore the value of K could not be considered valid. Furthermore, there is

www.EngineeringEBooksPdf.com

no guarantee that the components of K computed in this way would satisfy the constraints (8.100). Note also that not all five electrical parameters R_S, L_S, R_R, L_R, and M can be retrieved from the K_i's. The four parameters K_4, K_6, K_8, and K_{14} determine only the four independent parameters R_S, L_S, σ, and T_R by

$$R_S = \frac{K_6 - K_4}{K_{14}},\ T_R = K_8,\ L_S = \frac{1 + K_4 K_8^2}{K_{14} K_8},\ \sigma = \frac{1}{1 + K_4 K_8^2}. \quad (8.101)$$

As $T_R = L_R/R_R$ and $\sigma = 1 - M^2/(L_S L_R)$, only L_R/R_R and M^2/L_R can be obtained and not M, L_R and R_R independently. This situation is inherent to the identification problem when some of the state variables (in this case the rotor flux linkages) are unknown and is not specific to the method. If the rotor flux linkages are not measured, machines with different R_R, L_R, and M, but identical L_R/R_R and M^2/L_R, will have the same input/output (i.e., voltage to stator currents and speed) characteristics. However, machines with different K_i parameters, yet satisfying the nonlinear relationships (8.100), will be distinguishable. (For a related discussion of this issue see Bellini et al. [88], where parameter identification is performed using torque–speed and stator current–speed characteristics.)

8.5.2 Nonlinear Least-Squares Identification

In this section, it is shown how the linear least-squares method described in Chapter 2 is modified to account for the constraint (8.100). Recall from Chapter 2 that the least-squares problem is to minimize

$$E^2(K) = \sum_{n=1}^{N} \left| y(nT) - W(nT)K \right|^2 = R_y - 2R_{Wy}^T K + K^T R_W K \quad (8.102)$$

subject to the constraints

$$\begin{aligned} K_1 &= K_6 K_8, K_2 = K_4 K_8^2, K_3 = K_8 K_{14}, K_5 = 1/K_8, \\ K_7 &= K_4 K_8, K_9 = K_6 K_8^2, K_{10} = K_4 K_8^3, K_{11} = K_8^2, \\ K_{12} &= K_6 K_8^3, K_{13} = K_{14} K_8^3, K_{15} = K_{14} K_8^2. \end{aligned} \quad (8.103)$$

On physical grounds, the parameters K_4, K_6, K_8, and K_{14} are constrained to

$$0 < K_i < \infty \quad \text{for } i = 4, 6, 8, 14. \quad (8.104)$$

www.EngineeringEBooksPdf.com

Also, based on physical grounds, the squared error $E^2(K)$ will be minimized in the interior of this region. Let

$$E^2(K_p) \triangleq \sum_{n=1}^{N} \left| y(nT) - W(nT)K \right|^2_{\substack{K_1=K_6K_8 \\ K_2=K_4K_8^2}} \\ \vdots \\ = R_y - 2R_{Wy}^T K \Big|_{\substack{K_1=K_6K_8 \\ K_2=K_4K_8^2}} + \left(K^T R_W K\right)\Big|_{\substack{K_1=K_6K_8 \\ K_2=K_4K_8^2}} \qquad (8.105) \\ \vdots \qquad\qquad \vdots$$

where

$$K_p \triangleq \begin{bmatrix} K_4 & K_6 & K_8 & K_{14} \end{bmatrix}^T.$$

As just explained, the minimum of (8.105) must occur in the interior of the region and therefore at an extremum point. This then entails solving the four equations

$$r_1(K_p) \triangleq \frac{\partial E^2(K_p)}{\partial K_4} = 0 \qquad (8.106)$$

$$r_2(K_p) \triangleq \frac{\partial E^2(K_p)}{\partial K_6} = 0 \qquad (8.107)$$

$$r_3(K_p) \triangleq \frac{\partial E^2(K_p)}{\partial K_8} = 0 \qquad (8.108)$$

$$r_4(K_p) \triangleq \frac{\partial E^2(K_p)}{\partial K_{14}} = 0. \qquad (8.109)$$

The partial derivatives in (8.106)–(8.109) are *rational* functions in the parameters K_4, K_6, K_8, and K_{14}. Defining

$$p_1(K_p) \triangleq K_8 r_1(K_p) = K_8 \frac{\partial E^2(K_p)}{\partial K_4} \qquad (8.110)$$

$$p_2(K_p) \triangleq K_8 r_2(K_p) = K_8 \frac{\partial E^2(K_p)}{\partial K_6} \qquad (8.111)$$

$$p_3(K_p) \triangleq K_8^3 r_3(K_p) = K_8^3 \frac{\partial E^2(K_p)}{\partial K_8} \qquad (8.112)$$

$$p_4(K_p) \triangleq K_8 r_4(K_p) = K_8 \frac{\partial E^2(K_p)}{\partial K_{14}} \qquad (8.113)$$

results in the $p_i(K_p)$ being *polynomials* in the parameters K_4, K_6, K_8, and K_{14} and having the same positive zero set (i.e., the same roots satisfying $K_i > 0$) as the system (8.106)–(8.109). The degrees of the polynomials p_i

www.EngineeringEBooksPdf.com

are given in the following table.

	$\deg K_4$	$\deg K_6$	$\deg K_8$	$\deg K_{14}$
$p_1(K_p)$	1	1	7	1
$p_2(K_p)$	1	1	7	1
$p_3(K_p)$	2	2	8	2
$p_4(K_p)$	1	1	7	1

All possible solutions to this set may be found using elimination theory as is now summarized.

Solving Systems of Polynomial Equations [89][90]

The question at hand is "Given two polynomial equations $a(K_1, K_2) = 0$ and $b(K_1, K_2) = 0$, how does one solve them simultaneously to eliminate (say) K_2?". A systematic procedure to do this is known as *elimination theory* and uses the notion of *resultants* (see the appendix at the end of this chapter). Briefly, one considers $a(K_1, K_2)$ and $b(K_1, K_2)$ as polynomials in K_2 whose coefficients are polynomials in K_1. Then, for example, letting $a(K_1, K_2)$ and $b(K_1, K_2)$ have degrees 3 and 2, respectively, in K_2, they may be written in the form

$$\begin{aligned} a(K_1, K_2) &= a_3(K_1)K_2^3 + a_2(K_1)K_2^2 + a_1(K_1)K_2 + a_0(K_1) \\ b(K_1, K_2) &= b_2(K_1)K_2^2 + b_1(K_1)K_2 + b_0(K_1). \end{aligned}$$

The $n \times n$ *Sylvester* matrix, with

$$n \triangleq \deg_{K_2}\{a(K_1, K_2)\} + \deg_{K_2}\{b(K_1, K_2)\} = 3 + 2 = 5$$

is defined by

$$S_{a,b}(K_1) \triangleq \begin{bmatrix} a_0(K_1) & 0 & b_0(K_1) & 0 & 0 \\ a_1(K_1) & a_0(K_1) & b_1(K_1) & b_0(K_1) & 0 \\ a_2(K_1) & a_1(K_1) & b_2(K_1) & b_1(K_1) & b_0(K_1) \\ a_3(K_1) & a_2(K_1) & 0 & b_2(K_1) & b_1(K_1) \\ 0 & a_3(K_1) & 0 & 0 & b_2(K_1) \end{bmatrix}.$$

The *resultant* polynomial is then defined by

$$r(K_1) = \mathrm{Res}\Big(a(K_1, K_2), b(K_1, K_2), K_2\Big) \triangleq \det S_{a,b}(K_1) \qquad (8.114)$$

and is the result of *eliminating* the variable K_2 from $a(K_1, K_2) = 0$ and $b(K_1, K_2) = 0$. In fact, the following is true (see Refs. [89] and [90]).

Theorem Any solution (K_1^0, K_2^0) of $a(K_1, K_2) = 0$ and $b(K_1, K_2) = 0$ must satisfy $r(K_1^0) = 0$.

Though the converse of this theorem is not necessarily true, the finite number of solutions of $r(K_1) = 0$ are the *only* possible candidates for the

www.EngineeringEBooksPdf.com

first coordinate (partial solutions) of the common zeros of $a(K_1, K_2)$ and $b(K_1, K_2)$. Whether or not such a partial solution results in a full solution is easily determined by back solving and checking the solution (see the Appendix).

Using the polynomials (8.110)–(8.113) and a computer algebra software program (e.g., MATHEMATICA [91]), the variable K_4 is eliminated first to obtain three polynomials in three unknowns as

$$r_{p1p2}(K_6, K_8, K_{14}) \triangleq \text{Res}\Big(p_1(K_4, K_6, K_8, K_{14}), p_2(K_4, K_6, K_8, K_{14}), K_4\Big)$$
$$r_{p1p3}(K_6, K_8, K_{14}) \triangleq \text{Res}\Big(p_1(K_4, K_6, K_8, K_{14}), p_3(K_4, K_6, K_8, K_{14}), K_4\Big)$$
$$r_{p1p4}(K_6, K_8, K_{14}) \triangleq \text{Res}\Big(p_1(K_4, K_6, K_8, K_{14}), p_4(K_4, K_6, K_8, K_{14}), K_4\Big)$$

where

	$\deg K_6$	$\deg K_8$	$\deg K_{14}$
r_{p1p2}	1	14	1
r_{p1p3}	2	22	2
r_{p1p4}	1	14	1

Next K_6 is eliminated to obtain two polynomials in two unknowns as

$$r_{p1p2p3}(K_8, K_{14}) \triangleq \text{Res}\Big(r_{p1p2}(K_6, K_8, K_{14}), r_{p1p3}(K_6, K_8, K_{14}), K_6\Big)$$
$$r_{p1p2p4}(K_8, K_{14}) \triangleq \text{Res}\Big(r_{p1p2}(K_6, K_8, K_{14}), r_{p1p4}(K_6, K_8, K_{14}), K_6\Big)$$

where

	$\deg K_8$	$\deg K_{14}$
r_{p1p2p3}	50	2
r_{p1p2p4}	28	1

Finally K_{14} is eliminated to obtain a single polynomial in K_8 as

$$r(K_8) \triangleq \text{Res}\Big(r_{p1p2p3}(K_8, K_{14}), r_{p1p2p4}(K_8, K_{14}), K_{14}\Big)$$

where

$$\deg_{K_8}\{r(K_8)\} = 104.$$

The parameter K_8 was chosen as the variable *not* eliminated because its degree was the highest at each step, meaning it would have a larger (in dimension) Sylvester matrix than using any other variable. The positive roots of $r(K_8) = 0$ are found, which are then substituted into $r_{p1p2p3} = 0$ (or $r_{p1p2p4} = 0$) and which in turn are solved to obtain the partial solutions (K_8, K_{14}). The partial solutions (K_8, K_{14}) are then substituted into $r_{p1p2} = 0$ (or $r_{p1p3} = 0$ or $r_{p1p4} = 0$), which are solved to obtain the partial solutions (K_6, K_8, K_{14}) so that they in turn may be substituted into $p_1 = 0$ (or $p_2 = 0$, or $p_3 = 0$, or $p_4 = 0$) which is then solved to obtain the candidate

www.EngineeringEBooksPdf.com

solutions (K_4, K_6, K_8, K_{14}). These candidate solutions are then checked to see which ones satisfy the complete system of polynomials equations (8.110)–(8.113) and those that do constitute the *candidate* solutions for the minimization. Based on physical considerations, the set of candidate solutions is nonempty. From the set of candidate solutions, the one that gives the smallest squared error is chosen.

Computational Issues

Due to the high degrees of the resultant polynomials, care must be taken to compute their roots. The data set is collected and brought into MATHEMATICA [91]. The matrices R_y, R_W, and R_{Wy} are then computed and their entries converted to *rational* form. Finally the roots of the resultant polynomials are computed in MATHEMATICA using rational arithmetic with 16 digits of precision.

Numerical Conditioning of the Nonlinear Least-Squares Solution

After finding the solution that gives the minimal value for $E^2(K_p)$, one needs to know if the solution makes sense. For example, in the *linear* least-squares problem, there is a unique well-defined solution provided that the regressor matrix R_W is non singular (or in practical terms, its condition number is not too large). In the nonlinear case here, a Taylor series expansion about the computed minimum point $K_p^* = [K_4^*, K_6^*, K_8^*, K_{14}^*]^T$ to obtain $(i, j = 4, 6, 8, 14)$

$$E^2(K_p) = E^2(K_p^*) + \frac{1}{2}\left[K_p - K_p^*\right]^T \frac{\partial^2 E^2(K_p^*)}{\partial K_i \partial K_j}\left[K_p - K_p^*\right] + \cdots \quad (8.115)$$

One then checks that the Hessian matrix $\dfrac{\partial^2 E^2(K_p^*)}{\partial K_i \partial K_j}$ is positive definite to ensure that the data set is sufficiently rich to identify the parameters. Its condition number is also computed to obtain a measure of the numerically reliability of the computations [92].

8.5.3 Calculating the Parametric Error Indices

The expression for the error index in Chapter 2 is still applicable for the nonlinear case. However, the method for computing the parametric error indices must be modified for the nonlinear least-squares estimation problem. Here, the parametric error index is defined as the *maximum* value of δK_i for $i = 4, 6, 8, 14$ such that

$$E^2(K_p^* + \delta K_p) = 1.25 E^2(K_p^*) \quad (8.116)$$

where $\delta K_p \triangleq \begin{bmatrix} \delta K_4 & \delta K_6 & \delta K_8 & \delta K_{14} \end{bmatrix}^T$. Recall that in Chapter 2, $E^2(K_p^* + \delta K_p) = 2E^2(K_p^*)$ was used rather than (8.116). The choice is somewhat arbitrary as explained in Chapter 2.

www.EngineeringEBooksPdf.com

In words, for all δK_p that result in a 25% increase in the residual error, the parametric index is the maximum possible value of δK_i. Mathematically, for $i = 4, 6, 8$, and 14, one maximizes

$$\delta K_i$$

subject to (8.116). This is straightforwardly setup as an unconstrained optimization using Lagrange multipliers by maximizing

$$\delta K_i + \lambda\Big(E^2(K_p^* + \delta K_p) - 1.25E^2(K_p^*)\Big) \tag{8.117}$$

over all possible $\delta K_p \triangleq \left[\begin{array}{cccc} \delta K_4 & \delta K_6 & \delta K_8 & \delta K_{14} \end{array}\right]^T$ and λ. For example, with $i = 4$, the extrema are solutions to

$$\begin{aligned}
1 + \lambda \frac{\partial\left(E^2(K_p^* + \delta K_p) - 1.25E^2(K_p^*)\right)}{\partial \delta K_4} &= 0 && (8.118)\\
\lambda \frac{\partial\left(E^2(K_p^* + \delta K_p) - 1.25E^2(K_p^*)\right)}{\partial \delta K_6} &= 0 && (8.119)\\
\lambda \frac{\partial\left(E^2(K_p^* + \delta K_p) - 1.25E^2(K_p^*)\right)}{\partial \delta K_8} &= 0 && (8.120)\\
\lambda \frac{\partial\left(E^2(K_p^* + \delta K_p) - 1.25E^2(K_p^*)\right)}{\partial \delta K_{14}} &= 0 && (8.121)\\
E^2(K_p^* + \delta K_p) - 1.25E^2(K_p^*) &= 0. && (8.122)
\end{aligned}$$

The equations (8.118) through (8.122) are transformed to five polynomial equations in the five unknowns $\delta K_4, \delta K_6, \delta K_8, \delta K_{14}$, and λ, and elimination theory is then used to solve this set.

8.5.4 *Mechanical Parameters*

Once the electrical parameters have been found, the two mechanical parameters J, f ($\tau_L = -f\omega$) can be found using a linear least-squares algorithm. To do so, equations (8.95) and (8.96) are solved for $M\psi_{Rx}/L_R$ and $M\psi_{Ry}/L_R$, resulting in

$$\begin{aligned}
\left[\begin{array}{c} M\psi_{Rx}/L_R \\ M\psi_{Ry}/L_R \end{array}\right] = \sigma L_S \frac{1}{(1/T_R)^2 + n_p^2\omega^2} \left[\begin{array}{cc} 1/T_R & -\omega \\ \omega & 1/T_R \end{array}\right] \\
\times \left[\begin{array}{c} di_{Sx}/dt - u_{Sx}/(\sigma L_S) + \gamma i_{Sx} - n_p\omega i_{Sy} \\ di_{Sy}/dt - u_{Sy}/(\sigma L_S) + \gamma i_{Sy} + n_p\omega i_{Sx} \end{array}\right]. \qquad (8.123)
\end{aligned}$$

Noting that

$$\gamma = \frac{R_S}{\sigma L_S} + \frac{1}{\sigma L_S}\frac{1}{T_R}\frac{M^2}{L_R} = \frac{R_S}{\sigma L_S} + \frac{1}{\sigma L_S}\frac{1}{T_R}(1-\sigma)L_S, \tag{8.124}$$

www.EngineeringEBooksPdf.com

it is seen that the quantities on the right-hand side of (8.123) are all known once the electrical parameters have been computed. With $K_{16} \triangleq n_p/J, K_{17} \triangleq f/J$, equation (8.94) may be rewritten as

$$\frac{d\omega}{dt} = \begin{bmatrix} (M/L_R)\left(\psi_{Rx} i_{Sy} - \psi_{Ry} i_{Sx}\right) & -\omega \end{bmatrix} \begin{bmatrix} K_{16} \\ K_{17} \end{bmatrix}$$

so that the standard linear squares approach of Chapter 2 is directly applicable. Then

$$J \triangleq n_p/K_{16}, f \triangleq n_p K_{17}/K_{16}. \tag{8.125}$$

8.5.5 *Simulation Results*

The algorithm is first applied to simulated "data" to see how it performs under ideal conditions. In particular, the simulations are helpful in evaluating the usefulness of the parametric error indices. Here, a two pole-pair ($n_p = 2$), three-phase induction motor model was simulated using SIMULINK with parameter values chosen to be

$$\begin{aligned} R_S &= 9.7\ \Omega, R_R = 8.6\ \Omega, L_S = L_R = 0.67\ \text{H} \\ M &= 0.64\ \text{H}, \sigma = 0.088, J = 0.011\ \text{kg-m}^2, \tau_L = 3.7\ \text{N-m}. \end{aligned}$$

A 2048-line position encoder and 12-bit A/D converters were included in the simulation model in order to make the simulation data closer to actual experimental measurements. These values correspond to a 1/2-kW machine with a synchronous frequency of 50 Hz. These machine parameter values correspond to the following K values:

$$\begin{aligned} K_1 &= 299.15, K_2 = 10.42, K_3 = 17.05, K_4 = 1717.18, K_5 = 12.84 \\ K_6 &= 3839.8, K_7 = 133.78, K_8 = 0.0779, K_9 = 23.31, K_{10} = 0.8120 \\ K_{11} &= 0.0061, K_{12} = 1.82, K_{13} = 0.1035, K_{14} = 218.83, K_{15} = 1.328 \end{aligned}$$

for the electrical parameters and to

$$K_{16} = 181.82, \quad K_{17} = 336.36$$

for the mechanical parameters.

Figure 8.30 shows the simulated speed response (from standstill) of the induction motor after a balanced (open-loop) set of three-phase voltages of amplitude 466.7 V and frequency 50 Hz was applied to the machine.

The "data" $\{u_{Sa}, u_{Sb}, i_{Sa}, i_{Sb}, \theta\}$ were collected between 0 sec and 0.2 sec. The quantities $u_{Sx}, u_{Sy}, du_{Sx}/dt, du_{Sy}/dt, i_{Sx}, i_{Sy}\ di_{Sx}/dt, di_{Sy}/dt, d^2 i_{Sx}/dt^2$, $d^2 i_{Sy}/dt^2$, $\omega = d\theta/dt$, and $d\omega/dt$ were calculated and the regressor matrices R_W, R_y, and R_{Wy} were computed. The procedure explained in Section 8.5.2 was then carried out to compute K_4, K_6, K_8, and K_{14}. In this case,

www.EngineeringEBooksPdf.com

there was only one extremum point that had *positive* values for all the K_i. The table

Parameter	True Value	Estimated Value	Parametric Error Index
K_4	1717.2	1743.4	13.23
K_6	3839.8	3917.5	24.59
K_8	0.0779	0.0780	0.00031
K_{14}	218.8	222.2	8.27

compares the electrical parameter values determined from the nonlinear least-squares procedure to their actual values (which are known only because this is simulation data). Also given in the table are the corresponding parametric error indices. The residual error index for the parameters K_4, K_6, K_8, and K_{14} was computed to be 3.15%.

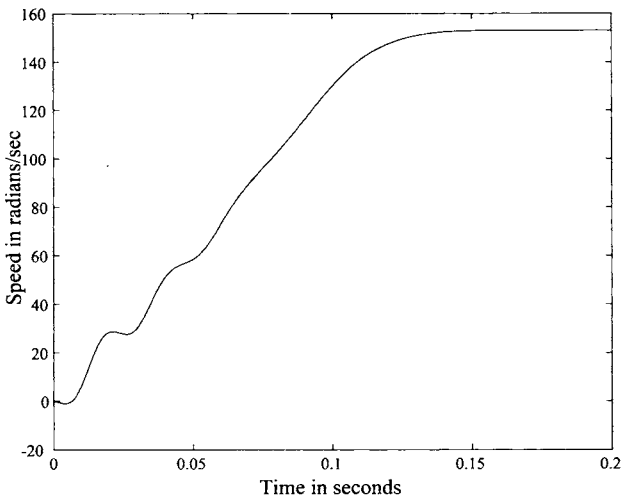


FIGURE 8.30. Rotor speed versus time.

Using these values, the scaled flux linkages $M\psi_{Rx}/L_R$ and $M\psi_{Ry}/L_R$ were reconstructed according to (8.123) to estimate the mechanical parameters K_{16} and K_{17}. The table

Parameter	True Value	Estimated Value	Parametric Error Index
K_{16}	181.8	195.3	4.29
K_{17}	336.4	359.3	9.78

compares the mechanical parameter values determined from the least-squares procedure to their actual values along with the corresponding parametric

www.EngineeringEBooksPdf.com

error indices. The residual error index for the mechanical parameters K_{16} and K_{17} was computed to be 4.26%.

The Hessian matrix for the identification of the parameters K_4, K_6, K_8, and K_{14} was calculated at the minimum point according to (8.115), resulting in

$$\left\{\frac{\partial^2 E^2(K_p^*)}{\partial K_i \partial K_j}\right\} = \begin{bmatrix} 7.534 & 0.2175 & 40.33 & -89.39 \\ 0.2175 & 18.04 & 10.17 & -44.35 \\ 40.33 & 10.17 & 5.308 \times 10^4 & 1.112 \times 10^3 \\ -89.39 & -44.35 & 1.112 \times 10^3 & 1.876 \times 10^3 \end{bmatrix}$$

which is positive definite and has a condition number of 1.88×10^4. The table below compares the estimated machine parameters to their actual values.

Parameter	True Value	Estimated Value
T_R	0.0779 sec	0.0780 sec
σ	0.088	0.086
L_S	0.67 H	0.6698 H
R_S	9.7 ohms	9.8 ohms
J	0.011 kg-m^2	0.010 kg-m^2
τ_L	3.7 N-m	3.68 N-m

8.5.6 *Experimental Results*

A three-phase, 0.5-Hp, 1735-rpm ($n_p = 2$ pole-pair) induction machine was used for the experiments. A 4096-pulse/rev optical encoder was attached to the motor for position measurements. The motor was connected to a three-phase, 60-Hz, 230-V source through a switch with no load on the machine. When the switch was closed, the stator currents and voltages along with the rotor position were sampled at 4 kHz. Filtered differentiation (using digital filters) was used for calculating the acceleration and the derivatives of the voltages and currents. Specifically, the signals were filtered with a low-pass digital Butterworth filter followed by reconstruction of the derivatives using $dx(t)/dt = (x(t) - x(t-T))/T$, where T is the sampling interval. The voltages and currents were put through a 3–2 transformation to obtain the two-phase equivalent voltages u_{Sa} and u_{Sb} which are plotted in Figure 8.31.

The sampled two-phase equivalent current i_{Sa} and it simulated response i_{Sa_sim} are shown in Figure 8.32 (the simulated current i_{Sa_sim} is discussed below). The phase b current i_{Sb} is similar, but shifted by $\pi/(2n_p)$. The calculated speed ω (from the position measurements) and the simulated speed ω_{sim} are shown in Figure 8.33 (the simulated speed ω_{sim} will also be discussed below).

www.EngineeringEBooksPdf.com

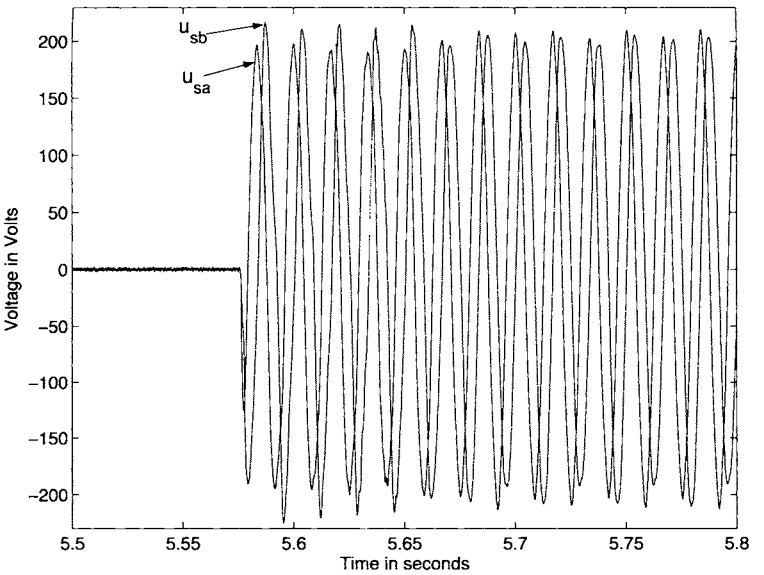


FIGURE 8.31. Sampled two-phase equivalent voltages u_{Sa} and u_{Sb}.

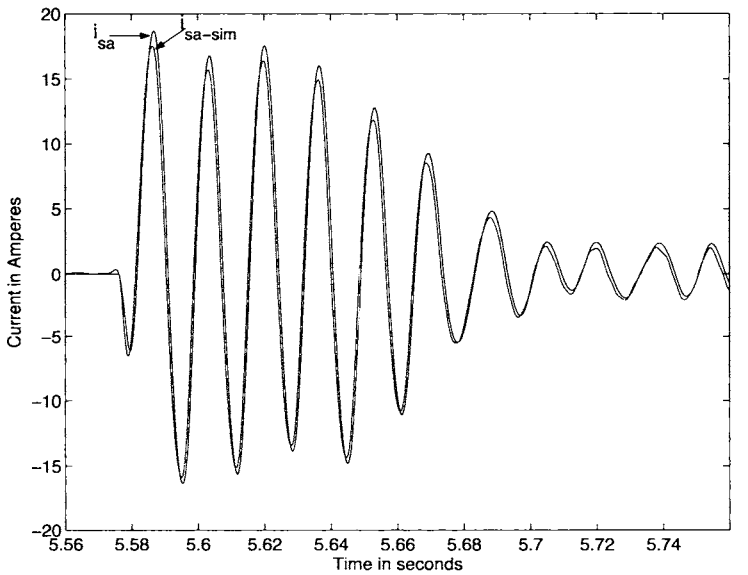


FIGURE 8.32. Phase a current i_{Sa} and its simulated response i_{Sa_sim}.

www.EngineeringEBooksPdf.com

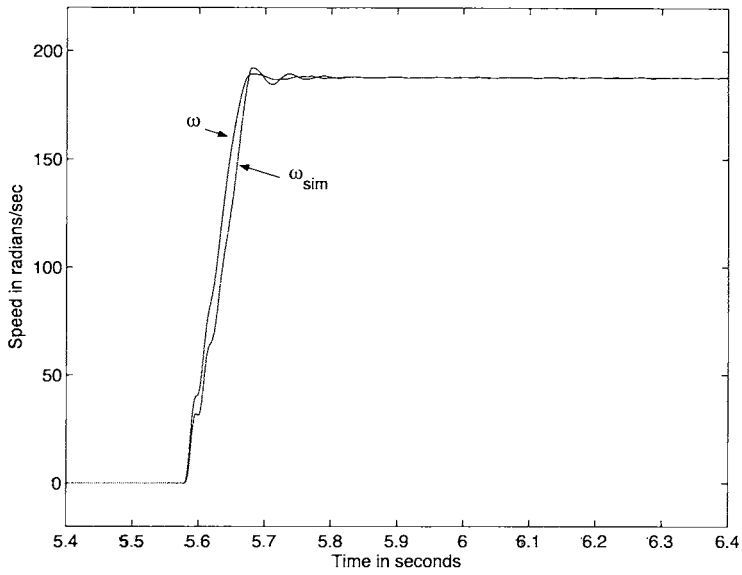


FIGURE 8.33. Calculated speed ω and simulated speed ω_{sim}.

Using the data $\{u_{Sa}, u_{Sb}, i_{Sa}, i_{Sb}, \theta\}$ collected between 5.57 sec to 5.8 sec, the quantities $u_{Sx}, u_{Sy}, du_{Sx}/dt, du_{Sy}/dt, i_{Sx}, i_{Sy}\, di_{Sx}/dt, di_{Sy}/dt, d^2i_{Sx}/dt^2$, d^2i_{Sy}/dt^2, and $\omega = d\theta/dt$, $d\omega/dt$ were calculated and the regressor matrices R_W, R_y, and R_{Wy} were computed. The procedure explained in Section 8.5.2 was then carried out to compute K_4, K_6, K_8, and K_{14}. In this case, there was only one extremum point that had *positive* values for all the K_i. The table below presents the parameter values determined using the nonlinear least-squares methodology along with their corresponding parametric error indices.

Parameter	Estimated Value	Parametric Error Index
$K4$	519.7	185.8
$K6$	1848.3	796.4
$K8$	0.1311	0.0103
$K14$	259.5	59.4

The residual error index was calculated to be 13.43%. The motor's electrical parameters are computed using (8.101) to obtain

$$R_S = 5.12 \text{ ohms} \tag{8.126}$$
$$T_R = 0.1311 \text{ sec} \tag{8.127}$$
$$L_S = 0.2919 \text{ H} \tag{8.128}$$
$$\sigma = 0.1007 \tag{8.129}$$

www.EngineeringEBooksPdf.com

By way of comparison, the stator resistance was measured using an ohmmeter giving the value of 4.9 ohms and a no-load test was also run to compute the value of L_S resulting in 0.33 H.

The Hessian matrix for the identification of the parameters K_4, K_6, K_8, and K_{14} was calculated at the minimum point according to (8.115), resulting in

$$\left\{\frac{\partial^2 E^2(K_p^*)}{\partial K_i \partial K_j}\right\} = \begin{bmatrix} 0.0574 & 0.1943 & -0.0034 & -0.7655 \\ 0.1943 & 2.584 & 10.17 & -44.35 \\ -0.0034 & 10.17 & 631.4 & 193.8 \\ -0.7655 & -44.35 & 193.8 & 3012 \end{bmatrix}$$

which is positive definite and has a condition number of 8.24×10^4.

Using the electrical parameters, the rotor flux linkages $(M/L_R)\psi_{Rx}$ and $(M/L_R)\psi_{Ry}$ were reconstructed and used to identify the mechanical parameters. The table below gives the estimated values and the parametric error indices.

Parameter	Estimated Value	Parametric Error Index
K_{16}	952.38	126.92
K_{17}	0.5714	0.1528

The residual error index was calculated to be 18.6%. The corresponding values for the motor parameters J and f are then computed using (8.125) to obtain

$$J = n_p/K_{16} = 0.0021 \text{ kg-m}^2 \tag{8.130}$$

$$f = n_p K_{17}/K_{16} = 0.0012 \text{ N-m/rad/sec.} \tag{8.131}$$

Simulation of the Experimental Motor

Another useful way to evaluate the identified parameters (8.126)–(8.129) and (8.130)–(8.131) is to simulate the motor using these values with the measured voltages as input. One then compares the simulation's output (stator currents) with the measured outputs. To proceed in this manner, recall that only R_S, T_R, L_S, and σ can be identified, but this is all that is needed for the simulation. Specifically, defining

$$\phi_{Ra} \triangleq \frac{M}{L_R}\psi_{Ra}, \quad \phi_{Rb} \triangleq \frac{M}{L_R}\psi_{Rb}$$

www.EngineeringEBooksPdf.com

the model (8.88) may be rewritten as

$$\begin{aligned}
\frac{d\omega}{dt} &= \frac{n_p}{J}\left(i_{Sb}\phi_{Ra} - i_{Sa}\phi_{Rb}\right) - \frac{\tau_L}{J} \\
\frac{d\phi_{Ra}}{dt} &= -\frac{1}{T_R}\phi_{Ra} - n_p\omega\phi_{Rb} + \frac{1}{T_R}\frac{M^2}{L_R}i_{Sa} \\
\frac{d\phi_{Rb}}{dt} &= -\frac{1}{T_R}\phi_{Rb} + n_p\omega\phi_{Ra} + \frac{1}{T_R}\frac{M^2}{L_R}i_{Sb} \\
\frac{di_{Sa}}{dt} &= \frac{1}{\sigma L_S T_R}\phi_{Ra} + \frac{1}{\sigma L_S}n_p\omega\phi_{Rb} - \gamma i_{Sa} + \frac{1}{\sigma L_S}u_{Sa} \\
\frac{di_{Sb}}{dt} &= \frac{1}{\sigma L_S T_R}\phi_{Rb} - \frac{1}{\sigma L_S}n_p\omega\phi_{Ra} - \gamma i_{Sb} + \frac{1}{\sigma L_S}u_{Sb}
\end{aligned} \tag{8.132}$$

where

$$\frac{M^2}{L_R} = (1-\sigma)\,L_S, \gamma = \frac{R_S}{\sigma L_S} + \frac{1}{\sigma L_S}\frac{1}{T_R}\frac{M^2}{L_R}$$

The model (8.132) uses only parameters that can be estimated. The experimental voltages shown in Figure 8.31 were then used as input to a simulation of the model (8.132) using the parameter values from (8.126)–(8.129) and (8.130)–(8.131). The resulting phase a current i_{Sa_sim} from the simulation is shown in Figure 8.32, and corresponds well with the actual measured current i_{Sa}. Similarly, the resulting speed ω_{sim} from the simulation is shown in Figure 8.33, where it is seen that the simulated speed is somewhat more oscillatory than the measured speed ω.

Remarks As explained above, M is not identifiable by the above method. However, it can be (and often is) estimated by assuming that $L_R = L_S$ (rotor and stator leakages are equal) so that $M = \sqrt{L_S L_R(1-\sigma)} = L_S\sqrt{1-\sigma}$. For the above experimental motor, this gives $M = 0.2768$ H. Under this same assumption, an estimate for the rotor resistance is given by $R_R = L_R/T_R = L_S/T_R = 2.23$ ohms.

The combined parameter identification and velocity estimation problem is considered in Refs. [93][94][95][96] while in Ref. [97] the sensitivity of measurable outputs to the machine parameters are discussed.

During operation of the machine, the values of the rotor time constant $T_R = L_R/R_R$ and the stator resistance R_S change due to ohmic heating. If one is only concerned with the online identification (tracking) of these two parameter values, then the problem simplifies considerably. This particular case has been developed in [98] (see also [99]).

www.EngineeringEBooksPdf.com

Appendix

Elimination Theory and Resultants

Given two polynomials $a(x_1, x_2)$ and $b(x_1, x_2)$, how does one find their common zeros? That is, the values (x_{10}, x_{20}) such that

$$a(x_{10}, x_{20}) = b(x_{10}, x_{20}) = 0.$$

Consider $a(x_1, x_2)$ and $b(x_1, x_2)$ as polynomials in x_2 whose coefficients are polynomials in x_1. For example, let $a(x_1, x_2)$ and $b(x_1, x_2)$ have degrees 3 and 2, respectively, in x_2 so that they may be written in the form

$$\begin{aligned} a(x_1, x_2) &= a_3(x_1)x_2^3 + a_2(x_1)x_2^2 + a_1(x_1)x_2 + a_0(x_1) \\ b(x_1, x_2) &= b_2(x_1)x_2^2 + b_1(x_1)x_2 + b_0(x_1). \end{aligned}$$

Then there exist polynomials $\alpha(x_1, x_2)$ and $\beta(x_1, x_2)$ of the form

$$\begin{aligned} \alpha(x_1, x_2) &= \alpha_1(x_1)x_2 + \alpha_0(x_1) \\ \beta(x_1, x_2) &= \beta_2(x_1)x_2^2 + \beta_1(x_1)x_2 + \beta_0(x_1) \end{aligned}$$

that is, satisfying

$$\begin{aligned} \deg_{x2}\{\alpha(x_1, x_2)\} &= \deg_{x2}\{b(x_1, x_2)\} - 1 \\ \deg_{x2}\{\beta(x_1, x_2)\} &= \deg_{x2}\{a(x_1, x_2)\} - 1 \end{aligned}$$

and a polynomial $r(x_1)$ in one variable such that

$$\alpha(x_1, x_2)a(x_1, x_2) + \beta(x_1, x_2)b(x_1, x_2) = r(x_1).$$

The polynomial $r(x_1)$ is called the *resultant polynomial*. So if $a(x_{10}, x_{20}) = b(x_{10}, x_{20}) = 0$, then $r(x_{10}) = 0$. That is, if (x_{10}, x_{20}) is a *common zero* of the pair $\{a(x_1, x_2), b(x_1, x_2)\}$, then the first coordinate x_{10} is a zero of $r(x_1) = 0$. The roots of $r(x_1)$ are easy to find (numerically) as it is a polynomial in one variable. To find the common zeros of $\{a(x_1, x_2), b(x_1, x_2)\}$, one computes all roots x_{1i}, $i = 1, ..., n_1$, of $r(x_1)$. Next, for each such x_{1i}, one (numerically) computes the roots of

$$a(x_{1i}, x_2) = 0 \tag{8.133}$$

and the roots of

$$b(x_{1i}, x_2) = 0. \tag{8.134}$$

Any root x_{2j} that is in the solution set of both (8.133) and (8.134) for a given x_{1i} results in the pair (x_{1i}, x_{2j}) being a common zero of $a(x_1, x_2)$ and $b(x_1, x_2)$. Thus, this gives a method of solving polynomials in one variable to compute the common zeros of $\{a(x_1, x_2), b(x_1, x_2)\}$.

www.EngineeringEBooksPdf.com

To see how one obtains $r(x_1)$, let

$$\begin{aligned} a(x_1,x_2) &= a_3(x_1)x_2^3 + a_2(x_1)x_2^2 + a_1(x_1)x_2 + a_0(x_1) \\ b(x_1,x_2) &= b_2(x_1)x_2^2 + b_1(x_1)x_2 + b_0(x_1). \end{aligned} \tag{8.135}$$

Next, one sees if polynomials of the form

$$\begin{aligned} \alpha(x_1,x_2) &= \alpha_1(x_1)x_2 + \alpha_0(x_1) \\ \beta(x_1,x_2) &= \beta_2(x_1)x_2^2 + \beta_1(x_1)x_2 + \beta_0(x_1) \end{aligned} \tag{8.136}$$

can be found such that

$$\alpha(x_1,x_2)a(x_1,x_2) + \beta(x_1,x_2)b(x_1,x_2) = r(x_1). \tag{8.137}$$

Proceeding, the expressions (8.135) for $a(x_1,x_2)$ and $b(x_1,x_2)$ as well as the expressions (8.136) for $\alpha(x_1,x_2)$ and $\beta(x_1,x_2)$ are substituted into (8.137). Equating powers of x_2, equation (8.137) may then be represented in matrix form as

$$\begin{bmatrix} a_0(x_1) & 0 & b_0(x_1) & 0 & 0 \\ a_1(x_1) & a_0(x_1) & b_1(x_1) & b_0(x_1) & 0 \\ a_2(x_1) & a_1(x_1) & b_2(x_1) & b_1(x_1) & b_0(x_1) \\ a_3(x_1) & a_2(x_1) & 0 & b_2(x_1) & b_1(x_1) \\ 0 & a_3(x_1) & 0 & 0 & b_2(x_1) \end{bmatrix} \begin{bmatrix} \alpha_0(x_1) \\ \alpha_1(x_1) \\ \beta_0(x_1) \\ \beta_1(x_1) \\ \beta_2(x_1) \end{bmatrix} = \begin{bmatrix} r(x_1) \\ 0 \\ 0 \\ 0 \\ 0 \end{bmatrix}.$$

The 5×5 matrix on the left-hand side is called the *Sylvester* matrix and is denoted here by $S_{a,b}(x_1)$. The inverse of $S_{a,b}(x_1)$ has the form

$$S_{a,b}^{-1}(x_1) = \frac{1}{\det S_{a,b}(x_1)} \mathrm{adj}\Big(S_{a,b}(x_1)\Big)$$

where $\mathrm{adj}(S_{a,b}(x_1))$ is the adjoint matrix and is a 5×5 *polynomial* matrix in x_1. Solving for $\alpha_i(x_1), \beta_i(x_1)$ gives

$$\begin{bmatrix} \alpha_0(x_1) \\ \alpha_1(x_1) \\ \beta_0(x_1) \\ \beta_1(x_1) \\ \beta_2(x_1) \end{bmatrix} = \frac{\mathrm{adj} S_{a,b}(x_1)}{\det S_{a,b}(x_1)} \begin{bmatrix} r(x_1) \\ 0 \\ 0 \\ 0 \\ 0 \end{bmatrix}.$$

If $r(x_1)$ is chosen as $r(x_1) = \det S_{a,b}(x_1)$, then

$$\begin{bmatrix} \alpha_0(x_1) \\ \alpha_1(x_1) \\ \beta_0(x_1) \\ \beta_1(x_1) \\ \beta_2(x_1) \end{bmatrix} = \mathrm{adj} S_{a,b}(x_1) \begin{bmatrix} 1 \\ 0 \\ 0 \\ 0 \\ 0 \end{bmatrix}.$$

www.EngineeringEBooksPdf.com

This then guarantees that

$$\alpha_0(x_1), \alpha_1(x_1), \beta_0(x_1), \beta_1(x_1), \beta_2(x_1)$$

are polynomials in x_1. That is, the *resultant polynomial* is defined by $r(x_1) \triangleq \det S_{a,b}(x_1)$ and is the polynomial required for (8.137) to hold.

In summary, the polynomials $\{a(x_1, x_2), b(x_1, x_2)\}$ have a common zero at (x_{10}, x_{20}) only if $r(x_{10}) \triangleq \det S_{a,b}(x_{10}) = 0$. For an arbitrary pair of polynomials $\{a(x), b(x)\}$ of degrees n_a and n_b in x, respectively, the *Sylvester* matrix $S_{a,b}$ is of dimension $(n_a + n_b) \times (n_a + n_b)$ (see Refs. [89][90][100]).

Remark It was just shown that if $a(x_{10}, x_{20}) = b(x_{10}, x_{20}) = 0$, then $r(x_{10}) \triangleq \det S_{a,b}(x_{10}) = 0$ as a simple consequence of (8.137). Does

$$r(x_{10}) \triangleq \det S_{a,b}(x_{10}) = 0$$

imply that there exists x_{20} such that

$$a(x_{10}, x_{20}) = b(x_{10}, x_{20}) = 0?$$

Not necessarily. However, the answer is yes if either of the leading coefficients in x_2 of $a(x_1, x_2), b(x_1, x_2)$ are not zero at x_{10}, that is, $a_3(x_{10}) \neq 0$ *or* $b_2(x_{10}) \neq 0$ (see [89][90][100] for detailed explanations).

Example Let

$$\begin{aligned} a(x_1, x_2) &= x_2^2 + x_2 + x_1 \\ b(x_1, x_2) &= -x_1 x_2^2 + x_2 + 1. \end{aligned}$$

The resultant matrix is

$$S_{a,b}(x_1) = \begin{bmatrix} a_0(x_1) & 0 & b_0(x_1) & 0 \\ a_1(x_1) & a_0(x_1) & b_1(x_1) & b_0(x_1) \\ a_2(x_1) & a_1(x_1) & b_2(x_1) & b_1(x_1) \\ 0 & a_2(x_1) & 0 & b_2(x_1) \end{bmatrix} = \begin{bmatrix} x_1 & 0 & 1 & 0 \\ 1 & x_1 & 1 & 1 \\ 1 & 1 & -x_1 & 1 \\ 0 & 1 & 0 & -x_1 \end{bmatrix}$$

and the resultant polynomial is

$$r(x_1) = \det S_{a,b}(x_1) = \left(3 + x_1^2\right) x_1^2$$

with roots

$$\left\{0, 0, j\sqrt{3}, -j\sqrt{3}\right\}.$$

The root at $x_1 = 0$ gives

$$\begin{aligned} a(0, x_2) &= x_2^2 + x_2 = 0 \\ b(0, x_2) &= x_2 + 1 = 0 \end{aligned}$$

making

$$\{(0, -1)\}$$

www.EngineeringEBooksPdf.com

a common zero.

The root at $x_1 = j\sqrt{3}$ gives

$$a(j\sqrt{3}, x_2) = x_2^2 + x_2 + j\sqrt{3} = 0$$

with roots

$$\left\{\frac{1}{2} - j\frac{\sqrt{3}}{2}, -\frac{3}{2} + j\frac{\sqrt{3}}{2}\right\}$$

and

$$b(j\sqrt{3}, x_2) = -i\sqrt{3}x_2^2 + x_2 + 1 = 0$$

with roots

$$\left\{\frac{1}{2} - j\frac{\sqrt{3}}{2}, -\frac{1}{2} + j0.2887\right\}.$$

The only common zero is then

$$\left(j\sqrt{3}, \frac{1}{2} - j\frac{\sqrt{3}}{2}\right).$$

Similarly, the root at $x_1 = -j\sqrt{3}$ results in the common zero

$$\left(-j\sqrt{3}, \frac{1}{2} + j\frac{\sqrt{3}}{2}\right).$$

The set of common zeros of $a(x_1, x_2)$ and $b(x_1, x_2)$ is

$$\left\{(0, -1), \left(j\sqrt{3}, \frac{1}{2} - j\frac{\sqrt{3}}{2}\right), \left(-j\sqrt{3}, \frac{1}{2} + j\frac{\sqrt{3}}{2}\right)\right\}.$$

Problems

Mathematical Models of the Induction Motor

Problem 1 State Space Form

Derive the state-space representation (8.5) from the representation (8.4).

Problem 2 Induction Motor Model in the Space Vector Formulation

The derivation of the model (8.4) is easier using the space vector representation

$$\begin{aligned} R_S\underline{i}_S + L_S\frac{d}{dt}\underline{i}_S + M\frac{d}{dt}\left(\underline{i}_R e^{jn_p\theta}\right) &= \underline{u}_S \\ R_R\underline{i}_R + L_R\frac{d}{dt}\underline{i}_R + M\frac{d}{dt}\left(\underline{i}_S e^{-jn_p\theta}\right) &= 0 \\ n_p M\,\mathrm{Im}\{\underline{i}_S(\underline{i}_R e^{jn_p\theta})^*\} - \tau_L &= J\frac{d\omega}{dt}. \end{aligned}$$

www.EngineeringEBooksPdf.com

To see this, define new (fictitious) flux linkages as

$$\underline{\psi}_R \triangleq \psi_{Ra} + j\psi_{Rb} \triangleq \underline{\lambda}_R e^{jn_p\theta} = L_R \underline{i}_R e^{jn_p\theta} + M\underline{i}_S$$

and show that system of equations for the induction motor can rewritten in the space vector form as

$$\begin{aligned} \frac{d}{dt}\underline{\psi}_R &= \left(-\frac{1}{T_R} + jn_p\omega\right)\underline{\psi}_R + \frac{M}{T_R}\underline{i}_S \\ \underline{u}_S &= \frac{M}{L_R}\frac{d}{dt}\underline{\psi}_R + \sigma L_S \frac{d}{dt}\underline{i}_S + R_S\underline{i}_S \\ \frac{d\omega}{dt} &= \mu\,\mathrm{Im}\{\underline{i}_S(\underline{\psi}_R)^*\} - \frac{\tau_L}{J} \end{aligned}$$

where $\mu \triangleq n_p M/(JL_R)$, $\sigma \triangleq 1 - M^2/L_S L_R$ *is the leakage factor, and* $T_R \triangleq L_R/R_R$ *is the rotor time constant. This problem illustrates the power of the space vector representation as the manipulations of the equations are carried out using (complex) scalar variables rather than dealing with matrix multiplications, matrix inverses, and so on.*

Problem 3 Induction Motor Model in Terms of the Flux Linkages

With $\lambda_{Sa}, \lambda_{Sb}$ *the flux linkage in stator phases a and b respectively, define*

$$\underline{\lambda}_S \triangleq \lambda_{Sa} + j\lambda_{Sb} \triangleq L_S\underline{i}_S + M\underline{i}_R e^{+jn_p\theta}.$$

Similarly, let λ_{Ra} *and* λ_{Rb} *be the flux linkage in rotor phases a and b, respectively, and define*

$$\underline{\lambda}_R \triangleq \lambda_{Ra} + j\lambda_{Rb} \triangleq L_R\underline{i}_R + M\underline{i}_S e^{-jn_p\theta}.$$

(a) Show that the electrical equations of the induction motor may be written as

$$\begin{aligned} R_S\underline{i}_S + \frac{d}{dt}\underline{\lambda}_S &= \underline{u}_S \\ R_R\underline{i}_R + \frac{d}{dt}\underline{\lambda}_R &= 0. \end{aligned}$$

(b) Using the fact that

$$\begin{bmatrix} \underline{i}_S \\ \underline{i}_R e^{+jn_p\theta} \end{bmatrix} = \frac{1}{L_S L_R - M^2}\begin{bmatrix} +L_R & -M \\ -M & +L_S \end{bmatrix}\begin{bmatrix} \underline{\lambda}_S \\ \underline{\lambda}_R e^{+jn_p\theta} \end{bmatrix}$$

show that

$$\begin{aligned} \frac{R_S}{L_S L_R - M^2}\left(L_R\underline{\lambda}_S - M\underline{\lambda}_R e^{+jn_p\theta}\right) + \frac{d}{dt}\underline{\lambda}_S &= \underline{u}_S \\ \frac{R_R}{L_S L_R - M^2}\left(-M\underline{\lambda}_S e^{-jn_p\theta} + L_S\underline{\lambda}_R\right) + \frac{d}{dt}\underline{\lambda}_R &= 0 \\ \frac{M}{L_S L_R - M^2}\,\mathrm{Im}\{\underline{\lambda}_S(\underline{\lambda}_R e^{+jn_p\theta})^*\} - \tau_L &= J\frac{d\omega}{dt} \end{aligned}$$

www.EngineeringEBooksPdf.com

is a representation of the induction motor in terms of $\underline{\lambda}_S \triangleq \lambda_{Sa}+j\lambda_{Sb}, \underline{\lambda}_R \triangleq \lambda_{Ra}+j\lambda_{Rb}$, *and* ω.

Problem 4 Field-Oriented Induction Motor Model

The space vector model of the induction motor

$$\begin{aligned}\frac{d}{dt}\underline{\psi}_R &= \left(-\frac{1}{T_R}+jn_p\omega\right)\underline{\psi}_R+\frac{M}{T_R}\underline{i}_S\\ \underline{u}_S &= \frac{M}{L_R}\frac{d}{dt}\underline{\psi}_R+\sigma L_S\frac{d}{dt}\underline{i}_S+R_S\underline{i}_S\\ \frac{d\omega}{dt} &= \mu\,\mathrm{Im}\{\underline{i}_S(\underline{\psi}_R)^*\}-\frac{\tau_L}{J}\end{aligned}$$

is derived in problem 2. Let $\underline{\psi}_R \triangleq \psi_{Ra}+j\psi_{Rb}=\psi_d e^{j\rho}$ *where* $\psi_d \triangleq \sqrt{\psi_{Ra}^2+\psi_{Rb}^2}, \rho \triangleq \tan^{-1}(\psi_{Rb}/\psi_{Ra})$ *and further let* $\underline{i}_{dq} \triangleq i_d+ji_q=\underline{i}_S e^{-j\rho}$, *and* $\underline{u}_{dq} \triangleq u_d+ju_q=\underline{u}_S e^{-j\rho}$.

(a) Find the field-oriented space vector representation of the induction motor, that is, in terms of $\psi_d, \rho, \underline{i}_{dq} \triangleq i_d+ji_q$, *and* $\underline{u}_{dq} \triangleq u_d+ju_q$

(b) Use the answer from part (a) to find a state space representation of the field-oriented induction motor model, that is, in terms of the state variables $i_d, i_q, \psi_d, \rho, \omega$, *and* θ *and the inputs* u_d *and* u_q.

Problem 5 Stator Flux Induction Motor Model

(a) The stator flux linkage is given by

$$\underline{\lambda}_S = L_S\underline{i}_S+M\left(\underline{i}_R e^{jn_p\theta}\right)=\lambda_S e^{j\rho_S}.$$

Rewrite the system model

$$\begin{aligned}R_S\underline{i}_S+L_S\frac{d}{dt}\underline{i}_S+M\frac{d}{dt}\left(\underline{i}_R e^{jn_p\theta}\right) &= \underline{u}_S\\ R_R\underline{i}_R+L_R\frac{d}{dt}\underline{i}_R+M\frac{d}{dt}\left(\underline{i}_S e^{-jn_p\theta}\right) &= 0\\ n_pM\,\mathrm{Im}\left\{\underline{i}_S\left(\underline{i}_R e^{jn_p\theta}\right)^*\right\}-\tau_L &= J\frac{d\omega}{dt}\end{aligned}$$

in terms of $\underline{\lambda}_S, \underline{i}_S$, *and* ω.

(b) Put the result from part (a) in state space form.

Problem 6 ψ_d and ψ_q

Show that $\cos(\rho)=\psi_{Ra}/\psi_d$, $\sin(\rho)=\psi_{Rb}/\psi_d$, *and*

$$\begin{bmatrix}\psi_d\\ \psi_q\end{bmatrix} \triangleq \begin{bmatrix}\cos(\rho) & \sin(\rho)\\ -\sin(\rho) & \cos(\rho)\end{bmatrix}\begin{bmatrix}\psi_{Ra}\\ \psi_{Rb}\end{bmatrix}$$

where $\psi_q \equiv 0$.

www.EngineeringEBooksPdf.com

Feedback Control and Reference Trajectories

Problem 7 Tracking a Constant Flux Reference

Let $e_0 = \int_0^t (\psi_{d0} - \psi_d)dt$ *and* $e_1 = \psi_{d0} - \psi_d$ *and assuming that* $\psi_{d0} = Mi_{d0}$, *show how to choose the gains* $K_{\psi P}$ *and* $K_{\psi I}$ *in (8.20) so that* $e_0(t) \to 0, e_1(t) \to 0$ *as* $t \to \infty$.

Problem 8 Trajectory Tracking via Field-Oriented Control

Let $e_0 = \int_0^t (\theta_{ref} - \theta)dt$, $e_1 = \theta_{ref} - \theta$, $e_2 = \omega_{ref} - \omega$, *and, assuming that* $\psi_d = \psi_{d0}$, *show how to choose the gains* K_0, K_1, *and* K_2 *in (8.19) so that the closed-loop poles are in the open left-half plane located at* $-r_1, -r_2, -r_3$ $(r_1 > 0, r_2 > 0, r_3 > 0)$. *If* τ_L *is constant, show that* $e_1(t) \to 0, e_2(t) \to 0$ *as* $t \to \infty$. *(Hint: Review Chapter 2.)*

Problem 9 Back Emf

With reference to the field-oriented model (8.9) of the induction motor, explain why $Mn_p\omega\psi_d/L_R$ *is the* back emf. *(The term "back emf" refers to the voltage* $v_{backemf}$ *that results in energy conversion from electrical to mechanical, that is,* $i_q v_{backemf} = \tau\omega$.*)*

Problem 10 Tracking a Time Varying Flux Reference

Consider the input-output linearization controller presented in Section 8.2.4. Let $\psi_{dref}(t)$ *be a desired flux reference with* i_{dref} *chosen to satisfy*

$$d\psi_{dref}/dt = -\eta\psi_{dref} + \eta M i_{dref}.$$

Choose

$$u_1 = i_{dr} = K_{\psi P}(\psi_{dref} - \psi_d) + K_{\psi I}\int_0^t (\psi_{dref} - \psi_d)dt + i_{dref}$$

and with $e_0 = \int_0^t (\psi_{dref} - \psi_d)dt, e_1 = \psi_{dref} - \psi_d$, *show how to choose the gains* $K_{\psi P}$ *and* $K_{\psi I}$ *such that* $e_0(t) \to 0, e_1(t) \to 0$ *as* $t \to \infty$. *(In practice,* i_{dref} *is usually set to zero with no significant deterioration in tracking.)*

Problem 11 Trajectory Tracking Via Input-Output Linearization

With $e_0 = \int_0^t (\theta_{ref} - \theta)dt$, $e_1 = \theta_{ref} - \theta$, $e_2 = \omega_{ref} - \omega$ *show how to choose the gains* K_0, K_1, *and* K_2 *in (8.32) so that the closed-loop poles are in the open left-half plane located at* $-r_1, -r_2, -r_3$ $(r_1 > 0, r_2 > 0, r_3 > 0)$. *Show that if* τ_L *is constant, then* $e_1(t) \to 0, e_2(t) \to 0$ *as* $t \to \infty$.

Problem 12 Field Weakening

Explain why field weakening is only needed when the induction machine is motoring (accelerating). That is, even if the motor is running at high speed, but one wants to decelerate *it down to zero (so it is generating rather than motoring), then the voltage limit* V_{max} *is not a constraint in bringing the flux* ψ_d *back up to* ψ_{d0}. *(However, most amplifiers are switching amplifiers and the blocking voltage rating of the switches must be respected.)*

www.EngineeringEBooksPdf.com

Problem 13 Maximum Torque

In steady state the currents in a two-phase motor are of the form $i_{Sa} = I\cos(\omega_S t+\phi_S), i_{Sb} = I\cos(\omega_S t+\phi_S-\pi/2)$ *so that* $i_{d0}^2+i_{q0}^2 = i_{Sa}^2+i_{Sb}^2 = I^2$. *Show that the steady-state torque* $\tau = J\mu\psi_{d0}i_{q0} = J\mu M i_{d0}i_{q0}$ *subject to* $i_{d0}^2 + i_{q0}^2 \leq I_{max}^2$ *is maximized by choosing* $i_{d0} = i_{q0} = I_{max}/\sqrt{2}$. *This is used only at lower speeds where the voltage constraint* $u_{Sa}^2+u_{Sb}^2 \leq V_{max}$ *will not be violated. (Note that if, for example,* $I_{max} = 6.0$ *A, then one might choose* $i_{d0} = 5.5/\sqrt{2}$ *so as to not operate at the current limit.)*

Problem 14 Closed-Loop Poles of the Field-Oriented and Input-Output Controller

(a) Using the motor parameters given in Section 8.2.2 and the gains of the field-oriented controller given by (8.22) and (8.23), compute the closed loop poles of the mechanical trajectory tracking error system as well as the closed-loop poles of the flux tracking error system.

(b) Repeat part (a) using the gain values of the input-output controller of Section 8.2.5.

Problem 15 Simulation of an Input-Output Linearization Controller

Let the parameters of the system be $n_p = 3$, $M = 0.0117$ *H*, $R_R = 3.9$ Ω, $R_S = 1.7$ $\Omega, L_R = 0.014$ *H*, $L_S = 0.014$ *H*, $f = 0$ *N-m/rad/sec,and* $J = 0.00011$ *kg-m*^{2}, $i_{d0} = 5.5/\sqrt{2}$, $\psi_{d0} = Mi_{d0}$, $\omega_{base} = 250$ *rad/sec*, $I_{max} = 6$ *A*, $V_{max} = 60$ *V [42].*

Simulate the complete input−output linearization controller for the induction motor. To simplify the matter, do the complete simulation in continuous time and assume that both speed and position measurements are available. Specifically,

Add the flux observer using equations (8.37). Check that this is working by comparing ρ *and* ψ_d *from the estimator with* $\tan^{-1}(\psi_{Rb}/\psi_{Ra})$ *and* $\sqrt{\psi_{Rb}^2+\psi_{Ra}^2}$ *from the simulation of the motor. Note from (8.37) that the direct and quadrature currents* i_d *and* i_q *are computed in the flux estimator.*

Add the PI current controllers described by (8.12) to the simulation so that the setup of Figure 8.3 results. Check that current controllers are working by commanding constant currents $i_{dr} = i_{d0}$ *and* $i_{qr} = i_{q0}$ *to see if* $i_d \to i_{d0}, i_q \to i_{q0}$, *respectively.*

Choose i_{dr} *and* i_{qr} *as given in (8.27) where* u_1 *is chosen as given in (8.31) and* u_2 *is chosen as given in (8.32). Let the flux reference be given by (8.24) where* $\omega_{base} = 250$ *rads/sec and* $\psi_{d0} = Mi_{d0}$ *with* $i_{d0} = 5.5/\sqrt{2}$. *Also, just take* $i_{dref} = 0$.

Add the trajectory generator to the simulation.

(a) Try a trajectory specified by $\omega_{\max} = 75$ *rads/sec*, $t_1 = 0.025$ *sec and* $\theta_f = \pi$. *Set the gains of the system to obtain tracking of the mechanical trajectory* $(\theta_{ref}, \omega_{ref})$ *and the flux reference* ψ_{d0}, *and run the simulation. Do you need to let the flux* ψ_d *build up before starting the* 180° *turn?*

(b) Try a high-speed trajectory specified by $\omega_{\max} = (2\pi/60)8000 = 838$

www.EngineeringEBooksPdf.com

rads/sec, $t_1 = 1.5$ seconds, $t_2 = t_1 + 0.1$ sec ($\theta_f = \omega_{\max} t_2$). Set the gains of the system to obtain tracking of the mechanical trajectory $(\theta_{ref}, \omega_{ref})$ and the flux reference ψ_{dref}, and run the simulation.

Problem 16 i_{dref}

Given a mechanical trajectory mechanical trajectory $(\theta_{ref}, \omega_{ref}, \alpha_{ref})$, show how to obtain the reference current i_{dref} corresponding to the flux reference ψ_{dref} specified by (8.24).

Problem 17 Nested Loop Control Structure [2]

Consider the (nested loop) control structure of Figure 8.34 following Figures 12.14 *and* 12.27 *of Ref.* [2]. *The block labeled "induction motor" is considered to be the model (8.9) with the decoupling feedback (8.10) applied, that is, the system (8.11). Using the model (8.11), and the controller given in Figure 8.34 with ψ_{dref} given by (8.24), do an analysis of this controller. In particular, with ψ_{dref} constant, can you show how to specify the controller gains so that the closed-loop system is stable? What if ψ_{dref} is not constant?*

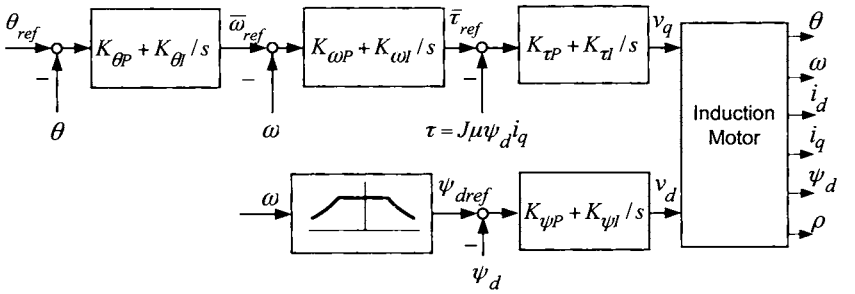


FIGURE 8.34. Nested loop control structure for the induction motor.

Field Energy and Torque

Problem 18 Torque from Conservation of Energy

(a) Multiply the fourth equation of (8.9) by $\sigma L_S i_d$, the fifth equation of (8.9) by $\sigma L_S i_q$ and add to obtain

$$\begin{aligned} i_d u_d + i_q u_q &= \frac{1}{2}\sigma L_S \frac{d}{dt}\left(i_d^2 + i_q^2\right) + \sigma L_S \gamma \left(i_d^2 + i_q^2\right) - (\eta M / L_R)\psi_d i_d \\ &\quad + (n_p M / L_R)\omega \psi_d i_q. \end{aligned}$$

(b) In Chapter 6 *it was shown that the field energy (the energy stored in the magnetic field of the air gap) is given by*

$$\begin{aligned} W_{field}(i_{Sa}, i_{Sb}, i_{Ra}, i_{Rb}, \theta) &\triangleq \frac{1}{2}L_S(i_{Sa}^2 + i_{Sb}^2) + \frac{1}{2}L_R(i_{Ra}^2 + i_{Rb}^2) \\ &+ M i_{Sa}\Big(i_{Ra}\cos(\theta) - i_{Rb}\sin(\theta)\Big) + M i_{Sb}\Big(i_{Ra}\sin(\theta) + i_{Rb}\cos(\theta)\Big). \end{aligned}$$

www.EngineeringEBooksPdf.com

Show that in the $(i_{Sa}, i_{Sb}, \psi_{Ra}, \psi_{Rb}, \theta, \omega)$ *coordinate system, the field energy is given by*

$$W_{field} = \frac{1}{2}L_S(i_{Sa}^2 + i_{Sb}^2) + \frac{1}{2}\frac{1}{L_R}\left(\psi_{Ra}^2 + \psi_{Rb}^2\right) - \frac{1}{2}\frac{M^2}{L_R}\left(i_{Sa}^2 + i_{Sb}^2\right)$$

and therefore in the dq coordinate system it is given by

$$W_{field} = \frac{1}{2}\sigma L_S(i_d^2 + i_q^2) + \frac{1}{2}\frac{1}{L_R}\psi_d^2.$$

(c) Conservation of energy (power) requires that

$$\frac{d}{dt}W_{field} + R_S\left(i_{Sa}^2 + i_{Sb}^2\right) + R_R(i_{Ra}^2 + i_{Rb}^2) + \tau\omega = i_{Sa}u_{Sa} + i_{Sb}u_{Sb}$$

where $\tau\omega$ *is the mechanical power produced. Rewrite this in the field-oriented coordinate system and compare with the answer to part (a) to conclude that* $\tau = (n_p M/L_R)\psi_d i_q$.

Observers

Problem 19 Discretization of the Flux Observer

Using Euler's approximation for the derivatives, that is,

$$\begin{aligned}\dot{\psi}_{Ra}(kT) &\approx \left(\psi_{Ra}((k+1)T) - \psi_{Ra}(kT)\right)/T \\ \dot{\psi}_{Rb}(kT) &\approx \left(\psi_{Rb}((k+1)/T) - \psi_{Rb}(kT)\right)/T\end{aligned}$$

a discretized version of (8.34) is given by

$$\begin{aligned}\psi_{Ra}((k+1)T) &= (1-\eta T)\psi_{Ra}(kT) - n_p T\omega(kT)\psi_{Rb}(kT) + \eta M T i_{Sa}(kT \\ \psi_{Rb}((k+1)T) &= n_p T\omega(kT)\psi_{Ra}(kT) + (1-\eta T)\psi_{Rb}(kT) + \eta M T i_{Sb}(kT\end{aligned}$$

An observer for this discretized system is then a discretized version of (8.35) given by

$$\begin{aligned}\hat{\psi}_{Ra}((k+1)T) &= (1-\eta T)\hat{\psi}_{Ra}(kT) - n_p T\omega(kT)\hat{\psi}_{Rb}(kT) + \eta M T i_{Sa}(kT \\ \hat{\psi}_{Rb}((k+1)T) &= n_p T\omega(kT)\hat{\psi}_{Ra}(kT) + (1-\eta T)\hat{\psi}_{Rb}(kT) + \eta M T i_{Sb}(kT\end{aligned}$$

Simulate this discrete *version of the observer (8.35) with the inputs to the motor given by* $u_{Sa} = V\cos(\omega_S t)$, $u_{Sb} = V\sin(\omega_S t)$, $\omega_S = (2\pi)60$ *rad/sec,* $V = 80$ *V, and* $\tau_L = 0$. *Plot out the discrete estimates* $\hat{\psi}_{Ra}$ *and* $\hat{\psi}_{Rb}$ *and compare with the actual values* ψ_{Ra} *and* ψ_{Rb}, *respectively. Try sample rates of* 2 *kHz,* 10 *kHz, and* 20 *kHz.*

Problem 20 Stability of a Discrete Flux Observer

Consider the stability of the discrete-time flux estimator of problem 19, define

$$\begin{aligned}e_{Ra}((k+1)T) &\triangleq \psi_{Ra}((k+1)T) - \hat{\psi}_{Ra}((k+1)T) \\ e_{Rb}((k+1)T) &\triangleq \psi_{Rb}((k+1)T) - \hat{\psi}_{Rb}((k+1)T)\end{aligned}$$

www.EngineeringEBooksPdf.com

and show that these error variables satisfy

$$\begin{bmatrix} e_{Ra}((k+1)T) \\ e_{Rb}((k+1)T) \end{bmatrix} = \begin{bmatrix} 1-\eta T & -n_p\omega(k)T \\ n_p\omega(k)T & 1-\eta T \end{bmatrix} \begin{bmatrix} e_{Ra}(kT) \\ e_{Rb}(kT) \end{bmatrix}.$$

Next, define the discrete-time function $V(kT)$ *as*

$$V(kT) \triangleq e_{Ra}^2(kT) + e_{Rb}^2(kT)$$

and show that

$$V((k+1)T) = \left((1-\eta T)^2 + (n_p\omega(kT)T)^2\right) V(kT).$$

Use this to find the conditions on the sample period T *and speed* ω *such that* $V(kT) \to 0$ *as* $t \to \infty$. *In particular, find the value of* T *that minimizes* $(1-\eta T)^2 + (n_p\omega_{\max}T)^2$, *where* $\omega_{\max}$ *is the maximum speed the motor is to be run. With* $\omega_{\max} = 2\pi(60)$ *rads/sec and sample rates of* 330 *Hz,* 1 *kHz, and* 10 *kHz, is the system (8.35) stable? Are your results consistent with your simulation?*

Problem 21 Discretization of the Flux Observer in the Field-Oriented Coordinate System

Simulate a discrete-time version of the equations (8.37). Plot out the discrete estimates $\hat{\rho}$ *and* $\hat{\psi}_d$, *compute* $\hat{\psi}_{Ra} = \hat{\psi}_d\cos(\hat{\rho})$ *and* $\hat{\psi}_{Rb} = \hat{\psi}_d\sin(\hat{\rho})$ *and compare with* ψ_{Ra} *and* ψ_{Rb}, *respectively. Try sample rates of* 330 *Hz,* 1 *kHz, and* 10 *kHz.*

Problem 22 Discretization of the Flux Observer Equations [73]

Consider another discretization of the flux equations (8.34) by writing them in the form

$$\frac{d}{dt}\begin{bmatrix} \psi_{Ra} \\ \psi_{Rb} \end{bmatrix} = \begin{bmatrix} -\eta & -n_p\omega \\ n_p\omega & -\eta \end{bmatrix} \begin{bmatrix} \psi_{Ra} \\ \psi_{Rb} \end{bmatrix} + \eta M \begin{bmatrix} i_{Sa} \\ i_{Sb} \end{bmatrix}$$

(a) Assuming that $\omega(t), i_{Sa}(t)$, *and* $i_{Sb}(t)$ *are constant over the sample period* T, *show that*

$$\begin{bmatrix} \psi_{Ra}((k+1)T) \\ \psi_{Rb}((k+1)T) \end{bmatrix} = e^{(-\eta\mathbf{I}+n_p\omega(kT)\mathbf{J})T} \begin{bmatrix} \psi_{Ra}(kT) \\ \psi_{Rb}(kT) \end{bmatrix} + \left(\int_0^T e^{(-\eta\mathbf{I}+n_p\omega(kT)\mathbf{J})(T-t)}\eta M dt\right) \begin{bmatrix} i_{Sa}(kT) \\ i_{Sb}(kT) \end{bmatrix}$$

where $\mathbf{I} \triangleq \begin{bmatrix} 1 & 0 \\ 0 & 1 \end{bmatrix}, \mathbf{J} \triangleq \begin{bmatrix} 0 & -1 \\ 1 & 0 \end{bmatrix}$.

www.EngineeringEBooksPdf.com

(b) Using the expressions

$$\begin{aligned}
\int e^{at}\cos(bt)dt &= \frac{e^{at}}{a^2+b^2}\left(a\cos(bt)+b\sin(bt)\right)\\
\int e^{a(T-t)}\cos(b(T-t))dt &= -\frac{e^{a(T-t)}}{a^2+b^2}\left(a\cos(b(T-t))+b\sin(b(T-t))\right)\\
\int e^{at}\sin(bt)dt &= \frac{e^{at}}{a^2+b^2}\left(a\sin(bt)-b\cos(bt)\right)\\
\int e^{a(T-t)}\sin(b(T-t))dt &= -\frac{e^{a(T-t)}}{a^2+b^2}\left(a\sin(b(T-t))-b\cos(b(T-t))\right)
\end{aligned}$$

show that

$$e^{(-\eta\mathbf{I}+n_p\omega(kT)\mathbf{J})T} = \begin{bmatrix} e^{-\eta T} & 0\\ 0 & e^{-\eta T}\end{bmatrix}\begin{bmatrix}\cos(n_p\omega(kT)) & -\sin(n_p\omega(kT)\\ \sin(n_p\omega(kT)) & \cos(n_p\omega(kT))\end{bmatrix}$$

and

$$\int_0^T e^{(-\eta\mathbf{I}+n_p\omega(kT)\mathbf{J})(T-t)}dt = \frac{1}{\eta^2+(n_p\omega(kT))^2} \times \begin{bmatrix} e^{-\eta T}d_1(kT)+\eta & -e^{-\eta T}d_2(kT)-n_p\omega(kT)\\ e^{-\eta T}d_2(kT)+n_p\omega(kT) & e^{-\eta T}d_1(kT)+\eta\end{bmatrix}$$

where

$$\begin{aligned}
d_1(kT) &\triangleq -\eta\cos(n_p\omega(kT)T)+n_p\omega(kT)\sin(n_p\omega(kT)T)\\
d_2(kT) &\triangleq -\eta\sin(n_p\omega(kT)T)-n_p\omega(kT)\cos(n_p\omega(kT)T).
\end{aligned}$$

(c) Use this discretization of the flux linkage equations to define an observer.

(d) With the flux estimate error defined by

$$\begin{aligned}
e_{Ra}((k+1)T) &\triangleq \psi_{Ra}((k+1)T)-\hat{\psi}_{Ra}((k+1)T)\\
e_{Rb}((k+1)T) &\triangleq \psi_{Rb}((k+1)T)-\hat{\psi}_{Rb}((k+1)T)
\end{aligned}$$

use the (Lyapunov) function

$$V(kT) \triangleq e_{Ra}^2(kT)+e_{Rb}^2(kT)$$

to show that

$$V((k+1)T) = e^{-2\eta T}V(kT).$$

(e) Simulate this discrete-time flux observer with the inputs to the motor given by $u_{Sa} = V\cos(\omega_S t)$, $u_{Sb} = V\sin(\omega_S t)$ *where* $\omega_S = (2\pi)60$ *rad/sec and* $V = 80$ *V*, $\tau_L = 0$. *Plot out the discrete estimates* $\hat{\psi}_{Ra}$ *and* $\hat{\psi}_{Rb}$, *and compare with their actual values* ψ_{Ra} *and* ψ_{Rb}. *Try sample rates of* 330 *Hz*, 1 *kHz, and* 10 *kHz.*

www.EngineeringEBooksPdf.com

Problem 23 Flux Observer Based on Position Measurements [67]

Consider the flux observer (8.37). Make a change of variables from (ρ, ψ_d) *to* (s, ψ_d) *where* $s(t) \triangleq \rho(t) - n_p\theta(t)$ *and show that*

$$\begin{aligned} \frac{d\hat{s}}{dt} &= \eta M \left(-i_{Sa} \sin(\hat{\rho}) + i_{Sb} \cos(\hat{\rho}) \right) / \hat{\psi}_d \\ \frac{d\hat{\psi}_d}{dt} &= -\eta \hat{\psi}_d + \eta M \left(i_{Sa} \cos(\hat{\rho}) + i_{Sb} \sin(\hat{\rho}) \right) \end{aligned}$$

where

$$\hat{\rho}(t) \triangleq n_p\theta(t) + \hat{s}(t)$$

is an estimator for ρ, ψ_d*. Note that this flux estimator requires the stator currents and rotor position, but not the rotor speed.*

Problem 24 Speed Observer

(a) Implement a discretized version of the speed observer

$$\begin{aligned} \frac{d\hat{\theta}}{dt} &= \hat{\omega} + \ell_1(\theta_c - \hat{\theta}) \\ \frac{d\hat{\omega}}{dt} &= \mu \hat{\psi}_d \hat{i}_q + \ell_2(\theta_c - \hat{\theta}) \end{aligned}$$

using the Euler approximation for the derivatives where $\theta_c(t) \triangleq \frac{2\pi}{2000} N(t)$ *in which* $N(t)$ *is the position of the motor in encoder counts. Set the inputs to the motor as* $u_{Sa} = V\cos(\omega_S t)$, $u_{Sb} = V\sin(\omega_S t)$ *(*$\omega_S = (2\pi)60$ *rad/sec, and* $V = 80$ *V). To simulate the encoder count* N*, simply set* $N =$ `floor`$(\frac{2000}{2\pi}\theta)$*, where* `floor(x)` *is the largest integer less than or equal to* x*.*

(b) Compare the speed estimate $\hat{\omega}$ *from the observer with that obtained from numerically differentiating the output of the encoder as* $\hat{\omega}_1(kT) = (\theta_c(kT) - \theta_c((k-1)T))/T$*. Also, compare with the actual speed* ω*. Try sample rates of* 1 *kHz,* 2 *kHz, and* 10 *kHz.*

(c) Show that a (Euler) discretized version of the error *equations for the above speed observer are given by*

$$\begin{bmatrix} e_1(k+1) \\ e_2(k+1) \end{bmatrix} = \begin{bmatrix} 1 - \ell_1 T & T \\ -\ell_2 & 1 \end{bmatrix} \begin{bmatrix} e_1(k) \\ e_2(k) \end{bmatrix}$$

where T *is the sample period,* ℓ_1 *and* ℓ_2 *are the observer gains,* $e_1(k) = \theta_c(kT) - \hat{\theta}(kT)$ *and* $e_2(k) = \omega(kT) - \hat{\omega}(kT)$*. Compute the eigenvalues of the error system in terms of* T*,* ℓ_1*, and* ℓ_2*. Is the discretized speed observer stable, that is, are the magnitudes of the eigenvalues less than* 1 *for the gains and sample rates chosen in your simulation?*

www.EngineeringEBooksPdf.com

Problem 25 Speed and Load-Torque Observer

Consider a modification of the speed observer to estimate any constant (or, slowly varying) load torque. Specifically, with the load torque τ_L assumed constant, consider a speed and load-torque estimator given by

$$\begin{aligned} \frac{d\hat{\theta}}{dt} &= \hat{\omega} + \ell_1(\theta - \hat{\theta}) \\ \frac{d\hat{\omega}}{dt} &= \mu\hat{\psi}_d\hat{i}_q - \hat{\tau}_L/J + \ell_2(\theta - \hat{\theta}) \\ \frac{d(\hat{\tau}_L/J)}{dt} &= 0 + \ell_3(\theta - \hat{\theta}). \end{aligned}$$

(a) With $e_1 = \theta - \hat{\theta}, e_2 = \omega - \hat{\omega}$, and $e_3 = \tau_L/J - \hat{\tau}_L/J$, find the equations describing the error system assuming $\hat{\psi}_d\hat{i}_q = \psi_d i_q$. For an appropriate choice of the observer gains ℓ_1, ℓ_2, and ℓ_3, show that $e(t) = (e_1(t), e_2(t), e_3(t)) \to 0$ as $t \to \infty$.

(b) Assume that $\hat{\psi}_d\hat{i}_q \neq \psi_d i_q$, but that their difference is constant. That is, let $\varepsilon_{\tau/J} \triangleq \mu\hat{\psi}_d\hat{i}_q - \mu\psi_d i_q$ be constant. Show that it still true that $e_1(t) = \theta(t) - \hat{\theta}(t) \to 0$ and $e_2(t) = \omega(t) - \hat{\omega}(t) \to 0$ as $t \to \infty$.

Problem 26 Flux and Speed Observer

Consider the following approach to estimating the flux linkages and speed simultaneously. The stator currents i_{Sa} and i_{Sb} and flux linkages ψ_{Ra} and ψ_{Rb} are rotated by the angle $n_p\theta$ to obtain

$$\begin{bmatrix} i_{Sx} \\ i_{Sy} \end{bmatrix} \triangleq \begin{bmatrix} \cos(n_p\theta) & \sin(n_p\theta) \\ -\sin(n_p\theta) & \cos(n_p\theta) \end{bmatrix} \begin{bmatrix} i_{Sa} \\ i_{Sb} \end{bmatrix}$$

$$\begin{bmatrix} \psi_{Rx} \\ \psi_{Ry} \end{bmatrix} \triangleq \begin{bmatrix} \cos(n_p\theta) & \sin(n_p\theta) \\ -\sin(n_p\theta) & \cos(n_p\theta) \end{bmatrix} \begin{bmatrix} \psi_{Ra} \\ \psi_{Rb} \end{bmatrix}.$$

The currents i_{Sx} and i_{Sy} are known *as the angle θ is measured. Note also that $\psi_{Rx} = \lambda_{Ra}$ and $\psi_{Ry} = \lambda_{Rb}$, that is, they are the actual flux linkages in the rotor windings as given in (8.2). In order to estimate the load torque, it is modeled as a constant so that its dynamic equation is taken to be $d(\tau_L/J)/dt = 0$.*

(a) In terms of the new state variables $i_{Sx}, i_{Sy}, \psi_{Rx} = \lambda_{Ra}$, and $\psi_{Ry} =$

www.EngineeringEBooksPdf.com

λ_{Rb}, *show that*

$$\begin{aligned}
\frac{d\psi_{Rx}}{dt} &= -\frac{R_R}{L_R}\psi_{Rx} + \frac{MR_R}{L_R}i_{Sx} \\
\frac{d\psi_{Ry}}{dt} &= -\frac{R_R}{L_R}\psi_{Ry} + \frac{MR_R}{L_R}i_{Sy} \\
\frac{d\theta}{dt} &= \omega \\
\frac{d\omega}{dt} &= \mu(i_{Sy}\psi_{Rx} - i_{Sx}\psi_{Ry}) - \frac{f}{J}\omega - \tau_L/J \\
\frac{d(\tau_L/J)}{dt} &= 0.
\end{aligned}$$

The key point here is that in this state-space representation, the (unmeasured) speed ω *has been eliminated from the flux equations.*

(b) Define an estimator for the flux linkages, speed, and load torque by

$$\begin{aligned}
\frac{d\hat{\psi}_{Rx}}{dt} &= -\frac{R_R}{L_R}\hat{\psi}_{Rx} + \frac{MR_R}{L_R}i_{Sx} \\
\frac{d\hat{\psi}_{Rx}}{dt} &= -\frac{R_R}{L_R}\hat{\psi}_{Ry} + \frac{MR_R}{L_R}i_{Sy} \\
\frac{d\theta}{dt} &= \hat{\omega} + \ell_1(\theta - \hat{\theta}) \\
\frac{d\omega}{dt} &= \mu(i_{Sy}\hat{\psi}_{Rx} - i_{Sx}\hat{\psi}_{Ry}) - \frac{f}{J}\omega - \frac{\hat{\tau}_L}{J} + \ell_2(\theta - \hat{\theta}) \\
\frac{d(\hat{\tau}_L/J)}{dt} &= 0 + \ell_3(\theta - \hat{\theta}).
\end{aligned}$$

With $e_{Rx} \triangleq \psi_{Rx} - \hat{\psi}_{Rx}, e_{Ry} \triangleq \psi_{Ry} - \hat{\psi}_{Ry}$, $e_\theta \triangleq \theta - \hat{\theta}$, $e_\omega \triangleq \omega - \hat{\omega}$, *and* $e_{\tau_L} \triangleq \tau_L/J - \hat{\tau}_L$, *show that the error system is given by*

$$\begin{aligned}
\frac{de_{Rx}}{dt} &= -\frac{R_R}{L_R}e_{Rx} \\
\frac{de_{Ry}}{dt} &= -\frac{R_R}{L_R}e_{Ry} \\
\frac{de_\theta}{dt} &= e_\omega - \ell_1(\theta - \hat{\theta}) \\
\frac{de_\omega}{dt} &= \mu(i_{Sy}e_{Rx} - i_{Sx}e_{Ry}) - \frac{f}{J}e_\omega - e_{\tau_L} - \ell_2(\theta - \hat{\theta}) \\
\frac{de_{\tau_L}}{dt} &= 0 - \ell_3(\theta - \hat{\theta}).
\end{aligned}$$

(c) As long as the currents i_{Sx} *and* i_{Sy} *are bounded (consistent with the assumed current-command operation), show that the error system is stable. Note that the rate of convergence of the error dynamics of this observer is still limited by the rotor time constant* $T_R = L_R/R_R = 1/\eta$ *[73].*

www.EngineeringEBooksPdf.com

Flux Observers with an Arbitrary Rate of Convergence

Martin and Rouchon [74][75] have developed an observer that generalizes the results of Verghese and Sanders [73] presented in Section 8.3.3. Specifically, their method results in an error system with complex eigenvalues whose rate of convergence can be arbitrarily specified. This is outlined in the next problem.

Problem 27 Martin-Rouchon Observer [74][75]

The equations in space vector form may be written as

$$\begin{aligned} R_S \underline{i}_S + \frac{d}{dt}\underline{\lambda}_S &= \underline{u}_S \\ R_R \underline{i}_R + \frac{d}{dt}\underline{\lambda}_R &= 0 \end{aligned} \tag{8.138}$$

where $\underline{i}_S = i_{Sa} + j i_{Sb}$, *and so on, and the flux linkages and currents are related by*

$$\begin{aligned} \underline{\lambda}_S &\triangleq \lambda_{Sa} + j\lambda_{Sb} \triangleq L_S \underline{i}_S + M \underline{i}_R e^{+j\theta_R} \\ \underline{\lambda}_R &\triangleq \lambda_{Ra} + j\lambda_{Rb} \triangleq L_R \underline{i}_R + M \underline{i}_S e^{-j\theta_R}. \end{aligned} \tag{8.139}$$

(a) Rearrange the first equation of (8.139) to obtain

$$\underline{i}_R e^{j\theta_R} = \frac{1}{M}\left(\underline{\lambda}_S - L_S \underline{i}_S\right)$$

and show that substituting this into the second equation of (8.139) results in

$$\underline{\lambda}_R e^{j\theta_R} = \frac{L_R}{M}\underline{\lambda}_S + \sigma M \underline{i}_S$$

where $\sigma = 1 - M^2/(L_S L_R)$.

(b) Multiply the second equation of (8.138) by $e^{-j\theta_R}$ *and substitute the expressions for* $\underline{i}_R e^{j\theta_R}$ *and* $\underline{\lambda}_R e^{j\theta_R}$ *from part (a) into (8.138) to show that the electrical equations have the equivalent form*

$$\begin{aligned} \frac{d}{dt}\underline{\lambda}_S &= -R_S \underline{i}_S + \underline{u}_S \\ \frac{d}{dt}\underline{i}_S &= \frac{(R_R - j\omega L_R)\underline{\lambda}_S - (R_R L_S + R_S L_R - j\omega\sigma L_R L_S)\underline{i}_S + L_R \underline{u}_S}{\sigma L_R L_S}. \end{aligned}$$

(c) Consider the observer proposed in Refs. [74][75] given by

$$\begin{aligned} \frac{d}{dt}\hat{\underline{\lambda}}_S &= -R_S \underline{i}_S + \underline{u}_S + c_1(\underline{i}_S - \hat{\underline{i}}_S)(R_R - j\omega L_R) \\ \frac{d}{dt}\hat{\underline{i}}_S &= -\frac{(R_R - j\omega L_R)\hat{\underline{\lambda}}_S - (R_R L_S + R_S L_R - j\omega\sigma L_R L_S)\underline{i}_S + L_R \underline{u}_S}{\sigma L_R L_S} \\ &\quad + \frac{c_2(\underline{i}_S - \hat{\underline{i}}_S)(R_R - j\omega L_R)}{\sigma L_R L_S} \end{aligned}$$

www.EngineeringEBooksPdf.com

where c_1 and c_2 are complex *gains to be chosen.*

(d) Set $\underline{\varepsilon}_\lambda = \underline{\lambda}_S - \hat{\underline{\lambda}}_S$ and $\underline{\varepsilon}_i = \underline{i}_S - \hat{\underline{i}}_S$ and show the error system is given by

$$\begin{aligned} \frac{d}{dt}\underline{\varepsilon}_\lambda &= -(R_R - j\omega L_R)c_1\underline{\varepsilon}_i \\ \frac{d}{dt}\underline{\varepsilon}_i &= \frac{(R_R - j\omega L_R)}{\sigma L_R L_S}(\underline{\varepsilon}_\lambda - c_2\underline{\varepsilon}_i). \end{aligned}$$

More compactly, one may write

$$\begin{aligned} \frac{d}{dt}\begin{bmatrix} \underline{\varepsilon}_\lambda \\ \underline{\varepsilon}_i \end{bmatrix} &= (R_R - j\omega L_R)\begin{bmatrix} 0 & -c_1 \\ \dfrac{1}{\sigma L_R L_S} & -\dfrac{1}{\sigma L_R L_S}c_2 \end{bmatrix}\begin{bmatrix} \underline{\varepsilon}_\lambda \\ \underline{\varepsilon}_i \end{bmatrix} \\ \frac{d}{dt}\underline{\varepsilon} &= (R_R - j\omega L_R)A\underline{\varepsilon} \end{aligned} \tag{8.140}$$

with the obvious definitions for $\underline{\varepsilon}$ and A.

(e) Show the eigenvalues of A can be arbitrarily assigned by choosing c_1 and c_2 appropriately.

(f) Show that the solution to (8.140) is given by

$$\underline{\varepsilon}(t) = e^{(R_R t - j\theta(t)L_R)A}\underline{\varepsilon}(0).$$

(g) Show that c_1 and c_2 can be chosen so that $s_1 = s_{1a} + js_{1b}sign(\theta(t))$ and $s_2 = s_{2a} + js_{2b}sign(\theta(t))$ are the eigenvalues of A with $s_{1a} < 0$, $s_{1b} \leq 0$, $s_{2a} < 0$, $s_{2b} \leq 0$. That is, they are the roots of the polynomial

$$s^2 + \frac{c_2}{\sigma L_R L_S}s + \frac{c_1}{\sigma L_R L_S}.$$

(As c_1 and c_2 are complex gains, this is possible to do with s_1 and s_2 not *being complex conjugates.)*

(h) Assuming $s_1 \neq s_2$, show that the error $\varepsilon(t)$ is a linear combination of the complex exponentials

$$e^{s_{1a}R_R t + s_{1b}sign(\theta(t))L_R\theta(t) + j\left(s_{1b}sign(\theta(t))\,R_R t - s_{1a}L_R\theta(t)\right)}$$
$$e^{s_{2a}R_R t + s_{2b}sign(\theta(t))L_R\theta(t) + j\left(s_{2b}sign(\theta(t))\,R_R t - s_{2b}L_R\theta(t)\right)}$$

which decay to zero.

Remark *One may choose $s_{1b} = s_{2b} = 0$ to simplify the expressions in part (h). However, as explained in [74][75], there is an advantage in choosing c_1 and c_2 such that s_1 and s_2 are not real. After the rotor position increases, $L_R\theta(t)$ typically is much larger than $R_R t$ so that a faster convergence rate results by having s_{1b} and s_{2b} both negative.*

www.EngineeringEBooksPdf.com

Dynamic Feedback Linearization

The concept behind feedback linearization is to find a coordinate system transformation such that the nonlinear dynamics represented in the new coordinate system can be canceled out by state feedback. This is a quite appealing approach when such a transformation exists. This theory has been worked out in that (checkable) necessary and sufficient conditions exist to determine the existence of such a transformation (see the excellent books by A. Isidori [52], H. Nijmeijer and A. J. van der Schaft [101], and R. Marino and P. Tomei [102] that described this theory is detail). However, it turns out that the system model (8.5) [or equivalently, the system model (8.9)] of the induction motor is *not* feedback linearizable [64]. Furthermore, the reduced-order model (8.13)–(8.16) with inputs i_{dr}, i_{qr} and state variables ω, ψ_d, ρ is also *not* feedback linearizable. However, a quite interesting result is that for some dynamic systems which are not feedback linearizable, the addition of integrators in some of the inputs can result in the (higher-order) system being feedback linearizable [103][104][105]. This is a phenomenon of multi-input systems, in that a single-input system is dynamically feedback linearizable if and only if it is (statically) feedback linearizable [105]. This approach is explored in the next two problems.

Problem 28 Addition of an Integrator to the d-axis Input [106][107]

Consider the current command induction motor model as given in the system model (8.13)–(8.16) whose inputs are taken to be i_{dr} and i_{qr}. A so-called dynamic feedback linearization controller can be found by the addition of an integrator to the d axis of field-oriented model. Specifically, define $x_1 \triangleq \omega$, $x_2 \triangleq \psi_d$, $x_3 \triangleq \rho$ and $x_4 \triangleq i_{dr}$, $dx_4/dt \triangleq v_1$, $v_2 \triangleq i_{qr}$ so that the equations are now

$$\begin{aligned} dx_1/dt &= \mu x_2 v_2 - \tau_L/J \\ dx_2/dt &= -\eta x_2 + \eta M x_4 \\ dx_3/dt &= n_p x_1 + \eta M v_2/x_2 \\ dx_4/dt &= v_1. \end{aligned}$$

More compactly, this may be written as

$$\frac{dx}{dt} = f(x) + g_1 v_1 + g_1 v_2$$

with

$$f(x) = \begin{bmatrix} -\tau_L/J \\ -\eta x_2 + \eta M x_4 \\ n_p x_1 \\ 0 \end{bmatrix}, \; g_1 = \begin{bmatrix} 0 \\ 0 \\ 0 \\ 1 \end{bmatrix}, \; g_2 = \begin{bmatrix} \mu x_2 \\ 0 \\ \eta M/x_2 \\ 0 \end{bmatrix} \in \mathbb{R}^4.$$

www.EngineeringEBooksPdf.com

(a) Consider the nonlinear state-space transformation given by

$$\begin{aligned} z_1 &= x_2 \\ z_2 &= -\eta x_2 + \eta M x_4 \\ z_3 &= x_1 - \mu x_2^2 x_3/\eta M \\ z_4 &= \frac{2\mu}{M} x_2 x_3 (x_2 - M x_4) - \frac{\mu n_p}{\eta M} x_2^2 x_1 - \tau_L/J. \end{aligned}$$

Show that in these new coordinates, the system equations become

$$\begin{aligned} \frac{dz_1}{dt} &= z_2 \\ \frac{dz_2}{dt} &= a_1(x) + v_1 b_{11} + v_2 b_{12}(x) \\ \frac{dz_3}{dt} &= z_4 \\ \frac{dz_4}{dt} &= a_2(x) + v_1 b_{21} + v_2 b_{22}(x) \end{aligned}$$

where

$$\begin{aligned} a_1(x) &= -\eta(-\eta x_2 + \eta M x_4) \\ a_2(x) &= -2\eta M \mu x_3 x_4^2 + 6\eta\mu x_2 x_3 x_4 - 4\mu n_p x_1 x_2 x_4 + \frac{\mu n_p}{\eta M J} \tau_L x_2^2 \\ &\quad + \frac{1}{M}(-4\eta\mu x_2^2 x_3 + 4\mu n_p x_1 x_2^2) \end{aligned}$$

and $b_{11} = \eta M, b_{12}(x) = -2\mu x_2 x_3, b_{21} = 0, b_{22}(x) = -2\mu(-\eta x_2 + \eta M x_4) - \frac{\mu^2 n_p}{\eta M} x_2^3$.

(b) Show that application of the feedback

$$\begin{bmatrix} v_1 \\ v_2 \end{bmatrix} = \begin{bmatrix} b_{11} & b_{12} \\ b_{21} & b_{22} \end{bmatrix}^{-1} \begin{bmatrix} u_1 - a_1(x) \\ u_2 - a_2(x) \end{bmatrix}$$

results in two decoupled second-order linear *systems*

$$\begin{aligned} dz_1/dt &= z_2 \\ dz_2/dt &= u_1 \\ dz_3/dt &= z_4 \\ dz_4/dt &= u_2. \end{aligned}$$

(c) The controller is singular when

$$\det\begin{bmatrix} b_{11} & b_{12} \\ b_{21} & b_{22} \end{bmatrix} = -2\eta M \mu(-\eta x_2 + \eta M x_4) - \mu^2 n_p x_2^3 = 0.$$

www.EngineeringEBooksPdf.com

Rewrite this singularity condition in the dq coordinates and show that it becomes

$$-(2\eta M\mu)d\psi_d/dt - \mu^2 n_p \psi_d^3 = 0.$$

Remark 1 *This singularity can be avoided by choosing, for example, the input u_1 to regulate ψ_d to a positive constant so that $d\psi_d/dt = 0$. On the other hand, during field weakening when ψ_d is reduced, this condition just restricts how fast ψ_d can be decreased, that is,*

$$0 \geq d\psi_d/dt > -(\frac{\mu n_p}{2\eta M})\psi_d^3 = -(\frac{n_p^2}{2JR_R})\psi_d^3.$$

At start-up of the motor, when the flux is brought up from zero to its nominal value, the singularity is not encountered as $d\psi_d/dt > 0$.

Remark 2 *Note that none of the state variables z_i are linearly related to the speed ω. Consequently, $d\theta/dt = \omega$ is* not *a linear function of the z_i so that the position cannot be appended to the coordinate system defining the z_i's without losing linearity of the system. That is, if $d\theta/dt = \omega = x_1$ is appended to the z_i coordinate transformation, then it is straightforward to show that the resulting system is* not *feedback linearizable (a similar situation arises in the case of a shunt-connected DC motor [55]). This situation also complicates the speed control design, as the speed is indirectly controlled through the input u_2 vis-a-vis $z_3 = x_1 - \mu x_2^2 x_3/(\eta M) = \omega - \mu\psi_d^2\rho/(\eta M)$. For example, if a constant speed ω_0 is desired, $z_3 = \omega_0 - \mu\psi_d^2\rho/(\eta M)$ must be tracked using the input u_2. This is sensitive to errors in the parameter values, as well as errors in the estimation of the state variables ψ_d and ρ.*

Problem 29 Addition of an Integrator to the q-axis Input [106][107]

It is quite natural to consider adding an integrator in the q axis of the system model (8.13)–(8.16) rather than the d axis for comparison. To proceed, let $x_1 = \omega$, $x_2 = \psi_d$, $x_3 = \rho$ and $x_4 = i_{qr}$, $dx_4/dt = v_2, v_1 = i_{dr}$ so that the system (8.13)–(8.16) becomes

$$\begin{aligned} dx_1/dt &= \mu x_2 x_4 - \tau_L/J \\ dx_2/dt &= -\eta x_2 + \eta M v_1 \\ dx_3/dt &= n_p x_1 + \eta M x_4/x_2 \\ dx_4/dt &= v_2. \end{aligned}$$

More compactly, this may be written as

$$\frac{dx}{dt} = f(x) + g_1 v_1 + g_1 v_2$$

with

$$f(x) = \begin{bmatrix} \mu x_2 x_4 - \tau_L/J \\ -\eta x_2 \\ n_p x_1 + \eta M x_4/x_2 \\ 0 \end{bmatrix},\ g_1 = \begin{bmatrix} 0 \\ \eta M \\ 0 \\ 0 \end{bmatrix},\ g_2 = \begin{bmatrix} 0 \\ 0 \\ 0 \\ 1 \end{bmatrix} \in \mathbb{R}^4.$$

www.EngineeringEBooksPdf.com

A feedback linearizing transformation is then

$$\begin{aligned} z_1 &= x_1 \\ z_2 &= \mu x_2 x_4 - \tau_L/J \\ z_3 &= x_3 \\ z_4 &= n_p x_1 + \eta M x_4/x_2. \end{aligned}$$

(a) Show that in these new coordinates, the system equations become

$$\begin{aligned} \frac{dz_1}{dt} &= z_2 \\ \frac{dz_2}{dt} &= a_1(x) + v_1 b_{11} + v_2 b_{12} \\ \frac{dz_3}{dt} &= z_4 \\ \frac{dz_4}{dt} &= a_2(x) + v_1 b_{21} + v_2 b_{22} \end{aligned}$$

where

$$\begin{aligned} a_1(x) &= -\eta\mu x_2 x_4 \\ a_2(x) &= \mu n_p x_2 x_4 + \eta^2 M \frac{x_4}{x_2} - \frac{n_p \tau_L}{J} \end{aligned}$$

and $b_{11} = \eta M \mu x_4, b_{12} = \mu x_2, b_{21} = -\eta^2 M^2 x_4/x_2^2, b_{22} = \eta M/x_2$.

(b) Show that application of the feedback

$$\begin{bmatrix} v_1 \\ v_2 \end{bmatrix} = \begin{bmatrix} b_{11} & b_{12} \\ b_{21} & b_{22} \end{bmatrix}^{-1} \begin{bmatrix} u_1 - a_1(x) \\ u_2 - a_2(x) \end{bmatrix}$$

results in two decoupled second-order linear *systems*

$$\begin{aligned} dz_1/dt &= z_2 \\ dz_2/dt &= u_1 \\ dz_3/dt &= z_4 \\ dz_4/dt &= u_2. \end{aligned}$$

results in two decoupled second-order systems as in the d-axis case.

Remark *This controller is singular when*

$$\det \begin{bmatrix} b_{11} & b_{12} \\ b_{21} & b_{22} \end{bmatrix} = 2\eta^2 M^2 \mu \frac{x_4}{x_2} = 2\eta^2 M^2 \mu \frac{i_{qr}}{\psi_d} = 0.$$

This singularity condition is comparable to the condition that the torque $\tau = J\mu\psi_d i_q = J\mu x_2 x_4 \neq 0$ *given in Ref.* [108]. *However, in contrast to Ref.* [108], *the approach here requires only a single transformation, and the resulting controller requires relatively little feedback computation. A drawback*

www.EngineeringEBooksPdf.com

here is the requirement that the quadrature current be nonzero ($\psi_d > 0$ is straightforward to maintain and is common to other controllers [1][64][70]*). Consequently, to use this controller would require switching to another control strategy when it is desired to change the sign of the torque. Note that, in contrast to the case where the integrator was in the d axis, one of the transformed state variables is the speed, which is easily controlled using the input u_1. By appending the state variable $z_0 = \theta$ to the z-coordinate transformation gives a feedback linearizing controller for* position *control. However, to avoid the singularity of the controller, it is still required that $i_q \neq 0$.*

Problem 30 The Induction Motor is a Flat System [74][109]

Another way of viewing dynamic feedback linearization is through the notion of flatness *of a system. The concept of a system being* flat *is due to Michel Fliess* [109] *and has been applied to the induction motor by Martin and Rouchon* [74]*. The book* [110] *by H. Sira-Ramírez and S. K. Agrawal presents a nice introduction to the theory of flat systems in terms of applications and the book* [111] *by G. Conte, C. H. Moog and A. M. Perdon presents a nice introduction to the underlying mathematics. To motivate the concept of flatness, consider the Chua circuit example discussed by Sira-Ramírez and Agrawal* ([110], *p. 196*)*, which is modeled by the third-order nonlinear system*

$$\frac{dx_1}{dt} = p\left(-x_1 + x_2 - x_1\left(1 - x_1^2\right)\right) \tag{8.141}$$

$$\frac{dx_2}{dt} = x_1 - x_2 + x_3 \tag{8.142}$$

$$\frac{dx_3}{dt} = -qx_2 + u \tag{8.143}$$

where p and q are known constant parameters. Let the (flat) output be $y = x_1$. The state can be written as function of y and its derivatives as follows:

$$\begin{aligned} x_1 &= y \\ x_2 &= \dot{y}/p + y + y(1 - y^2) && \textit{(rearranging (8.141))} \\ x_3 &= \frac{d}{dt}\left(\dot{y}/p + y + y(1 - y^2)\right) + \left(\dot{y}/p + y + y(1 - y^2)\right) - y \\ &= \ddot{y}/p + (2 + 1/p)\,\dot{y} - 3y^2\dot{y} + y(1 - y^2) && \textit{(rearranging (8.142))} \end{aligned}$$

or, more compactly,

$$x = \varphi(y, \dot{y}, \ddot{y}) \in \mathbb{R}^3.$$

Also, the input u can be written as function of y and its derivatives by

www.EngineeringEBooksPdf.com

rearranging (8.143) to obtain

$$\begin{aligned} u &= \frac{d}{dt}\left(\ddot{y}/p + (2+1/p)\,\dot{y} - 3y^2\dot{y} + y(1-y^2)\right) + q\left(\dot{y}/p + y + y(1-y^2)\right) \\ &= \dddot{y}/p + (2+1/p)\ddot{y} - 6y\dot{y} - 3y^2\ddot{y} + \dot{y} - 3y^2\dot{y} + (q/p)\dot{y} + qy + qy(1-y^2) \\ &= \phi(y, \dot{y}, \ddot{y}, \dddot{y}) \in \mathbb{R}. \end{aligned} \tag{8.144}$$

The notion of flatness refers to defining an output variable y such that both the state and the input can be written as a function of this output and its derivatives. Thus, the Chua circuit model is a flat system. To see why the notion of flatness is useful, in the Chua circuit example define the new state variables $z_1 = y, z_2 = \dot{y}$, and $z_3 = \ddot{y}$ so that

$$\begin{aligned} \frac{dz_1}{dt} &= z_2 \\ \frac{dz_2}{dt} &= z_3 \\ \frac{dz_3}{dt} &= \dddot{y}. \end{aligned}$$

However, by equation (8.144),

$$\dddot{y} = pu - p\left((2+1/p)\ddot{y} - 6y\dot{y} - 3y^2\ddot{y} + \dot{y} - 3y^2\dot{y} + (q/p)\dot{y} + qy + qy(1-y^2)\right)$$

so that setting

$$u = (2+1/p)\ddot{y} - 6y\dot{y} - 3y^2\ddot{y} + \dot{y} - 3y^2\dot{y} + (q/p)\dot{y} + qy + qy(1-y^2) + v/p$$

the system becomes

$$\begin{aligned} \frac{dz_1}{dt} &= z_2 \\ \frac{dz_2}{dt} &= z_3 \\ \frac{dz_3}{dt} &= v \end{aligned}$$

which is a linear system. Furthermore, the flatness property allows a straightforward design of the reference trajectory and reference input. Specifically, let $y_{ref}(t)$ be the desired reference output so that

$$\begin{aligned} x_{ref} &= \varphi\left(y_{ref}, \dot{y}_{ref}, \ddot{y}_{ref}\right) \in \mathbb{R}^3 \\ u_{ref} &= \phi\left(y_{ref}, \dot{y}_{ref}, \ddot{y}_{ref}, \dddot{y}_{ref}\right) \in \mathbb{R} \\ z_{ref} &= \left[y_{ref}, \dot{y}_{ref}, \ddot{y}_{ref}\right]^T \in \mathbb{R}^3 \end{aligned}$$

are the reference signals.

www.EngineeringEBooksPdf.com

Remark *For single-input systems, flatness is equivalent to feedback linearizability of which the Chua circuit is an example. For multi-input systems, flatness implies the system is dynamically feedback linearizable* [110].

(a) Consider the space vector formulation of the induction motor model, that is,

$$\begin{aligned} R_S\underline{i}_S + L_S\frac{d}{dt}\underline{i}_S + M\frac{d}{dt}\left(\underline{i}_R e^{jn_p\theta_R}\right) &= \underline{u}_S \\ R_R\underline{i}_R + L_R\frac{d}{dt}\underline{i}_R + M\frac{d}{dt}\left(\underline{i}_S e^{-jn_p\theta_R}\right) &= 0 \\ n_pM\,\mathrm{Im}\left\{\underline{i}_S(\underline{i}_R e^{jn_p\theta_R})^*\right\} - \tau_L &= J\frac{d\omega_R}{dt} \end{aligned}$$

where $\underline{i}_S \triangleq i_{Sa} + ji_{Sb}$, $\underline{i}_R \triangleq i_{Ra} + ji_{Rb}$, $\underline{u}_S \triangleq u_{Sa} + ju_{Sb}$. *With*

$$\begin{aligned} \underline{\lambda}_S &\triangleq \lambda_{Sa} + j\lambda_{Sb} \triangleq L_S\underline{i}_S + M\underline{i}_R e^{+jn_p\theta_R} \\ \underline{\lambda}_R &\triangleq \lambda_{Ra} + j\lambda_{Rb} \triangleq L_R\underline{i}_R + M\underline{i}_S e^{-jn_p\theta_R} \end{aligned}$$

the electrical equations of the induction motor may be written as

$$\begin{aligned} R_S\underline{i}_S + \frac{d}{dt}\underline{\lambda}_S &= \underline{u}_S \\ R_R\underline{i}_R + \frac{d}{dt}\underline{\lambda}_R &= 0. \end{aligned}$$

In problem 8 of Chapter 6, *it was shown that using*

$$\begin{bmatrix} \underline{i}_S \\ \underline{i}_R e^{+jn_p\theta_R} \end{bmatrix} = \frac{1}{L_SL_R - M^2}\begin{bmatrix} +L_R & -M \\ -M & +L_S \end{bmatrix}\begin{bmatrix} \underline{\lambda}_S \\ \underline{\lambda}_R e^{+jn_p\theta_R} \end{bmatrix},$$

a model for the induction motor in terms of the flux linkages is

$$\begin{aligned} \frac{R_S}{\sigma L_SL_R}\left(L_R\underline{\lambda}_S - M\underline{\lambda}_R e^{+jn_p\theta_R}\right) + \frac{d}{dt}\underline{\lambda}_S &= \underline{u}_S \\ \frac{R_R}{\sigma L_SL_R}\left(-M\underline{\lambda}_S e^{-jn_p\theta_R} + L_S\underline{\lambda}_R\right) + \frac{d}{dt}\underline{\lambda}_R &= 0 \\ \frac{M}{\sigma L_SL_R}\,\mathrm{Im}\{\underline{\lambda}_S(\underline{\lambda}_R e^{+jn_p\theta_R})^*\} - \tau_L &= J\frac{d\omega_R}{dt} \\ \frac{d\theta_R}{dt} &= \omega_R. \end{aligned}$$

Show that

$$\frac{M}{\sigma L_SL_R}\,\mathrm{Im}\{\underline{\lambda}_S(\underline{\lambda}_R e^{+jn_p\theta_R})^*\} = -\,\mathrm{Im}\,\{\underline{i}_R\underline{\lambda}_R^*\}.$$

www.EngineeringEBooksPdf.com

(b) Show that

$$\begin{aligned} J\frac{d\omega}{dt} &= -\operatorname{Im}\{\underline{i}_R\underline{\lambda}_R^*\} - \tau_L \\ &= -\frac{1}{R_R}\operatorname{Im}\left\{\frac{d\underline{\lambda}_R}{dt}\underline{\lambda}_R^*\right\} - \tau_L \\ &= -\frac{1}{R_R}\lambda_R^2\frac{d}{dt}\rho_R - \tau_L \end{aligned}$$

where $\underline{\lambda}_R \triangleq \lambda_R e^{j\rho_R}$.

(c) Show that

$$\begin{bmatrix} y_1 \\ y_2 \end{bmatrix} \triangleq \begin{bmatrix} \theta \\ \rho_R \end{bmatrix}$$

is a flat output. *That is, show that*

$$\begin{aligned} \underline{\lambda}_R &= \underline{\varphi}_1(y, \dot{y}, \ddot{y}) \\ \underline{\lambda}_R &= \underline{\varphi}_2(y, \dot{y}, \ddot{y}, \dddot{y}) \\ \underline{u}_S &= \underline{\phi}(y, \dot{y}, \ddot{y}, \dddot{y}, \ddddot{y}) . \end{aligned}$$

Explicitly compute the functions $\underline{\varphi}_1, \underline{\varphi}_2$, *and* $\underline{\phi}$.

(d) When is the transformation singular?

Optimal Field Weakening

Problem 31 Torque Expressions

Show that with $\omega_S = n_p\omega + \delta/T_R$ *the electrical frequency,* $S_p = 1/(\sigma\omega_S T_R)$ *the normalized pull out slip,* $S = (\omega_S - n_p\omega)/\omega_S = (\delta/T_R)/\omega_S$ *the normalized slip, and letting* $R_S \to 0$, *the torque expression*

$$\tau = \frac{n_p M^2}{L_R R_S^2} V^2 \frac{\delta}{\left(1 - \sigma T_S \delta\left(n_p\omega + \delta/T_R\right)\right)^2 + \left(\delta + T_S\left(n_p\omega + \delta/T_R\right)\right)^2}$$

reduces to

$$\tau = n_p \frac{3}{2}\frac{1-\sigma}{\sigma}\frac{U_S^2}{\omega_S^2 L_S}\frac{2}{S/S_p + S_p/S}$$

where $U_S \triangleq \sqrt{\frac{2}{3}}\frac{V}{\sqrt{2}}$. *(*$V/\sqrt{2}$ *is the two-phase equivalent rms voltage so that* $\sqrt{2/3}\left(V/\sqrt{2}\right)$ *is the line-to-neutral rms voltage in the three-phase machine.)*

Problem 32 Positive root of $p(\delta) = 0$

Use the Routh-Hurwitz test and the expression (8.68) to show that $p(\delta) = 0$ *has exactly one root in the right-half plane for all* $\omega \geq 0$.

Problem 33 Base Speed

Use the Routh-Hurwitz test to show that equation (8.85) has only one root satisfying $\omega > 0$ *for* $\delta_1 = \pm 1$.

www.EngineeringEBooksPdf.com

This Page Intentionally Left Blank

www.EngineeringEBooksPdf.com

9

PM Synchronous Motor Control

Starting with a mathematical model of the PM synchronous machine, a field-oriented controller is developed for high-performance control. Experimental results are presented to illustrate the methodology. Following this, a systematic approach to field weakening is developed based on maximizing the torque obtainable from the machine without violating the voltage or the current constraints. Next, it is shown how the least-squares identification procedure developed in Chapter 2 can be used to determine the parameters of a PM synchronous machine. Finally, the structure and operation of PM stepper motors are described.

9.1 Field-Oriented Control

The approach presented here for high-performance control of a PM synchronous machine is based on the development in [72][112]. To proceed, the two-phase model of a PM synchronous machine with sinusoidally wound stator phases and n_p pole pairs is given by (see equation (6.40) of Chapter 6 where $n_p = 1$)

$$\begin{aligned} L_S \frac{di_{Sa}}{dt} &= -R_S i_{Sa} + K_m \sin(n_p\theta)\omega + u_{Sa} \\ L_S \frac{di_{Sb}}{dt} &= -R_S i_{Sb} - K_m \cos(n_p\theta)\omega + u_{Sb} \\ J\frac{d\omega}{dt} &= K_m(-i_{Sa}\sin(n_p\theta) + i_{Sb}\cos(n_p\theta)) - \tau_L \\ \frac{d\theta}{dt} &= \omega. \end{aligned} \tag{9.1}$$

This is also the two-phase equivalent model of a three-phase PM synchronous machines [see equation (7.81) in Chapter 7]. Equation (9.1) is the starting point for the design of a field-oriented controller for the PM synchronous machine. For synchronous machines, the dq transformations of the phase voltages and currents are given by

$$\begin{bmatrix} u_d \\ u_q \end{bmatrix} \triangleq \begin{bmatrix} \cos(n_p\theta) & \sin(n_p\theta) \\ -\sin(n_p\theta) & \cos(n_p\theta) \end{bmatrix} \begin{bmatrix} u_{Sa} \\ u_{Sb} \end{bmatrix} \tag{9.2}$$

$$\begin{bmatrix} i_d \\ i_q \end{bmatrix} \triangleq \begin{bmatrix} \cos(n_p\theta) & \sin(n_p\theta) \\ -\sin(n_p\theta) & \cos(n_p\theta) \end{bmatrix} \begin{bmatrix} i_{Sa} \\ i_{Sb} \end{bmatrix}. \tag{9.3}$$

www.EngineeringEBooksPdf.com

The direct current i_d corresponds to the component of the stator magnetic field along the axis of the rotor magnetic field, while the quadrature current i_q corresponds to the orthogonal component. The application of the dq transformation to the original system (9.1) yields the system of equations

$$L_S \frac{di_d}{dt} = -R_S i_d + n_p \omega L_S i_q + u_d \tag{9.4}$$

$$L_S \frac{di_q}{dt} = -R_S i_q - n_p \omega L_S i_d - K_m \omega + u_q \tag{9.5}$$

$$J \frac{d\omega}{dt} = K_m i_q - \tau_L \tag{9.6}$$

$$\frac{d\theta}{dt} = \omega \tag{9.7}$$

where u_d is the direct voltage, u_q is the quadrature voltage, i_d is the direct current, i_q is the quadrature current, ω is the angular velocity, and θ is the angular position. In this coordinate system, the transformed currents i_d and i_q vary approximately at the *mechanical* frequency of the motor. These variables typically have bandwidths in the range of 0–100 Hz compared with 0–5 kHz bandwidth for u_{Sa}, u_{Sb}, i_{Sa} and i_{Sb}.

The resulting dq system model (9.4)–(9.7) is still nonlinear, however the nonlinear terms can now be canceled by state feedback. Specifically, choosing u_d and u_q to be of the form

$$u_d = R_S i_d - n_p \omega L_S i_q + L_S v_d \tag{9.8}$$

$$u_q = R_S i_q + n_p \omega L_S i_d + K_m \omega + L_S v_q \tag{9.9}$$

results in the *feedback linearized* system

$$\frac{di_d}{dt} = v_d \tag{9.10}$$

$$\frac{di_q}{dt} = v_q \tag{9.11}$$

$$\frac{d\omega}{dt} = (K_m/J) i_q - \tau_L/J \tag{9.12}$$

$$\frac{d\theta}{dt} = \omega. \tag{9.13}$$

Note that the original fourth-order system has been transformed into a first-order linear system (9.10) and a third-order linear system (equations (9.11)–(9.13)) which are decoupled from each other. As a consequence, *linear* control techniques can be used for the system (9.10)–(9.13) in these new variables.

9.1.1 *Design of the Reference Trajectory and Inputs*

The linearized system (9.10)–(9.13) is decoupled. However, constraints on the magnitude of the voltages introduce couplings. To achieve a desired

www.EngineeringEBooksPdf.com

(reference) speed ω_{ref} and acceleration α_{ref}, the required quadrature current is found from equation (9.6) to be

$$i_{qref} = \frac{J}{K_m}\alpha_{ref} + \frac{f}{K_m}\omega_{ref}$$

where $\tau_L = -f\omega$ is now assumed. The quadrature component i_q of the current produces torque while the direct component i_d does not produce any torque. However, in order to attain higher speeds, it is necessary to apply a *negative* direct current to cancel the effect of the back emf of the motor. Specifically, note from equation (9.5), the back-emf term in the dq coordinates is $K_m\omega$ and a decoupling control law as in (9.9) requires that u_q *cancel* this back-emf term. For example, in the experiments to be presented below, $K_m = 0.19$ V/rad/sec so that the back-emf voltage at a speed of 2000 rpm (209 radians/sec) is about 41 V. However, the source voltage for this motor is only 40 V, so that cancellation of the back emf would lead to saturation at the input. However, if i_d were forced to be negative (field-weakening) by the correct choice of v_d, the term $-n_p\omega L_S i_d$ would help to cancel the back-emf term $-K_m\omega$ [see equation (9.5) or, equivalently, equation (9.9)]. The design of an appropriate reference for i_d is thus essential to avoid saturation of the phase voltages at high rotor speeds.

The desired (reference) direct current i_{dref} is found by maximizing the torque, that is, $K_m i_q$ at constant speed subject to the constraint $u_d^2 + u_q^2 = u_{Sa}^2 + u_{Sb}^2 \leq V_{\max}^2$ where $V_{\max}$ is fixed. In order to obtain a tractable solution, the optimization is carried out at constant speed under steady-state conditions. Under steady-state conditions, the relations (9.4)–(9.7) become

$$\begin{aligned} u_d &= R_S i_d - n_p\omega L_S i_q \\ u_q &= R_S i_q + n_p\omega L_S i_d + K_m\omega \\ K_m i_q &= \tau_L. \end{aligned}$$

The actual physical constraints for u_{Sa}, u_{Sb} are of the form $|u_{Sa}| \leq V_{max}$, $|u_{Sb}| \leq V_{max}$ rather than $u_{Sa}^2 + u_{Sb}^2 \leq V_{\max}^2$. However, in steady-state operation, these conditions are equivalent (see problem 1). Using standard optimization techniques, the maximum is found to correspond to

$$u_{qref}(\omega) = \frac{R_S}{\sqrt{R_S^2 + (n_p\omega L_S)^2}} V_{\max} \tag{9.14}$$

$$\frac{u_{dref}(\omega)}{u_{qref}(\omega)} = -\frac{n_p\omega L_S}{R_S} \tag{9.15}$$

$$i_{dref}(\omega) = -\frac{n_p L_S K_m \omega^2}{R_S^2 + (n_p\omega L_S)^2}. \tag{9.16}$$

The inverse tangent of (9.15) is often referred to as the optimal lead angle [113][114][115]. It is the angle advance that the phase voltages u_{Sa} and

www.EngineeringEBooksPdf.com

u_{Sb} need to be commanded relative to $n_p\theta$ (corresponding to the position of the rotor) to achieve the maximum torque at any given speed ω without violating the voltage constraints. The relationship (9.16) gives the corresponding direct current as a function of speed required to obtain the maximum torque. Although (9.14) through (9.16) were derived assuming constant speed, it will be seen below that they are very useful even under dynamic conditions.

Choosing the direct current to be negative as in (9.16) is referred to as *field weakening*. This comes from considering the terms

$$-n_p\omega L_S i_d - K_m\omega = -\left(n_p L_S i_d + K_m\right)\omega$$

in (9.5) where, as the value of K_m is proportional to the strength of rotor's magnetic field, making $i_d < 0$ is viewed as weakening this field. A more general approach to obtaining the current references that also take into account the current constraints is given in Section 9.2.

After specifying a desired mechanical reference trajectory $\theta_{ref}, \omega_{ref}, \alpha_{ref}$, the corresponding state trajectory $i_{dref}, i_{qref}, \omega_{ref}, \theta_{ref}$ and reference input voltages u_{dref}, u_{qref} are computed. They are chosen to satisfy the system equations (9.4)–(9.7), that is,

$$L_S\frac{di_{dref}}{dt} = -R_S i_{dref} + n_p\omega_{ref}L_S i_{qref} + u_{dref} \tag{9.17}$$

$$L_S\frac{di_{qref}}{dt} = -R_S i_{qref} - n_p\omega_{ref}L_S i_{dref} - K_m\omega_{ref} + u_{qref} \tag{9.18}$$

$$J\frac{d\omega_{ref}}{dt} = K_m i_{qref} - f\omega_{ref} \tag{9.19}$$

$$\frac{d\theta_{ref}}{dt} = \omega_{ref} \tag{9.20}$$

The desired quadrature current is found by solving (9.19) for i_{qref} and its derivative di_{qref}/dt is then found by differentiating this expression. The desired direct current i_{dref} is given by (9.16) with ω replaced by ω_{ref}, and its derivative is found by simply differentiating this expression. Doing these calculations gives

$$i_{dref} = \frac{-n_p L_S K_m \omega_{ref}^2}{R_S^2 + (n_p\omega_{ref}L_S)^2} \tag{9.21}$$

$$i_{qref} = \frac{J}{K_m}\alpha_{ref} + \frac{f}{K_m}\omega_{ref} \tag{9.22}$$

$$\frac{di_{dref}}{dt} = \frac{-2K_m n_p\omega_{ref}L_S R_S^2}{(R_S^2 + (n_p\omega_{ref}L_S)^2)^2}\alpha_{ref} \tag{9.23}$$

$$\frac{di_{qref}}{dt} = \frac{J}{K_m}\frac{d\alpha_{ref}}{dt} + \frac{f}{K_m}\alpha_{ref}. \tag{9.24}$$

www.EngineeringEBooksPdf.com

Solving (9.17) and (9.18) for v_{dref} and v_{qref} results in

$$u_{dref} = L_S\frac{di_{dref}}{dt} + R_S i_{dref} - n_p\omega_{ref}L_S i_{qref} \quad (9.25)$$

$$u_{qref} = L_S\frac{di_{qref}}{dt} + R_S i_{qref} + n_p\omega_{ref}L_S i_{dref} + K_m\omega_{ref} \quad (9.26)$$

where the expressions in (9.21) through (9.24) are substituted into their respective places on the right-hand sides of (9.25) and (9.26). An important point here is that these references are chosen so as to not violate the current and voltage constraints, which typically requires some trial and error. For example, if i_{qref} is too large, then the mechanical trajectory must be modified so that α_{ref} is decreased [see equation (9.22)].

Remark Note that u_{dref}, u_{qref} are *not* given by (9.14) and (9.15) because these are constant speed values for the voltages. Rather, one *sets* (9.21) as the desired direct current and (9.21) as the desired quadrature current, and then chooses the reference input voltages according to (9.25) and (9.26).

9.1.2 State Feedback Controller

Subtracting the system model (9.4)–(9.7) from the reference model (9.17)–(9.20) gives

$$L_S\frac{d}{dt}(i_{dref} - i_d) = -R_S(i_{dref} - i_d) + n_p\omega_{ref}L_S i_{qref} - n_p\omega L_S i_q + u_{dref} - u_d \quad (9.27)$$

$$L_S\frac{d}{dt}(i_{qref} - i_q) = -R_S(i_{qref} - i_q) - n_p\omega_{ref}L_S i_{dref} + n_p\omega L_S i_d - K_m(\omega_{ref} - \omega) + u_{qref} - u_q \quad (9.28)$$

$$J\frac{d}{dt}(\omega_{ref} - \omega) = K_m(i_{qref} - i_q) - f(\omega_{ref} - \omega) \quad (9.29)$$

$$\frac{d}{dt}(\theta_{ref} - \theta) = \omega_{ref} - \omega. \quad (9.30)$$

The first step in specifying the state feedback control law is to use a *feedback linearizing* controller given by

$$u_d = -n_p\omega L_S i_q + u_{dref} + n_p\omega_{ref}L_S i_{qref} - L_S v_d \quad (9.31)$$

$$u_q = +n_p\omega L_S i_d + u_{qref} - n_p\omega_{ref}L_S i_{dref} - L_S v_q \quad (9.32)$$

where v_d and v_q are new inputs yet to be defined. Substituting equations (9.31) and (9.32) for u_d and u_q into (9.27)–(9.30) results in the *linear*

www.EngineeringEBooksPdf.com

system of equations

$$L_S \frac{d}{dt}(i_{dref} - i_d) = -R_S(i_{dref} - i_d) + v_d \tag{9.33}$$

$$L_S \frac{d}{dt}(i_{qref} - i_q) = -R_S(i_{qref} - i_q) - K_m(\omega_{ref} - \omega) + v_q \tag{9.34}$$

$$J \frac{d}{dt}(\omega_{ref} - \omega) = K_m(i_{qref} - i_q) - f(\omega_{ref} - \omega) \tag{9.35}$$

$$\frac{d}{dt}(\theta_{ref} - \theta) = \omega_{ref} - \omega. \tag{9.36}$$

Define the tracking error as

$$e = \begin{bmatrix} e_1 \\ e_2 \\ e_3 \\ e_4 \\ e_5 \end{bmatrix} \triangleq \begin{bmatrix} i_{dref} - i_d \\ i_{qref} - i_q \\ \omega_{ref} - \omega \\ \theta_{ref} - \theta \\ \int_0^t (\theta_{ref}(\tau) - \theta(\tau))d\tau \end{bmatrix} \tag{9.37}$$

where the integrator is added to the controller to eliminate any steady-state error due to constant disturbances (see Chapter 2). Using (9.33)–(9.36), the error (9.37) satisfies

$$\frac{de}{dt} = \begin{bmatrix} -R_S/L_S & 0 & 0 & 0 & 0 \\ 0 & -R_S/L_S & -K_m/L_S & 0 & 0 \\ 0 & K_m/J & -f/J & 0 & 0 \\ 0 & 0 & 1 & 0 & 0 \\ 0 & 0 & 0 & 1 & 0 \end{bmatrix} e + \begin{bmatrix} 1/L_S & 0 \\ 0 & 1/L_S \\ 0 & 0 \\ 0 & 0 \\ 0 & 0 \end{bmatrix} v. \tag{9.38}$$

where $v \triangleq \begin{bmatrix} v_d & v_q \end{bmatrix}^T$. More compactly,

$$\frac{de}{dt} = Ae + Bv$$

with the obvious definitions for A and B. Through the use of a nonlinear state transformation, input transformation, and nonlinear feedback, a *linear time-invariant* error system has been obtained. The input v is chosen as the linear state feedback

$$v = -Ke \tag{9.39}$$

where K is taken to be of the form

$$K = \begin{bmatrix} k_{11} & 0 & 0 & 0 & 0 \\ 0 & k_{22} & k_{23} & k_{24} & k_{25} \end{bmatrix}. \tag{9.40}$$

The closed-loop error system is then

$$\frac{de}{dt} = (A - BK)\, e.$$

Using the techniques of Chapter 2, one can choose K such that the closed-loop poles of $A - BK$ are placed at any desired location (see problem 2).

www.EngineeringEBooksPdf.com

9.1.3 *Speed Observer*

The above controller design assumed full state measurements. However, a typical hardware setup provides only the current measurements and the position measurements. In order to estimate the speed from the position measurement (optical encoder) and current measurements, a reduced-order observer can be implemented according to

$$\frac{d\hat{\theta}}{dt} = \hat{\omega} + \ell_1(\theta - \hat{\theta}) \tag{9.41}$$

$$\frac{d\hat{\omega}}{dt} = (K_m/J)i_q - (f/J)\hat{\omega} + \ell_2(\theta - \hat{\theta}) \tag{9.42}$$

where ℓ_1 and ℓ_2 are the observer gains and i_q is a known input to the observer as i_{Sa}, i_{Sb}, and θ are measured. Subtracting (9.41) from (9.7) and (9.42) from (9.6) results in

$$\frac{d\varepsilon_1}{dt} = \varepsilon_2 - \ell_1\varepsilon_1 \tag{9.43}$$

$$\frac{de_2}{dt} = -(f/J)\varepsilon_2 - \ell_2\varepsilon_1 \tag{9.44}$$

where $\varepsilon_1 \triangleq \theta - \hat{\theta}$, $\varepsilon_2 \triangleq \omega - \hat{\omega}$. One can then choose the observer gains ℓ_1, ℓ_2 such that $\varepsilon_1(t) \to 0, \varepsilon_2(t) \to 0$ at any prescribed rate (see problem 3 and Chapter 2).

A block diagram illustrating the state feedback controller for a PM synchronous motor is given in Figure 9.1.

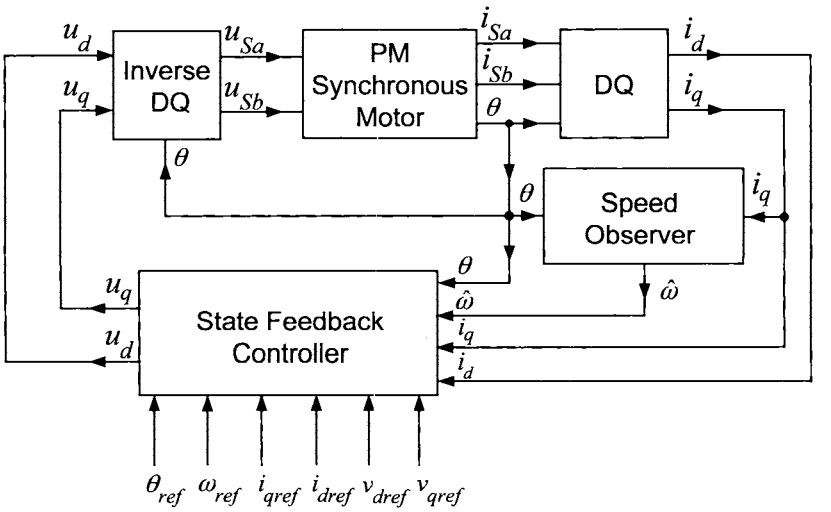


FIGURE 9.1. Controller block diagram. The state feedback controller is the composition of (9.31) and (9.32) with (9.39).

www.EngineeringEBooksPdf.com

9.1.4 *Experimental Results*

The PM motor used in the experiments has $n_p = 50$ pole pairs, two stator phases, and the following parameter values $I_{\max} = 6.0$ A, $V_{\max} = 40$ V, $R_S = 0.55\ \Omega$, $L_S = 1.5$ mH, $K_m = 0.19$ N-m/A, $J = 4.5 \times 10^{-5}$ kg-m^2, and $f = 0.0008$ N-m/rads/sec. The hardware setup used to implement the feedback controller consisted Motorola's Advanced Development System (ADS) including a Motorola DSP56001 digital signal processor, a DSP extension board, two Aerotech 20-kHz PWM amplifier, and the above PM motor with a 2000-counts/rev optical encoder.

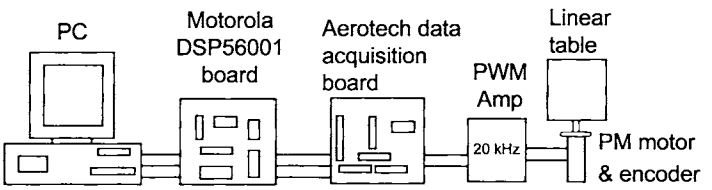


FIGURE 9.2. Experimental setup. The motor is connected to a linear positioning table through a ball screw.

The data acquisition board was built by Aerotech, Inc. and has four 8-bit A/D converters for sampling the voltages and currents, two 12-bit D/A converters to output the control voltages and a timer chip that is used to set the sample rate and to count the optical encoder pulses.

The control algorithm described above was tested on two different trajectories. The first one was a fast point-to-point move in which the motor turned 0.9π radians in 30 msec. The second move forces the motor up to a speed of 3000 rpm and brings it back down into position. This move was chosen to study high-speed control of the PM motor where the use of the reference trajectory (9.21) is required.

Sample Period and Observer Gains

A sample rate of 10 kHz ($T = 100\ \mu$sec) is required due to the high number of pole pairs. Specifically, the motor reaches speeds up to 3000 rpm, which corresponds to an electrical frequency of $(2\pi/60) \times 3000 \times n_p = 1.57$ kHz for $n_p = 50$.

The observer gains for both moves were chosen as $\ell_1 = 5272$ and $\ell_2 = 7.0 \times 10^6$, resulting in both closed-loop poles at -2646. The observer computation, that is, the integration of the system (9.41), (9.42) as well as the control algorithm is carried out every $T = 0.1$ msec (10 kHz).

As shown below (see Figure 9.5), the observer performed well and was essential to get the controller to track the particular demanding trajectories used (see Figures 9.3 and 9.5). It is reported in Ref. [72] that a speed

www.EngineeringEBooksPdf.com

estimator based on the backward difference estimate $\omega(kT) = [\theta(kT) - \theta((k-1)T)]/T$ did not result in closed-loop tracking for these same trajectories. As explained in Ref. [72], this is due to the fact when the velocity is computed by differentiating the position, the resolution of the velocity depends on the sample rate as well as the resolution of the encoder. Note that a 2000-counts/rev encoder gives a minimum velocity resolution of $(2\pi/2000)/T$ (see Chapter 2), which for $T = 1/10^4$ sec, gives a resolution of 31.4 rads/sec or 300 rpm! As the reference trajectory for speed (Figure 9.5) requires the motor to go from zero to 141 rads/sec (1350 rpm) in 10 msec, a sample rate of 10 kHz results in 100 iterations through the control loop in this time. On the other hand, a sample rate of 1 kHz would give a speed resolution of 3.14 rads/sec, but only 10 control loop iterations! The simple difference algorithm will work if a 50,000-counts/rev encoder is used (see Ref. [112]). However, this is not a practical choice for an industrial setup due to the cost and the fact that such an encoder is typically limited to lower motor speeds to work properly. (See Chapter 2 for more details on how an optical encoder works.)

Control of a 1.8-mm Move

A typical high-performance application for a PM synchronous motor is in a positioning system. Specifically, consider the requirement to have the motor move (point-to-point) a small linear positioning table 1.8 mm under 30 msec using a smooth mechanical trajectory so as to not excite vibrations in the table. The specified position θ_{ref}, speed $\omega_{ref} = d\theta_{ref}/dt$ and acceleration $\alpha_{ref} = d\omega_{ref}/dt$ are chosen to make the table move 1.8 mm. This turns out to be a 0.9π radian turn of the motor as the motor is attached to the linear stage through a ball screw. Figures 9.3 and 9.5 show the desired position and speed references θ_{ref} and ω_{ref}, respectively. That this move represents a very stringent performance requirement can be seen in Figure 9.6, which shows that the corresponding the reference input v_{dr} goes below -25 V leaving less than 15 V for the feedback controller. Furthermore, the current i_{qref} is shown in Figure 9.8 and is over 4 A (limit of 6 A) in order to achieve the required torque $K_m i_q$.

In the implementation, the gains for the 1.8-mm move were set as

$$K = \begin{bmatrix} 1.06 \times 10^4 & 0 & 0 & 0 & 0 \\ 0 & 1.78 \times 10^4 & 3.40 \times 10^2 & 3.80 \times 10^6 & 1.07 \times 10^7 \end{bmatrix}$$

to place the closed-loop poles at -18178 for the first-order subsystem and at $-11047, -28.3, -54.89 \pm j1190.7$ for the fourth-order subsystem. Figure 9.3 gives the actual and desired position response for the 1.8-mm move of the positioning table (corresponding to a 0.9π radian rotation of the motor) using the state feedback controller of Figure 9.1. The last part of the position response is shown in more detail in Figure 9.4, showing that the motor achieves the required final position within one encoder count.

www.EngineeringEBooksPdf.com

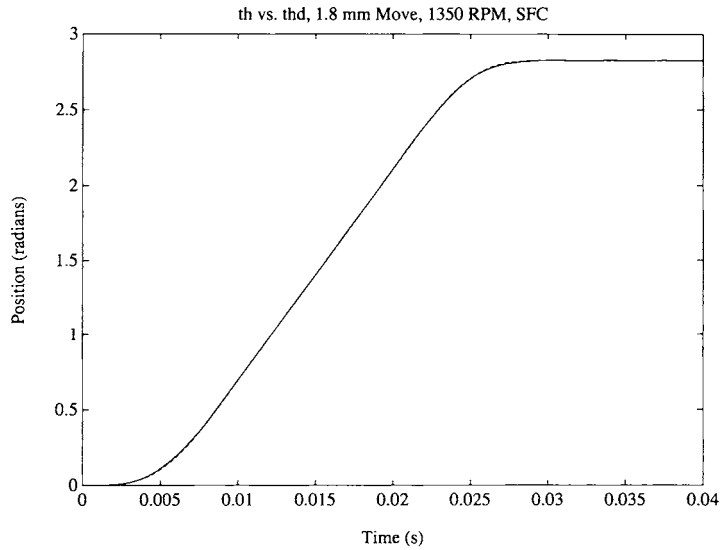


FIGURE 9.3. θ and θ_{ref} for the 1.8 mm move. From Bodson et al. [72], © 2004 IEEE.

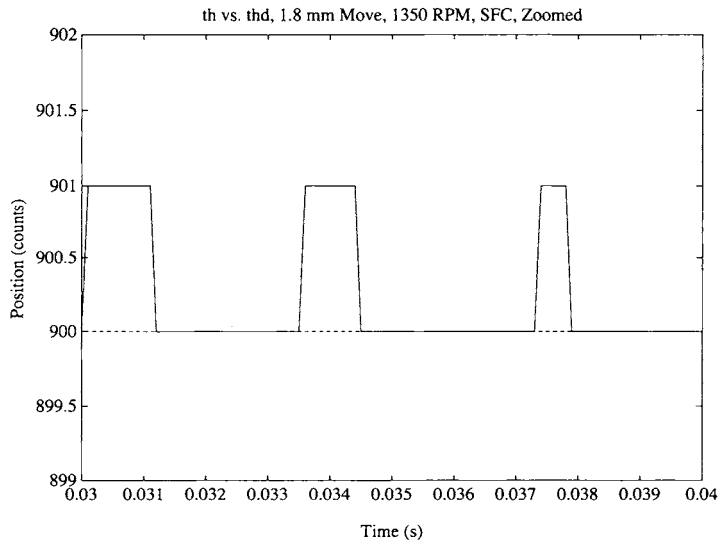


FIGURE 9.4. θ in counts after 30 msecs. Desired position is 900 counts ($= 2\pi \times 900/2000 = 0.9\pi$). From Bodson et al. [72], © 2004 IEEE.

www.EngineeringEBooksPdf.com

The desired and estimated (observer) speeds are shown in Figure 9.5.

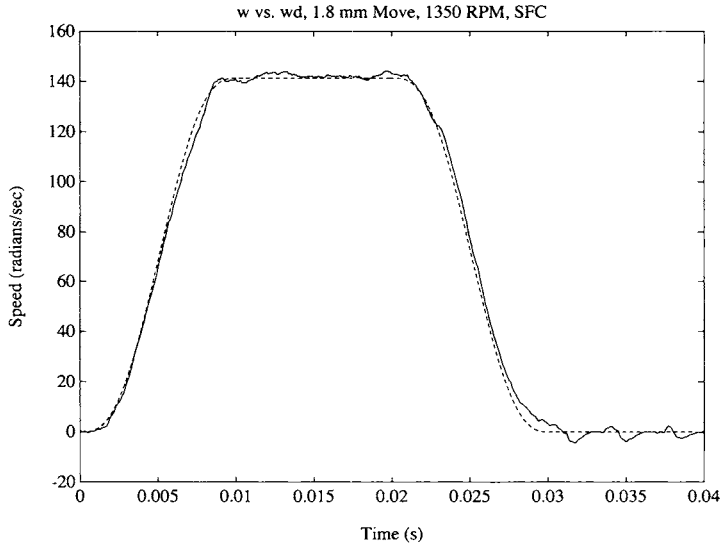


FIGURE 9.5. $\hat{\omega}$ and ω_{ref} for the 1.8-mm move. From Bodson et al. [72], © 2004 IEEE.

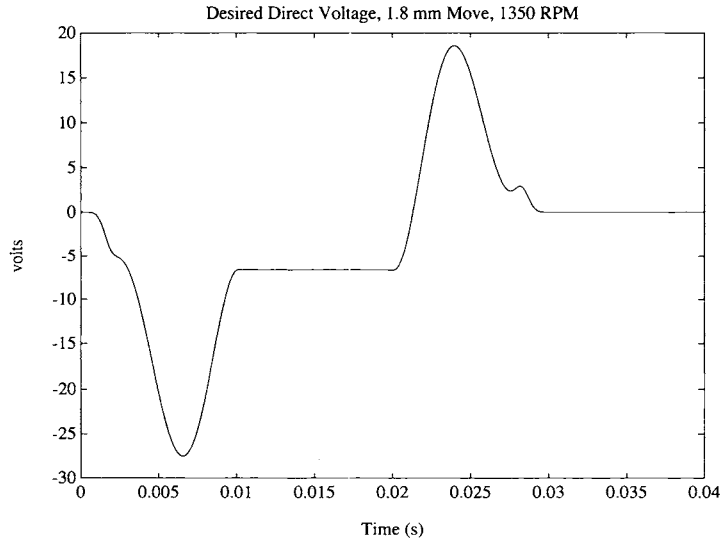


FIGURE 9.6. v_{dref} for the 1.8-mm move. From Bodson et al. [72], © 2004 IEEE.

www.EngineeringEBooksPdf.com

Figures 9.7 and 9.8 show the tracking of the currents i_d and i_q.

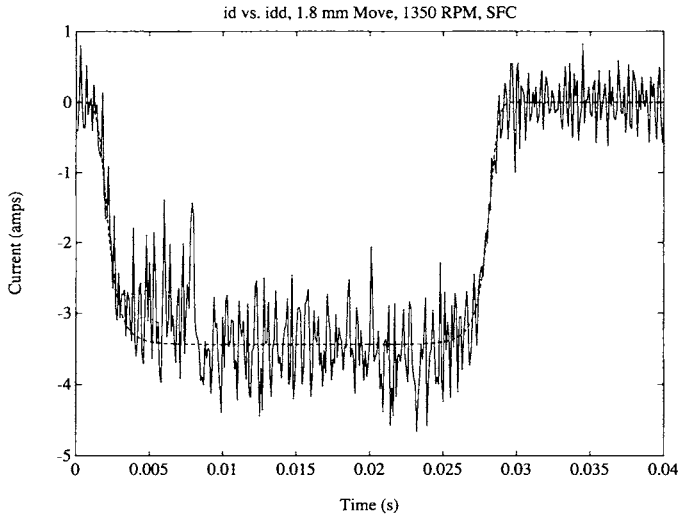


FIGURE 9.7. i_d and i_{dref} for the 1.8-mm move. From Bodson et al. [72], © 2004 IEEE.

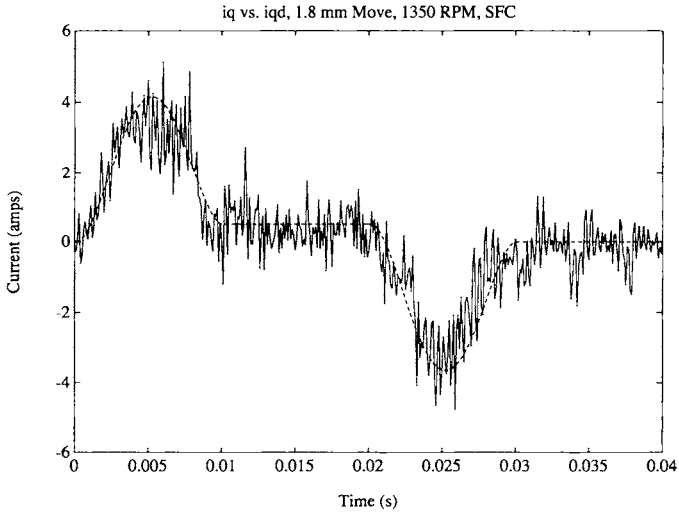


FIGURE 9.8. i_q and i_{qref} for the 1.8-mm move. From Bodson et al. [72], © 2004 IEEE.

www.EngineeringEBooksPdf.com

The position and speed tracking are very good despite large fluctuations in the measured/calculated currents i_d and i_q.

Current Fluctuations in i_d and i_q

Simulations show that the fluctuations in the currents shown in Figures 9.7 and 9.8 are due to the limited resolution of the position measurement (2000-counts/rev encoder) and not to the PWM noise [72]. Specifically, the oscillatory behavior is present in the simulation when a 2000 counts/rev encoder was modeled, but not when a 50,000-counts/rev encoder was modeled. As pointed out above, Figure 9.4 (note the units are in *counts* not radians) shows that the motor stays within one encoder count of the final position after 30 msec, which is the highest accuracy the controller can achieve with any given encoder. The oscillatory behavior of $\hat{\omega}$ at the end of the run in Figure 9.5 is a direct result of integrating the oscillating quadrature current i_q, that is, the noise due to quantization of the position θ. Consequently, the estimate of speed $\hat{\omega}$ is responding to the noisy oscillations in i_q and does not indicate that the controller is not maintaining the correct final position.

Remark It is straightforward to show that a permanent magnet DC brush motor with a torque constant of $K_T = 0.2$ N-m/A ($K_m = 0.19$ N-m/A for the stepper motor used here), a moment of inertia $J = 3.6 \times 10^{-4}$ kg-m^2 (the inertia is much larger than the stepper motor due to windings on the rotor), voltage ceiling limits of ± 80 V, and a peak current limit of 22 A is unable to make such a move under 30 msec. This is due to the fact that field weakening is not possible. However, the above PM synchronous motor with voltage limits of ± 40 V and current limits of 6 A can indeed make such a move.

Control of a 3000-rpm Run

Figure 9.9 shows the actual and desired (reference) position using the controller to bring the motor up to 3000 rpm. The actual and estimated speeds are shown in Figure 9.10. Again, the tracking of the mechanical trajectory is quite good despite oscillatory behavior in i_d and i_q (see Figures 9.12 and 9.13). These oscillations are again attributed to the lack of resolution in the 2000-counts/rev encoder. Note also that the reference input v_{dref} (Figure 9.11) reaches -30 V, leaving less than 10 V for the feedback controller.

In the implementation, the gains for the 3000-rpm run were set as

$$K = \begin{bmatrix} 2.587 \times 10^4 & 0 & 0 & 0 & 0 \\ 0 & 2.446 \times 10^4 & 6.031 \times 10^2 & 2.935 \times 10^6 & 1.004 \times 10^7 \end{bmatrix}$$

to place the closed-loop poles at -26314 for the first-order subsystem and at $-24727, -3.4, -101 \pm j893$ for the fourth-order subsystem.

www.EngineeringEBooksPdf.com

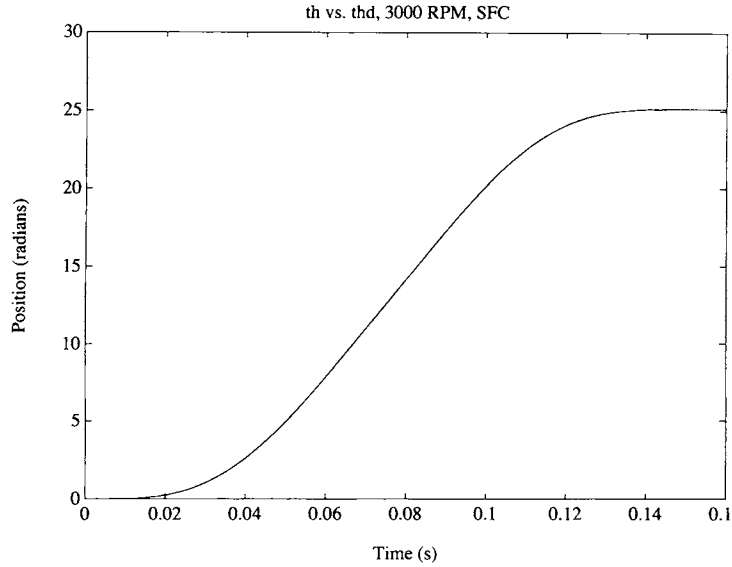


FIGURE 9.9. θ and θ_{ref} for the 3000-rpm move. From Bodson et al. [72], © 2004 IEEE.

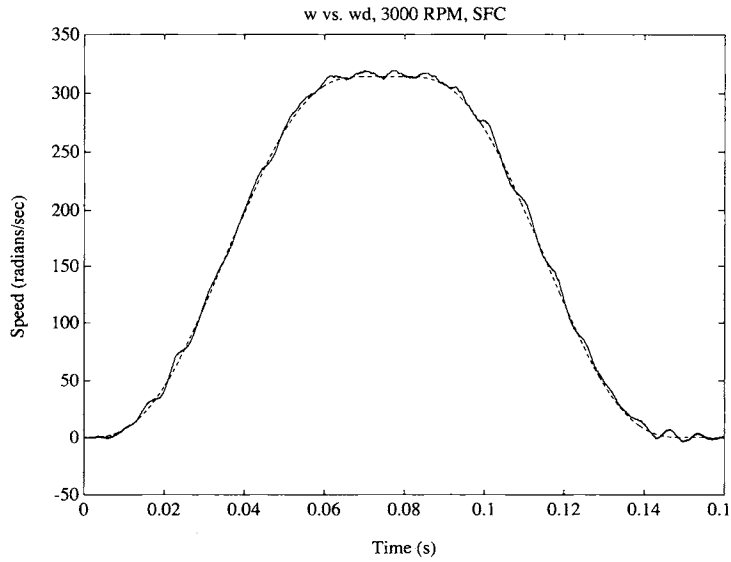


FIGURE 9.10. $\hat{\omega}$ and ω_{ref} for the 3000-rpm move. From Bodson et al. [72], © 2004 IEEE.

www.EngineeringEBooksPdf.com

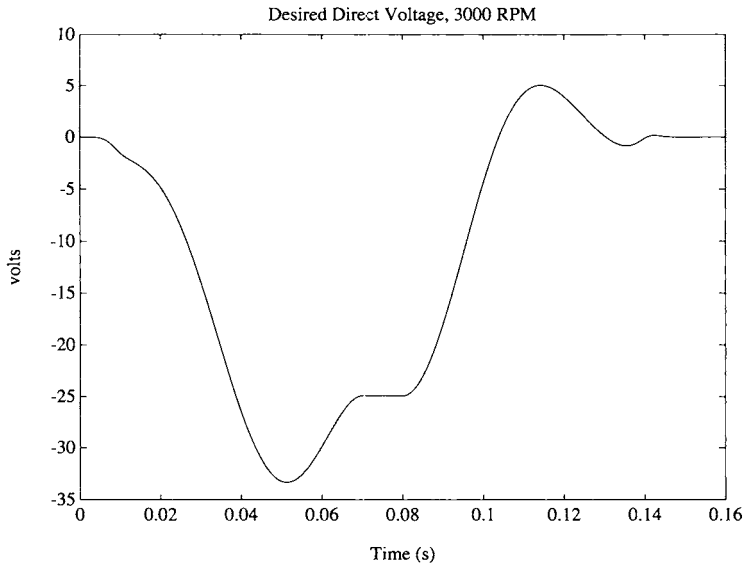


FIGURE 9.11. v_{dref} for the 3000-rpm move. From Bodson et al. [72], © 2004 IEEE.

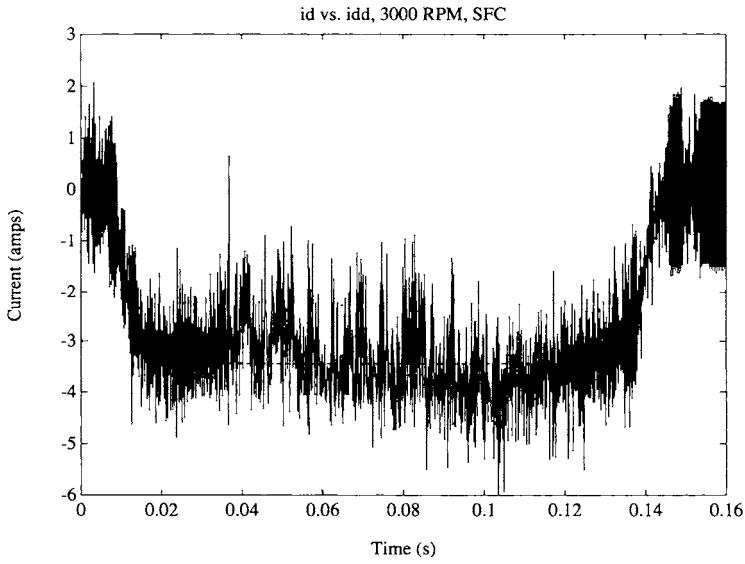


FIGURE 9.12. i_d and i_{dref} for the 3000-rpm move. From Bodson et al. [72], © 2004 IEEE.

www.EngineeringEBooksPdf.com

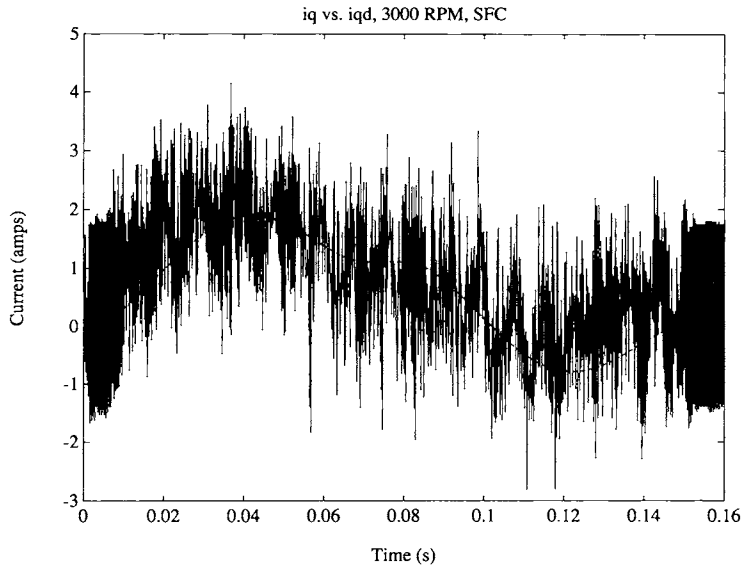


FIGURE 9.13. i_q and i_{qref} for the 3000-mm move. From Bodson et al. [72], © 2004 IEEE.

9.1.5 *Current Command Control*

In the previous section the motor was voltage-controlled. The experiments presented there used a PM synchronous motor with $n_p = 50$ pole pairs, making voltage control essential to obtain high performance. To explain, the equations of the PM machine are (9.4)–(9.7) which are repeated below.

$$L_S \frac{di_d}{dt} = -R_S i_d + n_p \omega L_S i_q + u_d \tag{9.45}$$

$$L_S \frac{di_q}{dt} = -R_S i_q - n_p \omega L_S i_d - K_m \omega + u_q \tag{9.46}$$

$$J \frac{d\omega}{dt} = K_m i_q - \tau_L \tag{9.47}$$

$$\frac{d\theta}{dt} = \omega \tag{9.48}$$

Equations (9.45) and (9.46) show that $n_p \omega L_S$ is an impedance to changing i_d, i_q through the input voltages u_d, u_q. With n_p large, the time it takes to change a current through an input voltage can be of the same order of time it takes to change the speed through i_q. This made it essential in the previous section (where $n_p = 50$) to design a voltage controller that accounts for the impedances $n_p \omega L_S$ in the current equations. However, it is also common to find PM synchronous motors with $n_p = 2$ rather than

www.EngineeringEBooksPdf.com

$n_p = 50$. In this case, the impedance is 25 times less and one does not usually need to use voltage control, but, rather, current control methods can be employed. That is, using a PI current controller of the form

$$u_q = K_p(i_{qref} - i_q) + K_I \int_0^t (i_{qref} - i_q)dt \tag{9.49}$$

$$u_d = K_p(i_{dref} - i_d) + K_I \int_0^t (i_{dref} - i_q)dt \tag{9.50}$$

and adjusting the gains appropriately, $i_{qref} \to i_q, i_{dref} \to i_d$ fast enough that one can consider $i_q \approx i_{qref}, i_d \approx i_{dref}$. Then a (mechanical) trajectory tracking controller can be designed based on the reduced-order system model

$$\frac{d\omega}{dt} = (K_m/J)\, i_{qref} - \tau_L/J \tag{9.51}$$

$$\frac{d\theta}{dt} = \omega \tag{9.52}$$

where i_{qref} is now considered as the input. Figure 9.14 is a block diagram illustrating a current command configuration. Experience shows that this works quite well if the number of pole pairs n_p is small. Equations (9.51) and (9.52) are identical in form to a DC motor so that, as in Chapter 2, one can choose a trajectory tracking controller in the form

$$i_{qref} = \frac{J}{K_m}\left(K_0 \int_0^t (\theta_{ref} - \theta)dt + K_1(\theta_{ref} - \theta) + K_2(\omega_{ref} - \omega) + \alpha_{ref}\right)$$

and choose the gains K_0, K_1, and K_2 such that $\theta \to \theta_{ref}, \omega \to \omega_{ref}$ despite any constant load torque τ_L acting on the motor.

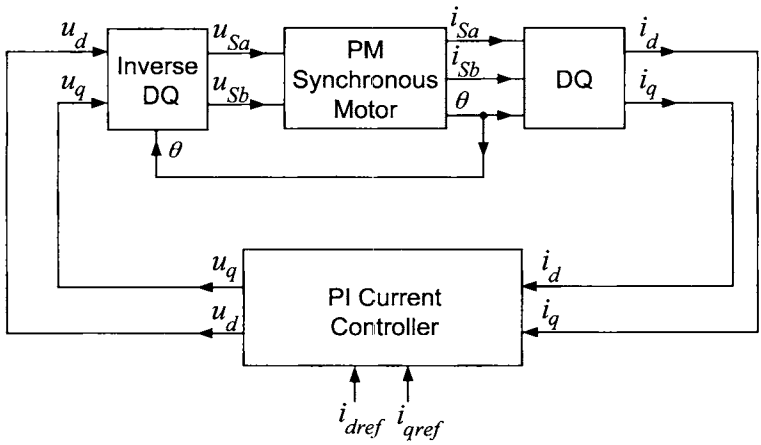


FIGURE 9.14. Current command control of a PM synchronous motor.

www.EngineeringEBooksPdf.com

One often chooses $i_{dref} \equiv 0$ in (9.49) if the speeds are not too high. However, field weakening may be required if one desires to run the machine at high speeds. In this case, the general approach to field weakening given in the next section would be a useful way to specify i_{dref}.

9.2 Optimal Field Weakening*

Maximization of the torque produced by electric motors is an important practical consideration, as optimization may yield the use of a smaller motor for a given application, or higher performance for a given motor. In this section, the problem of extracting all the available torque from a PM synchronous motor is considered. More specifically, given any fixed speed ω as well as the current and voltage constraints $I_{\max}$ and $V_{\max}$, respectively, it is shown how the voltages and currents in the machine must be chosen to obtain the optimum torque without violating the constraints. The approach here is from the development in Refs. [116][117].

As shown in the previous section, one of the reasons the available torque of electric motors decreases at high speed is due to the voltage limits. This is because the source voltage must overcome the increasing back-emf voltage to the detriment of building up the stator currents. Maximization of the torque at high speeds requires the use of field-weakening which, for synchronous motors, may be achieved optimally using a relatively simple strategy. At low speeds, the current limits restrict how much torque can be produced and the voltage limits play no role. At intermediate speeds as well as higher speeds, both the voltage and the current limits are active or just the voltage limits. This section provides algorithms to compute the speeds at which transitions occur between these modes, and describes control strategies required in each case.

9.2.1 Formulation of the Torque Maximization Problem

The state-space model in the dq coordinates is

$$L_S \frac{di_d}{dt} = -R_S i_d + n_p \omega L_S i_q + u_d \tag{9.53}$$

$$L_S \frac{di_q}{dt} = -R_S i_q - n_p \omega L_m i_d - K_m \omega + u_q \tag{9.54}$$

$$J \frac{d\omega}{dt} = K_m i_q - \tau_L \tag{9.55}$$

$$\frac{d\theta}{dt} = \omega. \tag{9.56}$$

www.EngineeringEBooksPdf.com

For a constant speed ω, equations (9.53)–(9.55) yield

$$u_d = R_S i_d - n_p \omega L_S i_q \tag{9.57}$$

$$u_q = R_S i_q + n_p \omega L_S i_d + K_m \omega \tag{9.58}$$

$$K_m i_q = \tau_L. \tag{9.59}$$

The objective here is the maximization of the electrical torque $K_m i_q$ within the voltage and current constraints. The voltage and current constraints are incorporated into the problem statement by using the fact that, at constant speed, the phase voltages and the phase currents are sinusoidal, with peak magnitudes given by $\sqrt{u_d^2 + u_q^2}$ and $\sqrt{i_d^2 + i_q^2}$, respectively. Therefore, the phase voltages bounded by V_{max} and the phase currents bounded by I_{max} yield constraints in the dq variables given by

$$V \triangleq \sqrt{u_d^2 + u_q^2} \leq V_{max} \tag{9.60}$$

$$I \triangleq \sqrt{i_d^2 + i_q^2} \leq I_{max}. \tag{9.61}$$

9.2.2 Speed Ranges and Transition Speeds

Because the torque may, in theory, be made arbitrarily large by increasing the voltage and current levels, optimal operation under constraints is always achieved with the limits on either the currents, the voltages or both being reached. A typical motor is characterized by three ranges of speed: a low-speed range where operation is constrained by the current limit only, an intermediate speed range where operation is constrained by both the voltage and the current limit, and a high-speed range where operation is constrained by the voltage limit only.

At a specific speed, torque maximization will be achieved for a specific choice of i_d and i_q for a current controlled drive, or a specific choice of u_d and u_q for a voltage controlled drive. The optimal values are denoted by i_d^*, i_q^*, u_d^*, and u_q^*. At each such speed, the torque optimization will result in the machine being at one of the three constraint conditions: (i) $V = V_{\max}$, (ii) $I = I_{\max}$, or (iii) $V = V_{\max}, I = I_{\max}$. Knowing what the solution is for each of these three possible constraint conditions, it remains to determine the speeds at which the system transitions from one constraint to another. The speed at which the system transitions between $V = V_{\max}$ and $V = V_{\max}, I = I_{\max}$ is referred to as the *first transition speed* and is denoted by ω_1. Similarly, the speed at which the system transitions between $I = I_{\max}$ and $V = V_{\max}, I = I_{\max}$ is referred to as the *second transition speed* and is denoted by ω_2. These speeds can be calculated after having obtained the form of the optimal solution in each speed range. In the analysis that follows, only the case $\omega \geq 0$ is considered because straightforward symmetry arguments easily yield the case $\omega \leq 0$.

www.EngineeringEBooksPdf.com

Case 1: Optimization under just Current Constraints

First consider the case where only the current constraint is active. In this case, the optimum i_d^* must be zero and $i_q^* = \pm I_{\max}$ to optimize the torque. The overall solution is simply

$$\begin{aligned} i_d^*(\omega) &= 0 && (9.62)\\ i_q^*(\omega) &= \pm I_{max} && (9.63)\\ u_d^*(\omega) &= \pm(-n_p\omega L_S I_{max}) && (9.64)\\ u_q^*(\omega) &= \pm R_S I_{max} + K_m\omega. && (9.65) \end{aligned}$$

where the positive sign is chosen for positive torque and the negative sign is chosen for negative torque.

Case 2: Maximization under just Voltage Constraints

Torque maximization under the voltage constraint alone yields a solution which is referred to as *optimal field-weakening* and is well known (cf. Ref. [1], p. 266, and Ref. [114]). To obtain the solution, one solves (9.57) and (9.58) for i_d and i_q, so that

$$\begin{bmatrix} i_d \\ i_q \end{bmatrix} = \frac{1}{Z_S^2(\omega)} \begin{bmatrix} R_S u_d + n_p\omega L_S(u_q - K_m\omega) \\ -n_p\omega L_S u_d + R_S(u_q - K_m\omega) \end{bmatrix}, \tag{9.66}$$

where $Z_S^2(\omega) \triangleq R_S^2 + (n_p\omega L_S)^2$. Choosing ϕ so that $u_d = V\cos(\phi), u_q = V\sin(\phi)$, the current i_q is given by

$$i_q = \frac{-n_p\omega L_S V\cos(\phi) + R_S V\sin(\phi) - R_S K_m\omega}{Z_S^2(\omega)}. \tag{9.67}$$

Equation (9.67) shows that the maximum current i_q, and therefore the maximum electrical torque, is obtained for

$$\begin{aligned} V &= \pm V_{max}\\ \frac{d}{d\phi}(-n_p\omega L_S\cos(\phi) + R_S\sin(\phi)) &= 0 \end{aligned}$$

where the positive sign is chosen for positive torque and the negative sign is chosen for negative torque. Solving the second of these equations gives $\tan(\phi^*) = -R_S/(n_p\omega L_S)$. The optimal u_d^* and u_q^* therefore satisfy

$$\frac{u_d^*}{u_q^*} = -\frac{n_p\omega L_S}{R_S} = \frac{1}{\tan(\phi^*)}. \tag{9.68}$$

This equation gives the value of the *optimal lead angle* for voltage-controlled drives. Equation (9.68) yields

$$\begin{aligned} \sin(\phi^*) &= R_S/Z_S(\omega)\\ \cos(\phi^*) &= -n_p\omega L_S/Z_S(\omega) \end{aligned}$$

www.EngineeringEBooksPdf.com

and therefore

$$u_d^*(\omega) = \pm\frac{-n_p\omega L_S}{Z_S(\omega)}V_{max} \tag{9.69}$$

$$u_q^*(\omega) = \pm\frac{R_S}{Z_S(\omega)}V_{max}. \tag{9.70}$$

where the + sign is for positive torque and the − sign is for negative torque. Using these values for the voltages, one finds the resulting direct current i_d^* is given by [see (9.66) and (9.68)]

$$i_d^*(\omega) = -\frac{(n_p\omega L_S)(K_m\omega)}{Z_S^2(\omega)} = \frac{-n_p L_S K_m\omega^2}{R_S^2 + (n_p\omega L_S)^2}, \tag{9.71}$$

which can be viewed as the *optimal field weakening current* (compare with (9.21)). Similarly, the quadrature current is given by

$$i_q^*(\omega) = \frac{\pm V_{max}Z_S(\omega) - K_m\omega R_S}{Z_S^2(\omega)}. \tag{9.72}$$

Note that if $R_S = 0$, then the motoring and braking quadrature currents are the negative of each other.

Case 3: Maximization under Voltage and Current Constraints

In the case where both the voltage and the current constraints are active, the optimization reduces to the solution of a system of algebraic equations, because there are as many constraints as degrees of freedom. The steady-state equations (9.57) and (9.58) are substituted into $u_d^2 + u_q^2 = V_{max}^2$ and after some rearranging, results in

$$Z_S^2(\omega)(i_d^2 + i_q^2) + K_m^2\omega^2 + 2R_S K_m\omega i_q + 2n_p L_S K_m\omega^2 i_d = V_{max}^2. \tag{9.73}$$

Eliminating i_d using $i_d^2 + i_q^2 = I_{max}^2$ leads to a quadratic equation for i_q^* of the form

$$\alpha(\omega)\, i_q^{*2} + \beta(\omega)\, i_q^* + \gamma(\omega) = 0, \tag{9.74}$$

where

$$\alpha(\omega) \triangleq 4R_S^2\omega^2 K_m^2 + 4n_p^2\omega^4 L_S^2 K_m^2 \tag{9.75}$$

$$\beta(\omega) \triangleq -4R_S K_m\omega(V_{max}^2 - K_m^2\omega^2 - Z_S^2(\omega)I_{max}^2) \tag{9.76}$$

$$\gamma(\omega) \triangleq (V_{max}^2 - K_m^2\omega^2 - Z_S^2(\omega)I_{max}^2)^2 - 4I_{max}^2 n_p^2\omega^4 L_S^2 K_m^2. \tag{9.77}$$

In this case, where both the voltage and the current constraints are active, $\beta^2(\omega) - 4\alpha(\omega)\gamma(\omega) \geq 0$ (see problem 4) and equation (9.74) has two real roots

$$i_q^*(\omega) = \frac{-\beta(\omega) \pm \sqrt{\beta^2(\omega) - 4\alpha(\omega)\gamma(\omega)}}{2\alpha(\omega)} \tag{9.78}$$

www.EngineeringEBooksPdf.com

with the positive sign for motoring and the negative sign for braking. It then follows that

$$i_d^*(\omega) = -\sqrt{I_{max}^2 - i_q^{*2}(\omega)} \tag{9.79}$$

$$u_d^* = R_S i_d^* - n_p \omega L_S i_q^* \tag{9.80}$$

$$u_q^* = R_S i_q^* + n_p \omega L_S i_d^* + K_m \omega. \tag{9.81}$$

Again note that if $R_S = 0$ ($\Rightarrow \beta(\omega) = 0$), the motoring and braking quadrature currents are just the negative of each other.

First Transition Speed ω_1

As previously explained, the speed at which the system transitions between $V = V_{\max}$ and $V = V_{\max}, I = I_{\max}$ is referred to as the *first transition speed* and is denoted by ω_1. To calculate ω_1, consider the machine to be operating under the current constraint only so that $i_q = \pm I_{\max}$ and find the value of the speed for which the voltage limit is first encountered. Specifically, substitute (9.64) and (9.65) into $u_d^2(\omega) + u_q^2(\omega) = V_{max}^2$ and rearrange to obtain the following equation for the first transition speed:

$$(K_m^2 + (n_p L_S I_{max})^2)\omega_1^2 + 2K_m K_m I_{max}\omega_1 = V_{max}^2. \tag{9.82}$$

The equation has two real roots $\omega_{1pos} > 0$ and $\omega_{1neg} < 0$ (see problem 5). The positive root ω_{1pos} corresponds to the case of positive torque. The negative root corresponds to the braking mode, that is, $|\omega_{1neg}|$ is the transition speed when $i_q = -I_{\max}$ (see problem 5). If $R_S = 0$, $\omega_{1neg} = -\omega_{1pos}$.

Second Transition Speed ω_2

Similarly, the speed at which the system transitions between $I = I_{\max}$ and $V = V_{\max}, I = I_{\max}$ is referred to as the *second transition speed* and is denoted by ω_2. To calculate ω_2, consider the machine to be operating under the voltage constraint only so that u_d^*, u_q^* are given by (9.69) and (9.70) resulting in the currents (9.71) and (9.72), then find the value of the speed for which the current limit is first encountered. Specifically, substitute the currents (9.71) and (9.72) into $i_d^2(\omega) + i_q^2(\omega) = I_{max}^2$ and rearrange to obtain

$$Z_S^2(\omega_2)\left(V_{max}^2 + (K_m\omega_2)^2 - Z_S^2(\omega_2) I_{max}^2\right) = \pm 2K_m\omega_2 R_S V_{max} Z_S(\omega_2). \tag{9.83}$$

Upon canceling $Z_S(\omega_2)$ and squaring both sides, one obtains

$$Z_S^2(\omega_2)\left((V_{max}^2 - R_S^2 I_{max}^2) - (n_p^2 L_S^2 I_{max}^2 - K_m^2)\omega_2^2\right)^2 = (2K_m R_S V_{max})^2 \omega_2^2. \tag{9.84}$$

This is a cubic equation in ω_2^2 of the form

$$(x-a)^2(x+b) = cx, \tag{9.85}$$

www.EngineeringEBooksPdf.com

where

$$x \triangleq \omega_2^2 \tag{9.86}$$

$$a \triangleq \frac{V_{max}^2 - R_S^2 I_{max}^2}{n_p^2 L_S^2 I_{max}^2 - K_m^2} \tag{9.87}$$

$$b \triangleq \frac{R_S^2}{(n_p L_S)^2} \tag{9.88}$$

$$c \triangleq \frac{(2K_m R_S V_{max})^2}{(n_p L_S)^2 (n_p^2 L_S^2 I_{max}^2 - K_m^2)^2}. \tag{9.89}$$

To study the roots of equation (9.85), rearrange it as

$$1 - c\frac{x}{(x-a)^2(x+b)} = 0. \tag{9.90}$$

Its root locations can then be found using the properties of the *complementary root locus* [37][46][81], that is, the root locus corresponding to a zero at $x = 0$, a pole at $x = -b$, a double pole at $x = a$, and a *negative* gain $k = -c$. This analysis is now broken down into two cases.

Case 1: $a > 0$

The most common situation is the one in which $a > 0$. The quantity $V_{max}^2 - R_S^2 I_{max}^2 > 0$ for any practical motor, so that the case $a > 0$ actually means that $n_p^2 L_S^2 I_{max}^2 - K_m^2 > 0$. In this case, the complementary root locus is shown in Fig. 9.15. For $c > 0$, there is one negative root $x < -b$, a positive root $x < a$, and a positive root $x > a$. As $x = \omega_2^2$, the root $x < -b$ is extraneous and therefore ignored. To understand which of the other two roots may apply, rearrange equation (9.83) to obtain

$$Z_S^2(\omega)\left(n_p^2 L_S^2 I_{max}^2 - K_m^2\right)\left(\frac{V_{max}^2 - R_S^2 I_{max}^2}{n_p^2 L_S^2 I_{max}^2 - K_m^2} - \omega^2\right) = \pm 2K_m \omega R_S V_{max} Z_S(\omega). \tag{9.91}$$

This expression shows that the root satisfying $x < a$ corresponds to positive torque $(+V_{max})$ while the root satisfying $x > a$ corresponds to the negative torque $(-V_{max})$.

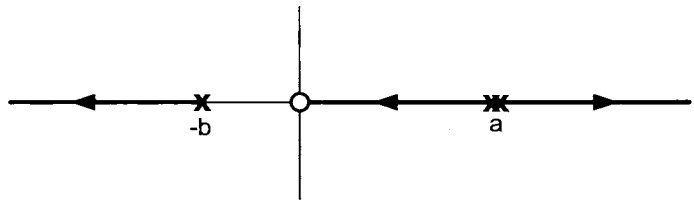


FIGURE 9.15. Locus of roots for $x = \omega_2^2$ of (9.90) with $a > 0$.

www.EngineeringEBooksPdf.com

Case 2: $a < 0$

The solutions of (9.90), or equivalently (9.85), when $a < 0$ are now considered. This case requires $K_m > n_p L_S I_{max}$. In this case, there is never a second transition speed in brake mode, while in the motor mode, there is either *no* second transition speed, or *two* second transition speeds (that is, *two* speeds ω_{21} and ω_{22} where the system transitions between the $V = V_{\max}$ constraint region and the $V = V_{\max}, I = I_{\max}$ constraint region.

In the case $a < 0$, there are two possibilities for the complementary root locus as shown in Figure 9.16. These two possibilities are determined by the break-away points which are the roots of

$$\frac{dc}{dx} = \frac{d}{dx}\frac{(x-a)^2(b+x)}{x} = \frac{(x-a)(2x^2+bx+ab)}{x^2} = 0. \tag{9.92}$$

The solutions of this equation that belong to the complementary root locus are

$$\begin{aligned} x_{b1} &= a \\ x_{b2} &= \frac{-b+\sqrt{b^2-8ab}}{4} \\ x_{b3} &= \frac{-b-\sqrt{b^2-8ab}}{4} \quad \text{if } -a > b. \end{aligned} \tag{9.93}$$

The second root x_{b2} is the only break-away point on the positive real axis and therefore the only one that has physical significance. For roots of (9.90) to be real and positive, the given value of c must be greater than or equal to the value corresponding to the break-away point x_{b2}. In other words, there are two positive roots x_{21}, x_{22} of (9.90) satisfying $x_{21} < x_{b2}$ and $x_{22} > x_{b2}$ if and only if

$$1 - c\frac{x_{b2}}{(x_{b2}-a)^2(b+x_{b2})} > 0. \tag{9.94}$$

Note that, as $a < 0$ (that is, $n_p^2 L_S^2 I_{max}^2 - K_m^2 < 0$), both x_{21} and x_{22} satisfy (9.91) [equivalently (9.83)], with + sign chosen ($+V_{\max}$) rather than the − sign ($-V_{\max}$). In other words, *both* transition speeds $\omega_{21} = \sqrt{x_{21}}, \omega_{22} = \sqrt{x_{22}}$ are associated with the motoring mode in contrast to the case $a > 0$ where they were split between the two modes. As a result, there is no second transition speed in the brake mode. In motor mode, there are actually *four* speed ranges in this case. They are, in order of increasing speed, constrained by (1) current limits (2) current and voltage limits (3) voltage limits and (4) current and voltage limits.

www.EngineeringEBooksPdf.com

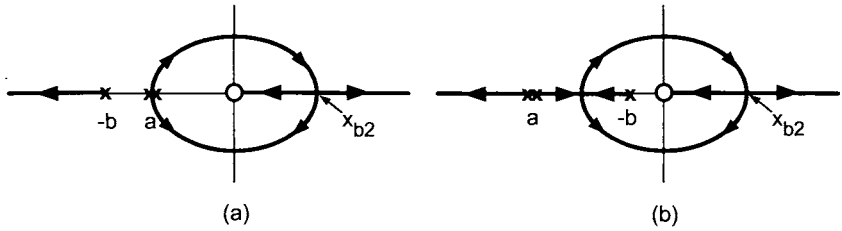


FIGURE 9.16. Locus of roots for $x = \omega_2^2$ of (9.90) with $a < 0$. (a) $-a < b$. (b) $-a > b$.

Although hypothetical motor parameters can be selected to obtain the case with $a < 0$ and two second transition speeds, they do not correspond to realistic motors. The typical case is the one in which (9.94) is *not* satisfied, and there is no second transition speed in either motor or brake mode. Then, there are only two speed ranges for torque optimization: a low-speed range constrained by current limits, and a high-speed range constrained by voltage and current limits. Examples of both the typical case (Figure 9.15) and the atypical case (Figure 9.16) are given next.

9.2.3 Two Examples

The motor chosen for consideration is a three-phase PM synchronous motor (BM 500 from Aerotech Inc., Pittsburgh, PA) whose parameter values are given by $L = 9.3 \times 10^{-4}$ H, $R_S = 0.25$ ohms, $J = 13.9 \times 10^{-5}$ kg-m^2, $K = 0.198$ N-m/A and $n_p = 4$. The limits are given by $I_{\max}$ (continuous) $= 18$ A, $I_{\max}$ (peak) $= 55$ A, and V_{bus} (bus voltage) $= 160$ V. The motor bearings are rated for 10,000 rpm or about 1000 rads/sec, which is taken to be the maximum speed of the motor. The corresponding equivalent two-phase parameters are (see the first appendix at the end of this chapter) $L_S = L + L/2 = 14 \times 10^{-4}$ H, $K_m = (\sqrt{3/2})K = 0.243$ N-m/A, $I_{\max}$(continuous) $= (\sqrt{3/2})i_{\max}$ (continuous) $= 22$ A, $I_{\max}$ (peak) $= \sqrt{3/2}i_{\max}$ (peak) $= 67.4$ A, $V_{\max} = \sqrt{3/2}(2/\pi)V_{bus} = 124.8$ V.

Continuous Current Limit

With $I_{\max} = 22$ A and $V_{\max} = 124.8$ V, Figure 9.17 is a plot of the maximum torque for $V = V_{\max}$, Figure 9.18 is a plot of the maximum torque for $I = I_{\max}$, and Figure 9.19 is a plot of the maximum torque for $V = V_{\max}$ and $I = I_{\max}$, all as a function of the speed ω (see the second appendix at the end of this chapter). Both positive and negative torques are given. The curves give the torques obtained by the three strategies, accounting for the voltage and current limits.

www.EngineeringEBooksPdf.com

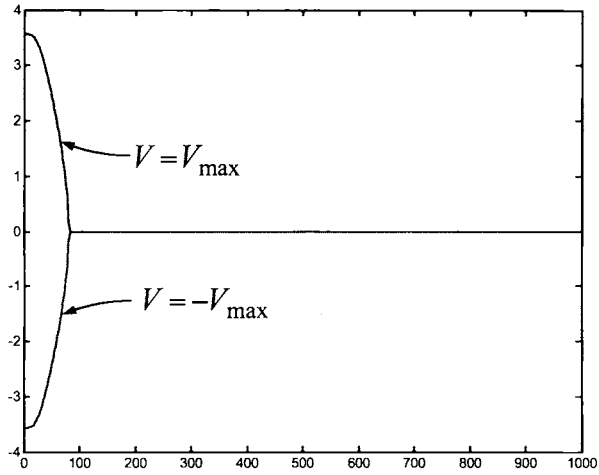


FIGURE 9.17. Maximum torque in N-m versus speed in rad/sec with $V = V_{\max}$.

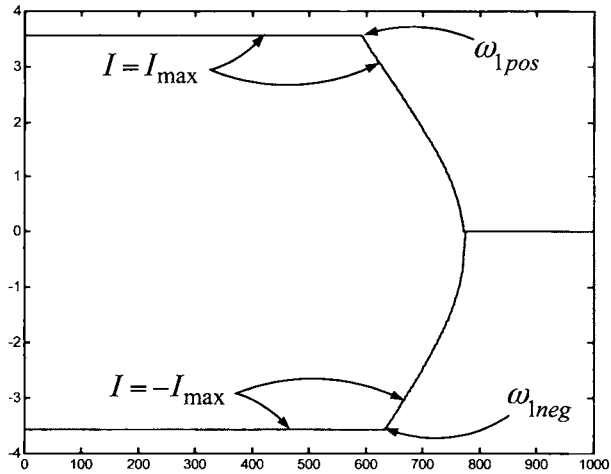


FIGURE 9.18. Maximum torque in N-m versus speed in rad/sec with $I = I_{\max}$.

www.EngineeringEBooksPdf.com

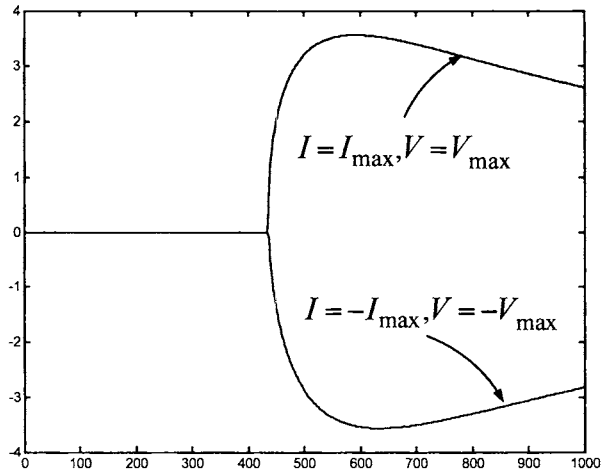


FIGURE 9.19. Maximum torque in N-m versus speed in rad/sec with $I = I_{max}$ and $V = V_{max}$.

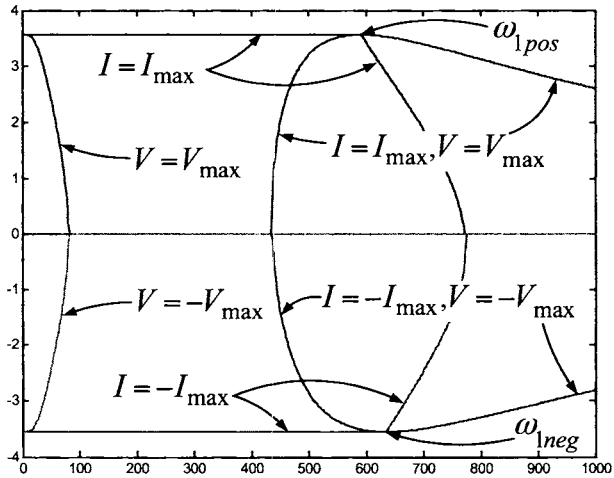


FIGURE 9.20. All three torque components in N-m versus speed in rad/sec.

Figure 9.20 is a plot of all three torque components where it is seen that the actual maximum (minimum) torque attainable is the largest (smallest)

www.EngineeringEBooksPdf.com

of the three curves at each speed (the outer envelope of the curves).

In this case, the first transition speed for the motor mode is $\omega_{1pos} = 592$ rads/sec (see Figures 9.18 and 9.20), while the first transition speed for the brake mode is $\omega_{1neg} = 635$ rads/sec (see Figures 9.18 and 9.20). Note that there are no second transition speeds. As one can see from Figure 9.17, the reason for this situation is that the torque curve obtained with optimal field-weakening (that is, operating at the voltage limit $V = V_{\max}$) falls rapidly due to the current limit. The torque is zero at the speed where the optimal field-weakening current is equal to the maximum current, leaving no torque-producing current. For this reason, a solution accounting for both current and voltage limits must be used at high speed.

Peak Current Limit

Now consider the peak current limit so that $I_{\max} = 67.4$ A and $V_{\max} = 124.8$ V. Figure 9.21 is a plot of the maximum torque for $V = V_{\max}$, Figure 9.22 is a plot of the maximum torque for $I = I_{\max}$, and Figure 9.23 is a plot of the maximum torque for $V = V_{\max}$ and $I = I_{\max}$, all as a function of the speed ω. Both positive and negative torques are given. The curves give the torques obtained by the three strategies, accounting for the voltage and current limits.

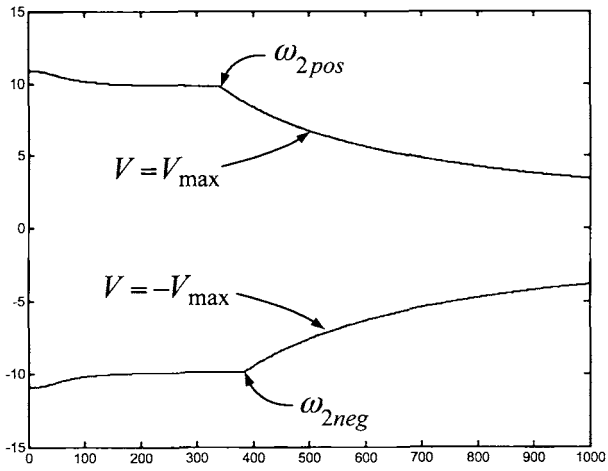


FIGURE 9.21. Maximum torque in N-m versus speed in rad/sec with $V = V_{\max}$.

www.EngineeringEBooksPdf.com

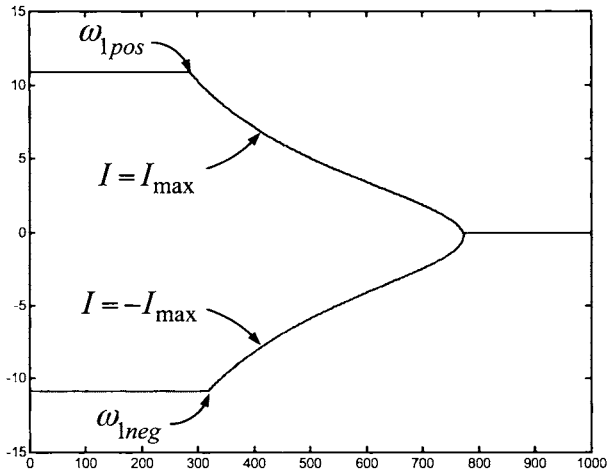


FIGURE 9.22. Maximum torque in N-m versus speed in rad/sec with $I = I_{\max}$.

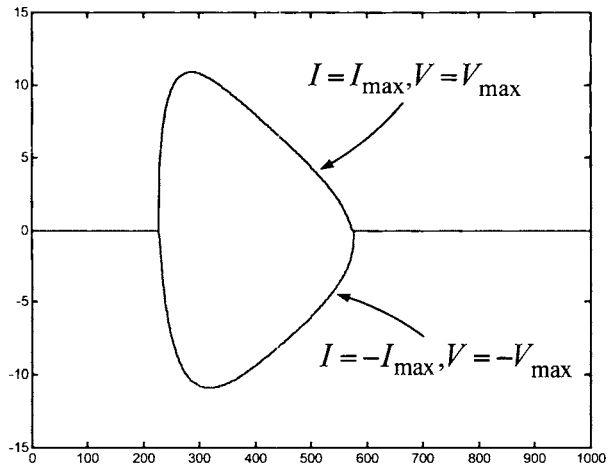


FIGURE 9.23. Maximum torque in N-m versus speed in rad/sec with $I = I_{\max}$ and $V = V_{\max}$.

www.EngineeringEBooksPdf.com

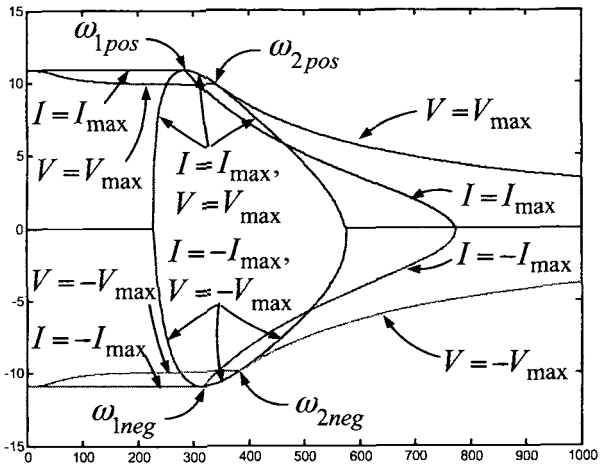


FIGURE 9.24. All three torque components in N-m versus speed in rad/sec.

Figure 9.24 is a plot of all three torque components. Again, the actual maximum (minimum) torque is simply the maximum (minimum) of the three curves at each speed. In this case, the first transition speed for the motor mode is $\omega_{1pos} = 288$ rads/sec (see Figures 9.22 and 9.24) while the second transition speed for the motor mode is $\omega_{1pos} = 320.6$ rads/sec (see Figures 9.21 and 9.24). The first transition speed for the brake mode is $\omega_{1neg} = 340.8$ rads/sec (see Figures 9.22 and 9.24) while the second transition speed for the brake mode is $\omega_{2neg} = 383$ rads/sec (see Figures 9.21 and 9.24).

Simulation

The above analysis assumed constant speed, steady-state conditions. To see how this approach works under non-constant speed conditions, a time-domain simulation can be performed (see problem 8). In this simulation, the continuous current limit of $I_{\max} = 22$ A and voltage limit of $V_{\max} = 124.8$ V are used with the motor driven by the maximum possible torque until the speed reaches approximately the maximum speed 1000 rads/sec (10,000 rpm or the rated speed of the motor bearings). As shown above, this motor with the continuous current limit of 22 A has only the two modes

$$V = V_{\max} \tag{9.95}$$

$$i_d^*(\omega) = 0 \tag{9.96}$$

$$i_q^*(\omega) = \pm I_{\max} \tag{9.97}$$

www.EngineeringEBooksPdf.com

and

$$V = V_{\max}, \quad I = I_{\max} \tag{9.98}$$

$$i_q^*(\omega) = \frac{-\beta(\omega) \pm \sqrt{\beta^2(\omega) - 4\alpha(\omega)\gamma(\omega)}}{2\alpha(\omega)} \tag{9.99}$$

$$i_d^*(\omega) = -\sqrt{I_{max}^2 - i_q^{*2}} \tag{9.100}$$

with

$$\begin{aligned}
\alpha(\omega) &\triangleq 4R_S^2\omega^2K_m^2 + 4n_p^2\omega^4L_S^2K_m^2 \\
\beta(\omega) &\triangleq -4R_SK_m\omega(V_{max}^2 - K_m^2\omega^2 - Z_S^2(\omega)I_{max}^2) \\
\gamma(\omega) &\triangleq (V_{max}^2 - K_m^2\omega^2 - Z_S^2(\omega)I_{max}^2)^2 - 4I_{max}^2n_p^2\omega^4L_S^2K_m^2
\end{aligned}$$

where the positive sign is for motoring and the negative sign is for braking. Consequently, for maximum positive torque, the current commands are (9.96) and (9.97) with the + sign up to $\omega_{1pos} = 592$ rads/sec and then (9.99) and (9.100) are used as the current commands with the + sign for higher speeds. For negative torque, the current commands are (9.96) and (9.97) (with the − sign) up to $\omega_{1neg} = 635$ rads/sec and then (9.99) and (9.100) are used as the current commands (with the − sign) for higher speeds. A basic block diagram for running the motor with maximum torque is given in Figure 9.25.

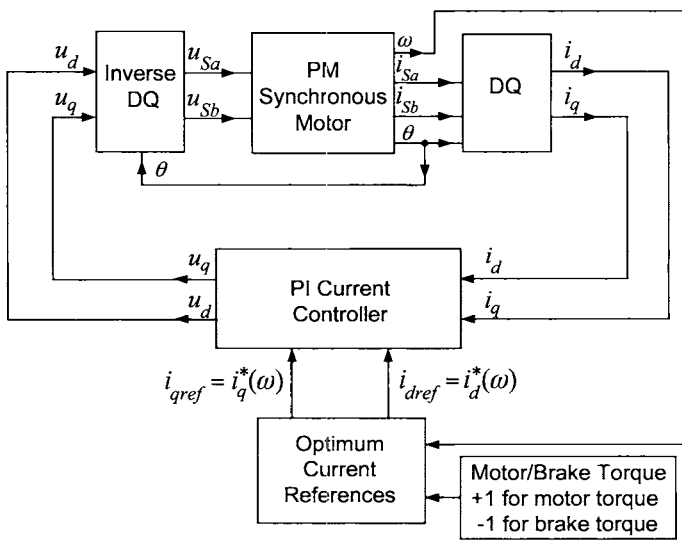


FIGURE 9.25. Block diagram for commanding maximum torque.

www.EngineeringEBooksPdf.com

The normalized optimal values $i_d^*/I_{\max}$ and $i_q^*/I_{\max}$ are graphed in Figure 9.26 corresponding to the normalized speed $\omega_{\text{normalized}} \triangleq \omega/(2\pi 10000/60))$ given in Figure 9.27.

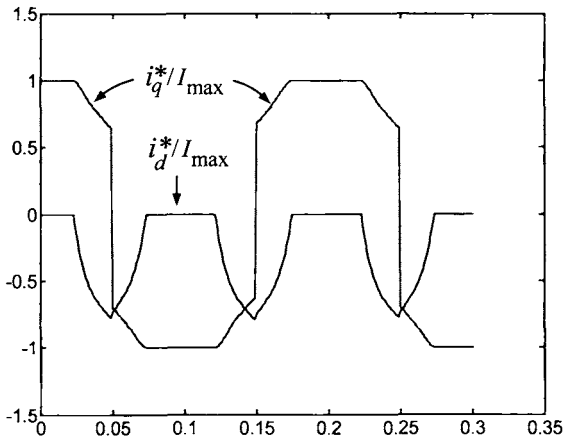


FIGURE 9.26. Optimal direct and quadrature currents versus time in seconds.

Figure 9.27 shows that the motor reaches the speed of 10,000 rpm in about 40 msec.

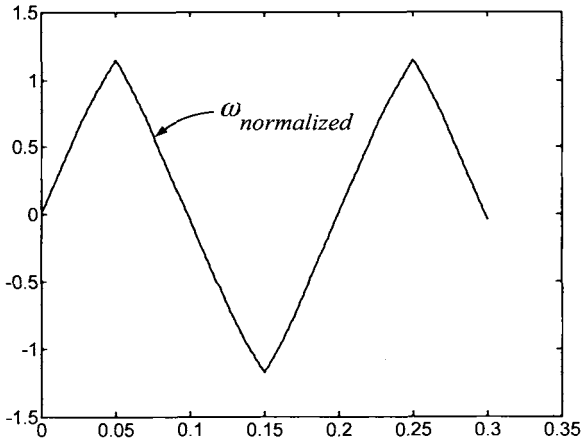


FIGURE 9.27. Normalized speed versus time in seconds.

www.EngineeringEBooksPdf.com

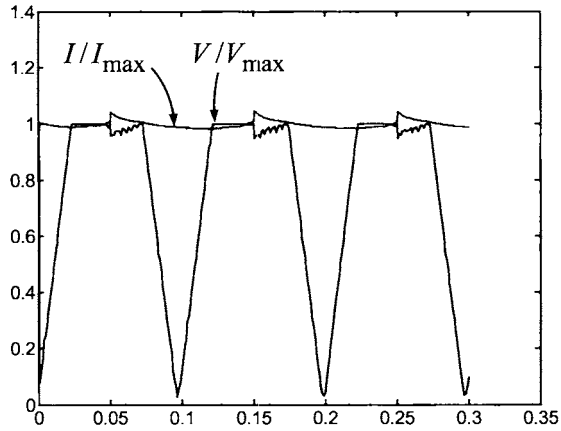


FIGURE 9.28. Normalized current and voltage versus time in seconds.

The normalized magnitude of the voltage $V/V_{\max}$ where $V = \sqrt{u_d^2 + u_q^2}$ and the normalized current $I/I_{\max}$ where $I = \sqrt{i_d^2 + i_q^2}$ are shown in Figure 9.28. Note that the voltage has peaks which are greater than the normalized limit of 1 at those times when the commanded current i_q^* undergoes step changes from the maximum positive value to the minimum negative value (or vice versa). The PI current controller given by $u_q = K_p(i_q^* - i_q) + K_I \int_0^t (i_q^* - i_q)dt$ [see equation (9.49)] is commanding a large voltage due to the large step change in the error $i_q^* - i_q$ at these points in time. However, the voltage actually applied to the motor in the simulation was limited to $V_{\max}$, indicating that these commanded overvoltage peaks have no effect on the performance.

Remarks Of course, the general situation is that one is not always requesting maximum torque from the machine. One possibility is to set the direct current $i_d = i_d^*(\omega)$ so that the maximum torque is always readily available.

Note that the most complicated calculations are square roots and cubic roots so that the whole set of computations could be performed in real-time if the motor parameters were determined online, using an identification procedure such as described in the next section.

In general, there is an intermediate speed range where both the voltage and the current limits are reached. Consideration of this speed range not only provides the complete solution to the problem, but also provides a smooth connection between the solutions for the low and high speed regimes. Further, there are cases where the optimal operation at high speed is determined solely by the joint voltage/current limit solution. In such

www.EngineeringEBooksPdf.com

cases, the conventional optimal field weakening formula never provides the optimum torque.

9.3 Identification of the PM Synchronous Motor Parameters*

This section requires an understanding of the material in Chapter 2 on least-squares identification. The identification of the parameters of a PM synchronous machine are conveniently carried out with the model in the dq coordinate system given by

$$L_S\frac{di_d}{dt} = -R_S i_d + n_p\omega L_S i_q + u_d \tag{9.101}$$

$$L_S\frac{di_q}{dt} = -R_S i_q - n_p\omega L_S i_d - K_m\omega + u_q \tag{9.102}$$

$$K\frac{d\omega}{dt} = K_m i_q - \tau_L. \tag{9.103}$$

For the identification of the motor parameters, the load torque is now taken to be a linear combination of viscous friction and coulomb friction given by

$$\tau_L = -f\omega - f_c\text{sgn}(\omega)$$

where

$$\text{sgn}(\omega) = \begin{cases} 1, & \omega > 0 \\ 0, & \omega = 0 \\ -1, & \omega < 0. \end{cases}$$

The model (9.101), (9.102), (9.103) is rewritten in regressor form as

$$y(nT) = W(nT)K \tag{9.104}$$

where the *output vector* y, *regressor matrix* W, and *parameter vector* K are defined as

$$y(nT) \triangleq \begin{bmatrix} u_d(nT) \\ u_q(nT) \\ 0 \end{bmatrix} \in \mathbb{R}^3,$$

$$W(nT) \triangleq \begin{bmatrix} i_d(nT) & \dfrac{di_d(nT)}{dt} - n_p\omega(nT)i_q(nT) & 0 \\ i_q(nT) & \dfrac{di_q(nT)}{dt} + n_p\omega(nT)i_d(nT) & \omega(nT) \\ 0 & 0 & -i_q(nT) \end{bmatrix}$$

$$\begin{bmatrix} 0 & 0 & 0 \\ 0 & 0 & 0 \\ \dfrac{d\omega(nT)}{dt} & \omega(nT) & -\text{sgn}(\omega(nT)) \end{bmatrix} \in \mathbb{R}^{3\times 6}$$

www.EngineeringEBooksPdf.com

and

$$K \triangleq \begin{bmatrix} R_S & L_S & K_m & J & f & f_c \end{bmatrix}^T \in \mathbb{R}^6.$$

As the model (9.101), (9.102), (9.103), or equivalently (9.104), is *linear* in the parameters, the linear least-squares technique of Chapter 2 applies directly. The *error equation* (9.105) is formed by subtracting the actual (measured) output $y(nT)$ from the estimated output $W(nT)K$ to obtain

$$e(nT) \triangleq W(nT)K - y(nT) \in \mathbb{R}^2. \tag{9.105}$$

If the model (9.104) of the motor were exact, and the voltages, currents, position, and speed could be measured exactly, then there is a parameter vector K such that $e(nT) = 0$ for all time. However, (9.104) is not exactly satisfied due to modeling errors, nor can the voltages, currents, and so on. be measured exactly. In other words, the error $e(nT)$ is never zero for all time. By definition, for any value of the parameter vector K, the *residual error* $E^2(K)$ is equal to the sum of the norm squared error $e^T(nT)e(nT)$ over an interval $[n_0T, n_1T]$, that is,

$$E^2(K) = \sum_{n=n_0}^{n_1} e^T(nT)e(nT) \tag{9.106}$$

$$= \sum_{n=n_0}^{n_1} \Big(W(nT)K - y(nT)\Big)^T \Big(W(nT)K - y(nT)\Big). \tag{9.107}$$

The *least-squares estimate* K^* is the one that minimizes the residual error. Expanding (9.107), the residual error becomes

$$\begin{aligned} E^2(K) = \sum_{n=n_0}^{n_1} \Big(& y^T(nT)y(nT) - y^T(nT)W(nT)K - K^TW^T(nT)y(nT) \\ & + K^TW^T(nT)W(nT)K\Big) \\ = \sum_{n=1}^{N} & y^T(nT)y(nT) - \left(\sum_{n=1}^{N} y^T(nT)W(nT)\right)K \\ & - K^T\left(\sum_{n=1}^{N} W^T(nT)y(nT)\right) + K^T\left(\sum_{n=1}^{N} W^T(nT)W(nT)\right)K. \end{aligned}$$

Making the definitions

$$R_W \triangleq \sum_{n=n_0}^{n_1} W^T(nT)W(nT) \in \mathbb{R}^{6\times 6}, \quad R_{Wy} \triangleq \sum_{n=n_0}^{n_1} W^T(nT)y(nT) \in \mathbb{R}^{6\times 1}$$

$$R_{yW} \triangleq \sum_{n=n_0}^{n_1} y^T(nT)W(nT) \in \mathbb{R}^{1\times 6}, \quad R_y \triangleq \sum_{n=n_0}^{n_1} y^T(nT)y(nT) \in \mathbb{R}$$

www.EngineeringEBooksPdf.com

it is written compactly as

$$\begin{aligned} E^2(K) &= R_y - R_{yW}K - K^T R_{Wy} + K^T R_W K \\ &= R_y - R_{yW}R_W^{-1}R_{Wy} + \left(K - R_W^{-1}R_{Wy}\right)^T R_W \left(K - R_W^{-1}R_{Wy}\right) \end{aligned} \tag{9.108}$$

where it is assumed R_W is invertible (The machine is sufficiently excited). The residual error is then minimized by choosing

$$K = K^* \triangleq R_W^{-1}R_{Wy}. \tag{9.109}$$

This approach is the standard least-squares approach presented in Chapter 2.

Error Index

The residual error indicates how well the measured output $y(nT)$ fits the linear model $W(nT)\hat{K}$. A residual error of zero would indicate a perfect match for every point n. However, as noted above, due to noise, quantization errors, and unmodeled dynamics, the actual residual error is greater than zero. To quantify this fact, recall that the notion of an error index was developed in Chapter 2. Specifically, if all the parameters were set to zero, the residual error would be equal to $E^2(0) = R_y$. As $E^2(K^*)$ is the minimum residual error, it must be less than or equal to R_y. Using these two facts, an indication of how well the least-squares solution fits the data is found by defining a residual error index as

$$\text{Error Index} \triangleq \sqrt{\frac{E^2(K^*)}{E^2(0)}} = \sqrt{\frac{R_y - R_{yW}R_W^{-1}R_{Wy}}{R_y}} \leq 1. \tag{9.110}$$

Multiplying this by 100, the error index can be viewed as a percentage of how well the data fits the linear relationship (9.104).

Parametric Error Index

The residual error index indicates how well the data set fits the model, but gives no indication as to how well the parameters are determined from the data. In Chapter 2, the idea of a parametric error index was developed to address this issue. Recall that to define the parametric error index, variations in the parameters that cause the residual error to double were considered. The residual error due to a variation of $\delta K = K - K^* = K - R_W^{-1}R_{Wy}$ in the parameters is given by $E^2(K) = E^2(K^*) + \delta K^T R_W \delta K$, which follows directly from (9.108). Setting $E^2(K)$ equal to $2E^2(K^*)$ yields

$$E^2(K^*) = \delta K^T R_W \delta K. \tag{9.111}$$

www.EngineeringEBooksPdf.com

If there were just a single parameter (so that R_W is a scalar), this would give an estimate of the parametric sensitivity as

$$\delta K = \sqrt{\frac{E^2(K^*)}{R_W}}.$$

The general solution to (9.111) for $K \in \mathbb{R}^n$ was derived in Chapter 2 and is given by

$$\delta K_i = \sqrt{E^2(K^*)(R_W^{-1})_{ii}}$$

and is taken to be the *parametric error* index. The percent parametric error index is then defined by

$$PE_i \triangleq \frac{\delta K_i}{K_i^*} \times 100. \tag{9.112}$$

This index is equal to the percentage change in the parameter K_i corresponding to a doubling of the residual error and provides an indication of how sensitive the residual error is to each parameter estimate. For example, if $PE_i = 10\%$, then the residual error $E^2(K)$ is doubled for only a 10% change in the ith parameter relative to the optimal estimate K_i^* and therefore $E^2(K)$ is relatively sensitive to the estimated value of K_i. PE_i can be interpreted as a measure of the order of magnitude of the errors on the parameters.

The parametric error indices were chosen to correspond to a doubling of the residual error. As pointed out in Chapter 2, this is an arbitrary as well as a conservative choice; it means that one looks for a parametric variation that would lead to an increase of error equal to 100% of the minimum residual error. If another level had been chosen, all the parametric error indices would have been scaled by the same constant factor. The parametric error indices are especially useful to compare relative sensitivities of different parameters and to give some idea of the values of the errors to be anticipated.

9.3.1 Experimental Results

Experimental results from Refs. [118][119] are now presented to illustrate the identification procedure. A 50-pole-pair ($n_p = 50$) PM synchronous machine is used with a 2000-pulses/rev encoder. Input voltages were commanded to the motor so that it would accelerate reasonably fast while not going over their limits. The sampling frequency is $T = 50$ kHz (see the subsection below on signal processing). Figure 9.29 shows both the current i_q resulting from the input voltages and the simulated current $i_{q\text{sim}}$ resulting from a simulation using the identified parameters and the same input as the experiment. Similarly, Figure 9.30 shows the corresponding speed response ω and the simulated speed ω_{sim}.

www.EngineeringEBooksPdf.com

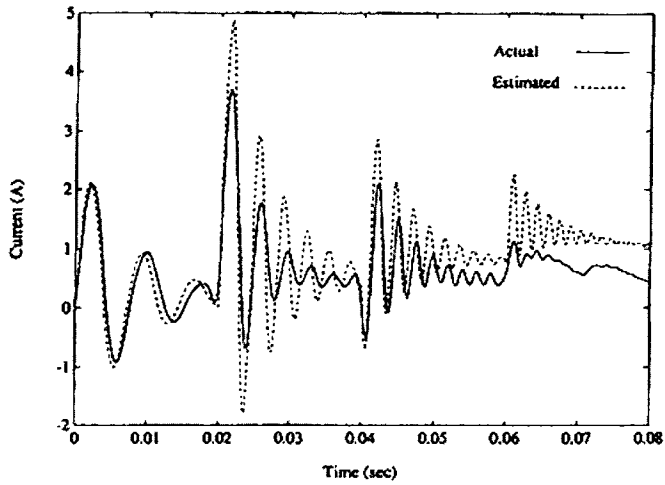


FIGURE 9.29. i_q and i_{qsim} for the identification experiment. From Blauch et al. [119], © 2004 IEEE.

Using the data collected between 0.01 sec and 0.03 sec, the parameters were computed according to (9.109) and their percent parametric error according to (9.112) and are given in the table below. The residual error computed using (9.110) was found to be 12%.

Parameter	Estimate	Parametric Error
R_S ohms	0.269	399%
L_S H	0.0027	47.6%
K_m N-m/A	0.515	19.8%
J kg-m^2/sec^2	0.000187	312%
f N-m/rad/sec	0.0032	5040%
f_c N-m	0.0693	4500%

For comparison, the resistance R_S was measured using an ohmmeter and was found to be 0.6 ohm. By locking the rotor at $\theta = 0$, phase a is just a simple RL circuit [see equation (9.1)] with a time constant of L_S/R_S. Commanding step voltages to phase a and computing the decay rate (time constant) in the current response, L_S/R_S, was found to be $0.0024/0.6 = 0.004$, giving a value of $L_S = 0.0024$ H for the inductance. The value of the resistance computed using the static rotor tests is further from its least-squares value than the value of the inductance. This is simply due to the fact that the value of R_S is not very significant compared to the value of $n_p\omega L_S$ if the speed is just a little above zero. Note that in Figure 9.30 the speed is

www.EngineeringEBooksPdf.com

10 rad/sec or higher after 0.01 sec so that $n_p\omega L_S \geq 50 \times 10 \times 0.0024 = 1.2$ while $R_S = 0.27$ ohm. That is, the value of R_S does not impact the value of the residual error compared to the value of L_S, and this is reflected in the relative values of their parametric errors.

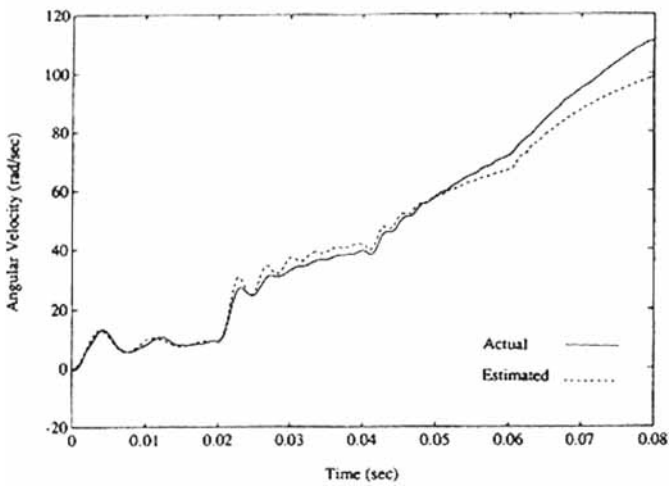


FIGURE 9.30. ω and ω_{sim} for the identification experiment. From Blauch et al. [119], © 2004 IEEE.

Note that the corresponding simulations in Figures 9.29 and 9.30 show a good correspondence with the actual measured data.

Two-Stage Identification

Note from the table above that values of the parametric indices of the friction parameters f and f_c indicate that they are much more uncertain than the stator resistance value, and that the moment of inertia J appears to be almost as uncertain as R_S. However, recall that the parametric indices are not absolute indicators of error. In fact, by doing the identification in two stages (i.e., first identifying the electrical parameters R_S, L_S, and K_m and then using these values to identify the mechanical parameters J, f, and f_c), the values of the parametric indices are significantly reduced though

www.EngineeringEBooksPdf.com

the computed values of J, f, and f_c remain the same. In more detail, let

$$W_{elec}(nT) \triangleq \begin{bmatrix} i_d(nT) & \dfrac{di_d(nT)}{dt} - n_p\omega(nT)i_q(nT) & 0 \\ i_q(nT) & \dfrac{di_q(nT)}{dt} + n_p\omega(nT)i_d(nT) & \omega(nT) \end{bmatrix}$$

$$y_{elec}(nT) = \begin{bmatrix} u_d(nT) \\ u_q(nT) \end{bmatrix}, \quad K_{elec} \triangleq \begin{bmatrix} R_S \\ L_S \\ K_m \end{bmatrix}$$

so that

$$y_{elec}(nT) = W_{elec}(nT)K_{elec}.$$

Defining

$$\begin{aligned} R_{W_{elec}} &\triangleq \sum_{n=n_0}^{n_1} W_{elec}^T(nT)W_{elec}(nT) \in \mathbb{R}^{2\times 2} \\ R_{W_{elec}y} &\triangleq \sum_{n=n_0}^{n_1} W_{elec}^T(nT)y_{elec}(nT) \in \mathbb{R}^{3\times 1} \\ R_{yW_{elec}} &\triangleq \sum_{n=n_0}^{n_1} y_{elec}^T(nT)W_{elec}(nT) \in \mathbb{R}^{1\times 3} \\ R_{y_{elec}} &\triangleq \sum_{n=n_0}^{n_1} y_{elec}^T(nT)y_{elec}(nT) \in \mathbb{R}, \end{aligned}$$

the optimal estimate in the least-squares sense is then given by

$$K_{elec} = R_{W_{elec}}^{-1}R_{W_{elec}y}.$$

Using the same data as above, the parameters and parametric errors were computed and are given in the table below. The values of the parameters are essentially the same as before.

Parameter	Estimate	Parametric Error
R_S ohms	0.268	399%
L_S H	0.0027	47.6%
K_m N-m/A	0.515	19.8%

Next, using the value of K_m just found, the mechanical parameters are identified. To proceed, let

$$W_{mech}(nT) \triangleq \begin{bmatrix} \dfrac{d\omega(nT)}{dt} & \omega(nT) & \text{sgn}(\omega(nT)) \end{bmatrix}$$

$$y_{mech}(nT) = K_m i_q(nT), K_{mech} \triangleq \begin{bmatrix} J \\ f \\ f_c \end{bmatrix}$$

www.EngineeringEBooksPdf.com

so that

$$y_{mech}(nT) = W_{mech}(nT)K_{mech}.$$

Also, let

$$\begin{aligned}
R_{W_{mech}} &\triangleq \sum_{n=n_0}^{n_1} W_{mech}^T(nT)W_{mech}(nT) \in \mathbb{R}^{2\times 2} \\
R_{W_{mech}y} &\triangleq \sum_{n=n_0}^{n_1} W_{mech}^T(nT)y_{mech}(nT) \in \mathbb{R}^{3\times 1} \\
R_{yW_{mech}} &\triangleq \sum_{n=n_0}^{n_1} y_{mech}^T(nT)W_{mech}(nT) \in \mathbb{R}^{1\times 3} \\
R_{y_{elec}} &\triangleq \sum_{n=n_0}^{n_1} y_{mech}^T(nT)y_{mech}(nT) \in \mathbb{R},
\end{aligned}$$

so that optimal estimate in the least-squares sense is given by

$$K_{mech} = R_{W_{mech}}^{-1} R_{W_{mech}y}.$$

The parameter estimates and their parametric errors are

Parameter	Estimate	Parametric Error
J kg-m^2/sec^2	0.000187	13.2%
f N-m/rad/sec	0.0032	214%
f_c N-m	0.0693	191%

The error index was 10%. Note that parameter estimates are the same as before, but the parametric errors are significantly reduced and the error index is reduced slightly. However, the parametric errors still show the same *relative* uncertainty in that the estimate of J is much more certain than the values of f and f_c.

Signal Processing

A few words about processing the signals i_d, i_q, and θ when n_p is large are in order. Recall that the currents i_{Sa} and i_{Sb} are sampled and i_d and i_q computed according to

$$\begin{bmatrix} i_d \\ i_q \end{bmatrix} = \begin{bmatrix} \cos(n_p\theta) & \sin(n_p\theta) \\ \sin(n_p\theta) & \cos(n_p\theta) \end{bmatrix} \begin{bmatrix} i_{Sa} \\ i_{Sb} \end{bmatrix}. \tag{9.113}$$

As the number of pole pairs is $n_p = 50$, a mechanical speed of 3000 rpm corresponds to an electrical frequency of 1.57 kHz. So, even if one samples at 50 kHz, a delay of one sampling period corresponds to a rotor movement of $n_pT \times \left(3000 \text{ rpm}/60\frac{\text{sec}}{\text{min}}\right) \times 360^\circ = 18^\circ$ for $n_p = 50, T = 1/\left(50 \times 10^3\right)$, and, therefore, a phase lag in i_d and i_q of this same amount. A phase shift in

www.EngineeringEBooksPdf.com

the measurement of the phase currents leads to a rotation by the same angle in the dq coordinates. Consequently, as the electrical torque is proportional to i_q only, such a shift could significantly affect the torque. For this reason, the delays present in the system must be accounted for precisely [119]. Due to the zero-order holds, the D/A converters create a delay between the commanded and actual voltages equal to half the sampling period. A delay is also caused by the time required to measure the state variables, calculate the dq transformation, and send the new commanded voltages. The PWM circuit also contains a low-pass filter to reduce circulation in the voltage regulator of the high-frequency noise. The filter has a DC gain of 1 and a cutoff frequency of 10 kHz. The delays due to the filter, PWM inverter, and zero-order hold were combined into a single delay of approximately $1.6T$. If the commanded voltages are used (rather than the measured voltages), they must be delayed by this amount to reflect the voltages effectively applied to the motor. However, if n_p is small, these delays are typically of no significance.

Another issue of significance in the experiments is the filtering of the noise before processing by the least squares algorithm. The collected currents and voltages were transformed into the dq coordinate system according to (9.113) and were filtered in order to remove as much of the measurement (PWM) noise as possible. A third-order Butterworth filter was used with a cutoff frequency of 500 Hz for the dq currents and 100 Hz for the dq voltages. This filtering was performed twice, forward and backward, to avoid the introduction of delays using the MATLAB function *filtfilt* (see Chapter 2). To obtain all the necessary signals for the identification procedure, the derivatives were reconstructed using the backward difference calculation $dx(kT)/dt \triangleq (x(kT) - x((k-1)T))/T$. As such a reconstruction enhances high-frequency noise, the derivatives are filtered again using a third-order Butterworth with a cutoff frequency of 500 Hz.

9.4 PM Stepper Motors*

Motion (servo) control systems often use a particular type of permanent magnet machine called the stepper motor. Permanent magnet stepper motors are synchronous electric machines, but have a quite different construction than the PM synchronous machine described in Chapters 6 and 7. A typical PM stepper motor consists of a stator made of soft iron equipped with windings/coils and a permanent magnet rotor. As shown in Figure 9.31, the rotor has two sets of teeth (left and right in Figure 9.31) which are out of alignment with each other by a tooth width. Typically, there are 50 teeth in each set; one set is magnetized as south poles and the other set is magnetized as north poles, resulting in $n_p = 50$ pole pairs.

www.EngineeringEBooksPdf.com

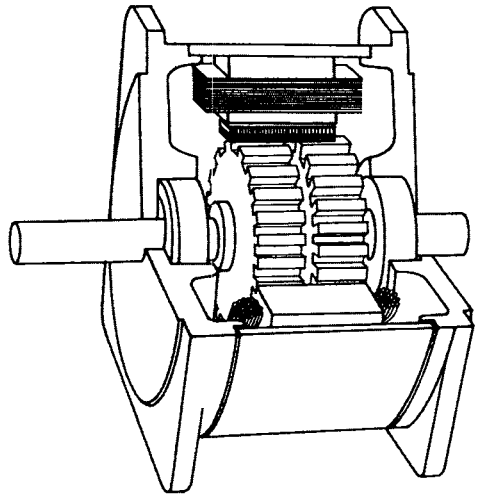


FIGURE 9.31. Cutaway view of a PM stepper motor. Drawn by Sharon Katz. From Section 9.7 of Ref. [120] and reproduced with permision of Marcel Dekker.

A photograph of a PM stepper motor is shown in Figure 9.32 where the rotor has been pulled out for viewing purposes.

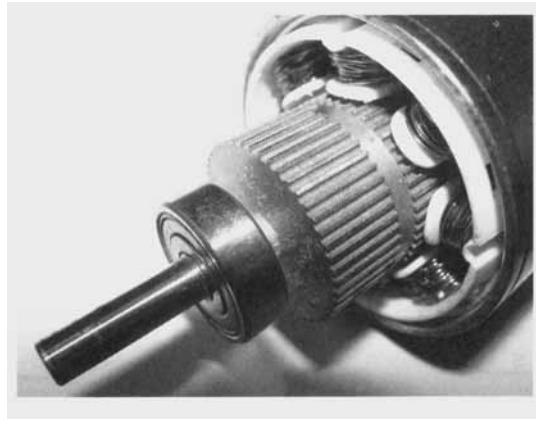


FIGURE 9.32. Photograph of a PM stepper motor with the rotor pulled out from the stator. Courtesy of Prof. J. Douglas Birdwell of The University of Tennessee.

The stator by itself is shown in Figure 9.33 and has eight windings. Four of these windings make up phase a and the other four windings make up phase b. The four windings of phase a are each separated by a winding of phase b and vice versa.

www.EngineeringEBooksPdf.com

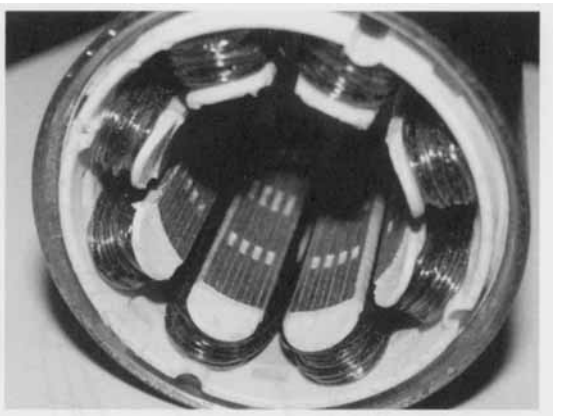


FIGURE 9.33. Stator windings of a PM stepper motor. Four of the windings make up phase a and the other four windings make up phase b. Courtesy of Prof. J. Douglas Birdwell of The University of Tennessee.

Figure 9.34 shows a cross-sectional view of both the left and right sides of a simplified PM stepper motor with only 5 rotor teeth on each side and a stator with four windings. Here the left side of the PM rotor is magnetized as a south pole and the right side of the PM rotor is magnetized as a north pole. The rotor is made of a cylindrical permanent magnet core with the sets of teeth made of soft iron pressed onto either end.

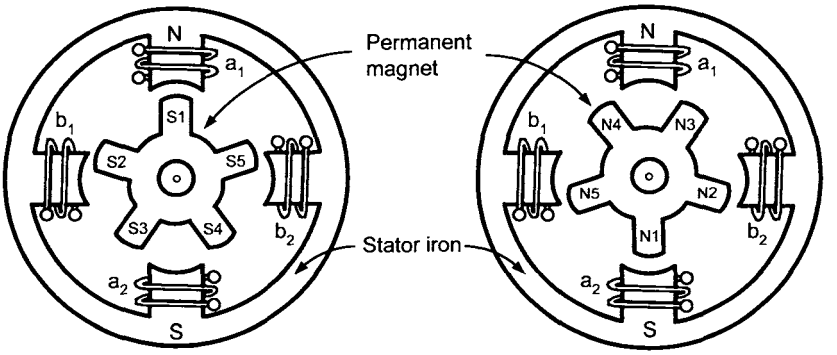


FIGURE 9.34. Cross-sectional views of the left and right sides of a PM stepper motor. Adapted from Deltoro [29] and drawn by Sharon Katz. From Section 9.7 of Ref. [120] and reproduced with permision of Marcel Dekker.

The permanent magnet magnetizes the soft iron of the rotor teeth, making one set a south pole and the other a north pole. The motor is operated as a two-phase machine by connecting windings (coils) a_1 and a_2 in series to make phase a and windings b_1 and b_2 in series to make phase b. This

www.EngineeringEBooksPdf.com

connection as a two-phase machine is now assumed is all that follows.

9.4.1 *Open-Loop Operation of the Stepper Motor*

Stepper motors were originally designed to be used in open-loop [113][114][29]. Their inherent *stepping* ability allows for accurate positioning to a set of discrete positions without feedback. To explain this, consider Figure 9.35(a) with the motor at $\theta = 0$. The direction for positive current for phase a is as shown in the figure. As indicated there, when positive current is in phase a, winding a_1 of the stator is magnetized as a north pole and winding a_2 is magnetized as a south pole. Conversely, when negative current is in phase a, winding a_1 of the stator is magnetized as a south pole and winding a_2 is magnetized as a north pole. Similar remarks hold for phase b. Following the development in Ref. [29], the stepping motion is illustrated in Figures 9.35(a)–(e), which are adapted from Figure 9–23 of Deltoro [29]. Figure 9.35(a) illustrates the starting point with phase a having positive current for a north–south (NS) orientation for windings $a_1 - a_2$ and phase b having no current. In steady-state with $u_{Sa} = u_0$, it follows that $i_{Sa} = i_0$ ($u_0 = R_S i_0$, where R_S is the resistance of phase a) and the motor is held by magnetic attraction at this location. For the first step, i_{Sa} is set to zero and $i_{Sb} = i_0$ so that rotor tooth $N2$ of (the right side) Figure 9.35(a) is attracted to stator winding b_2 [see the right side of Figure 9.35(b)]. Similarly, the rotor tooth $S2$ on the left side of Figure 9.35(a) is attracted to stator winding b_1 [see the left side of Figure 9.35(b)].

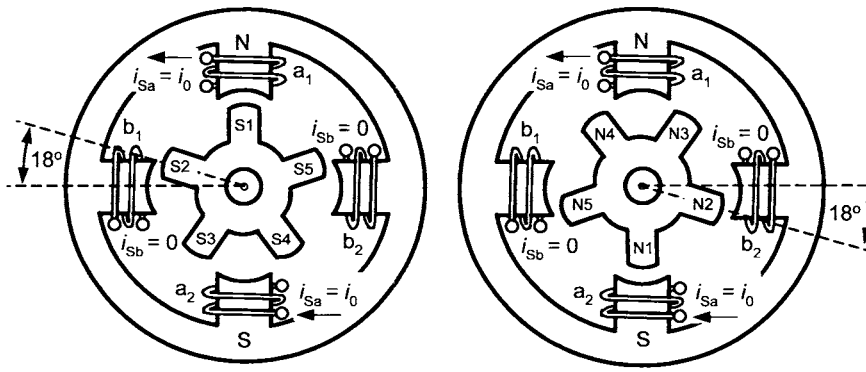


FIGURE 9.35. (a) Starting point with $\theta = 0$ where $u_{Sa} = u_0$, $u_{Sb} = 0$, $i_{Sa} = i_0$, and $i_{Sb} = 0$. Adapted from Deltoro [29] and drawn by Sharon Katz. From Section 9.7 of Ref. [120] and reproduced with permision of Marcel Dekker.

There are $360°/5 = 72°$ between each rotor tooth and, by the geometry of the right side of Figure 9.35(a), $N2$ is 18° from being aligned with winding b_2. The rotor then rotates counterclockwise 18° and, after a short transient

www.EngineeringEBooksPdf.com

period, ends up in the position shown in Figure 9.35(b).

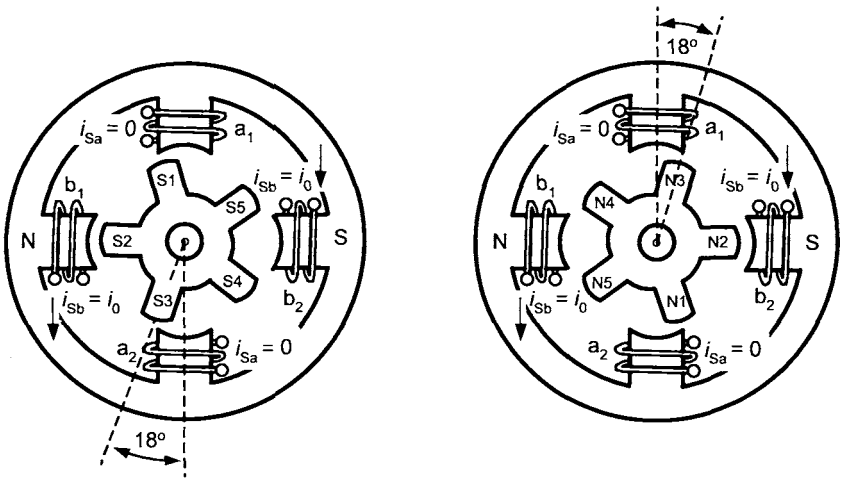


Figure 9.35(b) First step where $\theta = 18°$ with
$u_{Sa} = 0$, $u_{Sb} = u_0$, $i_{Sa} = 0$, $i_{Sb} = i_0$.

For the second step, one sets $u_{Sa} = -u_0$, $u_{Sb} = 0$, $i_{Sa} = -i_0$, and $i_{Sb} = 0$ so that winding a_1 is now a south pole and winding a_2 is a north pole [Figure 9.35(c)]. Rotor tooth $N3$ is then attracted to stator winding a_1 and rotor tooth $S3$ is attracted to stator winding a_2. The rotor then rotates another 18°; after a transient period, θ is 36°, ending up in the position shown in 9.35(c).

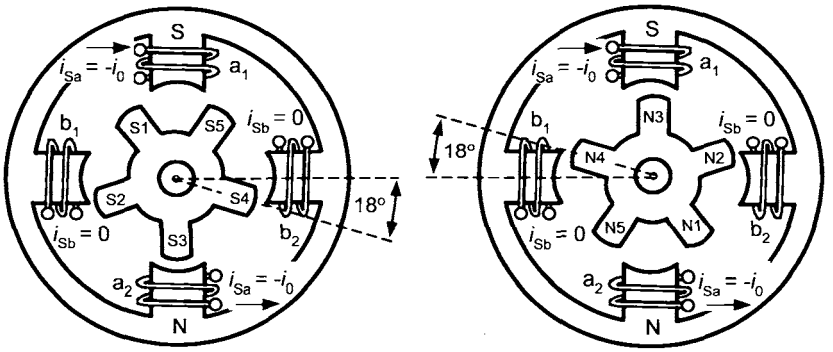


Figure 9.35(c) Second step where $\theta = 36°$ with
$u_{Sa} = -u_0$, $u_{Sb} = 0$, $i_{Sa} = -i_0$, $i_{Sb} = 0$.

For the third step, one sets $u_{Sa} = 0$, $u_{Sb} = -u_0$, $i_{Sa} = 0$, and $i_{Sb} = -i_0$ so that winding b_1 is now a south pole and winding b_2 is a north pole [Figure 9.35(d)]. Rotor tooth $N4$ is then attracted to stator winding b_1 and rotor tooth $S4$ is attracted to stator winding b_2. The rotor then rotates another 18°; after a transient period, θ is 54° as shown in 9.35(d).

www.EngineeringEBooksPdf.com

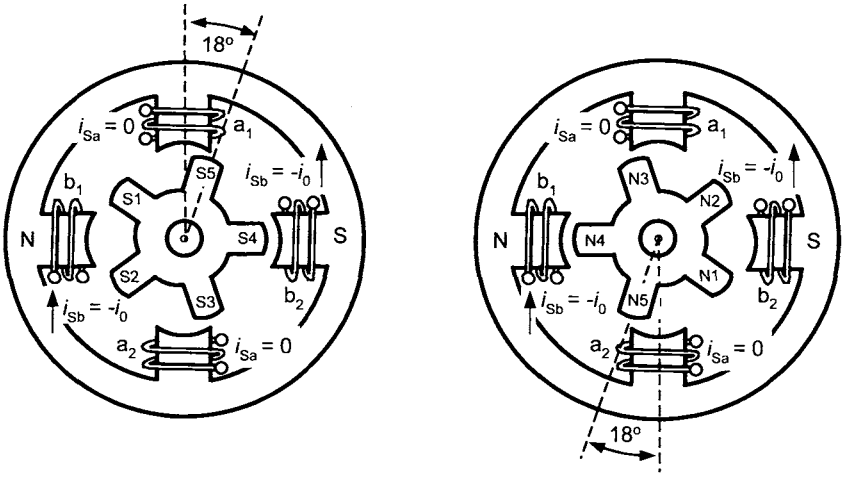


Figure 9.35(d) Third step where $\theta = 54°$ with $u_{Sa} = 0$, $u_{Sb} = -u_0$, $i_{Sa} = 0$, $i_{Sb} = -i_0$.

For the fourth step, one sets $u_{Sa} = u_0$, $u_{Sb} = 0$, $i_{Sa} = i_0$, and $i_{Sb} = 0$ so that winding a_1 is now a north pole and winding a_2 is a south pole [Figure 9.35(e)]. Rotor tooth $S5$ is then attracted to stator winding a_1 and rotor tooth $N5$ is attracted to stator winding a_2. The rotor then rotates another 18°; and after a transient period, θ is 72° as shown in 9.35(e).

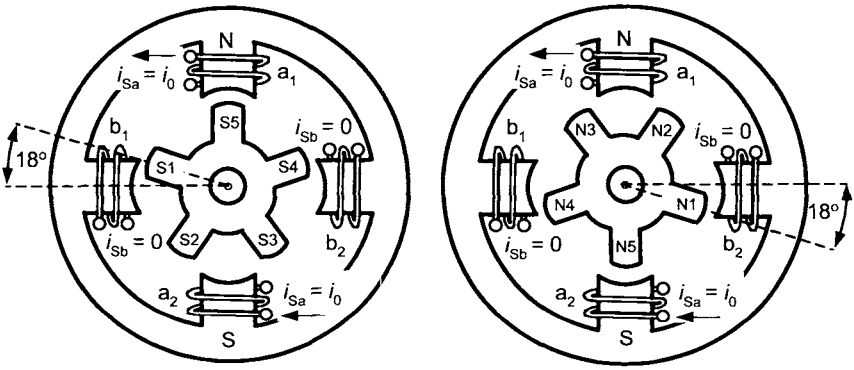


Figure 9.35(e) Fourth step where $\theta = 72°$ with $u_{Sa} = u_0$, $u_{Sb} = 0$, $i_{Sa} = i_0$, $i_{Sb} = 0$.

Note that Figure 9.35(e) is identical to Figure 9.35(a) except for the labeling of the rotor teeth. That is, after four steps, the rotor has moved by an angular distance equal to the angle between two successive rotor teeth. In general, the step size is given by $360°/(4n_p)$. In this particular example, $n_p = 5$ so that the step size is $360°/20 = 18°$ and, with $n_p = 50$, it follows that the step size is 1.8°.

A typical step response of a PM stepper motor with $n_p = 50$ is shown

www.EngineeringEBooksPdf.com

in Figure 9.36, in which the motor rotates 1.8°. For example, starting with the motor as shown in Figure 9.35(a), set $u_{Sa} = 0$ and $u_{Sb} = u_0$, and the response shown in Figure 9.36 results. This oscillatory behavior is due to the fact that the rotor motion (for small steps) is approximately the same as that of a pendulum with the only damping due to the viscous friction of the bearings (see below). To run the motor open loop at constant speed requires the stepping motion illustrated in Figures 9.35(a) through 9.35(e). If a step is initiated before the transient from the previous step have settled out sufficiently, the motor can lose synchronism, resulting in the position being off by a step or more, from which it cannot recover [114]. In fact, the motor can even reverse its direction [121]. As a result, the open-loop operation is traded off with a relatively long settling time and low-speed performance. Fast and precise positioning requires closed-loop control.

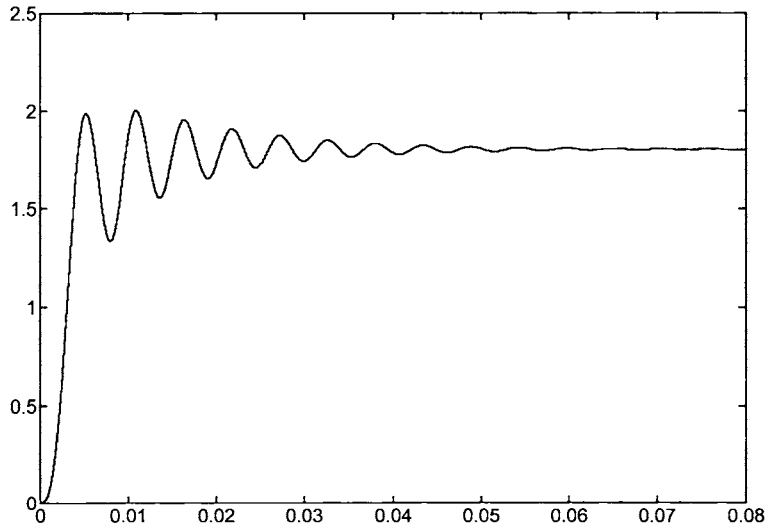


FIGURE 9.36. Step response showing rotor position going from the position in Figure 9.35(a) to the position in Figure 9.35(b). (θ in degrees versus time in seconds.)

www.EngineeringEBooksPdf.com

9.4.2 Mathematical Model of a PM Stepper Motor

Following the developments in Refs. [113][114][115], the mathematical model is now derived using conservation of energy. With L_S the self inductance of each phase winding, the total flux linkage in the windings of the stator phases is given by

$$\begin{aligned} \lambda_{Sa} &= L_S i_{Sa} + \phi_a(\theta) \\ \lambda_{Sb} &= L_S i_{Sb} + \phi_b(\theta) \end{aligned}$$

where $\phi_a(\theta)$ and $\phi_b(\theta)$ are the flux linkages in stator phases a and b, respectively, produced by the rotor's permanent magnet. The surfaces of the rotor and stator teeth are shaped so that the flux linkages $\phi_a(\theta)$ and $\phi_b(\theta)$ are given by (see Refs. [113][115][114])

$$\begin{aligned} \phi_a(\theta) &= \lambda_M \cos(n_p\theta) \\ \phi_b(\theta) &= \lambda_M \sin(n_p\theta) \end{aligned}$$

where λ_M is a constant and $\theta = 0$ corresponds to the rotor as shown in Figure 9.35. By Faraday's law, Ohm's law, and Kirchhoff's voltage law,

$$\begin{aligned} u_{Sa} - R_S i_{Sa} - \frac{d}{dt}\lambda_{Sa} &= 0 \\ u_{Sb} - R_S i_{Sb} - \frac{d}{dt}\lambda_{Sb} &= 0 \end{aligned}$$

or

$$\begin{aligned} L_S \frac{di_{Sa}}{dt} &= -R_S i_{Sa} + K_m \omega \sin(n_p\theta) + u_{Sa} \\ L_S \frac{di_{Sb}}{dt} &= -R_S i_{Sb} - K_m \omega \cos(n_p\theta) + u_{Sb} \end{aligned}$$

where $K_m \triangleq n_p \lambda_M$ and $\omega = d\theta/dt$ is the rotor's angular speed. The power supplied by the source voltages u_{Sa} and u_{Sb} is $i_{Sa}u_{Sa} + i_{Sb}u_{Sb}$ and thus

$$\begin{aligned} i_{Sa}u_{Sa} + i_{Sb}u_{Sb} &= R_S i_{Sa}^2 + R_S i_{Sb}^2 + L_S i_{Sa}\frac{di_{Sa}}{dt} + L_S i_{Sb}\frac{di_{Sb}}{dt} \\ &\quad - (i_{Sa}e_{Sa} + i_{Sb}e_{Sb}) \\ &= R_S\left(i_{Sa}^2 + i_{Sb}^2\right) + \frac{d}{dt}\frac{1}{2}L_S\left(i_{Sa}^2 + i_{Sb}^2\right) - (i_{Sa}e_{Sa} + i_{Sb}e_{Sb}) \end{aligned}$$

where the back-emf voltages e_{Sa} and e_{Sb} are defined by

$$\begin{aligned} e_{Sa} &\triangleq -\frac{d}{dt}\phi_a(\theta) = K_m \omega \sin(n_p\theta) \\ e_{Sb} &\triangleq -\frac{d}{dt}\phi_b(\theta) = -K_m \omega \cos(n_p\theta). \end{aligned}$$

www.EngineeringEBooksPdf.com

The term $R_S\left(i_{Sa}^2 + i_{Sb}^2\right)$ represents ohmic losses in the resistance of the phases ultimately appearing as heat while the term $\dfrac{d}{dt}\dfrac{1}{2}L_S\left(i_{Sa}^2 + i_{Sb}^2\right)$ represents the power stored in the inductance of the phases. The only other power in the system is the mechanical power $\tau\omega$ and thus the term $-\left(i_{Sa}e_{Sa} + i_{Sb}e_{Sb}\right)$ must be the mechanical power delivered to the rotor. That is,

$$\tau\omega = -\left(i_{Sa}e_{Sa} + i_{Sb}e_{Sb}\right)$$

so that the torque is given by

$$\begin{aligned}\tau &= -\left(i_{Sa}e_{Sa} + i_{Sb}e_{Sb}\right)/\omega \\ &= -i_{Sa}K_m\sin(n_p\theta) + i_{Sb}K_m\cos(n_p\theta). \qquad (9.114)\end{aligned}$$

With J the rotor's moment of inertia and τ_L the load torque, the equations of a PM stepper motor are given by

$$\begin{aligned}L_S\frac{di_{Sa}}{dt} &= -R_Si_{Sa} + K_m\omega\sin(n_p\theta) + u_{Sa} \\ L_S\frac{di_{Sb}}{dt} &= -R_Si_{Sb} - K_m\omega\cos(n_p\theta) + u_{Sb} \\ J\frac{d\omega}{dt} &= -i_{Sa}K_m\sin(n_p\theta) + i_{Sb}K_m\cos(n_p\theta) - \tau_L \\ \frac{d\theta}{dt} &= \omega.\end{aligned}$$

Oscillatory Behavior of the Open-Loop PM Stepper Motor

Figure 9.36 shows the oscillatory behavior of a PM stepper motor about it final equilibrium position. To understand the nature of this oscillation, consider the torque expression (9.114) around $\theta = 0$. Specifically, let the stepper motor be in the position shown in Figure 9.35(a), where $\theta = 0$ and with $u_{Sa} = u_0$, $u_{Sb} = 0$, $i_{Sa} = i_0$, $i_{Sb} = 0$. Then

$$\tau \approx -i_{Sa}K_m\sin(n_p\theta) \approx -i_0n_pK_m\theta \qquad (9.115)$$

for θ close to zero. The slope of the torque vs. θ curve at $\theta = 0$ is $-i_0n_pK_m$ which is large for n_p large (e.g., $n_p = 50$). That is, a slight disturbance of the rotor position θ from 0 results in a corresponding large increase in the restoring torque. Also, with $\tau_L = -f\omega$ a viscous friction load torque, the equation describing the rotor position for $|\theta|$ small is given by

$$J\frac{d^2\theta}{dt^2} = -\left(i_0n_pK_m\right)\theta - f\frac{d\theta}{dt}$$

or, with $\omega_n^2 \triangleq i_0n_pK_m/J$, $2\zeta\omega_n \triangleq f/J$, this may be rewritten as

$$\frac{d^2\theta}{dt^2} + 2\zeta\omega_n\frac{d\theta}{dt} + \omega_n^2\theta = 0.$$

This is simply the equation of a pendulum (simple harmonic motion) with viscous damping and, as such, the response is oscillatory.

www.EngineeringEBooksPdf.com

9.4.3 *High-Performance Control of a PM Stepper Motor*

As the mathematical model of the PM stepper motor is identical to that of a standard PM synchronous machine, the control is identical. In fact, the experimental motor used in Section 9.1.4 is a PM stepper motor.

Appendices

Two-Phase Equivalent Parameters

In this Appendix, the calculation of the motor parameters from the manufacturer's data sheet is given. The manufacturer's parameters (Aerotech, Inc., Pgh PA) for their $BM500$ PM synchronous motor are given as follows: line-to-line inductance $L_{\ell-\ell} = 0.028$ H, line-to-line resistance $R_{\ell-\ell} = 0.5$ ohms, line-to-line back-emf constant $K_b^{\ell-\ell} = 23.6$ V(peak)/krpm, torque constant $K_T = 0.28$ N-m/A(rms).

From Chapter 7, equation (7.83), the electrical equations of a three-phase PM synchronous machine are given by ($n_p = 1$)

$$L\frac{di_{S1}}{dt} - \frac{L}{2}\frac{di_{S2}}{dt} - \frac{L}{2}\frac{di_{S3}}{dt} = K\omega\sin(\theta) - R_S i_{S1} + u_{S1} \tag{9.116}$$

$$-\frac{L}{2}\frac{di_{S1}}{dt} + L\frac{di_{S2}}{dt} - \frac{L}{2}\frac{di_{S3}}{dt} = K\omega\sin(\theta - 2\pi/3) - R_S i_{S2} + u_{S2} \tag{9.117}$$

$$-\frac{L}{2}\frac{di_{S1}}{dt} - \frac{L}{2}\frac{di_{S2}}{dt} + L\frac{di_{S3}}{dt} = K\omega\sin(\theta - 4\pi/3) - R_S i_{S3} + u_{S3} \tag{9.118}$$

The line-to-line inductance and resistance measurements are done with the rotor held fixed and applying voltage between phase 1 and 2 with phase 3 open-circuited. Subtracting equation (9.117) from equation (9.116), with $i_{S2} = -i_{S1}, i_{S3} = 0, \omega = 0$ gives

$$3L\frac{di_{S1}}{dt} = u_{S1} - u_{S2} - 2R_S i_{S1}.$$

Consequently, $3L = 0.028$ H and as $L = (2/3)L_S$ one obtains

$$L_S = \frac{3}{2}\frac{0.028}{3}\text{ H} = 0.014\text{ H}$$

while $2R_S = 0.5$ ohm gives

$$R_S = 0.25\text{ ohm}.$$

The line-to-line back-emf voltage is measured by externally driving the motor shaft at constant speed with the phases open circuited and measuring

www.EngineeringEBooksPdf.com

the voltage between two-phases. In this setup, the voltages are given by

$$\begin{aligned} u_{S1} &= -K\omega\sin(\theta) \\ u_{S2} &= -K\omega\sin(\theta - 2\pi/3) = -K\omega\Big(-0.5\sin(\theta) - \sqrt{3}/2\cos(\theta)\Big) \\ u_{S3} &= -K\omega\sin(\theta - 4\pi/3) = -K\omega\Big(-0.5\sin(\theta) + \sqrt{3}/2\cos(\theta)\Big) \end{aligned}$$

where $\theta = \omega t$. Then

$$\begin{aligned} u_{S2} - u_{S3} &= \sqrt{3}K\omega\cos(\theta) \\ \frac{(u_{S2} - u_{S3})_{\text{peak}}}{\omega} &= \sqrt{3}K\,\frac{\text{V}}{\text{rads/sec}} \end{aligned}$$

and

$$K_b^{\ell-\ell} = \sqrt{3}K\frac{2\pi/60 \text{ rads/sec}}{\text{rpm}}\frac{1000 \text{ rpm}}{\text{krpm}}. \tag{9.119}$$

From Chapter 7 (see the remark on page 456), $K = \sqrt{2/3}K_m$ so that

$$\begin{aligned} K_m &= \sqrt{\frac{3}{2}}K = \frac{1}{\sqrt{2}}K_b^{\ell-\ell}\frac{\text{V(peak)}}{\text{krpm}}\frac{\text{krpm}}{1000 \text{ rpm}}\frac{\text{rpm}}{2\pi/60 \text{ rads/sec}} \\ &= \frac{1}{\sqrt{2}}23.6\frac{1}{1000}\frac{60}{2\pi} = 0.159\,\frac{\text{V(peak)}}{\text{rads/sec}} \end{aligned} \tag{9.120}$$

To compute the torque constant (which must equal the back-emf constant), consider the steady-state situation in which the currents are given by

$$\begin{aligned} i_{S1} &= I_{3ph}\cos(\omega t) \\ i_{S2} &= I_{3ph}\cos(\omega t - 2\pi/3) \\ i_{S3} &= I_{3ph}\cos(\omega t - 4\pi/3) \end{aligned}$$

where I_{3ph} is the peak current. The $3-2$ phase transformation results in

$$\begin{bmatrix} i_{Sa} \\ i_{Sb} \end{bmatrix} = \begin{bmatrix} \sqrt{3/2}I_{3ph}\cos(\omega t) \\ \sqrt{3/2}I_{3ph}\sin(\omega t) \end{bmatrix}$$

so that the torque is given by

$$\begin{aligned} \tau &= -\sqrt{\frac{3}{2}}Ki_{Sa}\sin(n_p\theta) + \sqrt{\frac{3}{2}}Ki_{Sb}\cos(n_p\theta) \\ &= \sqrt{\frac{3}{2}}K\sqrt{\frac{3}{2}}I_{3ph}\sin(\omega t - n_p\theta) \\ &= \sqrt{2}\frac{3}{2}KI_{3ph\_rms}\sin(\omega t - n_p\theta) \\ &= K_TI_{3ph\_rms}\sin(\omega t - n_p\theta) \end{aligned}$$

www.EngineeringEBooksPdf.com

where I_{3ph_rms} is the rms current. The manufacturer's value for the torque constant K_T is the torque per unit of rms phase current which this expression shows is equal to $K_T = \sqrt{2}\frac{3}{2}K$ N-m/A(rms) or

$$K = \frac{1}{\sqrt{2}}\frac{2}{3}K_T.$$

K_T is given in units of N-m/A(rms) while K_m is in N-m/A(peak). Finally, putting in the numerical values gives

$$K_m = \sqrt{\frac{3}{2}}K = \frac{K_T}{\sqrt{3}} = \frac{0.28}{\sqrt{3}}\frac{\text{N-m}}{\text{A(peak)}} = 0.162\frac{\text{N-m}}{\text{A(peak)}}. \tag{9.121}$$

Consequently, computing K_m using the back-emf constant (9.120) gives the same value (within numerical accuracy) as computing K_m using the torque constant (9.121) as it must be.

Current Plots

In this appendix, the procedure used to compute the *dq* currents given in Figures 9.17–9.24 is described in detail.

Case 1

Here $i_d^* = 0, i_q^* = \pm I_{max}$ and the magnitude of the voltage required to achieve the maximum current I_{max} must satisfy

$$\begin{aligned} u_d^{*2} + u_q^{*2} &= (-n_p\omega L I_{max})^2 + (R_S I_{max} + K_m\omega)^2 \\ &= Z_S^2(\omega)I_{max}^2 + 2R_S K_m\omega I_{\max} + K_m^2\omega^2 \leq V_{\max}^2. \end{aligned}$$

For higher speeds, this constraint cannot be satisfied and the current i_q^* must be reduced below $I_{\max}$. Setting $i_q^* = I$, the maximum current available for i_q^* is found by solving

$$Z_S^2(\omega)I^2 + 2R_S K_m\omega I + K_m^2\omega^2 = V_{\max}^2.$$

Solving,

$$I_{\pm}(\omega) = \frac{-R_S K_m\omega \pm \sqrt{(R_S K_m\omega)^2 + V_{\max}^2 - Z_S^2(\omega)(K_m\omega)^2}}{Z_S^2(\omega)}$$

www.EngineeringEBooksPdf.com

where the + sign is for motoring and the − sign is for braking. In summary, $i_d^* \equiv 0$ is the direct current reference and

$$i_q^* = \begin{cases} \pm I_{\max}, & u_d^{*2} + u_q^{*2} \le V_{\max}^2 \\ I_{\pm}(\omega), & u_d^{*2} + u_q^{*2} \ge V_{\max}^2 \text{ and} \\ & (R_S K_m \omega)^2 + V_{\max}^2 - Z_S^2(\omega)(K_m\omega)^2 > 0 \\ 0 & \text{otherwise} \end{cases}$$

with + for motoring and − braking.

Case 2

Operating under only the voltage constraint, the optimal field weakening current is given by

$$i_d^* = -\frac{(n_p \omega L_S)(K_m \omega)}{Z_S^2(\omega)}$$

and the corresponding quadrature current is

$$i_q^* = \frac{\pm V_{max} Z_S(\omega) - K_m \omega R_S}{Z_S^2(\omega)}.$$

This is the overall optimum as long as

$$i_d^{*2} + i_q^{*2} \le I_{\max}^2.$$

If this constraint is violated for $-I_{\max} < i_d^* < 0$, then the quadrature current is limited to

$$i_q^* = \pm\sqrt{I_{\max}^2 - i_d^{*2}}$$

otherwise $i_q^* = 0$. In summary, with $i_d^* = -(n_p \omega L)(K_m \omega)/Z_S^2(\omega)$ the direct current reference, the corresponding quadrature current is

$$i_q^* = \begin{cases} \dfrac{\pm V_{max} Z_S(\omega) - K_m \omega R_S}{Z_S^2(\omega)}, & i_d^{*2} + i_q^{*2} \le I_{\max}^2 \\ \pm\sqrt{I_{\max}^2 - i_d^{*2}}, & i_d^{*2} + i_q^{*2} \ge I_{\max}^2 \text{ and } -I_{\max} < i_d^* < 0 \\ 0 & \text{otherwise} \end{cases}$$

with + for motoring and − braking.

www.EngineeringEBooksPdf.com

Case 3

This case gives a direct current reference as $i_d^* = -\sqrt{I_{\max}^2 - i_q^{*2}}$ and the corresponding quadrature current is

$$i_q^* = \begin{cases} \dfrac{-\beta(\omega) \pm \sqrt{\beta^2(\omega) - 4\alpha(\omega)\gamma(\omega)}}{2\alpha(\omega)}, & \beta^2(\omega) - 4\alpha(\omega)\gamma(\omega) \geq 0 \\ 0 & \text{otherwise} \end{cases}$$

with + for motoring and − braking.

Problems

Problem 1 Maximum Torque Under the Voltage Constraint

(a) With the PM synchronous machine at constant speed in steady state so that

$$\begin{aligned} u_d &= R_S i_d - n_p \omega L_S i_q \\ u_q &= R_S i_q + n_p \omega L_S i_d + K_m \omega \\ K_m i_q &= \tau_L \end{aligned}$$

hold, show that the torque is maximized under the constraint $u_d^2 + u_q^2 \leq V_{max}^2$ by choosing the voltages and currents as in (9.14)–(9.16).

(b) Explain why in steady state the physical constraints $|u_{Sa}| \leq V_{max}$, $|u_{Sb}| \leq V_{max}$ are equivalent to $u_{Sa}^2 + u_{Sb}^2 \leq V_{max}^2$.

Problem 2 State Feedback

Show how to choose the state feedback gain (9.40) such that the state feedback specified by (9.39) places the poles of the system (9.38) at any arbitrary location.

Problem 3 Observer

Show how to choose the gains ℓ_1, ℓ_2 in (9.43) and (9.44) so that the error state $e(t) = \begin{bmatrix} e_1(t) & e_2(t) \end{bmatrix}^T \to 0$ at any given prescribed rate.

Problem 4 Maximum Torque Reference with $V = V_{max}, I = I_{max}$

Show that $\beta^2(\omega) - 4\alpha(\omega)\gamma(\omega) \geq 0$ with $\alpha(\omega)$, $\beta(\omega)$, and $\gamma(\omega)$ given by (9.75), (9.76), and (9.77).

Problem 5 First Transition Speed

(a) Show that equation (9.82) has one positive root and one negative root.

(b) Show that $|\omega_{1neg}|$, where ω_{1neg} is the real negative root of (9.82), is the transition speed for $i_q = -I_{max}$.

www.EngineeringEBooksPdf.com

Problem 6 Open-Loop Simulation of a PM Synchronous Machine

Let a two-phase PM machine have parameter values $n_p = 50$ *rotor teeth,* $I_{max} = 6.0$ *A,* $I_{max} = 6.0$ *A,* $V_{max} = 40$ *V,* $R_S = 0.55\ \Omega$, $L_S = 1.5$ *mH,* $K_m = 0.19$ *N-m/A,* $J = 4.5 \times 10^{-5}$ *kg-m*^{2}, *and* $f = 0.0008$ *N-m/rad/sec. Simulate the machine based on equations (9.1). Can you get it to run open loop?*

Problem 7 Closed-Loop Control of a PM Synchronous Machine

Using the parameter values of problem 6, simulate the complete closed-loop controller of Figure 9.1. Do this for two trajectories.

(a) Do a fast turn of the motor from $\theta = 0$ *to* $\theta = 0.9\pi$ *radians using the trajectories of Figures 9.3–9.8.*

(b) Do a high speed move from 0 *to* 25π *radians using the trajectories of Figures 9.9–9.13.*

Problem 8 Simulation of a PM Synchronous Machine Producing Maximum Torque

Let a three-phase PM synchronous motor have parameters values given by $L = 9.3 \times 10^{-4}$ *H,* $R = 0.25$ *ohms,* $J = 13.9 \times 10^{-5}$ *kg-m*^{2}, $K = 0.198$ *N-m/A,* $n_p = 4$. *The limits are given by* i_{max} *(continuous)* $= 18$ *A,* i_{max} *(peak)* $= 55$ *A, and* V_{bus} *(bus voltage)* $= 160$ *V. The motor bearings are rated for* $10,000$ *rpm or about* 1000 *rads/sec which is taken to be the maximum speed of the motor. The corresponding equivalent two-phase parameters are* $L_S = L + L/2 = 14 \times 10^{-4}$ *H,* $K_m = (\sqrt{3/2})K = 0.243$ *N-m/A,* I_{max}*(continuous)* $= (\sqrt{3/2})i_{max}$ *(continuous)* $= 22$ *A,* I_{max} *(peak)* $= \sqrt{3/2}i_{max}$ *(peak)* $= 67.4$ *A,* $V_{max} = \sqrt{3/2}(2/\pi)V_{bus} = 124.8$ *V.*

Do a simulation that implements the block diagram of Figure 9.25. Run the simulation for both the continuous current limit and the peak current limit.

Problem 9 Controlling Two PM Motors with One Amplifier [122]

Consider a situation in which two identical PM synchronous machines are connected in parallel to the same amplifier. This means that the same voltages u_{Sa}, u_{Sb} *are simultaneously applied to both motors. The dq voltages of each motor are given by*

$$\begin{bmatrix} u_{d1} \\ u_{q1} \end{bmatrix} = \begin{bmatrix} \cos(n_p\theta_1) & \sin(n_p\theta_1) \\ -\sin(n_p\theta_1) & \cos(n_p\theta_1) \end{bmatrix} \begin{bmatrix} u_{Sa} \\ u_{Sb} \end{bmatrix}$$

$$\begin{bmatrix} u_{d2} \\ u_{q2} \end{bmatrix} = \begin{bmatrix} \cos(n_p\theta_2) & \sin(n_p\theta_2) \\ -\sin(n_p\theta_2) & \cos(n_p\theta_2) \end{bmatrix} \begin{bmatrix} u_{Sa} \\ u_{Sb} \end{bmatrix}$$

and note that these dq voltages are not the same as the angle of the two motors may not be equal. The model of the two motors in the dq-coordinate

www.EngineeringEBooksPdf.com

system are then

$$\begin{aligned} L\frac{di_{d1}}{dt} &= -R_S i_{d1} + n_p \omega_1 L i_{q1} + v_{d1} \\ L\frac{di_{q1}}{dt} &= -R_S i_{q1} - n_p \omega_1 L i_{d1} - \omega_1 K_{eq} + v_{q1} \\ J\frac{d\omega_1}{dt} &= K_{eq} i_{q1} - \tau_{L1} \\ \frac{d\theta_1}{dt} &= \omega_1 \end{aligned}$$

and

$$\begin{aligned} L\frac{di_{d2}}{dt} &= -R_S i_{d2} + n_p \omega_2 L i_{q2} + v_{d2} \\ L\frac{di_{q2}}{dt} &= -R_S i_{q2} - n_p \omega_2 L i_{d2} - \omega_2 K_{eq} + v_{q2} \\ J\frac{d\omega_2}{dt} &= K_{eq} i_{q2} - \tau_{L2} \\ \frac{d\theta_2}{dt} &= \omega_2. \end{aligned}$$

Show that using the feedback

$$\begin{bmatrix} v_{q1} \\ v_{q2} \end{bmatrix} = \begin{bmatrix} -\sin(n_p\theta_1) & \cos(n_p\theta_1) \\ -\sin(n_p\theta_2) & \cos(n_p\theta_2) \end{bmatrix} \begin{bmatrix} u_{Sa} \\ u_{Sb} \end{bmatrix}$$

and current command control

$$\begin{aligned} v_{q1} &= K_p(i_{q1ref} - i_{q1}) + K_I \int_0^t (i_{q1ref} - i_{q1})dt \\ v_{q2} &= K_p(i_{q2ref} - i_{q2}) + K_I \int_0^t (i_{q2ref} - i_{q2})dt \end{aligned}$$

that the position and speed of each motor can be forced to track a trajectory. Is there any singularity in the controller? How should i_{q1ref}, i_{q2ref} be specified?

Problem 10 Half-Stepping of a PM Stepper Motor

Assume that the stepper motor starts out in the position shown in Figure

www.EngineeringEBooksPdf.com

9.35. Fill in the table below to show the stepping of the motor.

u_{Sa}	u_{Sb}	θ *(degrees)*
u_0	0	0
u_0	u_0	
0	u_0	
$-u_0$	u_0	
$-u_0$	0	
$-u_0$	$-u_0$	
0	$-u_0$	
u_0	$-u_0$	
u_0	0	

Problem 11 PM Synchronous Motor with a Salient Rotor [51]

Some PM synchronous motors are constructed in such a way that the rotor exhibits significant saliency due to a nonuniform air gap. In this case, the flux linkages in the stator phases due to the stator currents depends on the rotor position. Specifically, the stator flux linkages are given by

$$\begin{aligned}\lambda_{Sa} &= L_S i_{Sa} + K_m \cos(n_p\theta) + L_g\left(i_{Sa}\cos(2n_p\theta) + i_{Sb}\sin(2n_p\theta)\right)\\ \lambda_{Sb} &= L_S i_{Sb} + K_m \sin(n_p\theta) + L_g\left(i_{Sa}\sin(2n_p\theta) - i_{Sb}\cos(2n_p\theta)\right)\end{aligned}$$

where the third term in each expression is due to the nonuniform air gap (saliency) of the rotor. Notice that these terms have a period of π/n_p while the flux linkage due to the permanent magnet rotor has a period of $2\pi/n_p$.

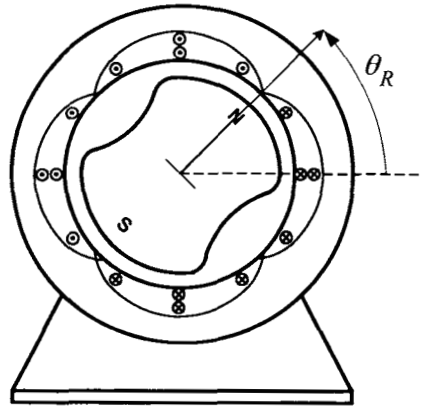


FIGURE 9.37. PM sychronous motor with a salient rotor ($n_p = 1$).

(a) Use a conservation of energy (power) argument to show that the

www.EngineeringEBooksPdf.com

motor torque is given by

$$\begin{aligned}\tau &= 2n_pL_g\Big((i_{Sa}^2 - i_{Sb}^2)\sin(2n_p\theta) + 2i_{Sa}i_{Sb}\cos(2n_p\theta)\Big) \\ &\quad + n_pK_m\Big(-i_{Sa}\sin(n_p\theta) + i_{Sb}\cos(n_p\theta)\Big).\end{aligned}$$

(b) Show that using the dq transformation given by

$$\begin{bmatrix} i_d \\ i_q \end{bmatrix} = \begin{bmatrix} \cos(n_p\theta) & \sin(n_p\theta) \\ -\sin(n_p\theta) & \cos(n_p\theta) \end{bmatrix} \begin{bmatrix} i_{Sa} \\ i_{Sb} \end{bmatrix}$$
$$\begin{bmatrix} u_d \\ u_q \end{bmatrix} = \begin{bmatrix} \cos(n_p\theta) & \sin(n_p\theta) \\ -\sin(n_p\theta) & \cos(n_p\theta) \end{bmatrix} \begin{bmatrix} u_{Sa} \\ u_{Sb} \end{bmatrix}$$

that the equations of the salient PM synchronous motor are given by

$$\begin{aligned}L_d\frac{di_d}{dt} &= -Ri_d - n_p\omega L_qi_q + u_d \\ L_q\frac{di_q}{dt} &= -Ri_q - n_p\omega L_di_d - n_p\omega K_m + u_q \\ J\frac{d\omega}{dt} &= n_p\left(K_mi_q + (L_d - L_q)i_qi_d\right) \\ \frac{d\theta}{dt} &= \omega\end{aligned}$$

where

$$\begin{aligned}L_d &\triangleq L_S + L_g \\ L_q &\triangleq L_S - L_g.\end{aligned}$$

(c) Consider the change of coordinates

$$\begin{aligned}\theta &= \theta \\ \omega &= \omega \\ \alpha &= \frac{n_p}{J}\left(K_mi_q + (L_d - L_q)i_qi_d\right) \\ i_d &= i_d\end{aligned}$$

and show that the motor model is then of the form

$$\begin{aligned}\frac{d\theta}{dt} &= \omega \\ \frac{d\omega}{dt} &= \alpha \\ \frac{d\alpha}{dt} &= f_1(\omega, i_d, i_q) + 2L_gn_pu_d/L_d + n_p\left(K_m + 2L_gi_d\right)u_q/L_q \\ \frac{di_d}{dt} &= f_2(\omega, i_d, i_q) + u_d/L_d.\end{aligned}$$

www.EngineeringEBooksPdf.com

Give the explicit expressions for f_1 *and* f_2.

(d) Show that the nonlinear feedback

$$\begin{bmatrix} u_d \\ u_q \end{bmatrix} = \begin{bmatrix} \dfrac{2L_g n_p}{L_d} & \dfrac{n_p\,(K_m + 2L_g i_d)}{L_q} \\ \dfrac{n_p\,(K_m + 2L_g i_d)}{L_q} & 0 \end{bmatrix}^{-1} \begin{bmatrix} -f_1 + v_d \\ -f_2 + v_q \end{bmatrix}$$

results in a linear *system.*

(e) Under what conditions is the nonlinear feedback of part (d) singular? Is it a practical problem? Explain.

www.EngineeringEBooksPdf.com

10

Trapezoidal Back-Emf PM Synchronous Motors (BLDC)

In this chapter a mathematical model of a trapezoidal back-emf synchronous motor is derived and a control scheme for it is developed. This machine is also known as the brushless DC (BLDC) motor, and this terminology will be explained in Section 10.8.1. Despite the name "brushless DC motor", this is a PM *synchronous* machine where the magnetic fields are *uniformly* distributed in the air gap (rather than sinusoidally distributed). With the motor running at constant speed, this results in a back emf that has a trapezoidal shape in time, and hence the name *trapezoidal back emf* motor.

10.1 Construction

Figure 10.1 shows the basic construction of a three-phase BLDC motor [25]. Figure 10.2 is a redrawing of Figure 10.1 without the rotor so as to show the layout of the three stator phases more clearly.

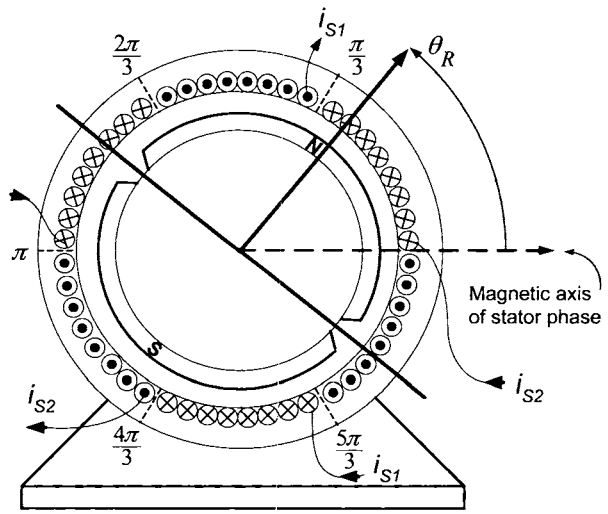


FIGURE 10.1. Construction of a PM trapezoidal back-emf machine. Adapted from Mohan [25].

www.EngineeringEBooksPdf.com

Figure 10.2 shows that there are three sets of windings which are uniformly wound[1] on the inside surface of the stator. Phase 1 with current i_{S1} has its turns uniformly wound between $\pi/3$ and $2\pi/3$ on one side of the stator's inside surface and between $4\pi/3$ and $5\pi/3$ on the other side of the stator. Similarly, phase 2 with current i_{S2} has its turns uniformly wound between π and $4\pi/3$ and between 0 and $\pi/3$ while phase 3 with current i_{S3} has its turns uniformly wound between $2\pi/3$ and π and between $5\pi/3$ and 2π.

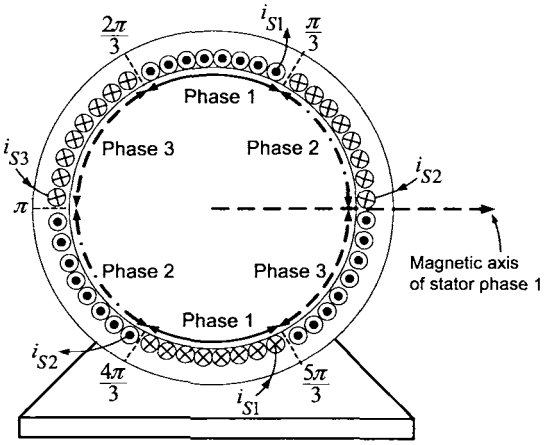


FIGURE 10.2. Three uniformly wound stator phases in a BLDC machine.

Figure 10.3 shows the PM rotor of Figure 10.1 by itself [25].

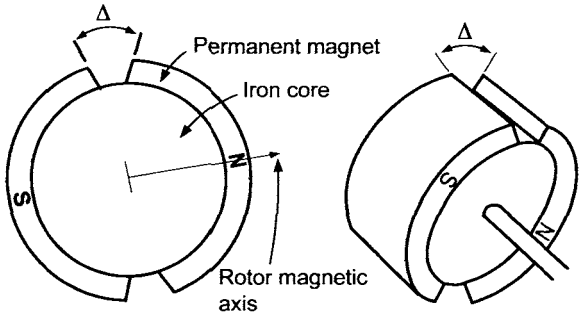


FIGURE 10.3. Rotor of a single pole-pair PM magnet rotor for a BLDC motor. Adapted from Mohan [25].

[1] By *uniformly wound*, it is meant that the number of turns between θ and $\theta + d\theta$ is constant independent of the angle θ.

www.EngineeringEBooksPdf.com

The magnetic axis of the rotor as well as the angle Δ between the north and south poles are indicated. The permanent magnet rotor is constructed by bonding permanent magnets on the surface of a cylindrical core of laminated soft iron. As usual, the rotor position is taken to be along the magnetic axis of the rotor (see Figure 10.3). The permanent magnets on the rotor set up a uniformly (in θ) distributed magnetic field in the air gap given by

$$\vec{\mathbf{B}}_R(r, \theta - \theta_R) =$$

$$\begin{cases} B_{R0}\dfrac{r_R}{r}\hat{\mathbf{r}} & \text{for} \quad -\dfrac{\pi}{2}+\dfrac{\Delta}{2} \le \theta-\theta_R \le \dfrac{\pi}{2}-\dfrac{\Delta}{2} \\ -B_{R0}\dfrac{r_R}{r}\dfrac{(\theta-\theta_R-\pi/2)}{\Delta/2}\hat{\mathbf{r}} & \text{for} \quad \dfrac{\pi}{2}-\dfrac{\Delta}{2} \le \theta-\theta_R \le \dfrac{\pi}{2}+\dfrac{\Delta}{2} \\ -B_{R0}\dfrac{r_R}{r}\hat{\mathbf{r}} & \text{for} \quad \dfrac{\pi}{2}+\dfrac{\Delta}{2} \le \theta-\theta_R \le \dfrac{3\pi}{2}-\dfrac{\Delta}{2} \\ B_{R0}\dfrac{r_R}{r}\dfrac{(\theta-\theta_R-3\pi/2)}{\Delta/2}\hat{\mathbf{r}} & \text{for} \quad \dfrac{3\pi}{2}-\dfrac{\Delta}{2} \le \theta-\theta_R \le \dfrac{3\pi}{2}+\dfrac{\Delta}{2} \end{cases} \tag{10.1}$$

where the parameter Δ represents the angular distance between the north and south pole magnets on the rotor. Also, the factor r_R/r ensures that conservation of flux holds in the air gap. The radial magnetic field distribution in the air gap due to the rotor's permanent magnet is illustrated in Figure 10.4.

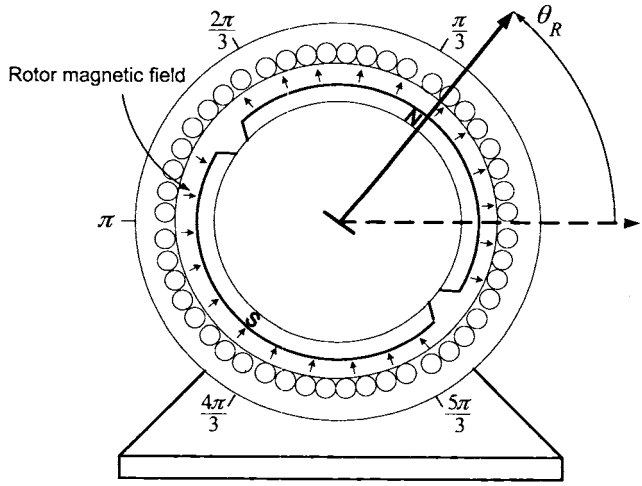


FIGURE 10.4. The radial magnetic field distribution $\vec{\mathbf{B}}_R(r, \theta - \theta_R)$.

www.EngineeringEBooksPdf.com

In Sections 10.2 through 10.7, Δ will be taken to be zero to simplify the analysis with no significant impact on the resulting mathematical model. In this case, (10.1) simplifies to

$$\vec{\mathbf{B}}_R(r,\theta-\theta_R)=\begin{cases} B_{R0}\dfrac{r_R}{r}\hat{\mathbf{r}} & \text{for} \quad -\pi/2 \le \theta-\theta_R \le \pi/2 \\ -B_{R0}\dfrac{r_R}{r}\hat{\mathbf{r}} & \text{for} \quad +\pi/2 \le \theta-\theta_R \le 3\pi/2. \end{cases} \tag{10.2}$$

10.2 Stator Magnetic Field $\vec{\mathbf{B}}_S$

The magnetic field $\vec{\mathbf{B}}_S$ produced stator currents is now derived. As illustrated in Figure 10.1, the stator winding density of a BLDC is uniform over inner periphery of the stator. Specifically, stator phase 1 has a winding density given by

$$N_{S1}(\theta) = \begin{cases} \dfrac{N_S}{\pi/3} & \text{for } \dfrac{\pi}{3} \le \theta \le \dfrac{2\pi}{3} \text{ and } \dfrac{4\pi}{3} \le \theta \le \dfrac{5\pi}{3} \\ 0 & \text{elsewhere.} \end{cases}$$

The total number of windings (turns or loops) making up phase 1 is then

$$\int_{\pi/3}^{2\pi/3} \frac{N_S}{\pi/3} d\theta = N_S.$$

Similarly, $N_{S2}(\theta) = N_{S1}(\theta - 2\pi/3)$ and $N_{S3}(\theta) = N_{S1}(\theta - 4\pi/3)$. To determine the radial magnetic field in the air gap produced by the current in stator phase 1, Ampère's law with $\vec{\mathbf{H}} \equiv 0$ in the iron is applied to the path 1–2–3–1 of Figure 10.5 to obtain [by symmetry, $H_{S1}(i_{S1}, \pi+\theta) = -H_{S1}(i_{S1},\theta)$]

$$2gH_{S1}(i_{S1},\theta) = \begin{cases} N_S i_{S1}, & -\pi/3 \le \theta \le \pi/3 \\ \displaystyle\int_\theta^{2\pi/3} \frac{N_S i_{S1}}{\pi/3} d\theta - \int_{4\pi/3}^{\theta+\pi} \frac{N_S i_{S1}}{\pi/3} d\theta, & \pi/3 \le \theta \le 2\pi/3 \\ -N_S i_{S1}, & 2\pi/3 \le \theta \le 4\pi/3 \\ \displaystyle\int_\theta^{5\pi/3} -\frac{N_S i_{S1}}{\pi/3} d\theta + \int_{7\pi/3}^{\theta+\pi} \frac{N_S i_{S1}}{\pi/3} d\theta, & 4\pi/3 \le \theta \le 5\pi/3 \end{cases}$$

www.EngineeringEBooksPdf.com

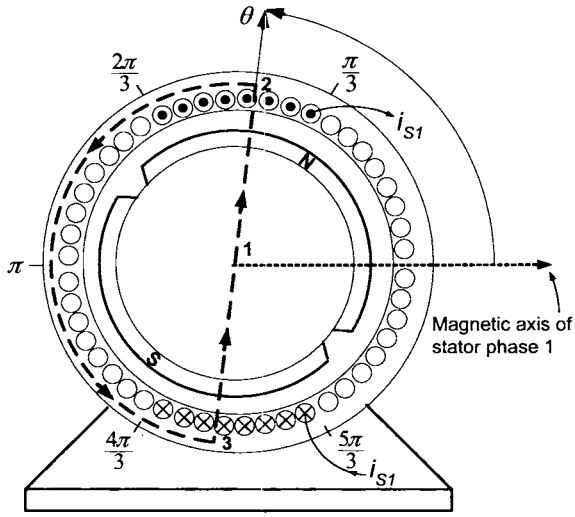


FIGURE 10.5. Path 1–2–3–1 for applying Ampère's law. Note that for the path drawn, $\pi/3 \leq \theta \leq 2\pi/3$.

or

$$\vec{\mathbf{H}}_{S1}(i_{S1},\theta) = \begin{cases} \dfrac{N_S i_{S1}}{2g}\hat{\mathbf{r}} & \text{for} \quad -\pi/3 \leq \theta \leq \pi/3 \\ \dfrac{N_S i_{S1}}{2g}\dfrac{6}{\pi}\left(\dfrac{\pi}{2}-\theta\right)\hat{\mathbf{r}} & \text{for} \quad \pi/3 \leq \theta \leq 2\pi/3 \\ -\dfrac{N_S i_{S1}}{2g}\hat{\mathbf{r}} & \text{for} \quad 2\pi/3 \leq \theta \leq 4\pi/3 \\ \dfrac{N_S i_{S1}}{2g}\dfrac{6}{\pi}\left(\theta-\dfrac{3\pi}{2}\right)\hat{\mathbf{r}} & \text{for} \quad 4\pi/3 \leq \theta \leq 5\pi/3 \end{cases}$$

where it was assumed that $\vec{\mathbf{H}}_{S1}$ is constant across the air gap. Then $\vec{\mathbf{B}}_{S1} = \mu_0 \vec{\mathbf{H}}_{S1}$ in the air gap. A factor of r_R/r is now included to ensure that $\vec{\mathbf{B}}_{S1}$ satisfies conservation of flux in the air gap. Consequently, the magnetic field $\vec{\mathbf{B}}_{S1} = B_{S1}(i_{S1}, r, \theta)\hat{\mathbf{r}}$ at any point (r, θ) in the air gap due to the current

www.EngineeringEBooksPdf.com

i_{S1} in phase 1 is given by

$$B_{S1}(i_{S1},r,\theta)\hat{\mathbf{r}} = \begin{cases} \dfrac{\mu_0 N_S i_{S1}}{2g}\dfrac{r_R}{r}\hat{\mathbf{r}} & \text{for} \quad -\pi/3 \le \theta \le \pi/3 \\ \dfrac{\mu_0 N_S i_{S1}}{2g}\dfrac{r_R}{r}\dfrac{6}{\pi}\left(\dfrac{\pi}{2}-\theta\right)\hat{\mathbf{r}} & \text{for} \quad \pi/3 \le \theta \le 2\pi/3 \\ -\dfrac{\mu_0 N_S i_{S1}}{2g}\dfrac{r_R}{r}\hat{\mathbf{r}} & \text{for} \quad 2\pi/3 \le \theta \le 4\pi/3 \\ \dfrac{\mu_0 N_S i_{S1}}{2g}\dfrac{r_R}{r}\dfrac{6}{\pi}\left(\theta-\dfrac{3\pi}{2}\right)\hat{\mathbf{r}} & \text{for} \quad 4\pi/3 \le \theta \le 5\pi/3. \end{cases} \tag{10.3}$$

Similarly,

$$\begin{aligned} B_{S2}(i_{S2},r,\theta) &= B_{S1}(i_{S2},r,\theta-2\pi/3) \\ B_{S3}(i_{S3},r,\theta) &= B_{S1}(i_{S3},r,\theta-4\pi/3). \end{aligned}$$

A plot of the normalized radial magnetic field $B_{S1}(i_{S1},r,\theta)/\left(\frac{\mu_0 N_S i_{S1}}{2g}\frac{r_R}{r}\right)$ due to the current in stator phase 1 for $-\pi/3 \le \theta \le 2\pi$ is in Figure 10.6.

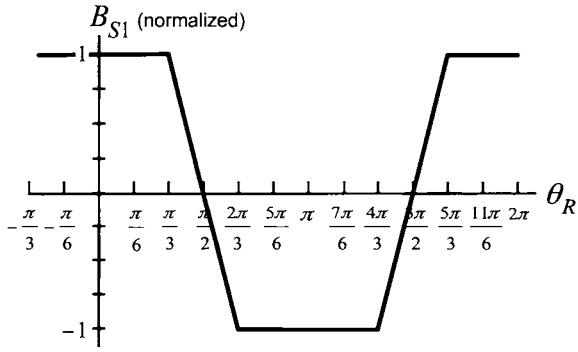


FIGURE 10.6. Normalized magnetic field $B_{S1}(i_{S1},r,\theta)/\left(\frac{\mu_0 N_S i_{S1}}{2g}\frac{r_R}{r}\right)$.

This is also illustrated in Figure 10.7 which shows the direction of radial magnetic field distribution $B_{S1}(i_{S1},r,\theta)$ in the air gap at each angular position θ. In particular, the magnetic field due to i_{S1} is radially out to the right of the dashed vertical line and radially in to the left of the vertical line.

www.EngineeringEBooksPdf.com

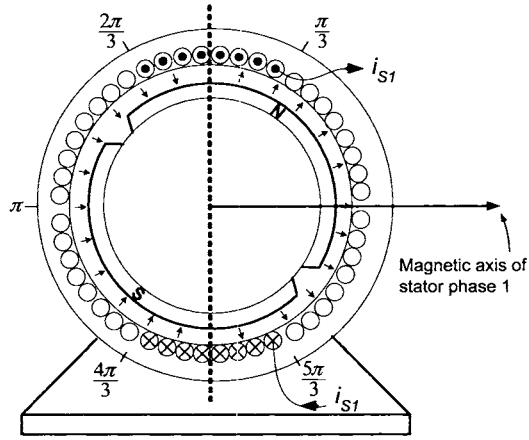


FIGURE 10.7. The radial magnetic field distribution $\vec{\mathbf{B}}_{S1}(i_{S1}, r, \theta)$ in the air gap due to the current i_{S1} in stator phase 1.

10.3 Stator Flux Linkage Produced by $\vec{\mathbf{B}}_S$

The flux $\phi_{11}(i_{S1}, \theta)$ in a winding of stator phase 1 at the angle θ where $\pi/3 \leq \theta \leq 2\pi/3$, due to the current in stator phase 1, is now computed using the flux surface shown in Figure 10.8.

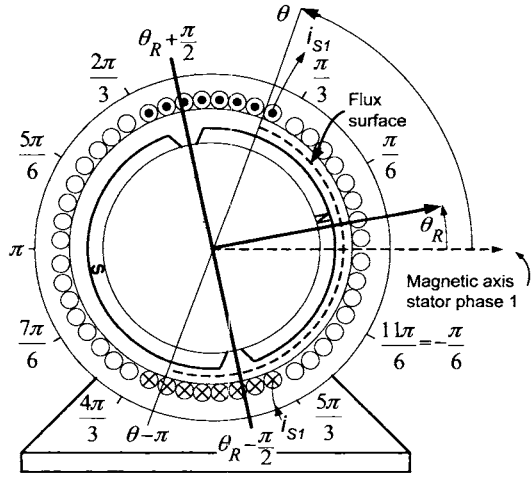


FIGURE 10.8. Flux surface for a winding of stator phase 1 to calculate the flux produced by the magnetic field of i_{S1}.

www.EngineeringEBooksPdf.com

Using the expression (10.3) for $\vec{\mathbf{B}}_{S1}$, the flux produced by $\vec{\mathbf{B}}_{S1}$ in a winding of stator phase 1 with one side at θ and the other at $\theta-\pi$ is given by

$$\begin{aligned}
\phi_{11}(i_{S1},\theta) &= \int_0^{\ell_1}\int_{\theta-\pi}^{\theta} \vec{\mathbf{B}}_{S1}(i_{S1},r_S,\theta')\cdot\left(r_S d\theta' d\ell\hat{\mathbf{r}}\right)\\
&= r_S\ell_1\int_{-\pi/3}^{\pi/3}\frac{\mu_0 N_S i_{S1}}{2g}\frac{r_R}{r_S}d\theta' + r_S\ell_1\int_{\pi/3}^{\theta}\frac{\mu_0 N_S i_{S1}}{g\pi/3}\frac{r_R}{r_S}\left(\frac{\pi}{2}-\theta'\right)d\theta'\\
&\quad + r_S\ell_1\int_{\theta+\pi}^{5\pi/3}\frac{\mu_0 N_S i_{S1}}{g\pi/3}\frac{r_R}{r_S}\left(\theta'-\frac{3\pi}{2}\right)d\theta'\\
&= \frac{\mu_0 r_R\ell_1 N_S i_{S1}}{2g}\left(\frac{2\pi}{3}-\frac{1}{2}\frac{6}{\pi}\left(\frac{\pi}{2}-\theta'\right)^2\Big|_{\pi/3}^{\theta}+\frac{1}{2}\frac{6}{\pi}\left(\theta'-\frac{3\pi}{2}\right)^2\Big|_{\theta+\pi}^{5\pi/3}\right)\\
&= \frac{\mu_0 r_R\ell_1 N_S i_{S1}}{2g}\left(\frac{2\pi}{3}-\frac{3}{\pi}\left(\left(\frac{\pi}{2}-\theta\right)^2-\left(\frac{\pi}{6}\right)^2\right)\right.\\
&\quad \left.+\frac{3}{\pi}\left(\left(\frac{\pi}{6}\right)^2-\left(\theta-\frac{\pi}{2}\right)^2\right)\right)\\
&= \frac{\mu_0 r_R\ell_1 N_S i_{S1}}{2g}\left(-\frac{6}{\pi}\left(\theta-\frac{\pi}{2}\right)^2+\frac{5\pi}{6}\right).
\end{aligned}$$

As the outward normal was used to compute the flux, $-d\phi_{11}/dt>0$ means that this induced emf in stator phase 1 will push current in the same direction as that chosen for positive current flow in stator phase 1.

The total flux linkage $\lambda_{S1}(i_{S1},0,0)$ in stator phase 1 due to the current in phase 1, is then found by adding up the fluxes in each winding of phase 1. That is,

$$\begin{aligned}
\lambda_{S1}(i_{S1},0,0) &= \int_{\pi/3}^{2\pi/3}\phi_{11}(i_{S1},\theta)\frac{N_S}{\pi/3}d\theta\\
&= \frac{\mu_0 r_R\ell_1 N_S^2 i_{S1}}{2g}\frac{3}{\pi}\int_{\pi/3}^{2\pi/3}\left(-\frac{6}{\pi}\left(\theta-\frac{\pi}{2}\right)^2+\frac{5\pi}{6}\right)d\theta\\
&= \frac{\mu_0 r_R\ell_1 N_S^2 i_{S1}}{2g}\left(-\frac{18}{\pi^2}\frac{1}{3}\left(\theta-\frac{\pi}{2}\right)^3\Big|_{\pi/3}^{2\pi/3}+\frac{5}{2}\left(\frac{2\pi}{3}-\frac{\pi}{3}\right)\right)\\
&= \frac{\mu_0 r_R\ell_1 N_S^2 i_{S1}}{2g}\left(-\frac{\pi}{18}+\frac{5}{2}\frac{\pi}{3}\right) = \frac{\mu_0 r_R\ell_1\pi N_S^2 i_{S1}}{2g}\left(\frac{14}{18}\right)\\
&= L_S i_{S1}
\end{aligned}$$

where $(r_R=\ell_2/2)$

$$L_S \triangleq \left(\frac{7}{3}\right)\frac{\mu_0\ell_1\ell_2\pi}{12g}N_S^2.$$

The flux $\phi_{21}(i_{S1},\theta)$ in a winding of stator phase 2 at an angle θ $(\pi\le\theta\le 4\pi/3)$, produced by the magnetic field of stator phase 1, is computed using

www.EngineeringEBooksPdf.com

the flux surface shown in Figure 10.9. With $\pi \leq \theta \leq 4\pi/3$, this flux is computed as

$$\begin{aligned}
\phi_{21}(i_{S1},\theta) &= \int_0^{\ell_1}\int_{\theta-\pi}^{\theta} \vec{\mathbf{B}}_{S1}(i_{S1},r_S,\theta')\cdot\left(r_S d\theta' d\ell\hat{\mathbf{r}}\right) \\
&= r_S\ell_1\int_{\theta-\pi}^{\pi/3}\frac{\mu_0 N_S i_{S1}}{2g}\frac{r_R}{r_S}d\theta' + r_S\ell_1\int_{\pi/3}^{2\pi/3}\frac{\mu_0 N_S i_{S1}}{g\pi/3}\frac{r_R}{r_S}\left(\frac{\pi}{2}-\theta'\right)d\theta' \\
&\quad + r_S\ell_1\int_{2\pi/3}^{\theta} -\frac{\mu_0 N_S i_{S1}}{2g}\frac{r_R}{r_S}d\theta' \\
&= \frac{\mu_0 r_R\ell_1 N_S i_{S1}}{2g}\left(\frac{4\pi}{3}-\theta-\frac{6}{\pi}\frac{1}{2}\left(\theta'-\frac{\pi}{2}\right)^2\Big|_{\pi/3}^{2\pi/3} - \left(\theta-\frac{2\pi}{3}\right)\right) \\
&= \frac{\mu_0 r_R\ell_1 N_S i_{S1}}{g}(\pi-\theta). \qquad (10.4)
\end{aligned}$$

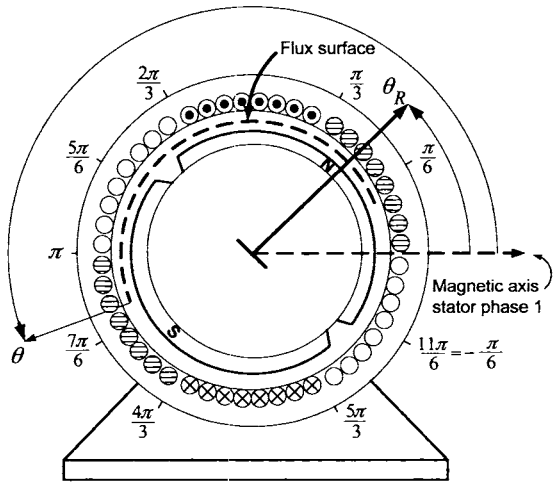


FIGURE 10.9. Flux surface for a winding of stator phase 2 to calculate the flux produced by the magnetic field of i_{S1}. The windings of phase 2 are shown shaded.

The total flux linkage $\lambda_{S2}(i_{S1},0,0)$ in stator phase 2 produced by the current in stator phase 1 is then

$$\begin{aligned}
\lambda_{S2}(i_{S1},0,0) &= \int_{\pi}^{4\pi/3}\phi_{21}(i_{S1},\theta)\frac{N_S}{\pi/3}d\theta = -\frac{3}{\pi}\frac{\mu_0 r_R\ell_1 N_S^2}{g}i_{S1}\frac{1}{2}(\pi-\theta)^2\Big|_{\pi}^{4\pi/3} \\
&= -\frac{\mu_0 r_R\ell_1\pi N_S^2}{6g}i_{S1} = -Mi_{S1}
\end{aligned}$$

www.EngineeringEBooksPdf.com

where ($r_R = \ell_2/2$)

$$M \triangleq \frac{\mu_0 \ell_1 \ell_2 \pi}{12g} N_S^2.$$

The flux $\phi_{31}(i_{S1}, \theta)$ in a winding of stator phase 3 at an angle θ where $5\pi/3 \leq \theta \leq 2\pi$ produced by the magnetic field of stator phase 1 is computed using the flux surface shown in Figure 10.10.

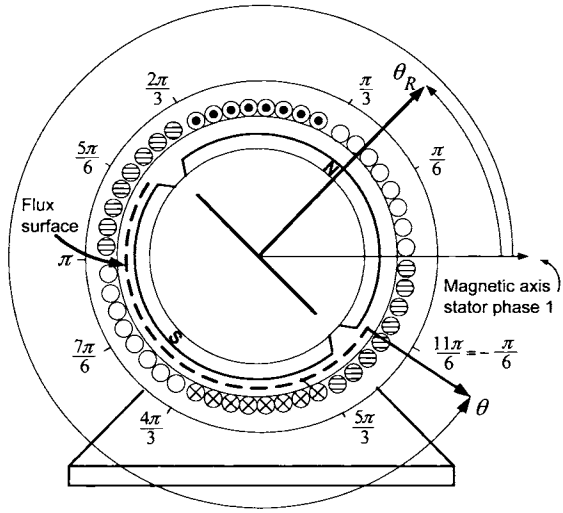


FIGURE 10.10. Flux surface for a winding of stator phase 3 to calculate the flux produced by the magnetic field of i_{S1}. The windings of phase 3 are shown shaded.

Proceeding, with $5\pi/3 \leq \theta \leq 2\pi$,

$$\begin{aligned}
\phi_{31}(i_{S1}, \theta) &= \int_0^{\ell_1} \int_{\theta-\pi}^{\theta} \vec{\mathbf{B}}_{S1}(i_{S1}, r_S, \theta') \cdot \left(r_S d\theta' d\ell \hat{\mathbf{r}}\right) \\
&= r_S \ell_1 \int_{\theta-\pi}^{4\pi/3} -\frac{\mu_0 N_S i_{S1}}{2g} \frac{r_R}{r_S} d\theta' + r_S \ell_1 \int_{4\pi/3}^{5\pi/3} \frac{\mu_0 N_S i_{S1}}{g\pi/3} \frac{r_R}{r} \left(\theta' - \frac{3\pi}{2}\right) d\theta' \\
&+ r_S \ell_1 \int_{5\pi/3}^{\theta} \frac{\mu_0 N_S i_{S1}}{2g} \frac{r_R}{r_S} d\theta' \\
&= \frac{\mu_0 r_R \ell_1 N_S i_{S1}}{2g} \left(-\left(\frac{7\pi}{3} - \theta\right) + \frac{6}{\pi} \frac{1}{2} \left(\theta' - \frac{3\pi}{2}\right)^2 \Big|_{4\pi/3}^{5\pi/3} + \left(\theta - \frac{5\pi}{3}\right) \right) \\
&= \frac{\mu_0 r_R \ell_1 N_S i_{S1}}{g} (\theta - 2\pi). \qquad (10.5)
\end{aligned}$$

The total flux linkage in stator phase 3 produced by the current in stator

www.EngineeringEBooksPdf.com

phase 1 is then

$$\lambda_{S3}(i_{S1},0,0) = \int_{5\pi/3}^{2\pi} \phi_{31}(i_{S1},\theta)\frac{N_S}{\pi/3}d\theta = \frac{3}{\pi}\frac{\mu_0 r_R \ell_1 N_S^2}{g} i_{S1}\frac{1}{2}(\theta-2\pi)^2\Big|_{5\pi/3}^{2\pi}$$
$$= -\frac{\mu_0 r_R \ell_1 \pi N_S^2}{6g} i_{S1} = -M i_{S1}$$

with

$$M \triangleq \frac{\mu_0 \ell_1 \ell_2 \pi}{12g} N_S^2.$$

The other phases are computed similarly. In summary, the flux linkages in the stator phases due to the stator currents are given by

$$\begin{aligned}
\lambda_{S1}(i_{S1},i_{S2},i_{S3}) &= +L_S i_{S1} - M i_{S2} - M i_{S3} \\
\lambda_{S2}(i_{S1},i_{S2},i_{S3}) &= -M i_{S1} + L_S i_{S2} - M i_{S3} \\
\lambda_{S3}(i_{S1},i_{S2},i_{S3}) &= -M i_{S1} - M i_{S2} + L_S i_{S3}
\end{aligned}$$

where

$$L_S = \frac{7}{3}\frac{\mu_0 \ell_1 \ell_2 \pi}{12g} N_S^2, \qquad M = \frac{\mu_0 \ell_1 \ell_2 \pi}{12g} N_S^2. \tag{10.6}$$

In matrix form, the flux linkages are given by

$$\begin{bmatrix} \lambda_{S1} \\ \lambda_{S2} \\ \lambda_{S3} \end{bmatrix} = \begin{bmatrix} L_S & -M & -M \\ -M & L_S & -M \\ -M & -M & L_S \end{bmatrix} \begin{bmatrix} i_{S1} \\ i_{S2} \\ i_{S3} \end{bmatrix}.$$

The inverse of the inductance matrix on the right is

$$\frac{1}{(L_S-2M)(M+L_S)} \begin{bmatrix} L_S-M & M & M \\ M & L_S-M & M \\ M & M & L_S-M \end{bmatrix}$$

where by (10.6), $L_S = (7/3)M$ results in $(L_S-2M)(M+L_S) > 0$.

10.4 Stator Flux Linkage Produced by $\vec{\mathbf{B}}_R$

The flux linkage $\lambda_{S1\_R}(\theta_R)$ in the windings of phase 1 due to the magnetic field of the PM rotor is now computed. The first step is to compute the flux $\phi_{S1\_R}(i_{S1},\theta)$ in each of the windings of stator phase 1 produced by the rotor's magnetic field. Recall that the top sides of the windings of phase 1 are located in the interval $\pi/3 \le \theta \le 2\pi/3$.

Case 1. As Figure 10.11 illustrates, in this case the computation of the flux in a loop of stator phase 1 produced by the rotor's magnetic field is done with rotor angle in the interval $\pi/6 \le \theta_R \le 5\pi/6$.

www.EngineeringEBooksPdf.com

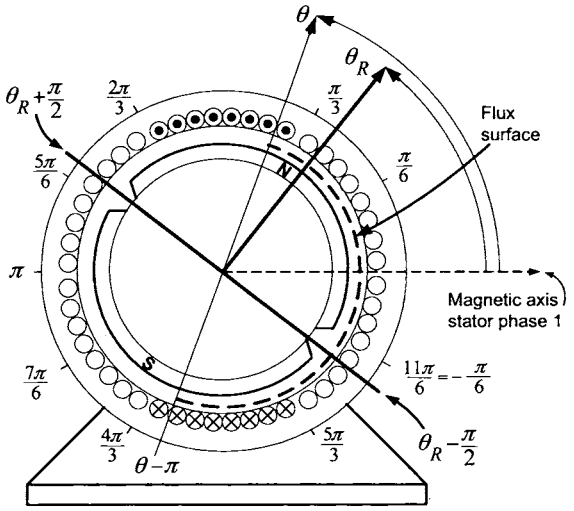


FIGURE 10.11. Computation of the flux in a loop of stator phase 1 produced by the rotor's magnetic field when $\pi/6 \leq \theta_R \leq 5\pi/6$.

Case 2. Figure 10.12 illustrates the computation of the flux in a loop of stator phase 1 produced by the rotor's magnetic field when $-\pi/6 \leq \theta_R \leq \pi/6$ and $\theta_R + \pi/2 \leq \theta \leq 2\pi/3$.

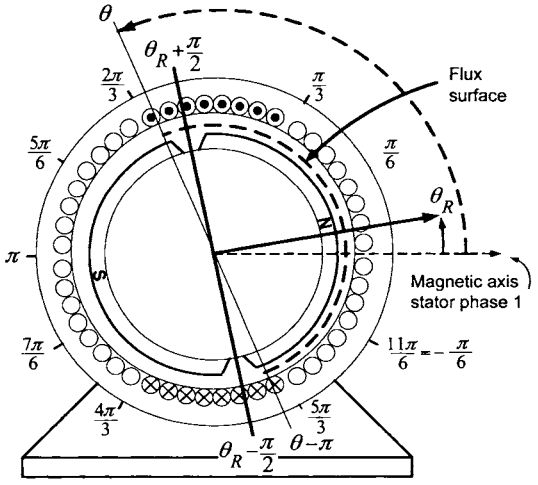


FIGURE 10.12. Computation of the flux in a loop of stator phase 1 produced by the rotor's magnetic field when $-\pi/6 \leq \theta_R \leq \pi/6$ and $\theta_R + \pi/2 \leq \theta \leq 2\pi/3$.

Case 3. Figure 10.13 illustrates the computation of the flux in a loop of

www.EngineeringEBooksPdf.com

stator phase 1 produced by the rotor's magnetic field when $-\pi/6 \leq \theta_R \leq \pi/6$ and $\pi/3 \leq \theta \leq \theta_R + \pi/2$.

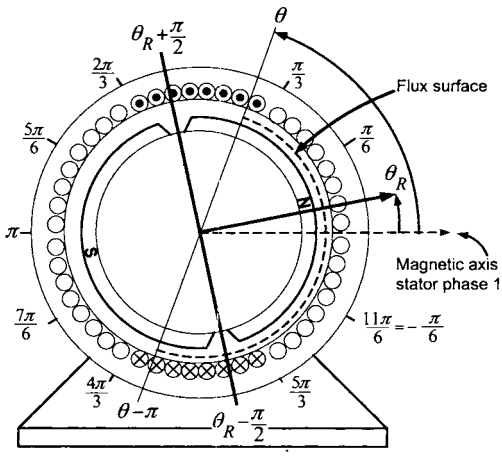


FIGURE 10.13. Computation of the flux in a loop of stator phase 1 produced by the rotor's magnetic field when $-\pi/6 \leq \theta_R \leq \pi/6$ and $\pi/3 \leq \theta \leq \theta_R + \pi/2$.

With reference to Figures 10.11, 10.12 and 10.13, and using the expression (10.2) for the magnetic field produced by the rotor, it follows that

$$\phi_{S1\_R}(i_{S1},\theta) = \int_0^{\ell_1}\int_{\theta-\pi}^{\theta} \vec{\mathbf{B}}_R(r_S,\theta'-\theta_R)\cdot\left(r_S d\theta' d\ell \hat{\mathbf{r}}\right)$$

$$= \begin{cases} \displaystyle\int_0^{\ell_1}\int_{\theta_R-\pi/2}^{\theta} B_{R0} r_R d\theta' d\ell + \int_0^{\ell_1}\int_{\theta-\pi}^{\theta_R-\pi/2} -B_{R0} r_R d\theta' d\ell \\ \qquad\qquad \text{for } \pi/6 \leq \theta_R \leq 5\pi/6 \\ \displaystyle\int_0^{\ell_1}\int_{\theta_R+\pi/2}^{\theta} -B_{R0} r_R d\theta' d\ell + \int_0^{\ell_1}\int_{\theta-\pi}^{\theta_R+\pi/2} B_{R0} r_R d\theta' d\ell \\ \qquad\qquad \text{for } \theta_R+\pi/2 \leq \theta \leq 2\pi/3 \\ \qquad\qquad \text{and } \ -\pi/6 \leq \theta_R \leq \pi/6 \\ \displaystyle\int_0^{\ell_1}\int_{\theta_R-\pi/2}^{\theta} B_{R0} r_R d\theta' d\ell + \int_0^{\ell_1}\int_{\theta-\pi}^{\theta_R-\pi/2} -B_{R0} r_R d\theta' d\ell \\ \qquad\qquad \text{for } \pi/3 \leq \theta \leq \theta_R+\pi/2 \\ \qquad\qquad \text{and } \ -\pi/6 \leq \theta_R \leq \pi/6. \end{cases}$$

www.EngineeringEBooksPdf.com

Simplifying, this becomes

$$\phi_{S1\_R}(i_{S1},\theta) = \begin{cases} 2r_R\ell_1 B_{R0}\,(\theta-\theta_R) & \text{for} \quad \pi/6 \le \theta_R \le 5\pi/6 \\ -2r_R\ell_1 B_{R0}\,(\theta-\theta_R-\pi) & \text{for} \quad \theta_R+\pi/2 \le \theta \le 2\pi/3 \\ & \text{and} \quad -\pi/6 \le \theta_R \le \pi/6 \\ 2r_R\ell_1 B_{R0}\,(\theta-\theta_R) & \text{for} \quad \pi/3 \le \theta \le \theta_R+\pi/2 \\ & \text{and} \quad -\pi/6 \le \theta_R \le \pi/6. \end{cases}$$

The total flux linkage $\lambda_{S1\_R}(\theta_R)$ in stator phase 1 produced by the rotor's magnetic field is then

$$\lambda_{S1\_R}(\theta_R) = \int_{\pi/3}^{2\pi/3} \phi_{S1\_R}(i_{S1},\theta)\frac{N_S}{\pi/3}d\theta.$$

Evaluating, this becomes

$$\lambda_{S1\_R}(\theta_R)$$

$$= \begin{cases} \displaystyle\int_{\pi/3}^{2\pi/3} 2r_R\ell_1 B_{R0}\,(\theta-\theta_R)\,\frac{N_S}{\pi/3}d\theta & \text{for } +\pi/6 \le \theta_R \le 5\pi/6 \\ \displaystyle\int_{\pi/3}^{\theta_R+\pi/2} 2r_R\ell_1 B_{R0}\,(\theta-\theta_R)\,\frac{N_S}{\pi/3}d\theta & \\ \quad + \displaystyle\int_{\theta_R+\pi/2}^{2\pi/3} -2r_R\ell_1 B_{R0}\,(\theta-\theta_R-\pi)\,\frac{N_S}{\pi/3}d\theta & \text{for } -\pi/6 \le \theta_R \le \pi/6. \end{cases}$$

Simplifying, this becomes

$$\lambda_{S1\_R}(\theta_R) = \begin{cases} \dfrac{3}{\pi}r_R\ell_1 N_S B_{R0}\,(\theta-\theta_R)^2\Big|_{\pi/3}^{2\pi/3} & \text{for } +\pi/6 \le \theta_R \le 5\pi/6 \\ r_R\ell_1 B_{R0}\dfrac{N_S}{\pi/3}\left((\theta-\theta_R)^2\Big|_{\pi/3}^{\theta_R+\pi/2} - (\theta-\theta_R-\pi)^2\Big|_{\theta_R+\pi/2}^{2\pi/3}\right) & \\ & \text{for } -\pi/6 \le \theta_R \le \pi/6 \end{cases}$$

which reduces to

$$\lambda_{S1\_R}(\theta_R) = \begin{cases} r_R\ell_1 N_S B_{R0}\left(2(\dfrac{\pi}{3}-\theta_R)+\dfrac{\pi}{3}\right) & \text{for} \quad +\pi/6 \le \theta_R \le 5\pi/6 \\ r_R\ell_1 N_S B_{R0}\left(-\dfrac{6}{\pi}\theta_R^2+\dfrac{5\pi}{6}\right) & \text{for} \quad -\pi/6 \le \theta_R \le \pi/6. \end{cases}$$

www.EngineeringEBooksPdf.com

By symmetry, $\lambda_{S1\_R}(\theta_R \pm \pi) = -\lambda_{S1\_R}(\theta_R)$ so that the total flux linkage in stator phase 1 due to the rotor's magnetic field may be written as

$$\lambda_{S1\_R}(\theta_R) = \begin{cases} +r_R \ell_1 N_S B_{R0}\left(-\frac{6}{\pi}\theta_R^2 + \frac{5\pi}{6}\right), & -\frac{\pi}{6} \le \theta_R \le \frac{\pi}{6} \\ +r_R \ell_1 N_S B_{R0}\left(2(\frac{\pi}{3} - \theta_R) + \frac{\pi}{3}\right), & \frac{\pi}{6} \le \theta_R \le \frac{5\pi}{6} \\ -r_R \ell_1 N_S B_{R0}\left(-\frac{6}{\pi}(\theta_R - \pi)^2 + \frac{5\pi}{6}\right), & \frac{5\pi}{6} \le \theta_R \le \frac{7\pi}{6} \\ -r_R \ell_1 N_S B_{R0}\left(2\left(\frac{\pi}{3} - (\theta_R - \pi)\right) + \frac{\pi}{3}\right), & \frac{7\pi}{6} \le \theta_R \le \frac{11\pi}{6}. \end{cases}$$

Define $\lambda_R(\theta_R)$ as

$$\lambda_R(\theta_R) \triangleq \lambda_{S1\_R}(\theta_R)/M_{SR}$$

where $M_{SR} \triangleq 2r_R \ell_1 N_S B_{R0}$ is the *coefficient of mutual inductance* between the stator and the rotor. A plot of $\lambda_R(\theta_R)$ versus θ_R is given in Figure 10.14.

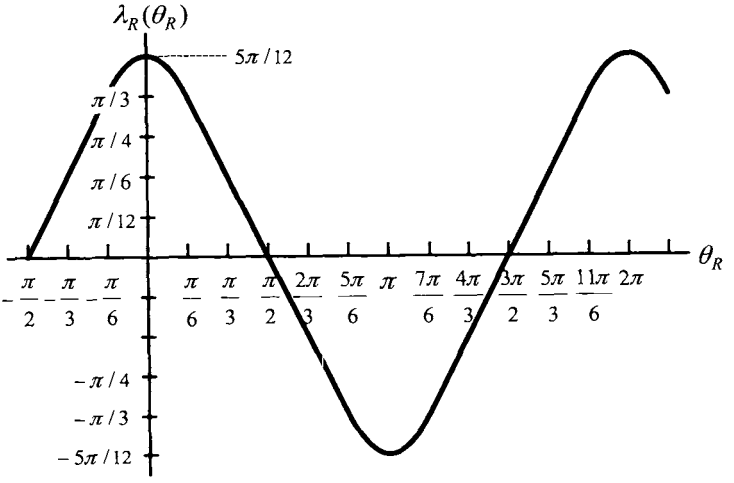


FIGURE 10.14. $\lambda_R(\theta_R)$ versus θ_R.

A simple computation shows that

$$-1 \le \frac{\partial \lambda_R(\theta_R)}{\partial \theta_R} \le 1.$$

www.EngineeringEBooksPdf.com

The total flux linkage in each stator phase may now be written in terms of $\lambda_R(\theta_R)$ as

$$\begin{aligned}\lambda_{S1\_R}(\theta_R) &= M_{SR}\lambda_R(\theta_R)\\ \lambda_{S2\_R}(\theta_R) &= M_{SR}\lambda_R(\theta_R - 2\pi/3)\\ \lambda_{S3\_R}(\theta_R) &= M_{SR}\lambda_R(\theta_R - 4\pi/3).\end{aligned}$$

10.5 Emf in the Stator Windings Produced by $\vec{\mathbf{B}}_R$

By Faraday's law, the back emf induced in the windings of phase 1 by rotor's magnetic field is given by

$$e_{S1} \triangleq -\frac{d}{dt}M_{SR}\lambda_R(\theta_R) = \begin{cases} +M_{SR}\dfrac{6\theta_R}{\pi}\omega_R, & -\pi/6 \le \theta_R \le \pi/6 \\ +M_{SR}\omega_R, & \pi/6 \le \theta_R \le 5\pi/6 \\ -M_{SR}\dfrac{6\,(\theta_R - \pi)}{\pi}\omega_R, & 5\pi/6 \le \theta_R \le 7\pi/6 \\ -M_{SR}\omega_R, & 7\pi/6 \le \theta_R \le 11\pi/6 \end{cases} \tag{10.7}$$

where $\omega_R = d\theta_R/dt$. With $e_p \triangleq M_{SR} = 2r_R\ell_1 N_S B_{R0}$ and

$$e(\theta_R) \triangleq \frac{e_{S1}}{M_{SR}\omega_R} = -\frac{\partial\lambda_R(\theta_R)}{\partial\theta_R}, \tag{10.8}$$

the back emf in each stator phase may now be written succinctly as

$$\begin{aligned}e_{S1} &= e_p e(\theta_R)\omega_R\\ e_{S2} &= e_p e(\theta_R - 2\pi/3)\omega_R\\ e_{S2} &= e_p e(\theta_R - 4\pi/3)\omega_R.\end{aligned}$$

As $-1 \le e(\theta_R) \le 1$, $e_p\omega_R$ is the peak value of the back emf. A plot of the back emfs $e_{S1}(\theta_R), e_{S2}(\theta_R)$, and $e_{S3}(\theta_R)$ at constant angular speed ω_R are given in Figures 10.15, 10.16, and 10.17, respectively. Note that each one has a trapezoidal shape and is the reason this machine is referred to as a *trapezoidal back-emf* synchronous motor.

www.EngineeringEBooksPdf.com

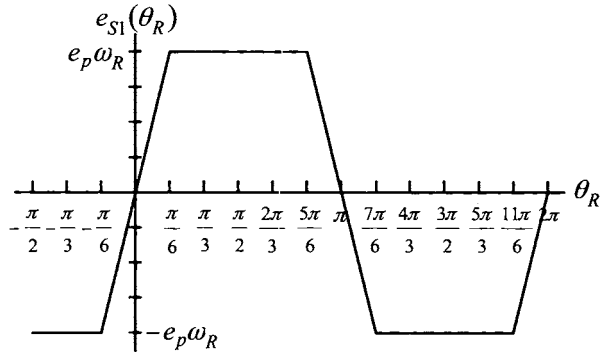


FIGURE 10.15. $e_{S1}(\theta_R)$ versus θ_R.

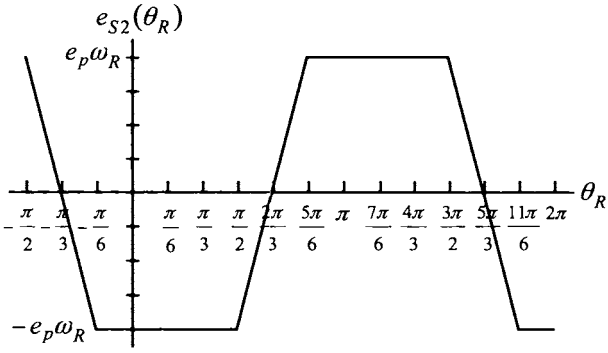


FIGURE 10.16. $e_{S2}(\theta_R)$ versus θ_R.

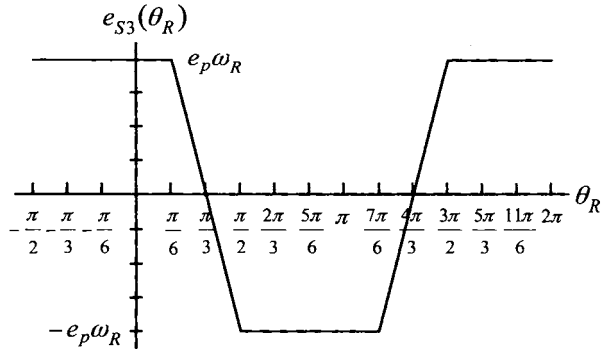


FIGURE 10.17. $e_{S3}(\theta_R)$ versus θ_R.

www.EngineeringEBooksPdf.com

10.6 Torque

The magnetic force exerted by the rotor's magnetic field $\vec{\mathbf{B}}_R(r_S, \theta - \theta_R)$ on the top axial side (i.e., $\pi/3 \leq \theta \leq 2\pi/3$) of a winding of phase 1 is (see Figure 10.18)

$$\begin{aligned}\vec{\mathbf{F}}_{S1}(r, \theta - \theta_R) &= i_{S1}\,(\ell_1 \hat{\mathbf{z}}) \times \vec{\mathbf{B}}_R(r_S, \theta - \theta_R) \\ &= i_{S1}\ell_1 B_R(r_S, \theta - \theta_R)\hat{\mathbf{z}} \times \hat{\mathbf{r}} \\ &= i_{S1}\ell_1 B_R(r_S, \theta - \theta_R)\hat{\boldsymbol{\theta}}.\end{aligned}$$

On the bottom side (i.e., $4\pi/3 \leq \theta \leq 5\pi/3$) the force is

$$\begin{aligned}\vec{\mathbf{F}}_{S1}(r, \theta - \theta_R) &= i_{S1}\,(-\ell_1 \hat{\mathbf{z}}) \times \vec{\mathbf{B}}_R(r_S, \theta - \theta_R) \\ &= -i_{S1}\ell_1 B_R(r_S, \theta - \theta_R)\hat{\mathbf{z}} \times \hat{\mathbf{r}} \\ &= -i_{S1}\ell_1 B_R(r_S, \theta - \theta_R)\hat{\boldsymbol{\theta}}.\end{aligned}$$

The total torque on the axial sides of the windings of phase 1 produced by the rotor's magnetic field is then

$$\begin{aligned}\tau_{S1} &= \int_{\pi/3}^{2\pi/3} \vec{\mathbf{r}} \times \vec{\mathbf{F}}_{S1} \frac{N_S}{\pi/3} d\theta + \int_{4\pi/3}^{5\pi/3} \vec{\mathbf{r}} \times \vec{\mathbf{F}}_{S1} \frac{N_S}{\pi/3} d\theta \\ &= \int_{\pi/3}^{2\pi/3} i_{S1}\ell_1 B_R(r_S, \theta - \theta_R) r_S \frac{N_S}{\pi/3} d\theta \hat{\mathbf{r}} \times \hat{\boldsymbol{\theta}} \\ &\quad - \int_{4\pi/3}^{5\pi/3} i_{S1}\ell_1 B_R(r_S, \theta - \theta_R) r_S \frac{N_S}{\pi/3} d\theta \hat{\mathbf{r}} \times \hat{\boldsymbol{\theta}} \\ &= i_{S1}\ell_1 \frac{N_S}{\pi/3} \left(\int_{\pi/3}^{2\pi/3} r_S B_R(r_S, \theta - \theta_R) d\theta \right. \\ &\quad \left. - \int_{4\pi/3}^{5\pi/3} r_S B_R(r_S, \theta - \theta_R) d\theta \right) \hat{\mathbf{z}} \\ &= 2 i_{S1}\ell_1 \frac{N_S}{\pi/3} \int_{\pi/3}^{2\pi/3} r_S B_R(r_S, \theta - \theta_R) d\theta \hat{\mathbf{z}}\end{aligned}$$

where the fact that $B_R(r_S, \theta - \theta_R) = -B_R(r_S, \theta - \theta_R \pm \pi)$ was used to obtain the last expression.

www.EngineeringEBooksPdf.com

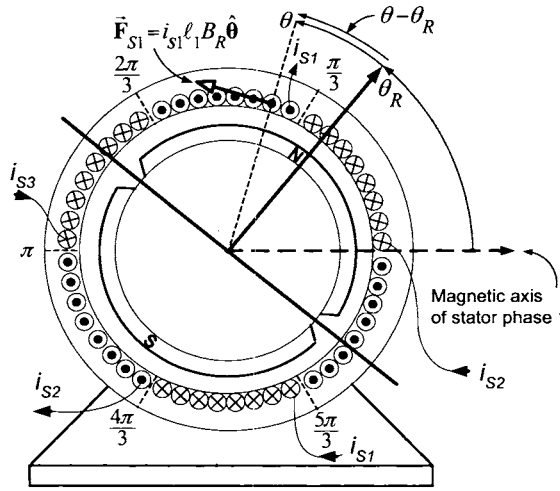


FIGURE 10.18. The force $\vec{\mathbf{F}}_{S1}(r, \theta - \theta_R) = -i_{S1}\ell_1 B_R(r_S, \theta - \theta_R)\hat{\boldsymbol{\theta}}$ exerted on a winding on the top side of stator phase 1 by the magnetic field of the rotor's permanent magnet.

Using the expression for the rotor's magnetic field given in (10.2), the integral is broken up as

$$\int_{\pi/3}^{2\pi/3} r_S B_R(r_S, \theta - \theta_R)\, d\theta$$

$$= \begin{cases} \displaystyle\int_{\pi/3}^{\theta_R+\pi/2} r_R B_{R0}\, d\theta + \int_{\theta_R+\pi/2}^{2\pi/3} -r_R B_{R0}\, d\theta & \text{for} \quad -\dfrac{\pi}{6} \le \theta_R \le \dfrac{\pi}{6} \\ \displaystyle\int_{\pi/3}^{2\pi/3} r_R B_{R0}\, d\theta & \text{for} \quad \dfrac{\pi}{6} \le \theta_R \le \dfrac{5\pi}{6} \\ \displaystyle\int_{\pi/3}^{\theta_R-\pi/2} -r_R B_{R0}\, d\theta + \int_{\theta_R-\pi/2}^{2\pi/3} r_R B_{R0}\, d\theta & \text{for} \quad \dfrac{5\pi}{6} \le \theta_R \le \dfrac{7\pi}{6} \\ \displaystyle\int_{\pi/3}^{2\pi/3} -r_R B_{R0}\, d\theta & \text{for} \quad \dfrac{7\pi}{6} \le \theta_R \le \dfrac{11\pi}{6} \end{cases}$$

which simplifies to

www.EngineeringEBooksPdf.com

$$\int_{\pi/3}^{2\pi/3} r_S B_R(r_S, \theta - \theta_R) d\theta$$

$$= \begin{cases} +r_R B_{R0}(\theta_R + \pi/6) - r_R B_{R0}(\pi/6 - \theta_R), & -\dfrac{\pi}{6} \le \theta_R \le \dfrac{\pi}{6} \\ +r_R B_{R0}\pi/3, & \dfrac{\pi}{6} \le \theta_R \le \dfrac{5\pi}{6} \\ -r_R B_{R0}(\theta_R - 5\pi/6) + r_R B_{R0}(7\pi/6 - \theta_R), & \dfrac{5\pi}{6} \le \theta_R \le \dfrac{7\pi}{6} \\ -r_R B_{R0}\pi/3, & \dfrac{7\pi}{6} \le \theta_R \le \dfrac{11\pi}{6} \end{cases}$$

Combining terms results in

$$\int_{\pi/3}^{2\pi/3} r_S B_R(r_S, \theta - \theta_R) d\theta = \begin{cases} +2r_R B_{R0}\theta_R, & -\pi/6 \le \theta_R \le \pi/6 \\ +r_R B_{R0}\pi/3, & \pi/6 \le \theta_R \le 5\pi/6 \\ -2r_R B_{R0}(\theta_R - \pi), & 5\pi/6 \le \theta_R \le 7\pi/6 \\ -r_R B_{R0}\pi/3, & 7\pi/6 \le \theta_R \le 11\pi/6. \end{cases}$$

Thus, the total torque exerted on the axial windings of phase 1 is then

$$\tau_{S1} = \begin{cases} +2\ell_1 r_R N_S B_{R0} \dfrac{6\theta_R}{\pi} i_{S1} & \text{for} \quad -\pi/6 \le \theta_R \le \pi/6 \\ +2\ell_1 r_R N_S B_{R0} i_{S1} & \text{for} \quad \pi/6 \le \theta_R \le 5\pi/6 \\ -2\ell_1 r_R N_S B_{R0} \dfrac{6(\theta_R - \pi)}{\pi} i_{S1} & \text{for} \quad 5\pi/6 \le \theta_R \le 7\pi/6 \\ -2\ell_1 r_R N_S B_{R0} i_{S1} & \text{for} \quad 7\pi/6 \le \theta_R \le 11\pi/6. \end{cases}$$

The torque exerted on the rotor by the magnetic field produced by the stator currents of phase 1 is then $\tau_{R1} = -\tau_{S1}$, that is,

$$\tau_{R1} = \begin{cases} -2\ell_1 r_R N_S B_{R0} \dfrac{6\theta_R}{\pi} i_{S1} & \text{for} \quad -\pi/6 \le \theta_R \le \pi/6 \\ -2\ell_1 r_R N_S B_{R0} i_{S1} & \text{for} \quad \pi/6 \le \theta_R \le 5\pi/6 \\ +2\ell_1 r_R N_S B_{R0} \dfrac{6(\theta_R - \pi)}{\pi} i_{S1} & \text{for} \quad 5\pi/6 \le \theta_R \le 7\pi/6 \\ +2\ell_1 r_R N_S B_{R0} i_{S1} & \text{for} \quad 7\pi/6 \le \theta_R \le 11\pi/6. \end{cases}$$

www.EngineeringEBooksPdf.com

With $\tau_p = 2\ell_1 r_R N_S B_{R0}$ (note that $\tau_p = M_{SR} = e_p$), this may be rewritten compactly as

$$\tau_{R1}(\theta_R, i_{S1}) = \begin{cases} -\tau_p \dfrac{6\theta_R}{\pi} i_{S1} & \text{for} \quad -\pi/6 \le \theta_R \le \pi/6 \\ -\tau_p i_{S1} & \text{for} \quad \pi/6 \le \theta_R \le 5\pi/6 \\ +\tau_p \dfrac{6\,(\theta_R - \pi)}{\pi} i_{S1} & \text{for} \quad 5\pi/6 \le \theta_R \le 7\pi/6 \\ +\tau_p i_{S1} & \text{for} \quad 7\pi/6 \le \theta_R \le 11\pi/6. \end{cases}$$

However, by (10.7) and (10.8), it follows that

$$\tau_{R1}(\theta_R, i_{S1}) = -\tau_p e(\theta_R) i_{S1}$$

and similarly

$$\begin{aligned} \tau_{R2}(\theta_R, i_{S2}) &= -\tau_p e(\theta_R - 2\pi/3) i_{S2} \\ \tau_{R3}(\theta_R, i_{S3}) &= -\tau_p e(\theta_R - 4\pi/3) i_{S2}. \end{aligned}$$

10.7 Mathematical Model

The stator flux linkages are given by

$$\begin{aligned} \lambda_1(i_{S1}, i_{S2}, i_{S3}) &= +L_S i_{S1} - M i_{S2} - M i_{S3} + e_p \lambda_R(\theta_R) \\ \lambda_2(i_{S1}, i_{S2}, i_{S3}) &= -M i_{S1} + L_S i_{S2} - M i_{S3} + e_p \lambda_R(\theta_R - 2\pi/3) \\ \lambda_3(i_{S1}, i_{S2}, i_{S3}) &= -M i_{S1} - M i_{S2} + L_S i_{S3} + e_p \lambda_R(\theta_R - 4\pi/3) \end{aligned}$$

and the phase torques are

$$\begin{aligned} \tau_{R1}(\theta_R, i_{S1}) &= -\tau_p e(\theta_R)\, i_{S1} \\ \tau_{R2}(\theta_R, i_{S2}) &= -\tau_p e(\theta_R - 2\pi/3) i_{S2} \\ \tau_{R3}(\theta_R, i_{S3}) &= -\tau_p e(\theta_R - 4\pi/3) i_{S3}. \end{aligned}$$

With R_S the resistance in each stator phase and u_{S1}, u_{S2}, and u_{S3} the voltages applied to each stator phase, the mathematical model is then

$$\begin{aligned} \frac{d}{dt}\lambda_1(i_{S1}, i_{S2}, i_{S3}) &= -R_S i_{S1} + u_{S1} \\ \frac{d}{dt}\lambda_2(i_{S1}, i_{S2}, i_{S3}) &= -R_S i_{S2} + u_{S2} \\ \frac{d}{dt}\lambda_3(i_{S1}, i_{S2}, i_{S3}) &= -R_S i_{S3} + u_{S3} \\ J\frac{d\omega}{dt} &= \tau_{R1}(\theta_R, i_{S1}) + \tau_{R2}(\theta_R, i_{S2}) + \tau_{R3}(\theta_R, i_{S3}) - \tau_L \\ \frac{d\theta_R}{dt} &= \omega_R \end{aligned}$$

www.EngineeringEBooksPdf.com

or

$$\begin{aligned}
\frac{d}{dt}\left(L_S i_{S1} - M i_{S2} - M i_{S3} + e_p \lambda_R(\theta_R)\right) &= -R_S i_{S1} + u_{S1} \\
\frac{d}{dt}\left(-M i_{S1} + L_S i_{S2} - M i_{S3} + e_p \lambda_R(\theta_R - 2\pi/3)\right) &= -R_S i_{S2} + u_{S2} \\
\frac{d}{dt}\left(-M i_{S1} - M i_{S2} + L_S i_{S3} + e_p \lambda_R(\theta_R - 4\pi/3)\right) &= -R_S i_{S3} + u_{S3} \\
J\frac{d\omega_R}{dt} &= \tau - \tau_L \\
\frac{d\theta_R}{dt} &= \omega_R
\end{aligned}$$

with

$$\tau \triangleq -\tau_p e(\theta_R)\, i_{S1} - \tau_p e(\theta_R - 2\pi/3)\, i_{S2} - \tau_p e(\theta_R - 4\pi/3)\, i_{S3}.$$

This system is often written in the form $\left(e(\theta_R) = -\partial\lambda_R(\theta_R)/\partial\theta_R\right)$

$$\begin{aligned}
\begin{bmatrix} u_{S1} \\ u_{S2} \\ u_{S3} \end{bmatrix} &= \begin{bmatrix} L_S & -M & -M \\ -M & L_S & -M \\ -M & -M & L_S \end{bmatrix} \frac{d}{dt} \begin{bmatrix} i_{S1} \\ i_{S2} \\ i_{S3} \end{bmatrix} + R_S \begin{bmatrix} i_{S1} \\ i_{S2} \\ i_{S3} \end{bmatrix} \\
&\quad - e_p \begin{bmatrix} e(\theta_R) \\ e(\theta_R - 2\pi/3) \\ e(\theta_R - 4\pi/3) \end{bmatrix} \omega_R \\
J\frac{d\omega_R}{dt} &= -\tau_p e(\theta_R)\, i_{S1} - \tau_p e(\theta_R - 2\pi/3)\, i_{S2} - \tau_p e(\theta_R - 4\pi/3)\, i_{S3} - \tau_L \\
\frac{d\theta_R}{dt} &= \omega_R.
\end{aligned}$$

With *balanced* stator currents, this may be rewritten as (see problem 1)

$$\begin{aligned}
\begin{bmatrix} u_{S1} \\ u_{S2} \\ u_{S3} \end{bmatrix} &= \begin{bmatrix} L_S + M & 0 & 0 \\ 0 & L_S + M & 0 \\ 0 & 0 & L_S + M \end{bmatrix} \frac{d}{dt} \begin{bmatrix} i_{S1} \\ i_{S2} \\ i_{S3} \end{bmatrix} + R_S \begin{bmatrix} i_{S1} \\ i_{S2} \\ i_{S3} \end{bmatrix} \\
&\quad - e_p \begin{bmatrix} e(\theta_R) \\ e(\theta_R - 2\pi/3) \\ e(\theta_R - 4\pi/3) \end{bmatrix} \omega_R \\
J\frac{d\omega_R}{dt} &= -\tau_p e(\theta_R)\, i_{S1} - \tau_p e(\theta_R - 2\pi/3)\, i_{S2} - \tau_p e(\theta_R - 4\pi/3)\, i_{S3} - \tau_L \\
\frac{d\theta_R}{dt} &= \omega_R.
\end{aligned}$$

www.EngineeringEBooksPdf.com

In state-space form this becomes

$$\begin{aligned}
\frac{di_{S1}}{dt} &= \frac{e_p}{L_S+M}\omega_R e(\theta_R) - \frac{R_S}{L_S+M}i_{S1} + \frac{1}{L_S+M}u_{S1} \\
\frac{di_{S2}}{dt} &= \frac{e_p}{L_S+M}\omega_R e(\theta_R - 2\pi/3) - \frac{R_S}{L_S+M}i_{S2} + \frac{1}{L_S+M}u_{S2} \\
\frac{di_{S3}}{dt} &= \frac{e_p}{L_S+M}\omega_R e(\theta_R - 4\pi/3) - \frac{R_S}{L_S+M}i_{S3} + \frac{1}{L_S+M}u_{S3} \\
\frac{d\omega_R}{dt} &= -(\tau_p/J)e(\theta_R)\, i_{S1} - (\tau_p/J)e(\theta_R - 2\pi/3)\, i_{S2} \\
&\quad -(\tau_p/J)e(\theta_R - 4\pi/3)\, i_{S3} - \tau_L/J \\
\frac{d\theta_R}{dt} &= \omega_R
\end{aligned}$$

where $e_p = \tau_p$.

Remark

In this formulation of the mathematical model, $e(\theta_R) = -\partial\lambda_R(\theta_R)/\partial\theta_R$ was used [see equation (10.8)] so that the back emfs in each phase $e_{S1} = e_p e(\theta_R)$, $e_{S2} = e_p e(\theta_R - 2\pi/3)$, and $e_{S3} = e_p e(\theta_R - 4\pi/3)$ have the *same* sign convention as the corresponding applied stator voltages u_{S1}, u_{S2}, and u_{S3}, respectively. This is consistent with Faraday's law and with the sign conventions chosen for the back emf in the induction and synchronous machines. However, in the literature, it is common to use $\varepsilon(\theta_R) \triangleq \partial\lambda_R(\theta_R)/\partial\theta_R$ for the back emf [15]; that is, the sign convention is opposite to that used here. This formulation is explored in problem 4. (In Chapter 1, both sign conventions were considered for the back emf of the DC motor.)

10.8 Operation and Control

At constant angular speed, Figure 10.19 is a graphical representation of the relationships between the back emf voltages (note their trapezoidal shape)

$$\begin{aligned}
e_{S1} &= e_p e(\theta_R)\omega_R \\
e_{S2} &= e_p e(\theta_R - 2\pi/3)\omega_R \\
e_{S3} &= e_p e(\theta_R - 4\pi/3)\omega_R,
\end{aligned} \tag{10.9}$$

the phase currents i_{S1}, i_{S2}, and i_{S3}, the power absorbed in each phase by the back emfs $p_{S1} \triangleq e_{S1}i_{S1}, p_{S2} \triangleq e_{S2}i_{S2}, p_{S3} \triangleq e_{S3}i_{S3}$, and the total power absorbed by the back emfs $p \triangleq e_{S1}i_{S1} + e_{S2}i_{S2} + e_{S3}i_{S3}$. In order to obtain the current profile i_{S1} shown in Figure 10.19, the current reference i_{S1r} for the current in phase 1 is chosen as

$$i_{S1r} = \begin{cases} -I_p & \text{if} \quad e_{S1} = +E_p = +e_p\omega_R \\ +I_p & \text{if} \quad e_{S1} = -E_p = -e_p\omega_R \\ 0 & \text{otherwise} \end{cases}$$

www.EngineeringEBooksPdf.com

or, from the expressions (10.7) and (10.8) for e_{S1}, it is seen that i_{S1r} may be written as

$$i_{S1r}(\theta_R) = I_p i_S(\theta_R)$$

where

$$i_S(\theta_R) \triangleq \begin{cases} 0 & \text{for} \quad -\pi/6 \leq \theta_R \leq \pi/6 \\ -1 & \text{for} \quad \pi/6 \leq \theta_R \leq 5\pi/6 \\ 0 & \text{for} \quad 5\pi/6 \leq \theta_R \leq 7\pi/6 \\ 1 & \text{for} \quad 7\pi/6 \leq \theta_R \leq 11\pi/6. \end{cases} \tag{10.10}$$

Choosing the gains in the PI current controller

$$u_{S1} = K_P(i_{S1r} - i_{S1}) + K_I \int_0^t (i_{S1r}(\tau) - i_{S1}(\tau))d\tau \tag{10.11}$$

appropriately results in $i_{S1} \to i_{S1r}$. Similarly, one chooses $i_{S2r} = I_p i_S(\theta_R - 2\pi/3)$ and $i_{S3r} = I_p i_S(\theta_R - 4\pi/3)$ and then employs PI current controllers of the form (10.11) to force $i_{S2} \to i_{S2r}, i_{S3} \to i_{S3r}$.

Figure 10.19 shows that the current is commutated (i.e., is switched from one phase to another) every $\pi/3$ radians or 60°. For example, at $\theta_R = \pi/6$ the current $-I_p$ in phase 3 goes (is commutated) to phase 1. After another $\pi/3$ radians so that $\theta_R = \pi/2$, the current I_p in phase 2 is commutated to phase 3. Note that one need only know the rotor position at the discrete locations $30°, 60°, 90°, 150°, 210°, 270°$, and $330°$ to carry out the commutation of the phases, i.e., to implement $i_{S1r}, i_{S2r}, i_{S3r}$. Usually these motors are equipped with Hall effect sensors that detect these discrete rotor positions for current commutation.

To determine torque produced using these current references, consider the electrical power absorbed by the back emfs which is given by

$$\begin{aligned} e_{S1}i_{S1} + e_{S2}i_{S2} + e_{S3}i_{S3} &= e_p e(\theta_R)\omega_R i_{S1} + e_p e(\theta_R - 2\pi/3)\omega_R i_{S2} \\ &\quad + e_p e(\theta_R - 4\pi/3)\omega_R i_{S3}. \end{aligned}$$

Choosing the current references as just described, it is seen from the plots in Figure (10.19) that this last expression reduces to

$$\begin{aligned} e_{S1}i_{S1} + e_{S2}i_{S2} + e_{S3}i_{S3} &= e_p e(\theta_R)\omega_R i_{S1r} + e_p e(\theta_R - 2\pi/3)\omega_R i_{S2r} \\ &\quad + e_p e(\theta_R - 4\pi/3)\omega_R i_{S3r} \\ &= -2e_p\omega_R I_p \end{aligned}$$

which is negative for $\omega_R > 0, I_p > 0$. Where does this power go? It is converted into mechanical power as is now shown (see also problem 2).

www.EngineeringEBooksPdf.com

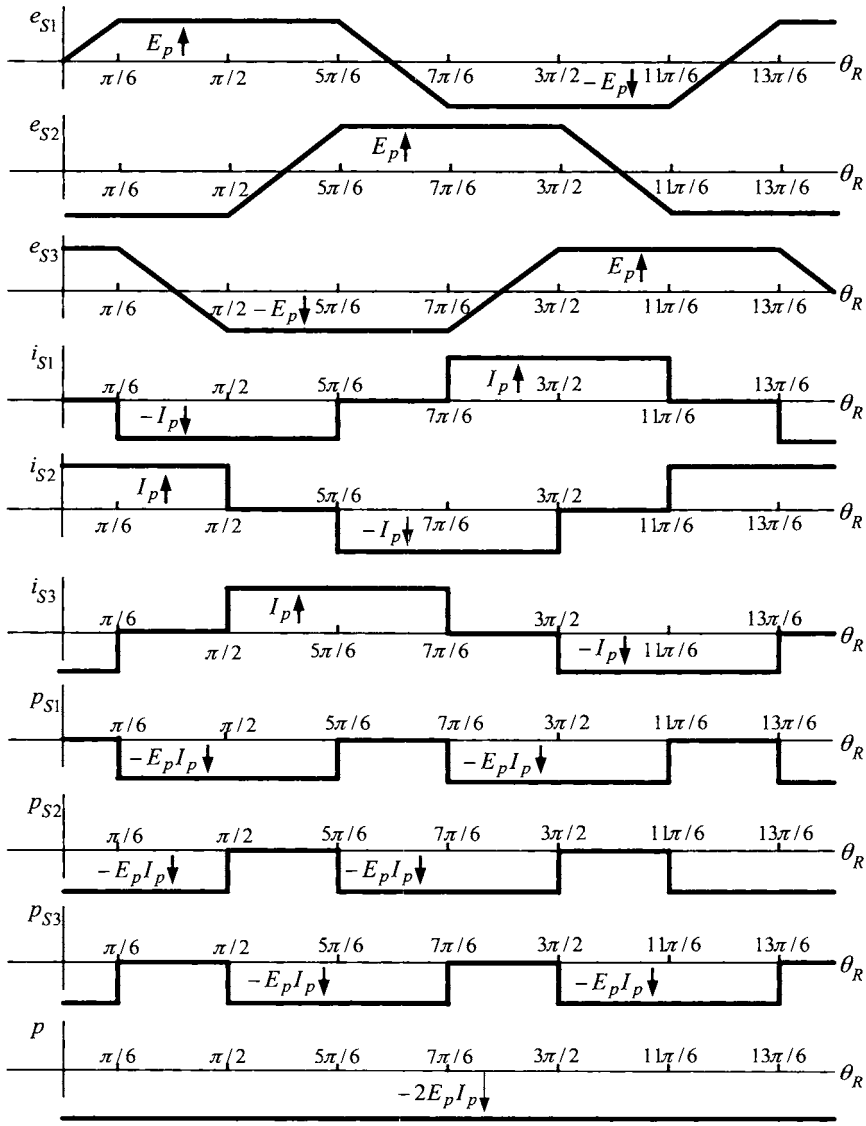


FIGURE 10.19. Back emf, currents, and power waveforms ($E_p \triangleq e_p\omega_R$). Note that the commutation of the phase currents occurs every $\pi/3$ radians at $\pi/6, \pi/2, 5\pi/6, 7\pi/6, 9\pi/6$, and $11\pi/6$. Adapted from Krishnan [15].

www.EngineeringEBooksPdf.com

Specifically, with the currents chosen as above, the mechanical power is

$$\begin{aligned}\tau\omega_R &= -\tau_p e\,(\theta_R)\omega_R i_{S1} - \tau_p e\Big(\theta_R - \frac{2\pi}{3}\Big)\omega_R i_{S2} - \tau_p e\Big(\theta_R - \frac{4\pi}{3}\Big)\omega_R i_{S3} \\ &= -e_p e\,(\theta_R)\omega_R i_{S1r} - e_p e\Big(\theta_R - \frac{2\pi}{3}\Big)\omega_R i_{S2r} - e_p e\Big(\theta_R - \frac{4\pi}{3}\Big)\omega_R i_{S3r} \\ &= 2e_p\omega_R I_p \\ &= 2\tau_p I_p\omega_R.\end{aligned}$$

That is, the torque is simply given by

$$\tau = 2\tau_p I_p.$$

This suggests a control scheme in which the current references are chosen as

$$\begin{aligned} i_{S1r} &= I_p i_S(\theta_R) \\ i_{S2r} &= I_p i_S(\theta_R - 2\pi/3) \\ i_{S3r} &= I_p i_S(\theta_R - 4\pi/3) \end{aligned} \tag{10.12}$$

and

$$\begin{aligned} u_{S1} &= K_P(i_{S1r} - i_{S1}) + K_I\int_0^t (i_{S1r}(\tau) - i_{S1}(\tau))d\tau \\ u_{S2} &= K_P(i_{S2r} - i_{S2}) + K_I\int_0^t (i_{S2r}(\tau) - i_{S2}(\tau))d\tau \\ u_{S1} &= K_P(i_{S3r} - i_{S3}) + K_I\int_0^t (i_{S3r}(\tau) - i_{S3}(\tau))d\tau. \end{aligned} \tag{10.13}$$

If the PI current controller performs well enough to assume $i_{S1} = i_{S1r}$, $i_{S2} = i_{S2r}$ and $i_{S3} = i_{S3r}$, then

$$\frac{d\omega}{dt} = \frac{\tau}{J} - \frac{\tau_L}{J} = \frac{2\tau_p}{J}I_p - \frac{\tau_L}{J}.$$

One then simply chooses

$$I_p = \frac{J}{2\tau_p}\alpha_r \tag{10.14}$$

$$\begin{aligned}\alpha_r &= K_I\int_0^t \Big(\theta_{ref}(\tau) - \theta(\tau)\Big)\,d\tau + K_P\Big(\theta_{ref}(t) - \theta(t)\Big) \\ &\quad + K_D\Big(\omega_{ref}(t) - \omega(t)\Big) + \alpha_{ref}.\end{aligned} \tag{10.15}$$

With $e_0(t) \triangleq \int_0^t(\theta_{ref}(\tau) - \theta(\tau))d\tau, e_1(t) \triangleq \theta_{ref}(t) - \theta(t)$, and $e_2(t) \triangleq \omega_{ref}(t) - \omega(t)$, the closed-loop system for the mechanical variables is

$$\frac{d}{dt}\begin{bmatrix} e_0 \\ e_1 \\ e_2 \end{bmatrix} = \begin{bmatrix} 0 & 1 & 0 \\ 0 & 0 & 1 \\ -K_I & -K_P & -K_D \end{bmatrix}\begin{bmatrix} e_0 \\ e_1 \\ e_2 \end{bmatrix} + \begin{bmatrix} 0 \\ 0 \\ 1/J \end{bmatrix}\tau_L.$$

www.EngineeringEBooksPdf.com

With $r_1 > 0, r_2 > 0, r_3 > 0$, set the gains as

$$\begin{aligned} K_D &= r_1 + r_2 + r_3 \\ K_P &= r_1 r_2 + r_1 r_3 + r_2 r_3 \\ K_I &= r_1 r_2 r_3 \end{aligned}$$

so that the closed-loop characteristic polynomial is

$$\begin{aligned} a(s) &= \det\left(sI - \begin{bmatrix} 0 & 1 & 0 \\ 0 & 0 & 1 \\ -K_I & -K_P & -K_D \end{bmatrix} \right) \\ &= s^3 + K_I s^2 + K_P s - K_I \\ &= s^3 + (r_1 + r_2 + r_3)s^2 + (r_1 r_2 + r_1 r_3 + r_2 r_3)s + r_1 r_2 r_3 \\ &= (s + r_1)(s + r_2)(s + r_3). \end{aligned}$$

With this choice of gains, the closed-loop poles are $p_1 = -r_1$, $p_2 = -r_2$, and $p_3 = -r_3$. As shown in Chapter 2, if the load torque is constant, then $e_1(t) \to 0, e_2(t) \to 0$ as $t \to \infty$. Of course, this controller assumes that $i_{S1} \to i_{S1r}, i_{S2} \to i_{S2r}$, and $i_{S3} \to i_{S3r}$ fast enough that it can be assumed that currents are *equal* to their reference values.

Remark

Note that the set of currents $i_{S1r} = I_p i_S(\theta_R), i_{S2r} = I_p i_S(\theta_R - 2\pi/3)$, and $i_{S3r} = I_p i_S(\theta_R - 4\pi/3) i_{S1r}$ are balanced, that is,

$$I_p i_S(\theta_R) + I_p i_S(\theta_R - 2\pi/3) + I_p i_S(\theta_R - 4\pi/3) \equiv 0.$$

However, the back emf voltages $e_{S1}(\theta_R)$, $e_{S2}(\theta_R)$ and $e_{S3}(\theta_R)$ are not balanced as

$$\begin{aligned} e_{S1}(\theta_R) + e_{S2}(\theta_R) + e_{S3}(\theta_R) &= -e_p \omega_R \Big(e(\theta_R) + e\,(\theta_R - 2\pi/3) \\ &\quad + e\,(\theta_R - 4\pi/3) \Big) \end{aligned}$$

is not identically zero (see Figure 10.19). This is in contrast to a three-phase PM synchronous machine with sinusoidally distributed windings in which the back emf voltages are balanced.

10.8.1 The Terminology "Brushless DC Motor"

The terminology *brushless DC motor* or *BLDC* is used for this machine because usually the motor is combined with an optical encoder, current measurements, Hall sensors for current commutation, an amplifier and feedback controller so that it behaves like a DC motor. That is, as indicated in Figure 10.20, the currents and motor position are fed back to the controller;

www.EngineeringEBooksPdf.com

the controller then uses PI current loops of the form (10.11) to force the currents to track the references

$$\begin{aligned} i_{S1r}(\theta_R) &= I_p i_S(\theta_R) \\ i_{S2r}(\theta_R) &= I_p i_S(\theta_R - 2\pi/3) \\ i_{S3r}(\theta_R) &= I_p i_S(\theta_R - 4\pi/3) \end{aligned} \tag{10.16}$$

where $i_S(\theta_R)$ is given by (10.10). The input to the controller is simply I_p so that with the inner current control loops working properly, the equations of the motor become

$$\begin{aligned} J\frac{d\omega}{dt} &= 2\tau_p I_p - \tau_L \\ \frac{d\theta}{dt} &= \omega \end{aligned}$$

which is the same form as current command DC motor with torque constant $K_T = 2\tau_p$.

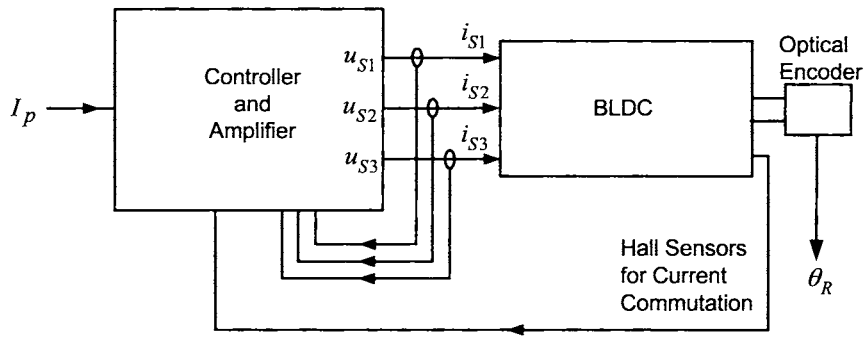


FIGURE 10.20. Block diagram for a brushless DC motor.

The system of Figure 10.20 is what one refers to as a "brushless DC motor" which the user obtains as a complete system from the manufacturer. Then, in the same way as for a DC motor, one simply chooses the "DC current" I_p as in equations (10.14) and (10.15) to use the BLDC as a servo (positioning) system.

Remark Typically, the position sensor for the current commutation, that is, for tracking the current references (10.16), is done with Hall effect sensors rather than an encoder. This is because to track the current references (10.16), the phase current plots in Figure 10.19 show that one only needs to determine the position of the rotor at multiples of $\pi/3$ or 60° as the current in any particular phase changes only at some multiple of 60°. Hall effect sensors provide a simple inexpensive way to detect the rotor position at multiples of 60°.

www.EngineeringEBooksPdf.com

10.9 Microscopic Viewpoint of BLDC Machines*

The microscopic viewpoint of the Physics of BLDC machine is described in this section. In this analysis, the system will be assumed to be in steady-state so that $\theta_R = \omega_R t - \delta, i_{S1} = I_S \cos(\omega_S t), i_{S2} = I_S \cos(\omega_S t - 2\pi/3), i_{S3} = I_S \cos(\omega_S t - 4\pi/3)$, and $\omega_S = \omega_R$.

10.9.1 Axial Electric Field $\vec{\mathbf{E}}_R$

It is now shown that the rotating radial magnetic field of the PM rotor produces an axial electric field in the air gap. Recall that the magnetic field produced by the rotor magnet is

$$\vec{\mathbf{B}}_R(r, \theta - \theta_R) = \begin{cases} B_{R0}\dfrac{r_R}{r}\hat{\mathbf{r}} & \text{for } -\dfrac{\pi}{2} + \dfrac{\Delta}{2} \le \theta - \theta_R \le \dfrac{\pi}{2} - \dfrac{\Delta}{2} \\ -B_{R0}\dfrac{r_R}{r}\dfrac{(\theta - \theta_R - \pi/2)}{\Delta/2}\hat{\mathbf{r}} & \text{for } \dfrac{\pi}{2} - \dfrac{\Delta}{2} \le \theta - \theta_R \le \dfrac{\pi}{2} + \dfrac{\Delta}{2} \\ -B_{R0}\dfrac{r_R}{r}\hat{\mathbf{r}} & \text{for } \dfrac{\pi}{2} + \dfrac{\Delta}{2} \le \theta - \theta_R \le \dfrac{3\pi}{2} - \dfrac{\Delta}{2} \\ B_{R0}\dfrac{r_R}{r}\dfrac{(\theta - \theta_R - 3\pi/2)}{\Delta/2}\hat{\mathbf{r}} & \text{for } \dfrac{3\pi}{2} - \dfrac{\Delta}{2} \le \theta - \theta_R \le \dfrac{3\pi}{2} + \dfrac{\Delta}{2} \end{cases} \tag{10.17}$$

where the parameter $\Delta > 0$ is now taken to be small, but nonzero. Maxwell's equations require that the divergence of the magnetic induction field $\vec{\mathbf{B}}_R$ be identically zero. In cylindrical coordinates with $\vec{\mathbf{B}} = B_r\hat{\mathbf{r}} + B_\theta\hat{\boldsymbol{\theta}} + B_z\hat{\mathbf{z}}$, the divergence is written as

$$\nabla \cdot \vec{\mathbf{B}} = \frac{1}{r}\frac{\partial}{\partial r}(rB_r) + \frac{1}{r}\frac{\partial B_\theta}{\partial \theta} + \frac{\partial B_z}{\partial z}.$$

A straightforward calculation (note that $B_{R\theta} = 0$, $B_{Rz} = 0$) shows that $\nabla \cdot \vec{\mathbf{B}}_R = 0$.

The rotor's magnetic field in the air gap induces an *axial* electric field in the air gap. This electric field can be computed using Faraday's law in differential form, that is,

$$\nabla \times \vec{\mathbf{E}}_R = -\frac{\partial \vec{\mathbf{B}}_R}{\partial t}.$$

In cylindrical coordinates, the curl of $\vec{\mathbf{E}}_R$ is given by $\nabla \times \vec{\mathbf{E}}_R =$

$$\left(\frac{1}{r}\frac{\partial E_{Rz}}{\partial \theta} - \frac{\partial E_{R\theta}}{\partial z}\right)\hat{\mathbf{r}} + \left(\frac{\partial E_{Rr}}{\partial z} - \frac{\partial E_{Rz}}{\partial r}\right)\hat{\boldsymbol{\theta}} + \left(\frac{1}{r}\frac{\partial (rE_{R\theta})}{\partial r} - \frac{1}{r}\frac{\partial E_{Rr}}{\partial \theta}\right)\hat{\mathbf{z}}.$$

www.EngineeringEBooksPdf.com

Then

$$-\frac{\partial \vec{\mathbf{B}}_R(r,\theta-\theta_R)}{\partial t}=\begin{cases} 0 & \text{for} \quad -\frac{\pi}{2}+\frac{\Delta}{2}\le\theta-\theta_R\le\frac{\pi}{2}-\frac{\Delta}{2} \\ -B_{R0}\frac{r_R}{r}\frac{2}{\Delta}\omega_R\hat{\mathbf{r}} & \text{for} \quad \frac{\pi}{2}-\frac{\Delta}{2}\le\theta-\theta_R\le\frac{\pi}{2}+\frac{\Delta}{2} \\ 0 & \text{for} \quad \frac{\pi}{2}+\frac{\Delta}{2}\le\theta-\theta_R\le\frac{3\pi}{2}-\frac{\Delta}{2} \\ B_{R0}\frac{r_R}{r}\frac{2}{\Delta}\omega_R\hat{\mathbf{r}} & \text{for} \quad \frac{3\pi}{2}-\frac{\Delta}{2}\le\theta-\theta_R\le\frac{3\pi}{2}+\frac{\Delta}{2}. \end{cases}$$

Now,

$$\frac{\partial E_{R\theta}}{\partial z}=0 \quad \text{and} \quad \frac{\partial E_{Rr}}{\partial z}=0$$

as it is assumed there is no dependence in z. Thus,

$$\nabla\times\vec{\mathbf{E}}_R=\frac{1}{r}\frac{\partial E_{Rz}}{\partial\theta}\hat{\mathbf{r}}$$

and Faraday's law in differential form reduces to

$$\frac{1}{r}\frac{\partial E_{Rz}}{\partial\theta}=-\frac{\partial B_R(r,\theta-\theta_R)}{\partial t}.$$

The solution is

$$E_{Rz}(\theta-\theta_R,t)=-\int_{\theta_R+\pi/2}^{\theta} r\frac{\partial B_R(r,\theta-\theta_R)}{\partial t}d\theta$$

where $\theta_R+\pi/2$ was chosen as the reference position for the integration as $E_{Rz}(\theta-\theta_R,t)|_{\theta=\theta_R+\pi/2}=0$ (see Figure 10.21 and problem 7). Evaluating the integral gives

$$E_{Rz}(\theta-\theta_R,t)$$
$$=\begin{cases} -\frac{2r_RB_{R0}}{\Delta}\omega_R\,(\theta-\theta_R-\pi/2) & \text{for} \quad \frac{\pi}{2}-\frac{\Delta}{2}\le\theta-\theta_R\le\frac{\pi}{2}+\frac{\Delta}{2} \\ -r_RB_{R0}\omega_R & \text{for} \quad \frac{\pi}{2}+\frac{\Delta}{2}\le\theta-\theta_R\le\frac{3\pi}{2}-\frac{\Delta}{2} \\ \frac{2r_RB_{R0}}{\Delta}\omega_R\,(\theta-\theta_R-3\pi/2) & \text{for} \quad \frac{3\pi}{2}-\frac{\Delta}{2}\le\theta-\theta_R\le\frac{3\pi}{2}+\frac{\Delta}{2} \\ r_RB_{R0}\omega_R & \text{for} \quad -\frac{\pi}{2}+\frac{\Delta}{2}\le\theta-\theta_R\le\frac{\pi}{2}-\frac{\Delta}{2}. \end{cases}$$

www.EngineeringEBooksPdf.com

Letting $\Delta \to 0$, this becomes

$$E_{Rz}(\theta - \theta_R, t)\hat{\mathbf{z}} = \begin{cases} +r_R B_{R0} \omega_R \hat{\mathbf{z}} & \text{for} \quad -\pi/2 \le \theta - \theta_R \le \pi/2 \\ -r_R B_{R0} \omega_R \hat{\mathbf{z}} & \text{for} \quad \pi/2 \le \theta - \theta_R \le 3\pi/2 \end{cases} \tag{10.18}$$

which is illustrated in Figure 10.21.

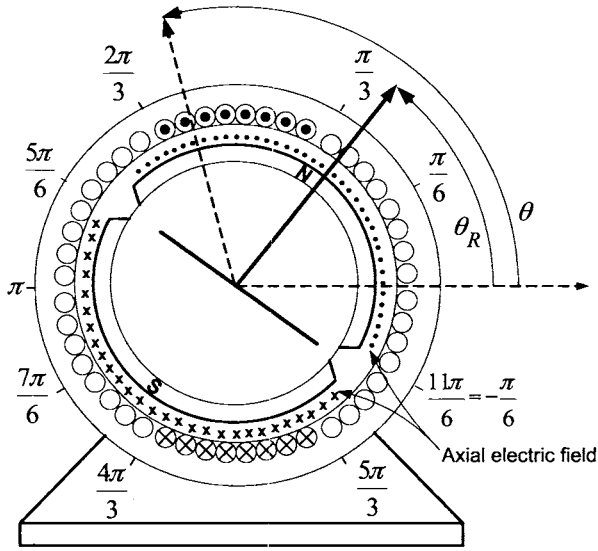


FIGURE 10.21. Axial electric field $\vec{\mathbf{E}}_R$ produced by $\vec{\mathbf{B}}_R$.

10.9.2 Emf Induced in the Stator Phases

Consider a winding of phase 1 where the axial side 1 is at the location θ with $2\pi/3 \le \theta \le \pi/3$ and the other axial side $1'$ of the winding is at $\theta + \pi$. To compute the emf $\zeta_{S1}(\theta)$ in this winding, let

$$d\vec{\ell} = \begin{cases} d\ell\hat{\mathbf{z}} & \text{for side 1} \\ -d\ell\hat{\mathbf{z}} & \text{for side } 1'. \end{cases}$$

For $\pi/3 \le \theta \le 2\pi/3$ and using (10.18), it follows that

www.EngineeringEBooksPdf.com

$$\zeta_{S1}(\theta) = \int_{\substack{\text{stator winding whose} \\ \text{sides are at } \theta \text{ and } \theta+\pi}} \vec{\mathbf{E}}_R(\theta) \cdot d\vec{\ell}$$

$$= \begin{cases} +2r_R\ell B_{R0}\omega_R & \text{for} \quad \pi/6 \le \theta_R \le 5\pi/6 \\ -2r_R\ell B_{R0}\omega_R & \text{for} \quad \theta_R + \pi/2 \le \theta \le 2\pi/3 \\ & \qquad -\pi/6 \le \theta_R \le \pi/6 \\ +2r_R\ell B_{R0}\omega_R & \text{for} \quad \pi/3 \le \theta \le \theta_R + \pi/2 \\ & \qquad -\pi/6 \le \theta_R \le \pi/6 \\ -2r_R\ell B_{R0}\omega_R & \text{for} \quad 7\pi/6 \le \theta_R \le 11\pi/6 \\ -2r_R\ell B_{R0}\omega_R & \text{for} \quad \pi/3 \le \theta \le \theta_R - \pi/2 \\ & \qquad 5\pi/6 \le \theta_R \le 7\pi/6 \\ +2r_R\ell B_{R0}\omega_R & \text{for} \quad \theta_R - \pi/2 \le \theta \le 2\pi/3 \\ & \qquad 5\pi/6 \le \theta_R \le 7\pi/6. \end{cases}$$

The total emf ξ_{S1} induced in stator phase 1 due to the rotor's magnetic field is then

$$\xi_{S1} = \int_{\substack{\text{All windings of} \\ \text{stator phase 1}}} \vec{\mathbf{E}}_R \cdot d\vec{\ell} = \int_{\pi/3}^{2\pi/3} \zeta_{S1}(\theta) \frac{N_S}{\pi/3} d\theta.$$

Evaluating the integral gives

$$\xi_{S1} = \begin{cases} \displaystyle\int_{\pi/3}^{2\pi/3} 2r_R\ell B_{R0}\omega_R \frac{N_S}{\pi/3} d\theta & \text{for} \quad \pi/6 \le \theta_R \le 5\pi/6 \\ \displaystyle\int_{\theta_R+\pi/2}^{2\pi/3} -2r_R\ell B_{R0}\omega_R \frac{N_S}{\pi/3} d\theta & \\ \displaystyle + \int_{\pi/3}^{\theta_R+\pi/2} 2r_R\ell B_{R0}\omega_R \frac{N_S}{\pi/3} d\theta & \text{for} \quad -\pi/6 \le \theta_R \le \pi/6 \\ \displaystyle\int_{\pi/3}^{2\pi/3} -2r_R\ell B_{R0}\omega_R \frac{N_S}{\pi/3} d\theta & \text{for} \quad 7\pi/6 \le \theta_R \le 11\pi/6 \\ \displaystyle\int_{\pi/3}^{\theta_R-\pi/2} -2r_R\ell B_{R0}\omega_R \frac{N_S}{\pi/3} d\theta & \\ \displaystyle + \int_{\theta_R-\pi/2}^{2\pi/3} 2r_R\ell B_{R0}\omega_R \frac{N_S}{\pi/3} d\theta & \text{for} \quad 5\pi/6 \le \theta_R \le 7\pi/6. \end{cases}$$

www.EngineeringEBooksPdf.com

This simplifies to

$$\xi_{S1} = \begin{cases} 2r_R \ell N_S B_{R0} \omega_R & \text{for} \quad \frac{\pi}{6} \le \theta_R \le \frac{5\pi}{6} \\ -2r_R \ell B_{R0} \omega_R \frac{N_S}{\pi/3} \left(\frac{2\pi}{3} - \theta_R - \frac{\pi}{2} \right) & \\ +2r_R \ell B_{R0} \omega_R \frac{N_S}{\pi/3} \left(\theta_R + \frac{\pi}{2} - \frac{\pi}{3} \right) & \text{for} \quad -\frac{\pi}{6} \le \theta_R \le \frac{\pi}{6} \\ -2r_R \ell N_S B_{R0} \omega_R & \text{for} \quad \frac{7\pi}{6} \le \theta_R \le \frac{11\pi}{6} \\ -2r_R \ell B_{R0} \omega_R \frac{N_S}{\pi/3} \left(\theta_R - \frac{\pi}{2} - \frac{\pi}{3} \right) & \\ +2r_R \ell B_{R0} \omega_R \frac{N_S}{\pi/3} \left(\frac{2\pi}{3} - \theta_R + \frac{\pi}{2} \right) & \text{for} \quad \frac{5\pi}{6} \le \theta_R \le \frac{7\pi}{6} \end{cases}$$

or, finally

$$\xi_{S1} = \int_{\substack{\text{All windings of} \\ \text{stator phase 1}}} \vec{\mathbf{E}}_R \cdot d\vec{\ell}$$

$$= \begin{cases} +2r_R \ell N_S B_{R0} \omega_R & \text{for} \quad \pi/6 \le \theta_R \le 5\pi/6 \\ +2r_R \ell N_S B_{R0} \omega_R \frac{6\theta_R}{\pi} & \text{for} \quad -\pi/6 \le \theta_R \le \pi/6 \\ -2r_R \ell N_S B_{R0} \omega_R & \text{for} \quad 7\pi/6 \le \theta_R \le 11\pi/6 \\ -2r_R \ell N_S B_{R0} \omega_R \frac{6(\theta_R - \pi)}{\pi} & \text{for} \quad 5\pi/6 \le \theta_R \le 7\pi/6 \end{cases}$$

which is the same expression as (10.7) derived in the macroscopic case.

www.EngineeringEBooksPdf.com

Problems

Problem 1 BLDC Motor Model

The electrical equations for the BLDC were derived as

$$\begin{bmatrix} u_{S1} \\ u_{S2} \\ u_{S3} \end{bmatrix} = R_S \begin{bmatrix} i_{S1} \\ i_{S2} \\ i_{S3} \end{bmatrix} + \frac{d}{dt} \begin{bmatrix} L_S & -M & -M \\ -M & L_S & -M \\ -M & -M & L_S \end{bmatrix} \begin{bmatrix} i_{S1} \\ i_{S2} \\ i_{S3} \end{bmatrix} + e_p \begin{bmatrix} e(\theta_R) \\ e(\theta_R - 2\pi/3) \\ e(\theta_R - 4\pi/3) \end{bmatrix} \omega_R.$$

Assuming the stator currents are balanced, show that

$$\begin{bmatrix} u_{S1} \\ u_{S2} \\ u_{S3} \end{bmatrix} = R_S \begin{bmatrix} i_{S1} \\ i_{S2} \\ i_{S3} \end{bmatrix} + \frac{d}{dt} \begin{bmatrix} L_S + M & 0 & 0 \\ 0 & L_S + M & 0 \\ 0 & 0 & L_S + M \end{bmatrix} \begin{bmatrix} i_{S1} \\ i_{S2} \\ i_{S3} \end{bmatrix} - e_p \begin{bmatrix} e(\theta_R) \\ e(\theta_R - 2\pi/3) \\ e(\theta_R - 4\pi/3) \end{bmatrix} \omega_R.$$

Problem 2 Conservation of Energy

The model of the BLDC may be written as

$$\frac{d}{dt}\Lambda \begin{bmatrix} i_{S1} \\ i_{S2} \\ i_{S3} \end{bmatrix} - e_p \begin{bmatrix} e(\theta_R) \\ e(\theta_R - 2\pi/3) \\ e(\theta_R - 4\pi/3) \end{bmatrix} \omega_R + R_S \begin{bmatrix} i_{S1} \\ i_{S2} \\ i_{S3} \end{bmatrix} = \begin{bmatrix} u_{S1} \\ u_{S2} \\ u_{S3} \end{bmatrix}$$

$$-\tau_p e(\theta_R) i_{S1} - \tau_p e(\theta_R - 2\pi/3) i_{S1} - \tau_p e(\theta_R - 4\pi/3) i_{S1} - \tau_L = J \frac{d\omega_R}{dt}.$$

Do an energy balance based on these equations to account for the energy stored in the magnetic fields in the air gap/iron due to the stator currents, the ohmic losses in the stator windings, the energy stored in the rotational motion of the rotor and the energy converted to mechanical power. In particular, show that $e_p = \tau_p$ must hold for energy conservation to hold.

Problem 3 Power Density in PM Synchronous Machines [15]

Consider two PM motors, one is a three-phase BLDC motor and the second one is a three-phase PM synchronous (sinusoidally wound stator) motor. Let both motors have the same stator resistance R_S and the same torque/back-emf constants ($\tau_p = K_T$ or, equivalently, $e_p = K_m$), and rotate at the same constant speed. Let I_{bldc} and I_{synch} be the peak *current limit in the BLDC and the PM synchronous motor, respectively.*

(a) Show that the rms current in each phase of the BLDC is $\sqrt{2/3} I_{\text{bldc}}$ while in the PM synchronous motor it is $I_{synch}/\sqrt{2}$.

www.EngineeringEBooksPdf.com

(b) Let the peak currents in the motors be chosen so they both have the same ohmic losses, that is,

$$3R_S\left(\sqrt{\frac{2}{3}}I_{bldc}\right)^2 = 3R_S\left(\frac{I_{synch}}{\sqrt{2}}\right)^2$$

or

$$I_{bldc} = \frac{\sqrt{3}}{2}I_{synch}.$$

Choose the current references in the BLDC according to (10.12) in order to obtain the maximum torque out of the machine for a given current. In this case, the steady-state power produced by the BLDC is constant and equal to

$$2e_pI_p.$$

Assume in the PM synchronous motor that it is possible to have the stator currents in phase with their corresponding stator voltages (unity power factor) so that the steady-state power produced by the PM motor is

$$3\frac{K_m}{\sqrt{2}}\frac{I_{synch}}{\sqrt{2}}$$

where $K_m = K_T$ is the back emf constant. Show that, under these conditions, the ratio of the output power of the BLDC machine to the PM synchronous machine is 1.155.

Problem 4 Mathematical Model of the BLDC

In the literature, the normalized back emf is usually taken to be $\varepsilon(\theta_R) \triangleq \partial\lambda_R(\theta_R)/\partial\theta_R$ rather than $e(\theta_R) \triangleq -\partial\lambda_R(\theta_R)/\partial\theta_R$ as in equation (10.8). That is, the back emfs are then taken to be

$$\begin{aligned}\varepsilon_{S1} &= e_p\varepsilon(\theta_R)\omega_R\\ \varepsilon_{S2} &= e_p\varepsilon(\theta_R - 2\pi/3)\omega_R\\ \varepsilon_{S3} &= e_p\varepsilon(\theta_R - 4\pi/3)\omega_R\end{aligned}$$

(compare with 10.9). This is just a different sign convention for the back emfs; that is, these back emfs have a sign convention that is opposite to that of the applied phase voltages u_{S1}, u_{S2}, and u_{S3}.

(a) Rewrite the mathematical model of the motor in terms of $\varepsilon(\theta_R)$.

(b) How do the waveforms in Figure 10.19 change as a result of using $\varepsilon(\theta_R)$?

Problem 5 Simulation of a BLDC

Simulate an open-loop three-phase trapezoidal back-emf synchronous motor. Set the parameters as $R_S = 0.7\ \Omega$, $L_S = 2.72\ mH$, $M = 0.15\ mH$, $\tau_p = e_p = 0.5128\ N\text{-}m/A$, $J = 0.0002\ kg\text{-}m^2$, $f = 0.002\ N\text{-}m/rad/sec$, $n_p =$

www.EngineeringEBooksPdf.com

1, $\omega_S = (2\pi)10$ *rad/sec,* $V = V_{max} = 200$ *V (peak),* $I_{max} = 10$ *A, and* $\tau_L = 0$ *[15]. Apply a three-phase set of trapezoidal voltages to the motor with a peak of* V_{max} *and plot (a)* i_{Sa} *and* i_{Sb}*, (b)* ω*, and (c)* θ*. Does the speed* ω *need to be initialized to a value close to the synchronous speed value* ω_S *in order to run open loop?*

Problem 6 Closed-Loop Control of a BLDC

Add the closed-loop controller (10.13), (10.14), and (10.15) to the simulation of the BLDC in problem 5. Use only proportional control in the current controller. Have the motor do a point-to-point move in which it goes from 0 *to* 240 *radians and achieves a maximum speed of* 400 *rads/sec in* 0.5 *sec.*

Problem 7 Rotor Electric Field

Show that at $\theta = \theta_R + \pi/2$ *the axial electric field due to motion of the rotor magnet is zero, that is,*

$$E_{Rz}(\theta - \theta_R, t)|_{\theta=\theta_R+\pi/2} = 0.$$

Hint: Consider a half-cylindrical-shaped loop containing the rotor with one axial side fixed *at the angular position* θ_0 *in the air gap and, consequently, the other side fixed at* $\theta_0 + \pi$ *(the loop does not rotate). Use Faraday's law to show that the emf generated in this loop by the rotor's magnetic field is zero when the position of the rotor is such that* $\theta_0 = \theta_R + \pi/2 \pm n\pi$*.*

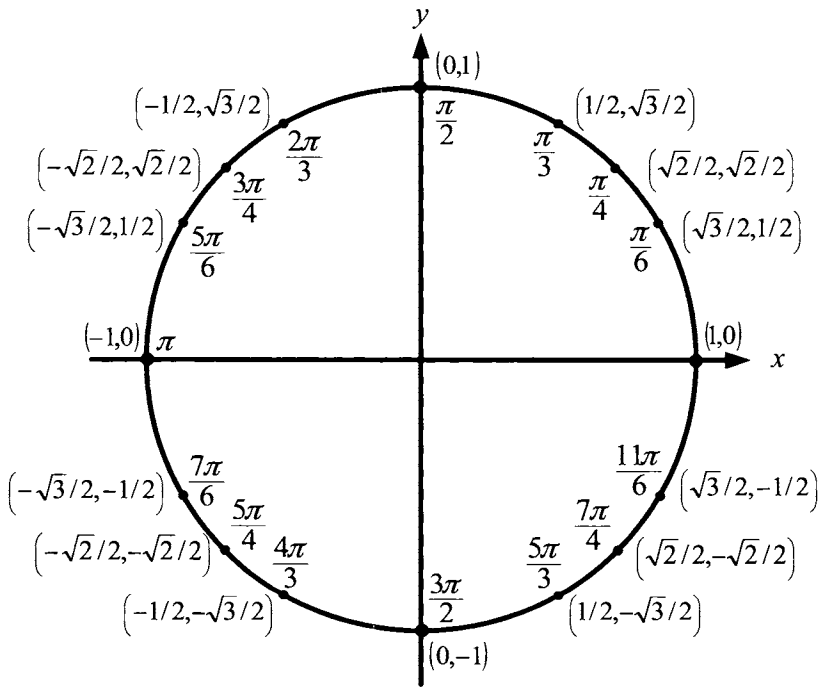
Problem 8 Permeability of a Permanent Magnet

Explain why, as far as the stator magnetic field $\vec{\mathbf{B}}_S$ *is concerned, the permeability of the permanent magnets on the rotor is* $\mu = \mu_0\mu_r = \mu_0$*. Show that this implies that the "effective" air gap (i.e., the value for g) is the sum of the actual air-gap length and the thickness of the PM magnets on the rotor surface.*

www.EngineeringEBooksPdf.com

Trigonometric Table and Identities

Trigonometric Table



www.EngineeringEBooksPdf.com

Trigonometric Identities

$$
\begin{aligned}
e^{j\theta} &= \cos(\theta) + j\sin(\theta) \\
a\cos(\theta) + b\sin(\theta) &= \sqrt{a^2+b^2}\cos\left(\theta + \tan^{-1}(b/a)\right) \\
\sin(2\theta) &= 2\sin(\theta)\cos(\theta) \\
\cos(2\theta) &= \cos^2(\theta) - \sin^2(\theta) = 2\cos^2(\theta) - 1 \\
&= 1 - 2\sin^2(\theta) \\
\cos^2(\theta) &= \frac{1+\cos(2\theta)}{2} \\
\sin^2(\theta) &= \frac{1-\cos(2\theta)}{2} \\
\cos(\theta_1 \pm \theta_2) &= \cos(\theta_1)\cos(\theta_2) \mp \sin(\theta_1)\sin(\theta_2) \\
\sin(\theta_1 \pm \theta_2) &= \sin(\theta_1)\cos(\theta_2) \pm \cos(\theta_1)\sin(\theta_2)
\end{aligned}
$$

$$
\begin{aligned}
\cos(\theta_1)\cos(\theta_2) &= \frac{1}{2}\cos(\theta_1+\theta_2) + \frac{1}{2}\cos(\theta_1-\theta_2) \\
\sin(\theta_1)\sin(\theta_2) &= \frac{1}{2}\cos(\theta_1-\theta_2) - \frac{1}{2}\cos(\theta_1+\theta_2) \\
\sin(\theta_1)\cos(\theta_2) &= \frac{1}{2}\sin(\theta_1+\theta_2) + \frac{1}{2}\sin(\theta_1-\theta_2) \\
\cos(\theta_1)\sin(\theta_2) &= \frac{1}{2}\sin(\theta_1+\theta_2) - \frac{1}{2}\sin(\theta_1-\theta_2)
\end{aligned}
$$

$$
\begin{aligned}
\frac{3}{2} &= \cos^2(\theta) + \cos^2(\theta - 2\pi/3) + \cos^2(\theta - 4\pi/3) \\
\frac{3}{2} &= \sin^2(\theta) + \sin^2(\theta - 2\pi/3) + \sin^2(\theta - 4\pi/3) \\
0 &= \sin(\theta)\cos(\theta) + \sin(\theta - 2\pi/3)\cos(\theta - 2\pi/3) \\
&\quad + \sin(\theta - 4\pi/3)\cos(\theta - 4\pi/3) \\
0 &= \cos(\theta) + \cos(\theta - 2\pi/3) + \cos(\theta - 4\pi/3) \\
0 &= \sin(\theta) + \sin(\theta - 2\pi/3) + \sin(\theta - 4\pi/3)
\end{aligned}
$$

www.EngineeringEBooksPdf.com

$$\frac{3}{2}\cos(5\theta_1+\theta_2) = \sin(5(\theta_1+\pi/2))\cos(\theta_2) + \sin(5(\theta_1+\pi/2-2\pi/3))\cos(\theta_2-2\pi/3) + \sin(5(\theta_1+\pi/2-4\pi/3))\cos(\theta_2-4\pi/3)$$

$$-\frac{3}{2}\cos(7\theta_1-\theta_2) = \sin(7(\theta_1+\pi/2))\cos(\theta_2) + \sin(7(\theta_1+\pi/2-2\pi/3))\cos(\theta_2-2\pi/3) + \sin(7(\theta_1+\pi/2-4\pi/3))\cos(\theta_2-4\pi/3)$$

$$\frac{3}{2}\sin(\theta_1-\theta_2) = \sin(\theta_1)\cos(\theta_2) + \sin(\theta_1-2\pi/3)\cos(\theta_2-2\pi/3) + \sin(\theta_1-4\pi/3)\cos(\theta_2-4\pi/3)$$

$$\frac{3}{2}\cos(\theta_1-\theta_2) = \sin(\theta_1)\sin(\theta_2) + \sin(\theta_1-2\pi/3)\sin(\theta_2-2\pi/3) + \sin(\theta_1-4\pi/3)\sin(\theta_2-4\pi/3)$$

$$-\frac{3}{2}\sin(\theta_1-\theta_2) = \cos(\theta_1)\sin(\theta_2) + \cos(\theta_1-2\pi/3)\sin(\theta_2-2\pi/3) + \cos(\theta_1-4\pi/3)\sin(\theta_2-4\pi/3)$$

$$\frac{3}{2}\cos(\theta_1-\theta_2) = \cos(\theta_1)\cos(\theta_2) + \cos(\theta_1-2\pi/3)\cos(\theta_2-2\pi/3) + \cos(\theta_1-4\pi/3)\cos(\theta_2-4\pi/3)$$

$$\frac{3}{2}\sin(\theta_1+\theta_2) = \sin(\theta_1)\cos(\theta_2) + \sin(\theta_1-4\pi/3)\cos(\theta_2-2\pi/3) + \sin(\theta_1-2\pi/3)\cos(\theta_2-4\pi/3)$$

$$-\frac{3}{2}\cos(\theta_1+\theta_2) = \sin(\theta_1)\sin(\theta_2) + \sin(\theta_1-4\pi/3)\sin(\theta_2-2\pi/3) + \sin(\theta_1-2\pi/3)\sin(\theta_2-4\pi/3)$$

$$\frac{3}{2}\sin(\theta_1+\theta_2) = \cos(\theta_1)\sin(\theta_2) + \cos(\theta_1-4\pi/3)\sin(\theta_2-2\pi/3) + \cos(\theta_1-2\pi/3)\sin(\theta_2-4\pi/3)$$

www.EngineeringEBooksPdf.com

This Page Intentionally Left Blank

www.EngineeringEBooksPdf.com

References

[1] Werner Leonhard, *Control of Electrical Drives*, Springer-Verlag, Berlin, 1985.

[2] Werner Leonhard, *Control of Electrical Drives*, 3rd Edition, Springer-Verlag, Berlin, 2001.

[3] Paul C. Krause, *Analysis of Electric Machinery*, McGraw-Hill, New York, 1986.

[4] Paul C. Krause, Oleg Wasynczuk, and Scott D. Sudhoff, *Analysis of Electric Machinery and Drive Systems*, 2nd Edition, John Wiley & Sons, New York, 2002.

[5] C. B. Gray, *Electrical Machines and Drive Systems*, Longman Scientific & Technical, New York, 1989.

[6] Chee-Mun Ong, *Dynamic Simulation of Electric Machinery using Matlab/Simulink*, Prentice-Hall, Upper Saddle River, NJ, 1998.

[7] D. W. Novotny and T. A. Lipo, *Vector Control and Dynamics of AC Drives*, Oxford University Press, New York, 1996.

[8] Peter Vas, *Vector Control of AC Machines*, Clarendon Press, Oxford, 1990.

[9] J. M. D. Murphy and F. G. Turnbull, *Power Electronic Control of AC Motors*, Pergamon, Elmsford, NY, 1988.

[10] I. Boldea and S. A. Nasar, *Vector Control of AC Drives*, CRC Press, Boca Raton, FL, 1992.

[11] B. Adkins and R. G. Harley, *The General Theory of Alternating Current Machines*, Chapman and Hall, New York, 1975.

[12] A. M. Trzynadlowski, *The Field Orientation Principle in Control of Induction Motors*, Kluwer Academic Publishers, Hingham, MA, 1994.

[13] M. P. Kazmierkowski and H. Tunia, *Automatic Control of Converter Fed Drives*, Elsevier, Amsterdam, 1994.

www.EngineeringEBooksPdf.com

[14] B. K. Bose, *Modern Power Electronics and AC Drives*, Prentice-Hall, Upper Saddle River, NJ, 2002.

[15] R. Krishnan, *Electric Motor Drives: Modeling, Analysis, and Control*, Prentice-Hall, Upper Saddle River, NJ, 2001.

[16] Romeo Ortega, Antonio Loria, Per Johan Nicklasson, and Hebert Sira-Ramírez, *Passivity-Based Control of Euler–Lagrange Systems: Mechanical, Electrical and Electromechanical Applications*, Springer-Verlag, Berlin, 1998.

[17] Darren M. Dawson, Jun Hu, and Timothy C. Burg, *Nonlinear Control of Electric Machinery*, Marcel Dekker, New York, 1998.

[18] F. Khorrami, P. Krishnamurthy, and H. Melkote, *Modeling and Nonlinear Adaptive Control of Electric Motors*, Springer-Verlag, Berlin, 2003.

[19] Stephen J. Chapman, *Electric Machinery Fundamentals*, McGraw-Hill, New York, 1985.

[20] H. H. Woodson and J. Melcher, *Electromechanical Dynamics: Part 1 Discrete Systems*, John Wiley & Sons, New York, 1968.

[21] L. W. Matsch and J. Derald Morgan, *Electromagnetic and Electromechanical Machines*, 3rd edition, John Wiley & Sons, New York, 1986.

[22] George McPherson and Robert D. Laramore, *An Introduction to Electrical Machines and Transformers*, 2nd edition, John Wiley & Sons, New York, 1990.

[23] D. V. Richardson, *Rotating Electric Machinery and Transformer Technology*, Reston Publishing Co., Reston, VA, 1978.

[24] Paul C. Krause and O. Wasynczuk, *ELECTROMECHANICAL Motion Devices*, McGraw-Hill, New York, 1989.

[25] Ned Mohan, *ELECTRIC DRIVES: An Integrative Approach*, MNPERE, Minneapolis, 2001.

[26] G. R. Slemon and A. Straughen, *Electric Machines*, Addison-Wesley, Reading, MA, 1980.

[27] J. Sokira and W. Jaffe, *Brushless DC Motors Electronic Commutation and Controls*, TAB Books, Blue Ridge Summit, PA, 1990.

[28] George J. Thaler and Milton L. Wilcox, *Electric Machines: Dynamics and Steady State*, John Wiley & Sons, New York, 1966.

www.EngineeringEBooksPdf.com

[29] Vincent Deltoro, *Electric Machines and Power Systems*, Prentice-Hall, Englewood Cliffs, NJ, 1985.

[30] Mohamed E. El-Hawary, *Principles of Electric Machines with Power Electronic Applications*, John Wiley & Sons, New York, 2002.

[31] P.C. Sen, *Principles of Electric Machines and Power Electronics*, John Wiley & Sons, New York, 1989.

[32] G. R. Slemon, *Electric Machines and Drives*, Addison-Wesley, Reading, MA, 1992.

[33] Uri Haber-Schaim, John H. Dodge, Robert Gardner, and Edward Shore, *PSSC Physics*, 7th Edition, Kendall/Hunt, Dubuque, IA, 1991.

[34] D. Halliday and R. Resnick, *Physics Volume II*, John Wiley & Sons, New York, 1962.

[35] Melvin Schwartz, *Principles of Electrodynamics*, Dover Publications, New York, 1972.

[36] Roald K. Wangsness, *Electromagnetic Fields*, John Wiley & Sons, New York, 1979.

[37] K. Ogata, *Modern Control Engineering*, Prentice-Hall, Englewood Cliffs, NJ, 1970.

[38] A. R. Bergen and V. Vittal, *Power Systems Analysis*, 2nd Edition, Prentice-Hall, Upper Saddle River, NJ, 2000.

[39] C. W. deSilva, *Control Sensors and Actuators*, Prentice-Hall, Englewood Cliffs, NJ, 1989.

[40] C. W. deSilva, *Mechatronics: An Integrative Approach*, CRC Press, Boca Raton, FL, 2004.

[41] T. Kailath, *Linear Systems*, Prentice-Hall, Englewood Cliffs, NJ, 1980.

[42] J. Stephan, M. Bodson, and J. Chiasson, "Real-time estimation of induction motor parameters", *IEEE Transactions on Industry Applications*, vol. 30, no. 3, pp. 746–759, May/June 1994.

[43] Alan V. Oppenheim and Alan S. Willsky, *Signals & Systems*, 2nd Edition, Prentice-Hall, Englewood Cliffs, NJ, 1997.

[44] E. W. Kamen and B. S. Heck, *Fundamentals of Signals and Systems using the Web and Matlab*, 2nd Edition, Prentice-Hall, Upper Saddler River, NJ, 2000.

www.EngineeringEBooksPdf.com

[45] Michael J. Roberts, *Signals and Systems – Analysis using Transform Methods and MATLAB*, McGraw-Hill, New York, 2003.

[46] G. F. Franklin, J. D. Powell, and A. Emami-Naeini, *Feedback Control of Dynamic Systems*, Addison-Wesley, Reading, MA, 1986.

[47] William A. Wolovich, *Automatic Control Systems*, Saunders College Publishing, Fort Worth, TX, 1994.

[48] Peter Dorato, *ANALYTICAL FEEDBACK SYSTEM DESIGN An Interpolation Approach*, Brooks/Cole, Pacific Grove, CA, 1999.

[49] Graham C. Goodwin, Stefan F. Graebe, and Mario E. Salgado, *Control System Design*, Prentice-Hall, Upper Saddle River, NJ, 2001.

[50] Vladimir Kučera, *Discrete Linear Control: The Polynomial Approach*, John Wiley & Sons, New York, 1979.

[51] M. Bodson and J. Chiasson, "Differential-geometric methods for control of electric motors", *International Journal of Robust and Nonlinear Control*, vol. 8, pp. 923–954, 1998.

[52] A. Isidori, *Nonlinear Control Systems*, Springer-Verlag, Berlin, 1989.

[53] J. Chiasson, "Nonlinear differential-geometric techniques for control of a series DC motor", *IEEE Transactions on Control Systems Technology*, vol. 2, no. 1, pp. 35–42, March 1994.

[54] Samir Mehta and John Chiasson, "Nonlinear control of a series DC motor: Theory and experiment", *IEEE Transactions on Industrial Electronics*, vol. 45, no. 1, pp. 134–141, February 1998.

[55] J. Chiasson and M. Bodson, "Nonlinear control of a shunt DC motor", *IEEE Transactions on Automatic Control*, vol. 38, no. 11, pp. 1662–1665, November 1993.

[56] Bodine Electric Co., *HANDBOOK: Small Motor, Gearmotor and Control*, Bodine Electric Company, Chicago, IL, 1993.

[57] John Kassakian, Martin Schlecht, and George Verghese, *Principles of Power Electronics*, Addison-Wesley, Reading, MA, 1991.

[58] A. E. Fitzgerald, C. Kingsley Jr., and S. D. Umans, *Electric Machinery*, McGraw-Hill, New York, 1983.

[59] Kaiyu Wang, John Chiasson, Marc Bodson, and Leon M. Tolbert, "A nonlinear least-squares approach for estimation of the induction motor parameters", in *Proceedings of the IEEE Conference on Decision and Control*, December 2004, pp. 3856–3861.

www.EngineeringEBooksPdf.com

[60] Joachim Holtz, "On the spatial propagation of transient magnetic fields in ac machines", *IEEE Transactions on Industry Applications*, vol. 32, no. 4, pp. 927–937, July/August 1996.

[61] E. R. Laithwaite and L. L. Freris, *Electric Energy: Its Generation, Transmission and Use*, McGraw-Hill, New York, 1980.

[62] Frank Wicks, "How George Westinghouse changed the world", *Mechanical Engineering*, pp. 74–79, October 1996.

[63] Marc Bodson, "Induction machines as generators", Private communication, May 2003, Denali National Park, Alaska.

[64] R. Marino, S. Peresada, and P. Valigi, "Adaptive input-output linearizing control of induction motors", *IEEE Transactions on Automatic Control*, vol. 38, no. 2, pp. 208–221, February 1993.

[65] M. Bodson, J. Chiasson, and R. Novotnak, "High performance induction motor control via input-output linearization", *IEEE Control Systems Magazine*, vol. 14, no. 4, pp. 25–33, August 1994.

[66] R. Lessmeier, W. Shumacher, and W. Leonhard, "Microprocessor-controlled ac-servo drives with synchronous or induction motors: Which is preferable?", *IEEE Transactions Industry Applications*, vol. IA-22, no. 5, pp. 812–819, September/October 1986.

[67] M. Bodson, J. Chiasson, and R. Novotnak, "Nonlinear speed observer for high-performance induction motor control", *IEEE Transactions on Industrial Electronics*, vol. 42, no. 4, pp. 337–343, August 1995.

[68] Marc Bodson and John Chiasson, "A systematic approach to selecting optimal flux references in induction motors", in *Record of the 27th Annual Meeting of the Industry Applications Society*, October 1992, Houston, TX.

[69] M. Bodson, J. Chiasson, and R. Novotnak, "A systematic approach to selecting flux references for torque maximization in induction motors", *IEEE Transactions on Control Systems Technology*, vol. 3, no. 4, pp. 388–997, December 1995.

[70] Z. Krzeminski, "Nonlinear control of the induction motor", in *10th IFAC World Congress*, 1987, pp. 349–354.

[71] G. S. Kim, I. J. Ha, and M. S. Ko, "Control of induction motors for both high dynamic performance and high-power efficiency", *IEEE Transactions on Industrial Electronics*, vol. 39, no. 4, pp. 323–333, August 1992.

www.EngineeringEBooksPdf.com

[72] M. Bodson, J. Chiasson, R. Novotnak, and R. Rekowski, "High performance nonlinear control of a permanent magnet stepper motor", *IEEE Transactions Control Systems Technology*, vol. 1, no. 1, pp. 5–14, March 1993.

[73] George C. Verghese and Seth Sanders, "Observers for flux estimation in induction machines", *IEEE Transactions on Industrial Electronics*, vol. 35, no. 1, pp. 85–84, February 1988.

[74] Phillipe Martin and Pierre Rouchon, "Two remarks on induction motors", in *CESA'96 IMACS Multiconference, Symposium on Control, Optimization and Supervision*, Lilles, 1996, pp. 76–79.

[75] Phillipe Martin and Pierre Rouchon, "Two simple flux observers for induction motors", *International Journal of Adaptive Control and Signal Processing*, vol. 14, pp. 171–175, 2000.

[76] X. Xu and D. W. Novotny, "Selection of the flux reference for induction machines in the field weakening region", *IEEE Transactions on Industry Applications*, vol. 28, no. 6, pp. 1353–1358, 1992.

[77] F. M. H. Khater, R. D. Lorenz, D. W. Novotny, and K. Tang, "Selection of the flux reference in field oriented induction machine controllers with consideration of magnetic saturation effects", *IEEE Transactions on Industry Applications*, vol. 23, no. 2, pp. 276–282, 1987.

[78] V. R. Stefanovic and T. H. Barton, "Static torque characteristics of an induction motor with variable frequency supply", in *Proceedings of the IEEE PES Winter Meeting*, 1972, pp. 1–3, New York.

[79] I. T. Wallace, D. W. Novotny, R. D. Lorenz, and D. M. Divan, "Increasing the dynamic torque per ampere capability of induction machines", *IEEE Transactions on Industry Applications*, vol. 30, no. 1, pp. 146–153, January/February 1994.

[80] S. H. Kim, S. K. Sul, and M. H. Park, "Maximum torque control of an induction machine in the field weakening region", in *Conference Record of the Industrial Applications Society*, 1993, pp. 401–407.

[81] B. C. Kuo, *Automatic Control Systems*, Prentice-Hall, Englewood Cliffs, NJ, 1987.

[82] R. Novotnak, J. Chiasson, and M. Bodson, "High-performance motion control of an induction motor with magnetic saturation", in *Proceedings of the 34th IEEE Conference on Decision and Control*, December 1995, pp. 2145–2150, New Orleans, LA.

www.EngineeringEBooksPdf.com

[83] R. Novotnak, *Nonlinear Control of an Induction Motor with Saturation: Theory and Experiment*, PhD thesis, University of Pittsburgh, 1995.

[84] R. Novotnak, J. Chiasson, and M. Bodson, "High-performance motion control of an induction motor with magnetic saturation", *IEEE Transactions on Control Systems Technology*, vol. 7, no. 3, pp. 315–327, May 1999.

[85] A. Khambadkone and J. Holtz, "Vector-controlled induction motor drive with a self-commissioning scheme", *IEEE Transactions on Industrial Electronics*, vol. 38, no. 5, pp. 322–327, October 1991.

[86] G. Heinemann and W. Leonhard, "Self-tuning field-oriented control of an induction motor drive", in *Proceedings of the 1990 International Power Electronics Conference*, April 1990, Tokyo, Japan.

[87] J. Stephan, "Real-time estimation of the parameters and fluxes of induction motors", Master's thesis, Carnegie Mellon University, 1992.

[88] A. Bellini, A. De Carli, and M. La Cava, "Parameter identification for induction motor simulation", *Automatica*, vol. 12, pp. 383–386, 1976.

[89] David Cox, John Little, and Donal O'Shea, *IDEALS, VARIETIES, AND ALGORITHMS An Introduction to Computational Algebraic Geometry and Commutative Algebra*, 2nd Edition, Springer-Verlag, Berlin, 1996.

[90] Joachim von zur Gathen and Jürgen Gerhard, *Modern Computer Algebra*, Cambridge University Press, Cambridge, UK, 1999.

[91] Stephen Wolfram, *Mathematica, A System for Doing Mathematics by Computer*, 2nd Edition, Addison-Wesley, Reading, MA, 1992.

[92] David Kincaid and Ward Cheney, *Numerical Analysis: Mathematics of Scientific Computing*, 3rd edition, Brooks/Cole, Pacific Grove, CA, 2002.

[93] Miguel Vélez-Reyes, W. L. Fung, and J. E. Ramos-Torres, "Developing robust algorithms for speed and parameter estimation in induction machines", in *Proceedings of the IEEE Conference on Decision and Control*, 2001, pp. 2223–2228, Orlando, Florida.

[94] M. Vélez-Reyes, K. Minami, and G. Verghese, "Recursive speed and parameter estimation for induction machines", in *Proceedings of the IEEE Industry Applications Conference*, 1989, pp. 607–611, San Diego, California.

www.EngineeringEBooksPdf.com

[95] Miguel Vélez-Reyes and George Verghese, "Decomposed algorithms for speed and parameter estimation in induction machines", in *Proceedings of the IFAC Nonlinear Control Systems Design Symposium*, 1992, pp. 156–161, Bordeaux, France.

[96] Miguel Vélez-Reyes, *Decomposed algorithms for parameter estimation*, PhD thesis, Massachusetts Institute of Technology, 1992.

[97] Miguel Vélez-Reyes, Milan Mijalković, Aleksandar M. Stanković, Silva Hiti, and James Nagashima, "Output selection for tuning of field-oriented controllers: Steady-state analysis", in *Conference Record of Industry Applications Society*, October 2003, pp. 2012–2016, Salt Lake City, UT.

[98] Kaiyu Wang, John Chiasson, Marc Bodson, and Leon M. Tolbert, "Tracking the rotor time constant of an induction motor traction drive for HEVs", in *Proceedings of the IEEE Workshop on Power Electronics in Transportation (WPET)*, October 2004, pp. 83–88.

[99] John Chiasson, Kaiyu Wang, Mengwei Li, Marc Bodson, and Leon M. Tolbert, "Algebraic methods for nonlinear systems: Parameter identification and state estimation", in *Current Trends in Nonlinear Systems and Control.* Laura Menini, Luca Zaccarian and Chaouki T. Abdallah, Eds., 2005, pp. 57–76, Birkhäuser.

[100] David Cox, John Little, and Donal O'Shea, *Using Algebraic Geometry*, Springer-Verlag, Berlin, 1998.

[101] Henk Nijmeijer and A. J. van der Schaft, *Nonlinear Dynamical Control Systems*, Springer-Verlag, 1990.

[102] R. Marino and P. Tomei, *Nonlinear Control Design - Geometric, Adaptive and Robust*, Prentice-Hall, Englewood Cliffs, NJ, 1995.

[103] B. Charlet, J. Levine, and R. Marino, "Two sufficient conditions for dynamic feedback linearization", in *Analysis and Optimization of Systems, Lecture Notes in Control and Information Sciences.* A. Bensoussan and J. L. Lions, Eds., 1988, vol. 111, pp. 181–192, Springer-Verlag, Berlin.

[104] B. Charlet, J. Levine, and R. Marino, "On dynamic feedback linearization", *Systems and Control Letters*, vol. 13, no. 2, pp. 143–151, August 1989.

[105] B. Charlet, J. Levine, and R. Marino, "Sufficient conditions for dynamic feedback linearization", *SIAM Journal on Control and Optimization*, vol. 29, no. 1, pp. 38–57, January 1991.

www.EngineeringEBooksPdf.com

[106] J. Chiasson, "Nonlinear controllers for induction motors", in *Proceedings of the IFAC Conference on System Structure and Control*, July 1995, pp. 572–583, Nantes, France.

[107] J. Chiasson, "A new approach to dynamic feedback linearization control of an induction motor", *IEEE Transactions on Automatic Control*, pp. 391–397, March 1998.

[108] J. Chiasson, "Dynamic feedback linearization of the induction motor", *IEEE Transactions on Automatic Control*, vol. 28, no. 10, pp. 1588–1594, 1993.

[109] M. Fliess, J. Levine, P. Martin, and P. Rouchon, "Flatness and defect of nonlinear systems: introductory theory and applications", *International Journal of Control*, vol. 61, no. 6, pp. 1327–1361, 1995.

[110] Hebertt Sira-Ramírez and Sunil K. Agrawal, *Differentially Flat Systems*, Marcel-Dekker, New York, 2004.

[111] G. Conte, C. H. Moog, and A. M. Perdon, *Noninear Control Systems, Lecture Notes in Control and Information Sciences, Volume 242*, Springer-Verlag, 1999.

[112] R. Novotnak, "A state feedback tracking controller for a PM stepper motor", Master's thesis, University of Pittsburgh, 1991.

[113] B. Kuo and J. Tal, *Incremental Motion Control, Step Motors and Control Systems, Vol. II*, SRL Publishing, Champaign, IL, 1987.

[114] P. P. Acarnley, *Stepping Motors: A Guide to Modern Theory and Practice*, Peter Peregrinus, Ltd., London, 1982.

[115] T. Kenjo, *Stepping Motors and Their Microprocessor Control*, Clarendon, New York, 1984.

[116] A. Verl and Marc Bodson, "Torque maximization for permanent magnet synchronous motors", *IEEE Transactions on Control Systems Technology*, vol. 6, no. 6, pp. 740–745, November 1998.

[117] Marc Bodson, John Chiasson, and Leon M. Tolbert, "A complete characterization of torque maximization for permanent magnet nonsalient synchronous motors", in *Proceedings of the American Control Conference*, June 2001, Arlington, VA.

[118] A. Blauch, "High-speed parameter estimation of step motors", Master's thesis, Carnegie Mellon University, 1992.

[119] A. Blauch, M. Bodson, and J. Chiasson, "High-speed parameter estimation of stepper motors", *IEEE Transactions on Control Systems Technology*, vol. 1, no. 4, pp. 270–279, April 1993.

www.EngineeringEBooksPdf.com

[120] Marc Bodson and John Chiasson, "Open and closed loop control of a permanent magnet stepper motor", in *Handbook of Electric Motors*. Richard H. Engelmann and William H. Middendorf, Eds., 1995, pp. 540–552, Marcel Dekker, New York.

[121] Marc Bodson, Jeffrey S. Sato, and Stephen R. Silver, "Spontaneous speed reversals in stepper motors", in *Proceedings of the 2003 Conference on Decision and Control*, December 2003, Maui, Hawaii.

[122] J. Chiasson, D. Seto, F. Sun, A. Stanković, and S. Bortoff, "Independent control of two PM motors using a single inverter: Application to elevator doors", *International Journal of Mechatronics*, vol. 15, no. 1, pp. 95–110, February 2005.

www.EngineeringEBooksPdf.com

Index

36-slot machine, 287

Air-gap voltage
  Induction motor, 478
Ampère's law, 194, 249, 259, 264, 269
  Examples, 196
  Ideal transformer, 228
  Modification to account for 1/r dependence, 286
Amplifier
  Saturation, 152
  Voltage limit, 71
Arbitrary rotating reference frame
  Induction motor, 478
Armature reaction
  DC motor, 38
Armature winding
  Definition, 315
Azimuthal magnetic field, 269, 292

B-H curve
  Definition, 207
Back emf
  Trapezoidal back-emf PM synchronous motor, 666
Backward difference speed estimator
  DC motor, 77, 153
Balanced conditions
  Induction motor
    Three-phase, 421
Base speed
  DC motor, 47
  Induction motor, 509, 541
Block diagram
  Block Diagram Reduction, 74
Blocked-rotor test
  Induction motor, 481
Bodson, M., 483
Bound current, 191
Brushless DC motor (BLDC), *see* Trapezoidal back-emf PM synchronous motor
Butterworth filter, 116, 163

Chapman, S. J., 213, 214
Clarke's transformation, 433
Classical control
  Internal model principle, 149
  PID, 131, 140
  Tracking and disturbance rejection, 129
Co-energy, 393, 411
  Induction motor, 393
    Torque from co-energy, 397
  Wound rotor synchronous motor, 411
Coercive force
  Definition, 208
Coercivity
  Definition, 208
Commutation
  BLDC motor, 674
  Multiloop DC motor, 32
  Single-loop DC motor, 9
Conservation of flux, 186, 252, 254, 365
Control
  Trapezoidal back-emf PM synchronous motor, 673
Current

www.EngineeringEBooksPdf.com

Drift speed, 28
Current command
DC motor, 74, 152
Current command control
PM synchronous motor, 606
Cylindrical coordinates
Definition, 7

DC motor
Arcing, 20
Armature flux, 17, 41, 63
Multiloop motor, 42
Armature reaction, 38
Armature winding
Definition, 315
Back emf, 15
Backward difference speed estimator, 77, 153
Base speed, 47
Block diagram, 74
Brush shifting, 62
Commutation
Multiloop motor, 32
Single-loop motor, 9
Current command, 74
Field flux linkage, 40
Field weakening, 46
Field winding
Definition, 315
Mathematical model, 20, 71
Microscopic viewpoint, 23
Single-loop motor, 26
Multiloop DC motor, 31
Nested loop controller, 90, 158
Neutral plane, 62
Parameter identification, 96, 160
Permanent magnet DC motor
Mathematical model, 43
Schematic diagram, 22
Self-inductance, 18
Separately excited DC motor, 166
Conservation of energy, 64
Field control, 168
Mathematical model, 44
Series DC motor, 166
Feedback linearization, 171
Field weakening, 171
Mathematical model, 64
Speed and load-torque observer, 172, 173
Shunt DC motor, 166
Feedback linearization, 174
Input-output linearization, 174
Mathematical model, 65
Simulation
Closed-loop simulation, 155
Open-loop simulation, 62
Single-loop, 5
Skewing of armature windings, 62
Speed and load-torque observer, 153
Speed controller, 77
Speed observer, 79
State feedback control, 86, 155
Integrator for load torque disturbance rejection, 157
Stator iron construction, 37
Tachometer, 29
Single-loop motor, 30
Torque, 6
Voltage and current limits, 22
Distributed windings, 245
Approximate sinusoidally wound, 249, 280
Flux linkage, 284
Self-inductance, 283
Two-phase machine, 284
Sinusoidailly wound
Radial magnetic field, 259
Sinusoidally wound, 257
Three-phase
36-slot machine, 287
Uniformly distributed winding, 285
Drift speed, 28

www.EngineeringEBooksPdf.com

Electric and magnetic fields
In the air gap, 276
Electric field
In the air gap, 275
Electromotive force (emf)
Definition, 12, 28
Elimination theory, 554
Encoder
Current fluctuations due to encoder resolution, 603
Encoder noise, 109
How it works, 72
End turn, 246

Faraday's law, 11, 57
Example
Linear DC machine, 14
Single-loop DC motor, 15
Ideal transformer, 229
Microscopic viewpoint, 323
Sign convention for the induced emf, 13
Surface element vector, 12
Feedback linearization
Induction motor
Dynamic feedback linearization, 582
Input-output linearization, 511
PM synchronous motor, 592, 595
Experimental results, 599, 603
Series DC motor, 171
Shunt DC motor, 174
Field weakening
DC motor, 46, 171
Induction motor
Comparison of the optimal with the standard approach, 544
Current constraints, 529
Optimal approach, 528
Standard approach, 509
Voltage and current constraints, 537
Voltage constraints, 530
PM synchronous motor, 592, 608
Example, 615
Simulation, 620
Transition speed, 609
Field winding
DC motor
Definition, 315
Synchronous motor
Definition, 315
Field-oriented control
Induction motor
Current command, 501
Experimental results, 506, 514
Input-output linearization, 511
Voltage command, 512
PM synchronous motor, 591
Field-oriented model
Induction motor, 497
Filtering, 108, 162
Bilinear transformation, 121
Butterworth filters, 116
Causality, 112
Digital filters, 122
Discretization using the trapezoidal rule, 120
Distortion, 114
filtfilt, 126, 165
Frequency response, 112
Implementation, 118
Low-pass filter, 113
Noncausal filtering, 126
Representations, 111
Signal flow diagram, 164
State-space representation, 124
The filter command, 164
Final value theorem, 156
Flat systems, 586
Fliess, M., 586
Flux linkage

www.EngineeringEBooksPdf.com

Definition, 40, 266
Trapezoidal back-emf PM synchronous motor, 661
Flux linkages in AC machines, 370
Fourier series expansion, 279
Free current, 206

Gauss's law, 183, 281
Divergence of the magnetic field, 292
Gears, 52
Global coupling factor, 369
Gray, C. B., 274

Hysteresis, 209
Loss, 223

Ideal filter, 162
Ill conditioned, 551
Induction motor
Air-gap voltage, 478
Arbitrary rotating reference frame, 478
Armature winding
Definition, 315
Base speed, 509, 541
Control problem, 494
Dynamic feedback linearization, 582
Equivalent circuit, 436, 446
Experimental results, 506
Field-oriented control, 501
Field-oriented model, 497
Flatness, 586
Flux observer, 519
Input-output linearization, 511
Leakage on the rotor side, 479, 484
Leakage on the stator side, 480, 484
Magnetic field energy, 393
Mathematical model, 363, 493
Microscopic viewpoint, 317, 326
Energy conversion, 321
Torque, 321
Multiple pole-pairs, 387
Nested loop controller, 573
Neutral, 423
Optimal flux reference, 545
Parameter identification, 548
Physics of, 296
Radial air-gap magnetic field, 364
Simulation
Input-output linearization controller, 572
Open-loop, 481
Space vector, 402
Squirrel cage rotor, 386
Comparison with a sinusoidally wound rotor, 344
Emfs, 336
Equivalent rotor circuit, 341
Rotor fluxes, 336
Rotor magnetic field, 342
Steady-state analysis, 334
Torque, 337
Stator and rotor magnetic fields rotate synchronously, 391
Steady-state analysis, 434
Blocked-rotor test, 481
Circle diagram, 438
Efficiency, 448
Equivalent circuit, 484
Impressed stator currents, 489
Maximum mechanical power, 489
No-load test, 481
Power factor, 439
Power factor angle, 439
Power transfer, 444
Pull-out slip, 443
Pull-out torque, 443
Rated current, 440
Rated slip, 439
Theory versus experiment, 448
Torque, 441

www.EngineeringEBooksPdf.com

Torque-slip curve, 442
Three-phase
Balanced conditions, 421
Mathematical model, 413
Motor neutral, 416
Rotor flux linkages, 420
Simulation using a two-phase equivalent model, 430
Sinusoidal windings, 415
Stator flux linkages, 419
Symmetric, 415
Two-phase equivalent model, 425, 430
Two-phase equivalent parameters, 420
wye-connected, 416
Three-phase to two-phase transformation, 424, 432
Torque
Three-phase, 427
Torque from co-energy, 393, 397
Torque from magnetic field energy, 396
Torque optimization, 528
Two-phase
Mathematical model, 383
Two-phase equivalent model, 430
Direct axis, 433, 478
Quadrature axis, 433, 478
Zero sequence, 425
Input-output linearization
Induction motor, 497, 511
Series DC motor, 171
Shunt DC motor, 174
Internal model principle, 149

Laplace transform
Final value theorem, 156
Reference trajectory, 159
Leakage, 366
Lenz's law, 14
Leonhard, W., 434
Long-pitched winding, 291

Magnetic field energy
Induction motor, 393
Magnetic field intensity
Definition, 207
Motivation for the definition, 204
Magnetic fields
B is normal to the surface of soft iron, 217
Computing B and H in magnetic circuits, 211
Conservation of flux, 186
Continuity of the normal component of B, 188
DC motor
Air-gap magnetic field, 6
Definition, 183
Experimental field distribution, 177
Solenoid, 198
Magnetic force
Definition, 3
Magnetic force law
Definition, 185
Magnetic materials, 177
B is normal to the surface of soft iron, 217
Bound current, 191
Continuity of the normal component of B, 188
Dipole moments, 192
H = 0 in ideal magnetic materials, 212, 217
Hysteresis loop, 209
Hysteresis loss, 223
Magnetic field intensity H
Definition, 207
Motivation for the definition, 204
Modeling, 190
Permanent magnets, 219
Permeability, 204
Quantum mechanics, 193
Rare earth materials for PM machines, 225

www.EngineeringEBooksPdf.com

Relating B to M, 201
Silicon steel, 225
Relative permeability, 225
Magnetization
Definition, 194
Magnetization vector, 195
Magnetizing inductance
Transformer, 230
Magnetomotive force (mmf), 264
Martin, P., 528
Mathematical model
Trapezoidal back-emf PM synchronous motor, 671
Matrix
Postive definite, 101
Postive semidefinite, 101
Symmetric, 101
Microscopic viewpoint, 315, 356
Axial electric field, 316
DC motor, 23
Single-loop motor, 26
Induction motor, 317, 326
Energy conversion, 321
Torque, 321
Trapezoidal back-emf PM synchronous motor, 679
Wound rotor synchronous machine, 334
Moment of inertia
Definition, 47
Multiple pole-pairs
Induction motor, 387, 405
Wound rotor synchronous motor, 408

Nested loop controller
DC motor, 90, 158
Induction motor, 573
Neutral
Induction motor, 416, 423
No-load test
Induction motor, 481
Numerical conditioning, 556

Observers
DC motor, 79
Comparison of a speed observer with a backward difference estimator, 154
Discretization of the speed observer equations, 82
Position cannot be estimated from speed, 154
Recovery from a disturbance, 153
Speed and load-torque observer, 153
Speed observer, 79
Induction motor
Flux observer, 519, 574
Load-torque observer, 578
Martin-Rouchon flux observer, 580
Speed observer, 521
Verghese-Sanders flux observer, 524
PM synchronous motor, 597
Series DC motor
Speed and load-torque observer, 172
Speed and load-torque observer in field weakening, 173
Oersted, Hans, 183

Parameter identification
DC motor, 96, 160
Error Index
DC motor, 103
Error index
Induction motor, 556
PM synchronous motor, 626
Induction motor, 548
Experimental results, 560
Mechanical parameters, 557
Nonlinear least-squares, 552
Overparameterized model, 549
Simulation, 558

www.EngineeringEBooksPdf.com

Least-squares approximation, 99
Parametric error indices, 161
DC motor, 103
Induction motor, 556
PM synchronous motor, 626
PM synchronous motor, 624
Experimental results, 627
Sufficient excitation
DC motor, 99
Induction motor, 556
PM synchronous motor, 626
Permanent magnets, 219
Relative permeability, 234
Permeability
Permanent magnet, 234
PM synchronous motor, 390
Armature winding
Definition, 315
Experimental results, 598, 599, 603
Mathematical model, 363, 591
Two-phase, 408
Parameter identification, 624
Radial air-gap magnetic field, 364
Simulation
Closed-loop control, 646
Open-loop control, 646
Three-phase
Mathematical model, 449, 456
Six pole, 288
Stator flux linkages, 451
Torque, 454
Pole-pairs
Definition, 67
Power factor
Induction motor, 439
Power factor angle
Induction motor, 439

Rated conditions
Interpretation, 440
Rated current, 440
Rated slip, 439
Rated torque, 443
Rational arithmetic, 556
Reluctance
Definition, 215
Remanence
Definition, 208
Resultants, 554
Retentivity
Definition, 208
Rotating magnetic fields, 245, 262, 293
Rotor flux linkage, 375
Rouchon, P., 528

Salient rotor, 313
Sanders, S., 524
Schwartz, M., 193, 265
Separately excited DC motor, 166
Armature control, 166
Field control, 168
Mathematical model, 44
Series DC motor, 166
Feedback linearization, 171
Mathematical model, 64
Speed and load torque observer, 172
Speed and load-torque observer, 173
Short-pitched winding
Self-inductance, 291
Short-pitched windings, 361
Flux linkage, 289
Shunt DC motor, 166, 173
Mathematical model, 65
Slip rings, 247
Slip speed, 302
Solenoid
Experimental field distribution, 180
Magnetic field, 198
Radial magnetic field, 227
Space vector
Flux linkage model, 569

www.EngineeringEBooksPdf.com

Induction motor model, 402, 430, 476, 477, 568
Rotor flux model, 570
Stator flux model, 570
Spatial harmonics, 282
Special theory of relativity
Transformation of the electromagnetic field, 327
Squirrel cage rotor, 386
Steady-state analysis, 334
State feedback control
DC motor, 86, 155
Block diagram, 89
Integator for load torque disturbance rejection, 157
PM synchronous motor, 595
Stator flux linkage, 370
Stator magnetic field
Trapezoidal back-emf PM synchronous motor, 654
Steady-state analysis
Induction motor
Circle diagram, 481
Efficiency, 448
Equivalent circuit, 436, 446, 484
Impressed stator currents, 489
Maximum mechanical power, 489
Power transfer, 444
Rated torque, 443
Torque, 441
Torque-slip curve, 442
Squirrel cage rotor, 334
Stepper motors, 632
Surface current density, 200, 205
Sylvester matrix, 554
Symmetric three-phase AC machine, 415
Synchronous motor
Armature winding
Definition, 315
Field winding
Definition, 315
Mathematical model, 388
Physics of, 302

Tachometer
DC motor, 29
Single-loop motor, 30
Three-phase generator
Induced voltage, 66
Three-phase to two-phase transformation, 432
Induction motor, 424
PM synchronous motor, 453
Toroid
Solenoid, 200
Torque, 380
Definition, 47
Induction motor
Three-phase, 427
Torque from co-energy, 393
Induction motor, 397
Torque from magnetic field energy
Induction motor, 396
Trapezoidal back-emf PM synchronous motor, 668
Wound rotor synchronous motor
From co-energy, 411
Torque optimization
Induction motor, 528
Current constraints, 529
Generator mode, 538
Motoring mode, 539
Optimal flux reference, 545
Voltage and current constraints, 537
Voltage constraints, 530
Synchronous motor, 608
Total leakage factor, 385
Tracking and disturbance rejection, 129
Trajectory generation, 82, 93
Continuous jerk, 155
Transformer
Ideal, 228, 229

www.EngineeringEBooksPdf.com

Magnetizing inductance, 230
Trapezoidal back-emf PM synchronous motor, 651
Back emf, 666
BLDC terminology, 677
Construction, 651
Control, 673
Flux linkage, 657, 661
Mathematical model, 671
Microscopic viewpoint, 679
Operation, 673
Stator magnetic field, 654
Torque, 668
Two stage identification
PM synchronous motors, 629
Two-phase machine
Approximate sinusoidal winding, 284

Verghese, G., 524
Voltage
Definition, 28

Why 60 Hz?, 474
Why AC?, 471
Why sinusoidal voltages?, 472
Why three-phase?, 458
Wound rotor synchronous machine, 489
dq model, 409
Mathematical model, 409
Multiple pole-pairs, 408

Zero component
Induction motor, 431

www.EngineeringEBooksPdf.com